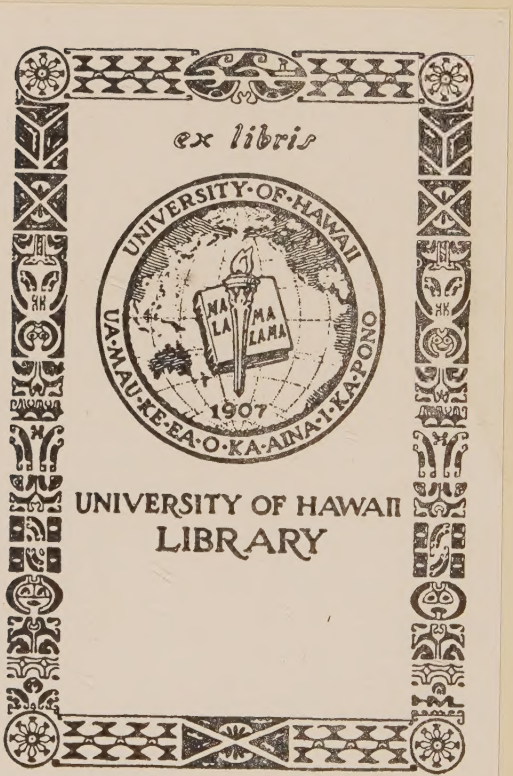
ex libris
UNIVERSITY·OF·HAWAII
NA LA MA LAMA
1907
UA·MAU·KE·EA·O·KA·AINA·I·KA·PONO
UNIVERSITY OF HAWAII
LIBRARY

FIFTH SYMPOSIUM

(INTERNATIONAL)

ON

COMBUSTION

5th, University of Pittsburgh, 1954.

Combustion in Engines and Combustion Kinetics

At The University of Pittsburgh
Pittsburgh, Pennsylvania
August 30–September 3, 1954

Published for
THE COMBUSTION INSTITUTE
Under the auspices of
THE STANDING COMMITTEE ON COMBUSTION SYMPOSIA

REINHOLD PUBLISHING CORPORATION
New York
CHAPMAN & HALL, Ltd., LONDON
1955

UNIVERSITY OF HAWAII LIBRARY

Copyright 1955 by

The Combustion Institute

All rights reserved

Brief quotations from this book for purposes of scientific discussion will be permitted.

Library of Congress Catalog Card Number: 55–9170

Printed in the United States of America
By The Waverly Press, Inc.

QD516
S92
1954

PREFACE

The Fifth Symposium (International) on Combustion was the last in the series of three postwar symposia to be sponsored by the Standing Committee on Combustion Symposia. At the 1952 symposium, held at Massachusetts Institute of Technology, it was suggested that serious thought be given to the formation of a permanent organization devoted to the interests of the science of combustion. Such an organization, it was felt, could put the important work done by the Standing Committee on a firm footing and better meet the needs of the rapidly expanding group of chemists, physicists, and engineers engaged in research and development in this field. It would also provide a responsible body for dealing legally and effectively with various problems. Accordingly a subcommittee of ten, with representatives from industry, government, and universities in the United States, was formed to consider the advisability and feasibility of establishing a permanent society. After a year and a half of careful study and discussion with numerous individuals and professional groups, the subcommittee—in conjunction with similar committees headed by the honorary members of the Standing Committee in Belgium, France, Great Britain, and the Netherlands—recommended the formation of The Combustion Institute.

On July 1, 1954, The Combustion Institute was incorporated in the State of Delaware as a nonprofit professional society, whose purpose is to promote the science and application of combustion and to disseminate knowledge in this field. Its activities include the organization of symposia and publication of the proceedings, and related projects consistent with its stated purpose. It is not intended that the Institute will compete with other societies either in its meetings or publications. Its interests embrace a wide field of scientific activity not covered by the meetings of established societies.

The first business meeting of Institute members was held September 1, during the Fifth Combustion Symposium. A Board of Directors of 15 members was elected from a list submitted by a nominating committee. Subsequently the Board of Directors elected officers, determined the location of the executive office of the Institute, appointed an executive secretary, and established two working committees: The Executive Committee and the Combustion Institute Committee. This latter committee comprises representatives from industry, government, and universities in Australia, Austria, Belgium, Canada, France, Germany, Great Britain, India, Italy, Japan, the Netherlands, Spain, Sweden, Switzerland, and the United States. It is the function of The Combustion Institute Committee to organize and conduct future symposia and to arrange for the publication of symposia proceedings.

The technical meetings of the Fifth Symposium, held at the University of Pittsburgh, emphasized the chemical aspects of combustion, especially combustion kinetics. In recognition of the role of combustion in the development and design of engines of all types, a series of invited papers was arranged to discuss unsolved problems in engines, including spark and compression ignition engines, liquid and solid rockets, turbojet and ramjet engines, as well as basic kinetic problems, including high temperature kinetics of importance to the field of combustion. Ninety papers were accepted for presentation, which with the invited papers total 101. Of these, one was from Australia; two from Belgium; one from Canada, six from France; two from Germany; twenty-four from Great Britain; six from Japan; and fifty-nine from the United States. The Papers Subcommittee is to be commended for carrying out the difficult task of arranging the multiple review of each manuscript submitted, which resulted in the presentation of an outstanding series of papers.

Two panel discussions were scheduled:

1. Heterogeneous Burning. Presiding, Professor H. C. Hottel. Discussion Leaders: Drs. David Altman, Glenn C. Williams, and Sabri Ergun.

2. Status of the Theory of the Kinetics of Combustion Reactions. Presiding, Professor A. R. Ubbelohde. Discussion Leaders: Drs. George Porter, John M. Richardson, and Kurt E. Shuler.

Because of space limitations, these stimulating discussions have been summarized by the chairmen.

There were 575 registrants. Representation from other countries was as follows: 1 from Belgium, 11 from Canada, 9 from France, 3 from

Germany, 30 from Great Britain, 4 from Japan, 4 from the Netherlands, and 4 from Sweden.

In addition to the General Committee and the Papers Subcommittee, two other subcommittees worked diligently to ensure the success of the symposium. To the Subcommittee on Arrangements much credit is due for the efficient organization of physical facilities and an entertainment program that added appreciably to the enjoyment of those attending the symposium.

The Finance Subcommittee enlisted the cooperation of government agencies and industry which made possible the participation of combustion experts from abroad, and the partial subsidy of this volume. The Department of the Air Force and the Advisory Group for Aeronautical Research and Development (NATO) generously provided transportation for many of the overseas visitors. It is desired to acknowledge the partial support of this symposium by the United States Department of the Air Force through the Office of Scientific Research of the Air Research and Development Command, by the United States Department of the Army through the Office of Ordnance Research, and by the United States Department of the Navy through the Office of Naval Research.

The Symposium Committee also gratefully acknowledges support received from:

Air Reduction Company
American Cyanamid Company
American Gas Association
American Gas and Electric Service Corporation
American Machine & Foundry Company
The Atlantic Refining Company
Atlantic Research Corporation
Avco Manufacturing Corporation—Lycoming Division
Battelle Memorial Institute
Bechtel Corporation
Bendix Aviation Corporation—Scintilla and Products Divisions
Bethlehem Steel Company
Boeing Airplane Company
C. F. Braun & Company
Buffalo Electro-Chemical Company, Inc., Division of Food Machinery and Chemical Corporation
Godfrey L. Cabot
California Research Corporation
Catalytic Construction Company
Caterpillar Tractor Company
Chrysler Corporation
Cities Service Research & Development Company
Combustion and Explosives Research, Inc.
Consolidated Vultee Aircraft Corporation—Convair Company
Continental Aviation & Engineering Corporation
Continental Oil Company
Cummins Engine Company
Curtiss-Wright Corporation
The Dow Chemical Corporation
E. I. du Pont de Nemours & Company
Ethyl Corporation
Engine and Airplane Corporation—Fairchild Engine Division
Experiment Incorporated
Fairbanks, Morse & Company
Fisher Scientific Company
The Fluor Corporation
Ford Motor Company
The Garrett Corporation
General Electric Company—Aircraft Gas Turbine Division
General Motors Corporation—Allison and Research Laboratories Divisions
Gulf Research & Development Company
Hercules Motor Corporation
Hercules Powder Company
Houdry Process Corporation
International Harvester Company
The M. W. Kellogg Company
Koppers Company, Inc.
Linde Air Products Company (Union Carbide & Carbon Corporation)
Arthur D. Little, Inc.
The Lummus Company
Marquardt Aircraft Company
Mellon Institute of Industrial Research
Mine Safety Appliances Company
National Airoil Burner Company, Inc.
National Fireworks Ordnance Corporation
Olin Industries Incorporated
Peabody Engineering Corporation
Phillips Petroleum Company
Pittsburgh Plate Glass Foundation
The Pure Oil Company
Reaction Motors Incorporated
Richfield Oil Corporation
A. V. Roe Canada Limited
Shell Development Company
Sinclair Refining Company
Socony-Vacuum Oil Company
Southwest Research Institute of San Antonio

Standard Oil Company of Indiana
Standard Oil Company of Ohio
Standard Oil Development Company
Sun Oil Company
The Texas Company
Thompson Products, Inc.
Tide Water Associated Oil Company
Union Oil Company of California
United Aircraft Corporation—Pratt and Whitney Division
United States Steel Corporation
Universal Oil Products Company
Westinghouse Electric Corporation

The grateful appreciation of all who attended the symposium is extended to Chancellor Rufus H. Fitzgerald and Dean Herbert E. Longenecker, of the University of Pittsburgh, for their cooperation in making available the facilities of the University and to Dr. Edward R. Weidlein for use of the Mellon Institute Auditorium. Special mention is made, also, of the untiring efforts of Mr. Frederick E. Lange and Mr. Viers Adams of the University's Extension Division, which contributed greatly to the success of the meeting.

The U. S. Bureau of Mines arranged an interesting coal mine explosion demonstration at the Experimental Station in Bruceton and provided the services of Mrs. Ruth F. Brinkley who assisted in editing and translating a number of the foreign papers.

Members of the technical staffs of the Westinghouse Research Laboratories and the U. S. Bureau of Mines aided in reading proof of this book.

Standing Committee on Combustion Symposia:

Bernard Lewis, *Chairman*
Combustion and Explosives Research, Inc.
200 Alcoa Building
Pittsburgh 19, Pennsylvania

Hoyt C. Hottel, *Secretary*
Massachusetts Institute of Technology
Cambridge 39, Massachusetts

A. J. Nerad
General Electric Company
Schenectady 5, New York

Digitized by the Internet Archive
in 2026

https://archive.org/details/symposium-international-on-combustion_1955

STANDING COMMITTEE ON COMBUSTION SYMPOSIA

Chairman—Bernard Lewis
Secretary-Treasurer—Hoyt C. Hottel
Member—A. J. Nerad

Honorary Members

Dr. J. J. Broeze, Holland
Professor K. Clusius, Switzerland
Sir Alfred C. Egerton, Great Britain
Professor Wilhelm Jost, Germany
Mr. W. B. Kennedy, Australia
Professor Paul Laffitte, France
* Professor Heinrich Mache, Austria
Dr. D. C. MacPhail, Canada
Professor Eugène Mertens, Belgium
Dr. Gregorio Millán, Spain
Dr. Ernst H. W. Weibull, Sweden
Professor Sakae Yagi, Japan

1954 SYMPOSIUM COMMITTEE

Chairman

Dr. Bernard Lewis	Combustion and Explosives Research, Inc.
Dr. Herbert E. Longenecker	University of Pittsburgh

Papers Subcommittee

Dr. Stewart Way } *Co-*	Westinghouse Research Laboratories
Dr. Glenn C. Williams } *Chairmen*	Massachusetts Institute of Technology
Dr. David Altman	California Institute of Technology
Dr. W. H. Avery	The Johns Hopkins University
Dr. George Glockler	Office of Ordnance Research
Professor Newman A. Hall	University of Minnesota
Dr. J. O. Hirschfelder	University of Wisconsin
Professor H. C. Hottel (ex officio)	Massachusetts Institute of Technology
Professor Keith Laidler	Catholic University of America
Dr. Bernard Lewis (ex officio)	Combustion and Explosives Research, Inc.
Dr. J. P. Longwell	Esso Research and Engineering Company
Professor R. G. W. Norrish	Cambridge University, England
Professor Robert N. Pease	Princeton University
Dr. Guenther von Elbe	Combustion and Explosives Research, Inc.
Dr. Lloyd L. Withrow	General Motors Corporation

Finance Subcommittee

Mr. J. B. Macauley, *Chairman*	Ethyl Corporation
Mr. Richard C. Alden	Phillips Petroleum Company
Mr. John M. Campbell	General Motors Corporation
Mr. A. T. Colwell	Thompson Products, Inc.
Mr. L. O. Crockett	Gulf Oil Company
Mr. David E. Day	Richfield Oil Corporation
Mr. Hugh W. Field	Atlantic Refining Company
Dr. John M. Gaines	Linde Air Products Company
Mr. William E. Hanford	The M. W. Kellogg Company
Dr. J. Bennett Hill	Sun Oil Company
Mr. William M. Holaday	Socony-Vacuum Oil Company, Inc.
Mr. George J. Huebner, Jr.	Chrysler Corporation
Mr. Roy T. Hurley	Curtiss-Wright Corporation

* Deceased September 1, 1954.

Finance Subcommittee (Continued)

Mr. Edward W. Isom	Sinclair Refining Company
Dr. W. E. Kuhn	The Texas Company
Mr. Earle S. MacPherson	Ford Motor Company
Mr. John T. McCoy	Tide Water Associated Oil Company
Mr. A. J. Nerad (ex officio)	General Electric Company
Mr. Wright A. Parkins	Pratt & Whitney Aircraft
Mr. Charles M. Ridgway	Pure Oil Company
Mr. Joseph K. Roberts	Standard Oil Company of Indiana
Mr. C. G. A. Rosen	Caterpillar Tractor Company
Mr. J. R. Sabina	E. I. du Pont de Nemours & Company, Inc.
Mr. Walter W. Scheumann	Cities Service Oil Company
Dr. Monroe E. Spaght	Shell Development Company
Dr. William J. Sweeney	Esso Research and Engineering Company
Mr. Howard G. Vesper	California Research Corporation

Subcommittee on Arrangements

Mr. Frederick E. Lange, *Chairman*	University of Pittsburgh
Mr. Viers W. Adams	University of Pittsburgh
Mr. E. A. Batchelder	University of Pittsburgh
Dr. Theodore W. Biddle	University of Pittsburgh
Dr. John R. Bowman	University of Pittsburgh
Dr. S. R. Brinkley, Jr.	Combustion and Explosives Research, Inc.
Mr. Max Elder	University of Pittsburgh
Mr. Charles Elliott, Jr.	University of Pittsburgh
Dr. G. R. Fitterer	University of Pittsburgh
Dr. Henry Frank	University of Pittsburgh
Dr. David Halliday	University of Pittsburgh
Dr. Herbert E. Longenecker	University of Pittsburgh
Mr. G. Edward Lyness	University of Pittsburgh
Mr. Charles W. Shaffer	Pittsburgh Convention Bureau, Inc.

Other Members

Mr. Ralph E. Albright	Socony-Vacuum Laboratories
Dr. D. L. Armstrong	Aerojet-General Corporation
Mr. Everett M. Barber	The Texas Company
Dr. Daniel P. Barnard	Standard Oil Company of Indiana
Mr. Bernard F. Beckelman	Boeing Airplane Company
Mr. William J. Bennet	Marquardt Aircraft Company
Dr. L. G. Bonner	Allegany Ballistics Laboratory
Prof. Cecil E. Boord	Ohio State University
Prof. F. Philip Bowden	Cambridge University, England
Dr. H. P. Broida	National Bureau of Standards
Mr. Edmund D. Brown	United Aircraft Corporation
Dr. Hartwell F. Calcote	Experiment Incorporated
Mr. D. E. Carr	Phillips Petroleum Company
Dr. A. G. Cattaneo	Shell Development Company
Mr. C. E. Chapman	Consolidated Vultee Aircraft Corporation
Mr. J. L. Cooley	California Research Corporation
Prof. L. G. Crocco	Princeton University
Dr. Glenn H. Damon	U. S. Bureau of Mines
Dr. B. deB. Darwent	Olin Mathieson Chemical Corporation
Dr. L. Deffet	Centre de Recherches des Produits Explosifs, Brussels, Belgium

Other Members (Continued)

Mr. Floyd G. Dougherty	General Motors Corporation
Mr. Cyrus G. Dunkle	Picatinny Arsenal, Dover
Dr. Rudolph Edse	Ohio State University
Dr. M. A. Elliott	Illinois Institute of Technology
Prof. Howard W. Emmons	Harvard University
Dr. Marjorie Evans	Stanford Research Institute
Dr. John B. Fenn	Project SQUID, Princeton University
Dr. Ernest F. Fiock	National Bureau of Standards
M. l'Ingénieur-Général Fleury	Directeur Central des Poudres, Paris, France
Dr. Charles E. Frank	National Distillers Chemical Company
Dr. Joseph H. Frazer	Ballistic Research Laboratories, Aberdeen Proving Ground
Dr. H. A. Fremont	General Electric Company
Dr. Sidney Golden	Brandeis University
Dr. W. A. Gruse	Mellon Institute
Mr. William V. Hanzalek	Wright Aeronautical Corporation
Prof. John Happel	New York University
Dr. Amos G. Horney	Office of Scientific Research, Air Research and Development Command
Dr. L. S. Kassel	Universal Oil Products Company
Dr. R. M. Kennedy	Sun Oil Company
Mr. Bertrand A. Landry	Battelle Memorial Institute
Prof. Maurice Letort	Université de Nancy, Nancy, France
Dr. Robert S. Levine	North American Aviation, Inc.
Dr. J. W. Linnett	Queen's College, Oxford England
Mr. W. G. Lovell	Ethyl Corporation
Dr. G. H. Markstein	Cornell Aeronautical Laboratory
Dr. Frederick J. Martin	The M. W. Kellogg Company
Mr. G. V. McGurl	Koppers Company
Mr. David J. Miller	Bureau of Aeronautics
Dr. C. W. Montgomery	Gulf Research & Development Company
Prof. D. L. Mordell	McGill University, Quebec, Canada
Dr. E. C. Noonan	Naval Ordnance Laboratory
Dr. W. T. Olson	National Advisory Committee for Aeronautics
Dr. Frank A. Parker	Detroit Controls Corporation
Dr. S. S. Penner	California Institute of Technology
Dr. John M. Richardson	Ramo-Wooldridge Corporation
Mr. T. L. Robey	American Gas Association
Prof. Ernst H. W. Schmidt	Technische Hochschule Munich, Germany
Dr. Edward H. Seymour	Office of Naval Research
Mr. M. S. Silverstein	Frankford Arsenal
Dr. A. W. Sloan	Atlantic Research Corporation
Dr. Robert L. Smith	Sinclair Research Laboratories, Inc.
Dr. B. M. Sturgis	E. I. duPont de Nemours & Company
Prof. Martin Summerfield	Princeton University
Prof. H. Austin Taylor	New York University
Sir Hugh S. Taylor	Princeton University
Dr. James Taylor	Imperial Chemical Industries, Ltd., London, England
Dr. Sumner B. Twiss	Chrysler Corporation
Prof. A. R. Ubbelohde	Imperial College of Science and Technology, London, England
Mr. W. van Loon	Netherlands State Mines, Gêleen, Holland
Dr. Donald S. Villars	U. S. Naval Ordnance Test Station

Other Members (Continued)

Dr. Theodore von Kármán	Advisory Group for Aeronautical Research & Development, NATO, Paris, France
Dr. A. D. Walsh	University of Leeds, Leeds, England
Mr. E. P. Walsh	Experiment Incorporated
Dr. E. A. Watson	Joseph Lucas Ltd., Birmingham, England
Mr. R. L. Wehrli	Robertshaw-Fulton Controls Company
Prof. Kurt Wohl	University of Delaware
Mr. Warren W. Woods	Continental Oil Company
Dr. William P. Yant	Mine Safety Appliances Company
Prof. M. J. Zucrow	Purdue University

THE COMBUSTION INSTITUTE

Officers

President ..... Bernard Lewis
Vice President ..... Hoyt. C. Hottel
Treasurer ..... Stewart Way
Assistant Treasurer ..... Bernard M. Sturgis
Secretary ..... Glenn C. Williams

Executive Office

200 Alcoa Building, Pittsburgh 19, Pennsylvania
Mrs. Helen G. Barnes, Executive Secretary

Board of Directors

Mr. J. L. Cooley, Vice President (2)
California Research Corporation
200 Bush Street
San Francisco 4, California

Professor Newman Hall (2)
Department of Mechanical Engineering
University of Minnesota
Minneapolis 14, Minnesota

Dr. Amos G. Horney (1)
Chief, Chemistry Division
Office of Scientific Research
Deputy Commander/Technical Operations
Air Research and Development Command
P. O. Box 1395
Baltimore 3, Maryland

Professor H. C. Hottel (2)
Department of Chemical Engineering
Massachusetts Institute of Technology
Cambridge 39, Massachusetts

*Dr. Bernard Lewis, President (3)
Combustion and Explosives Research, Inc.
200 Alcoa Building
Pittsburgh 19, Pennsylvania

Mr. J. B. Macauley (3)
Director of Research
Ethyl Corporation
1600 West Eight Mile Road
Ferndale 20, Detroit, Michigan

*Mr. A. J. Nerad (1)
Research Laboratory
General Electric Company
P. O. Box 1088
Schenectady, New York

Dr. Walter T. Olson (3)
Chief, Fuels and Combustion Research Division
National Advisory Committee for Aeronautics
Lewis Flight Propulsion Laboratory
Cleveland 11, Ohio

Professor Robert N. Pease (1)
Frick Chemical Laboratory
Princeton University
Princeton, New Jersey

Dr. Edward H. Seymour (2)
Power Branch, Office of Naval Research
Department of the Navy
Washington 25, D. C.

Dr. Bernard M. Sturgis (3)
Organic Chemicals Department
E. I. du Pont de Nemours & Company, Inc.
P. O. Box 1671
Wilmington, Delaware

Dr. W. J. Sweeney, Vice President (1)
Esso Research and Engineering Company
15 West 51st Street
New York 19, New York

* Executive Committee
(1) Term expires September 1956.
(2) Term expires September 1958.
(3) Term expires September 1960.

Board of Directors (Continued)

*Dr. Stewart Way (1)
Manager, Thermodynamics Section
Research Laboratories
Westinghouse Electric Corporation
East Pittsburgh, Pennsylvania

Professor Glenn C. Williams (3)
Department of Chemical Engineering
Massachusetts Institute of Technology
Cambridge 39, Massachusetts

Dr. Lloyd L. Withrow (2)
Head, Fuels & Lubricants Department
Research Laboratories Division
General Motors Corporation
Detroit 2, Michigan

The Combustion Institute Committee

United States

Professor Glenn C. Williams, Chairman
Massachusetts Institute of Technology
Cambridge 39, Massachusetts

Dr. David Altman
California Institute of Technology
Pasadena 3, California

Mr. J. L. Cooley
California Research Corporation
San Francisco 4, California

Dr. George Glockler
Office of Ordnance Research
Durham, North Carolina

Dr. J. P. Longwell
Esso Research and Engineering Company
Linden, New Jersey

Dr. Walter T. Olson
Lewis Flight Propulsion Laboratory
National Advisory Committee for Aeronautics
Cleveland 11, Ohio

Great Britain

Sir Alfred C. Egerton
Imperial College of Science and Technology
London, S.W.7

Dr. J. Stanley Clarke
Joseph Lucas Limited
Burnley, Lancs.

Dr. Peter Lloyd
National Gas Turbine Establishment
Pyestock, Farnborough, Hampshire

Australia

Mr. W. B. Kennedy
Aeronautical Research Laboratories
Department of Supply
Melbourne

Austria

(To be selected)

Belgium

Dr. Louis Deffet
Centre de Recherches Scientifiques et Techniques pour l'Industrie des Produits Explosifs
Bruxelles

Canada

(To be selected)

France

Professeur Paul Laffitte
Faculté des Sciences
L'Université de Paris
Laboratoire de Chimie Générale
1, rue Victor-Cousin
Paris V°

Germany

Professor Dr. Wilhelm Jost
Chemisches Institut der Universität
Göttingen

India

Dr. M. S. Thacker
Director, Indian Institute of Science
Bangalore 3

Italy

Professor Cesare Codegone
Istituto di Fisica Tecnica
Politecnico di Torino

Japan

Professor Sakae Yagi
University of Tokyo

Netherlands

Professor Ir. J. J. Broeze
Director of Research
Royal Dutch/Shell Company
Delft

Spain

Dr. Gregorio Millán
Instituto Nacional di Tecnica Aeronautica
Madrid

Sweden

Professor Dr. Ernst H. W. Weibull
Bockamöllan, Brösarps Station

Switzerland

Professor Dr. K. Clusius
Physikalisch-Chemisches Institut der Universität
Zürich

CONTENTS

Introduction to the Fifth Symposium (International) on Combustion, University of Pittsburgh, Pittsburgh, Pennsylvania, August 30–September 3, 1954, by Hoyt C. Hottel xxv

REVIEW OF PROBLEMS ON COMBUSTION IN ENGINES AND KINETICS OF COMBUSTION PROCESSES

I. Combustion Problems in Internal Combustion Engines. *W. G. Lovell* 1
II. Combustion Problems in Diesel Engines. *P. H. Schweitzer* 7
III. Combustion Problems in Liquid-Fuel Rocket Engines. *S. S. Penner and P. P. Datner* .. 11
IV. Unsolved Problems in Solid-Propellant Combustion. *Richard D. Geckler* 29
V. Problems of Turbo-Jet Combustion. *Peter Lloyd* 40
VI. Combustion Problems in Ramjets. *J. P. Longwell* 48
VII. On the Kinetics of Elementary Gas Phase Reactions at High Temperatures. *Kurt E. Shuler* 56
VIII. Survey of Collision Processes in the Combustion of Hydrocarbons. *A. R. Ubbelohde* 74
IX. Chemical Kinetics of Hydrocarbon Combustion. *Guenther von Elbe* 79
X. Space Heating Rates and High Temperature Kinetics. *W. H. Avery* 86
XI. A Theory of Space Requirements for Combustion Behind Grids in a Closed Duct. *Joseph Jennissen* 91

COMBUSTION OF FUEL DROPLETS

1. Combustion of Droplets of Heavy Liquid Fuels. *H. C. Hottel, G. C. Williams, and H. C. Simpson* 101
2. Combustion of Fuel Droplets in a Vibrating Air Field. *Seiichiro Kumagai and Hiroshi Isoda* 129
3. The Effects of Chemical and Physical Parameters on the Burning Rate of a Liquid Droplet. *Henry Wise, Jack Lorell, and Bernard J. Wood* 132
4. An Experimental Study on the Combustion of a Fuel Droplet. *Kiyosi Kobayasi* 141
5. Kinetics of Liquid Combustion Processes: Evaporation and Ignition Lag of Fuel Droplets. *Niichi Nishiwaki* 148
6. Effect of Fuel Droplets on Flame Stability, Flame Velocity, and Inflammability Limits. *J. A. Browning and W. G. Krall* 159

PROPELLANT BURNING

7. Preliminary Measurements of the Combustion Time Lag in a Monopropellant Rocket Motor. *Luigi Crocco, Jerry Grey, and George B. Matthews* 164
8. Study of the Ignition Lag of Liquid Propellants. *M. Barrére and A. Moutet* 170
9. Studies of the Rates of Combustion of Hypergolic Fluids. *Foy McCullough, Jr. and H. P. Jenkins, Jr.* 181
10. Oscillation of the Flame Front Between Two Unlike Droplets in a Bipropellant Liquid System. *C. C. Miesse* 190
11. A Study of Fast Reactions in Fuel-Oxidant Systems: Anhydrous Hydrazine with 100 Per Cent Nitric Acid. *Martin Kilpatrick and Louis L. Baker, Jr.* 196
12. Mechanism of Burning of Nitrate Esters. *Rudolph Steinberger* 205
13. Measurement of the Temperature Distribution in Burning Liquid Strands. *D. L. Hildenbrand and A. Greenville Whittaker* 212
14. Surface Properties of Liquid Bipropellants and Their Effects on the Kinetics of Ignition. *Michel L. J. Bernard* 217
15. The Application of Kinetics to the Hazardous Behavior of Ammonium Nitrate. *R. M. Hainer* 224

COMBUSTION OF SOLIDS

16. Studies on Combustion of Carbon Particles in Flames and Fluidized Beds. *Sakae Yagi and Daizo Kunii* ... 231
17. Contributions to the Combustion Mechanism of Carbon. *E. Wicke* ... 245
18. Combustion Rate of Pulverized Coal in a Jet Stream. *Kenjiro Saji* ... 252
19. The Absolute Thermal Decomposition Rates of Solids. *Robert D. Schultz and Albert O. Dekker* ... 260
20. Some Physical Aspects of the Combustion of Magnesium Ribbons. *Kenneth P. Coffin* ... 267
21. Pre-Ignition and Ignition Reactions of the Pyrotechnic System Zn-C_6Cl_6-$KClO_4$. *Saul Gordon and Clement Campbell* ... 277

DIFFUSION FLAMES AND CARBON FORMATION

22. On the Ions in Diffusion Flames. *Tosirô Kinbara and Junji Nakamura* ... 285
23. The Height of Diffusion Flames and the Relative Importance of Mixing and Reaction Rates. *H. N. Powell* ... 290
24. Formation of Carbon and Related Materials in Diffusion Flames. *J. R. Arthur and D. H. Napier* ... 303
25. Mechanism of Smoke Formation in Diffusion Flames. *Rose L. Schalla and Glen E. McDonald* 316
26. Carbon Formation from C_2H_2 and CO in Discharge Tubes. *A. G. Gaydon and A. R. Fairbairn* 324

COMBUSTION IN ENGINES

27. The Effect of Heat Transfer on the Maximum Reaction Rates of a Homogeneous Reactor. *E. A. DeZubay and E. C. Woodward* ... 329
28. Rational Prediction of Combustion Efficiency for Baffle-Type Combustors. *Gilbert S. Bahn* 336
29. Mixing and Combustion at High Turbulence in Combustion Chambers. *Ernst H. W. Schmidt and Fritz Schoppe* ... 343
30. Correlation of Autoignition Phenomena in Internal Combustion Engines and Rapid Compression Machines. *J. C. Livengood and P. C. Wu* ... 347
31. Combustion of Hydrogen and Carbon Monoxide as Related to Knock. *W. F. Anzilotti and V. J. Tomsic* ... 356
32. Photographic Studies of Cool Flames and Knock in an Engine. *George A. Ball* ... 366
33. Multistage Autoignition of Engine Fuels. *William J. Levedahl* ... 372
34. A Study of Cool Flames and Associated Reactions in an Engine. *E. W. Malmberg, M. L. Smith, J. E. Bigler, and J. A. Bobbitt* ... 385

SPECIAL TECHNIQUES

35. A New Shock Tube Technique for the Study of High Temperature Gas Phase Reactions. *H. S. Glick, W. Squire, and A. Hertzberg* ... 393
36. Polarographic Study of Cool-Flame Oxidation Products of Hydrocarbons. *W. M. MacNevin, P. F. Urone, M. L. B. Omietanski, and M. L. Dunton* ... 402
37. Microwave Studies in the Ionization of Alkali Metals in Flame Gases and Related Phenomena. *T. M. Sugden* ... 406
38. Temperature Measurements from Iodine Absorption Spectrum. *N. J. Beck, Simon K. Chen, O. A. Uyehara, J. G. Winans, and P. S. Myers* ... 412
39. Studies of Ionization in Flames by Means of Langmuir Probes. *H. F. Calcote and I. R. King* 423

KINETICS OF COMBUSTION REACTIONS

40. Kinetics of the Gas-Phase Oxidation of Formaldehyde. *Milton D. Scheer* ... 435
41. Early Oxidation Products of Acetaldehyde and Propane: Interpretation. *Joseph Grumer* ... 447
42. The Kinetics of the Thermal and Photochemical Oxidation of Acetaldehyde. *C. A. McDowell and J. B. Farmer* ... 453
43. The Oxidation of Weak Methane-Air Mixtures at High Temperatures. *J. R. Simonson and N. P. W. Moore* ... 458
44. The Oxidation of Methane. *D. E. Hoare and A. D. Walsh* ... 467

45. The Kinetics of the Slow Combustion of Methane at High Temperature. *M. Vanpée and F. Grard* 484
46. On the Combustion of Paraffin Hydrocarbons. *P. Dugleux and E. Freling* 491
47. The Fast and Slow Reactions of Hydrogen-Oxygen-Propane Mixtures. *Arthur Levy* 495
48. The Inhibition of the Hydrogen-Oxygen Reaction by Hydrocarbons. *R. R. Baldwin, N. S. Corney, and R. F. Simmons* 502
49. The Role of Propylene in the Partial Oxidation of Propane. *Charles N. Satterfield and Robert C. Reid* 511
50. The Oxidation of Olefins. *C. E. H. Bawn and G. Skirrow* 521
51. Cool Flames in Butane Oxidation. *J. Bardwell* 529
52. Free Radicals in Combustion Processes: Thermochemistry of the Alkoxy Radicals RO. *Peter Gray* 535
53. The Vapor Phase Oxidation of 2,4,4-Trimethylpentene-1 (α-Di-isobutylene) and Mixtures of this with *n*-Heptane. *F. H. Garner, R. Long, and G. A. Webster* 541
54. The Kinetics of the Oxidation of Some Tertiary Aliphatic Amines. *C. F. Cullis and D. J. Waddington* 545
55. A Kinetic Comparison of the Combustion of Methyl Alcohol and Methane. *Wendell H. Wiser and George Richard Hill* 553
56. The Slow Oxidation of Some Aliphatic Alcohols. *E. J. Newitt* 558
57. Effect of Temperature, Pressure, and Composition on Ignition Delays for Propane Flames. *Richard S. Brokaw and Joseph L. Jackson* 563
58. Effect of Atomic Radiation on the Combustion of Hydrocarbon Air Mixtures. *Robert E. Cullen and Martin E. Gluckstein* 569
59. The Combination of Hydrogen Isotopes and Oxygen Initiated by Tritium Beta-Radiation. *Leon M. Dorfman* 578
60. Stabilization and Temperature Measurement of Flat Cool Flames. *Roy J. Foresti* 582
61. Effect of Preflame Reaction on Flame Velocity of Propane-Air Mixtures. *Gordon L. Dugger, Robert C. Weast, and Sheldom Heimel* 589
62. A Study of the Ethylene Oxide Decomposition Flame. *Raymond Friedman and Edward Burke* 596
63. Second Limits in Mixtures of Hydrogen, Carbon Monoxide and Oxygen. *G. Dixon-Lewis* 603
64. The Problem of the Second Explosion Limit in the Carbon Monoxide-Oxygen System. *Guenther von Elbe, Bernard Lewis and Walter Roth* 610
65. The Influence of Inert Gases on the Explosion Limits of Cyanogen. *P. Laffitte and H. James* 616
66. Regions of Flammability of Binary Mixtures of Hydrocarbons with Nitrous Oxide: Action of Nitrous Oxide as Oxidant. *Guy Pannetier and Adrien Sicard* 620
67. Self-Combustion of Acetylene. I. Pre-Ignition Kinetics. *W. W. Robertson, E. M. Magee, Janice Fain, and F. A. Matsen* 628
68. Self-Combustion of Acetylene. II. Reactions in Flame Propagation. *E. A. Westbrook, Katherine Hellwig, and Robbin C. Anderson* 631
69. Chain-Branching Activation Energy in Acetylene-Oxygen Flames. *J. Van Wonterghem and A. Van Tiggelen* 637
70. The Effect of Lead Oxide and Copper Surfaces on the Thermal Decomposition of Ethyl Nitrate Vapor. *W. R. Ellis, B. M. Smythe and E. D. Treharne* 641
71. The Effect of Methyl Bromide on the Combustion of Some Fuel-Air Mixtures. *M. C. Burdon, J. H. Burgoyne and F. J. Weinberg* 647
72. Kinetic Studies of Gaseous Explosions. *R. G. W. Norrish, G. Porter and B. A. Thrush* 651
73. Flame Propagation in Methyl and Ethyl Nitrate Vapors. *G. K. Adams and J. Scrivener* 656
74. The Ignition of Combustible Mixtures by Shock Waves. *M. Steinberg and W. E. Kaskan* 664
75. The Structure of the Reaction Zone in a Detonation Explosive. *S. Paterson* 672
76. Recombination of Oxygen Atoms on Surfaces. *D. G. H. Marsden and J. W. Linnett* 685
77. Explosive Decomposition and Combustion of Hydrazine. *Peter Gray and J. C. Lee* 692
78. Sensitized Ignitions in Mixtures of Hydrogen and Chlorine. *P. G. Ashmore* 700

79. Combustion Studies of Alkylsilanes. *Rose L. Schalla, Glen E. McDonald and Melvin Gerstein* 705
80. Combustion of Diborane-Oxygen Mixtures at the Second Explosion Limit. *Walter Roth and Walter H. Bauer* 710
81. Spectra and Combustion Mechanism of Flames Supported by the Oxides of Nitrogen. *H. G. Wolfhard and W. G. Parker* 718
82. Prediction of the Quenching Effect of Various Surface Geometries. *A. L. Berlad and A. E. Potter, Jr.* 728
83. Stationary Flames in Cylindrical Flow of Homogeneous Air-Hydrogen Mixtures. *C. Fouré* .. 736
84. Kinetics of Oxygen Uptake by Cyclohexene in the Liquid Phase. *Anis T. Touma and Frank H. Verhoek* 741

FLAME SPECTRA AND DISSOCIATION ENERGIES

85. Spectrophotometric Traverses Through Flame Fronts. *K. Wohl and F. Welty* 746
86. Atomic Flames: Spectra, "Temperatures," and Products. *R. E. Ferguson and H. P. Broida* 754
87. Infrared Emission from Cool Flames. Stabilized Cool Flames; Engine Cool Flame Reactions; Gas Temperatures Deduced from Infrared Emission. *W. G. Agnew, J. T. Agnew, and K. Wark, Jr.* 766
88. Ultraviolet Spectrophotometry of Low Pressure Explosions. *G. J. Minkoff, A. J. Everett, and H. P. Broida* 779
89. Photodecomposition of Formaldehyde. *L. Schoen* 786
90. Spectroscopic Determination of the Dissociation Energy of the OH Radical. *George A. Hornbeck* 790

PANEL DISCUSSIONS

1. Heterogeneous Burning. Panel Members: Hoyt C. Hottel, *Chairman,* David Altman, Sabri Ergun, and Glenn C. Williams 795
2. Status of the Theory of the Kinetics of Combustion Reactions. Panel Members: A. R. Ubbelohde, *Chairman,* George Porter, John M. Richardson, and Kurt E. Shuler 799

LIST OF AUTHORS

Adams, G. K., Explosives Research and Development Establishment, Ministry of Supply, Waltham Abbey, Essex, England 656
Agnew, J. T., School of Mechanical Engineering, Purdue University, Lafayette, Indiana 766
Agnew, W. G., Research Laboratories Division, General Motors Corporation, Detroit 2, Michigan 766
Altman, David, Jet Propulsion Laboratory, California Institute of Technology, Pasadena 3, California 795
Anderson, Robbin C., Department of Chemistry, The University of Texas, Austin 12, Texas 631
Anzilotti, W. F., Jackson Laboratory, E. I. du Pont de Nemours & Company, Inc., Post Office Box 1671, Wilmington 99, Delaware 356
Arthur, J. R., The British Coal Utilisation Research Association, Randalls Road, Leatherhead, Surrey, England 303
Ashmore, P. G., Department of Physical Chemistry, University of Cambridge, Free School Lane, Cambridge, England 700
Avery, W. H., Applied Physics Laboratory, The Johns Hopkins University, Silver Spring, Maryland 86
Bahn, Gilbert S., Marquardt Aircraft Company, 7801 Hayvenhurst Avenue, Van Nuys, California 336
Baker, Jr., Louis L., Department of Chemistry, Illinois Institute of Technology, Chicago 16, Illinois 196
Baldwin, R. R., Chemistry Department, The University, Hull, England 502
Ball, George A. (Research and Engineering Department) Research Laboratories, Ethyl Corporation, 1600 West Eight Mile Road, Ferndale 20, Detroit, Michigan 366
Bardwell, J., Department of Chemistry, University of Saskatchewan, Saskatoon, Canada 529
Barrére, M., Office National D'Études et de Recherches Aéronautiques, 25, Avenue de la Division-Leclerc, Chatillon-sous-Bagneux (Seine) France 170
Bauer, Walter H., Department of Chemistry, Rensselaer Polytechnic Institute, Troy, New York 710
Bawn, C. E. H., Department of Inorganic and Physical Chemistry, The University, Liverpool 3, England 521
Beck, N. J., Douglas Aircraft Company, Santa Monica, California 412
Berlad, A. L., National Advisory Committee for Aeronautics, Lewis Flight Propulsion Laboratory, Cleveland, Ohio 728
Bernard, Michel L. J., Laboratoire de Recherches Balistiques et Aérodynamiques de Vernon, (Eure) France 217
Bigler, J. E., Department of Chemistry, The Ohio State University, Columbus 10, Ohio 385
Bobbitt, J. A., Department of Chemistry, The Ohio State University, Columbus 10, Ohio .. 385
Broida, H. P., National Bureau of Standards, Washington 25, D.C. 754, 779
Brokaw, Richard S., National Advisory Committee for Aeronautics, Lewis Flight Propulsion Laboratory, Cleveland, Ohio 563
Browning, J. A., Thayer School of Engineering, Dartmouth College, Hanover, New Hampshire 159
Burdon, M. C., Department of Chemical Engineering and Applied Chemistry, Imperial College of Science and Technology, Prince Consort Road, London, S.W. 7, England 647
Burgoyne, J. H., Department of Chemical Engineering and Applied Chemistry, Imperial College of Science and Technology, Prince Consort Road, London, S.W. 7, England 647
Burke, Edward, 5412 Bartlett Street, Pittsburgh 17, Pennsylvania 596
Calcote, H. F., Experiment Incorporated, P. O. Box 1-T, Richmond 2, Virginia 423

Campbell, Clement, Pyrotechnics Chemical Research Laboratory, Picatinny Arsenal, Dover, New Jersey ... 277
Chen, Simon K., Industrial Power Division, International Harvester Company, Melrose Park, Illinois ... 412
Coffin, Kenneth P., National Advisory Committee for Aeronautics, Lewis Flight Propulsion Laboratory, Cleveland, Ohio ... 267
Corney, N. S., British Iron and Steel Research Association, London, England ... 502
Crocco, Luigi, Department of Aeronautical Engineering, Princeton University, Princeton, New Jersey ... 164
Cullen, Robert E., Aircraft Propulsion Laboratory, University of Michigan, Ypsilanti, Michigan ... 569
Cullis, C. F., Department of Chemistry, Imperial College of Science and Technology, Imperial Institute Road, London, S.W. 7, England ... 545
Datner, P. P., Aerojet-General Corporation, Azusa, California ... 11
Dekker, Albert O., Aerojet-General Corporation, Azusa, California ... 260
DeZubay, E. A., Westinghouse Research Laboratories, East Pittsburgh, Pennsylvania ... 329
Dixon-Lewis, G., The Gas Research Laboratory, The University, Leeds 2, England ... 603
Dorfman, Leon M., Knolls Atomic Power Laboratory, General Electric Company, Schenectady, New York ... 578
Dugger, Gordon L., National Advisory Committee for Aeronautics, Lewis Flight Propulsion Laboratory, Cleveland, Ohio ... 589
Dugleux, P., C.N.R.S., 5 Square de Port-Royal, Paris 13°, France ... 491
Dunton, M. L., Department of Chemistry, The Ohio State University, Columbus 10, Ohio ... 402
Ellis, W. R., Chemical and Physical Research Laboratories, Department of Supply, Commonwealth of Australia, Salisbury, South Australia ... 641
Ergun, Sabri, U. S. Bureau of Mines, Pittsburgh 13, Pennsylvania ... 795
Everett, A. J., Chemical Engineering Department, Imperial College of Science and Technology, Prince Consort Road, London, S.W. 7, England ... 779
Fain, Janice, Department of Chemistry, The University of Texas, Austin 12, Texas ... 628
Fairbairn, A. R., Department of Chemical Engineering and Applied Chemistry, Imperial College of Science and Technology, Prince Consort Road, London, S.W. 7, England ... 324
Farmer, J. B., Department of Inorganic and Physical Chemistry, The University, Liverpool 7, England ... 453
Ferguson, R. E., National Bureau of Standards, Washington 25, D.C. ... 754
Foresti, Roy J., Monsanto Chemical Company, Dayton, Ohio ... 582
Fouré, C., Office National D'Études et de Recherches Aéronautiques, 25, Avenue de la Division-Leclerc, Chatillon-sous-Bagneux (Seine) France ... 736
Freling, E., C.N.R.S., 5, Square de Port-Royal, Paris 13°, France ... 491
Friedman, Raymond, Westinghouse Research Laboratories, East Pittsburgh, Pennsylvania ... 596
Garner, F. H., Department of Chemical Engineering, The University, Edgbaston, Birmingham 15, England ... 541
Gaydon, A. G., Department of Chemical Engineering and Applied Chemistry, Imperial College of Science and Technology, Prince Consort Road, London, S.W. 7, England ... 324
Geckler, Richard D., Director of Quality Control, Aerojet-General Corporation, Azusa, California ... 29
Gerstein, Melvin, National Advisory Committee for Aeronautics, Lewis Flight Propulsion Laboratory, Cleveland, Ohio ... 705
Glick, H. S., Cornell Aeronautical Laboratory, Inc., 4455 Genesee Street, Buffalo 21, New York ... 393
Gluckstein, Martin E., Aircraft Propulsion Laboratory, University of Michigan, Ypsilanti, Michigan ... 569
Gordon, Saul, Pyrotechnics Chemical Research Laboratory, Picatinny Arsenal, Dover, New Jersey ... 277
Grard, F., Institut National des Mines, 60, Rue Grande, Paturages, Belgium ... 484

GRAY, PETER, Department of Chemical Engineering, University of Cambridge, Tennis Court Road, Cambridge, England 535, 692
GREY, JERRY, Department of Aeronautical Engineering, Princeton University, Princeton, New Jersey 164
GRUMER, JOSEPH, Explosives and Physical Sciences Division, U. S. Bureau of Mines, Pittsburgh 13, Pennsylvania 447
HAINER, R. M., Arthur D. Little, Inc., Memorial Drive, Cambridge 42, Massachusetts 224
HEIMEL, SHELDON, National Advisory Committee for Aeronautics, Lewis Flight Propulsion Laboratory, Cleveland, Ohio 589
HELLWIG, KATHERINE, Department of Chemistry, The University of Texas, Austin 12, Texas .. 631
HERTZBERG, A., Cornell Aeronautical Laboratory, Inc., 4455 Genessee Street, Buffalo 21, New York 393
HILDENBRAND, D. L., U. S. Naval Ordnance Test Station, Inyokern, China Lake, California .. 212
HILL, GEORGE RICHARD, Department of Fuel Technology, University of Utah, 220 Mines Building, Salt Lake City, Utah 553
HOARE, D. E., University of Swansea, Swansea, South Wales, U. K. 467
HORNBECK, GEORGE A., National Bureau of Standards, Washington 25, D.C. 790
HOTTEL, H. C., Department of Fuel Engineering, Massachusetts Institute of Technology, Cambridge 39, Massachusetts 101, 795
ISODA, HIROSHI, Department of Aeronautics, University of Tokyo, Bunkyo-ku Tokyo, Japan .. 129
JACKSON, JOSEPH L., R. O. Hull & Company, Inc., 1300 Parsons Court, Rocky River, Ohio .. 563
JAMES, H., Laboratoire de Chimie Générale, Sorbonne; 224 Avenue du Maine, Paris xiv, France 616
JENKINS, JR., H. P., U. S. Naval Ordnance Test Station, Inyokern, China Lake, California .. 181
JENNISSEN, JOSEPH, Ordnance Missile Laboratories, Redstone Arsenal, Huntsville, Alabama .. 91
KASKAN, W. E., Aircraft Gas Turbine Division, General Electric Company, Evendale, Ohio .. 664
KILPATRICK, MARTIN, Department of Chemistry, Illinois Institute of Technology, Chicago 16, Illinois 196
KINBARA, TOSIRÔ, College of General Education, University of Tokyo, 865 Komaba-cho, Meguro-ku, Tokyo, Japan 285
KING, I. R., Experiment Incorporated, P. O. Box 1-T, Richmond 2, Virginia 423
KOBAYASI, KIYOSI, Engineering Department, Tohoku University, Katahira-cho, Sendai, Japan 141
KRALL, W. G., Thayer School of Engineering, Dartmouth College, Hanover, New Hampshire .. 159
KUMAGAI, SEIICHIRO, Department of Aeronautics, University of Tokyo, Bunkyo-ku, Tokyo, Japan 129
KUNII, DAIZO, Department of Chemical Engineering, Tokyo University, Tokyo, Japan 231
LAFFITTE, P., Laboratoire de Chimie Générale, Sorbonne, 1, rue Victor-Cousin, Paris, v, France 616
LEE, J. C., Department of Chemical Engineering, University of Cambridge, Tennis Court Road, Cambridge, England 692
LEVEDAHL, WILLIAM J., Engine Fuels Section National Bureau of Standards, Washington 25, D.C. 372
LEVY, ARTHUR, Battelle Memorial Institute, 505 King Avenue, Columbus 1, Ohio 495
LEWIS, BERNARD, Combustion and Explosives Research, Inc., 200 Alcoa Building, Pittsburgh 19, Pennsylvania 610
LINNETT, J. W., The Queen's College, Oxford, England 685
LIVENGOOD, J. C., Massachusetts Institute of Technology, Cambridge 39, Massachusetts 347
LLOYD, PETER, National Gas Turbine Establishment, Pyestock, Farnborough, Hampshire, England 40
LONG, R., Department of Chemical Engineering, The University, Edgbaston, Birmingham 15, England 541
LONGWELL, J. P., Esso Research and Engineering Company, Linden, New Jersey 48
LORELL, JACK, Jet Propulsion Laboratory, California Institute of Technology, 4800 Oak Grove Drive, Pasadena 3, California 132
LOVELL, W. G., Research Laboratories, Ethyl Corporation, Ferndale 20, Detroit, Michigan ... 1

McCullough, Jr., Foy, Properties Section, Code 40121, Area R, U. S. Naval Ordnance Test Station, Inyokern, China Lake, California 181
McDonald, Glen E., National Advisory Committee for Aeronautics, Lewis Flight Propulsion Laboratory, Cleveland, Ohio 316, 705
McDowell, C. A., Department of Inorganic and Physical Chemistry, The University, Liverpool 7, England 453
MacNevin, W. M., Department of Chemistry, The Ohio State University, Columbus 10, Ohio 402
Magee, E. M., Department of Chemistry, The University of Texas, Austin 12, Texas 628
Malmberg, E. W., Department of Chemistry, The Ohio State University, Columbus 10, Ohio 385
Marsden, D. G. H., National Research Council, Div. of Pure Chemistry, Ottawa 2, Canada. 685
Matsen, F. A., Department of Chemistry, The University of Texas, Austin 12, Texas 628
Matthews, George B., Department of Aeronautical Engineering, Princeton University, Princeton, New Jersey 164
Miesse, C. C., Aerojet-General Corporation, Azusa, California 190
Minkoff, G. J., Chemical Engineering Department, Imperial College of Science and Technology, Prince Consort Road, London S.W. 7, England 779
Moore, N. P. W., Department of Mechanical Engineering, City and Guilds College, The Imperial College of Science and Technology, Exhibition Road, London S.W. 7, England. 458
Moutet, A., Office National D'Études et de Recherches Aéronautiques, 25, Avenue de la Division-Leclerc, Chattilon-sous-Bagneux (Seine) France 170
Myers, P. S., Mechanical Engineering Department, University of Wisconsin, Madison 6, Wisconsin 412
Nakamura, Junji, College of General Education, University of Tokyo, 865 Komaba-cho, Meguro-ku, Tokyo, Japan 285
Napier, D. H., The British Coal Utilisation Research Association, Randalls Road, Leatherhead, Surrey, England 303
Newitt, E. J., Department of Chemistry, Imperial College of Science and Technology, Imperial Institute Road, London S.W. 7, England 559
Nishiwaki, Niichi, Faculty of Engineering, Tokyo University, Bunkyo-ku, Tokyo, Japan 148
Norrish, R. G. W., Department of Physical Chemistry, University of Cambridge, Free School Lane, Cambridge, England 651
Omietanski, M. L. B., Department of Chemistry, The Ohio State University, Columbus 10, Ohio 402
Pannetier, Guy, Faculté des Sciences, Université de Dijon, 51, rue Monge, Dijon, France ... 620
Parker, W. G., R. A. E., Rocket Propulsion Department, Ministry of Supply, Westcott, near Aylesbury, Bucks, England 718
Paterson, S., Nobel Division, Research Department, Imperial Chemical Industries Limited, Stevenston, Ayrshire, Scotland 672
Penner, S. S., Jet Propulsion Center, California Institute of Technology, Pasadena 4, California 11
Porter, G., Department of Physical Chemistry, University of Cambridge, Free School Lane, Cambridge, England 651, 799
Potter, Jr., A. E., National Advisory Committee for Aeronautics, Lewis Flight Propulsion Laboratory, Cleveland 11, Ohio 728
Powell, H. N., Aircraft Gas Turbine Division, General Electric Company, Post Office Box 196, Cincinnati 15, Ohio 290
Reid, Robert C., Department of Chemical Engineering, Massachusetts Institute of Technology, Cambridge 39, Massachusetts 511
Richardson, John M., Ramo-Wooldridge Corporation, 8820 Bellanca Avenue, Los Angeles 45, California 799
Robertson, W. W., Department of Chemistry, The University of Texas, Austin 12, Texas 628
Roth, Walter, General Physics Research Department, General Electric Company, Knolls Research Laboratory, Schenectady, New York 610, 710

Saji, Kenjiro, Central Research Laboratory, Nihon Cement Company, Ltd., 8, 1-Chome Fukagawa-Kiyosumicho Koto-Ku, Tokyo, Japan 252
Satterfield, Charles N., Department of Chemical Engineering, Massachusetts Institute of Technology, Cambridge 39, Massachusetts 511
Schalla, Rose L., National Advisory Committee for Aeronautics, Lewis Flight Propulsion Laboratory, Cleveland 11, Ohio 316, 705
Scheer, Milton D., General Electric Company, Cincinnati, Ohio 435
Schmidt, Ernst H. W., Technische Hochschule, Walter von Dyck-Platz 1, Munich, Germany .. 343
Schoen, L., Olin-Mathieson Chemical Corporation, New Haven, Connecticut 786
Schoppe, Fritz, Technische Hochschule, Walter von Dyck-Platz 1, Munich, Germany 343
Schultz, Robert D., Aerojet-General Corporation, Azusa, California 260
Schweitzer, P. H., Pennsylvania State College, University Park, Pennsylvania 7
Scrivener, J., Explosives Research and Development Establishment, Ministry of Supply, Waltham Abbey, Essex, England 656
Shuler, Kurt E., Applied Physics Laboratory, The Johns Hopkins University, Silver Spring, Maryland 56, 799
Sicard, Adrien, Faculté des Sciences de Dijon, Dijon, France 620
Simmons, R. F., Rocket Propulsion Department, Ministry of Supply, Westcott, Aylesbury, Buckinghamshire, England 520
Simonson, J. R., Department of Mechanical Engineering, City and Guilds College, The Imperial College of Science and Technology, Exhibition Road, London S.W. 7, England 458
Simpson, H. C., Imperial Chemical Industries, Ltd., Stevenston, Ayrshire, Scotland 101
Skirrow, G., Department of Inorganic and Physical Chemistry, The University, Liverpool 3, England 521
Smith, M. L., Department of Chemistry, The Ohio State University, Columbus 10, Ohio 385
Smythe, B. M., Chemical and Physical Research Laboratories, Department of Supply, Commonwealth of Australia, Salisbury, South Australia 641
Squire, W., Cornell Aeronautical Laboratory, Inc., 4455 Genesee Street, Buffalo 21, New York 393
Steinberg, M., Aircraft Gas Turbine Division, General Electric Company, Evendale, Ohio .. 664
Steinberger, Rudolph, Hercules Powder Company, Inc., Allegany Ballistics Laboratory, Cumberland, Maryland 205
Sugden, T. M., Department of Physical Chemistry, University of Cambridge, Free School Lane, Cambridge, England 406
Thrush, B. A., Department of Physical Chemistry, University of Cambridge, Free School Lane, Cambridge, England 651
Tomsic, V. J., Petroleum Laboratory, E. I. du Pont de Nemours & Company, Inc., Wilmington 99, Delaware 356
Touma, Anis T., University of Beirut, Beirut, Lebanon 741
Treharne, E. D., Chemical and Physical Research Laboratories, Department of Supply, Commonwealth of Australia, Salisbury, South Australia 641
Ubbelohde, A. R., Department of Chemical Engineering, Imperial College of Science and Technology, Prince Consort Road, London, S.W. 7, England 74, 799
Urone, P. F., State Health Laboratory, Ohio Department of Health, Columbus 10, Ohio 402
Uyehara, O. A., Mechanical Engineering Department, University of Wisconsin, Madison 6, Wisconsin 412
Vanpée, M., Institut National des Mines, 60, Rue Grande, Paturages, Belgium 484
Van Tiggelen, A., Université de Louvain, 98, Rue de Namur, Louvain, Belgium 637
Van Wonterghem, J., Université de Louvain, 98, Rue de Namur, Louvain, Belgium 637
Verhoek, Frank H., Dept. of Chemistry, The Ohio State University, Columbus 10, Ohio 741
von Elbe, Guenther, Combustion and Explosives Research, Inc., 200 Alcoa Building, Pittsburgh 19, Pennsylvania 79, 610
Waddington, D. J., Department of Chemistry, Imperial College of Science and Technology, Imperial Institute Road, London S.W. 7, England 545

Walsh, A. D., The University, Leeds 2, England 467
Wark, Jr., K., Purdue University, Lafayette, Indiana 766
Weast, Robert C., Case Institute of Technology, Cleveland, Ohio 589
Webster, G. A., Department of Chemical Engineering, The University, Edgbaston, Birmingham 15, England 541
Weinberg, F. J., Department of Chemical Engineering and Applied Chemistry, Imperial College of Science and Technology, Prince Consort Road, London S.W. 7, England 647
Welty, F., Department of Chemical Engineering, University of Delaware, Newark, Delaware 746
Westbrook, E. A., Department of Chemistry, The University of Texas, Austin 12, Texas 631
Whittaker, A. Greenville, U. S. Naval Ordnance Test Station, Inyokern, China Lake, California 212
Wicke, E., Institut für Physikalische Chemie, Universität Hamburg Jungiusstrasse 9, Hamburg, 36, Germany 245
Williams, G. C., Department of Chemical Engineering, Massachusetts Institute of Technology, Cambridge 39, Massachusetts 101, 795
Winans, J. G., Department of Physics, The University of Wisconsin, Madison 6, Wisconsin .. 412
Wise, Henry, Jet Propulsion Laboratory, California Institute of Technology, 4800 Oak Grove Drive, Pasadena 3, California 132
Wiser, Wendell H., Department of Fuel Technology, University of Utah, 220 Mines Building, Salt Lake City, Utah 553
Wohl, K., Department of Chemical Engineering, University of Delaware, Newark, Delaware .. 746
Wolfhard, H. G., R. A. E., Rocket Propulsion Department, Ministry of Supply, Westcott, Near Aylesbury, Bucks, England 718
Wood, Bernard J., Jet Propulsion Laboratory, California Institute of Technology, 4800 Oak Grove Drive, Pasadena 3, California 132
Woodward, E. C., Westinghouse Research Laboratories, East Pittsburgh, Pennsylvania 329
Wu, P. C., Massachusetts Institute of Technology, Cambridge 39, Massachusetts 347
Yagi, Sakae, Department of Chemical Engineering, Tokyo University, Tokyo, Japan 231

INTRODUCTION TO THE FIFTH SYMPOSIUM (INTERNATIONAL) ON COMBUSTION

University of Pittsburgh, August 30—September 3, 1954

By HOYT C. HOTTEL

The frequency of combustion symposia and the number of papers accepted together constitute some sort of measure of progress in combustion, imperfect though the measure may be. The numbers representing the quotient of papers by time-lapse since the previous symposium, within this series, are 3, 9, 28, and 50, the last figure representing the 100 papers of this Volume divided by the two-year lapse between the Fourth and Fifth Symposia. Add to this the restriction of field covered in the last two symposia to keep them from becoming unmanageably large and the excellent volumes covering AGARD combustion meetings, and one sees here the evidence of what specialists in combustion would be tempted to call an "explosion" of learning. Some of the dangers of explosions are that they are incompletely understood, and that they sometimes get out of hand and develop in unprofitable directions (and if they are set off in a mixed group including scientists and engineers, there may further be some argument as to the meaning of "profitable").

The Third Symposium of this series—the first of the postwar series and the one which set the precedent of publication in a single volume—covered the whole field of combustion. The Fourth Symposium focused on the physics of combustion. The Fifth, with papers herein, attempted the compromise assignment of complementing the Fourth by concentration on the chemical kinetics of combustion reactions (half of the papers) while at the same time rounding out the program by the inclusion of 14 papers on engine combustion, 20 about equally spread among the burning of droplets, liquid propellants, and solids, and 16 on diffusion flames, special techniques, spectra and dissociation energies.

The series of six invited papers on unsolved problems of engine combustion remind us that knowledge of engine knock is still primarily empirical; that the Diesel engine still delivers objectionable combustion products; that combustion instability and carbon formation in liquid-fuel rockets are still largely unexplained; that there is need of a guiding theory of the burning of composite-propellants analagous to that for colloidal propellants; that the turbojet lacks a working set of model laws and adequate knowledge of the kinetics of hydrocarbon burning, and that these deficiencies in our understanding are emphasized by the need of the turbojet combustion chamber to operate over a 120-fold pressure range. In the ramjet field it is pointed out that although a fairly sound basis for combustion chamber design exists, present performance is significantly poorer than the limits set by presently developed theory, in that neither the potential ability of recirculation to stabilize flame nor the ability of turbulence to spread flame is being realized.

Papers like the invited series just mentioned have an important place in these symposia. Let us hope that those concerned primarily with fundamental studies will continue to listen to those responsible for putting combustion to work, will sympathize with and understand their urge to attack problems sometimes of a more mixed character than the scientist considers most profitable, and be guided (just the right amount!) in their choice of problems to attack. Consider the redefinition of the scope of the term "fundamental combustion studies" which has come about, in the past 15 years, from the practical demands that combustion processes be carried out in high-velocity turbulent streams.

The adequacy of our knowledge of combustion is for engineering purposes in large measure tested by our ability to determine the space requirement for combustion; and this is directly or indirectly the subject of several of the papers of this volume. How does one set up a combustion model which allows, as flow rates increase, for the transition from combustion in a laminar flame front to combustion in a wrinkled flame front to combustion in stirred islands or pockets, for recirculation as a means of feeding chain carriers or heat into the stream along its main flow path, for the possibly

profound change in the kinetics of combustion in the progression from laminar to turbulent burning? The mathematics of steady laminar flame propagation becomes so complex, when allowance is made for diffusion and reaction of all the chemical species present, as to have produced from Dr. Lewis a suggestion in the Introduction to the Fourth Symposium on Combustion that more attention might justifiably be devoted to mathematical methodology of flame propagation. Combustion progress in a high-output combustion chamber is even more complex, with problems of jet-mixing, flow around baffles, and feeding of combustion products into the flame jet added to the problems in chemical kinetics; but chemically the process is probably not as complex as laminar flame propagation. Here also is a field where mathematical methodology needs attention. It is a problem which the purists in combustion shy away from as unprofitable to attack, but one which must be attacked if high-output combustors are to be designed on other than an empirical basis. One illuminating approach to the problem is made in this volume in the analysis of combustion progress in a multi-layered system of air and fuel-gas where partial allowance can be made for the influence of both mixing and chemical reaction rates.

Education in chemical kinetics in colleges still shows the influence of the dominant interest most kineticists have in isothermal processes. One of the survey papers underlines the important differences between low-temperature kinetics and the kinetics of combustion processes: the adiabatic rather than the isothermal process, the departure from Maxwellian energy distribution, the modification of radical mechanism caused by the high concentration of chain carriers, the influence of temperature-sensitive inter- and intra-phase transport processes on the reaction mechanism. Encouraging progress is being made in correlating the reactivity of complex hydrocarbon molecules with the processes of energy transfer among the bonds within the molecule. Of the 44 contributed papers on chemical kinetics, exactly half are concerned with the combustion of hydrocarbons. Progress in this field is summarized in one of the survey papers, which holds out to the engineer the hope that a generalized description of hydrocarbon combustion mechanism may some day be available which is markedly simpler in application at high temperatures than under the conditions of many laboratory experiments. Flash photolysis as means of initiating homogeneous gaseous explosions permits a spectroscopic examination of products formed; and a time resolution of 1 μsec has been achieved. This should constitute one of the prime means of identifying the transient intermediate processes responsible for build-up of reaction to rates identifiable by other means.

Returning to the suggestion that "explosions" can develop in unprofitable directions, there is no evidence in this volume of such a tendency. The writer did have the feeling in examining the papers that the purpose of these Combustion Symposia would be better served and the many small areas of progress put in better perspective if somewhat greater emphasis were put on the interpretation of accumulated facts, on the search for the big truths to be built up from the little ones.

Review of Problems on Combustion in Engines and Kinetics of Combustion Processes

I

COMBUSTION PROBLEMS IN INTERNAL COMBUSTION ENGINES

By W. G. LOVELL

Why the Problems are Important

The problems of combustion in engines are interesting principally for three reasons: first, they have great economic and social significance: second, the solution of them is limited by our lack of fundamental knowledge of the processes going on in the engines and especially of the chemical kinetics; and third, some of the problems can be solved with great rewards. They seem to indicate a good place to work.

The economic significance of combustion in engines is easy to understand. As indicated in Figure 1, of all the energy that we liberate or use in this country, a little less than 40 per cent comes from coal, a little less than 60 per cent from petroleum, and only 4 per cent from water power. This does not include the energy that is immediately derived from sunshine, but only our so-called mechanical or heat energy. Almost all of it comes from what we call combustion and this means that we have to have oxygen in addition to the fuel. Now the almost 60 per cent of the total that comes from petroleum out of holes in the ground is of special interest. For of this 60 per cent, nearly one-third is used for internal combustion engines, almost all of it in the form of gasoline.

There are many engines in this country—most of them in automobiles and trucks of which there are about 55 million. If we would think of their installed horsepower as being about 100 each, then the total amounts to about 50 times the entire installed central-station horsepower in this country. If we could increase the efficiency of these engines by even one per cent we would save enormous amounts of fuel and in effect increase our total fuel supply.

We think these engines are going to be with us a long time yet; they are quite reliable, convenient and cheap in automobiles. There are more and more of them doing most of the hauling on railroads and on the farms as tractors and in many other places doing odd jobs. So the engines continue to increase in numbers, and it is hard to see a replacement for them in the foreseeable future.

What is wrong with them, and can they be improved or made more efficient? As indicated before, they can be improved; but a principal obstacle is our ignorance about the chemical kinetics of combustion.

Chemical Kinetics in Spark-Ignition Engines

There are two main avenues of approach toward improved engine performance. The first is by increasing the engine compression ratio; this results in more power because of increased thermal efficiency. The second way is by putting more fuel-air mixture into the cylinder by geared supercharging; this results in increased power output but the same thermal efficiency. Both of these methods encounter the important phenomenon called fuel knock. Knock limits both the permissible compression ratio and the permissible amount of supercharge.

THE KNOCK

The knock occurs because as the charge of gasoline vapor and air is compressed by the piston in the cylinder, chemical reactions may occur

in the mixture. Then, after the mixture has been ignited by the spark plug, the expanding gases compress the unburned mixture still further, and during this further compression it undergoes additional reactions. With many gasoline hydrocarbons the reactions proceed to a critical state in the last portion of the unburned charge or the "end-gas" so that it autoignites, and this last portion burns extremely rapidly. It knocks. The knock is thus a definite limitation, because it is not mechanically practical to run an engine with any significant amount of knock. If knock could be completely eliminated, engine efficiencies would be greatly increased. This is no small matter for even a 10 per cent relative increase in efficiency is like discovering whole new oil fields, or decreasing the total required amount of engine power by hundreds of millions

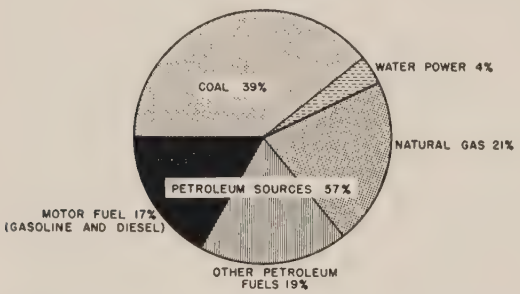

FIG. 1. U. S. energy sources expressed in per cent equivalent Btu's. (Data from "Petroleum Facts and Figures," 10th Ed., 1952.)

of horsepower, or considerably extending our petroleum reserves.

I would like to digress for a moment, now that the importance of the phenomenon of knock is apparent, to consider it briefly. We think about it as autoignition of a fuel-air mixture ahead of the flame, and that sounds simple, even though the steps leading up to autoignition are quite complex. The autoignition is complex, also. If we photograph the autoigniting volume at high speed by means of the light it emits, or by observing its density gradients (as by schlieren photography) one comes up with some important observations. One is that it is an extremely nonhomogeneous thing (and this is possibly a rational idea because we are dealing with very short time intervals) both as to temperature and extent of reaction. In fact it is convenient to think of a succession of autoignitions of little volumes. And if one thinks of the nonhomogeneities, and rates of heat transfer, and reaction-rate temperature coefficients, there is a lot to think about. Yet, one is encouraged to do some thinking about it because of the potential economic advantage in doing something about reducing the knock.

REDUCTION OF KNOCK

While there has been a good deal of thought given to using the knock, this approach has to date shown little promise. On the other hand, there are several possibilities for lessening the limitation of knock. Since the knock occurs in the end-gas, elimination of end-gas would remove the knock. This may be accomplished by modifying the cycle somewhat and putting the fuel in at the same rate as it burns, so that the flame is stationary with respect to the engine cylinder but moving through a controlled swirling gas. The ingenious mechanism for doing this is the result of straight-forward research, and there can be no doubt of its effectiveness for the complete elimination of knock.

This method for eliminating knock competes with another one which consists of changing the fuel. Which method may be better can only be determined by experience and by new knowledge of how best to go on both routes. For the present, modification of the cycle would be the best route only when fuel cost is high relative to engine cost. But for most engine-propelled automobiles, depreciation of the value of engine and mechanism accounts for over three quarters of the total operating cost.

Other special attention may be given the end-gas by mechanical means. Keeping it cool, diluting it, or shortening its time of existence in the engine cycle are methods that have been used successfully to reduce knock. These features of engine and combustion chamber design are sometimes termed "mechanical octane numbers." They move the barrier of knock ahead, but they do not eliminate it.

FUEL VARIABLES

So it is worth while to look at alternative methods for achieving the potentialities which can result from the elimination of knock. Knock can be eliminated by changing the molecular structure of the fuel to one which does not knock. Consider the two isomers, *n*-heptane and triptane (2,2,3-trimethylbutane). Although they have identical composition and the same heat of combustion within a third of a per cent, their difference in combustion is so great that when they are used in an engine of varied knock-limited

compression ratio, the thermal efficiency may vary almost twofold. The relationship between molecular structure and incidence of knock has been worked out on an empirical basis for some 300 pure hydrocarbons by an American Petroleum Institute Research project, so that firm fundamental data are available. The importance of fuel structure is evidenced by the fact that while the octane number scale of 0 to 100 covers only a part of the total range, it represents about a fivefold variation in the knock-limited power to be obtained by supercharging an engine.

Thus, the useful work to be obtained from a gasoline depends not only on the heat content (which cannot be changed very much) but also on the molecular structure of its hydrocarbon constituents. Hydrocarbons of some molecular structures can be used at higher compression ratios without knock because of the variations in the rate of chemical reactions in the end-gas ahead of the flame. Although it is probably not the original fuel that knocks or goes suddenly into autoignition, still it is the original fuel that determines to a large extent whether knock will occur or not. Consequently, the kinetics of some of these intermediate reactions are the determining factor in the utility of the fuel.

EARLY COMBUSTION REACTIONS

Let us consider for a moment how important some of these intermediate reactions may be. These early reactions (or precombustion reactions, so-called because they do not necessarily result in the formation of the final combustion products), which are chemical changes occurring in the fuel-air mixture ahead of the flame front, have been shown to play an important role in engine operation. One of the most important aspects of these changes is that they are accompanied by the release of appreciable amounts of heat—perhaps exceeding 10 per cent of the total heat of combustion. Since the release of this heat alters the character of the entire combustion process, it is essential that we be able to determine the progress of such precombustion reactions in order to evaluate their effect on engine operation.

A convenient way of doing this is by the use of pressure-time records, comparing different fuels, and with the spark ignition delayed in the cycle. One comes up with the ideas that the heat evolution may be a considerable amount, and that it depends on the fuel, but does not necessarily correlate with the tendency of the fuel to knock. These are important concepts. They do not simplify the picture very much, but they enable one to do things to the combustion cycle, in the way of timing the heat release for better advantage.

Another way of looking at some of these early reactions is to consider not primarily their heat evolution but their effect on knock. One way to do this experimentally is to use two engines, one motored to compress and expand the fuel-air charge without ignition, the other firing this motored charge. What one observes is that as autoignition conditions are approached in the first engine, some reactions take place which do not evolve more than 1 per cent of the heat of combustion but which very significantly increase the tendency of the mixture to knock in the second engine. As the point of autoignition is approached closer, more extensive reactions take place, and the mixture has less tendency to knock in the second engine than even the original fuel-air mixture, probably because it is significantly decreased in heating value. One can do similar experiments in which the fuel and air are passed through a heated tube instead of an engine and come up with similar general ideas.

In summary, then, we can state the general concept that many reactions may occur before the flame occurs. The extent of these reactions are important, not only in determining the thermodynamics of the cycle, but also in determining what happens ahead of the flame and whether knock occurs or not. These factors complicate the consideration of the combustion cycle, of course, but add intriguing possibilities for exploitation.

CONTROL OF KNOCK REACTIONS

More knowledge of the gross physical control of these reactions will help also. Knowledge of how to influence the pressure and also the temperature of the reacting gas and the temperature of the surrounding walls has already resulted in great progress in reducing knock. Such progress goes by the name of "mechanical octane numbers", as mentioned previously. These gains are real, but they will not go far enough in permitting higher compression ratios to make us stop wanting better fuels, or more octane numbers, or more extensive catalytic control of the chemical reactions of knock.

Catalytic control of the knock reactions is gained by the use of so-called antiknocks, metallic or nonmetallic, such as tetraethyllead or

aromatic amines. They reduce knock when added to the fuel in small amounts. The chemical mechanism by which antiknocks or products of their decomposition or oxidation function can only be expressed in quite vague and general terms such as surface deactivation of chain carriers. In spite of our lack of knowledge of the mechanism by which lead catalysts operate, they are used in various amounts in over 98 per cent of the gasoline burned today in this country. If more were known about the chemical mechanism of antiknocks, they might be made more effective, since it is known that their effectiveness varies severalfold with changes in fuel composition, in contaminants such as sulfur compounds in the fuel, and with engine operating conditions. Certainly new knowledge on this subject would seem to offer great potentialities for practical improvement in the use of gasolines whether they contain commercially known antiknocks or new ones. Here again with antiknocks, as with fuels, we are concerned not with equilibrium states, but with the kinetics of combustion.

FLAME VELOCITY

Kinetics are also important in the control of flame velocity, and residence time of the charge is important in determining the incidence of knock. There would be less time for the knock-inducing reactions to take place ahead of the flame if the flame were to get there sooner. So far we have not been able to change flame velocity very much by reasonable amounts of additives or without gross fuel changes. We have been able to influence flame velocity importantly only by modifying physical factors such as turbulence. While turbulence reduces the knock, too much turbulence results in excessive heat loss to the walls. On the other hand an increase of flame velocity without increased turbulence would help reduce knock and would also probably make a small, but important, contribution to engine thermal efficiency because of less heat transfer at the walls. What the fundamentals are which determine flame velocity are not entirely clear. Certain it is that we run engines at 600 rpm and also 10 times as fast at 6000 rpm. Over this range of speed there is only about a two-fold range in the degrees of crankshaft revolution required for the flame to consume the charge, and at the high-speed conditions, the flame travels about five times as fast in terms of feet per second. It is this phenomenon that makes possible flexible engines, ones that will operate over a wide range of speed and load. This increase in flame speed is, of course, due to turbulence; and that is something, again, about which we have little useful knowledge.

ENGINE DEPOSITS

So far, in thinking about engine combustion, little direct attention has been paid to the walls of the combustion chamber. They influence combustion and engine operation, and they are especially important because they accumulate deposits. These deposits consist of carbonaceous residues from the fuel and the oil and lead salts from the combustion catalyst, tetraethyllead. These deposits are bad, for two principal reasons.

The first reason is that they have a pronounced effect on heat transfer; they get hot from one cycle, and transfer heat to the incoming charge on the next cycle. This is the most important reason that engines with deposits knock more than clean engines.

A second important bad effect of deposits is that they induce ignition of the charge. This comes about because many lead salts catalyze the combustion of carbon and carbonaceous materials, and under some conditions the deposits will glow and ignite the charge. This uncontrolled ignition of the charge may cause knock when it is early enough in the cycle, for example before the spark. This random ignition of the charge by the deposits takes the control of ignition time away from the designed spark timing and location, and, of course greatly disturbs the order of the engine cycle.

Various materials may be added to the fuel to correct this. Many of them contain phosphorus, which acts as a "poison" for the catalytic action of some lead salts, and such additives are currently quite widely used.

Compression-Ignition Engines

When we turn to the diesel cycle, another set of problems faces us in engine-fuel relationships; and here, again, is a situation where more knowledge of chemical kinetics may lead to improvements in fuel utilization. In the diesel cycle, a charge of air is compressed in the engine cylinder and then the fuel is injected. The air is so hot, because of the approximately adiabatic compression, that the injected fuel ignites and burns. In the spark ignition engine, it is desirable to run at high compression ratios, but this cannot be done because of a kind of ignition ahead

of the flame. But in the compression-ignition engine, high compression ratios must be used in order to get the air hot enough to ignite the fuel in a reasonable time and before too much fuel is injected, so that too much will not burn at once. In fact, the required compression ratios are possibly a little higher than the ideal, not from the standpoint of thermodynamic efficiency, but from the standpoint of mechanical and metallurgical design required to withstand the high pressures. Thus, in the spark ignition engine a form of spontaneous ignition (knock) is undesirable, but in the compression-ignition engine it is essential.

FUEL CHARACTERISTICS

In general, the autoignition characteristics of fuels for spark-ignition engines (characteristics which are roughly measured by knock ratings or octane numbers) are about the opposite of combustion characteristics for fuels used in compression-ignition engines, characteristics measured in terms of cetane numbers. Usually, high cetane number in a fuel goes with low octane number, and vice versa. Generally, compact structural formulas for hydrocarbons go with low cetane numbers (or high octane numbers), and long-chain formulas are typical of high cetane numbers (or low octane numbers). If the individual hydrocarbons of petroleum and its products could be separated into two classes, high and low cetane numbers, compression-ignition engines could be operated on one class, and the spark-ignition engines on the other class. The two types of engines would then run at about the same compression ratios and consequently at about the same thermodynamic efficiencies. The choice of which of the two to use would then depend upon the type of service and the costs of manufacture of the two types of engines. But we do not know how to make such a separation of hydrocarbons, based not on physical properties but on combustion or autoignition characteristics. A separation on the basis of combustion inevitably destroys the material, and a suitable method of separation based on structure has not yet been devised. Perhaps in the future the equivalent of such a separation may be accomplished, even though it may entail the development of processes for manufacturing specific and fairly pure hydrocarbons.

Present fuels for compression-ignition or diesel engines are imperfect primarily because of deficiencies in their ignition. Better and faster ignition would be an improvement for many applications. The gains, however, from better ignition or higher cetane numbers in diesel fuels are not comparable to those from higher octane numbers in gasolines. Higher octane numbers offer the potentiality of higher compression ratios, with better efficiency and more power. Higher cetane numbers fundamentally enable lower compression ratios to be used with a consequent loss in thermodynamic efficiency. And so, the gains resulting from superior diesel fuels are gains in the operations of engines and not those of fundamental thermodynamics.

IGNITION PHENOMENA

The word ignition, as used here in relation to diesel fuels, covers a multitude of ignorances about how soon and how much vaporization occurs and how fast some undefined chemical reactions of oxidation take place after the injection of the fuel into the hot air. We do know that ignition is greatly influenced by fuel composition and by the addition of small amounts of materials such as some organic nitrates. An early and definite ignition would insure control of the diesel cycle, since too much fuel could not then be injected before burning.

Our ignorances about ignition in the diesel cycle also extend to what is included in the word burning. The mixture in the diesel combustion chamber is far from homogeneous since it consists of air, and some exhaust-gas from the previous cycle, and into this mixture liquid fuel is injected. It is easy to imagine droplets of fuel surrounded by vapor undergoing oxidation reactions leading to ignition and more complete combustion with a range of fuel-air ratios giving various products of combustion. On a larger scale of volumes, we can imagine fairly large places where there is no fuel and other places where there is too much. As a practical matter, one cannot burn all the air in all parts of the combustion chamber because if the average fuel-air ratio is made sufficiently rich to accomplish this, there will be some volumes where there is so much excess fuel that smoke results. The practical power rating of a diesel combustion chamber depends not upon how much air there is available for combustion but rather upon how much fuel can be put in without there being some volumes or pockets which are so rich that smoke results, even though there is an over-all average excess of air. For these reasons, it is obvious that any progress that can be made in

sorting out the simultaneous and consecutive phenomena of fuel injection, dispersion, vaporization, ignition, and burning will lead to important advances in fuel utilization. A practical end, of course, is a more powerful, smaller and smoother operating engine. This requires a fairly fundamental approach.

What Kind of Research

The kind of information we might wish for on this kind of problem of chemical kinetics of combustion is quite fundamental. We would like to know the chemical equations and rates of all the oxidation and other reactions involved in

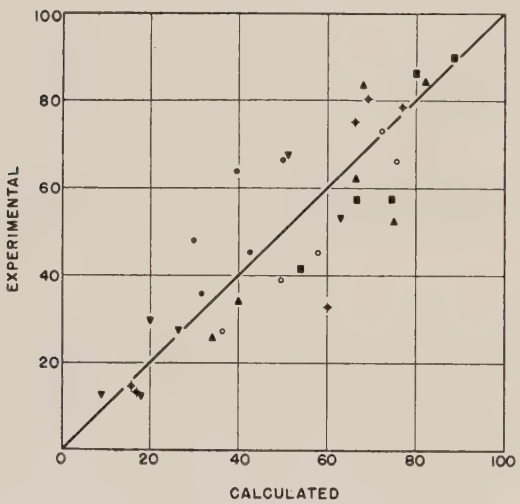

FIG. 2. Correlation of calculated and experimental values of TEL decomposition expressed as per cent undecomposed. Different symbols represent different fuel-additive combinations.

the burning of many different hydrocarbons, expressed as a function of temperature and pressure. This is too much information to obtain in any reasonable time, inasmuch as the combustion of a relatively simple substance such as hydrogen is far from being completely understood. Consequently, the attack must be on several fronts: the slow frontal attack on the fundamentals by relatively indirect methods, and the logical, or intuitive, or empirical utilization of an individual piece of fundamental or basic information.

However, it is possible to make quite specific and practical use of combustion kinetics in engine combustion. I have mentioned a specific application to engine deposits. A later paper in this symposium discusses the application of rapid-compression machine data on ignition delay to problems of engine knock. Other papers discuss the analyses of intermediate products from an engine, and the correlation of cool flame reactions. There will be photographs of cool flames and their spectra in engines.

As an interesting specific example of how it is possible to apply kinetics to the engine cycle, I would like to mention some work, which will be in a forthcoming paper, on the decomposition of tetraethyllead in the engine. This decomposition is interesting because the products of the decomposition are the effective antiknock catalysts and they must be present at the right time in the engine cycle to be most effective.

An engine, with certain modifications, can be a useful research tool, because with modern instrumentation one can measure the basic parameters of time, temperature, and pressure. Therefore, an engine is a reactor, more complex, it is true, than a simple heated vessel or a flow tube, but particularly useful. Furthermore, an engine has certain advantages for the investigation of rapid high-temperature reactions, in that cycles are repetitive and permit the use of devices like stroboscopes or sampling valves. Also, an engine permits the measurement of very high-temperature reactions which cannot be measured in conventional ways, because flow systems take longer to heat up the material than desired. Finally, if an engine is used as an experimental tool, there is less trouble in correlating the data with engine conditions.

For the study of the decomposition of tetraethyllead we may use a motored engine and avoid some of the difficulties with the nonhomogeneity of the charge when a flame goes through it; and we may determine the amount of tetraethyllead decomposed by sampling the exhaust. We may also compute the extent of decomposition by assuming a first-order homogeneous reaction, as has been reported in the literature, and using an Arrhenius equation:

$$\ln \frac{n_1}{n_2} = -\int_{t_1}^{t_2} k\,dt = -A\int_{t_1}^{t_2} e^{-B/T}\,dt$$

where n_1 and n_2 represent the concentration of TEL at the start and end of the cycle, respectively; k is the reaction-rate constant expressed in terms of the two constants A and B and the variable temperature T; and t is the time. We can use temperature values obtained from accurate pressure records and gas laws. By trial we may find consistent values of the constants.

Figure 2 shows the results of 33 engine tests in which the amount of tetraethyllead decomposed was calculated from accurate pressure-time data, and compared with the experimental values for TEL decomposition. These tests covered a wide range of fuel types and engine temperatures, and the calculated values differ from the experimental results by an average of less than 10 per cent, which is considered satisfactory for this type of investigation. It would be quite difficult to carry out this work in a reactor other than an engine. The half life of tetraethyllead at the temperatures of interest is of the order of milliseconds, and conventional apparatus for kinetic studies under these conditions is not completely satisfactory.

The important thing about this may be that there is nothing unusually mysterious about an engine. Chemical reactions go on in it about the same as they do anywhere else. But it is particularly important that we consider the rapidly changing temperatures and pressures.

We can, consequently, see a good deal of light ahead, and although we have largely used up, in the field of combustion in engines, our available stock of fundamental information we see several ways to apply new fundamental concepts. And finally, any new pieces of information are almost certain to have practical significance in this field in which, as has been indicated, the economic rewards are so great.

II

COMBUSTION PROBLEMS IN DIESEL ENGINES

P. H. SCHWEITZER

The topic assigned is Combustion Problems in Diesel Engines. The following presentation is intended to highlight briefly some of these problems as they appear to this observer.

It should first of all be pointed out that when we discuss problems of combustion, it is in order to ask whose problems we are talking about.

Various groups are affected by engine combustion. The principal interest of the scientists is in such things as flame and preflame kinetics, of the engineers in thermal efficiency, of the owners of the machine in operating economy and reliability; but a party intensely interested in combustion is seldom mentioned and usually completely forgotten: the general public.

A little reflection on the situation as it affects the public leads us to pinpoint certain diesel combustion problems. Noise, smoke and odor are the principal complaints, and the diesel excells in all three of them.

Even enlightened self-interest should induce the industry to take this matter seriously, more seriously than it has in the past. It is easy to predict that government—state or municipal—will soon act if we do nothing about it. An incensed public may force legislators to enact unwise laws to the detriment of all of us.

Noise, smoke, and odor are the problems concerning which the public looks to us for solution. Just where are we in these items?

A good deal of the engine noise is combustion knock. Combustion knock is some function of the rate of combustion or the rate of cylinder pressure rise. While it is not a rule, it is a fairly valid observation that if the rate of pressure rise per degree crank angle exceeds a certain value, the engine is sure to be rough. Why the pressure rise per degree should be the controlling factor instead of pressure rise per sec is a puzzle.

Another puzzle that may be mentioned in passing pertains to ignition temperature. It is a common observation that a liquid spray ignites more easily than gas or dry vapor. There is still a school in Germany which maintains that ignition takes place from the liquid phase. The self-ignition temperature is lower in the liquid phase than in the vapor phase. In fact, it is often below the vaporization temperature. Chemists correctly object that no ignition can take place in the liquid phase. Yet you will find that, although a

mixture of air and fuel vapor fails to ignite at a certain border compression ratio, injection of a jet of the same fuel will ignite it.

The confusion can perhaps be traced to the uncertainty in the definition of self-ignition temperature. R. O. King, of the Defense Research Board in Canada, has developed a nuclear theory of ignition which requires the presence of nuclei, such as carbon flakes, for ignition to occur.

Coming back to combustion knock, the desire to get more power from a given cylinder volume demands that we burn large quantities of fuel as rapidly as possible. Economy demands that we burn it close to the top dead center position of the piston. Both of these things aggravate engine noise. At least we thought so until recently, when we came across the new MAN engine called the "Flustermotor," whisper motor, in Germany.

This engine was demonstrated to the writer by its inventor, Dr. Meurer. We drove trucks with it and inspected it on the test stand. It was an impressive demonstration.

The engine is very quiet for a diesel by any standard and the difference from the old MAN is striking. The Meurer combustion system not only stops combustion knock but adds some 15 per cent to the low rpm bmep without injecting more fuel, indicating the improvement of thermal efficiency at low rotating speeds. This gives a "lugging" torque characteristic to the engine. It took three attempts to stall the engine uphill at high gear. The (112 x 140 mm 2000 rpm) engine was running at 200 rpm, the truck moving at five miles per hour uphill, and the engine did not stall. When it was on the point of stalling and then given fuel, it picked up immediately and noiselessly. Few engines could pass such a test.

The explanation is a new kind of combustion system, which, according to Professor Pischinger, is likely to revolutionize the automotive diesel field.

Dr. Meurer has been prominent in diesel development for many years. Long ago he concluded that for autoignition the fuel needs such a high temperature that it cracks into hydrogen and carbon early in the combustion process. First the hydrogen burns with noise; then the carbon burns with smoke. This picture is oversimplified. Dr. Meurer told of his calculations based on reaction kinetics leading finally to the Meurer combustion system where the above sequence is eliminated. Instead, he creates a narrow layer of fuel vapor, particles of which, in contact with fast moving air, ignite, crack and burn, in minute quantities, divided in space and time. The fuel vapor burns in nascendi, so to speak, and has a similarity in this respect to the Barber combustion system and even to the Fiedler engine where a slug of oil injected with no atomization produced a quiet engine. But the fortunate aspect is that Meurer produced this effect with only insignificant changes in the existing MAN engine.

As is well known the MAN combustion chamber used to consist of a spherical chamber in the piston receiving a well-atomized spray from an offset nozzle. Meurer made the combustion chamber in the piston shallower, about hemispherical. On the edge of this half-sphere he has a small ear-like cavity. Into that cavity the nozzle tip protrudes. Two jets issue and hit the combustion chamber at a very acute angle, approximately 5 degrees directed somewhat downward. The jets impinge on the wall but are not reflected from it. Instead they wet the wall, about ¾ around. In the same direction he has a vigorous air swirl, produced by shrouded valves and displacement of air by the top of the piston (0.040 in. clearance between piston top and cylinder head).

The piston temperature is important. The wetted wall must have a temperature between 400 and 750°F, high enough for vaporization but not high enough for cracking. The jet impinges on a lukewarm piston. The piston temperature is controlled by spraying luboil (2 liter/min) under it and by the latent heat of the vaporized fuel over it. It is remarkable that under widely varying operating conditions these limits are never transgressed, except for a few seconds.

The combustion process is then as follows. As the piston approaches top center on the compression stroke a vigorous air swirl (the bigger the better) sweeps the piston cavity. The jets penetrate into this and they (or at least one of the two) form a little cloud before they hit the wall. This could act as the initiator of ignition, as the fuel oil in a dual-fuel engine. In the meanwhile the rest of the fuel is smeared on the combustion chamber wall and becomes vaporized at a controlled rate. As the fuel is vaporized it ignites and burns in a narrow layer near the wall. Then more fuel hits the wall and burns. A flame front never has a chance to develop and a large amount of fuel never has a chance to crack at any one time.

It would not be surprising if this explanation were modified or repudiated by Dr. Meurer, who has not yet put down his thoughts in a paper. But the engine works and the diesel industry in Germany is excited about it. The MAN organization is now concentrating on this new system.

The engine can digest a wide range of fuels. Best results were obtained with 75 per cent gasoline and 25 per cent gas oil. Ordinary diesel oil is all right. The engine can even handle straight gasoline, below 80 octane.

Whether the Meurer system will be the final answer to the diesel combustion knock problem, no one knows, but it appears to be a fine advance. One wishes it were possible to report similar progress on the smoke problem.

Some may remember that in 1947 the author gave a paper before the Society of Automotive Engineers under the title "Must Diesel Engines Smoke?", concluding then that they need not smoke. Now, seven years later, they smoke more than ever. The European diesels are no better. The British vehicles smoke slightly less, the Germans more than ours. Passing some trucks on the up-grade is definitely dangerous because the sight is obstructed by black smoke. What made the diesel smoke tend to increase? The truck loads apparently went up faster than engine powers and too many trucks are now underpowered. The driver is tempted to overload his engine to speed his delivery. Every diesel smokes if one injects enough fuel and the maximum load exceeds the clear exhaust load by at least 20 per cent.

The smoke caused by overloading or, what is the same, by over-rich mixture is black or brownish gray soot. This we call hot smoke. Engines frequently smoke, however, under idling conditions. Then the smoke is usually wet fog from unburned fuel and has a white or light gray color. This we call cold smoke. Although at times cold smoke and hot smoke may appear side by side, their natures are almost opposite and require opposite remedies for their elimination.

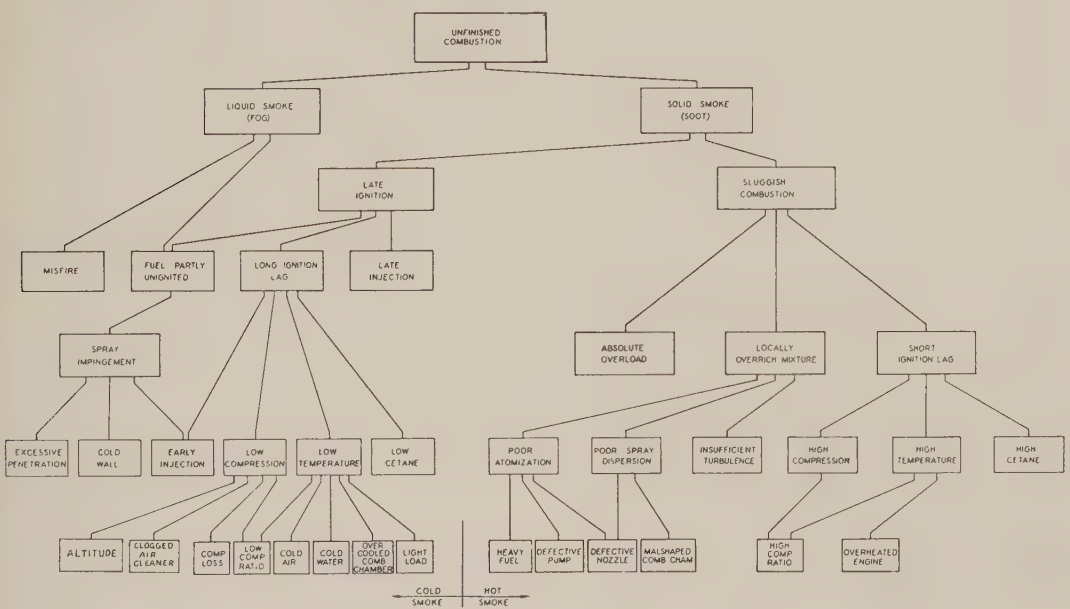

FIG. 1. Smoke chart.

Discoloration of the exhaust is always caused by the presence of liquid or solid particles in the exhaust gas. Liquid particles (fog) consist of unburned fuel (or occasionally luboil or condensed water vapor); solid particles (soot) are generally carbon particles resulting from incomplete combustion of the thermally decomposed hydrocarbons.

So exhaust smoke may be caused either by misfire, that is, fuel at least partly unignited (cold smoke), or by late burning when all the fuel in the cylinder is ignited but had not time to finish its burning when the exhaust opens (hot smoke).

Late burning, again, may be caused either by late ignition or by sluggish combustion. Late

ignition is the result of too late an injection or too long an ignition lag. Sluggish combustion means too low a burning rate which results from a deficiency of oxygen; that is, an over-rich mixture.

An over-rich mixture in a diesel engine may actually have 50 per cent excess air which would make it over-lean in a spark-ignition engine. The mixture in a spark-ignition engine is uniform; in a diesel it is highly stratified. The mixture needs only be locally over-rich to produce exhaust smoke even if the rest is extra lean.

To reduce exhaust smoke of the hot variety it is usually helpful to improve the distribution of the fuel in the air by better atomization, dispersion, and turbulence. Measures that help ignition, like heat or high cetane fuel, will help to eliminate cold smoke. A smoke diagnosis on the basis of the smoke chart reproduced in FIG. 1, is a good first step in attacking the problem.

Odor or nose and eye irritating fumes frequently accompany cold smoke. They involve intermediate combustion products such as aldehydes. They appear more frequently at idling than at heavy loads and measures directed against cold smoke usually relieve exhaust odor and lacrimation.

While the diesel exhaust is frequently obnoxious, there is no proof that it is noxious. The very noxious CO gas is conspicuously absent from the diesel exhaust.

Diesel engineers generally tend to subscribe to two traditional concepts. The first is that a diesel engine must always get a full charge of air and only the fuel quantity must vary according to the load. The second is that all of the fuel must mix with the air inside of the cylinder. Neither proposition should be regarded as a necessity.

Twenty years ago, in discussing the diesel with some spark ignition engineers, one of them asked "Compression ignition is all right but why don't you have a constant air-fuel ratio?" The diesel engineers would smile condescendingly; "The poor fellow is not a diesel engineer and does not know what he is talking about." Today it appears that the spark ignition engineer was talking sense! The diesel engine would be better off if it would get less air at light load. Then most troubles with cold smoke and odor associated with idling would disappear.

As to mixing, the spark ignition engine would be better off if its charge were less homogeneous. If it were rich near the spark plug, the rest could be lean, the fuel economy would be better and the range of ignitable mixture strength wider.

The diesel engine, on the other hand, would be better off if its charge would be less heterogeneous. Just because it is so heterogeneous, we now need 50 to 100 per cent excess air at full load to burn the fuel without excessive hot smoke. Suppose that you introduce a part of the fuel into the air already in the intake manifold. That part will be well mixed when the injection takes place. The fuel spray has an easier job and we may get by with half as much excess air. This is what McLaughlin and others are doing in California, Lyn in England and Havemann in India. The result is less smoke with the same load or more load with the same smoke. We may look forward to more progress in this direction.

Just to be sure that no one shall misinterpret the intent of the author's remarks, let it be emphasized that the better we understand the mechanism of combustion the better position we will be in to combat the nuisances that accompany it. We therefore look to combustion scientists for major contributions. A plea is made, however, for a concerted effort in directing combustion research to objectives that scientists can easily lose sight of, but which are tremendously important to our fellow citizens, namely the elimination of noise, smoke and odor from diesel engine combustion.

III

COMBUSTION PROBLEMS IN LIQUID-FUEL ROCKET ENGINES[a]

By S. S. PENNER AND P. P. DATNER

I. Introduction

The design and development of liquid-propellant rocket engines with high combustion efficiency, stable motor operation, and reasonable heat transfer characteristics often involves more art than science. At the present stage of our knowledge, an attempt at scientific interpretation of combustion in rocket engines may therefore appear to be a fruitless task. Nevertheless, useful guides for further work are often evolved by a critical study of our state of ignorance. This study will be our task with emphasis on classification of important problems in combustion, rather than on the remedies for specific ills of a given piece of hardware. By approaching the subject from a unified point of view, we hope to show that sometimes seemingly unrelated facts connected with motor operation fall into an intelligible pattern.

Before proceeding with a discussion of combustion problems, we present a brief summary of theoretical estimates for motor performance based on thermodynamic considerations (Section I-A). Next the relation between nozzle flow characteristics and performance is mentioned (Section I-B). We conclude the introductory considerations by examining the complexities of heterogeneous combustion problems in general terms, emphasizing the relation between injection system and rate-controlling reaction steps in the combustion reactions (Section I-C).

I-A. THEORETICAL PERFORMANCE EVALUATION FOR CHEMICAL PROPELLANTS

The performance of propellants is generally described in terms of specific impulse, I_{sp}, which is defined as the ratio of thrust to weight flow rate and is expressed in sec. Quantitative calculations involve the following important assumptions: (a) thermodynamic equilibrium is reached in the combustion chamber after adiabatic reaction;[b] (b) expansion of the combustion products through the de Laval nozzle is adiabatic; (c) the products of combustion behave as ideal gases; (d) the expansion process involves one-dimensional flow of nonviscous ideal gases[1, 2]. It is customary to make performance calculations for nozzle flow without chemical change (frozen-flow calculations) and for nozzle flow in which chemical equilibrium is maintained at all times (equilibrium-flow calculations). For the hottest propellant systems (e.g., stoichiometric H_2-F_2 motor), the calculated I_{sp} for equilibrium flow corresponds to a value some 12 per cent higher than for frozen flow. For the propellant systems encountered in ordinary rocket practice, the performance difference is at most a few per cent.

On the basis of extensive development work, with a wide variety of propellants, the conclusion may be drawn that the experimentally observed performance approaches but never exceeds the calculated value of I_{sp}.[c] Thus the approach to the calculated performance for frozen flow or for equilibrium flow, depending on the propellants and nozzle dimensions involved, may be used as a convenient estimate for combustion efficiency.

Following a suggestion by Zwicky[3], isothermal combustion under flow conditions has been studied theoretically. The adiabatic work cycle appears to be preferable to an isothermal work cycle[4], aside from the difficulties involved in the proper design of the latter.

The possibility that combustion efficiency, defined in terms of conventional equilibrium- or frozen-flow calculations, may depend on thermodynamic considerations has been emphasized recently[5]. For the propellant system RFNA-AN,[d] slight nonhomogeneous mixing in the chamber will give theoretical performance exceeding the calculated value for the design mixture ratio,

---

[a] Supported, in part, by the Office of Ordnance Research, U. S. Army, under Contract DA 04-495-Ord-446 with the California Institute of Technology. Supported, in part, by the USAF Office of Scientific Research, Air Research and Development Command, under Contract No. AF 18(600)-799 with the Aerojet-General Corporation.

[b] Heat loss corrections, which are small for large motors, can be incorporated in theoretical performance estimates without difficulty.

[c] Exceptional cases, in which the observed performance exceeds the calculated values by a few per cent or less, have been noted. These can probably be accounted for in terms of uncertainties in the thermodynamic constants used for calculation or else in terms of relaxation effects.

[d] RFNA = red fuming nitric acid, AN = aniline.

provided $d^2I_{sp}/dg^2 > 0$ for weight fractions of oxidizer g near the design value. This requirement for improved performance is often met for fuel-rich propellant mixtures.

The development of conventional chemical propellants has been carried to the point where significant increases in theoretical or experimental I_{sp} can probably not be achieved through the discovery of new stable compounds. However, interest has been focused recently on application of metastable compounds, the successful development of which can lead to propellants with greatly improved performance[6].

FIG. 1. Schematic representation of reaction paths in bipropellant rocket engines.

I-B. NOZZLE-FLOW STUDIES AND THEORETICAL PERFORMANCE CALCULATIONS[7]

For some propellant systems it is possible to supplement the theoretical performance calculations by kinetic studies of chemical changes and internal relaxtion effects during nozzle flow. Since the maximum calculated performance differences between equilibrium and frozen flow are small, the required corrections to theoretical I_{sp} and combustion efficiency are also small.

Nozzle-flow phenomena influence estimates of theoretical I_{sp}, and hence of combustion efficiency, differently for motors of different size. For all chemical reactions near-frozen flow obtains in sufficiently small nozzles. For each propellant system there is a minimum nozzle size which will permit a transition from near-frozen to near-equilibrium flow. Whether or not this critical nozzle size is of reasonable dimens ons, and will permit practical utilization of the increase in performance associated with near-equilibrium flow, depends on the rates of the chemical reactions which are characteristic for each propellant system. Although specific reaction rate constants are generally not available, useful approximate estimates of the interrelation between nozzle dimensions and chemical reaction rates can be obtained frequently by utilizing simple analytic flow criteria[7]. It appears that for conventional nozzle sizes, many chemical reactions are either so rapid as to assure near-equilibrium flow or else so slow as to favor near-frozen flow.

In conventional rocket practice no allowance is made, in estimating combustion efficiency, for the relation between theoretical performance and motor dimensions.

I-C. GENERAL CONSIDERATIONS RELATING TO COMBUSTION IN LIQUID-PROPELLANT ROCKET ENGINES

The relations between the physico-chemical processes (evaporation, diffusion, heat conduction) during stable combustion in rocket engines is generally so complex that it is not possible to select a single transport process or chemical reaction rate as the slow or rate-controlling step. A schematic diagram of some of the important reaction paths for bipropellant systems is shown in Figure 1 and can be made applicable to monopropellants with slight modification. The possible reaction steps are not meant to be all inclusive (e.g., surface catalysis of chemical reaction rates is not indicated explicitly) but can be used as a model either for the transitory ignition processes or for steady combustion.

The design of the injection system exerts a profound effect on the subsequent combustion reactions. For this reason we present in Table 1 a summary of important injection systems[8] together with some remarks concerning desirable and undesirable features of the various injector types. The last row of Table 1 contains a classification of injection systems in terms of their probable influence on rate-controlling reaction steps in motor combustion.

Study of Figure 1 and Table 1 sometimes suggests useful injection methods for selected bipropellants. We proceed to illustrate this remark by several examples.

For nonhypergolic[e] propellants, mixing in the liquid phase can have little or no effect in accelerating the combustion rate, which is probably controlled by gas-phase chemical reactions. Hence a showerhead injector, which gives fine sprays and rapid evaporation rates, should be useful. In accord with this conclusion, such systems as RFNA-hydrocarbons, which are often nonhypergolic, can be operated successfully with random showerhead injectors.

The following remarks apply for many small rocket engines but are apparently not applicable to large motors. For hypergolic bipropellant systems the combustion rate, and hence the combustion efficiency for a given motor size, should be increased by facilitating liquid-liquid collisions and liquid-phase chemical reaction rates. For systems of this type, the use of liquid-liquid impingement injectors is therefore indicated. In accord with this conclusion, we find, for example, successfully operating units employing the spontaneously reacting mixture RFNA-AN, based on liquid-liquid impingement injectors.

For some propellant combinations the chemical decomposition and reaction rates can sometimes be accelerated by surface catalysis. For systems of this type the use of a splash plate should be beneficial. Practical examples verifying this conclusion are available.

Simple methods for categorizing motor performance characteristics are subject to error, insofar as the rate-controlling reaction step is not necessarily affected adversely by modifying injection procedure. Thus a liquid-liquid impingement injector would not be expected to reduce the combustion efficiency of nonhypergolic mixtures, compared to a showerhead injector, provided both injectors give equally rapid evaporation and gas-phase reaction rates. The point is rather that the impingement injectors for nonhypergolic systems are not necessarily superior to showerhead injectors.

We have attempted in the present section to present a summary of basic qualitative ideas relating to motor design and performance. We now turn our attention in Section II to representative fundamental studies which may ultimately prove to be of value in working out analytical procedures for motor design. In Section III we examine some typical engineering problems in an effort to obtain some insight into the nature of rate-controlling reaction steps in motor operation.

[e] Hypergolic = spontaneously igniting.

II. Fundamental Studies

A number of experimental and theoretical studies have been carried out in recent years on the burning characteristics of simple heterogeneous systems under controlled conditions. This work may prove to be useful in evolving a rational system of classification for rate-controlling reaction steps in liquid-fuel rocket engines. For this reason we present brief summaries of some of the results of the heterogeneous burning of single droplets (Section II-A), spray combustion (Section II-B), burning rate of liquid monopropellants in tubes (Section II-C), fundamental studies on carbon formation (Section II-D), laboratory measurements of ignition delay for hypergolic bipropellant systems (Section II-E), and experimental studies on local compositions and gas temperatures in jet engines (Section II-F).

II-A. HETEROGENEOUS BURNING OF SINGLE DROPLETS

The heterogeneous burning of single stationary droplets of hydrocarbon fuel in a gaseous oxidizing medium has been studied both experimentally[9-14] and theoretically[10, 15, 16] by several investigators. As a result of this work it has become apparent that a useful description for the burning rate is obtained on the assumption that the liquid droplet is surrounded by a spherical diffusion flame whose position is determined, in first approximation, by the condition that the rates of delivery of fuel and oxidizer to the flame front are in stoichiometric proportions[10, 16].

It is customary to base the analysis on the assumption that the droplet and flame surfaces are concentric spherical surfaces, that radiant heat transfer is relatively unimportant, that the rates of mass and energy transfer are rate-controlling with the chemical reactions occurring instantaneously at the flame surface. Without making proper allowance for (a) a distributed reaction front of finite width and (b) dissociation at the highest temperatures and reassociation at lower temperatures, the theoretical model leads to very high fictitious temperatures at the flame front and to excessively large combustion radii[16]. Nevertheless, a compensation of errors occurs which produces useful estimates for the burning rate. Thus the burning rate is ultimately determined by temperature and concentration gradients near the droplet surface; these gradients, in turn, seem to be predicted almost correctly by

TABLE 1. TYPICAL INJECTOR CONFIGURATIONS USED IN LIQUID-PROPELLANT ROCKET ENGINES

	Propellants Mix in the Combustion Chamber						Propellants Mix Upstream of the Combustion Chamber;
	Showerhead	Coaxial-stream	Atomizing	Fuel-on-oxidizer impinging	Splash-plate	Like-on-like	Premix
	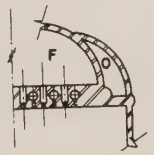		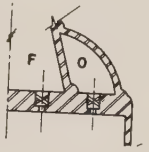	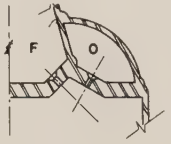	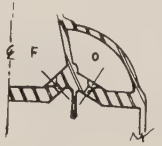	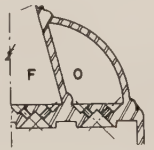	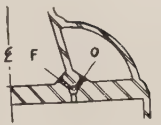
	Without atomization aids		With atomization aids				
Description	Injection through orifices parallel to the axis of the combustion chamber resulting in fuel & oxidizer streams parallel to each other	Propellants are injected in coaxial streams parallel to the axis of the combustion chamber	Propellants are injected in well atomized streams parallel to each other and to the axis of the combustion chamber	Injection is accomplished by orifices inclined to the chamber axis & arranged so that fuel & oxidizer streams impinge upon each other	Injection through orifices inclined to the chamber axis, propellant jets impinge upon splash plates	Injection through orifices inclined to the chamber axis so that each fuel stream impinges upon another fuel stream & each oxidizer stream impinges upon another oxidizer stream	The propellants are mixed upstream of the combustion chamber & are injected as premixed liquids
Salient performance characteristics	Fair combustion efficiency with both hypergolic & non-hypergolic propellants; low heat transfer rates & generally smooth combustion. Requires moderately large L*, at least for chambers of small size	There is relatively little experience with this type of injector. Satisfactory operation can be obtained only with relatively few propellant combinations	Moderate combustion efficiency, L* requirements & heat transfer rates	Combustion efficiency is, as a rule, high for both hypergolic & non-hypergolic propellants. Requires low L* values but heat transfer rates are high. With certain propellant combinations high-frequency combustion instability occurs	Combustion efficiency & heat transfer rates are high, L* requirements low. With certain propellant combinations leads to combustion oscillations of high frequency	Combustion efficiency fair, heat transfer rates & L* requirements are moderate. Usually smooth combustion	There is little experience with this type of injector; explosion of propellants in the premixing chamber is often experienced. This danger can be minimized by high injection pressure drops

Relation to rate-controlling reaction steps in combustion	The rate-controlling steps in combustion are, in all probability, determined by diffusion processes. The slow steps are probably the same as occur during the burning of either fuel droplets in gaseous oxidizer or of oxidizer droplets in gaseous fuel, if one of the propellants is relatively much more volatile than the other. It appears that this injector should be employed only for propellants, the combustion of which is not affected significantly by liquid-phase & surface reactions	This design facilitates liquid-phase reactions to a greater extent than the showerhead injector. It appears that the nature of the processes & reactions taking place during combustion depends to a great extent upon the relative volatility of the propellants	Similar to showerhead injector	Diffusion & other physical processes required for preparing a combustible mixture are greatly accelerated because of the intimate mixing of liquid droplets; simultaneously, liquid-phase reactions are enhanced	Facilitates jet disintegration, evaporation & also liquid-phase mixing & surface catalysis. In addition, splash plates may act as flame holders. This injector should be useful for propellants for which liquid-phase chemical reactions are rate-controlling in combustion	Similar to showerhead injector	Mixing in the combustion chamber & gas-phase diffusion processes are eliminated as rate-controlling reaction steps. Liquid-phase chemical reactions should be greatly accelerated. This type of injector should give optimum performance for all propellant combinations & notably improved performance, compared with other injectors, for propellant combinations for which chemical reaction rates are not the rate-controlling steps in combustion

the conventional model of the heterogeneous diffusion flame.

In order to emphasize the utility of the theoretical model, we reproduce in Table 2 a comparison between observed and theoretical evaporation constants K' for a number of hydrocarbon

Table 2. Comparison of Calculated and Observed Evaporation Constants for Various Fuels Burning in Air

(The Data are Taken from Reference 16)

Compound	Observed Value of K′	Calculated Value of K′
	(cm^2/sec)	(cm^2/sec)
Benzene	0.0097	0.0100
Ethyl alcohol	0.0081	0.0079
Ethyl benzene	0.0086	0.0085
n-Heptane	0.0097	0.0086
Toluene	0.0076	0.0087

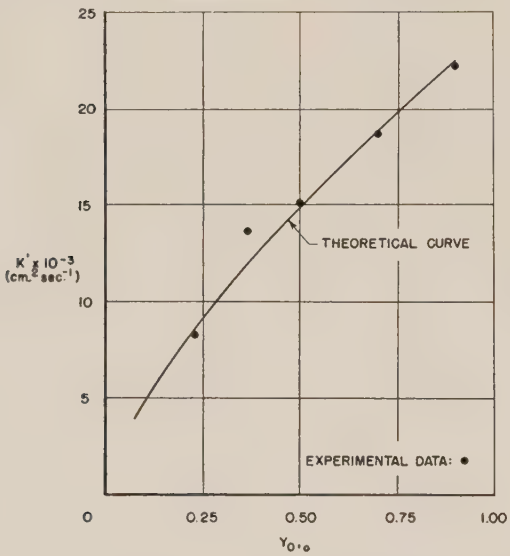

Fig. 2. Dependence of the evaporation constant K' on the weight fraction of oxygen Y_0 for the burning of *n*-heptane in oxygen-nitrogen mixtures (the data are taken from reference 13).

fuels burning in air. The calculated results were obtained from the equations of Goldsmith and Penner[16] which contain no adjustable parameters, although considerable uncertainty remains in estimating "best values" for the transport coefficients. The evaporation constant K' is independent of droplet radius and is defined by the relation

$$K' = 4\dot{m}_F/\pi D\rho_l \qquad (1)$$

where $\dot{m}_F$ is the mass burning rate of a fuel droplet of diameter D and density ρ_l. In Figure 2 we present some experimental and theoretical results[13] on the variation of K' for *n*-heptane with oxygen concentration in oxygen-nitrogen mixtures. Again we note impressive agreement between theory and experiment.

The effect of pressure on burning rate has been studied experimentally by Hall and Dieterichsen[12] and can be understood qualitatively in terms of the known variation of convective heat transfer coefficients with pressure.

The preceding considerations support the idea that the rate of heterogeneous burning of hydrocarbon fuels in oxidizing atmospheres is controlled by transport phenomena. Extrapolation of the results to other chemical systems is admittedly dangerous. However, it appears likely that the problem is reversible with respect to the roles played by the fuel and oxidizer.

In terms of the general combustion scheme for liquid-propellant rocket engines considered in Section I, it is now appropriate to ask for what type of propellant and injection system the physico-chemical environment may conceivably simulate the heterogeneous burning of single fuel droplets. It appears that heterogeneous diffusion flames with mass and energy transport as rate-controlling steps could arise for nonhypergolic bipropellant systems injected with a showerhead injector. If one of the components of the bipropellent system is relatively much more volatile, then it is possible that single droplet combustion will be simulated, except that the droplets are not stationary and that the proximity of many droplets may modify the combustion reactions extensively. It is therefore of obvious interest to proceed by studying the relation between single droplet and spray combustion of fuels in oxidizing atmospheres.

If the rate-controlling steps in the burning of nonhypergolic propellants injected with a showerhead injector are, in fact, a series of transport processes, then the following conclusion is inescapable: nonhypergolic propellants should give optimum combustion rate with premix-injectors. For miscible components, the rate-controlling steps will then again become chemical reaction rates; for immiscible components, "pre-mixing" will produce foams which will minimize transport control of combustion rate. Practical experience to verify the preceding conclusions does not appear to be available.

II-B. Burning of Fuel Sprays

A basic theoretical study for correlating combustion characteristics of fuel sprays has been

published by Probert[17]. The two most important assumptions in Probert's analysis are:

(a) The spray particle size follows the Rosin-Rammler distribution law

$$w = \exp\left[-\left(D/\overline{D}\right)^n\right] \tag{2}$$

where w equals the volume or weight fraction of the spray composed of drops with diameter greater than D, $\overline{D}$ is called the size constant, and n is usually referred to as the distribution constant.

(b) The rate of burning of each droplet is taken to be proportional to the first power of the droplet diameter, in which case the droplet diameter at any time D is given by the expression

$$D^2 = D_0^2 - K't; \tag{3}$$

here K' is the evaporation constant discussed in Section II-A and t represents the time.

Probert defines a mean droplet diameter, D_m, in such a way that a single droplet per unit volume of diameter D_m burns at the same rate as the liquid in unit volume of the spray. Convenient plots are provided for estimating the mean diameter of the injected spray, and also of the spray in a combustion chamber at steady burning, as a function of size constant ($\overline{D}$) and distribution constant (n). In good approximation

$$D_m = \overline{D}/\sqrt{2} \text{ for steady-burning.} \tag{4}$$

Finally, the percentage of unburnt liquid after time t_r, from which the combustion efficiency can be computed, is given as a function of the group $\sqrt{K't_r}/\overline{D}$ for values of n between two and four.

The preceding qualitative summary of Probert's work shows that the combustion efficiency for a given residence time t_r is determined by the spray distribution (through $\overline{D}$ and n) and by the evaporation constant K'. Very high combustion efficiency for fixed values of t_r is favored by small values of $\overline{D}$ and large values of n, although small values of n give a high initial combustion rate.

A question of fundamental importance for combustion analysis in all types of engines is the following: can the values of the evaporation constant determined from studies on stationary single drops be used, in conjunction with Probert's analysis, to predict the burning characteristics of sprays? An attempt to answer this question has been made recently by Graves and Gerstein[18].

Graves[19] determined experimentally the dependence of combustion efficiency for a single tubular combustor for a range of inlet oxygen concentrations, using iso-octane as fuel. A comparison between the observed dependence of combustion efficiency on oxygen concentration, and the dependence determined from the known variation of burning rate with oxygen concentration for quiescent single droplets, can then be used to obtain an empirical estimate for the utility of single droplet studies in predicting burning rates of sprays.

Graves and Gerstein[18] determined drop-size distribution constants for their atomizer and fuel flow rates from empirical correlations of Bowen and Joyce[20]. Next they calculated the theoretical combustion efficiency according to Probert's analysis as a function of oxygen concentration using mean values for the evaporation constant determined from single-drop studies.

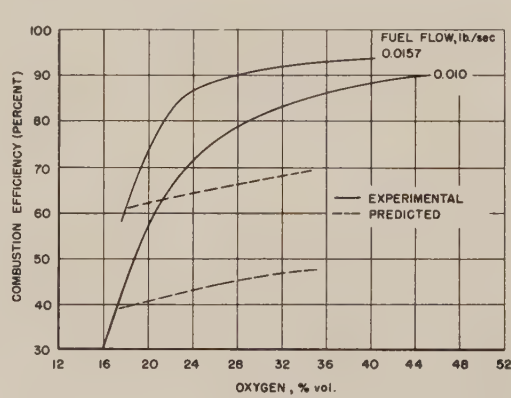

FIG. 3. Comparison between calculated and observed changes in combustion efficiency for the burning of iso-octane in a tubular combustor at various oxygen concentrations (the data are taken from reference 18).

The results of the experimental and theoretical studies are contrasted in Figure 3. Reference to Figure 3 shows that the experimentally determined combustion efficiency increases rapidly with inlet oxygen concentration for the lower oxygen concentrations, whereas the calculated values depend only weakly on oxygen concentration. The observed change in combustion efficiency with fuel flow rate can be understood in terms of a decrease in drop size for the spray with increased fuel flow rate. Graves and Gerstein[18] conclude from their investigation that "no single factor which has been shown to be important in the simpler diffusion flames is sufficient to correlate all of the data obtained" and "it would appear that the chemistry of the reaction, ignored

in diffusion flame theories, may be a significant factor in determining combustion efficiency".

Reference to Figure 3 shows that for oxygen concentrations above about 24 per cent by volume, the predicted and experimental curves have similar slopes. It is therefore apparent that "theory" and experiment on combustion efficiency can be made to agree for large oxygen concentrations by suitable adjustment of the unknown burning time t_r, which is assumed to be constant with variations in inlet oxygen concentrations. In this case one might argue that the disparity between theory and experiment results from incomplete combustion for lower oxygen concentrations. The choice of the proper value of K' for spray combustion is obviously complex. Thus single droplet studies are always carried out with excess of oxygen under conditions of negligible oxygen depletion and without heating of the reactant gases. It is clear that these conditions may be approximated in sprays with considerable excess of oxygen but do not apply for low oxygen concentrations.

Although one can make a case for the applicability of single-droplet studies to spray combustion in oxygen-rich mixtures, we are inclined to agree with Graves and Gerstein that chemical rate processes usually play a vital role in the burning of sprays. The preceding incomplete discussion on spray combustion emphasizes the need for additional work along the lines sketched. The discussion was not meant to be exhaustive but was designed to show possible relations between single-droplet and spray combustion. Additional references to recent work on spray combustion will be found in the literature cited by us.

II-C. BURNING OF MONOPROPELLANTS IN TUBES

Burning rate measurements on liquid monopropellants in tubes[21] may or may not provide useful phenomenological information on the rates of liquid-phase reactions for monopropellants in rockets which, in turn, may constitute slow or even rate-controlling reaction steps.

Experimental studies on mixtures of 2-nitropropane and nitric acid[21] show that the measured rate of regression of the liquid in narrow tubes (the burning rate r) can be expressed as a function of pressure (p) according to the relation

$$r = p^n \tag{5}$$

where $n = 1.1$ for pressures below about 1000 psia and $n = 4.3$ for pressures above about 1000 psia. Near the transition pressure, the burning rate was found to vary erratically between two different values, corresponding to the two different branches of the burning rate vs pressure curve. The erratic behavior of the burning rate may be associated with oscillations of the liquid column and changes in surface area with time. Any connection between this phenomenon and motor oscillations during unstable combustion appears to be remote. The physical properties of the reacted gases changed drastically with pressure.

Some experiments on the effect of tube diameter on burning rate showed lower burning rates for narrower tubes, thereby suggesting possible wall-quenching effects.

For the range 25 weight per cent less to 25 weight per cent greater than stoichiometric, the burning rate was found to be insensitive to the amount of nitric acid added to the nitropropane.

Thus far insufficient experimental and interpretative work has been done to assess fully the utility of burning rate measurements on liquid monopropellants. Additional work, particularly on the decomposition rate of single droplets in heated gases (i.e., in inert gases, heated combustion products, or partially burnt gases) is warranted. Work along similar lines for mixed bipropellant systems may be said to constitute a fundamental approach also to the combustion characteristics in bipropellant systems utilizing premix-injectors.

II-D. CARBON FORMATION

One of the troublesome phenomena occasionally encountered in the operation of both monopropellant and bipropellant rockets is the formation of solid deposits consisting of carbonaceous residue. The chemical processes responsible for the formation of carbon have been the subject of basic studies by several investigators.

Porter[22] has suggested that carbon formation involves a series of decomposition reactions of hydrocarbons which leads eventually to the formation of acetylene and hydrogen. Carbon is then formed by condensation and dehydrogenation of the acetylene. Porter believes that the proposed reaction scheme is applicable to all types of flames. Experimental studies on carbon formation in acetylene are in progress[23] and suggest that residue formation results from reaction between acetylene and hot carbon particles.

Parker and Wolfhard[24] favor the idea that high molecular weight polymers are formed in the precombustion zone and that subsequent carbon

formation involves a solid-phase dehydrogenation reaction. Porter[22] considers the experimental conditions, under which Wolfhard and Parker observed the formation of large particles, to be unrelated to conditions in flames, where the time spent in the preheating zone is very short.

Additional references to fundamental studies on carbon formation may be found in the literature.[25-29]

Work on carbon formation in engine combustion under controlled conditions has been carried out for turbomachines[30, 31] in which the operating temperatures are generally much lower than in rocket engines. Extrapolation to rocket conditions is therefore not feasible, particularly since the extent of carbon formation depends on both chemical and motor design features. Nevertheless, a survey of empirical results, obtained under controlled conditions, is instructive.

Rough correlations between the rate of carbon formation and the physico-chemical properties of the fuel can be obtained for (a) boiling temperatures of families of hydrocarbons, (b) fuel density, (c) carbon to hydrogen ratio or number of carbon atoms in a hydrocarbon molecule, (d) average carbon-carbon bond strength[30-32]. The coking tendencies increase from paraffinic to naphthenic to aromatic fuels; for a given ratio of carbon to hydrogen, deposits decrease as fuel volatility increases and as fuel density decreases[30]. The greater the average strength of the carbon-carbon bonds in the fuel molecule, the greater is the smoking tendency during combustion[32].

For a given combustion chamber, experimental data for a wide variety of hydrocarbons can be correlated by an expression of the form

$$c = (1/K_3)\ln(K_1R - K_2) + (T_b/K_4) - K_5 \quad (6)$$

where c is the rate of carbon deposition, R equals the carbon to hydrogen ratio, T_b represents the boiling temperature of the fuel, and K_1 to K_5 are empirically determined constants for each chamber[30].

A great deal of experimental work has been done on the kinetics of oxidation of carbon, which constitutes an integral part also of the problem of carbon deposition[33].

Some interesting results on carbon formation during the burning of single droplets have been described recently[13]. It appears that the burning of benzene and toluene droplets in oxygen-nitrogen mixtures containing more than about 20 per cent of oxygen leads to incipient residue formation near the cooled tip of the diffusion flame, which is exposed to the supporting quartz fiber from which the liquid droplet is suspended. The formation of carbonaceous residues progresses from the tip down, roughly along the surface of maximum luminosity surrounding the burning droplet.

Carbon formation in engines may be the result of gas-phase and liquid-phase reactions, and may also involve the motor walls directly as a catalytic surface. Fouré quotes some experimental studies in tubes heated to 500°C containing pure CO in which the extent of carbon formation was strongly dependent on the material used for construction. Yet these same materials were found to differ little in their tendency to produce carbon in burners[31]. Results of this type emphasize the importance of both chemical and motor design features in carbon formation for engines.

II-E. LABORATORY MEASUREMENTS OF IGNITION DELAY

A survey of the unclassified literature relating to laboratory methods for ignition delay measurements in rocket engines has been prepared recently[34] and need not be repeated for the present purposes. It is sufficient to note here that the results of laboratory ignition delay studies can be described in terms of a nonstationary reaction scheme of the type sketched in Figure 1 and that the numerical values obtained are generally not dependent only on the hypergolic propellants involved, but are functions also of injector configuration, chamber volume and construction, and other design features of the test apparatus. In other words, ignition lag tests are not fundamental studies and are most useful in connection with the development of a specific piece of hardware.

As examples of the type of correlations obtained, we quote the following summary statements[34].

In laboratory tests for the determination of ignition delay in unconfined systems, the measuring techniques often emphasize the contributions to the total delay of liquid-phase mixing and reaction. Hence a correlation with performance in motor combustion chambers is to be expected only if liquid-phase reactions control the rate of ignition in the motor. An extreme example of this type of measurement is the twin-jet apparatus[35], in which separate streams of fuel and oxidizer are allowed to impinge. The angle between the liquids is chosen in such a way that a single continuous stream results after collision, with relatively little carry-through. The ignition delay (ID) is then

defined as the time elapsed between impingement of the oxidizer streams and the first occurrence of rapid chemical reaction[35]. Open-cup tests in which a fuel drop or sheet is poured into a dish of oxidizer (or conversely), and in which the ID is defined as the time between mixing and the first occurrence of vigorous exothermic reaction (as measured by a sizable pressure rise or by the emission of luminous radiation) are still popular[36].

Measurements of ID in semi-enclosed chambers or in small rocket motors are generally the more useful the closer the test conditions approximate service rocket design.[34]

Although absolute values of the ID show little correlation for different test conditions, the *relative* changes in ID with propellant composition, ignition catalysts, pressure, temperature, etc., are often similar in laboratory tests and in motor operation. For hypergolic bipropellant systems it is sometimes possible to obtain useful correlations between chemical structure, reactivity, and ID[34].

Monopropellants are conveniently divided into three classes, viz., (a) monopropellants which contain both oxidizer and fuel constituents in the same molecule (e.g., CH_3NO_2 and H_2O_2); (b) monopropellants which would be classified as oxidizers (e.g., NO) or as fuels (e.g., N_2H_4 and C_2H_2) in bipropellant operation; (c) synthetic mixtures of fuel and oxidizers (e.g., CH_3NO_2 mixed with CH_3OH, the German "Myrol"). There is an unavoidable correlation between explosive power and high performance for many monopropellants. Monopropellant ignition, like that of nonhypergolic bipropellants, requires an external energy source (e.g., a heated surface or a spark) or else a small amount of added fuel or oxidizer which produces a hypergolic mixture[34].

Ignition in rocket engines at high altitudes poses a special problem. As a qualitative guide for the expected performance, laboratory ignition tests on small units and at reduced pressure may be useful.

Finally, reference should be made to extensive ignition delay measurements on fuels injected into an air stream[37], as well as to studies on combustion in vitiated air[38] and at high altitudes[39]. Although this work was carried out primarily in connection with the problem of air-fuel combustion, some of the results are relevant also for liquid-propellant rocket engines.

II-F. LOCAL COMPOSITION AND TEMPERATURE ANALYSIS IN ROCKET ENGINES

Experimental determination of local gas compositions and temperatures in the combustion chamber is of obvious interest in connection with efforts at understanding combustion processes in engines. A survey of experimental techniques useful for this purpose has been published recently in a "Special Instrumentation Issue"[40] of the Journal of the American Rocket Society. We refer to the papers in this issue and other selected references[41-45] for details concerning composition and temperature analysis. The available information is as yet insufficient to provide a detailed description of engine combustion processes, although some useful conclusions concerning, for example, combustion patterns (see Section III-B) and motor oscillations (compare Section III-C) are possible.

III. Engineering Problems in Rocket Engine Combustion

After surveying theoretical methods for estimating motor performance (Section I) and reviewing some basic work on heterogeneous combustion (Section II), we turn now to a discussion of some of the important problems encountered in rocket engineering. Although we are unable to present a detailed quantitative analysis of the physical and chemical processes involved in rocket combustion, liquid-propellant rocket engines are being developed successfully on an empirical basis. We shall make no attempts at classifying specific problems associated with motor operation for which no intelligent summary remarks can be made beyond the observation that we are dealing with a problem which is a sensitive function of physico-chemical parameters and motor design features. Thus we omit any further discussions of carbon formation, ignition delay studies, motor cooling problems (even though they are related to combustion operations if, for example, a propellant is used for sweat cooling).

In Section III-A we consider the design difficulties associated with ignition failure, shut-down problems, and flame-out problems, from a thermodynamic point of view, in an effort to estimate peak pressures during transient operation. Combustion chamber volume requirements and their relation to possible rate-controlling reaction steps are discussed in Section III-B. Combustion oscillations are reviewed in Section III-C. Motor scaling and similarity analysis form the contents of Section III-D.

III-A. COMBUSTION UNDER TRANSIENT CONDITIONS

Experience indicates that the problems arising during combustion under transient conditions are

often more troublesome than those connected with steady-state operation. Unburned propellants may accumulate in the combustion chamber during starting and shutdown and cause "hard starts", which are characterized by pressure peaks exceeding the steady-state combustion pressure. The pressure peaks may be sufficiently high to destroy the rocket chamber. Depending upon the intensity of the transient pressures generated, the vehicle propelled by the rocket may be subjected to excessive accelerations, which can damage instruments or even structural members. In practice the rocket engineer must control combustion during starting and after shutdown in such a manner as to satisfy specified requirements concerning the variations in thrust with time.

Upper limits for the peak pressures produced during transient motor operation can be calculated from thermodynamic considerations. Unfortunately, the estimated upper limits are often so high as to be useless for predicting motor performance. Similarly, neither the dynamic loads which the rocket chamber can withstand, nor the peak acceleration which a missile can tolerate, can be predicted accurately. For these reasons, the performance of a liquid-propellant rocket engine during transient operation must ultimately be tested empirically.

In concluding the present incomplete discussion, we present a summary of methods for estimating peak pressures during transient motor operation, which may be useful in some cases. A conservative upper limit for the transient chamber pressure during ignition, as a function of equilibrium chamber pressure, ignition delay, and motor design characteristics, has been published for monopropellant operation[34]. With suitable modifications, expressions can be obtained also for the expected peak pressures in bipropellant rockets and after shutdown or flame-out followed by reignition.

Peak pressures following ignition delay in bipropellant rockets

The initial total mass flow rate into the chamber ($\dot{m}$) of both oxidizer (identified by the subscript O) and fuel (identified by the subscript F) is less than, or equal to, the equilibrium injection rate into a chamber at ambient pressure p^0, i.e.,

$$\dot{m} \leqslant A_F \sqrt{2(p_F - p^0)/\delta_F} + A_O \sqrt{2(p_O - p^0)/\delta_O} \tag{5}$$

where A, p, and δ denote, respectively, the cross-sectional area of the injector, injector gauge pressure, and liquid density. In the worst possible case all of the injected propellants remain unreacted in the chamber for a time t_{ID} if t_{ID} is the ignition delay time. Hence the following upper limit obtains for propellant accumulated in the combustion chamber during the ignition delay period

$$\dot{m}t_{\mathrm{ID}} \leqslant (A_F \sqrt{2(p_F - p^0)/\delta_F} + A_O \sqrt{2(p_O - p^0)/\delta_O})\, t_{\mathrm{ID}} \tag{6}$$

The maximum transient chamber pressure, p_{tr}, cannot exceed the value corresponding to instantaneous combustion of all of the propellant accumulated in the combustion chamber prior to ignition. Therefore,

$$p_{\mathrm{tr}} \leqslant \dot{m}t_{\mathrm{ID}}(RT_c/\overline{M}V_c) \tag{7}$$

where R, T_c, $\overline{M}$, and V_c denote, respectively, the molar gas constant, adiabatic flame temperature, average molecular weight of combustion products, and chamber volume.

During steady-state operation the required equilibrium flow rate of propellant $\dot{m}_e$ is

$$\dot{m}_e = A_F \sqrt{2(p_F - p_c)/\delta_F} + A_O \sqrt{2(p_O - p_c)/\delta_O} = p_c f_t/c^* \tag{8}$$

where p_c represents the equilibrium (design) chamber pressure, f_t is the cross-sectional area at the nozzle throat, and c^* equals the characteristic velocity, which is easily calculated from thermodynamic considerations[1]. From equations (6) to (8) the following useful result is obtained:

$$\frac{p_{\mathrm{tr}}}{p_c} \leqslant \frac{t_{\mathrm{ID}}}{c^*}\frac{RT_c}{\overline{M}L^*} \frac{A_F \sqrt{2(p_F - p^0)/\delta_F} + A_O \sqrt{2(p_O - p^0)/\delta_O}}{A_F \sqrt{2(p_F - p_c)/\delta_F} + A_O \sqrt{2(p_O - p_c)/\delta_O}} \tag{9}$$

with $L^* = V_c/f_t$ representing the ratio of chamber volume to nozzle throat area. By the use of a well-known expression for c^*[46], ... ref. 46, equation (9) can be written also in the form

$$\frac{p_{\mathrm{tr}}}{p_c} \leqslant \frac{c^*\Gamma}{L^*}\, t_{\mathrm{ID}} \frac{A_F \sqrt{2(p_F - p^0)/\delta_F} + A_O \sqrt{2(p_O - p^0)/\delta_O}}{A_F \sqrt{2(p_F - p_c)/\delta_F} + A_O \sqrt{2(p_O - p_c)/\delta_O}} \tag{10}$$

where

$$\Gamma = \sqrt{\gamma}\left(\frac{2}{\gamma + 1}\right)^{(\gamma+1)/2(\gamma-1)} \tag{11}$$

and γ represents a suitably chosen average heat capacity ratio.

Reference to equation (10) emphasizes the importance of obtaining small values for t_{ID} in order to assure peak pressure ratios p_{tr}/p_c which do not exceed the chamber design limits.

Peak pressures following motor shutdown

The analysis proceeds as for the discussion concerning peak ignition pressures, except that the upper limit for total propellant accumulation is now the sum of a term corresponding to equation (6), $\dot{m}\, t'_{ID}$ with t'_{ID} usually smaller than t_{ID}, and a term representing the total propellant accumulation during and after shutdown.

Peak pressures following flame-out

If burning has ceased for a flame-out time t_{FO} the following upper limit obtains for unburnt propellant accumulated in the chamber

$$\dot{m}t_{FO} \leqslant \left(A_f \sqrt{2(p_F - p')/\delta_F} + A_O \sqrt{2(p_O - p')/\delta_O}\right) t_{FO} \tag{12}$$

where p' is an average pressure in the chamber during flame-out. Proceeding as before, it is now found that

$$\frac{p'_{tr}}{p_c} \leqslant \frac{c^*\Gamma}{L^*}\, t_{FO} \frac{A_F \sqrt{2(p_F - p')/\delta_F} + A_O \sqrt{2(p_O - p')/\delta_O}}{A_F \sqrt{2(p_F - p_c)/\delta_F} + A_O \sqrt{2(p_O - p_c)/\delta_O}}. \tag{13}$$

III-B. COMBUSTION CHAMBER VOLUME REQUIREMENTS

One of the most important design parameters which must be determined in the development of liquid-propellant rocket engines is the minimum combustion chamber volume required to obtain reasonably complete burning of the propellants. Since the beginning of German rocket development more than 20 years ago, attempts have been made to relate the minimum required chamber volume to the time required for the conversion of the propellants into more or less completely burned gases[47]. For instantaneous evaporation and chemical reaction, the stay time t'_s of propellants in the combustion chamber equals the ratio of chamber volume V_c to the product of propellant flow rate and average specific volume of the propellant gases at the adiabatic flame temperature T_c. Thus[48, 49]

$$t'_s = L^* \sqrt{\left(\frac{\bar{M}}{\gamma R T_c}\right)\left(\frac{\gamma + 1}{2}\right)^{(\gamma+1)/(\gamma-1)}} \tag{14}$$

where L^* is the characteristic length (cm) defined in Section III-A, $\bar{M}$ is the average molecular weight of the combustion products (g/mole), γ is the ratio of specific heat at constant pressure to specific heat at constant volume, R is the molar gas constant (ergs/mole − °K), and the adiabatic flame temperature T_c is expressed in °K. Since $\bar{M}$, γ, and T_c do not vary greatly for related propellant systems, L^* is a convenient measure of the stay time t'_s provided the combustion reactions occur very rapidly. The actual relationship between time in the chamber and L^* must depend on the rates of the complex physico-chemical processes occurring during combustion, which have been summarized schematically in Figure 1. Nevertheless, the characteristic length L^* has become an accepted and useful parameter for indicating the approximate residence time requirements with injectors of different design and/or combustion chambers of different shapes and sizes. Altseimer[45] and Berman and Logan[44], using photographic techniques, were able to make time traces of eddies and luminous tracks traveling from the injector face downstream in transparent combustion chambers. Their data can be utilized to establish the time-travel history of reactants in the combustion chambers and thus to make rough estimates of the residence time. It is of interest to note that the data published by Altseimer indicate that the residence time in a constant-area section (8.9 in long, 4.375 in high and 0.47 in wide) of a two-dimensional thrust chamber with $L^* = 57$ in varied between 3.0 and 7.3 msec, depending upon the injector employed. On the other hand, the "stay time" computed from Equation (14) is found to be smaller by roughly a factor of two. These results are in agreement with the observation that the calculated values for t'_s must constitute lower limits.

For a given propellant system, the value of L^* required for complete combustion varies with total thrust and slightly with the operating pressure level. Typical requirements for L^* are about 125 cm for a nitric-acid aniline motor[48], 120 to 300 cm for liquid oxygen-ethyl alcohol motors using outdated injection methods[49], and more than 500 cm for some chambers utilizing nitromethane as monopropellant[49]. Some attempts have been made to relate the L^* requirements to rate-controlling reaction steps in combustion.

For example, Summerfield[50] has stressed the possibility that the thermal decomposition of nitric oxide, or reactions involving nitric oxide, may be rate-controlling reaction steps in motors utilizing nitric acid as oxidizer. Minimum evaporation times for representative propellant droplets in combustion chambers are sometimes not much shorter than the calculated stay times t_s'[51].

Transparent motor studies by Altseimer[45] and by Berman and Logan[44] provide useful qualitative information on the burning processes in rocket engines. The combustion chamber contents are heterogeneous with respect to composition, temperature, and velocity. A single planar flame front perpendicular to the combustion chamber axis does not exist. Instead, there are longitudinal flame columns which suggest that the flow through the combustion chamber is stratified. Circulation of combustion products from the combustion zones back toward the injector face, referred to as recirculation, was observed, but the intensity of the transverse flows was not sufficient for the longitudinal stratification patterns to be erased. It is likely that the intensity of recirculation influences the combustion chamber volume and the characteristic chamber length L^*, required for complete combustion, differently in motors of different shapes and sizes. The transparent motor studies emphasize the importance of complex three-dimensional flow phenomena in determining minimum requirements for L^* and show that a universal classification of rate-controlling reaction steps may not be feasible even for a given propellant system.

III-C. COMBUSTION INSTABILITY

Combustion instabilities in liquid-propellant rockets have plagued scientists and engineers since the beginning of modern rocket development. A review of the available information reveals that combustion instability (also referred to as rough burning, chugging, humming, groaning, motor-boating, organing, screaming, screeching, buzzing, squealing, combustion oscillations unstable combustion, oscillatory combustion etc.) can occur in every kind of liquid-propellant rocket engine regardless of the size and shape of the combustion chamber, propellants used, or feed system employed.

To date, after more than ten years of concentrated work in the United States, no complete theory or explanation exists, although significant contributions have been made to our understanding of some instability phenomena. This situation is particularly embarrassing since the design of larger units than those currently investigated, and even slight modifications of existing units, may necessitate extended and costly trial-and-error development programs. Although some empirical rules for correcting the difficulties are recognized, it is generally agreed that they are inadequate and have relatively low probabilities of success.

Combustion instability manifests itself as uncontrolled cyclic variations of pressure in the propellant feed system and combustion chamber concurrently, or in the combustion chamber alone, depending upon the frequency of the oscillations. High frequencies (i.e., 1000 cps or more) are almost always confined to the combustion chamber whereas oscillations having frequencies below about 600 cps generally reflect simultaneous variations in the feed system. The classification of combustion instabilities should be based on the physical mechanism responsible for the oscillations[52]. At least two types of combustion instability are recognized, in both of which the combustion reactions deliver the energy necessary to sustain the oscillations. Types of combustion instability are the following:

(a) Low-frequency instabilities resulting from interactions of propellant-feed system oscillations and combustion-chamber gas vibrations. Unstable operation is characterized by pulsations in the rate of propellant injection; the variations in combustion chamber pressure appear to be a forced vibration driven by the pulsations of the propellant flow. Because of the inertia of the mass of liquid propellant participating in the vibrations, the frequency of the pressure oscillations is relatively low (less than about 600 cps); for this reason, this type of oscillatory combustion is usually referred to as "low-frequency instability" or "chugging".

(b) High-frequency combustion oscillations appear to be confined to the gases in the combustion chamber, whose inertia is small compared to that of the liquid propellants in the feed lines. The high-frequency instability or "screaming" is probably connected with the combustion or injection processes themselves. Pulsations in propellant flow do not appear to be important in "screaming" and, when they are observed, their frequency and amplitude are much lower than those occurring in the combustion chamber.

High-frequency oscillatory combustion is accompanied by a significant increase in the amount

of heat transferred from the combustion gases to the walls of the chamber and to the injector face, resulting in serious burnouts; low-frequency instabilities, on the other hand, do not alter the heat transfer rates to any significant extent.

The integrated values of thrust and propellant consumption indicate a reduction in combustion efficiency of the rocket engine during low-frequency combustion instability; on the other hand, high-frequency oscillatory combustion results in a performance increase compared with normal operation.[f]

Theoretical studies

A theory regarding the conditions necessary for sustaining vibrations of a gas column in a cavity resonator was developed by Rayleigh almost 80 years ago[53]. Relevant thermodynamic considerations are due to Putnam and Dennis[54]. Vibrations in a confined mass of gas can be sustained by a periodic release of heat in the gas, if the oscillating component of heat release is in phase with the oscillating component of pressure (positive feedback). On the other hand, the gas vibrations will be impeded if the fluctuations in heat release and pressure are out of phase (negative feedback). In order to maintain vibration in a gas mass by periodic addition of heat, a space condition of resonance must also be satisfied, viz., in order to sustain vibrations, the energy must be released near the point of maximum effectiveness. Thus velocity disturbances must be added near a region where the particle velocity is at a maximum and pressure disturbances must be added in the vicinity of the loci of maximum pressure amplitude. Some experimental evidence for the validity of the space criterion of resonance is reported by Putnam and Dennis[54] and by Coward and associates[55].

The fact that a feedback mechanism is operative in combustion instability serves as the basis of the theoretical work in which the establishment of criteria for stable motor operation is attempted analytically[56-65]. Another common feature of the theoretical studies is that liquid-propellant rockets are considered to be dynamic systems with a delayed action involving a time lag, which must exist between any arbitrary change in propellant feed rate and the corresponding change in propellant consumption rate, as well as between a change in propellant consumption rate and the resulting change in chamber pressure. This time interval is usually referred to as a combustion time lag or time delay. The fact that the existence of the time delay may be instrumental in producing combustion instability was recognized[58] by Th. von Kármán in 1941. The time lag may be responsible for creating a phase shift in the over-all process, thus establishing conditions under which oscillatory variations in combustion rate can occur. The existence of a combustion time lag seems to have been confirmed experimentally[45].

Analytical problems concerned with the stability of dynamic systems with time lag have been studied by Minorsky[66] and Ansoff[67]. Criteria for stability can be obtained conveniently by using the methods of Nyquist[68] and Satche[69]. Analysis of the equations derived in the treatment of combustion instability in liquid-propellant rocket systems[56-65], by means of which the regions of stable operation can be determined, indicate that they are essentially of the same structure as the equations studied by Minorsky and Ansoff. Nyquist and Satche diagrams have been used for establishing the conditions of stable operation in rocket engines[57, 60-62]. Owing to the work of Crocco, Tsien, and others, elegant mathematical methods are now in use for determining stability criteria. In the early theoretical studies on combustion instability, the flow through the nozzle was assumed to be in phase with pressure variations in the combustion chamber. Tsien[70] has shown how to make proper allowance for inertia effects during nozzle flow, which can be included through a simple correction in existing theories[52, 64]. Crocco and Cheng have obtained analytical results for several types of rocket engines[59, 63, 64]. Tsien[60] and Marble and Cox[61] have discussed requirements of servostabilizers for eliminating low-frequency oscillations during motor operation.[g]

High-frequency instability has been defined as an effect of reactive waves, which may develop into shock waves.[52, 71] In general, there are at least three distinct possible sources of dissipation: shock waves, work needed to force the pressure waves through the nozzle, and increased heat transfer to the motor walls. It is apparent from

[f] There appears to be some question about this conclusion and a contrary opinion has been expressed by M. Barrère. *AGARD Selected Combustion Problems*, pp. 394–396, London, Butterworths, Ltd., 1954. Barrère has also proposed an extended classification of combustion instabilities.

[g] For a detailed discussion see also H. S. Tsien: *Engineering Cybernetics*, Chapter 8. New York, McGraw-Hill Book Co., 1954.

the work of Crocco and Cheng[63, 64] that the detailed description of the combustion processes will influence profoundly the stability limits in high-frequency combustion.

We may summarize the theoretical studies on combustion instability with the remarks that a valid conceptual framework has been evolved for understanding the principal types of unstable engine combustion. Crocco[52] has listed the reasons for possible discrepancies between calculated and observed oscillation frequencies. These are: (a) the calculations utilize linearized theories and show incipient instability whereas experimental data refer to fully developed unstable operation; (b) several of the parameters entering into the theoretical analysis are not known; (c) the mechanism producing oscillation may be different from that assumed in the theoretical analysis. For additional remarks concerning the theory of unstable combustion we refer to the survey paper of Ross and Datner[71]; for an exhaustive quantitative evaluation of the analytical work, reference should be made to a paper by Crocco and Cheng[72] or to the references cited previously.

Experimental studies

For a complete account of published experimental work relating to unstable combustion we refer to the review paper of Ross and Datner[71]. For the present purposes it will be sufficient to list some representative experimental results.

Instructive experimental data on the high-frequency type of combustion oscillations has been obtained by Berman and Cheney[43] and by Ellis and associates[73]. Photographs obtained by means of continuous-strip and high-speed motion picture cameras suggest that the vibrations of the gases occurring during the oscillatory combustion correspond to the propagation of finite pressure disturbances in the combustion chamber, which appear to originate in the combustion zone. Similar resonance phenomena of confined flames have been investigated photographically by Dunlap[74] and Shonerd[75].

The possibility that instabilities occurring either in the injection orifices, or in the propellant jets downstream from the injector face, are responsible for combustion instability has been considered. Northrup[76] found that straight, sharp-edged orifices with length to diameter ratios in the ranges normally used for rocket injectors may produce unstable flow. Discontinuities occurring in the flow vs. pressure drop curves are dependent on the density of the gaseous atmosphere into which the liquid streams are discharging. Heidmann and Humphrey[77] and Stehling[8] found that impinging jets of water formed a ruffled sheet of liquid which disintegrated intermittently to form droplet waves propagating from the point of impingement. The frequencies of these formations indicate that the propellant flow rate in the spray may vary with sufficient rapidity to promote high-frequency or "screaming" combustion oscillations. On the other hand, Stehling[8] reports some evidence relating the 90 cps frequency, which is present in the "Christmas tree" or "pagoda" pattern of fluid ligaments, with unstable low-frequency combustion.

The relation of observed oscillation frequencies to fundamental acoustic frequencies in organ pipes has been discussed at length by Ross and Datner[71]. Pressure variations and particle velocities characteristic of the fundamental tangential mode of gas vibrations, "sloshing" back and forth across the combustion chamber, have been described by Morse[78] and by Smith and Sprenger[79]. It has been found in many instances that the burning away of the walls of the combustion chamber, resulting from high-frequency instability, leaves helical grooves, thus indicating an apparent rotation of the gases in the chamber. These results are evidence for the occurrence of the tangential modes of vibrations in the combustion chamber.

The conclusion that the phenomenon of high-frequency oscillatory combustion is the result of reactive waves in the combustion chamber may explain burning of the chamber walls and injector face. Excessive heating may be caused either by the interaction between waves or by interaction between the waves with the walls and injector face, since it is well known that these phenomena produce extremely high temperatures[80, 81].

III-D. MOTOR SCALING AND SIMILARITY ANALYSIS

We have seen in the preceding discussion that the detailed combustion processes in rocket engines are so complex that a complete analytical description of engine performance does not appear to be feasible at the present time. Combustion in liquid-fuel rocket engines is therefore seen to be one of the many engineering problems for which a similarity analysis may prove to be of value, particularly as far as the basic problem of motor scaling is concerned.

Similarity studies on heterogeneous chemical reactions in enclosed chambers were first considered by Damköhler[82] and have been discussed

also by other investigators[83, 84]. Although the importance of similarity analysis in rocket motor design has been stressed repeatedly by Th. von Kármán, no published work on rocket engines has come to our attention.

Damköhler's pioneering studies led to the following five basic similarity constants, which must have the same values in engines of different sizes in order to yield similar combustion patterns:

$$\gamma_v = \frac{\text{rate of generation of each substance by chemical reaction}}{\text{rate of removal of each substance by convection}},$$

$$\gamma_d = \frac{\text{rate of generation of each substance by chemical reaction}}{\text{rate of removal of each substance by diffusion}}$$

$$R_e = \frac{\text{inertial force acting per unit volume}}{\text{viscous force acting per unit volume}},$$

$$q_v = \frac{\text{rate of generation of heat per unit volume by chemical reaction}}{\text{rate of removal of heat per unit volume by convection}}$$

$$q_c = \frac{\text{rate of generation of heat per unit volume by chemical reaction}}{\text{rate of removal of heat per unit volume by conduction}}.$$

Constancy of the number γ_v assures that the same fraction of the chemical reaction is completed in corresponding volume elements of the reactor. Diffusion processes (in a combustion chamber we deal normally with turbulent diffusion transport) determine the departures of the local composition from the mean. Hence a constant value of γ_v assures similar variations in combustion pattern for chambers of different size. For turbulent transfer, constancy of the Reynold's number R_e implies the same numerical values for the turbulent transfer coefficients. Finally, fixed values of q_v and q_c will produce similar heat generation patterns in chambers of different size. Actually Damköhler's similarity criteria are incomplete since the Mach number, Froude number, and other dimensionless groups must also remain invariant in order to maintain strict similarity in flow systems with chemical reactions. However, for a variety of low-velocity flow problems, Damköhler's criteria are sufficient, in good approximation.

For ordinary chemical production processes the five similarity conditions cannot be satisfied simultaneously because, in general, there are only four disposable design variables, viz., vessel size, temperature, pressure, and flow rate. According to Edgeworth-Johnstone[83], Damköhler[82] overestimated the number of degrees of freedom of a continuous reactor by ignoring the Arrhenius relationship between reaction velocity and temperature. However, Bosworth[84] has pointed out that for ordinary chemical processes the effective activation energy for the reaction is a property of the chemical system and does not vary with reactor size. Thus there is, in general, still an insufficient number of variables to satisfy all of the similarity conditions. For a reactor with a catalyst bed, on the other hand, the effective activation energy can be varied by changing catalyst activity. Hence, in this case, the similarity requirements can be met. The implications of this last conclusion have been studied by Bosworth[84].

It appears from the preceding discussion that the five similarity criteria of Damköhler can be satisfied in the scaling of liquid-fuel rocket engines only if the reaction rate as a function of motor size can be varied independently, for example, by suitable modification of injector design. We leave the details of a similarity analysis in the combustion of liquid-fuel rocket engines to a subsequent publication and conclude here with the observation that the logical development and application of motor scaling criteria, based on similarity analysis, constitutes one of the most important directions for future rocket development.

REFERENCES

1. For a discussion of analytical procedures involved in making performance estimates see, for example, Penner, S. S.: Am. J. Phys., *20*, 26 (1952).
2. A convenient summary of propellant characteristics and performance has been prepared by the Bell Aircraft Corporation, *Pocket data for Rocket Engines*, December 1953.

3. Zwicky, F.: J. Am. Rocket Soc., *84*, 3 (1951).
4. Scheller, K., and Bierlein, J. A.: J. Am. Rocket Soc., *22*, 245 (1952).
5. Altman, D., and Lorell, J.: J. Am. Rocket Soc., *22*, 252 (1952).
6. Zwicky, F.: J. Am. Rocket Soc., *84*, 3 (1951).
7. For a critical summary of the work on reactions during nozzle flow, see Penner, S. S.: Technical Report No. 1, Contract DA 04-495-Ord-446, Calif. Inst. of Tech., May 1953 or *Proceedings of the 1953 Iowa Thermodynamics Symposium*. Earlier papers appear, for example, in J. Chem. Phys., *19*, 377 (1951) and *20*, 341 (1952).
8. Stehling, K. R.: J. Am. Rocket Soc., *22*, 132 (1952).
9. Godsave, G. A. E.: National Gas Turbine Establishment Report No. R 87, 1951.
10. Spalding, D. B.: Fuel, *29*, 2, 25 (1950); *Selected Combustion Problems—Fundamentals and Aeronautical Applications*, pp. 340–351. London, Butterworths, Ltd., 1954.
11. Tanasawa, Y., and Kobayashi, K.: Technology Reports of Tohoku University, vol. 14, No. 2, 1950; Kumugai, S., and Isoda, H.: Science of Machine, *3*, 431 (1951) and *4*, 337 (1952).
12. Hall, A. R., and Diederichsen, J.: *Fourth (International) Symposium on Combustion*, pp. 837–46. Baltimore, The Williams and Wilkins Co., 1953.
13. Goldsmith, M., and Perkins, C. K.: Technical Report No. 4, Contract DA 04-495-Ord-446, Calif. Inst. of Tech., Pasadena, May 1954.
14. Topps, J. E. C.: J. Inst. Petrol., *37*, 535 (1951). This work is concerned with falling droplets.
15. Godsave, G. A. E.: National Gas Turbine Establishment Report No. R 66, 1950; Report No. R 88, 1952.
16. Goldsmith, M., and Penner, S. S.: Technical Report No. 2, Contract DA 04-495-Ord-446, Calif. Inst. of Tech., Pasadena, October 1953; Jet Prop., *24*, 245 (1954).
17. Probert, R. P.: Phil. Mag., *37*, 94 (1946).
18. Graves, C. C., and Gerstein, M.: *Some Aspects of the Combustion of Liquid Fuel*, paper presented before the AGARD Combustion Panel, Scheveningen, The Netherlands, May 1954.
19. Graves, C. C.: Preprint of paper from Proceedings of the Third Midwestern Conference on Fluid Mechanics, Univ. of Minn., Minneapolis, 1953.
20. Bowen, I. G., and Joyce, J. R.: Shell Petroleum Co., Ltd., Technical Report No. I.C.T./17.
21. Tait, C. W., Whittaker, A. E., and Williams, H.: J. Am. Rocket Soc., *85*, 83 (1951).
22. Porter, G.: *The Mechanism of Carbon Formation*, paper presented before the AGARD Combustion Panel, Scheveningen, The Netherlands, May 1954.
23. Frazee, J. D., and Anderson, R. C.: Univ. of Texas, Technical Report No. 8, Contract No. AF 18, (600)-430.
24. Parker, W. G., and Wolfhard, H. G.: J. Chem. Soc., p. 2038 (1950).
25. Gaydon, A. G., and Wolfhard, H. G.: *Flames*. London, Chapman and Hall, 1953.
26. Porter, G.: *Fourth (International) Symposium on Combustion*, p. 248. Baltimore, The Williams and Wilkins Co., 1953.
27. Norrish, R. W. G., Porter, G., and Thrush, B. A.: Proc. Roy. Soc. (London), *216A*, 165 (1953).
28. Behrens, H.: *Fourth (International) Symposium on Combustion*, p. 538. Baltimore, The Williams and Wilkins Co., 1953.
29. Thomas, N.: J. Chem. Phys., *20*, 899 (1952).
30. Starkman, E. S., Cattaneo, A. G., and McAllister, S. H.: Ind. & Eng. Chem., *43*, 2822 (1951).
31. Fouré, C.: *Formation and Deposition of Carbon in Aircraft Turbine Machines*, paper presented before the AGARD Combustion Panel, Scheveningen, The Netherlands, May 1954.
32. Schalla, R. L., and McDonald, G. E.: National Advisory Committee for Aeronautics, RM E 52122, December 1952, Washington, D. C.
33. For extensive discussion of carbon reactions see the group of papers published in Ind. & Eng. Chem., *44*, May (1952).
34. Altman, D., and Penner, S. S.: *Combustion of Liquid Propellants*, in Section L, vol. VII of the Princeton Series on *High Speed Aerodynamics* (in press). This paper should be consulted for extensive references to the literature as well as for a discussion of motor performance characteristics of selected monopropellants and bipropellants.
35. Broatch, J. D.: Fuel, *29*, 106 (1950).
36. See, for example, Gunn, S. V.: J. Am. Rocket Soc., *22*, 33 (1952).
37. Mullins, B. P., Fuel, *32*, 451, 467, 481 (1953) and earlier papers.
38. Lloyd, P., and Mullins, B. P.: *Selected Combustion Problems—Fundamentals and Aeronautical Applications*, p. 405. London, Butterworths Ltd., 1954.
39. Mullins, B. P.: *Ibid*, p. 447.
40. J. Am. Rocket Soc., *23*, 123–183 (1953).
41. Neumann, R. K., Dembrow, D., Berl, W. G., and Prescott, R.: J. Am. Rocket Soc., *23*, 244 (1953).

42. Heidmann, M. F., and Priem, R. J.: *Ibid.*, *23*, 248 (1953).
43. Berman, K., and Cheney, S. H., Jr.: *Ibid.*, *23*, 89 (1953).
44. Berman, K., and Logan, S. E.: *Ibid.*, *22*, 78 (1952).
45. Altseimer, J. H.: *Ibid.*, *22*, 86 (1952).
46. Zucrow, M. J.: *Jet Propulsion and Gas Turbines*. New York, John Wiley and Sons, Inc., 1948.
47. Sänger, E.: Recent Results in Rocket Flight Technique. NACA TM No. 1012, Washington 1942 (translated from a German manuscript).
48. Seifert, H. S., Mills, M. M., and Summerfield, M.: Am. J. Phys., *15*, 121 (1947).
49. Sutton, G. P.: *Rocket Propulsion Elements*, pp. 133–140. New York, John Wiley and Sons, Inc., 1949.
50. Summerfield, M.: J. Am. Rocket Soc., *21*, 79 (1951).
51. Penner, S. S.: J. Am. Rocket Soc., *23*, 85 (1953).
52. Crocco, L.: *AGARD Selected Combustion Problems*, pp. 397–400. London, Butterworths, Ltd., 1954.
53. Rayleigh, Lord: *The Theory of Sound*. Dover Publications, New York, 1945.
54. Putnam, A. A., and Dennis, W. R.: *Fourth Symposium (International) on Combustion*, pp. 566–75. Baltimore, The Williams and Wilkins Co., 1953.
55. Coward, F., Hartwell, F. J., and Georgeson, E. H. M.: J. Chem. Soc. (London), *part II*, 1482 (1937).
56. Yachter, M.: M. W. Kellogg Co. Report No. SPD-241, 1949; J. Appl. Mech., *18*, 114 (1951).
57. Gunder, D. F., and Friant, D. R.: J. Appl. Mech., *17*, 327 (1950).
58. Summerfield, M.: J. Am. Rocket Soc., *21*, 108 (1951).
59. Crocco, L.: J. Am. Rocket Soc., *21*, 163 (1951); *22*, 7 (1952).
60. Tsien, H. S.: J. Am. Rocket Soc., *22*, 256 (1952).
61. Marble, F. E., and Cox, D. W., Jr.: J. Am. Rocket Soc., *23*, 63 (1953).
62. Lee, Y. C., Gore, M. R., and Ross, C. C.: J. Am. Rocket Soc., *23*, 75 (1953).
63. Crocco, L., and Cheng, S. I.: *Fourth Symposium (International) on Combustion*, pp. 865–880. Baltimore, The Williams and Wilkins Co., 1953.
64. Cheng, S. I.: J. Am. Rocket Soc., *24*, 27, 102 (1954).
65. Sabersky, R. H.: Jet Propulsion, *24*, 172 (1954).
66. Minorsky, N.: J. Appl. Mech., *9*, 65 (1942).
67. Ansoff, H. I.: J. Appl. Mech., *16*, 185 (1949).
68. Nyquist, H.: Bell System Tech. J., *11*, 126 (1932).
69. Satche, M.: J. Appl. Mech., *16*, 418 (1949).
70. Tsien, H. S.: J. Am. Rocket Soc., *22*, 139 (1952).
71. Ross, C. C., and Datner, P. P.: *AGARD, Selected Combustion Problems*, pp. 352–76. London, Butterworths, Ltd., 1954.
72. Crocco, L., and Cheng, S. I.: AGARDograph on *Combustion Instability in High Propellant Rockets*, in preparation.
73. Ellis, H., Odgers, I., Stosick, A. J., and Van de Verg, N.: *Fourth Symposium (International) on Combustion*, pp. 880–85. Baltimore, The Williams and Wilkins Co., 1953.
74. Dunlap, R. A.: Report No. UMM-43, Aeronautical Research Center, Univ. of Mich., Ann Arbor, March 1950.
75. Shonerd, D. E.: Report No. 3-18, Jet Propulsion Laboratory, C. I. T., Pasadena, June 1952.
76. Northrup, R. P.: Am. Rocket Soc. Reprint No. 49–51, 1951.
77. Heidmann, M. F., and Humphrey, J. C.: J. Am. Rocket Soc., *22*, 127 (1952).
78. Morse, P. M.: *Vibrations and Sound*, 2nd Ed. New York, McGraw-Hill Book Co., Inc., 1948.
79. Smith, R. P., and Sprenger, D. F.: *Fourth Symposium (International) on Combustion*, pp. 893–906. Baltimore, The Williams and Wilkins Co., 1953.
80. Rand, F. F., Jr.: Aeron. Eng. Rev., *11*, 22 (1952).
81. Perry, R. W., and Kantrowitz, A.: J. Appl. Phys., *22*, 878 (1951).
82. Damköhler, G.: Z. Elektrochem., *42*, 846 (1936); *43*, 1, 8 (1937).
83. Edgeworth-Johnstone, R.: Trans. Inst. Chem. Engrs., *17*, 129 (1939).
84. Bosworth, R. C. L.: Trans. Faraday Soc., *43*, 399 (1947).

Discussion by Luigi Crocco*

This lucid and synthetic presentation of an obscure and complicated subject deserves certainly full appreciation. There are only a few points on which I would like to comment:

(1) I fully agree with the authors that the combustion instability, once generated, is a non-linear phenomenon. However, this recognition is far from implying that the cause for instability resides in a non-linear process; and in fact the linear theory furnishes a large number of possibilities for unstable operation. These theories provide important indications on the effects on

* Robert H. Goddard Professor of Jet Propulsion, Princeton University.

instability of the parameters of the system, and these effects are likely to be preserved even in the presence of non-linear effects. It is not possible to exclude the possibility of some non-linear types of instability characterized by the fact that only disturbances above a certain level would not decay and would, therefore, produce unstable operation. But these cases, even if they exist, cannot be for the moment the subject of theoretical analysis. I do not consider this to be a deficiency of the linear theories, which still apply to a large class of cases, but only a limitation, because certain cases may be excluded from the theoretical treatment.

(2) I think that the subdivision of all types of instability into the high frequency and the low frequency types is too restrictive. The low frequency type, where the feeding system plays an important role, should generally be confined to frequencies below 100 c.p.s., while the high frequency type, connected to acoustical modes in the chamber, is generally above 1000 c.p.s. (except for very special geometries or dimensions of the chamber). Any instability observed between the two frequencies must be related to different causes and classified separately as an intermediate frequency type. Theoretical studies are now in progress on this type of instability and on its causes.

IV

UNSOLVED PROBLEMS IN SOLID-PROPELLANT COMBUSTION

By RICHARD D. GECKLER

The invitation to present a review of current problems in the combustion of solid propellants at this symposium affords a welcome opportunity to discuss several topics not covered in the writer's review presented at the Cambridge Colloquim last year[1]. Parr has extended the theory of normal deflagration to include diffusion in the gase phase[2]. Additional theoretical work on unstable combustion has been published by Cheng[3]. The original brief discussion of a thermal theory of ignition given by Frazer and Hicks[4] has been amplified in a recent paper by Hicks[5]. These topics, together with some remarks on erosive burning, constitute the subject matter of the present review. It will become apparent in each case that in the writer's opinion the "unsolved problems" consist essentially in the lack of sufficient experimental data.

Steady-State Deflagration

The currently accepted views of the mechanism of combustion of colloidal propellants are based upon a model of the combustion zone proposed by Rice and Ginell[6]. This model is shown in Figure 1. The combustion reaction is postulated to occur in four successive steps:

(1) In the foam zone a solid-phase reaction occurs with the evolution of heat Q_0. This would raise the temperature of the solid propellant from T_0 to a value T_s' given by

$$T_s' = T_0 + Q_0/c_0 \tag{1}$$

where c_0 is the specific heat capacity of the solid. However, since heat is also conducted back from the gas-phase reactions, the actual surface temperature T_s is higher than T_s'.

(2) In the so-called fizz zone next to the propellant surface a second-order reaction occurs in

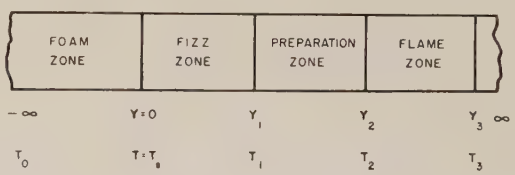

FIG. 1. Structure of combustion region for colloidal propellants.

which a quantity of heat Q_1 is evolved. This would raise the gas temperature to

$$T_1' = T_s' + Q_1/c_1 = T_0 + Q_0/c_0 + Q_1/c_1 \tag{2}$$

However, the actual temperature at the end of the fizz zone is T_1 which is greater than T_1' because heat is conducted back from later regions.

(3) In the preparation zone following the fizz zone no heat is evolved, but active species build up to a critical concentration required to initiate

further reactions. When heat is conducted back from the last zone, the temperature T_2 at the end of the preparation zone will be greater than T_1.

(4) In the flame zone a final reaction of second order occurs in which the quantity of heat Q_3 is evolved. This heat raises the gases to the isobaric flame temperature T_3 given by

$$T_3 = T_1' + Q_3/c_3 = T_0 + Q_0/c_0 + Q_1/c_1 + Q_3/c_3 \quad (3)$$

The central problem of the theory of deflagration is to compute the linear burning rate r as a function of the pressure p of the gases in contact with the burning surface. This Rice and Ginell were able to do using the model just described, and they established that the problem is considerably simpler at low pressures (say less than 50 to 100 atm) because the effect on the fizz reaction of the heat evolved in the flame zone is negligible and can be ignored. The methods these authors employed were highly approximate, but Parr and Crawford[7] succeeded in adapting the more fundamental method of Boys and Corner[8] to the low-pressure case in which the flame zone is neglected. In their treatment diffusion in the fizz zone was not considered.

This was where matters stood when the subject was reviewed for the Combustion Colloqium at Cambridge University, December 7–11, 1953.[1] However, Parr has now succeeded in including the effect of diffusion in the fizz zone.[2] He starts with the two differential equations

$$\frac{d\epsilon_1}{dT} = \frac{\lambda_1}{\rho_1 D_1} \frac{\epsilon_1 - G_1}{(1 - \delta_1 - G_1)Q_1 - c_1(T_1 - T)} \quad (4)$$

$$\frac{dG_1}{dT} = \frac{\lambda_1(1 - \epsilon_1)^2 \rho_1^2 B_1 \exp(-A_1/RT)}{m^2[(1 - \delta_1 - G_1)Q_1 - c_1(T_1 - T)]} \quad (5)$$

which express the results of heat and mass balances for the region under consideration.[a] The boundary conditions are

$$G_1 = \epsilon_1 = 1 - \delta_1 \quad \text{when } T = T_1 \quad (6)$$

$$G_1 = \epsilon_1 = 0 \quad \text{when } T = T_s \quad (7)$$

It will be noted that the very small positive number δ_1 is the device introduced by Parr and Crawford to separate the reaction zones. When the extent of the fizz reaction has reached $1 - \delta_1$ then the next reaction is supposed to start. Since in the present instance we assume that no reactions occur after the fizz reaction, δ_1 disappears from the final result. Nevertheless, it should not be regarded as simply a mathematical artifice used to avoid singular points and then allowed to vanish.

Equations (4) and (5) cannot be solved exactly, but the method of successive approximation developed by Corner[9] can be used. Discussion of the solution is simplified if we employ the following combinations of parameters:

$$\alpha_1 = c_1 m^2 R^2 T_1^2 (1 + N_1)^2 / \lambda_1 B_1 p^2 \bar{M}_s^2 \exp(-A_1/RT_1) \quad (8)$$

$$\mathfrak{L} = \lambda_1/\rho_1 c_1 D_1 \quad (9)$$

The latter is the dimensionless parameter called the Lewis number. In equation (8) N_1 is the molecular weight parameter

$$N_1 = (\bar{M}_s/\bar{M}_1) - 1 \quad (10)$$

where $\bar{M}_s$ and $\bar{M}_1$ are the average molecular weights of the reactants and products of the fizz reaction. N_1 is used in the perfect gas law to eliminate the density from equations (4) and (5), thus

$$\rho = p\bar{M}_s/(1 + N_1\epsilon_1)RT \quad (11)$$

The solution to a second degree of approximation of the differential equations is given by the implicit equation

$$\chi f(T_s) = \int_0^{\eta_s} [1 - \{N_1/(1 + N_1)\}\xi]^2 \, d\eta \quad (12)$$

where

$$\xi = 1 - \epsilon_1 \quad (13)$$

$$\eta = (c_1/Q_1)(T_1 - T) \quad (14)$$

$$f(T_s) = (c_1 T_1/Q_1)(T_1 R/A_1) [1 - \exp(-A_1/RT_s) \exp(A_1/RT_1)] \quad (15)$$

The integral on the right-hand side of equation (12) is given in terms of functions tabulated by

[a] The symbols are defined in the list at the end of the paper. The derivation of these equations needs no discussion since they are treated so voluminously in the literature. An intimate knowledge of these equations and the conditions of their validity is a prerequisite to any discussion of combustion theory.

Corner[9] as follows:

$$\int_0^{\eta_s}\left[1-\left(\frac{N_1}{1+N_1}\right)\xi\right]^2 d\eta = \eta_s - \left[\frac{2N_1}{1+N_1}\right]\int_0^{\eta_s}\xi\, d\eta + \left(\frac{N_1}{1+N_1}\right)^2\int_0^{\eta_s}\xi^2\, d\eta \tag{16}$$

Each term is a function of α_1 and $\mathcal{L}$, Corner employing $\mathcal{L}$ and $(\mathcal{L}/\alpha_1)/(\mathcal{L}+15)$ as the independent variables in double-entry tables. To partially compensate for the approximations employed in solving the differential equations, Parr uses $0.8\mathcal{L}$ to replace $\mathcal{L}$ throughout his computations. The relation between our terminology and Corner's is as follows:

η_s is Corner's $\gamma E_0/\beta$

$\int_0^{\eta_s}\xi\, d\eta$ is Corner's $\left(\frac{\gamma}{\beta}\right)^2\int_0^{E_0} N\, dE$

$\int_0^{\eta_s}\xi^2\, d\eta$ is Corner's $\left(\frac{\gamma}{\beta}\right)^3\int_0^{E_0} N^2\, dE$

The quantity χ in equation (12) is another adjustable parameter introduced to partially compensate for the approximations employed in solving the differential equations. Its value is obtained as in the case of zero diffusion,[7] by requiring equation (12) to hold in the low-pressure limit $p = 0$, where $T_s = T_s'$:

$$\chi = \frac{\left(\int_0^{\eta_s}[\{1-(N_1/(1+N_1)\}\xi]^2\, d\eta\right)_{p=0}}{f(T_s')} \tag{17}$$

The manner in which equation (12) represents a solution of the fizz reaction problem is easily seen by noting that for a given set of values for $\mathcal{L}$, T_s, and T_1 only one value of α_1 will permit the equation to be satisfied. This value of α_1 immediately relates a value of the mass burning rate m to a value of the pressure p by equation (8). T_s is of course established by an analogous equation for the foam zone. T_1 would be determined by reactions occurring in regions following the fizz zone. In the present case these reactions are neglected, and T_1 established by thermodynamic methods is substituted.

For practical computations Parr tabulates as a function of T_s'/T_s a quantity Z defined by

$$Z = \log\left[\frac{0.8\mathcal{L}\chi\alpha_1}{0.8\mathcal{L}+15}\right] \tag{18}$$

Z plays the same role in the theory with diffusion that Y does in the theory without diffusion.[1, 7] An abridgment of Parr's results computed for $\mathcal{L} = 1.25$ and $N_1 = 1.0$ from equations (8) to (18) is shown in Table 1.

From equation (8) it is apparent that one can write

$$Z = 2\log m - 2\log p + \log\left[\frac{\chi c_1 R^2 T_1^2(1+N_1^2)}{\lambda_1 B_1 M_s^2 \exp(-A_1/RT_1)}\right] + \log\frac{0.8\mathcal{L}}{0.8\mathcal{L}+15} \tag{19}$$

For the corresponding quantity X defined for the foam zone, one has a similar relationship[1, 7]

$$X = -2\log m + \log p + \log\left(\lambda_0 B_0 \bar{M}_s/c_0 R T_s'\right) \tag{20}$$

An abridgment of Parr and Crawford's results giving X as a function of T_s'/T_s is shown in Table 2. Using X and Z, m and p may be found as functions of T_s'/T_s and hence of each other by the formulas:

$$\log m' = \log k_m m = -(X + Z/2) \tag{21}$$

$$\log p' = \log k_p p = -(X + Z) \tag{22}$$

where

$$k_m = \left[\frac{c_0\lambda_1^{1/2}B_1^{1/2}T_s'}{c_1^{1/2}\lambda_0 B_0 T_1(1+N_1)}\right]\left[\frac{0.8\mathcal{L}+15}{0.8\mathcal{L}}\right]^{1/2}\cdot\frac{\exp(-A_1/2RT_1)}{\chi^{1/2}} \tag{23}$$

$$k_p = \left[\frac{c_0\lambda_1 B_1 T_s'\bar{M}_s}{c_1\lambda_0 B_0 T_1^2 R(1+N_1)^2}\right]\left[\frac{0.8\mathcal{L}+15}{0.8\mathcal{L}}\right]\cdot\frac{\exp(-A_1/RT_1)}{\chi} \tag{24}$$

The values of the parameters found by Parr to fit the experimental burning rate data best for HES 4016 propellant[7] are compared in Table 3 for $\mathcal{L} = 1.25$ and for $\mathcal{L} = \infty$ (diffusion neglected). Consideration of diffusion lowers the value of T_1' from 1100°K to 900°K and the value of A_1 from 30 kcal·mol^{-1} to 20 kcal·mol^{-1}. However, the burning rate data are fitted equally well by either theory.

Since the available equations describing the mechanism of burning of solid propellants contain a great many adjustable parameters, it is not sur-

prising that any given burning rate vs pressure curve can be fitted very closely. The merit of the theories therefore cannot be rightly judged by the degree of correspondence between experimental and theoretical burning rates. In the writer's opinion this fact calls for an exhaustive study of propellants with deliberately varied parameters. Comparison of experimental and theoretical burning-rate curves for propellants having different sets of values of the temperatures T_s^1, T_1', T_2', and T_3 and different sets of values of the activation energies A_0, A_1, and A_3 for example, ought to readily discover the truth or falsity of the theories. While such a program would not be easy to carry through, it offers an interesting challenge to the ingenious investigator. Without this type of study there would appear to be little point in continuing recondite theoretical investigations.

The foregoing conclusion does not apply to the case of composite propellants. In a heterogeneous mixture of a powdered, crystalline oxidizer dispersed in an organic fuel matrix it is not likely that the assumptions permissible for colloidal propellants could be used. The linear dimensions of a single oxidizer crystal, for example, can be larger than the thickness of the entire combustion region predicted for a colloidal propellant. Under such conditions a crude one-dimensional model would appear to be an over-simplification. Since the problems peculiar to composite propellants have been scarcely touched on in the literature, there is clearly a need for the theoretical study of

TABLE 1. Z AS A FUNCTION OF T_s'/T_s

Q_0/c_0	$T_1' - T_0$	A_1/R	T_s'/T_s					
			$T_0 = 298$			$T_0 = 323$		
			0.98	0.90	0.80	0.98	0.90	0.80
102	702	0	2.215	1.999	0.506	2.202	1.977	0.475
		8000	6.356	5.242	4.318	5.961	(4.876)	3.955
		14000	9.950	8.450	6.917	9.241	7.796	6.350
	1002	0	2.293	1.313	0.678	2.282	1.298	0.655
		8000	7.158	6.044	5.120	6.728	5.643	4.764
		14000	11.354	9.853	8.320	10.584	9.139	6.693
	1302	0	2.340	1.373	0.764	2.327	1.361	0.748
		8000	7.659	6.545	5.621	7.212	6.127	5.248
		14000	12.230	10.730	9.197	11.431	9.986	8.540
402	702	0	1.834	0.506	−0.838	1.819	0.456	−0.917
		8000	2.875	1.790	0.649	2.800	1.694	0.507
		14000	3.746	2.587	1.373	3.612	2.459	1.210
	1002	0	2.078	0.970	0.133	2.067	0.952	0.102
		8000	3.711	2.766	—	3.606	2.662	—
		14000	5.153	(4.175)	(4.125)	4.960	(4.025)	(3.900)
	1302	0	2.180	1.145	0.422	2.172	1.132	0.401
		8000	4.216	3.350	—	4.095	3.170	—
		14000	6.030	4.916	3.991	5.808	4.710	3.810
702	1002	0	1.668	0.133	—	1.658	0.101	—
		8000	2.226	0.913	−1.257	2.192	0.856	−1.446
		14000	2.695	1.415	−0.691	2.617	1.343	−0.913
	1302	0	1.965	0.764	−0.266	1.956	0.749	−0.312
		8000	2.850	1.858	1.007	2.810	1.802	0.941
		14000	3.601	2.582	1.708	3.520	2.502	1.622

the mechanism of combustion of solid propellants. But here again, such work will only be of value if ample experimental data become available for comparison with the theories.

Before leaving the topic of steady-state deflagration, the problems associated with erosive burning should be mentioned. That the linear burning rate of a solid propellant is increased by an increase in the velocity of the combustion gases parallel to the burning surface was first discovered by Muraour[10]. This was explained semi-quantitatively by Corner[11] as a result of an increase in the effective thermal conductivity of the gas phase arising from turbulence. Because no additional information has appeared since the writer's previous review[1], there is no need for further discussion. However, since the matter is of considerable importance to rocket designers, there is perhaps some point in emphasizing the great need for more accurate experimental data. So difficult are the necessary measurements that only a rough approximation to the nature of the dependence of burning rate on gas velocity has been gained for any propellant. There is truly an excellent opportunity for the experimenter to display originality by devising a method of accurately studying erosive burning.

Table 2. X as a Function of T_s'/T_s

δ_0	A_0/R	Q_0/c_0	T_s'/T_s					
			$T_0 = 298$			$T_0 = 323$		
			1.00	0.90	0.80	1.00	0.90	0.80
e^{-16}	14,000	102	15.783	15.411	14.205	14.827	14.573	13.464
		402	9.413	9.317	8.758	9.079	9.026	8.500
		702	6.742	6.803	6.511	6.569	6.653	6.373
	20,000	102	22.475	21.446	19.560	21.138	20.266	18.511
		402	13.301	12.884	11.901	12.844	12.440	11.541
		702	9.514	9.335	8.766	9.280	9.130	8.583
e^{-24}	14,000	102	15.783	15.574	14.378	14.827	14.740	13.634
		402	9.413	9.462	8.924	9.079	9.171	8.666
		702	6.742	6.934	6.672	6.569	6.783	6.540
	20,000	102	22.475	21.613	19.752	21.138	20.432	18.698
		402	13.301	12.994	12.067	12.844	12.591	11.707
		702	9.514	9.476	8.929	9.280	9.271	8.747

Table 3. Best Values of Parameters for HES 4016 Propellant* at 25°C

$\mathfrak{L}$	∞	1.25
T_s', °K	700	700
T_1', °K	1100	900
A_0 kcal·mol^{-1}	20	20
A_1 kcal·mol^{-1}	30	20
δ_0	e^{-24}	e^{-24}

* HES 4016 propellant consists of 54.0 wt per cent nitrocellulose (13.25 wt per cent N) 43.0 wt per cent nitroglycerin, and 3.0 wt per cent centralite.

Periodic Deflagration

Certain propellants occasionally exhibit an abnormal increase in burning rate, when fired in rocket motors, that causes an irregular and unpredictable increase in chamber pressure. This phenomena is known as resonant burning or unstable combustion. By using instrumentation capable of responding to chamber pressure oscillations with a frequency up to 25,000 cycles per second, Smith and Sprenger[12] were able to show that the disturbances in the mean chamber pressure were always accompanied by high-frequency, high-amplitude pressure oscillations.

If we consider the equations of motion for the gas in the combustion chamber and assume that the flow is isentropic and that all velocity components and derivatives are small compared to the velocity of sound a, then we can derive the

wave equation which in cylindrical co-ordinates r, φ, and x is:

$$\frac{\partial^2\rho}{\partial t^2} = a^2\left[\frac{\partial^2\rho}{\partial r^2} + \frac{1}{r}\frac{\partial\rho}{\partial r} + \frac{1}{r^2}\frac{\partial^2\rho}{\partial\varphi^2} + \frac{\partial^2\rho}{\partial x^2}\right] \quad (25)$$

In solving this partial differential equation for the density ρ, one assumes that the general solution can be expressed as an infinite series of products of four independent, complex-valued functions:

$$\rho(r, \varphi, x, t) = \Sigma[R(r)\cdot\Phi(\varphi)\cdot X(x)\cdot T(t)] \quad (26)$$

and finds

$$R(r) = c_1 J_\beta(\eta r) + c_2 Y_\beta(\eta r) \quad (27)$$

$$\Phi(\varphi) = c_3 e^{i\beta\varphi} + c_4 e^{-i\beta\varphi} \quad (28)$$

$$X(x) = c_5 e^{i\xi x} + c_6 e^{-i\xi x} \quad (29)$$

$$T(t) = c_7 e^{i\alpha a t} + c_8 e^{-i\alpha a t} \quad (30)$$

where

$$\alpha^2 = \xi^2 + \eta^2 \quad (31)$$

J_β and Y_β are Bessel functions of the first and second kinds, respectively, and the $c_1, \cdots, c_8$ are arbitrary, complex-valued constants. The summation in equation (26) is carried out over the parameters α, β, ξ, η, which are subject only to the restriction given by equation (31). Further restrictions on these parameters and on the arbitrary constants are determined by the application of initial and boundary conditions.

If we are dealing with a hollow cylinder closed at the end $x = 0$ then c_2 must be zero in order that ρ be bounded at $r = 0$, since $Y_\beta(0) = \infty$. Moreover, β must be an integer in order that $\rho(\varphi) = \rho(\varphi + 2\pi)$, and $\partial\rho/\partial x = 0$ at $x = 0$ requires $c_5 = c_6$. Both c_1 and c_5 can be assigned the value unity without loss of generality, and a typical term of equation (26) written for a density variation $\delta\rho$ then appears in the form

$$\delta\rho = c_i c_j J_\beta(\eta r)\cos(\xi x)e^{i\beta\varphi}e^{i\alpha a t} \quad (32)$$

where $i = 3, 4$; $j = 7, 8$. This much of the solution to the wave equation is common to all the available treatments of unstable combustion in a cylindrically perforated propellant grain burning only on the inner surface. They differ, however, in the boundary conditions employed at the cylindrical propellant burning surface $r = R$ and at the open end $x = L$.

If we take the simplest assumption that might be made; namely, that both the cylindrical surface and the open end behave as rigid boundaries, then $\partial\rho/\partial r = 0$ at $r = R$ and $\partial\rho/\partial x = 0$ at $x = L$. The first condition requires that η be a root of the equation

$$J'_\beta(\eta R) = 0 \quad (33)$$

and the second restricts values of ξ to the set

$$\xi = q\pi/L \quad (34)$$

where q is an integer. If $\eta_{\beta\sigma}$ is written for the σth root of $J'_\beta(\pi\eta_{\beta\sigma}R) = 0$ and the real and imaginary parts of equation (32) separated [remembering that $e^{x+iy} = e^x(\cos y + i\sin y)$], then the following alternative form of equation (32) is obtained

$$\delta\rho = J_\beta(\pi\eta_{\beta\sigma}r/R)\cos(\pi q x/L)\cdot[A_1\cos(\beta\varphi + \omega t - \delta_1) + A_2\cos(\beta\varphi - \omega t - \delta_2)] \quad (35)$$

Here, β, σ, and q are integers, $\omega = \alpha a$ is the circular frequency, A_1 and A_2 are real, arbitrary amplitude constants, and δ_1 and δ_2 are real, arbitrary phase constants. Since in cycles per second the frequency of oscillation $\nu = 2\pi\omega$, one obtains from equation (31)

$$\nu = \frac{a}{2}\sqrt{\left(\frac{\eta_{\beta\sigma}}{R}\right)^2 + \left(\frac{q}{L}\right)^2} \quad (36)$$

The frequencies observed by Smith and Sprenger appeared to be adequately represented by equations (35) and (36) with $\beta = 1, 2, \cdots 5$, $\sigma = q = 0$; and $A_2 = 0$; i.e., the gas oscillated in the pure, traveling, tangential mode. The tentative identification of a mode of oscillation that exists during unstable burning marked a definite step forward in our understanding of the phenomenon. Nevertheless, the important question remained as to how the oscillations are excited.

The explanation investigated by all writers to date is that the oscillation is self-excited, the driving force arising out of the oscillation itself. If a small periodic disturbance is superimposed upon steady-state flow, then self-excitation will lead to amplification and reamplification of the oscillation until the driving force is counterbalanced by other factors. To explain behavior of this type one looks for a means of obtaining values of α having a negative imaginary part.

The mechanism of self-excitation is ordinarily sought in the effect of a time lag in the combustion process. Thus, Grad[13] postulated that combustion of the solid propellant requires a constant, small time τ for completion. The rate m at

which propellant is completely burned at any given instant t depends upon the equilibrium rate at which burning was initiated at the previous instant $t - \tau$. Therefore, we can write

$$m(t - \tau) = m(t) + \tau \frac{d}{dt} m(t) \tag{37}$$

Now the burning rate $m(t - \tau)$ must be considered as a function of the pressure p and temperature T of the combustion gas near the surface: $-\rho v = m = f(p, T)$. Hence, if a density variation of the form $\rho = \bar{\rho} + \epsilon e^{i\alpha a t}$ is superimposed upon the steady-state flow so that the pressure variation is $p = \bar{p} + a^2 \epsilon e^{i\alpha a t}$ and the temperature variation is $T = \bar{T} + (a^2/c_p \bar{\rho}) \epsilon e^{i\alpha a t}$, then

$$f(p, T) = f(\bar{p}, \bar{T}) + ba\epsilon e^{i\alpha a t} \tag{38}$$

where

$$b = \left(\frac{\partial f}{\partial p} + \frac{1}{c_p \bar{\rho}} \frac{\partial f}{\partial T} \right) a \tag{39}$$

The dimensionless parameter b is a measure of the stability of the propellant. Grad derives a boundary condition in terms of b and τ to replace the equation $\partial \rho / \partial r = 0$ which holds for the case of rigid walls. Thus

$$a \frac{\partial \rho}{\partial r} = \left(\frac{b}{1 + i\alpha a \tau} + \frac{v}{a} \right) \frac{\partial \rho}{\partial t} \tag{40}$$

He also substitutes for the rigid-wall condition $\partial / \partial x = 0$ at $x = L$ the equation

$$a \frac{\partial \rho}{\partial x} + k \frac{\partial \rho}{\partial t} = 0 \tag{41}$$

where k is a complex-valued function of frequency. Equation (40) leads to the condition

$$\eta J'_\beta(\eta R) = i\alpha \left(b + \frac{v}{a} \right) J_\beta(\eta R) \tag{42}$$

and equation (41) leads to

$$\xi \tan (\xi L) = i\alpha k \tag{43}$$

By expert analysis of equations (31), (42), and (43) Grad is able to show that the mode of oscillation which builds up most rapidly is characterized approximately by

$$\eta = \beta / R \tag{44}$$

$$\xi = \pi / 2L \tag{45}$$

where

$$\beta = \frac{R}{a\tau} \left\{ \left[\left(\frac{b}{\mathfrak{M}} \right)^2 + 3 \left(\frac{b}{\mathfrak{M}} \right) \right]^{1/2} - \left(\frac{b}{\mathfrak{M}} \right) - 1 \right\}^{1/2} \tag{46}$$

and the Mach number $\mathfrak{M} = -v/a$ of the flow at the surface of the grain is approximately

$$\mathfrak{M} = R/4L \tag{47}$$

at the closed end of the grain increasing to double this value at the open exit.

This mode of oscillation is by no means identical with the traveling, tangential mode apparently identified by Smith and Sprenger although it is somewhat similar. In Grad's words: "The wave of maximum blow up . . . is one which, so to speak, spirals around the tube . . . while slowly moving downstream and back and forth across the tube . . . a wave of this kind will 'stick' to the burning surface (moving radially around it), and will thereby allow the burning condition to exert a maximum effect." Fitting the experimental frequencies with equations (31), and (44) to (47) is of course not difficult in view of the two adjustable parameters b and τ, neither of which can presently be computed. For example, Smith and Sprenger report an observed frequency of 11,900 cycles per second for their Propellant A fired in Rocket No. 1 when $R = 2.5$ cm and $L = 76$ cm. For this propellant $a = 1.02 \times 10^5$ cm·sec^{-1}. Using these data it is a straightforward computation to deduce the following examples of pairs of values of τ and b that would give the same frequency.

τ, 10^{-6} sec.	b
4.21	0.0123
5.40	.0164
7.64	.0410
8.50	.0820
8.96	.164
9.26	.410

Only one pair of values will reproduce the observed decrease in frequency as the perforation diameter increases. In the present case $\tau = 4.21 \times 10^{-6}$ sec., $b = 0.0123$ appear to be adequate, and, in fact, somewhat superior to the inverse proportionality given by equation (36) that was used by Smith and Sprenger. Such a small value of b is not inconsistent with Green's statement[14]

that the propellant exhibited "plateau" burning behavior, i.e., in the burning rate equation $m = cp^n$ that $n = 0$, for in this case the first term of equation (39) is $\partial f/\partial p = n(m/p)$. Unfortunately, there is no way of estimating the term $\partial f/\partial T$.

More recently Cheng[3] has published a theory of unstable combustion that is based upon a variable time lag. Following the hypothesis of Crocco[15] advanced for unstable combustion in liquid-propellant rockets, Cheng supposes that τ is inversely proportional to the μth power of the pressure: i.e.

$$\tau p^{\mu} = \text{const.} \tag{48}$$

If the pressure is oscillating, it changes during the time lag, and it is the integrated effect that is important. The definition that τ must satisfy is thus really

$$\int_{t-\tau}^{t} [p(s)]^{\mu}\, ds = \text{const.} \tag{49}$$

Now a mass balance shows that the amount of propellant burned completely in time dt must equal the amount on which burning had started during the time $d(t - \tau)$. Therefore, $m(t)dt = m(t - \tau)d(t - \tau)$, and we can write

$$m(t) = \frac{d(t-\tau)}{dt}\, m(t-\tau) \tag{50}$$

Differentiation of equation (49) gives $[p(t)]^{\mu} - [p(t-\tau)]^{\mu} \cdot d(t-\tau)/dt = 0$. Moreover, the pressure dependence of burning rate is usually written

$$m = cp^n \tag{51}$$

where n and c are independent of pressure. With these results, equation (50) gives for the instantaneous burning rate at time t

$$m(t) = c[p(t-\tau)]^n \cdot \left[\frac{p(t)}{p(t-\tau)}\right]^{\mu} \tag{52}$$

Cheng's boundary condition at the burning surface is found by equating this expression for $m(t)$ to the mass rate of flow of combustion gases away from the propellant surface $-\rho v$. In so doing, we utilize again a density variation of the form $\rho = \bar{\rho} + \epsilon e^{i\alpha a t}$ and a pressure variation of the form $p = \bar{p} + a^2 \epsilon e^{i\alpha a t}$ together with a velocity variation of the form $v = \bar{v} + \zeta e^{i\alpha a t}$. Neglecting products of the second order, using a mean value $\bar{\tau}$ for the time lag, and remembering that $a^2\bar{\rho}/\bar{p} = \gamma$, we obtain for the boundary condition at $r = R$ Cheng's result

$$\zeta\bar{\rho}/\epsilon = -[1 - \gamma\mu + \gamma(\mu - n)e^{-i\alpha a\bar{\tau}}]v = -B\bar{v} \tag{53}$$

With some further computation this equation can be put in the form

$$a\frac{\partial \rho}{\partial r} = \left(\frac{b}{1 + i\alpha a\tau} + \frac{\bar{v}}{a} + \frac{\mu}{n}\, bi\alpha a\bar{\tau}\right)\frac{\partial \rho}{\partial t} \tag{54}$$

which is similar to equation (40) used by Grad. However, the term $\partial f/\partial T$ in equation (39) is neglected.

For the boundary condition at $x = L$, Cheng uses the equation

$$a\frac{\partial \rho}{\partial x} + A\left(\frac{u_e}{a}\right)\frac{\partial \rho}{\partial t} = 0 \tag{55}$$

where u_e is the gas velocity in the x-direction at the exit of the perforation. This equation is similar to equation (41) used by Grad. The complex-valued function A is the admittance of the nozzle and is given by Cheng in graphical form as a function of frequency.

Application of these boundary conditions leads to

$$\xi \tan(\xi L) = i\alpha A(u_e/a) \tag{56}$$

and

$$\eta J_{\beta}'(\eta R) = i\alpha B\bar{v} J_{\beta}(\eta R) \tag{57}$$

Cheng's analysis of equations (31), (55) and (56) shows that for an unstable oscillation to be possible, the value of a parameter $S = \mu - (n/2)$ called the index of interaction must be greater than a certain minimum value $S_{\min}$. In the case of a simple tubular grain burning on the inner surface only, the minimum index of interaction is

$$S_{\min} = \frac{1}{2\gamma}\,[1 + 5.15A_r A_i (L/R)^2 \mathfrak{M}] \tag{58}$$

where A_r and A_i are the real and imaginary parts of the nozzle admittance A. For small ratios of L/R the minimum index of interaction is about 0.5. However, for $L/R > 15$ the minimum index of interaction increases quite rapidly. In the latter case Cheng states that his analysis is no longer valid.

Since L/R decreases during burning, it is to be expected that unstable oscillations would be less likely to occur at the beginning of burning than later. Although Cheng cites this point in support of his theory, Green (14) mentions that some rocket motors show instability only at the start

of burning. Nevertheless, the type of grain configuration to which Green refers is not stated, and it is clear that Cheng's conclusion applies only to the case of a cylindrically perforated grain burning only on the inner surface.

If $S_{\min}$ is exceeded, then Cheng's theory shows that unstable oscillations will occur if the mean time lag $\bar{\tau}$ falls within specific ranges of values that differ by $(2\ h\pi/\omega)$ seconds where ω is the angular frequency for the mode of oscillation and h is an integer. The most unstable mode is that composed of the three fundamental components in the circumferential, radial and axial directions. The frequency β of the circumferential component is identical with the frequency of the acoustical circumferential mode given by equation (35). The frequency η of the radial component differs but slightly from the frequency of the acoustical radial mode. However, the frequency ξ of the axial component is significantly different from $q\pi/L$ for the acoustical axial mode.

It is apparent that the frequencies observed by Smith and Sprenger for tubular grains are compatible with the frequency of Cheng's fundamental spiral mode. We cannot draw any conclusions about $S_{\min}$ from their data, however, because the ratio L/R in the rockets they employed was beyond the range in which Cheng's analysis is valid.

Cheng extends his analysis to other propellant grain configurations and is able to predict the observed stabilizing effect of resonance rods, i.e., a noncombustible rod within the cylindrical perforation. He also predicts that rod-in-tube grain configurations should be more stable than the simple perforated grain and that a rod grain alone burning on the exterior surface should be still more stable. The predicted stability of the rod-in-tube type of propellant grain is contested by Green[14] who states that in static tests it has been found less stable than simple tubular grains.

In attempting to reach any conclusions regarding the application of theory to unstable combustion, we are hindered by the lack of experimental data. As in the case of ordinary solid-propellant deflagration, it appears that an extensive program of measurements planned to deliberately explore wide ranges of values of the significant parameters appearing in the different theories would yield substantial returns. Even so, it is unlikely that one could reach satisfying results from rocket motor firings alone. Methods of measuring the time lag $\bar{\tau}$ and the parameter b independently of rocket motor firings would be especially gratifying.

Notwithstanding the apparent success of the time lag concept in accounting for self-excited oscillations, it must be recognized as an artificial concept used to simplify the complexities that would attend a more fundamental analysis. No general studies of transient processes in solid-propellant combustion have yet appeared. It must be expected that when they do, many of the current ideas will be modified. The familiar steady-state burning law $m = cp^n$, for example, ought not to hold when p is varying rapidly, but how it should be modified is not known. For reasons such as this it seems wise to regard our present views of unstable combustion as possibly somewhat primitive.

Before leaving the subject of periodic deflagration, it is interesting to note that Huffington[16] has accumulated evidence which tends to show that even normal deflagration proceeds in a periodic fashion. His experiments on the burning of double-base propellants indicated that the combustion proceeds in jumps, consuming a layer of propellant about 3 microns thick at each jump. How these data are to be interpreted is not yet clear, and additional work is desirable.

Transient Combustion

As we have already noted, the problems of the general transient state of solid-propellant combustion do not appear to have been discussed in the literature. However, the particular process of ignition has received some attention. The results are well worth studying in view of the great practical importance of the ignition process.

Frazer and Hicks[4] first published in 1950 the preliminary results of some computations for a thermal model of ignition. They considered a semi-infinite slab of propellant in which an exothermic zero-order reaction occurs. The heat conduction equation for their model is

$$\frac{\partial T}{\partial t} = \frac{\lambda_0}{c_0\rho_0}\frac{\partial^2 T}{\partial y^2} + Q_0 B_0 \exp\left(-A_0/RT\right) \quad (y > 0,\ t > 0) \tag{59}$$

The initial temperature is uniform

$$T = T_0 \qquad (y \geqslant 0,\ t = 0) \tag{60}$$

and the propellant is ignited by being heated at the plane $y = 0$ through contact with a hot gas at a temperature $T_g^{(1)}$ for a time t_0. Heat transfer is governed by a constant convection coefficient

h so that the boundary condition at $y = 0$ is

$$-\lambda_0 \frac{\partial T}{\partial y} = h(T_g^{(1)} - T) \qquad (x = 0, 0 < t < t_0) \tag{61}$$

After t_0 the gas temperature is lowered to $T_g^{(2)}$ and the boundary condition is

$$-\lambda_0 \frac{\partial T}{\partial y} = h(T_g^{(2)} - T) \qquad (x = 0, t_0 < t) \tag{62}$$

The time t_0 thus corresponds to the duration of the igniter blast. In the region far removed from

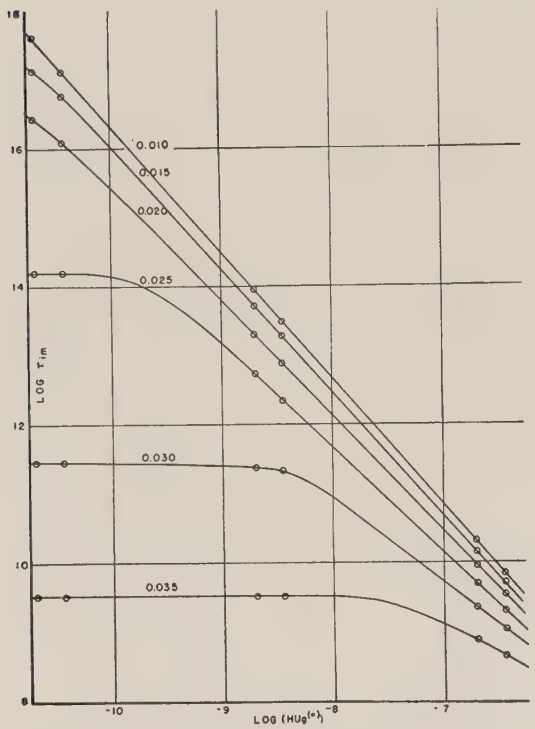

FIG. 2. Minimum ignition time of solid propellants as a function of igniter intensity.

the heated surface there is no heat flow and another boundary condition is

$$-\lambda_0 \frac{\partial T}{\partial y} = 0 \qquad (x \to \infty, t \geqslant 0) \tag{63}$$

In solving the heat conduction problem, Frazer and Hicks employed the following dimensionless variables:

$$\text{temperature} \qquad \mathfrak{U} = \frac{T}{(A_0/R)} \tag{64}$$

$$\text{time} \qquad \mathfrak{I} = t\left(\frac{Q_0 B_0}{c_0 \rho_0 A_0/R}\right) \tag{65}$$

$$\text{distance} \qquad \mathfrak{Y} = y\left(\frac{Q_0 B_0}{\lambda_0 A_0/R}\right)^{1/2} \tag{66}$$

$$\text{convection coefficient } \mathfrak{C} = h\left(\frac{A_0/R}{\lambda_0 Q_0 B_0}\right)^{1/2} \tag{67}$$

and integrated equation (59) numerically. Their results were extended in a more recent paper by Hicks[5] who summarized the data in the graphical form shown in Figure 2.

The minimum ignition time $\mathfrak{I}_{im}$ is defined as the shortest time required for the surface temperature $\mathfrak{U}$ to reach the value 0.045. $\mathfrak{I}_{im}$ is also the longest time $\mathfrak{I}_0$ that the igniter blast at a temperature $\mathfrak{U}_g^{(0)}$ is applied. Should $\mathfrak{I}_0$ be any shorter than $\mathfrak{I}_{im}$ then ignition will not occur for a substantially long time after shut-off of the igniter blast. Figure 2 shows $\log \mathfrak{I}_{im}$ as a function of $\log \mathfrak{C}\mathfrak{U}_g^{(0)}$. The individual lines are for constant values of the initial propellant temperature $\mathfrak{U}^{(0)}$.

As an example of the use of Figure 2 the following problem can be considered. Assume

$$Q_0 = 140 \text{ cal}\cdot\text{gm}^{-1}$$
$$c_0 = 0.4 \text{ cal}\cdot\text{gm}^{-1}\cdot{}^\circ K^{-1}$$
$$\lambda_0 = 0.0005 \text{ cal}\cdot\text{cm}^{-1}\cdot\text{sec}^{-1}\cdot{}^\circ K^{-1}$$
$$\rho_0 = 1.6 \text{ gm}\cdot\text{cm}^{-3}$$
$$A_0 = 20{,}000 \text{ cal}\cdot\text{gm-mol}^{-1}$$
$$B_0 = 10^{14} \text{ sec}^{-1}$$
$$h = 0.01 \text{ cal}\cdot\text{cm}^{-2}\cdot\text{sec}^{-1}\cdot{}^\circ K^{-1}$$
$$T_0 = 300^\circ\text{K}$$
$$T_g^{(0)} = 1500^\circ\text{K}$$

Then

$$\mathfrak{U}^{(0)} = 0.030$$
$$\mathfrak{U}_g^{(0)} = 0.15$$
$$\mathfrak{C} = 3.8 \times 10^{-7}$$
$$\mathfrak{C}\mathfrak{U}_g^{(0)} = 0.57 \times 10^{-7}$$

From Figure 2 we read that $\log \mathfrak{I}_{im} = 10$, and equation (65) then gives $t = 0.004$ sec. This is not a necessarily unreasonable result. However, at the present time information about the parameters required in the use of the theory is uncertain. In the writer's opinion there is a great need for an experimental program undertaken to provide the necessary data for correlating ignition

data on a quantitative basis. Once such data have been obtained, the theory of Frazer and Hicks ought to be of substantial value to the practical designer.

Conclusions

Each of the theoretical studies touched on in this review represents a considerable achievement in the application of mathematics to the solution of difficult physical problems. The skill that the theoretical investigators have exhibited, however, contrasts forcefully with the relative meagerness of our experimental data and the crudeness of our experimental methods. Until the experimental data have been markedly increased there is little that can be done with the best of the theories.

Symbols

Latin

a	velocity of sound, cm·sec^{-1}
A	nozzle admittance, cm·sec^{-1}·atm^{-1}
A_i	activation energy in Arrhenius law for ith zone, cal·gm-mol^{-1}; also amplitude constants
b	dimensionless parameter, equation (39)
B	function in boundary condition at burning surface, equation (53)
B_i	frequency factor in Arrhenius law for ith zone, (gm·cm^{-3})$^{1-n}$·sec^{-1}
c_i	specific heat capacity of propellant in i-th zone, cal·gm^{-1}·°K^{-1}.
D_1	diffusion coefficient in fizz zone, cm^2·sec^{-1}
G_1	fraction of mass rate of flow in fizz zone made up of reactant
h	heat transfer coefficient, cal·cm^{-2}·sec^{-1}·°K^{-1}; also an integer
$\mathfrak{H}$	dimensionless heat transfer coefficient, equation (67)
i	$\sqrt{-1}$
k	admittance parameter, equation (41)
L	length of propellant grain, cm
$\mathfrak{L}$	Lewis number, $\lambda/\rho cD$
m	mass rate of burning, gm·cm^{-2}·sec^{-1}
M_s, M_1	average molecular weights at beginning and end of fizz zone, gm-mol^{-1}
$\mathfrak{M}$	Mach number at burning surface, $-v/a$
n	burning rate exponent in $m = cp^n$; also order of chemical reaction
N_1	reduced change in molecular weight in fizz zone, equation (10)
p	pressure, atm
$\bar{p}$	mean pressure, atm
q	integer
Q_i	heat of reaction in ith zone, cal·gm^{-1}
r	linear burning rate, cm·sec^{-1}; also radial coordinate
R	universal gas constant, 82.054 cm^3·atm·°K^{-1}·gm-mol^{-1}, or 1.9869 cal·°K^{-1}·gm-mol^{-1}; also radius of cylindrical perforation
S	$\mu - n/2$
t	time, sec
T	temperature, °K
T_0	initial propellant temperature, °K
$\bar{T}$	mean temperature, °K
T_s	propellant surface temperature, °K
$\mathfrak{T}$	dimensionless time, equation (65)
$\mathfrak{T}_{im}$	dimensionless ignition time
u	velocity in x-direction, cm·sec^{-1}
v	velocity in r-direction at propellant surface, cm·sec^{-1}
$\bar{v}$	mean velocity in r-direction, cm·sec^{-1}
$\mathfrak{U}$	dimensionless temperature, equation (64)
$\mathfrak{U}_0$	dimensionless initial propellant temperature
$\mathfrak{U}_g^{(0)}$	dimensionless temperature of igniter blast
x	axial coordinate, cm
X	tabulated function
y	coordinate perpendicular to burning surface, cm
Y	tabulated function
$\mathfrak{Y}$	dimensionless distance, equation (66)
Z	tabulated function

Greek

α	$(\xi^2 + \eta^2)^{1/2}$
α_1	dimensionless burning rate parameter, equation (8)
β	characteristic constant for circumferential oscillations
γ	ratio of specific heats
δ	variation
δ_1, δ_2	phase constants
ϵ	density variation in $\rho = \bar{\rho} + \epsilon e^{i\alpha at}$
ϵ_i	extent of reaction in ith zone
ζ	velocity variation in $v = \bar{v} + \zeta e^{i\alpha at}$
η	$(c_1/Q_1)(T_1 - T)$; also characteristic constant of radial oscillations

λ_i thermal conductivity in ith zone, cal·cm^{-1}·sec^{-1}·°K^{-1}
μ pressure index of interaction between combustion and oscillation in gas phase
ν frequency, $2\pi\omega$
ξ $1 - \delta_1$; also characteristic constant of axial oscillations
ρ_i mass density in ith zone, gm·cm^{-3}
$\bar{\rho}$ mean density, gm·cm^{-3}
σ integer
τ time lag, sec
$\bar{\tau}$ mean time lag, sec
φ angular coordinate
χ numerical factor
ω angular frequency

REFERENCES

1. Geckler, R. D.: *Selected Combustion Problems*, pp. 289–339. London, Butterworths Scientific Publications, 1954.
2. Parr, R. G.: Private communication (1953).
3. Cheng, S. I.: Jet Propulsion, *24*, 27–32, 102–109 (1954).
4. Frazer, J. H., and Hicks, B. L.: J. Phys. & Colloid Chem., *54*, 872–876 (1950).
5. Hicks, B. L.: J. Chem. Phys., *22*, 414–429 (1954).
6. Rice, O. K., and Ginell, R.: J. Phys. & Colloid Chem., *54*, 885–917 (1950).
7. Parr, R. G., and Crawford, B. L.: J. Phys. & Colloid Chem., *54*, 929–954 (1950).
8. Boys, S. F., and Corner, J.: Proc. Roy. Soc. (London), *A197*, 90–106 (1949).
9. Corner, J.: Proc. Roy. Soc. (London), *A198*, 388–402 (1949).
10. Muraour, H.: Bull. Soc. Chim. Fr., *41*, 1451–1461 (1927).
11. Corner, J.: Trans. Faraday Soc., *43*, 635–642 (1947).
12. Smith, R. P., and Sprenger, D. F.: *Fourth Symposium (International) on Combustion*, pp. 893–906. Baltimore, The Williams & Wilkins Co., 1953.
13. Grad, H.: Comm. Pure Applied Math., *2*, 79–102 (1949).
14. Green, L.: Jet Propulsion, *24*, 252–253 (1954).
15. Crocco, L.: J. Am. Rocket Soc., *21*, 163–178 (1951); *22*, 7–16 (1952).
16. Huffington, J. D.: Trans. Faraday Soc., *47*, 864–876 (1951). *cf. 50*, 942–952 (1954).

V

PROBLEMS OF TURBO-JET COMBUSTION

By PETER LLOYD

Introduction

The last 10 years have seen great advances both in the development of turbo-jet combustion systems to meet increasingly arduous requirements and in the understanding of the underlying processes. But in spite of this it is very clear that there are still many unsolved problems. Consider, for instance, the following questions: (1) What is the relative importance of the physical and chemical factors? (2) What are the parameters defining the effects of temperature, pressure and velocity on combustion efficiency? (3) What is the relationship between the performance of a model and that of a full scale combustion chamber? (4) What are the factors that limit the rating of combustion chambers? All of these are legitimate questions which can now be answered only in a vague and qualitative way. Discussion of them would be bound to bring up big differences of opinion.

The incompleteness of our understanding of turbo-jet combustion may be further illustrated by considering to what extent combustion chambers are designed by a logical process based on the application of knowledge of underlying principles. It has to be admitted that no such design procedure is followed and that instead combustion systems are developed by a step-wise and empirical process.

Peculiarities of Turbo-Jet Combustion

This situation is not unique to turbo-jet combustion, and the main reason for the unsatisfactory state of affairs is that all applied combustion

processes, whether in furnaces, boilers or engines, involve a complex combination of factors physical, aerodynamic, chemical, thermodynamic and mechanical, which are difficult to disentangle. Incidentally there are plenty of other technological processes to which similar criticism applies: the development of alloys, the design of structures, and the forecasting of weather.

maximum thrust downwards. The present range of operation from high speed flight at ground level to windmilling conditions at altitudes already extends from about 12 atm and 600°K to $\frac{1}{10}$ atm and 240°K, but flight in the supersonic regime is now beginning to extend this range still further especially in the direction of higher temperatures.

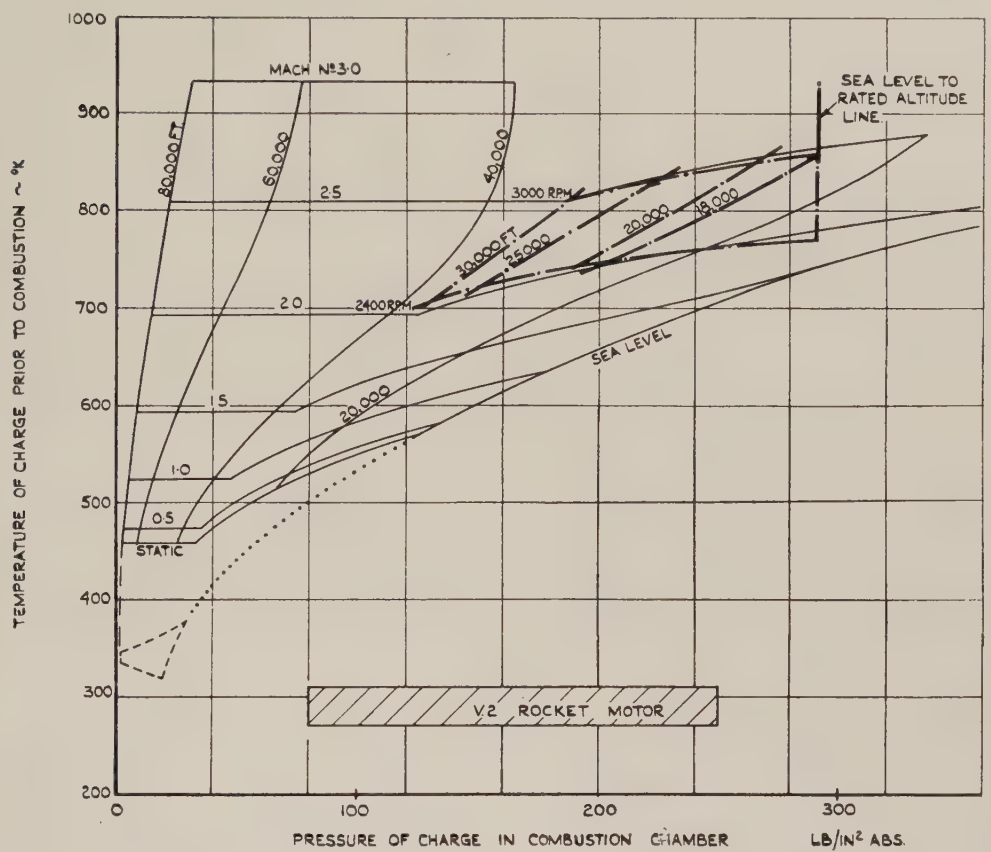

Fig. 1. A comparison of the range of engine operating conditions. Notes: (1) The turbo-jet range is for an 8:1 compression engine and the full lines refer to the full engine speed condition. Approximate idling conditions are indicated by broken lines, thus — — —. (2) The reciprocating engine figures refer to the Rolls Royce Merlin 46 and are shown by chain dotted lines, thus — . — . — . (3) The envelope represents the operating range of the German V2 rocket motor.

But while this complexity and the empiricism to which it leads are common to all technological combustion processes, the turbo-jet case involves some particular factors which distinguish it from most others.

The first of these is the wide range of pressure and temperature over which the system is called upon to operate. This range of conditions results from the need to fly over a range of forward speeds and altitudes and from the fact that the engine operation must also be capable of variation from

This trend is illustrated by Figure 1 which shows the temperatures and pressures at inlet to the combustion system of a turbo-jet engine of 8:1 compression ratio at speeds up to twice that of sound. By contrast the operating range of a typical reciprocating aero engine, which is also shown in Figure 1, is considerably less, and that of a liquid fuelled rocket is narrower still.

This variety of operating conditions does not merely raise practical problems for engine designers; it also implies that in studying funda-

mental aspects of turbo-jet combustion and its component processes we have to cover a wide span of pressures and temperatures.

Another characteristic of the turbo-jet requirement is operation outside the normal limits of inflammability. It is this factor which brings about the need for using separate primary combustion zones with subsequent mixing operations and which is largely responsible for the flame chilling effects to which gas turbine combustion is prone.

The last factor which need be mentioned is the high loading of gas turbine combustion systems. The reaction times available are from 4 to 10 msec only in main combustion systems and much nearer to the lower figure for reheat. These figures are not so very different from those which characterize spark ignition engines, diesel engines, and rockets, but in turbo-jet engines (at high altitude and low speed) they are associated with much lower pressure and temperature levels. It is this combination of short reaction time with low pressure and temperature that is important, for the controlling parameter in high speed combustion processes is the ratio of residence time to time required for reaction, and in turbo-jet relighting and idling conditions this falls to a very low value.

This then is the background to the problem. As a field for research it is full of interest and opportunity, all the more so because of its intrinsic difficulty and since it overlaps the boundaries of several academic divisions of science. As a matter of engineering development the requirements have been hard to satisfy but so far they have been met effectively enough, though at a high cost in time and effort. Apart from a difficult time at the beginning of turbo-jet history in 1940 combustion has not often been a real bottleneck in engine development. But current trends in aeronautics towards higher speeds and greater altitudes involve increased aerodynamic and thermal loading, and improved techniques will be required to prevent combustion from setting a limit to engine performance.

The Elementary Processes

Though it is not the only approach to a complex phenomenon, the study of its elementary component processes in isolation is an obvious first step, and this is the method that most of us have adopted in this field. It does not, of course, take us the whole way, for even a full understanding of the parts will not, in itself, amount to an explanation of the whole, but it is a necessary preliminary.

How far have we got in this attempt at an exact treatment of turbo-jet combustion? Here is my own assessment.

In the first place we have listed the elementary processes which may be involved and we have ideas, some well founded and others tentative, as to which are the most important. Simple though it sounds, this qualitative analysis has, in fact, taken some time to complete. The relative importance of the different processes depends upon operating conditions and is still perhaps a matter of opinion, but in my own view the more important ones are: (1) The flow of fluid past stalled baffles and other obstructions, and the recirculation and mixing in their wakes; (2) The mixing of hot and cold streams; (3) The mixing of fuel droplets and air, either in separate piloting zones or when fuel is injected direct into the primary zone; (4) The break-up of liquid fuel into droplets; (5) The reaction of mixtures of fuel and air, including air vitiated with combustion products.

The less important factors are: (1) The effects of compressibility in the flow. (In the main combustion systems of turbo-jets, pressure losses are generally limited to about 10 per cent on thermodynamic grounds and velocities are low. But compressibility must be taken into account in reheat pipes in which high subsonic speeds are reached); (2) Convectional heat transfer to walls; (3) Evaporation of fuel droplets in air; (4) Burning of fuel droplets; (5) Radiation from flames to walls and to fuel droplets; (6) Propagation of flame from hot burnt gas to fresh combustible mixtures; (7) The reactions of fuels when heated in the absence of air.

In the second place we have amassed a good deal of information about these processes. Many of them are familiar physical or chemical effects which already have a long history of research and investigation and on which there is text book data; but in almost every case it has been necessary to extend past work, and in some an entirely fresh approach has been necessary, as, for instance, in the work of Godsave and Spalding on the burning of fuel droplets, and in the work of Mullins on the spontaneous ignition of hydrocarbon fuels at high temperatures. The process continues for there are still notable blanks on the map.

In particular we need to know a good deal more about the effects of pressure and temperature on

some of these processes such as the break-up of liquid fuel into droplets and the reaction of fuel air mixtures. There is scope for quite a lot of work of this kind at both the high and low extremes of pressure.

In the third place we are just beginning to experiment with the application of this knowledge to more complex processes. We have shown, for instance, that if air:fuel ratio and inlet temperature remain fixed, and if the spray parameters are correctly chosen, then a model of linear fractional size f should reproduce in most respects the performance of a full sized chamber when tested at the same air velocity and at $1/f \times$ the pressure level and we have confirmed by experiment that this conclusion is substantially borne out in practice.

We have also begun to use our quantitative understanding of the elementary processes to devise experiments to estimate the relative importance of the different elementary processes. We expect, for instance, that the combustion chamber Reynolds number will be a secondary factor, but we can only prove this by devising an experiment which will keep all other factors constant and allow this to vary independently. This third stage of the process, the integration and application of knowledge derived from a study of the idealized components, is only just beginning.

Reaction in the Turbo-jet and the Bunsen Flame

To illustrate the state of our ignorance it may be worthwhile to discuss quite briefly some aspects of the relationship between the bunsen flame, which of all the idealized combustion systems has been most intensively studied, and the turbo-jet.

The propagation of flame in the bunsen cone is simply the successive inflammation of adjacent elements of combustible mixture. It is directional and non-isothermal.

In the spark ignited reciprocating engine, in which a recognizable combustion wave in an essentially pre-mixed system traverses the combustion chamber, a similar process of flame propagation is clearly a factor of significance. But in the continuously burning turbo-jet combustion system, with flame stabilisation brought about by a deliberately reduced aerodynamic recirculation, we have a different situation. Here fresh mixture (or the components of an inflammable mixture) is continuously mixed into an already burning charge. Here again there is no directional flame propagation, but each element of fresh mixture undergoes a "three-dimensional" process of ignition and continuing reaction in the turbulent system, and when, as is commonly the case, the fluid surrounding the combustion zone is air and not a premixed inflammable gas, there can be no question of the flame propagation from the combustion zone into the surrounding gas stream.

Thus in turbo-jet combustion the flame speed in ft/sec is of no direct significance, its only value being as an index of reaction rate, and this reaction rate is only of significance when linked to a particular volume of reaction zone and to a particular temperature level.

Herein lie the difficulties of making practical use of laboratory determinations of flame speed. Firstly the effective reaction volume is difficult to specify uniquely, and once specified is still less easy to determine experimentally at normal or elevated pressures. Secondly, since the process is essentially non-isothermal, it is impossible to define a temperature level.

In turbo-jet combustion it is the rate of heat release per unit volume at any given pressure level that is of interest, and this is one of the criteria defining the loading of the system. The rate of heat release in relation to the rate of heat loss is also a critical factor determining the stability of this and other self-sustaining combustion systems. In alternative and simpler terms the fundamental combustion parameter is the time required for reaction. When this is known both combustion efficiency and stability may be examined in terms of the ratio of available residence time to required reaction time.

Using these parameters how do the characteristics of the pre-mixed linear flame compare with those of the turbo-jet?

In the case of a simple one-dimensional flame, the mean reaction time is deduced, subject to the difficulties of measurement, from the reaction zone thickness and the cold flow velocity corrected for temperature changes. Similarly assuming complete combustion, the mean heat release rate per unit volume of the reaction zone is proportional to the mass flow per unit area divided by the reaction zone thickness.

Calculation on this basis shows that the apparent intensity of reaction in linear flame propagation is much higher than in contemporary turbo-jet systems. Thus using the results of Gaydon and Wolfhard[1] for a butane-oxygen-nitrogen mixture at atmospheric pressure, we

have:

Thickness of luminous reaction zone = 0.02 cm

Flame velocity = 40 cm/sec

If, for simplicity, we identify the luminous flame zone with the reaction zone considered in the present analysis, then, using data for the initial composition of the mixture and the heat of combustion of butane, we may calculate the corresponding heat release rate to be

$$550 \times 10^6 \text{ CHU/hr/ft}^3$$

This value is clearly an optimum depending, as it does, upon a minimal estimation of the reaction zone width. Such assessments as there are of the extension of the region of exothermic reaction beyond the luminous region (see for instance Gaydon and Wolfhard[1]) would perhaps halve the calculated value of the mean volumetric heat release rate. We may note that this conclusion is broadly confirmed by Longwell's values[2] of limiting heat release rate measured in a flowing system devised to give extremely rapid mixing, his figure being:

$$220 \times 10^6 \text{ CHU/hr/ft}^3\text{/atm}^2$$

It will be noticed that the statement of the reaction rate in these terms implies acceptance of the view that the volumetric heat release rate varies as the square of the pressure. Incidentally the confirmation of this generalization, by measurements over a wide pressure range, is much to be desired.

These values may be compared with the conventionally calculated combustion ratings of present day turbo-jet chambers. At one atmosphere pressure these normally operate at about 2.0×10^6 CHU/hr/ft^3. Similarly reheat systems are typified by a heat release rate at one atmosphere of 1.5×10^6 CHU/cu ft/hr. But in terms of the pressure corrected parameter the rating of turbo-jets is not a fixed characteristic of the design but is a function of altitude, forward speed and engine conditions and the most arduous requirement is given by low forward speed, low engine speed and high altitude. The figures given above, therefore, need correction as follows.

For the main combustion system the pressure corrected heat release rate for a 6:1 engine cruising at 60,000 ft becomes 4×10^6 CHU/cu ft/hr/atm^2 and the corresponding reheat requirement at full engine speed Mach No. 0.9 and 60,000 ft becomes 4.4×10^6 CHU/cu ft/hr/atm^2. At idling and relighting conditions the combustion requirement can become more arduous still, but the fact remains that even the worst-condition requires less than one-tenth of the heat-release rate which occurs in the bunsen flame.

This comparison, however, needs much qualification. In the laminar flame the volumetric heat release, just calculated, measures the optimum reaction rate of a pre-mixed stoichiometric system and the volume used in the calculation has been measured from a point already at a high temperature level and after ignition has taken place. In the turbo-jet system the residence time provided must allow not only for the high temperature reaction but also for mixture preparation and ignition, secondary mixing and dilution, for in this case the initial reactants are admitted at a temperature level well removed from their ignition point. It is also relevant that stability and efficiency must be retained at air:fuel ratios other than stoichiometric.

Longwell's experiment is in an intermediate category; in this case the reactants are admitted at low temperature and ignition is effected by mixing, but in other respects the conditions are idealized.

But in spite of these qualifications we must conclude that chemical reaction rate does not at present, and will not in the immediate future, impose any absolute limit to the corrected heat release rates which can be achieved.

In terms of time we can use the available data on temperature distribution in simple flames (see Gaydon and Wolfhard,[1] and Klaukens and Wolfhard,[3]) to estimate a temperature correction factor for the flow velocity of the order of 5, and we thus see from previous results that for the laminar butane air flame the mean reaction time at one atmosphere is of the order:

$$\Delta t_{\text{react.}} = 0.2/(40 \times 5) \text{ sec}$$

$$= 0.1 \text{ msec}$$

This approximate figure may be compared with the available residence times in turbo-jet combustion systems which vary from about 4 to 10 msec according to loading.

In this comparison the influence of pressure must again be borne in mind. Available residence time in a turbo-jet engine is largely independent of altitude but required reaction time is, of course, pressure dependent and on the evidence available we take it to be inversely proportional. It follows that under high altitude conditions the

margin between available residence time and required reaction time will be reduced. Taking the same example of the cruising condition at 60,000 ft with a conventional 6:1 engine we have an unchanged residence time of 10 msec and a reaction time of 0.2 msec giving a ratio of 50.

The validity and usefulness of this approach to combustion processes in terms of available residence time and required reaction time has been confirmed by the results of a recent theoretical treatment of baffle stabilization by B. P. Mullins at N. G. T. E. Using preflame reaction rates as a criterion of reaction time he was able to predict qualitatively the observed effects of fuel:air ratio, static pressure, baffle diameter and inlet temperature on the blow-out velocity of a simple stabilizing baffle.

All this argument refers to the laminar bunsen flame and it is worth considering briefly what are the effects of turbulence on pre-mixed flames and on the comparison between these and turbo-jet combustion systems.

Turbulence in the aerodynamic sense is on a supra-molecular scale, and thus cannot increase the molecular collision rate and subsequent reaction of an element of mixture of dimensions comparable to the molecular mean free paths, since these rates are determined by the fundamental conditions of concentration, pressure and temperature. Turbulence, however, will speed up the process of mixture preparation in an imperfectly mixed system, and also the transfer of heat and active species, thus promoting the processes of mixture heating and ignition. Turbulence will also help to convey fresh fuel and oxygen to the burning zone.

In the special case of a propagating flame in a homogeneous mixture it has been suggested that small scale turbulence (the index of scale here being the thickness of the laminar flame zone) acts as above by promoting the transfer of heat and active species, whereas large scale turbulence distorts the flame front and so increases the area available for reaction (see for instance Scurlock and Grover[4]). The latter process, it will be noted, increases the absolute mass reaction rate, and hence the speed of linear propagation, but since the folded flame front occupies more volume the effective flame zone is also increased, so that, as is indeed to be expected, the volumetric reaction rate is not increased beyong the limit set by the fundamental molecular-scale reaction rate.

One new factor underlies this discussion of reaction rates in turbo-jet combustion and in the idealized bunsen flame and this is that we have a great need of further data on the reactions of hydrocarbons at high temperature levels. Examination of bunsen flames may or may not be the best way of studying these high temperature processes, but in one way or another we must fill in the gap of our knowledge. For practical purposes we are, of course, much more interested in the effective rates of reaction (whether measured as times or as rates of heat release) than in the chemical mechanisms involved. The present situation is broadly illustrated by Figure 2 in which the logarithm of reaction time is plotted against the reciprocal of the absolute temperature. The area in the top right hand corner indicates the long reaction times and low temperatures characteris-

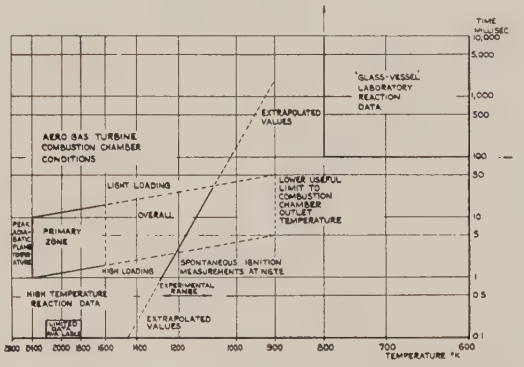

Fig. 2. Disparity between engine conditions and laboratory reaction data. (Differences in pressure level not included.)

tic of glass-vessel laboratory kinetic studies. The conditions obtaining in aero gas turbine combustion chambers are shown in the middle of the diagram. A typical time-temperature plot is also shown for the spontaneous ignition of a spray of kerosine at atmospheric pressure, as measured by the N. G. T. E. method.[5] In the bottom left-hand corner of the diagram we have only limited data available at high temperatures and short reaction times. For example, a spot point could be put in to represent the butane flame data previously discussed.

Techniques of Combustion

I have made the familiar points that turbo-jet combustion, like much other applied combustion, is a complex affair in which the mere listing of the underlying physical and chemical processes is a matter of difficulty, and that development, though guided by much experience and helped by

various experimental methods, is still an *ad hoc* process, but there is another aspect of the matter that is worth touching upon. The intractability of turbo-jet combustion as a scientific problem is partly due to the fact that it does not employ, not at any rate in a systematic way, the simpler and more easily analyzed processes such as the idealized bunsen and diffusion flames. Instead it uses a variety of flow patterns designed to give

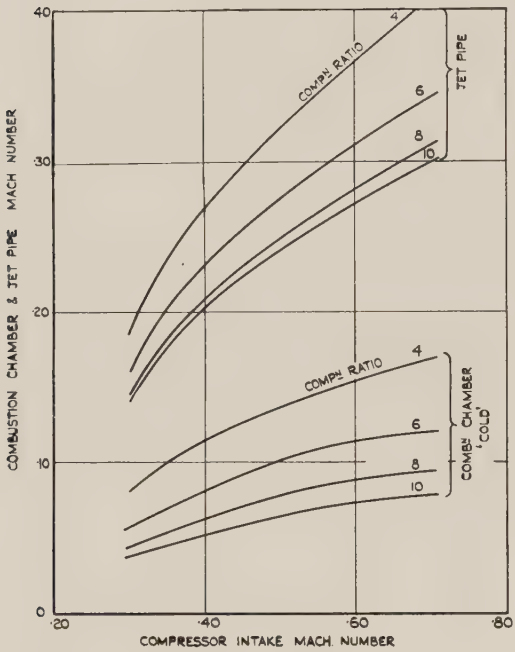

Fig. 3. Variation of combustion chamber and jet pipe mach. no. with compressor intake no. Notes: The basis of the curves is a hypothetical series of engines having a combustion annulus equal in area to the compressor entry annulus and a jet pipe diameter equal to the diameter of the engine intake. Also, hub/tip ratio = 0.5; compressor polytropic $\eta = 0.87$; combustion temperature = 1150°K; turbine isentropic $\eta = 0.88$.

flow reversal recirculating hot gases to a piloting zone and techniques of localized fuel injection giving arbitrary variation in concentration throughout the burning zone. The flow reversal is difficult to analyze theoretically or to measure experimentally and the non-uniform fuel distribution (which also varies with operating conditions) is an obvious handicap in any theoretical treatment.

The use of these awkward techniques is no mere caprice; they have real advantages and there is, as yet, no alternative which does not involve some loss of efficiency. Nevertheless, it is fair to ask whether these techniques, which are at present universal, are indeed essential. A system which through greater simplicity made possible a more exact analysis and an effective design procedure and which gave model tests an exact significance would be worthwhile even though it gave no improvement in performance.

Problems of Development

The dominant trends in the evolution of turbo-jet engines are towards increased thrust per unit frontal area and lower specific weight. The most important developments contributing to these ends are increasing the air flow through the engine and raising the cycle temperature. Both tendencies are important from the point of view of combustion design.

Increased air flow through the engine means, in practice, higher air speeds through the combustion zone. It is true that by using a higher compression ratio this increase in air speed could be avoided, but there are good reasons against achieving the desired effect in this way. In the first place greater compression means more weight and complication; in the second place the use of increased compression in the supersonic flight regime would not be justified on thermodynamic grounds.

Figure 3 gives some idea of how combustion chamber and jet pipe Mach number will vary in a given engine configuration (hub:tip diameter at compressor intake of 0.5 and similar diameter ratio for the combustion annulus, with jet pipe diameter equal to intake diameter). It is clear from this that combustion chamber Mach number may well reach 0.10 and jet pipe Mach number 0.275.

The effects of this demand for increased air flow are far reaching. In the first place it requires a big improvement in the aerodynamic efficiency of combustion systems, i.e., a marked reduction in the overall pressure loss which is compounded of parasitic losses in the intake and in changes of section plus the losses involved in generating the flow reversal system and in carrying out the mixing processes. This point is well illustrated by Figure 4 which summarizes the aerodynamic characteristics of a contemporary design of combustion chamber. Above the flow Mach number of 0.05 the pressure loss soon becomes excessive.

In the second place the combination of higher air speed with lower pressure loss factor and lower turbulence level means much more arduous

conditions from the point of view of the combustion processes.

Figure 5 illustrates this point by indicating how the time available for reaction in the wake of a stabilizing baffle might vary in response to change of inlet velocity. Since we do not have exact knowledge of the size of the flow reversal region or of the rate of air flow through it, the best we can do is to use as ordinate the function d/v, baffle dimension/stream velocity, which has the

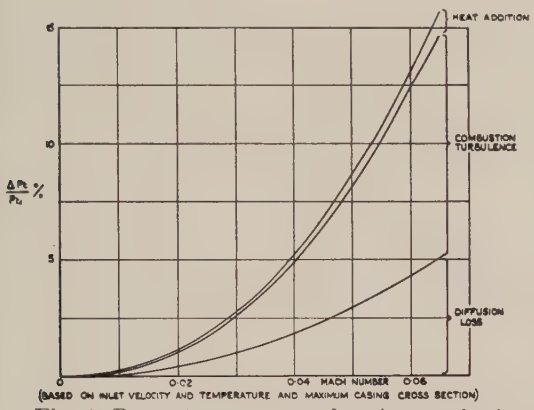

Fig. 4. Percentage pressure loss in a turbo-jet combustion system as a function of the aerodynamic loading.

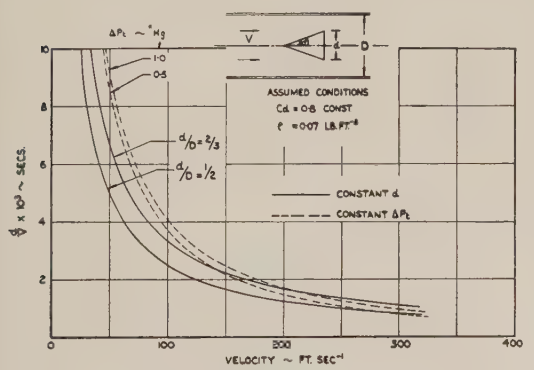

Fig. 5. Variation of the residence time parameter d/v with velocity for a simple flame holder.

dimension of time and which for a given flow pattern will be proportional to the residence time in the wake. Two cases are considered, constant geometry which, of course, gives a simple hyperbola, and constant pressure drop. The latter case, which implies reduction in baffle size at the higher velocities, shows how big the effect can be.

Increased cycle temperature is important in quite a different way. While higher air speeds mean more arduous combustion requirements without qualification, higher gas temperatures have two opposing effects, favorable and unfavorable. The favorable effect is, of course, the acceleration of combustion reactions and the diminution of flame chilling phenomena, the shifting of the operating mixture strength nearer to the optimum stoichiometric values. The adverse effect is on cooling and mixing. The higher the cycle temperature the less the air available for cooling the flame tube wall against enhanced heat transfer rates. And the higher the temperature was due to combustion the greater the difficulty of achieving uniformity of outlet temperature traverse. It is not yet clear which of these two effects will be dominant.

Conclusions

I would like to conclude by reiterating the fields of research which seem to me most worthwhile at the present time from the point of view of the turbo-jet application.

(1) The first is that of reaction kinetics, the well chosen first topic of this year's international symposium, and, most important in practice, the kinetics of the high temperature reaction in the system hydrocarbon-air-recirculated combustion products.

(2) The second is the extension of our knowledge of the other component processes such as atomization, droplet combustion and turbulent flame propagation to cover a wider range of temperature, pressure and, where relevant, linear scale.

(3) The third is analytical examination of combustion systems, either practical or idealized, to assess which are the rate controlling factors over different ranges of operation. This is a necessary preliminary to the use of model testing techniques.

(4) The last is that of mixing, for I have shown that reaction rate, though important, does not impose a fundamental limit on combustion systems as at present loaded, and it follows that there is scope for the use of improved mixing techniques.

Acknowledgments

I am indebted to the Chief Scientist of the (British) Ministry of Supply for permission to present this paper. I am also glad to acknowledge the help, in the preparation of the paper, of G. A. E. Godsave and J. M. Hawkins of the National Gas Turbine Establishment.

REFERENCES

1. Gaydon, A. G., and Wolfhard, H. G.: Proc. Roy. Soc., *A196*, 105 (1949).
2. Longwell, J. P.: *Selected Combustion Problems*, AGARD, p. 508. London, Butterworth Scientific Publications, 1954.
3. Klaukens, K., and Wolfhard, H. G.: Proc. Roy. Soc., *A193*, 512 (1948).
4. Scurlock, A. C., and Grover, J. H.: *Selected Combustion Problems*, AGARD, p. 215. London, Butterworth Scientific Publications, 1954.
5. Mullins, B. P.: Fuel, *32*, 211 (1953).

Discussion by Gilbert S. Bahn*

Any comprehensive consideration of combustion problems in engines must make note of pressure loss considerations, since these are so fundamental to development of satisfactory performance. On the other hand, in a combustion symposium concerned primarily with reaction kinetics, too detailed a story regarding pressure loss would be inappropriate. The author has struck a nice balance in his presentation. From the engine standpoint, a fairly detailed statement of combustor pressure loss problems has been made by Bahn and Koffer.†

To recognize the importance of pressure loss is the most important aspect. To recognize the necessity for treating the flow as three-dimensional is the next most important. Dr. Lloyd has done both. It should be added, however, that full-scale engine designs are extremely complex, and make three-dimensional flow calculations very complicated and uncertain. Furthermore, many instances exist where test data do not follow theory even as to trend. It would be unfortunate to permit the implication that pressure loss data for full-scale engines are readily predictable.

* Marquardt Aircraft Co.

† G. S. Bahn and G. W. Koffer: Problems in Formulation of Design Procedures for Continuous-Flow Combustion of Hydrocarbons, ASME Paper No. 54-SA-22 (March 1954).

VI

COMBUSTION PROBLEMS IN RAMJETS

By J. P. LONGWELL

Introduction

For purposes of discussion, combustion in ramjets can be conveniently divided into two zones: the flame stabilization or piloting zone and the flame spreading zone. In this first zone, a relatively small flame is established which is fed into the main body of material to be burned. This stabilizing flame is generally maintained in a recirculation zone behind a baffle or in the dome of a can type burner. In this zone, intense mixing occurs and fresh unburned fuel and air mixture enter continuously and are mixed with hot combustion products. The hot combustion products leaving the recirculation zone cause ignition of the main body of fuel and air. The rate at which the main body of fuel and air is consumed determines the length of combustion chamber required and is thus of considerable interest.

Quantitative information on the high temperature chemical reaction rate of hydrocarbons and air has recently become available. This allows comparison of the ultimate performance of combustion devices, as limited by chemical reaction rate, with performance as now reported. This review will be devoted to a description of the operation of typical ramjet combustion devices and comparison of what is considered to be the limiting performance with that actually obtained.

Flame Stabilization

In order for a mixture of fuel and air to react rapidly, it is necessary for the mixture to be raised to a high temperature or to come in contact with active particles from a nearby reaction zone. In practical equipment this is accomplished by feeding back some of the heat and combustion products generated by previously reacted fuel and air into the unburned mixture. In a laminar flame front this is accomplished by molecular transport of heat and material. Because very high rates of heat liberation are required of ramjet engines, the engine is built so that this feedback is aided

by the turbulent mixing of burned products. The two most important devices for doing this are shown in Figure 1. These devices are the familiar baffle and can. Flow is shown diagrammatically, and it is seen that flow of fresh unburned material into the reaction zone and escape of hot gases downstream takes place. Intense mixing occurs in this zone which is generally called the recirculation zone.

Stabilization by Baffles

The intensity of mixing in the wake of baffles has been illustrated by Nicholson and Field[1] who took high speed motion pictures of this zone. Using particles of sodium acetate as tracers they found that, in one run, for example, the average residence time of a particle in the recirculation zone was 0.008 sec (for a 0.75-in gutter in a 200 ft/sec stream). However, the sodium vapor from entering particles appeared to diffuse completely throughout the zone in about 0.0002 sec giving a ratio of mixing time to residence time of about 1 in 40.

Some further detail on combustion in the wake of the baffle is shown in Figure 2.[2] Time average measurements of oxygen consumption in a stoichiometric fuel-air mixture are shown. It is seen that a zone of high combustion efficiency approximately the width of the baffle exists in the wake of the baffle. This zone narrows somewhat as one proceeds downstream but still further downstream it expands again. By probing with a salt covered rod, it was found that the combustion zone upstream of the rod was colored yellow if the rod was not more than about 10.5 in downstream from the baffle. This recirculation zone length of 4–5 baffle diameters seems to hold for both 1.0 and 2.25-in gutters. It is felt that this general pattern is typical of large size baffles in high velocity air streams.

While some material at a distance of 4-5 baffle widths downstream flows upstream, flow in this direction is sporadic and is estimated to occur about 10 per cent of the time. A typical time average velocity at this distance downstream (for other conditions), as shown in Figure 3, is almost as high as the main stream velocity. From such velocity distribution and efficiency data, it is possible to estimate the fuel burned upstream of this point. In this case, burned mixture amounts to the equivalent of an unburned airstream about 0.33 in wide if it can be considered to be traveling at the air velocity upstream from the baffle.

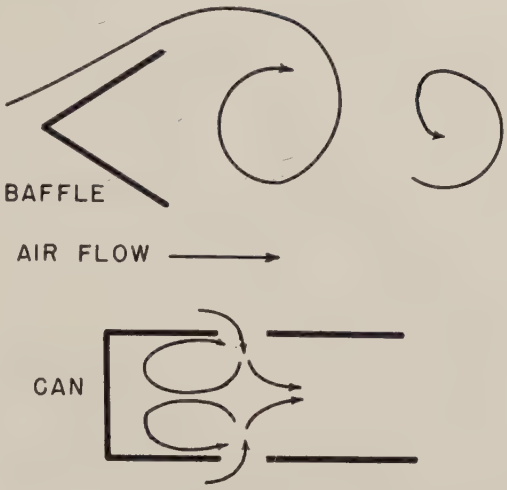

Fig. 1. Diagrammatic sketch of flame stabilizing devices.

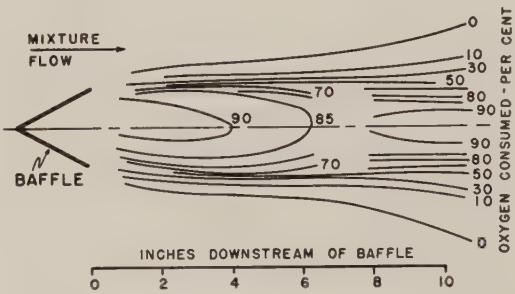

Fig. 2. Combustion efficiency pattern in the wake of a baffle.
Velocity = 300 ft/sec
Fuel = No. 1 solvent naphtha
Pressure = 1 atmosphere
Temperature = 250°F
Equivalence ratio = 1.0

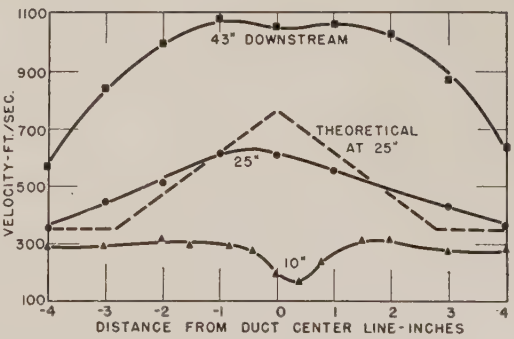

Fig. 3. Velocity distribution downstream from a V-gutter.
Equivalence ratio = 1.0
Temperature = 250°F
Pressure = 10″ Hg abs.
Velocity = 170 ft/sec
2¼″ V-gutter
Fuel = No. 1 solvent naphtha

The above discussion gives some idea of the time average velocity and temperature distribution downstream from a large baffle; this distribution would probably be considerably different for very small baffles or low velocities. At very low pressures, it is also probable that the pattern might deviate somewhat; however, such data are not presently available.

A large number of observations of conditions under which blowouts occur have appeared in the literature.[3, 4, 5, 6, 7, 8, 11] These have given rise to the now familiar correlations where the mixture ratio at blowout is plotted as a function of u/D^nP^m. Here u is the velocity past the baffle, D a characteristic dimension of the baffle and P the pressure. The exponent n varies from 0.45 to 1.0 and m is approximately 0.9. These correlations are discussed in more detail later.

Recent work by Fristrom and Avery[9] and by Weiss and Longwell[10] has indicated that the rate of heat liberation can be empirically described by a second order rate equation for reaction of fuel and air using an activation energy of approximately 40,000 cal/mol. The existence of such an expression makes possible estimation of the effectiveness of stabilizing devices, if one can describe the flow. Longwell, Frost and Weiss[2] and DeZubay[11] have carried out such calculations assuming that the recirculation zone in the wake of the baffle is so intensely mixed as to be homogeneous.

For such a situation the rate of combustion can be represented by the equation:[10]

$$\left.\begin{array}{l}\text{Lean: } A\phi\epsilon/4.76 \times 29 \\ \text{Rich} \quad A\epsilon/4.76 \times 29\end{array}\right\} = Vk\sqrt{T}\, e^{-E/RT} \left(\frac{P}{RT}\right)^r x_{\text{Fuel}}^{f}\, x_{O_2}^{r-f}$$

where A = mass flow rate of air into the reaction zone
ϕ = equivalence ratio
ϵ = oxygen combustion efficiency (oxygen consumed divided by oxygen which would be consumed were combustion complete)
V = reaction volume
k = rate constant
T = absolute temperature
E = activation energy
R = gas constant
P = pressure
r = overall reaction order
f = fuel exponent
x_{Fuel}, x_{O_2} = volume fractions in combustion gases of fuel and oxygen, respectively.

This equation balances the rate of oxygen disappearance between inlet and outlet of the reaction zone (the left side) to the rate of chemical reaction within the zone (the right side)—a bimolecular reaction of r order with an Arrhenius term for temperature. The $\sqrt{T}$ is added (from collision theory) presumably to make k temperature independent; this term has little effect on the final results. Constants on the left side convert pounds of air to pound-moles of oxygen. In working with these rate equations, it is simpler to deal with oxygen disappearance than with fuel disappearance because of the formation of cracked and incompletely burned combustibles from the original fuel.

The volume fractions of fuel and oxygen can be expressed in terms of efficiency (ϵ) if assumptions are made about the nature of the reaction. For example, one may assume that for lean mixtures a fraction ϵ of original fuel burns to CO_2 and H_2O, and a fraction $(1 - \epsilon)$ remains unchanged. Similarly, a fraction $\epsilon\phi$ of original O_2 is consumed and $(1 - \epsilon\phi)$ remains. Thus, for octane and air

$$x_{C_8H_{18}} = \frac{.08\phi(1 - \epsilon)}{4.76 + \phi(0.28\epsilon + .08)},$$

$$x_{O_2} = \frac{(1 - \epsilon\phi)}{4.76 + \phi(0.28\epsilon + .08)}$$

For rich mixtures, the expression is more complex because of the known presence of CO and H_2. One may then assume that fractions ϵ of original C_8H_{18} and O_2 are consumed to give CO_2, CO, H_2 and H_2O in water gas equilibrium at the reaction temperature T. Fractions $(1 - \epsilon)$ of C_8H_{18} and O_2 remain giving

$$x_{C_8H_{18}} = \frac{.08\phi(1 - \epsilon)}{4.76 - \epsilon + .08\phi(1 + 16\epsilon)},$$

$$x_{O_2} = \frac{1 - \epsilon}{4.76 - \epsilon + .08\phi(1 + 16\epsilon)}$$

for octane and air.

If these fractions are substituted in the rate equations, rearranged, and the usual assumptions made that $r = 2$ and $f = 1$, then the results are

$$\text{Lean:} \quad \frac{A}{VP^2} = \frac{4.76 \times 29 \times k}{R^2} \frac{e^{-E/RT}}{T^{3/2}} \frac{.08(1 - \epsilon)(1 - \epsilon\phi)}{\epsilon[4.76 + \phi(0.28\epsilon + .08)]^2}$$

$$\text{Rich: } \frac{A}{VP^2} = \frac{4.76 \times 29 \times k}{R^2} \frac{e^{-E/RT}}{T^{3/2}}$$

$$\frac{.08\phi}{\epsilon} \left(\frac{1 - \epsilon}{4.76 - \epsilon + .08\phi(1 + 16\epsilon)} \right)^2$$

For a given fuel, knowing the products of combustion, one can calculate the temperature as a function of equivalence ratio and efficiency. Efficiency can then be found as a function of A/VP^2 giving results as shown in Figure 4. Starting from complete combustion, as A/VP^2 is increased, less time is available for reaction and it is seen that the efficiency decreases. The rate of heat release is higher, however, since the efficiency does not decrease as rapidly as fuel and air flow increase. The higher reaction rate is made possible by the increase in concentration of reactants. As A/VP^2 is increased further, however, a point is reached where the decrease in temperature due to the decrease in efficiency reduces the rate more rapidly than can be compensated for by increased reactant concentration and the efficiency drops to essentially zero. This point is the blowout commonly observed when a combustion zone is overloaded because of an increase in mass flow, a decrease in pressure, or a change in mixture ratio.

The group A/VP^2 must be related to the quantities usually observed in order to compare the results of this treatment with a variety of experimental results. The variation of blowout velocity with pressure and baffle width, as discussed below, is not firmly established; however, for purposes of comparison it was assumed that flow, A, into the recirculation zone of the baffle is proportional to velocity, u, inversely proportional to density (i.e., pressure, P) and to the baffle width, D, raised to some power, c, we have $A/VP^2 \sim u/PD^c$ which is identical to the customary correlating group. The proportionality constant can be estimated from temperature and velocity distributions such as shown in Figures 2 and 3. If it is assumed that the volume, V, is a volume the width of the baffle extending 4.5 baffle diameters downstream, conditions for blowout can be calculated using rate expressions such as those given in Avery[9] and Weiss and Longwell.[10] Using that of Weiss and Longwell,[10] the calculated blowout curve shown in Figure 5 is obtained. Also shown are the correlating curves taken from DeZubay[3] and Longwell, *et al.*[6] The calculated curve could be superimposed on the experimental curves by dividing by factors of approximately 3 to 6 giving fair qualitative agreement. The reasons for the poor performance relative to what appears possible is not accurately known. It is fairly certain that the volume employed in the calculation is not completely utilized and this might easily account for a factor of 2 or 3; however, it is also probable, that in this case, too high an air flow into the mixed zone

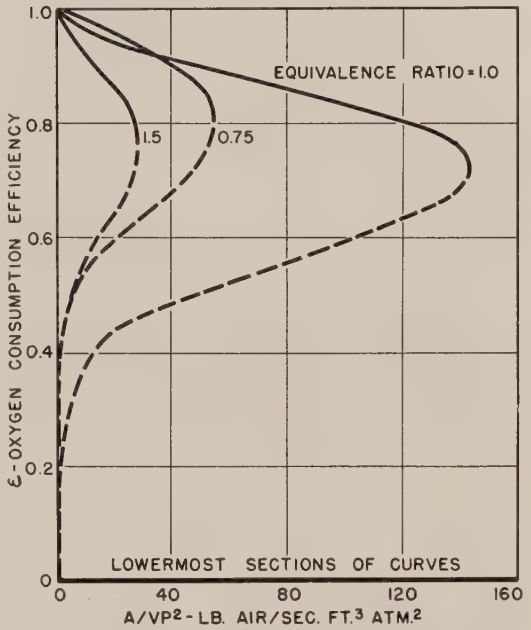

FIG. 4. Calculated combustion efficiency for a homogeneous reaction.
Hydrocarbon fuels and air Temperature = 260°F

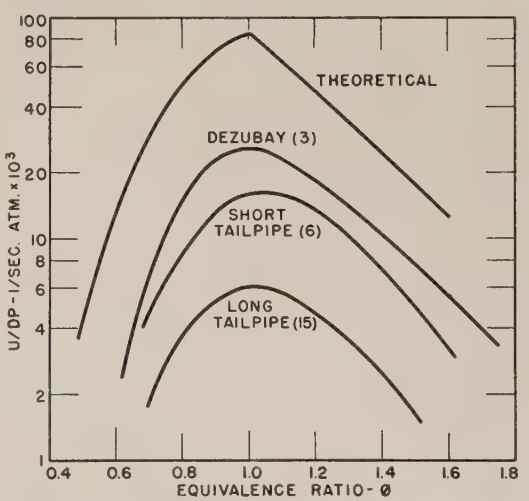

FIG. 5. Calculated and measured stability limits of baffles.

was assumed. High speed pictures show that the mixing pattern undergoes large fluctuations, eddies break off, and there are probably large changes in the rate of addition of fresh mixture and of loss of burned mixture. Heat losses from the combustion zone have a large effect. For example, 5 per cent heat loss, according to the rate expression used in this discussion, will reduce the maximum combustion rate by a factor of 1.4 and 10 per cent loss will reduce it by a factor of 2. The curve labeled long tailpipe[15] was taken using

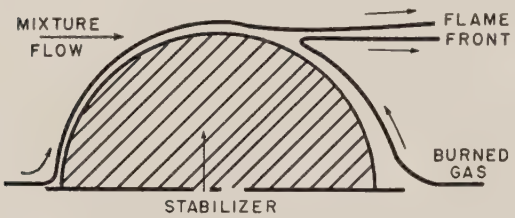

FIG. 6. Proposed flame anchoring mechanism[12].

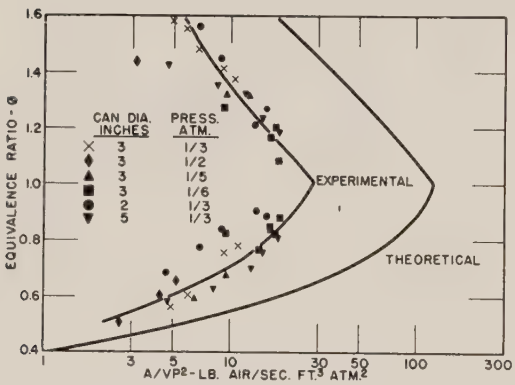

FIG. 7. Calculated and measured stability limits of can stabilizers.
Temperature = 200°F Fuel = No. 1 solvent naphtha

1½ and 2¼ in gutters at pressures ranging from ⅓ to 1 atm. Combustion was essentially complete in this tailpipe, which is in contrast with the other two curves where very short tailpipes were used and precautions were taken to avoid pressure and flow pulsations. This pronounced reduction of stability has also been noted by Scurlock[4] and others and is presumably due to flow fluctuation set up by the interaction of the flame and the flow. This problem of flow pulsation is obviously of great practical importance and, while considerable discussion of this subject has appeared in the literature, the variables determining the amplitude of the fluctuations are not well understood.

A comparison of the results available in the literature was given by Longwell[7] and more recently by Zukoski.[21, 22] The work of Haddock[5] and Zukoski[21, 22] indicates that the nature of flow at the boundary immediately downstream from the baffle changes from laminar to turbulent at a Reynolds' number, based on baffle width, of approximately 2×10^4. This was shown by photographs where the change in the nature of the flow was quite obvious and was also indicated by a change in the slope of the blowout velocity vs. Reynolds' number curve in this region. Further evidence of the change in flow is given by the shift in the equivalence ratio of maximum blowout velocity observed at low Reynolds' numbers. It has been found by Williams and Shipman[13] and Zukoski[21, 22] that for fuels which diffuse more slowly than oxygen the fuel/air ratio is lower in the recirculation zone than in the main air stream. This accounts for the shift in limits and is of importance below Reynolds' numbers of 10^4. Zukowski has shown that if the transition region around Reynolds' numbers of 10^4 is neglected, the results of all investigators examined, except Longwell, can be correlated by $U/D^{0.5}$. Longwell's data[6] require an exponent of 1.0. Since these data were taken in a more turbulent air stream than the others and since the flame stabilizers were large and were of such a design as to develop a more turbulent boundary layer, it may be that, as Zukoski points out, a third, more turbulent, regime exists.

For a mechanism of stabilization as described by Barrère and Mestre[12] and by Spalding[14] may be important. As illustrated by Figure 6, a laminar or turbulent flame front is assumed to start at the point of separation, ignition being caused by the hot recirculated gases. Reaction in this case takes place in a much smaller zone and stabilization by this mechanism would not be as effective as by one in which the total volume behind the baffle was used efficiently.

Can Stabilizers

In the can type stabilizer as illustrated in Figure 1, a recirculation zone exists upstream from the holes through which the air enters. Part of the air and fuel from the impinging jets flows upstream and mixes with hot combustion products in the recirculation zone. The hot gases flow out between the jets and ignite the mixture flowing downstream. This type of stabilizer is used in turbojet combustors and is particularly useful in can type ramjet combustors.

A few studies[15] have been made in which the stability of cans of this type was determined under conditions where a known amount of homogeneous fuel-air mixture flowed through the holes in 2–5-in diameter cylindrical cans similar to that shown in Figure 1. It was found that if the air rate were increased above a certain value for a given pressure and fuel/air ratio a blowout similar to that observed for baffles occurred. It was possible to estimate the amount of mixture flowing upstream by velocity and composition measurements. The analysis of blowout discussed above applies to this case if it is assumed that the system is adiabatic and that mixing is complete in the region upstream of the inlet holes. A comparison of predicted and observed performance can again be made as shown in Figure 7. It is seen that the group A/VP^2 correlates the data for the pressures used, and that the curves have the same shape as the predicted stability curves. The predicted curve, however, is translated to higher values of A/VP^2 by a factor of approximately 4. Again there appears to be considerable room for improvement before the final limitation of chemical kinetics is reached. One suspects, of course, that the mixing in the reaction zone is not perfect so that parts of this zone are not fully utilized. Heat losses from the can walls are also important; however, detailed studies of flow and combustion in this device are not available.

Flame Spreading

The baffle or the can type flame stabilizers just discussed both liberate a relatively small amount of heat compared to the requirements of a ramjet. This burned material then serves as a nucleus from which the flame that consumes the major amount of fuel develops. The flame downstream from a baffle grows by propagation through the unburned mixture. Flow is quite turbulent so that propagation is more rapid than would be predicted from the laminar burning velocity of the mixture. In some cases the mixing is so intense that the flame has many of the characteristics typical of a reaction rate controlled system. The rate of mixing in this type of flame depends on the nature of the flow and of the flame. Much better control of mixing and combustion rate can be obtained by use of a can type combustor where the flame zone is confined by a metal partition as shown in Figure 8. Unburned mixture enters through holes in the can at a rate determined by the designer.

Very few data on rate of flame propagation downstream from baffles have been published and none are available on cans. In the case of baffles, this study has been inhibited by the pronounced tendency for rough and unstable burning encountered in laboratory equipment with small baffles and a homogeneous air-fuel mixture. With care it is possible to avoid excessive pressure pulsations; however, the rate of mixing and therefore the rate of burning are dependent on the flow oscillations so a variety of results and considerable confusion can be expected in the early phases of this study.

A few data are available which give a general description of the flame downstream from a baffle.[1] Composition and velocity traverses have been made at a number of positions downstream from the 2¼ in gutter for which traverses in the recirculation zone were previously discussed. This baffle was 5 in long and mounted centrally between the walls of a 9 by 5-in rectangular duct. A homogeneous and vaporized mixture of petroleum naphtha and air flowed through the duct. Figure 3 shows velocity profiles at 10, 25 and 43 in downstream from the baffle and it is seen that the burned material in the center accelerates more rapidly than the mixture near the wall. The dashed line was calculated using the relations developed by Scurlock[4] and Tsien[16] for the velocity profile downstream from a line source. The experimental profile is much more rounded than the calculated one because the calculations assume no momentum transfer in the radial direction.

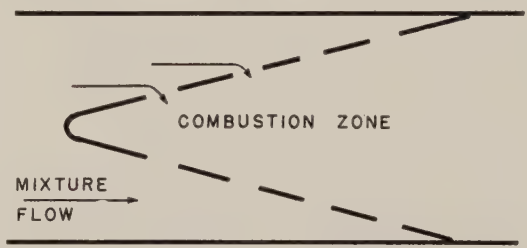

FIG. 8. Diagrammatic sketch of a can type combustor.

Figure 9 shows the time average efficiency for the same positions. The efficiency is highest in the wake of the baffle and decreases smoothly toward the walls showing that photographic studies would define the flame front with difficulty. Instantaneous photographs of a flame such as this[4, 12, 17] show that the luminous part of the

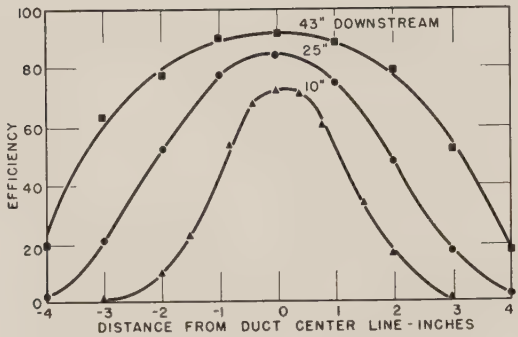

FIG. 9. Efficiency profiles downstream from a V-gutter.
Equivalence ratio = 1.0 Velocity = 170 ft/sec
Temperature = 250°F 2¼" V-gutter
Pressure = 10" Hg abs. Fuel = No. 1 solvent naphtha

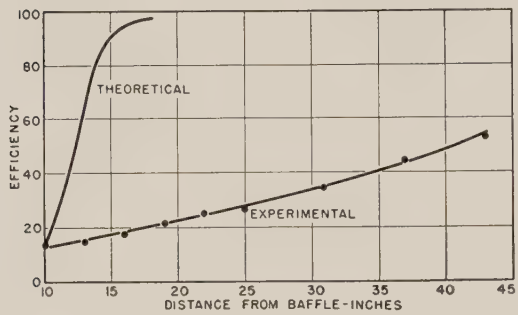

FIG. 10. Rate of combustion in 9 x 5 inch duct.
Equivalence ratio = 1.0 Velocity = 170 ft/sec
Temperature = 250°F Pressure = 10" Hg abs.
Fuel = No. 1 solvent naphtha

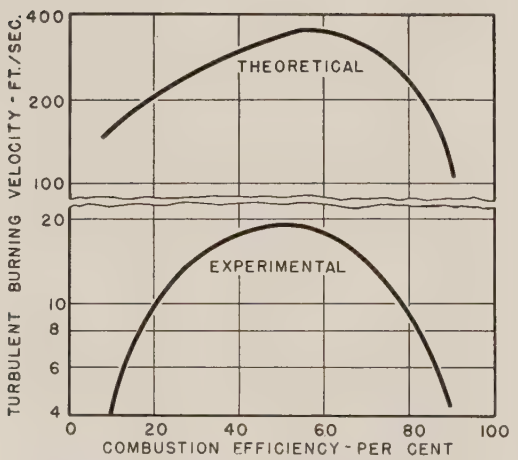

FIG. 11. Turbulent burning velocities.

flame is very irregular in shape with large changes in radial position with time. The efficiency is therefore a time average of unburned and burned pockets of mixture and possibly some partly burned material from regions of very intense mixing. The information from Figures 3 and 9 can be combined to give the average efficiency as a function of distance downstream from the baffle as shown in Figure 10. The curve is concave upward showing an increase in burning rate with distance.

It is possible to convert the slope of this curve to a burning velocity analogous to the turbulent burning velocity commonly used by the following relation:

$$S_t = \frac{d\epsilon}{dx} \frac{Vo \cos\theta}{W}$$

where S_t is the turbulent burning velocity

$\frac{d\epsilon}{dx}$ is the rate of change of efficiency with distance

Vo is the total volumetric flow rate

W is the width of the duct

θ is the angle of the imaginary flame front to the duct walls ($\cos\theta \cong 1$ for this case).

The burning velocity calculated from Figure 10 is shown in Figure 11. The curve rises to a maximum value of 19 ft/sec and drops to zero at 100 per cent combustion efficiency. The high efficiency part of the curve is drawn in from similarity with other curves since the data, in this case, did not extend beyond 60 per cent efficiency. The maximum value of 19 ft/sec is about 15 times the laminar burning velocity of 1.3 ft/sec. This indicates a very high rate of mixing well beyond the range described by the current theories of turbulent flame propagation by wrinkled flame fronts. It has not been possible to account for such high burning rates by considering the effect of turbulence in the incoming air stream and a number of investigators have discussed mechanisms by which the flame itself can increase turbulence to account for this increase in burning rate. Westenberg[18] has measured turbulent intensity in such a confined flame and has found essentially no increase in the turbulent intensity as determined by dispersion of a small helium jet. It is probable that the large eddies, shown in photographs of these flames, which are caused by flow pulsations and by shear due to velocity gradients are responsible for a large part of the mixing with the turbulence doing the finer scale mixing within these larger areas. Quantitative descriptions of this process are, however, lacking.

It is interesting to compare this rate of combustion with that estimated to be the maximum possible. This maximum rate can be estimated using an approach similar to that used by Avery and Hart[19] in their discussion of can combustor performance. The reaction rate expression is the same as that used in the discussion of stability.

As shown in Figure 12, the reaction rate expression describing combustion predicts a maximum combustion rate at an efficiency of approximately 75 per cent. This gives the optimum combination of high concentrations of reactants and high temperature. If one wishes to liberate heat at the maximum rate then fresh material should be mixed into burned material at a rate such that this efficiency is maintained. If R_m is this maximum reaction rate on a volume basis, then

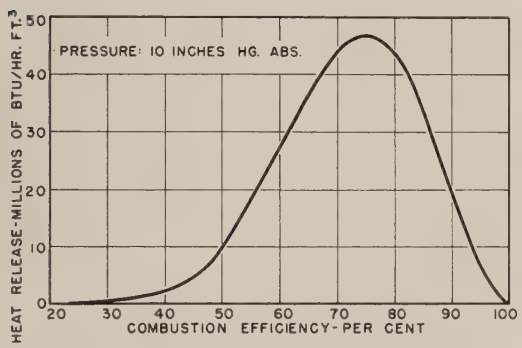

FIG. 12. Predicted heat release rate as a function of efficiency.

$$\mathring{m} = \frac{R_m V}{\epsilon}$$

where $\mathring{m}$ is the maximum rate of addition of fresh material

V is the volume of burned material into which $\mathring{m}$ is mixed.

Since V increases as more material is added to the combustion zone, the rate of addition increases until all the material is mixed into the combustion zone. The efficiency then rises as fuel and oxygen react and the rate as shown in Figure 12 drops off approaching zero at 100 per cent efficiency. A calculation of the rate for conditions corresponding to the experimental conditions of Figure 10 gives the theoretical curve in Figures 10 and 11. It is seen that this curve has much the same shape as the experimental curve both that the rates are higher by a factor of about 20. This indicates, as one might expect, that the local efficiency is not at the optimum value at all points, and that improvements in the mixing would cause an increase in rate. The possibility of doing this is indicated by the work of Mullen, Fenn and Garmon[20] who obtained reasonably high efficiencies with a 2-in ramjet in a length of 14 in as compared to the 48 in in the example chosen.

Conclusion

The availability of an empirical expression for reaction rate of fuel and air as a function of efficiency makes it possible to evaluate the possibilities for improvement of flame stabilizing and spreading devices. Such a comparison shows that by improved mixing it is possible to gain considerably in performance and that present performance must be very sensitive to changes in the mixing rate and mixing patterns. This is illustrated by the great sensitivity of stability to the flow fluctuations that are set up by the flame as it spreads through the air-fuel mixture. For an adequate understanding then, the interaction of flame spreading and flame stabilization must be studied. The problem of flame spreading has received relatively little attention and should be a fertile field for research. A considerably more detailed knowledge of the mechanism of flame stabilization without the complication of flow pulsations is also needed.

Acknowledgment

The author is indebted to the Bureau of Ordnance, Department of the Navy, and to the Standard Oil Development Company for permission to publish the data on can flame stability and on flame spreading in a duct.

REFERENCES

1. NICHOLSON, H. M., AND FIELD, J. P.: *Third Symposium on Combustion, Flame and Explosion Phenomena*, p. 44. Baltimore, The Williams & Wilkins Co., 1949.
2. LONGWELL, J. P., FROST, E. E., AND WEISS, M. A.: Ind. & Eng. Chem., *45*, 1629 (1953).
3. DEZUBAY, E. A.: Aero Digest, *61*, 54 (1950).
4. SCURLOCK, A. C.: Mass. Inst. of Tech., Meteor Report. 19 (1948).
5. HADDOCK, G. H.: Calif. Inst. of Tech., J.P.L Report. 3-24 (1951).
6. LONGWELL, J. P., ET AL.: *Third Symposium on Combustion, Flame and Explosion Phenomena*, p. 40. Baltimore, The Williams & Wilkins Co., 1953.
7. LONGWELL, J. P.: *Fourth Symposium (Inter-*

national) on Combustion, p. 90. Baltimore, The Williams & Wilkins Co., 1953.
8. Weir, A., Jr., et al.: Univ. of Mich., Report, UMM-74 (1950).
9. Avery, W. H.: To be published.
10. Longwell, J. P., and Weiss, M. A.: To be published.
11. DeZubay, E. A.: Paper 54-SA-27, presented at Semi-Annual Meeting, Am. Soc. Mech. Engrs., Pittsburgh (June 1954).
12. Barrère, M., and Mestre, A.: *Selected Combustion Problems, AGARD*. London, Butterworth Scientific Publications, 1954.
13. Williams, G. C., and Shipman, C. W.: *Fourth Symposium (International) on Combustion*, p. 733. Baltimore, The Williams & Wilkins Co., 1953.
14. Spalding, D. B.: Aircraft Engineering, *25*, 264 (1953).
15. Unpublished data, Standard Oil Development Company.
16. Tsien, H. S.: J. Appl. Mech., *18*, 188 (1951).
17. Shonerd, D. E.: California Institute of Technology, Jet Propulsion Laboratory Report 3-18 (June 4, 1952).
18. Westenberg, A. A.: J. Chem. Phys., *22*, 814 (1954).
19. Avery, W. H., and Hart, R. W.: Ind. & Eng. Chem., *45*, 1634 (1953).
20. Mullen, J. W., II., et al.: Ind. & Eng. Chem., *43*, 195 (1951).
21. Zukoski, E.: Calif. Inst. of Tech. Ph.D. Thesis (1954).
22. Zukoski, E.: Calif. Inst. of Tech., Jet Propulsion Lab. Progress Report 20-220, April 12, 1954.

Discussion by Luigi Crocco*

The influence on the stability of the flame of the downstream geometry can be quite important, as Dr. Longwell has shown, because of the appearance of oscillatory flow conditions that have a tendency to decrease substantially the blowout velocity. The suppression or the limitation of these oscillatory conditions is therefore quite important for the best operation of the flame holder.

Any self-sustained oscillation is the result of two contrasting factors: an exciting mechanism which produces energy to entertain the oscillation, and a damping mechanism which absorbs energy. As far as ramjets are concerned, the first mechanism is still obscure, though there is no doubt it is related to the combustion process. However, certain aspects of the damping mechanism have been recently made clear by theoretical analysis which shows the importance of the exhaust nozzle and of its geometry in damping energy. It seems to me that this property has not been sufficiently investigated experimentally, and that it could provide a simple and inexpensive means of getting rid of disturbing oscillations.

* Robert H. Goddard Professor of Jet Propulsion, Princeton University.

VII

ON THE KINETICS OF ELEMENTARY GAS PHASE REACTIONS AT HIGH TEMPERATURES[a]

By KURT E. SHULER

Introduction

In writing a survey paper on a topic as extensive as that indicated by the above title, an author is usually faced with such a plethora of accumulated data that the main problem reduces to that of judicious selection. This problem is usually solved by treating most exhaustively those aspects of the field in which the author is particularly interested and then giving a less detailed treatment of some of the other phases, proceeding all the while in the fervent hope that the end product will give a properly weighted and fairly comprehensive picture of the whole field.

In writing about high temperature kinetics which is somewhat arbitrarily defined here as chemical kinetics in the region from about 1000°K to 3000°K the problem is, however, quite different. There is at present still a great dearth of data regarding the more fundamental aspects of this field and the author is thus limited by ne-

[a] This work was supported by the Bureau of Ordnance, Department of the Navy, under Contract NOrd-7386.

cessity to a discussion which is neither properly weighted nor at all comprehensive. It so happens that the facet of the field in which most of the research has been carried out, namely the study of non-equilibrium distributions in chemical reactions at high temperatures, coincides with the special interest of the author so that a fairly detailed treatment could be presented. For some of the other topics, however, data and/or theoretical treatments are either scarce or altogether lacking so that it has been possible only to indicate the nature of the problem rather than to discuss the work that has been done toward its clarification. Among these problems are the following: the development of "energy chain" reactions involving vibrationally and/or electronically excited species; modifications in the reaction mechanism due to the high concentration of atoms and radicals in high temperature systems; and changes in reaction mechanisms due to the change in the relative efficiency of intra- and intermolecular energy transfer with increasing temperature.

This survey on the kinetics on elementary gas phase reactions at high temperatures is thus divided essentially into two main parts. The first part consists of a rather detailed discussion of the origin, the nature and the effects of the non-equilibrium distribution of energy in high temperature chemical reactions; in the second part there is given a less detailed discussion of the other topics listed above. Throughout this discussion, the author has tried, as a leitmotif, to focus his and the reader's attention on what he considers to be the most characteristic property of reactions at high temperatures, namely, the large amount of energy which is added to and contained in the reaction system. This large amount of energy, whether it be added externally from a heat bath or furnished internally by the exothermicity of the reaction, is probably responsible for most of the characteristic kinetic phenomena which require specific consideration in high temperature reaction systems. It is the author's hope that even a short discussion of these problems will stimulate some of the research which is so necessary for our further progress in this interesting and difficult field.

I. Non-equilibrium Distributions in High-Temperature Reaction Systems

GENERAL BACKGROUND

It has been recognized for many years that by its very nature a chemical reaction must produce a perturbation in the (initial) Maxwell-Boltzmann distribution of energy in a reaction system and that this perturbation will persist until the system, after the completion of the reaction, has returned to its thermodynamic equilibrium by inelastic collisions with the surrounding heat bath[1]. The extent of the departure from equilibrium in the system will depend upon the relative magnitudes of the rates of chemical reactions (i.e., the rate of transformation of reactants to product) and the rates of energy exchange between the molecules in the reaction system. If the rate of the chemical transformation is small compared with the rate of energy exchange, the perturbation of the initial equilibrium distribution will be small and the reaction system can be treated as an equilibrium system which is not affected by the unfolding of the chemical reaction. Such a time invariant equilibrium hypothesis is the basis of both the collision theory and the absolute (quantum-statistical) theory of reaction rates. If, however, the rate of the chemical transformation exceeds the rate of intra- and intermolecular energy exchange, there may develop a large-scale perturbation of the initial Maxwell-Boltzmann distribution of energy. Under these conditions the equilibrium hypothesis underlying the present theories of chemical kinetics may no longer be tenable and its application to these systems may lead to an incorrect interpretation of the experimental observations.

In some theoretical studies on these questions, to which more detailed reference will be made below, it was found[2-4] that the perturbation of the initial equilibrium distribution during the course of a chemical reaction will probably be serious only for reactions in which the activation energy is of about the order of kT, i.e., $E_{act}/kT \leqslant 5$. Since for most homogeneous unimolecular and bimolecular reactions at around room temperature up to about 1000°K one has $E_{act}/kT \gg 5$, the perturbation of the initial Maxwell-Boltzmann distribution will most probably be negligible and does not have to be taken into account in formulating the rate equations. In high temperature elementary reactions involving atoms and/or radicals it is, however, quite possible that $E_{act}/kT \leqslant 5$. Thus, for instance, the reaction $O + H_2 \rightarrow OH + H$ taking place in a flame at about 2500°K would have an E_{act}/kT of about unity. In reactions of this type it is clearly advisable to investigate in some detail the possible departure from equilibrium and to study the distribution of energy in the reaction system during the course of the chemical reaction.

Before considering the experimental evidence relating to the non-equilibrium distribution of energy in high temperature reaction systems and before presenting some of the theoretical studies which have been devoted to this question, it will perhaps be worthwhile to examine this problem in its more general aspects. When a fast chemical reaction takes place in a high temperature reaction system, the energy-rich reactant molecules may be transformed into products (or intermediates) more rapidly than they can be replenished by the inelastic collisions in the reaction mixture. At the same time, particularly if the reaction is strongly exothermic, the product molecules may be formed initially with a mean energy in excess above that corresponding to the thermal equilibrium of the heat bath. Under these circumstances the reaction system would be characterized in the early stages of the reaction by an energy distribution of reactants in which there is a depletion of molecules in the high energy tail of the distribution and in which there is an excess of product molecules with abnormally high energy. The temporal behavior of such a non-equilibrium system will depend upon whether it is a closed or an open one. In a closed system in contact with an isothermal heat bath the energy distribution will adjust in time to the equilibrium Boltzmann distribution with a final temperature equal to that of the heat bath. In an open reaction system, the non-equilibrium distribution brought about by the chemical reaction may persist under certain circumstances as the (time invariant) steady state distribution[5]. In either case, the resulting non-equilibrium distribution of reactant and product molecules in their various internal and translational energy levels prevents the specification of the reaction system by its *temperature* and a different specification will be necessary to describe the energy distribution of the system.

This can at present be done only in a rather formal manner. To specify the molecular distribution, for both equilibrium and non-equilibrium systems, we can write

$$n = f(p_1 \cdots q_r , t)\delta p_1 \cdots \delta q_r \qquad (1)$$

for the number of molecules which have coordinates and momenta $p_1 \cdots q_r$ in the region of space $\delta p_1 \cdots \delta q_r$. The distribution function $f(p_1 \cdots q_r , t)$ depends upon the coordinates and momenta of the molecules and on the time t, since the distribution in a non-equilibrium system will in general be a function of time. For a Boltzmann equilibrium distribution, the distribution function f becomes

$$f = f(\epsilon_1 \cdots \epsilon_r , T) = nCe^{-\epsilon(p_1 \ldots q_r)/kT} \qquad (2)$$

where C is a constant entering into the normalization of the distribution. This distribution, being the equilibrium distribution, is independent of time and depends only upon the energy ϵ as a function of the coordinates and momenta. The temperature T is the single parameter required in this expression to specify the distribution of molecules among the various energy levels. It can now readily be shown by combining equations (1) and (2) and integrating over all space that n_i, the number of molecules in the state i, is given in an equilibrium system, by the well known expression

$$n_i = n \frac{e^{-\epsilon_i/kT}}{\sum_i e^{-\epsilon_i/kT}} \qquad (3)$$

where the distribution of the molecules among the (known) energy levels is then again specified unequivocally by the temperature T of the system. In a non-equilibrium system it is, however, not possible to write a distribution function such as given in equation (2). About the best that can be done in the absence of any detailed and specific information about the reaction system is to write

$$f = f(\epsilon_1 \cdots \epsilon_s , k_{12} \cdots k_{sr} , t) \qquad (4)$$

where the distribution now depends upon the position of the energy levels $\epsilon_1 \cdots \epsilon_s$ the transition probabilities $k_{12} \cdots k_{sr}$ for the transition between any and all levels, and the time t at which the observation is made. Such a non-equilibrium distribution can, in general, no longer be characterized by a *single* parameter such as the "temperature" but requires instead explicit introduction of all the transition probabilities for a complete specification of the system. In a formal and incomplete way such a non-equilibrium system could be specified as a function of time, by the mean energy $\bar{\epsilon}$

$$\bar{\epsilon}(t) = \frac{\int \cdots \int \epsilon f(p_1 \cdots q_r , t) dp_1 \cdots dq_r}{\int \cdots \int f(p_1 \cdots q_r , t) dp_1 \cdots dq_r} \qquad (5)$$

where $\epsilon = \epsilon(p_1 \cdots q_r)$. This expression can however, be evaluated only if the distribution function and the dependence of the energy on the

momenta and coordinates are known for the system under study.[b]

In the absence of any specific information on the mean energy of non-equilibrium reaction systems, it is important to ascertain how far the concept of a "temperature" can be carried over to these systems. Strictly speaking, a system whose energy in all degrees of freedom is not distributed according to the Boltzmann law can not be characterized by its "temperature" as given in equation (2). It is, however, possible in many of the experimentally studied examples of non-equilibrium systems to determine a quantity which is related to the equilibrium temperature. From equation (3) we find for a Boltzmann equilibrium system that

$$\frac{n_i}{n_0} = e^{(\epsilon_0 - \epsilon_i)/kT}. \qquad (6)$$

From equation (6) it follows that for an equilibrium system a plot of $\ln(n_i/n_0)$ vs. $(\epsilon_0 - \epsilon_i)$ will give a straight line with a slope of $1/kT$. We may adopt this also as an operating definition of temperature for non-equilibrium systems and say that whenever a relationship of this type is found to hold, the system is at the temperature T. The reason why a relationship such as given in equation (6) may obtain in systems which deviate from a Boltzmann distribution is connected fundamentally with the fact that the distribution function relates to the *probability* that the energy in a system consisting of a *very large number* of *nearly independent particles* is distributed in a certain way. Such types of probability distributions often have an exponential form as witness for instance the Gaussian and Poisson distributions. It would, therefore, not be too surprising if an exponential distribution similar to the Boltzmann distribution of equation (6) would also obtain for some non-equilibrium reaction systems. An exponential energy distribution which results in a linear relationship between $\ln(n_i/n_0)$ and $(\epsilon_0 - \epsilon_i)$ with a concomitant effective temperature T may be called a pseudo-Boltzmann distribution.

For diatomic and polyatomic radicals and molecules it is necessary to consider in some detail the distribution of energy in and between the various degrees of freedom. As long as it is permissible to write the total energy of a species in a given level as the sum of the energies of all the various degrees of freedom, i.e.,

$$\epsilon = \epsilon_{\text{transl}} + \epsilon_{\text{int}}$$
$$= \epsilon_{\text{transl}} + \epsilon_{\text{rot}} + \epsilon_{\text{vibr}} + \epsilon_{\text{electr}} + \epsilon_{\text{ioniz}} + \ldots$$

the argument given above can be applied to all of the degrees of freedom so that it is possible to speak of rotational "temperatures", vibrational "temperatures", etc., in the reaction systems depending upon whether one is studying the distribution of molecules in the rotational or the vibrational energy levels. In an equilibrium system, these temperatures are all identical and the energy distribution in the system is defined uniquely by its equilibrium temperature T. This is, however, not necessarily the case in a non-equilibrium or non-equipartition system where it is possible to have different temperatures corresponding to the different degrees of freedom. Such an energy distribution could conceivably arise in a non-equilibrium reaction system with a pseudo-Boltzmann distribution when the rate of energy transfer within each degree of freedom is much more rapid than the transfer of energy between different degrees of freedom[6]. It is, therefore, necessary when studying energy distributions in chemically reacting systems, to investigate *separately* the distribution of molecules in their translational, rotational, vibrational and electronic energy states[7].

In a reaction system, in which the chemical reaction has perturbed the initial Maxwell-Boltzmann distribution of energy, one might thus have any one of the following cases of a non-equilibrium energy distribution; some of these have been observed experimentally.

(A) *The perturbation of the Boltzmann distribution is not too strong so that a pseudo-Boltzmann distribution of energy is maintained in the system.* It is then possible, from the operational definition of temperature given above, to measure a "temperature" for the reaction system. This temperature may be quite different from the initial equilibrium temperature which obtained prior to the initiation of the reaction. In general, the measured "temperature" of the non-equilibrium system will be higher than that of the initial equilibrium distribution since the energy added to

[b] In an equilibrium system with a Boltzmann distribution of energy one has $\bar{\epsilon} = \frac{1}{2}\, kT$ so that in this case there is a simple and direct connection between the mean energy and the temperature.

or released in the system may go preferentially into exciting the molecules or radicals into the higher energy levels.

(1) The transfer of energy by inelastic collisions within in each degree of freedom is much more rapid than the transfer of energy between the different degrees of freedom. There may then obtain a pseudo-Boltzmann distribution of energy in each degree of freedom, but the "temperatures" corresponding to the different degrees of freedom will be different[6], i.e., $T_{trans} \neq T_{rot} \neq T_{vibr} \neq T_{electr}$ etc.

(2) The transfer of energy by inelastic collisions in one particular degree of freedom is very rapid, while the transfer of energy in the other degrees of freedom and between the different degrees of freedom is less efficient. There may then obtain a pseudo-Boltzmann distribution of energy in that one degree of freedom with a corresponding "temperature", while the distribution of energy in the other degrees of freedom departs so radically from a Boltzmann-like distribution that no temperatures can be assigned to them. The degrees of freedom which most rapidly adjust to a Boltzmann or pseudo-Boltzmann distribution of energy are the translational and rotational ones since the quanta of energy which have to be adjusted by inelastic collisions are relatively small. A pseudo-Boltzmann distribution and its corresponding "temperature" are thus most likely to be found for the translation and the rotation of the molecules[7].

(B) *The perturbation of the Boltzmann distribution is very strong and no Boltzmann-like distribution is maintained in the system.* It is then not possible to measure or assign any "temperatures" for any of the degrees of freedom in the reaction system. The energy distribution in the various degrees of freedom can be specified only by calculating, if the prerequisite data are at hand, the mean energy $\bar{\epsilon}(t)$ residing in the translation and in the internal modes of motion. It may be possible in this case also to distinguish between subcases 1 and 2 above where now the mean energy $\bar{\epsilon}$ replaces the temperature in the above arguments.

EXPERIMENTAL RESULTS

The experimental study of the energy distribution in chemically reacting systems can be carried out most readily by spectroscopic means[8, 9]. The reaction systems on which most of the work along these lines has been done are various types of flames such as premixed flames, self-decomposition flames, diffusion flames, atomic flames, and the like. These are high temperature reaction systems, where the (adiabatic) temperature, depending upon the flame gases, is usually of the order of 1500°K to 3000°K. Since these flames are steady state flow systems, any non-equilibrium distribution of the reactants, intermediates, or products brought about by the chemical reactions will persist to some extent as the steady state distribution and will thus be amenable to spectroscopic analysis[5].

The results obtained in recent years in the spectroscopic study of the energy distribution in flames agree in general with the theoretically predicted behavior as outlined in the preceeding section. There can be little doubt that the chemical reactions which constitute a flame do give rise, in many cases, to non-equilibrium distributions of reactants, intermediates and products among their energy levels. Non-equilibrium energy distributions of flame constituents have been observed for all the internal degrees of freedom, i.e., for rotational, vibrational and electronic ones. Since the data have been collected and discussed at some length in a recent paper[5] (see also Gaydon and Wolfhard[9]), we will content ourselves here principally with a listing of the most pertinent observations and with a short discussion of the most recent work in this field.

Nonthermal ionization

There is some evidence that the ionization of various flame constituents in the reaction zone is in excess (by a factor of about 10^2) over that calculated for a reaction system in thermal equilibrium[10, 11]. Recent microwave attenuation measurements, which gave data averaged over both the reaction zone and the surrounding hot gases, indicated, however, that the ionization of the flame constituents (for a H_2-O_2 and C_2H_2-Q_2 flame) was thermal[12]. Additional research will be necessary to clarify this question.

Electronic non-equilibrium

(a) The formation of CO_2 in the electronically excited $CO_2(^3\Pi)$ state in the carbon monox-

ide flame by the reaction

$$O(^3P) + CO\ (^1\Sigma^+) + M \rightarrow CO_2^*(^3\Pi) + M \quad (7)$$

gives rise to CO_2* in large excess over that calculated for a system in thermal equilibrium[13, 14, 15].

(b) The formation of Na in the electronically excited Na* (^2P) state by vibrationally excited NaCl in dilute atomic flames

$$NaCl + Na(^2S) \rightarrow NaCl + Na^*(^2P) \quad (8)$$

gives rise to Na*(^2P) in large excess over that calculated from thermal considerations.[14, 16, 17]

(c) The excitation of Fe to very high energy levels when Fe in the form of traces of iron carbonyl is added to various hydrocarbon flames supported by oxygen or nitric oxide is another example of an electronic non-equilibrium distribution. The excitation of Fe to the upper electronic levels in these flames is considerably stronger than would be expected from purely thermal excitation[18, 19].

(d) In some recent work reported in this volume, Drs. Wolfhard and Parker have studied the spectra of various flames supported by the oxides of nitrogen[19]. They found that in the acetylene-nitric oxide flame the NH bands and the CH band at 3143 A appeared in *emission* against the radiation of the anode of a carbon arc [see plate 2 E of Wolfhard and Parker[19]]. Since the carbon arc is at an effective temperature of at least 3800°K, the concentration of electronically excited NH and CH must have corresponded to an electronic "temperature" in excess of 3800°K in order for the bands to appear in emission. The adiabatic equilibrium flame temperature of the C_2H_2-NO flame is between 2850°K and 3100°K depending upon the mixture ratio. It is clear, therefore, that the NH and CH radicals must have been formed by some chemical reaction in their excited electronic states in a concentration which considerably exceeds that given by a Boltzmann distribution with the equilibrium flame temperature. The OH radicals, which are also formed in this flame reaction, appear in absorption under the above condition. The above finding constitutes one of the most clear-cut examples yet observed of electronic non-equilibrium conditions in a high temperature reaction system.

Vibrational non-equilibrium

Owing to the theoretical and computational difficulties involved in obtaining accurate vibrational radiative transition probabilities, not too much work has been done on the vibrational distribution of energy. From the data that has been analyzed (H_2-O_2 and C_2H_2-O_2 flames) it appears that chemical reactions can and do give rise to non-equilibrium distributions of OH radicals among their vibrational energy states[7, 20].

Rotational nonequilibrium

There has now accumulated a large body of data which indicates quite strongly that chemical reactions in flames give rise to rotational non-equilibrium distributions of some of the reacting species. Among the species which have been studied, primarily in hydrocarbon flames, are OH,[7, 21] CH[22, 23] and C_2[24]. Some of the rotational "temperatures" which have been determined for these species range as high as 9000°K for OH in the low pressure (~3 mm) oxy-acetylene flame[21] and most of the rotational "temperatures" measured in these studies are from about 100°K to 1000°K higher than the adiabatic flame temperatures. The above cited work relates to the rotational distribution of electronically excited species. Recently, the rotation-vibration temperature of OH in an oxy-acetylene flame has been measured in the infrared for ground state OH($^2\Pi$)[25] and was found to be about 300 to 500°K lower than the rotational temperature measured in the $^2\Sigma^+$-$^2\Pi$ electronic transition. Since the radiative lifetime for the infrared emission of OH($^2\Pi$) is about 10^{-2} sec as compared with about 10^{-6} sec for the electronic $^2\Sigma^+ \rightarrow {}^2\Pi$ transition, it is evident that on the average an OH radical in the $^2\Pi$ state undergoing an infrared radiative transition must have suffered about 10^4 times as many collisions prior to and during the radiation as an electronically excited OH($^2\Sigma^+$) making an electronic radiative transition. There is thus a much greater opportunity for OH($^2\Pi$) to have reached thermodynamic equilibrium by inelastic collisions than is the case for OH($^2\Sigma^+$). The fact that the rotation-vibration "temperature" is much higher for the electronic transition than for the infrared one can then plausibly be interpreted to indicate that there is an abnormal excitation of the rotational-vibrational degrees of freedom of OH in the reaction $O_2 + C_2H_2$ which has been

brought back close to the thermodynamic equilibrium distribution after about 10^4 collisions. This figure stands in a reasonable relationship to some recent calculations which indicate that about 10^3 to about 10^6 collisions are required on the average to deactivate rotationally or vibrationally excited molecules to their lower quantum levels[26, 27].

THEORETICAL TREATMENTS

There have been several attempts to develop theoretical treatments which would give some information about the perturbation brought about in equilibrium systems by chemical reactions. Since the field of non-equilibrium statistical mechanics, on which a general treatment of this problem must be based, is to a large extent still *terra incognita*, the treatments and calculations which have been presented so far have been based on existing equilibrium techniques which were then applied to simplified models of reaction systems. To anticipate the results presented below one may say that a really satisfactory general solution of the problem of the perturbation introduced into a Maxwell-Boltzmann distribution by a chemical reaction has yet to be given and that much work remains to be done in this field.

The Curtiss-Prigogine kinetic theory model[3, 4, 28]

The theory of Curtiss and of Prigogine is concerned exclusively with the perturbation of the distribution of velocities, i.e., the Maxwell distribution, by a chemical reaction; they do not consider the effects of the reaction on the internal degrees of freedom. Their treatment consists of an extension of the Boltzmann integro-differential equation to include the effects of chemical reactions such as the change of concentration (density) of the various constituents by inelastic collisions as a function of time and the addition of energy by the heat of reaction. The extended distribution equation is then solved by a generalization of the Chapman-Enskog method[c] using a perturbed distribution function f of the form

$$f = f^0(1 + \phi) \tag{9}$$

where f^0 is the Maxwell distribution given by

$$f^0 = n\left(\frac{m}{2\pi kT}\right)^{3/2} e^{-mc^2/2kT} \tag{10}$$

[c] Professor Prigogine has informed me in a private communication that he has also solved the Boltzmann integro-differential equation by Grad's moment method [H. Grad: Commun. pure appl. Math. *5*, 455 (1952)] and has arrived at the identical solution with much less effort.

and ϕ is the correction introduced by the chemical reaction. The internal degrees of freedom could not be included in this treatment owing to the lack of detailed information on the nature and the extent of the intermolecular forces governing the collisional exchange and adjustment of internal energy. The correction term ϕ is found to have the form

$$\phi = -\frac{AkT}{E_{\text{act}}} \tag{11}$$

where A is a numerical constant involving the Sonine polynomials in terms of which the solution to the Boltzmann equation is obtained. Equation (11) which is due to Prigogine, shows that the the departure from equilibrium depends upon the the ratio of the temperature (or rather kT, the mean energy) to the activation energy. For reactions at high temperature and with a low activation energy, such as elementary processes involving atoms and radicals, the perturbation of the initial equilibrium can be quite pronounced. On the other hand, for reactions which take place at low temperatures and which have a fairly high activation energy, the perturbation of the Maxwell equilibrium distribution may be quite small. The numerical evaluation of the above results in terms of the reaction velocity by both Prigogine and Curtiss indicates that the departure from equilibrium becomes serious only when $E_{\text{act}}/kT \leqslant 5$.

It should be noted that the above correction term is expressed as a function of the temperature T even though it refers to a distribution which is no longer Maxwellian. This arises from the fact that the Curtiss-Prigogine treatments are perturbation calculations in which the zeroth order solution is the Maxwell distribution. The correction terms are then expressed in terms of the parameters of the Maxwell distribution. This points up the fact that this solution will only hold for distributions which are close to equilibrium. When the perturbed distribution function f is written out as

$$f = n\left(\frac{m}{2\pi kT}\right)^{3/2} e^{-E/kT}\left(1 - \frac{AkT}{E}\right) \tag{12}$$

it furnishes a good example of a pseudo-equilibrium distribution; in the above case it should be referred to as a pseudo-Maxwellian distribution. Since AkT/E must be much smaller than unity in order for the perturbation calculation to be valid, we can write

$$f \sim n\left(\frac{m}{2\pi kT}\right)^{3/2} e^{-E/kT} e^{-AkT/E} \tag{13}$$

which after some rearrangement becomes

$$f \sim n\left(\frac{m}{2\pi kT}\right)^{3/2} e^{-\{E/kT[1+A(kT/E)2]\}}$$
$$\sim n\left(\frac{m}{2\pi kT}\right)^{3/2} e^{-[E/kT(1+\delta)]} \tag{14}$$

where $\delta \ll 1$. The distribution is thus still essentially exponential and a translational temperature can be determined from the operational definition of temperature given above. The temperature T appearing in equations (12) to (14) is the equilibrium temperature corresponding to the initial Maxwell distribution of velocities. If we now define a new quantity T_{tr} by

$$T_{tr} = \frac{T}{1+\delta} \tag{15}$$

and substitute this expression into equation (14), we find

$$f \sim n\left(\frac{m}{2\pi kT}\right)^{3/2} e^{-E/kT_{tr}} \tag{16}$$

where T_{tr} is then the translational temperature corresponding to the perturbed Maxwell distribution. It will be noted from equation (15) that $T_{tr} < T$. This result is a restatement of the findings of Curtiss and Prigogine that the reaction velocity obtained from the perturbed Maxwell distribution is less than the rate which is calculated from the initial equilibrium Maxwell distribution.

The Zwolinsky-Eyring discrete energy level model[29]

A different approach to this problem was taken by Zwolinsky and Eyring. They investigated the (time dependent) distribution of reactants and products among a set of discrete energy levels and then computed the ratio of the actual rate to the equilibrium rate for various special cases. These special cases were arrived at by using different values for the concentrations in the initial and final states and for the ratio of the transition probabilities governing the rate of transitions between the energy levels. If the reaction to be studied is first order, it is possible to write a set of n linear rate equations

$$\frac{dA_i}{dt} = \sum_j (k_{ji}A_j - k_{ij}A_i); \qquad i = 1, 2, \cdots n \tag{17}$$

which govern the rate of transition of species A between the n energy levels of the system, the k_{ji}'s being the transition probabilities (rate constants) for transition between levels j and i. The mathematical technique used in solving this set of linear equations with constant coefficients is identical with that used in studying the vibration of polyatomic molecules[30]. The solution is given formally by

$$A_i = \sum_{k=1}^{n} B_{ik}e^{\lambda_k t}, \qquad i = 1, 2, \cdots n \tag{18}$$

where the λ_k's are the characteristic roots of the matrix (secular determinant) obtained by setting $A_i = B_i e^{\lambda t}$ and where the B_{ik} are the eigenvectors of the matrix. It would be most reasonable to assume that the n energy levels $i = 1, \cdots n$ are vibrational ones in which case equation (18) would then give the distribution of reactants and products in their vibrational levels as a function of time.

As is well known from the related case of the vibrations of polyatomic molecules it has not proved possible so far to give an analytical solution for the eigenvalues λ_k and the eigenvectors B_{ik} for the general n level model. The solution to this n level problem would provide the distribution function of chemically reacting species (as a function of time) and would permit its comparison with the equilibrium Boltzmann distribution to ascertain the departure from equilibrium introduced by the chemical reaction. It is important to note that equation (18) contains all the transition probabilities k_{ij} since both λ_k and B_{ik} are explicit functions of k_{ij}. This is in line with the statement made earlier that any explicit expression for a non-equilibrium distribution must involve the detailed specification of all the transition probabilities between the energy levels. In this model the specification is made by means of the rate constants k_{ij} for the transfer of the molecults between the different energy levels; in the Curtiss-Prigogine model the specification is made in terms of the collision cross sections governing the transfer between the various translational energy states. It is this feature which distinguishes a non-equilibrium distribution function from the equilibrium one, since in the latter, *one* parameter, namely the temperature T, suffices for the complete specification of the distribution.

In the absence of any explicit expression for the distribution function $f(A_i, k_{ij}, t)$, Zwolinsky and Eyring evaluated equation (18) numerically for a 4 level model ($n = 4$) by choosing different values for the rate constants k_{ij} and for the initial concentrations at $t = 0$. Their results, which are

expressed in terms of the ratio Γ of the non-equilibrium rate to the equilibrium one, indicate that the chemical reaction does indeed perturb the equilibrium distribution in the reaction system as evidenced by the fact that the ratio $\Gamma \neq 1$. In agreement with the results of Curtiss and Prigogine it was found that the non-equilibrium rate was less than that calculated for a time-invariant equilibrium system and that the lowering of the reaction velocity amounted to about 20 per cent.

It should be emphasized here, however, that the calculations of both Curtiss and Prigogine as well as those of Zwolinsky and Eyring will not necessarily give a good picture of the condition to be expected for fast reactions taking place at high temperatures. The author is presently engaged in extending the scope of the Zwolinsky-Eyring model in order to determine the distribution function of reactants and products in a chemical reaction under more severe conditions of temperature and specific rates; the results will be published at a later time.

The Kramers diffusion model[31, 32]

An ingenious approach to this problem was taken by Kramers. He represented a chemical reaction by the diffusion over a potential barrier of particles moving in an external field of force and subject to Brownian motion. The rate of the reaction is then given by the diffusion current across the potential barrier and the energy distribution of the reacting species along the reaction coordinate q is given by the density distribution in momentum space. Mathematically speaking, this approach is based on the construction and solution of the equation of diffusion obeyed by a density distribution of particles in phase space.

Owing to the mathematical difficulties involved in a general solution, Kramers restricted his discussion to the case where the height Q of the potential barrier is very large compared with the mean thermal energy kT of the particles. His results are, therefore, not strictly applicable to high temperature reactions where the above condition does not necessarily hold. Thus, for instance, Kramers assumed that the rate of the reaction would be slow enough for the diffusion to be treated as a quasi-stationary process where the diffusion current (i.e., the rate of the reaction) and the energy distribution are time-invariant. This also means that the diffusion is slow enough so that the initial Boltzmann distribution of reactants will not be perturbed and will remain a Boltzmann distribution all during the reaction. These are, however, precisely the points about which some detailed information is desired. To make the Kramers model applicable to fast, high temperature reactions it would be necessary to solve the Kramers diffusion equation (equation (9) in Kramers[31]) without the assumption of a quasi-stationary state. Professor Prigogine in a private communication has indicated that such a program should be feasible; it might be added, however, that attempts of the present author along these lines have been singularly unsuccessful.

The Hulburt-Hirschfelder hydrodynamic model[33]

In the treatment of Hulburt and Hirschfelder, a chemical reaction is represented by the motion of a fluid in the configuration space of the reaction complex. The fluid here corresponds to the assembly of mass points which represent the reaction complex in configuration space, the motion of the fluid in space then corresponds to the chemical reaction. In this model of a chemical reaction all references to the details of molecular interactions are omitted and one is dealing with a continuum theory whose solution is to be found in the relevant equations of hydrodynamics. By making certain assumptions regarding the pressure and the viscosity of the fluid, it is possible to determine various macroscopic properties of the mass points (i.e., the reaction complexes) such as their average density, average momentum, and their average energy. It is not possible, however, from this treatment to obtain explicitly any detailed "microscopic" information about the *distribution* of energy in the reaction system. This approach, therefore, does not appear to be too well suited for the problem under discussion.

THE EFFECTS OF NONEQUILIBRIUM DISTRIBUTIONS OF ENERGY ON THE RATES OF ELEMENTARY REACTIONS

It is now of interest to consider some of the possible modifications introduced in the kinetics of chemical reactions by the occurrence of non-equilibrium distributions in a reaction system. Since the present quantitative theories of chemical kinetics, i.e., the collision theory and absolute rate theory, are based on the assumption that there is a time invariant Maxwell-Boltzmann distribution of energy in the reaction system, it is

evident that they cannot correctly represent the rates in systems where the basic assumption of time invariant energy equilibrium is no longer valid. This point has been discussed from the theoretical side in some detail in the papers referred to above[3,4, 28, 31]. An example of the type of effect which may be expected is furnished by the work of Prigogine and Mahieu[28]. They found that for a reaction of the type $A_0 + B \rightarrow A_1 + B$, which could represent a case of chemical quenching, the initial rate v will be given by

$$v = v^{(0)}(1 + 1.2\, x_{A0} x_B \Delta H / E_{act}) \qquad (19)$$

where $v^{(0)}$ is the equilibrium rate for a time invariant Maxwell distribution of velocities, x_{A_0} and x_B are the mole fraction of A_0 and B, ΔH is the heat of reaction, and E_{act} is the activation energy. It is evident from equation (19) that for a reaction which is very exothermic and has a low activation energy the measured initial rate v may be considerably larger than the calculated equilibrium rate $v^{(0)}$. This result may be explained in the following manner. In a fast exothermic reaction accompanied by a perturbation of the Maxwell distribution, the product molecules may be formed with a translational energy in excess of that given by the Maxwell distribution. By collisions, this excess energy is then transferred in part to the reactants with the consequence that the reaction rate is increased over that expected for a time invariant equilibrium system. The higher the exothermicity of the reaction, the larger would be the expected effect. A higher activation energy would, however, decrease its magnitude since it would bring about an overall decrease in the rate of the reaction and would thus permit a more rapid establishment of equilibrium conditions in the reaction system. The increase in the rate due to the exothermicity of the reaction can then be attributed to the operation of an energy chain occasioned by the perturbation of the Maxwell distribution which gives rise to products with a higher average energy than that predicted by equilibrium theory[d].

[d] This increase in the reaction velocity of an exothermic reaction is of a quite different type from that found in thermal explosions as treated for instance by Rice and his co-workers [A. O. Allen and O. K. Rice: J. Am. Chem. Soc., *57*, 310 (1935); H. C. Campbell and O. K. Rice: Ibid, *57*, 1044 (1935); O. K. Rice, A. O. Allen and H. C. Campbell: Ibid., *57*, 2212 (1935)] where the enhancement of the rate is considered to be due to the *equilibrium* rise in temperature in the reaction mixture (self-heating) when the heat produced by the fast exothermic reaction cannot be conducted away sufficiently rapidly by the walls of the container.

The above result, which refers to the non-equilibrium distribution of translational energy in a single step reaction, can be generalized to chain reactions of several steps and broadened to include the energy distribution in the internal degrees of freedom. In a sequence of elementary reactions which comprise the overall mechanism it is quite possible that the products of a very exothermic step are formed with an energy in excess of that given by an equilibrium Boltzmann distribution. If these species with higher than equilibrium average energy now react with another component of the reaction mixture in a subsequent step, the rate of that reaction could be considerably higher than predicted by equilibrium rate theory for the equilibrium "temperature". If this effect is sufficiently pronounced the rate of the overall reaction may be considerably larger than that given by equilibrium theory and its dependence on temperature may be quite different from that predicted by an Arrhenius type rate equation $v = A\exp(-E/kT)$. The picture developed here would seem to have some application to the theory of steady state flame propagation. It is assumed in most of these theories[34] that the rate of the overall chemical reaction is given by an equilibrium type rate equation. In view of the discussion given above it may, however, be worthwhile to consider the formulation of a flame propagation theory which takes into account the effects of non-equilibrium conditions in the reaction zone on the form of the rate equations. What is suggested here then is that in high temperature flame reactions one may be dealing with non-equilibrium energy chains which may require a somewhat different kinetic formulation for the overall rate than that given for radical chains by an equilibrium theory[36].

II. Energy Chains in High Temperature Reaction Systems

GENERAL BACKGROUND

It has been pointed out in the preceding discussion that one of the most characteristic features of high temperature reactions is the large amount of energy which is contained in the reaction system. As a consequence of this, the system will contain a rather large concentration

of high energy species. These atoms, radicals, and molecules with high translational and internal energy may be present either in their equilibrium concentration as given by the Boltzmann equation or they may be present, as discussed in Section I, in excess of equilibrium. In either case, it will be of interest to consider the possible modifications introduced in the reaction kinetics and the reaction mechanism by the presence of these high energy species.

It is now commonly accepted that chain reactions in the temperature region between 300°K and 1000°K take place by elementary reactions involving the participation of atoms and radicals in the reaction mechanism. The high reactivity of these species is due to the presence of an unpaired electron which makes for strong specific intermolecular forces and low activation energies. In high temperature reaction systems it is necessary, in addition, to consider the possibility of energy chains. In these types of chains the high reactivity of the species participating in the elementary steps is due to their high energy content. In energy chains, or for elementary reactions involving species of high energy, it is not necessary that the reacting species be an atom or a radical; it is only necessary that the species have a sufficiently high translational and/or internal energy to overcome the energy barrier of the reaction. The high reactivity of these species is thus not brought about by *specific* chemical affinities as in the case of radical reactions but rather by the *general* property of their high energy content. In essence, one of the central problems of flame propagation, namely whether the self-sustaining propagation of steady state flames is controlled by radical diffusion or by thermal conduction could well be rephrased according to the above discussion in terms of radical chains vs. energy chains. The occurrence of energy chains and reactions of energetic molecules has also been examined recently in connection with some radio-chemical and photochemical reactions where the energy is added to the reaction system by light quanta or nuclear radiation[37].

There are four types of processes about which additional information is required in order to obtain some understanding about the mechanism and the kinetics of energy chain reactions. These are the processes of excitation by which the highly energetic species are formed, the processes of intermolecular energy transfer by which the energy is transferred and transformed by inelastic collisions, the processes of physical quenching and radiation by which the excitation energy is removed, and the various chemical processes such as dissociation reactions, metathetical reactions, etc., which are initiated by the excited species. It is the interplay of these processes, some of which are presented schematically in Table 1, which will determine the relative importance of energy chains as compared with radical ones. Electronically and vibrationally excited species may under certain conditions be more efficient in initiating or propagating a chemical reaction than the corresponding radicals so that an energy chain may seem to be indicated. On the other hand, the lifetime of the energetically excited species will, on the average, be shorter than that of atoms and radicals since the processes of physical quenching and radiative deactivation, which play no role in radical chains, contribute to the removal of high energy particles from the reaction system. The chain length in an energy chain would thus be expected to be shorter than that of a radical one so that radical chains would appear to be more efficient from this consideration.

In order to ascertain the relative importance of these factors it would be necessary to study in detail all of the possible inelastic collision processes and elementary chemical reactions which may enter into a given energy chain. Various aspects of these studies have been reviewed recently. Thus, for instance, Massey and Burhop[38] have given a thorough discussion of the processes of collisional excitation, energy transfer, and physical quenching; Laidler[39] has discussed the problem of energy transfer and transformation in molecular collisions, Laidler and Shuler[14] have presented a detailed discussion of elementary chemical reactions involving excited electronic states, and the present author has developed some of the general correlation rules which govern the reactions of electronically and vibrationally excited species[40]. In view of the availability of these surveys it would only be repetitious to give another general review at this point. In place of this we will consider here primarily one important aspect of the problem which has not been treated explicitly by previous authors, namely, the influence of temperature on the efficiency of some of the processes listed in Table 1.

EXCITATION PROCESSES (PROCESSES 1 TO 4 OF TABLE 1)

Electronic excitation

The efficiency of electronic excitation by inelastic collisions (Process 1 of Table 1) where the relative kinetic energy of translation is changed into the internal energy of electronic excitation of one of the collision partners is at best rather small. Under the usual gas kinetic conditions, the relative velocity of the collision partners will be small compared with the velocity of the orbital electronic motion. The electrons therefore have sufficient time to readjust themselves during a collision to the slowly changing conditions without undergoing transitions between the electronic levels. The usual collision in chemically reacting systems will thus approximate to adiabatic conditions. Since the perturbation introduced by the gradual approach of the collision partners is rather weak it follows that if an electronic transition is to take place during the collision the energy difference between the electronic levels will have to be quite small. The efficiency of an electronic excitation by inelastic collisions will thus be a function of the energy difference, ΔE, between the electronic levels involved in the transition and of the relative velocity, v, of the colliding species. It can readily be shown[41] that a high efficiency for an electronic transition will be found only when

$$\frac{a\Delta E}{vh} \leq 1 \qquad (19)$$

where a is the range of interaction between the colliding species. This formula simply states that for a high efficiency of transfer of translational into electronic energy the time of collision, a/v, should be of the same order of magnitude as the natural frequency $\Delta E/h$ of the oscillator which has been chosen to represent the collision system. Since $v \sim (T)^{1/2}$ it follows that condition (19) is fulfilled more readily at higher temperatures and that the efficiency of collisional electronic excitation will increase, other things being equal, with increasing temperature[e].

[e] It should be realized that equation (19) has been obtained from quite general considerations rather than from a detailed analysis of the collision processes. Equation (19) thus represents a qualitative rather than a quantitative relationship between the temperature and the efficiency of excitation.

In electronic excitations brought about by chemical reactions (Reactions 2 and 3 of Table 1) the influence of temperature manifests itself in two ways. If equilibrium is maintained during the reaction the influence of the temperature on the rates of the reaction and thus on the efficiency of the production of excited products is given by the usual Arrhenius expression. The rate of formation of excited species thus increases exponentially with temperature. An added factor, in the case of non-adiabatic excitation reactions, is the requirement that the reactive collisions must be sufficiently vigorous. The probability, P, for a non-adiabatic reaction leading to electronic excitation is given by the expression (14, 38)

$$P = e^{-(4\pi^2\epsilon^2/hv|s_1-s_2|)} \qquad (20)$$

where ϵ is the resonance energy at the crossing of the potential surfaces, $|s_1 - s_2|$ is the absolute magnitude of the difference of the slopes at the crossing point of the surfaces and where v is the relative velocity of the colliding species in the neighborhood of the crossing point. In the absolute rate theory formulation of reaction kinetics the probability, P, for a non-adiabatic reaction will be contained in the transmission coefficient

TABLE 1. ATOMIC AND MOLECULAR COLLISION PROCESSES INVOLVING HIGH ENERGY SPECIES

Type	Schematic Representation
(1) Excitation	$A + B \rightarrow A + B^*$
(2) Excitation	$A + B + M \rightarrow AB^* + M$
(3) Excitation	$A + B + C \rightarrow AB + C^*$
(4) Physical quenching	$A^* + B \rightarrow A + B$
(5) Energy transfer	$A^* + B \rightarrow A + B^*$
(6) Dissociation reaction	$AB^* \rightarrow A + B$
(7) Dissociation reaction	$AB^* + M \rightarrow A + B + M$
(8) Metathetical reaction	$A^* + BC \rightarrow AB + C$
(9) Chemical quenching	$A^* + BC \rightarrow A + B + C$
(10) Association reaction	$A^* + B + M \rightarrow AB + M$

The asterisk indicates electronic, vibrational or rotational excitation.

A, B, C, and M may be either atoms or molecules depending upon the type of excitation.

κ. As can be seen from equation (20), P increases with increasing temperature since $v \sim T^{1/2}$; an increase in temperature may thus increase the rate of production of electronically excited species somewhat over that predicted solely on the basis of the exponential Arrhenius factor. For a detailed discussion of some of the other factors which influence the rates of chemical reactions leading to electronically excited species reference may be had to the papers quoted above[14, 38].

Vibrational excitation

Under the heading of vibrational excitation we consider the transfer of translational into vibrational energy. It is necessary here to treat three different cases, namely inelastic collisions with no chemical affinity between the collision partners, inelastic collision where there is a strong chemical interaction between the colliding species and chemical reactions leading to vibrationally excited species.

The influence of temperature on the efficiency of vibrational excitation by inelastic collisions involving species which have no strong chemical affinities (such as N_2 and O_2) can most readily be understood by following the treatment of Bethe and Teller[42] which is based on the semi-classical theory of inelastic molecular collisions put forth by Landau and Teller[43]. The effectiveness χ of a collision for the excitation of a vibrational degree of freedom is related to the ratio

$$\chi = \frac{\tau_c}{\tau_v} \tag{21}$$

where τ_c is the effective duration of the collision and τ_v the natural period of the vibration. Writing τ_c as

$$\tau_c = \frac{a}{v} \tag{21a}$$

where a is again the range of intermolecular forces ($a \sim 2$ to $5 \cdot 10^{-9}$ cm) and v is the relative velocity of the colliding species, and setting

$$\tau_v = \frac{1}{2\pi\nu} \tag{21b}$$

where ν is the natural frequency of the vibration, one obtains

$$\chi = \frac{2\pi\nu a}{v} . \tag{22}$$

The effectiveness of a collision in the excitation of a molecular vibration is then given by the condition $\chi \leq 1$ which states that the duration of the collision should be of the same order of magnitude or smaller than the period of the vibration. It will be noted that equation (22) and the order of magnitude condition imposed upon it is analogous to equation (19) for electronic excitation by inelastic collisions. This analogy arises from the fact that for an effective interchange of energy in inelastic collisions it is necessary that the collisions approach the conditions of nonadiabacity where the relative velocity of the encounter is comparable to the natural period of the degree of freedom concerned.

It will be seen from equation (22) that the condition $\chi \leq 1$ is more readily fulfilled for high relative velocities of the collision partners so that the effectiveness of vibrational excitation by inelastic collision involving the transfer of translational to vibrational energy increases with increasing temperature. To put this statement on a more quantitative basis we consider the case where the kinetic energy of the relative motion of the colliding molecules is kT, i.e.,

$$\tfrac{1}{2}\mu v^2 = kT \tag{23}$$

where μ is the reduced mass of the colliding molecules. For the velocity v given by equation (23), the values of χ is given by

$$\chi = 2\pi\nu a \left(\frac{\mu}{2kT}\right)^{1/2} . \tag{24}$$

This can be rewritten after some rearrangement as

$$\begin{aligned} \chi &= \left(\frac{a}{\sqrt{2}}\right)\left(\frac{h\nu}{kT}\right)^{1/2}\left(\frac{4\pi^2\mu\nu}{h}\right)^{1/2} \\ &= \left(\frac{a}{A\sqrt{2}}\right)\left(\frac{h\nu}{kT}\right)^{1/2} \end{aligned} \tag{25}$$

were $A = (h/4\pi^2\mu\nu)^{1/2}$ is the amplitude of the molecular vibration in the lowest quantum state. The first factor, which is temperature independent, shows that the efficiency of vibrational excitation depends upon the ratio a/A of the range of intermolecular forces to the amplitude of vibration. Since this ratio a/A is usually much larger than unity for collisions between weakly interacting molecules, the probability of the transfer of translational to vibrational energy is in general rather small. The second factor shows, as mentioned above, that the efficiency of vibrational excitation increases with increasing temperature. If one considers $h\nu$ as the energy of the

vibrational quantum excited in the collision, it follows furthermore from equation (25) that the efficiency of the vibrational excitation is enhanced, for a given temperature, for a collisional transition between higher lying vibrational levels where Δv is small. This is important since in chemical reactions involving vibrationally excited species it will be the molecules with high vibrational energy which will be most effective in bringing about the reaction.

The classical collision theory of Landau and Teller has been extended, among others, by Schwartz and Herzfeld[26] who treated the problem of energy exchange by inelastic collisions quantum mechanically by the method of distorted waves. They derived an explicit formula for the probability, $P_{1\to 0}$, of a vibrational de-excitation from quantum levels 1 to 0 during a single collision[f] and evaluated this expression for various gases as a function of temperature. Their results, which are given in Table 2, indicate quite clearly the marked effect of temperature on the efficiency of vibrational excitation. For some other calculations on the effect of temperature on the efficiency of vibrational de-excitation by inelastic collisions the paper by Castellan and Hulburt[44] may be consulted.

Table 2. Calculated Probabilities $P_{1\to 0}$ (Fractions of Effective Collisions) for Vibrational De-excitation in Inelastic Collisions as a Function of Temperature[26]

	T(°K)						
Gases	288	600	900	1200	1800	2400	3000
N_2 in N_2	10^{-12}	2×10^{-10}	3.2×10^{-9}	5×10^{-8}	1.1×10^{-6}	8×10^{-6}	1.6×10^{-5}
O_2 in O_2	3.0×10^{-9}	3×10^{-7}	3×10^{-6}	1.3×10^{-5}	8.6×10^{-5}	5.5×10^{-4}	1.5×10^{-3}
O_2 in N_2	2×10^{-8}	3×10^{-6}	3×10^{-5}	1.2×10^{-4}	7×10^{-4}	2×10^{-3}	4×10^{-3}

The above developed theory does not hold when the colliding molecules have a "chemical affinity" in the sense that there are strong attractive forces such as, for instance, between H_2O and CO_2. It would lead too far afield to go into any extended discussion of the resulting phenomena and the reader is referred instead to the paper by Widom and Bauer[45], who have discussed in some detail various aspects of this problem. The essential result for the purpose of this discussion is that the excitation of the vibrational degrees of freedom by inelastic collisions is much more efficient when there are attractive forces between the colliding species. In a chemical reaction where the colliding species have, by the very nature of the system, a chemical affinity, there is thus a good chance that collisions which do not bring about a chemical transformation may at least lead to vibrational excitation of one of the collision partners. In regard to the problem of the influence of temperature on the efficiency of this type of excitation, there are at present not sufficient data to permit one to draw any general conclusions. From the results obtained by Eucken and Küchler[46] on the CO_2-H_2 and the CO_2-H_2O system it appears that the excitation efficiency for molecules with "chemical affinity" is not a monotone function of the temperature but shows maxima and minima at various temperatures. This is a problem which deserves much additional research.

In chemical reactions in which the products are formed in vibrationally excited states (Reactions 2 and 3 of Table 1) the influence of temperature manifests itself in two ways. At higher temperatures there will be more reactive species with high translational energy whose collisions will lead to a chemical reaction. This is taken account of by the exponential Arrhenius factor $\exp(-E/kT)$. Secondly, the species with high translational energy will give rise in the chemical reaction to vibrationally excited products. The efficiency of this energy transfer in a chemical reaction depends upon the geometry of the potential energy surface and its temperature dependence is included in the pre-exponential transmission coefficient. This point has been discussed at some length by various authors[1, 44, 47, 48]. While a quantitative theory has not yet been developed, it would appear from an intuitive examination of this problem that for a given curvature of the surface the reflection of mass points

[f] The efficiency of the vibrational *excitation* is given by the principle of detailed balancing as

$$P_{0\to 1} = P_{1\to 0} \exp(-h\nu_{1\to 0}/kT).$$

with high translational velocity along the walls of the potential valley would lead to correspondingly high vibrational excitation. It would thus appear that both of the two temperature dependent factors in the reaction rate expression, i.e., the Arrhenius factor and the transmission coefficient, predict an increase in the rate of production of vibrationally excited species in a chemical reaction with increasing temperature.

The problem of the influence of temperature on the rotational excitation by inelastic collisions and by chemical reactions could be discussed at this point. However, the energies involved in these processes are so small compared with the usual activation energies that it is highly doubtful whether rotationally excited species play any role in initiating or propagating chemical reactions. No further development of this topic thus appears to be necessary for the purpose of this discussion.

Reactions involving excited species (Processes 6 to 10 in Table 1)

An extensive survey of chemical reactions involving electronically excited species has been presented recently[14]. It was pointed out there that it is necessary to distinguish between reactions which are allowed in the sense that the reactants and products correlate in regard to both electronic spin and orbital angular momenta[40] and those which are forbidden or only weakly allowed since they violate one or both of these correlation rules. These latter reactions have a very low rate and it would not be expected that they play any important role in the development of energy chains. An increase in temperature would bring about some increase in the rate of these reactions owing to the operation of the Arrhenius factor; the increase in temperature would, however, have very little, if any, effect in overcoming the restrictions imposed by the correlation rules. This is due to the fact that the perturbations, which may give rise to violations of the correlation rules, are brought about by the interaction of the electric fields of the reacting molecules and since an increase in temperature is manifested primarily in the motion of the nuclei rather than that of the electrons, it is evident that the influence of temperature on the correlation rules is at best a second order effect. Reactions involving excited electronic species which have a low rate owing to a possible violation of spin and/or orbital correlation rules would thus be expected to have a relatively low rate even at high temperatures.

The reactions which may be of importance in the development of energy chains are those in which the states of the reactant and product species correlate adiabatically such as, for instance, reaction (7) leading to electronically excited CO_2. In investigating the influence of higher temperatures on the rates of these reactions it is necessary to consider collectively all the degrees of freedom of the reacting molecules. When electronically excited species are formed, either thermally by inelastic collisions or in a chemical reaction, they will also have, except in the case of excited atoms, a certain amount of energy in the other degrees of freedom. Since the excited electronic levels for most simple molecules are rather far apart energetically, an increase of temperature will bring about primarily an increase in the translational, rotational, and vibrational energy of the electronically excited molecule. This is no different from the conditions which obtain for molecules in their electronic ground states; the influence of temperature on the rates of reactions involving electronically excited species will thus be governed by the Arrhenius factor $\exp(-E/kT)$ and the rate of these reactions will increase with increasing temperature.

There is, however, one feature of elementary reactions involving excited species at high temperatures which is quite specific to such systems. Suppose that in a chemical reaction the products are formed with high energy content in excess of their equilibrium concentration. These high energy products will then have an effective "temperature" in excess of the equilibrium temperature of the reaction system. If these high energy molecules now undergo a subsequent reaction whose activation energy is lower than the mean energy of the excited reactants, then an increase of temperature of the reaction system would not bring about any further increase in the rate of the reaction. To illustrate, in the possible sequence of reactions,

(a) $A + B + C \rightarrow AB + C^*(\bar{\epsilon} \sim 40 \text{ kcal})$; $\Delta H = 100$ kcal

(b) $C^* + DG \rightarrow CD + G$; $E_{act} = 20$ kcal

where C* is formed in *excess of its equilibrium concentration* with a mean energy of about 40 kcal, the rate of Reaction (b) would not be affected by an increase in the temperature of the initial reac-

tion system A, B, C, DG. These types of reactions ("hot" radical reactions) have been discussed previously in connection with radio-chemical and photochemical systems[37] where there is some evidence for their occurrence[49]. There are, however, not sufficient data as yet on high temperature reaction systems such as flames to ascertain whether they also play an important role in these systems.

SUMMARY

The discussion given in this section (Section II) is of necessity quite sketchy. As has been pointed out already in the introduction, there is a dearth of quantitative data and of basic theoretical studies which, it is hoped, may be remedied by the present activity in the field of high temperature kinetics. It appears from the data available at present and from reasonable extrapolations on low temperature systems that excited species with high energy content may play an important role in reactions taking place at elevated temperatures. The importance of "energy chains" as compared with radical chains in the overall mechanisms of high temperature reactions is a question which cannot be answered at present and which deserves much further study.

III. Radical Reactions in High Temperature Systems

In chain reactions in the temperature range from 300°K to about 1000°K the concentration of atoms and radicals is usually quite small. In writing out the reaction mechanism it is therefore not necessary to consider the various possible gas phase reactions between atoms and/or radicals except as chain termination steps by bimolecular or termolecular recombinations. In high temperature reaction systems the situation may, however, be somewhat different and may require some special consideration.

An increase in temperature in a reaction system will bring about an increased concentration of atoms and radicals. For an equilibrium system this increase in atom and radical concentration, which is due to the higher degree of dissociation of the various molecular species at elevated temperatures, can readily be calculated. Owing to the high a priori probability of the dissociated state (increase in entropy accompany the proliferation of species) the effect of temperature on the degree of dissociation is considerably larger than would be expected solely from the operation of the Boltzmann factor $\exp(-D/kT)$ where D is the dissociation energy. Thus, for instance, the degree of dissociation α of O_2 is 1.4 per cent at 3000°K when $\exp(-D/kT) \sim 10^{-9}$ and 15 per cent at 4000°K when $\exp(-D/kT) \sim 10^{-6}$. Further examples of the relatively high concentrations of atoms and radicals in equilibrium high temperature reaction systems may be found in the tables of Hottel, Williams and Satterfield[50]. In high temperature flame reactions where, as pointed out in Section I, non-equilibrium conditions may obtain in the reaction system, atoms and radicals may be produced in considerable excess of their equilibrium concentrations. In some calculations on the ozone self-decomposition flame it has been found, for instance, that the concentration of oxygen atoms near the hot boundary is higher by a factor of about 10,000 than the thermal equilibration concentration at the equilibrium flame temperature[51]. The observation of the abnormal excitation of $OH(^2\Sigma^+)$ to the $v' = 2$ state in the oxy-hydrogen and oxy-acetylene flames is also an indication of the presence of H and/or O atoms in excess of their equilibrium concentrations[7, 40, 52]. As has been pointed out by Hirschfelder[51], it may be expected that for many different flame reactions the concentration of free radicals (near the hot boundary) is, in general, greatly in excess of the thermal equilibrium value.

When a high temperature reaction system contains a large concentration of atoms and/or radicals, either in their thermal equilibrium concentration or in excess of equilibrium, it may be necessary to consider the possibility of different reaction mechanisms from those which prevail in low temperature pyrolysis and oxidation reactions. If the concentration of atoms and/or radicals is sufficiently large, the probability of radical-radical or atom-radical collisions may be correspondingly high enough for these types of processes to play a significant role in the reaction mechanism. At high temperature, recombination reactions involving atoms and/or radicals will, however, not be very efficient processes since the equilibrium has shifted toward the dissociated product side. Metathetical reaction of radicals (or atoms with radicals) may, however, be important under these conditions. Some *speculative* examples of this type of reaction are

$$CH + OH \rightarrow CO + H_2$$

$$C_2 + OH \rightarrow CH + CO$$

$$NH + NH \rightarrow N_2 + H_2$$

$$NH + OH \rightarrow NO + H_2 \text{ etc.}$$

There are at present unfortunately not sufficient data on elementary reactions at high temperatures to permit any more detailed consideration of this interesting class of reactions. Some research along these lines would be very helpful in furthering our knowledge of elementary reactions in systems with high concentration of atoms and radicals.

IV. Unimolecular Reactions at High Temperatures

A large amount of work has been carried out, both experimentally and theoretically, on the influence of pressure on the rate and order of unimolecular reactions. One of the aims of this research has been to determine the pressure regimes at which unimolecular reactions change from first to second order kinetics. These data give some insight into the relative efficiency of intermolecular and intramolecular energy exchange since the order of a unimolecular reaction depends, in the last analysis, upon the relative magnitude of these two factors.

The rate of activation, which is determined by the efficiency of intermolecular energy transfer, and the rate of decomposition of the activated complex, which is determined by the efficiency of the intramolecular energy transfer are, however, not only pressure dependent but are also functions of temperature. The question therefore arises whether a change in temperature will have an effect similar to that of pressure on the rate and order of a unimolecular reaction. There have been no explicit investigations of this point, either experimentally or theoretically, of which the author is aware. In the absence of such studies we can only speculate here on the influence of temperature on the mechanism of unimolecular reactions.

It has been pointed out in Section II that the rates of vibrational excitation, which are the important ones for unimolecular reactions, will increase with increase in temperature. The rates of intramolecular energy transfer which govern the kinetics of unimolecular decomposition are those of the transfer of vibrational energy among the various vibrational degrees of freedom of the activated species. In particular, decomposition will occur when a sufficient amount of energy has passed from the various normal modes of vibration into the vibrational mode along the reaction coordinate. Since the coupling of the vibrational degrees of freedom increases with the anharmonicity of the excited vibration it is quite likely that the transfer of vibrational energy within the molecule will be more efficient at higher temperatures. The central question then would seem to be whether at high temperatures the increase in the rate of vibrational excitation by inelastic collisions is less than, about equal to, or greater than the increase in the rate of intramolecular transfer of energy brought about by the stronger coupling of the anharmonic vibrations in the molecule. To this problem there does not seem to be an answer at the present time.

For a reaction system at constant volume an increase in temperature will bring about a corresponding increase in pressure and it would be necessary in that case to disentangle, if possible, the temperature from the pressure effects. This difficulty would, however, not be found for systems at constant pressure such as flow systems. In such a system the following circumstances could conceivably arise. The reaction system is at a pressure where the rate of the unimolecular decomposition obeys strict first order kinetics. As the temperature T is now raised, the collision frequency will decrease as $T^{-3/2}$ but the collisions will be more energetic so that the activated species formed in the inelastic collisions will have, on the average, a higher energy content than the activated species produced at lower temperatures. Since the efficiency of activation in inelastic collisions increases at least exponentially with temperature, and probably even somewhat more rapidly if all the normal modes of vibration are taken into consideration, the rate of activation, which is given essentially by the product of the collision frequency and the activation efficiency, will certainly increase with increasing temperature. If now the rate of intramolecular energy transfer, or to be more precise, if the rate of transfer of vibrational energy from the different modes of vibrations into the vibration corresponding to the reaction coordinate increases more rapidly with temperature than the rate of activation, then the overall unimolecular reaction will show a decline from its limiting first order rate and will change to second order kinetics. Under these conditions, the effect of an increase in temperature at constant pressure would be analogous to that produced by the lowering of the pressure at constant temperature. If experiments along these lines should prove feasible it would be very interesting to see whether temperature effects similar to the one discussed above

will show up in unimolecular reactions at high temperatures[g].

REFERENCES

1. See, e.g., Fowler, R., and Guggenheim, E. A.: *Statistical Thermodynamics*, ch. XII. Cambridge, Cambridge University Press, 1949; and Eyring, H., Walter, J., and Kimball, G. E.: *Quantum Chemistry*, ch. XVI. New York, John Wiley and Sons, Inc., 1944.
2. Kramers, H. A.: Physica, *7*, 284 (1940).
3. Curtiss, C. F.: University of Wisconsin, Naval Research Laboratory, CM-476, June 8, 1948.
4. Prigogine, I., and Xhrouet, E.: Physica, *15*, 913 (1949).
5. Shuler, K. E.: J. Phys. Chem., *57*, 396 (1953).
6. Shuler, K. E.: J. Chem. Phys., *18*, 1466 (1950).
7. Broida, H. P., and Shuler, K. E.: J. Chem. Phys., *20*, 168 (1952); Shuler, K. E., and Broida, H. P.: Ibid., *20*, 1383 (1952).
8. *Energy Transfer in Hot Gases*, National Bureau of Standards Circular 523, Washington, D. C. (1954).
9. Gaydon, A. G., and Wolfhard, H. G.: *Flames, Their Structure, Radiation and Temperature*. London, Chapman and Hall, Ltd., 1953.
10. Calcote, H.: *Third Symposium on Combustion, Flame and Explosion Phenomena*, p. 245. Baltimore, The Williams and Wilkins Co., 1949.
11. Karlovitz, B., et al.: *Fourth Symposium (International) on Combustion*, p. 613. Baltimore, The Williams and Wilkins Co., 1953.
12. Shuler, K. E., and Weber, J.: J. Chem. Phys., *22*, 491 (1954).
13. Griffing, V. F., and Laidler, K. J.: *Third Symposium on Combustion, Flame and Explosion Phenomena*, p. 432. Baltimore, The Williams and Wilkins Co., 1949.
14. Laidler, K. J., and Shuler, K. E.: Chem. Rev., *48*, 153 (1951).
15. Broida, H. P., and Gaydon, A. G.: Trans. Faraday Soc., *49*, 1190 (1953).
16. Polanyi, M.: *Atomic Reactions*. London, Williams and Norgate, 1932.
17. Magee, J. L.: J. Chem. Phys., *8*, 687 (1940).
18. Gaydon, A. G., and Wolfhard, H. G.: Proc. Roy. Soc. (London), *205A*, 118 (1951).
19. Wolfhard, H. G., and Parker, W. G.: This volume.
20. Shuler, K. E.: J. Chem. Phys., *18*, 1221 (1950).
21. Gaydon, A. G., and Wolfhard, H. G.: Proc. Roy. Soc. (London), *194A*, 169 (1948).
22. Gaydon, A. G., and Wolfhard, H. G.: Proc. Roy. Soc. (London), *199A*, 89 (1949).
23. Broida, H. P.: J. Chem. Phys., *21*, 340 (1953).
24. Gaydon, A. G., and Wolfhard, H. G.: Proc. Roy. Soc. (London), *201A*, 561 (1950).
25. Benedict, W. S., Plyler, E. K., and Humphreys, C. J.: J. Chem. Phys., *21*, 398 (1953).
26. Schwartz, R. N., and Herzfeld, K. F.: J. Chem. Phys., *22*, 767 (1954).
27. Brout, R.: J. Chem. Phys., *22*, 934 (1954).
28. Prigogine, I., and Mahieu, M.: Physica, *16*, 51 (1950).
29. Zwolinsky, B. J., and Eyring, H.: J. Am. Chem. Soc., *69*, 2702 (1947).
30. Matsen, F. A., and Franklin, J. L.: J. Am. Chem. Soc., *72*, 3337 (1950).
31. Kramers, H. A.: Physica, *7*, 284 (1940).
32. Chandrasekhar, S.: Revs. Modern Phys., *15*, 1 (1943); see especially pp. 63 to 68.
33. Hulburt, H. M., and Hirschfelder, J. O.: J. Chem. Phys., *17*, 964 (1949).
34. For a recent review see Evans, M. W.: Chem. Rev., *51*, 363 (1952).
35. Richardson, J. M.: *Fourth Symposium (International) on Combustion*, p. 920. Baltimore, The Williams and Wilkins Co., 1953.
36. For a discussion of the importance of proper rate expressions in the theory of flame propagation see also *Selected Combustion Problems, AGARD*, pp. 167–191. London, Butterworth Scientific Publications, 1954.
37. Hamill, W. H., et al.: University of Notre Dame, Radiation Chemistry Project, AECU-1321, March 1, 1951.
38. Massey, H. S. W., and Burhop, E. H. S.: *Electronic and Ionic Impact Phenomena*, Ch. VII. London, Oxford University Press, 1952.
39. Laidler, K. J.: *Chemical Kinetics*, Ch. 13. New York, McGraw-Hill Book Co., 1950.
40. Shuler, K. E.: J. Chem. Phys., *21*, 624 (1953).
41. See, e.g., Massey, H. S. W.: Reports on Progress in Physics, *12*, 248 (1949).
42. Bethe, H. A., and Teller, E.: Ballistic Research Labs., Report X-117, 1941.
43. Landau, L., and Teller, E.: Physik. Zeits. d. Sowjetunion, *10*, 34 (1936).
44. Castellan, G. W., and Hulburt, H. M.: J. Chem. Phys., *18*, 312 (1950).
45. Widom, B., and Bauer, S. H.: J. Chem. Phys., *21*, 1670 (1953).
46. Eucken, A., and Küchler, L.: Physik. Zeits., *39*, 831 (1938).

[g] A short discussion of the effect of temperature on the rate and order of unimolecular reactions has been given by N. B. Slater: Trans. Roy. Soc., *246A*, 57 (1953), par. 7d; this discussion, however, refers to different effects from the ones discussed above.

47. Hirschfelder, J. O., and Wigner, E.: J. Chem. Phys., *7*, 616 (1939).
48. Hulburt, H. M., and Hirschfelder, J. O.: J. Chem. Phys., *11*, 276 (1943).
49. See, e.g., Schultz, R. O., and Taylor, H. A.: J. Chem. Phys., *18*, 194 (1950).
50. Hottel, H. C., Williams, G. C., and Satterfield, C. N.: *Thermodynamic Charts for Combustion Processes*, part 2, Table 10. New York, John Wiley and Sons, Inc., 1949.
51. Hirschfelder, J. O., Curtiss, C. F., and Campbell, D. E.: J. Phys. Chem., *57*, 403 (1953).
52. Gaydon, A. G., and Wolfhard, H. G.: Proc. Roy. Soc., *208A*, 63 (1951).

VIII

SURVEY OF COLLISION PROCESSES IN THE COMBUSTION OF HYDROCARBONS

By A. R. UBBELOHDE

The early triumphs of the kinetic theory of the velocity of gas reactions can be compactly summarized by the formulae:[1]

Number of molecules entering into collision

$$\text{per cc per sec} = Z = n_1 n_2 \sigma_{12}^2 \left\{ 8\pi RT \left(\frac{1}{m_1} + \frac{1}{m_2} \right) \right\}^{\frac{1}{2}} \quad (1)$$

Number of molecules reacting

$$= PZ \exp(-E/RT) \quad (2)$$

In this expression, σ_{12} is the Gas-kinetic collision diameter, between molecules of species 1 and 2, n_1, n_2 are the number of molecules of each kind per cc. P is a steric or probability factor, E is an activation energy.

While great progress has been achieved in terms of the quite simple physico-chemical concepts associated with these formulae, it seems timely to review their meaning, and to examine the need for extensions and refinements, in dealing with the reactions of polyatomic molecules, such as hydrocarbons.

Activation Energy

Experimentalists have been remarkably fortunate with the simple Arrhenius expression: Rate constant $= A_{\exp} - E/RT$, since practically any physico-chemical process that shows a marked temperature coefficient at all can be fitted to give an exponential slope, at any rate over a moderate range of temperatures. It is not always easy, however, to identify the activation energy calculated from experiment, with specific processes during the reaction. For simple molecules with only very few atoms, the transition state theory gives a working model. From this, the activation energy of a chemical bond-rearrangement AB + CD → AC + BD can be calculated if the potential energy-distance curves are known for all the combinations AB, AC, AD, BC, BD, CD.

Hypothesis of the Independent Reactivity of Molecular Segments

A natural extension of the transition state theory to the reaction kinetics of hydrocarbons would be to regard each of the various C—H and C—C bonds as effectively independent, to a zero-order approximation. By way of example, the reaction kinetics of any chemical process such as

$$\begin{array}{l} \qquad\qquad\quad CH_3 \\ \qquad\qquad\quad | \\ CH_3—CH_2—CH_2\text{–}CH—CH_3 + X \rightarrow \\ \qquad\qquad\qquad\qquad\qquad X\,H + (C_6H_{13})— \end{array}$$

can then be regarded as the sum of the reaction rates of each of the individual CH bonds with the body X. The overall reaction rate constant is the sum of the individual reaction rates.

Even this zero-order hypothesis of independent bond reactivity calls for extension of the simplest kinetic theory concepts in two ways.

(1) It is necessary to know how the —C—H potential energy curves differ for the carbon atoms bonded in different ways.

A frequently made assumption is that the relative activation energies for different C—H bonds

will differ in the same way as the —C—H bond disruption energies differ. At present, the fruitfulness of even this simplifying assumption is greatly reduced by lack of reliable information about the different —C—H bond disruption energies. Some of the values published are given in Table 1.[2]

—C—H Bond-Disruption Energies in Different Hydrocarbons

The most prominent fact emerging from this table, in the form as at present available, is that in aliphatic hydrocarbons tertiary —C—H bonds should exhibit notably smaller activation energies than secondary —C—H bonds, which in turn require less disruption energy than primary —C—H bonds. This conclusion should affect the overall kinetic reaction-rate constants of hydrocarbons accordingly. Generally speaking, a tertiary C—H should be a focus of reactivity. How far this applies in practise is discussed in Small and Ubbelohde.[2a]

In aromatic hydrocarbons, it seems likely that bond-disruption energies of different aromatic C—H bonds will be influenced by their position in the aromatic nucleus, relative to any orienting substituents. Up to the present, however, there is little or no information available on possible differences of disruption energies of various aromatic —C—H bonds. Possible methods of measurement are discussed in a forthcoming publication.[3]

(2) Only a fraction of collisions between X and the hydrocarbon molecule can lead to reaction with any particular bond, for steric reasons. If the hydrocarbon molecule can be regarded as substantially rigid, as is probably permissible for many aromatic hydrocarbons, steric factors for each of the C—H bonds can be calculated with reasonable confidence. When the number of collisions between X and the hydrocarbon has been calculated by formula (1), using values of collision diameters to be further discussed below, the steric factor appropriate to each C—H bond can be inserted. However, if the hydrocarbon molecule is flexible, and can crumple into various configurations, much more careful analysis of the possibilities is required. These are further discussed below (cf. Ubbelohde and McCoubrey[4]).

Availability of Activation Energy Within a Complex Molecule

So long as the number of atoms in a molecule is small, it seems feasible to regard internal energy distributed in the various degrees of freedom as available for permitting a specific bond-rearrangement in a specific collision. In some way, not always clearly specified, the internal energy in the various degrees of freedom contributes to the probability of finding sufficient activation for one specific bond change. This idea that the internal energy in the different internal degrees of freedom is available for promoting reaction in one specific bond is the foundation of the well-known

Table 1. —C—H Bond Disruption Energies in Different Hydrocarbons

	Kcal/mole	References
Primary aliphatic		
$D(CH_3—H)$	101–2	b_1 , b_2
$D(C_2H_5—H)$	98	c
$D(C_3H_7—H)$	95	d
Secondary aliphatic		
$D(CH_3)_2CH—H$	89–94	d_1 , d_2
Tertiary aliphatic		
$D(CH_3)_3C—H$	86–89	d_1 , d_2 , e
Aromatic		
—C—H	101.4	a

(a) Ladachi and Szwarc: Proc. Roy. Soc., *219A*, 341 (1953).

(b_1) Andersen and Kistiakowsky: J. Chem. Phys., *11*, 6 (1943).

(b_2) Roberts and Skinner: Transactions Faraday Society, *45*, 339 (1949).

(c) Andersen and Van Artsdalen: J. Chem. Phys., *12*, 479 (1944).

(d_1) Butler and Polanyi: Trans. Faraday Soc., *48*, 220 (1952).

(d_2) Mortimer, Pritchard, and Skinner: Trans. Faraday Soc., *48*, 220 (1952).

(e) Van Artsdalen: J. Chem. Phys., *22*, 28 (1954).

factor:

$$\frac{(E/RT)^{\frac{1}{2}n-1}}{(\frac{1}{2}n-1)!} \qquad (3)$$

by which $\exp(-E/RT)$ must be multiplied when the activation energy is distributed among n quadratic terms (cf. Hinshelwood,[1] p. 53, 79). For some characteristic thermal decompositions of fairly simple organic molecules, $n = 10$ for $(CH_3)_2O$, $n = 18$ for $(C_2H_5)_2O$, $n = 25$ for azomethane, and $n = 9$ for germanium tetraethyl.

But however this naive assumption about the availability of internal energy for chemical activation may apply in molecules with only a few

atoms, when the molecule forms an extensive system of vibrators, as is true for the higher hydrocarbons, the availability of activation energy at any one bond calls for much more detailed study. To focus the discussion, two extreme cases can be described. In one extreme, all the bond vibrations and valency angle vibrations would be regarded as completely independent, so that there is no coupling of vibrations throughout the complex molecule. This extreme model corresponds with the assumption of independent reactivities of the —C—H and —C—C bonds already referred to. At the other extreme, all the molecular vibrations would be treated as strongly coupled. Internal energy of vibration would flow freely from any one part of a hydrocarbon molecule to any other, so that the remotest portions of the molecule can affect bond-rearrangement resulting from a collision at any specific C—H or C—C bond. Formula (3) assumes that this effectively applies. However, the fact that first order change to second order rate constants at sufficiently low collision rates is clear evidence that even in fairly simple molecules there is a relaxation time for the transfer of internal energy within the molecule. For time delays short compared with this relaxation time, the internal energy is not freely available from the different degrees of freedom, and the reaction rate would be expected to fall.

In reality, different hydrocarbons probably break up into a system of groups of coupled vibrators. Within any one group of coupled vibrators, the relaxation time for transfer of internal energy is small, and factor (3) applies down to low collision rates. Between the groups there may be quite large barriers to the transfer of energy. The relaxation time for such transfer between groups of coupled vibrators may be so large that these groups behave as effectively independent in a chemical reaction. For example, in a normal paraffin the unbranched C—C skeleton almost certainly forms one group of coupled vibrators. Some of the CH vibrations may lie sufficiently close to the proper frequencies of the coupled skeleton to link up with it, but others may differ so much in frequency that they behave as practically independent. In a branched paraffin, each branch may be expected to belong to a separate group of vibrators not strongly coupled with the neighboring branch.[5] In an aromatic hydrocarbon the vibrations of the aromatic nucleus may or may not couple strongly with the —C—H vibrations and with vibrators in substituents in the nucleus, according to whether the frequencies overlap sufficiently.

Transfer of Internal Energy in Molecular Collisions

Though the coupling or independence of bond-vibrations in hydrocarbons must be of considerable importance for the reactivity of individual bonds, no really adequate theoretical or experimental study of this problem is yet available. At present, the experimental evidence which is being obtained about the role of internal energy distribution for the reactivity of hydrocarbons is still rather indirect:

(1) In self-collisions, the number of encounters Z_{eff} needed for each transfer translational $\rightarrow$ internal energy is small for paraffins. This has been established both from ultrasonic measurements on gaseous hydrocarbons[6] and from calculations[4] of the Eucken coefficient a in the expression $K = a\eta C_v$ where K is the thermal conductivity, η the viscosity and C_v the specific heat of the gas. For olefins, the transfer of vibrational energy can be considerably less efficient. With self-collisions in ethylene, $Z_{\text{eff}} \approx 2500$. However, when aliphatic groups are linked to the double bond, as in propylene, Z_{eff} drops to quite small values again.

For benzene, there is ultrasonic relaxation around 5×10^{-8} sec.[7] While the information obtainable from such ultrasonic studies is limited to much lower vibrational energies than are generally necessary for chemical activation, they indicate that at least in the paraffins most collision-approaches result freely in the transfer of vibrational energy. No obvious restrictions on internal energy flow can be inferred from observations of this kind.

(2) More discriminating tests on internal energy flow during a collision can be obtained when a molecule such as ethylene, for which the transfer translational $\rightarrow$ vibrational energy is rather inefficient, encounters other molecules. Encounters with molecules such as O_2, N_2, or propane are not appreciably more efficient for the transfer of internal energy than self collisions. However, encounters with the higher paraffins are much more effective, as is shown in Table 2.[8] For reasons further discussed below, it seems likely that differences can be expected, for example amongst paraffins of different structure, according to the degree of molecular flexibility. Flexible hydrocarbons are much more efficient in

promoting the transfer translational $\rightleftharpoons$ internal energy in a collision, than molecules of practically identical mass and structure, but in which the valency bonds are so distributed that the molecule is stiffened.[9]

A tentative interpretation is that the flexible molecules smear the quantum restrictions for the transfer translational $\rightarrow$ vibrational energy, by virtue of their wide range of configurations with only moderately different potential energies. As is shown in Table 2, the flexible paraffins are even more efficient than hydrogen itself in promoting energy transfer.

(3) It has frequently been suggested that some of the peculiarities of the oxidation kinetics of hydrocarbons could be explained if energy chains play a significant role in the reaction mechanism.[2a] The difficulties in pinning down evidence for the specific transfer of internal energy in a reaction chain have long hindered the full substantiation of energy chains. However, the role of hydrogen as an inhibitor at the very early stages of oxidation seems to indicate specific transfer of internal energy. New techniques for studying reaction kinetics are required to develop the study of energy chains. In this connection, a recent development in the study of energy transfer may be important:

The Hydrogen-Effect in Molecular Collisions

One kind of evidence that has recently been growing in bulk follows from the discovery of the hydrogen-effect in molecular collisions. From a theoretical discussion by Pidduck[10] it follows that if internal energy can be efficiently transferred in molecular collisions, the effective molecular collision diameter is increased. In this approach, collision diameters are merely to be regarded as parameters defined by the well known gas-kinetic equations for the transport of mass or momentum, in which the symbols have their usual significance:

$$\text{momentum } \pi\sigma^2 = \tfrac{2}{3}\sqrt{k/N\pi} \times \sqrt{MT/\eta} \ldots \quad (4)$$

$$\text{mass } [D_{12}]_1 = \frac{3}{8n\sigma_{12}^2}\left\{\frac{kT(m_1+m_2)}{2\pi m_1 m_2}\right\}^{\frac{1}{2}} \quad (5)$$

Experimentally, definite hydrogen effects are found, when one of the molecules in the collision is flexible and can crumple readily. One way of showing this is to calculate the difference $\Delta\{\sigma_{H_2} - \sigma_{N_2}\}$ for various molecules, from gas kinetic measurements on diffusion. Here, σ_{H_2} is the apparent collision diameter when hydrogen is the gas transporting the hydrocarbon and σ_{N_2} the apparent diameter when another transporting gas is used, such as argon or nitrogen. As shown in Table 4 the hydrocarbon molecules show large Δ's particularly when they can readily crumple by rotation about C—C bonds. On the other hand, if the hydrocarbon molecules are stiff, Δ is small or negligible, showing that the transfer of internal energy in molecular collisions is repressed by the stiffness of the molecular configuration.

Table 2. Number of Encounters with Ethylene Required for One Transfer (Translational $\rightarrow$ Vibrational Energy) at 288°K

	Z_{eff} (approx.)
Air	5000
Propane	2500
Helium	2500
Ethylene (self collisions)	2500
Hydrogen	250
H_2O	85
Isopentane	50
n-Pentane	40
Isohexane	40
n-Hexane	30

Table 3. Contrast Between Stiff and Flexible Hydrocarbons for the Transfer of Internal Energy to Ethylene Z_{eff} at 298° K

Hydrocarbons

Flexible $\longrightarrow$ Inflexible

n-pentane	50	isopentane	60	neopentane	120	cyclopentane	3300
n-hexane	30	isohexane	40	cyclohexane	100		

Other Effects of Molecular Crumpling on Collision Diameters

In the simple formula for reaction rates the collision diameters used are often taken from somewhat crude kinetic theory calculations. As already stated, when multi-bonded molecules are involved it is possible to allow to some extent for the specific reactivities of the different bonds, by introducing steric factors to represent the fraction of the solid angle 4π in which collisions can be fruitful for any particular bond. Such corrections may give adequate representation of the kinetics in the case of rigid molecules, such as the aromatic hydrocarbons. More accurately defined collision diameters can be computed, if necessary, for such rigid molecules, by the methods described by Hirschfelder and his co-workers.[11]

Table 4. Apparent Collision Diameters of Hydrocarbons in Mass Transport[10]

Compound	σ_{N_2}	$\Delta\{\sigma_{H_2} \cdot \sigma_{N_2}\}$ (in A.U.)
C_2 series		
*Ethylene	3.67	+1.13
Ethane	4.49	−0.02
C_6 series		
n-Hexane	6.48	+0.25
2:3-Dimethylbutane	6.53	+0.03
Benzene	5.70	+0.04
Cyclohexane	6.47	−0.15
Methyl cyclopentane	6.41	−0.11
C_8 series		
n-Octane	7.03	+0.37
2:2:4-Trimethylpentane	7.07	+0.03
C_{10} series		
n-Decane	7.50	+0.71
2:3:3-Trimethylheptane	8.73	+0.18
C_{12} series		
n-Dodecane	8.45	+0.46

* The σ for ethylene may need revision in the light of recent findings.

Table 5. Ratios of Collision Areas of Paraffins (Momentum Transfer Parameters[11])

	$\sigma^2_{normal}/\sigma^2_{iso}$
C_4 series	
n-Butane: Isobutane	1.00
C_5 series	
n-C_5H_{12}: $(C_2H_5)CH(CH_3)_2$	1.03
C_7 series	
n-C_7H_{16}: $(CH_3)_2CH \cdot C(CH_3)_3$	1.07
C_8 series	
n-C_8H_{18}: $(CH_3)_2\ CH \cdot CH_2\ C(CH_3)_3$	1.05

However, no crude use of collision diameters is permissible for molecules such as the higher normal paraffins, which can assume a wide range of molecular configurations not differing much in energy, by crumpling through rotations about single C—C bonds. The results of a collision between a reacting species and the hydrocarbon are likely to depend considerably[4] upon whether the paraffin behaves as a fully extended molecule

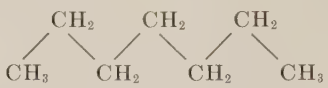

in the gas phase, or whether most of the collisions take place with extensively crumpled hydrocarbons such as

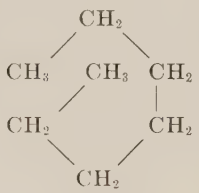

Experiments have not yet established how the different configurations behave in actual chemical reactions. However, underlying gas-kinetic measurements have been completed for a number of hydrocarbons, for various types of collision diameter. These show, that on average, even the normal hydrocarbons are extensively crumpled in the gas phase, at ordinary temperatures. The most direct illustration of this is to compare the collision parameter σ^2 for various hydrocarbons with the same number of carbon atoms.

A possible reconciliation of this finding with the barriers computed in other ways for rotation about single C—C bonds has been proposed.[12] The present purpose, however, is to discuss which value of the collision diameter to use for such flexible hydrocarbons. From what has been stated, it seems clear:

(1) The geometry of the reactivity of different C—H and C—C— bonds in hydrocarbons must be carefully discussed for specific examples, particularly when extensive crumpling can occur.

(2) Smooth transfer of internal energy in collisions may play an important part in reaction kinetics, particularly for flexible hydrocarbons.

(3) Secondary effects of molecular crumpling

on the reactivity of groups apparently remote in the molecule must also be kept in mind. For example, by bending around on itself a hydrocarbon molecule can surround a reacting group with a solvent atmosphere in a kind of autosolvent effect.

This survey indicates considerable caution in applying crude reaction-kinetic concepts to hydrocarbon reactions, particularly when the hydrocarbons can crumple. However, if the other partners in the reactions are sufficiently simple, the effects of molecular complexity discussed above may be only subsidiary. For example, studies of the monochlorination of the higher paraffins have recently been made in Belfast[13] to determine how far molecular structure affects reaction rates. It is noteworthy that lengthening the paraffin chain accelerates monochlorinations, and branching the chain slows it down, just as for oxidation at low temperatures in the gas phase. However, these influences of molecular structure are much less marked for a simple reaction chain such as:

$$\begin{aligned} Cl_2 &\rightarrow Cl + Cl \\ Cl + RH &\rightarrow R + ClH \\ R + Cl_2 &\rightarrow RCl + Cl \end{aligned}$$

than for the oxidation reactions. To a fair approximation, it is found that the reactivities of the individual C—H bonds can be treated as independent of one another, and can be summed for the molecules as a whole. Only for the longer normal paraffins does a departure from the additivity rule become evident. Probably, the effects of molecular crumpling on reaction rates becomes just appreciable for such hydrocarbons.

REFERENCES

1. Hinshelwood, C. N.: *Kinetics of Chemical Change*, pp. 14, 51. Oxford, Oxford University Press, 1949.
2. C—H bond disruption energies are taken from references (a) quoted in Small, N. J. H., and Ubbelohde, A. R.: J. Appl. Chem., (1954); and (b) from references at the foot of Table 1.
3. Graham, W. S., Nichol, R. J., and Ubbelohde, A. R.: J. Chem. Soc., in publication.
4. Ubbelohde, A. R., and McCoubrey, J. C.: Disc. Faraday Soc., *10*, 94 (1951).
5. cf. Ubbelohde, A. R.: Proc. Roy. Soc., *A152*, 361 (1935).
6. Lambert, J. D., and Rowlinson, J. S.: Proc. Roy. Soc., *204A*, 424 (1950).
7. Cheng, L. M.: J. Chem. Phys., *19*, 693 (1951).
8. McCoubrey, J. C., Parke, J. B., and Ubbelohde, A. R.: Proc. Roy. Soc., *A223*, 155 (1954).
9. McGrath, W. D., and Ubbelohde, A. R.: Proc. Roy. Soc. *A227*, 1 (1954).
10. References quoted by Cummings, G. A. McD., and Ubbelohde, A. R.: J. Chem. Soc., 3751 (1953).
11. References quoted in McCoubrey, J. C., McCrea, J. N., and Ubbelohde, A. R.: J. Chem. Soc., 1961 (1951).
12. Ubbelohde, A. R., and Woodward, I.: Trans. Faraday Soc., *48*, 113 (1952).
13. Chambers, G., and Ubbelohde, A. R.: J. Chem. Soc. In publication.

IX

CHEMICAL KINETICS OF HYDROCARBON COMBUSTION

By GUENTHER VON ELBE

Considerable progress has been made in unravelling the complex chemical processes of hydrocarbon oxidation. As it would be futile to attempt to follow the vast subject matter in its entirety, the present survey is limited to a discussion of the kinetics of the oxidation of methane and of certain general kinetic and chemical aspects of the oxidation of higher alkyl hydrocarbons. Consideration is given to some of the new material presented at this symposium. For a more detailed presentation of the subject, the reader is referred to a previous publication[1].

Methane Oxidation

The latest information on methane and oxygen, as represented by contributions to this sym-

posium, does not yield the much-desired clarification of the kinetic picture, but instead raises doubts concerning the validity of previous concepts. It may be asked whether perhaps an overly fine-grained mapping of the facts, coupled with the unfortunate side-by-side occurrence of reactions of methane and accumulated carbon monoxide, may not be partly or largely responsible for this situation. It seems in order, therefore, to describe the kinetic picture suggested by the older literature and to examine, as far as possible, whether or not the new data are so radically contradictory as to force a change of concepts.

According to Bone and Gardner[2], on admitting a mixture of methane and oxygen to a silica vessel at ~390–420°C a parallel increase occurs of the rate of methane consumption and of the concentration of formaldehyde in the reacting mixture. The increase is at first exponential with time and then tapers off. This parallelism between reaction rate and formaldehyde concentration is understandable if a chain reaction is assumed in which (1) minute traces of formaldehyde are formed spontaneously from methane and oxygen, (2) chain carriers are formed by reaction of formaldehyde and oxygen, (3) formaldehyde is formed as a consequence of reaction between methane and chain carriers, and (4) formaldehyde is destroyed by reaction with chain carriers. In such a mechanism, the formaldehyde concentration increases at first exponentially with time (induction period) and later attains a steady-state value at which the rates of formation and destruction are equal, and the reaction rate is at any instant proportional to the concentration of formaldehyde since the latter determines the number of chains that are generated per second.

On this basis one may, for example, propose the following chain-initiating step:

$$HCHO + O_2 = CHOO + OH \qquad I$$

There are other conceivable formulations of this reaction, the essence being that the product formed by direct association of formaldehyde and oxygen is capable of splitting in such manner that a chemical bond is broken and free valences are formed. A radical possessing a free valence is then supposed to react with methane, as

$$OH + CH_4 = H_2O + CH_3 \qquad II$$

This is an inherently plausible reaction. The radical CH_3 is considered to react further with oxygen to yield formaldehyde, possibly via the short-lived methyl peroxide radical CH_3OO,

$$CH_3 + O_2 (= CH_3OO) = HCHO + OH \qquad III$$

The fourth reaction concerns the destruction of HCHO in collisions with free radicals:

$$OH + HCHO = H_2O + CHO \qquad IV$$

However, the four reactions provide only a part of the total reaction mechanism. Additional guidance for the completion of the mechanism is provided by the reaction rate data of Norrish and Foord[3] and Norrish and Reagh[4], provided that we grant that these data apply substantially to the steady-state phase of the reaction—i.e., that during the period of rate measurement in the individual runs the rates of formation and destruction of formaldehyde were essentially in equilibrium, and that neither the exhaustion of reactants nor the simultaneous carbon monoxide-oxygen reaction had a significant effect on the data. Accepting this premise, one must supplement the mechanism by additional reactions so that the theoretical expression for the steady-state rate conforms to the experimentally determined dependence of the rate on vessel diameter, pressure and mixture composition.

The data of Norrish and coworkers can be summarized by the following empirical equation:

$$-\frac{d[CH_4]}{dt} = \frac{ad^2}{1 + bd^2} \qquad (1)$$

where d is the vessel diameter and a and b are functions of pressure and mixture composition. The coefficient a is proportional to the fourth power of the pressure and the coefficient b, as far as one can judge from the data, to the first power of the pressure, although a second power might be tolerated. a is furthermore proportional to the square of the mole fraction of methane and the first power of the mole fraction of oxygen. b appears to be independent of mixture composition, as far as the data permit judgment. Experiments with added nitrogen show the rate to increase with increasing partial pressure of inert gas but the curve of reaction rate versus inert gas pressure has a declining slope, as is expected if both a and b increase with pressure. The data of Norrish and Foord[3] agree with those of Norrish and Reagh[4] in smaller vessels, whereas in larger vessels Norrish and Reagh observed significantly larger rates. The discrepancy may be ascribed to an erratic influence of the nature of the vessel sur-

face on the rate, which is not easily eliminated. Thus, Norrish and Foord report that they obtain concordant and reproducible results only by carrying out a complete series of experiments without allowing the reaction vessel to cool, and pumping out the vessel between successive experiments. Previous admittance of air lowered the rate considerably. In the later experiments of Norrish and Reagh, the previous experience was fully utilized so that these data may be more representative of a trouble-free surface.

Another observation is that there exists a critical lower limit of vessel diameter below which reaction is not observed at all and the methane-oxygen system appears to be stable for an indefinite period.

In order to accommodate these data we introduce the reaction

$$\mathrm{OH} \xrightarrow{\text{wall}} \text{destruction} \qquad \text{V}$$

This formulation implies that the free radical OH may diffuse to the wall where it is adsorbed and ultimately destroyed by heterogeneous recombination with another free radical. The fact that inert gas accelerates the reaction rate is interpreted as being due to the decrease of the rate of diffusion of OH to the surface. According to the diffusion theory this implies further that the chain-breaking efficiency ϵ of the wall, i.e., the number of times a chain carrier must on the average collide with the wall before it is destroyed, is much larger than the ratio of mean free path to the vessel diameter; the rate of reaction V is in this case inversely proportional to the pressure and to the square of the vessel diameter. Writing the rate of reaction V as being equal to the product of the average concentration of OH and a coefficient K_5, the dependence of the rate on pressure and vessel diameter is thus given by the equation

$$K_5 = k_5/[\mathrm{M}]d^2 \qquad (2)$$

where k_5 is a mild function of temperature and is insensitive to changes in the nature of the surface, and [M] is the total concentration of all the molecules. With increasing vessel diameter K_5 becomes smaller and the reaction rate, therefore, becomes larger. However, since the data show that with increasing vessel diameter the rate does not increase indefinitely but tends to taper off to a constant value, there must be another chain-breaking reaction which is independent of the vessel diameter and thus arrests the rise of reaction rate with increasing diameter. Reaction IV will serve in this role if it is assumed that the radical CHO does not continue the chain. We shall investigate the kinetic consequences of the latter assumption, specifying at present merely that CHO radicals disappear in some manner. The reaction scheme thus becomes

$$\mathrm{HCHO} + \mathrm{O_2} \rightarrow \text{free radicals} \rightarrow \mathrm{OH} \qquad \text{I}$$

$$\mathrm{OH} + \mathrm{CH_4} = \mathrm{H_2O} + \mathrm{CH_3} \qquad \text{II}$$

$$\mathrm{CH_3} + \mathrm{O_2} = \mathrm{HCHO} + \mathrm{OH} \qquad \text{III}$$

$$\mathrm{OH} + \mathrm{HCHO} = \mathrm{H_2O} + \mathrm{CHO} \qquad \text{IV}$$

$$\begin{aligned} \mathrm{OH} &\xrightarrow{\text{wall}} \text{destruction} \\ \mathrm{COH} &\longrightarrow \text{destruction} \end{aligned} \qquad \text{V}$$

This scheme leads to the following equations for the steady-state concentrations of OH and formaldehyde.

$$[\mathrm{OH}] = \frac{k_1[\mathrm{HCHO}][\mathrm{O_2}]}{K_5 + k_4[\mathrm{HCHO}]} \qquad (3)$$

$$[\mathrm{HCHO}] = \frac{k_2[\mathrm{CH_4}] - K_5}{2k_4} \qquad (4)$$

The rate of methane consumption is $k_2[\mathrm{CH_4}][\mathrm{OH}]$ and on inserting equation (2), the steady-state reaction rate is given by

$$-\frac{d[\mathrm{CH_4}]}{dt} = \frac{k_1k_2}{k_4}[\mathrm{CH_4}][\mathrm{O_2}]\frac{\frac{k_2}{k_5}[\mathrm{CH_4}][\mathrm{M}]d^2 - 1}{\frac{k_2}{k_5}[\mathrm{CH_4}][\mathrm{M}]d^2 + 1} \qquad (5)$$

This equation is of the form

$$\frac{-d[\mathrm{CH_4}]}{dt} = a'\frac{b'd^2 - 1}{b'd^2 + 1} \qquad (6)$$

where, at constant mixture composition, a' and b' are each proportional to the square of the total pressure.

It is seen that the theoretical equation (6) is of a form somewhat similar to the empirical equation (1). In order to modify the scheme so that the theoretical equation completely takes the form of equation (1), it is merely necessary to assume with Norrish (5) that the radicals CHO usually continue the chain and only occasionally disappear without chain continuation. If γ represents the relative probability of the chain-

continuing versus the chain-breaking reaction path of CHO, one obtains in place of equation (6) the equation

$$\frac{-d[CH_4]}{dt} = \frac{0.5a'(b'd^2 - 1)}{0.5(b'd^2 - 1)\gamma + 1} \qquad (7)$$

For $\gamma = 1$ this equation reduces to equation (6), while the empirical equation (1) is obtained if the conditions $b'd^2 \gg 1$ and $\gamma \ll 1$ are both fulfilled. It is seen that in this scheme the coefficient a becomes $0.5\ a'b'$ and the coefficient b becomes $0.5\ b'\gamma$.

The dependence of the factor γ on experimental variables is determined by the specific reactions of the radical CHO. It appears to be premature to speculate on these reactions beyond the remark that they should not introduce an additional diameter term into the scheme, and, hence, that γ is presumably insensitive to changes in the nature of the vessel surface.

If destruction of HCHO at the vessel surface occurred at a significant rate, the numerator of the rate equation would change from the form ad^2 to the form $ad^2 - c/d$, the coefficient c being sensitive to changes in the nature of the surface. It would seem, therefore, that Norrish and coworkers have succeeded in establishing experimental conditions in which c is rather small. At the same time, it is seen that at some critical small diameter the numerator becomes zero, that is, the reaction rate should become unobservably small, as has in fact been observed.

The simplicity and logical coherence of the kinetic picture, coupled with its ability to explain a wide variety of observations, strongly suggests that it is basically correct. The new data presented at this symposium do not seem sufficiently at variance with the former data to discredit this picture. The orders of pressure and mixture composition effects reported by Hoare and Walsh[6] do not seem out of proportion, particularly since the data do not permit a breakdown in terms of numerator and denominator of the rate equation; furthermore, the theoretically postulated steady state is possibly in practice only a gross approximation, because of the continuous change of reactant concentrations, and precise agreement with theory is therefore not obtainable. The incompatibility of the theory with data obtained at high temperatures as reported by Hoare and Walsh[6] and by Vanpée and Grard[7], seems to be sufficiently explained by the remark that here one deals with the simultaneous CH_4- and CO-oxidation, which constitutes a highly complex reaction and is beyond the scope of this survey.

Higher Hydrocarbons

1. CHEMICAL ASPECTS OF THE OXIDATION MECHANISM

It is generally agreed that free radical chains are involved both in the pyrolysis and oxidation of higher hydrocarbons and related compounds. Pyrolysis is catalyzed by traces of oxygen, presumably because oxygen assists in the process of chain initiation by reactions such as

$$RH + O_2 = R + HO_2 \qquad \text{VI}$$

where R denotes a monovalent radical group. At higher oxygen concentrations, the free radicals R react with oxygen in various ways, forming oxygenated free radicals, which continue the chain by attacking other molecules, and saturated compounds such as peroxides, aldehydes and olefins which participate in the reaction and affect its course in various ways.

The nature of the reaction products and hence the course of the overall reaction is largely determined by the structure of the hydrocarbon molecule and by the point of attack of a free radical on the carbon skeleton.

Thus, in studies of the propane oxidation between 260° and 300°C, Pease[8] obtained methyl alcohol as a prominent product of the reaction, the amount of which tended to approximate the amount of propane reacting as the percentage of oxygen in the initial mixture was decreased. Acetaldehyde and formaldehyde in a total yield comparable to that of methanol were also obtained; according to data of Newitt and Thornes[9] acetaldehyde is a primary and formaldehyde is a secondary product of propane oxidation. In explanation of these facts, it has been suggested[10] that free radicals attack propane mainly at the middle carbon atom, removing one hydrogen atom and forming the isopropyl radical which subsequently reacts according to

$$CH_3CHCH_3 \xrightarrow{O_2} CH_3CH(OO)CH_3 \rightarrow CH_3CHO + CH_3O \xrightarrow{CH_3CH_2CH_3} CH_3OH + CH_3CHCH_3. \qquad \text{VII}$$

In this way, one molecule of methyl alcohol and one molecule of acetaldehyde are formed for each molecule of propane reacting. Formaldehyde conceivably arises from the further reaction of

acetaldehyde. From experiments at low temperature (below ~200°C), it is rather well established[11, 12] that free-radical attack on acetaldehyde produces the acetyl radical CH_3CO; the latter is capable of combining with O_2 to form the peracetyl radical CH_3CO_3 which in turn may acquire an H-atom by attack on another molecule CH_3CHO to form peracetic acid CH_3CO_3H and the radical CH_3CO. At higher temperatures CH_3CO decomposes readily into CO and CH_3[13, 14], and the latter presumably reacts with O_2 to form CH_3OO which may decompose into formaldehyde HCHO and OH (reaction III above); on the other hand, CH_3CO may possibly persist even at high temperatures sufficiently long—there is no compelling evidence to the contrary—to combine with O_2 to CH_3CO_3 and subsequently to decompose into HCHO, CO and OH; or even to form peracetic acid CH_3CO_3H which subsequently decomposes into HCHO, CO and H_2O[a].

If the scheme VII is applied to an *n*-paraffin of more than three carbon atoms, it would seem that initial attack is possible with equal facility on any of the CH_2 groups. One would therefore write in general

$$R'CHCH_2R'' \xrightarrow{O_2} R'CH(OO)CH_2R'' \rightarrow R'CHO + R''CH_2O. \qquad \text{VIII}$$

Unlike propane, where the methoxyl radical CH_3O is stable and can react further to form methyl alcohol, the higher oxyalkyl radicals formed in this fashion are not stable but decompose according to the reaction[15]

$$R''CH_2O \rightarrow R'' + HCHO. \qquad \text{IX}$$

This explains the observation that formaldehyde appears among the first oxidation products of higher *n*-paraffins in the ratio of one molecule HCHO for every molecule of higher aldehyde[16].

In propane oxidation, propylene appears in quantity early in the reaction[9]. To explain its formation, one may propose either that some of the propyl radicals C_3H_7 decompose into C_3H_6 and H instead of reacting with O_2, or that the reaction of C_3H_7 with O_2 may occasionally take the course

$$C_3H_7 + O_2 = C_3H_7O_2 \rightarrow C_3H_6 + HO_2. \qquad \text{X}$$

Studies on the inhibition of the hydrogen-oxygen reaction by propane[17] suggest that the latter is the case since such inhibition demands removal of free hydrogen atoms and their replacement by the comparatively inert radicals HO_2. There is evidence that the yield of propylene increases relative to the yield of oxygenated products as the temperature is increased[9, 18], hence, it appears that with increasing temperature reaction X becomes relatively more frequent than the reaction sequence VII.

The formation of olefins is a general phenomenon in the oxidation of paraffin hydrocarbons and may be ascribed to reactions of paraffin radicals with O_2 analogous to reaction X. Olefins themselves appear to be more prone to chain initiation than paraffins, but their free radicals seem to be less reactive than paraffinic free radicals because of stabilization by resonance between the alternative structures[19]

$$R\dot{C}HCH = CHR \quad \text{and} \quad RCH = CH\dot{C}HR'$$

The most interesting group of intermediates, and at the same time the most significant for an understanding of the kinetics of hydrocarbon oxidation, are the various peroxidic compounds. In the following paragraphs, an attempt is made to discuss their role in the oxidation mechanism.

2. KINETIC ASPECTS OF THE OXIDATION MECHANISM

Alkyl hydrocarbons and related compounds exhibit the phenomenon of two-stage ignition in which each stage is preceded by an induction period. Depending on experimental conditions, the first induction period τ_1 may terminate in the appearance of cool flames, and the second induction period τ_2 in explosion. An investigation by Prettre[20] of the τ_1-period in pentane-oxygen mixtures showed that the accumulation of reaction

[a] The formation of methanol in the thermal oxidation of acetaldehyde, reported by Grumer[12], is equally explained by

$$CH_3OO + CH_3CHO = CH_3OH + CH_3O + CO,$$

or

$$CH_3CO_3 + CH_3CHO = CH_3OH + CH_3O + 2CO,$$

or

$$CH_3CO_3H + CH_3CHO = 2CH_3OH + 2CO.$$

This author also corroborates the earlier conclusion of Pease[8] that in the oxidation of propane both methanol and acetaldehyde appear as primary products, in accord with the postulated reaction chain VII.

products (measured by the pressure rise ΔP in the reaction vessel) follows over a considerable range of observation the equation

$$\Delta P \sim e\varphi^t - 1, \tag{8}$$

where t is the time from the start of reaction. This may be taken as evidence that during the τ_1-regime chain-branching occurs, φ being the net branching factor, and cool flames are, therefore, of the nature of branched-chain explosions except that in some manner the reaction is arrested or at least substantially slowed down before a large part of the chemical enthalpy is liberated.

Chain branching presumably occurs by occasional breaking (fission) of the —O—O— bond either in peroxidic free radicals or in saturated peroxides that result from occasional acquisition by such radicals of a hydrogen atom from a hydrocarbon or other molecule. By such fission, two new free valences and hence two new reaction chains are released. In order to explain the accelerating effect of aldehydes on the reaction in the τ_1 regime, it has been suggested[21] that association of an aldehyde molecule R′CHO with an alkyl peroxide molecule such as R″CH_2OOH, to form the oxydialkyl peroxide R′C(OH)$OOCH_2$R″, prevents the decomposition of the peroxide by reaction VII or some similar reaction and thus increases the chance of fission of the peroxide bond. This concept may have to be revised in the light of the most recent work[11] on the acetaldehyde-oxygen reaction, which has shown rather conclusively that chain-branching occurs at low temperatures by fission of peracetic acid formed in the previously mentioned chain reaction

$$CH_3CO \xrightarrow{O_2} CH_3CO_3 \xrightarrow{CH_3CHO} CH_3CO_3H + CH_3CO. \tag{XI}$$

In view of the fact that acetaldehyde is capable of producing cool flames and that aldehydes, including acetaldehyde, are intermediate products of hydrocarbon oxidation, it may be suggested that even at higher temperatures the probability of —O—O— bond fission of peracids is not negligible compared to other modes of decomposition and that the branching process in the τ_1-regime occurs largely via oxidation of aldehydes to peracids.

The question arises in which manner the reaction is slowed down in the τ_1-period and accelerates again to explosion in the τ_2-period. The answer seems to lie in the gradual replacement, during the course of the reaction, of readily fissionable peroxides by less fissionable ones. Specifically, it may be suggested, in accord with the previously described reaction schemes, that in the course of the oxidative degradation of hydrocarbon formaldehyde replaces the higher aldehydes, and that, therefore, the peroxide population of the system becomes preponderantly performic acid or hydrogen peroxide, which latter results from performic acid by loss of CO. Judging from the experience on the formaldehyde-oxygen system, where chain-branching seems to play no role[22], the probability of performic acid fission or H_2O_2-fission is negligible compared to decomposition into neutral molecules such as CO, H_2O and O_2. Hence, the chain-branching probability decreases below the chain breaking probability so that the net branching factor φ (equation 8) becomes zero and the reaction rate vanishes except for the residual spontaneous formation of chain carriers from neutral molecules. In passing from the τ_1 to the τ_2-regime, the system thus is in a state analogous to the methane-oxygen system: formaldehyde and presumably the remaining higher aldehydes react spontaneously with O_2 to form chain carriers; more aldehydes are produced by the ensuing reaction chains, and if effective chain-breaking does not occur the overall reaction again accelerates and finally becomes explosive.

According to this concept, formaldehyde acts as an inhibitor of the reaction in the τ_1-regime but promotes the reaction in the τ_2-regime. This accords well with experimental observations on the effect of addition of formaldehyde to hydrocarbon-oxygen mixtures. The inhibiting effect has been noted, for example, in studies of the low-temperature oxidation of propane[23], pentane and hexane[16], whereas a recent study of the butane-oxygen system has demonstrated both the inhibition of the reaction in the early phase and the promotion of the reaction in the late stages[24].

It is reasonable to suppose that with increasing temperature, peracid decomposes with increasing probability into lower aldehyde, CO and H_2O instead of yielding free radicals by fission; hence, an aldehyde RCHO that is being oxidized to peracid will less frequently generate chain carriers plus molecules of higher aldehydes (the latter being the result of chain carrier attacks on hydrocarbon molecules) and instead more frequently be merely degraded to lower aldehyde. As a consequence of such temperature increase, therefore, the aldehyde population of the system will already in an early stage of the reaction become

predominantly formaldehyde, and the τ_1-regime will terminate before much reaction has taken place. This seems to explain the various facts concerning the effect of temperature on the course of hydrocarbon oxidation. Thus, since acetaldehyde probably always constitutes the most significant part of the higher aldehyde population, the vanishing of the τ_1-regime with increasing temperature should take place in approximately the same temperature range for all hydrocarbons, and this is born out by the fact that the well-known cool flame and explosion limit peninsula (in a pressure-temperature diagram) has approximately the same upper temperature bound for all hydrocarbons. When the hydrocarbon has a condensed structure, like isooctane, the aldehyde formed in the chain reaction is largely formaldehyde; consequently, the τ_1-regime may be expected to be only weakly developed, as is indeed the case. Furthermore, an explanation is provided for the well-known fact that in the pressure and temperature range of two-stage ignition an increase of the initial temperature of the system increases the period τ_2, because less aldehyde will have been produced during the preceding τ_1-period and, hence, the rate of chain initiation in the τ_2-regime will be initially lower.

The cool-flame phenomenon occurs as a result of the accumulation of chain carriers due to chain branching, as the system passes through the τ_1-regime. The characteristic light emission is attributable to the production of molecules of electronically excited formaldehyde. Because of the high energy of the electronic states responsible for the radiation, the appearance of such molecules points to the occurrence of highly exothermic free-radical reactions, as for example, $CH_3 + HO_2 = HCHO^* + H_2O$.

Binary reactions of this type, involving two free radicals in the gas phase, become increasingly frequent as the free-radical concentration increases. Various details of the kinetics of cool flames, particularly their periodic recurrence in closed-vessel systems, remain at present obscure. They are further complicated by the fact that cool flames propagate as waves and, hence, both physical and chemical processes are involved.

REFERENCES

1. Lewis, B., and von Elbe, G.: *Combustion, Flames and Explosions of Gases*. New York, Academic Press, 1951.
2. Bone, A. W., and Gardner, J. B.: Proc. Roy. Soc. (London), *A154*, 297 (1936).
3. Norrish, R. G. W., and Foord, S. G.: Proc. Roy. Soc. (London), *A157*, 503 (1936).
4. Norrish, R. G. W., and Reagh, J. D.: Proc. Roy. Soc. (London), *A176*, 479 (1940).
5. Norrish, R. G. W.: Ann. Comb. Liquides, *4*, 16 (1949).
6. Hoare, D. E., and Walsh, A. D.: *Fifth Symposium on Combustion*, p. 467. New York, Reinhold Publishing Corp., 1955.
7. Vanpée, M., and Grard, F.: *Fifth Symposium on Combustion*, p. 484. New York, Reinhold Publishing Corp., 1955.
8. Pease, R. N.: J. Am. Chem. Soc., *57*, 2296 (1935).
9. Newitt, D. M., and Thorne, L. S.: J. Chem. Soc., 1656, 1669 (1937).
10. Lewis, B., and von Elbe, G.: *Combustion, Flames and Explosions of Gases*, pp. 131–132. New York, Academic Press, 1951.
11. McDowell, C. A., and Farmer, J. B.: *Fifth Symposium on Combustion*, p. 453. New York, Reinhold Publishing Corp., 1955.
12. Grumer, J.: *Fifth Symposium on Combustion*, p. 447. New York, Reinhold Publishing Corp., 1955.
13. Feldman, M. H., Ricci, J. E., and Burton, M.: J. Chem. Phys., *10*, 618 (1942).
14. Pitts, J. N., Jr., and Blacet, F. E.: J. Am. Chem. Soc., *74*, 455 (1952).
15. Rice, F. O., and Rodowskas, F. L.: J. Am. Chem. Soc., *57*, 350 (1935).
16. Cullis, C. F., and Hinshelwood, C. N.: Disc. Faraday Soc., *2*, 117 (1947).
17. Baldwin, R. R., Corney, N. S., and Simmons, R. F.: *Fifth Symposium on Combustion*, p. 502. New York, Reinhold Publishing Corp., 1955.
18. Satterfield, C. N., and Reid, R. C.: *Fifth Symposium on Combustion*, p. 511. New York, Reinhold Publishing Corp., 1955.
19. Jost, W.: *Explosions und Verbrennungsvorgänge in Gasen*, p. 489. Berlin, Springer, 1939.
20. Prettre, M.: *Third Symposium on Combustion, Flame and Explosion Phenomena*, p. 397. Baltimore, The Williams & Wilkins Co., 1949.
21. Lewis, B., and von Elbe, G.: *Combustion, Flames and Explosions of Gases*, p. 173. New York, Academic Press, 1951.
22. Scheer, M. D.: *Fifth Symposium on Combustion*, p. 435. New York, Reinhold Publishing Corp., 1955.
23. Harris, E. J., and Egerton, A.: Chem. Rev., *21*, 287 (1937).
24. Bardwell, J.: *Fifth Symposium on Combustion*, p. 529. New York, Reinhold Publishing Corp., 1955.

X

SPACE HEATING RATES AND HIGH TEMPERATURE KINETICS

By W. H. AVERY[a]

In recent years military needs for high speed aircraft and missiles have resulted in development of engines with space heating rates far exceeding those hitherto acceptable for commercial use. The magnitude of the improvement is shown by the comparison in Figure 1 of the heat outputs of some typical furnaces and combustors with recently published data on jet engines. The progress that has been made leads naturally to the consideration of whether further improvements are possible with conventional fuels. In actual furnaces and engines no evident decision can be made as to whether attainable space heating rates are limited by time required for mixing as is generally assumed, or whether reaction rates are of primary importance. It is clear, however, that even if mixing were instantaneous a limit on heating rates would exist due to the finite time required for the reaction of fuel and oxygen molecules. It is of interest, therefore, to determine quantitatively whether reaction rates would be slow enough under practical engine operating conditions to be of significance in limiting the performance.

	HEAT OUTPUT Btu/ft³/hr	OPERATING PRESSURE Atm	SPACE HEATING RATE Btu/ft³/hr/atm²
HOUSEHOLD OIL BURNER	10,000-100,000	1	10,000-100,000
NAVY BOILER	250,000	1	250,000
TURBOJET	30,000,000	3.8	2,000,000
RAMJET	136,000,000	4.3	7,500,000

FIG. 1. Heat output of typical combustors.

Instantaneous Mixing

In a typical continuous flow burner or engine, combustible materials enter the combustion zone in jets, or through a duct partially blocked with some form of grid, and the burning is accomplished by flame-spreading from a stable region at the base of the jet or flame holder.

We may consider that this type of combustor contains at any instant three types of material: (a) unburned combustible at a temperature near that of the incoming feed; (b) burned material at approximately the flame temperature of the reaction; and (c) burning material disposed over more or less continuous flame "fronts" or combustion zones which divide burned from unburned material. Flames propagating in laminar flow have a thickness of the combustion zone of the order of one millimeter at atmospheric pressure. With turbulent flow the thickness of the visible flame zone increases. It has usually been assumed that the increased combustion rate is due to a wrinkling of the flame front that gives an apparent increased volume of reacting material but that the flame sheet at any instant is continuous and gives a rather sharp division of unburned from burned material.

Since only the volume occupied by the flame zone is used for liberation of heat, it appears that considerable gains should be possible if a combustor could be operated so that the entire volume was given over to the combustion reaction. Such a combustor could exist in principle if incoming material could be mixed instantaneously with the material in the combustion zone. In practice, substantially the same operation might be observed if mixing could be made rapid compared to the time required for reaction of the combustible material. Such a combustor would show no flame front. Instead the temperature would be uniform throughout.

For stable adiabatic operation of the combustor with instantaneous mixing it is evident that the heat liberated by reaction would just balance the heat required to warm incoming combustible to the operating temperature, which would be uniform throughout the combustor.

Quantitatively, for stoichiometric fuel-air input,

$$\dot{m}CT_u + dq = \dot{m}CT \text{ (heat balance)} \quad (1)$$

$$\dot{m} = \dot{m}\alpha + \delta\dot{m} \text{ (mass balance)} \quad (2)$$

[a] This work was supported by the Bureau of Ordnance, Department of the Navy, under Contract NOrd 7386.

$$dq = H\delta\dot{m} = H\dot{m}(1 - \alpha)$$

$$= HV\left(\frac{a+f}{f}\right)C_F^k C_A^S B' e^{-E/RT} \quad (3)$$

Noting that

$$C_F = \left(\frac{f}{a+f}\right)\rho\alpha = \left(\frac{f}{a+f}\right)\frac{PM}{RT}\alpha \quad (4)$$

$$C_A = \frac{a}{f}C_F \quad (5)$$

$$\dot{m}(1 - \alpha) = V\left(\frac{a+f}{f}\right)\left[\frac{f}{a+f}\rho\alpha\right]^k \cdot\left[\left(\frac{a}{f}\right)\left(\frac{f}{a+f}\right)\rho\alpha\right]^S B' e^{-E/RT} \quad (6)$$

$$\dot{m} = V\left(\frac{f}{a+f}\right)^{k+S-1}\left(\frac{a}{f}\right)^S \cdot\rho^{k+S}\frac{(\alpha)^{k+S}}{1-\alpha}B' e^{-E/RT} \quad (7)$$

Substituting

$$B = B'\left(\frac{f}{a+f}\right)^{k+S-1}$$

$$1 - \alpha = \frac{T - T_u}{T_f - T_u} \qquad \alpha = \frac{T_f - T}{T_f - T_u}$$

$$\rho = \frac{PM}{RT} \qquad n = k + S = \text{reaction order}$$

$$\dot{m} = V\left(\frac{a}{f}\right)^S\left(\frac{PM}{RT}\right)^n \cdot\frac{(T_f - T)^n}{(T_f - T_u)^{n-1}}\frac{1}{(T - T_u)}Be^{E/RT} \quad (8)$$

In the above

α = fraction of unburned mass in combustor
ρ = gas density
a/f = air fuel ratio
$\dot{m}$ = injection rate = throughput
$\delta\dot{m}$ = mass burning rate
dq = heat liberated per second
$Be^{-E/RT}$ = reaction rate constant
C = average heat capacity of combusting gases (assumed constant)
C_A = air concentration wt/unit volume
C_F = fuel concentration wt/unit volume
$-dC_F/dt = C_F^k C_A^S Be^{-E/RT}$ = assumed reaction rate equation
H = heat of combustion of unit mass of air-fuel mixture = $C(T_f - T_u)$
M = molecular weight (assumed constant)
P = pressure
R = gas constant
T = combustor temperature
T_f = adiabatic flame temperature
T_u = temperature of unburned fuel
V = combustor volume

If $\dot{m}$ is plotted as a function of temperature, a curve of the form shown in Figure 2 is obtained. We see that there is a maximum value of mass injection rate or throughput for stable operation, which for an activation energy of 30–40 kcal occurs at a temperature about ¾ that of the flame temperature for complete combustion, and also that the operation is unstable if the temperature falls below that corresponding to maximum throughput. The portion of the curve near T_u is not associated with significant heat release.

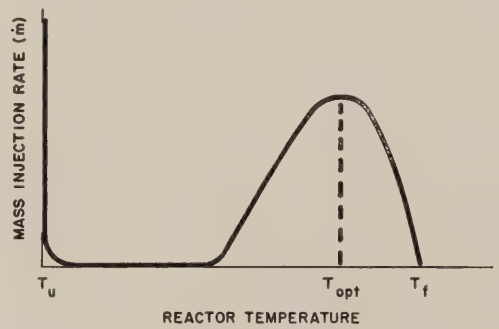

FIG. 2. Variation of reaction temperature with throughput in homogeneous combustor.

It is easily shown that the temperature of maximum throughput is

$$T_{\text{opt}} = \frac{T_f}{1 + \frac{nRT_f}{E}}$$

Thus, measurement of the combustion efficiency at the blowout limit gives directly the activation energy of the reaction (presumed to be of order n). Also, the reaction rate constant B may be derived from the value of the throughput mass at blowout.

Measurements of kinetic parameters by this interesting method have been made by the group at Esso and will be discussed further in the concluding section of this talk.

In a jet engine, in which the momentum of the exhaust gases provides the motive force, unburned material enters the combustor at the upstream end. Practical requirements of minimum duct area and high thrust coefficient lead

to a requirement for axial speeds of flow through the combustor of 200 to 400 ft/sec. For such combustors ignition of a small part of the material is provided by a flame stabilized on a baffle or by a separately controlled pilot flame, from which flame spreads to the remaining combustible.

We now consider the behavior of an adiabatic combustor in which the material to be burned is added in successive increments beginning at the pilot exit, each increment being mixed instantaneously with the burning material at the corresponding station. It is clear from the above analysis that there will be an optimum mass addition rate at any station downstream of the pilot, to give maximum heat release at that station. This mass rate will lead to approximately the same total temperature as that found appropriate for the combustor described above.[b] Optimum heat release will then be achieved when the entire combustor operates at the optimum total temperature[1].

For this combustor with a matched pilot, isothermal operation leads to a curve similar to that presented in Figure 2, with the difference that $1/\dot{m}\ d\dot{m}/dx$ replaces $\dot{m}$ as the independent variable. Increase of injection rate uniformly along the length in the isothermal combustor causes blowout except for the pilot. However, the pilot heat will induce reaction for some distance downstream. If the mass injection rate at any particular station exceeds the critical value, the temperature in that section drops and the rate falls off rapidly at successive stages downstream of that section. However, it is clear that recovery is possible if less than critical mass is injected downstream until the temperature rises to the optimum value again.

The instantaneous mixing concept has implications with regard to combustor design which have been presented elsewhere[1, 2]. Here we wish to consider only the information that may be deduced about the maximum space heating rate. The theory indicates the form of the dependence of the space heating rate (SHR) on pressure, input temperature, and flow velocity, but does not supply actual numbers for the reaction order, activation energy or maximum SHR. Attempts to obtain this information, which must be obtained experimentally, are discussed in the next section.

[b] The conversion of part of the thermal energy to kinetic energy changes the situation slightly.

Flame Temperature Profiles[c]

The initial attempt to derive reaction rate data from a measurement of flame temperature profile appears to have been made in 1948 by Klaukens and Wolfhard[3] who studied acetylene flames in oxygen and air at a pressure of about 15 mm of Hg. They used a thermocouple to determine the temperature. Their work demonstrated that the major amount of reaction occurred in the luminous zone of their flames but they did not attempt to compute quantitative values of the rate. Dixon-Lewis and Wilson[4] in 1951 obtained the temperature profile in a methane flame at atmospheric pressure by a schlieren technique and computed the rate of heat liberation as a function of distance normal to the flame front. They found that heat liberation began at a temperature of about 1200°K and increased rapidly as the flame temperature was approached. However, the small thickness of the flame prevented them from making quantitative estimates of the rate of heat liberation. Recently, the thermocouple method has been further developed and refined by Friedman and Burke[5] who have established experimental conditions and techniques that permit measurements of flame temperature profiles of sufficiently high accuracy to permit quantitative estimates of heat evolution rates. Their investigation was made on a flat propane-air flame maintained by a burner of the Edgerton-Powling type. The propane-air ratio was 29.2 (equivalence ratio = 0.535) and the pressure 0.0594 atm. The adiabatic flame temperature for this composition is 1332°C. Curves of the temperature profile and of the heat release pattern, taken from the Friedman and Burke paper[5], are presented in Figures 3 and 4. The maximum heat release rate, 1.2 cal/cm^{3}sec (4.8×10^5 BTU/ft^{3}hr), was found at a plane slightly beyond the beginning of the luminous zone at a temperature of 1100°C. Data are not available to permit accurate calculation on the basis of this value of the variation of heat release rate with pressure and equivalence ratio. However, for a rough comparison with other work discussed in this paper, it is of interest to compute the rates that may be obtained by extrapolation of Friedman

[c] Lack of space requires us to discuss here only investigations in which attempts have been made to measure space heating rates.

Temperature profiles in flames have been the subject of a rather large number of investigations, which have been reviewed recently by Linnett[6].

and Burke's result. Thus, if one assumes that the pressure dependence of the reaction may be inferred from the flame velocity dependence, the apparent reaction order is 1.4. This would lead to a heat release rate of one atmosphere of 60 cal cm^3 sec, or 2×10^7 BTU/ft^{3}hr. If the rate should vary as the square of the pressure the value would be 1×10^8 BTU/ft^{3}hr at atmospheric pressure.

Finally, Burgoyne and Weinberg[7] have just published a study of the temperature profile in a dilute ethylene-air flame at atmospheric pressure and have presented curves showing the variation of rate of heat release with distance normal to the flame front. No numerical values of the heat release rate are presented[7].

Flame Composition Profiles

An alternative to the derivation of heat release rates from the temperature profile is to use the composition profile and the known heats of reaction. This technique is being developed at the Applied Physics Laboratory. In principle, much more direct information about the chemical kinetics is obtainable by this method than by temperature profile measurements, but at present the experimental technique is less well developed.

The method involves use of a fine probe to withdraw gas samples at various depths in the flame zone, the composition being determined by direct passage of the gas into a mass spectrometer. The high sensitivity of the mass spectrometer makes possible the use of probes small enough so that little disturbance of the flow results, and the ability of the mass spectrometer to give direct information about the entire composition makes this method attractive. At present, only a single complete determination of composition profile is available. This is obtained with a propane-air flame at an equivalence ratio of 0.93 burning at a pressure of 0.265 atm (8.0 in of mercury)[8]. The observed composition profile is presented in Figures 5 and 6. The temperature profile for the same propane-air mixture and pressure has been obtained by the particle track method[9].

From the variation of oxygen content with distance, one can estimate the reaction rate of oxygen through use of the equation for conservation of mass of a particular component[10, 11].

$$\frac{d}{dx}\left(D\rho \frac{dC}{dx}\right) - S\rho \frac{dC}{dx} + W(x) = 0 \qquad (9)$$

Here D is the diffusion coefficient of oxygen in the

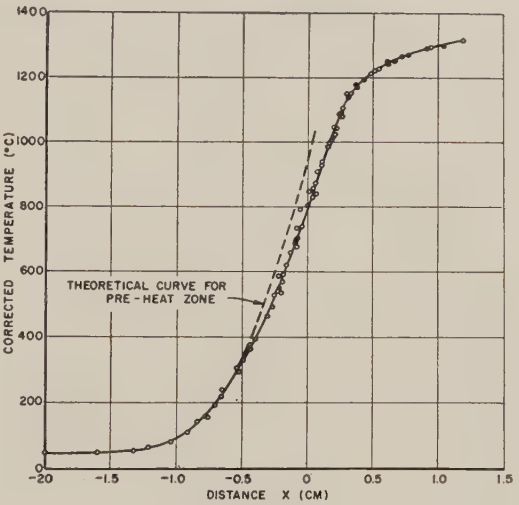

FIG. 3. Corrected temperature vs. distance through flame. (From reference 5.)

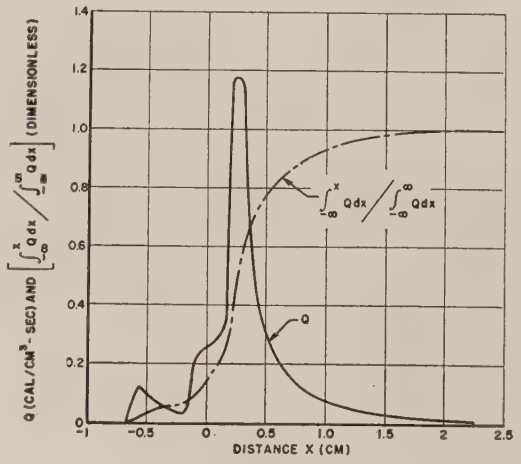

FIG. 4. Instantaneous and integrated heat release as functions of distance through flame. (From reference 5.)

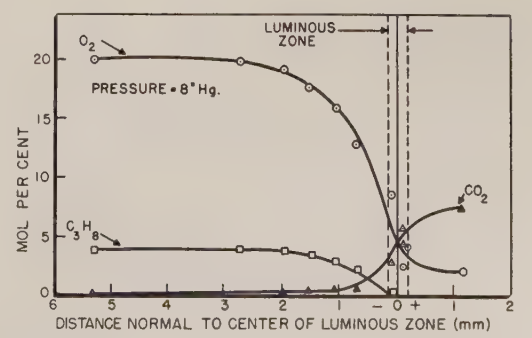

FIG. 5. Composition profile of a propane-air flame.

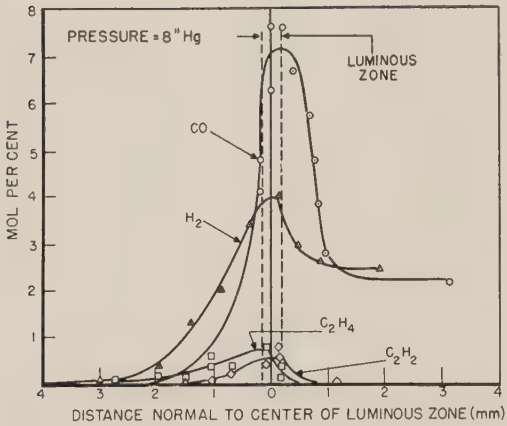

FIG. 6. Composition profile of a propane-air flame.

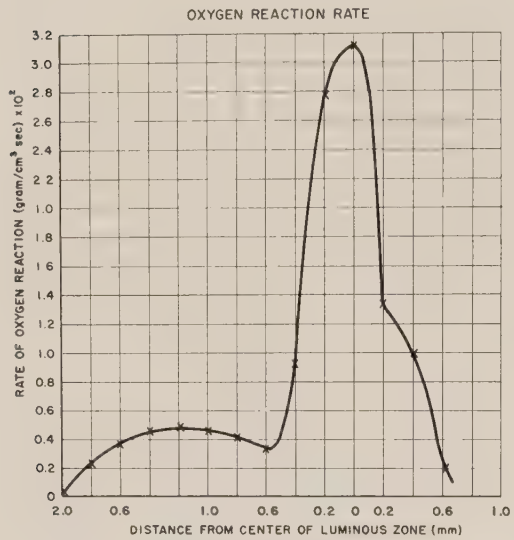

FIG. 7. Variation of oxygen reaction rate with distance from center of luminous zone.

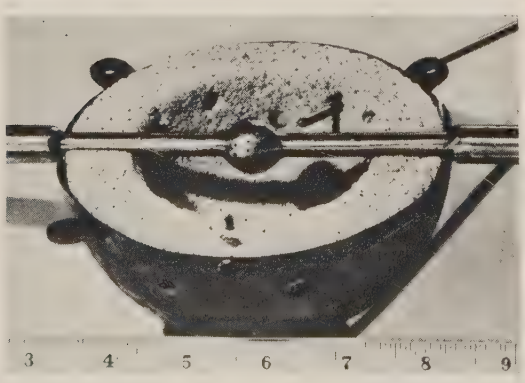

FIG. 8. Spherical reactor. (From reference 5.)

reacting mixture, ρ is the density, C is the oxygen concentration, $\rho S = \rho_0 S_0$ is the product of density and flame velocity, and W is the mass of oxygen reacting at distance x. Values of the diffusion coefficient of oxygen in air may be accurately calculated from the tables provided by Hirschfelder and Curtiss[11]. These values have been used for the propane-air mixture, since the mixture contains nitrogen in large excess and the average molecular weight changes only a few per cent with reaction. Values for the density are derived directly from the temperature profile and composition. The calculation leads to the reaction rate curve shown in Figure 7 which is very similar in shape to that found by Friedman and Burke[5] and Burgoyne and Weinberg[7]. The maximum reaction rate is found at a temperature of 1375°K at the center of the luminous zone. At this temperature and at $\frac{1}{4}$ atmosphere the apparent space heating rate is 4×10^7 BTU/hr ft^3. The value is provisional and may be subject to appreciable error.

It is immediately apparent from Figures 5 and 6 that the composition of the reacting mixture varied markedly with the amount of reaction, so that one might expect the reaction to show an apparent reaction order and activation energy that would depend on the amount reacted. If the reaction had an apparent order of 2, the maximum heating rate at one atmosphere would be 6×10^8 BTU/ft^{3}hr. It is hoped that further development of this method will be possible, to extend the data and to establish the limits of accuracy.

Spherical Reactor

A third method of obtaining reaction rate data at high temperatures involves the use of a new reactor designed at Esso to give extremely rapid rates of mixing[12]. If the mixing rates can be made rapid enough in such a reactor so that mixing times are small compared to the residence time of material in the reactor, and the heat losses can be made negligible, the theory developed for instantaneous mixing should apply and the reaction kinetics could be inferred from the blow-out limits.

In the Esso reactor, shown in Figure 8, premixed fuel-air mixture is injected at high velocity into a spherical shell, insulated on the inside, through a number of jets equally spaced over the surface of the sphere or through jets in a small internal sphere concentric with the reactor. Burned material is ejected through other holes

also uniformly distributed over the reactor surface.

It is found that the reactor operates smoothly over a wide pressure range and that blow-out limits are sharp and reproducible, and independent of the velocity of the entering jets. By observation of blow-out limits at a variety of compositions and pressures, the dependence of reaction rate on pressure and composition may be inferred and the activation energy may be computed from the temperature at which blow-out occurs. The experiments give a value of approximately 40 kcal for the activation energy of hydrocarbon air reaction and a maximum space heating rate of 3 to 5 $\times$ 10^8 BTU/ft^{3}hr at atmospheric pressure[12].

Conclusion

Definite progress has been made in the last two years in investigations undertaken to elucidate reaction kinetics and space heating rates at high temperatures. Methods now exist which offer promise of providing kinetic data of useful accuracy in this field. Estimates of space heating rates indicate a maximum value for hydrocarbon air mixtures of about one-half billion BTU/ft^{3}hr at atmospheric pressure.

Acknowledgment

The writer wishes to thank Drs. Friedman and Longwell for permission to use figures and data from their publications in this paper. He wishes also to express his appreciation to Drs. Fristrom, Westenberg and Rosen of the Applied Physics Laboratory for helpful discussions of the material, and to Mr. Neumann for computational assistance.

REFERENCES

1. Avery, W. H., and Hart, R. W.: Ind. & Eng. Chem., *45*, 1634 (1953).
2. Rosen, P., and Hart, R. W.: J. Aero. Sci., *20*, 549 (1953).
3. Klaukens, H., and Wolfhard, H.: Proc. Roy. Soc. (London), *A-193*, 512 (1948).
4. Dixon-Lewis, G., and Wilson, M. J. G.: Trans. Faraday Soc., *47*, 1106 (1951).
5. Friedman, R., and Burke, E.: J. Chem. Phys., *22*, 824 (1954).
6. Linnett, J. W.: *Selected Combustion Problems, AGARD*, p. 92. London, Butterworth Scientific Publications, 1954.
7. Burgoyne, J. H., and Weinberg, F. J.: Proc. Roy. Soc. (London), *224*, 286 (1954).
8. Prescott, R., Hudson, R. L., Foner, S. N., and Avery, W. H.: J. Chem. Phys., *22*, 145 (1954).
9. Fristrom, R. M., Prescott, R., and Godard, G.: Forthcoming publication.
10. Friedman, R., and Burke, E.: J. Aero Sci., *18*, 239 (1951).
11. Hirschfelder, J. O., Curtiss, C. F., and Bird, R. B.: *Molecular Theory of Gases and Liquids*. New York, J. Wiley & Sons Inc., 1954.
12. Longwell, J. P., and Weiss, M. A.: Forthcoming publication. We are indebted to them for making this information available to us before publication.

XI

A THEORY OF SPACE REQUIREMENTS FOR COMBUSTION BEHIND GRIDS IN A CLOSED DUCT

By JOSEPH JENNISSEN

Introduction

The space requirements for combustion of a steady flowing combustible mixture in a closed duct may be calculated in two ways, by using the concept of a second-degree chemical reaction and by using the concept of flame velocity.

Avery and Hart[1] and Rosen and Hart[2] recently published two papers in which the concept of a second degree chemical reaction was used to calculate the length of combustion chambers. Two basic factors, the frequency and the energy factor, must be known in order to use this concept. In these factors are integrated the kind, arrangement, and the dimensions of burner and duct, as well as the temperature and pressure range and the quality of the fuel used. Conse-

quently, this theory is applicable to designs that are similar geometrically and thermally.

In this paper the concept of flame velocity will be used to calculate the dimensions of combustion chambers and the efficiency of the combustion process behind plane grids in the case of a continuous one dimensional flow. The application of this theory is not restricted as is the second-degree chemical reaction concept. Stability limits of the combustion are not discussed in connection with this theory.

The decisive flame velocity depends on the turbulent properties of the flow produced by means of a grid installed in a duct. To produce a controlled intensity of turbulence the grid has two purposes—to destroy the turbulence of the incoming flow and to generate the wanted turbulence. The energy necessary to maintain the flow through the grid can be expressed by the drag coefficient of the grid.

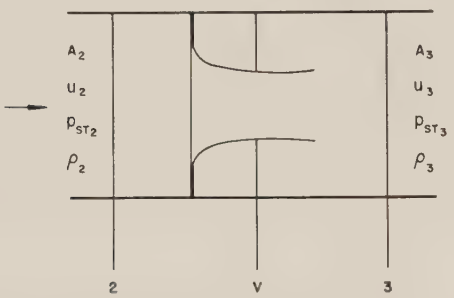

FIG. 1. Flow through an aperture or sudden enlargement.

In the first section of this paper the flow behind a grid without combustion is treated and the correlation between the intensity of turbulence produced and the drag coefficient is shown. In the second part the flow with combustion behind the grid is discussed and the effective flame velocity calculated, the length of the reaction zone estimated and the efficiency of the combustion process determined. The remaining space conditions for combustion behind grids in a closed duct have been related to the results already gained in the third section.

1. Drag Coefficient of Grids or Plane Combustors

It is supposed that the holes of a grid are distributed uniformly and narrowly together and produce an isotropic turbulence in a certain distance behind the grid. In this case, it is sufficient to take into consideration the flow in a duct through a sharp aperture, as shown in Figure 1.

The drag coefficient is defined[3] by the equation

$$C_d = \frac{\Delta p_{st}}{(\rho/2)u_2^2} \tag{1}$$

where Δ_p represents the static pressure difference between 2 and 3, and the denominator represents the dynamic pressure.

In the case of incompressible flow the equations of continuity, energy and momentum yield[4, 5]

$$C_{d_{inc}} = (1/\alpha\psi - 1)^2 \tag{2}$$

where α represents the coefficient of contraction, and ψ represents a ratio of areas

$$\begin{aligned} \psi &= (A_2 - A_{block})/A_2 = 1 - \varphi \\ \alpha &= A_v/(A_2 - A_{block}) \\ \varphi &= A_{block}/A_2 \end{aligned} \tag{3}$$

As equation (2) shows, the drag coefficient does not depend upon the velocity of the flow but upon the product $\alpha\psi$.

The edges of the holes in the grid are well rounded when many small openings cover the grid, as in sieves. The relative magnitude of the roundness has the effect that the contraction coefficient is $\alpha \approx 1$, and on the other hand a strong correlation between the Reynolds number and the drag coefficient occurs. The openings in the grids used as flame holders are bigger and sharp edged. A remarkable change in the order of magnitude for the contraction coefficient results as a function of the kind and form of the single openings and the irregular form of openings at the wall of the duct. Also, the influence of the Reynolds number ceases because complete flow separation occurs at the sharp edges of the openings even when the velocity of the flow is low. Therefore, boundary layers do not have any effect on the flow and the combustion process behind such grids.

The velocities before the flame holder may be high, and therefore the compressibility affects the coefficient of drag. In this case the equations of energy, state, momentum, and continuity yield

$$C_{d_{Co}} = 2/(\kappa Ma_2^2) \left[1 - \frac{\dfrac{(u/a^*)_v}{(u/a^*)_2}(Ma_2/Ma_v)^2 \dfrac{1}{\alpha\psi}}{1 - \kappa Ma_2^2\left(\dfrac{(u/a^*)_v}{(u/a^*)_2} - 1\right)} \right] \tag{4}$$

The coefficient of drag is not only a function of the product $\alpha\psi$ but also of the entrance velocity Ma_2 in this equation.

The influence of the turbulence on the drag has to be investigated next. In the case of incompressible flow, van Driest[6] showed that the turbulence does not influence the statements of the continuity equation but the results of the momentum equation. The steady-turbulent flow equation takes into consideration fluctuations in the flow direction only.

By definition the velocity consists of the mean velocity $\bar{u}$ and the fluctuation u^*. The effective velocity is

$$u = \bar{u} + u^* \tag{5}$$

The application of the momentum, the continuity and energy equation yields the drag coefficient

$$C_{d_t} = (1/\alpha\psi - 1)^2 - 2[(u'/\bar{u})_v^2 1/\alpha\psi - (u'/\bar{u})_3^2] \tag{6}$$

In addition to the term on the right side of equation (2), which is independent of the velocity, two more terms have been found which give corrections for the turbulence in the cross sections A_v and A_3.

Normally the intensity of turbulence given by the expression $(u'/\bar{u})_v^2$ for the narrowest cross section A_v may be neglected because the contraction from A_2 to A_v depresses[7] the intensity of turbulence in the incoming flow so that the fluctuations u_2' do not have a major effect upon the flow behind the grid. In this case, the equation (5) applied to cross section 2 reduces to

$$u_2 = \bar{u}_2 \tag{7}$$

But when the fluctuations are of considerable magnitude, as in the so-called subsonic diffuser of a ramjet behind the last series of shocks, and the product $\alpha\psi$ is unfavorable, the influence of the turbulence may be important. In such a case the flame holder is defective because the turbulence produced by the grid is uncontrolled.

The most important term of equation (6) in regard to turbulence is the intensity of turbulence given by the expression $(u'/\bar{u})_3$. Because of this intensity the flame velocity of the combustible air-fuel mixture will be multiplied, and the mixing of the cold and hot gases will be intensified.

In Figure 2 the correlation between the product $\alpha\psi$ and $C_{d_{Co}}$ with Ma_2 as parameter is shown and in Figures 3 and 4 a graphical representation of equation (6) shows the function between $\alpha\psi$ and C_{d_t} with $(u'/\bar{u})_v = 0$. A comparison of drag coefficients calculated according to the equations (4) and (6) shows that the values of the drag coefficients for constant $\alpha\psi$ approach the same value of $C_{d_{inc}}$ both for $C_{d_{Co}}$ with $Ma_2 \to 0$ and C_{d_t} with $(u'/\bar{u})_3 \to 0$, as must be expected. The differences between $C_{d_{inc}}$ and $C_{d_{Co}}$ increase with higher Mach numbers, especially in the region where $\alpha\psi$ is low and C_d is high. The opposite procedure takes place in the case of turbulent

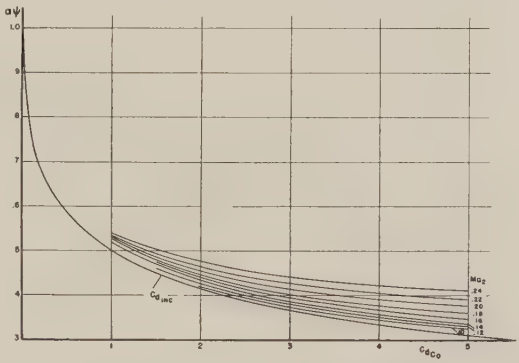

FIG. 2. Influence of the compressibility upon the drag coefficient of grids. (Equation 4)

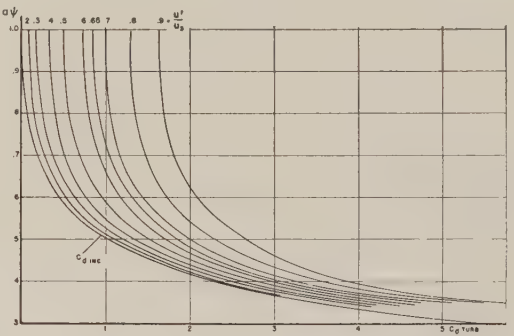

Fig. 3. Influence of the intensity of turbulence upon the drag coefficient of grids. (Equation 6), when $(u'/\bar{u})_v = 0$.

flow, where the difference between $C_{d_{inc}}$ and C_{d_t} is greater when $\alpha\psi \to 1$ and $C_{d_t} \to 0$.

The quality of grids to produce turbulence can be checked with the aid of equation (2). When the drag coefficient of a grid is lower than the equation for $C_{d_{inc}}$ indicates, it is obvious that the turbulence of the incoming flow plays an undesirable role and the grid should be replaced by a grid with a smaller mesh size. The effect of the compressibility, even in the range of $\alpha\psi \approx 0.4$ and $Ma_2 \leqslant 0.25$, is small because nearly an equal increase of the drag coefficient occurs in either case, the compressible without turbulence and

the incompressible with turbulence effect. But the influence of turbulence on the drag coefficient is by far greater than the influence of compressibility in the range of higher $\alpha\psi$ values. Therefore,

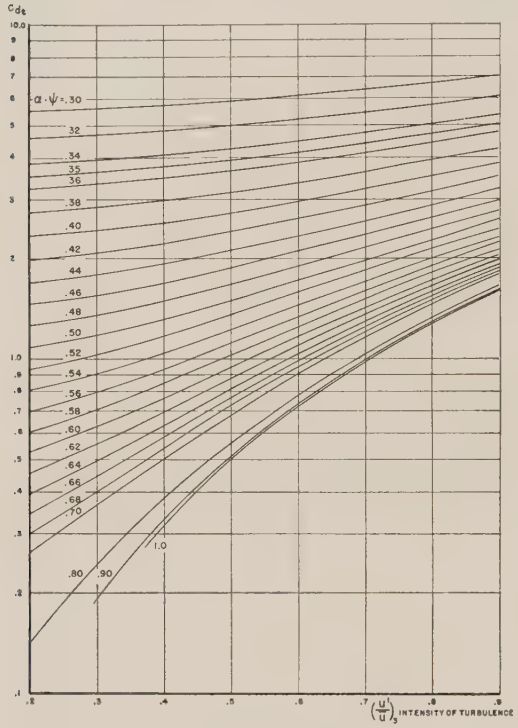

FIG. 4. Influence of the intensity of turbulence upon the drag coefficient of grids. (Equation 6), when $(u'/\bar{u})_v = 0$.

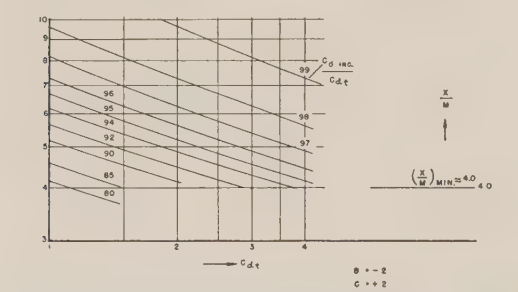

FIG. 5. Distance behind a grid as function of the turbulent drag coefficient. (Equation 9)

Figure 4 may be used to find the intensity of turbulence in a first approximation when $\alpha\psi$ and the drag coefficient of a grid are given.

In the case of isotropic turbulence Taylor[8] expressed the function between the decay of the intensity of turbulence and the distance behind the grid in a useful manner. The general equation is

$$1/(u'/\bar{u}) = B + (5/C^2)(x/M) \qquad (8)$$

where B and C are constants, M is the mesh size, and x is the distance behind the grid. This equation is restricted to the distance $x \geqslant x_{\min}$ when the anisotropy in the x and y direction of the flow is nearly 10 per cent. The ratio x/M means the distance behind the grid made dimensionless by the mesh size M, but the distance may be made dimensionless by any other characteristic length.

The relation of this distance factor x/M to the drag coefficient C_{d_t}, of the grid can be found by introduction of equation (6) into equation (8) under the assumption that $(u'/\bar{u})_v = 0$ and $C = 2$. The result is

$$x/M = 4/5 \left[-B + \left(\frac{2}{C_{d_t}(1 - C_{d_{\text{inc}}}/C_{d_t})} \right)^{1/2} \right] \qquad (9)$$
$$\geqslant (x/M)_{\min}$$

A grid which has a B value of -2, is demonstrated in Figure 5 by use of equation (9). It can be seen that in the distance $x/M \geqslant 4$ a high degree of equalization, expressed by the ratio $(C_{d_{\text{inc}}}/C_{d_t})_3$ has already been attained. But with increasing equalization the distance factor x/M increases, especially when the effective drag coefficient is low. This means that the distance behind the grid, where isotropic turbulence exists, may be defined by prescribing the drag ratio $(C_{d_{\text{inc}}}/C_{d_t})$ or the intensity of turbulence.

In some cases the intensity of turbulence produced by the grid varies from the intensity expected.

Von Bohl[9] shows an undesirable attribute of the decay of turbulence behind grids. He investigated the flow behind flat, sharp-edged, parallel strips in a closed duct and found that under certain conditions two jets fuse together rather than mix. This phenomenon is a function of the area ratio ψ; when ψ is great the jet may stay parallel and mix, but when is small the flow is unstable, and the jets fuse together and generate long wave disturbances which die away slowly. The critical ratio in his experiments is

$$0.54 \leqslant \psi \leqslant 0.63 \qquad (10)$$

but is very sensitive in respect to small changes of the geometry of the grid. It may be expected that the contraction coefficient is also important in this case.

The combination of several grids placed one behind the other changes the drag of the first one,

because the formation of the vortex streets is partly prevented by the presence of the next grid[10]. When the arrangement of grids does not affect the formation of the vortex streets, the drag of the different single grids may be added to calculate the total drag.

The drag of grids can be reduced by tilting against the flow direction, but this reduction results from a decrease in turbulence. Since the generation of turbulence is the purpose of the installed grid, the resulting reduction impairs the intensity of turbulence and the combustion chamber has to be lengthened to give the same combustion efficiency as with the nontilted grid.

The equalization of flow temperature behind a grid consisting of heated bars takes place in a shorter time than the equalization of the flow velocities. Reichardt[11] gives a general relation between temperature and velocity in case of free turbulence.

$$T_x/T_{\max} = (u_x/u_{\max})^{1/2} \tag{11}$$

In this equation the scale of the velocity and temperature has to be adjusted so that the reference points, where $u = 0$ and $T = 0$, correspond to each other.

According to this equation, the pre-reaction process in a combustible mixture behind a grid will be determined by the temperature reached rather than by the local velocity of the flow, assuming that the velocity of reaction is sufficiently high.

2. Combustion of a Combustible Mixture Behind a Grid

Now the flow in the wake of the quasi-stationary eddies immediately behind the baffles shall be investigated. The findings of Section 1 make it possible to form a conception about the flow in this region, as shown in Figures 6 and 7.

The mixture flowing through the grid and not controlled by the quasi-stationary eddies will be heated and ignited by the completely burned hot gases shedded by the eddies. The mixture will be heated to a temperature high enough to induce the decisive reaction of the mixture and to release an appreciable amount of heat. Combustion will be maintained by repeating the process. The zone in which the reaction temperature is reached expands according to the mechanism of turbulence in the wind-shadow region and the temperature reached in the pre-reaction zone. The rate of reaction of the fresh mixture will be slightly diminished by mixing with the burned gases shedded by the eddies, but on the other hand the intensity of turbulence produced by the grid multiplies the laminar burning velocity to a high degree.

The flow rate through the reaction zone is therefore

$$A_2 u_2 (p_{st_2}/p_{st_3})(T_R/T_{st_2}) = S_R v_t \tag{12}$$

where S_R is the reaction surface, v_t the turbulent flame velocity, and T_R the reaction temperature.

For an arrangement of flat strips in a rectangular duct as shown in Figure 6 the length of the

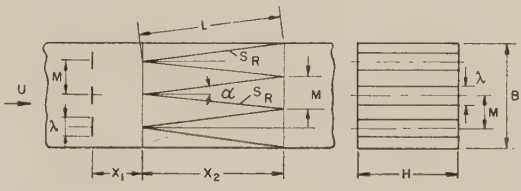

FIG. 6. Flow of a combustible mixture behind a flat grid with parallel slits.

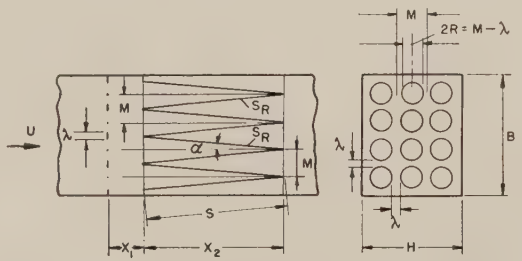

FIG. 7. Typical flow of a combustible mixture behind a flat grid with holes.

reaction zone can be calculated and is

$$x_2 = \frac{1}{2} \frac{1}{p_{st_3}/p_{st_2}} \frac{T_R}{T_{st_2}} \frac{\lambda}{1 - \psi} \frac{u_2}{v_t} \tag{13}$$

If the grid has round holes instead of rectangular slits, the reaction surface consists of conical surfaces in the first approximation as indicated in Figure 7. In this case the length of the reaction zone is

$$x_2 = \frac{1}{2} \frac{T_R/T_{st_2}}{p_{st_3}/p_{st_2}} \frac{M(1 - \lambda/M)}{\psi} \frac{u_2}{v_t} \tag{14}$$

The temperature T_{st_2} is practically the total temperature determined by the flight velocity, as far as the ramjet is concerned, or the temperature behind the last stage of the turbojet. In the pressure range of 2 atm and in the presence of high intensity of turbulence, the reaction temperature of hydrocarbon fuels can be expected to

be $T_R \approx 800°K$[12, 13]. Therefore the temperature ratio T_R/T_{t_2} can be changed only slightly by different fuels. The pressure ratio p_{st_3}/p_{st_2} is in the order of 0.7–0.8 when the combustion chambers are cylindrical. The terms $(\lambda/1 - \psi)$ and $[M(1 - \lambda/M)/\psi]$ are design factors of the grid used.

If the combustion chamber consists of a number of cylindrical tubes, as in ceramic tubes, the length of the reaction zone is

$$x_2 = \frac{1}{4} \frac{T_R/T_{st_2}}{p_{st_3}/p_{st_2}} \frac{M(1 - \lambda/M)}{\psi} \frac{u_2}{v_{app}} \tag{15}$$

where v_{app} shall be an apparent flame velocity.

The next step is to determine the turbulent flame velocity behind the grid when the laminar flame velocity, depending on temperature and pressure, is given.

The turbulent motion behind the grid or obstacle is determined by the magnitude of the intensity of turbulence and the scale. Equation (6) gives the relation between the drag coefficient, the grid constants and the intensity of turbulence produced. This intensity of turbulence is assumed to be distributed uniformly in the cross-sectional area with the index 3. Therefore, this intensity is a mean value reached in a certain distance behind the grid and caused by eddies whose axis are mainly perpendicular to the x direction. The region of these spreading eddies is well defined and may be expressed as a function of the distance behind the grid. When the contours of these eddy fields fuse together, the production of the isotropic turbulence begins and a correlation exists between the components of the velocity fluctuations at any given point. The contours of these fields are surfaces of discontinuity which are associated with the existence of vortices together with the circulatory irrotational motion of the flow of the fresh mixture. In this surface of discontinuity the correlation factor is naturally

$$R_{uv} = 0 \tag{16}$$

It can be assumed that the combustion process in general does not change the intensity of turbulence in a distance $x/M \leqslant (x/M)_{min}$ behind the grid, especially in the surfaces of discontinuity. The conditions may be described by the relations

$$(x/M)_{min} \approx (x/M)_3 < (x/M)_{(x1+x2)C} \tag{17}$$

and

$$(u'/u)_{(x/M)_{min}} \approx (u'/\bar{u})_3 = (u_3'/\bar{u}_2) \approx (u'/u)_{(x1+x2)C}$$

Therefore, as a first approximation the intensity of turbulence may be taken as a constant and to be equal to the mean value according to equation (6). The perception of this essential flow quality permits the calculation of the turbulent flame velocity in the surfaces of discontinuity. The result is

$$v_t/v_l = 1 + [2(u'/\bar{u})_3(u_2/v_l)]^{1/2} \tag{18}$$

This is the same result as in the case of large turbulence found by Karlovitz et al.[14] considering equation (7) when an efficient grid is used to depress the fluctuation of the incoming flow and the assumption

$$\bar{u}_2/\bar{u}_3 = 1$$

is made to find equation (6).

The scale depends on the form and the mesh size of the grid and not on the cross section of the bars. In the distance $x/M \geqslant (x/M)_{min}$ the average size of the smallest eddies is found by Taylor to be

$$d/M = B(\nu/Mu')^{1/2} \tag{19}$$

This equation shows that the diameter d of the eddies is proportional to the kinematic viscosity. Assuming as before that the combustion process does not affect the basic flow pattern, it can be expected that in the case of flow with combustion d is proportional to

$$\left[\frac{T_{st_3}/T_{st_2}}{p_{st_3}/p_{st_2}}\right]_C^{1/2}$$

if the combustion is completed in the isotropic region.

Now equations (13) and (14) can be evaluated, and the minimum length of the combustion chamber can be estimated. The length of the combustion chamber is

$$L_{cc} = x_1 + x_2 = x_R \tag{20}$$

because only a very small amount of the fuel will be burned in the distance x_1 and where

$$x_1 \approx 3\lambda$$

The relation between the length of the combustion chamber and the combustion efficiency is of special interest to the designer.

By definition, the combustion efficiency is the ratio of heat released effectively to the heat released possibly, or expressed in terms of the

reaction surfaces S_R and $S_{R\,\mathrm{eff}}$

$$\eta_{co} = \frac{S_{R\ \mathrm{eff}} v_{t\gamma R\ \mathrm{eff}} (F/A) H_i}{S_R v_{t\gamma R} (F/A) H_i} \tag{21}$$

When all conditions that may affect the combustion process are held constant and the difference between $\gamma_{R\,\mathrm{eff}}$ and γ_R is small because the supposed change of the length stays within reasonable limits, the efficiency is

$$\eta_{co} = \frac{x_{R\,\mathrm{eff}}}{x_R} \leqslant 1 \tag{22}$$

3. Combustion Efficiency and Volume of Combustion Chamber

In Section 2 it has been shown that the length of the combustion chamber depends mainly on the characteristics of the flow behind the grid and of the temperature ratio T_R/T_{st_2} when the reaction begins. But the relation between the flow characteristics, the combustion process, and the volume of the combustion chamber has to be determined yet.

The combustion process may be governed by the well-known equation

$$\eta_{co}\, H_i = \dot{W}_A/\dot{W}_F(1 + \dot{W}_F/\dot{W}_A)h \tag{23}$$

when

$$h = C_{pm}\, \Delta T = C_{pm}\, T_{t2}\, (T_{t3}/T_{t2} - 1)$$

and

$$\dot{W}_A/\dot{W}_F = \nu^+ L$$

then this equation yields the enthalpy

$$h = \eta_{co} \frac{H_i}{\nu^+ L + 1} \tag{24}$$

The residence time of the combustion gases in the combustion chamber is

$$t = \frac{V_{cc}}{A_m \bar{u}_{cc}} \tag{25}$$

where V_{cc} is the volume of the combustion chamber, A_m is the mean cross-sectional area and $\bar{u}_{cc}$ is the mean velocity. A supplemented form of equation (25) reads

$$t = (V_{cc}/h\dot{W}_A) \frac{h\dot{W}_A}{A_2/4(A_3/A_2 + 1)} \frac{1}{u_2(u_3/u_2 + 1)}$$

and the length of the combustion chamber is

$$L_{cc} = t(u_2/2)(u_3/u_2 + 1) = \frac{2}{A_3/A_2 + 1} \frac{h\dot{W}_A/A_2}{h\dot{W}_A/V_{cc}} \tag{26}$$

The length of the combustion chamber is already given by equation (20), and therefore, the heat loading capacity of the burner plane is

$$\frac{h\dot{W}_A}{A_2} = \frac{L_{cc}}{2}\left(\frac{A_3}{A_2} + 1\right)\frac{h\dot{W}_A}{V_{cc}} \tag{27}$$

The heat loading capacity per unit volume is

$$\frac{h\dot{W}_A}{V_{cc}} = \eta_{co} \frac{H_i}{\nu^* L + 1} \frac{A_2 u_2 \gamma_2}{V_{cc}} = \left(\frac{\kappa g}{R}\right)^{1/2} \eta_{co} \frac{H_i}{\nu^+ L + 1} \frac{p_{st2}}{(T_{st2})^{1/2}} \frac{Ma_2}{\dfrac{V_{cc}}{A_2}} \tag{28}$$

When the combustion chamber is a cylindrical one, the equation reads

$$\frac{h\dot{W}_A}{V_{cc}} = \left(\frac{\kappa g}{R}\right)^{1/2} \eta_{co} \frac{H_i}{\nu^+ L + 1} \frac{p_{st2}}{(T_{st2})^{1/2}} \frac{Ma_2}{L_{cc}} \tag{29}$$

But

$$\frac{\dot{W}_A}{A_2} = \left(\frac{\kappa g}{R T_{st2}}\right)^{1/2} p_{st2} Ma_2$$

and therefore

$$\frac{h\dot{W}_A}{V_{cc}} = \eta_{co} \frac{H_i}{\nu^+ L + 1} \frac{\dfrac{\dot{W}_A}{A_2}}{L_{cc}} \tag{30}$$

If equation (30) is solved with respect to the combustion efficiency, there are several possibilities of describing the correlation between η_{co} and the design data.

$$\eta_{co} = \frac{h\dot{W}_A}{V_{cc}} \frac{\nu^+ L + 1}{H_i} \frac{L_{cc}}{\dfrac{\dot{W}_A}{A_2}}$$

$$\eta_{co} = \left(\frac{R}{\kappa g}\right)^{1/2} \frac{h\dot{W}_A}{V_{cc} p_{st2}} \frac{\nu^+ L + 1}{H_i} \frac{(T_{st2})^{1/2} L_{cc}}{Ma_2} \tag{31}$$

$$\eta_{co} = \left(\frac{R}{\kappa g}\right)^{1/2} \frac{h\dot{W}_A}{A_2 p_{st2}} \frac{\nu^+ L + 1}{H_i} \frac{(T_{st2})^{1/2}}{Ma_2}$$

These equations make it possible to evaluate burners from different viewpoints and to compare them with each other.

Under the assumption that $L_{cc} \approx x_2$ the length of the combustion chamber is

$$L_{cc} \approx \frac{\left(\dfrac{\kappa g}{R}\right)^{1/2}}{2\dfrac{p_{st3}}{p_{st2}}} \frac{T_R}{(T_{st2})^{1/2}} \underbrace{M\left(1 - \frac{\lambda}{M}\right)}_{\psi} \frac{Ma_2}{v_t}$$

and the combustion efficiency is

$$\eta_{co} = \frac{R\dfrac{\nu^+ L + 1}{H_i}}{2\dfrac{p_{st3}}{p_{st2}}} \frac{M\left(1 - \dfrac{\lambda}{M}\right)}{\psi} \frac{T_R}{v_t} \frac{h\dot{W}_A}{V_{cc} p_{st2}} \tag{32}$$

as a function of the fuel burned, the fuel-air ratio, the burner data, the turbulent flame velocity, and the heat loading per unit volume as a function of the pressure before the grid with holes.

The cross-sectional area of the burner plane can be found by combining equations (22) and (31) to be

$$A_2 = \frac{h\dot{W}_A}{\left(\dfrac{\kappa g}{R}\right)^{1/2} \dfrac{H_i}{\nu^+ L + 1} \dfrac{p_{st2} Ma_2}{(T_{st2})^{1/2}} \dfrac{x_{R\,\mathrm{eff}}}{x_R}} \tag{33}$$

Equation (33) shows that the area of the burner plane can be calculated directly from the design data, as can the volume of the combustion chamber.

$$V_{cc} = \frac{h\dot{W}_A}{\left(\dfrac{\kappa g}{R}\right)^{1/2} \dfrac{H_i}{\nu^+ L + 1} \dfrac{p_{st2} Ma_2}{(T_{st2})^{1/2}} \dfrac{1}{x_R}} \tag{34}$$

Summary

A theory of space requirements for the combustion of a premixed air-fuel mixture behind plane grids in a closed duct is presented in the case of a continuous one-dimensional flow. The concept of flame velocity is used to calculate the cross sectional area of the burner plane, the length and the volume of the combustion chamber and the efficiency of the combustion process. Relations between the design factors of the flow, the flame holder, the kind of fuel, the air-fuel ratio, the temperatures before and after combustion are given.

The theory is not restricted to designs that are similar geometrically and thermally, so the factors that influence the performance of the combustion chamber may be considered as the status of the design requires. Stability limits of combustion are not discussed in connection with this theory.

Nomenclature

A Cross-sectional area
A Air
a^* Critical velocity
B Constant
B Width of the duct
C Constant
C_d Drag coefficient
d Diameter
F Fuel
g Acceleration of gravity
H Height of the duct
H Heating value of the fuel
h $c_{pm}\Delta T$ or enthalpy
K Kelvin, degree
L Length
L Theoretical weight of air for stoichiometric combustion of unit weight of fuel
Ma Mach number
M Mesh size
p Pressure
R Gas constant of air
R Reynolds number
S_R Reaction surface
T Absolute temperature
u Velocity of the flow
$\bar{u}$ Mean velocity
u' $(\overline{u^{*2}})^{1/2}$, intensity of isotropic turbulence
u^* Fluctuating component of velocity
V Volume
v Velocity
$\dot{W}$ Weight per second
x Distance behind the grid
α Angle in degree
γ Specific weight
Δ Difference
η Efficiency
κ Specific heat ratio
λ Width of the bar of the grid
ν Kinematic viscosity
ν^+ Air ratio number
ρ Density
ψ Ratio of free area
φ Ratio of blockage area

$$\frac{u}{a^*} \quad Ma \left[\frac{(\kappa + 1)/2}{1 + \dfrac{\kappa - 1}{2} Ma^2}\right]^{1/2}$$

SUBSCRIPTS

2 Combustion chamber inlet
3 Combustion chamber outlet
A Air
app Apparent
C Caused by the combustion process
cc Combustion chamber
Co Compressible
co Combustion

eff Effective contrary to theoretical
F Fuel
fl Flame
i In H_i: lower heating value
inc Incompressible
l Laminar
p Pressure
R Reaction
st Static
t Turbulent
v Vena contracta

REFERENCES

1. Avery, W. H., and Hart, R. W.: Ind. & Eng. Chem., *8*, 1634 (1953).
2. Rosen, P., and Hart, W.: J. Aero. Sci., *20*, 549 (1953).
3. Ergebnisse der Aerodynamischen Versuchsanstalt Göttingen, IV Lief., 112 (1932).
4. Strömungslehre L. Prandtl, Vieweg und Sohn Braunschweig, *36*, 153 (1949).
5. Eckert, B., und Pflüger. F.: Lufo *18*, 4 (1941).
6. van Driest, E. R.: J. Appl. Mech., *13*, A231 (1946).
7. Ribner, H. S., and Tucker, M.: Proc. Second Midwestern Conference on Fluid Mechanics, 57 (1952).
8. Taylor, C. I.: Proc. Roy. Soc., *A151*, 421 (1935).
9. von Bohl: Ing. Arch., *11*, 295 (1940).
10. Hoerner, S. H.: Aerodynamic Drag, p. 94. Dayton, Ohio, Otterbein Press, 1951.
11. Reichardt, H.: Zeitschrift f. a. Mathematik und Mechanięk, *15*, 35 (1935).
12. Jost, W.: Explosion and Combustion Processes in Gases, p. 486. New York, McGraw-Hill Book Co., 1946.
13. Gaydon, A. G., and Wolfhard, H. G.: Proc. Roy. Soc., *A196*, 105 (1949).
14. Karlovitz, B., Denniston, D. W., and Wells, F. E.: J. Chem. Phys., *19*, 541 (1951).

Discussion by Stewart Way and E. C. Woodward

(1) The object of the paper is to calculate the dimensions of combustion chambers for continuous tubulent combustion with sloping flame fronts such as might be expected behind a flame holder or grid. The author dismisses, at the outset, all questions of stability. Hence, he does not know whether burning at the flow conditions postulated can exist or not. Consequently, the calculated lengths required for combustion may be fictitious. The theory should in no sense be compared to heat release theories that attempt to predict a maximum rate of heat release for continuous stable combustion. It seems, therefore, that the author rather attempts to answer questions such as "How long would the burning zone be providing there is combustion and turbulent flames anchor at or near to the grid, and burn downstream from it in sloping flame fronts?"

(2) In Figures 3 and 4 the values of turbulence intensity given seem to be extraordinarilly large for the approximately isotropic turbulence downstream of a grid.

(3) Equation (12), which forms the basis of the subsequent derivations, assumes

$$S_R v_t \rho_R = A_2 u_2 \rho_2$$

where ρ is density, and the other symbols are as defined by the author. This implies that the tubulent burning velocity is the normal component of mean flow velocity in the reaction region where density is ρ_R and temperature is T_R. In other words, the author appears to follow the unconventional practice of referring burning velocities to the conditions of the gas in the reaction zone rather than to the state of the unburned mixture. There appears to be an inconsistency here since the formula 18 refers to the rate of advancement of a turbulent flame into unburned mixture.

(4) One wonders what is meant by the state designated by subscript R. It is termed a reaction region. Does the author perhaps mean ignition region, and if so, what is the definition?

(5) It is said that equation (14) applies to flame fronts of the type of Figure 7. The latter are conical flames of base diameter M. A check of the derivation of equation (14) indicates that it applies to conical flames of base diameter equal to the hole diamter M-λ. Perhaps we have misinterpreted some aspect of the assumed flame geometry here.

(6) With regard to equation (15), it is not clear to us what configuration of grid or flameholder is assumed, and what the term, apparent flame velocity, means.

(7) An equation such as (23) is generally taken as the definition of combustion efficiency. In that case the author's equation (22) would be a definition of $x_{R\ \mathrm{eff}}$. If the author chooses to define η_{co} by way of equations (21) and (22), then what is the meaning of $S_{R\ \mathrm{eff}}$ and $x_{R\ \mathrm{eff}}$?

(8) Equations(28), (29), (30) appear to be all simple identities which follow at once from continuity and the definition of efficiency via equation (23). They seem to tell nothing new about possible heat loading capacities.

(9) The various forms of equation (31) appear to give no correlation between η_{co} and the design data, but simply reduce to the equation (23) again, with the rest of the coefficients in the right

hand members all combining to give the value unity.

(10) In equation (32), the terms $h(\nu^{+}L + 1)/H_i$ may be grouped together and they are η_{co} by definition. The remaining terms combine to give unity, by equation (14) and the assumption $L_{cc} = x_2$.

(11) Equation (33), by virtue of equations (22) and (24), and elementary relations, seems to reduce to the identity $A_2 = A_2$, and does not appear to produce any new information. Similarly, equation (34) reduces to $V_{cc} = V_{cc}$.

(12) The assumption of approximately conical flame fronts in the calculation of x_2 may be considerably in error if the turbulent flame front itself is distorted by gross eddies in the wake of the grid, or by large velocity gradients in the transverse direction. Such effects have been mentioned by Longwell in this Symposium.

The writers believe the author's approach can yield interesting information, and for this reason hope that some reconsideration in line with the points mentioned above will be given.

Author's Reply

(1) The aim of this paper is clearly indicated in the introduction.

The stability of a flame behind a bluff body may and has been treated as a special problem separated from the combustion process outside the wake or the recirculation zone. The space requirements for combustion behind grids, as discussed in this paper, are not determined by space requirements for combustion in the recirculation zone because only a very small amount of the fuel present in the mixture will be burned there.

(2) The theoretical values of turbulence intensity cover a wider range than the values produced by grids.

(3) Equation (12) states,

$$S_R \cdot \gamma_R \cdot v_t = S_2 \cdot \gamma_2 \cdot u_2$$

where γ is the specific weight and states that the combustion takes place in the surfaces of discontinuity or the reaction surfaces behind the grid where the turbulent flame velocity is present. It is an unconventional practice to use the concept of reaction temperature T_R. Its use produces simple equations in the subsequent analysis. With this concept, the mixture flowing in the conical cores can be regarded as unburned gases. Equation 18 gives the ratio between the turbulent and laminar flame velocities related to the intensity of turbulence produced by the grid. Therefore, there is no inconsistency in the use of T_R and of the application of equation (18).

(4) The reaction zone is defined as the zone where the temperature is high enough to induce the decisive reaction of the mixture and to release an appreciable amount of heat. The reaction temperature, T_R, is nearly 800°K for hydrocarbons[12, 13]. Below 800°K, slow or partial oxidation takes place which in general does not have any influence on the space requirements discussed. It is known that the introduction of an ignition temperature in the treatment of the burning or reaction zone is not advisable in any case.

(5) It is said that if the grid has round holes the reaction surface consists of conical surfaces *in the first approximation*. The base has the diameter equal to the hole diameter in accordance to tests. Figure 7 is simplified and not correct in this respect.

(6) It is assumed that in a ceramic tube the apparent reaction surface equals π times the average inner diameter of the tube. The apparent flame velocity is defined as the volume of gas per unit time entering divided by the reaction surfaces.

(7) Under the assumptions made in the text, equation (22) is an approximate definition of the combustion efficiency. When the combustion chamber length, i.e., $x_{R\ eff}$, is insufficient the mixture partly flows unburned through the areas cut open at the tips of the cones, shown in Figure 7. Only if the length of the combustion chamber is equal to the theoretical value, x_R, does the mixture flow completely through the reaction surfaces. Equation (21) is the exact definition of the efficiency for the combustion process assumed in this paper.

(8–11) Section 3 is written for design or test engineers and gives relations which may be used in engineering work. Possible heat loading values are specific values for grids used and depend on stability limits of combustion. Useful values cannot be presented on account of security reasons. Part III also aids in visualization of the effect of the different variables in combustion chamber design of this type.

(12) It is true that large velocity gradients would destroy the symmetry of the flow pattern assumed. However, behind a useful, or properly designed, grid such large gradients do not exist in region x_2. When gross eddies in the wake of a grid occur, the flow is unstable. In such a case, the grid should be replaced because the intensity of turbulence produced is uncontrolled and not reproducible. A single rod in a duct is not comparable to a properly designed grid as assumed in this paper.

Combustion of Fuel Droplets

1

COMBUSTION OF DROPLETS OF HEAVY LIQUID FUELS

By H. C. HOTTEL, G. C. WILLIAMS, AND H. C. SIMPSON

Introduction

The combustion of sprays of liquid fuels involves a number of complex processes, most of which are only incompletely understood, but which can be summarized as follows: As the oil droplets enter the furnace, they receive heat by convection from preheated combustion air and from recycled combustion products. They also absorb energy radiated from the furnace walls and from the flame. This addition of heat causes the droplets to evaporate and, in some cases, to polymerize and crack. The major portion of the combustion occurs in the gas phase with the production of a diffusion flame lying either at the O_2-rich boundaries of eddies containing many vaporizing droplets or, depending on mixing conditions, a diffusion flame at least partly surrounding each droplet; and transition from the first to the second state may occur along the flame path in a furnace. This flame is often made luminous by the formation of carbon due to cracking reactions in the gas-phase. A minor, but often important, portion of the fuel burns heterogeneously.

It is clear that the rate of combustion of the fuel spray is a complicated function of the size and velocity distribution of the droplets, the physical and chemical properties of the fuel, its environment, and the character of the mixing process of the spray with air and with combustion products. One aspect of the problem is reported here, viz., the combustion of individual droplets of heavy residual oils and of pure hydrocarbons similar to those occurring in the heavy oils.

In the burning of fuel droplets the physical processes of heat and mass transfer to the droplets are as important as the chemical reactions. Comparatively little study has been made of the overall combustion problem, but much work has been done on the related problem of heat and mass transfer to spheres.

A heated sphere immersed in an infinite, stagnant cooling medium transfers heat by conduction from its surface radially through the medium at a rate

$$\dot{Q} = (4\pi R^2)(h_c)(T_R - T_\infty) \qquad (1)$$

Motion of the fluid medium past the sphere increases the Nussel number, $2h_c R/k_g$, above its theoretical minimum of 2.0. Theoretical attempts to calculate forced convection coefficients by assuming simple flow patterns for the fluid about the sphere[18, 22] have been mainly of qualitative value, while more rigorous theoretical investigations of heat transfer in the boundary layer surrounding the sphere are incomplete[29]. However, empirical equations have been presented in which the Nusselt number (Nu) corresponding to the overall heat transfer coefficient defined by equation (1) has been related to the Prandtl number ($\mathrm{Pr} = c_g\mu_g/k_g$) and Reynolds number ($\mathrm{Re} = 2RV\rho_g/\mu_g$) of the stream. For low Reynolds numbers, these correlations are of the form[21, 25, 30].

$$(\mathrm{Nu}) = 2 + a\,(\mathrm{Pr})^p\,(\mathrm{Re})^q \qquad (2)$$

Perhaps the most reliable of these correlations is the recent one of Ranz and Marshall[25]

$$(\mathrm{Nu}) = 2 + 0.6\,(\mathrm{Pr})^{0.33}\,(\mathrm{Re})^{0.5} \qquad (3)$$

Equation (3) was used in the work described below.

Mass transfer from a sphere into a medium with no large temperature gradients has also been the subject of considerable investigation. In quiescent surroundings only radial diffusion is permitted, and the Langmuir equation[23] can be used to describe the steady-state rate mass

transfer:

$$-\dot{M} = \frac{4\pi R\mathfrak{D}(MW)}{R'T}(p_R - p_\infty) \qquad (4)$$

This equation has been amply verified[14, 16, 17, 24] for large spheres, but has been found to be invalid for vaporization of droplets of diameter less than 20 μ. Such small spheres vaporize at a rate less than that given by equation (4) due to a vaporization resistance[18] as well as to a diffusion resistance in the surrounding medium[2, 8]. However, for the work described below, it was not necessary to include these refinements. For droplets less than 1 μ[32] the increase of vapor pressure due to surface tension must be included in evaluating p_R. These facts emphasize that even the vaporization of a sphere cannot be described by one simple equation, valid for all drop diameters of interest. It is likewise brought out below that the mechanism of combustion of droplets depends on the size range of droplets considered.

The equation for the vaporization of a sphere can be written in a form similar to equation (1), viz.,

$$-\dot{M} = (4\pi R^2)(b)(\rho_R - \rho_\infty) \qquad (5)$$

where ρ_R and ρ_∞ are the mass per unit volume of the diffusing material at the droplet surface and far from the droplet surface, respectively, and b is a mass transfer coefficient. The Sherwood number (Sh) for mass transfer is defined to be $(2bR/\mathfrak{D})$ and has a value of 2.0 for radial diffusion from a sphere into a quiescent medium. Attempts have been made to predict from theory the Sherwood number for mass transfer from a sphere into a flowing medium[22] but more reliable estimates are provided by empirical equations[7, 25, 31] relating the Sherwood number to the Reynolds number (Re) and the Schmidt number (Sc = $(\mu_g/\rho_g\mathfrak{D})$) in the form

$$(\mathrm{Sh}) = 2 + a\,(\mathrm{Sc})^p\,(\mathrm{Re})^q \qquad (6)$$

Probably the most reliable estimate for mass transfer from a sphere moving at a low Reynolds number is that provided by Ranz and Marshall[25]

$$(\mathrm{Sh}) = 2 + 0.6\,(\mathrm{Sc})^{0.33}\,(\mathrm{Re})^{0.5} \qquad (7)$$

The similarity between equations (3) and (7) is obvious.

The most extensive studies of the combustion of individual oil droplets have been carried out by three groups of investigators: workers at M.I.T.[3, 9, 27], at the National Gas Turbine[10] and Royal Aircraft Establishments[5] in England, and the work of Spalding[28] in England.

The earliest quantitative work on single droplets was carried out by Chang[3] and Gerald[9]. They burned droplets of a Bunker C fuel oil by dropping them through a vertical tubular furnace, catching and extinguishing them at the bottom. By comparing the weight of the residual droplet with that of the original droplet, a measure of its degree of combustion was obtained. By measuring the falling velocity of the droplet at different known points along its path through the furnace, with intermittent flash photography, an estimate of the residence time of the droplet in the furnace was obtained. The effective length of the furnace was readily changeable and it was thus possible to subject the droplets to the high temperature atmosphere for different lengths of time. They studied the combustion of heavy oil droplets of mass 10–30 μg. (i.e., diameter 270 μ to 380 μ) at furnace temperatures of 800°–1100°C. The information obtained by these experiments is substantially in agreement with the more recent work forming the basis of this paper.

Godsave[10] suspended single droplets, 1500 μ to 2000 μ in diameter, of some sixteen light fuels on a silica fibre, ignited them, and followed the progress of the combustion photographically. He showed that, for his limited range of variables, the mass rate of vaporization of the droplets was proportional to the first power of the droplet radius R according to the equation,

$$-\dot{M} = \frac{\rho_l \pi \beta}{2} R \qquad (8)$$

where ρ_l is the density of the liquid fuel and β is the evaporation constant, shown to depend mainly on the heat required to vaporize unit mass of fuel. The similarity between equation (8) and Langmuir's equation (4)) is obvious. Similar experiments by Diederichsen and Hall[5] indicated that β was proportional to the fourth root of the atmospheric pressure, the effect being attributed to change in latent heat of the fuel associated with pressure change. Godsave calculated β on the basis of a very much simplified picture of the combustion process. He considered the droplet to be spherical, of radius R, surface temperature T_R, and surrounded concentrically by an infinitesimally thin flame of radius R_F and temperature T_F. Then assuming steady-state, radial heat transfer from the flame to the droplet against the outward-diffusing, vaporized fuel with the prop-

erties of the gaseous medium independent of temperature, it was simple to solve the Fourier-Poisson equation to give

$$-\dot{M} = 4\pi R \frac{k_g}{c_g} \frac{R_F}{R_F - R} \log_e \left\{ 1 + \frac{c_g(T_F - T_R)}{\lambda'} \right\} \quad (9)$$

Although Godsave showed that for his drop size range R_F/R varied between 2.4 and 3.0, the value of this ratio is unknown for smaller droplets; the value of T_F is also unknown.

While attempts have been made to predict theoretically the effect of gas motion about the droplet on the vaporization and combustion of that droplet, e.g., Gohrbandt[11], the most interesting investigation was that of Spalding[28] in which attention was focused on combustion in a diffusion flame close to a surface of liquid fuel. By assuming the properties of the gas surrounding the fuel surface to be everywhere equal to the values at the fuel surface, Spalding was able to apply boundary layer theory to predict burning of liquid fuel off some simple geometrical shapes, particularly the flat plate parallel to a flowing air stream. This last problem has recently been more carefully solved by Emmons[6]. Spalding did not solve the problem of liquid fuel burning off a sphere in a flowing gas stream but did state that the rate of vaporization of a liquid sphere into a medium in which only radial flow was possible (the diffusion flame concentric with the droplet) was given by an equation similar to equation (9),

$$-\dot{M} = 4\pi R \frac{k_g}{c_g} \log_e (1 + G') \quad (10)$$

where G' is the transfer number of the fuel, defined as,

$$G' = \frac{b_\infty - b_R}{\lambda'} \quad (11)$$

Here b_R and b_∞ are the total enthalpies of unit mass of the gas mixtures at the droplet surface and far from the droplet surface, respectively, above a base in which zero enthalpy is assigned to the fuel, nitrogen and products CO_2 and H_2O (g) at a base temperature T_0. On this basis, oxygen at T_0 has a positive enthalpy equal to the heat of combustion of a stoichiometric mixture of oxygen and fuel. This parameter G' entered into all the solutions obtained by Spalding for fuel burning from surfaces of different shapes. Clearly equation (10) provides yet another definition of β in equation (8). Comparison of the flat-plate theory with data obtained by Spalding for fuel burning off ½ in to 1½ in diameter spheres in a flowing air stream showed encouraging agreement. Both the theories of Gohrbrandt[11] and Spalding[28] predict that the mass rate of vaporization of a droplet is proportional to the square root of the Reynolds number. Spalding's work indicates that the mass rate of vaporization of a sphere is given by an equation of the form,

$$-\dot{M} = 4\pi R \frac{k_g}{c_g} G' f(G', \mathrm{Pr}) \sqrt{\mathrm{Re}} \quad (12)$$

where the form of the function f is unknown for spheres.

The experimental data described above were of low accuracy and covered small ranges of the relevant variables. Also, most of the more recent work has been on light fuels under conditions different from those encountered in industrial furnaces. The objective of the experimental work described below was to measure, under conditions of high radiation heat flux similar to that encountered in commercial furnaces, combustion rates of droplets of heavy oils of diameter small enough to be at least approaching the size used industrially. An attempt was made to extend and examine the theories of Godsave and Spalding and consideration was given to heat transfer within the droplet during the combustion process, a feature incompletely considered in recent literature.

Experimental Procedure

Droplet burning was studied by projecting a stream of uniform droplets up into an electric furnace and allowing these droplets to follow their trajectories inside the furnace and out through the bottom of the furnace. A diagram of the equipment is shown in Figure 1. The droplets were extinguished as they left the furnace, and the weight of the residual droplets was compared with that of the original droplets. Residence time of the droplets in the furnace was measured by recording photoelectrically the instants at which the droplets entered and left the furnace. By changing the position of atomizer underneath the furnace it was possible to change the height to which the droplet was projected into the furnace. Thus, curves of degree of combustion versus residence time in furnace were built up for each fuel for a range of initial drop sizes and furnace tem-

peratures. This technique was considered to offer five advantages: (1) The furnace had all major heat sinks at the bottom; thus the combustion space was free from convection currents and nearly isothermal. (2) Residence time of the droplets in the furnace was measured directly. (3) The narrow stream of droplets on being projected into the furnace fanned out to a certain extent. Slight variations in drop size, velocity, or the combustion properties of the fuel accentuated

As shown in Figure 1, the equipment was made up of four main parts: the furnace, the atomizer, the timer, and the extinguisher. The furnace was in the form of a rectangular parallelepiped, 18 in tall, 8 in wide, and 3 in deep, well-insulated on the top and vertical sides. The bottom of the furnace was closed off by a slice of firebrick roughly $\frac{3}{4}$ in thick, containing a slot $\frac{1}{2}$ in wide and 5 in long for entrance and exit of the droplets. Energy was supplied to the furnace through coils

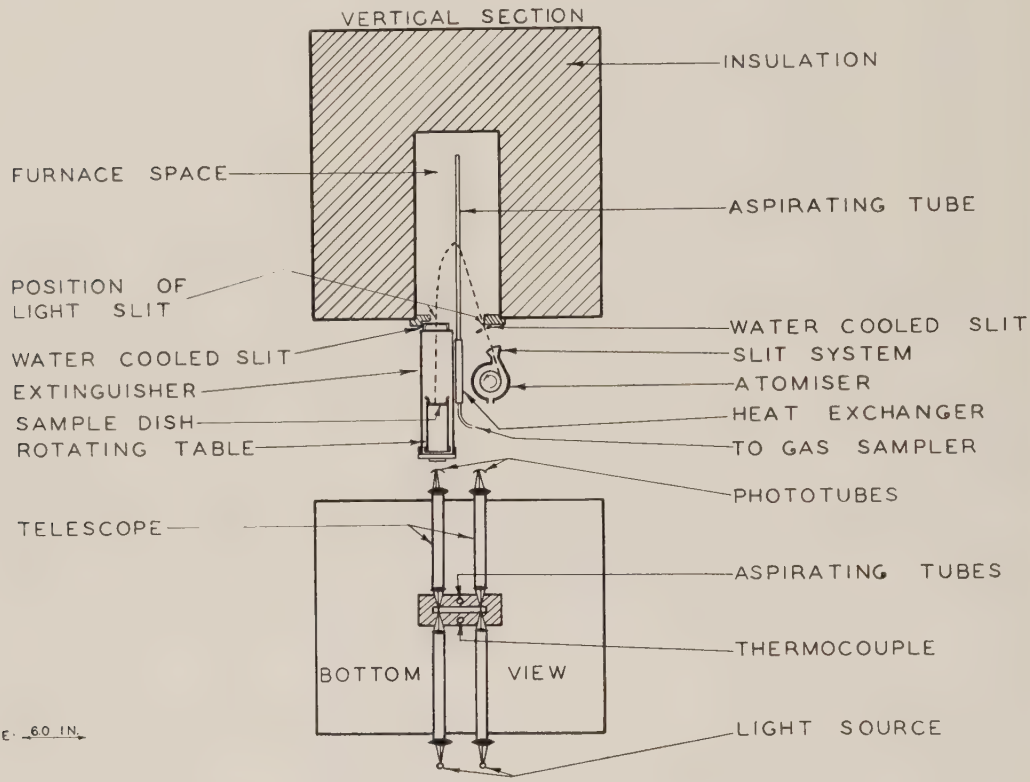

Fig. 1. Diagram of apparatus

this. By collecting only a narrow width of the downward spray of droplets, selection was made of rigidly controlled droplets. (4) The degree of combustion of the droplets was found directly from the mass of the residual droplets, not from measurement of diameter. As shown below, the density of droplets of residual fuels changed markedly during combustion. Consequently, the diameter of the residual droplet did not provide a reliable measure of the degree of combustion. (5) The droplets were projected into high temperature air and were submitted to intense thermal radiation in a manner similar to that encountered in industrial practice.

of number 8 gauge Kanthal A1 wire arranged, as far as possible, to compensate for the major heat sink at the bottom of the furnace. Furnace temperature was measured by means of a platinum, platinum-rhodium thermocouple mounted in an alundum tube vertically in the furnace. The furnace gases were aspirated for analysis through a second similar alundum tube mounted vertically in the furnace and leading out through the bottom brick to a small tubular heat exchanger.

A flat, steel, spinning disc atomizer was used to project a stream of uniform droplets upwards into the furnace. This disc, 1.6 in in diameter, $\frac{1}{8}$

in thick, was mounted in the vertical plane underneath the furnace as shown in Figure 1, and was driven through a simple system of changeable gears by a synchronous motor. Coaxial with the disc was a cylindrical steel cover of outside diameter 3 in which contained a slit parallel to its axis ¼ in wide in the plane of the disc face. A small fraction of the droplets from the periphery of the disc passed through this slit to form the droplet stream. The remaining droplets impinged on the wall of the cover and were drained off at the bottom into a sump. The fuel was held in a steel reservoir of capacity roughly 1000 cc and was fed on to the center of the disc through a filter gauze and then a horizontal feed tube. Nitrogen pressure was used to drive the oil and a capillary meter to measure the flow rate of nitrogen and hence of the oil. The whole atomizer unit (i.e., atomizer, atomizer housing, synchronous motor and gears, oil reservoir and feed tube) was mounted on to a heavy metal arm which could be moved horizontally and vertically underneath the furnace with screw adjustment. To change the angle of projection of the droplets into the furnace the cover, and hence the slit, was rotated by a screw adjustment. A converging-diverging system of slits mounted on the atomizer slit (Fig. 1) was used to define the droplet stream to a width of roughly 0.10 in. Since highly viscous oils and hydrocarbons solid at room temperature were under investigation, six heating coils were mounted on the atomizer system to keep the fuel fluid, and five iron-constantan thermocouples were distributed about the atomizer system for fuel temperature control.

The timer consisted of two photometers, one in the path of droplets entering the furnace, the other in the path of those leaving. Each photometer consisted of: (1) a light source, (2) a system of lenses and a collimator to focus the light to a slit, roughly ¼ in wide and 0.05 in thick in the plane of the droplet trajectory, (3) a similar system of lenses to pick up the light after the trajectory plane and focus it on to a phototube, and (4) an amplifier. These photometers were placed so that the light slits were as close to the furnace bottom as possible, and the bottom brick was shaped to the light beam. Signals from the photometers were observed on oscilloscopes mounted close to the furnace and were recorded on a Heiland mechanical oscillograph. To ensure that each droplet entering or leaving the furnace traversed a light beam, a water-cooled slit, roughly ¼ in wide, was placed before each light beam, one attached to the inlet photometer, and the other to the extinguisher. Both slits were shaped to the contour of the light beams. Slit positions are shown in Figure 1.

The extinguisher was a brass cylinder 12 in tall and outside diameter 3 in. The outside of the cylinder was water-jacketed, and the inside could be partially evacuated and filled with nitrogen. On top of the cylinder was a housing containing two opposed glass windows through which the light beam of the exit photometer could pass, and a roof forming the water-cooled slit mentioned above. This slit was ¼ in square with a metal strip running on rails across the top to close it. On the outside of the bottom of the extinguisher was mounted a 60 rpm motor with its shaft attached to an aluminum table mounted inside the extinguisher. Residue samples were collected in a glass culture dish on this rotating aluminum table and the vertical position of the dish inside the extinguisher could be changed by supporting the dish on one of a series of aluminum cylinders. Flat droplet trajectories required the collecting dish to be high in the extinguisher. Some of the residues were quite fluid and it was necessary to freeze these droplets as soon as they hit the collecting dish. For this, a brass pan, similar to the aluminum one, was constructed with copper fins projecting downwards into a Dewar flask filled with a freezing mixture. The whole unit was mounted on top of the aluminum pan and could be rotated inside the extinguisher.

In operation, the best atomizing conditions for each fuel were determined, the atomizer was calibrated for a series of disc angular velocities by weighing a representative sample of droplets, the atomizer was placed in the desired vertical position underneath the furnace and the extinguisher, water-cooled slits, and atomizer were aligned with the trajectory of the droplets. Depending on the type of residue, dry or sticky, the sample was collected either on a dry culture dish or a circular disc of weighed aluminum foil spread across the bottom of the dish. For low viscosity residues the freezing unit was used with the aluminum foil. When the equipment was satisfactorily aligned, the extinguisher slit was opened, a sample of the residues was collected on the rotating dish for 5 to 10 min, and a representative series of signals from the photometers were recorded for ½ to 1 min on photosensitive paper moving at roughly 2 in/sec. At the end of a run, the gases from the furnace were aspirated and analyzed. In no case was more than 0.1 per cent

CO_2 ever detected in these gases. The average mass of the residual particles was found by weighing 50 to 100 of them on an assay balance to within ± 10 μg. Consequently, the precision of the average weight of a particle was no better than ± 0.1 μg. The residence time of the droplets was found by measuring, to within 0.01 in, the distance between corresponding inlet and exit pulses recorded on the photographic paper. Despite the fact that less than 10 per cent of the droplets entering the furnace passed through the exit light beam, little trouble was found in identifying corresponding pulses if the rate of projection of droplets into the furnace was low (e.g., 100–200 droplets per minute). A minimum of ten exit pulses was used to establish the residence time of the droplets with the atomizer in a given position. Thus, an average residence time of the droplets in the furnace was determined, with a scatter of ± 5 millisec from droplet to droplet in a good run. Other details of the equipment and operating procedure are given by Simpson[27].

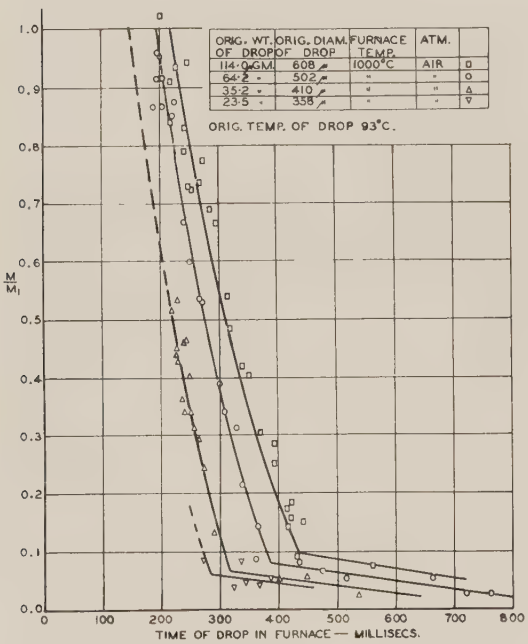

FIG. 2. Effect of drop size on combustion of Type A production oil at 1000°C.

For each run, the basic measurements made were degree of combustion of the droplet, residence time, furnace temperature, distance of atomizer from the furnace entrance, initial droplet size; and, where possible, photomicrographs were taken of a sample of the residual particles. From these, the average diameter of the particles was estimated. Since only 6 to 40 particles per sample were so measured, these data are of low accuracy.

Experimental Results

Residual fuel oils and pure hydrocarbons were investigated. All experiments were at atmospheric pressure. The range of drop sizes and furnace temperatures capable of being investigated with the equipment described above was established with a residual fuel oil called Type A Production which was typical of its class. It was found possible to obtain combustion curves for droplets initially of diameter roughly 350 μ, 400 μ, 500 μ, and 600 μ, burning in air at temperatures of 900°C, 1000°C, and 1100°C. These data are presented in Figures 2, 3, and 4. In Figure 2, where M is the mass of the droplet at time t, and M_1 is its original mass, the effect of initial drop size on the fractional combustion of the fuel is shown at a furnace temperature of 1000°C. In Figure 3, $M^{2/3}$ versus residence time shows the effect of furnace temperature on the combustion of the 400 μ, 500 μ and 600 μ droplets.

To investigate the possible effect of the flame surrounding the burning oil droplet, a series of runs was carried out in which the furnace was filled with nitrogen so that the vaporizing fuel did not ignite. The vaporization of droplets of Type A oil of initial diameter roughly 500 μ in the inert nitrogen atmosphere at 1000°C is compared in Figure 4 with the combustion in 1000°C air of the same oil atomized to the same drop diameter. Some data were also taken with another residual fuel oil, Type B oil, reputed to have a high tendency for the formation of stack solids. These data compare closely with the data taken on the Type A production oil. Some of the data obtained by Chang[3] and Gerald[9] on the combustion of their fuel oil are shown in Figures 5 and 6. These curves include data taken with the droplets burning in atmospheres containing 5 per cent and 10 per cent oxygen.

The inspection data and the available analyses for each of these three residual oils are given in Table 1. The distillation curve, corrected to atmospheric pressure, of the Type A production oil calls for 5 per cent off at 180°C, 50 per cent off at 526°C and 75 per cent off at 630°C.

The measured diameters of the cold, dry residual particles of the Type A production oil

are shown in Figure 7 as R/R_1, the fractional radius after residence time t, plotted against M/M_1, the corresponding fractional mass. Within the scatter of the data, the experimental points can be divided into three groups corresponding to initial droplet diameters of roughly 400 μ, 500 μ and 600 μ irrespective of the furnace temperature in the range 900°C to 1100°C. The separation into three groups of data is indicated by lines in Figure 7. Also shown is the line of constant initial oil density.

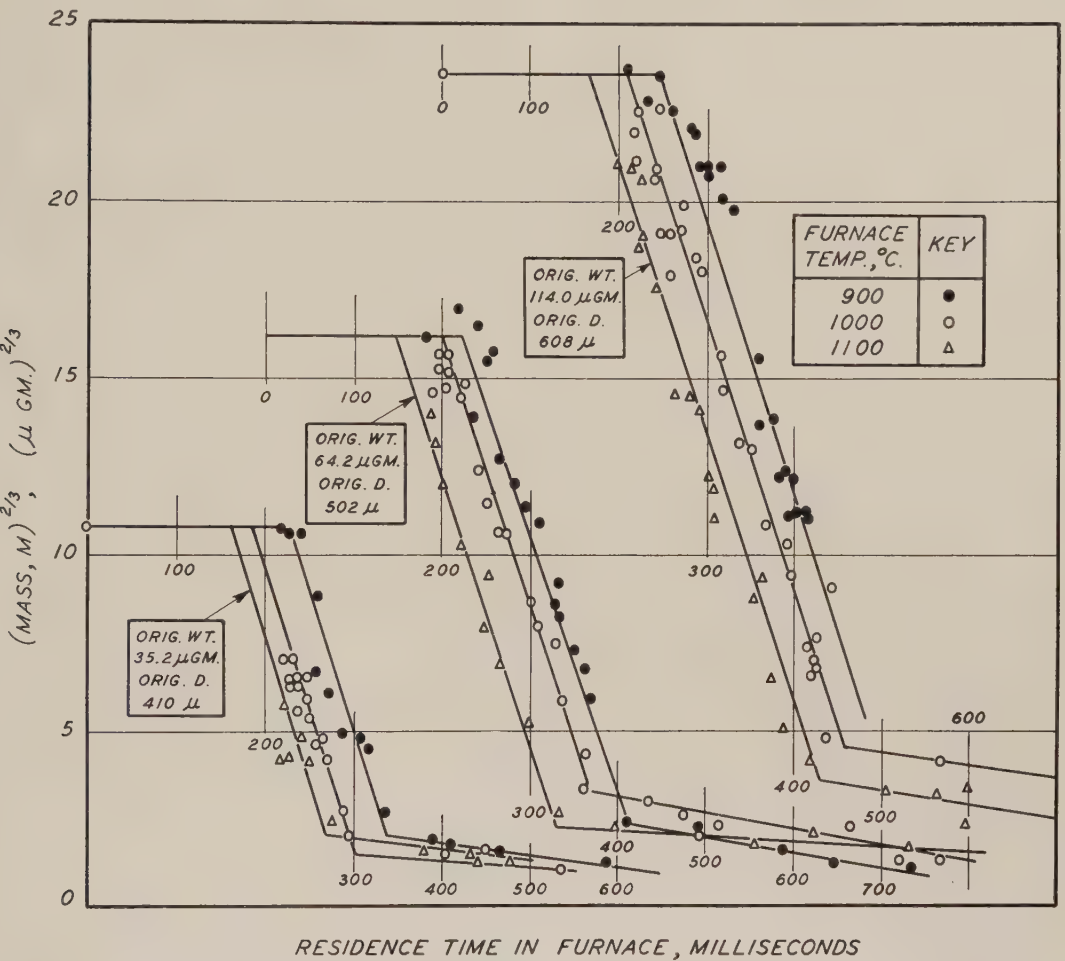
(MASS, M)^2/3 , (μ GM.)^2/3
RESIDENCE TIME IN FURNACE, MILLISECONDS
FURNACE TEMP., °C.
KEY
900
1000
1100
ORIG. WT. 114.0 μGM. ORIG. D. 608 μ
ORIG. WT. 64.2 μGM. ORIG. D. 502 μ
ORIG. WT. 35.2 μGM. ORIG. D. 410 μ

FIG. 3. Effect of furnace temperature and drop size on combustion time for Type A production oil. (Note displaced time-scales for the 3 drop sizes.)

Experiments were also made on the combustion of six hydrocarbons, three paraffinic and three aromatic, similar to those which occur in residual fuel oils. There is evidence[27] that residual fuel oils contain polynuclear aromatic and naphthenic hydrocarbons with long paraffinic side chains, the number of rings per molecule ranging from two or three up to more than ten in the resinous and asphaltic constituents, with as high as sixteen carbon atoms in the side chains. It was difficult to obtain such hydrocarbons in pure form. Thus the six hydrocarbons were chosen to give as wide a range of boiling points, latent heats, and carbon-hydrogen ratios as possible and still be related to the residual fuel oil. A reasonably low melting point was also necessary for easy atomization.

The hydrocarbons were burned only at a furnace temperature of 1000°C and in an air atmosphere. The hydrocarbons investigated were cetane (i.e., *n*-hexadecane), *n*-eicosane, a very narrow cut wax estimated to be *n*-hexacosane from its melting point, *m*-terphenyl, phenanthrene, and acenaphthene. Some of the properties are listed in Table 2. Liquid properties were

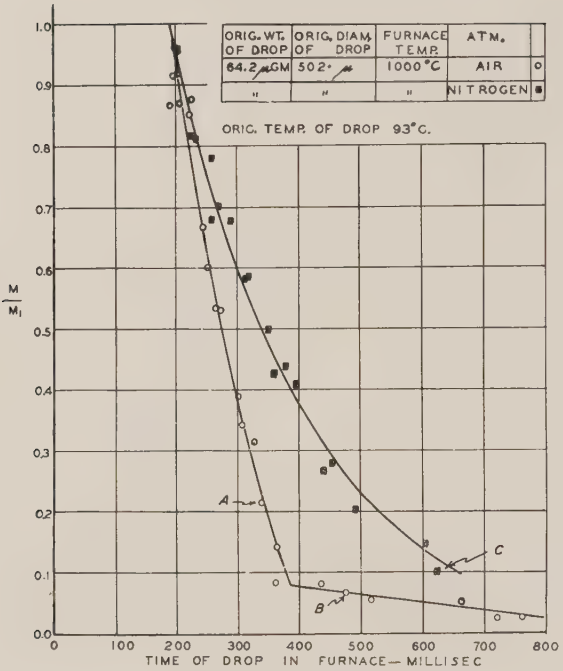

FIG. 4. Comparison of mass reduction rate of 500 micron drops vaporizing in a nitrogen atmosphere with burning rate in air. Photographs of residues corresponding to points A, B, and C are shown in Fig. 19 A, B and C, respectively.

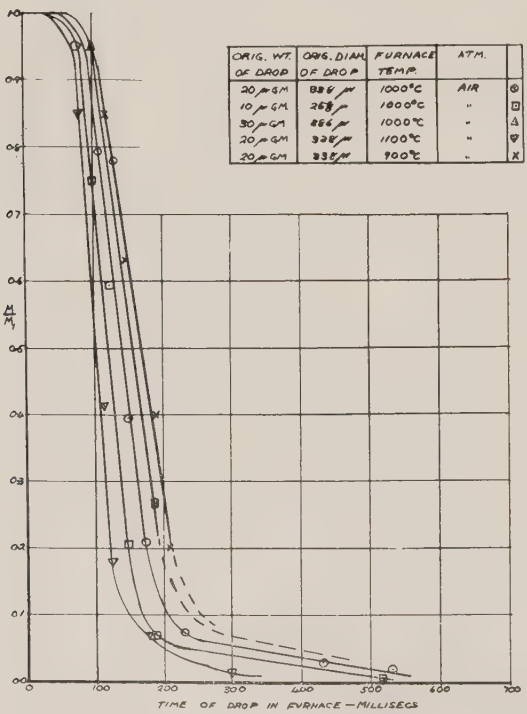
ORIG. WT. OF DROP
ORIG. DIAM. OF DROP
FURNACE TEMP.
ATM.
20 μGM 338 μ 1000°C AIR
10 μ GM. 268 μ 1000°C "
30 μ GM 386 μ 1000°C "
20 μ GM 338 μ 1100°C "
20 μ GM 338 μ 900°C "
M/M1
TIME OF DROP IN FURNACE — MILLISECS

FIG. 5. Combustion of Bunker C fuel oil, data of Chang[8].

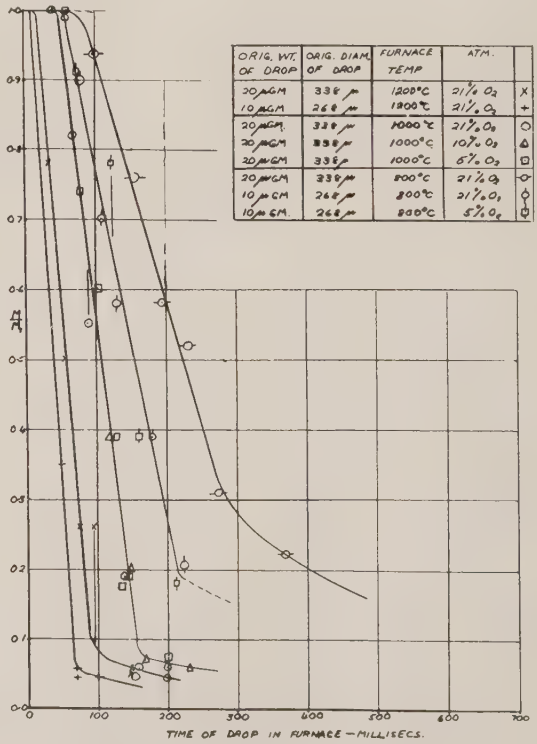
ORIG. WT. OF DROP
ORIG. DIAM. OF DROP
FURNACE TEMP.
ATM.
20 μGM 338 μ 1200°C 21% O2 X
10 μGM 268 μ 1200°C 21% O2 +
20 μGM 338 μ 1000°C 21% O2 ○
20 μGM 338 μ 1000°C 10% O2 △
20 μGM 338 μ 1000°C 5% O2 □
20 μGM 338 μ 800°C 21% O2 ◇
10 μ GM 268 μ 800°C 21% O2 ◇
10 μ GM 268 μ 800°C 5% O2 □
M/M1
TIME OF DROP IN FURNACE — MILLISECS.

FIG. 6. Combustion of Bunker C fuel oil, data of Gerald[9].

evaluated at a temperature midway between the boiling point of the fuel and the temperature of atomization; vapor properties were evaluated at the pure hydrocarbons, for reasons that are given below, are presented in Figure 9 in the form of (mass of the droplet)$^{2/3}$ versus residence time of

TABLE 1. INSPECTION DATA FOR THE RESIDUAL FUEL OILS

	Type A	Type B	Chang and Gerald fuel
Gravity, °A.P.I.	13.7	14.8	10.7
Viscosity, Furol at 122°F, sec	186	173	128
Flash, P.M., °F	208	250	180
Pour, max, °F	—	20	—
Water by distillation, wt per cent	Trace	0.05	—
Sediment by extraction, wt per cent	—	0.01	—
Sediment by hot filtration, wt per cent	0.10	0.01	0.23
Ash, wt per cent	0.08	0.05	—
Water soluble ash, wt per cent	—	0.05	—
Sulfur, wt per cent	2.53	2.85	—
Insoluble in 86° naphtha (modified), wt per cent	10.1	12.1	10.37
Stack solids, wt per cent	1.1–1.2 (est)	1.7	—
Analysis:			
Carbon, wt per cent	85.31	85.99 (est)	
Hydrogen, wt per cent	10.91	11.16 (est)	
Sulphur, wt per cent	2.53	2.85 (est)	
Nitrogen, wt per cent	0.44	—	
Oxygen, wt per cent	0.43	—	
Ash, wt per cent	0.08	—	

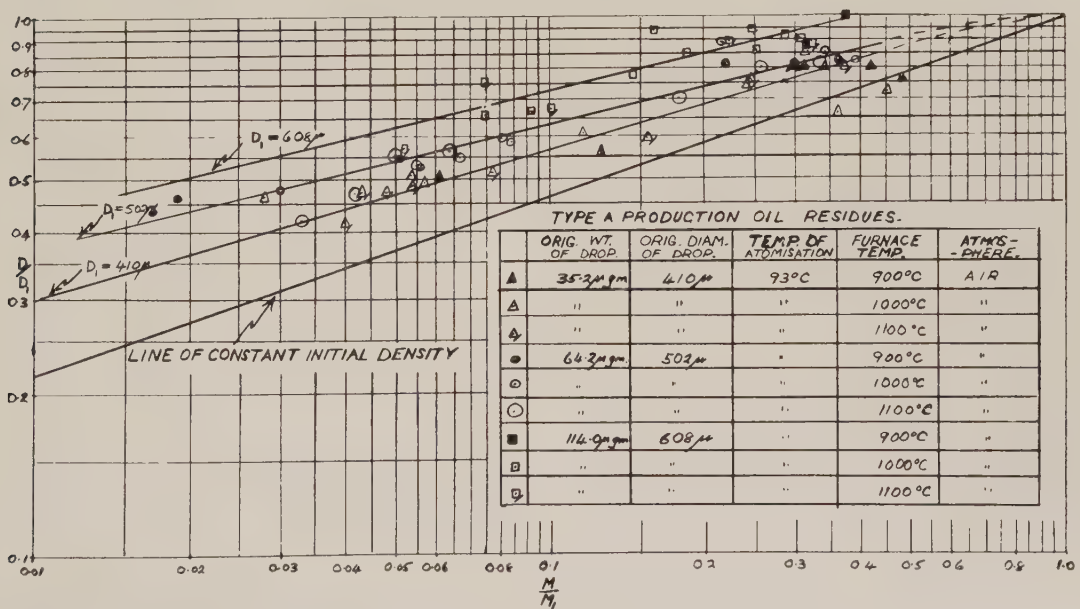

FIG. 7. Variation of drop diameter with fractional combustion, showing effect of initial drop size on density change with burning for Type A oil.

the boiling point of the fuel. Some of the results of these studies are presented in Figure 8 in the form of plots of M/M_1 versus the residence time of the droplet in the furnace. All of the data on the droplet in the furnace; the initial droplet diameters are given on each curve. Some of the curves are obviously more adequately defined by experimental points than others. These data

represent the range of initial droplet size and residence times in the furnace which could be covered by the equipment. The wax data were limited to the single curve shown because only a small amount was available.

Criticism of the Experimental Technique

Three difficulties were encountered: (1) the range of droplet sizes and furnace temperatures capable of investigation was low; (2) the droplets did not burn in a perfectly isothermal atmosphere; (3) the velocity of the droplet relative to its environment was not directly controllable and was unknown except within certain limits. It can be shown[27] that the necessary height of the trajectory of the droplets inside the furnace will probably vary as the fourth power of the initial droplet diameter. Thus the range investigated here (viz., 350 μ–650 μ) is as great as can be expected by this technique. Furnace temperature also had an important effect on combustion space requirements. Consequently, the range 900°C to 1100°C was the widest that could be studied for the above range of droplet diameters and fuels. The presence of the large heat sink at the bottom of the furnace introduced a temperature gradient there; furthermore, the velocity of a droplet changed markedly as it progressed through the furnace. Consequently, the exact temperature-time and velocity-time histories of the droplets were unknown. Since the heat transferred to the droplet depended on both the environment temperature and the droplet velocity, interpretation of the experimental data was difficult.

Table 2. Properties of the Fuels

Fuel	Formula	Molecular weight	C/H mole/mole	Melting point	Heat of comb.*	Liquid properties					Vapor properties at BP	
						Boiling point	Latent heat of vap.	Thermal conduct	Heat capacity	Specific gravity at 100°C	Thermal conduct	Heat capacity
				°C	kcal/g	°C	cal/g	Btu/ft hr °F	Btu/lb °F		Btu/ft hr °F	Btu/lb °F
Cetane	$C_{16}H_{34}$	226	0.471	18	10.6	288	52.9	0.0729	0.653	0.77	0.018	0.65
n-Eicosane	$C_{20}H_{42}$	282	0.476	38	10.59	350	47.6	0.0712	0.685	0.78	0.020	0.70
Wax	$C_{26}H_{54}$	366	0.482	57	10.54	418	41.1	0.0692	0.731	0.78	0.022	0.74
m-Terphenyl	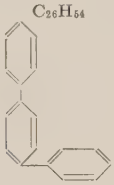	230	1.288	86	9.42	363	59.7	0.0687	0.550	1.03	0.021	0.54
Phenanthrene	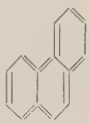	178	1.400	99	9.36	340	74.1	0.0689	0.537	1.05	0.022	0.50
Acenaphthene	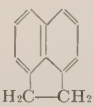	154	1.200	95	9.46	278	76.2	0.0710	0.497	1.05	0.019	0.43
Type A production	—	—	0.651	—	10.28	5% 180 50% 526 75% 630	—	—	—	0.974	—	—
Type B fuel	—	—	0.642		10.31	—	—	—	—	0.967	—	—

* Fuel as vapor at 25°C; products CO_2 and H_2O (g).

Theory of the Combustion of Single Component Fuels

An examination of Figures 8 and 9 shows that the combustion curves of the hydrocarbons are all of the same form. There is first preheating to such a temperature that significant vaporization occurs, followed by rapid vaporization in which

the droplet is surrounded by a flame envelope formed by the burning vaporized hydrocarbons. Any vaporization detected in the hot air-filled furnace was always accompanied by a flame surrounding the droplet. In Fig. 10 is presented a series of photographs of a droplet of Bunker C fuel oil burning as it falls through the vertical furnace of Chang[3] and Gerald[9]. The flame envelope attached to the droplet is luminous, and the major portion of gas-phase combustion takes place in the wake of the droplet. That this flame has a considerable effect in increasing the rate of

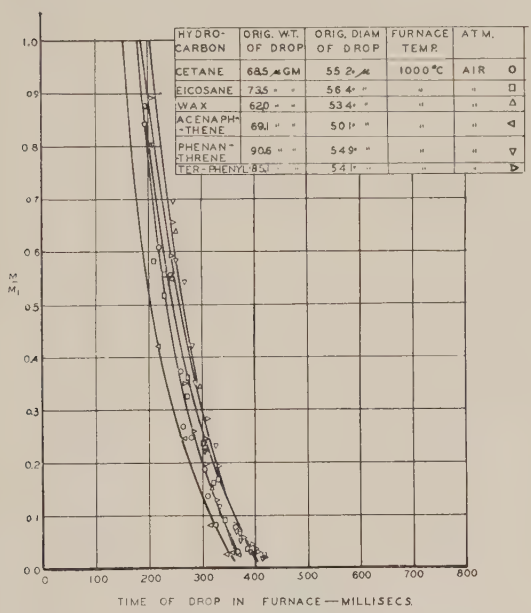

FIG. 8. Combustion of pure hydrocarbon drops (500–560 μ) at 1000°C

vaporization of the droplet is indicated by Figure 4, which indicates that the time from initiation of boiling to the production of a 10 per cent residue was more than doubled by the removal of the flame envelope.

The rate of consumption of the droplets is probably controlled by the heat transfer rate to the droplet. On entering the furnace, the droplet is first heated by radiation from the furnace walls and by convection from the hot air. Convection heats the droplet exterior, but some of the heat is transmitted to the interior by conduction or convection. Radiation, on the other hand, is absorbed at different depths within the droplet. Heating by these combined mechanisms continues until the outside of the droplet reaches such a temperature that vaporization becomes sufficient to produce a diffusion flame surrounding the droplet. This flame increases the rate of heat transfer to the vaporizing droplet by heat conduction from the flame front and by radiation from the luminous flame. This heat partly vaporizes the droplet and partly heats its interior. Radiation from the furnace walls and the luminous flame continues to be absorbed within the droplet. The vaporization rate is determined by the rate at which heat is transferred to the droplet surface and the simultaneous heat transfer from its surface to the interior.

Preliminary considerations[27] showed that for the small droplets encountered here and in practice it was a good assumption to treat the droplets as rigid spheres free from internal circulation due to air drag or internal convection currents. Also it was shown that radiation from the local flame surrounding the droplet was negligible in comparison with the total heat input to the droplet. However, in industrial practice the radiation from the flame formed by the entire spray is very much greater than that from a droplet's local flame.

The development of the theory can be divided into three parts: (1) heat transfer in the preheat region; (2) the effect of the flame envelope; (3) the vaporization process. Attention is focused here on the second and third parts; the theory of the first part is only summarized. A full report appears in the thesis of Simpson[27].

(1) HEAT TRANSFER IN THE PREHEAT REGION

Calling

$$h_r = \frac{\sigma T_\infty^4}{T_\infty - T_1}$$

the radiation coefficient to a sphere at temperature T_1 from black surroundings at T_∞, h_r/h_c is the ratio of the heat flux into the droplet due to radiation to that due to conduction. In Figure 11 h_r/h_c has been plotted against drop diameter for different temperature levels T_∞ of 1000°C, 2000°C, and 3000°C. A resaonable value of $T_1 = 100$°C was chosen and values of the thermal conductivity of air at temperatures $\frac{1}{2}(T_1 + T_\infty)$ were used[27]. The ranges of normal operation of rockets, open-hearth furnaces and many industrial furnaces are compared in Figure 11 with the more important experimental data obtained to date on the combustion of oil droplets. Note that Godsave[10] and Spalding[28] operated with room temperature air; thus their data are not strictly

comparable with those of Chang[3], Gerald[9] and the present experiments. Figure 11 shows how markedly the principal mode of heat transfer to the droplet depends on drop size; under industrial conditions h_r/h_c can vary from roughly 0.2 to 0.5; for the studies reported here h_r/h_c was as high as 0.8.

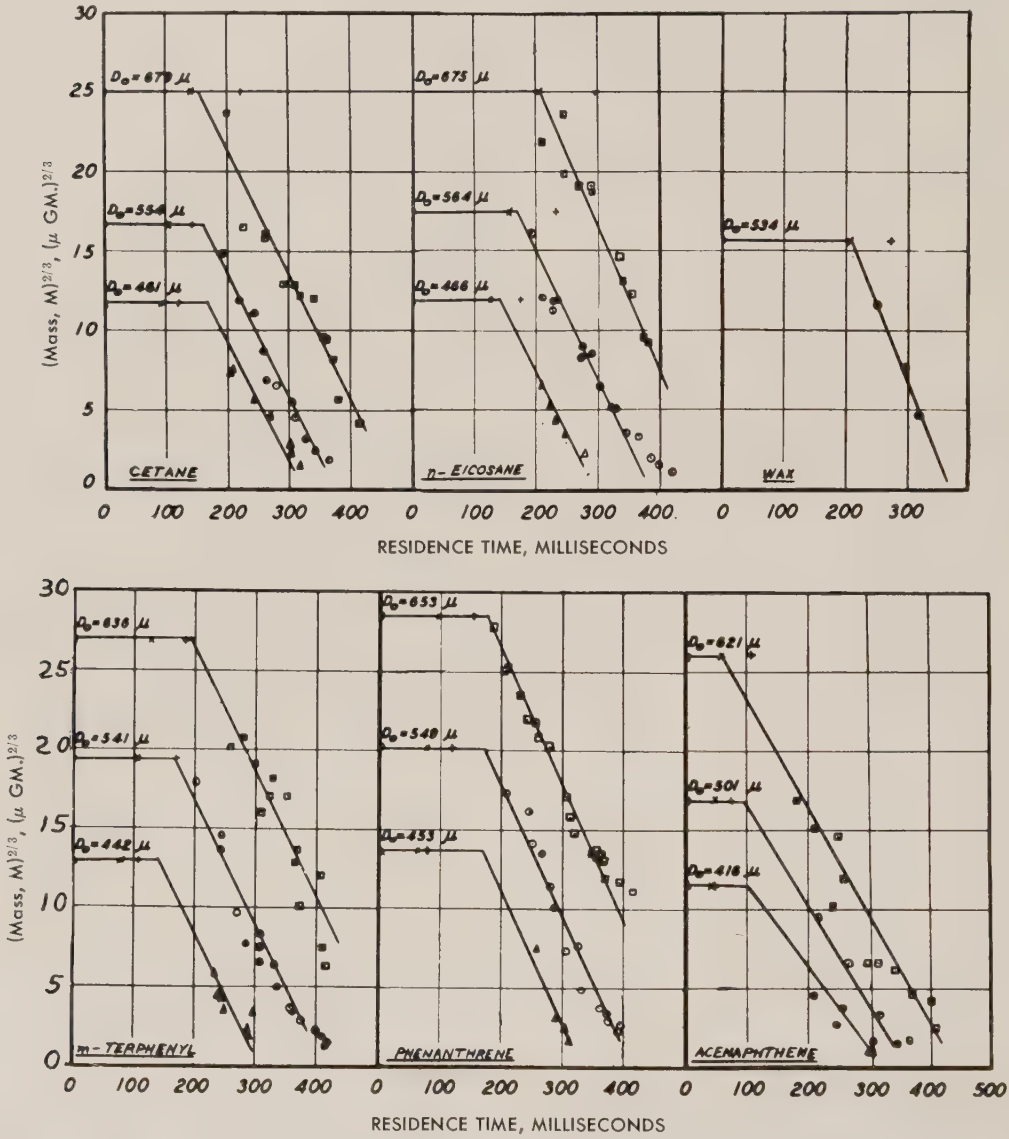

FIG. 9. Effect of hydrocarbon type and initial drop diameter on combustion of pure hydrocarbons at 1000°C. (Points marked × and + represent lower and upper limits of calculated preheat times.)

Of the radiation incident on the surface of a droplet, only a fraction is absorbed. Infrared absorption spectra of each of the fuels were measured and from this the absorptivities of droplets for 1000°C black body radiation were calculated. Not only was the total absorptivity of the spherical droplet found, but also the energy absorbed per unit volume within the droplet. In so doing, it was necessary to allow for the refraction of radiation by the liquid and for multiple reflections of the radiation at the droplet surface. These refinements had a minor effect on the total absorptivity of the droplet, but a major effect on the distribution of absorbed energy. If the absorptivity α of a film of liquid of thickness x

normal to plane, black body radiation is written as

$$\alpha = a\ (1 - e^{-kx}) \tag{13}$$

where k is the effective absorption coefficient, and a is a transparency constant less than 1.0, then the absorptivity α of a sphere of radius R and of refractive index n (taken to be independent of wavelength) is defined by the absorption group $C = kR$ and the constant a. Let the quantity κ be defined as the contribution of a unit volume at radius r within the droplet towards the surface area-total absorptivity product $4\pi R^2\alpha$. It may be shown that the dimensionless quantity κ/k is a function of (kR) and the fractional radius $z = r/R$.

Typical values of a and k for 1000°C black body radiation traveling through the fuels over distances between 350 μ and 700 μ were found to be $a = 0.658$ with $k = 29.2$ cm^{-1}, for the pure hydrocarbons, and $a = 0.877$ with $k = 38.9$ cm^{-1}, for the Type A production oil.

In Figure 12, the total absorptivity α has been plotted against (kR) with $a = 1$ and $n = 1.5$ for three special cases; absorption by the droplet with no refraction or external reflection, absorption with refraction but no external reflection, and absorption with both refraction and external reflection. It can be seen that refraction and reflection have a modest but significant effect on the total absorptivity of the droplet. In Figure 13 κ/k, proportional to the local absorptivity per unit volume, has been plotted against (r/R) with $n = 1.5$ and $(kR) = 1.0$ for the three special cases described above and for a series of values of the absorption group (kR), with both refraction and reflection effect taken into account. It is clear that refraction profoundly affects the distribution of absorbed radiant energy by focusing the radiation towards the droplet center. The marked concentration of radiation towards the center of the droplet for small values of (kR) is apparent. The relative radius $(r/R) = 1/n$ bounds a sphere through which every beam entering the droplet from the outside must pass. Related to the critical angle of reflection, it is a region of secondary maximum energy absorption which can exceed the surface values if the absorption is low enough; e.g., if the refractive index is 1.5, kR must be less than 3.0.

It can now be seen that the ratio of radiant energy absorbed in the droplet to the energy conducted from the gaseous environment to the

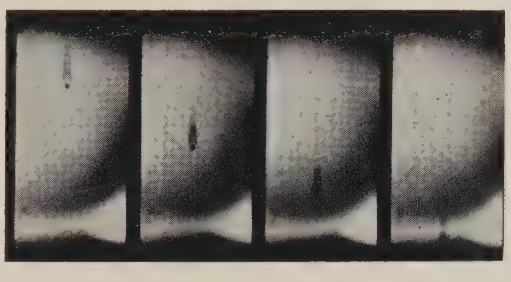

FIG. 10. A burning droplet of Bunker C fuel oil falling through 1200°C air, initial droplet mass—20 micrograms. From Gerald[9].

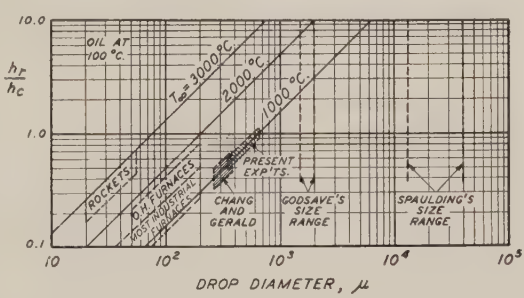

FIG. 11. The effect of drop size and surrounding temperature on the ratio of thermal radiation incident on a drop to heat transfer to the drop by convection.

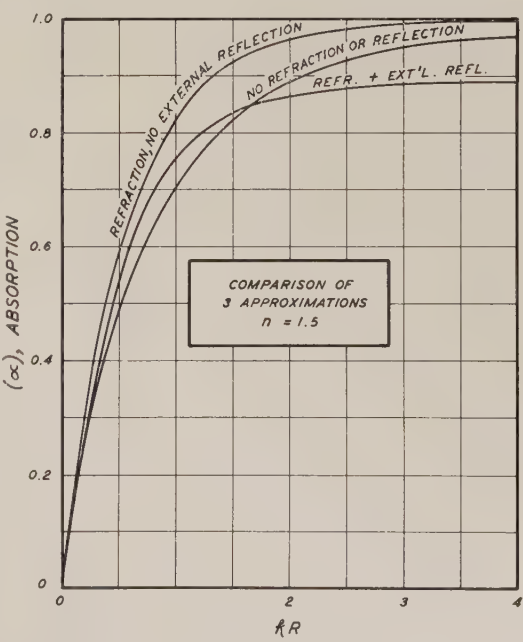

FIG. 12. The total absorptivity of liquid spheres, showing the effects of allowance for external and internal reflections and for refraction on the fraction α of the incident radiation which is abosrbed.

droplet, $(\alpha h_r/h_c)$ lies between 0.02 and 0.20 for droplets of industrial importance and is roughly 0.3 for the droplets of this study. In industrial practice only a minor portion of the energy supplied to the droplet is transferred by radiation; a small, but important, fraction of the total energy is supplied by radiation to the droplets studied here. This again emphasizes the major effect of drop size.

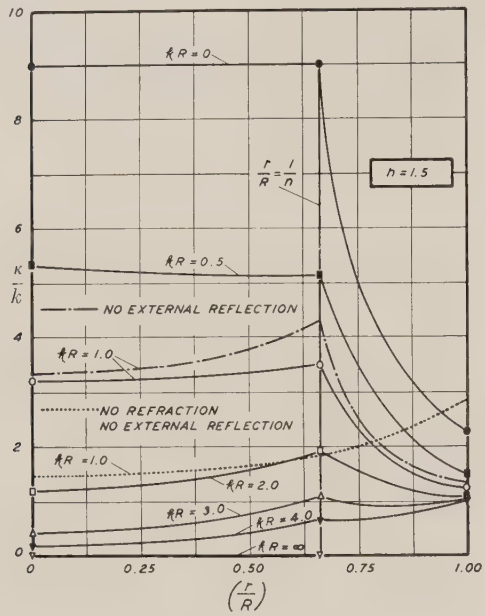

FIG. 13. The distribution of absorption of incident radiant energy within a sphere: solid lines allow for refraction and reflection; dotted and dash-lot lines for $kR = 1.0$ ignore refraction-and-reflection or reflection, respectively.

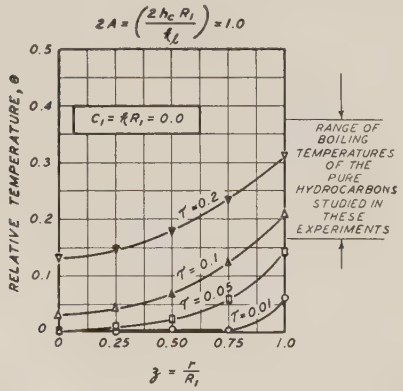
2A = (2h_c R_1/k_l) = 1.0
C_1 = kR_1 = 0.0
RANGE OF BOILING TEMPERATURES OF THE PURE HYDROCARBONS STUDIED IN THESE EXPERIMENTS
τ = 0.2
τ = 0.1
τ = 0.05
τ = 0.01
RELATIVE TEMPERATURE, θ
ζ = r/R_1

FIG. 14. Calculated temperature profiles within a droplet, radiation ignored.

Having established the heat transfer it was possible to calculate the temperature-time history of a droplet in the preheat region. Consider a droplet of radius R_1 and initial temperature T_1 suddenly immersed in and moving with constant velocity relative to a gas of temperature T_∞ and bathed in radiation from black walls at T_w. The Fourier equation for heat conduction within a rigid sphere is solved, with due allowance for absorption of radiation according to Figure 13 and conduction of heat from gas to droplet surface according to equation (1). The temperature T at any radius r in the droplet at time t is then expressible in the dimensionless form,

$$\Theta = f(A, B, C_1, z, \tau) \qquad (14)$$

Here Θ is the fractional accomplished temperature $(T - T_1)/(T_\infty - T_1)$, A is the convection group $(h_c R_1/k_l)$, B the radiation group $(\alpha h_r R_1/k_l)$, C_1 the absorption group (kR_1), τ the generalized time $K_l t/R_1^2$ and f a known function evaluated as the sum of two Fourier series. Here also k_l and K_l are the thermal conductivity and thermal diffusivity, respectively, of the liquid fuel. Plots of Θ for various values of the parameters A, B and C_1 have been made and two of these are shown in Figures 14 and 15. Both are for $2A = 1.0$ which corresponds roughly to a Nusselt number of 2. In Figure 14 the radiant heat transfer is zero; in Figure 15 the radiant heat transfer is high $(2B = 3.0)$. It can be seen that when radiant heat transfer predominates, the inside of the droplet can actually be hotter than the surface.

It is shown[27] to be a reasonable assumption that significant vaporization followed by ignition of the vapors and production of a diffusion flame around the droplet only occurs when the surface of the droplet is close to the boiling temperature. Plots such as Figures 14 and 15 can thus be used to determine the preheat time of a droplet and the temperature pattern within a droplet at the beginning of the vaporization stage. Under conditions where radiation heat transfer predominates, the inside of the droplet can reach boiling temperature before the outside. However, under normal conditions of industrial practice ($A \approx 0.5$, $B \approx 0.2$, $C_1 \approx 0.2$) and for the experiments reported here ($A > 0.5$, $B \approx 0.15$, $C_1 \approx 0.8$), this is not likely.

(2) HEAT TRANSFER FROM THE FLAME TO THE DROPLET

The heat transfer during vaporization is much more complex than that during the preheat. It is clear from Figure 4 that the local flame around

the droplet is an important if not major heat source for vaporization of the droplet. Although the outward flow of the vapors tends to decrease the inward flow of heat to the droplet, the presence of the local flame as a high temperature heat source compensates for this.

Two approaches were made in which the effect of relative velocity between droplet and air was neglected, the diffusional and thermal flow taken to be radial with the thermal diffusivity and molecular diffusivity equal, the flame assumed to be spherically symmetrical about the droplet, and the combustion reaction assumed to produce CO_2 and H_2O (g) everywhere.

In the first approach no assumptions were made about flame thickness, but the gaseous fuel, oxygen, products and inerts were assumed to have identical molecular weights, specific heats, and thermal conductivities. This approach was similar to that used by Spalding[28]. In the second, the flame was assumed to be thin and partial allowance was made for the variation of gas properties with composition.

First approach

Consider a liquid droplet of radius R vaporizing into an infinite mass of hot air in which only radial flow occurs. As the fuel diffuses from the droplet surface into the ambient air it starts burning. Combustion products and oxygen diffuse in opposite directions through nitrogen, with a superimposed outward bulk motion due to fuel consumption. At any given radius the gas mixture will in general contain fuel, oxygen, nitrogen and combustion products.

By considering a spherical shell of radius r and thickness dr, it is possible to write an energy balance on the element to give

$$4\pi \frac{d}{dr}\left(r^2 k_g \frac{dT}{dr}\right) - \frac{d(\dot{M}\tilde{h})}{dr} + 4\pi r^2 \cdot R_q = 0 \quad (15)$$

Similarly, balances of molecular oxygen, fuel and products can be written for this elementary shell. In normal isothermal diffusion the appropriate potential to use is the concentration gradient of the component of interest-concentration being defined as moles per unit volume. However, for molecular diffusion in a nonisothermal medium, the correct driving potential is the mole fraction of the component, as has been pointed out by Ackermann[1] and proved in the more advanced treatments of the kinetic theory of gases[4, 12]. With these precautions, and neglecting thermal diffusion[12] it is possible to write material balances on each component as shown below for oxygen.

$$4\pi \frac{d}{dr}\left(r^2 \frac{\mathfrak{D}_{O_2} P}{R'T} \frac{df_{O_2}}{dr}\right) - \frac{d}{dr}(\dot{M} f_{O_2}) - 4\pi r^2 \cdot \tilde{R}_{O_2} = 0 \quad (16)$$

The quantities $\tilde{R}_{O_2}$, $\tilde{R}_f$, and $\tilde{R}_p$ are, of course, related by the stoichiometry of the combustion chemical reaction, and $\tilde{R}_f$ is related to R_q by the molal heat of combustion of the fuel.

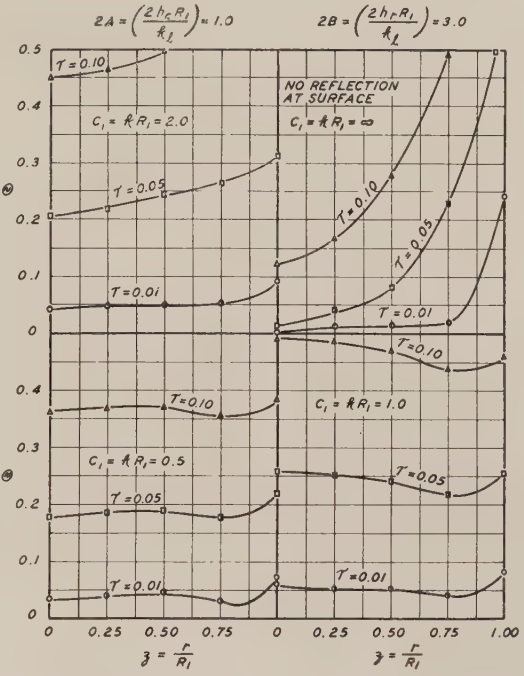

FIG. 15. Calculated temperature profiles within a droplet, radiation included.

In general, it is extremely difficult to solve equations (15) and (16) for T, f_{O_2}, f_f, and f_p because the terms $\tilde{R}_i$ are related to the component mole fractions and gas temperatures. Even a very simple bimolecular chemical reaction such that

$$\tilde{R}_f \propto e^{-E/R'T} f_{O_2} \cdot f_f \quad (17)$$

makes equations (15) to (17) non-linear. Some simplifying assumptions must be made to eliminate the $\tilde{R}$'s.

Now assume that

$$R_q = \tilde{Q}_{P,O_2} \tilde{R}_{O_2} \quad (18)$$

where $\tilde{Q}_{P,O_2}$ is the heat of combustion of the fuel at constant pressure per mole of oxygen con-

sumed. Eliminating R_q and $\tilde{R}_{O_2}$ from (15), (16) and (18), substituting $\tilde{h} = \tilde{c}_g (T - T_0)$, and assuming $\tilde{c}_g$ to be independent of the radius r gives:

$$4\pi \frac{d}{dr}\left[r^2 \left\{ \left(\frac{k_g}{\tilde{c}_g} \frac{d\tilde{h}}{dr} + \bar{\rho}_g \mathfrak{D}_{O_2} \frac{d(\tilde{Q}_{F,O_2} f_{O_2})}{dr} \right) \right\} \right] - \frac{d}{dr}\left[\dot{\tilde{M}} (\tilde{h} + \tilde{Q}_{F,O_2} f_{O_2}) \right] = 0 \tag{19}$$

Little is known about molecular diffusivities at elevated temperatures of the complex fuel-air-products mixtures encountered here, except that on the basis of very simple kinetic theory of gases the molecular diffusivity of a simple gas is roughly equal to its thermal diffusivity. Thus assume that

$$\mathfrak{D}_{O_2} = K_g = k_g / \rho_g c_g .$$

Now define $\tilde{b}$ by the relation,

$$\tilde{b} = \tilde{h} + Q_{F,O_2} f_{O_2} \tag{20}$$

where $\tilde{b}$ is the total enthalpy per mole of gas mixture above T_0 and the chemical base in which zero enthalpy is assigned to fuel, inerts and products CO_2 and H_2O (g). At a great distance from the droplet $\tilde{b}$ has the value corresponding to the enthalpy of one mole of air at T_∞ plus the enthalpy of combustion of the oxygen in it with stoichiometric fuel added at T_0. At the droplet surface, $\tilde{b}$ is the sensible enthalpy of one mole of fuel. Putting $\tilde{b}$ into (19) gives,

$$4\pi \frac{d}{dr}\left[r^2 \frac{k_g}{\tilde{c}_g} \frac{d\tilde{b}}{dr} \right] - \frac{d}{dr}\left(\dot{\tilde{M}} \tilde{b} \right) = 0 \tag{21}$$

with $\tilde{b} = \tilde{b}_R$, at $r = R$; and $\tilde{b} = \tilde{b}_\infty$, at $r = \infty$.

Now comes the really questionable step. To retain simplicity of derivation, it is assumed that the molecular weight of the mixture is independent of the radial position r; then the radial molal flow $\dot{\tilde{M}}$ is independent of r. Equation (21) can be integrated to give

$$\frac{\tilde{b} - \tilde{b}_R}{\tilde{b}_\infty - \tilde{b}_R} = 1 - \frac{1 - e^{-F/r}}{1 - e^{-F/R}} \tag{22}$$

with $F = (\dot{\tilde{M}} \tilde{c}_g / 4\pi k_g)$.

It is assumed that no oxygen reaches the surface of the droplet, i.e., at $r = R$, $f_{O_2} = (df_{O_2}/dr) = 0$. Thus if $\tilde{\lambda}'$ is the heat required to heat and vaporize one mole of the fuel,

$$\dot{\tilde{M}} = 4\pi R^2 \frac{k_g}{\tilde{\lambda}'} \left(\frac{dT}{dr} \right)_{r=R} = 4\pi R^2 \frac{k_g}{\tilde{\lambda}' c_g} \left(\frac{db}{dr} \right)_{r=R} \tag{23}$$

Combination of equations (22) and (23) yields the relation predicting burning rate,

$$\dot{\tilde{M}} = 4\pi R \frac{k_g}{\tilde{c}_g} \log_e (1 + G') \tag{24}$$

where

$$G' = \frac{\tilde{b}_\infty - \tilde{b}_R}{\tilde{\lambda}'}$$

This is Spalding's equation, and G' is the transfer number based on $\tilde{\lambda}'$ the heat required to vaporize one mole of fuel—the sum of the true latent heat and the heat transferred to the interior of the droplet per mole of fuel vaporized. In general, $\tilde{\lambda}'$ is time-dependent.

Equations (22) and (24) can be combined to give $\tilde{b}$ at any radius r external to the droplet.

$$\frac{\tilde{b} - \tilde{b}_R}{\tilde{b}_\infty - \tilde{b}_R} = \frac{(1 + G')^{(r-R)/r} - 1}{G'} \tag{25}$$

The value of enthalpy $\tilde{b}$ from equation (25) has been plotted versus relative position r/R in Figure 16 for G' of about 2. Such curves with ordinate normalized are unique, irrespective of the drop size R. Although equation (25) was derived with no commitments regarding kinetics of the combustion reaction, no information has been obtained about the temperature profile in the flame envelope. In Figure 16 possible temperature and oxygen profiles in the diffusion flame, expressed in enthalpy units, are roughly sketched. In zone AB, equation (21) reduces to

$$4\pi \frac{d}{dr}\left(r^2 k_g \frac{dT}{dr} \right) - \dot{\tilde{M}} \tilde{c}_g \frac{dT}{dr} = 0$$

with a solution

$$\dot{\tilde{M}} = 4\pi R \frac{k_g}{c_g} \frac{R_F}{R_F - R} \log_e \left[1 + \frac{\tilde{c}_g (T_F - T_R)}{\tilde{\lambda}'} \right] \tag{9}$$

This is Godsave's equation.

It is of interest to compare the effective heat transfer coefficient h_c' in the presence of flame, defined as

$$\left[k_g \left(\frac{dT}{dr} \right)_{r=R} \right]_{\text{with flame}} = h_c' (T_\infty - T_R), \tag{26}$$

with the heat transfer coefficient h_c in the preheat region, defined by equation (1). Eliminating $(dT/dr)_{r=R}$ from equations (23) and (26) and eliminating $\dot{\tilde{M}}$ by using (24) and (20), one has

$$\frac{h_c'}{h_c} = \frac{\log_e\left[1 + \dfrac{\tilde{c}_g(T_\infty - T_R) + \tilde{Q}_{P,O_2} f_{O_{2\infty}}}{\tilde{\lambda}'}\right]}{\dfrac{\tilde{c}_g(T_\infty - T_R)}{\tilde{\lambda}'}} \tag{27}$$

If $\tilde{c}_g\,(T_\infty - T_R)/\tilde{\lambda}'$ is significantly less than unity, $h_c'/h_c > 1$; if much greater than unity, $h_c'/h_c < 1$. For a fuel in cold surroundings and/or with high latent heat, the increased thermal gradient close to the droplet during combustion more than compensates for the enthalpy carried outward by the vapors. For a fuel with a low latent heat and/or in high temperature remote surroundings, the outflowing vapors reduce the heat transfer coefficient so effectively that the presence of the flame can only partially compensate for it.

Equation (24) is simple in form with few assumptions made regarding the kinetics of the combustion reactions. However, $\tilde{c}_g$, k_g and molecular weight of the gas mixture were assumed independent of r; consequently, of temperature and gas composition. Consider eicosane burning in pure air at 1000°C. Close to the droplet surface is almost pure fuel at its boiling point; far from the droplet, pure air at T_∞. Thus,

$$\text{at} \quad r = R, \frac{k_g}{\tilde{c}_g} = \frac{8.26 \times 10^{-5}}{197.4}$$

$$= 4.19 \times 10^{-7} \text{ g mole/cm sec}$$

$$\text{at} \quad r = \infty, \frac{k_g}{\tilde{c}_g} = \frac{188.8 \times 10^{-6}}{7.59}$$

$$= 2.49 \times 10^{-5} \text{ g mole/cm sec}$$

Clearly $k_g/\tilde{c}_g$ varies so widely that equation (24) is almost valueless for estimating the rate of vaporization of a fuel droplet. It is necessary to allow for variation of k_g, $\tilde{c}_g$ and molecular weight in the flame envelope.

Second approach

Consider equations (15) and (16) with the assumption that the chemical reaction is so fast that the flame is only infinitesimally thick. Then, as indicated in Figure 17, fuel will diffuse through stationary products and nitrogen to reach the flame front. Oxygen will diffuse from the air through stationary nitrogen and counter-diffusing products.

Assume the combustion reaction to be of the form:

One mole of fuel + m moles of $O_2 \rightarrow n$ moles of (CO_2 + H_2O). It is then possible to rewrite the basic energy and material balances

Fuel side

Fuel diffusion,

$$\dot{\tilde{M}} = 4\pi r^2 \frac{\mathfrak{D}_{f,p} P}{R'T}\left(-\frac{df_f}{dr}\right) + \dot{\tilde{M}} f_f \tag{28}$$

Vapor pressure,

$$f_{f,R} = exp.\left\{-\frac{\lambda}{R'}\left(\frac{1}{T_R} - \frac{1}{T_B}\right)\right\} \approx 1 - \frac{\tilde{\lambda}}{R'T_{av}^2}(T_B - T_R) \tag{29}$$

with $T_{av}^2 = T_R T_B = T_B^2$ here.

Energy diffusion,

$$\frac{d}{dr}\left(4\pi r^2 k_{g,f}\frac{dT}{dr} - \dot{\tilde{M}}\tilde{c}_{g,f}T\right) = 0 \tag{30}$$

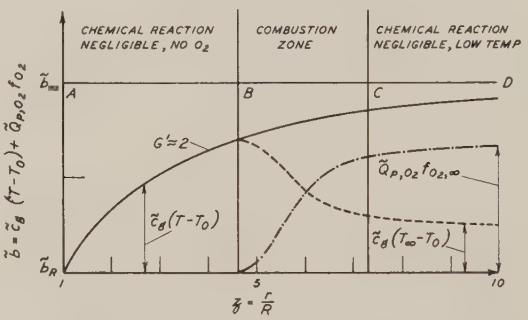

FIG. 16. Enthalpy profile, diffusion flame theory

Vaporization at the surface,

$$\dot{\tilde{M}} = (4\pi R^2)\frac{k_{g,R}}{\tilde{\lambda}'}\left(\frac{dT}{dr}\right)_{r=R+} \tag{31}$$

Air side

Oxygen diffusion, $-m\dot{\tilde{M}}$

$$= 4\pi r^2 \frac{\mathfrak{D}_{O_2,p} P}{R'T}\left(-\frac{df_{O_2}}{dr}\right) + (n-m)\dot{\tilde{M}} f_{O_2} \tag{32}$$

Product diffusion, $n\dot{\tilde{M}}$

$$= 4\pi r^2 \frac{\mathfrak{D}_{p,O_2} P}{R'T}\frac{df_p}{dr} + (n-m)\dot{\tilde{M}} f_p \tag{33}$$

Energy diffusion,

$$\frac{d}{dr}\left[4\pi r^2 k_{g,a}\frac{dT}{dr} - (n-m)\dot{\tilde{M}}\tilde{c}_{g,a}T\right] = 0 \tag{34}$$

Energy balance at flame,

$$\dot{\tilde{M}}\tilde{Q}_{f,T_0} = 4\pi R_F^2 k_{g,F}\left[\left(\frac{dT}{dr}\right)_{r=R_F-} - \left(\frac{dT}{dr}\right)_{r=R_F+}\right] + \dot{\tilde{M}}(T_F - T_0)\tilde{c}_{g,F}(n-m-1) \tag{35}$$

Equations (28), (32) and (33) are similar to equations (16), and equations (30) and (34) are equivalent to equation (15), both sets with source and sink terms removed. The gas molal specific heat is chosen so that $\tilde{c}_g T$ is the correct value of enthalpy above T_0.

The properties $\mathfrak{D}$, k_g, and $\tilde{c}_g$ depend on the temperature and composition of the gas mixture in a manner which is not simple[20]. Even simple dependence of k_g, $\mathfrak{D}$, and $\tilde{c}_g$ on temperature and composition makes equations (28) to (35) difficult to solve. However, the integration was performed for the special case of assumed linear variation of $k_g/\tilde{c}_g$ with radius, keyed to values at the drop surface, the flame, and remote surroundings. The reader not interested in details may pick up the argument at equation (48).

Let $\rho = R/r$ and assume, as above, that $\mathfrak{D}P/R'T = k_g/\tilde{c}_g$. Then let $k_g/\tilde{c}_g$ be a linear function of ρ on either side of the flame, with the correct values of $k_g/\tilde{c}_g$ selected at $r = R$, R_F, and ∞. Thus, on the fuel side

$$\frac{k_{g,f}}{\tilde{c}_{g,f}} = \alpha_f \rho + \beta_f \qquad \text{for} \qquad \rho < \rho_F = R/R_F$$

with the constants α_f and β_f defined by,

$$\begin{aligned} \alpha_f + \beta_f &= k_{g,R}/\tilde{c}_{g,R} \\ \alpha_f \rho_F + \beta_f &= k_{g,F}/\tilde{c}_{g,F} \end{aligned} \tag{36}$$

and on the air side,

$$\frac{k_{g,a}}{\tilde{c}_{g,a}} = \alpha_a \rho + \beta_a \qquad \text{for} \qquad \rho > \rho_F = R/R_F$$

with the constants α_a and β_a defined by,

$$\begin{aligned} \alpha_a \rho_F + \beta_a &= k_{g,F}/\tilde{c}_{g,F} \\ \beta_a &= k_{g,\infty}/\tilde{c}_{g,\infty} \end{aligned} \tag{37}$$

Then, with the above transformations equations (29), (31) and (35) reduce to

$$\dot{\tilde{M}} = -4\pi R \frac{k_{g,R}}{\tilde{\lambda}'} \left(\frac{dT}{d\rho}\right)_{\rho=1+} \tag{38}$$

$$f_{f,R} = 1 - \frac{\tilde{\lambda}}{R'T_B^2}(T_B - T_R) \tag{39}$$

$$\dot{\tilde{M}}\tilde{Q}_{f,T_0} = -4\pi R k_{g,F}\left[\left(\frac{dT}{d\rho}\right)_{\rho=\rho_F-} - \left(\frac{dT}{d\rho}\right)_{\rho=\rho_F+}\right] + \dot{\tilde{M}}(T_F - T_0)\tilde{c}_{g,F}(n-m-1) \tag{40}$$

and equations (28), (30), (32), (33) and (34) are integrated to give

$$\frac{1 - f_f}{1 - f_{f,R}} = \left(\frac{\alpha_f \rho + \beta_f}{\alpha_f + \beta_f}\right)^{-N_f} \tag{41}$$

$$\frac{T - T_\infty}{T_F - T_R} = \frac{1 - \left(\dfrac{\alpha_f \rho + \beta_f}{\alpha_f + \beta_f}\right)^{-N_f}}{1 - \left(\dfrac{\alpha_f \rho_F + \beta_f}{\alpha_f + \beta_f}\right)^{-N_f}} \tag{42}$$

$$\frac{m + (n-m)f_{O_2}}{m + (n-m)f_{O_{2,\infty}}} = \left(\frac{\alpha_a \rho + \beta_a}{\beta_a}\right)^{-(n-m)Na} \tag{43}$$

$$\frac{n - (n-m)f_p}{n - (n-m)f_{p,\infty}} = \left(\frac{\alpha_a \rho + \beta_a}{\beta_a}\right)^{-(n-m)Na} \tag{44}$$

$$\frac{T - T_\infty}{T_F - T_\infty} = \frac{1 - \left(\dfrac{\alpha_a \rho + \beta_a}{\beta_a}\right)^{-(n-m)Na}}{1 - \left(\dfrac{\alpha_a \rho_F + \beta_a}{\beta_a}\right)^{-(n-m)Na}} \tag{45}$$

where $N_f = \dot{\tilde{M}}/4\pi R\alpha_f$, $N_a = \dot{\tilde{M}}/4\pi R\alpha_a$.

Equations (42) and (45) permit elimination of (dT/dr) from equations (30) and (34) to give

$$1 - \left(\frac{\alpha_f \rho_F + \beta_f}{\alpha_f + \beta_f}\right)^{-N_f} = -\frac{k_{g,R}}{\tilde{\lambda}'}\frac{T_F - T_R}{\alpha_f + \beta_f} \tag{46}$$

$$\begin{aligned} \frac{Q_{f,T_0}}{k_{g,F}} = {} & \frac{T_F - T_\infty}{1 - \left(\dfrac{\alpha_a \rho_F + \beta_a}{\beta_a}\right)^{-(n-m)Na}} \cdot \left(\frac{\alpha_a \rho_F + \beta_a}{\beta_a}\right)^{-(n-m)Na} \frac{n-m}{\alpha_a \rho_F + \beta_a} \\ & - \frac{T_F - T_R}{1 - \left(\dfrac{\alpha_f \rho_F + \beta_f}{\alpha_f + \beta_f}\right)^{-N_f}} \left(\frac{\alpha_f \rho_F + \beta_f}{\alpha_f + \beta_f}\right)^{-N_f} \cdot \frac{1}{\alpha_f \rho_F + \beta_f} + (T_F - T_0)\frac{\tilde{c}_{g,F}}{k_{g,F}}(n - m - 1) \end{aligned} \tag{47}$$

In general T_B, T_∞, $f_{O_{2,\infty}}$, are known. Furthermore, at the flame front the oxygen and fuel concentrations are assumed to be negligible, i.e., $f_{O_2,F} = f_{f,F} = 0$. Thus, there are six unknowns $\dot{\tilde{M}}$, R_F (or ρ_F), T_R, T_F, $f_{f,R}$, and $f_{p,F}$ to be found from the six equations (41), (43), (44), (46), (47) and (39). We are primarily interested in $\dot{\tilde{M}}$, T_F, and R_F.

By use of equation (43) with $\rho = \rho_F$ and equation (44), N_f and N_a can be eliminated from equation (47) to give,

$$T_F = \frac{f_{O_2,\infty}}{f_{O_2,\infty}(n-m)+m} \left\{ T_R + \frac{m}{f_{O_2,\infty}} T_\infty + (n-m-1)T_0 + \frac{\tilde{Q}_{f,T_0}}{\tilde{c}_{g,F}} - \frac{\tilde{\lambda}'}{\tilde{c}_{g,R}} \right\} \quad (48)$$

Elimination of α_f and β_f from equation (46) with $\rho = \rho_F$ and equation (36) yields,

$$\frac{\dot{\tilde{M}}}{4\pi R} = \frac{R_F}{R_F - R} \left(\frac{k_g}{\tilde{c}_g}\right)_{RF} \log_e \cdot \left(1 + \frac{\tilde{c}_{g,R}(T_F - T_R)}{\tilde{\lambda}'}\right) \quad (49)$$

where $(k_g/\tilde{c}_g)_{R,F}$ is the logarithmic mean of the values of $(k_g/\tilde{c}_g)$ at the drop surface and at the flame.

The similarity between equation (49) and equation (9) of Godsave is obvious. Partial allowance has been made, however, for variation in gas properties with radial distance. Elimination of α_a and β_a from equation (43) with $\rho = \rho_F$ and equation (36) yields

$$\frac{\dot{\tilde{M}}}{4\pi R} = \frac{R_F}{R} \frac{1}{n-m} \left(\frac{k_g}{\tilde{c}_g}\right)_{F,\infty} \log_e \cdot \left(1 + f_{O_2,\infty} \frac{n-m}{m}\right) \quad (50)$$

where $(k_g/\tilde{c}_g)_{F,\infty}$ is the logarithmic mean of the values of $(k_g/\tilde{c}_g)$ at the flame and in the remote surroundings.

Solving equations (49) and (50) for $\dot{\tilde{M}}$ and R_F gives

$$\frac{\dot{\tilde{M}}}{4\pi R} = \left(\frac{k_g}{\tilde{c}_g}\right)_{F,\infty} \frac{\log_e}{n-m} \left(1 + f_{O_2,\infty} \frac{n-m}{m}\right) + \left(\frac{k_g}{\tilde{c}_g}\right)_{R,F} \log_e \left\{1 + \frac{\tilde{c}_{g,R}(T_F - T_R)}{\tilde{\lambda}'}\right\} \quad (51)$$

$$\frac{R_F - R}{R} = \frac{\left(\frac{k_g}{\tilde{c}_g}\right)_{R,F} \log_e \left\{1 + \frac{\tilde{c}_{g,R}(T_F - T_R)}{\tilde{\lambda}'}\right\}}{\left(\frac{k_g}{\tilde{c}_g}\right)_{F,\infty} \log_e \left\{1 + f_{O_2,\infty} \frac{n-m}{m}\right\}^{\frac{1}{n-m}}} \approx \frac{(k_g/\tilde{c}_g)_{R,F}}{(k_g/\tilde{c}_g)_{F,\infty}} \frac{m}{f_{O_2,\infty}} \cdot \log_e\{1 + \tilde{c}_{g,R}(T_F - T_R)/\tilde{\lambda}'\} \quad (52)$$

It is also of interest to determine the surface temperature of the droplet T_R and the concentration of the products at the flame $f_{p,F}$. Elimination of α_f, β_f, $\dot{\tilde{M}}$, and $f_{f,R}$ from equations (36), (43) and (49) at $\rho = \rho_F$ yields

$$(T_B - T_R) = \frac{R'T_B^2}{\tilde{\lambda}} \Big/ \left\{1 + \frac{\tilde{c}_{g,R}(T_F - T_R)}{\tilde{\lambda}'}\right\} \quad (53)$$

and combination of equations (43) and (45) at $\rho = \rho_F$ where $f_{O_2} = 0$, $f_p = f_{p,F}$ yields

$$f_{p,F} = \frac{n(1 - f_{O_2,\infty}) + m f_{p,\infty}}{n(1 - f_{O_2,\infty}) + m f_{O_2,\infty}} \quad (54)$$

If the gas specific heats are independent of temperature and composition, T_F in equation (48) is the non-dissociated adiabatic flame temperature of a stoichiometric mixture of ambient gas at T_∞ and liquid fuel at T_R. Thus in the first approach described above, if the flame is assumed to be thin, the adiabatic flame temperature corresponding to products CO_2 and H_2O (g) is attained. Further, if the gas thermal conductivities are also independent of temperature and composition and if there is no change in the number of moles of gas in the chemical reaction, equations (51) and (48) reduce to equation (24) of the first approach as is necessary.

Since $\dot{\tilde{M}}$, R_F, and T_R all depend on T_F, solution of equation (48) for T_F is by trial and error. Consider a droplet of eicosane burning in air at 1000°C and neglect heat transfer to the interior of the droplet so that $\tilde{\lambda}' = \tilde{\lambda}$. The parameters have the following values:

$$m = 30.5, \quad n = 41.0$$

$$T_0 = 25°C, \quad T_B = 350°C, \quad T_\infty = 1000°C$$

$$\tilde{\lambda}' = 13.4 \text{ kcal/g mole}, \quad Q_{f,T0} = 2{,}986 \text{ kcal/g mole}$$

$$f_{f,R} \approx 1, \quad T_R \approx T_B, \quad \tilde{c}_{g,R} \approx 197.4 \text{ cal/g mole °C}$$

$$k_{g,R} \approx 8.26 \times 10^{-5} \text{ cal/°C cm sec}$$

$$f_{O_2,\infty} = 0.21, \quad f_{N_2,\infty} = 0.79, \quad \tilde{c}_{g,\infty} = 7.59 \text{ cal/g mole °C}$$

$$k_{g,\infty} = 188.8 \times 10^{-6} \text{ cal/°C cm sec}$$

From equation (54) the gas at the flame was found to be 16.4 per cent N_2, 40.8 per cent CO_2, and 42.8 per cent H_2O. Using molal weighted means of $\tilde{c}_g$ for H_2O, CO_2, and N_2 at elevated temperatures[13], T_F from equation (48) was

2600°C. In using equation (48), it is a very good approximation to neglect the sensible and latent heats of the fuel and also the term $(n - m - 1)\,T_0$. The corresponding adiabatic flame temperature, with due allowance[13] being made for dissociation at elevated temperatures, was calculated to be 2410°C. Taking $(T_F - T_R)$ to be 2250°C, equation (53) yields $(T_B - T_R) = 1.7$°C; the assumption that the droplet surface is close to the boiling point is very good indeed. This does not, however, mean that it is allowable to assume $f_f = 1.0$ at the drop surface in equation (41).

Substitution of these values into equations (51) and (52) yields $R_F/R = 142$, and $\dot{\tilde{M}}/4\pi R = (2.83 \times 10^{-5})$ g mole/sec cm. Again, it is a good approximation to write equation (51) as,

$$\frac{\dot{\tilde{M}}}{4\pi R} = \left(\frac{k_g}{\tilde{c}_g}\right)_{R,F} \log_e \left\{1 + \frac{\tilde{c}_{g,R}(T_F - T_R)}{\tilde{\lambda}'}\right\} \qquad (55)$$

Use of $T_F = 2410$°C only changes R_F/R to 137 and $\dot{\tilde{M}}/4\pi R$ to (2.64×10^{-5}) g mole/sec cm.

The concentration and temperature profiles around a droplet of burning eicosane according to the above theory are shown in Figure 17. Also

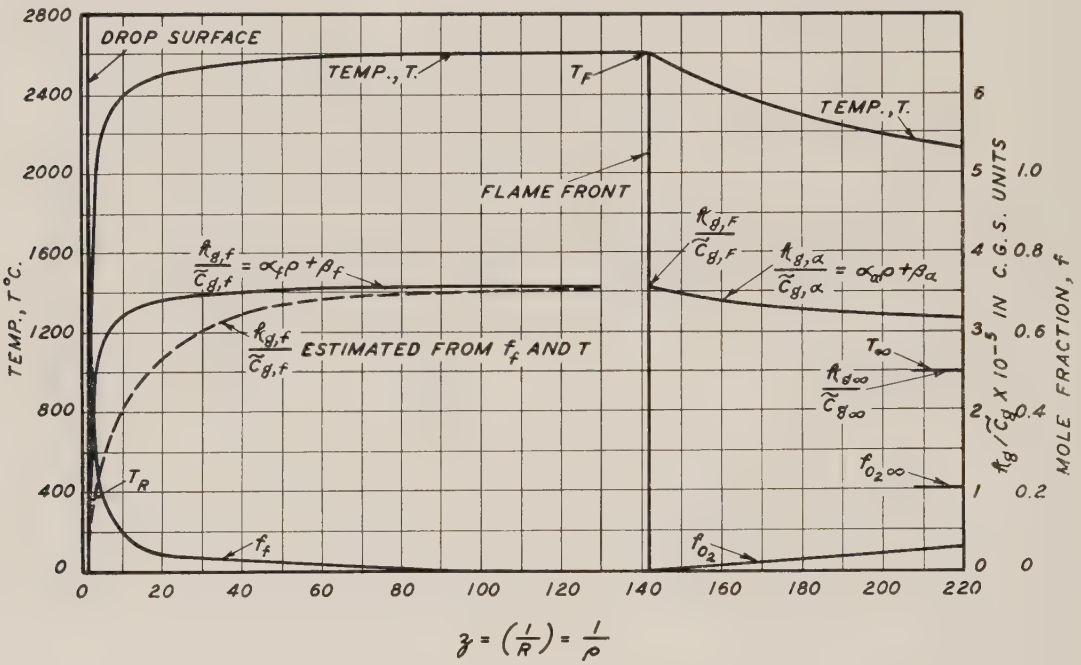

FIG. 17. Temperature, concentration and physical property profiles, thin flame theory

From the composition and temperature of the flame front both $\tilde{c}_{g,F}$ and $k_{g,F}$ are determined.

At $r = R$,

$$k_{g,R}/\tilde{c}_{g,R} = 8.26 \times 10^{-5}/197.4$$
$$= 0.419 \times 10^{-6} \text{ g mole/cm sec}$$

$r = R_F$,

$$k_{g,F}/\tilde{c}_{g,F} = 4.14 \times 10^{-6}/11.6$$
$$= 35.6 \times 10^{-6} \text{ g mole/cm sec}$$

$r = \infty$,

$$k_{g,\infty}/\tilde{c}_{g,\infty} = 188.8 \times 10^{-6}/7.59$$
$$= 24.9 \times 10^{-6} \text{ g mole/cm sec}$$

shown are the assumed variation of $(k_g/\tilde{c}_g)$ with (r/R) and the variation of $(k_g/\tilde{c}_g)$ estimated from the temperature and concentration patterns. It is apparent that the assumed variation of $(k_g/\tilde{c}_g)$ is of the proper shape but that the slope is too great close to the droplet surface.

It is striking that R_F/R is predicted to be 142 whereas it is apparent in Figure 10 that the flame envelope is less than two droplet radii away from the droplet surface. The simple diffusion theory given above calls for the flame front to be far from the droplet surface as a consequence of the facts that the number of moles of oxygen required for the combustion of one mole of heavy fuel is large and also that the increase in the number of

gas moles $(n - m)$ is considerable. In short, the oxygen must diffuse in at a high rate, relative to that of the fuel, against a heavy back-diffusing stream of products. Calculation indicates that the volume of gas contained within the flame front predicted by the above theory is so large that there is not enough fuel in a droplet for the calculated steady state pattern to be established!

Clearly the predicted value of R_F/R is impossible; it is apparent that air motion past the droplet cannot be neglected in any realistic theoretical model. Use of an eddy diffusivity to describe transport of oxygen from the air to the flame front instead of the molecular diffusivity used above would greatly reduce R_F/R in equation (52); but the burning rate from equation (51) would be affected only slightly.

Although the thin concentric flame theory is more likely to be valid for very small droplets than for the large droplets investigated here, R_F/R in equation (52) is independent of R and is still too high. It may thus be necessary to treat the problem in its unsteady state form in any realistic model.

However, it seems possible that a semi-theoretical description of the rate of vaporization of the droplet would be as follows:

$$\frac{\dot{\tilde{M}}}{4\pi R} = \underline{f}\left(\frac{k_{g,R}}{\tilde{c}_{g,R}}, \frac{k_{g,F}}{\tilde{c}_{g,F}}\right)\log_e\left\{1 + \frac{\tilde{c}_{g,R}(T_F - T_R)}{\tilde{\lambda}'}\right\} \tag{56}$$

where T_F is given by equation (48) and where $\underline{f}$ is a function predicted by the above theory to be the logarithmic mean, but likely to depend on the flow pattern about the droplet.

(3) HEAT TRANSFER WITHIN THE DROPLET DURING VAPORIZATION

In equation (56), the heat required to vaporize one mole of fuel, $\tilde{\lambda}'$, depends on the internal conduction of heat in the droplet during the vaporization process and is, in general, a function of time. For a droplet of radius R at time t and latent heat per mole $\tilde{\lambda}$,

$$\tilde{\lambda}' = \tilde{\lambda} + (4\pi R^2/\dot{\tilde{M}})k_l\left(\frac{\partial T}{\partial r}\right)_{r=R^-}$$

$$\text{with } \dot{\tilde{M}} = 4\pi R^2\tilde{\rho}_l\frac{dR}{dt}$$

where $\tilde{\rho}_l$ and k_l, the molal density and thermal conductivity of the liquid, are assumed to be constant throughout the vaporization process, and $(\partial T/\partial r)_{r=R-}$ is the temperature gradient in the liquid at the droplet surface. Then using the system of dimensionless variables,

θ = fractional accomplished temperature = $(T - T_1)/(T_\infty - T_1)$

z = fractional radius = r/R_1

z_s = value of z at droplet surface = R/R_1

τ = generalized time = kt/R_1^2

G = transfer number based on latent heat alone

$$\xi = f\left(\frac{k_{g,R}}{\tilde{c}_{g,R}}, \frac{k_{g,F}}{\tilde{c}_{g,F}}\right)\Big/\frac{k_l}{\tilde{c}_l}$$

and

$$J = \frac{\tilde{c}_l(T_\infty - T_1)}{\tilde{\lambda}},$$

the equations describing the conduction of heat within the droplet with its surface temperature maintained at the boiling point T_B can be written as,

$$\frac{\partial\theta}{\partial\tau} = \frac{\partial^2\theta}{\partial z^2} + \frac{2}{z}\frac{\partial\theta}{\partial z} + BC_1\psi(z/z_s, C)$$

$$\frac{dz_s}{d\tau} = \frac{\xi}{z_s}\log_e\left\{1 + \frac{G}{1 + \left[\frac{\left(\frac{\partial\theta}{\partial z_{z=z_s-}}\right)}{\frac{dz_s}{d\tau}}\right]J}\right\} \quad \text{at } z = z_s \tag{57}$$

$$\theta = \theta_B = \frac{T_B - T_1}{T_\infty - T_1} \quad \text{at } z = z_s$$

$$\left.\begin{aligned}\theta &= \phi_1(A, B, C_1, \theta_B, z)\\ z_s &= 1\end{aligned}\right\} \text{ when } \tau = 0$$

In equations (57), the function ϕ_1 is the temperature pattern at the end of the preheat regime and is calculated as described above. The function $\psi(z/z_s, C) = (d\alpha_n/d(kr))$ is given by Figure 13, and $C_1 = kR_1$ is the value of C at $\tau = 0$. It is desired to solve equations (57) for the position of the droplet surface z_s and the temperature distribution θ at any time during vaporization. A closed solution of these equations was found impossible, although numerical solution

was obtained for one case, as is described below. In general, the temperature pattern within the droplet depends on at least nine dimensionless groups,

$$\theta = \phi_2 (A, B, C_1, \Theta_B, G, \xi, J, z, \tau) \quad (58)$$

The number of curves required to describe precisely the combustion of fuel droplets over a reasonable range of these variables would be very large.

the radiation group B, and the absorption group C_1, and to use plots similar to those in Figures 14 and 15 to estimate the time required for the surface of the droplet to reach boiling temperature and the temperature pattern within the droplet at the end of that time. In Table 3, these calculated preheat times (t_B) are listed for each fuel and each initial droplet diameter. U refers to the upper estimate of the Reynolds number of a given fuel and droplet, L to the lower estimate.

Table 3. Preheat of the Pure Hydrocarbon Droplets

Fuel	Initial diam.	t_B, millisec		Q_s/Q_L		$\log_e (1 + G')$		$\log_e (1 + G')$ selected
		U	L	U	L	U	L	
	μ							
Cetane	461	93	121	0.946	0.809	2.74	2.81	2.7 ± 0.1
	554	106	144	1.122	0.934	2.66	2.75	
	679	140	223	1.142	0.851	2.64	2.78	
Eicosane	466	127	175	1.131	0.853	2.79	2.93	2.8 ± 0.1
	564	156	231	1.279	0.926	2.73	2.90	
	675	205	296	1.341	1.022	2.72	2.85	
Wax	534	207	274	1.459	1.148	2.82	2.95	2.9 ± 0.1
m-Terphenyl	442	80	109	0.766	0.636	2.55	2.62	2.5 ± 0.1
	541	105	170	0.794	0.600	2.54	2.64	
	636	129	185	0.841	0.721	2.51	2.57	
Phenanthrene	453	63	79	0.555	0.510	2.41	2.43	2.3 ± 0.1
	549	76	115	0.596	0.491	2.38	2.44	
	653	95	152	0.606	0.496	2.38	2.44	
Acenaphthene	416	41	46	0.426	0.424	2.35	2.35	2.3 ± 0.1
	501	46	75	0.469	0.378	2.33	2.38	
	621	60	101	0.469	0.396	2.33	2.37	

t_B = time for the outside of the droplet to reach boiling temperature

Q_s/Q_L = ratio of sensible heat required to raise the droplet to boiling temperature at end of preheat to the latent heat requirements of the liquid

$G' = \tilde{c}_{g,R}(T_F - T_R)/\tilde{\lambda}'$

Comparison of Theory with the Measured Combustion Rates of the Pure Hydrocarbons

From calculations of droplet trajectories for travel from atomizer to furnace and in the furnace, upper and lower estimates were made of the average Reynolds numbers during preheat. All of these Reynolds numbers were below 25[27]. From equation (3) upper and lower estimates of the Nusselt number were made; all of these Nusselt numbers were below 5.0. Consequently, it was possible to calculate the convection group A,

These estimates of the preheat time are compared with the experimental combustion curves of the pure hydrocarbons in Figure 9. The experimental curves are not in disagreement with the calculated preheat times, although the data are not precise enough to validate the assumed model of heat transfer. Also listed in Table 3 are the estimated ratios Q_s/Q_l of Q_s, the sensible heat required to raise the interior of the droplet to boiling temperature after the surface has reached that temperature to Q_l, the latent heat requirements of the droplet. During vaporization, between 25 per cent and 60 per cent of the total

heat supplied to the droplet must be used to raise the interior of the droplets studied to boiling temperature. Clearly, sensible heat requirements are appreciable during vaporization. Further details of these calculations are given by Simpson[27].

Equation (56) was also compared with the measured rates of vaporization of the single component fuels and for this G', the transfer number based on $\tilde{\lambda}'$ and defined by the equation

$$G' = \frac{\tilde{c}_{g,R}(T_F - T_R)}{\tilde{\lambda}'}$$

was calculated for each fuel, drop diameter, and upper (U) and lower (L) estimate of preheat conditions. In these calculations the heat required to vaporize one mole of fuel was taken to be the sum of the heat required to raise the interior of the droplet to boiling temperature at the beginning of vaporization plus the latent heat requirements of the fuel, both based on one mole of fuel. The group $\log_e (1 + G')$ is listed in columns 7 and 8 of Table 3. Although the sensible heat requirement of the droplet at the end of the preheat depends on the initial drop diameter and the motion of the droplet, grouping the variables in the form $\log_e (1 + G')$ indicates that over the range of variables studied here it is within experimental error to choose a constant value of the group for each fuel. These are listed in column 9 of Table 3. The group G' was also based on T_F determined by equation (48). Use of an adiabatic flame temperature which included the effect of high temperature dissociation of the combustion products changed $\log_e (1 + G')$ only slightly.

In Figure 9 the slope of the curve $M^{2/3}$ versus the residence time t is proportional to the group $(\dot{\tilde{M}}/4\pi R)$ the left-hand side of equation (56). All the experimental points could, within experimental error, be represented by straight lines the slopes of which were independent of initial droplet diameter. This is in agreement with the use of values of $\log_e (1 + G')$ independent of initial droplet diameter in Table 3. The right-hand side of equation (56) was then calculated for each of the hydrocarbons to give an upper limit

$$f\left(\frac{k_{g,R}}{\tilde{c}_{g,R}}, \frac{k_{g,F}}{\tilde{c}_{g,F}}\right) = \frac{k_{g,F}}{\tilde{c}_{g,F}},$$

a lower limit

$$f\left(\frac{k_{g,R}}{\tilde{c}_{g,R}}, \frac{k_{g,F}}{\tilde{c}_{g,F}}\right) = \frac{k_{g,R}}{\tilde{c}_{g,R}}$$

and a theoretical value

$$f\left(\frac{k_{g,R}}{\tilde{c}_{g,R}}, \frac{k_{g,F}}{\tilde{c}_{g,F}}\right) = \text{log mean } \frac{k_{g,R}}{\tilde{c}_{g,R}}, \frac{k_{g,F}}{\tilde{c}_{g,F}}$$

It is apparent from Table 4 that the upper and lower estimates of $(\dot{\tilde{M}}/4\pi R)$ bracket the measured values and that the value of $(\dot{\tilde{M}}/4\pi R)$ corresponding to the logarithmic mean function of the gas properties is from 2 to 4 times the experimental value.

Table 4. Comparison of Measured Vaporization Rates with Those Predicted by Equation (51)

Fuel	Measured		Predicted molal rates, $\dot{\tilde{M}}/4\pi R$		
	$\dot{\tilde{M}}/4\pi R$	$\dot{M}/4\pi R$	R	F	$L.M.$
Cetane	6.1	1.4	1.37	95.4	22.6
Eicosane	5.7	1.6	1.17	99.0	22.1
Wax	4.7	1.7	0.98	103.0	21.7
Terphenyl	6.7	1.5	1.75	79.0	20.4
Phenanthrene	9.4	1.7	2.35	72.6	20.4
Acenaphthene	12.7	1.9	2.72	72.6	21.3
Average ratio: measured/predicted			4.4 ±10%	0.09 ±50%	0.37 ±50%

$R = k_g/\tilde{c}_g$ evaluated at drop surface
$F = k_g/\tilde{c}_g$ evaluated at flame radius
$L.M. = k_g/\tilde{c}_g$ evaluated at logarithmic mean of drop surface and flame values
$\dot{\tilde{M}}/4\pi R$ = g moles/(sec)(cm) × 10^6
$\dot{M}/4\pi R$ = g/(sec)(cm) × 10^3

In the above calculations, $\tilde{\lambda}'$ was taken to be constant and the absorption of radiation during vaporization was neglected. This implies that the mass rate of combustion of the droplet is proportional to the first power of the droplet radius, a law proposed earlier by Godsave and others. Equations (57) were numerically integrated for one case. The vaue of ξ was chosen to fit Figure 9. In Figure 18, the generalized temperature θ is plotted versus the fractional radius $z = r/R_1$ for different generalized times τ. It can be seen that the interior of the droplet only reaches boiling point after most of the droplet has vaporized. The straight-line variation of z_s^2 vs. τ predicted by

equation (56) for a constant average value of $\tilde{\lambda}'$ differs little from the more rigorously determined values of z_s and τ taken from Figure 18.

Although equation (56) with $\tilde{\lambda}'$ treated as a constant predicts vaporization rates of the correct order of magnitude, any realistic theory must also include the effect of motion of the droplet. Furthermore, the above theoretical studies have accentuated the importance of allowing for the variation of combustion gas properties with temperature. In view of the complexity of the problem, a semiempirical correlation might be sought, viz.,

$$\frac{\dot{\tilde{M}}}{4\pi R} = f\left(\frac{k_{g,R}}{\tilde{c}_{g,R}}, \frac{k_{g,F}}{\tilde{c}_{g,F}}\right) \log_e (1 + G') \left\{1 + a(\mathrm{Re})^p(\mathrm{Sc})^q \left(\frac{D^2 k_r c^{n-1} \rho_g}{\mu_g}\right)^s\right\} \quad (59)$$

in which the group $(D^2 k_r c^{n-1}\rho_g)/\mu_g$ measures the rate of chemical reaction relative to the momentum transfer, with the kinetics of the combustion reaction represented by an equation of the form $(dc/dt) = k_r c^n$. In Table 4 the measured values of $\dot{\tilde{M}}/4\pi R$ and the calculated values corresponding to the three sets of

$$f\left(\frac{k_{g,R}}{\tilde{c}_{g,R}}, \frac{k_{g,F}}{\tilde{c}_{g,F}}\right) \log_e (1 + G')$$

considered are compared. The mass rate $(\dot{M}/4\pi R$ and ratio $(\dot{\tilde{M}}/4\pi R)$

$$\Big/ \left\{\frac{k_{g,R}}{c_{g,R}} \log_e (1 + G')\right\}$$

are almost independent of the fuel, the implication being that the mass rate of vaporization of the fuel is largely independent of its molecular weight. Thus $\tilde{M}$ and $k_g/\tilde{c}_g$ in equation (59) can be replaced by $\dot{M}$ and k_g/c_g.

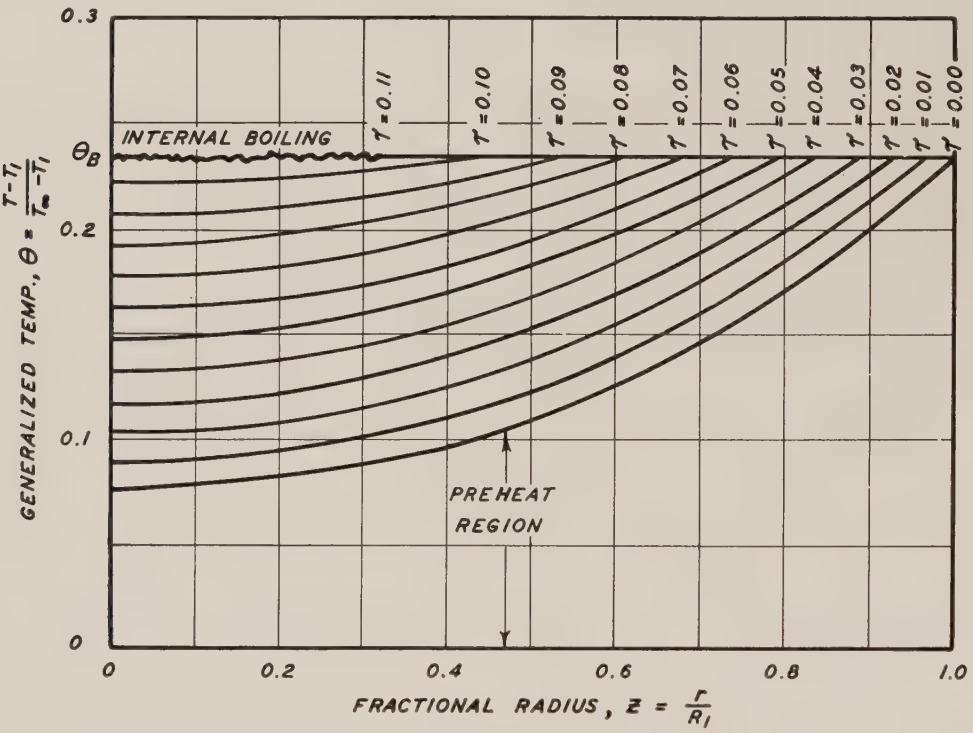

FIG. 18. Temperature pattern within a droplet during vaporization. $R_1 = 282\ \mu$, $T_1 = 52°C$, $T_\infty = 1322°C$, $T_w = 1000°C$, $T_B = 350°C$, $2B' = 0.336$, $C_1' = 0.826$, $G = 38.9$, $J = 18.3$, $\xi = 1.33$, $\tau = k_1 t/R_1^2$.

Combustion of Multicomponent Fuels

The combustion of multicomponent fuels presents a much more complex problem than that of single component fuels. Photomicrographs of the residues of Type A Production oil droplets are shown in Figure 19 A, B and C with the corresponding points shown in Figure 4. Limitations of space prevent the presentation and interpretation of a large mass of data on the burning of heavy resi-

A

Combustion in air at 1000°C.
$M_1 = 64.2\ \mu g$ $D_1 = 502\ \mu$
$M = 13.9\ \mu g$ $D = 449\ \mu$
$t = 340$ millisec

B

Combustion in air at 1000°C.
$M_1 = 64.2\ \mu g$ $D_1 = 502\ \mu$
$M = 4.3\ \mu g$ $D = 274\ \mu$
$t = 476$ millisec

C

Vaporization in nitrogen at 1000°C
$M_1 = 64.2\ \mu g$ $D_1 = 502\ \mu$
$M = 6.4\ \mu g$ $D = 1000\ \mu$
$t = 627$ millisec

FIG. 19. Photographs of drop residues, Type A oil, see points A, B, and C, Fig. 4.

dual fuel oil droplets in which the importance of a third stage of combustion—that of residual coke particles—is brought out. This will be the subject of a later paper.

Conclusions

Combustion of pure hydrocarbon droplets takes place in two stages, preheat and vaporization.

In the preheat region, heat is supplied by radiation from the furnace walls and by conduction (and radiation in industrial furnaces) from the hot ambient gases. For most industrial cases, radiation can be neglected. The radiation is focused towards the center of the droplet and the conduction of heat from the ambient gases heats up the outside of the droplet. If the droplet can be treated as a rigid sphere and if appreciable vaporization and subsequent ignition of the vapors takes place only when the droplet surface is close to boiling temperature, then the preheat time and the temperature pattern within the droplet is defined by a dimensionless equation of the form of equation (58) and the heat required in the subsequent vaporization region to raise the interior of the droplet to boiling temperature is comparable with the latent heat required to vaporize the droplet. The present data on preheat, though not adequate to prove the theory, are consistent with it; and they indicate that its use cannot introduce any significant error in prediction of total burning time.

In the vaporization region, the major heat source in single-droplet burning is the flame envelope surrounding the droplet and heat is transferred to the droplet surface by conduction against the vaporizing fuel. The assumption of radial heat and mass flow about the droplet, a spherical flame, radial diffusion only, and linear variation of physical properties from the flame inwards and outwards yields solutions for vaporization rate, flame temperature, and flame position. Although values of the vaporization rate based on limiting values of the physical properties bracket the data, a relation is proposed, (56), in which the precise form of allowance for the large variation of gas properties with radial distance from the droplet is unknown. The unmodified theory predicts a flame temperature which is too high, and a position of the flame front which is much too far from the droplet surface, A realistic theory of droplet combustion must include the effect of the motion of the main air stream past the droplet. Also, the mass rate of vaporization of the fuels was found to be largely independent of the fuel molecular weight. For these reasons, a relation of the form of equation (59), with molal quantities replaced by mass, is expected to offer a useful means of correlating data.

The assumption of a constant λ' equal to the total heat per unit mass required to vaporize the fuel in the vaporization region of combustion was shown to be good for the droplets of this paper but the detailed description of the temperature pattern within the droplet during vaporization would require an equation of the form of equation (58).

The experimental data of this paper cover a very limited range of relevant variables. More data must be accumulated before the above theories, and, in particular, the parameters a, p, a, n and s in equation (59) can be evaluated.

Data

Complete tables of data and details of experimental procedure are given by Simpson[27].

Acknowledgment

The research reported here was done in connection with Contract N6-ori-105, Task Order III for Project Squid, a cooperative research project in jet propulsion under the sponsorship of the office of Naval Research, Department of the Navy, the Office of Ordnance Research, Department of the Army and the Office of Air Research, Department of the Air Force. The authors acknowledge with thanks the sponsorship of this study and the permission to publish this paper. The junior author (H.C.S.) also wishes to acknowledge financial support from the management of the Nobel Division of Imperial Chemical Industries Limited, Scotland, who sponsored him during this research work.

Table of Nomenclature

$A = h_c R_1/k_l$	The convection group corresponding to an environment T_∞.
a	A constant
$B = \alpha h_r R_1/k_l$	The radiation group
b	The mass transfer coefficient in equation (5)
$b = \bar{h} + \bar{Q}_{P,O_2} f_{O_2}$	The total enthalpy of one mole of the gas mixture about the droplet above a base of zero enthalpy for fuel, CO_2,

H_2O (g) and inerts at T_0

$C = kR$ The absorption group

$C_1 = kR_1$ Value of C at $R = R_1$

c The concentration of a reactant in the equation $(dc/dt) = k_r c^n$

c_g Specific heat of gas

$\tilde{c}_g$ Molal specific heat of gas

c_l , $\tilde{c}_l$ Specific heat of liquid per unit mass and mole, respectively

D Diameter of droplet at any time t

D_1 Initial diameter of droplet

D_e Effective diameter of a coke residual particle

$\mathfrak{D}$ Molecular diffusivity

E Energy of activation

$F = \dot{\tilde{M}}\tilde{c}_g/4\pi k_g$

f Mole fraction in a gas mixture

$\underline{f}$ A function in equation (56)

G Transfer number based on $\tilde{\lambda}$

G' Transfer number based on $\tilde{\lambda}'$

h_c Heat transfer coefficient for convection

h_c' A fictitious h_c allowing for the flame

h_r Heat transfer coefficient for radiation

$\tilde{h}$ Sensible enthalpy of gas above T_0 , per mole

$J = \tilde{c}_l\,(T_\infty - T_1)/\tilde{\lambda}$

$K_g = k_g/c_g\rho_g$ Thermal diffusivity of gas

$K_l = k_l/c_l\rho_l$ Thermal diffusivity of liquid

k_g , k_l Gas and liquid thermal conductivities, respectively

k Effective absorption coefficient

k_r Reaction rate constant

M Mass of a droplet at time t

M_1 Initial mass of a droplet

$\dot{M} = dM/dt$ Mass rate of vaporization of a droplet

$\dot{\tilde{M}} = dM/dt$ Molal rate of vaporization of a droplet

(MW) Molecular weight

m Moles of oxygen required to burn 1 mole of fuel to H_2O (g) and CO_2

n Refractive index of a medium

n Moles of product when 1 mole of fuel is burned to produce H_2O (g) and CO_2

n The order of the gas-phase combustion reaction, $dc/dt = k_r c^n$

P Total pressure

p A constant when used as an exponent

$\tilde{Q}_{P,O_2}$ Heat of combustion of the fuel at constant pressure per mole of oxygen, with products CO_2 and H_2O (g)

$\tilde{Q}_{f,T_0}$ Heat of combustion at temperature T_0 and constant pressure of one mole of fuel to products CO_2 and H_2O (g)

$\dot{Q}$ Heat flux

q A constant when used as an exponent

R Radius of droplet at any time

R_1 Initial radius of droplet

R_F Flame radius

Rq Heat produced per unit volume and time by the gas-phase combustion of the fuel to CO_2 and H_2O (g)

R' Molal gas constant

$\tilde{R}_{O_2}$, $\tilde{R}_f$, $\tilde{R}_p$ Moles of oxygen, fuel (products) consumed (produced) per unit time and volume in the gas phase combustion reaction of fuel to CO_2 and H_2O (g)

r Radial distance

s A constant when used as an exponent

T Temperature

t Time

t_B Preheat time

V Velocity of gas stream relative to droplet

x A distance in equation (13)

$z = r/R_1$ Fractional radius

$z_s = R/R_1$ Ratio of radius of droplet at time t to initial radius of the droplet

α Absorptivity

α	A constant in equation $k_g/\tilde{c}_g = \alpha\rho + \beta$
β	Evaporation constant
β	A constant in equation, $k_g/\tilde{c}_g = \alpha\rho + \beta$
θ	Fractional accomplished temperature
κ	Contribution per unit volume, located at radius r, to the product, (total surface) (absorptivity).
λ, $\tilde{\lambda}$	Latent heat of fuel per unit mass and mole, respectively
λ', $\tilde{\lambda}'$	Heat required to vaporize unit mass and one mole of fuel, respectively
μ_g	Viscosity of gas
$\xi = f\left(\frac{k_{g,R}}{\tilde{c}_{g,R}}, \frac{k_{g,F}}{\tilde{c}_{g,F}}\right) \Big/ \frac{k_l}{\tilde{c}_l}$	
$\rho = R/r$	
ρ_g , $\tilde{\rho}_g$	Mass density and molal density of gas
ρ_l , $\tilde{\rho}_l$	Mass density and molal density of liquid
ρ_R , ρ_∞	Partial densities of diffusing component in equation (5)
σ	Stefan-Boltzmann constant
$\tau = K_l t/R_1^2$	Generalized time
$\tau_B = K_l t_B/R_1^2$	Generalized preheat time
ϕ_1 , ϕ_2	Functions in equation after (57) and in (58)
ψ	A function in equation (57)

SUBSCRIPTS

a	On air side of flame
B	At the atmospheric boiling point of the fuel
f	Properties of the fuel
F	At the flame
g	In the gas phase
O_2	Of oxygen
p	Of combustion products
q	Heat
R	At the drop surface
∞	At a great distance from the drop surface

REFERENCES

1. Ackermann, G.: V.D.I., Forshungsheft, 382 (1937).
2. Bradley, R. S., Evans, H. G., and Whytlaw-Gray, R. W.: Proc. Roy. Soc., *A186*, 368 (1946).
3. Chang, T. Y.: Sc.D. Thesis, Chem. Eng. Dept., M.I.T., 1941.
4. Chapman, S., and Cowling, T. G.: *The Mathematical Theory of Nonuniform Gases*. Cambridge University Press, 1939.
5. Diederichsen, J., and Hall, A. R.: *Fourth Symposium (International) on Combustion*, p. 837. Baltimore, The Williams & Wilkins Co., 1953.
6. Emmons, H. W.: Harvard University, Division of Applied Sciences, Combustion Aerodynamics Laboratory, Interim Technical Report No. 6, June, 1953.
7. Frössling, N.: Gerlands Beiträge zur Geophysik, *52*, 170 (1938).
8. Fuchs, N.: Phys. Z. Sowjet, *6*, 225 (1934); Trans. N.A.C.A.T.M. 1160, 1947.
9. Gerald, C. F.: Sc.D. Thesis, Chem. Eng. Dept., M.I.T., 1940.
10. Godsave, G. A. E., Report No. R.66, N.G.T.E., England, March, 1950; Report No. R.87, N.G.T.E., England, April, 1951; Report No. R.88, N.G.T.E., England, August, 1952; Report No. R.125, N.G.T.E., England, October, 1952; Report No. R.126, N.G.T.E., England, November, 1952; Memo. No. M95, N.G.T.E., England, October, 1950; *Fourth Symposium (International) on Combustion*, p. 818. Baltimore, The Williams & Wilkins Co., 1953.
11. Gohrbandt, W.: Memo. No. M110, N.G.T.E., England, April, 1951.
12. Grew, K. E., and Ibbs, T. L.: *Thermal Diffusion in Gases*. Cambridge University Press, 1952.
13. Hottel, H. C., Williams, G. C., and Satterfield, C. N.: *Thermodynamic Charts for Combustion Processes*. New York, John Wiley & Sons, Inc., 1949.
14. Houghton, H. G.: Physics, *4*, 419 (1933).
15. Ingebo, R. D.: N.A.C.A., T.N. 2368 (1951).
16. Jeffreys, H.: Phil. Mag. (London), *35*, 270 (1918).
17. Johnson, J. C.: J. Appl. Physics, *21*, 22 (1950).
18. Johnstone, H. F., Pigford, R. L., and Chapin, J. H.: Trans. A.I.Ch.E., *37*, 95 (1941).
19. Kennard, E. H.: *Kinetic Theory of Gases*. New York, McGraw-Hill Book Co., Inc., 1938.
20. Klibanovr, T. M., Pomerantsev, V. V., and Frank-Kamenetsky, D. A.: J. of Tech. Physics (U.S.S.R.), *12*, 14 (1942).
21. Kramers, H.: Physica, *12*, 61 (1946).
22. Krönig, R., and Bruijsten, J.: Applied Scientific Research, *A2*, 439 (1949–51).

23. Langmuir, I.: Physical Review, Series 2, *12*, 368 (1918).
24. Morse, H. W.: Proc. Am. Acad. Sci., *45*, 1909.
25. Ranz, W. E., and Marshall, W. R.: Chem. Eng. Prog., *48*, 141 (1952); Chem. Eng. Prog., *48*, 173 (1952).
26. Sherwood, T. K.: *Absorption and Extraction*. New York, McGraw-Hill Book Co., Inc., 1937.
27. Simpson, H. C.: Sc.D. Thesis, Chem. Eng. Dept., M.I.T., 1954.
28. Spalding, D. B.: Fuel, *29*, 2 (1950); Fuel, *29*, 25 (1950); Fuel, *30*, 121 (1951); Fuel, *32*, 169 (1953); Combustion on Fuels Subcommittee, Aeronautical Research Council, 13, 711, C.F. 159, Jan. 24, 1951; *Fourth Symposium (International) on Combustion*, p. 847. Baltimore, The Williams & Wilkins Co., 1953.
29. Squire, H. B.: *Modern Developments in Fluid Dynamics*, Vol. II, Chap. XIV. Edited by L. Howarth. Oxford, 1953.
30. Tang, Y. S., Duncan, J. M., and Schweyer, H. E.: N.A.C.A. T.N. 2867, 1953.
31. Tverskaya, N. P.: Izvestiga Akademii Nauk, Seria Geograficheskaya i Geofizicheskaya, *14*, 164 (1950). Trans. by H. Goyer in R.A.E., Farnborough, Hants., England, Library Translation No. 367, March, 1951.
32. Williams, G. C.: Sc.D. Thesis, Chem. Eng. Dept., M.I.T., 1942.

Discussion by F. Schultz-Grunow*

The forms of evaporating or burning droplets shown in this paper seem to coincide very closely to surfaces of constant temperature and concentration caused by a point source of heat and mass in a parallel flow. The expression for this distribution is

$$\vartheta = \frac{C}{r} e^{-V(r-y)/2a}$$

where ϑ is the temperature or concentration, C a constant, V the flow velocity, a the thermometric conductivity, r the radial and y the distance in the direction of flow from the heat source.

* Technische Hochschule, Aachen, Germany.

2

COMBUSTION OF FUEL DROPLETS IN A VIBRATING AIR FIELD

By SEIICHIRO KUMAGAI and HIROSHI ISODA

Introduction

In recent years evaporation and combustion of fuel droplets have formed a field of study of combustion phenomena. These problems are important as a first step in understanding the combustion process in compression ignition engines, gas turbines and jet engines. This paper presents the program of research on evaporation and combustion of fuel droplets of one of the authors. Some of the results have already been published[1, 2]. Combustion in a vibrating air field at room temperature and atmospheric pressure is investigated in relation to the effect of air turbulence on the burning rate of fuel droplets.

Apparatus and Procedure

The experimental apparatus is shown in Figure 1. A droplet of *n*-heptane is suspended from a silica filament about 0.1 mm in diameter. Ignition is produced by bringing a small burner flame close to the droplet. The driving unit of a dynamic speaker is used as the vibrator. A circular diaphragm, 25 mm in diameter, is fixed to the voice-coil which is supported by a corrugated damper. The vibrator is set so that the diaphragm may be

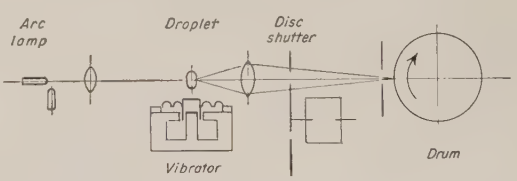

Fig. 1

placed horizontally exactly below the droplet. An RC audio-oscillator of variable frequency is used to excite the vibrator. Frequency calibration is performed by means of a tuning fork oscillator (1000 cycles/sec) and an electromagnetic oscillograph. The amplitude of the diaphragm is measured with a comparator.

The amplitude of air vibration (peak-to-peak) at a point at any distance from the diaphragm is determined directly as the amplitude of the flame tip of a small Bunsen burner with the vibrator set in a vertical position. Application of this method, however, is restricted to a narrow range of frequency. The hot-wire anemometer method generally is employed.

A burning droplet is photographed on the film of a rotating drum with intermittent illumination by a carbon arc. For this purpose, a slotted disc driven by a synchronous motor is used, giving exposure intervals of 0.12 second. The magnification is usually about 7:1.

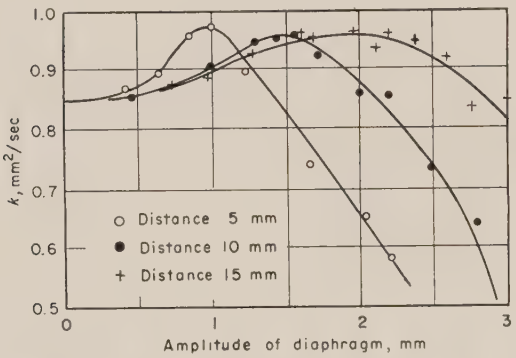

FIG. 2

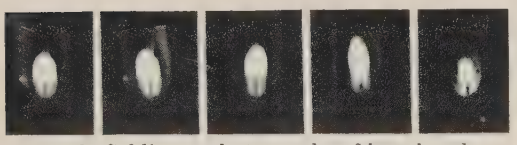

FIG. 3. Schlieren photographs of burning droplets. From left to right the amplitude of air vibration is 0, 0.4, 0.7, 0.85 and 1.2 mm with the frequency of 156 cycles per second.

The lateral diameter of a burning droplet is measured by using a comparator. The error of measurement is almost negligible, although the longitudinal diameter on the photograph is a little less than the real value owing to the exposure time of the order of several millisec. In the present investigation the droplet is treated as a sphere of corresponding diameter. The error due to such a treatment is acceptable except for the later period of the combustion. The relation between the diameter of a burning droplet and time is obtained in this way.

Results and Discussion

It is found that the relation between the diameter of a burning droplet, D, and time, t, is the same as in combustion in quiescent air, namely

$$D_0^2 - D^2 = kt,$$

where

D = initial diameter (mm),

k = constant (mm²/sec).

Hence, we can use the value of k also as a measure of the burning velocity in combustion in a vibrating air field.

As the amplitude of the diaphragm is increased, keeping the frequency and the distance from the diaphragm to the droplet constant, the value of k increases, reaches a maximum and then drops to zero (Fig. 2). The maximum value of k is about 15 per cent greater than the value of k in still air. With a smaller amplitude, the flame boundary takes on an oval shape much the same as in combustion in still air. As the amplitude increases further, the flame boundary is disturbed and its lower half diminishes (Fig. 3). This corresponds to the rather sudden decrease of the value of k.

As the distance increases, the amplitude of air vibration decreases exponentially except near the diaphragm where it is independent of the distance. The distance has the same influence upon the value of k as that of the amplitudes of the diaphragm as regards the intensity of air vibration around the droplet. Thus, for a constant frequency, the value of k is expressed uniquely by the amplitude of air vibration around the droplet (Fig. 4). This relation is formulated empirically as follows:

$$k = k_0 + ma^2(n - a^2),$$

where

k = value of k in still air (mm²/sec),
a = amplitude of air vibration around droplet (mm),
m, n = constants.

The amplitude corresponding to the maximum value of k decreases with increasing frequency (Fig. 5). Variations of the maximum value of k for various frequencies fall within the experimental accuracy. Finally, the value of k is expressed empirically as follows (Fig. 6):

$$k = k_0 + Afa^2(B - fa^2),$$

where

f = frequency (cycle per second),
A, B = constant.

From this equation it is concluded that the maximum value of k is independent of the frequency.

Assuming conduction of heat and diffusion of mass of spherical symmetry, the following equations can readily be derived.

$$C_0 = 1 - \exp[-(dm/dt)(1/R_0 - 1/R_f)/4\pi\rho_1 D_1] \quad (1)$$

$$C'_\infty = n(\exp[(dm/dt)/4\pi\rho_2 D_2 R_f] - 1) \quad (2)$$

$$T_f - T_0 = (\exp[c_1(dm/dt)(1/R_0 - 1/R_f)/4\pi\lambda_1] - 1)L/c_1 \quad (3)$$

$$T_f - T_\infty = (\exp[c_2(dm/dt)/4\pi\lambda_2 R_f] - 1)[(H - L)/c_2 - (T_f - T_0)] \quad (4)$$

where

C_0 = concentration of fuel vapor at drop surface,
C'_∞ = concentration of oxygen at infinite distance,
dm/dt = burning rate (g/sec),
R_0 = radius of drop (cm),
R_f = radius of flame front (cm),
ρ = density of gas (g/cm³),
ρ' = density of liquid (g/cm³),
D = diffusion coefficient of gas (cm²/sec),
c = specific heat at constant pressure of gas (cal/g°C),
λ = thermal conductivity of gas (cal/sec °C cm),
L = latent heat of fuel (cal/g),
T_f = temperature of flame front (°K),
T_0 = temperature of drop surface (°K),
T_∞ = temperature at infinite distance (°K),
H = calorific value of fuel (cal/g),
n = mass of oxygen required for combustion of unit mass of fuel,
1 (suffix) = inside of flame front,
2 (suffix) = outside of flame front.

Equation (3) becomes

$$dm/dt = [4\pi\lambda_1 R_0/c_1(1 - R_0/R_f)] \log [1 + c_1(T_f - T_0)/L]. \quad (5)$$

Since dm/dt is equal to $\pi k R_0 \rho'/2$,

$$k = [8\lambda_1/c_1\rho'(1 - R_0/R_f)] \log [1 + c_1(T_f - T_0)/L]. \quad (6)$$

Combining equations (1) and (3),

$$T_f - T_0 = [(1 - C_0)^{-c_1\rho_1 D_1/\lambda_1} - 1]L/c_1. \quad (7)$$

From equations (2) and (3) it follows that

$$R_f/R_0 = 1 + (\lambda_1/c_1\rho_2 D_2) \log [1 + c_1(T_f - T_0)/L]/\log (1 + c_2/n). \quad (8)$$

Equations (7) and (8) mean that $T_f - T_0$ and R_f/R_0 are independent of the change of thermal conductivity and diffusion coefficient, if they change similarly. Finally, it follows that k is directly proportional to the diffusivity (molecular or eddy).

The dimension of fa is that of velocity, and

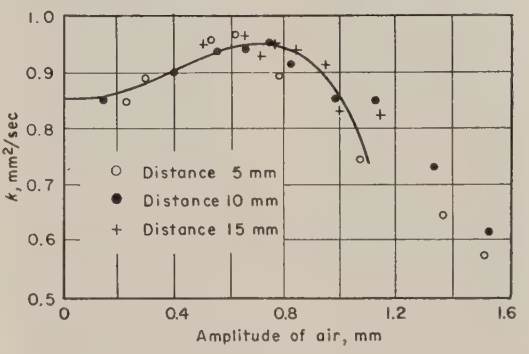

FIG. 4

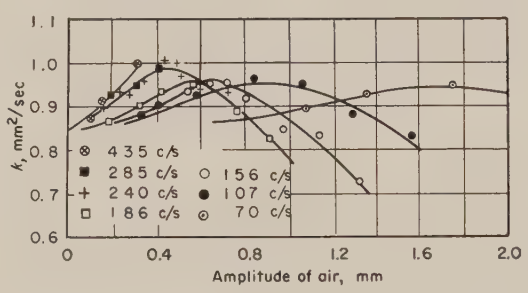

FIG. 5

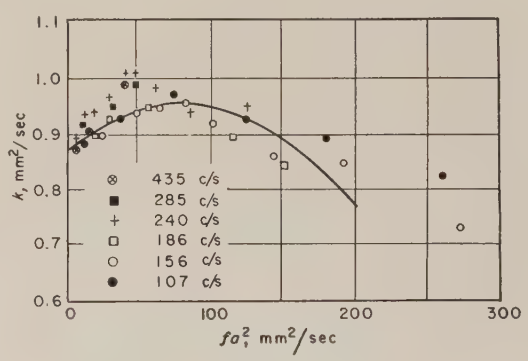

FIG. 6

consequently fa^2 may be considered to be a kind of diffusivity. Thus, we obtain

$$k = k_0 + \text{constant } fa^2.$$

This equation explains the experimental results with smaller values of fa^2.

The increase of the value of k with fa^2 is presumably due to the increased diffusivity. Furthermore, the decrease of the value of k with further

increase of fa^2 may be ascribed to the deformation of flame boundary by violent air vibration.

Conclusion

An empirical expression for the effect of air vibration velocity, i.e., the amplitude and frequency on the burning of fuel droplets, is given. It seems that the value of k cannot exceed some limit, however violent the air vibration may be. It is reasonable to suppose that the knowledge obtained in this investigation applies to the case of a turbulent air field. When fine fuel particles are injected into a turbulent air or gas, their relative velocity will vanish rapidly, and they will burn, if ignited, at a rate much the same as that attained in still air. Nevertheless, air turbulence probably has a considerable influence upon the combustion of droplet-vapor systems, such as in jet engines and gas turbines, where the combustion of gas mixtures plays a role more or less.

REFERENCES

1. Kumagai, S., and Isoda, H.: Nature, *166*, 1111 (1950).
2. Kumagai, S., and Isoda, H.: Science of Machine (Japan), *4*, 337 (1952).

3

THE EFFECTS OF CHEMICAL AND PHYSICAL PARAMETERS ON THE BURNING RATE OF A LIQUID DROPLET[a]

By HENRY WISE, JACK LORELL, and BERNARD J. WOOD

Introduction

Recent papers have reported certain experimental and theoretical aspects of the combustion of liquid propellants dispersed as aerosols in gaseous reactants. The experimental procedures employed in these fundamental studies of the burning rate of liquid droplets may be grouped into the following three categories: (1) the process of nonstationary, nonsteady-state combustion in which a free-falling droplet is allowed to come in contact with a reacting gas[1, 2]; (2) the process of stationary, nonsteady-state combustion in which the combustion rate of a droplet suspended in a reacting medium is determined from the variation of droplet size with time;[2, 3] and (3) the process of stationary, steady-state combustion in which the geometric dimensions of a supported droplet are maintained constant during combustion[4].

Theoretical considerations[5] indicate that the burning rate of a liquid drop is controlled by a steep temperature gradient near the droplet surface. The liquid reactant evaporates from the wet sphere and feeds the homogeneous, vapor-phase reaction zone located at some distance from the liquid surface. Therefore the interior of the droplet has little effect on the combustion process. Consequently in the study of the kinetics of material transport in heterogeneous systems, a wetted, noncatalytic sphere may be employed to simulate adequately the burning of a liquid drop. Thus the conditions of steady-state combustion of a stationary droplet can be realized experimentally by feeding liquid reactant into a porous sphere at a rate determined by the physical and chemical parameters of the system under study. Such an experimental procedure is particularly suited to an evaluation of the fundamental principles governing the mechanism of combustion of iquid droplets.

Experimental Procedure

The apparatus used in the study of the burning rate of liquid droplets is shown schematically in Figure 1. A porous alundum[b] sphere of known size is contained in a cylindrical pyrex chamber (6-in D and 24-in height). This sphere is supported by a stainless-steel feed line through which liquid reactant is fed at a measured rate. The test liquid is displaced into the sphere from a syringe

[a] This paper presents the results of one phase of research carried out at the Jet Propulsion Laboratory, California Institute of Technology, under Contract No. DA-04-495-ORD 18, sponsored by the Department of the Army, Ordnance Corps.

[b] Catalyst support spheres manufactured by Norton Company, Worcester 6, Mass.

whose piston is advanced at the desired rate by means of a servo-controlled motor furnished with worm-gear drive and vertical-screw arrangement. Gaseous reactants are introduced into the cylindrical chamber at a measured rate of mass flow through the conical section at the bottom of the reaction chamber. This gas stream flows past the liquid body, thereby replenishing gaseous reactant and removing reaction products from the homogeneous vapor-phase burning zone. As is shown in Figure 2, a diffusion flame having a liquid surface as a flame holder is established at some distance from the wet sphere. Ignition of the

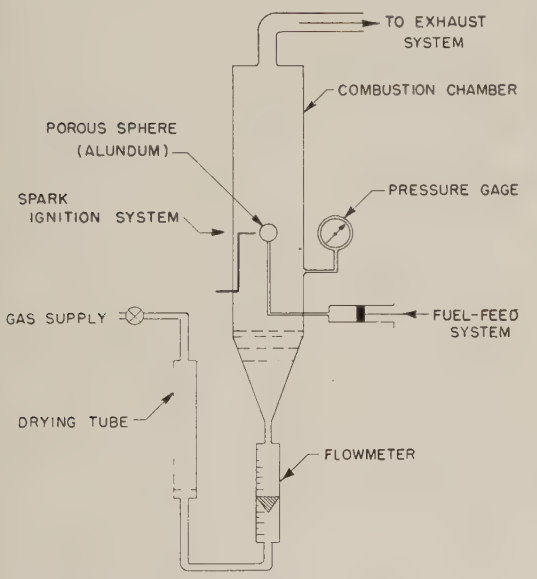

FIG. 1. Schematic diagram of apparatus for study of droplet burning rates.

reactants is accomplished by means of a pilot flame or a high-voltage spark discharge.

It is apparent that this experimental procedure may be applied to fuel-oxidizer systems having either reactant in the liquid or the gaseous state. In this investigation liquid alcohols and gaseous oxygen as well as liquid nitric acid and gaseous ammonia have been employed. However, the method may be extended to the study of the burning rate of liquid monopropellants (e.g., hydrazine) which sustain chemical transformation by their own exothermic heats of reaction. Practical considerations limit the extension of this procedure to spheres with radii of less than 1000 μ. However, the agreement observed between the experimental results thus obtained for relatively large droplets and those reported for smaller droplets[3] suggests that the mechanism which governs mass and energy transfer during the combustion process is not materially affected by the dimensions of the liquid phase.

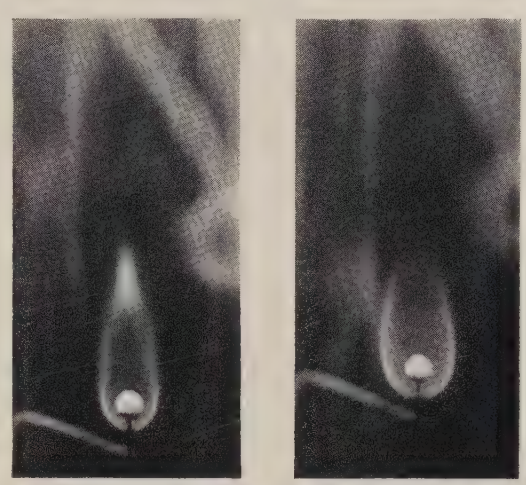

FIG. 2. Burning of liquid-fuel droplet (ethanol) in air at a pressure of 650 mm Hg (*left*) and 240 mm Hg (*right*).

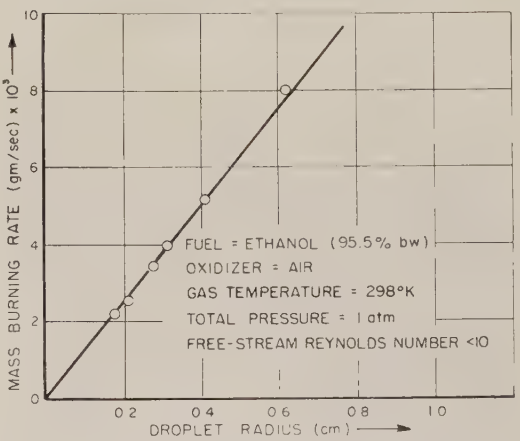

FIG. 3. Droplet burning rate as a function of droplet radius.

Experimental Results

BURNING RATE AS A FUNCTION OF DROPLET RADIUS

The linear variation of mass-burning rate $\dot{m}_F$[c] with droplet radius as observed experimentally by Godsave[3] for droplets less than 1000 μ in radius has been found to apply equally well to droplets as large as 6000 μ in radius (Fig. 3). It is of interest to note that for this propellant combination (ethyl alcohol-air) the slope of the curve

[c] The nomenclature used in this report is given at the end of the chapter.

yields an evaporation constant[d] ϵ equal to 0.0098 which is about 15 per cent higher than that reported for measurements carried out under non-steady-state conditions[3]. This increase in ϵ may be partially due to the imposed gas velocity of the oxidizer stream (free-stream Reynolds number <10) flowing past the sphere in these experiments. Also the higher absorptivity of the porous

Table 1. Distance Between Luminous Flame Zone and Droplet Surface for System Ethanol-Air

r_l (cm)	$\dot{m}_F$ (gm/sec)10^3	r_c (cm)	Δr (cm)
0.178	2.21	0.430	0.23
0.216	2.49	0.450	0.23
0.276	3.24	0.485	0.21
0.310	3.95	0.558	0.25
0.414	5.14	0.656	0.24
0.623	8.08	0.870	0.25

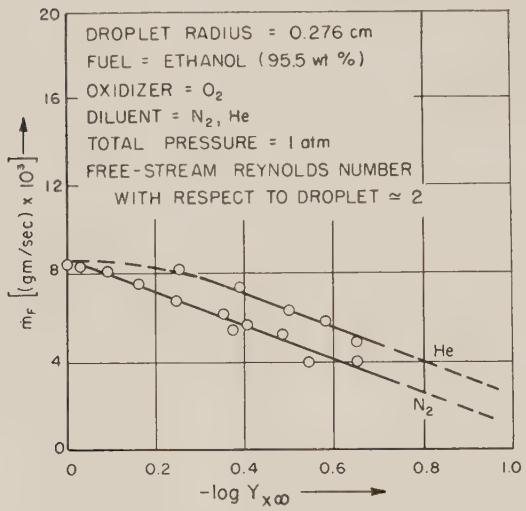

Fig. 4. Droplet burning rate as a function of gas-phase composition.

sphere relative to that of the liquid results in a larger contribution of radiative heat transfer. Quantitative information on the effect of gas velocity on liquid-burning rate is not available as yet. However, preliminary determinations have shown that the burning rate is a function of the free-stream Reynolds number.

The experimental measurements indicate the existence of a well defined luminous region at some distance from the liquid-droplet surface (Fig. 2). This zone probably represents the region of maximum temperature resulting from the chemical reaction between fuel and oxidizer. Although this region is not sphericosymmetrical because of axial convection and does not necessarily represent the completion of chemical reaction, the maximum distance between the drop and the luminous section of the flame appears to remain constant and independent of droplet radius (Table 1). Such an observation is in agreement with the suggestion made by Hall and Diederichsen[2].

Burning Rate as a Function of Gas-Phase Composition

Since the heterogeneous combustion process is governed by the transport rate of energy and mass to and from the liquid droplet, the composition of the vapor phase has a marked effect on the liquid-burning rate. Thus at constant total pressure of 1 atm the mass combustion rate of ethanol (95.5 per cent bw) diminishes exponentially as the weight fraction of gaseous oxygen Y_{X_∞} is decreased (Fig. 4). With nitrogen as a diluent in the gas phase, Y_{X_∞} attains a limiting value of 0.21 (corresponding to 17 per cent bw) below which the droplet surface does no longer sustain stable combustion.

Substitution of helium for nitrogen as the diluent in the gas stream carrying the oxidizer causes a pronounced rise in the burning rate (Fig. 4). This relative change in $\dot{m}_F$ becomes more pronounced as the concentration of diluent in the gas mixture is increased.

The increase in burning rate with rising weight fraction of gaseous oxidizer is reflected also in the gradual approach of the luminous region of the flame towards the liquid surface. As a result the rate of heat transfer per unit area becomes greater, and the attainment of steady-state combustion becomes more difficult, especially as the droplet radius is diminished. Under these conditions disruptive boiling is observed together with the intermittent ejection of liquid fuel from the drop surface.

Burning Rate as a Function of Liquid-Phase Composition

The effect of the physical properties of the liquid phase on the burning rate of a fuel droplet was investigated in a series of experiments in which a binary liquid solution composed of

[d] The evaporation constant[3] is calculated from $\epsilon = 2\dot{m}_F/\pi\rho_l r_l$.

ethanol and water was employed. In these measurements the weight fraction of oxygen in the gas stream was varied over a wide range. The results (Fig. 5) demonstrate the logarithmic increase in burning rate with rising oxidizer concentration for each of the liquid mixtures studied, as was previously observed for the mixture containing 95.5 per cent (bw) ethanol (Fig. 4). As the fuel becomes more dilute with water (>60 per cent bw of H_2O), some difficulty is encountered in completely vaporizing the liquid during the burning process. Under these conditions the loss of liquid material from the wetted sphere was noted. It appears that as a result of the low heat flux per unit area, separation of the components by distillation occurs for those solutions highly dilute with respect to fuel. Thus the composition of the vapor reaching the combustion surface differs widely from that of the liquid solution. Consequently the less volatile constituent begins to accumulate in the liquid phase until its mass can no longer be supported by the spherical surface. On the other hand, at high rates of heat transfer flash-vaporization of the nonideal solution is preferred. As a result, the same composition is maintained in the liquid and vapor phases, thereby yielding steady-state combustion.

The separation of components from a binary liquid mixture by distillation during combustion became further evident in the burning-rate measurements employing isopropanol as the fuel and water as the diluent. This two-component system forms an azeotrope containing 87.9 per cent (bw) isopropanol. The pure material as well as the binary azeotrope indicated complete vaporization of the liquid phase during the burning process. However, liquid solutions displaced in composition from the azeotrope (41.5 per cent bw and 71.7 bw isopropanol), so that under equilibrium conditions the vapor composition was widely different from that of the liquid, clearly demonstrated incomplete vaporization with loss of liquid material from the spherical surface.

BURNING RATE OF SYSTEM: LIQUID NITRIC ACID-GASEOUS AMMONIA

The experimental procedure has been extended to include measurements of the burning rate of a liquid oxidizer and a gaseous fuel. For this purpose the system composed of liquid nitric acid and gaseous ammonia was chosen. Burning-rate measurements for this system are of practical importance because of the application of such a fuel-oxidizer combination in rocket propulsion. Moreover, the thermal instability of liquid nitric acid at temperatures near its boiling point adds to the interest of this reactant from the standpoint of chemical kinetics and combustion. A

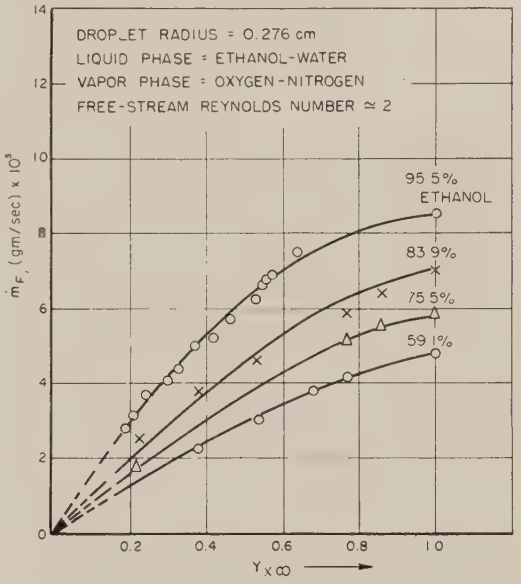

FIG. 5. Droplet burning rate as a function of liquid-phase composition.

FIG. 6. Nitric acid droplet burning in ammonia atmosphere.

representative photograph of a nitric acid droplet burning in an ammonia atmosphere is shown in Figure 6. Visual observation indicates the existence of three distinct zones ranging from dark brown to blue to yellow between the droplet surface and the outer luminous region of the flame. It is apparent that the decomposition of the acid occurs near the liquid surface and subsequently

interaction of the decomposition products with ammonia in the homogeneous diffusion flame takes place.

The temperature-labile characteristics of the liquid nitric acid caused burning instability for droplets of relatively small radii. However, since the heat flux per unit area is inversely proportional to the droplet radius, an increase in droplet size made possible the attainment of steady-state combustion. Similarly the addition of small amounts of water to the liquid phase reduced the rate of thermal decomposition of nitric acid sufficiently to observe a stable flame.

Table 2. Burning Rate of Nitric Acid Droplet in Gaseous Ammonia*

Composition, Liquid Phase (per cent *bw*)			Burning Rate $(gm/sec)10^3$
HNO_3	NO_2	H_2O	
100	0	0	18.1
90	0	10	14.6
86	13	1	23.4

* Droplet radius = 0.414 cm. Free-stream Reynolds number $\simeq 2$. Total pressure = 1 atm.

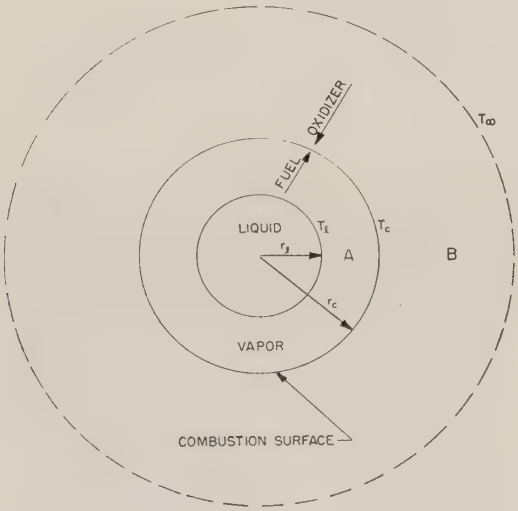

Fig. 7. Schematic presentation of burning liquid droplet.

The results of the burning-rate measurements for this system are summarized in Table 2. The retarding effect of water and the accelerating influence of nitrogen dioxide on $\dot{m}_F$ are clearly demonstrated. In the presence of large concentrations of NO_2 in the acid, intermittent loss of reactant caused by ejection of liquid material from the drop surface was observed. The trajectory of the atomized liquid through the gaseous atmosphere of ammonia could be traced by the smoke trail it produced. This instability was presumably the result of very rapid vaporization of NO_2 from the liquid surface. It is to be expected that during the life time of a droplet the increase in heat flux per unit area with diminishing droplet size causes the breakup of the droplet by means of disruptive boiling as a critical radius is reached.

Theoretical Analysis

The theoretical analysis of the burning rate of a droplet is based on a sphericosymmetrical model[3, 6] in which gaseous reactant is produced by evaporation from a liquid spherical source as a result of energy transfer from the flame front. As a first approximation, convective effects due to thermal gradients are neglected. However, the influence of free convection on the combustion process is subsequently introduced as a semi-empirical correction to this treatment. The spherical-liquid source gives rise to radial displacement of vapor towards the flame front at which the weight fraction of reactants approaches zero. The location of this flame front is governed by the transport characteristics and the chemical kinetics of the system. Thus for a bipropellant liquid-vapor system composed of fuel and oxidizer the flame front may be considered as a mathematical surface at which the ratio of the mass-flow rates of fuel and oxidizer is stoichiometric. For a monopropellant liquid-aerosol system, on the other hand, the position of the flame front is located at a distance where the chemical reaction has practically gone to completion and the gas temperature has essentially attained the adiabatic-flame temperature. The case of the monopropellant droplet resembles in many respects the problem of linear-flame propagation in homogeneous systems except for the spherical-coordinate system and the existence of a flame holder at the cold boundary which is the liquid-droplet surface. Because of the differences in the treatment of the problem, the theoretical analysis has been restricted to the burning rate of a liquid droplet in a bipropellant system. The burning rate of a liquid-monopropellant droplet forms the subject of a separate publication.

The sphericosymmetrical model of a burning droplet is schematically depicted in Figure 7. In region A ($r_l < r < r_c$) enclosed by the diffusion-flame interface, the fuel vapor is diluted by means

of combustion products and inert gas for which no sink is available in this shell. Since the weight fraction of oxidizer approaches zero at the combustion surface ($r = r_c$), it may be assumed that the entire heat release as a result of chemical interaction between fuel and oxidizer occurs at the flame front. However, in its passage from the liquid surface to the surface of active combustion, the fuel molecule may undergo endothermic reactions such as thermal cracking which alters the temperature distribution in this region. Such effects are neglected in the analysis that follows.

The mathematical derivation includes the following assumptions: (1) spherical symmetry with neglect of relative motion of droplet and surrounding medium; (2) entire heat release at the flame surface of infinitesimal thickness where the weight fractions of fuel and oxidizer approach zero; (3) averaged values with respect to temperature for the transport parameters and the physical properties of the system; (4) liquid-surface temperature ($T = T_l$) equal to the boiling point of the liquid; (5) independence of the ratio of specific heat to thermal conductivity (C/λ), and the product of density and diffusion coefficient (ρD) on weight fraction and temperature; (6) steady-state combustion under isobaric conditions; (7) stoichiometric mass-flow rate of fuel and oxidizer at the combustion surface ($r = r_c$); (8) no conduction of heat into the interior of the droplet; and (9) neglect of radiation effects.

EQUATIONS FOR CONSERVATION OF MASS AND ENERGY[e]

Consider the region A lying between r_l and r_c. The mass-flow rate[f] of fuel vapor leaving the liquid surface is given by

$$\dot{m}_F = 4\pi r^2 \rho (Y_F v - D_A Y_F') \tag{1}$$

Since no sink is available for the products (including the inert gas), the mass-flow rate of products in this region is zero; i.e.,

$$\dot{m}_P = 4\pi r^2 \rho (Y_P v - D_A Y_P') = 0 \tag{2}$$

Under steady-state conditions the total enthalpy flux H_F at any point within this region must be equal to the total enthalpy flux at the liquid surface H_{F_l}, or

$$H_F = \dot{m}_F h_F - 4\pi r^2 \lambda_A T'$$

$$H_{F_l} = \dot{m}_F h_{F_l} - 4\pi r^2 \lambda_A T_l'$$

Therefore

$$\dot{m}_F (h_F - h_{F_l}) = 4\pi r^2 \lambda_A T' - \dot{m}_F L \tag{3}$$

where

$$4\pi r^2 \lambda_A T_l' = \dot{m}_F L = \dot{m}_F [L^* + C_l (T_l - T^*)] \tag{4}$$

since, in the absence of a source or sink of heat within the liquid droplet, the total rate of heat transfer at the spherical surface r_l must be equal to the rate of vaporization of liquid fuel. In region B, where $r_c < r < \infty$, the mass-flow rate of oxidizer is

$$\dot{m}_X = 4\pi r^2 \rho (Y_X v - D_B Y_x') \tag{5}$$

Since it is assumed that combustion takes place at stoichiometric-mixture ratio (equal to the wt frac ratio of oxidizer to fuel)

$$\dot{m}_X = -i\dot{m}_F \tag{6}$$

Similarly the mass-flow rate of products in this region is given by the difference in mass-flow rates of fuel and oxidizer. Therefore,

$$\dot{m}_P = \dot{m}_F - \dot{m}_X = 4\pi r^2 \rho (Y_P v - D_B Y_p') \tag{7}$$

Based on the principle of conservation of energy, the following energy balance obtains

$$\dot{m}_X h_X + \dot{m}_P h_P - \dot{m}_F h_{F_l} = 4\pi r^2 \lambda_B T' - \dot{m}_F L \tag{8}$$

THERMODYNAMIC RELATIONSHIPS

$$h_F + i h_X = q + (1 + i) h_P$$

$$h_P = C_P (T - T^*)$$

$$h_X = C_X (T - T^*) + q/i$$

$$h_F = C_F (T - T_l) + L$$

where T^* is an arbitrary reference temperature. It is assumed that

$$C_P = C_F = C_X = C$$

BOUNDARY CONDITIONS

$r = r_l$	$T = T_l$		
$r = r_c$	$T^+ = T^-$[g]	$Y_X = 0$	$Y_F = 0$
$r = \infty$	$T = T_\infty$	$Y_X = Y_{X_\infty}$	

INTEGRATION OF DIFFERENTIAL EQUATIONS

Based on these relationships for motion and heat conduction appropriate to the problem, the

[e] The same basic equations were used by Goldsmith and Penner[6]. However, the physical model permits both the simplification of assumptions and an alternate mathematical treatment.

[f] The prime notation indicates space derivatives; the dotted quantities are time derivatives.

[g] T is continuous, but T' may be discontinuous.

following differential equations are obtained for the condition $T^* = T_l$: For shell of radius r where $r_l < r < r_c$,

$$Y_F' = \dot{m}_F(Y_F - 1)/4\pi\rho D_A r^2 \tag{9}$$

$$(T - T_l)' = \dot{m}_F[C(T - T_l) + L]/4\pi\lambda_A r^2 \tag{10}$$

For shell of radius r where $r_c < r < \infty$,

$$Y_X' = \dot{m}_F(Y_X + i)/4\pi\rho D_B r^2 \tag{11}$$

$$(T - T_l)' = \dot{m}_F[C(T - T_l) + (L - q)]/4\pi\lambda_B r^2 \tag{12}$$

These equations may be integrated in closed form if the assumption is made that C/λ and ρD are constant and independent of Y and T. The results of the integration yield the following explicit solutions for the mass and flow rate of fuel $\dot{m}_F$, the temperature at the combustion surface T_c, and the radius of the combustion surface r_c:

$$\dot{m}_F = \frac{4\pi\lambda_B r_l}{C_B} \ln\left[\frac{q}{L}\left(1 + \frac{Y_{X_\infty}}{i}\right)^{\alpha\lambda_B/\lambda_A} - \frac{C_B}{L}\left(\frac{q - L}{C_B} + T_l - T_\infty\right)\cdot\left(1 + \frac{Y_{X_\infty}}{i}\right)^{\alpha[(\lambda_B/\lambda_A)-1]}\right] \tag{13}$$

$$T_c - T_l = \frac{q - L}{C_B} - \left(\frac{q - L}{C_B} + T_l - T_\infty\right)\cdot\left(1 + \frac{Y_{X_\infty}}{i}\right)^{-\alpha} \tag{14}$$

$$\frac{r_c}{r_l} = \ln\left[\frac{q}{L}\left(1 + \frac{Y_{X_\infty}}{i}\right)^{\alpha\lambda_B/\lambda_A} - \frac{C}{L}\left(\frac{q - L}{C} + T_l - T_\infty\right)\cdot\left(1 + \frac{Y_{X_\infty}}{i}\right)^{\alpha[(\lambda_B/\lambda_A)-1]}\right] \Big/ \alpha\frac{\lambda_B}{\lambda_A}\ln\left(1 + \frac{Y_{X_\infty}}{i}\right) \tag{15}$$

where $\alpha = Cp D_B/\lambda_B$. This ratio of the Prandtl to Schmidt number is near unity for most gases having a specific heat ratio between 1.3 and 1.4.[h]

In order to examine the functional relationships between the various parameters it is desirable to further simplify the equations by assuming the same values for the transport parameters in regions A and B. Thus the modified equations read

$$\dot{m}_F = \frac{4\pi\lambda r_l}{C} \ln\left[\frac{q}{L}\left(1 + \frac{Y_{X_\infty}}{i}\right) - \frac{C}{L}\left(\frac{q - L}{C} + T_l - T_\infty\right)\right] \tag{16}$$

or

$$\dot{m}_F \simeq \frac{4\pi\lambda r_l}{C} \ln\left(\frac{q}{L}\frac{Y_{X_\infty}}{i}\right) \tag{17}$$

$$T_c - T_l = \frac{q - L}{C} - \left[\frac{q - L}{C} + T_l - T_\infty\right] \Big/ \left[1 + \frac{Y_{X_\infty}}{i}\right] \tag{18}$$

$$\frac{r_c}{r_l} = \frac{\ln\left[\frac{q}{L}\left(1 + \frac{Y_{X_\infty}}{i}\right) - \frac{C}{L}\left(\frac{q-L}{C} + T_l - T_\infty\right)\right]}{\ln\left(1 + \frac{Y_{X_\infty}}{i}\right)} \tag{19}$$

or

$$\frac{r_c}{r_l} \simeq \ln\left(\frac{q}{L}\frac{Y_{X_\infty}}{i}\right) \Big/ \ln\left(1 + \frac{Y_{X_\infty}}{i}\right) \tag{20}$$

It also can be shown that the weight fraction of fuel at liquid surface is given by

$$Y_{F_l} \simeq 1 - \frac{L}{q}\left(1 + \frac{i}{Y_{X_\infty}}\right) \tag{21}$$

It is apparent that the value of T_c calculated from equation (18) is identical to the adiabatic flame temperature. However, it may exceed the adiabatic flame temperature if the ratio of molecular to thermal diffusivity is greater than unity (equation 14).

Correlation with Experimental Measurements

An examination of the experimental results on the basis of the theoretical equations indicates that the sphericosymmetrical model qualitatively predicts the variation of the burning rate of the liquid droplet as a function of the droplet radius and the chemical properties of the system. Thus the linear dependence of $\dot{m}_F$ on droplet radius (equation 17) is borne out by the data presented

[h] Based on Eucken's equation[7] for thermal conductivity $\lambda = \frac{1}{4}[9 - (5/\gamma)]C\eta$ and Maxwell's equation for the diffusion coefficient $D = 1.34\ \eta/\rho$, the ratio $\lambda/C\rho D = 1.68 - (0.931/\gamma) \simeq 1$ for γ between 1.3 and 1.4.

in Figure 3. Similarly the exponential change in burning rate with variations in the weight fraction of oxidizer in the gas stream Y_{X_∞} has been verified (Fig. 4). Equation (17) is also in qualitative agreement with the experimental measurements of the effect of changes in extensive properties of the liquid fuel on mass-burning rate. In these experiments the physical properties of the fuel (ethanol) were altered by the addition of varying amounts of water, and the burning rate was measured over a wide range of weight fractions of gaseous oxidizer. The results originally presented in Figure 5 have been recalculated in accordance with equation (17). As is seen by the data in Figure 8, the mass-burning rate is proportional to $\log\left(\frac{q}{L}\frac{Y_{X_\infty}}{i}\right)$

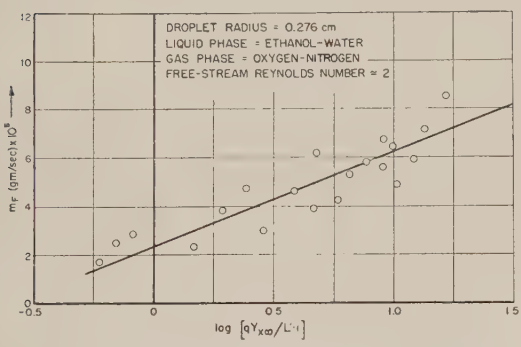
DROPLET RADIUS = 0.276 cm
LIQUID PHASE = ETHANOL-WATER
GAS PHASE = OXYGEN-NITROGEN
FREE-STREAM REYNOLDS NUMBER ≈ 2
$\dot{m}_F$ (gm/sec) x 10^5
log $[qY_{X\infty}/L^{-1}]$

FIG. 8. Mass-burning rate as a function of physical properties of fuel.

(equation 17). It is of particular interest that on the basis of equation (17) the limiting value of Y_{X_∞} for steady-state combustion of a fuel droplet may be calculated. This value is given by $\lim_{\dot{m}_F \to 0} (Y_{X_\infty}/i) = (L/q)$. For the ethanol-air system $L/q = 0.028$, corresponding to a weight fraction of oxygen equal to ~0.1 with nitrogen as the diluent. The experimental value of $\lim Y_{X_\infty}$ is 0.21 (see Section III). It is obvious that an increase in the magnitude of L/q raises the lower limit of oxygen concentration at which stable combustion occurs.

However, examination of the experimental results as a function of the transport properties of the system shows certain defects of the sphericosymmetrical model. Thus, to a first approximation, the theory predicts the burning rate to be proportional to the ratio[i] λ/C of the gas (equation 13). It is apparent that such a change in the transport properties would exert its main influence in region B where the weight fraction of inert gas is high relative to that in region A. The experimental measurements, on the other hand, indicate that $\dot{m}_F$ is affected to a lesser degree than predicted by the theoretical analysis of the change in interdiffusion coefficient (Fig. 4). The inadequacy of the theoretical model is further demonstrated by the change in burning rate with total pressure. The model suggests that $\dot{m}_F$ is independent of total pressure, whereas the investigation by Hall and Diederichsen[2] demonstrates a weak dependence on pressure.

The cause for these discrepancies between theory and experiment may in part be attributed to the contribution of axial convection to the transport properties of the system. Such an effect is demonstrated by the nonspherical appearance of the combustion zone surrounding the droplet (Fig. 2). The magnitude of the contribution of axial convection to the mass-burning rate is difficult to evaluate. However, semi-empirically this effect may be introduced into the theoretical analysis by replacing the parameters for diffusive transport of mass and energy with appropriate mass and heat-transfer coefficients which include free convective flow in an axial direction. Thus the total rate of mass and energy transfer in region B is the sum of transfer by radial flow, diffusion, and free convection. The latter two terms may be combined into a single mass-transfer coefficient k and heat-transfer coefficient h. These physical relations[8] may be defined in terms of dimensionless groups; i.e.,

$$hd/\lambda = N_u = \delta(Gr \cdot Pr)^{1/4} \tag{22}$$

$$kd/D = N'_u = \beta(Gr \cdot Sc)^{1/4} \tag{23}$$

where d is the linear dimension of the heating surface, and the dimensionless groupings represent the Nusselt number for heat transfer N_u, the Nusselt number for mass transfer N'_u, the Grashof number Gr, the Prandtl number Pr, and the Schmidt number Sc. The terms δ and β are empirical constants. Consequently the heat-transfer coefficient is given by

$$h = \delta\lambda(\sigma C\rho^2/\eta\lambda d)^{1/4} \tag{24}$$

where the term σ contains the product of spherical expansion, the gravitational constant, and the temperature difference between the two shells across which heat transfer occurs. The term η represents the viscosity of the medium. Therefore the value for the thermal conductivity of the gas is modified by a coefficient (equation 24) which

[i] The ratio is equal to ρD.

represents the contribution of free convection to the process of heat transfer. Therefore based on the heat-balance equation, $\dot{Q} = \dot{m}_F L = 4\pi r^2 h \Delta T$, which upon substitution from equation (24) makes $\dot{m}_F$ proportional to the one-half power of the total pressure. Experimental observations[2] have shown that $\dot{m}_F$ is approximately proportional to $\rho^{1/4}$. It is to be remembered that the exponent in the Grashof-Nusselt correlation is a function of the Grashof number and has a maximum value of $\frac{1}{4}$. It approaches zero for very low Grashof numbers.[i] Thus the empirical pressure exponent for the mass burning rate suggest the contribution of free convection to the over-all process of heat transfer.

The contribution of free convection also yields some interesting information on the variation of the distance between the combustion surface and the liquid-droplet surface (Fig. 7) with total pressure. By combining equations (13) and (15), it can be shown that the sphericosymmetrical model yields the relationship

$$r_c = \dot{m}_F \Big/ \left[4\pi\rho D \ln\left(1 + \frac{Y_{X_\infty}}{i}\right)\right] \qquad (25)$$

which makes r_c independent of the total pressure. However, the location of this mathematical surface is governed by the diffusive transport of the reactants. By means of the Nusselt analogy for mass transport, the mass-flow rate in such a diffusion-controlled process is proportional to the mass-transfer coefficient. In the presence of free convection this coefficient

$$k = D(\beta\sigma\rho/\eta D d)^{1/4} \qquad (26)$$

is inversely proportional to the square root of the total pressure. Consequently the variation of r_c (equation 25) with pressure exhibits the same dependency. Experimental measurements carried out in a pressure range from 1 to 20 atm have shown that such a relationship between combustion radius and total pressure exists[2]. Therefore it may be concluded that the inclusion of free convection in the sphericosymmetrical model satisfactorily describes the phenomena associated with the combustion of a liquid droplet as measured in this investigation.

Nomenclature

C_F = specific heat of fuel vapor at constant pressure (cal/gm °K).
C_P = specific heat of gaseous products at constant pressure (cal/gm °K).
D = diffusion coefficient (sq cm/sec).
h = enthalpy per unit mass of gaseous component (cal/gm).
i = stoichiometric-mixture ratio = $(Y_X/Y_F)_{\text{stoichiometric}}$.
L^* = heat of vaporization (cal/gm).
$\dot{m}_F$ = mass-flow rate of fuel (gm/sec).
q = heat of reaction (cal/gm).
r_l = droplet radius (cm).
r_c = radius of flame zone (cm).
T = temperature (°K).
T^* = arbitrary reference temperature (°K).
T_{X_∞} = temperature of gaseous reactant at infinite distance from droplet surface
v = velocity = dr/dt (cm/sec) (°K).
Y_F = mole fraction of liquid reactant.
Y_P = mole fraction of product.
Y_X = mole fraction of gaseous reactant.
γ = specific heat ratio.
η = viscosity (gm/cm sec).
λ = thermal conductivity (cal/cm sec °K).
density (gm/cc).

SUBSCRIPTS:

l = liquid surface.
A = transport parameters in region A.
B = transport parameters in region B.
F = fuel.
X = oxidizer.
P = products.

[i] The authors acknowledge clarification on this point by the reviewer of the manuscript.

REFERENCES

1. Gregory, C. A., Jr., and Calcote, H. F.: *Fourth Symposium (International) on Combustion*, p. 830. Baltimore, The Williams & Wilkins Co., 1953.
2. Hall, A. R., and Diederichsen, J.: *Fourth Symposium (International) on Combustion*, p. 837. Baltimore, The Williams & Wilkins Co., 1953.
3. Godsave, G. A. E.: *Fourth Symposium (International) on Combustion*, p. 818. Baltimore, The Williams & Wilkins Co., 1953.
4. Spalding, D. B.: *Fourth Symposium (International) on Combustion*, p. 847. Baltimore, The Williams & Wilkins Company, 1953.
5. Godsave, G. A. E.: *The Burning of Single Drops of Fuel. Part I: Temperature Distribution and Heat Transfer in the Preflame Region.* Report No. R. 66. London, National Gas Turbine Establishment of the Ministry of Supply, June (1950).
6. Goldsmith, M., and Penner, S. S.: *On the*

Burning of Single Drops of Fuel in an Oxidizing Atmosphere. Technical Report No. 2. Pasadena, Calif. Inst. of Tech., November (1953).

7. KENNARD, E. H.: *Kinetic Theory of Gases*. New York, McGraw-Hill Book Co., 1942.
8. MCADAMS, W. H.: *Heat Transmission*. New York, McGraw-Hill Book Co., 1942.

DISCUSSION BY F. SCHULTZ-GRUNOW*

It seems that the aforementioned eigenvalue problem could be fitted better to the problem by using the solution of a point heat source in a parallel flow. One could assume the flame front to be the constant temperature surface at which the evaporated liquid is burned.

* Technische Hochschule, Aachen, Germany.

4

AN EXPERIMENTAL STUDY ON THE COMBUSTION OF A FUEL DROPLET

By KIYOSI KOBAYASI

Introduction

In research on combustion in gas turbines or diesel engines, it is essential to know the combustion mechanism of individual fuel droplets, because the ignition lag and the burning velocity of the injected fuel spray which have an important bearing on the design and performance of these engines can be determined from the combustion of a single droplet. Many workers had investigated the combustion of injected fuel sprays in diesel engines prior to the time when in recent years, prompted by the use of gas turbines, the study of combustion of a single droplet was initiated and expanded in theoretical work by Spalding[1, 2], Okazaki and Gomi[3], and experimental work by Godsave[4], Spalding[5], Topps[6], Kumagai et al.[7, 8], and Nishiwaki et al.[9].

The present paper describes an attempt to study by means of motion-picture recordings the combustion mechanism of a fuel droplet suspended from a quartz fiber. It represents a continuation of a previous study on the rate of evaporation velocity of a liquid droplet[10].

Experimental Procedure

In the experimental apparatus shown in Figure 1, the liquid droplet [1] (0.7–1.7 mm in diameter) is suspended by a quartz fiber, 0.1–0.2 mm in diameter. An electric furnace [2] mounted on rails can be moved so as to surround the hanging droplet completely. The moment at which the droplet enters the furnace is indicated by the closing of an electric circuit [3] with a lamp [4] mounted in series. Evaporation and combustion of the droplet in the furnace is recorded by motion pictures as shadowgraphs using a light source [6], a liquid filter [7], a telephoto lens [8], and a 16-mm movie camera [9]. The process is observed through the quartz window [5] in the side wall of

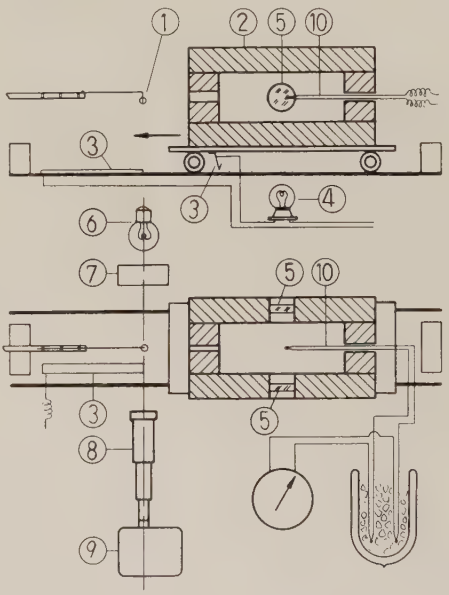

FIG. 1. Experimental apparatus

the furnace. The temperature measured by the thermocouple [10], whose hot junction is located near the droplet when it enters the furnace, is taken as the temperature of the air in the furnace. The dimensions of the droplet are measured on the motion pictures under a traveling microscope.

In these experiments the droplet at the tip of

the quartz fiber underwent such marked oval deformation as it decreased that it had to be corrected to an equivalent sphere as shown in Figure 2. This can be done: (a) by equating the

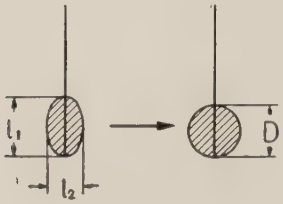

FIG. 2. Conversion from ellipsoid to equivalent sphere.

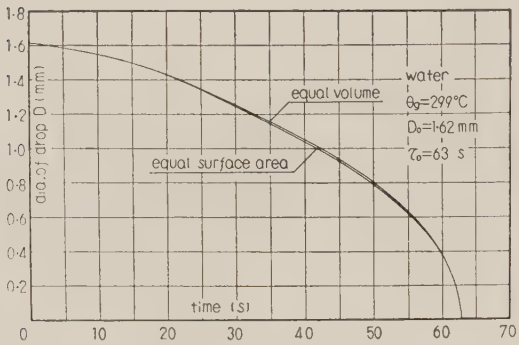

FIG. 3. Comparison of two conversion methods for measured example.

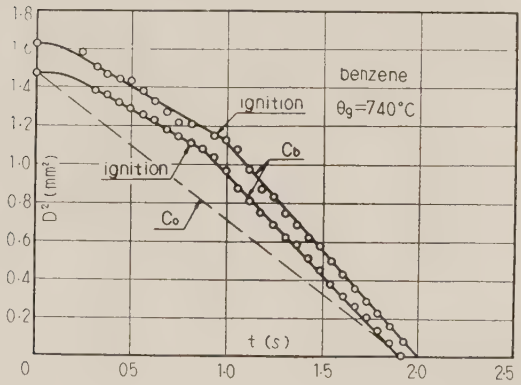

FIG. 4. Ignition and combustion of benzene droplet—"*true and apparent droplet burning velocity coefficients.*"

volumes;

$$D = \sqrt[3]{l_1 l_2^2} \tag{1}$$

or (b) by equating the surface areas;

$$D = l_2 \sqrt{\frac{1}{2}\left[1 + \frac{(l_1/l_2)^2}{\sqrt{(l_1/l_2)^2 - 1}} \sin^{-1} \frac{\sqrt{(l_1/l_2)^2 - 1}}{(l_1/l_2)}\right]} \tag{2}$$

Figure 3 shows the comparison of the two methods for a numerical example. The difference between them is so small (not more than 1.5 per cent) that equation (1) was used as easier to calculate.

Experimental Results

PURE LIQUID FUELS

As the temperature of the surrounding air increases, evaporation of the fuel droplet becomes more rapid, culminating in combustion by spontaneous ignition. An example of this process is shown in Figure 4 based on measurements of shadowgraph pictures, such as Figure 12b.

The relation between the droplet diameter D and the time t for the combustion at constant air temperature is given by:

$$\frac{dD^2}{dt} = \text{const.} = -C_b \tag{3}$$

This is similar to the equation for evaporation, and the slope of the curve is greater after ignition than during evaporation. This means that for a volatile fuel the law of evaporation holds at the surface of the burning droplet with diffusion of a suitable vapor-air mixture from the droplet to the outer flame. The inner diffusion zones of the flames may be seen in Figure 12b–f, and especially in Figure 12c which shows the comparison between shadowgraph and dark-field photographs. In Figures 12 and 13 (except Fig. 12c) the first frame is the initial state of the droplet just before introduction into the furnace, and its introduction is indicated by an arrow. The increase of the slope of the diameter-time curve which follows ignition is due to the increase in the amount of heat transferred to the droplet from the flame, and is analogous to the increase of the temperature θ_g of the surrounding air in the case of evaporation.

It is convenient to represent the burning velocity of the droplet by the slope C_b of that part of the curve. C_b may be called the true droplet burning velocity coefficient, by analogy to the evaporation of the droplet[10]. Moreover, the relation:

$$\frac{\tau_0}{D_0^2} = \text{const.} = \frac{1}{C_0} \tag{4}$$

exists between the initial diameter D_0 of the droplet and its life τ_0 in the case of combustion, too. The ignition lag decreases with the increase of the air temperature (Fig. 4). The life of the

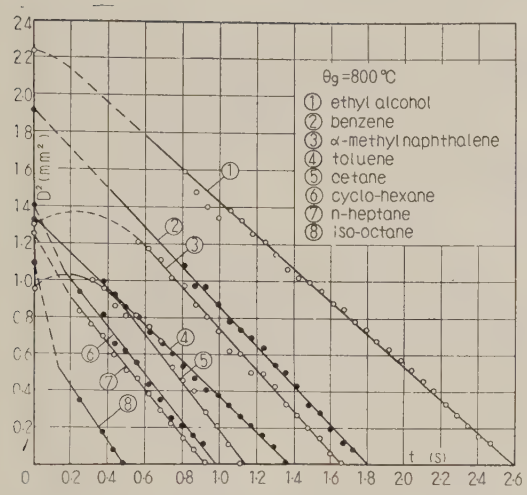

FIG. 5. Combustion of droplets of various pure fuels.

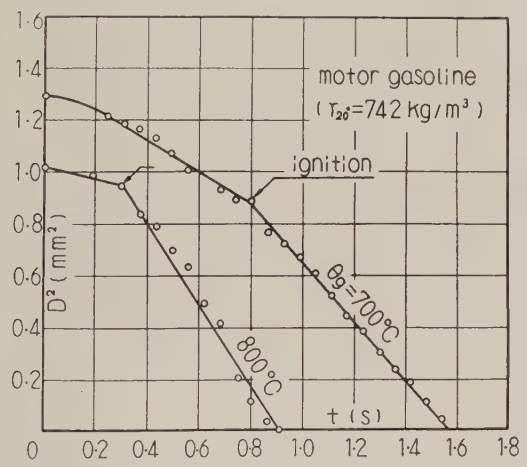

FIG. 6. Combustion of motor gasoline droplet

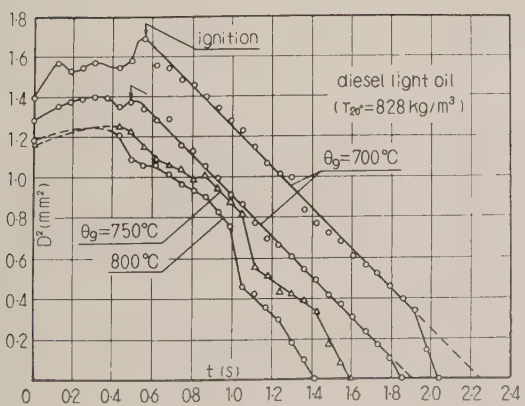

FIG. 7. Combustion of light diesel oil droplet

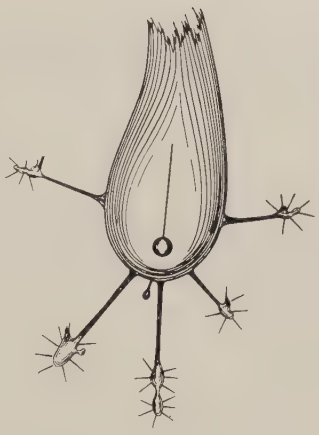

FIG. 8. Splashes in combustion of heavy oil droplet.

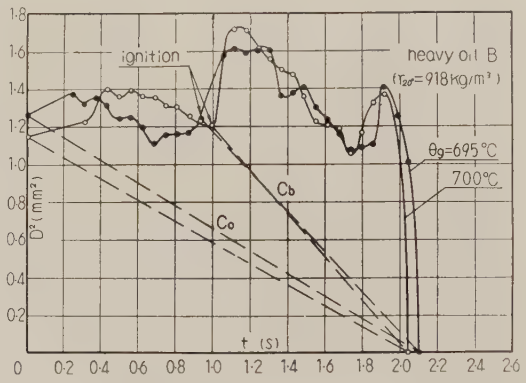

FIG. 9. Change of droplet diameter in combustion of heavy oil B.

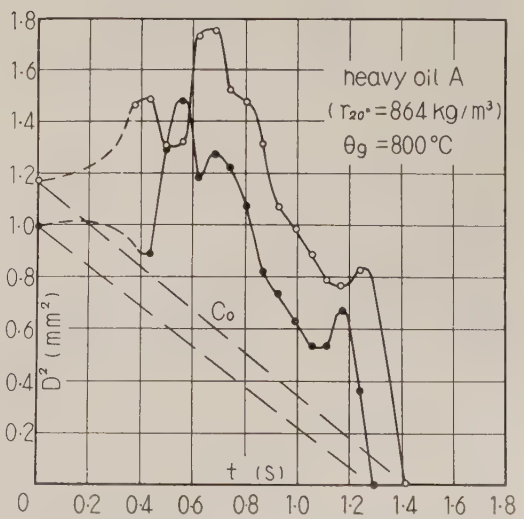

FIG. 10. Change of droplet diameter in combustion of heavy oil A.

droplet which is necessary for practical applications may be determined rapidly by using C_0 which may be called the apparent droplet burning velocity coefficient. If the ignition lag is negligible, as in the case of a fuel droplet with low boiling point injected into sufficiently hot air, C_0 becomes nearly equal to C_b. The combustion of droplets of various pure fuels at the air temperature θ_g = 800°C are compared in Figure 5. It will be seen that the relation of equation (3) is satisfied. Fuels with low carbon content burn with dark flames as shown in Figure 12a, but the fuels with high carbon content burn with luminous flames and smoke due to vapor-phase cracking in the flames (Fig. 12b–f). Formation of soot is especially apparent in Figure 12d.

Table 1. Coefficients of Combustion Velocity of Droplet

θ_g°C	C_b $\frac{mm^2}{s}$	C_0 $\frac{mm^2}{s}$
Methyl alcohol		
800	1.72	1.14
800	1.48	1.19
Nitrobenzene		
700	1.02	0.94
800	1.00	0.95
Benzene		
705	0.65	0.88
710	1.00	—
730	1.05	0.82
730	1.08	0.72
730	0.90	0.87
735	1.01	0.87
740	1.05	0.77
740	1.07	0.81
750	0.87	0.87
750	0.91	0.91
750	0.96	0.85
750	1.11	0.98
800	1.16	1.08
800	1.37	—
995	1.40	1.03
Heavy oil B		
695	1.05	0.60
700	1.14	0.56
800	—	0.86
800	—	0.91
Heavy oil B (*cont.*)		
800	—	0.78
Ethyl alcohol		
700	0.99	0.90
800	—	0.87
Isooctane		
700	0.90	1.03
900	1.30	1.43
900	1.30	1.26
995	1.35	1.76
n-Heptane		
700	—	1.37
700	1.21	1.15
700	1.10	0.96
800	—	1.61
800	1.24	1.35
800	—	1.59
Heavy oil A		
700	0.82	0.56
700	1.04	0.67
800	—	0.76
800	—	1.00
800	—	0.94
800	—	0.83
800	—	1.02
Cyclohexane		
700	1.02	0.90
Cyclohexane (*cont.*)		
800	1.50	1.27
Methylnaphthalene		
695	0.90	0.47
700	1.04	0.56
705	—	0.56
800	0.97	0.65
800	1.15	0.79
Motor gasoline		
695	—	0.71
695	1.00	0.66
700	1.10	0.82
705	1.14	0.87
710	1.00	0.87
800	1.45	1.08
800	1.49	1.02
Kerosene		
650	1.03	0.59
700	1.15	0.75
700	1.09	0.72
740	1.28	0.99
750	—	0.85
785	1.47	0.90
795	1.47	1.18
Toluene		
735	0.91	0.74
800	—	0.95
Cetane		
600	—	0.57
600	1.05	0.57
700	1.44	0.86
800	1.55	0.86
898	2.50	0.93
900	2.30	0.93
990	2.60	0.98
Diesel light oil		
628	1.29	—
655	1.12	0.59
700	1.09	0.74
700	1.31	0.70
700	1.01	0.63
700	1.01	0.68
710	1.04	0.71
740	1.36	0.99
740	1.28	0.73
750	1.10	0.75
790	1.15	0.63
795	1.22	0.89
800	1.18	0.83
900	1.90	0.89
904	2.00	0.81
995	2.15	1.08

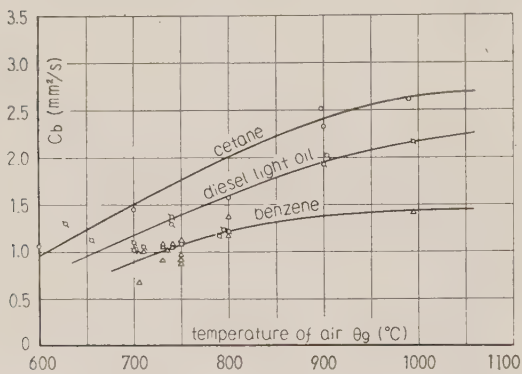

Fig. 11. Effects of ambient air temperature on the "*true droplet burning velocity coefficients.*"

Mechanism of Ignition of Fuel Droplets

The ignition of a benzene droplet was recorded by high-speed photography at 64 frames/sec. Figure 14 clearly shows the details of transition from ignition to steady-state combustion. Ignition sets in at some point on one of the concentric layers of vapor-air mixtures surrounding the droplet where the ratio is suitable. The flame propagates circumferentially and almost uniformly within the diffusion zone. For fuels having a high carbon content, the mixtures in this zone are so rich that the particles of soot are produced

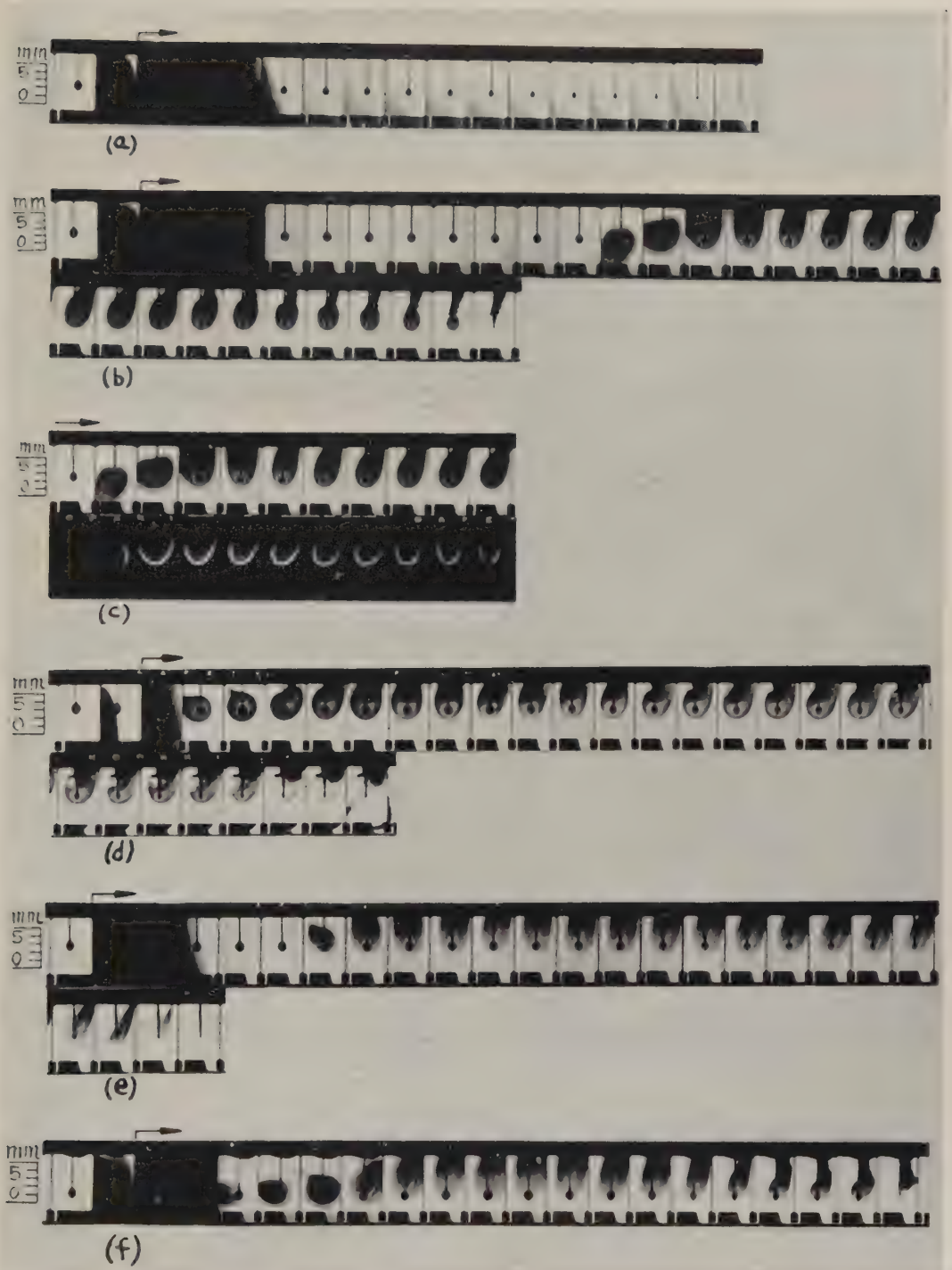

FIG. 12. (a) n-Heptane, $\theta_g = 800°C$, $D_0 = 1.12$ mm, $\tau_0 = 0.92$s, time interval $\Delta t = 61.8$ ms.
(b) Benzene, $\theta_g = 740°C$, $D_0 = 1.21$ mm, $\tau_0 = 1.91$s, $\Delta t = 61.8$ ms.
(c) Benzene, $\theta_g = 740°C$, $\Delta t = 61.8$ ms. (Upper) Shadowgraphs. (Lower) Dark field photographs.
(d) Nitrobenzene, $\theta_g = 700°C$, $D_0 = 1.26$ mm, $\tau_0 = 1.68$ s, $\Delta t = 61.8$ ms.
(e) Light diesel oil, $\theta_g = 735°C$, $D_0 = 1.04$ mm, $\tau_0 = 1.62$ s, $\Delta t = 61.8$ ms.
(f) Heavy oil A, $\theta_g = 800°C$, $D_0 = 1.05$ mm, $\tau_0 = 1.17$ s, $\Delta t = 61.8$ ms.

immediately by vapor-phase cracking, but convection does not yet occur. When convection finally sets in as the result of the heat liberated, the combustion products in the original diffusion zone are carried upward by fresh air supplied from below until a steady combustion is reached in which combustion in the inner diffusion zone is

On the other hand, light oil burns in a different way as shown in Figure 7. Here, for low air temperatures, the relation between the square of droplet diameter and the time follows the same curve as before, but during the evaporation and heating period before ignition, the droplet diameter fluctuates as a result of the superposed

FIG. 13. Heavy oil B in N_2, $\theta_g = 700°C$, $D_0 = 1.00$ mm, $\Delta t = 62.5$ ms.

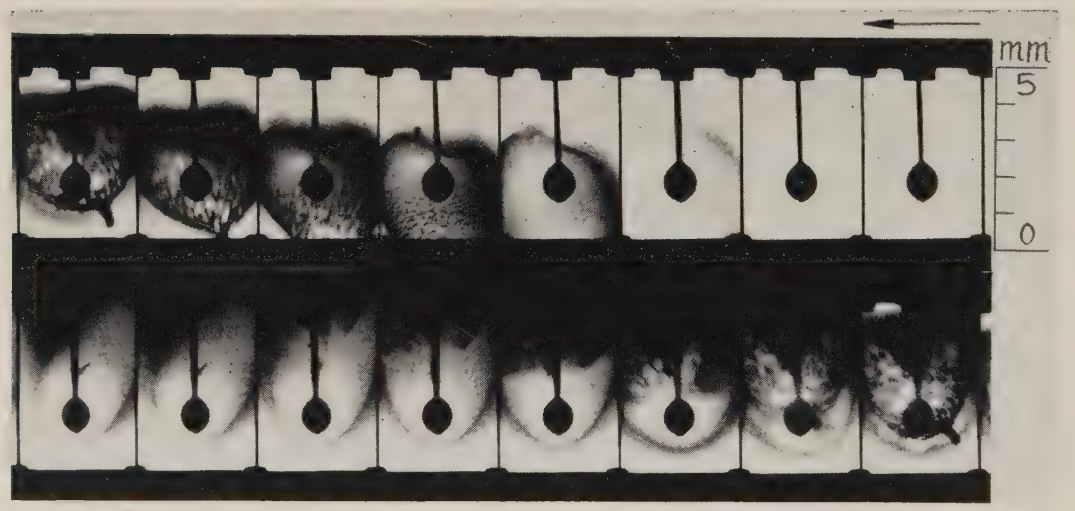

FIG. 14. Transient state from ignition to steady combustion. Benzene, $\theta_g = 680°C$, $\Delta t = 15.6$ ms.

incomplete due to the high consumption of oxygen at the flame front. Droplets of toluene, nitrobenzene, α-methylnaphthalene, light diesel oil, kerosene, and heavy oil, all were observed to behave in the same way as benzene. The rate of droplet diameter change during transition from ignition to steady combustion is relatively low.

FUELS FROM PETROLEUM

Motor gasoline burns in the same way as pure fuels (Fig. 6) with evaporation as the governing factor.

effects of thermal expansion and evaporation. Moreover, after ignition, the droplet diameter decreases more rapidly due to liquid-phase cracking caused by overheating through thermal conduction from the quartz fiber. When the quartz fiber is absent, combustion of the droplet follows the dotted line in Figure 7. This means that the temperature of the burning droplet is near the cracking temperature. If the air temperature increases, the linear relation is disturbed by liquid-phase cracking from the moment the tem-

perature in the droplet exceeds the cracking temperature.

Heavy oil shows an even more anomalous behavior. After evaporation of the lighter constituents, a viscous semi-solid residue remains. Vapor bubbles form by internal vaporization and by liquid-phase cracking in the droplet. These burst, producing large splashes of viscous residue which fly through the flame front, and which in turn produce secondary splashes at the droplet surface, like sparks formed by grinding carbon steel.

This phenomenon is shown in the sketch of Figure 8 and in the photograph of Figure 15 in which the secondary splashes do not appear. For such combustion, the change in the droplet diameter is complex as shown in Figures 9 and 10 where the peaks and troughs indicate respectively the formation of internal bubbles and release of scattering splashes. A characteristic of the burning heavy oil droplet is that it vanishes suddenly after a final expansion (Figs. 9 and 10). This is caused by the combustion of the final splashes which have solidified to carbon.

As the rate of peroxidation increases with the molecular weight of the fuel, the increase in diameter of the heavy oil droplet and the scattering might be attributed to peroxidation or internal combustion. To test this, heavy oil was evaporated in nitrogen at high temperature (Fig. 13). The formation and bursting of numerous bubbles in the droplet, following the evaporation of the lighter constituents, are clearly visible in Figure 16 which is a detail of Figure 13. As the temperature of the droplet is less in nitrogen than in air, due to the absence of the surrounding flame, the splashes are small, and the diameter of the expanded droplet is about 1.7 times as large as that of the original droplet, and the carbon skeleton persists. The changes in the droplet diameter are similar to those in air.

This indicates that the increase in diameter and the splashing which accompanies the combustion of heavy oil droplets are the result of frothing due to thermal cracking rather than of peroxidation and inner combustion.

Since the relation of equation (4) is satisfied even in such complex cases as the combustion of light or heavy oil, the droplet burning velocity coefficient C_b or C_0 may be taken as the mean value.

DROPLET BURNING VELOCITY COEFFICIENTS FOR VARIOUS TYPES OF FUELS AND AS FUNCTIONS OF AMBIENT TEMPERATURE

The true and apparent droplet burning velocity coefficients measured by the motion pictures (Fig. 12) for various kinds of fuels are listed in Table 1. Given the initial droplet diameter, the life of the droplet may be found by using these coefficients. Figure 11 shows the effects of the ambient air temperature on them. These effects are less than for evaporation, because the flame temperature has a direct influence on the combustion velocity.

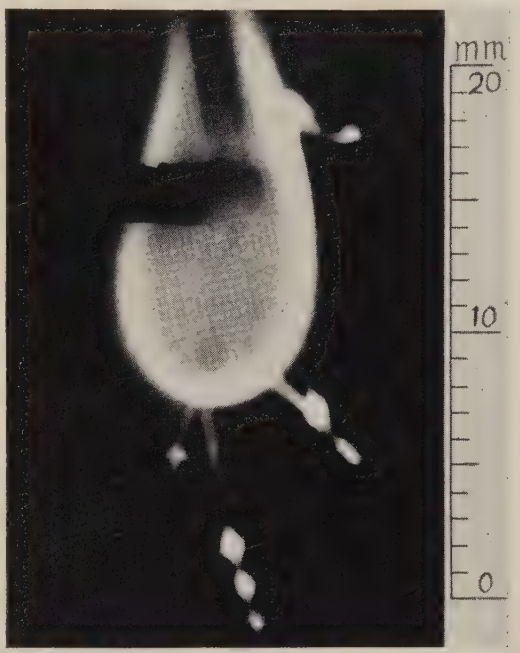

FIG. 15. Splashes in combustion of heavy oil A. $\theta_g = 800°C$.

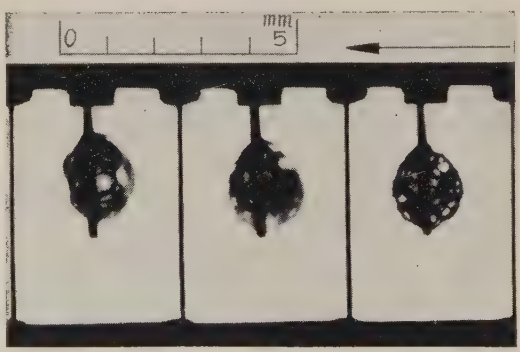

FIG. 16. Frothing and fully expanded droplet. Heavy oil B in N_2, $\theta_g = 700°C$, $\Delta t = 62.5$ ms.

Conclusions

The combustion of fuel droplets was investigated experimentally by means of motion pictures with the following results:

(1) In the combustion of pure fuel droplets, the decrease of the square of the droplet diameter is proportional to the time. Therefore, it may be convenient to represent the burning velocity of the droplet by a proportional constant known as the true droplet burning velocity coefficient by analogy to the evaporation of the droplet[10]. This fact shows that the law of evaporation also holds at the surface of the droplet for the combustion of pure fuels.

As the ignition lag of the droplet is almost equal to the initial evaporation period and cannot be neglected in many cases, the life of the droplet may be found conveniently by using the apparent droplet burning velocity coefficient as shown in equation (4). These true and apparent burning velocity coefficients were measured for various fuels and the effect of the ambient temperature upon them was determined.

(2) The mechanism of droplet ignition was established.

(3) The gasoline droplet burns in the same way as pure fuels.

Light oil and kerosene burn with liquid-phase cracking at higher air temperatures, but at lower air temperatures there is only evaporation without liquid-phase cracking.

Heavy oil burns with frothing and splashing of burning viscous residue which in turn produces secondary splashes that solidify into carbon particles, making the change of droplet diameter associated with combustion a complex one. However, it is virtually established that the life of the droplet is proportional to the square of its initial diameter. It was shown that the increase in diameter and the splashes of heavy oil were caused by frothing and the bursting of bubbles formed by thermal cracking, rather than by peroxidation and internal combustion.

Acknowledgments

The author wishes to express his hearty thanks to Professor Yasusi Tanasawa of the Tohoku University for his kind direction and valuable aid, and to Professor Hirosi Tokuhisa of the same University who supplied the pure fuels and gave helpful advice. Further, the author desires to express his thanks to Mr. Mituaki Okuyama and to Mr. Shozi Amano and to Mr. Nobuki Nagai for their assistance in the experimental work, and to the Ministry of Education of Japan for its financial aid.

REFERENCES

1. Spalding, D. B.: Fuel, *29*, 25 (1950).
2. Spalding, D. B.: Fuel, *30*, 121 (1951).
3. Okazaki, T., and Gomi, M.: Trans. Japan Soc. Mech. Engr., *19*, 88 (1953).
4. Godsave, G. A. E.: Nature, *164*, 708 (1949).
5. Spalding, D. B.: Fuel, *29*, 32 (1950).
6. Topps, J. E. C.: J. Inst. Petroleum, *37*, 535 (1951).
7. Kumagai, S., and Kimura, I.: Science of Machine *3*, 431 (1951).
8. Kumagai, S., and Isoda, H.: Science of Machine, *4*, 337 (1952).
9. Nishiwaki, J., Hagi, H., and Kinosita, M.: Annual Meeting, Japan Soc. Mech. Engr., April, 1951.
10. Kobayasi, K.: Technology Rept. of Tohoku University. XVIII, 2 (1954).

5

KINETICS OF LIQUID COMBUSTION PROCESSES: EVAPORATION AND IGNITION LAG OF FUEL DROPLETS

By NIICHI NISHIWAKI

Many experimental and theoretical studies have been published on the combustion of fuel droplets[1-6]. To these, the present paper adds a study on the evaporation and ignition lag of fuel droplets at various ambient air temperatures observed by photographical methods.

Apparatus and Procedure

Figure 1 shows the experimental apparatus. The combustion chamber (a furnace with two windows), shown in detail in Figure 2, is movable on rails. A fuel droplet suspended from a silica filament was quickly introduced into the com-

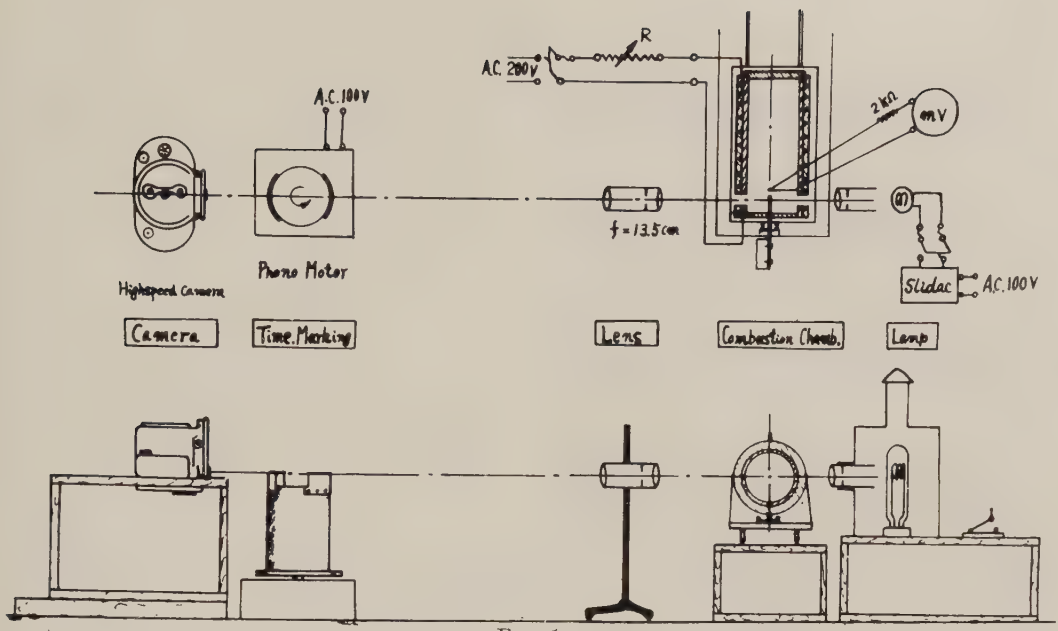
A.C. 200V
R
A.C. 100V
2 kΩ
mV
f = 13.5 cm
Slidac
A.C. 100V
Highspeed Camera
Phono Motor
Camera
Time Marking
Lens
Combustion Chamb.
Lamp

FIG. 1

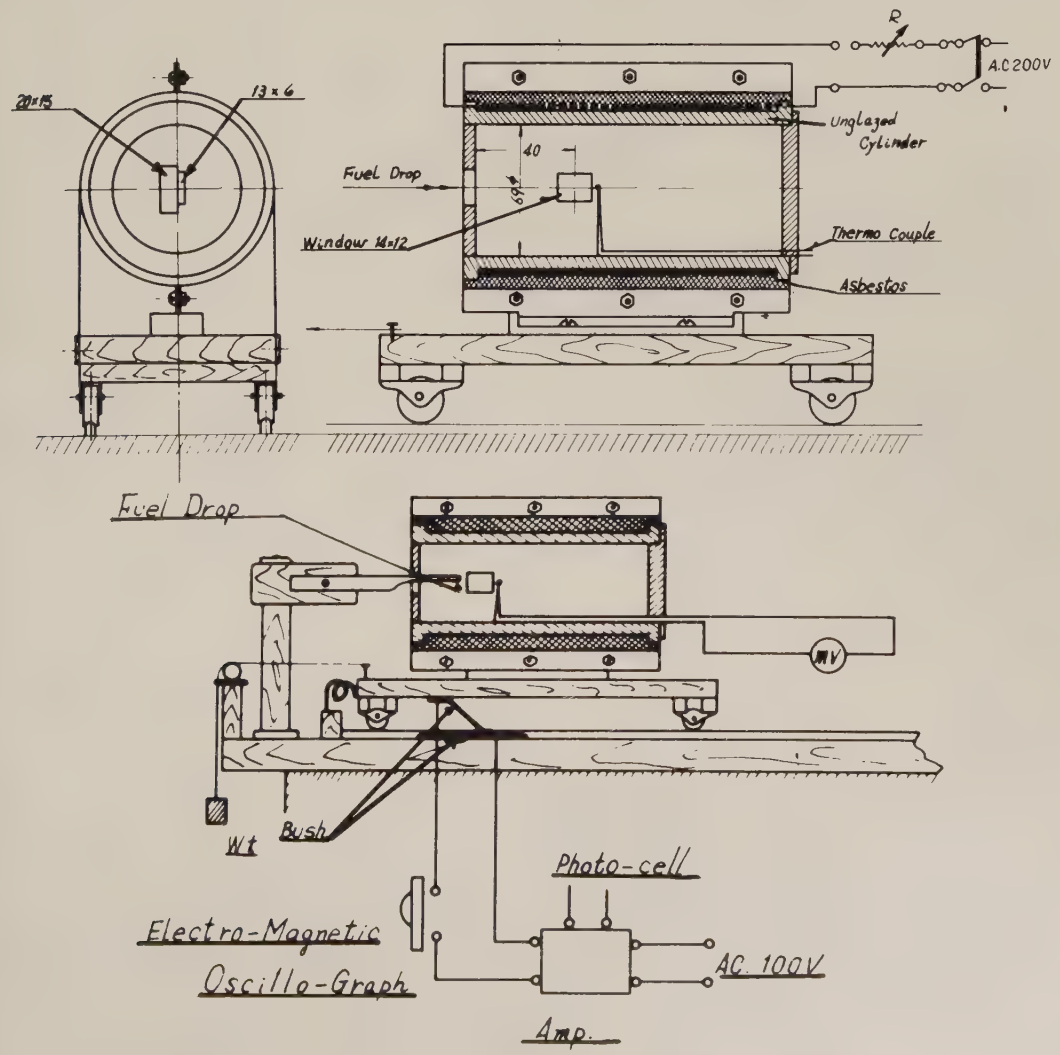
R
A.C 200V
20×15
13×6
Unglazed Cylinder
40
Fuel Drop
Window 14×12
Thermo Couple
Asbestos
Fuel Drop
mV
Wt
Bush
Photo-cell
Electro-Magnetic
Oscillo-Graph
AC. 100V
Amp.

FIG. 2

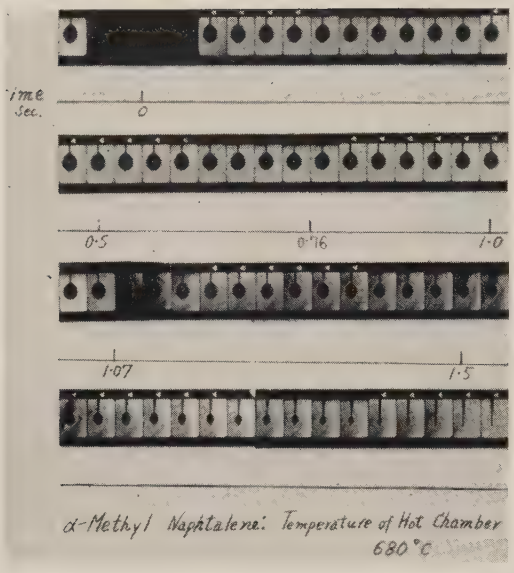

FIG. 3

In this investigation, the fuel droplet which is of ellipsoidal shape, was treated as a sphere of equal volume. As the droplet considered is almost spherical, its measured diameter is approximately equal to that of a sphere having the same surface area as the droplet.

From Figure 4, it will be seen that during evaporation and combustion the square of the diameter D varies linearly with time. In these curves, τ_1 is the time required to bring the droplet to the temperature at which evaporation begins; τ_2 is the time between the start of evaporation and the ignition; $\tau_{1+2}(= \tau_1 + \tau_2)$ is the ignition lag.

Evaporation

The evaporation, ignition and burning of fuel droplets were observed also by the schlieren method. The optical system shown in Figure 5 was used to obtain photographs of the type

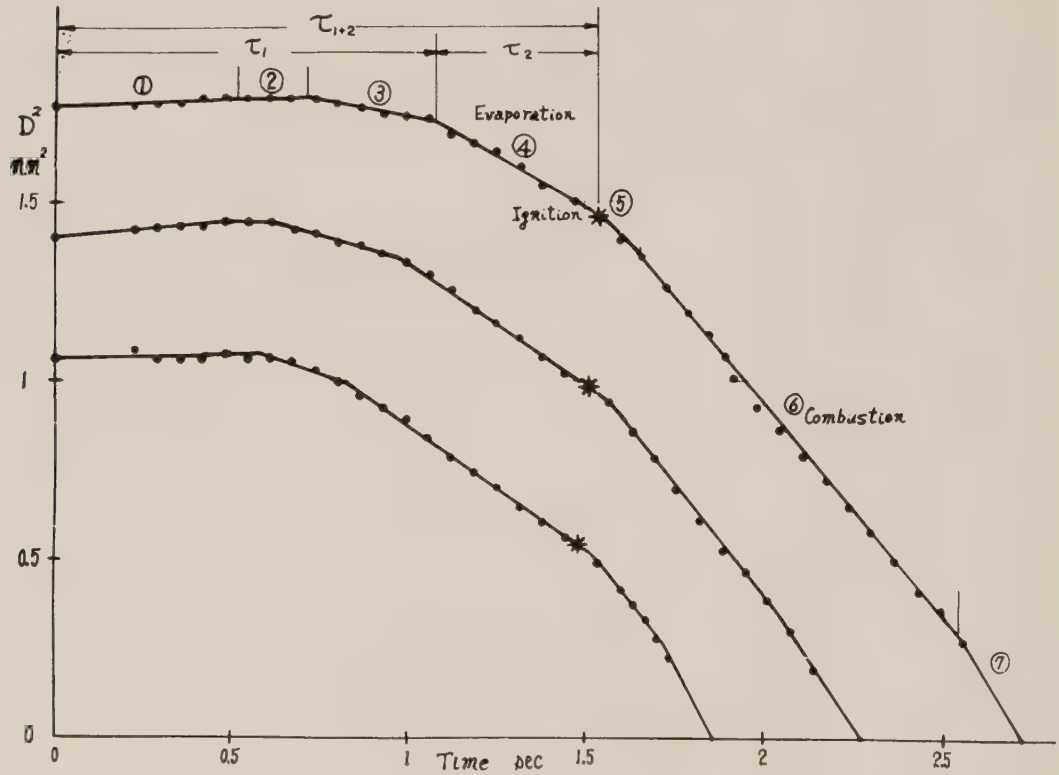

FIG. 4. Pure α-methylnaphthalene. (Furnace temperature, 713 ± 5°C)

bustion chamber which was moved around it and heated rapidly. The rates of evaporation were obtained from shadow photographs of fuel droplets taken with a motion-picture camera (Fig. 3).

shown in Figure 6. A hot-air stream flows downward around the heated droplet. Vapor from the droplet forms a boundary layer around it. After ignition, the direction of the vapor stream changes and it flows upward.

This vapor stream can be clearly observed by addition of droplets of brilliant scarlet (Fig. 7). The thickness of the vapor layer is proportional to the diameter of droplets (Fig. 8).

HEAT TRANSFER TO FUEL DROPLET

Neglecting evaporation during τ_1 and assuming uniform temperature distribution in the droplet,

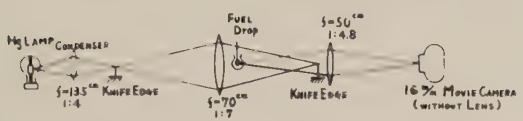

FIG. 5. Diagram of schlieren photography

the following equation can be derived:

$$4\pi r_0^2 \cdot \alpha(T_a - T_l)\, d\tau + 4\pi r_0^2 \cdot \sigma B(T_w^4 - T_l^4)\, d\tau = \tfrac{4}{3}\pi r_0^3 \rho_l c_{pl} \frac{dT_l}{d\tau}\, d\tau \quad (1)$$

where

r_0 = radius of fuel droplet
α = coefficient of heat transfer from surrounding air to droplet
T_a = temperature of surrounding air
T_l = temperature of droplet
τ = time
T_w = temperature of the wall of the combustion chamber
σ = Stefan-Boltzmann constant
B = absorption coefficient for heat radiation
ρ_l = specific weight of liquid fuel
c_{pl} = specific heat at constant pressure of liquid fuel

Integrating equation (1), we have:

$$\tau_1 = \tfrac{1}{3} r_0 \rho_l c_{pl} \int_{T_{l_0}}^{T_{l_1}} \frac{dT_l}{\alpha(T_a - T_l) + \sigma B(T_w^4 - T_l^4)} \quad (2)$$

where

T_{l_0} = initial temperature of droplet

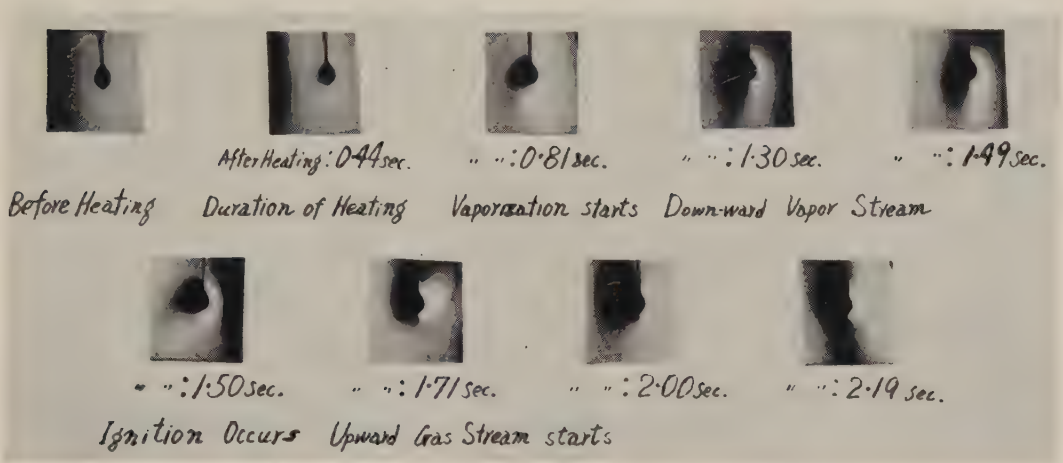

FIG. 6. Cetane: Temperature of combustion chamber 590°C.

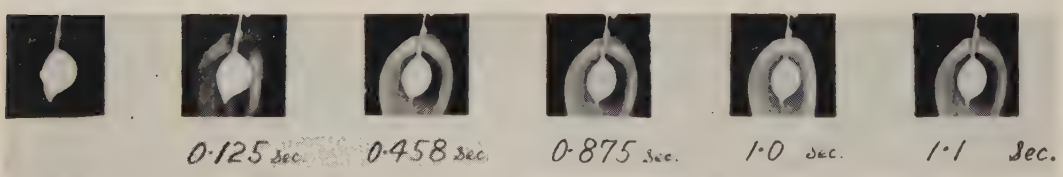

FIG. 7. Time after evaporation. Brilliant Scarlet 3R plus $Ba(NO_3)_2$. Temperature of combustion chamber 720°C.

T_{l_1} = Temperature of droplet at the start of evaporation

By approximation, equation (2) can be written:

$$\tau_1 \doteq \tfrac{1}{3} r_0 \rho_l c_{pl} \frac{1}{\alpha} \left\{ \ln \frac{\alpha(T_a - T_{l_0}) + \sigma B T_w^4}{\alpha(T_a - T_{l_1}) + \sigma B T_w^4} \right\}$$

Droplet temperatures T_{l_1} are observed by suspending the droplet at the end of a small copper-constantan thermocouple (diam., 1.6 mil). The value of T_{l_1} remains constant during the period of steady evaporation. Figure 9 shows the observed values for various air temperatures. Time

τ_1 is observed for various initial diameters D_0 of droplets and for various air temperatures (Fig. 10). Using experimental values of T_{l_1} and assuming Nu = 2.0, values of τ_1 are calculated from equation (2), as shown in Figure 10. In this calculation, the rate of heat transfer to the droplets is assumed to be equal to the rate of heat transfer in natural convection to solid spheres.

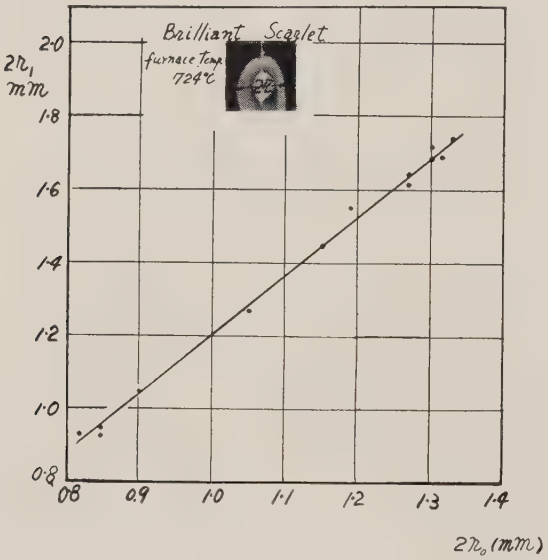

FIG. 8

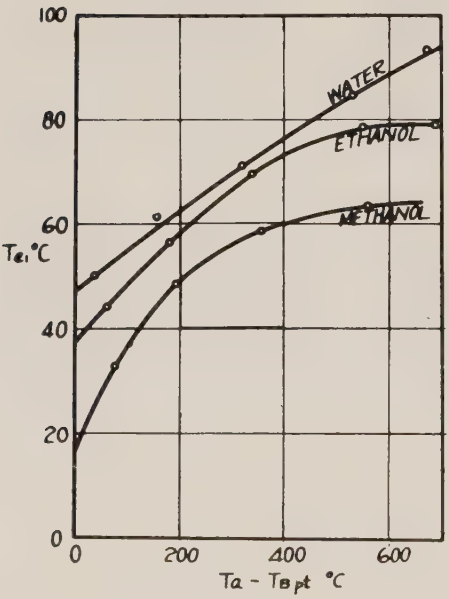

FIG. 9

CALCULATION OF EVAPORATION RATE OF FUEL DROPLETS

For simplicity, the flow model shown in Figure 11 (right) is substituted for the real vapor flow around fuel droplets (Fig. 11, left). In this treatment, it is assumed that the downward velocity

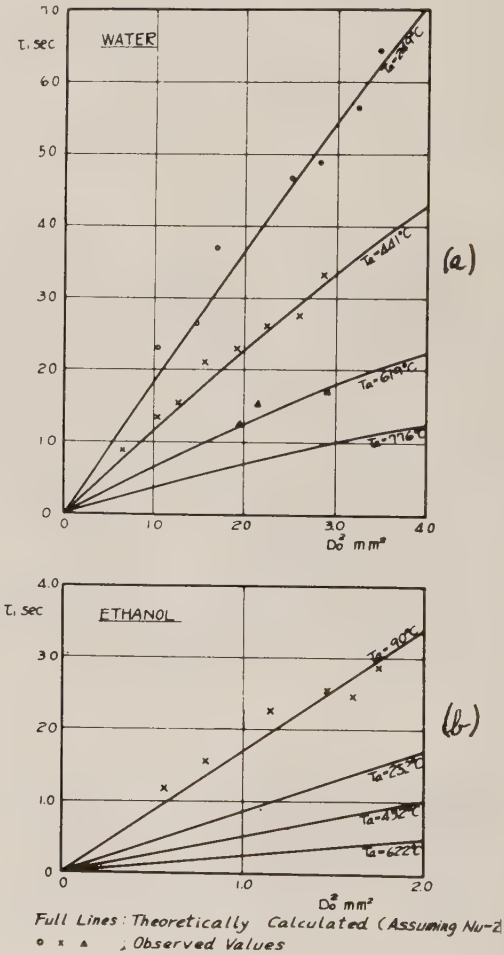

FIG. 10

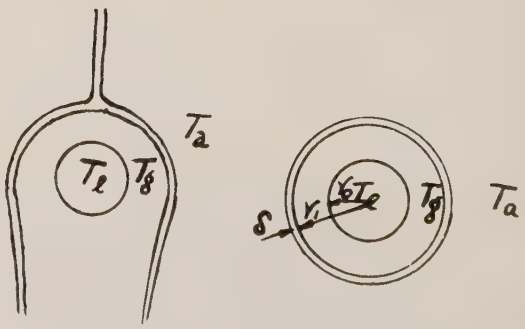

FIG. 11

of the vapor is very small compared with its radial velocity. Thus the following approximate calculations become possible for (a) the heat balance:

$$4\pi r_0^2 k_g \left(\frac{dT_g}{dr}\right)_{r=r_0} d\tau + 4\pi r_0^2 \sigma B(T_w^4 - T_l^4)\, d\tau = 4\pi r_0^2 \rho_l L \left(-\frac{dr_0}{d\tau}\right) d\tau + \tfrac{4}{3}\pi r_0^3 \rho_l c_{pl} \frac{dT_l}{d\tau}\, d\tau \tag{3}$$

where

k_g = thermal conductivity of fuel vapor
T_g = temperature of fuel vapor
L = latent heat of liquid fuel

and (b) the mass flow,

$$4\pi r^2 V_r \rho_g\, d\tau = 4\pi r_0^2 \rho_l \left(-\frac{dr_0}{d\tau}\right) d\tau \tag{4}$$

where

ρ_g = specific weight of fuel vapor
V_r = radial velocity of vapor

The equation for heat balance in the vapor layer is

$$\frac{d}{dr}\left(4\pi r^2 k_g \frac{dT_g}{dr} - 4\pi r^2 V_r \rho_g c_{pg} T_g\right) = 0 \tag{5}$$

where

c_{pg} = specific heat at constant pressure of fuel vapor.

Assuming $dT_l/d\tau = 0$ in equation (3), the following relations are derived from equations (3–5):

$$r^2 k_g \left(\frac{dT_g}{dr}\right) = \left\{r_0^2 \rho_l L\left(-\frac{dr_0}{d\tau}\right) - r_0^2 \sigma B(T_w^4 - T_l^4)\right\} + r_0^2 \rho_l \left(-\frac{dr_0}{d\tau}\right) c_{pg}(T_g - T_l) \tag{6}$$

$$\therefore \frac{1}{r_0}\left(1 - \frac{r_0}{r_1}\right) = \int_0^{T_{g1}-T_l} \frac{k_g\, d(T_g - T_l)}{\left[r_0^2 \rho_l L\left(-\frac{dr_0}{d\tau}\right) - r_0^2 \sigma B(T_w^4 - T_l^4)\right] + r_0^2 \rho_l \left(-\frac{dr_0}{d\tau}\right) c_{pg}(T_g - T_l)}$$

$$= \frac{k_g}{r_0^2 \rho_l \left(-\frac{dr_0}{d\tau}\right) c_{pg}} \left[\log\left\{1 + \frac{r_0 \rho_l \left(-\frac{dr_0}{d\tau}\right) c_{pg}(T_g - T_l)}{r_0^2 \rho_l \left(-\frac{dr_0}{d\tau}\right) - r_0^2 \sigma B(T_w^4 - T_l^4)}\right\}\right]^{T_{g1}-T_l} \tag{7}$$

$$\fallingdotseq 2 \frac{k_g}{r_0^2 \rho_l \left(-\frac{dr_0}{d\tau}\right) - r_0^2 \sigma B(T_w^4 - T_l^4)} \cdot \frac{T_{g1} - T_l}{2 + \frac{r_0 \rho_l \left(-\frac{dr_0}{d\tau}\right) c_{pg}(T_{g1} - T_l)}{r_0^2 \rho_l \left(-\frac{dr_0}{d\tau}\right) - r_0^2 \sigma B(T_w^4 - T_l^4)}}$$

where T_{g1} is the value of T_g corresponding to r_1 and T_l and c_{pg} are assumed to be constant.

Equation (7) becomes

$$-r_0 \frac{dr_0}{dt} \fallingdotseq \frac{2}{\rho l\{2L + c_{pg}(T_{g1} - T_l)\}} \left\{\frac{k_g(T_{g1} - T_l)}{(1 - r_0/r_1)} + r_0 \sigma B(T_w^4 - T_l^4)\right\} \tag{8}$$

Furthermore, if $(T_a - T_{g1})$ and r_0/r_1 are virtually independent of time, and the second term in equation (8) is small compared with the first term, $-dr_0^2/d\tau$ is approximately constant. This can be confirmed experimentally as shown in Figure 12. The observed values of $k_1 = -(d(2r_0)^2/d\tau) = -(dD^2/d\tau)$ were plotted against $(T_a - T_{\text{B.pt.}})$ for water, methanol and ethanol as shown in Figure 13, where full lines show the values calculated from equation (8). In making this calculation, values of r_1/r_1 were measured on schlieren photographs, and all found to be approximately equal to 0.3, regardless of the kind of liquid, for various temperatures and times. T_g is assumed to be equal to T_a.

EVAPORATION TIME OF A DROPLET

The time required for a droplet of a given diameter to vaporize completely were calculated from equations (2) and (8). The calculated values are compared with the experimental ones in Figure 4.

EVAPORATION OF DROPLET IN HOT-AIR STREAM

Evaporation rates of liquid droplets in hot-air streams were observed and compared with the theoretical values. For this purpose, a liquid droplet was suspended at the end of a silica filament, (diam., 0.04 mm) and placed in a hot-air stream. Shadow photographs of the droplet

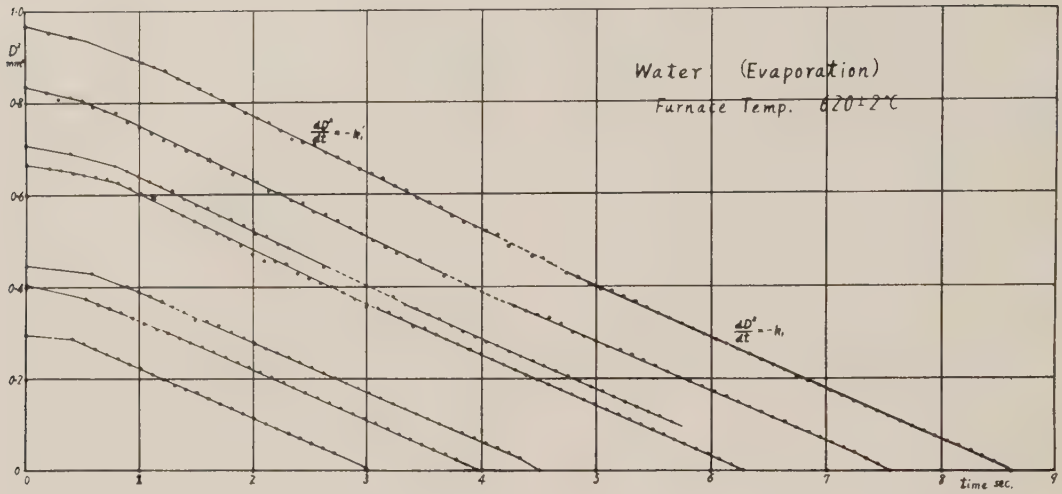

FIG. 12

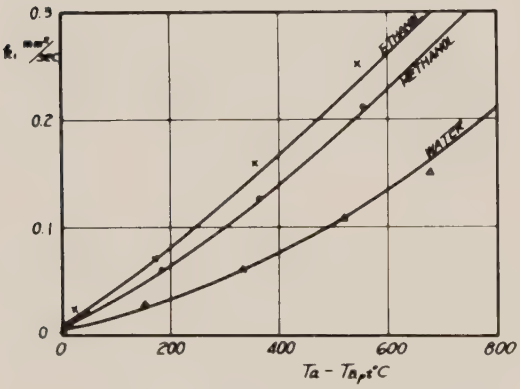

FIG. 13. Full lines: theoretically calculated $\left(\text{assuming } 1 - \frac{Y_0}{Y_1} = 0.7\right)$. x, ○, ▲: observed values.

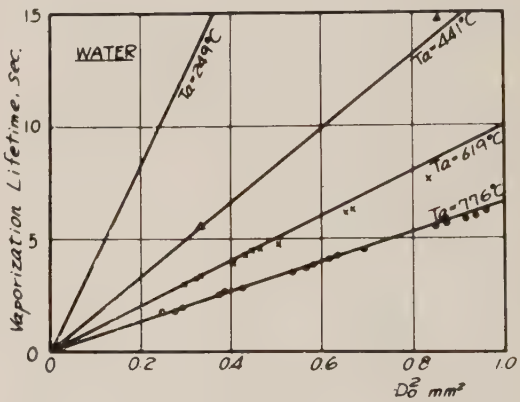

FIG. 14. Full lines, theoretically calculated. x, ○, ▲: observed values.

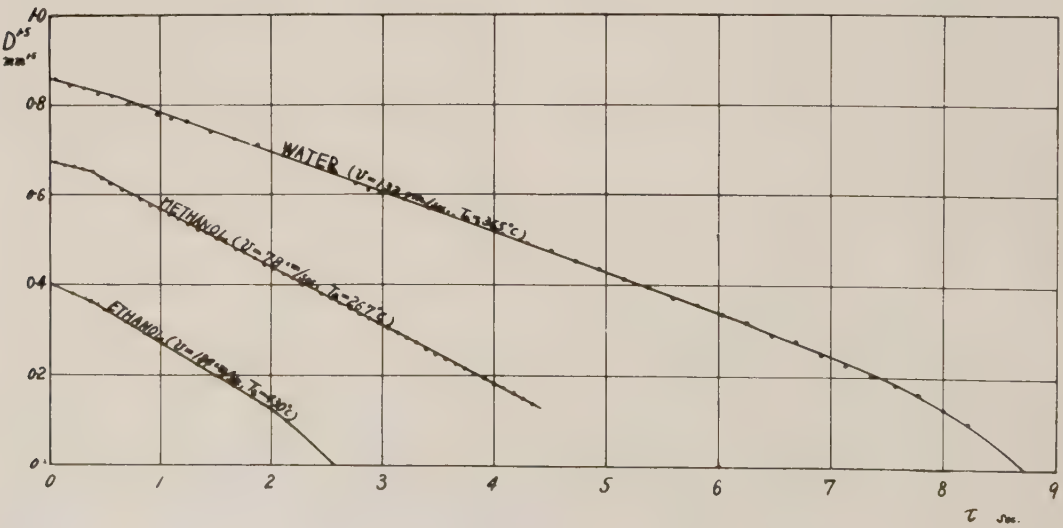

FIG. 15

were taken with a motion-picture camera and the change in the droplet diameter was observed.

To determine the droplet temperature, T_{l_1}, it is suspended at the end of a thermocouple of copper-constantan wires (diam., 0.04 mm) and the temperatures are measured by an electromagnetic oscillograph.

From Figure 15, it will be seen that $D^{1.5}$ varies linearly with time during steady evaporation. In these experiments, it is difficult to obtain accurate values of τ_{l_1} as T_{l_1} varies with Reynolds number as shown in Figure 16. The rates of heat transfer to droplets are shown in Figure 17; they are

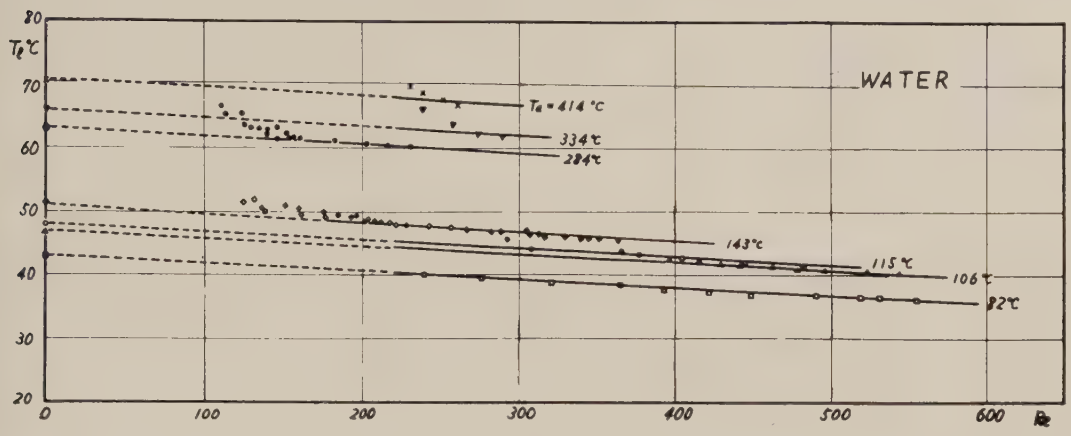

FIG. 16

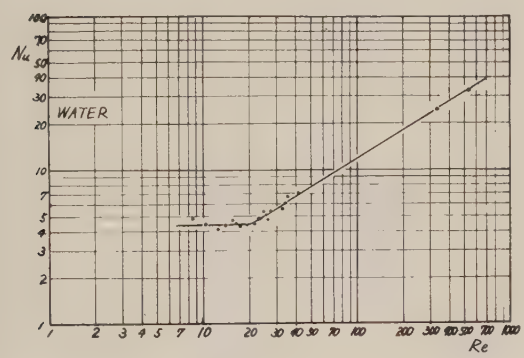

FIG. 17

higher than the corresponding values for solid spheres. Assuming $4\pi r_0^2 \sigma B(T_w^4 - T_l^4)d\tau = 0$ and $(dT_{l_1}/d\tau) \fallingdotseq 0$, the following relation is obtained from equations (3)–(5):

$$\left(1 - \frac{r_0}{r_1}\right) r_0 \frac{dr_0}{d\tau} = \frac{k_g}{\rho_l c_{pg}} \ln\left\{1 + \frac{c_{pg}}{L}(T_g - T_{l_1})\right\} \tag{9}$$

The values of $(1 - r_0/r_1)$ are measured from the schlieren photographs as shown in Figure 18 and are plotted against the Reynolds number in Figure 19.

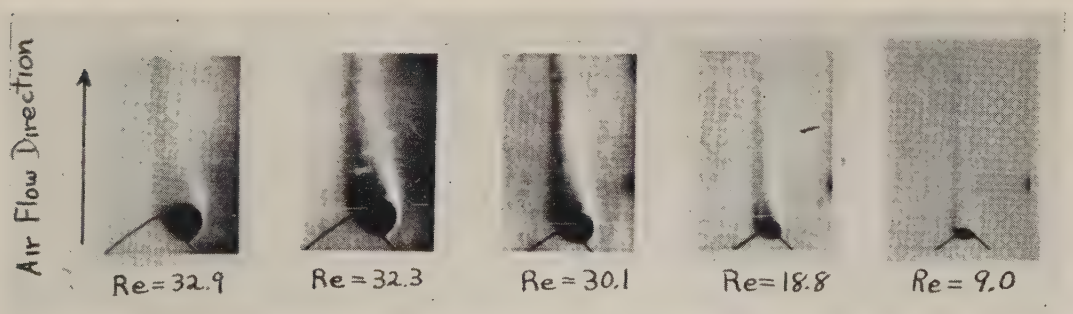

FIG. 18. Cetane: V = 130.2 cm/sec., T_a = 355°C

In Figure 20, the observed values of $(dD^{1.5}/d\tau)$ are compared with the values calculated from equation (9), using observed values of $\left(1 - \frac{r_0}{r_1}\right)$.

Ignition Lags

Figure 21 shows the relation between the time lag and initial diameter D_0 for alpha-methyl-naphthalene. From these curves it is found that τ_1 is proportional to D_0, τ_2 decreases and τ_{1+2} $(= \tau_1 + \tau_2)$ increases with increasing D_0.

The ignition lags of alpha-methyl-naphthalene and cetane droplets were observed for various oxygen contents (Fig. 22). The oxygen content

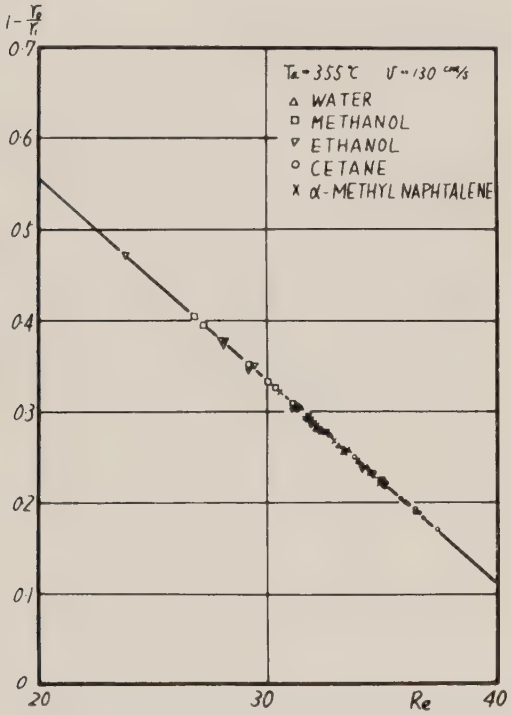

FIG. 19

has no effect on τ_1, but it has considerable effect on τ_2.

Ignition lags were observed for two fuel droplets of about 1 mm diameter placed side by side at various distances. Figure 23 gives the mean values of ignition lags from 40–50 trials, plotted against the distances between two cetane droplets. It will be seen that the ignition lags are shortest for the case of 4–5 mm distance, i.e., where the vapor layers of the two droplets are close together. As the temperature of the surrounding air increases, the distance corresponding to the minimum ignition lags increases. This is probably due to the greater thickness of the vapor layers at higher air temperatures.

Acknowledgments

The author wishes to acknowledge the kind comments and suggestions of Professor Seiichiro Kumagai of University of Tokyo. He is indebted to Messrs. Sanni Hagi, Tsutomu Kanai, Tsuneo Matsuzaki, Masaru Hirata and many co-workers for their help in this investigation.

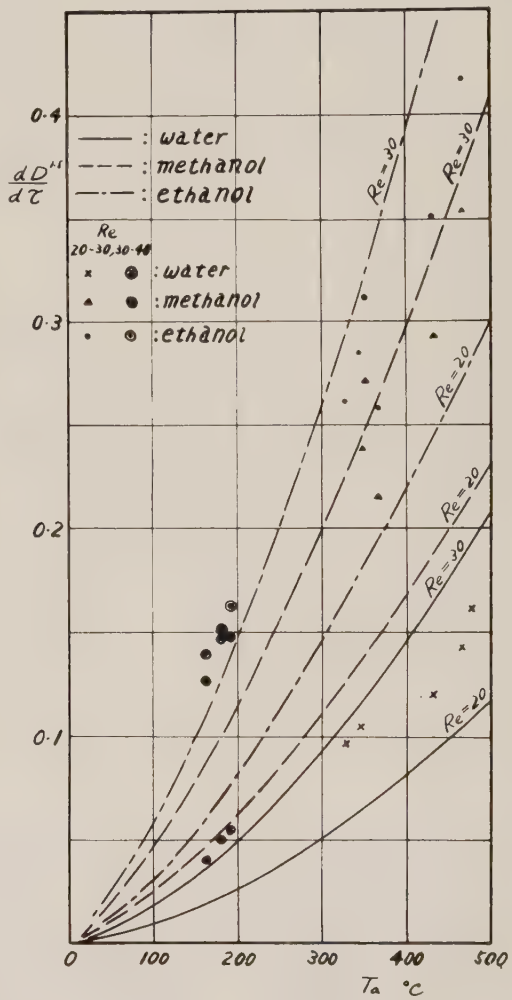

FIG. 20

Nomenclature

D = diameter of liquid droplet, mm
r_0 = radius of liquid droplet, mm
r_1 = radius of vapor layer, mm
r = radius at center of liquid droplet, mm
k_1 = evaporation rate of liquid droplet, $-dD^2/d\tau$ mm²/sec

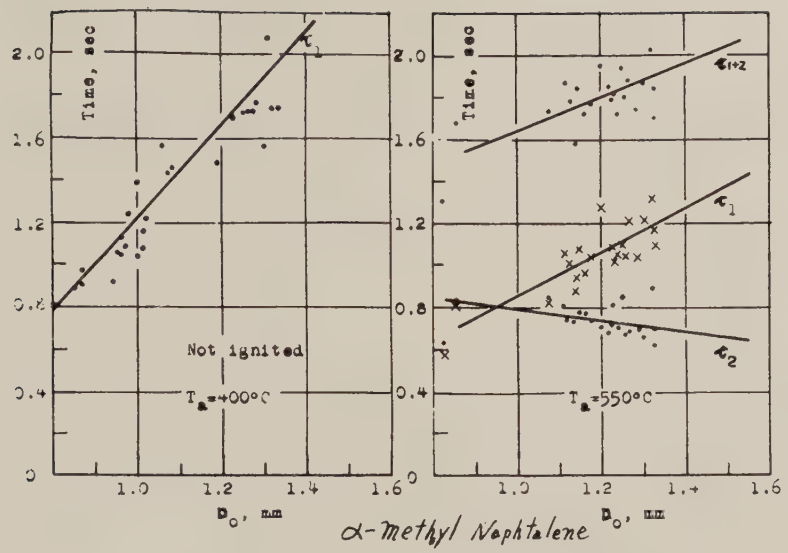
Time, sec
Not ignited
T_a=400°C
T_a=550°C
D_0, mm
α-Methyl Naphtalene

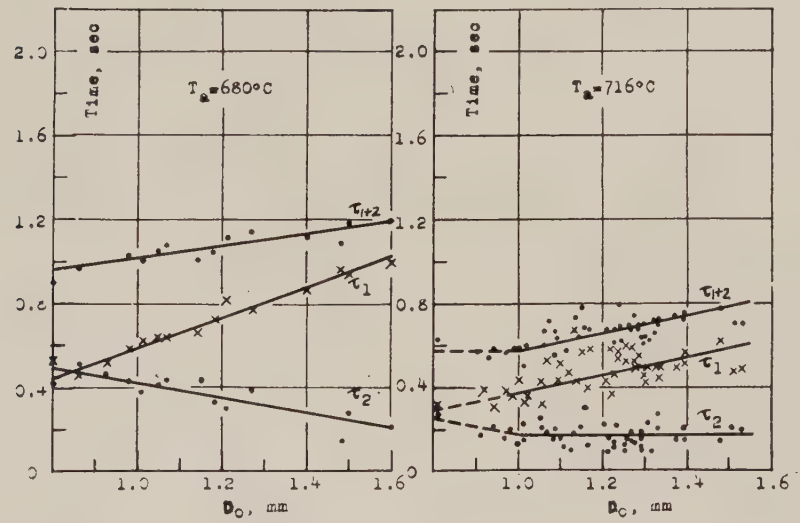
Time, sec
T_a=680°C
T_a=716°C
D_0, mm

FIG. 21

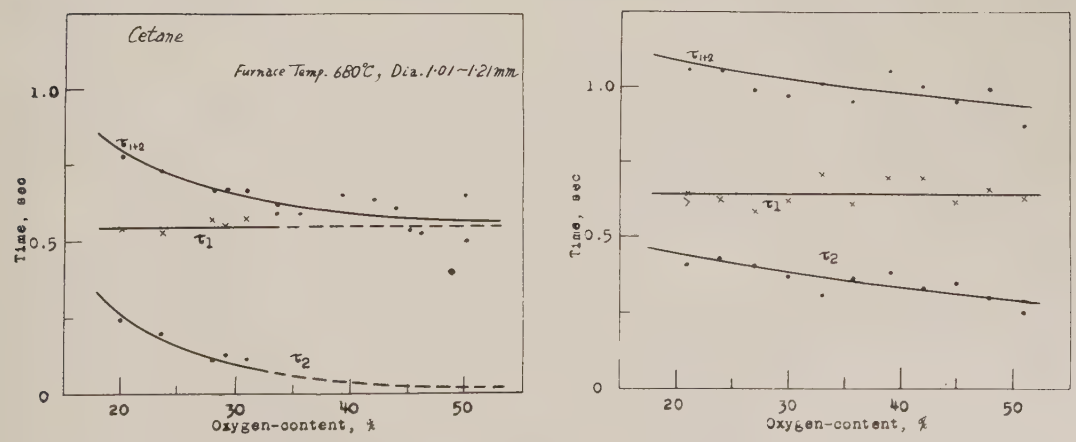
Cetane
Furnace Temp. 680°C, Dia. 1·01~1·21mm
Time, sec
Oxygen-content, %
α-Methylnaphthalene

FIG. 22

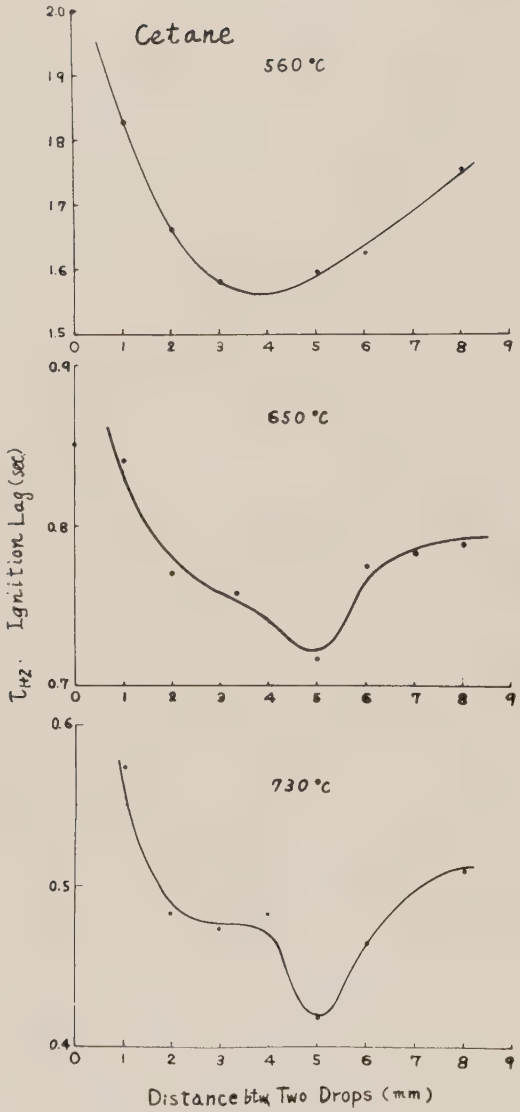

FIG. 23

k_2 = combustion rate of liquid droplet, $-dD^2/d\tau mm^2/sec$

α = coefficient of heat transfer from surrounding air to droplet, kcal/h/m²/deg

T_l = temperature of droplet, °C

T_{l_0} = initial temperature of droplet, °C

T_{l_1} = temperature of droplet during steady evaporation, °C

T_g = temperature of vapor, °C

T_{g_1} = values of T_g corresponding to r_1, °C

T_a = temperature of surrouding air, °C

T_w = temperature of the wall of the combustion chamber, °C

τ = time, sec

τ_1 = time required for heating a droplet, sec

τ_2 = time from start of steady evaporation to time of ignition, sec

$\tau_{1+2} = \tau_1 + \tau_2$

ρ_l = specific weight of liquid, kg/m³

ρ_g = specific weight of vapor, kg/m³

c_{pl} = specific heat at constant pressure of liquid, kcal/kg/deg

c_{pg} = specific heat at constant pressure of vapor, kcal/kg/deg

V_r = radial velocity of vapor, m/sec

V = velocity of air stream, cm/sec

k_g = thermal conductivity of vapor, kcal/h/m/deg

L = latent heat of liquid, kcal/kg

σ = Stefan-Boltzmann constant, 4.96×10^{-8} kcal/h/m/deg

B = absorption coefficient for heat radiation.

REFERENCES

1. RANZ, W. E., AND MARSHALL, W. R.: J. Chem. Eng. Progress, *3*, 48 (1952).
2. INGEBO, R. D.: J. Chem. Eng. Progress, *8*, 48 (1952).
3. GODSAVE, G. A. E.: *Fourth Symposium (International) on Combustion*, p. 818. Baltimore, The Williams & Wilkins Co., 1952.
4. NISHIWAKI, N., AND HAGI, S.: Proc. 1st Japan National Congress for Appl. Mech., 1951.
5. OKAZAKI, T., AND GOMI, M.: Trans. J. S. M. E., *88*, 19 (1953).
6. KUMAGAI, S., AND ISODA, H.: Nature, *166*, 1111 (1950); Science of Machine, *6*, 4 (1952).
   KUMAGAI, S.: AND KIMURA, I.: Science of Machine, *8*, 3 (1951); Trans. J. S. M. E., *67*, 18 (1952).

6

EFFECT OF FUEL DROPLETS ON FLAME STABILITY, FLAME VELOCITY, AND INFLAMMABILITY LIMITS[a]

By J. A. BROWNING AND W. G. KRALL

Introduction

The combustion characteristics of fuel droplets are largely determined by the size of the particles being burned. Figure 1 shows a portion of a laminar Bunsen flame which has been originally established by the combustion of a mixture of gaseous fuel and air. Imagine that an instantaneous interchange of fuels may be effected, and the liquid droplets of a known uniform size be substituted for the gaseous fuel. If these droplets are sufficiently small they will be vaporized completely prior to the zone of visible combustion and the laminar flame front will continue to exist. Conversely, the substitution of large droplets in place of the gaseous fuel will result in the collapse of the laminar flame front and the establishment of a combustion system wherein each droplet is surrounded by its own diffusion flame. An intermediate range of droplet sizes may produce both types of combustion, provided that a sufficiently rich mixture is used. Burgoyne[1] and Cohen have stabilized inverted flames of monodisperse tetralin aerosols on a port. For droplets less than 10 μ in diameter the flame front is similar to that for a gaseous mixture. Larger droplets lead to a "brush" type of flame in which the droplets burn separately.

In order to evaluate and compare the combustion characteristics of mixtures composed of gaseous fuels on the one hand and liquid fuel droplets on the other, it is necessary to obtain basic data such as flame velocity and stability and inflammability limits. In the measurement of each of these quantities it is important that the reactants be uniform in distribution. Also, the fuel droplets in the mixture being tested must all be of about the same size. These requirements may be met by the use of a mist of sub-micron diameter droplets formed by the rapid condensation of fuel vapor in cool air.

[a] This research was conducted under the auspices of Project SQUID, jointly sponsored by the Office of Naval Research, Department of the Navy, Office of Scientific Research, Department of the Air Force, and Office of Ordnance Research, Department of the Army.

Experimental

Standard experimental techniques were employed to obtain controlled mixtures of fuel and air for both the Bunsen tube and ignition "bomb". Mist was produced by introducing the superheated vapor of a high boiling point liquid fuel from a boiler into the cool primary stream of air. The flame stability tests were conducted both in the open atmosphere and in a Smithells separator (a glass tube fitted over the top of a Bunsen tube in such a manner that the primary and secondary flame cones are separated).

A $\frac{5}{8}$-in diameter nozzle was used for the determination of average flame velocities (v_f). The schlieren image of a flame produced above

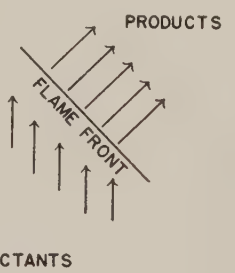

FIG. 1. Schematic sketch of a portion of a Bunsen flame front.

this nozzle had straight sides which indicated a relatively flat velocity profile of the mixture stream. The average stream velocity (v_s) was calculated by use of the perfect gas laws, the continuity equation, and an area correction factor of 0.935 determined from boundary layer measurements. The relationship $v_f = v_s \sin \alpha$ is applicable in this case where 2α is the angle between the two straight sides of the flame cone. Measurements of this angle were made by both shadow and schlieren photography. The two methods gave nearly identical flame velocities provided the outer edge of the shadow was used. Flame velocities calculated using the value of α for the inner edge of the shadow were about 10 per cent too low. (Linnett and Hoare[2] give a detailed discussion of the use of shadowgraphs for this application.)

Optical scattering techniques were used in the determination of droplet size. Preliminary use of this equipment in the study of kerosine mist showed that the average diameter of the droplets was between 0.5 and 1.0 μ. The use of kerosine, a mixture of compounds, precludes the attainment of more accurate measurements. Pure compounds are presently being tested.

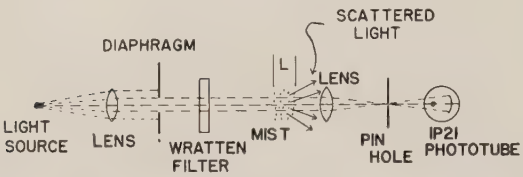

FIG. 2. Optical system used for determination of droplet size.

FIG. 3. Typical shadow picture of laminar propane-air flame.

Figure 2 is a sketch of the arrangement of the optical diffraction apparatus used. The light scattering properties of a mist depend on the uniformity of droplet size, the individual droplet size, the index of refraction of the liquid forming the mist, the concentration (n) of the droplets per unit volume of mixture, the path length (l) through which the light must pass, and the wavelength (λ) of the light beam. A relationship between the incident light and transmitted light is given by the Lambert-Beer equation: $I = I_0 e^{-KAnl}$ where I = intensity of transmitted light; I_0 = intensity of incident light; K = scattering coefficient; A = geometric cross-sectional area of an individual particle. The scattering coefficient is a function of the mean particle size, the index of refraction of the liquid, and the wavelength of the light beam. Two independent quantities, A and n, are unknown. The use of different wavelengths of the incident light give simultaneous equations which may be solved. (References 3 through 8 give a thorough treatment of the diffraction theory and its application.)

Results and Discussion

Flame velocity measurements were made for both propane vapor and kerosine mist in air. The value of the flame velocity for the propane mixture was found to be 44 $\pm$ 1 cm/sec at a stream temperature of 73°F, while that for the mist was 47 $\pm$ 2 cm/sec at 93°F. At a stream temperature of 285°F the flame velocity for the propane mixture was 75 $\pm$ 3 cm/sec, while that for the kerosene vapor was 79 $\pm$ 3 cm/sec. The propane-air flame velocities obtained for both stream temperatures are in good agreement with those reported by Dugger.[9] Similar values for the mist suggest that any quenching action due to heat supplied from the reaction zone for fuel vaporization is negligible. (Shadow photographs of the type used for these velocity determinations are shown in Figures 3 and 4.)

The blow-off curves for mixtures of both propane vapor and kerosine mist burning above a Bunsen tube are shown in Figure 5. The difference between these curves is due to the period of time required for vaporization of the mist. A Bunsen flame is initially stabilized at its base; thus, a combustible mixture must be available above the rim of the Bunsen tube. The propane can more readily supply the necessary amount of fuel vapor in this zone. The mist which issues from the tube is nearly free of vapor, as evident from the fact that there is no wetting of kerosene on a cold piece of metal held in the stream.

Blow-off data for a Smithells separator are shown in Figure 6. Results similar to those for blow-off in free air are obtained for lean mixtures. Beyond a fuel content slightly richer than stoichiometric the blow-off curve for propane reaches

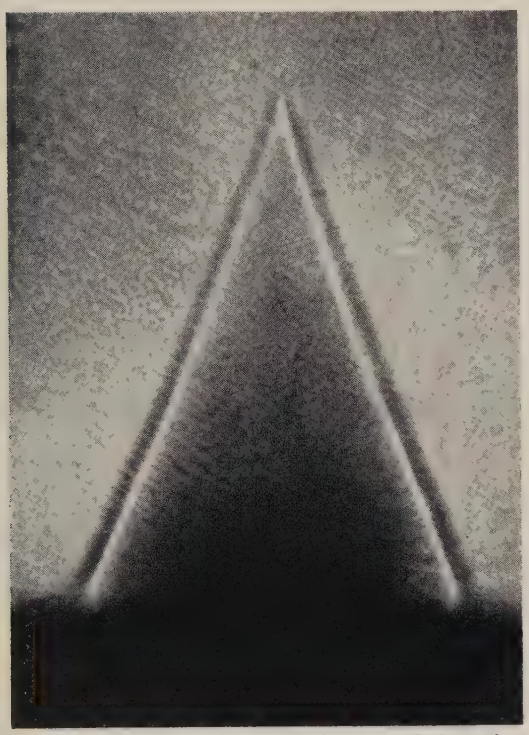

FIG. 4. Typical shadow picture of kerosine mist-air flame.

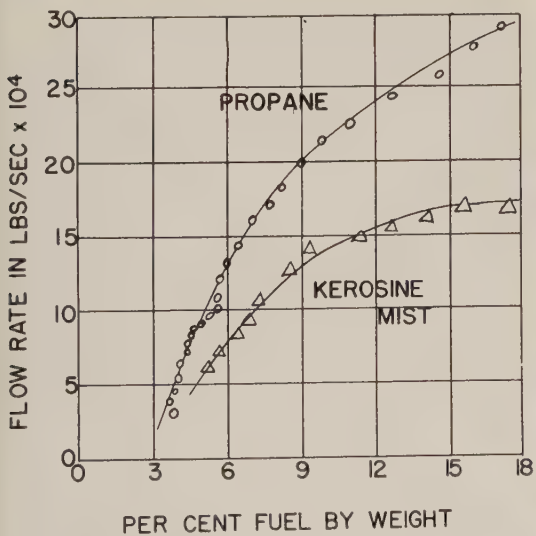

FIG. 5. Blow-off curves for propane-air and kerosine mist-air mixtures in the free atmosphere. Tube diameter: ½ inch.

a peak, after which it falls. This peak corresponds to that mixture which gives maximum flame velocity. At richer mixtures the flame velocity becomes lower, and since there is no diffusion of secondary air into the stabilizing zone at the

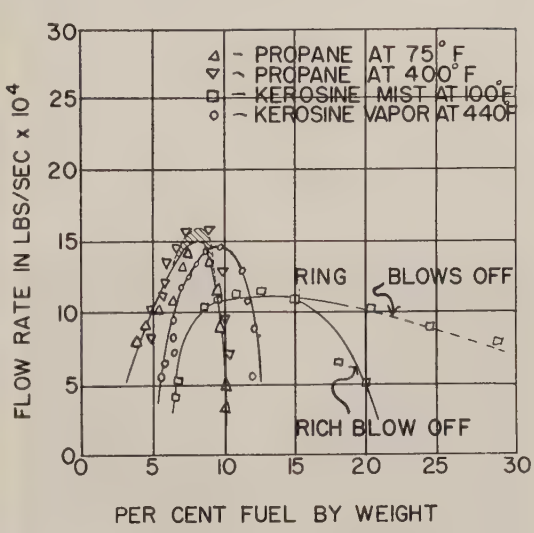

FIG. 6. Blow-off curves for propane-air and kerosine mist-air and kerosine-vapor-air mixtures in Smithells separator. Bunsen tube diameter: ½ inch; outer tube diameter: 1 inch; rim of outer tube 5 inches above rim of Bunsen tube.

FIG. 7. Direct photograph of rich kerosine mist-air flame.

base of the flame, the blow-off curve must drop. Blow-off data for propane mixtures at both 75°F and 400°F are shown. The shaded portion between the two curves may be accounted for by a slightly greater than linear increase of flame velocity with temperature.[9]

The difference between the propane vapor

and kerosine mist blow-off curves is more evident in the Smithells separator than when the flames are burned in the open atmosphere. The percentage fuel range over which the flame burns stably is much higher in the case of the mist. A comparison between kerosine mist at 100°F and kerosine vapor at 440°F shows that

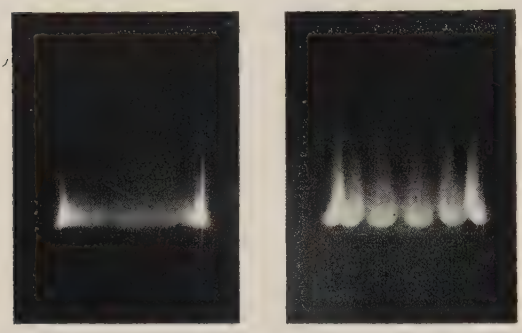

(a) (b)

FIG. 8. Flame ring (a) and flame filaments (b) for rich kerosine mist-air mixture burning in a Smithells separator.

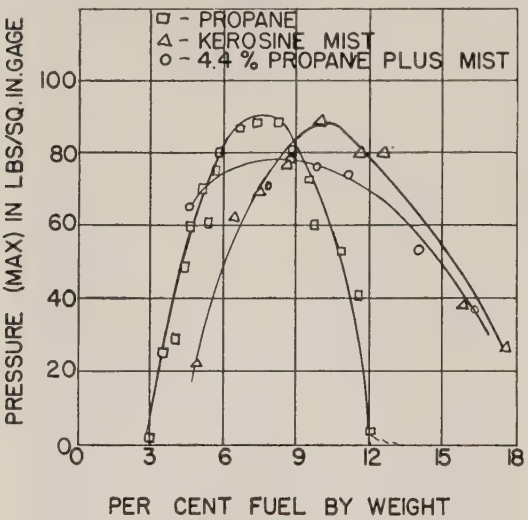

FIG. 9. Maximum pressure curves for propane-air and kerosine mist-air mixtures in constant volume combustion "bomb."

the blow-off curve for the vapor is quite similar to that for propane; thus, the wide stability range for the mist is due to physical characteristics.

Laminar flames of mists which are relatively lean appear quite similar to those for propane. At richer mixtures a distinct difference may be noted. The first appearance of a yellow diffusion flame in the propane-air mixture occurs at the peak of the secondary cone at a fuel content of 10 per cent. The mist produces a yellow fringe of flame just above the primary cone at a fuel content of only 8 per cent. It appears that the flame establishes itself within that region of the vaporizing mist which produces the optimum air-fuel vapor ratio for rapid combustion. The remaining droplets vaporize beyond this region (perhaps within the visible cone itself), and this vapor in turn burns as a diffusion flame above the primary cone and within the normal secondary envelope.

Figure 7 is a direct photograph of a mist flame burning in the open atmosphere. The flow velocity in this case is much greater than that used for flame velocity measurements. The low flame velocities near the base of the flame are indicated by the steep slope of the flame cone in this region. At a point well above the burner rim the mixture burns at its maximum rate.

The low flame velocity above the burner rim is due to the lean vapor mixture present. The distance above the rim at which a combustible mixture is formed is not only dependent on the time required for vaporization of the mist, but on the mixture velocity out of the tube. If this distance is too great, the stabilizing effect of the rim is lost and the flame blows-off.

At a fuel content of approximately 15 per cent the Smithells tube blow-off data split into two separate curves. At this point the large rich flame within the Smithells tube lifts to a new position above the rim of the outer tube leaving a pale blue ring of flame attached to the inner rim. This ring (Fig. 8a) experiences rich blow-off as shown by the solid curve in Figure 4. A higher blow-off range results from an increase in the flow velocity. The ring for any one fuel percentage is stable only between certain flow velocity limits. There appears to be a balance between the supply of vaporized fuel at the burner rim and an allowable wall velocity gradient for stable combustion. A decrease in the flow velocity allows more time for droplet vaporization, and the vapor-air mixture becomes too rich to support combustion. An increase in the stream velocity not only allows less time for vaporization, but increases the velocity gradient to a point where the flame can no longer exist.

The kerosine mist-air flame ring breaks into individual flame filaments at the richest mixtures tested (Fig. 8b). This type of polyhedral flame which is open at the cone tip has been obtained by Behrens[10] and Garside[11] for lean mixtures of hydrogen and air. Such a ring could not be pro-

duced by the combustion of kerosine vapor and air. The difference between the diffusivity of the vapor and mist in relation to that of the combustion air is probably the principal reason for the appearance of this type of flame only in the mist system. (See Markstein[12] for a more thorough description of polyhedral flames.)

The maximum pressure obtained during combustion in the closed ignition "bomb" is plotted as a function of fuel content in Figure 9. The propane limits of ignition are again much narrower than those obtained for the mist. The peak pressures are the same for both systems. Addition of kerosine mist to a lean mixture of propane results in a much wider range of ignition limits; however, the peak pressure is reduced. The lean limit of combustion for both propane vapor and kerosine mist was found to be approximately 3 per cent by weight of the total mixture.

REFERENCES

1. Burgoyne, J. H.: Discussion at end of section on Solid and Liquid Propellants, *Selected Combustion Problems*, Combustion Colloquium, pp. 392–394. Cambridge University, 1954.
2. Linnett, J. W., and Hoare, M. F.: *Third Symposium on Combustion and Flame and Explosion Phenomena;* discussion by Kurt Wohl, pp. 203–204. Baltimore, The Williams & Wilkins Co., 1949.
3. Durbin, E. J.: NACA TN 2441, August (1951).
4. Gumprecht, R. O., and Sliepcevich, C. M.: J. Phys. Chem., *57*, 95 (1953).
5. Gumprecht, R. O., Sung, N., Chin, J. H., and Sliepcevich, C. M.: J. Optical Soc. Am., *42*, 226–231, April (1952).
6. Gumprecht, R. O., and Sliepcevich, C. M.: J. Phy. Chem., *57*, 90 (1953).
7. *Tables of Scattering Function for Spherical Particles*. Department of Commerce, National Bureau of Standards, Applied Mathematics Series 4.
8. Sinclair, D.: J. Optical Soc. Am., *37*, 475, June (1947).
9. Dugger, G. L.: NACA TN 2374, May (1951).
10. Behrens, H.: *Fourth Symposium (International) on Combustion*, p. 538. Baltimore, The Williams & Wilkins Co., 1953.
11. Garside, J. E., and Jackson, B.: *Fourth Symposium (International) on Combustion*, p. 545. Baltimore, The Williams & Wilkins Co., 1953.
12. Markstein, G. H.: *Fourth Symposium (International) on Combustion*, p. 44. Baltimore, The Williams & Wilkins Co., 1953.

Propellant Burning

7

PRELIMINARY MEASUREMENTS OF THE COMBUSTION TIME LAG IN A MONOPROPELLANT ROCKET MOTOR[a]

By LUIGI CROCCO, JERRY GREY, AND GEORGE B. MATTHEWS

Introduction

The problem of combustion instability in liquid propellant rocket motors has long been recognized as one of the major difficulties in their development. In particular, the effect of extreme rates of heat transfer which have been shown to result from the high-frequency oscillations commonly called screaming will become even more significant as the industry progresses to the use of higher thrust, higher performance rocket engines.

In view of the present lack of correlation among so many of the recorded instances of instability, a program directed by the senior author was instituted at Princeton under the sponsorship of the Bureau of Aeronautics to examine the fundamental nature of this phenomenon from both theoretical and experimental viewpoints. One of the primary objects of this research is to obtain information about the combustion process under stable operating conditions. It is believed that such information can be of help in the explanation of unstable phenomena.

This paper presents the first step in the experimental program, describing the techniques which have been developed to conduct the investigation and some of the results of preliminary tests performed on a monopropellant rocket motor.

Conceptual Background

The concept of time lag, which has had so many useful applications, can be rationalized in the particular case of a rocket motor in such a way that it represents not a mere schematic assumption without a close connection to the real events, but a well-defined mathematical quantity which allows a close description of the actual behavior of the combustion process to be made[1]. The transformation of a given element of propellant (or two elements of two propellants destined to react together) from the instant of injection to final appearance as hot gases is a gradual process. In most cases, however, the largest energy release and volume change for a given element are likely to take place in a relatively short interval of time toward the end of the transformation. No great error can therefore derive in the overall picture if we replace the gradual transformation with a discontinuous one, where no volume or energy change takes place before a certain instant at which the whole increase of volume and energy occurs discontinuously; after this instant the propellant may be considered to be completely transformed into the final burned gases. The interval from injection to burned-gas generation is the time lag of the element considered. Now, every propellant element has a different value of time lag, so that in physical terms one cannot speak of a single time lag for the whole system. It has been shown, however[1, 2, 3], that if one introduces a small sinusoidal modulation into the flow rate of the propellants, the resulting chamber pressure will also undergo a small sinusoidal oscillation; and that in the first approximation, this oscillation will be the same as if all the propellant elements had the same value of the time lag. In other words, if one replaces the nonuniform distribution of time lags among the various elements with a single average value, the resulting chamber pressure oscillation will still

[a] Work performed under sponsorship of the Bureau of Aeronautics, USN. (*Note*: Some of the material contained herein was presented at the Second Symposium on Rocket Combustion Instability, Brooklyn, New York, October 28 and 29, 1953 (*Confidential*).

be the same provided the time lag spread around the average value is not appreciable. If this condition is satisfied, it has also been shown that the stability behavior of the actual system can be well approximated by that of a system in which the time lag is uniform and equal to the aforementioned average value. This result is particularly important in that all the theoretical work based on the assumption of a uniform time lag[4, 5, 6, 7, 8] can be applied to the practical cases in which the time lag is certainly not uniform. It also implies that the value of this average time lag upon which the instability behavior depends can be found experimentally by means of the previously mentioned technique of modulating the injection flow. This technique appears to be superior to a method, used by several experimenters, which involves the introduction of a single sharp pulse in the flow rate through one of the propellant feed lines. The single pulse technique is an excellent one for comparison between several different propellant combinations, for example; however, it is not suitable for accurate time lag measurements because of the uncertainty of relationship between corresponding points on the propellant feed line and chamber pressure pulses.

In the case of modulated injection, let us suppose that the injection rate $\dot{m}_i$ to a rocket chamber undergoes a sinusoidal oscillation of angular frequency ω around its mean value $\overline{\dot{m}}$. This can be written as

$$\frac{\dot{m}_i - \overline{\dot{m}}}{\overline{\dot{m}}} = \mu_i = \tilde{\mu} e^{i\omega t} \tag{1}$$

where μ_i represents the fractional oscillation, and $\tilde{\mu}$ the scalar amplitude, assumed to be small compared to unity. Here we have used the complex representation of oscillating quantities; in other words the oscillating quantity is considered to be a rotating vector in the complex plane, with only the real component having a physical meaning.

As a result the chamber pressure p will also oscillate around its mean value $\overline{p}$, and its fractional oscillation can be expressed as

$$\varphi = \frac{p - \bar{p}}{\bar{p}} = \tilde{\varphi} e^{i(\omega t - \beta)} \tag{2}$$

where $\tilde{\varphi}$ is the corresponding amplitude (small with respect to unity), and a phase lag β has been explicitly introduced.

Other important quantities will also oscillate. For instance both the burning rate $\dot{m}_b$ and the exhaust rate $\dot{m}_e$ will oscillate around their mean value $\overline{\dot{m}}$ (the same as for the injection rate) and their fractional oscillations

$$\mu_b = \frac{\dot{m}_b - \overline{\dot{m}}}{\overline{\dot{m}}}; \qquad \mu_e = \frac{\dot{m}_e - \overline{\dot{m}}}{\overline{\dot{m}}} \tag{3}$$

will be small sinusoidal quantities. Also, the amount of gas contained in the chamber, $M_g = \rho V$, will oscillate around its mean value $\overline{M}_g = \overline{\rho} V$ (where V is the chamber volume) and its fractional oscillation is the same as the fractional oscillation of density:

$$\frac{M_g - \overline{M}_g}{\overline{M}_g} = \frac{\rho - \bar{\rho}}{\bar{\rho}} = \frac{\varphi}{\gamma}, \tag{4}$$

the last relation being obtained within the assumption of isentropic oscillations.

A mass balance tells us that the rate of gas accumulation must be equal at each instant to the difference between the burning rate and the exhaust rate:

$$\frac{dM_g}{dt} = \dot{m}_b - \dot{m}_e$$

Introducing equations (3) and (4), we obtain

$$\frac{\overline{M}_g}{\gamma \overline{\dot{m}}} \frac{d\varphi}{dt} = \mu_b - \mu_e \tag{5}$$

The problem now is to relate μ_b and μ_e to φ and μ_i. Obviously, if A is the cross-sectional area at the entrance of the nozzle and u is the corresponding gas velocity, we can write

$$\dot{m}_e = A \rho u$$

from which, within the assumption of small variations, we find

$$\mu_e = \frac{\rho - \bar{\rho}}{\bar{\rho}} + \frac{u - \bar{u}}{\bar{u}} = \frac{\varphi}{\gamma} + \nu \tag{6}$$

Here, $(\rho - \bar{\rho})/\bar{\rho}$ has been replaced by φ/γ (equation 4). The fractional variation ν of velocity around the mean value $\bar{u}$ is related to φ by the behavior of the exhaust nozzle, a problem which has been solved by Crocco and Cheng[1], Tsien[9], and Crocco[10]. For frequencies well below the range of screaming, this relation can be written

$$\frac{\gamma \nu}{\varphi} = \frac{\gamma - 1}{2} + i\omega a \tag{7}$$

where the quantity a is a known function of the nozzle shape[10]. At zero frequency the second member of equation (7) becomes $(\gamma - 1)/2$ and

represents the corresponding quantity in a steady state nozzle when the conditions are changed isentropically. It is easily shown that in this case it coincides with the condition that the Mach number at the entrance of the nozzle does not vary, because it is determined by the contraction ratio of the nozzle only. Thus, equation (6) can be written

$$\mu_e = \varphi\left(\frac{\gamma+1}{2\gamma} + i\,\frac{\omega a}{\gamma}\right) \tag{8}$$

For the burning rate, observe that if the time lag $\bar{\tau}_T$ were perfectly constant, the burning rate at each instant t would be exactly equal to the injection rate at the instant $(t - \bar{\tau}_T)$. If, on the contrary, the combustion process is affected by the oscillating condition, there will be a variation from this equality. This can be written as

$$\mu_b(t) = \mu_i(t - \bar{\tau}_T) + \Delta\mu \tag{9}$$

It is not necessary to make any explicit assumptions about the quantity $\Delta\mu$ other than that it is likely to be of the same order as φ and should increase proportionally with it. This means that if we write

$$\Delta\mu = B\varphi, \tag{10}$$

the modulus of B (in general a complex quantity) will be of order unity. This quantity can be called the interaction function. In the present assumption of sinusoidal oscillations, we can also write

$$\begin{aligned} \mu_i(t - \bar{\tau}_T) &= \mu_i(t)e^{-i\omega\bar{\tau}_T} \\ \frac{d\varphi}{dt} &= i\omega\varphi \end{aligned} \tag{11}$$

Finally, substituting equations (8, 9, 10, 11) into equation (5) and solving for μ_i/φ we obtain

$$\frac{\mu_i}{\varphi} = \frac{\tilde{\mu}}{\tilde{\varphi}}\,e^{i\beta} = \left(i\omega\theta_g + \frac{\gamma+1}{2\gamma} - B\right)e^{i\omega\bar{\tau}_T} \tag{12}$$

where

$$\theta_g = \frac{1}{\gamma}\left(\frac{\bar{M}_g}{\bar{\dot{m}}} + a\right)$$

is a characteristic time of the system which is of the same order as the mean gas residence time in the chamber. For a given system, θ_g and $\bar{\tau}_T$ have well-defined values. If one had the necessary information to evaluate the interaction function B in the relation (10), then equation (12) would give the value of the ratio of the amplitudes of fractional oscillation of pressure and injection rate and the relative phase difference as a function of ω. However, our information about B and $\bar{\tau}_T$ is practically zero, and even the theoretical value of θ_g is subject to caution. In this case it is better to use equation (12) for the inverse operation. Experimentally one can determine, for the given system, $\tilde{\mu}/\tilde{\varphi}$ and β as functions of ω; then equation (12) provides the evaluation of θ_g and $\bar{\tau}_T$ and the determination of the interaction function $B(\omega)$, from which, in principle, valuable information on the mechanism of combustion can be obtained.

Observe that if $\omega\theta_g \gg 1$, the second and third terms on the right side of equation (12), being of the order of unity, can be neglected. In this case the solution of equation (12) gives

$$\left.\begin{aligned} \theta_g &= \left(\frac{\tilde{\mu}}{\tilde{\varphi}\omega}\right)_{\omega\theta_g\gg1} \\ \bar{\tau}_T &= \left(\frac{\beta - \dfrac{\pi}{2}}{\omega}\right)_{\omega\theta_g\gg1} \end{aligned}\right\} \tag{13}$$

and the unknown values of θ_g and $\bar{\tau}_T$ can be determined for sufficiently high frequencies no matter what value the interaction function B may take.

It is clear that if one plots the experimental values of the right-hand members of equation (13) as a function of the frequency of modulation, one must expect a constant value at sufficiently high frequencies, corresponding to the actual values of θ_g and $\bar{\tau}_T$ (which must be unaffected by the frequency). At lower frequencies, however, when $\omega\theta_g$ or $\tilde{\mu}/\tilde{\varphi}$ become comparable with unity, one must expect a departure from constancy. It is precisely this departure which, in principle, allows the determination of the interaction function B.

We see that the determination of θ_g and $\bar{\tau}_T$ does not require very great accuracy in the measurements, because these values are obtained from the general level of $\tilde{\mu}/\tilde{\varphi}$ and β. On the contrary, the evaluation of B, based on the shape of the variations in the level of $\tilde{\mu}/\tilde{\varphi}$ and β, requires higher experimental accuracy. In the preliminary measurements described below the obtained level of accuracy was sufficient for the first purpose but was not yet suitable for determination of B.

Apparatus

The equipment used to obtain experimental data consists basically of a gas-pressurized pro-

pellant feed system, a rocket motor, flow and pressure sensing elements, and electronic recording equipment. In the intent of simplifying the initial experiments tests were conducted on a monopropellant rocket motor. The propellant was ethylene oxide, selected for its known and safe properties and the relatively low temperature of combustion (approximately 1000°C).

In the propellant feed system, inert gas is used to pressurize ethylene oxide in a high-pressure tank, forcing it through a flowmeter, a cavitating venturi, the flow modulating unit, and into the rocket motor injectors. All components downstream of the propellant valve are mounted on a flexure-type thrust stand (Fig. 1) which uses leaf springs to provide one degree of frictionless freedom. The rocket motor shown in the figure is of stainless steel and has an inner diameter of 5 in. It is of sectional construction, using 8 radial injectors of the full-cone spray type. Combustion is facilitated by a small amount of gaseous oxygen injected through an orifice located on the motor axis at the head end, and ignition is accomplished by means of standard spark plugs.

The flow modulating unit is mounted in the propellant feed line between the rocket motor and the cavitating venturi. The venturi serves to maintain a constant mean value of the flow rate independent of disturbances traveling upstream from the modulating unit and the injectors. The flow modulating unit itself is a straightforward crank-piston arrangement with 0.20-in stroke and interchangeable pistons to provide different displacements. The data included in this report have been taken using a piston with 0.802-in diameter and a resulting displacement of 0.1 cubic in. The unit was driven at speeds ranging from 50 to 125 rps by a U. S. Motors ¾ HP Varidrive.

The mean propellant flow rate is measured with a Potter turbine-type flowmeter. Two Li-Liu pressure pickups are used to record instantaneous pressures at the injector and in the chamber. This type of pickup is a double catenary diaphragm, water-cooled, strain-gage transducer which is designed to be flush mounted in a rocket combustion chamber. Detailed descriptions of this device are presented by Li[11] and Matthews[12].

One of the pickups is mounted so that its diaphragm is flush with the inner combustion chamber wall, and the other is installed in one of the propellant lines about an inch from the injector orifice. The signals from the pickups are recorded simultaneously on a recording potentiometer (through a cathode follower which serves to isolate the low impedance potentiometer) and on a four-beam oscilloscope screen which is photographed by a continuous strip-film camera. The recording potentiometer provides data on the mean values of injector and chamber pressures, and the oscilloscope camera records amplitudes and phase angles of the oscillating portions of these pressures. A typical oscilloscope record is shown in Figure 2.

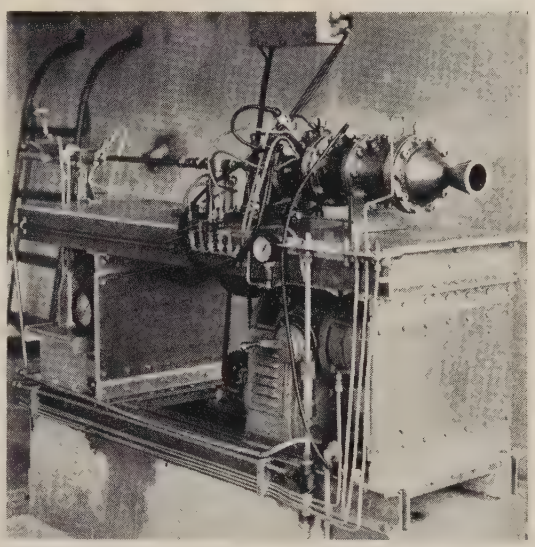

FIG. 1. Monopropellant rocket motor and thrust stand.

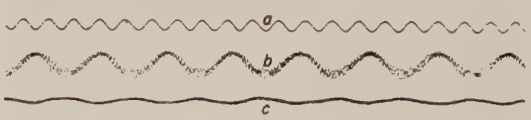

FIG. 2. Typical oscilloscope pressure data: (a) 200 c.p.s. timing trace, (b) injector pressure, (c) chamber pressure.

Discussion of Results

As illustrated previously, the quantities necessary for computation of the combustion time lag and related parameters are the frequency of oscillation ω of the propellant flow rate, the amplitude ratio $\tilde{\mu}/\tilde{\varphi}$ of the fractional injection rate and chamber pressure oscillations, and the phase difference β between them. The quantity $\tilde{\varphi}$ is

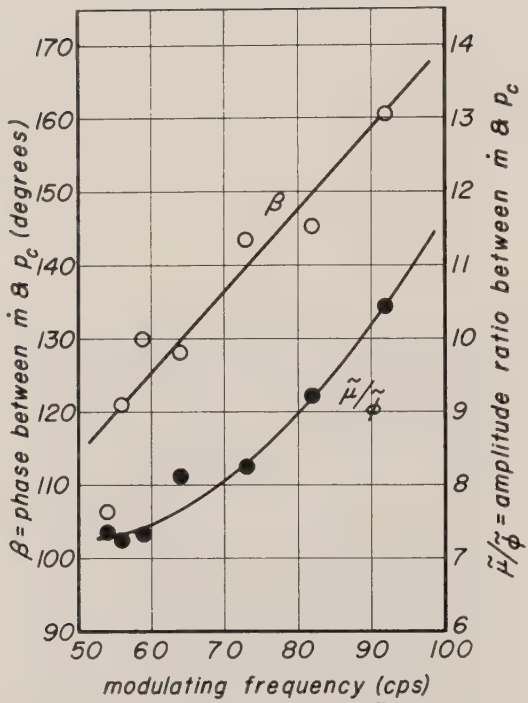

FIG. 3. Experimental data points ($\bar{P}_c = 630$ psia)

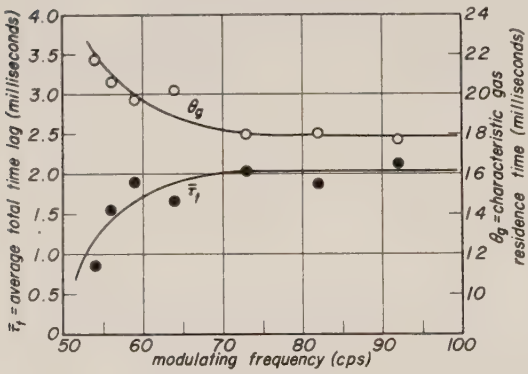

FIG. 4. Experimental values of characteristic gas residence time and average total time lag for $\bar{P}_c = 630$ psia (based on approximation of $\omega\theta_g \gg 1$).

obtained from the trace of the chamber pressure[b] on the oscilloscope and on the recording potentiometer. Similarly one can obtain from the traces of the injector and chamber pressure the instantaneous pressure drop Δp through the injector ports, that is, its mean value $\overline{\Delta p}$ and its oscillating part $(\Delta p - \overline{\Delta p})$. From this, the amplitude of the fractional oscillation of the pressure drop can be obtained and also the phase lag β' of the chamber pressure oscillation with respect to the pressure drop oscillation. From these quantities one can obtain the values of $\tilde{\mu}$ and β, as indicated briefly below.

If the frequencies were very low (quasi-steady conditions) the flow rate would at every instant be proportional to the square root of the pressure drop. For small oscillations this means that $\tilde{\mu}$ would be half of the amplitude of fractional oscillation of the pressure drop, and that there would be no phase shift between the two quantities, so that $\beta = \beta'$. If, however, the frequency increases, inertial effects in the injector passage produce a distortion from the quasi-steady condition, with the consequence that a phase shift exists, increasing with frequency, and also that the ratio of the fractional amplitudes of oscillation is affected. These two effects can be computed[13] and the corresponding correction taken into account to evaluate $\tilde{\mu}$ and β.

Figure 3 is a plot of $\tilde{\mu}/\tilde{\varphi}$ and β evaluated in this way at a given chamber pressure. The corresponding values of $\bar{\tau}_T$ and θ_g obtained from equations (13) are plotted in Figure 4 as functions of the modulating frequency. The behavior of the curves corresponds exactly to the previous discussion of equations (13). In the range of frequencies where $\tilde{\mu}/\tilde{\varphi}$ is sufficiently larger than unity, θ_g and $\bar{\tau}_T$ take constant levels; these values are to be considered as the correct values for the corresponding physical quantities. In the lower range of frequencies the values vary considerably, and the corresponding variation could be taken as a basis for calculating the interaction function B. It is apparent, however, that the scatter of the points does not allow the deduction of a well defined curve. Higher accuracy and extension of the tests to lower frequencies are advisable and will be performed before reliable data for the calculation of B can be obtained.

Observe that the value of $\bar{\tau}_T$ is much smaller than θ_g, which, as already observed, must be of the order of the residence time. This means that the combustion chamber is unnecessarily large for the present combustion conditions. A word of explanation seems necessary. This series of tests was especially directed at the purpose of establishing the possibility of practical use of the flow modulation method, and also to overcome the

[b] Note that at flow modulating frequencies below 100 cps, the location of the chamber pressure tap is immaterial, since the wave travel time throughout the chamber is negligible compared with the period of the oscillation, and hence changes in chamber pressure caused by the flow modulating unit may be considered to occur simultaneously at all points in the chamber.

difficulties of the instrumentation. It was originally intended to operate the motor as a monopropellant chamber alone, which required a large combustion chamber. The oxygen was intended to be used only during the ignition and warming-up phases; however, difficulties were encountered in obtaining regular decomposition when the flow of oxygen was stopped. It was then decided to make no effort to overcome these combustion difficulties, but simply to maintain the oxygen flow during the entire test. Due to the marked effect of the small amounts of oxygen used (less than 5 per cent) in enhancing the decomposition of ethylene oxide, the chamber size could have been reduced appreciably. In this preliminary phase this change was not considered necessary.

Another result can be obtained from the preliminary measurements, despite their relative inaccuracy. A series of tests was performed at varying mean chamber pressures and injector pressure drops. For the reasons described below these data appeared too rough for the precise evaluations previously described. However, it is still possible to obtain a reliable evaluation of the phase lag between injector pressure and chamber pressure, as follows:

Due to the large chamber volume, the chamber pressure has a relatively small oscillation compared to the oscillation produced at the injector. Consequently, the variation in pressure drop coincides very nearly with that of the injector pressure, and the phase difference β' between pressure drop and chamber pressure coincides approximately with the phase difference between the injector pressure oscillation itself and the chamber pressure oscillation. The values of $\bar{\tau}_T$ computed in this manner are plotted as a function of mean chamber pressure in Figure 5. We see by this figure that the time lag is sensitive to chamber pressure in an approximately inverse relation, as has been postulated by qualitative consideration of the physical processes occurring in the chamber[2].

In view of the fact that the conclusions indicated by Figures 4 and 5 are considered by the authors to be of a preliminary nature, some discussion concerning the accuracy of the measurements is pertinent here.

The combustion chamber used in these tests has a characteristic length $L^* = 570$ in. Consequently, if the flow rate oscillations are kept small, the resulting variations in chamber pressure are not sufficiently large to be observed with proper accuracy. For example, in order to obtain a chamber pressure oscillation of the order of 3 per cent in amplitude, it was necessary to increase the injector pressure drop amplitude of oscillation to the order of 50 per cent for a typical chamber pressure and modulating frequency. This means that the flow rate-pressure drop correlation is out of the approximately linear range. Moreover, the pressure drop oscillation sometimes becomes too large for proper range of operation of the cavitating venturi, with the result that disturbances affecting the sinusoidal nature and general regularity of the modulation can appear at each cycle. This is especially true at the higher frequencies.

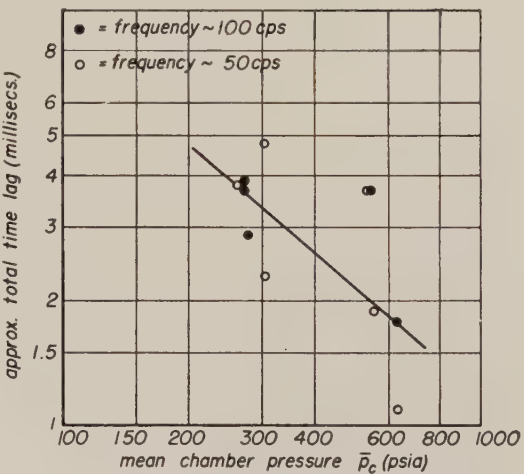

FIG. 5. Experimental variation of average total time lag with chamber pressure.

Elimination of these causes of error is now under way. In the monopropellant case, refinement of instrumentation techniques and reduction in L^* can supply higher orders of accuracy together with larger amplitudes of oscillation in chamber pressure. In the bipropellant rocket chamber which is now being used to extend this investigation, the situation is made easier by the much smaller value of L^*.

REFERENCES

1. CROCCO, L., AND CHENG, S. I.: *Combustion Instability in Liquid Rockets.* Monograph prepared by AGARD, NATO, published by USAF (1954).
2. CROCCO, L.: J. Am. Rocket Soc., *21*, 163 (1951), and *22*, 7 (1952).
3. CHENG, S. I.: Princeton Univ. Aeronautical Eng. Rept. 216f, Appendix A (1953).

4. Gunder, D. F., and Friant, D. R.: J. Appl. Mech., *17*, 327 (1950).
5. Yachter, M.: J. Appl. Mech., *18*, 114 (1951).
6. Summerfield, M.: J. Am. Rocket Soc., *21*, 108 (1951).
7. Tsien, H. S.: J. Am. Rocket Soc., *22*, 256 (1952).
8. Marble, F. E., and Cox, D. W.: J. Am. Rocket Soc., *23*, 63 (1953).
9. Tsien, H. S.: J. Am. Rocket Soc., *22*, 139 (1952).
10. Crocco, L.: Aerotecnica, *33*, 46 (1953).
11. Li, Y. T.: J. Am. Rocket Soc., *23*, 124 (1953).
12. Matthews, G. B.: Princeton Univ. Aeronautical Eng. Rept. 216f, Appendix C (1953).
13. Crocco, L., and Grey, J.: Princeton Univ. Aeronautical Eng. Rept. 216h, Appendix A (1954).

8

STUDY OF THE IGNITION LAG OF LIQUID PROPELLANTS

By M. BARRÈRE and A. MOUTET

(1) Introduction

The measurement of ignition lag is very important for the rating of the propellants used in combustion chambers of liquid-propellant rockets[1].

The initial ignition lag and the operation ignition lag[2] will be studied separately:

(1) The main purpose in the study of the initial ignition lag of a propellant is to establish a simple method of comparison between the various reactants and to determine the effect on this lag of the main physical and chemical parameters. At the firing of the rocket, explosion hazard must be reduced and a progressive pressure rise without dangerous oscillations must be obtained (the pressure rise must be shorter and shorter).

(2) The study of the operation ignition lag, that is to say the period between the admission of a propellant droplet into the combustion chamber and its combustion, is closely related to the chamber size and the disturbances in this chamber. It is well established now[3] that the time for the preparation of the propulsive mixture in a rocket combustor is very high with respect to the time required for combustion and for the establishment of chemical equilibrium. This lag has a great influence on the determination of the combustion chamber size. Consequently, it is important to determine the main factors which act upon this lag which can be considered as a dead time from the standpoint of combustion. Moreover, the ignition lag is related to combustion stability[4]. Some of the fluctuations observed are due to the transformation process of the propellant into combustion gases which occurs when combustion does not directly follow the injection and may initiate auto-oscillations.

Several experimental setups have been devised for the study of ignition lag but no reliable correlation has been obtained between the corresponding measurements and the results in actual rocket combustion chambers. The first part of this paper will be devoted to a method of ignition lag measurement which is a good approximation of the actual test conditions and of the results obtained.

The second part will be devoted to the study of operation ignition lag which is very complex. The effects on this lag of the numerous governing factors are not yet well understood and it is not possible to act on them individually in the combustion chamber itself. Special test chambers in which it would be possible to analyze this phenomenon with more certainty than in actual operation have not been developed. We shall only study operation lag with regard to its effects on combustion stability and especially on the low frequency instabilities which are directly associated with it.

(2) Study of the Ignition Lag

(2.1) definition

The study of initiation of combustion may be characterized by two lags[2]. Let ξ $(0 < \xi \leqslant 1)$ be the degree of advancement of the reaction, and 0 the point where the oxidizer and the liquid fuel are brought into contact by means of a suitable

device (Fig. 1). At this point, the reactants are at the temperature T_0 defined by experimental conditions. The segment OA represents the contact time of the injected liquids; no reaction is initiated up to point A. The temperature T_A is roughly equal to the temperature T_0. At A, an exothermic reaction begins in the liquid phase, which raises the mixture temperature, and smoke appears indicating the decomposition of the oxidizer and the fuel and the vaporization of certain intermediate products. This temperature rise within the mixture accelerates the reaction up to point B corresponding to an ignition temperature T_i and a degree of advancement of the reaction ξ_i. Starting at B, there is a sharp increase in the mean temperature of the mixture and in the degree of advancement of the reaction. We determine two ignition lags t_v and t_i according to the origin selected. The lag t_v is defined as the time lapse between the beginning of the first reactions and ignition; t_L is a total lag which includes the contact time of the reactants. The lag t_v is a function of the chemical nature of the oxidizer and the fuel, and of their reactivity; t_L depends not only on the parameters which characterize t_v, but on the physical properties of the reactants, such as surface tension, viscosity, etc. This definition mainly applies to hypergolic mixtures which ignite spontaneously without addition of any external energy. For most propellants, the ignition conditions, i.e., the energy conditions which characterize ignition must be given initially. Ignition is generally obtained by bringing the propellant to a temperature T_p, such that the heat provided at this temperature by the beginning of the reaction raises the temperature of the mixture to the ignition temperature. The temperature T_p determines new initial experimental conditions and the ignition lag is defined as previously.

(2.2) MEASURING DEVICES

All devices for measurement of the ignition lag consist of two parts which bear respectively on:

(1) The mixing of the oxidizer and the fuel;

(2) The measurement of the time between impingement of the liquids and appearance of a flame.

The main difficulty encountered in the choice of a measurement method is due to the process of impingement for the two liquids. As the accuracy is a function of the method used, it is advisable to approximate the actual operation conditions of the chamber. Accordingly, we developed a combustion chamber with a window having the following characteristics:

The rectangular chamber has two opposite walls made of Plexiglas (Fig. 2); the oxidizer injection system has two identical orifices positioned so that both jets impinge on the chamber axis at an angle of 90°. The fuel jet is directed along the nozzle axis and bisects this 90°-angle.

The feeding system is the same as for microrockets[5]. It consists essentially of a low-pressure nitrogen feeding system actuated by electrovalves which discharge the liquids into the chamber.

The time lapse between impingement of the two liquids and the appearance of a flame is

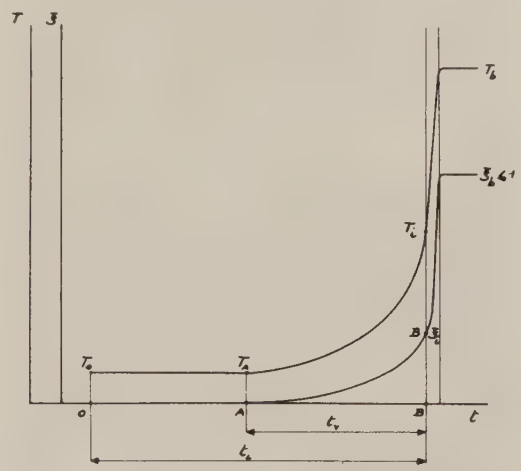

FIG. 1. Variation in temperature and reaction evolution during the ignition.

measured by two methods:

(1) A high-speed moving-picture Fastax camera (5000 frames/sec) records all phenomena developing in the combustion chamber during this time lapse (Fig. 2). It is possible with this method to observe delivery of the reactants into the chamber and to study the first combustion zones, the ignition and the initial frequencies of oscillation. The total lag t_L is measured from the point where fuel and oxidizer impinge.

(2) A temperature measuring device[6, 7] placed in front of the chamber is used to observe the following events at a point in the chamber which, in our experiments, is located ahead of the expansion zone:

the first appearance of smoke,

the moment when the chamber becomes opaque,

the first appearance of flame and the tem-

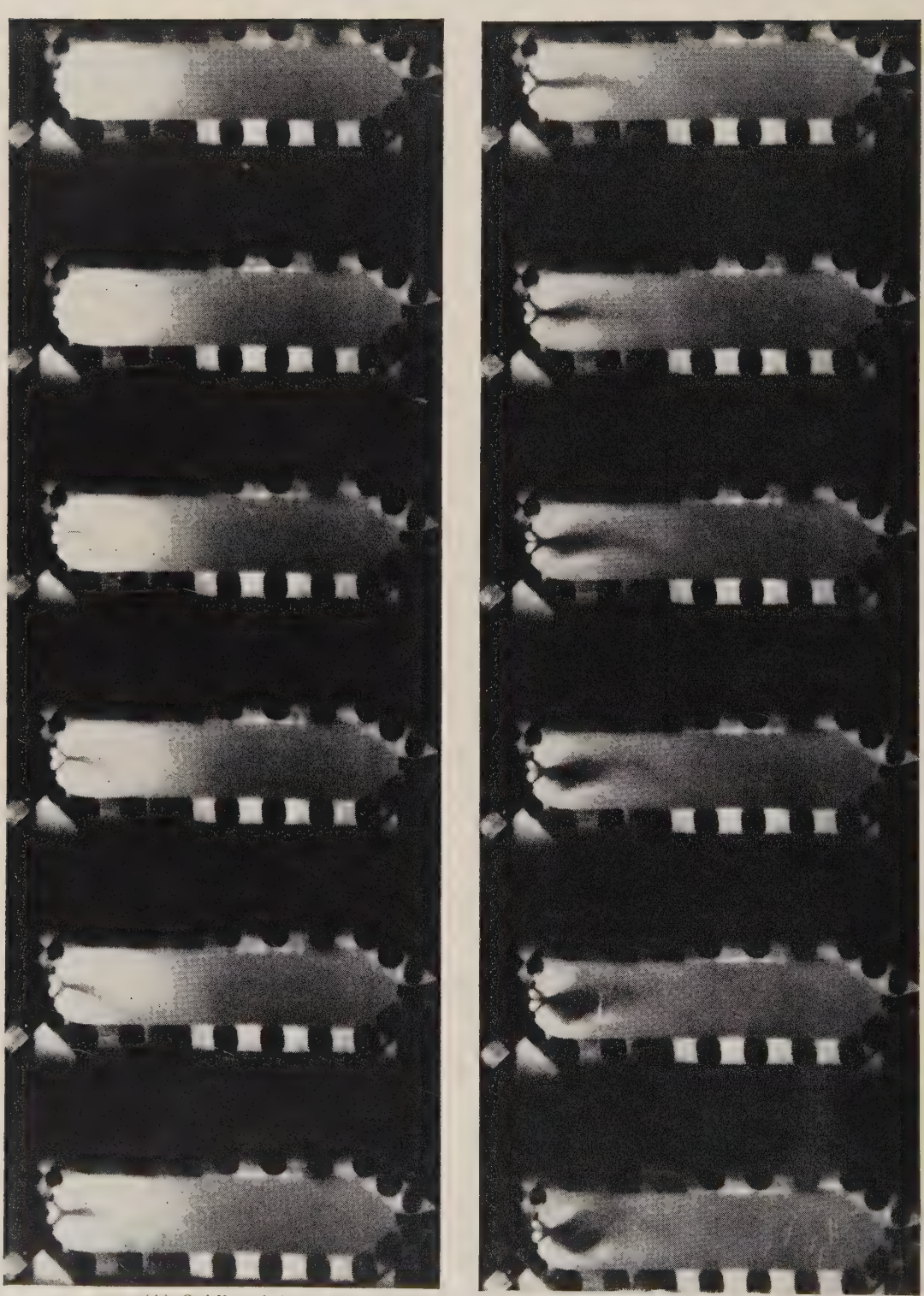

(A) Oxidizer injection (B) Fuel injection

FIG. 2. Motion-picture study of combustion initiation (1680 frames per second). Propellant: nitric acid–(50% furfuryl alcohol + 50% zylidine).

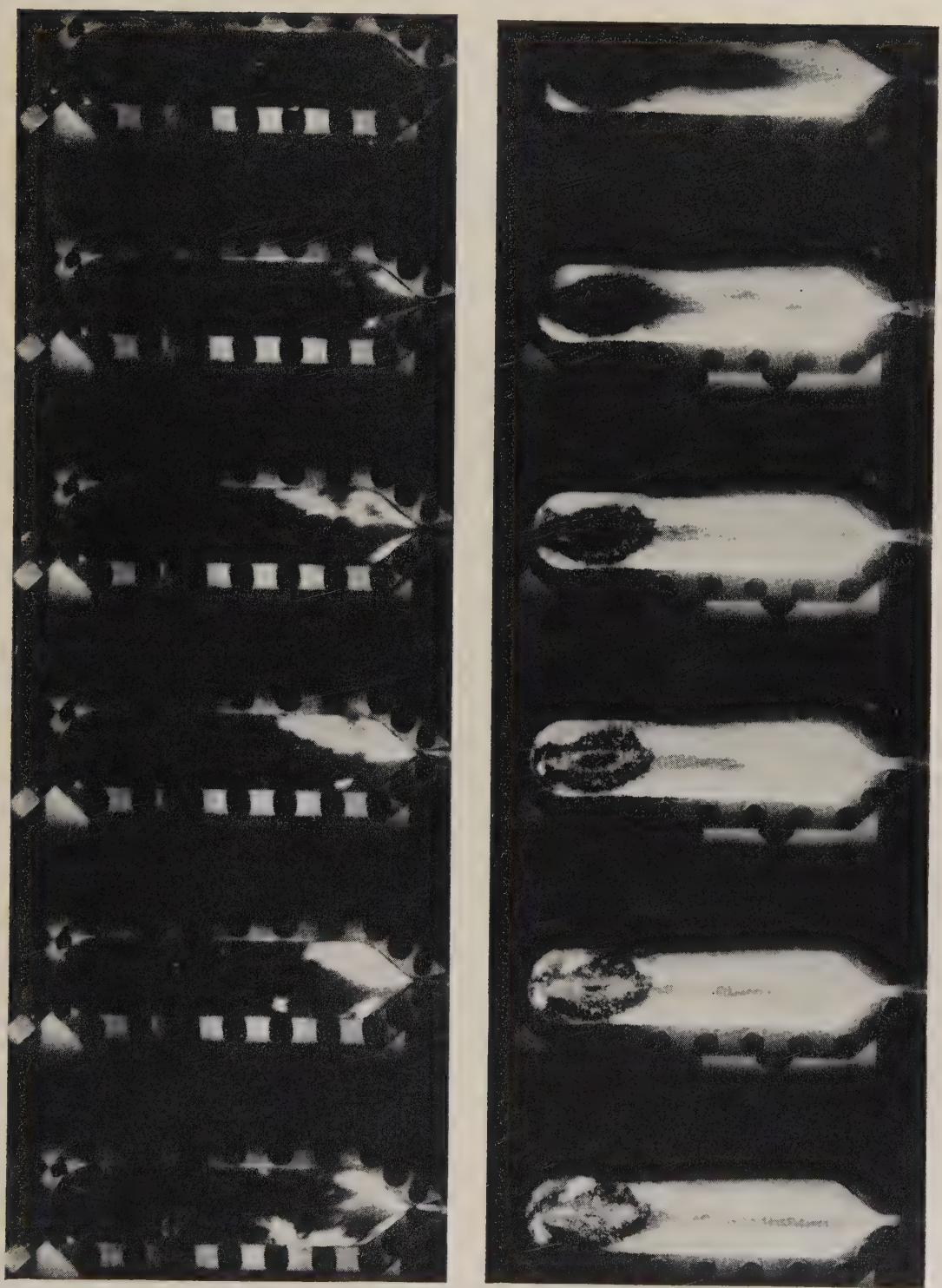

(C) and (D). Combustion initiation
FIG. 2 *continued*

perature during the first milliseconds following the ignition.

Figure 3 shows two oscillograms obtained with this procedure. Three traces corresponding respectively to the filament energy of a lamp taken as a reference, the flame energy alone, and the flame energy increased by the filament energy after crossing the flame are recorded separately. This last trace is used as reference for the appearance of the first smoke and the beginning of the chemical process which precedes ignition: during this time the chamber is opaque and the light beam is almost totally absorbed.

Oscillogram 3A shows the first absorption due to the introduction of propellants, followed by total absorption of the light beam and later by the appearance of a flame.

Oscillogram 3B shows the oscillations which accompany firing of the rocket.

Thus, temperature measurement complements the cinematographic method and gives the lag t_v. In this case, the time when absorption of the light beam becomes important is taken as zero point. As shown in Figure 3, this point is well determined.

(2.3) RESULTS

Before studying the different factors which act on the ignition lag, we shall make the following remark which applies to all tests. The appearance of the ignition zone and the initial ignition characteristics are a function only of the total ignition lag. Figure 4 corresponds to a total lag of 16 millisec: there is a progressive increase of the combustion zone over a period of 2 millisec; firing is not accompanied by explosion; the supersonic jet at the nozzle outlet is well initiated; and some low-amplitude oscillations appear. With a longer lag (46 millisec), the aspect of the combustion zone is modified: Figure 5 shows a sharp rise in luminous intensity corresponding to a sharp increase in combustor pressure; the jet bursts from the nozzle; the oscillations have a large amplitude; there is a momentary halt in combustion.

With a still longer lag (96 millisec), the accumulation of reactants is very important and ignition is spontaneous in the whole combustor where the pressure is so high that the transparent walls are broken (Fig. 6). In an actual rocket combustor so great a lag results in large oscillations at firing. The pressure recordings obtained under such

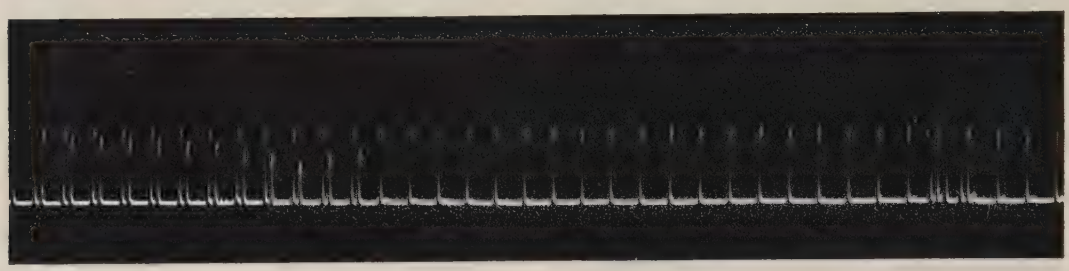

(A)

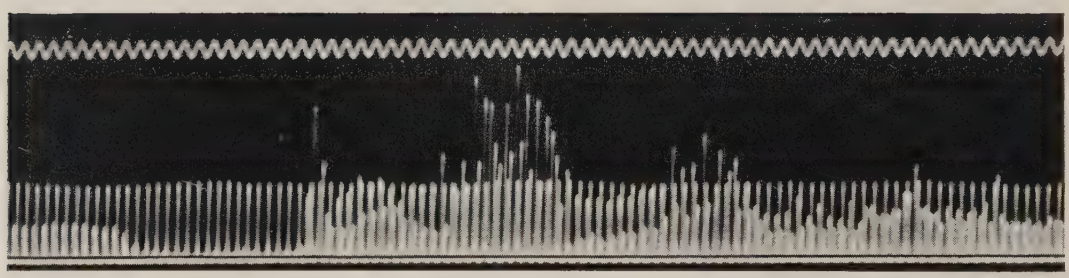

(B)

FIG. 3. (A) Oscillogram of the nitric acid-(25% aniline + 75% furfuryl alcohol) propellant; frequency of measurement 1470. (B) Oscillogram of the nitric acid-(50% xylidine + 50% furfuryl alcohol) propellant. Time frequency, 1000; $m^* = 1.39$.

conditions for a 100 kg-thrust rocket motor (Fig. 7) show the importance of these instabilities.

The physical and chemical factors acting upon the ignition lag have been studied by this method. We shall now consider them.

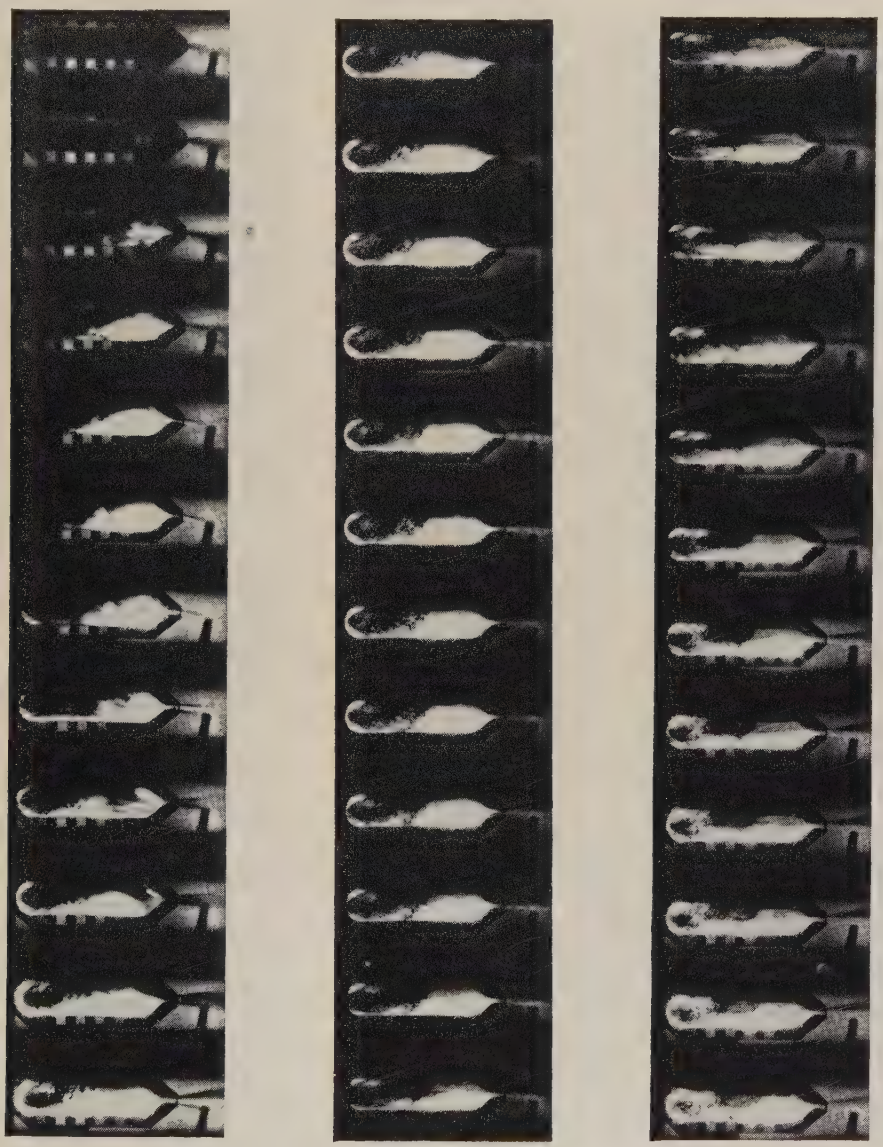

FIG. 4. Ignition characteristic for a lag of 16 millisec

(2.3.1) *Effect of injection*

With an actual rocket motor, it is critical to inject the oxidizer and the fuel together and the delay of one ergol with respect to the other may involve an increase in the total ignition lag. We have evaluated this increase in a first series of tests, taking a furfuryl alcohol-nitric acid mixture as a propellant which was injected into the chamber under a 10 kg/cm² pressure. Figure 8 shows the results obtained. The lag ratio t_v/t_{vo} (t_{vo} representing the minimum lag) is the ordinate and the lead time t_A of either the oxidizer with respect to the fuel (right in Figure 8) or the fuel with respect to the oxidizer (left in the same figure) is the abscissa. As the lag increases materially when the fuel is injected before the

oxidizer, it is advisable to inject the oxidizer first while tending toward simultaneous injection of the two ergols.

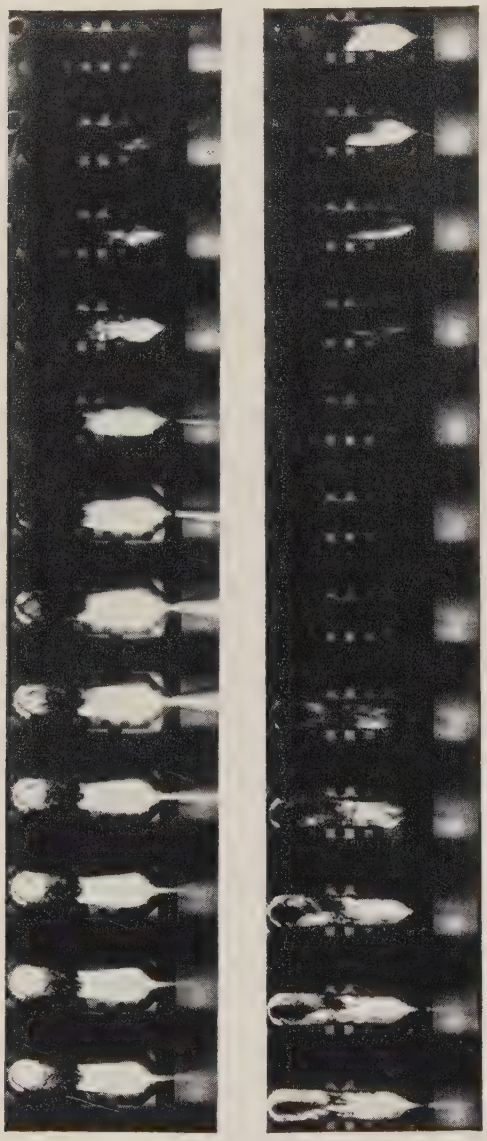

FIG. 5. Firing oscillations for a lag of 46 millisec

propellant, the mixture ratio at the injection of the initial hypergolic mixture does not correspond to optimum performance. Therefore, it is useful

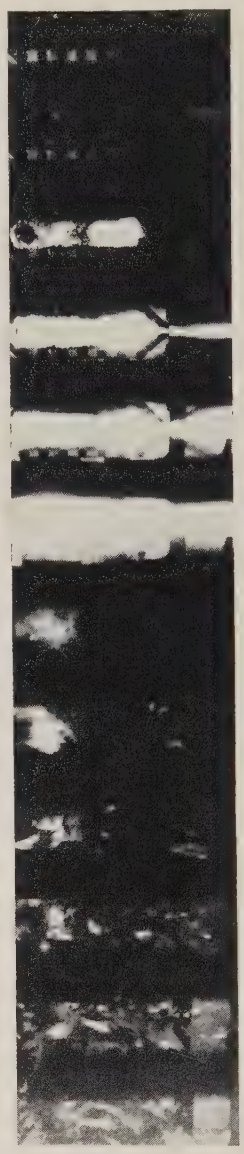

FIG. 6. Chamber explosion for a lag of 96 millisec

(2.3.2) *Effect of the mixture ratio m**

It is interesting from a practical point of view to determine the modification of the ignition lag in terms of the mixture ratio. In most cases, a hypergolic mixture is used to ignite a non-hypergolic mixture such as nitric acid and kerosene. However, as the injection head has been designed to obtain the best performance with the nitric acid-kerosene mixture which is the main to know the increase in ignition lag when the mixture ratio is very different from minimum lag conditions.

The mixture ratio m for an injection head is given by the expression:

$$m = \frac{\alpha_H A_H}{\alpha_o A_o} \sqrt{\frac{\rho_H \Delta p_H}{\rho_o \Delta p_o}}$$

where A_H and A_o are the injection head cross-

sections, α_H and α_o the flow-rate factors, ρ_H and ρ_o the specific gravities, and Δp_H and Δp_o the over-pressures, respectively, for the fuel (subscript H) and the oxidizer (subscript o). To vary

FIG. 7. Record of chamber pressure oscillations and injection pressure at firing

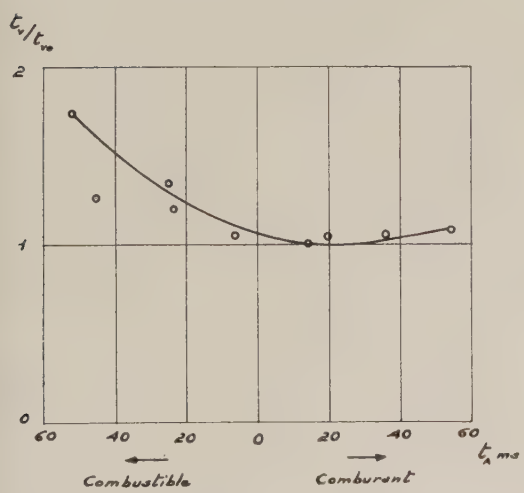

FIG. 8. Effect of injection lead of one ergol on the ignition lag.

m, we have employed a set of calibrated injector orifices with different (A_H/A_o) ratios, keeping Δp_H and Δp_o constant in order to keep the injection speed of the ergols constant.

Figure 9 shows the results obtained with the nitric acid-(50 per cent xylidine + 50 per cent furfuryl alcohol) mixture, the characteristic mixture ratio $m^* = m/m_s$ (m_s = corresponding stoichiometric mixture) being the variable. We have recorded on the same graph the total lag t_L and the chemical lag t_v obtained from the temperature measurement. We observe:

an increase in chemical lag for lean mixtures,

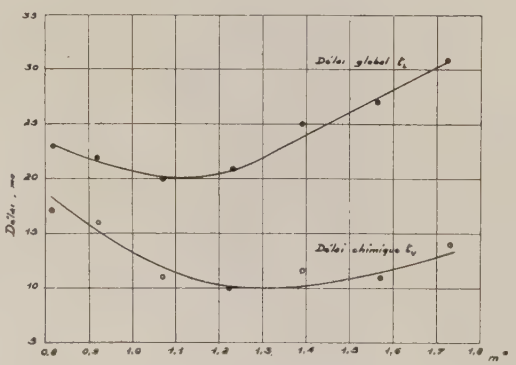

FIG. 9. Effect of the mixture ratio m^* on the ignition lag.

an increase in contact time for rich mixtures,
a minimum lag corresponding to $m^* = 1.1$ for the total lag and
$m^* = 1.3$ for the chemical lag.

(2.3.3) *Effect of the injection speed*

In order to vary the injection speed for a constant mixture ratio, the oxidizer and fuel injection speeds must be modified, leaving the ratio $\Delta p_H/\Delta p_o$ unmodified.

In our tests, the pressure varied from 10 to 20 kg/cm². Figure 10 represents the results for the same propellant as previously and a mixture ratio

$m^* = 1.39$. The lag becomes slightly longer with the increase in pressure. The total lag t_L and the chemical lag t_v vary in the same way.

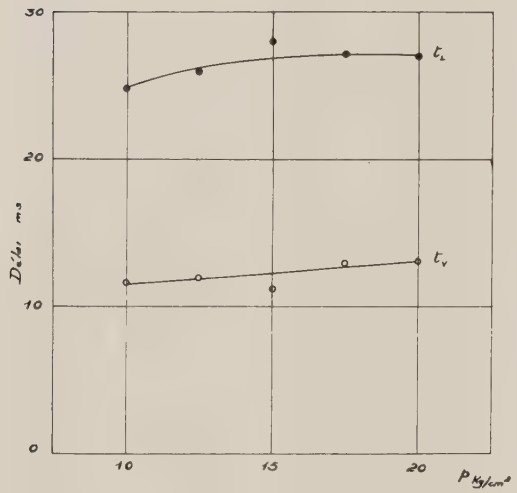

FIG. 10. Effect of the injection over-pressure on the ignition lag.

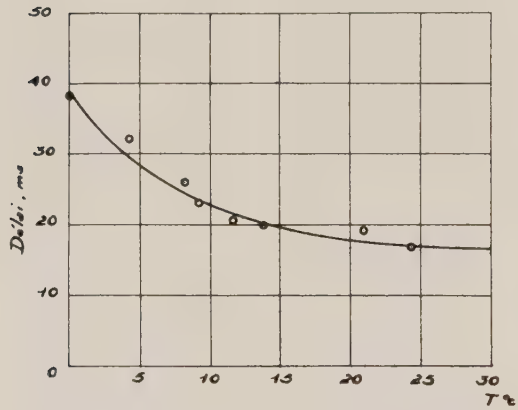

FIG. 11. Effect of the initial reactant temperature on the ignition lag.

(2.3.4) *Effect of the initial temperature of the reactants*

The ignition lags were determined in terms of the initial temperature for a mixture ratio m^* of about 1.07, using the nitric acid-(50 per cent xylidine + 50 per cent furfuryl alcohol) mixture and a feed pressure of 10 kg/cm². The results are summarized in Figure 11 where an important increase in lag with a decrease in ergol temperature can be observed.

(2.3.5) *Effect of the type of propellant*

Both the physical and chemical properties of the propellant act on the ignition lag.

As seen above (Section 2.3.2), the difference $t_L - t_v$ corresponding to the physical lag is far from negligible; thus, by modifying the physical properties of the reactant, it is possible to reduce this lag. Surface-active agents have been employed in order to reduce the contact time of the liquids[8] and decrease the ignition lag.

But the most important parameter is the reactivity of the propellant. Thus, with the furfuryl alcohol-nitric acid propellant, we obtain the following results by adding to the furfuryl alcohol various compounds of similar physical properties:

(Operation pressure, 10 kg/cm², initial propellant temperature, 11°–13°C)

		Millisec
Furfuryl alcohol-nitric acid	$m^* = 1.21$	$t_L = 33$
25 Per cent aniline + 75 per cent furfuryl alcohol, nitric acid	$m^* = 1.31$	$t_L = 18$
25 Per cent dimethylaniline + 75 per cent furf. alc., nitric acid	$m^* = 1.41$	$t_L = 96$
25 Per cent toluidine + 75 per cent furf. alc., nitric acid	$m^* = 1.32$	$t_L = 37$
25 Per cent xylidine + 75 per cent furf. alc., nitric acid	$m^* = 1.40$	$t_L = 20$
50 Per cent xylidine + 50 per cent furf. alc., nitric acid	$m^* = 1.57$	$t_L = 27$
25 Per cent diethylamine + 75 per cent furf. alc., nitric acid	$m^* = 1.17$	$t_L = 55$
25 Per cent triethylamine + 75 per cent furf. alc., nitric acid	$m^* = 1.75$	$t_L = 61$

This table points out the importance of addition products which have a significant effect on the lag.

Conclusions

In giving these few results, we intended to show the possibilities of this method which has the practical advantage of approximating actual test conditions.

In addition to the total lag generally used, we have defined a chemical lag, pointing out the im-

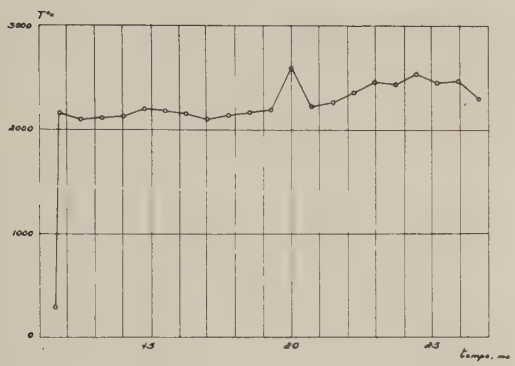

FIG. 12. Variation in firing temperature. Nitric acid-(50% xylidine + 50% furfuryl alcohol) propellant; $p_i = 10$ kg/cm^2; $m^* = 1.39$; $T_0 = 12$°C.

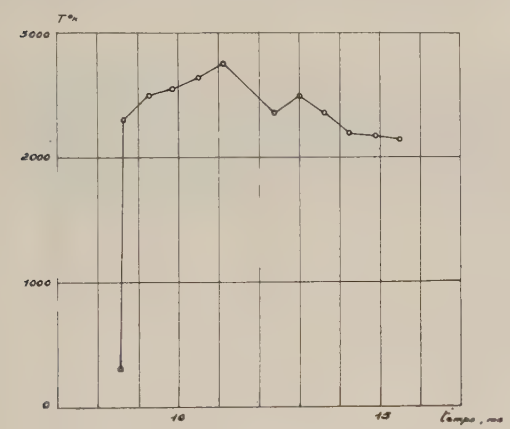

FIG. 13. Variation in firing temperature. Nitric acid-(50% xylidine + 50% furfuryl alcohol) propellant; $p_i = 10$ kg/cm^2; $m^* = 1.22$; $T_0 = 21$°C.

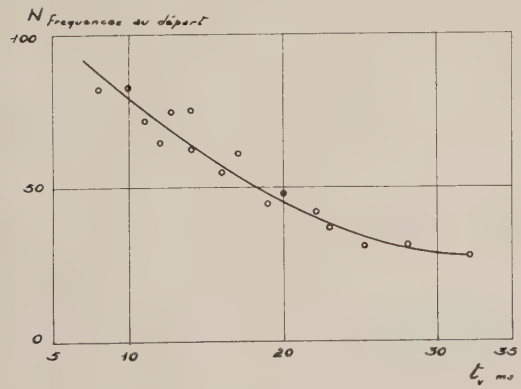

FIG. 14. Correlation between the ignition lag and the first-oscillation frequency at the firing.

portance of the first chemical reactions before ignition. Thus, it has been possible to determine the principal parameters which act upon both lags and study their importance. However, we have systematically neglected all parameters relative to the injection system (jet angle, injector position and shape, etc.) which ultimately result in a more or less homogeneous mixture, that

FIG. 15. Record of the chamber pressure fluctuations and the nitric acid flow rate. A, nitric acid flow rate; B, chamber pressure.

is to say a lag modification. Moreover, the above study deals only with an elementary injector, but the injector distribution on the chamber bottom may have a great influence on the ignition lag. This distribution can be studied by taking larger chambers of the same type with different distributions of the injector set.

It seemed interesting for us to complete this study by the examination of the temperature variation based on the ignition temperature.

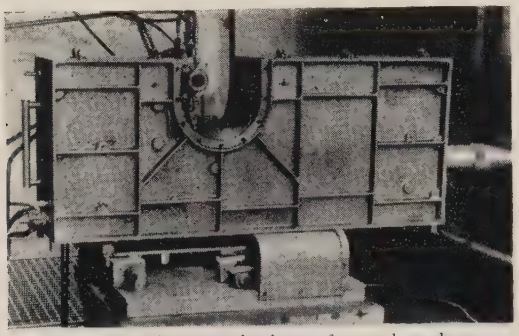

FIG. 16. External view of test bench

the results are given in Figure 14. The frequency increases and the amplitude decreases as t_v decreases.

Figures 15 and 17 give pressure, flow, and temperature fluctuations recorded in the chamber with an experimental set-up of this type (Fig. 16). They show the importance for a given injection system of the principal factors acting upon the recorded frequency: chamber pressure, characteristic length, and type of propergol . Figures 18 and 19 show the influence of these different factors. It will be seen that the frequency increases with the pressure but the results obtained for three characteristic lengths (2.10, 2.35 and 3.35 meters) show that the frequency increases as the characteristic length decreases. On the other

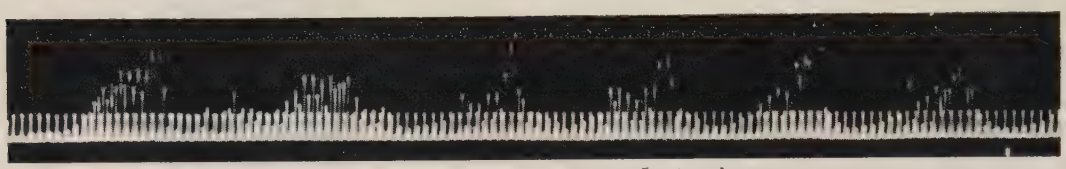

FIG. 17. Record of temperature fluctuations

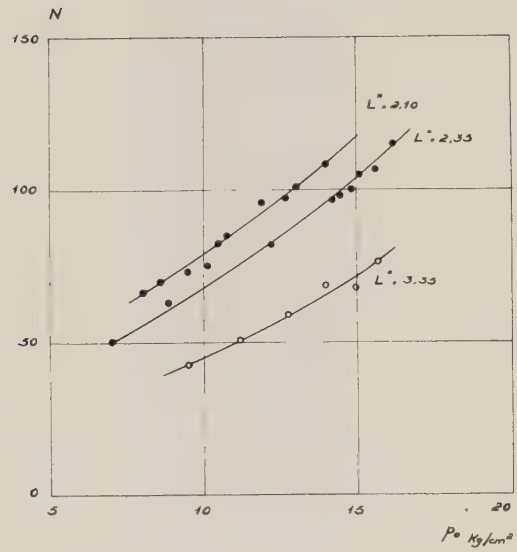

FIG. 18. Frequency variation in terms of the chamber pressure and characteristic length L^*. Nitric acid-furfuryl alcohol propellant.

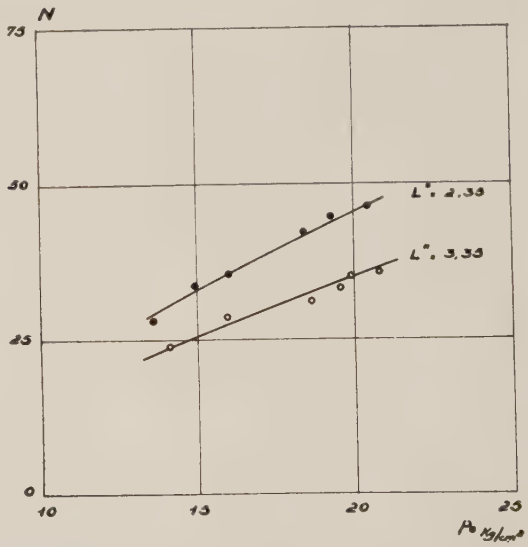

FIG. 19. Frequency variation in terms of chamber pressure and characteristic length L^*. Nitric acid-octane propellant.

Figures 12 and 13 give the results for the same propellant and two mixture ratios (m^* = 1.39, temperature 2300°K; m^* = 1.22, temperature 2600°K).

The oscillation frequency at firing has been studied. We have tried to derive a correlation between the frequency and the chemical lag t_v ; hand, the frequency is generally higher for the furfuryl alcohol-nitric acid mixture than for the octane-nitric acid mixture.

The frequency value seems to give some information about the operation ignition lag. Thus, for an evolution relation $\tau p^n = c^{te}$ between the lag τ and the pressure p, the present theories on

combustion instability [4, 9, 10] give the constant factor n in terms of the pulsation ω^* following the relation

$$n = \alpha + \beta\omega^{*2}$$

where the constant factors α and β are given by the experimental feed conditions and the geometry of apparatus. It is possible with this method to determine the order of the exponent n and check if it is a characteristic factor of the propellant, independent of the chamber pressure or characteristic length. In fact, n varies from 0.72 to 1.9 for the furfuryl alcohol-nitric acid propellant and from 0.47 to 0.69 for the octane-nitric acid propellant. However, as direct measurement of this exponent is not possible, it seemed interesting for us to give these first, albeit approximate, values obtained by this indirect method.

REFERENCES

1. Roy, M.: Thermodynamique des Systèmes Propulsifs à Réaction, p. 71–72. Paris, Dunod, 1947.
2. Barrére, M.: "Méthodes générales de mesure des délais d'inflammation des propergols liquides." IVe Congrès International du Chauffage Industriel, Groupe I, Section 12, n° 100, 1952.
3. Canright, R. B.: Chem. Eng. Progress, May 1950, p. 228–232.
4. Crocco, L.: J. Am. Rocket Soc., November 1951, p. 163–178; January–February 1952, p. 1–16.
5. Barrére, M.: La Recherche Aéronautique, *21*, 25–33 (1951).
6. Moutet, A.: La Recherche Aéronautique, *27*, 21–27, (1952); *28*, 21–30, (1952).
7. Moutet, A.: "Mesures et enregistrements des températures de flammes". IVe Congrès International du Chauffage Industriel, Groupe I, Section 14, no. 56, 1952.
8. Bernard, L.: C. R. Ac. Sc., November, 1952.
9. Summerfield, M.: *J. Am. Rocket Soc., 21*, September 1951, 108–114.
10. Gunder, D. F., and Friant, D. R.: *J. Appl. Mech.* (Trans. A.S.M.E.), *17*, 327–333 (1950).
11. Satche, M.: *J. Appl. Mech., 16*, 419–420 (1949).
12. Barrére, M. and Moutet, A.: *La Recherche Aéronautique, 38*, 15, 1954.

Discussion by John H. Hett*

If I understood this paper correctly, the authors gave instantaneous temperatures in a liquid fuel rocket by using a tungsten lamp for reference and by assuming that the rocket radiation was grey body radiation.

The writer, together with Mr. J. B. Gilstein, reported at the American Rocket Society meeting in New York City, December 1953, the necessity of examining the spectral radiation carefully to determine whether equilibrium radiation actually exists. Our spectral study of the background radiation of alcohol-oxygen rockets in the thrust range 150 to 1500 lbs showed that true equilibrium does not exist, and that consequently all rocket temperatures are highly qualified. We prefer to call them indicated temperatures.

* Research Associate, Jet and Flame Laboratory, New York University.

9

STUDIES OF THE RATES OF COMBUSTION OF HYPERGOLIC FLUIDS

By FOY McCULLOUGH, JR., and H. P. JENKINS, JR.

Introduction

The combustion of monofuels and miscible non-hypergolic liquid fuels and oxidizers has been studied for some time by means of the strand-burning technique.[1, 2] The *consumption rate,* inches per second, and the *burning rate,* inches per second per unit surface area, of such combustible combinations may be interpreted as measures of the combustion rate or overall reaction rate. In view of the desirability of extending the study of combustion to include hypergolic liquid combinations, an apparatus called the Micromix was developed for this purpose at the U. S. Naval Ordnance Test Station, Inyokern, China Lake, California.

The purpose of this paper is to (1) describe the Micromix apparatus; (2) describe two experimental techniques, with discussions of the limita-

tions and problems associated with each; and (3) present preliminary combustion rate data as obtained by the two different methods employed.

Apparatus Design

The design of the Micromix was based on the idea that by forcing a hypergolic fuel and oxidizer through a mixer into a small diameter glass

Figure 2 is a schematic diagram of its principal components. The Micromix consists essentially of (1) a 200-cu in stainless-steel combustion bomb that has an injector or mixer mounted in its base, two viewing ports, and fixtures for gas pressurization, venting, and water flushing; (2) two tanks for storage of the fuel and oxidizer; (3) a positive displacement pump and its power supply; (4) a pressurizing system; and (5) various

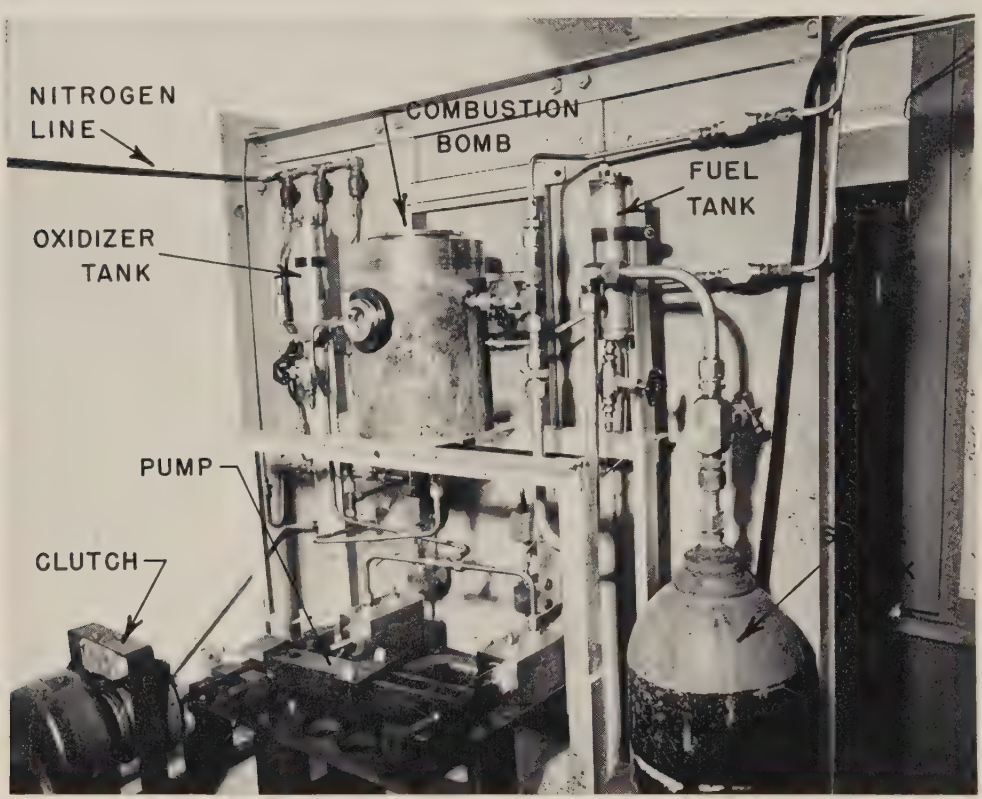

FIG. 1. The Micromix apparatus. The combustion bomb is 12 in tall. In this view the bomb is fitted with the original viewing ports (1¼ in diameter) intended for use with tube-burning. (Official photograph, U. S. Navy.)

or quartz tube it would be possible, by adjustment of the fluid flow rate, to obtain a steady state condition with the rate of flow of the mixed liquids equal to the consumption rate. Thus the flow rate at which this balanced condition was obtained could be considered as a measure of the propellant consumption rate at the existing pressure. Essentially then, the Micromix was designed to operate as a dynamic application of the strand-burning technique. This dynamic strand-burning of hypergolic mixtures was called *tube-burning*.

Figure 1 shows the apparatus of the Micromix; controls. The control panel (Fig. 3) is mounted on boiler plate, which shields the operator from the apparatus. Note that in Figure 1 the combustion bomb is equipped with the original viewing ports intended for use with the tube-burning technique; in Figure 3 the combustion bomb has been turned on its side and is equipped with four-inch diameter windows of Plexiglas for free-jet tests which are described later in the paper.

POSITIVE DISPLACEMENT PUMP

The key to the successful operation of the Micromix is a specially designed positive displace-

ment pump (shown in Figs. 1 and 2) with which the flow rate and injection ratio of the two fluids are controlled. This pump is a single-stroke device with two cylinder-and-piston assemblies fasted to a rigid base. Each assembly has a fluid side and a gas side with the gas side of each cylinder connected directly to the combustion bomb. Since the fluid sides are connected to the injector in the bomb, the pressures on either side of the pistons are nearly equal during operation of the apparatus. Thus, the power required to operate the pump is kept to a minimum, since only the pressure drop across the injector and mechanical friction must be overcome.

Motion is transmitted to the pistons by a common driving arm called the proportioning arm which swings about a pivot so that the pistons move in opposite directions. The pivot pin can be moved along a slot (perpendicular to the piston's center line) in the base plate of the pump in order to change the ratio between the delivered volumes of the two fluids. The proportioning arm is connected at one end to a traveling nut that moves along a drive shaft. Movement of the traveling nut from one end of the shaft to the other constitutes one pump load. The rotation of the drive shaft is reversed to refill the pump.

The distance from center line to center line of the pistons is 12.000 in; the distance from the drive shaft center line to the nearest piston is 2.250 in. With these two dimensions and the desired volume ratio, the pivot setting can be easily calculated. The pivot pin is adjusted to the setting with a pair of dividers. With this method the injection ratio can be adjusted to within about 0.1 per cent.

At any given pivot position, and at constant drive speed, the flow from each cylinder is linear with respect to time. The motions involved are, in a sense, the reverse of those of an automobile engine. In the internal combustion engine the motion of the pistons is a sine function with respect to time and the crankshaft rotates at constant angular velocity. Conversely, the pump pistons move at constant linear velocity and the angular motion of the proportioning arm around the pivot pin is a sine function with respect to time.

Variable speed power supply

Power to drive the pump is supplied by an electric motor with a variable speed transmission. The rotational speed of the output shaft of this transmission can be varied continuously from about 2 rpm in reverse to 195 rpm in forward drive and has the characteristic of a straight line speed curve; that is, equal divisions on the speed control dial correspond to equal changes in rotational speed. This transmission also provides overload protection—the output shaft may be completely stopped without damaging the trans-

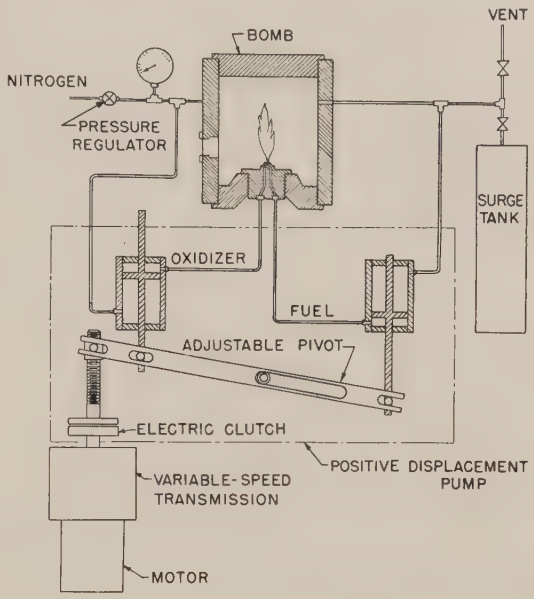

FIG. 2. Schematic diagram of Micromix apparatus. (Official photograph, U. S. Navy.)

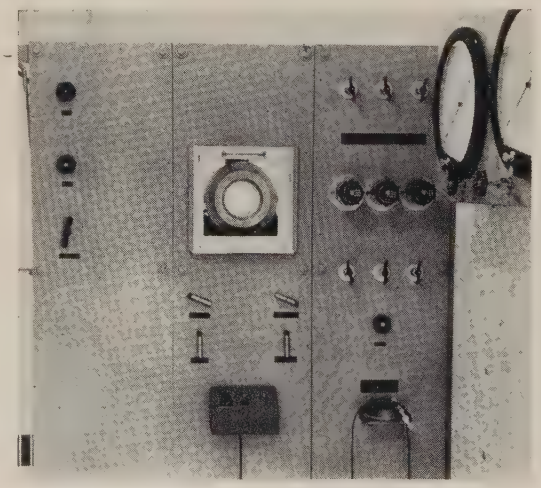

FIG. 3. Control panel of the Micromix. In this view the bomb has been turned on its side and is fitted with 4 in diameter windows for use with free-jet burning. The injector is mounted in a housing fitted in one of the sockets used for the small viewing ports. (Official photograph, U. S. Navy.)

mission. A micrometer remote speed control allows the speed to be changed from behind the barricade during a firing in order to match flow rate against burning rate.

Firing control

The transmission is coupled to the drive shaft of the pump with an electromagnetic clutch (Fig. 1). Control of the current to the electromagnet of this clutch is the firing control of the

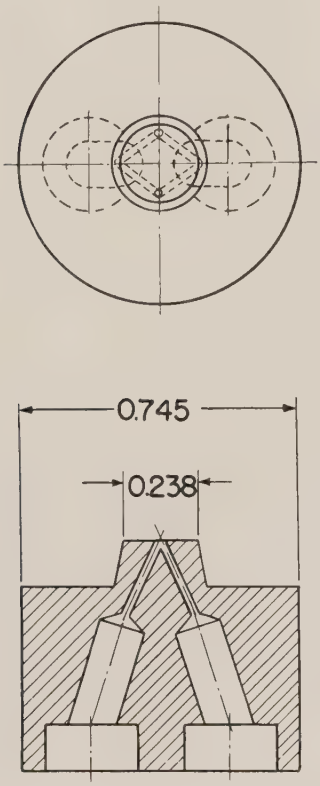

FIG. 4. Injector used for tube burning. Dimensions are in inches. (Official photograph, U. S. Navy.)

Micromix and enables the operator to have the motor and transmission running at any desired speed before firing. With this arrangement the pump delivers a full flow (corresponding to the speed of the transmission) almost instantaneously.

Pressure control system

Commercial nitrogen is used as the pressurizing gas. To regulate the pressure in the system three Grove loaders together with suitable valving were installed between the nitrogen supply and the bomb. These regulators are equipped with back pressure relief valves; which, together with a manually controlled vent valve, serve to keep the pressure constant at any selected value. As an additional aid in controlling the pressure, a large surge tank was connected directly to the combustion bomb as shown in Figure 1. Two Heise gauges were used to determine the pressure. The Micromix has a working pressure limit of 2500 psi.

Tube-Burning

INJECTOR FOR TUBE-BURNING

The injector used with the tube-burning technique was designed for quartz tubes of a nominal inside diameter of 6 mm. The quartz tubes were ground internally to a slight taper to fit tightly over the injector which was machined to the same taper. This injector, a double-impinging type, is shown in Figure 4. Impingement of the fuel and oxidizer streams occurs on the surface or face of the injector at an angle of about 60 degrees. The resultant streams then strike the wall of the quartz tube at an angle of about 25 degrees. These two factors account for the rapid and thorough mixing that results. The mixing characteristics of this arrangement were studied[3] with inert fluids by a modified schlieren technique. As a result of these studies it was shown that above a flow rate of about 3.5 in/sec (2.5 cc/sec in a 6 mm ID tube) mixing is essentially complete. The height of the turbulent or mixing zone immediately above the injector face was found to increase slightly as the flow rate was increased and approach a maximum of about 2 cm (approximately 0.75 in). These studies were made with injectors having fuel and oxidizer orifices 0.020 in in diameter.

EXPERIMENTAL

The hypergolic fluids studied were mixed butyl mercaptan (a by-product of the petroleum industry) and 95.6 per cent nitric acid. The mixed butyl mercaptan used for all tests described in this chapter had the following approximate composition.[4]

Propyl mercaptans	27.8 mole per cent
Butyl mercaptans	65.3
Amyl mercaptans	6.6
Hexyl mercaptans	0.3

By proper adjustment of the flow rate it was possible to stabilize the flame in the tube above

the mixing zone so that the rate of burning or consumption of the liquid hypergolic mixture was balanced by the flow rate of the incoming fluids. The flow rate, measured as velocity in the tube, was taken as the consumption rate at the pressure existing in the bomb.

Considerable difficulty was encountered in this work because of fumes released during ignition and burning which filled the interior of the bomb and prevented observation of the tube and flame. Droplets of the fluids being studied and the products of combustion damaged the Plexiglas windows to such an extent that installation of new windows was frequent. Both of these problems were solved by partially filling the bomb with water so that the window was covered. As a result the tube was surrounded by water and the tube and flame observed through a clear layer of water.

The turbulence in the fluid stream caused by ignition of the mixture was of sufficient magnitude to make it difficult to obtain a stable flame. It is to be noted that the terms "stable flame" and "stabilize" are used only to describe a steady state condition in the tube with the flame located above a column of the hypergolic mixture. The flame frequently flashed down the tube to the injector face and burning occurred at the points of impingement. When this occurred it was virtually impossible to "lift" or stabilize the flame by increasing the flow rate, because the injector face seemed to act like a flame holder. Stable flames were obtained most often when the initial flow rate was adjusted so that ignition occurred near the top of the tube.

The productivity of the tests was increased by the addition of a flame holder. The flame holder was a piece of iron wire (0.018 in diameter) bent to a U-shape about ½ in long. This was placed in the top of the quartz tube with the closed end of the U downward, and served to stabilize the flame at about the bottom of the U. To overcome the turbulence and unstable effects of spontaneous ignition, tests were conducted by setting the initial flow rate higher than that required to produce a stable flame. To insure ignition within the tube the flame holder was heated to a red heat by short intermittant firings at slow flow rates. With the clutch circuit open (no flow) the drive speed was increased to a point where the flow rate would be higher than the expected consumption rate and the firing switch closed again. If the flow rate was high enough the flame would establish itself on the flame holder. The flow rate was then slowly decreased until the first perceptible motion of the flame away from the flame holder was observed. The flow rate at this point was taken as a measure of the consumption rate at the existing pressure. Any catalytic or thermal effects of the flame holder were neglected.

Using the flame holder technique, consumption rates for nitric acid and mixed butyl mercaptan (oxidizer to fuel ratio of 4.4 by weight) were determined at pressures from 50 to 140 psia. These data are shown in Figure 5 which is a plot of the log of the consumption rate as a function of the log of the pressure.

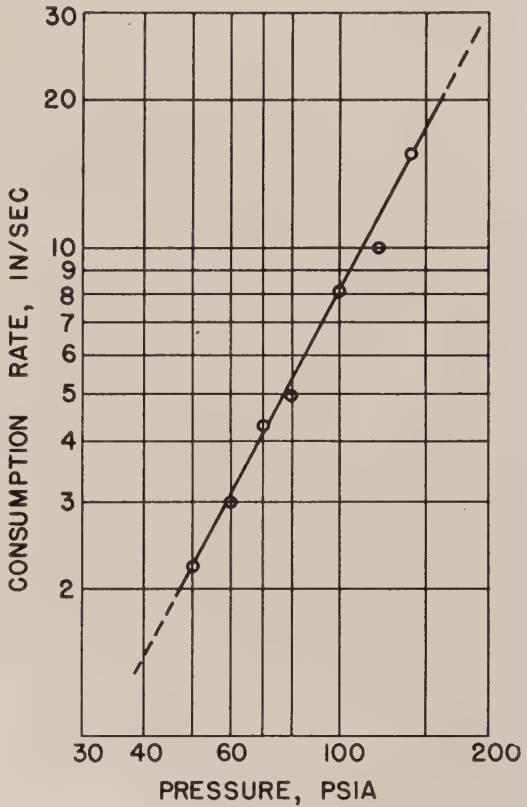

FIG. 5. Consumption rate of mixed butyl mercaptan and 95.6 per cent nitric acid. (Official photograph, U. S. Navy.)

When pressures of greater than 80 psia were employed stable flames could not be obtained with an injector having fuel and oxidizer orifices 0.020 in in diameter (No. 76 drill). Another injector of the same design with orifices 0.040 in in diameter (No. 60 drill) was found to be satisfactory from 80 to 140 psia. These injectors were designated the No. 76 and No. 60 respectively. At 60 psia the measured consumption rate was 3.0

in/sec using the No. 76 injector and 3.9 in/sec using the No. 60 injector. At 80 psia the consumption rates determined with the two injectors differed only by 0.1 in/sec which was within the constant experimental precision of plus or minus 0.2 in/sec.

The data obtained with the No. 76 injector from 50 through 80 psia is plotted with the data obtained with the No. 60 injector from 80 through 140 psia in Figure 5. As may be seen in Figure 5, the measurements made with the two injectors form a smooth curve.

Viewed through the burning-tube, stable flames of this system appeared to be red in color. That portion of the flame above the tube was blue-white and droplets of the mixture (unburned) were being blown out of the tube. In addition, when the flow of fluids was stopped, and the flame flashed down the tube, it was observed to be blue-white. The base of the flame (interface between the flame and the fluid mixture) was an elongated cone with the apex of the cone pointing downward toward the injector face. The interface was irregular with a continuously shifting shape and on occasions some frothing was evident in the fluid immediately below the flame. Stable flames had a fluid appearance and it was concluded from this, the difference in colors observed, and the shape of the interface that the wall of the tube was coated or lined with a layer of the fluid mixture. Since accurate measurements of the interface could not be made determinations of the burning rate with reference to the fluid surface exposed to the flame could not be made.

DISCUSSION

It was concluded that the inherent characteristics of fluid flow, as influenced by injection, mixing, flow and combustion in a tube, created an excessive amount of turbulence which made stabilization of the flame impossible above specific rates of flow. On the basis of the successful firings with injectors having different sized orifices (and thus proportionally different injection velocities) it was concluded that injection was the primary case of excessive turbulence. The injection velocity with either injector was several times greater than the average flow velocity in the tube. This might explain the shape of the interface and the propellants observed on the wall of the tube since the direction of injection is such as to produce a high flow velocity near or on the wall of the tube, leaving a more or less stagnant zone in the center of the tube. It is believed that the unstable condition that occurred above specific rates of flow with the two injectors was caused by the creation of eddies or regions of low axial velocity immediately above the face of the injector. This would, of course, result in secondary ignition in this region and prevent the formation of stable flames for more than a brief instant.

It was concluded that this technique was satisfactory for the comparison of the consumption rates of different hypergolic combinations provided the consumption rate was not more than about 15 in/sec at the highest pressure at which measurements were desired. Measurements of consumption rates greater than 15 in/sec could probably be made by increasing the size of the injector orifices. However, the maximum flow velocity obtainable with the present Micromix design is about 35 in/sec in 6 mm ID tubes. It is believed that consumption rate measurements could be made over a wider range by using tubes of smaller diameter together with an injector designed to eliminate regions of low axial velocity

Free-Jet Burning

The free-jet method of measuring combustion rates vs pressure was based on the ideas that (1) a small unconfined stream, or jet, of fluid would not have the turbulence of fluids fed into a tube and (2) it would have a small velocity gradient across the stream compared to flow in a tube. Originally free-jet burning was to be used in a manner similar to the tube-burning tests. A definite flow rate would stabilize the flame above the injector; and at a higher combustion pressure, if the combustion rate were higher, an increased flow rate would be required to stabilize the flame. This measurement would still have yielded a consumption rate in inches per second

FREE-JET INJECTOR

The injector designed for use with the free-jet burning studies was a confined impingement or premix type with an exit channel 0.375 in long. This injector is shown in Figure 6. The fuel, oxidizer and exit channels were made the same diameter (0.055 in) in an effort to eliminate regions of low axial velocity. Although this design is somewhat contrary to that required for rapid mixing, the small channels apparently mix the hypergolic fluids adequately above an exit ve-

locity of about 45 in/sec. The injector was tested with water, and it was found that an unbroken jet (with no spray formation) was produced up to a flow rate of about 700 in/sec through a 0.055-in orifice, which is the maximum obtainable with the pump. These jet-action tests were made only at atmospheric pressure. Similar tests with an injector having 0.0325-in diameter orifices resulted in a definite spray pattern above flow velocities of about 200 in/sec.

FREE-JET BURNING, PRELIMINARY TESTS

Preliminary tests of free-jet burning were made with nitric acid and mixed butyl mercaptan in the small-windowed bomb. Tests were conducted from 50 to 200 psia and it was found that stable flames could be obtained with an unconfined jet of the hypergolic mixture apparently supporting the flame. An increase in flow rate tended to cause the flame to rise on the unconfined jet. Attempts were made to determine the flow velocity required to stabilize the flame at some given point above the injector tip as a function of pressure. As a means of fixing this point a metal plate with a small hole through it was suspended in a horizontal position about ½ in above the top of the injector. The jet passed through the hole and the flow rate was adjusted until the base of the flame appeared to coincide with the metal reference marker. This was found to be difficult since the base of the flame was somewhat fuzzy in apparance and had a slight up and down motion.

It was found that between 50 and 200 psia the pressure had no appreciable influence on the flow velocity required to stabilize the flame a set distance above the injector exit. However, it was observed that the size of the flame decreased as the pressure was increased, and it appeared that this action might be used to describe rates of combustion. Unfortunately, observations of free-jet burning were hampered by the small size of the viewing ports and the fumes resulting from the combustion. The combustion bomb was then modified as shown in Figure 3 to permit better observation.

SPECIFIC CONSUMPTION RATE CONCEPT

Visual tests of free-jet burning, using red fuming nitric acid and mixed butyl mercaptan, suggested that there is a better measurement than the consumption rate in inches per second to describe the rate of combustion. This measurement, which has been termed *specific consumption rate*, is the ratio between the mass flow rate of the fluid mixture that is fed into the combustion zone and the volume of the combustion zone under steady state conditions. The idea for this measurement was the result of three observations:

(1) *At constant flow rate and constant pressure the flame was consistent in size and shape.* The flame usually had a cylindrical shape with a diameter of about ½ to ¾ in and a height varying from 2 to 5 in depending on flow rate. In addition, the flame appeared to be homogeneous in texture.

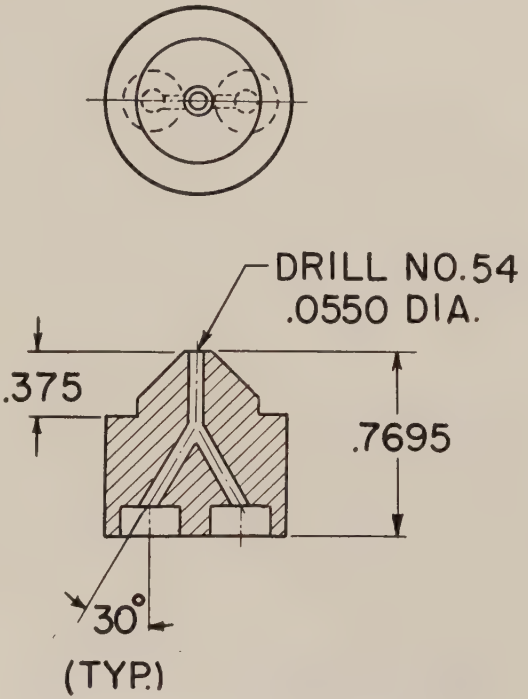

FIG. 6. Free-jet injector. Dimensions are in inches. (Official photograph, U. S. Navy.)

(2) *At constant combustion pressure an increased flow rate resulted in an increased flame volume* and an increase in the length of the unconfined liquid jet. A decrease in the flow rate resulted in the reverse.

(3) *At constant flow rate an increase in pressure resulted in a decreased flame volume* and a decrease in the length of the unconfined liquid jet. A decrease in pressure resulted in the reverse.

On the basis of the above observations it was concluded that for a given fuel and oxidizer combination at a fixed ratio, the flame volume under steady state conditions is a function of the mass flow rate and the pressure at which combustion

occurs. Since it is a fair assumption that at constant pressure the flame volume is directly proportional to the mass flow rate, the specific consumption rate is a valid measure of the combustion rate or overall reaction rate. The basic assumption can be verified experimentally. The reciprocal of the specific consumption rate, termed specific flame volume, volume of flame per unit mass flow rate at steady state conditions, is of equal interest and importance.

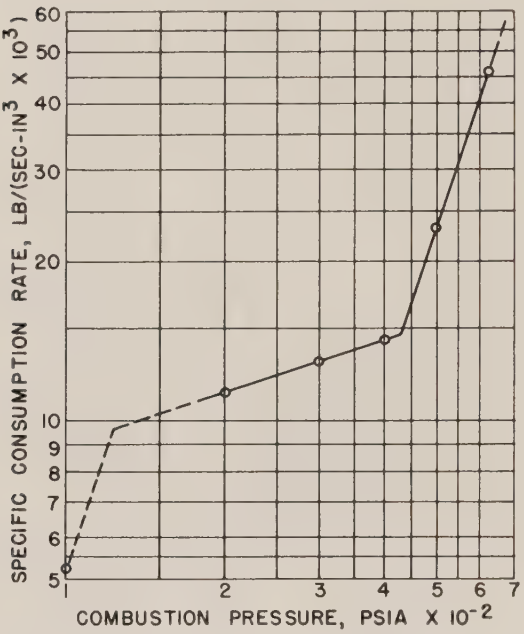

FIG. 7. Specific consumption rate of mixed butyl mercaptan and RFNA at an oxidizer/fuel ratio of 3.5. (Official photograph, U. S. Navy.)

EXPERIMENTAL

Tests were made to determine the specific consumption rate as a function of pressure for red fuming nitric acid and mixed butyl mercaptan at an oxidant to fuel ratio of 3.5 by weight. The red fuming nitric acid (RFNA) contained approximately 77.0 per cent nitric acid, 22.0 per cent nitrogen tetroxide and 1.0 per cent water.

The principal requirements set for these tests were that the flame be in a steady state condition and be stable with an unconfined jet of fluid between the injector exit and the flame. The requirement that the flame be stable was deemed necessary to avoid the effects of a heated injector on the rates of reaction. Photographs of the flame were taken to determine the volume of the flame as soon as the flame became steady so that each test was of short duration, usually lasting not more than 2 or 3 sec.

Flame volume determinations

The volumes of steady state flames were determined from photographs of the flames taken with a 4 x 5 in Speed Graphic camera. Both color (Kodak Ektachrome) and black and white film were used. Color film was found to be the better since the image of the flame was produced through the fumes in the bomb, provided they were not too dense; whereas with black and white film the fumes frequently obscured portions of the flame. The exposure times were $\frac{1}{100}$ sec for the color film and $\frac{1}{400}$ sec for the black and white film. For the purpose of obtaining the true size of the flame a vertical rod was placed on each side of the injector. These rods were two inches apart and provided the basis for correcting the photographic image to true size.

The determination of the flame volume from photographs of the flame is the most difficult part of the procedure. This is primarily due to the difficulty of obtaining clear photographs. Since the shape of the flame was more or less cylindrical, the volume of the flame was estimated on the basis of a cylindrical envelope. The outline of the flame was traced on paper (either from the negative or from an enlarged image) and a cylinder marked off over the outline. The dimensions of this cylinder were measured, corrected to true size, and the volume computed.

Effect of pressure

The effect of pressure on the specific consumption rate of mixed butyl mercaptan and red fuming nitric acid is shown in Figure 7. The specific consumption rate is apparently an exponential function of the pressure. The change in slope between 100 and 200 psia is questionable, and the curve is shown as a broken line in this region. The flame at 100 psia departed from the usual cylindrical shape which made volume determinations difficult. It is possible that inadequate mixing was obtained with the low flow rate used at 100 psia. The curve was plotted from average values, the average deviation being about plus or minus 13 per cent. Maximum deviation at any one pressure was about 25 per cent. The lower portion (200 to 430 psia) of the specific consumption rate curve may be represented by the equation:

$$R_f = 1.9 \times 10^{-3} P^{0.33} \qquad (1)$$

and the upper portion by:

$$R_f = 2.0 \times 10^{-10} P^{3.0} \quad (2)$$

where R_f = specific consumption rate (lb/sec/cu in) and P = pressure (psia).

Between 200 and 430 psia the flame was somewhat like a Bunsen burner flame except that it appeared more dense and more turbulent. The color was blue-white. Figure 8 shows a photograph of a free-jet flame at 200 psia with a flow rate of 0.008 lb/sec (3.63 gm/sec). The luminous zone at the top of the bomb above the flame was caused by the hot combustion products striking a carbon deposit.

FIG. 8. Free-jet flame of mixed butyl mercaptan and RFNA. The rods on each side of the flame are 2 in apart. Data in text. (Official photograph, U. S. Navy.)

At pressures above 430 psia the flow rate had to be increased markedly to maintain steady state combustion. If the flow rate was too low the flame pulsated. Whether or not the flame was actually extinguished and thus intermittent was not determined. Combustion could be made smooth and stable by increasing the flow rate sufficiently. Pulsating flames were observed frequently at 400 psia and occasionally at pressures as low as 350 psia. At combustion pressures below 350 psia no pulsations were obtained even at flow rates low enough to cause the flame to recede into the injector. This action served to emphasize the sudden increase in the pressure dependency of the specific consumption rate. For example, to maintain a flame of approximately the same volume when the pressure was increased from 300 to 400 psia, required an increase in the flow rate of about 20 per cent. With an increase in pressure from 400 to 500 psia, approximately a 100 per cent increase in the flow rate was required to maintain the same flame volume and achieve steady state burning.

Photographs of the flame, taken with the aid of a Strobo-lite, showed that at pressures below 430 psia the fluid jet extended a short distance (about ¼ in) into the flame and then broke up into droplets which appeared to extend throughout the flame. At pressures above 430 psia the fluid jet spread slightly immediately below the flame and did not extend into the flame as a jet. Definite droplets could not be found within the flame above 430 psia. It is possible that the jet broke up into a spray so fine that individual droplets could not be detected by the photographic technique used. Flames observed above 430 psia appeared to be more dense than flames obtained at lower pressure.

DISCUSSION

It is believed that the shift in the pressure dependency of the specific consumption rate that occurs at 430 psia represents a change in the reaction mechanism, probably a change in the rate controlling step. It is possible that this phenomenon is associated with the flow characteristics of a fluid jet discharging into a pressurized atmosphere. However, this seems doubtful since the shift in pressure dependency is rather abrupt. If the phenomenon were caused by the flow characteristics it should be a more gradual change.

Neglecting mixing effects, the time lapse between impingement and breakup of the fluid jet may be interpreted as a measure of the time required for liquid phase reactions. In cases where the jet breaks up into droplets, this time lapse might be considered as the reaction time of the fastest liquid phase reactions producing gaseous products in quantity. By considering the specific consumption rate as a vapor phase reaction rate, the relationship between the pressure dependence of the vapor and liquid phase reactions may be found. In addition, the specific consumption rate is convenient for kinetic interpretation and it is believed that overall energies of activation may be derived from it.

This paper was prepared to present techniques that may be used for the study of hypergolic

liquid combinations. The apparatus, with some modification, may also be used for the study of non-hypergolic liquid fuels and oxidizers and would be particularly advantageous for the study of non-miscible non-hypergolic combinations. The techniques and ideas presented herein may also find application in other fields of combustion research.

Acknowledgment

The permission of the Naval Ordnance Test Station to publish this work is gratefully acknowledged. Special acknowledgment is due Dr. H. K. Haussmann for his assistance.

REFERENCES

1. Stocks, G. W., and Wiseman, L. A.: Part I, ERDE Report No. 31/R/49.
2. Tait, C. W., Whittaker, A. G., and Williams, H.: J. Am. Roc. Soc., *85*, 83 (1951).
3. Kretschmar, G. G., and Wedaa, H. W.: J. Am. Optical Soc., *43*, 526 (1953).
4. Whitnack, G. C., et. al.: NOTS TM-319.

10

OSCILLATION OF THE FLAME FRONT BETWEEN TWO UNLIKE DROPLETS IN A BIPROPELLANT LIQUID SYSTEM[a]

By C. C. MIESSE

Introduction

One possible source of the oscillatory combustion which has been observed in the combustion chamber of a liquid-bipropellant system is oscillation of the flame front between a pair of fuel and oxidizer droplets. The object of this analysis

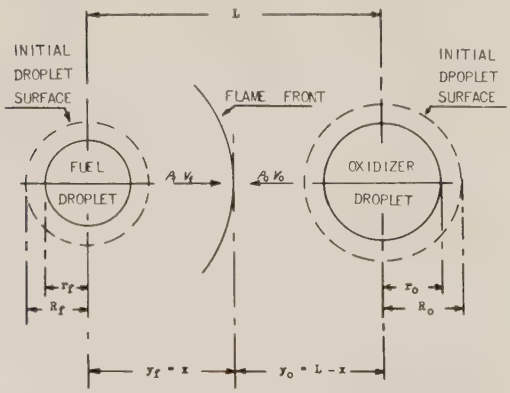

Fig. 1. Schematic diagram of flame configuration between fuel and oxidizer droplets.

is to investigate the stability of such a flame front under the following assumptions:

(1) Each of the droplets is spherical;

(2) The flame front is considered to be a surface;

(3) The phenomenon is controlled by the mass transfer of fuel and/or oxidizer vapors from the droplets to the flame front.

The idealized configuration under consideration is shown schematically in Figure 1.

From this diagram it is seen that the radii of the spherical fuel and oxidizer droplets are r_f and r_o respectively, that the distance between their centers is L, and that the distance from the center of the fuel droplet to the flame front is x. It will now be assumed that the position of the flame front is determined by the condition that the ratio of the diffusing vapors be stoichiometric.

Theoretical Analysis

Since there is a continual flow of vapors outward from the droplets, this stoichiometric condition can be expressed by the equation:

$$k\rho_f v_f = \rho_o v_o \tag{1}$$

where ρ_f and ρ_o are the densities and v_f and v_o are the linear velocities of the fuel and oxidizer vapors, respectively, at the flame front, and where k is the stoichiometric mixture ratio. The incremental area terms dA which should logically appear in equation (1) have been suppressed, since $dA_f = dA_o$. By considering each droplet to

[a] The work reported in this paper was performed under the sponsorship of the U. S. Air Force, Wright Air Development Center.

be a spherical vapor source, in the hydrodynamical sense, the velocities v can be expressed by the equation

$$v = \frac{M}{4\pi\rho y^2} \tag{2}$$

where M is the mass evaporation rate (considered as the strength of the vapor source), and y is the distance of the flame front from the center of the droplet. An approximation for the mass evaporation rate is given by Godsave[1] who equated the quantity of heat transferred to the droplet to the heat used in evaporating the liquid (in still air). The resultant equation for mass evaporation rate is

$$M = \frac{\ln (1 - c\Delta\theta/\Delta H)}{c(1/r - 1/y)/4\pi K} = \frac{D}{(1/r - 1/y)} \tag{3}$$

where $\Delta\theta$ is the difference between flame temperature and boiling temperature of the droplet, ΔH is the latent heat of vaporization of the droplet, c is the specific heat of the vapor, K is its thermal conductivity, and D is a function of the physical properties of the liquid and its vapor.

It must now be recognized that the flow of vapor from the evaporating droplet is not instantaneous, but requires a time lag, T, so that the vapor velocity at time t will be determined by the mass evaporation rate, M, for the previous time $(t - T)$. Hence, equation (2) can be rewritten as

$$v(t) = \frac{M(t - T)}{4\pi\rho[y(t)]^2} \tag{2a}$$

If y_f is represented by x, and y_o by $(L - x)$, substitution of equations (2a) and (3) into equation (1) results in the following equation for the flame position $x(t)$ as a function of time

$$\frac{x(t - T_f)\cdot r_f(t - T_f)}{[x(t - T_f) - r_f(t - T_f)][x(t)]^2} = \frac{k'[L - x(t - T_o)]\cdot r_o(t - T_o)}{[L - x(t - T_o) - r_o(t - T_o)][L - x(t)]^2} \tag{4}$$

where

$$k' = D_o/kD_f \tag{5}$$

Now let the flame position $x(t)$ be expressed as

$$x(t) = X(t) + g(t) \tag{6}$$

where $X(t)$ is the dominant component whose variation with time is due only to the shrinking of the droplets by evaporation, and where $g(t)$ is the small perturbation component due to the effect of the time-lag considerations. It is tacitly assumed that $g \ll X$. Substitution of equation (6) into equation (4) then leads to the following equations of the zero and first orders, respectively:

$$X^2(k'r_o - r_f) + Xr_f[2L - r_o(k' + 1)] - r_fL(L - r_o) = 0 \tag{7}$$

and

$$g(t - T) + A.g(t - T_o) + B.g(t) = 0 \tag{8}$$

where

$$A = 1/k' \tag{9}$$

and

$$B = 2L(L - r_o - X)/r_ok'X \tag{10}$$

In equations (9) and (10), it was assumed that the time lags T are sufficiently small so that $r(t - T) = r(t)$.

Zero-Order Solution

The solution of equation (7) is readily obtained as

$$X = \frac{r_f}{2(k'r_o - r_f)}\left[-2L + r_o(k' - 1) + \sqrt{4L^2 - 4Lr_o(k' + 1) + r_o^2(k' + 1)^2 + 4L(L - r_o)(k'r_o - r_f)/r_f}\right] \tag{11}$$

where the variation of the droplet radii with time can be expressed by the equation

$$r = \sqrt{R^2 - \lambda t/4} \tag{12}$$

where R is the original radius of the droplet, and λ is the "evaporation constant[2, 3, 4]." This equation, which was assumed by Probert[3], was confirmed experimentally by Godsave[2] and by Kumagai and Isoda[5]. Comparison of equations (3) and (12) indicates that, for $r \ll y$,

$$\lambda = 2D/\pi\rho' \tag{13}$$

where ρ' is the density of the liquid.

Obviously, the solution represented by equations (11) and (12) is non-oscillatory, and hence cannot be considered as a possible source of oscillatory combustion. However, it is necessary to examine this solution in order to ascertain what simplifying assumptions can be made for the solution of the non-linear transcendental equation (8). Accordingly, the typical values of $R_f = 0.0909$ cm, $R_o = 0.1074$ cm, $L = 0.762$ cm, and

$k' = 0.174$ were chosen, and the resultant variation of $X(t)$ was plotted in Figure 2. Inspection of this figure indicates that there is very little change in X until t_{crit} (for which $r_f = k'r_o$) is reached, at which time the flame front rapidly approaches the vanishing fuel droplet. In particular, it is noted that neither r_f, r_o, nor X varies by more than a few percent for the first half of the lifetime of the fuel droplet. Consequently, in the analysis that follows, these terms will be considered as essentially constant.

First-Order Solution

If essentially constant values of $r_f = R_f$, $r_o = R_o$, and $X(t) = X(O) = X$ are assumed,

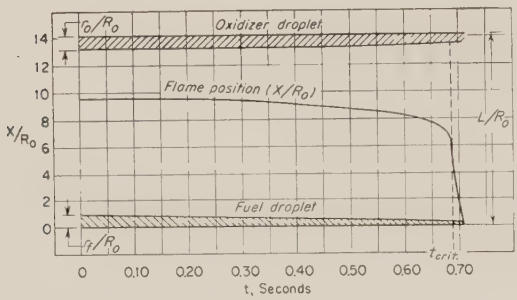

FIG. 2. Variation of flame front position between fuel and oxidizer droplets, assuming instantaneous transport processes.

equation (10) can be rewritten as

$$B = 2L(L - R_o - X)/k'R_oX$$
$$= 2L(bX - R_o)/k'R_oX \quad (10a)$$

where

$$b = (L - X)/X \quad (14)$$

This assumed constancy of the radii and of the gross flame position logically leads also to essentially constant values of T_f and T_o, so that these time lags can be related by the equation

$$T_o = qT_f = qT \quad (15)$$

Equation (8) thus becomes a finite difference equation with constant coefficients. It is well known that this type of equation can be satisfied by an exponential function with complex argument, the imaginary part of which represents an oscillation, and the real part of which prescribes the time rate of growth or decay of this oscillation. Hence, let

$$g(t) = N \exp\{(u + iw)t\}$$
$$= N e^{ut}[\cos(wt) + i \sin(wt)] \quad (16)$$

where N is the initial amplitude of the oscillation.

Substitution of equation (16) into equation (8) results in the following pair of equations, corresponding to the real and imaginary terms, respectively:

$$z \cos(wT) + Az^q \cos(qwT) = -B \quad (17)$$

and

$$z \sin(wT) + Az^q \sin(qwT) = 0 \quad (18)$$

where

$$z = e^{-uT} \quad (19)$$

From equations (17) and (18), it is seen that

$$\cos(wT) = \frac{A^2z^{2q} - z^2 - B^2}{2Bz} \quad (20)$$

and

$$\cos(qwT) = \frac{z^2 - A^2z^{2q} - B^2}{2ABz^q} \quad (21)$$

Solution of equations (20) and (21) for (wT) results in the equation

$$wT = 2n\pi - \cos^{-1}\left(\frac{A^2z^{2q} - z^2 - B^2}{2Bz}\right)$$
$$= \frac{1}{q}\left[2m\pi + \cos^{-1}\left(\frac{z^2 - A^2z^{2q} - B^2}{2ABz^q}\right)\right] \quad (22)$$

where m and n are integers, and where the reversal of the signs is necessitated by the conditions of equation (18). Equation (22) thus becomes an eigenvalue equation for z, which must be determined so that, for any given values of A, B, and q, and for any chosen integral value of m (which specifies the mode of oscillation), n will have an integral value.

The complex transcendental nature of this equation eliminates the possibility of an analytical solution, so that the permissible values of z must be determined by numerical methods. The range of values for z, however, can be obtained by setting equations (20) and (21) first equal to plus one, and then to minus one, since these are the limits of the cosine function. The resultant limiting equations can be represented by the single equation

$$z = \left|\frac{z + B}{A}\right|^{1/q} \quad (23)$$

Analysis of equation (23) reveals that the values of A and B determine the range of permissible values of z in the following manner:

(1) $B \leq (A - 1)$:

(a) $z \leq 1$, for $(2n - 1) \leq 1/q \leq 2n$

(b) $z > 1$ (24)

(2) $(A - 1) \leq B \leq (A + 1)$: $z \lesssim 1$

(3) $B > (A + 1)$: $z > 1$

Since $z > 1$ represents a decrease in the amplitude of oscillation, it will be useful to determine that value of L (designated by L_s) above which all oscillations will decay. From equations (7), (10a), and (24-3),

$$L_s = \left(\tfrac{1}{2}\right)\cdot(R_f + R_o \pm \sqrt{(R_f + R_o)^2 + 3R_fR_o(k' + 1)^2/k'}) \quad (25)$$

An upper limit on the value of n, for any chosen integral value of m, can be obtained by setting the angles of equation (22) equal to π. Hence,

$$n \leq m/q + (1 + 1/q)/2 \quad (26)$$

Since any solution of equation (22) will prescribe a value for (wT), as well as for z, the corresponding frequency of oscillation, f, for any mode, can be obtained readily from the equation

$$f = w/2\pi = \frac{1}{2\pi qT}\left\{2m\pi + \cos^{-1}\left(\frac{z^2 - A^2z^{2q} - B^2}{2ABz^q}\right)\right\} \quad (27)$$

The first order solution is now complete, except for the determination of the time lags T, which can obviously be represented by the equation

$$T = \int_r^y \frac{ds}{v} \doteq 4\pi \int_R^y \frac{\rho s^2 ds}{M} \quad (28)$$

If it is assumed that the vapors are flowing into vacuous surroundings, then the isothermal density will vary as the concentration, hence as the reciprocal of the radius. The reasonable assumptions (a) of a temperature distribution which increases linearly with the radius, and (b) of the validity of the perfect gas law, together with the above assumption regarding the isothermal density distribution, then lead to the following equation for the actual density distribution:

$$\rho \doteq R^2\rho''/s^2 \quad (29)$$

where ρ'' is the saturation density of the vapor on the surface of the droplet, and s is the radial distance from the center of the droplet. Substitution of equations (3) and (29) into equation (28) results in the following equations for the time lags:

$$T_f = \frac{4\pi R_f^2\rho_f''}{D_f}(1/R_f - 1/X)\int_{R_f}^{X} ds = \frac{4\pi R_f\rho_f''}{D_f}\cdot\frac{(X - R_f)^2}{X} \quad (30)$$

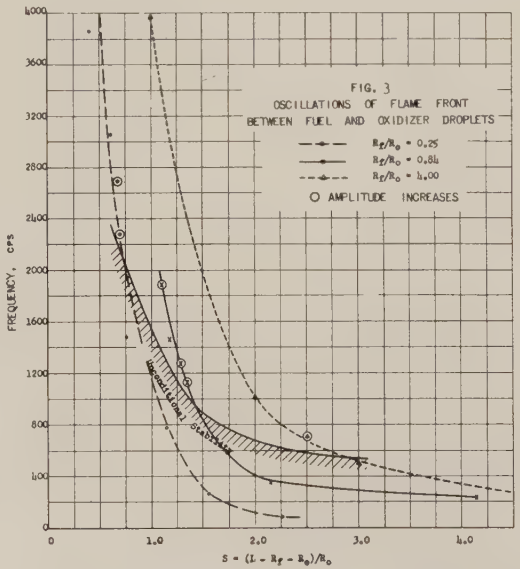

FIG. 3. Oscillations of flame front between fuel and oxidizer droplets.

and

$$T_o = \frac{4\pi R_o^2\rho_o''}{D_o}(1/R_o - 1/bX)\int_{R_o}^{bX} ds = \frac{4\pi R_o\rho_o''}{D_o}\cdot\frac{(bX - R_o)^2}{bX} \quad (31)$$

The value of the factor q can then be obtained by substituting equations (30) and (31) into equation (15):

$$q = T_o/T_f = \frac{R_o\rho_o''D_f}{bR_f\rho_f''D_o}\cdot\left(\frac{bX - R_o}{X - R_f}\right)^2 \quad (32)$$

Figure 3 shows the variation of zero-mode ($m = 0$) frequency with a relative separation

distance $(L - R_f - R_o)/R_o$, as predicted by equation (27). The previous value of the parameter $k' = 0.174$ was used in the computations. It is seen from this figure that the frequency spectrum is infinite, and that the frequency increases as the distance between the droplets decreases. Those frequencies for which an increase in amplitude is predicted are denoted by large circles, and the boundary of the region of unconditional stability (decay in amplitude of oscillation, for $B > A + 1$) is marked by a heavy line. This boundary line indicates that, for the assumed value of the parameter (k'), the stability region will increase as the fuel/oxidizer drop-size ratio is decreased.

The criterion for the growth of the stability region can actually be determined analytically by differentiation of equation (25a) with respect to the size ratio $(Q = R_f/R_o)$:

$$\frac{\partial(L_s/R_o)}{\partial Q} = \frac{1}{2}\left[\frac{1 + 2(Q + 1) + 3(1 + k')^2/k'}{2\sqrt{(Q + 1)^2 + 3Q(1 + k')^2/k'}}\right] > 0 \tag{33}$$

which indicates that, for a constant value of R_o, the limiting value L_s will increase as the size ratio increases, thus diminishing the size of the stability region. Conversely, for a constant value of R_f, the stability region will increase as R_o decreases.

The effect of varying the property value (k') can also be determined by differentiation of equation (25a) with respect to k':

$$\frac{\partial(L_s/R_o)}{\partial k'} = \frac{3Q(1 - 1/k'^2)}{4\sqrt{(Q + 1)^2 + 3Q(k' + 1)^2/k'}} \tag{34}$$

which is positive for $k' > 1$, and negative for $k' < 1$. Hence, for $k' < 1$, the stability region will increase with an increase in k', and the largest stability region will occur when $k' = 1$. Conversely, for $k' > 1$, the stability region will increase as k' decreases.

Conclusions

The following conclusions can now be drawn as a result of this analysis:

(1) Oscillations of any frequency can be established by the instability of the flame front between two unlike droplets in a bipropellant combustion chamber.

(2) As the distance between the droplets increases, the frequency decreases.

(3) The frequency increases with an increase in the size ratio of fuel to oxidizer droplets.

(4) The region of unconditional stability increases with a decrease in the size of either droplet.

(5) The region of unconditional stability reaches a maximum range for a value of $k' = 1$, and decreases in size as the value of the parameter k' differs from unity (in either direction).

Nomenclature

A = $1/k'$, constant coefficient
B = variable coefficient
b = $(L - X)/X$, ratio of flame distances
c = specific heat
D = $4\pi K[\ln (1 - c\Delta\theta/\Delta H)]/c$
dA = element of flame surface
e = Napierian logarithmic base
f = frequency of oscillation
g = $N \exp\{(u + iw)t\}$, oscillatory componponent of flame position
K = thermal conductivity of vapor
k = stoichiometric mixture ratio
k' = D_o/kD_f, parameter
L = distance between droplet centers
M = mass evaporation rate
m = integer, mode of oscillation
N = initial amplitude of oscillation
n = integer
Q = R_f/R_o, ratio of initial radii
q = T_o/T_f, ratio of time lags
R = initial radius of droplet
r = variable radius of droplet
S = $(L - R_f - R_o)/R_o$, dimensionless separation distance
s = radial distance from center of droplet
T = time lag
t = time
u = exponential rate of growth of oscillation
v = radial velocity of diffusing vapors
w = $2\pi f$, imaginary coefficient
X = non-oscillatory component of flame position
x = $X + g$, flame position
y = distance from flame front to center of droplet
z = e^{-uT}
ΔH = latent heat of vaporization
$\Delta\theta$ = temperature difference between flame and droplet
ρ = variable vapor denisty
ρ' = droplet density
ρ'' = saturation vapor density
λ = $2D/\pi\rho'$, evaporation constant

SUBSCRIPTS

f = fuel
o = oxidizer
s = stability limit

REFERENCES

1. Godsave, G. A. E.: National Gas Turbine Establishment Report No. R. 66, March 1950, Ministry of Supply, Millbank, London, TPA3/TIB.
2. Godsave, G. A. E.: National Gas Turbine Establishment Report No. R. 87, April 1951, Ministry of Supply, Millbank, London, TPA3/TIB.
3. Probert, R. P.: Phil. Mag., *37*, 94–105 (1936).
4. Godsave, G. A. E.: Nature, *166*, 1111 (1950).
5. Kumagai, S., and Isoda, H.: Nature, *166*, 1111 (1950).

Discussion by Luigi Crocco*

I do not intend to criticize any of the assumptions that have been introduced for the solution of this problem. These assumptions are extremely rough, but the problem cannot probably be treated without very drastic simplifications. I would like only to observe that the possibility of unstable solutions arises substantially from the introduction of the two time lags; this introduction has been made in a somewhat arbitrary way, but it should be possible to justify it on more rigorous grounds through the diffusion equations.

Accepting the results of this paper on the existence of oscillatory flames it is interesting to evaluate the possible implications for combustion instability. The frequency of the oscillatory flame between a pair of droplets would be determined by the local geometrical conditions, and would be therefore distributed, for the large number of droplets present in the chamber, on a certain range of values. Even assuming that the statistical distribution of the conditions could result in a preferred frequency, and supposing that this frequency coincides with one of the natural frequencies of the chamber, still the phases of oscillation of the different flames are distributed at random. In order that the oscillations of the flames and the acoustical modes of the chamber may interfere, a coordinating factor should be present to correlate the phases of oscillation.

However, the theory does not predict the possibility of any such coordinating factor. It seems to me, therefore, that the phenomenon studied in this paper cannot be connected with unstable operation, although it might possibly be responsible for rough operation, where the pressure oscillations are distributed more or less at random.

* Robert H. Goddard Professor of Jet Propulsion, Princeton University.

Author's Reply

The author is deeply indebted to Professor Crocco for pointing out that the mechanism proposed in subject paper allows for excitation sources over a wide range of frequencies. In an undamped system, the mere existence of an oscillation at the resonant frequency of the chamber is sufficient to excite resonance, which then provides the coordinating factor.* In a damped system, which requires sufficient energy to induce chamber resonance, the possibility of an additional phase-coordinating factor can be shown in the following manner: Let us suppose that two pairs of droplets, the flame fronts for which oscillate in phase opposition at the preferred frequency, include one droplet which is common to both pairs. Then, as the stronger of the two resultant flame fronts approaches the common droplet, the droplet's evaporation rate will increase over all of its surface, thus tending to push the stronger flame front away and, at the same time, tending to hold the weaker flame front at its remote position. This predominant effect of existing stronger (more rapidly-burning) flame fronts thus provides a mechanism for correlating the phases of oscillation.

* Combustion Instability in Rocket Motors, L. Crocco, Tech. Presentations before the AGARD Combustion Panel, Rome AGARD Conference, 1952, pp 32–53.

11

A STUDY OF FAST REACTIONS IN FUEL-OXIDANT SYSTEMS

Anhydrous Hydrazine with 100 per cent Nitric Acid[a]

By MARTIN KILPATRICK AND LOUIS L. BAKER, JR.

Introduction

Certain liquid fuels when brought into contact with strong oxidizing agents will ignite spontaneously. The ignition of such systems may take place instantaneously when the liquids are first brought into contact or there may be a time delay. Most of the studies of the ignition delay in such systems have employed methods designed to simulate conditions met in a rocket motor. In a typical rocket motor the two reactants are contacted by the impingement of a number of fuel and oxidant streams in a relatively unconfined area. Observation of the time required for ignition under such conditions does not differentiate between the delay created by the time required to achieve efficient mixing and the delay caused by an actual chemical induction period.

Methods have been devised to achieve the complete mixing of useful amounts of two liquids in a very short time. The work of Hartridge and Roughton,[1] Chance,[2] and McKinney and Kilpatrick[3] has proven conclusively that it is possible to effect the complete intermixing of two liquids and begin observation of the resulting mixture only a few milliseconds after the initial contact. These methods have not previously been applied to the study of the ignition of fuel-oxidant mixtures. The present research is an attempt to apply the mixing methods of Roughton, Chance, and McKinney and Kilpatrick to the problem of the self-ignition of fuel-oxidant systems and to study the associated reactions.

Ignition Delay Studies

Most of the impetus for the study of the ignition delay time of liquid fuel-oxidant systems is due to the potential use of such systems in rocket motors. Systems which do not ignite spontaneously can be used successfully in rocket motors if some external means of ignition can be found. From a practical standpoint, however, it is preferable to employ a system that will ignite spontaneously. In such a rocket motor it is imperative that ignition take place in a very short time after contact of the reactants. An excessive delay will cause the unreacted materials to accumulate in the motor chamber; ignition could then cause a destructive explosion. For this reason the study of hypergolic ignition (self-ignition) is of great practical importance in the field of rocket technology.

Some of the experimental variables which must be controlled for the precise measurement of ignition delay time include: (1) the reactant ratio, (2) the time required to effect complete mixing, (3) the chemical composition of the reactants, (4) the ambient temperature, and (5) the ambient pressure.

Studies of the ignition delay of the systems hydrazine-nitric acid, furfuryl alcohol-nitric acid, and liquid ammonia-hydrazine mixtures-nitric acid have been carried out in a small rocket motor.[4] The reactants were contacted by the impingement of a single fuel stream with a single oxidant stream. The nominal values obtained for optimum test conditions are given in Table 1.

The effect of reactant ratio on ignition delay time, however, is not clear under the uncertain mixing conditions resulting from the impingement of two streams in an unconfined space. If the complete intermixing could be effected in a time very short compared to the ignition delay time, then the measured delay would be the true chemical delay or induction period, and a change of the reactant ratio should lead to a different chemical delay time. When ignition takes place before mixing is completed, and the remainder of the fluid ignites, reactant concentrations of this igniting mixture cannot be known.

Table 2 makes evident the delay due to incomplete mixing by comparing the results obtained for furfuryl alcohol-white fuming nitric acid by a refined open-cup apparatus due to

[a] This research is part of the work being done in the Department of Chemistry of Illinois Institute of Technology, supported by the Office of Naval Research under Contract N7onr-32913. This paper is abstracted from part of the dissertation submitted by Louis L. Baker, Jr. to the Graduate School of Illinois Institute of Technology in partial fulfillment of the requirements for the degree of Doctor of Philosophy.

Gunn[5] with those of the impingement method.

The impingement method would be expected to yield smaller ignition delay times because of more efficient mixing than the open-cup method due to greater turbulence and impact associated with impinging streams.

The present study was undertaken on the premise that a fundamental approach to the phenomenon of ignition delay was possible only if complete mixing could be accomplished in a time shorter than the ignition delay time. Studies in this laboratory[3] had already shown that 1 ml of one reactant could be contacted and effectively mixed with 25 ml of a second reactant in less than 10 msec. It was, therefore, expected that a few milliliters of each of the reactants could be mixed in much less time than ignition delay times such as those reported in Tables 1 and 2.

Rapid Mixing Studies

The problem of rapid and efficient mixing of dilute solutions has been recently reviewed by Roughton and Chance,[6] and the mixing of liquids for reactions evolving gases investigated by McKinney and Kilpatrick.[3] In general, the mixers are of two shapes, T and Y, the T type being preferred. In the T-type mixer, the jets may be directly opposed or arranged so that the two liquids stream tangentially into the mixing area. The tangential arrangement was found to be better at low flow rates but both methods of contacting the liquids gave about equally efficient mixing at high flow rates. The method of opposing jets was adopted in our earlier studies.[3, 7, 8]

Our findings that the time for mixing by the use of the streaming method cannot readily be reduced below 0.1 msec seem to be confirmed by the fact that recent discussions of fast reactions[9] have emphasized relaxation methods for measuring fast reactions where mixing of the reactants is not involved. Such methods may well be developed for measurement of reactions having half-times of microseconds.

Experimental Methods

APPARATUS

The apparatus, which has been described previously,[8, 10] is referred to as Reactor II to distinguish it from an apparatus employed earlier in this laboratory for the study of fast reactions. Reactor II, in combination with the pneumatic injector of Neas, Raymond and Ewing,[3, 11] is capable of contacting and mixing a few cubic centimeters of two liquids in a few milliseconds. The operation of the apparatus will be briefly reviewed. A diagram of the fluid mechanical system of the reactor is shown in Figure 1. The pneumatic injector, not shown in the figure, is located above the reactor. It functions as a quick opening valve discharging nitrogen gas at pressures up to 2000 psi into the area P behind the driving piston. As the driving piston descends,

Table 1. Ignition Delay in a Small Rocket Motor[4]

Reactants	Temperature	Ignition Delay
	°C	*msec*
Hydrazine, 96 per cent—RFNA*	21	3.1 ± 1.4
Hydrazine, 96 per cent—WFNA†	21	5.0 ± 1.7
Furfuryl alcohol —WFNA	21	16.6 ± 2.4
Furfuryl alcohol—WFNA	−29	22 to 40
Hydrazine, 71.5 per cent—WFNA	25	ca. 37
Hydrazine, 71.5 per cent—RFNA	−48	ca. 37
Ammonia, 14.1 per cent hydrazine—RFNA	−36	6 to 10
Ammonia, 9.5 per cent hydrazine—RFNA	−35 to −40	ca. 14
Ammonia, 5.0 per cent hydrazine—RFNA	−37 to −47	37‡

* RFNA, red fuming nitric acid, 24 per cent NO_2.

† WFNA, white fuming nitric acid, 96 per cent HNO_3.

‡ Sporadic ignition.

Table 2. Ignition Delay for Furfuryl Alcohol-White Fuming Nitric Acid

Initial Temp.	Ignition Delay Time	
	Open-cup[5]	Impingement[4]
°C	*msec*	*msec*
Room	36	16.6
−15	180	—
−29	—	22–40

the two smaller pistons F_1 and F_1' are driven downward. This design was an improvement over that of Reactor I, giving a substantial hydraulic advantage in having the large piston drive the two smaller ones and insuring simultaneous descent of the two small pistons during injection. The liquids to be contacted are initially contained below the smaller pistons in the areas designated as P_1 and P_1'. During injection, the liquids flow through the lead tubes P_2 and P_2', the jets P_3 and

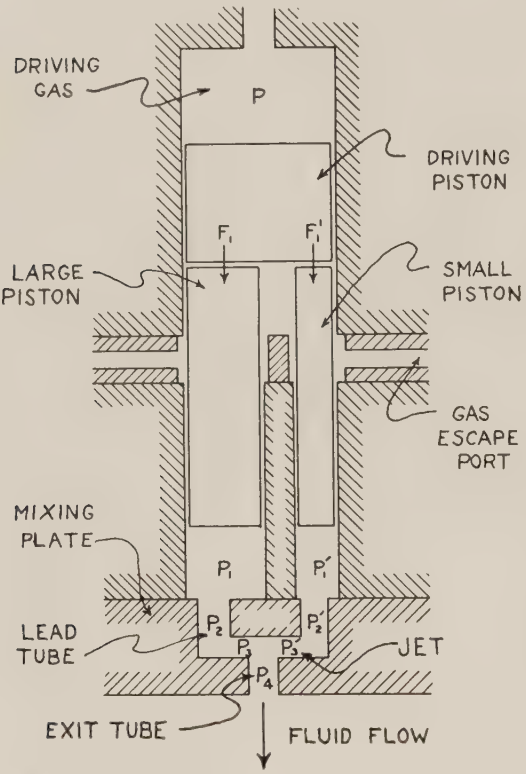

FIG. 1. Schematic diagram of fluid mechanical system of Reactor II.

P_3', and mix in the exit tube P_4. The mixed solution is then ejected into a closed volume of 339 cc where reaction occurs.

The reactor was designed to allow for immersion in a low temperature bath. The volume ratio of the reactants could be varied over a range from approximately 4:1 to 1:1 by the use of fittings and additional pistons. The mixing pattern could be varied by using additional mixing plates of differing design. For this study, a T-type mixing plate designed in accordance with the principles set forth by Roughton and Chance was used. The simultaneous descent of the two small pistons insured uniformity of the mixing.

The reactions under study were followed by several techniques, but mainly by measurement of the transient pressure. The pressure sensitive element was a diaphragm type strain gage manufactured by the Statham Laboratories, Inc. The strain gage is in the form of a balanced bridge, the output being supplied by an AC carrier wave, and frequencies of the order of 1000 cps were used. The unbalance of the bridge was amplified and applied to the vertical plates of a cathode-ray oscilloscope. It was found by calibration against known static pressures that the amplitude of the oscilloscope pattern was accurately proportional to the applied pressure. The natural frequency of the strain gage was stated by the manufacturer to be in excess of 2000 cps so that pressure events occurring in a time of the order of a millisecond should be accurately reproduced. The horizontal plates of the oscilloscope were connected to a single sweep generator which was triggered automatically by the closing of a contact located in the penumatic injector. The oscilloscope sweep normally began between 1 and 1.5 msec before the beginning of injection. The record of the transient pressure was obtained by photographing the screen of the oscilloscope.

Another method of following the reactions was by the measurement of light emission. The output of a vacuum phototube-amplifier combination was connected to the vertical plates of a second oscilloscope. The horizontal plates were driven by the same sweep generator used for the transient pressure recording system. In some cases, the time distribution of the light emission was obtained; in others, only the time corresponding to the onset of light emission. Simultaneous measurements of the transient pressure and the light emission were made possible through the use of an additional camera.

The progress of the injection could be followed by means of an electronic timer. The timer consisted of a serrated brass rod connected to the moving piston system. A light beam passing between the serrations on the rod was focussed on a phototube cathode. During injection, the serrations on the moving rod interrupted the beam and caused a varying light intensity to fall on the phototube, and the amplified output from the phototube was applied to the vertical plates of an oscilloscope. An analysis of the resulting oscilloscope trace gave the time corresponding to a number of positions of the pistons with respect to the stationary light beam. The timer was operated simultaneously with the

transient pressure measuring system to give a record of both the injection process and the pressure rise.

The final pressure of the product gases was measured by venting the reactor to a glass reservoir by means of a needle vave and measuring the pressure on a mercury manometer.

The ignition delay of the fuel-oxidant systems was determined by simultaneous injection and transient pressure measurements. The time between the beginning of the injection process (first contact of the reactants) and the beginning of the pressure rise was obtained with an accuracy of about ±0.5 msec. The observed delay had to be corrected for the time required for the first pressure pulse to travel from the reactor to the diaphragm of the strain gage, a distance of about 18 in. If the initial pressure pulse was propagated at the speed of sound in ordinary air, it would have required 1.3 msec. This value was used for the correction of the observed data. Even if the pulse were propagated as a shock wave, it it was unlikely that the pulse would have reached the gage in a significantly shorter time because of the irregular path.

Simultaneous light emission and transient pressure measurements were made to establish the fact that the beginning of the pressure rise and the onset of light emission occurred simultaneously. Again the experimental results had to be corrected for the transit time of the initial pressure pulse.

RATE OF INJECTION

A number of measurements were made of the injection rates obtainable when water was injected into the mixing area from both cylinders of the reactor. The runs were made with the 1:1 ratio, the stroke of the piston system being set at ⅞ in, and approximately 1.1 cc of water was ejected from each cylinder. Some of the data for different driving pressures are shown in Figure 2. The linearity of the plots indicated that the rate of descent of the piston system and hence the injection rate was constant throughout injection. The linearity further indicated that the moving parts accelerated very rapidly to the equilibrium velocity. The data obtained for the injection of water are shown in Table 3. The rate of injection is expressed as the time required for the pistons to descend ⅞ in. Runs 114 to 120 inclusive were made with loosely fitting neoprene piston gaskets and runs 123 and 124 with very tight gaskets, in order to test the effect of gasket resistance. The gasket resistance had only a small effect on the measured injection rate. Two runs, 73 and 98, were made using the 4:1 injection ratio. In this case, 2.84 cc of water was injected from the large cylinder and 0.74 cc from the small cylinder of the reactor.

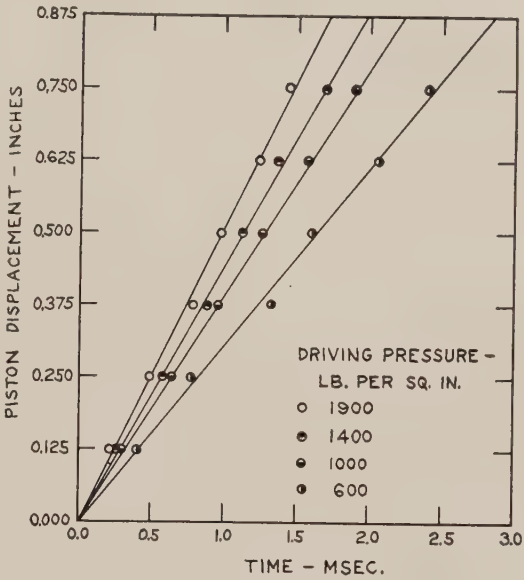

FIG. 2. Injection rate measurements, Reactor II

TABLE 3. INJECTION RATE MEASUREMENTS WITH WATER

Run	Reactant Ratio	Pressure of Driving Gas	Injection Time
		psi	*msec*
114	1:1	1950	1.79
119	1:1	1900	1.71
123	1:1	1700	1.91
124	1:1	1700	1.91
117	1:1	1400	1.96
116	1:1	1000	2.21
120	1:1	600	2.84
73	4:1	1800	4.27
98	4:1	1700	4.31

A rough calculation of the injection rates was made based upon empirical relations found in standard engineering treatises.[12, 13] The values calculated for the 1:1 ratio for the water injection are shown in Figure 3 as the dotted line. It is evident that the calculations predict a much more rapid injection rate than that observed. The calculations indicate that the flow rate should be roughly proportional to the square root of the driving gas pressure, and Chance[2] obtained in-

jection rates that were precisely proportional to the square root of the pressure drop using identical mixing systems but at much smaller pressure drops. It seemed likely, in view of the curvature of the observed plot, that the resistance to gas flow in the pneumatic injector might be slowing the injection. If this were the case, there would have been a pressure drop due to the nitrogen flow from the gas storage reservoir of the pneumatic injector to the driving cylinder, and the pressure

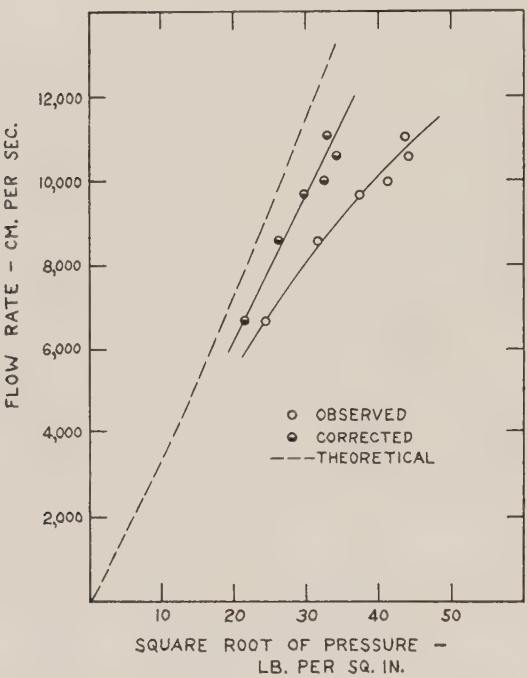

FIG. 3. Linear flow rate in the exit tube of Reactor II as a function of the square root of the driving gas pressure.

actually driving the large piston would then have been less than the value recorded.

A rough calculation of the pressure drop was made according to a method outlined by Beale and Docksey,[14] and the measured driving pressures for the runs plotted in Figure 3 were corrected for the pressure drop. The corrected data show much better proportionality between the injection rate and the square root of the driving gas pressure, although the corrected data still show a slower flow rate than those predicted by the fluid mechanical calculations. These calculations were made on the basis that the injection rate was determined entirely by the resistance to fluid flow and not by the gasket resistance.

RATE OF MIXING

The rate at which two reactants are contacted is not necessarily equal to the rate at which they are mixed. Reactor II has been applied to the study of the reaction of sodium-potassium alloy and water.[8] For this reaction it was found that the pressure rise, corresponding to hydrogen evolution, was completed in a time nearly equal to the measured time of completion of the injection. This would suggest that the mixing rate was nearly equal to the injection rate.

A number of previous investigations have been made of the efficiency obtainable for the mixing of equal volumes of reactant solutions in T-type mixers.[6] These studies indicate that the reactants should be thoroughly mixed in our reactor. In our reactor the mixing plate used has two jets of 2.5 mm diameter discharging into an exit tube of 3.9 mm diameter. A T-type mixer described by Roughton[6] and due to Trowse[15] also employs two jets. The diameter of the jets and the exit tube (observation tube) was 0.7 mm. Trowse found that the reactant solutions were 97 per cent mixed at a point 5.7 mm downstream from the jets. His measurements were made at a linear flow velocity at the exit tube of 440 cm/sec. Millikan[16] studied the extent of mixing in another T-type mixer as a function of the flow velocity. He found that the distance downstream to the point of 97 per cent mixing rapidly moved toward the point of first contact as the flow velocity increased. The linear flow velocities in the exit tube of our reactor ranged from 5,000 to 11,000 cm/sec so that mixing should be complete within the 8 mm length of the exit tube of the reactor used in the present study. To further insure the completeness of mixing, the stream emerging from the exit tube impinged on a baffle plate only 25 mm from the exit tube.

The time of residence of the stream in the exit tube of the reactor for the total range of flow velocities varied between 0.07 and 0.16 msec. For the study of ignition delay, the injection rate is of interest only as it affects the mixing efficiency. It is only the time between the contact and the completion of mixing of a given fluid element that is of importance, since presumably the first element of fluid to be injected is the one that will first ignite.

PREPARATION OF MATERIALS

Nitric acid

The acid was prepared by the vacuum distillation of an equal volume mixture of commercial 95 per cent nitric and sulfuric acids in an all-glass apparatus. The mixture was cooled to 0°C before reducing the pressure to 10^{-4} mm Hg, and the anhydrous nitric acid was collected in a trap cooled by a mixture of dry ice and trichloroethylene at a rate of 2 cc per hour. The acid, which consistently analyzed between 100.2 and 100.8 per cent HNO_3 by titration, was stored at dry ice temperature to avoid decomposition.

Hydrazine

The hydrazine was prepared from commercial anhydrous hydrazine, about 95 per cent N_2H_4, by refluxing in an all-glass distilling apparatus with an equal quantity of calcium or barium oxide at approximately 50 mm Hg. The hydrazine was then fractionally distilled, the first half collected, and analyzed by direct titration with HCl and by the iodate method using wool red as an internal indicator. The material was found to be 97.7 to 99.0 per cent N_2H_4.

Aniline

Aniline was purified by distillation from zinc dust. The product was colorless and distilled at 182°C under a pressure of 750 mm Hg. The refractive index was found to be 1.4791 at 32.5°C.

Hydrogen peroxide

High strength hydrogen peroxide was analyzed by titration with ceric sulfate and found to contain 84.5 per cent H_2O_2 by weight.

Ammonia-hydrazine mixtures

Anhydrous hydrazine was weighed into a small Erlenmeyer flask fitted with a ground glass joint, attached to the vacuum line, and the system evacuated after freezing in a liquid nitrogen bath. Anhydrous ammonia was transferred from a tank to a flask of known volume, the amount being determined by the gas pressure, and condensed into the flask with the hydrazine. The procedure was repeated until the desired amount of ammonia had been added and the mixture was stored at the temperature of dry ice.

Experimental Results

THE HYDRAZINE-NITRIC ACID REACTION

A typical simultaneous measurement of injection and transient pressure for a near stoichiometric mixture of hydrazine and nitric acid is shown in Figure 4. The pressure rise began 2.2 msec after the beginning of injection. Correcting by the 1.3 msec required for the pressure impulse

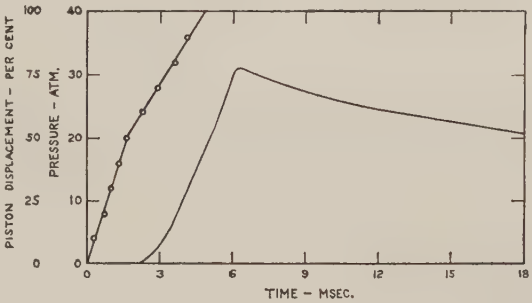

FIG. 4. Simultaneous measurement of injection rate and pressure rise in the reaction of one and one-half volumes of nitric acid with one volume of hydrazine, run 142, Reactor II.

TABLE 4. TRANSIENT PRESSURE AND INJECTION MEASUREMENTS. HYDRAZINE-NITRIC ACID REACTION

Volume HNO_3	Volume N_2H_4	Mole Ratio HNO_3: N_2H_4	Maximum Pressure Rise	Final Pressure	Overall Injection Time	Ignition Delay
cc	*cc*		*atm*	*atm*	*msec*	*msec*
2.84	0.74	2.87	23.4	2.66	9.2	0.2
1.59	0.74	1.61	31.6	2.21	5.4	0.5
1.11	0.74	1.12	31.7	1.80	4.9	0.9
1.11	1.11	0.75	46.7	3.35	4.7	0.1
0.74	1.11	0.51	43.2	3.57	4.6	0.2
0.74	1.59	0.352	51.3	5.26	6.4	0.4

to reach the diaphragm of the strain gage, the ignition delay was 0.9 msec. The average ignition delays for all of the ratios studied of the hydrazine-nitric acid reaction are given in the last column of Table 4. The maximum pressure rises obtained from the transient pressure record are given in the fourth column and the final pressures calculated from the manometer reading, in the fifth column.

The plot of piston displacement vs. time in Figure 4 showed a definite break in the slope. No such break was observed in any of the results obtained for the injection of water. The sudden slowing of the injection rate may be attributed to

the ignition of the reaction, and the constancy of the injection velocity near the completion of

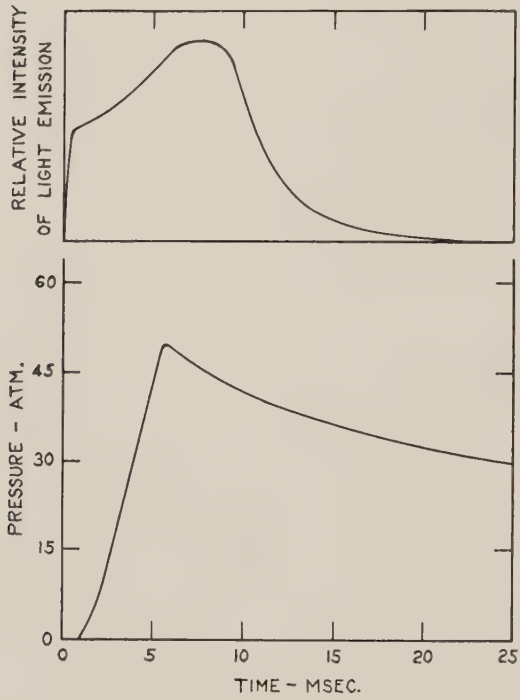

FIG. 5. Pressure rise and light intensity in reaction of two volumes of hydrazine with one volume of nitric acid, run 152, Reactor II.

TABLE 5. IGNITION DELAY BY TRANSIENT PRESSURE MEASUREMENTS

Run	Fuel	Oxidant	Mole Ratio Oxidant-to-Fuel	Maximum Pressure	Ignition Delay
				atm	*msec*
157	Aniline	Nitric	8.18	42	2.3
158		acid		25	1.2
163	Hydrazine	Hydrogen	1.15	42	0.1
165		peroxide		55	1.1
162				58	2.2
166	Hydrazine	Hydrogen	2.46	32	1.3
167		peroxide		41	1.7

injection suggests that a stable flame front was produced within the exit tube before the injection was completed. Because of this slowing of the injection rate, the overall injection time was substantially longer than the values obtained for the injection of water. The average values of the overall injection times are given in the sixth column of Table 4.

The simultaneous measurements of the transient pressure and the light emission showed that the light emission preceded the pressure rise by 0.2 to 1.6 msec. After correction for the transit time of the initial pressure pulse, it was concluded that the beginning of the pressure rise coincided, within experimental error, with the beginning of visible light emission. A typical result of the simultaneous measurement of light emission and transient pressure is shown in Figure 5 for the reaction of nitric acid with a slight excess of hydrazine.

THE HYDRAZINE-HYDROGEN PEROXIDE REACTION

The results for the hydrazine-hydrogen peroxide reaction are reported in Table 5, and the results of the simultaneous measurement of injection and transient pressure for two runs at oxidant-to-fuel ratio of 1.15 are shown in Figures 6 and 7. In run 163 the change in the injection rate is again apparent, but was not found in run 162, and this is interpreted to mean that here the ignition did not occur until injection was completed.

For the other run made at this same oxidant-to-fuel ratio the results were not conclusive. As shown in Table 5, the ignition delays reported for the 1.15 oxidant-to-fuel ratio were less consistent than those for the 2.46 ratio. In the latter case, ignition occurred during the course of injection. Simultaneous measurements of the light emission and the transient pressure for both reactant ratios showed that the beginning of visible light emission coincided with the beginning of the pressure rise.

THE ANILINE-NITRIC ACID REACTION

Table 5 also shows two runs for the reaction of aniline with nitric acid. The mixing plate was damaged in both of these runs. It is likely that during ejection, ignition was delayed and the flame may have flashed back with detonation velocity to the exit tube.

THE REACTION BETWEEN LIQUID AMMONIA-HYDRAZINE MIXTURES AND NITRIC ACID

For these studies the reactor was immersed in a low temperature bath, and the temperature before injection was measured by a thermocouple located close to the reactant solutions. Since injection rate measurements could not be made

with the reactor immersed in the bath, ignition delay data were obtained from simultaneous measurements of the transient pressure and the light emission. The results are reported in Table 6.

It was necessary to utilize the fact that injection began from 1.0 to 1.5 msec after the contact closed in the pneumatic injector. This was established from observations made under conditions where injection measurements could be made. An average value of 1.2 msec was taken as the time interval. It can be seen from the data that ignition occurred with a delay of only 2.9 msec at a concentration of only 2.7 per cent hydrazine although in two other runs no ignition occurred. A run was made of the reaction of nitric acid with pure ammonia and no ignition occurred.

Discussion

The longest ignition delay time observed for any of the reactions studied was 2.9 msec. This is so much shorter than the results by other methods (see Tables 1 and 2) that one can only conclude that the other methods do not give efficient mixing. From our results it cannot be concluded that we are measuring the rate of a homogeneous, thermal chemical reaction as this type of reaction should require an energy of activation and the igntion delay time appears to be independent of the initial temperature of the reactants, for the range −40° to 30°C. The actual temperature just before ignition may be of the order of several hundred degrees and a difference of seventy degrees in the initial temperature may not result in sufficient difference in the temperature of the reactants just before ignition when the mixing is efficient.

An unignited mixture of a fuel and oxidant such as hydrazine and nitric acid may be likened to a liquid explosive such as nitroglycerine. Nitroglycerine can be ignited by impact alone. Bowden et al.[17] have studied the ignition of nitroglycerine by impact. They found that thin sheets of the material on an anvil would not ignite even under the influence of a rather strong hammer blow unless gas bubbles were present in the liquid. These authors concluded that the high temperatures produced by the adiabatic compression of the bubbles were responsible for the ignition. It was possible to estimate crudely the minimum ignition energy required to ignite the material by estimating the size of the bubbles and the compression ratio.[18] A value of 10^{-8} calorie was obtained. This value is of the order of magnitude of the minimum ignition energy for gaseous mixtures found by more precise methods involving spark ignition.[18] It is thus reasonable to suppose that the impact and turbulence associated with the mixing process in Reactor II could have re-

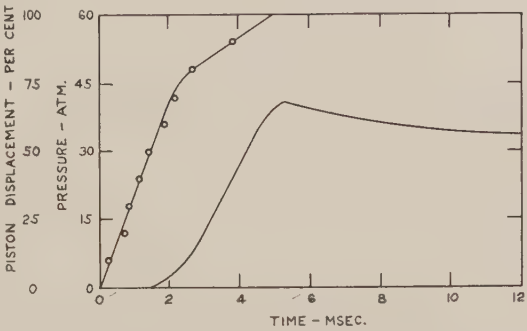

Fig. 6. Simultaneous measurement of injection rate and pressure rise in the reaction of equal volumes of hydrogen peroxide and hydrazine, run 163, Reactor II.

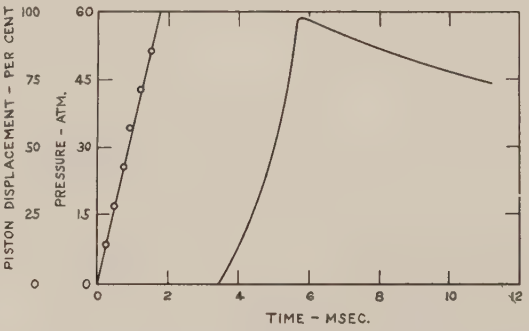

Fig. 7. Simultaneous measurement of injection rate and pressure rise in the reaction of equal volumes of hydrogen peroxide and hydrazine, run 162, Reactor II.

Table 6. Ignition Delay by Light Emission Measurements. Equal Volumes of Nitric Acid with Hydrazine-Liquid Ammonia Mixtures

Run	Hydrazine in Mixture	Temp.	Ignition Delay	Maximum Pressure
	Wt per cent	*°C*	*msec*	*atm*
174	9.0	−35	1.0	41
175	9.0	−33	1.4	41
176	2.7	−38	2.9	31
177	2.7	−41	—*	3.5
178	2.7	−41	—*	3.5

*No ignition.

sulted in immediate or nearly immediate ignition.

This conclusion also results from the failure to observe a systematic increase of the ignition delay as the hydrazine concentration was decreased in the hydrazine-ammonia mixtures. The ignition delay increased to only 2.9 msec for the mixture containing 2.7 per cent hydrazine. The runs made on this mixture that failed to ignite indicated that the impact energy was just insufficient to ignite this mixture. Instead of observing a longer and longer delay as the hydrazine concentration or the temperature was decreased, a point was reached where the mixture simply failed to ignite. Such behavior is more indicative of ignition by mechanical shock than it is of thermally initiated ignition showing an induction period due to the rate of a chemical reaction.

A study of the ignition delay of gaseous mixtures of hydrocarbons and oxygen was made by Jost and Teichmann[19] by a rapid compression method. They obtained a straight line when the logarithm of the ignition delay was plotted against the reciprocal of the reaction temperature. The plot was linear from delay values of a few milliseconds to over five seconds. The fact that the data could be represented by an Arrhenius equation indicates that the delay-determining factor was due to the rate of a chemical reaction. The experimental results obtained in the present study show, nevertheless, that fuel-oxidant systems previously thought to have long ignition delays will ignite in a very short time under violent mixing conditions.

The measured explosion pressures shown in Table 4 are much lower than those calculated by the thermodynamic method outlined in a treatise by Lewis and von Elbe. The calculations indicated an equilibrium pressure of the order of 90 atm. Analysis of the reaction products showed quantities of nitrogen oxides greatly exceeding that expected from thermodynamic considerations alone. These facts indicate that the reaction was quenched through contact with the metal parts of the reactor.

Conclusions

(1) A constant volume reactor was designed to rapidly contact and mix two liquid reactants in a volume ratio ranging from 4:1 to 1:4.

(2) The reactor was easily adapted to a change of the mixing pattern and could be immersed in a thermostatic bath. Satisfactory operation was obtained at temperatures as low as −40°C.

(3) A photoelectric method was devised to follow the course of the injection. The injection of 2.2 cc of water was achieved in 1.7 msec. A somewhat longer time was required for the injection of reacting fuel-oxidant systems because of the thrust created by the reaction process.

(4) Reactions were studied in the reactor by following the transient pressure and the light emission.

(5) The rate of mixing in the apparatus was shown to be very rapid by reference to measurements made by other investigators who employed geometrically similar mixing patterns.

(6) The ignition delay for certain reactant ratios of several fuel-oxidant systems was measured and found to be less than 3 msec in every case. The systems included: (a) Hydrazine vs. nitric acid; (b) Aniline vs. nitric acid; (c) Hydrazine vs. hydrogen peroxide; (d) Hydrazine-liquid ammonia mixtures vs. nitric acid. The delays were significantly lower than those observed by other investigators who employed mixing methods where the efficiency of mixing was most uncertain.

(7) The very short ignition delays were attributed to (a) the rapid rate of mixing in the apparatus, and (b) the impact and turbulence associated with the mixing process.

(8) There was a negligible effect of the initial temperature of the reactant or of the hydrazine concentration on the ignition delay time of the reaction with liquid ammonia-hydrazine mixtures with nitric acid. This result was more indicative of ignition by impact than it was of ignition controlled by the rate of a homogeneous chemical reaction.

REFERENCES

1. Hartridge, H., and Roughton, F. J. W.: Proc. Roy. Soc. (London), *104A*, 376 (1923), et seq.
2. Chance, B.: J. Franklin Inst., *229*, 455, 613, 737 (1940).
3. McKinney, C. D., Jr., and Kilpatrick, M.: Rev. Sci. Insts., *22*, 590 (1951).
4. Kellogg Co., M. W.: *Preliminary Experimental Studies of Liquid Fuel Systems, Final Report.* Report No. SPD 236, May 20, 1949, pp. 88, et seq.
5. Gunn, S. V.: J. Am. Rocket Soc., *22*, 33 (1952).
6. Roughton, F. J. W., and Chance, B.: *Investigations of Rates and Mechanisms of Reactions, Technique of Organic Chemistry*, Volume VIII, ed. A. Weissberger, p. 669. New York, Interscience Publishers, Inc., 1953.

7. Kilpatrick, M., and McKinney, C. D., Jr.: J. Am. Chem. Soc., *72*, 5474 (1950).
8. Kilpatrick, M., Baker, L. L., Jr., and McKinney, C. D., Jr.: J. Phys. Chem., *57*, 385 (1953).
9. Discussions of the Faraday Society, No. 17, 1954.
10. Baker, L., Jr., *Ignition Delay with Rapidly Mixed Liquid Reactants.* Tech. Rept. No. 7, Contract N7onr-32913, August 1954.
11. Neas, C. C., Raymond, M. W., and Ewing, C. O.: M. I. T. Report No. 11, DIC 6351, November 1, 1946.
12. Perry, J. H.: *Chemical Engineers' Handbook*, 2nd. ed., pp. 800 et seq. New York, McGraw-Hill Book Co., 1941.
13. Walker, W. H., Lewis, W. K., McAdams, W. H., and Gilliland, E. R.: *Principles of Chemical Engineering*, pp. 74 et seq. New York, McGraw-Hill Book Co., 1937.
14. Beale, E. S. L., and Docksey, P.: J. Institute of Petroleum, *34*, 602 (1948).
15. Trowse, F. W.: Dissertation. Leeds, 1952.
16. Roughton, F. J. W., and Millikan, G. A.: Proc. Roy. Soc. (London), *155A*, 258 (1936).
17. Bowden, F. P., Mulcahy, M. F. R., Vines, R. G., and Yoffe, A.: Proc. Roy. Soc. (London), *188A*, 291 (1947).
18. Lewis, B., and von Elbe, G.: *Combustion, Flames and Explosions of Gases*, p. 440. New York, Academic Press Inc., 1951.
19. Jost, W., and Teichmann, H.: Naturwissenschaften, *27*, 318 (1939).

12

MECHANISM OF BURNING OF NITRATE ESTERS

By RUDOLPH STEINBERGER[a]

Introduction

This paper represents part of an effort to determine the mechanism of burning of double-base propellants. These are highly complex mixtures, consisting of nitrocellulose, nitroglycerin, stabilizer, inert plasticizer, and usually other adulterants such as carbon black or inorganic salts. It has, therefore, been found to be more satisfactory to study simple liquid nitrate esters as models for the more complex system. These compounds exhibit burning behavior very similar to that of double-base powders; burning rate levels, pressure coefficients, and temperature coefficients are all comparable.

The chemistry of the combustion process of a nitrate ester is necessarily very involved. The compound must go through many stages of degradation, before the final products are formed. However, the system has one property which is highly useful from the point of view of establishing the general outline of the reaction sequence. This is the presence of a liquid-gas interface. Like any other phase change, the transport of material across this liquid surface imposes some very definite demands on the system as regards chemical and physical properties.

It is possible to postulate several different mechanisms by which the phase transition can occur. Each mechanism has different requirements as to temperature, so that, at least in principle, one can distinguish between them on the basis of temperature profiles, with special attention to the temperature in the liquid phase up to the surface.

The first postulated mechanism involves volatilization of the liquid, as suggested by Belajev[1] and others.[2, 3] In this case no chemical reaction takes place in the liquid phase, the liquid merely serving as a reservoir of combustible vapor. Under such conditions the temperature reached by the surface is simply a function of volatility. To vaporize the most volatile liquid studied by us, ethyl nitrate, would require a surface temperature of approximately 250°C at 1000 psi. Other less volatile nitrate esters would require surface temperatures up to 500°C at the same pressure. If this mechanism is correct, then no conclusions as to chemical reaction sequence can be drawn from liquid phase temperature profile data. It

[a] From the Allegany Ballistics Laboratory, a facility owned by the U. S. Navy and operated by the Hercules Powder Company under Contract NOrd 10431.

may be mentioned here that this mechanism is quite improbable on the basis of burning rate data. Materials with as widely differing volatilities as ethyl nitrate (BP 88°C) and triethylene glycol dinitrate (BP ~ 300°C) have burning rates at 1000 psi within ten per cent of each other. Moreover, the less volatile compound in this comparison, which also has the lower flame temperature, has the higher burning rate.

The second mechanism of accomplishing the phase transition involves the thermal decomposition of the nitrate ester into volatile compounds. This process has been studied in considerable

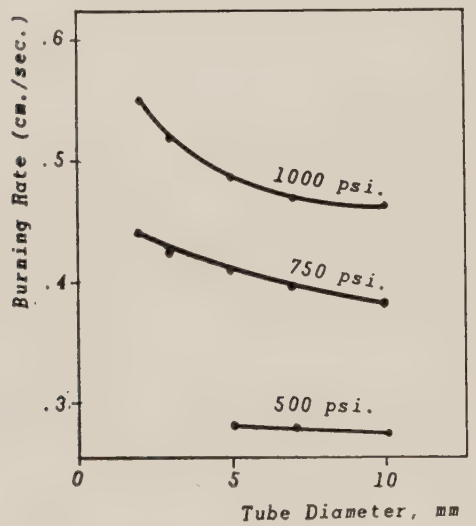

FIG. 1. Burning rate vs. tube diameter for triethylene glycol dinitrate at 25°C and various pressures.

detail[4] and has been shown to require an activation energy of 35–40 kcal/mol. Estimates vary[5, 6, 7, 8] as to the surface temperature necessary in order that this reaction may proceed at the observed rate; 500°C appears to be a reasonable figure. In discussions of the mechanism of burning of double-base propellants[9] thermal decomposition is generally postulated as the initial chemical reaction.

The third mechanism is also chemical in nature but involves a bimolecular reaction of nitrate ester, rather than a unimolecular decomposition. Depending on the nature of the other reagent, the activation energy, and consequently the required surface temperature of such a reaction can be quite low.

It should be noted that the first and second mechanisms on the one hand and the third mechanism on the other hand require different mechanisms of energy transfer to the propellant surface. The first two depend solely on the transfer of heat; it is merely necessary that enough heat flow back from the flame to volatilize the nitrate ester in the first case or to decompose it in the second case. The third mechanism, however, depends on the transfer of material as well. The second-order reaction requires a second reagent in addition to the nitrate ester, and this reagent must be supplied by diffusion from a more advanced stage of combustion. Thus the system under consideration offers a remarkably clear choice between a thermal and a diffusion mechanism of flame propagation.

An investigation of temperature profiles was therefore undertaken and has served to point out the essentials of the probable chemical reaction sequence. Further studies, intended to probe the mechanism in more detail, took the form of burning rate measurements to evaluate the effects of variations in composition. On the basis of this work a more definite reaction sequence can be postulated. However, it is doubtful whether any firm conclusions can be drawn without a detailed chemical analysis of the progressive reaction zones.

Temperature Profiles Study

In the study of the burning behavior of liquid nitrate esters we have followed the basic experimental technique developed by Adams and coworkers.[2, 3] The compounds were burned as liquid strands in 3 mm ID glass tubes usually under pressure (nitrogen) in a window bomb. Burning rates were measured by timing the progress of the liquid meniscus down the tube. These rates are higher than the true linear burning rates, inasmuch as the burning surface is curved. Data at different tube diameters (Fig. 1) show, however, that the necessary correction is small, and it was not applied in the comparison of rates of different materials at any given pressure. Quenching action by the tube walls is not an important effect except at low pressures, where it serves to dampen the effect of decreasing tube diameter and finally to extinguish the burning of the strand.

Temperature profiles were measured in an apparatus shown schematically in Figure 2. Fine wire thermocouples (0.0005-in platinum vs. platinum, 10 per cent rhodium) were cemented horizontally through the burning tube, which was connected to a relatively large liquid reservoir.

The reservoir served to feed liquid continually into the strand and thus to decrease the rate of travel of the burning surface by a large factor, usually about 13. The whole assembly was placed in a window bomb and the progress of the burning surface down the tube and over the thermocouple was recorded by a movie camera. The slow rate of travel of the surface (~0.03 cm/sec) made it possible to use relatively slow equipment and high magnification. A single movie frame, taken at 82 frames/sec is shown in Figure 3. At this speed the motion of the burning surface per frame is approximately one-fifth the diameter of the thermocouple bead, so that it is the latter which limits the accuracy of the experiment. The thermocouple output was recorded by an oscilloscope-drum camera combination. The oscillographic and movie records were synchronized by a flash bulb which was actuated by the drum camera shutter and served to blank out one frame of the movie film. A typical oscilloscope record, obtained with triethylene glycol dinitrate at 800 psi, is shown in Figure 4.

The point of greatest interest in these records is that at which the burning surface meets the thermocouple. This point, shown at A, Figure 4, has consistently been observed to be at room temperature. (Due to a small balancing error, the oscilloscope trace does not show an appreciable difference between room temperature and the 0°C reference mark.) With the present technique, this, then, is the best approximation of surface temperature obtainable. According to the discussion given in the Introduction, the low temperature rules out the first two mechanisms for the phase transition, but even if the third mechanism is correct, one would expect at least some small temperature rise at the surface. A considerable amount of effort has therefore been expended in order to find any systematic error in the measurement. Parameters such as volatility and viscosity of nitrate ester, size of strand, burning rate, pressure, arrangement of thermocouple, and coating of thermocouple were varied but were found to be without effect. It has been concluded, therefore, that within the limits of accuracy imposed by a thermocouple of finite dimensions the surface temperature of these burning liquids is equal to the conditioning temperature.

It would appear, therefore, that the phase transition mechanism involves a highly efficient chemical reaction which can proceed at the required high rate at room temperature. The initiating reagent for this reaction must almost certainly be a free atom or radical originating in the hotter regions of the combustion zone. Thus the evidence points quite clearly to a diffusion process as the fundamental mechanism of flame propagation.

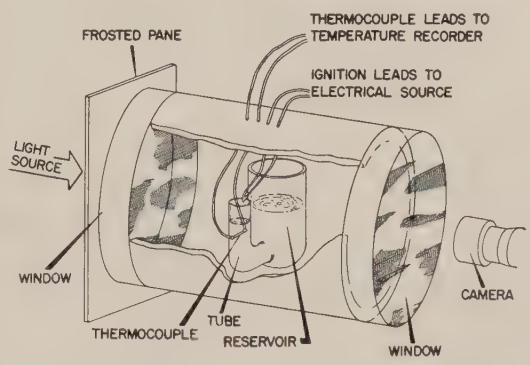

FIG. 2. Schematic sketch of apparatus used in determination of temperature profiles of burning liquids.

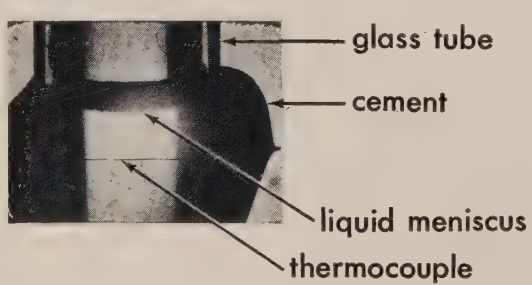

FIG. 3. Single frame of movie record

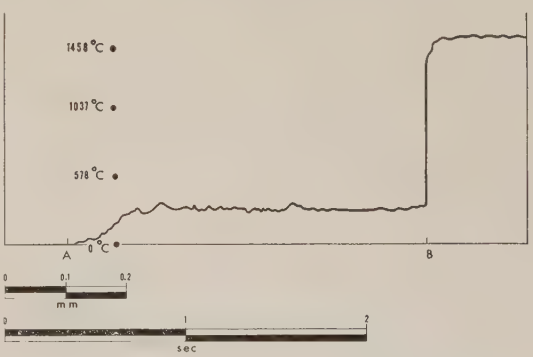

FIG. 4. Typical oscilloscope record.

With regard to the portion of the temperature profile following point A, Figure 4, it has been indicated by several experiments that a true picture of gas-phase temperature distribution is not provided by these data. It appears that, as the thermocouple wire attempts to rise out of the surface, it draws along a film of liquid by surface tension (Fig. 5). The temperature recorded be-

tween points A and B, therefore, approximates that of the (presumably burning) film. This is higher than the normal surface temperature, because the film projects into the flame and is

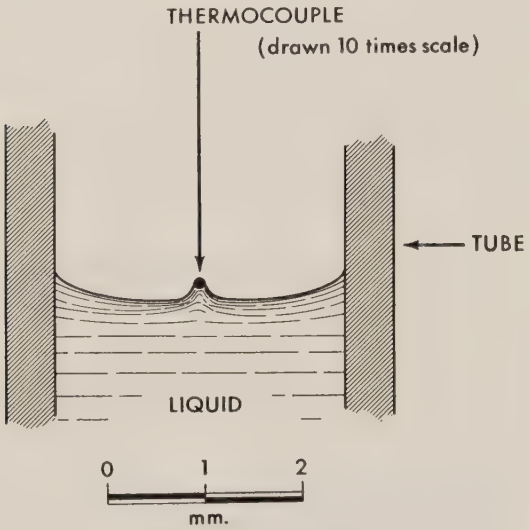

FIG. 5. Sketch of experimental situation between points A and B, Fig. 4.

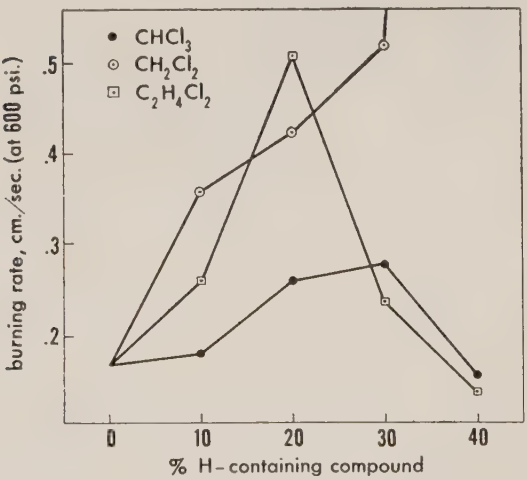

FIG. 6. Effect of substituting hydrogen-containing compounds for carbon tetrachloride in the tetranitromethane-carbon disulfide-carbon tetrachloride system.

thus exposed to a higher-than-normal temperature gradient. At point B, Figure 4, the liquid film finally drops back, and the thermocouple registers the flame temperature.

Atomic Hydrogen as a Key Reagent

On the supposition that the conclusions drawn from the temperature data are correct, it is now necessary to determine what the reagent is which diffuses back from the flame in order to react with the nitrate ester. The reagent must be capable of reacting with nitrate esters at great speed and must diffuse readily. The second requirement is best met by atomic hydrogen, and while we have as yet no specific information on the reactivity of atomic hydrogen with nitrate esters, it is reasonable to assume that the two react very readily. A considerably number of other reagents can be postulated, but this is certainly the most probable on an a priori basis.

HYDROGEN-POOR SYSTEMS

In order to check on the importance of hydrogen in the combustion of liquids, burning rate determinations were made on mixtures in which hydrogen was largely absent. The parent mixture consisted of tetranitromethane (30 per cent) carbon disulfide (30 per cent) and carbon tetrachloride (40 per cent). Except for absorbed moisture, this mixture thus contained no hydrogen. It has a measured heat of explosion of 830 cal/gm and a flame temperature, calculated on the basis of an arbitrarily assumed stoichiometry, of 4500°K. The actual flame temperature must be assumed to be much lower than this but still considerably higher than that of nitrate esters with the same heat of explosion. Nevertheless the burning rate was found to be comparatively low, 0.25 cm/sec at 1000 psi.

Three further sets of burning rate determinations were now made, in each of which the carbon tetrachloride was replaced by successive increments of one of the following hydrogen-containing compounds: chloroform, methylene chloride, and ethylene chloride. The resultant burning rates are shown in Figure 6. The extraordinary rate-boosting effect of even very small amounts of hydrogen is readily apparent. We are not prepared to explain the detailed shape of these curves; presumably they reflect the combined influence of an increasing hydrogen concentration and decreasing flame temperature. Nevertheless it is clear that hydrogen plays quite an important role in the combustion of these mixtures.

DEUTERATED NITRATE ESTERS

A second approach toward ascertaining the possible role of hydrogen involves the burning of completely deuterated nitrate esters. The effect of substituting deuterium for hydrogen can be

expected to be twofold. (1) Deuterium has a lower rate of diffusion than hydrogen. If we use the Tanford-Pease square-root law as a guide, we can expect a resultant lowering of the burning rate by a factor of about 1.2. (2) The deuterium must necessarily be introduced in the form of C—D bonds. Therefore, the kinetic effect of breaking a C—D bond, as compared to a C—H bond, is superimposed on the diffusion effect. The actual rate-lowering factor should therefore be greater than 1.2.

Deuterated ethyl nitrate and ethylene glycol dinitrate were prepared and burning rates measured. Results are shown in Figures 7 and 8. In the case of ethyl nitrate, the deuterated compound burned slower than the ordinary one by a factor of 1.4. Ethylene glycol dinitrate was burned as a 1:1 molar mixture with ethylene bromide. All four possible mixtures of the ordinary and deuterated forms of both compounds were measured. The ordinary mixture burned faster than the completely deuterated one by a factor of 1.7. The other two mixtures burned at intermediate rates. However, the mixture containing deuterated nitrate burned considerably slower than the one containing deuterated bromide, even though the overall deuterium content was the same in both cases. In view of the kinetic effect mentioned above, this fact is interpreted as showing that the breaking of a C—H bond of the nitrate ester is of considerable importance in the overall kinetic scheme. It is postulated, therefore, that this bond is broken in the first step of the combustion process and that the initial reaction is

$$RR'CHONO_2 + H \rightarrow RR'CONO_2 + H_2 \quad (1)$$

The subsequent reaction then depends on the fate of the radical $RR'CONO_2$.

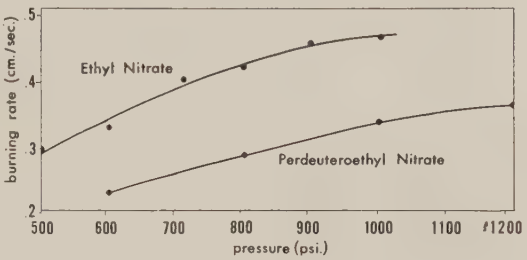

FIG. 7. Effect of substituting deuterium for hydrogen in ethyl nitrate.

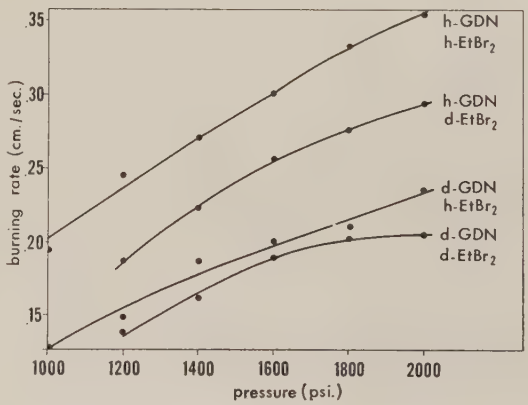

FIG. 8. Effect of substituting deuterium for hydrogen in 1:1 molar mixtures of ethylene glycol dinitrate (GDN) and ethylene bromide ($EtBr_2$).

Formulation in Terms of Chemical Kinetics

The evidence presented above is far from sufficient to establish reaction (1) firmly as the mechanism by which the breakdown of the nitrate ester is initiated. However, the reaction is in agreement with all the facts at our disposal. It now becomes useful to formulate the burning process in terms of chemical kinetics, following the approach of Wilfong, Penner, and Daniels,[5] and to use reaction (1) as the basis of this formulation.

Such an approach does not involve the assumption that reaction (1) is the rate-determining step in the combustion process. In fact it should be pointed out that in a system of this type, in which feedback of energy and material is very important, there exists no such thing as a rate-determining step. Each reaction proceeds at exactly the same rate as every other (if proper allowance is made for stoichiometry), and if a change in conditions imposes a change in the rate of any given reaction, then this effect is automatically transmitted to all the rest. By the same token it is possible to fix attention arbitrarily on any single reaction and to evaluate the effect of a given perturbation by estimating its effect on the reaction in question.

In the present case the mass burning rate is necessarily equal to the rate of consumption of nitrate ester, and we can write the rate law

$$\dot{m} = k\,[N]\,[H] \quad (2)$$

where $\dot{m}$ = mass rate of burning, mols/cm²-sec; k is a rate constant, l/mol-sec; [H] = concentration of nitrate ester at the surface, mols/cm²; and [H] = concentration of atomic hydrogen in the gaseous layer just outside the surface, mol/l. Use of these units gives k its usual significance but

involves the assumption that reaction takes place in a monomolecular layer at the surface only. This is clearly an oversimplification but is justified by the fact that the hydrogen atom concentration must go to zero very quickly inside the liquid. The true burning rate can be thought of as being merely proportional to that given by equation (2).

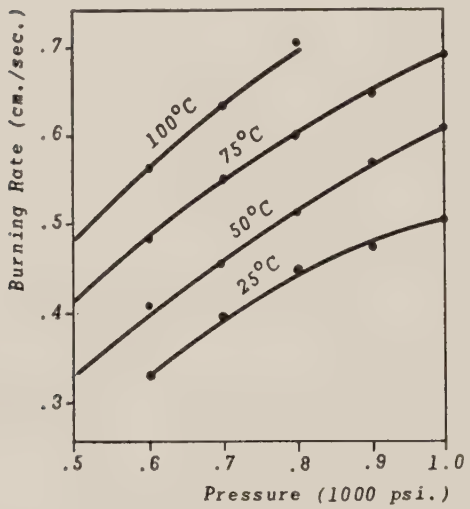

FIG. 9. Burning rate vs. pressure for triethylene glycol dinitrate at various temperatures.

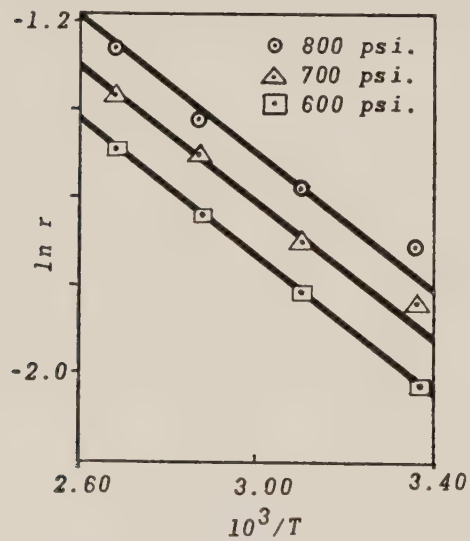

FIG. 10. Arrhenius plot of burning rate of triethylene glycol dinitrate at various pressures.

During steady-state burning, [N] is kept constant by volatilization of reaction products and exposure of fresh nitrate ester and is given by

$$(N) = \left(\frac{d}{M}\right)^{2/3} \tag{3}$$

where d = density, M = molecular weight. The linear burning rate, r (cm/sec), is related to the mass burning rate, $\dot{m}$, by

$$r = \dot{m}\,\frac{M}{d} \tag{4}$$

Therefore, we can relate k to r by substituting equations (3) and (4) in (2) to get

$$k = r\left(\frac{d}{M}\right)^{1/3}\frac{1}{[\mathrm{H}]} \tag{5}$$

Thus, k is directly proportional to r. The factor $1/[\mathrm{H}]$ serves in effect to lump together the total influence of the flame on the reaction rate. Since k is an ordinary rate constant, we can relate the temperature coefficient of r to the activation energy, E, which corresponds to k

$$\frac{d\ln k}{d(1/T)} = -\frac{E}{R} = \frac{d\ln r}{d(1/T)} - \frac{d\ln[\mathrm{H}]}{d(1/T)} \tag{6}$$

(The variation of $d^{1/3}$ with temperature is considered negligible.) Since the temperature, T, of the reaction zone is equal to the conditioning temperature, we can use burning rate data for triethyleneglycol dinitrate at various temperatures (Fig. 9) to calculate E, provided we assume that the last term of equation (6) is small. The value of E determined in this way (Fig. 10) is 1.6 kcal/mol. If we assume, instead, that [H] is proportional to the equilibrium concentration of atomic hydrogen at the flame temperature, then the last two terms of equation (6) cancel each other almost exactly, and we are left with zero activation energy.

A reasonable a priori estimate of the activation energy for reaction (1) is 5 kcal/mol. Thus it may be seen that this simple formulation yields a result in the right range, although, at this degree of approximation, it is far from exact.

Conclusions

The data presented show that a diffusion mechanism of flame propagation probably operates in the burning of liquid nitrate esters. The detailed chemical reaction sequence is still in doubt, but the initial reaction has been postulated as an attack by atomic hydrogen on the nitrate ester. A simple formulation of the burning process,

based on chemical kinetics, shows that the temperature coefficient of burning rate is quite simply related to the activation energy of the initial reaction, and that the value thus calculated on the basis of experimental data is in reasonable agreement with that expected for the postulated reaction.

Acknowledgment

The author is indebted to Mr. Kenneth E. Carder, who performed the greater part of the experimental work required in this study, and to Dr. Lyman G. Bonner and Dr. Frank H. Westheimer for their continued interest and many stimulating discussions. This work was sponsored by the United States Navy under Contract NOrd 10431.

REFERENCES

1. Belajev, A. F.: Acta Physicochim. U.R.S.S., *8*, 763 (1938).
2. Adams, G. K., and Stocks, G. W.: *Fourth Symposium (International) on Combustion*, p. 239. Baltimore, The Williams & Wilkins Company, 1953.
3. Adams, G. K., Parker, W. G., and Wolfhard, N. G.: Disc. Farad. Soc., *14*, 101 (1953).

4a. Levy, J. B.: NAVORD Reports #2169, 2313, 2608, 2897, Naval Ordnance Laboratory, Silver Spring, Maryland.

b. Phillips, L.: Nature, *160*, 753 (1947).

5. Wilfong, R. E., Penner, S. S., and Daniels, F.: J. Phys. & Colloid Chem., *54*, 863 (1950).
6. Rice, O. K., and Ginell, R.: Ibid., *54*, 885 (1950).
7. Parr, R. G., and Crawford, B. L., Jr.: Ibid., *54*, 929 (1950).
8. Olds, R. H., and Shook, G. B.: *Investigations Relating to Burning Rates of Solid Propellants. Part II, Theoretical Calculations*. U. S. Naval Ordnance Test Station, China Lake, Calif.
9. *Symposium on Kinetics of Propellants:* J. Phys. & Colloid Chem., *54*, 847–954 (1950).

Discussion by Peter Gray*

When studying the spontaneous ignition of alkyl nitrate vapours Yoffe and I felt that atoms and free radicals played an important part. The difficulty as I see it is to pin the effect down to hydrogen atoms: the ingenious experiments on isotopic substitution do not yet enable a firm choice to be made. Another difficulty is that for H atoms to reach the nitrate surface they may have to diffuse through a reactive mixture of aldehydes and nitrogen dioxide. Might not the reactions of RO· and NO_2 with unchanged ester contribute appreciably to the mechanism of burning?

Author's Reply

The question as to whether atomic hydrogen can, in fact, diffuse from the hot boundary to the burning surface cannot be answered definitely at this time. Information is lacking in general as to the distance involved, the composition of the intermediate flame gases, the temperature distribution, and the reaction kinetics of atomic hydrogen with the various possible intermediates. However, approximate calculations have been carried out for one set of conditions (ethylene glycol dinitrate burning at a pressure of 0.05 atm), using the assumption that all chemical loss of atomic hydrogen is by recombination. Under these conditions it appears that the atomic hydrogen concentration at the surface is more than 90 per cent that at the hot boundary. This situation is not changed appreciably by other hydrogen-removal reactions, unless these are at least two orders of magnitude faster than recombination.

The contributions to the burning mechanism of the reactions of RO· and NO_2 with unchanged ester do not appear to be important, inasmuch as these reactions do not compete successfully even in the slow thermal decomposition of nitrate esters.†

---

* Cambridge University.

† J. B. Levy, J. Am. Chem. Soc. *76*, 3254, 3790 (1954).

13

MEASUREMENT OF THE TEMPERATURE DISTRIBUTION IN BURNING LIQUID STRANDS[a]

By D. L. HILDENBRAND AND A. GREENVILLE WHITTAKER

Introduction

A number of theoretical treatments of the combustion of liquids have been carried out, but all of them employ certain simplifying assumptions concerning the physical and chemical details of the combustion process. This type of approach is largely due to the lack of experimental data on the detailed mechanism of the combustion of liquids. It is the primary purpose of this study to measure the temperature distribution in the liquid phase of a burning liquid in order to obtain some of the detailed information that is required to build a good theoretical treatment of liquid combustion. Also, the results of this study can be used to show which of the existing theoretical models contain assumptions that are unreal.

Two types of combustible liquids were investigated. One consisted of the homogeneous binary system 2-nitropropane-95 per cent nitric acid in which the oxidizer and fuel are in different molecules. The other type consisted of ethyl nitrate, and metriol trinitrate (i.e., methyl trimethylol methane trinitrate)-triacetin (i.e., glycerol triacetate) mixture in which the fuel and all the available oxygen are in the same molecule. Triacetin was used as a diluent to reduce the flame temperature below that of pure metriol trinitrate and to make the system safer to handle. Temperatures were measured with very fine thermocouples and the profiles obtained were quite reproducible. Surface temperatures could be measured to $\pm 15°C$ or less for all the liquids studied.

Experimental

Compounds used in this study were of varying degrees of purity. The 2-nitropropane was prepared by distillation of commercial grade material, and only the center fraction was used. This fraction had an index of refraction of 1.3950 at 20°C using the sodium D lines. The literature value is given as 1.3941[1]. Nitric acid was prepared by distillation of a 50-50 mixture of CP white fuming nitric acid and concentrated sulphuric acid at a pressure of less than two millimeters of mercury. The resulting acid was analyzed and then diluted to 95 per cent with distilled water. This acid contained less than 0.1 per cent nitrogen dioxide. Eastman white label ethyl nitrate was used without further purification. Similarly the purity of the metriol trinitrate-triacetin mixture was about the same as the ethyl nitrate.

A detailed description of the experimental technique used in this study has been given previously[2]. However, a brief description of the methods employed will be given here. Liquid to be burned was placed in a 3.7 mm inside diameter Pyrex tube about 4 cm long and sealed at one end. This tube was placed inside a two-window bomb which could be pressurized with nitrogen and held at a constant pressure during combustion of the liquid. The liquid was ignited by a piece of solid propellant which in turn was ignited by a hot wire. At a convenient location on the glass tube a thermocouple (0.0003 inch diameter Pt-Pt 10 per cent rhodium) was sealed diametrally through the tube. The junction of the couple was about 70 per cent larger in diameter than the wire. High-speed motion pictures were taken of the combustion wave traveling down the tube. From these pictures the consumption rate was obtained and the location of the couple relative to the surface at any given time could be determined also. At the same time the thermocouple signal was amplified and fed to a cathode ray oscilloscope, and the scope image was photographed with a continuous strip camera. Both photographic records were time synchronized through a common timing source and they had the same zero time reference. The data thus obtained were assessed in such a way that a plot of temperature vs. distance resulted, and the space relation of the temperature distribution to the burning surface was established experimentally. The thermocouples were calibrated against a bureau of standards calibrated Pt-Pt 10 per cent rhodium thermocouple to establish that they were working properly. The temperature measuring system was checked for time lag in the equipment, and it was found that the lag was less than

[a] Studies carried out in the Research Department of the U. S. Naval Ordnance Test Station, Inyokern, China Lake, California.

two millisec. Also, later experiments indicated that the couple itself was capable of following very rapid temperature changes. For reasons to be discussed later, this technique does not yield complete profiles. Consequently, the thermocouple amplifier gain was set to give about 600°C for full scale deflection (i.e., approximately four in. on the oscilloscope screen).

Occasionally temperature profiles were obtained using a Sanborn recording oscillograph instead of the cathode ray oscilloscope. Because of the lower sensitivity of this recorder the entire temperature record was obtained, but with correspondingly lower accuracy. These records were used to obtain maximum flame temperature and the position at which this temperature is reached with respect to the liquid surface.

Results and Discussion

Profiles for all the systems studied showed the same general characteristics. A copy of a Sanborn recording of the temperature distribution shown in Figure 1 illustrates a typical profile. As the combustion wave passed the thermocouple the temperature profile showed that there was a preheat region in the liquid about 100 to 300 μ deep. In this region the temperature rose exponentially to 100° to 300°C. This region was followed by a temperature plateau that extends from 0.3 to 1 mm. The temperature rise was only 20° to 50°C in this region. Photographs showed this plateau to be caused by the lifting of a filament of liquid by the thermocouple because of the surface tension of the liquid. The temperature plateau was followed by a very steep temperature rise with a gradient of about 200,000°C per sec which stopped near the final flame temperature. The reason for this appeared to be that by the time the filament of liquid broke away from the thermocouple, the thermocouple was well up into a fairly hot portion of the flame; hence, the temperature of the thermocouple environment suddenly changed from that of the relatively cool liquid to that of the hot gases which have nearly reached the final flame temperature. The rapid rise was then followed by a short distance of more slowly rising temperature until final flame temperature was reached. The extent of these various regions depended on the particular liquid studied and the pressure at which it was burned. The values given show only a representative range of values actually observed. Clearly, it is not possible to get complete temperature profiles of burning liquids by this method. Fortunately, only the preheat regions and surface temperature were of interest in this study. Most of these determinations were made with bare thermocouples, although few were made with the thermocouple covered with a very thin coat of teflon. Comparison of the results gave no evidence of catalysis in the liquid phase by the bare couples.

The 2-nitropropane and 95 per cent nitric acid were mixed in stoichiometric proportions to give carbon dioxide, water, and nitrogen as complete combustion products. This mixture has a calculated flame temperature of about 3000°K; hence, only the liquid phase portion was obtainable before the thermocouple melted. Color photographs showed that liquid phase reactions take place in the preheat zone of the system 2-nitropropane-95 per cent HNO_3. They also showed that there was much random motion under the

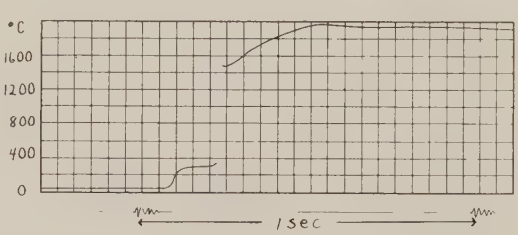

FIG. 1. EMF vs. time for metriol trinitrate-triacetin burning at 900 psig. Chart sensitivity: 1 Div. = 200°C. Chart speed: 1 div. = 0.05 second.

liquid surface which was probably due to convection currents in the preheat zone. This random motion showed up as irregularities on the temperature profile of the preheat region as shown in Figure 2. Because the thermocouple tended to dwell in the liquid surface it was possible to determine the surface temperature with fairly good accuracy in spite of the irregularities in the profile. For this system the temperature of the liquid surface was found to be 450 ± 15°K. This temperature corresponds to the point on the profile at which the exponential rise stops and the plateau portion due to filament formation starts. Increasing the viscosity of the liquid from 0.7 to 18 centipoises by adding about 0.5 per cent lucite caused these irregularities to be smoothed out so that a reproducible profile was obtained as shown in Figure 3. Photographs showed that the increased viscosity rather markedly damped the convection currents in the preheat zone. This supported the notion that the observed irregularities were due to the convection currents in the normal liquid perheat zone.

This system gave the interesting result that its surface temperature was independent of pressure over the range 300 to 700 psig. This pressure range covers the middle portion of the smooth burning region for this system.

A few profiles were determined in the turbulent burning region, but the turbulence causes the profile to be non-reproducible primarily in the filament pull out region of the profile. Consequently, it is not possible to determine a precise value for the surface temperature when turbulent combustion occurs in this system. Comparing these profiles with profiles obtained at 700 psig gives the impression that surface temperature

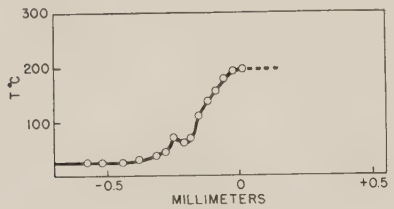

FIG. 2. Temperature vs. distance from burning surface for 2-nitropropane-95 per cent nitric acid burning at 300 psig.

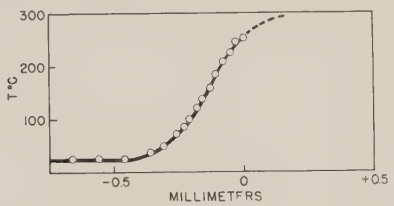

FIG. 3. Temperature vs. distance from burning surface for 2-nitropropane-95 per cent nitric acid plus 0.5 per cent Lucite burning at 300 psig.

was not appreciably different in the turbulent region compared to the smooth burning region. However, no precise statement of this can be made. The maximum temperature reached at any point on the liquid phase portion of a profile in the turbulent region was about 513 ± 15°K. Therefore, the surface temperature in this region cannot lie outside of the range 450° to 513°K. By measuring the variation of surface tension with temperature, the critical temperature of this mixture was found to be about 570°K. In general, this method of estimating liquid critical temperature gives values that are less than the true value; hence, the above value probably represents an estimate of the lower limit of the critical temperature. It had been proposed that the onset of turbulent burning may be associated with the reaching of the liquid critical temperature. Since the surface temperature in the turbulent combustion cannot exceed 513°K and the liquid critical temperature is probably not less than 570°K, it appears that this concept is untenable.

The metriol trinitrate-18 per cent triacetin mixture had a viscosity of about 25 centipoises, and it yielded smooth and very reproducible profiles of the preheat zone. Photographs showed only a thin zone of very mild convection currents in this region. Surface temperature was found to be 560 ± 10°K for this liquid. A more extensive study was made of the effect of pressure on this system, and again it was found that the surface temperature was independent of pressure. The results obtained are shown in Table 1. These data were recorded on the Sanborn oscillograph so that maximum flame temperature could be

TABLE 1. LIQUID SURFACE AND MAXIMUM FLAME TEMPERATURE AS A FUNCTION OF PRESSURE FOR THE SYSTEM METRIOL TRINITRATE-18 PER CENT TRIACETIN

Bomb Pressure	Liquid Surface Temp.	Max. Flame Temp.
psig	°K	°K
500	560	1900
500	550	1840
700	550	1880
900	560	1890
1100	550	1900
1300	560	1880
1460	570	1880

obtained also. Figure 1 shows a profile for this system. The transition from the exponential rise portion to the plateau was sharper for this liquid; hence, the surface temperature could be determined with somewhat greater precision. Within the accuracy of the experimental method both the temperatures indicated in Table 1 are constant over the pressure range studied. Metriol trinitrate-18 per cent triacetin burns smoothly up to about 2500 psig. At this pressure and above the combustion was turbulent. Hence, all the data in Table 1 applies to the smooth burning region for this system.

Ethyl nitrate had about the same viscosity as the 2-nitropropane-95 per cent nitric acid mixture, but it yielded smooth and highly reproducible profiles. Photographs of burning ethyl nitrate showed only very mild convection currents in the preheat zone as would be expected from the appearance of its temperature profile

shown in Figure 4. The results of other investigators indicate that no chemical reactions occur in the liquid phase of ethyl nitrate just ahead of the combustion wave. If this is correct, comparison of the profiles of ethyl nitrate and of the system 2-nitropropane-95 per cent nitric acid gives further support to the view that the combustion process of the latter system differs from that of the nitrate ester in that exothermic chemical reactions probably occur in the liquid phase just ahead of the combustion wave.

The study of the effect of pressure on surface temperature of burning ethyl nitrate has not been completed, but tentative results indicate a somewhat different behavior. The profiles for this liquid showed the sharpest transition at point A in Figure 4; hence, the surface temperature of ethyl nitrate could be determined with the highest precision. However, the surface temperature showed some variation with pressure for this burning liquid. The surface temperature changed from about 370°K at 100 psig to about 450°K at 700 psig. From this pressure to 1100 psig the surface temperature remains at 450°K. Apparently ethyl nitrate does show no pressure effect on surface temperature over a short range. It may be that the other liquids show only this range because they cannot be burned at low enough pressure. All the data on ethyl nitrate were obtained in the smooth burning region. This liquid starts to burn turbulent at about 1150 psig; hence, there is no relation between the constant surface temperature and the transition to turbulent combustion.

The variation of surface temperature with pressure in the low pressure region for ethyl nitrate may be due to the increase in boiling point because of the increase in pressure. A plot of log bomb pressure versus the reciprocal of the surface temperature for the present data yields a rather good straight line, and indicates an associated enthalpy change of about 8 kcal/mole. Unfortunately, vapor pressure data on ethyl nitrate has not been obtained in this pressure region; hence, it is not possible to say that this 8 kcal/mole is equal to the heat of vaporization. However, the indication is that the liquid surface may reach the boiling point in the low pressure region.

The constant surface temperature region may be due to attainment of the decomposition temperature of the ethyl nitrate. At this point it is possible that the heat sources and sinks maintain a balance over a pressure range in such a way as to result in a constant temperature at the surface. It is also possible that the Poynting effect on the liquid vapor pressure becomes sufficiently large at some pressure that an adequate supply of vapor can be maintained at constant surface temperature over a pressure range provided the total pressure is high enough. Similar remarks can be made about the other liquids studied. However, for these liquids it appears that certain conditions must be reached before combustion is self-sustaining. Either a particular reaction temperature must be reached or the pressure must be sufficiently high to produce an adequate amount of vapor to keep pace with vapor phase reactions. If this were the case, then the region in which surface temperature varies with pressure did not exist for these liquids.

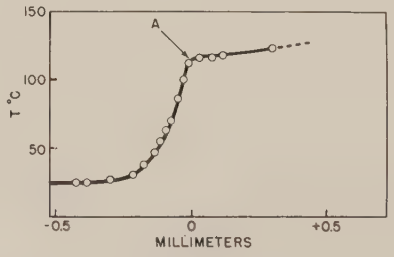

FIG. 4. Temperature vs. distance from burning surface for ethyl nitrate at 100 psig.

For liquids that burn with a constant surface temperature a theory as proposed by Rice and Ginell[3], in which the rate controlling process is related to the surface temperature, cannot be used to describe the combustion process. Results obtained in this study indicate that a theoretical model is required in which a variable amount of heat must be supplied to a liquid surface at constant temperature. The Sanborn recordings obtained on metriol trinitrate-18 per cent triacetin (and apparently ethyl nitrate also) showed that the distance between the surface and the location of maximum flame temperature decreased with increasing pressure according to the empirical equation (1)

$$S = \frac{2.63 \times 10^5}{P^{1.83}} \qquad (1)$$

where S is the distance in millimeters and P is the gage pressure in psi. In a general way this relation indicates that the temperature gradient just above the liquid surface increases with pressure. Unfortunately equation (1) cannot be used for

quantitative evaluation of the gradient just above the surface. To do this, it is necessary to know the exact shape of the temperature profile in the gas phase. This study did not give this information, but it is believed that a change in technique will make it possible to get the desired gas phase profile in future work. Factors other than temperature gradient influence the amount of heat reaching the liquid phase. Variation with pressure of radiation intensity and thermal conductivity of the gases above the liquid play a role in the transfer of heat to the liquid. However, these effects are likely to be second order compared to the variation of temperature gradient with pressure.

Although no theoretical treatment of the entire combustion process was considered, some interesting results were obtained when the profile of only the preheat zone in the liquid phase was examined by the theoretical treatment developed by Reid[4]. This treatment is restricted to a region in the condensed phase in which chemical reactions are negligible. Consequently, it is possible to solve the heat transfer problem analytically on the basis of a conduction-radiation model. Reid showed that temperature profile data could be used directly in equation (2)

$$v^2(u - u_\infty) = h^2(du/dt) + \frac{Av}{Dc} \exp(-as) \quad (2)$$

where v = steady state burning velocity
u = temperature taken from profile at point s
u_∞ = ambient temperature
h^2 = thermal diffusivity
du/dt = slope of profile at point s
A = radiation intensity
a = radiation absorption coefficient
s = distance variable
D = density of liquid
c = heat capacity of liquid

All the variables in equation (2) can be evaluated at various points along the profile to obtain a set of simultaneous equations that can be solved for h^2, A, and a. The data obtained on metriol trinitrate-triacetin was used in equation (2) and the values resulting from the solution of the equations were $h^2 = 3.6 \times 10^{-4}$ cm²/sec, $A = 17$ cal/cm²sec and $a = 121$ cm^{-1}. None of these parameters have been evaluated by independent experiment, but they are reasonable in the light of measurements made on these parameters for solid propellants. It has been found that equation (2) does not yield reasonable values for h^2, A, and a for all systems. Hence, the theoretical model used to derive equation (2) is not applicable to all burning systems. This may mean that the burning rates of all systems do not show primary dependence on the same parameters. Perhaps systems should be classified according to different models depending upon which parameters are most important; for example, a radiation and conduction model, a conduction only model, etc.

REFERENCES

1. Handbook of Chemistry and Physics, p. 1077. Chemical Rubber Pub. Co., 1933.
2. Hildenbrand, D. L., Whittaker, A. G., and Euston, C. B.: J. Phys. Chem. *58*, 1130 (1954).
3. Rice, O. K., and Ginell, R.: J. Phys. and Coll. Chem., *54*, 885 (1950).
4. Reid, W. P.: J. Phys. Chem., *57*, 242 (1953).

Discussion by Dr. Peter Gray*

The authors mention that variation of the pressure of the gases just above the burning liquid surface may influence both thermal conductivity and vapor pressure (Poynting effect). We believe these are secondary effects. We have carried out experiments in Cambridge on burning mono-fuels in capillary tubes under varying pressures and we find strong evidence for the importance of convective heat transfer from the outside walls of the tube. At high pressures heat loss through the walls to an external surface relatively well cooled by convection can actually extinguish a flame.

Author's Reply

Subsequent experimental results have shown that the Poynting effect, or the change in vapor pressure due to the effect of the pressurizing gas, is indeed negligible as regards combustion. The situation with respect to variation of thermal conductivity with pressure is not clear. However, we are inclined to agree that this may be a secondary effect. With regard to the effect of heat transfer from the tube walls, we have found from burning liquids in capillary tubes surrounded by a water bath that at sufficiently low pressures (or low rates of burning) the combustion wave cannot propagate below the level of the bath, presumably because heat transfer away from the wave at that point is more rapid than the rate of regression of the surface. On increasing the pressure (and rate of burning) up to ten atmospheres, the liquid appears to burn as it normally would in the absence of the bath.

* P. Gray and J. C. Kay: Selected Combustion Problems, p. 381, London, 1954, Butterworths.

14

SURFACE PROPERTIES OF LIQUID BIPROPELLANTS AND THEIR EFFECTS ON THE KINETICS OF IGNITION

By MICHEL L. J. BERNARD

Introduction

The importance of ignition lag on rocket performance is well known. Many studies have been published on the measurement of ignition lag under various test conditions.[1, 2, 3]

Attempts have been made to determine the effect on this lag of various factors, such as temperature, impurities, and the addition of metallic oxides or salts.[2] In the last war, German engineers were well acquainted with the effect of iron salts on the spontaneous ignition of a pair of bipropellants containing nitric acid, or with that of copper salts in the case of a bipropellant pair containing hydrogen peroxide.

It is evident that the action of these salts—Fe, Cu, Va—is catalytic in nature; in other words, they initiate the chemical reactions which precede ignition. The purpose of the present study is to establish the physical behavior of sprayed bipropellants and the influence of interfacial tension on ignition delays in a rocket combustion chamber.

Once combustion has been initiated, the theory can be readily extended to liquid bipropellants that do not ignite spontaneously, provided that the liquid phases of these substances react with one another under the new conditions of pressure and temperature prevailing in the rocket chamber.

Experimental

MEASUREMENT OF IGNITION LAG

Two procedures were used to ignite the bipropellants: (1) Drop by drop pouring into an open cup, in which a large drop (about 1 gm) of the liquid oxidizer falls from a height of 10 cm onto the surface of the fuel contained in an open cup whose capacity is 1 cc (Fig. 1); (2) Injection of two opposite concurrent jets, in which the propellants issuing from small pressure tanks are sprayed one against the other (Fig. 2).

Two methods were developed for the accurate measurement of the ignition lag: (1) In the open cup test, the phenomenon is recorded on a film at the rate of 64 shots per sec; (2) In the case of the concurrent jets, the lag is recorded by photographing the oscilloscope trace.

The principle of the latter method was developed by Gunn,[2] who applied it to checking the ignition lag of furfuryl alcohol poured into white fuming nitric acid. The procedure was adapted to the case of concurrent jets in the following way. The meeting of the two streams closes an electric circuit, producing a voltage pulse which is fed to one channel of a cathode-ray oscillograph with stationary locked scanning causing the spot to move horizontally across the screen. The emission of light from the reacting propellants generates a second pulse by means of a photoelectric cell and produces a sudden vertical deflection of the spot on the screen. With a sufficient remanence of the screen, the length of the horizontal trace is clearly defined and may be calibrated by comparison with the sine wave appearing on the next oscillograph channel if connected to the distributor system (50 Hz). Both the horizontal trace and the sine wave, can be recorded photographically (Figs. 2 and 3).

With the first method, the accuracy of the ignition lag measurement depends on the speed of the moving film. With the second method, it depends on the exact correlation of the trace with the time scale. In the open cup test, the accuracy is $\pm 0.5 \times 10^{-2}$ sec; in the case of the concurrent jets it is $\pm 0.25 \times 10^{-3}$ sec.

It may be stated that for a given bipropellant system, the ignition lags are not the same in all tests, but are spread along a Gaussian curve whose median ordinate is a salient feature of the system (Fig. 4).

ADDITION OF WETTING AGENTS TO BIPROPELLANT SYSTEMS

Effects upon the ignition lag of different additives

It has been found that so-called surface active substances improve the ignitability of a fuel mixed with an acid oxidizer.[4] The available fuels were furfuryl alcohol and dicyclopentadiene dissolved in oil in the proportion of 83 per cent and 37 per cent, respectively, which gave hypergolic ignition with 97 per cent nitric acid. Table 1

shows the ignition delays measured for these systems with and without addition of various surface active substances.

Delays measured for a 99.5 per cent nitric acid-

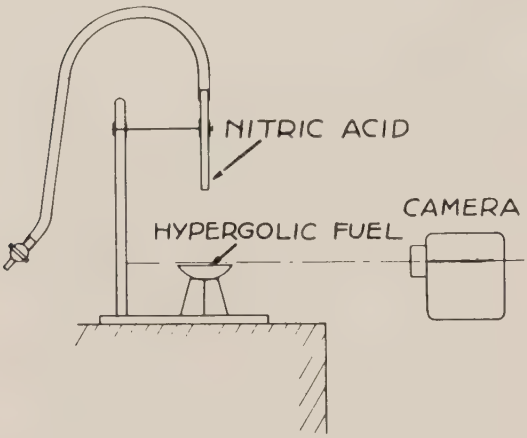

Fig. 1. Open cup method

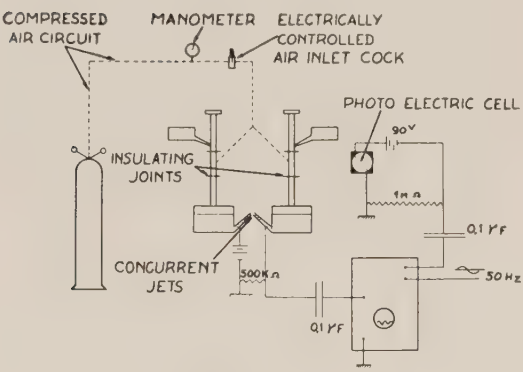

Fig. 2. Concurrent jets method

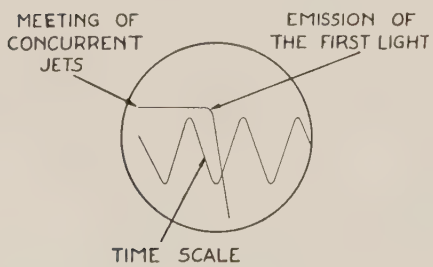

Fig. 3. Time measuring device

furfuryl alcohol system by the concurrent jets method are shown in Table 2.

Influence of the wetting agent concentration

Most of the surface active substances considered are not readily soluble in the fuels used. Consequently, the effect of increasing the concentration of the additive could be studied only for the following substances: sodium sulforicinate,

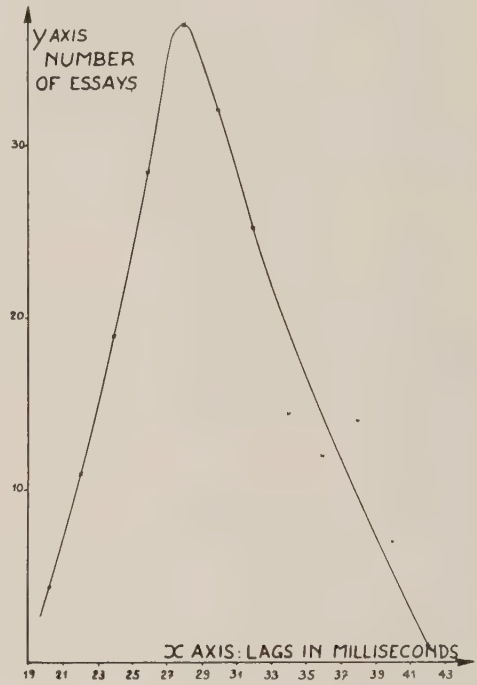

Fig. 4. Gaussian curve of ignition lags

Table 1. Ignition Delays (msec.) Measured with Open Cup Method

Additives	System with Furfuryl Alcohol	System with Dicyclopentadiene 83 per cent
No additive	31	70
0.5 per cent oleamide	23	39
0.5 per cent triethanolamine oleate	23	31
0.5 per cent glyceryl oleate	23	39
0.5 per cent glycolpropylene oleate	23	31
0.5 per cent cetyl pyridinium bromide	31	47
0.5 per cent sodium sulforicinate	16	47
0.5 per cent alkyl-aryl sodium sulfate	23	47
0.5 per cent alkyl sodium sulfate	23	31

polyoxyethylene glycol oleate, monoethanolamine.

The results are shown graphically in Figure 5.

It will be seen that the ignition lag drops to a minimum for a concentration of as little as 2 per cent, and remains there over a wide range of concentrations.

Symmetrical effect of adding surface active agents to one or the other bipropellant

The action of the wetting agent does not depend in any way on the hypergolic component in which it is dissolved as shown by the experiments with sodium alkyl sulfate (Table 3). This compound is one of the exceptional wetting agents which remain stable when mixed with highly concentrated nitric acid.

TABLE 2. IGNITION DELAYS (MSEC) MEASURED WITH CONCURRENT JETS METHOD

Additives	System with Furfuryl Alcohol
No additive	26.3
0.5 per cent glyceryl oleate	16.9
0.5 per cent cetyl pyridinium bromide	20
0.5 per cent sodium naphthalene sulfonate	18.4
0.5 per cent sodium sulforicinate	19.5
0.5 per cent alkyl sodium sulfate	19.2

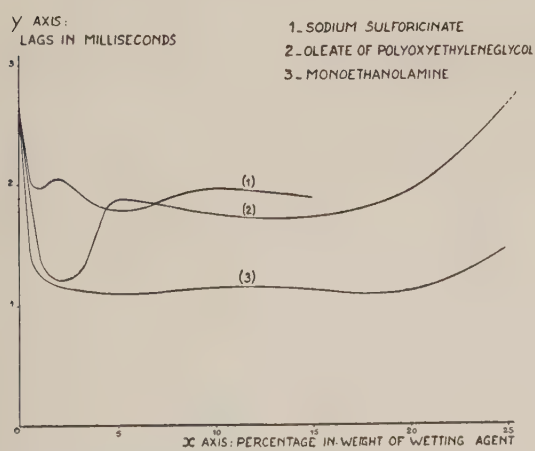

FIG. 5. Influence of concentrations of wetting agent upon ignition lags.

INFLUENCE OF SPRAYING RATE ON IGNITION LAG, WITH AND WITHOUT WETTING AGENTS

The ignition lag depends not only on the surface properties of the propellants, but also on the momentum of the sprayed particles. In the open cup method, where this momentum is least, the lag reaches its lowest value (Table 4).

Conversely, in the concurrent jets method, if the pressure drop through the injector increases, i.e., with intensified spraying, ignition is delayed. For every pair of hypergolic components there exists a maximum spraying rate, above which spontaneous ignition no longer occurs. For 37 per cent nitric acid-dicyclopentadiene, this limit corresponds to a spraying rate of about 6 kg/cm^2 (Fig. 6).

It is noteworthy that the increase in the spraying rate—necessary for further chemical reaction—has an unfavorable effect on the ignition lag which is highly dependent on the energy stored in the particles. Fortunately, these two opposite re-

TABLE 3. IGNITION DELAYS (MSEC.)

Additives	Open Cup Method	Concurrent Jets Method
A. System: Furfuryl alcohol-nitric acid concentrated at 98 per cent		
No additive	23	29.9
0.5 per cent alkyl sodium sulfate mixed with fuel component	23	14.4
0.5 per cent alkyl sodium sulfate mixed with acid component	23	22.7
B. System: Dicyclopentadiene-nitric acid concentrated at 98 per cent		
No additive	16	∞
0.5 per cent alkyl sodium sulfate mixed with acid component	16	12.5

TABLE 4. IGNITION LAGS (MSEC) FOR SYSTEMS CONTAINING 98 PER CENT NITRIC ACID AND VARIOUS FUELS

Various Fuels	Open Cup Method	Concurrent Jets Method
Furfuryl alcohol	23	29.9
Furfuramide saturated solution in furfuryl alcohol	23	20.3
Dicyclopentadiene, 83 per cent	23	∞
Dicyclopentadiene, 37 per cent	16	∞

quirements may be satisfied by the use of wetting agents which shift upward the demarcation between the two of ignitability and of non-ignitability.

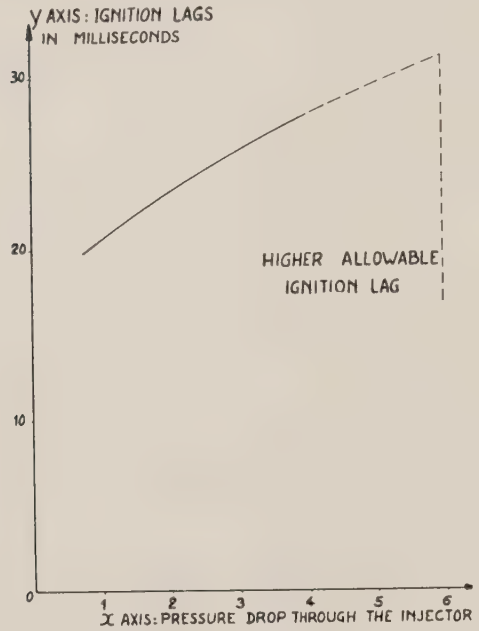

FIG. 6. Influence of spraying rate upon ignition lag of the pair: HNO_3-dicyclopentadiene at 37 per cent concentration.

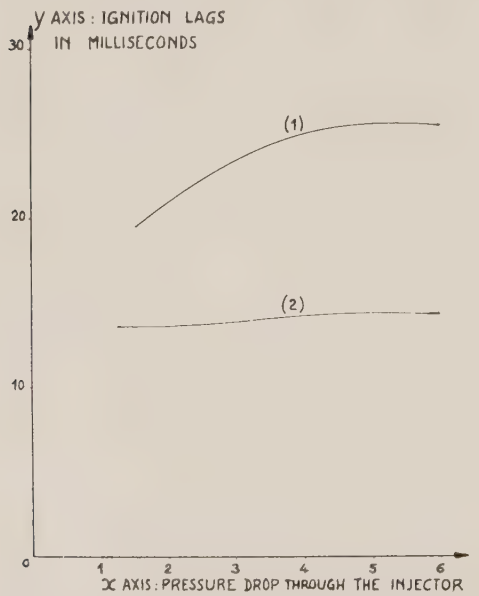

FIG. 7. Influence of spraying rate upon ignition lag of the pair: furfuryl alcohol-HNO_3. With (2) and without monoethanolamine as wetting agent.

Surprisingly enough, for a given bipropellant system the effect of these surface-active substances increases in the same proportion as the rate of spraying, with the result that ignition lag becomes nearly constant for all rates of spraying (Fig. 7).

Discussion of the Experimental Results

INFLUENCE OF WETTING AGENTS ON SURFACE TENSION OF BIPROPELLANTS

To investigate the possible physical or chemical action of wetting agents on the propellants tested, we determined the surface tension of the hypergolic components with and without the additives.[a]

It has been stated that the introduction of the additives produce no change in the surface tension of the individual components, nor can the effect be a chemical one. The wetting agents considered are not hypergolic; some of them are neutral toward nitric acid. Moreover, the relative weight of these additives is too low to reduce or increase the potential energy of the system appreciably.

EFFECT OF WETTING AGENTS UPON INTERFACIAL TENSION OF BIPROPELLANTS

The negative results of the preceding experiments led us to explain the effect of wetting agents as a reduction of interfacial tension between hypergolic components.

To check this theory by actual measurements was impractical, but the problem could be approached by studying the general property of surface active substances to lower the interfacial tension between a stable organic compound and nitric acid.

The organic compounds initially tried were gasoline, gasoil and toluene with nitric acid of increasing concentrations (Fig. 8). However, at concentrations above 50 per cent, nitric acid decomposes these hydrocarbons, which are partly olefinic, making their use impossible. On the other hand, petroleum ether and cyclohexane which have been adequately purified are stable toward anhydrous nitric acid. The results are shown in Figures 9 and 10. The wetting agent adopted was 1 per cent sodium alkyl sulfate dissolved in petroleum ether (Fig. 9) and cyclohexane (Fig. 10). It will be seen that the interfacial tension decreases as the acid concentration decreases, but does not drop to zero in the anhydrous acid.

If C_2 is the concentration by weight and γ the

[a] Measurements were made with the standard Lecomte de Noüy tensiometer.

interfacial tension, the function γ (C_2) has the same general character as the curve representing the effect of a wetting agent on the surface tension of water.[5] In particular, the slope of the tangent to the curve at the origin $d\gamma/dC_2$ may be

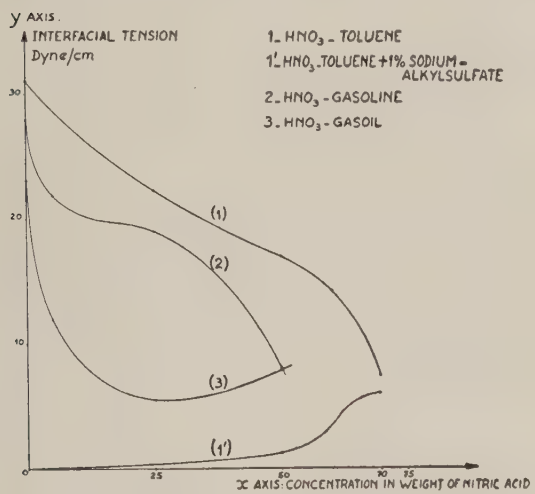

FIG. 8. Influence of acid concentrations

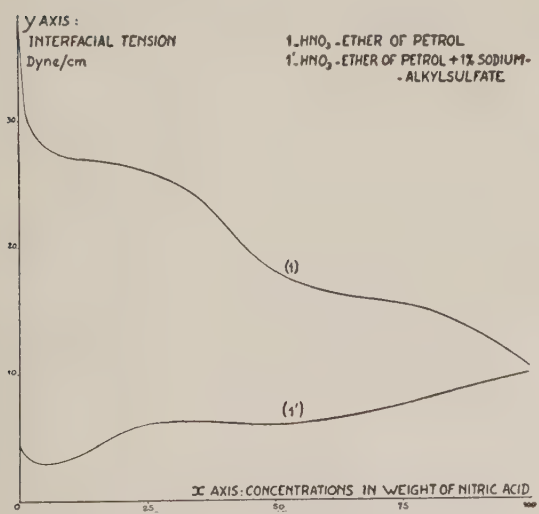

FIG. 9. Influence of acid concentrations upon interfacial tensions.

considered as a measure of the efficiency of the wetting agent (Fig. 11).

Moreover, this statement is of general value as shown by Table 5 which gives the effects of several wetting agents on the interfacial tension of the following pairs:

nitric acid–petroleum ether
nitric acid–cyclohexane

INFLUENCE OF THE RATE OF ADSORPTION UPON IGNITION LAG

The data in Figure 5 indicate that the ignition lag cannot be reduced to less than about 10 msec, even by adding large amounts of wetting agents.

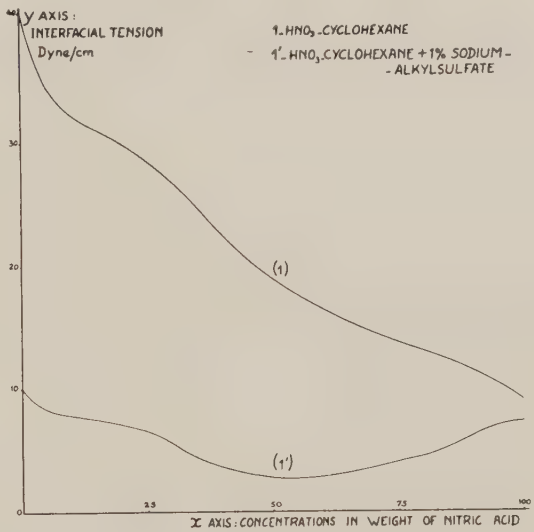

FIG. 10. Influence of acid concentrations upon interfacial tensions.

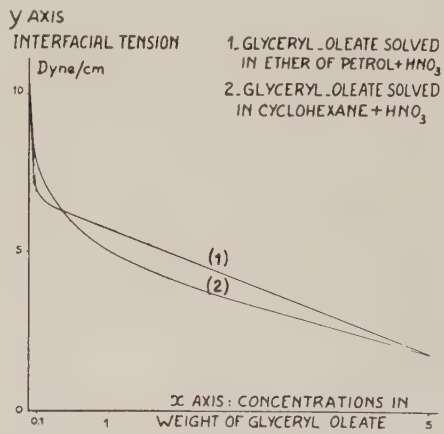

FIG. 11. Influence of concentration of wetting agent upon interfacial tension.

We suggest that this lowest limit is related to the threshold time required to adsorb the surface active substance and bring it into action at the interface. It may be assumed that after this interval of time the particles at the interface are saturated and that any further addition is ineffective.

The rate of adsorption of fatty alcohols in aqueous solution has been studied by Addison[6,7,8]

who reports that the delay for setting up a static surface tension ranges from 100 msec for secondary alcohol to 10 msec for isoamyl alcohol and is generally proportional to the molecular weight of dissolved substances.

Based on this theory we investigated wetting agents having a low molecular weight and the same structure as those already tried (Table 6).

To date the best surface active substance tested has been monoethanolamine. It was found

Table 5. Interfacial Tensions, dyne/cm

Additive (C_2 = 1 per cent)	System: Nitric Acid-Petroleum Ether	System: Nitric Acid-Cyclohexane
No additive	10.0	10.6
Sodium β-naphthalene sulfonate	11.5	10.5
Sodium sulforicinate	9.5	7.8
Sodium alkyl sulfate	7.6	7.0
Cetyl pyridinium bromide	8.9	10.0
Glyceryl oleate	5.7	5.0
Polyoxyethylene glycol oleate	6.9	4.9

Table 6. Ignition Lags of Bipropellants as a Function of Molecular Weight of Wetting Agents (msec.)

Added Wetting Agent C_2 = 0.5 per cent	Molecular Weight	Lags of Furfuryl Alcohol-Nitric Acid System
No additive	—	26.3
Polyoxyethylene glycol oleate	>500	20.6
Glyceryl oleate	357	16.9
Triethanolamine	149	16.7
Monoethanolamine	61	14.5

that by increasing the amount of this additive the ignition lag could be reduced to 11 msec. This would be the lowest limit obtained by action of a surface active substance on the nitric acid-furfuryl alcohol system.

THEORETICAL INTERPRETATION OF THE INFLUENCE OF WETTING AGENTS ON INTERFACIAL TENSION BETWEEN BIPROPELLANTS

The simplest explanation of the part played by a wetting agent in hypergolic ignition is to ascribe its action to the concentration of the wetting agent on the interfacial film between fuel and combustive, in the same way as at the fuel-water interface. We have already proposed this hypothesis elsewhere.[3] If this is the case, the best wetting agents would be anionic ones, such as soaps and the sulfates and sulfonates of fatty alcohols.

Due to their low solubility in the hypergolic fuels considered, the actual choice of these agents offers difficulties. However, as petroleum ether and cyclohexane are good solvents for the wetting agents, it was possible by measuring the interfacial tension between these solutions and nitric acid to classify the wetting agents according to their effect on surface tension, $\Delta\gamma/\Delta C_2$ for a given concentration (C_2 = 1 per cent). Table 5 shows that nonionic agents are by far the most efficient. This is supported by Figure 5 which gives ignition lags for concentrations, $0 \leqslant C_2 \leqslant 15$ per cent. Of the agents tried, the two nonionic compounds, oleate of polyoxyethylene glycol and monoethanolamine, are more efficient than sodium sulforicinate.

These results may be explained by the affinity between anhydrous nitric acid and organic compounds containing the OH radical. (The first fatty alcohols are soluble in HNO_3.)

In short, the best choice is a nonionic wetting agent of low molecular weight.

Interfacial Energy as a Factor of Hypergolic Ignition

The experimental evidence presented here indicates that the kinetics of the ignition of hypergolic components are strongly influenced by the magnitude of the total surface of all the particles of both components, which exerts a double action: (1) by its specific area, i.e., the sum of the interfaces of concurrent particles divided by the volume of the system (mass factor): (2) by the forces acting upon the said surface, i.e., the sum of the interfacial tensions (intensity factor).

Having introduced these two parameters, we are led to consider a new form of energy which plays an independent part in the tripping of ignition. This is the specific surface energy E_s defined as follows:

$$E_s = \gamma_i \cdot \Sigma_i$$

where γ_i is the interfacial tension, and Σ_i the specific area. The greater the force with which the components are sprayed, the more physical energy is stored in the blended particles. We have established that this stored energy increases the igni-

tion lag, which is therefore an increasing function of E_s and consequently of Σ_i .

Our experiments have shown that all other conditions being equal, Σ_i is an increasing function of the momentum of the concurrent jets and a decreasing function of the interfacial tension.

But $\Sigma(\gamma)$ has a finite value when $\gamma = 0$, as may be seen in the case of two concurrent jets of the same substance. Therefore E_s becomes equal to zero for $\gamma_i = 0$ and it will be assumed hereafter that the function $E_s(\gamma)$ is represented by a straight line within the range of our experiments.

Let $E_s^1(\gamma)$, $E_s^2(\gamma)$, $E_s^3(\gamma)$ be three straight lines representing the variation of specific surface energy of a given hypergolic pair at three different rates of spraying (Fig. 12). The point where the two components cease to be hypergolic is shown for each curve of this family, making it possible to plot a curve which defines the region of ignitability, $E = E_L$.

The geometrical representation enables us to formulate the following rules:

(1) If $\gamma_C C_3$ is a curve corresponding to a normal system of bipropellants (without wetting agent) and having an interfacial tension γ_C , the figurative point of a system for which the momentum of the jets is determined, may lie inside or outside of the said boundary;

(2) For a given rate of spraying—i.e., along E_s^3—the decrease of interfacial tension from γ_C to γ_B shifts the system from C_3 (nonignitability) to B_3 (ignitability), and decreases the ignition lag from B_3 to A_3 ;

(3) For a given decrease of γ—for instance $\gamma_B - \gamma_A$, the decrease of surface energy and consequently of ignition lag increases with the dispersion of the system: $\Delta E_3 > \Delta E_2 > \Delta E_1$.

Conclusion

The field of hypergolic components is a very broad one. We have not made an exhaustive investigation of this field, but have tested only some of the most usual bipropellants and a few additives. Nevertheless, our experiments have led us to a mathematical expression for the energy stored at the interface of a bipropellant system and have suggested a graphic representation of the ignition lag and the influence upon this coefficient of the addition of wetting agents. These rules appear to be generally applicable.

The preceding theory suggests that in actual practice the same ignition lag may be obtained—other conditions being equal—at a higher rate of spraying with added wetting agents than without such agents.

The specific area and the interfacial tension of the hypergolic components both act on the kinetics of the ignition. Although limited, the information obtained on these two parameters makes it possible to improve the ignition lag of any self-propelled engine operated with liquid propellants.

This theory will make it possible in some instances to increase the efficiency of many bipropellant systems where the phenomena associated with injection are of prime importance.

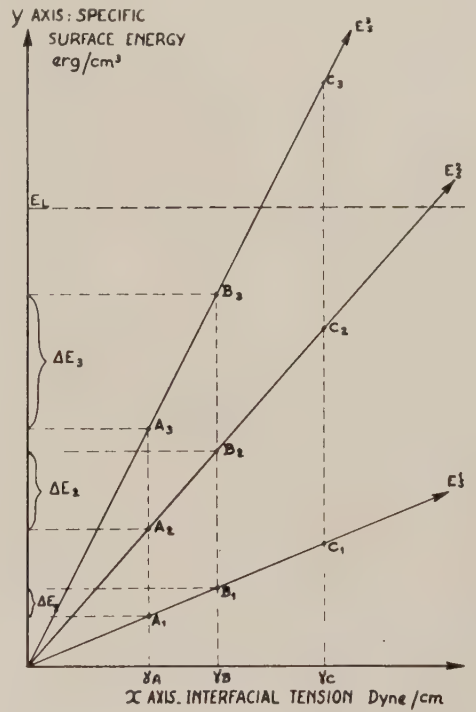

FIG. 12. Influence of interfacial tension upon specific surface energy.

REFERENCES

1. BROATCH, J. D.: Fuels, *29*, 106 (1950).
2. GUNN, S. V.: Rocket, *22*, 33 (1952).
3. BERNARD, M. L. J.: Comptes rendus de l'Academie des Sciences, *235*, 1646 (1952).
4. PENNER, S. S.: Rocket, *23*, 85 (1953).
5. DEFAY, R., AND PRIGOGINE, I.: *Tension Superficielle et Adsorption*, p. 145. Dunod, 1951.
6. ADDISON, C. C.: J. Chem. Soc., 535 (1943).
7. ADDISON, C. C.: J. Chem. Soc., 252 (1944).
8. ADDISON, C. C.: J. Chem. Soc., 477 (1944).

15

THE APPLICATION OF KINETICS TO THE HAZARDOUS BEHAVIOR OF AMMONIUM NITRATE[a]

By R. M. HAINER

Introduction

The hazardous behavior of ammonium nitrate (AN) has become well known in the past 40 years through a series of more than 25 major fires or explosions. These have involved more than 12,000 tons of ammonium nitrate and have resulted in death or injury to more than 5,000 people. Properties of ammonium nitrate have been extensively studied, particularly since the disaster at Texas City in 1947,[1] and this report is based on research initiated as a result of that disaster. The continued annual United States production of approximately 1.5 million tons (1952) of ammonium nitrate for fertilizers, propellants, and explosives continues the interest in the properties and hazards of ammonium nitrate. Knowledge of the kinetics and decomposition of ammonium nitrate is basic to the analysis of hazard.

There are two important aspects to the hazardous behavior of ammonium nitrate, and both can be intuitively understood from its rate of decomposition: the condition under which spontaneous or self-heating in ammonium nitrate can take place; and the development of explosion from fire in ammonium nitrate. The hazard in ammonium nitrate arises on the one hand from its exothermic decomposition, and on the other hand, from the release of gaseous products in considerable volume. The kinetic analysis which is herein applied to AN is equally applicable to other materials which are handled in sizable quantities, are exothermic, and on decomposition release gaseous products.

Measurements of the rate of decomposition of chemically pure ammonium nitrate (CPAN) and several commercially important ammonium nitrate products will first be compared with the published kinetic data and will then be applied to the analysis of the two aspects of hazard in ammonium nitrate.

[a] This paper is derived from research performed for and reported to the United States Coast Guard on Contract Teg-38525 (CG-20, 003-A) in a report entitled "An Investigation of the Properties and Hazards of Ammonium Nitrate and High-Percentage Ammonium Nitrate Fertilizers", November 14, 1952, and to the National Academy of Sciences under Contract Teg-38325 in "Hazards in the Handling, Storing, and Transporting of Ammonium Nitrate and High-Content Ammonium Nitrate Fertilizer: A Critical Interpretation and Review of the Literature"; 75 Abstracts and 170 References, April 30, 1953.

Kinetics of Decomposition

The rate of decomposition of CPAN has been measured by observing the volume of nitrous oxide released, and the loss in weight in the system, during the decomposition:

$$NH_4NO_3 \rightarrow N_2O + 2H_2O.$$

Samples of approximately 25 gm were heated over a 70°C temperature interval from 220–290°C. These data are plotted in Figure 1. The weight loss on a 300-gm sample at the "self-limiting" temperature was observed and was found to be first order. After correction for sublimation loss,[2] the rate constant was found to be 2.3×10^{-3} sec^{-1} at 290°C. In addition, the rate of gas release was measured over a three-week period on a solid sample of 100 pounds of CPAN held in a paper bag, insulated in santocel, and enclosed in an airtight drum. A temperature of about 130°–135°C was produced by careful electrical heating over the entire surface of the bag. The rate of decomposition was about 3×10^{-9} sec^{-1}.

The rate of decomposition of the 1:1 double salt, composed of 40 per cent ammonium nitrate and 60 per cent ammonium sulfate, was similarly observed on 25-gm samples; the data are shown in Figure 1.

Because of the commercial importance of the 3-per cent, wax-coated, fertilizer-grade ammonium nitrate (FGAN), which was involved in the Texas City disaster, the rate of decomposition was observed over as wide a temperature range as possible. Observations above the melting point (170°C) were made on 25-gm samples, but because of spontaneous ignition of this organic-coated AN in test-tube size apparatus, rates of gas evolution above 230°C were not possible. Below 170°C, several kilograms of FGAN were used, and the rate of decomposition was obtained by

measuring the change in gas pressure within a closed system of fixed volume. The rates of decomposition, from 70°–230°C, are plotted in Figure 1.

A preliminary investigation was made of the effect of certain common additives on the rate of decomposition of ammonium nitrate. Samples of approximately 25 gm of CPAN were observed after the addition of 5 per cent nitric acid and 1 per cent sodium chloride. With the addition of the nitric acid, the rate of reaction at 200°C is approximately 100 times that of CPAN. The sodium chloride also catalyzes the decomposition of CPAN, but not by a direct process. At 175°C, an induction period of more than an hour is required with 1 per cent sodium chloride in CPAN; during this period, Cl_2 is released, and the rate of reaction rapidly increases to approximately 1000 times that of CPAN at the same temperature. Tramm and Velde,[3] and more recently Bent and Powell,[4] have shown that if the NaCl-NH_4NO_3 mixture is prevented from turning acid, the catalytic effect can be delayed indefinitely, even at temperatures as high as 175°C.

Potassium dichromate has been indicated by Robertson[5] as one of the most effective catalysts for the decomposition of ammonium nitrate. The rate of decomposition was measured for a 1 per cent mixture of $K_2Cr_2O_7$ in CPAN; the data are given in Figure 2.

Because of the importance of paper in the fertilizer-grade ammonium nitrate, the effects on the rate of decomposition of the mixture were measured and were found to be approximately 100 times that of FGAN alone. The data obtained are shown in Figure 2.

The scatter of the data over the limited temperature range for the decomposition of CPAN does not allow a precise evaluation of the energy of activation or of the frequency factor, although this factor is greater than 10^{14} and the activation energy curve appears to be of the order of 50,000 calories. The remaining systems, as shown in Figures 1 and 2, are inhomogeneous, and direct adherence to straight-line decomposition on these plots is not expected. For the wax-coated FGAN, the rate constant is approximately linear over a 150°C temperature interval, and over a change in phase. It is clear that the catalysts, $K_2Cr_2O_7$, HNO_3, and the reaction products with NaCl, greatly enhance the rate of decomposition at low temperatures. However, the rates of decomposition extrapolated to near 300°C are not essentially different from that of CPAN alone. Thus, it appears that the catalysts act by reducing the activation energy for decomposition or by changing the products of decomposition, for example, to other oxides of nitrogen. Nitrogen dioxide can be observed in the higher temperature range of

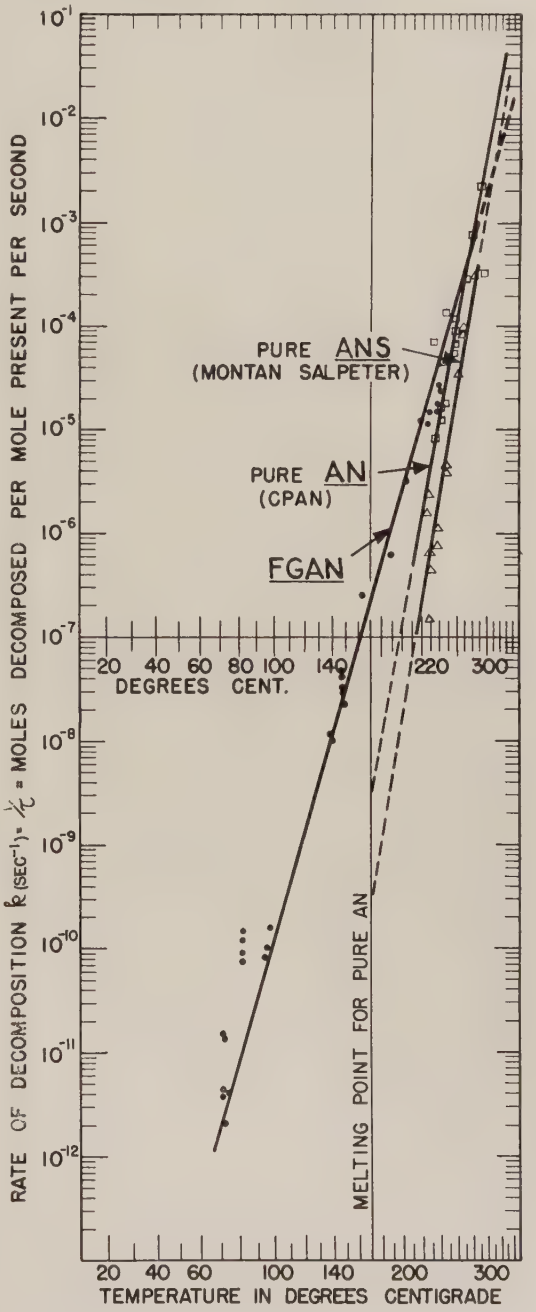

FIG. 1. The decomposition of chemically pure ammonium nitrate, fertilizer-grade ammonium nitrate, and montan salpeter.

the decomposition in the presence of these catalysts. Because of the high collision rate for the decomposition of ammonium nitrate in the high-temperature region, decomposition should be as rapid for pure ammonium nitrate as for any catalytic mixture. Presumably a catalyst acts as an active center for decomposition, and, at high reaction rates, requires diffusion to its active center. This process would involve inherently a lower collision rate than if the decomposition rate directly resulted from a vibration process. While these data do not prove the impossibility of an ammonium nitrate catalyst in the temperature range well above 300°C, no observation has been found in our work or in the literature to indicate markedly greater rates of decomposition than for CPAN alone.

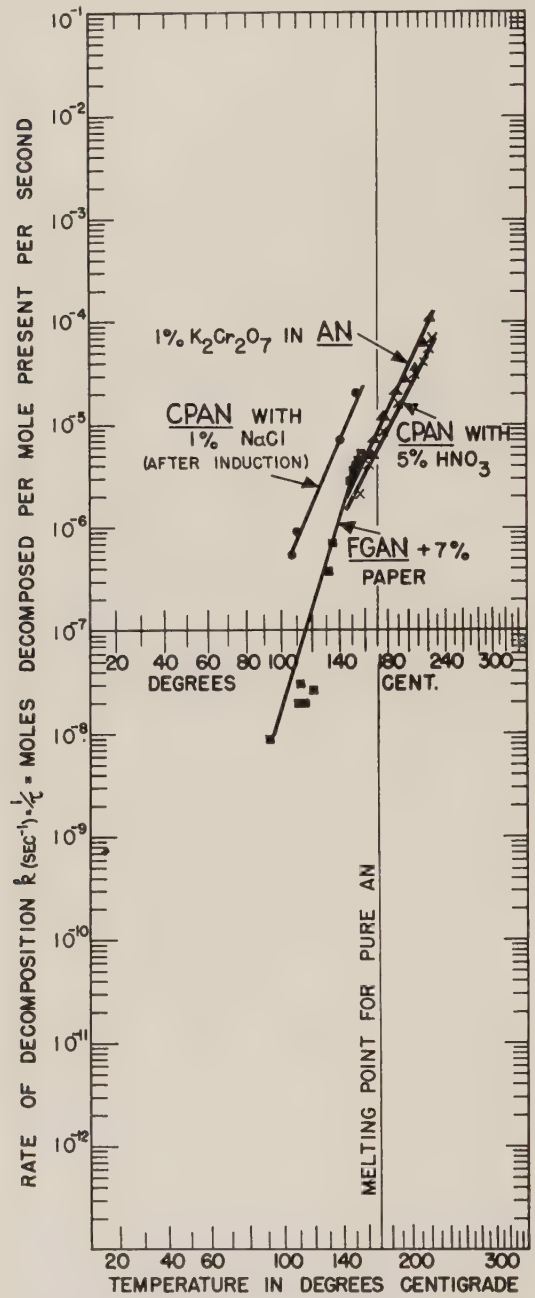
RATE OF DECOMPOSITION k (SEC⁻¹) = 1/τ = MOLES DECOMPOSED PER MOLE PRESENT PER SECOND
1% K2Cr2O7 IN AN
CPAN WITH 1% NaCl (AFTER INDUCTION)
CPAN WITH 5% HNO3
FGAN +7% PAPER
20 40 60 80 100 140 180 240 300
DEGREES CENT.
MELTING POINT FOR PURE AN
20 40 60 100 140 200 300
TEMPERATURE IN DEGREES CENTIGRADE

FIG. 2. The rate of decomposition of catalyzed ammonium nitrate.

Published Kinetic Data

Minor attention had been given to the rate of decomposition of ammonium nitrate prior to 1947. Saunders[6] in 1922 found the rate constant at 200°C as 4×10^{-7} sec^{-1}. Shah and Oza[7] made a careful study of the rate of decomposition on on 1-gm samples of ammonium nitrate over the temperature range of 230°–290°C. These data are plotted in Figure 3.

Within the last few years, the rate of decomposition of pure ammonium nitrate and catalyzed[8] ammonium nitrate has been investigated by a number of workers. Robertson[5] measured the rate of decomposition of ammonium nitrate over the range 242°–364°C by dropping samples of 2 to 123 mg on heated iron plates of known temperature. It was found that the data could be represented by $k = 10^{13.8} e^{-40{,}500/RT}$ sec^{-1}. These data are plotted in Figure 3.

Doeschner[9] measured the decomposition of ammonium nitrate over the range from 178°–203°C; his data are also given in Figure 3. Rice, Ransil, and Scherber[10] measured the decomposition over the range of 240°–260°C; their high and low values are plotted in Figure 3.

Recently, Bent and Powell[4] observed the decomposition of ammonium nitrate and the effect of acid over the temperature range 210°–250°C; also Wood and Wise[11] observed the decomposition and effect of acid over the range of 200°–300°C. These data are given in Figure 3.

All of these data agree fairly well except for those of Robertson, which are as much as 20 times greater in the region of about 250°C. Since his data are markedly higher, and at the same time are based on a rather unusual technique which utilizes only small samples, his results are believed to be anomalously high.[2] In the region above 250°C, the self-heating of ammonium nitrate due to its own rate of reaction and exothermal decomposition is significant. It may well

be that the spontaneous heating of the nitrate gave rise to a higher temperature than that of the metal plate and that the volatilization of the ammonium nitrate to ammonia and nitric acid was inadequately compensated.

Friedman and Biegeleisen[12] have reported that a thoroughly dried, evacuated, 3-gm sample of ammonium nitrate can be heated to 300°C without detectable decomposition, and that water is a catalyst for the decomposition. The decomposition of 3 gm of ammonium nitrate with water vapor present can be detected in their apparatus at 180°C. From the data of Figures 1 and 3, the decomposition of ammonium nitrate at 300°C is approximately $1 \times 10^{-2}(\text{sec}^{-1})$; at 180°C, it is approximately $1 \times 10^{-7}(\text{sec}^{-1})$. Thus the acceptance of their report necessitates that an attenuation of 10^5 be obtained in the rate of decomposition by carefully drying, in high vacuum (10^{-5}mm), a sample of ammonium nitrate whose decomposition product itself is 2 moles of water per mole of AN. Confirmation of this result has not yet been reported, but for the decomposition of bulk amounts of ammonium nitrate under conditions of possible hazard, adequate amounts of water are present for the decomposition to proceed as has been reported in Figures 1 and 3.

The Hazard of Spontaneous Heating

The hazard of spontaneous heating in ammonium nitrate can be understood by equating the heat released from the decomposition to the heat loss by conductivity through the sample. Above a given critical size, the heat released within the material is larger than the heat lost, and in consequence, spontaneous heating will take place. The quantitative conditions under which such spontaneous heating may develop have been considered in detail by Frank-Kamenetsky[13] and have been reviewed by Bowden and Yoffe.[14] Rice[15] repeated in English the Frank-Kamenetsky formulation and applied it to thermal explosion of gases. Recently, Robertson[16] has applied this treatment to several solid explosives. The Frank-Kamenetsky formulation for spontaneous heating has been quantitatively described in terms of a differential equation whose solution is given in terms of an arbitrary dimensionless constant, δ. The value of this constant for the condition of spontaneous heating must be equal to, or greater than, 3.32; thus:

$$\delta = \frac{r_0^2 nQkB}{\lambda RT^2} = 3.32$$

In terms of the critical radius for spontaneous heating, r_0, in centimeters,

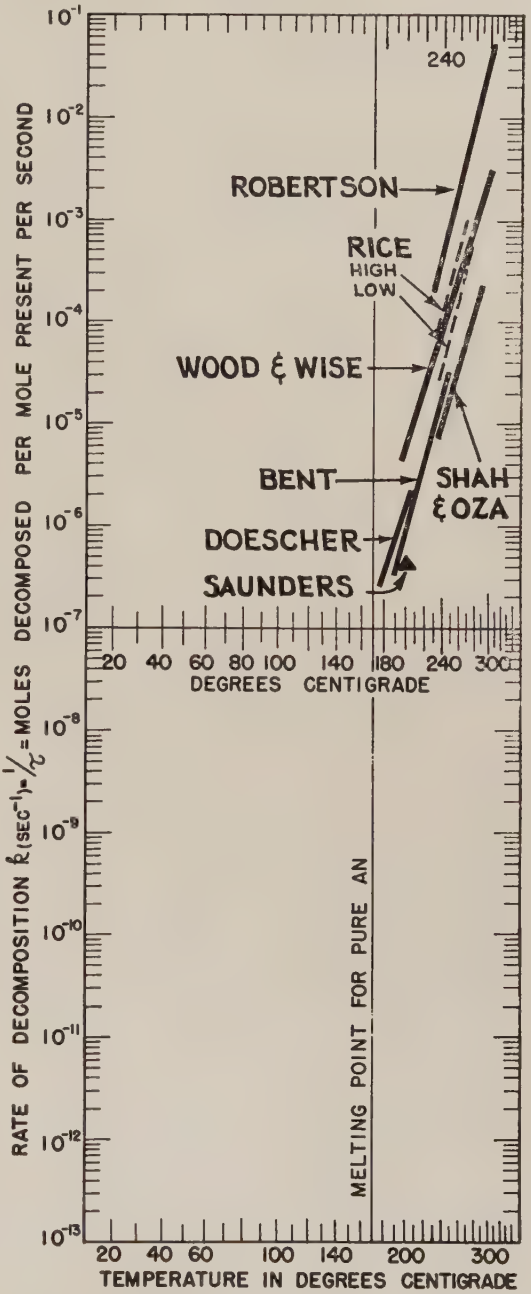

FIG. 3. The published rates of decomposition of ammonium nitrate.

$$r_0 = \left(\frac{3.32R\lambda T^2}{nQkB}\right)^{1/2}$$

where λ = thermal conductivity, 2.9 to 3.9 $\times$ 10^{-4} cal cm ^{1}C^{-1}sec^{-1};

R = gas constant, 1.987 cal°C^{-1} mole^{-1};
n = number of moles per cc, (0.8g cm^{-3}/80g mole^{-1}) = 1.0 × 10^{-2} mole cm^{-3};
Q = heat of reaction, 14,400 cal mole^{-1} at 170°C and 16,300 cal mole^{-1} at 300°C;
k = rate of reaction, sec^{-1} (see Figures 1, 2, and 3);
B = activation energy for reaction, 50,000 cal mole^{-1} (see Figures 1 and 3);
T = the initial uniform temperature, °K.

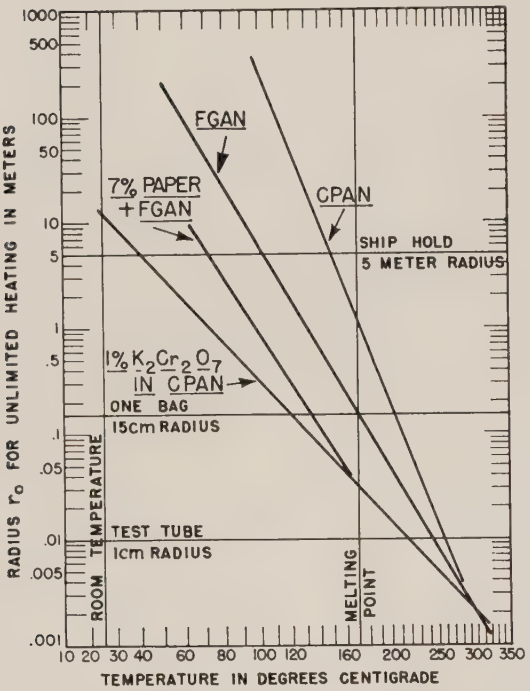

FIG. 4. The critical radius for spontaneous heating of several varieties of ammonium nitrate.

The critical radius, r_0, is thus a function of: δ and R, which are universal constants; λ and n, which are constants for a given sample of ammonium nitrate; Q, the heat of reaction; and B, the activation. Neither Q nor B has been found to have values which differ more than a factor of 2 from any available data, and their product does not change to an important extent for any reactions known. T, the temperature, changes only by a factor of 2 over the range of importance. The rate constant, k, is the only significant variable; over an important temperature range it may change by a factor of 10^{10}. Thus we may write $r_0 = C(k)^{-1/2}$. Since, to a very good approximation, $k = Ae^{-B/RT}$, we may conclude:

$$\ln r_0 = C' + C''/T.$$

Thus, the logarithm of the critical radius is, for practical purposes, a linear function of the reciprocal of the absolute temperature. The critical radii for spontaneous heating for various materials are plotted in Figure 4; the appropriate assumptions were made from Figures 1 and 2. The graph accents ordinants and abscissa which are important in evaluating the hazard of ammonium nitrate.

Lines on Figure 4 divide the region of safety from the region of hazard. To this approximation, chemically pure ammonium nitrate in a sphere of 5 meters in radius should gradually cool if the initial temperature is less than 150°C. The important fertilizer-grade ammonium nitrate (FGAN), with 3 per cent wax, has significantly greater hazard and, in the same size sample, may not be safe unless the initial temperature is below 100°C. For catalyzed ammonium nitrate, these values are only approximate, and suggest that with $K_2Cr_2O_7$, hazard may be experienced for an unventilated sphere of 5 meters radius at temperatures above approximately 40°–50°C.

In this analysis, nothing has been said concerning the time required for the development of unlimited self-heating for a given sample of ammonium nitrate initially at a uniform arbitrary temperature. The formal analysis is difficult, and any assumptions made in an approximate analysis are inadequate to describe the wide variation of practical circumstances.

The empirical affirmation of the correctness of the approximation given in Figure 4 for the hazard of ammonium nitrate is very difficult in larger than laboratory samples; however, considerable experimental evidence supporting the plot of Figure 4 has been obtained (see footnote *a*, page 224). The phenomenon can be easily demonstrated in the laboratory by observing the temperature rise of samples in a test tube, a beaker, or a Dewar flask.

Kistiakowsky and Guinn[17] have experimentally investigated the spontaneous heating of FGAN and have concluded that spontaneous heating is quite probable in shipload cargoes above 100°C.

The critical radius for defining the hazard of spontaneous heating in commercial ammonium nitrate clearly depends almost entirely upon the rate of chemical decomposition; once the rate of decomposition has been determined for the materials involved over the significant range of tem-

perature, the boundary of hazard for samples of various sizes can be deduced with only minor approximations.

The Hazard of Explosion from Fire

The knowledge that ammonium nitrate decomposes exothermically, that the products of decomposition are gases, and that the rate of reaction is an exponential function of temperature, would by itself, lead to the conclusion that fire in large quantities of ammonium nitrate should inevitably develop into explosion. This conclusion is supported by the experimental demonstration of spontaneous heating and by the explosion during the last seven years of four cargo vessels.[b] However, the fact that many fires[18] have existed in various commercial grades of ammonium nitrate without explosion has led to the conclusion that under some conditions, a secondary mechanism interrupts the self-accelerating decomposition in ammonium nitrate and limits its rise in temperature.

Berthelot,[19] as early as 1869, suggested the importance of the endothermic dissociation of ammonium nitrate into ammonia and nitric acid. At 300°C, this endothermic dissociation requires approximately 38 kcal/mole, which, in an isolated reaction, must be supplied from the exothermic decomposition. A heat balance can be formulated via the first law of thermodynamics which equates the endothermic heat of dissociation to the exothermic heat of decomposition; from this heat balance, and from the empirical vapor pressure of ammonium nitrate, an equilibrium or self-limiting temperature can be predicted which is a function of the external applied pressure of the system. This limiting temperature has been experimentally investigated[2] from 200°–350°C and can be approximately represented by the following equation:

$$\ln_{10} P = \frac{-4.71 \times 10^{+3}}{T} + 11.20,$$

where P is the external applied pressure in millimeters, and T is the limiting absolute temperature. The vapor pressure has been investigated,[a] and a full account of the results will be published by Feick and Hainer.[2] The limiting temperature defined by this relationship is not substantially changed, even in the presence of flame. If, however, inadequate venting of the product gases from decomposition raises the applied pressure of the system, the endothermic dissociation will be suppressed, and the rapid spontaneous heating of the ammonium nitrate will raise the temperature of the system until a new limiting temperature is reached. If the applied pressure is sufficiently high, the rate of decomposition may reach the critical range for explosion[c] for values of k in the range of 10 to 100 sec^{-1}.

By using this suggested range of k as the hazardous reaction rate of explosion, and by extrapolating the limiting temperature, the pressure required for the hazardous decomposition of ammonium nitrate can be estimated. A minimum temperature of approximately 450°C appears to be required to reach the necessary rate of reaction; the corresponding pressure is, therefore, of the order of 60 to 80 atmospheres for the hazard of explosion in AN. For FGAN, with its additional exothermy from the combustion of wax and paper, the attainment of 450°C may be possible with pressures as low as 20 atm. These values are consistent with independent measurements of the Bureau of Mines[20] and Picatinny Arsenal.[21]

The close-packed geometry within a ship, with the attendant inadequacy of venting for the rapid decomposition of a fire, leads to an internal pressure rise within perhaps a very small volume; the resulting self-heating and unrestricted acceleration of the decomposition rate probably leads to shock processes which set off the remaining material by detonation. By contrast, the geometry of a warehouse appears to preclude the attainment of the required pressure within a fire for the explosive reaction rate, and the ammonium nitrate is consumed in fire without explosion.

The phenomena described here as resulting from the unrestricted acceleration of the reaction rate appear to be in line with the description of the origin of detonation by Kistiakowsky,[22] by Bowden and Yoffe,[14] and by Eyring, Powell, Duffey, and Parlin.[19]

[b] S. S. Grandcamp, April 16, 1947, Texas City, Texas, 2000 tons FGAN. S. S. High Flyer, April 17, 1947, Texas City, Texas, 1000 tons FGAN. S. S. Ocean Liberty, July 28, 1947, Brest, France, 2000 tons FGAN. S. S. Tirrenia, January 24, 1953, Red Sea, 4000 tons AN.

[c] Spencer Chemical Company, October 19, 1949, Independence, Kansas. 1400 tons FGAN. E. I. du Pont (Repauno), April, 1940, Gibbstown, New Jersey. 300 tons AN. St. Stevens, Canada, 1947. 400 tons AN.

Acknowledgment

The work reported has in part been supported by group activity. I wish to acknowledge the contributions of Mr. G. Feick, Drs. A. G. Emslie, W. E. Gordon, H. O. McMahon, and W. C. Lothrop.

This work was performed under the auspices of the United States Coast Guard and the Advisory Committee on Hazards of Ammonium Nitrate Transportation of the National Research Council. Permission to publish this article has been granted by the United States Coast Guard, but neither of the sponsoring agencies necessarily approves the technical opinions or conclusions herein expressed.

REFERENCES

1. Kintz, G. M., Jones, G. W., and Carpenter, C. B.: Bureau of Mines, R. I. 4245, February, 1948.
   Lewis, B., and Jones, G. W.: Bureau of Mines, Problem PC-368, Report 3041-C, May 21, 1947.
2. Feick, G., and Hainer, R. M.: J. Am. Chem. Soc., *76*, 5860 (1954).
   Feick, G., and Hainer, R. M.: Nature, *173*, 1188 (1954).
   Feick, G.: J. Am. Chem. Soc., *76*, 5858 (1954).
3. Tramm, H., and Velde, H.: Angew. Catm., *47*, 782 (1934).
4. Bent, H., and Powell, R. E.: Thesis, Univ. of Calif., Berkeley, 1953.
5. Robertson, A. J. B.: J. Soc. Chem. Ind. (London), *67*, 221 (1948).
6. Saunders, H. L.: J. Chem. Soc., *121*, 698 (1922).
7. Shah, N. S., and Oza, T. N.: J. Chem. Soc., *131*, 725 (1932).
8. Clarke, R. P., King, S. M., and Calcote, H. F.: Experiment, Inc., TP No. 54 (June, 1952). Wright Development Center, AF 33 (038)-21837.
9. Doeschner, R. N.: Jet Propulsion Laboratory, C. I. T. Basic Research on Rocket Propellants, Progress Report 9-43 (March 14, 1950). Project TU 2-1, Contract W-04-200-ORT-1482.
10. Rice, F. O., Ransil, C., and Scherber, F.: Final Report to United States Coast Guard. Contract No. Teg-38529 with the Catholic University of America (November 15, 1952).
11. Wood, B. J., and Wise, H.: Jet Propulsion Laboratory, Calif. Inst. of Tech., Progress Report, No. 20-215 (January 29, 1954).
12. Friedman, L., and Biegeleisen, J.: J. Chem. Phys., *18*, 1325 (1950).
13. Frank-Kamenetsky, D. A.: Acta Phys. Chem. U. S. S. R., *10*, 365 (1939); Russian J. Phys. Chem., *13*, 738 (1939).
14. Bowden, F. P., and Yoffe, A. D.: *The Initiation and Growth of Explosives in Liquids and Solids*. Cambridge, Cambridge University Press, 1952.
15. Rice, O. K.: Chem. Phys., *8*, 727 (1940).
16. Robertson, A. J. B.: Thesis for Ph. D., Cambridge (1947).
17. Kistiakowsky, G. B., and Guinn, V. P.: *Spontaneous Ignition of Bagged FGAN*. Testimony in re Texas City Disaster Litigation, U. S. District Court for the Southern District of Texas (April 13, 1950).
18. Berthelot, M.: Ann. Chem. et Phys. (4), *18*, 5 (1869).
19. Eyring, H., Powell, R. E., Duffey, G. H., and Parlin, R. B.: Chem. Revs., *45*, 69 (1949).
20. Burns, J. J., Jones, G. W., and Lewis, B.: Bureau of Mines, Problem PC-368, Report 3099-C: 472, (December 8, 1947).
    Scott, F. E., Burns, J. J., Jones, G. W., and Lewis, B.: Bureau of Mines, Problem PC-368, Report 3099-C: 472 A, (April 1, 1948).
    Scott, F. E., Burns, J. J., Jones, G. W., and Lewis, B.: Bureau of Mines, Problem PC-368, Report 3099-C: 472 B, (December 14, 1948).
    Burns, J. J., Scott, G. S., Jones, G. W., and Lewis, B.: Bureau of Mines, Report of Investigations 4994, (May, 1950). (Compilation of the 3 reports mentioned above for the Bureau of Mines.)
21. Macy, P. F., Dudderar, T. D., Reese, E. F., and Eriksen, L. H.: Picatinny Arsenal Technical Report 1658 (July 11, 1947).
    Eriksen, L. H.: Picatinny Arsenal Technical Report 16775 (April 15, 1948).
22. Kistiakowsky, G. B.: *Third Symposium on Combustion, Flame and Explosion Phenomena*, pp. 560–565. Baltimore, The Williams & Wilkins Company, 1949.

16

STUDIES ON COMBUSTION OF CARBON PARTICLES IN FLAMES AND FLUIDIZED BEDS

By SAKAE YAGI AND DAIZO KUNII

General Theory

COMBUSTION OF SINGLE CARBON PARTICLE

Not only the chemical reaction rate coefficient of a carbon particle but the mass transfer coefficient through the boundary film surrounding it must be considered when studying the overall rate of combustion of a carbon particle, especially in the case of combustion in flames or in fluidized beds. The value of the chemical reaction rate coefficient k_{c1}[cm/s] is calculated, for example, by changing the unit of the specific combustion rate K_c in the following equation derived by Parker and Hottel[1].

$$10^3 K_c = (9.55 \times 10^9/\sqrt{T})P_1 \exp(-44{,}000/\mathbf{R}T) \quad (1)$$

The value of the mass transfer coefficient through the boundary film around the carbon particle, k_{f1}[cm/s], can be calculated by the following equation, derived from experimental data on mass transfer for various conditions by N. Froessling and by Ranz and Marshall[2].

$$\mathbf{N}_{Nu}{}' = k_f D_p \xi_f / \mathbf{D}_{vf} = 2.0 + 0.6(\mathbf{N}_{Sc})^{1/3}(\mathbf{N}_{ReM})^{1/2} \quad (2)$$

The combustion rate of a single carbon particle of radius r according to $C + O_2 \rightarrow CO_2$ can be described as follows:

$$-\frac{dr}{d\theta_p} = \alpha k_1 C_1 \qquad \frac{1}{k_1} = \frac{1}{k_{c1}} + \frac{1}{k_{f1}} \quad (3)$$

When a particle reacts with both oxygen and carbon dioxide during combustion, the subsequent equation can be given.

$$-\frac{dr}{d\theta_p} = \alpha \bar{z} \qquad \bar{z} = \bar{k}_1 \overline{C_1} + \bar{k}_2 \overline{(C_2 - C_2^*)} \quad (4)$$

In another ideal case where the ash layer remains around the unburned core of the particle and prevents the diffusion of gas (Fig. 1), the equations given by the authors can be used to obtain the combustion rate at the core[3]:

$$-\frac{dr}{d\theta_p} \doteqdot \alpha \bar{k}_1 C_1 \qquad \frac{1}{\bar{k}_1} = \frac{1}{k_{c1}} + \frac{1}{k_{d1}} + \frac{1}{3k_{f1}} \qquad k_{d1} = \frac{12\mathbf{D}_{vs}}{D_p} \quad (5)$$

Generally speaking, in this case, where the chemical reaction, the diffusion of gas through the solid layer, and the mass transfer through the boundary film must be taken into consideration, the radius-ratio of unburned core r/R can be expressed by the following equations given by the authors[3, 4].

$$\frac{\theta_p}{\theta_B} = 1 - \frac{\gamma(r/R) + 3\omega\gamma(r/R)^2 + \omega(1 - 2\gamma)(r/R)^3}{\omega + \omega\gamma + \gamma}$$

$$\omega = \frac{k_{c1}}{k_{d1}} \quad (6)$$

$$\theta_B = \frac{D_p}{2\alpha \bar{k}_1 C_1} = \text{time required for complete combustion of particle of diameter } D_p$$

The value of γ is also expressed as follows:

$$\gamma = \frac{3k_{f1}}{kd_1} = \left(\frac{\mathbf{N}_{Nu'}}{4\xi_f}\right)\left(\frac{\mathbf{D}_{vf}}{\mathbf{D}_{vs}}\right) \doteqdot \frac{\mathbf{N}_{Nu'}}{4e} \quad (7)$$

e = (total sectional area of small holes in the solid layer through which the gas can diffuse)/(unit area)

in case of boundary film controlling

$$k_{f1} \ll k_{c1}, k_{d1}\ \gamma \to 0\ \frac{\theta_p}{\theta_B} = 1 - \left(\frac{r}{R}\right)^3 \qquad (8)$$

diffusion through solid layer controlling

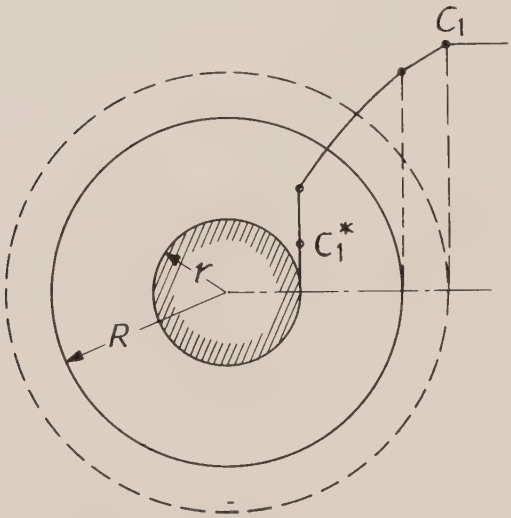

FIG. 1. Model of single particle, in which solid layer remains around unreacted core.

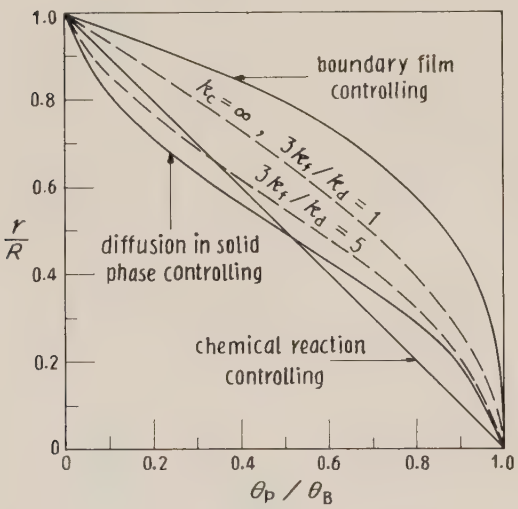

FIG. 2. Decrease of diameter of unreacted core with time, in case of single particle shown in Fig. 1.

$$k_{d1} \ll k_{c1}, k_{f1}\ \omega, \gamma \to \infty$$

$$\frac{\theta_p}{\theta_B} = 1 - 3\left(\frac{r}{R}\right)^2 + 2\left(\frac{r}{R}\right)^3 \qquad (9)$$

chemical reaction rate controlling

$$k_{c1} \ll k_{d1}, k_{f1}\ \omega \to 0\ \frac{\theta_p}{\theta_B} = 1 - \frac{r}{R} \qquad (10)$$

The ratio r/R vs. θ_p/θ_B, i.e., the decrease of unburned core with the time, can be calculated for some values of k_{c1}, k_{d1} and k_{f1}, which are shown in Figure 2.

In the case of a particle surrounded by a solid layer, where the value of e is generally less than 0.5, the value of γ is usually larger than 1, because $\mathbf{N}_{Nu'} \geqslant 2.0$. The larger the value of γ, the more the r/R vs. θ_p/θ_B curve approaches a straight line in Figure 2, and this is why approximations such as in equation (5) are possible.

When carbon particles are burned in flames, the turbulent diffusion of oxygen into the cloud of carbon particles must be considered. According to the authors' model (Fig. 3), the combustion rate of carbon particles per unit length of flame is:

$$\begin{aligned}(\pi D_F)(\bar{\epsilon}/\bar{\delta})(C_1 - C_1') &= (\pi/4)D_F^2 N_{Fp}(\pi D_p^2)k_1 C_1' \\ &= (\pi/4)D_F^2 N_{Fp}(\pi D_p^2)k_1^* C_1\end{aligned} \qquad (11)$$

where k_1^* is the overall rate coefficient of combustion for a single carbon particle, $\bar{\epsilon}$ is the modified eddy diffusivity of turbulent flames, $\bar{\delta}$ is the mean diffusion length of turbulent flame, D_F is the flame diameter, N_{FP} is the number of particles per unit volume of flame, and C_1' is the mean concentration of oxygen in the flame as shown in Figure 3.

Eliminating C_1' from equation (11), k_1^* can be expressed by the following equation:

$$\frac{1}{k_1^*} = \frac{1}{k_{c1}} + \frac{1}{k_{f1}} + \frac{1}{k_t}$$

in case of low ash content

$$\frac{1}{k_1^*} = \frac{1}{k_{c1}} + \frac{1}{k_{d1}} + \frac{1}{3k_{f1}} + \frac{1}{k_t} \qquad (12)$$

in case of high ash content

where k_t is defined by

$$k_t = \frac{4}{\pi N_{Fp} D_F D_p^2}\left(\frac{\bar{\epsilon}}{\bar{\delta}}\right). \qquad (13)$$

Considering the initial diameter of the particles before ignition D_{pi}, their diameter during combustion D_p, and the mean volume of flame gas corresponding to the unit weight of particle V, the number of particles per unit volume of the flame N_{Fp} can be given as follows:

$$N_{Fp} = 1 \Big/ \left(\frac{\pi}{6} D_p^3 \rho_s V\right) \qquad (14)$$

Using equation (14), the value of k_t is expressed by

$$k_t = \left(\frac{2V\rho_s}{3}\right)\left(\frac{D_{pi}}{D_p}\right)^2\left(\frac{D_{pi}}{D_F}\right)\left(\frac{\bar{\epsilon}}{\bar{\delta}}\right), \qquad (15)$$

where the mean values of the modified eddy diffusivity $\bar{\epsilon}$ and the diffusion length of the turbulent flame $\bar{\delta}$ can be calculated as follows[5]:

$$\begin{aligned} \bar{\epsilon} &= 2.74 \times 10^{-3}\bar{u}_F D_F \\ \bar{\delta}/D_F &= 0.0515 \end{aligned} \qquad (16)$$

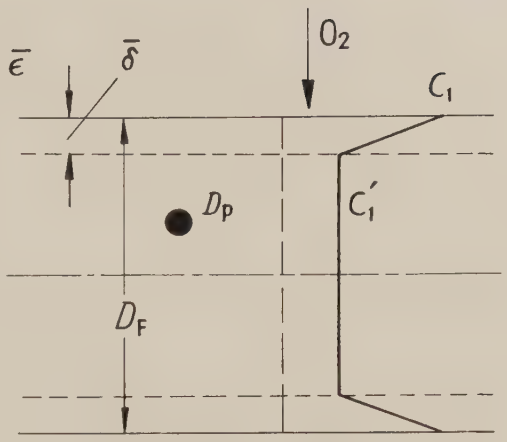

FIG. 3. Model of turbulent diffusion in flame of carbon particles.

COMBUSTION OF PURE CARBON PARTICLES IN FLUIDIZED BED

When pure carbon particles are fed continuously into a fluidized bed where they undergo steady-state combustion, both the combustion kinetics and the holding time of any carbon particle are fundamental to the understanding of the combustion phenomena in the bed, because the fluidized bed is the accumulation of many carbon particles which have been fed into it over a long period of time. If a given particle is observed, it appears to wander through the whole bed, reacting with both oxygen and carbon dioxide alternately in case of combustion with air. Its combustion rate can be calculated from equation (4), where C_1 or $\overline{C_2 - C_2^*}$ are the mean values of driving forces with respect to the total surface area of particles in the fluidized bed, taking into account the effects due to their agglomeration.

In a model of the fluidized bed in the steady state shown in Figure 4, the elutriation constant $\kappa_{(x)}$ for particles of diameter x can be calculated by the following equations which involve the carry-over rate J, the weight of the fluidized bed M, the size frequency distribution functions of carry-over $\mathbf{K}_{4(x)}$ and of the fluidized bed $\mathbf{K}_{2(x)}$.

$$\begin{aligned} J\mathbf{K}_{4(x)}\,dx &= \kappa_{(x)}M\mathbf{K}_{2(x)}\,dx \\ \kappa_{(x)} &= (J/M)\{\mathbf{K}_{4(x)}/\mathbf{K}_{2(x)}\} \end{aligned} \qquad (17)$$

The definition of the elutriation constant and the derivation of equation (17) are presented in Appendix I. In Figure 4, the particles fed into the bed during the time θ and $\theta + d\theta$ are marked, their diameters ranging between X and $X + dX$.

The probability distribution functions for overflow or carry-over particles, $f_{(X,\theta p)}$ or $g_{(X,\theta p)}$, are formulated as equation (50) in Appendix II, by integrating the fundamental differential equations for the fractional numbers of marked particles which leave the bed during the short time interval $d\theta_p$ after time θ_p as shown in Figure

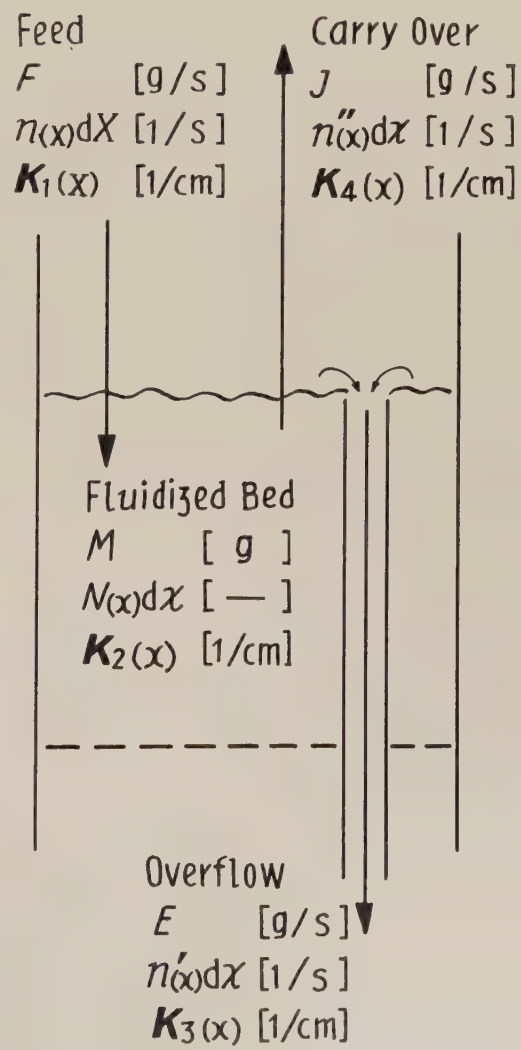

FIG. 4. Model of fluidized bed in steady state

5. With the aid of the above functions, the average holding time in the fluidized bed of carbon particles with initial diameters of between X and $X + dX$, is formulated as equation (18), equation (4) for combustion rate of a carbon particle being used for the unification of the independent variable.

$$\{\theta_{h(X)}\}_{\text{overflow}} \equiv \{\theta_{h(X)}\}_{\text{carry over}} = \frac{1}{2\alpha\tilde{z}} \int_{x=0}^{x=X} I_{(X,\,x)}\, dx \tag{18}$$

$$I_{(X,\,x)} = \exp\left\{\frac{-1}{2\alpha\tilde{z}} \int_{x=x}^{x=X} \left(\frac{E}{M}\psi_{(x)} + \kappa_{(x)}\right) dx\right\} \tag{19}$$

Similarly, the equations for the carry-over ratio,

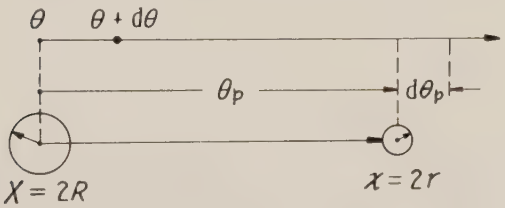

FIG. 5. Relation of particle diameter to time

(carry-over rate J)/(feed rate F), and for the weight of the fluidized bed M are given as follows.

$$\frac{J}{F} = \frac{1}{2\alpha\tilde{z}} \int_{X=0}^{X=X_{\max}} \mathbf{K}_{1(X)}\, dX \int_{x=x}^{x=X} \left(\frac{x}{X}\right)^3 \kappa_{(x)} I_{(X,\,x)}\, dx \tag{20}$$

$$M = \frac{F}{2\alpha\tilde{z}} \int_{X=0}^{X=X_{\max}} \mathbf{K}_{1(X)}\, dX \int_{x=x}^{x=X} \left(\frac{x}{X}\right)^3 \psi_{(x)} I_{(X,\,x)}\, dx \tag{21}$$

Furthermore, by proper application of probability distribution functions, the size-frequency distribution functions of the fluidized bed $\mathbf{K}_{2(x)}$, the overflow $\mathbf{K}_{3(x)}$ and the carry over $\mathbf{K}_{4(x)}$ are formulated as:

$$\mathbf{K}_{2(x)} = \left(\frac{F}{M}\right) \frac{1}{2\alpha\tilde{z}} \int_{X=x}^{X=X_{\max}} \mathbf{K}_{1(X)} \left(\frac{x}{X}\right)^3 I_{(X,\,x)}\, dX \tag{22}$$

$$\mathbf{K}_{3(x)} = \psi_{(x)}\mathbf{K}_{2(x)} \tag{23}$$

$$\mathbf{K}_{4(x)} = \kappa_{(x)}(M/J)\mathbf{K}_{2(x)} \tag{24}$$

Once the kinetics of the combustion of a single particle and the law of elutriation are established, it can be shown from equations (20), (21), (22), (23) and (24) that the overflow rate E, the carry-over rate J, the size frequency distribution functions for the bed itself, the overflow and the carry-over, are derivable from the feed rate F, size frequency distribution function for feed $\mathbf{K}_{1(X)}$ and assumed value of $\psi_{(x)}$ (mean value of $\psi_{(x)} \doteqdot 1$), when the bed weight M is determined by using an overflow pipe. When the overflow rate E is determined artificially by adequate adjustments, the weight of the bed M is similarly derived.

The value of $\tilde{z}$ in equation (4) can be obtained from the experimental data, by applying equation (25) which represents the consumption of carbon per unit time in the fluidized bed.

$$\frac{F - (E + J)}{12} = \left\{\frac{6M}{\rho_s \phi_s} \int_{x=0}^{x=x_{\max}} \frac{\mathbf{K}_{2(x)}}{x}\, dx\right\}\tilde{z} \tag{25}$$

The term presented in braces is the total surface area of the carbon particles, as shown in equation (26):

$$\int_{x=0}^{x=x_{\max}} \frac{M\mathbf{K}_{2(x)}\, dx(\pi x^2)}{(\pi/6)x^3\phi_s\rho_s} = \frac{6M}{\rho_s\phi_s} \int_{x=0}^{x=x_{\max}} \frac{\mathbf{K}_{2(x)}}{x}\, dx \tag{26}$$

CONSTANT DIAMETER OF PARTICLE

Where the diameter of a particle remains constant during the reaction in the fluidized bed, or the hard layer of solid persists around the unreacted core (Fig. 1), the elutriation constant $\kappa_{(x)}$ of particles of diameter x can be obtained in the same way as the preceding section, by using the feed rate F, the carry-over rate J, the weight of the bed M, the overflow rate E, the size frequency distribution functions of the feed and the bed, $\mathbf{K}_{1(x)}$ and $\mathbf{K}_{2(x)}$, and $\psi_{(x)} = \mathbf{K}_{3(x)}/\mathbf{K}_{2(x)}$ as previously reported by the authors[4].

$$\kappa_{(x)} = \frac{J}{M}\frac{\mathbf{K}_{4(x)}}{\mathbf{K}_{2(x)}} = \frac{\beta F}{M}\frac{\mathbf{K}_{1(x)}}{\mathbf{K}_{2(x)}} - \frac{E}{M}\psi_{(x)} \tag{27}$$

Now in Figure 4,

$$X = x \tag{28}$$

x is independent of time θ_p

Then the average holding time of overflow or carry-over particles $\theta_{h(x)}$, diameters of which are between x and $x + dx$, can be formulated with

regard to their number, as follows:

$$\{\theta_{h(x)}\}_{\text{overflow}} \equiv \{\theta_{h(x)}\}_{\text{carry over}} = \frac{1}{(E/M)\psi_{(x)} + \kappa_{(x)}} = \frac{M}{\beta F}\frac{\mathbf{K}_{2(x)}}{\mathbf{K}_{1(x)}}. \quad (29)$$

Tracing particles with diameters between x and $x + dx$, the combustion degree of the overflow or carry-over particles $y_{(x)}$ can be described, by employing the probability distribution functions, as shown in Appendix III.

$$\begin{aligned}\{y_{(x)}\}_{\text{overflow}} \equiv \{y_{(x)}\}_{\text{carry over}} &= 1 - 3\left(\frac{\theta_{h(x)}}{\theta_{B(x)}}\right) + 6\left(\frac{\theta_{h(x)}}{\theta_{B(x)}}\right)^2 \\ &- 6\left(\frac{\theta_{h(x)}}{\theta_{B(x)}}\right)^3 \{1 - \exp(\theta_{B(x)}/\theta_{h(x)})\} \\ &= 1 - \frac{1}{4}\left(\frac{\theta_{B(x)}}{\theta_{h(x)}}\right)\left\{1 - \frac{1}{5}\left(\frac{\theta_{B(x)}}{\theta_{h(x)}}\right)\right. \\ &\left. + \frac{1}{30}\left(\frac{\theta_{B(x)}}{\theta_{h(x)}}\right)^2 - \frac{1}{210}\left(\frac{\theta_{B(x)}}{\theta_{h(x)}}\right)^3 + \cdots\right\} \quad (30)\end{aligned}$$

$$y_{(x)} \doteqdot 1 - \frac{1}{4}\left(\frac{\theta_{B(x)}}{\theta_{h(x)}}\right) \text{ when}$$

$$\theta_{B(x)}/\theta_{h(x)} < 0.5$$

The average combustion degrees for overflow or carry-over can be obtained from the following equations:

$$\begin{aligned}(y)_{\text{overflow}} &= \int_{x=0}^{x=x_{\max}} y_{(x)}\mathbf{K}_{3(x)}\,dx \\ (y)_{\text{carry over}} &= \int_{x=0}^{x=x_{\max}} y_{(x)}\mathbf{K}_{4(x)}\,dx \end{aligned} \quad (31)$$

By analogy with equation (20), the ratio (carry-over rate J)/(feed rate F) can be calculated from the following equation.

$$\frac{J}{\beta F} = 1 - \frac{E}{\beta F} = \int_{x=0}^{x=x_{\max}} \mathbf{K}_{1(x)}\frac{\kappa_{(x)}}{(E/M)\psi_{(x)} + \kappa_{(x)}}\,dx \quad (32)$$

If the values of the elutriation constant $\kappa_{(x)}$ are given, the ratios of both overflow or carry-over rates to the feed rate, i.e., E/F or J/F, can be derived by solving the simple integral equation (32), and then the size frequency distribution functions of the bed itself or the carry-over can be obtained from equation (33).

$$\begin{aligned}\mathbf{K}_{2(x)} &= \left(\frac{\beta F}{M}\right)\frac{\mathbf{K}_{1(x)}}{(E/M)\psi_{(x)} + \kappa_{(x)}} \\ \mathbf{K}_{3(x)} &= \psi_{(x)}\mathbf{K}_{2(x)} \\ \mathbf{K}_{4(x)} &= \kappa_{(x)}(M/J)\mathbf{K}_{2(x)}\end{aligned} \quad (33)$$

The above equations can be employed not only for carbon particles with high ash content, but also for other solid particles provided their diameters remain unchanged. Thus, the experimental results obtained by the authors for pyrrhotite or zinc blend were effectively analyzed with these equations[3, 4].

Application of General Theory

COMBUSTION RATE OF PARTICLES IN FLAMES AND FLUIDIZED BEDS

The controlling factor for combustion under various conditions was estimated by comparing the value of the chemical reaction rate coefficient k_{c1} of a carbon particle with that of the mass transfer coefficient of boundary film around the particle k_{f1}.

Using equations (1), (2) and (3), the chemical reaction rate coefficient k_{c1}, and the overall rate coefficient for the combustion of single carbon particle k_1 were calculated for various temperatures, particle diameters, and relative velocities of the particle and the gas stream. The results are shown in Figure 6.

Figure 6 shows that the rate coefficient of the chemical reaction does not differ much from the transfer coefficient of the mass through the boundary film, when the temperature is about 1300°K and the diameter of the particle is 1 mm, assuming that the relative velocity between the particle and the gas stream are equal to the terminal velocity of the particle.

In the case of fluidized beds, where the formation of the boundary layer around the particle is apt to be prevented by the highly turbulent mixing, it may be assumed that the chemical reaction rate is controlling when $T < 1300$°K and $D_p < 1$ mm, if complete contact of all particles with the gas stream is assumed. For small particles with diameters of less than 0.1 mm, mass transfer numbers $\mathbf{N}_{Nu}'$ are not much larger than 2, the controlling factor for one of these small particles can be evaluated from the ABC line in Figure 7, for example, which is derived from the equation and shows that the rate coefficient of

the chemical reaction k_{c1} is equal to the mass transfer coefficient through the boundary film

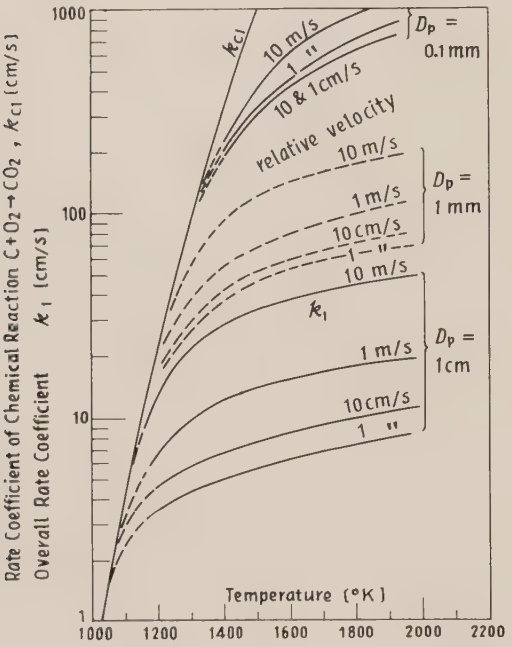

FIG. 6. Overall rate coefficient of combustion for pure carbon particle.

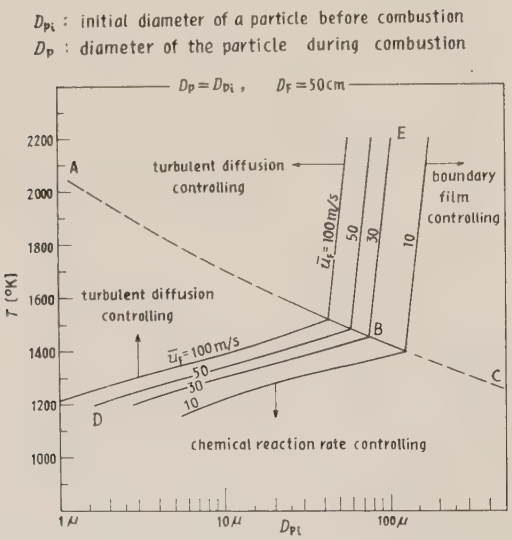
Dpi : initial diameter of a particle before combustion
Dp : diameter of the particle during combustion
Dp = Dpi , DF = 50cm
turbulent diffusion controlling
boundary film controlling
turbulent diffusion controlling
chemical reaction rate controlling
T (°K)
Dpi

FIG. 7. Figure for estimation of controlling factor in flame carbon particles. (In case of $D_p = D_{pi}$, $D_f = 50$ cm.)

k_{f1} , if that number is 2. However, when there is agglomeration of particles in the fluidized bed, the effect of turbulent diffusion of gas on all particles must be considered statistically. These problems are under study in the authors' laboratory and may help to explain the role of the turbulent diffusion.

In the case of combustion of carbon particles in

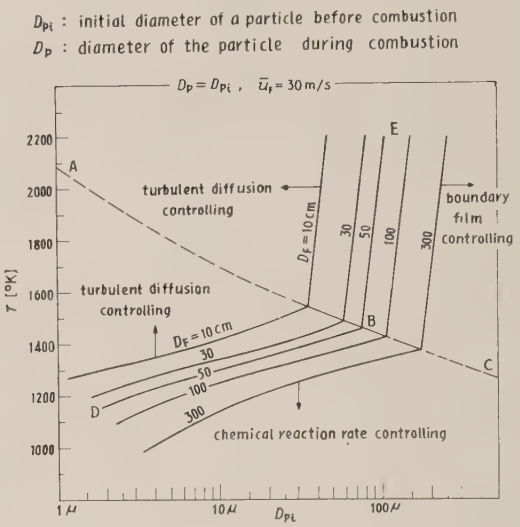
Dpi : initial diameter of a particle before combustion
Dp : diameter of the particle during combustion
Dp = Dpi , Uf = 30 m/s
turbulent diffusion controlling
boundary film controlling
turbulent diffusion controlling
chemical reaction rate controlling
T (°K)
Dpi

FIG. 8. Figure for estimation of controlling factor in flame of carbon particles. (In case of $D_p = D_{pi}$, $\bar{U}_f = 30$ m/s.)

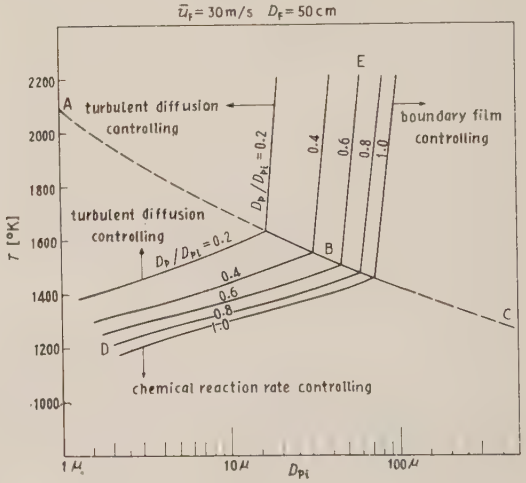

FIG. 9. Figure for estimation of controlling factor in flame of carbon particles. (In case of $\bar{U}_f = 30$ m/s, $D_f = 50$ cm.)

a flame, the mass transfer coefficient of turbulent diffusion k_t should be compared both with the chemical reaction rate coefficient k_{c1} and the mass transfer coefficient of the boundary film k_{f1}. In Figures 7, 8 and 9, the BD line is calculated from the relation $k_{c1} = k_t$, the BE line from $k_{f1} = k_t$ for particles with low ash content, and

the AB line from the relation $k_{c1} = k_{f1}$. Several examples of calculations are shown in Table 1. If the carbon weight is assumed to decrease exponentially along the path of the particles, the controlling factor changes with the distance from the burner, as shown in Figure 10. It is obvious from the above descriptions that turbulent diffusion becomes the controlling factor if the flame diameter is large, the flame velocity is low, the carbon particle is small, and the temperature is high.

TABLE 1. CONTROLLING FACTOR IN FLAMES OF CARBON PARTICLES

D_F[cm] = diameter of flame
D_{pi}[μ] = initial diameter of carbon particle before ignition
D_p[μ] = diameter of carbon particle during combustion
$\bar{u}_F$[m/s] = average velocity of flame gas
T[°K] = temperature

Conditions					Figure	Controlling Factor
D_F	D_{pi}	D_p	$\bar{u}_F$	T		
			10	1800	7	Turbulent diffusion
50	70	70	100	1800		Boundary film
			10	1400		Turbulent diffusion
			100	1400		Chemical reaction
10				1800	8	Boundary film
300	50	50	30	1800		Turbulent diffusion
10				1400		Chemical reaction
300				1400		Turbulent diffusion
		40		1800	9	Turbulent diffusion
50	40	8	30	1800		Boundary film
		40		1500		Turbulent diffusion
		8		1500		Chemical reaction or boundary film

COMBUSTION OF PITCH COKE IN FLUIDIZED BEDS

Analysis of experimental data by theoretical equations

The authors' experiment is outlined in Figure 11, where sized particles of pitch coke are fed continuously by a screw feeder and a pneumatic conveyer, and the carry-over is caught by three cyclone collectors and a bag filter. The experimental conditions and results are shown in Table 2. Examples of size frequency distribution

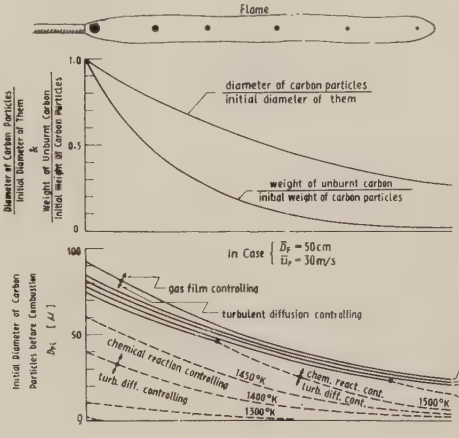

FIG. 10. Change of controlling factor along the length of flame. (In case of D_f = 50 cm, $\bar{U}_f$ = 30 m/s.)

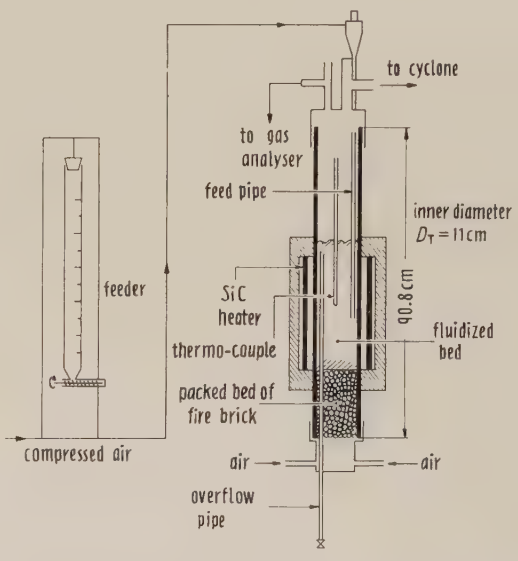

FIG. 11. Reactor used for experimental study of combustion of carbon particles with wide size distribution in fluidized bed.

curves for the bed and carry-over are shown in Figure 12. The ratio of carry-over rate to feed rate varies, owing to the superficial velocity of the gas (Fig. 13). The details of the experimental data will be presented in a later publication.

The experimental results are analyzed with the authors' theoretical equations as follows:

TABLE 2. OUTLINE OF EXPERIMENT*

PITCH COKE USED

Moisture, 0.14% Ash, 0.22% Volatile matter, 0.60% Fixed carbon, 99.04%

SIZE FREQUENCY DISTRIBUTION FUNCTION OF FEED

X [cm]		1×10^{-2}	2	3	4	5	6	8	10	11	12
$K_{1(X)}$[1/cm]	(a)	4.3	9.0	11.5	13.0	12.5	12.0	9.5	5.0	2.5	0
	(b)	3.2	9.3	14.8	16.8	15.4	13.4	9.0	1.6	0	0
	(c)	5.9	8.4	11.0	13.7	16.0	17.7	9.0	0	0	0

RANGE OF EXPERIMENT

Temperature	1000 ~ 1230°C
Velocity of gas (superficial)	27.7 ~ 105 cm/s
Feed rate	8.48 ~ 18.8/min

RANGE OF RESULTS

Overflow rate	0 ~ 5.28 g/min
Carry-over rate	0.0195 ~ 4.43 g/min
Weight of bed	310 ~ 2770 g
Composition of gas	
O_2	0.1 ~ 0.6 per cent
CO_2	14.7 ~ 18.8
CO	3.4 ~ 9.4

* Details of experimental conditions shall be presented in Chemical Engineering (Japan), perhaps in 1955.

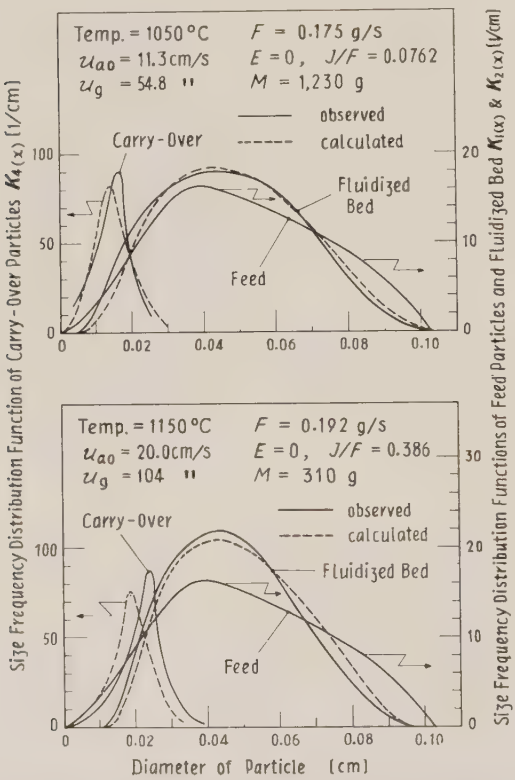

FIG. 12. Size frequency distribution functions for fluidized bed and carry-over, both experimental and theoretical results.

First, equation (17) is used to obtain the elutriation constant $\kappa_{(x)}$ from the experimental data presented in Table 3, making the next correlation possible under the conditions shown in Table 2.

$$\kappa_{(x)} \propto u_{ao}^4 M^{-1} \tag{34}$$

More approximate but effective mean values of $\kappa_{(x)}$ can be obtained by equation (35).

$$\kappa_{(x)} = 2.2 \times 10^{-4}(x/0.01)^{-3}(u_{ao}/10.5)^4 (M/1{,}100)^{-1}[1/\mathrm{s}]x[\mathrm{cm}], \tag{35}$$

u_{ao}[cm/s NTP], M[g]

Next, the values of $\tilde{z}$ are calculated from equation (25) (see Table 4). Taking the values of $\kappa_{(x)}$ represented in (a) of Table 3 as the standard value, calculated from equation (34), we can calculate the size frequency distribution functions of the fluidized bed or carry-over as shown in Figure 12 in good agreement with the experimental data. Similarly, the ratio (carry-over rate J)/(feed rate F) and the weight of the bed M can be calculated theoretically, applying equations (20), (21), (34) or (35), examples of which are presented in Table 4 and Figure 13. Using calculated values of elutriation constant κ_x for the constant bed weight (M = 1100 g), the evaluated line for J/F in Figure 13 explains the experimental data fairly well, suggesting the adequacy of the preceding

theoretical treatment. The average holding times for carbon particles with wide size distribution are calculated from equation (18) for experimental conditions, and several examples of results are presented in Figure 14. In fluidized beds operated in the steady state, whether the diameter of particles is constant or decreases with time, it is interesting that the average holding time of particles for the overflow is strictly equal to that for the carry-over with respect to the same diameter.

Summary

(1) The overall combustion rate of single carbon particles was obtained by using the simple equations (3), (4), (5), (12) and (15), and graphs for evaluating factors relating to the combustion rate of the particle in the fluidized bed and in the flame were plotted (Figs. 6, 7, 8, 9 and 10).

(2) The reaction of the carbon particles in the fluidized bed was studied theoretically for both the case of pure carbon particles and particles with constant diameter. Theoretical equations for the carry-over rate and average holding time of the particles in the fluidized bed were derived [equations (18), (20), (29) and (32)].

(3) The results of experimental studies on the combustion of pitch coke over a wide particle size distribution are outlined. It was found that the carry-over increases greatly with the gas velocity. These results were analyzed with the preceding theoretical equations. It was found that these equations adequately express combustion in fluidized beds and predict experimental data.

Appendix I

The definition of the elutriation constant κ' in the case of batch-type elutriation of narrow-cut fine particles, is described as follows, by Max Leva.[6]

$$\mathbf{C}_s = \mathbf{C}_{s0} \exp(-2.303\ \kappa'\theta) \tag{36}$$

For simplification, the authors modified this definition, as follows:

$$\mathbf{C}_s = \mathbf{C}_{s0} \exp(-\kappa\theta) \tag{37}$$

Differentiation of equation (37) gives

$$-\frac{d\mathbf{C}_s}{d\theta} = \kappa\mathbf{C}_s \tag{38}$$

Equation (38) can be extended as follows, using the weight of the fluidized bed M, the size frequency distribution function of the bed $\mathbf{K}_{2(x)}$, for particles with diameters between x and $x + dx$:

$$-\frac{d\{M\mathbf{K}_{2(x)}\,dx\}}{d\theta} = \kappa_{(x)}\{M\mathbf{K}_{2(x)}\,dx\} \tag{39}$$

The rate of carry-over within the diameter range considered is given by equation (40) for the steady state, as indicated in Figure 4, where J is the carry-over rate and $\mathbf{K}_{4(x)}$ is the size frequency distribution function for carry-over.

$$-\frac{d\{M\mathbf{K}_{2(x)}\,dx\}}{d\theta} = J\mathbf{K}_{4(x)}\,dx \tag{40}$$

Equation (17) is derived from equations (39) and (40).

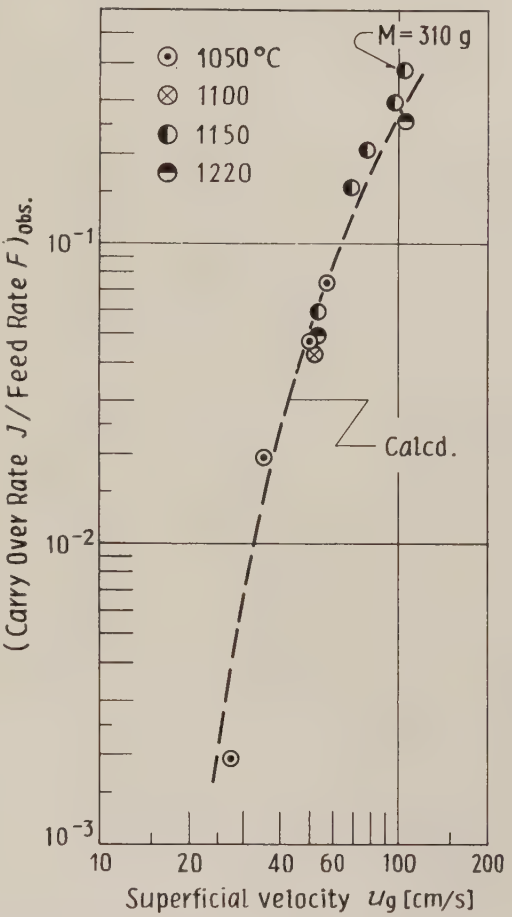

FIG. 13. Increase of carry-over rate with increase of gas velocity, both experimental and theoretical results.

Appendix II

In Figure 4, the particles fed into the bed during the time interval θ and $\theta + d\theta$ are marked. The diameters range from X and $X + dX$.

Table 3. Elutriation Constant $\kappa_{(x)}$

(A) Mean value of $\kappa_{(x)}$ observed for next conditions

u_{ao} = 9.9 ~ 11.3 cm/s [NTP], mean value 10.5 cm/s
M = 920 ~ 1320 g, mean value 1100 g
T = 1050 ~ 1150°C

x [cm]	8×10^{-3}	10	12	14	16	18	22	26	30
$\kappa_{(x)}$[1/s]	38×10^{-5}	26	17	11.5	7.5	4.7	1.6	0.55	0.10

(B) Calculation of $\kappa_{(x)}$ for next conditions

u_{ao} = 11.3 cm/s
M = 1,230 g
$\kappa_{(x)} = [\kappa_{(x)}]_{\text{presented in (A)}} \times (11.3/10.5)^4(1230/1100)^{-1}$

x [cm]	8×10^{-3}	10	12	14	16	18	22	26	30
$[\kappa_{(x)}]$calcd[1/s]	45.5×10^{-5}	31.1	20.4	13.8	9.0	5.63	1.92	0.66	0.12
$[\kappa_{(x)}]$obs[1/s]	45	26	16	10	7	4.8	1.8	0.60	—

(C) Calculation of $\kappa_{(x)}$ for next conditions

u_{ao} = 20.0 cm/s
M = 310 g
$\kappa_{(x)} = [\kappa_{(x)}]_{\text{presented in (A)}} \times (20.0/10.5)^4(310/1100)^{-1}$

x [cm]	10×10^{-3}	12	14	16	18	20	22	24
$[\kappa_{(x)}]$calcd[1/s]	122×10^{-4}	80	54	35	22	12.7	7.6	4.5
$[\kappa_{(x)}]$obs[1/s]	—	—	40	34	26	21	—	—

Table 4. Examples of Calculation

Assumption used: $\kappa_{(x)} = 2.2 \times 10^{-4}(x/0.01)^{-3}(u_{ao}/10.5)^4$[1/s]

Case	1	2	3	4	5	6
			Experimental Data*			
T[°C]	1050	1050	1100	1150	1050	1160
u_{ao}[cm/s NTP]	5.65	7.12	10.4	10.5	11.3	15.3
u_g[cm/s]	27.4	34.6	52.3	54.8	54.8	80.4
F [g/s]	1.68×10^{-1}	1.53	1.90	1.63	1.75	1.74
E[g/s]	8.8×10^{-2}	2.74	2.85	0	0	5.03
J[g/s]	0.325×10^{-3}	2.92	8.18	9.65	13.3	36.7
M[g]	630	1200	1050	1100	1230	970
			Calculated Results			
$\int[\mathbf{K}_{2(x)}]$obs/x (dx)[1/cm]	34.0	27.1	28.2	25.0	27.8	24.7
$\bar{z}$[mol/cm²s]	0.935×10^{-7}	0.947	1.29	1.38	1.18	0.91
M[g]	645	1240	1220	1110	1360	1080
J/F[−]	0.35×10^{-2}	1.94	4.86	5.84	6.31	18.0
$[M]$obs/$[M]$calcd[−]	0.98	0.97	1.16	0.99	0.91	0.90
$[J]$obs/$[J]$calcd[−]	0.55	0.98	0.89	1.02	1.21	1.17

* Size frequency distribution function of feed particles is (a) and (b) in Table 2.

The fraction of marked particles $-d\eta_{1(X)}$ or $-d\eta_{2(X)}$ that leaves the bed as overflow or carry-over respectively during the time increment $d\theta_p$ after the time θ_p (Fig. 5) can be described as follows:

Number of marked particles overflowing from the bed

$$-d\eta_{1(X)} = (n'_{(x)}\,dx)\,d\theta_p(\eta_{(X)}/N_{(x)}\,dx) \quad (41)$$

Number of marked particles elutriated from the bed

$$-d\eta_{2(X)} = (n''_{(x)}\,dx)\,d\theta_p(\eta_{(X)}/N_{(x)}\,dx) \quad (42)$$

Here, $\eta_{(X)}$ is the residual number of marked particles with diameters between x and $x + dx$ at the time θ_p after feeding into the bed, whose initial diameters ranged from X and $X + dX$ (Fig. 5). $(n'_{(x)}\,dx)\,d\theta_p$ is the number of all particles with diameters between x and $x + dx$ which overflow from the fluidized bed in the time increment $d\theta_p$, and $\eta_{(X)}/N_{(x)}\,dx$ is the relative amount of marked particles having the same diameter range. Since $-d\eta_{(X)}$ is the number of marked particles leaving the fluidized bed, we can write:

$$-d\eta_{(X)} = -(d\eta_{1(X)} + d\eta_{2(X)} \quad (43)$$

Next, employing the feed rate F, the size frequency distribution function of the feed $\mathbf{K}_{1(X)}$, and the density of the particle ρ_s, the number of particles fed into the fluidized bed per unit time can be expressed as follows (initial diameters between X and $X + dX$):

$$n_{(X)}\,dX = F\mathbf{K}_{1(X)}\,dX/(\pi/6)X^3\rho_s \quad (44)$$

In the fluidized bed, the number of particles with diameters between x and $x + dx$, can be expressed by the following equation:

$$N_{(x)}\,dx = M\mathbf{K}_{2(x)}\,dx/(\pi/6)x^3\rho_s \quad (45)$$

The number of particles overflowing from the fluidized bed per unit time can be written as follows (diameters between x and $x + dx$):

$$n'_{(x)}\,dx = E\mathbf{K}_{3(x)}\,dx/(\pi/6)x^3\rho_s \quad (46)$$

Applying the elutriation constant $\kappa_{(x)}$ to the particles of diameter x in the fluidized bed, the number of particles entrained by the gas from the fluidized bed per unit time is described as follows (diameters between x and $x + dx$):

$$n''_{(x)}\,dx = \kappa_{(x)}M\mathbf{K}_{2(x)}\,dx/(\pi/6)x^3\rho_s \quad (47)$$

Applying equations (41), (42), (44), (45), (46) and (47), equation (43) can be integrated as follows.

$$\eta_{(X)} = (n_{(X)}\,dX)\,d\theta \exp\left\{\int_{\theta_p=0}^{\theta_p=\theta_p}\left(\frac{E}{M}\psi_{(x)} + \kappa_{(x)}\right)d\theta_p\right\} \quad (48)$$

The probability distribution functions for overflow or carry-over particles, $f_{(X,\theta_p)}$ or $g_{(X,\theta_p)}$, are defined respectively as follows:

$$-d\eta_{1(X)} = (n_{(X)}\,dX)\,d\theta f_{(X,\theta_p)}\,d\theta_p$$
$$-d\eta_{2(X)} = (n_{(X)}\,dX)\,d\theta g_{(X,\theta_p)}\,d\theta_p \quad (49)$$

The probability distribution functions are derived from equations (48) and (49) as follows:

$$f_{(X,\theta_p)} = f_{(X,x)} = (E/M)\psi_{(x)}I_{(X,x)}$$
$$g_{(X,\theta_p)} = g_{(X,x)} = \kappa_{(x)}I_{(X,x)} \quad (50)$$
$$I_{(X,x)} = \exp\left\{-\frac{1}{2\alpha\bar{z}}\int_{x=x}^{x=X}\left(\frac{E}{M}\psi_{(x)} + \kappa_{(x)}\right)dx\right\}$$

Experimental Conditions Corresponding to Results of Calculation
Temp. 1,050 ~ 1,230°C

	F g/min	u_{ao} cm/s NTP	u_g cm/s	M g	$\frac{E}{F}$	$\frac{J}{F}$
①	10.5	11.3	54.8	1,230	0	0.0762
②	11.5	20.0	104	310	0	0.386
③	9.15	7.12	34.6	1,200	0.181	0.0191
④	11.4	10.4	52.3	1,050	0.150	0.043
⑤	9.28	20.0	111	640	0.169	0.253

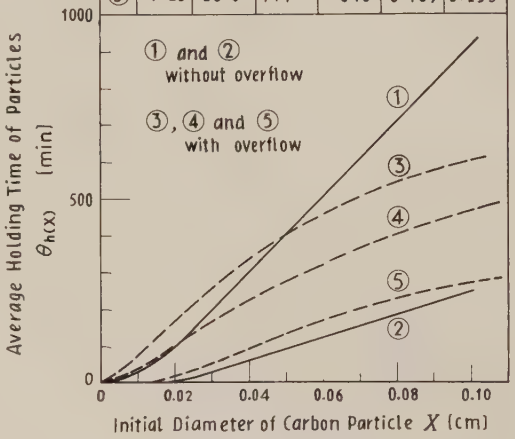

FIG. 14. Average holding time for carbon particles in fluidized bed, initial diameters of which are between X and $X + dX$, calculated theoretically with eq. (21), applying experimental conditions.

The average holding times for both overflow and carry-over particles, with initial diameters between X and $X + dX$, are described with the next equations:

$$\{\theta_{h(X)}\}_{\text{overflow}} = \frac{\int_{\theta_p=0}^{\theta_p=\theta_{B(X)}} [(n_{(X)}\, dX)\; d\theta_p f_{(X,\theta_p)}\; d\theta]\theta_p}{\int_{\theta_p=0}^{\theta_p=\theta_{B(X)}} (n_{(X)}\, dX)\; d\theta_p f_{(X,\theta_p)}\; d\theta} \tag{51}$$

$$\{\theta_{h(X)}\}_{\text{carry over}} = \frac{\int_{\theta_p=0}^{\theta_p=\theta_{B(X)}} [(n_{(X)}\, dX)\; d\theta_p g_{(X,\theta_p)}\; d\theta]\theta_p}{\int_{\theta_p=0}^{\theta_p=\theta_{B(X)}} (n_{(X)}\, dX)\; d\theta_p g_{(X,\theta_p)}\; d\theta_p} \tag{52}$$

Substituting equation (50) in equation (51) and (52), we obtain equation (18) for the holding time.

Applying the probability distribution function $g_{(X,\theta_p)}$, the ratio (carry-over rate J)/(feed rate F) can be obtained as follows:

$$\frac{J}{F} = \frac{\int_{X=0}^{X=X_{\max}} \int_{\theta_p=0}^{\theta_p=\theta_{B(X)}} (n_{(X)}\, dX)\; d\theta_p (\pi/6) x^3 g_{(X,\theta_p)}\; d\theta}{\int_{X=0}^{X=X_{\max}} (n_{(X)}\, dX)(\pi/6)X^3} \tag{53}$$

Applying equations (44) and (50), equation (53) can be reduced to equation (20).

The number of particles with diameters between x and $x + dx$ that overflow in the time increment $d\theta$ can be formulated as:

$$\frac{E\mathbf{K}_{3(x)}\, dx\, d\theta}{(\pi/6)x^3\rho_s} = \int_{X=0}^{X=x} \frac{F\mathbf{K}_{1(X)}\, dX}{(\pi/6)X^3\rho_s}\, d\theta_p f_{(X,\theta_p)}\; d\theta \tag{54}$$

Equation (22) is derived from equation (54).

Appendix III

In the case of constant diameter, probability distribution functions for overflow or carry-over particles with diameters between x and $x + dx$, i.e., $f_{(x,\theta_p)}$ or $g_{(x,\theta_p)}$, can be obtained by simplification of equation (50) as follows:

$$\begin{aligned} f_{(x,\theta_p)} &= (E/M)\psi_{(x)} I_{(x,\,\theta_p)} \\ g_{(x,\,\theta_p)} &= \kappa_{(x)} I_{(x,\theta_p)} \\ I_{(x,\theta_p)} &= \exp\left\{-\left(\frac{E}{M}\,\psi_{(x)} + \kappa_{(x)}\right)\theta_p\right\} \end{aligned} \tag{55}$$

The average holding time of overflow or carry-over particles $\theta_{h(x)}$ with diameters between x and $x + dx$, can be formulated with regard to their number as follows:

$$\{\theta_{h(x)}\}_{\text{overflow}} = \frac{\int_{\theta_p=0}^{\theta_p=\infty} [(n_{(x)}\, dx)\; d\theta_p f_{(x,\theta_p)}\; d\theta]\theta_p}{\int_{\theta_p=0}^{\theta_p=\infty} (n_{(x)}\, dx)\; d\theta_p f_{(x,\theta_p)}\; d\theta} \tag{56}$$

$$\{\theta_{h(x)}\}_{\text{carry over}} = \frac{\int_{\theta_p=0}^{\theta_p=\infty} [(n_{(x)}\, dx)\; d\theta_p g_{(x,\theta_p)}\; d\theta]\theta_p}{\int_{\theta_p=0}^{\theta_p=\infty} (n_{(x)}\, dx)\; d\theta_p g_{(x,\theta_p)}\; d\theta} \tag{57}$$

Equation (29) is derived from the above two equations.

Tracing particles with diameters between x and $x + dx$, the combustion degree of the overflow particles $y_{(x)}$ can be expressed in terms of the probability distribution function $f_{(x,\theta_p)}$, as follows:

$$y_{(x)} = 1 - \frac{\int_{\theta_p=0}^{\theta_p=\theta_{B(x)}} (4/3)\pi r^3 (n_{(x)}\, dx)\; d\theta_p f_{(x,\theta_p)}\; d\theta}{(4/3)\pi R^3 (n'_{(x)}\, dx)\; d\theta} \tag{58}$$

Using (5) and (58), the combustion degree $y_{(x)}$ of the overflow and the carry-over particles also can be calculated from equation (30).

Nomenclature

1	= subscript for oxidation or oxygen	
2	= subscript for reduction or carbon dioxide	
C_1	= concentration of oxygen	[mol/cm³]
C_1'	= average concentration of oxygen in flame	[mol/cm³]
C_2	= concentration of carbon dioxide	[mol/cm³]

C_2^* = concentration of carbon dioxide in equilibrium with carbon [mol/cm³]

$\mathbf{C}_s$ = concentration of fine particles, (weight of fine particles)/(weight of fluidized bed) [−]

$\mathbf{C}_{s0}$ = initial concentration of fine particles [−]

D_F = diameter of flame [cm]

D_p = diameter of particle during combustion [cm]

D_{pi} = initial diameter of particle before ignition [cm]

$\mathbf{D}_{vf}$ = diffusivity of gas in gas phase [cm²/s]

$\mathbf{D}_{vs}$ = diffusivity of gas in solid phase [cm²/s]

E = rate of overflow [g/s]

F = rate of feed [g/s]

$f_{(X,\theta_p)}$, $f_{(x,\theta_p)}$ = probability distribution function of overflow particles with initial diameter of X or x [1/s]

$g_{(X,\theta_p)}$, $g_{(x,\theta_p)}$ = probability distribution function of carry over particles with initial diameter of X or x [1/s]

$$I_{(X,\theta_p)} = I_{(X,x)} = \exp\left\{-\frac{1}{2\alpha\bar{z}}\int_{x=x}^{x=X}\left(\frac{E}{M}\psi_{(x)} + \kappa_{(x)}\right)dx\right\} \quad [-]$$

$$I_{(x,\theta_p)} = \exp\left\{-\left(\frac{E}{M}\psi_{(x)} + \kappa_{(x)}\right)\theta_p\right\} \quad [-]$$

J = rate of carry-over [g/s]

K_c = specific rate of combustion [g/cm²s]

$\mathbf{K}_{1(X)}$, $\mathbf{K}_{1(x)}$ = size frequency distribution function for feed [1/cm]

$\mathbf{K}_{2(x)}$ = size frequency distribution function for fluidized bed [1/cm]

$\mathbf{K}_{3(x)}$ = size frequency distribution for overflow [1/cm]

$\mathbf{K}_{4(x)}$ = size frequency distribution function for carry over [1/cm]

k_1 , k_1^* = overall rate coefficient of combustion $C + O_2 \rightarrow CO_2$ [cm/s]

k_c = rate coefficient of chemical reaction [cm/s]

k_d = mass transfer coefficient through solid layer [cm/s]

k_f = mass transfer coefficient through gas film [cm/s]

k_t = mass transfer coefficient of turbulent diffusion [cm/s]

M = weight of fluidized bed [g]

N_{Fp} = number of carbon particles in unit volume of flame gas [1/cm³]

$\mathbf{N}_{Nu'}$ = mass transfer number [−]

$\mathbf{N}_{ReM}$ = Modified Reynolds number [−]

$\mathbf{N}_{Sc}$ = Schmidt number [−]

$N_{(x)}\,dx$ = number of particles with diameter between x and $x + dx$ in fluidized bed [−]

$n_{(X)}\,dX$ = number of particles fed during unit time, diameters of which are between X and $X + dX$ [1/s]

$n'_{(x)}\,dx$ = number of overflow particles during unit time [1/s]

$n''_{(x)}\,dx$ = number of carry-over particles during unit time [1/s]

P_1 = partial pressure of oxygen [atm]

$\mathbf{R}$ = gas constant [cal/°K]

R = initial radius of a particle [cm]

r = radius of unburnt core in a particle during combustion [cm]

$-dr/d\theta_p$ = decrease rate of carbon radius [cm/s]

T = temperature [°K]
u_{ao} = superficial velocity of air in fluidized bed, represented in NTP [cm/s]
$\bar{u}_F$ = average velocity of flame gas [cm/s]
u_g = superficial velocity of gas in fluidized bed corresponding to its temperature [cm/s]
V = volume of flame gas per unit weight of particle [cm³/g]
X = diameter of particle in feed [cm]
x = diameter of particle [cm]
y = average combustion degree [−]
$y_{(x)}$ = combustion degree of particle with diameter of x [−]
$z = \bar{k}_1\bar{C}_1 + \bar{k}_2(\overline{C_2 - C_2^*})$ [mol/cm²s]
α = volume of particle corresponding for 1 mol of carbon [cm³/mol]
β = (density of particle after reaction)/(density before reaction) [−]
$\bar{\delta}$ = mean diffusion length of turbulent flame [cm]
$\bar{\epsilon}$ = modified eddy diffusivity of turbulent flame [cm²/s]
κ = elutriation constant, defined by authors [1/s]
κ' = elutriation constant, defined by Max Leva [1/s]
$\kappa_{(x)}$ = elutriation constant for particles with diameter x [1/s]
ϕ_s = shape factor for surface area [−]
$\psi_{(x)} = \mathbf{K}_{2(x)}/\mathbf{K}_{3(x)}$ [−]
θ = time [s]
θ_p = time after instant of feeding [s]
θ_B , $\theta_{B(X)}$, $\theta_{B(x)}$ = time required for complete combustion of one particle, which diameter is X or x [s]
$\theta_{h(X)}$ = average holding time of particles, initial diameters of which are between X and $X + dX$. [s]
$\theta_{h(x)}$ = average holding time of particle, having constant diameter x [s]
ρ_s = density of particle [g/cm³]
ξ_f = fraction of intransferable gas in boundary film [−]

REFERENCES

1. Parker, A. L. and Hottel, H. C.: Ind. & Eng. Chem., *28*, 1334 (1936).
2. Froessling, N.: Gerlands Beitr. Geophys., *52*, 170 (1938); Ranz, W. R. and Marshall, Jr., W. R.: Chem. Eng. Prog., *48*, 141 (1952).
3. Yagi, S., and Kunii, D.: J. Chem. Soc. (Japan), Industrial Chemistry Section, *56*, 131, 133, 213, 301 (1953).
4. Yagi, S., and Kunii, D.: Chem. Eng. (Japan), *16*, 283, 288 (1952).
5. Yagi, S. and Saji, K.: *Fourth Symposium (International) on Combustion*, p. 771. The Williams & Wilkins Co., Baltimore, (1953).
6. Leva, M.: Chem. Eng. Prog., *47*, 39 (1951).

17

CONTRIBUTIONS TO THE COMBUSTION MECHANISM OF CARBON

By E. WICKE

In technical studies on the combustion of coal and coke the chief point of interest is the mass and heat transfer at the outer surfaces of the solid fuel. The chemical mechanism, complicated by the influences of the volatile and ash content, is of secondary importance. In fundamental research, on the contrary, the emphasis is on the chemical interchanges of oxygen with carbon which is as pure as possible. The influence of transport processes and of secondary reactions are avoided in these cases by working at low gas pressures. Our own investigations lie half way between these two groups. We are interested in knowing to what extent the reacting gases penetrate by diffusion into the porous structure of graphitic carbon, and how far the inner surface of this structure is utilized by the chemical reactions. One is here concerned with the relationships between the size and shape of the inner surfaces, their accessibility to the gases diffusing into the porous structure, and of the reactions which take place at the walls of the pores. Under isothermal conditions these relationships are largely analogous to the combustion in oxygen or air and gasification by CO_2, the results complementing each other.

Two types of carbon, of very different porosity, were used in these experiments. One was a highly recrystallized electrode carbon (spectroscopically pure, ash content <0.01 per cent, inner surface 2 m^2/g); the other was a highly porous activated charcoal known as Supersorbon (ash content 0.15 per cent, inner surface approximately 700 m^2/g).

The first step was to measure the perceptible increase of the inner surface during gasification with CO_2. Secondly, we wished to determine the activation energies of combustion by O_2 and gasification by CO_2. Because of the influence of diffusion in the porous interior of the carbon, which had hitherto been neglected, the values of these activation energies recorded in literature do not correspond to the surface reactions. In reality, these values are higher by as much as a factor two. As we have shown, the experimental conditions may be arranged easily so as to measure in one case the true activation energy, with no diffusion effects and, in the other case, with full effect of diffusion, the half of the true value. The true activation energy is the same for the highly dispersed charcoal as for the dense electrode carbon; the frequency factor, reduced to unit inner surface, is even smaller by a factor of about ten. This indicates that the greater reactivity of the charcoal is not the result of any special thermodynamic activity, but is due solely to the larger inner surface.

Lastly, our interest was directed to the possibility of varying the rate of combustion and gasification by treating the carbon surface with molecules containing halogens, such as $POCl_3$ and others. The addition of these substances, known to be inhibitors of the homogeneous combustion of CO, decreases appreciably the rate of the surface reactions. During removal of the surface layers built up by these additives, the reaction rate rises far above its normal value, indicating a roughening of the surface caused by these halogenated molecules at the boundaries of the graphitic structure. Further studies of the relations between the surface structure and the rates of heterogeneous reactions with carbon are in progress.

Increase of the Inner Surface of the Electrode Carbon During Gasification by CO_2

The apparatus used for these experiments is shown in Figure 1. A carbon tube of 5 mm inner diameter, 2.5 mm wall thickness and 100 mm length is adjusted between two nozzles of quartz tubing. It is surrounded by another quartz tube of 15 mm inner diameter with a water-cooled ground joint at the upper end. The tube was heated electrically to temperatures between 900° and 1250°C, and CO_2 was passed through it at velocities between 0.1 and 3 m/sec. The degree of reduction to CO was analyzed by means of a gas interferometer, and the results were evaluated, using the following equation which assumes a first order reaction and takes into account the volume increase:

$$2 \ln \frac{2c_L/c_0}{1 + c_L/c_0} + \frac{1 - c_L/c_0}{1 + c_L/c_0} = -\frac{kOm}{v_0} \qquad (1)$$

Here c_0 and v_0 are, respectively, the concentration

and space velocity of CO_2 at the reaction tube inlet and, c_L is the CO_2-concentration at the outlet; m is the mass of carbon present, O is the whole surface of the carbon per unit mass, and k is the reaction rate constant related to the unit carbon surface. The value (kOm) goes through a maximum as the degree of gasification increases (Fig. 2). The same result was obtained using a bed of granulated electrode carbon. The solid curve in Figure 2 is based on the assumption that the maximum is the result only of competition between the increasing inner surface of the carbon and the decreasing carbon mass. The inner surface was determined by the BET-method (adsorption of butane at 0°C). During the entire gasification process it increased by a factor of 14 (see Fig. 3). This factor was found to depend on the temperature of the reaction and the type of carbon used. The good agreement of the curve in Figure 2 with actual measurements indicated that the rate constant k, related to the unit inner surface, did not change during gasification. The outer shape of the carbon tube or the granules remained unchanged even for fairly extensive carbon consumption, indicating that the chemical attack on the carbon structure is from within. This also was the case for the charcoal where despite its high initial value, the inner surface increased linearly with increasing carbon consumption, as shown by the amount of argon adsorbed physically. The determination of the inner surface and its changes during reaction therefore may be a useful method for characterizing the gasification of porous solid fuels.

On the other hand in investigating the reaction kinetics, it is necessary to work with carbon of approximately constant inner surface if reproducible results are to be obtained. Before each experimental run, described in the next section, the carbon was subjected to 20 to 30 per cent gasification, i.e., to the beginning of the maximum region in Figure 2, so as to insure that the

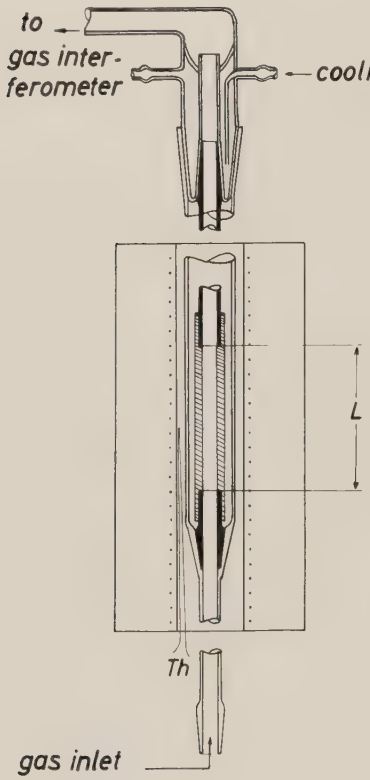

Fig. 1. Reaction apparatus with carbon tube (hatched). L = effective carbon tube length, Th = thermocouple.

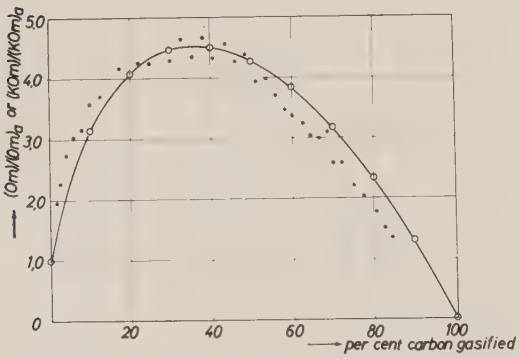

Fig. 2. The whole carbon surface as determined by butane adsorption (○), and the gasification velocity measured at 1026°C (●) dependent on the degree of carbon consumption.

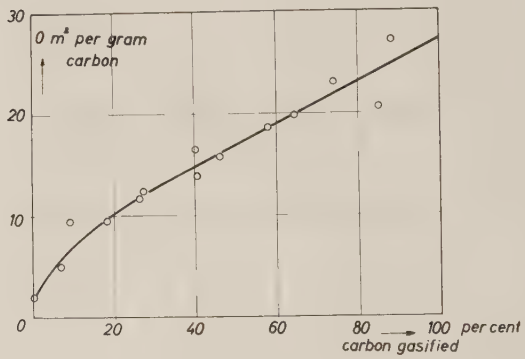

Fig. 3. The surface per gram carbon dependent on the ratio of carbon gasified (by butane adsorption at 0°C; BET method).

carbon surface remained approximately constant during the ensuing run in spite of decreasing amount of carbon.

True Activation Energies of O_2-Combustion and CO_2-Gasification of Carbon

In reactions with porous media, the consumption of the reacting gases and the resistance to their diffusional transport may diminish their concentration in the interior of the porous mass, so that only part of the inner surface participates in the chemical change. The retarding effect of diffusion has been calculated variously by Zeldowitsch[1], Thiele[2], Mayers[3], and Wagner[4]. The first experimental proof was undertaken successfully five years ago by the author in collaboration with Brötz[5], using simple gaseous reactions on porous catalysts of different structures and shapes. Since then, the diminishing influence of diffusion on the efficiency of porous catalysts has been verified a number of times under laboratory and technical conditions. Today, this effect has become a well-known factor which must be taken into consideration in designing catalytic equipment (see, for instance, Houghen[6]).

The surprising thing is that this effect has received little attention in the case of heterogeneous reactions of gases with porous solids, such as the combustion and gasification of carbon and coke. The line of attack formerly pursued with catalysts was applied to the case of these heterogeneous reactions[7, 8, 9], using the circulating apparatus shown in Figure 4. By action of the membrane pump P the gases were circulated through the reaction tube R, a liquid-air condensation trap F, and the exchangeable volume K. Burning experiments with air or oxygen were carried out at temperatures between 600° and 700°C. The only reaction product proved to be CO_2 which condensed in trap F. Thus, the reaction rate could be measured by the pressure drop in the manometer M. In the case of gasification by CO_2 between 1000° and 1100°C, the pressure increase was taken to measure the reaction velocity.

The reaction chamber R was constructed like a cooling trap with two concentric tubes. The carbon to be burned or gasified could be introduced two different ways:

(1) The carbon was crushed to granules, 0.4 to 1 mm in diameter, and packed in the inner tube, 3 to 4 cm high, between samples of quartz wool. The gas was passed directly through this layer. In this case the diffusion paths were short enough to prevent any diffusion effect either during combustion or gasification. The inner surface of the porous granules was utilized completely and uniformly by the reaction. The reaction velocities were not affected by the addition of inert gases, nor did changing from a packed to a fluidized bed alter these conditions. Accordingly, reaction rates and the activation energies measured in this way were the true values for the surface reactions.

(2) Finely pulverized carbon was compressed into the lower part of the outer tube so as to form a cylinder about 5 cm high, the inner tube remaining empty. The gases flowed past the upper end of this cylinder and were able to enter it only by diffusion. The compressed carbon bed was deeper than the reaction zone under operating condi-

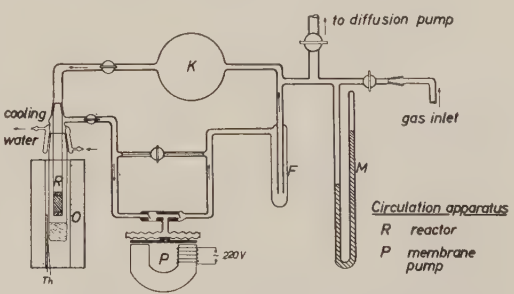

FIG. 4. Circulation apparatus: R = reactor, O = heating coil, P = membrane pump, F = cooling trap, M = manometer, Th = thermocouple, K = exchangeable volume.

tions, and consequently the lower part of it did not react at all. In this case, the measured rate constant k of a first-order reaction is given by the simple equation:

$$k = \frac{1}{l} \cdot \sqrt{\frac{r}{2} D k_0}\,, \qquad (2)$$

where k_0 is the reaction rate constant, determined in the absence of diffusion, by the procedure described in paragraph (1), D is the diffusion coefficient of the reacting gases in the pores of a compressed carbon cylinder of length l, and r is the mean radius of these pores. The influence of the diffusion coefficient was verified by measurements with added inert gases, such as He or N_2, and was found to agree with equation (2). The resulting activation energies were just half of the true values obtained for the measurements by procedure (1), as required by the root in equation (2). This relationship holds regardless of the real order of reaction.

Table 1 contains the results obtained for combustion and gasification of the electrode carbon, as well as the results for gasification of the charcoal obtained in a similar manner. The activation energies noted are the values of the slopes of the Arrhenius curves. As the results obtained with full effect of diffusion proved to be more reliable experimentally than the true values measured in the absence of diffusion effects, the frequency factors H were determined by the equations:

$$k_0 = H \times \exp(-58000/RT) \text{ (combustion)} \quad (3)$$

and

$$k_0 = H \times \exp(-86000/RT) \text{ (gasification)} \quad (4)$$

(3) The frequency factor of gasification obtained with the charcoal is lower by a factor of about 10. To clarify this difference is a problem of further study, but it suggests that the finely divided charcoal provides no more reactive spots per unit surface than the denser electrode carbon.

Between the two limiting cases of full and negligible effect of diffusion considered above, there exists an intermediate case where the apparent activation energies increase from one-half to the full true values as diffusion effect decreases. Experiments with carbon granules of different sizes and with carbon tubing fully verified theoretical expectations on this point. Accordingly,

Table 1. True Activation Energies and Frequency Factors of Carbon Combustion and Gasification

Type of Carbon Used	Electrode Carbon (Spectral Carbon, Ringsdorff)		Activated Charcoal (Supersorbon S, Bayer)
Inner surface, initially	2 m^2/gm		700 m^2/gm
Porosity, initially	29 per cent		77 per cent
Ash content, initially	<0.01 per cent		0.14–0.17 per cent
	Combustion $C + O_2 \rightarrow CO_2$		Gasification $C + CO_2 \rightarrow 2CO$
Temperature range	600–700°C	1000–1100°C	850–1000°C
Pressure range	0.1–0.2 atm O_2	0.1–0.7 atm CO_2	0.1–1 atm CO_2
A_E with diffusion	29 ± 1 kcal/mol	43 ± 1 kcal/mol	43 ± 1.5 kcal/mol
A_E without diffusion	58 ± 4 kcal/mol	85 ± 3 kcal/mol	84 ± 3 kcal/mol
Frequency factor H	2.9×10^9 cm/sec	2.6×10^9 cm/sec	3.4×10^8 cm/sec

They are related to the unit carbon surface, i.e., cc O_2 or cc CO_2 consumed per cm^2 carbon surface and sec.

Three important conclusions may be derived from the data in Table 1:

(1) The true activation energies do not depend on the dispersion of the carbon structure. The higher reactivity of the charcoal, therefore, is not the result of specially favoured active centers, but is due solely to its larger internal surface.

(2) The frequency factors obtained with the electrode carbon are the same for combustion and gasification. The values are not compatible with the concept of the activation energies produced by molecules impinging on the surface. On the contrary, the rate-determining step in both cases must be a reorientation or a dissociation process in an adsorbed layer or a desorption from the surface, energetically supported by thermal vibrations of the graphite lattice.

the various data for the activation energies reported in the literature may be interpreted as apparent values, corresponding to varying diffusion effects which have not been taken into consideration in comparing these results. Table 2 contains a list of such values which do not seem to be markedly influenced by catalytically active impurities. The *gasification* data extend over the whole range mentioned above going from one-half to the full true value determined in this investigation (43 and 86 kcal/mol). The low value obtained by Walker and co-workers[20] may be affected to some extent by the diffusion resistance of an outer gas layer which comes into play at the high temperatures used in their work. The values reported for *combustion* lie around the lower limit of our determination (29 kcal/mol), indicating that the rapid combustion reaction utilizes in general only a flat zone below the outer carbon surface. The low values of Kuchta and co-

workers[15] are due—as before—to the influence of diffusion through an outer gas layer.

Since the classical work on carbon combustion by Tu, Davis and Hottel[21], it has become customary to divide the overall reaction rate into two regions (Fig. 5). In the low-temperature range (A—C, Fig. 5) the rate is strongly dependent on temperature but practically independent of gas velocity, and is controlled by the surface reaction (region of chemical resistance). At high temperatures (A—B, Fig. 5), the rate is almost independent of temperature, but increases with the gas velocity and is controlled by the diffusion through the laminar gas layer outside the carbon particles (region of physical resistance). However in the case of porous media, these two regions are not contiguous. In this case, there is an intermediate section (B′—C′, Fig. 5) which must be taken into account. In the Arrhenius curve, the slope is one-half the value of that in the low-temperature region. The overall rate in this section is controlled by the competition between diffusion and reaction inside the porous mass, i.e., by the depth of the reaction zone. The points in Figure 5 are taken from a paper by Hunt and co-workers[22] on gasification by steam of high-temperature pitch coke, crushed to particles ranging from 0.8 to 2 mm. The authors themselves do not allow for the intermediate section B′—C′.

Effect of $POCl_3$ on the Reactivity of the Carbon Surface

Up to the time when Hinshelwood[23] first reported that small amounts of iodine greatly retard the conversion of CO to CO_2, halogens and halogenated compounds often were used to inhibit the homogeneous oxidation of CO following its primary formation at burning carbon sur-

Table 2. Activation Energies Recorded by Other Investigators

	Temperature Range, °C	Activation Energy, kcal/mol	Type and Shape of Carbon Used
Combustion with air or O_2			
Sihvonen[10]	800–1200	29	Carbon filaments
Meyer[11]	900–1300	20–30	Carbon filaments coated with graphite
Tu[12]	750–850	35	Electrode graphite, spheres
Tsuchanova[13]	500–1000	29	Electrode graphite, tubes
Baetke[14]	900–1100	28	Spectroscopic carbon, tubes
Kuchta, Kant and Damon[15]	1050–1300	20–25	Spectroscopic carbon, cylinders
Gasification by CO_2			
Clement, Adams and Haskins[16]	850–1300	42, 58	Charcoal and coke, packed beds
Drakeley[17]	950–1100	50–70	Several cokes, packed beds
Mayers[18]	950–1300	39	Spectroscopic carbon, tubes
Mayers[3]	850–1150	52	Acheson-graphite, packed beds
Long and Sykes[19]	700–900	59, 68	Coconut shell charcoal, packed beds
Walker, Foresti and Wright[20]	900–1200	48	Gas-baked petroleum
	1200–1400	26	Coke and graphitized carbon, rods

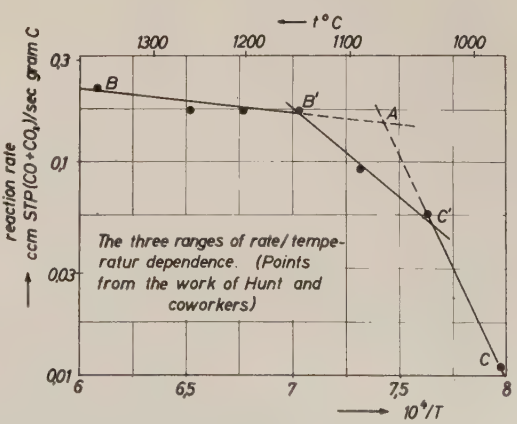

Fig. 5. The three ranges of rate/temperature dependence in reactions of gases with porous media. (Points from the work of Hunt and co-workers[22] on the gasification of coke by steam.)

faces. Inhibitors, such as Cl_2, CCl_4, PCl_3 and especially $POCl_3$, presumably act by capturing the chain carriers of the homogeneous CO combustion reaction—the H-atoms and the OH-radicals (Arthur and Bowring[24]). Moreover, the most efficient inhibitor, $POCl_3$, also captures H_2O molecules to form volatile HPO_3[24]. In addition to these well-known retarding effects on the CO-combustion, the inhibitors also diminish the rates of the heterogeneous reactions, as was shown for carbon combustion by Arthur[25] and for the CO_2-gasification by Bridger and Appleton[26]. To explain these findings it has been suggested that for heterogeneous reactions too, there is a radical chain mechanism with H and OH as chain carriers; (for combustion, see Arthur and Bangham[27]; for gasification by CO_2, Behrens[28]). We made a number of runs to verify these assumptions[8], but our results did not confirm them.

Table 3. Combustion of Electrode Carbon with Dry and Moist Air and with Added $POCl_3$ as Inhibitor

Run	Gas	t, °C	CO_2	O_2	CO	N_2	CO/CO_2
2	Dry air	647	7.2	6.8	11.2	74.8	1.56
3	Moist air	647	5.6	11.0	7.4	76.0	1.32
6	Dry air	827	6.6	0.1	23.6	69.7	3.58
7	Moist air	822	15.4	0.2	9.0	75.4	0.59
29	Dry air with $POCl_3$	830	2.2	8.6	16.8	72.4	7.65
31	Dry air with $POCl_3$	890	1.8	0.5	30.4	67.3	16.9
37*	Moist air with $POCl_3$	890	3.8	0.2	28.0	68.0	7.38
39†	Moist air with $POCl_3$	890	3.9	0.6	27.0	68.5	6.90

* $H_2O:POCl_3 \approx 1:1$.

† $H_2O:POCl_3 \approx 2:1$.

COMBUSTION

In these experiments we used the apparatus already shown in Figure 1. Instead of the carbon tube, a packed bed of 7 gm of spectroscopic carbon, crushed to a size range of 0.4 to 1 mm, was placed in the quartz tube between samples of quartz wool. The air stream was adjusted to 4.4 cc STP/sec in all runs. The residence time of the air stream in the bed varied from 0.1 to 1 sec. The results with dry and with moist air (about 2 per cent by volume of H_2O) and with inhibitor added (about 1 per cent by volume of $POCl_3$) are summarized for a number of characteristic runs in Table 3.

The first four runs were made without $POCl_3$ and the first two were just below the critical temperature of ignition (650°C under the conditions of investigation). In this case, moisture did not increase the reaction rate which was obviously diminished by water vapor adsorbed on part of the carbon surface. The CO/CO_2 ratio was little affected by the moisture, whereas at higher temperatures (runs 6 and 7) with moist air, as was expected, the CO/CO_2-ratio was much lower than with dry air. With added $POCl_3$, there was no reaction at all at 650°C, and it proved impossible at this temperature to remove the inhibiting material from the carbon bed by passing pure air. Even at 900°C this removal took several minutes. This marked retardation of carbon combustion raised the ignition temperature of the carbon bed about 200°C (see run 29, Table 3). The second effect of the inhibitor—the well-known retardation of the CO-combustion—produced the very high CO/CO_2-ratios of runs 29 and 31. Practically the same thing happened with moist air and added $POCl_3$ (see runs 37 and 39, Table 3). The general increase of the CO/CO_2-ratio at higher temperatures agrees approximately with the results of other investigations (see, for instance, Arthur[25]).

Adding the inhibitor markedly changed the structure of the carbon. It became soft and sticky, could be easily ground up, and fine flaky pieces were blown off the bed by the gas stream. It is obvious, therefore, that the heterogeneous reaction is not retarded by the breaking off of a radical chain mechanism, but by a very strong adsorption action, or rather by a chemical reaction between the inhibitor and the carbon sur-

face. As a result, the surface structure is partially destroyed, but simultaneously the products of this reaction form a coat which protects the carbon surface against attack by oxygen. At higher temperatures these reaction products desorb and their protective action diminishes. This concept is further confirmed by the results on gasification.

GASIFICATION

The procedure was similar to that used in the combustion runs. In all runs, the CO_2-input was maintained at 2.80 cc STP/sec and the temperature at 1105°C. Figure 6 shows a typical set of results. Without added $POCl_3$ the reaction proceded along the dashed line, the rate passing through a maximum value for increasing carbon gasification, as discussed in connection with Figure 2. With $POCl_3$ (about 1 per cent by volume), the reaction rate rose abruptly and then fell steeply below the normal value (see Fig. 6, at $t = 33$ min). This initial peak of the reaction rate is difficult to measure, but it appeared in each run, and there can be no doubt of its existence. After the $POCl_3$ input was stopped (at $t = 63$ min, in Fig. 6), the reaction rate again rose far above its normal value, but the rise was appreciably slower than the first time. The rate dropped once more as soon as the inhibitor was added again. This was repeated several times, producing a zigzag line as compared with the curve of normal reaction course (Fig. 6).

This behavior indicates a twofold action of the inhibitor. First, at the prevailing temperature the products of its reaction with the carbon surface partially protect this surface against the adsorption of CO_2. Second, the reaction of the inhibitor with the carbon roughens and disperses the surface, so that during the removal of the reaction products the gasification rate rises to twice its normal value. When the inhibitor is added for the first time, destruction of the carbon surface sets in, but there is not enough inhibitor material present to coat the splits and cracks formed by the first molecules striking the surface. This is the reason for the sharp peak in the gasification rate corresponding to the first addition of inhibitor (Fig. 6).

As stated above, it would be difficult to explain the action of $POCl_3$ on the heterogeneous reaction rates of combustion and gasification by any radical chain mechanism. On the other hand, the strong effects of $POCl_3$ on the structure of the carbon surface and its chemical behaviour limit the value of this and perhaps other inhibitors for use in studying the primary products of carbon combustion[29]. However, these effects offer unexpected possibilities for varying the conditions of combustion and gasification of graphitic carbon by treating it with molecules whose surface action can prevent or promote chemical attack by the reaction products.

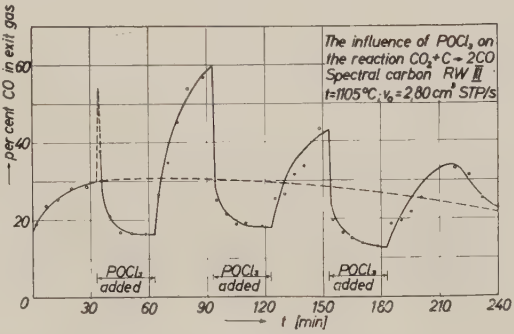

FIG. 6. The influence of 1 per cent of volume $POCl_3$ vapor added to the incoming CO_2 on the reaction: $CO_2 + C \rightarrow 2CO$. Spectral carbon RW III, reaction temperature 1105°C, gas velocity, 2.80 cm³ STP CO_2 per second.

Acknowledgment

The author is greatly indebted to Dr. K. Hedden for valuable criticism and to Mrs. M. Buschmann for her assistance in the preparation of this paper. Grateful acknowledgment is due the *Deutsche Forschungsgemeinschaft* for the scientific implements placed at our disposal, and to the *Fonds der Chemie* for effective financial support of the work.

REFERENCES

1. ZELDOWITSCH, J. B.: Acta Physicochim. (URSS), *10*, 583 (1939).
2. THIELE, E. W.: Ind. & Eng. Chem., *31*, 916 (1939).
3. MAYERS, M. A.: J. Am. Chem. Soc., *61*, 2053 (1939).
4. WAGNER, C.: Z. Physikal. Chem., (A) *193*, 1 (1944).
5. WICKE, E., AND BRÖTZ, W.: Chem.-Ing.-Techn., *21*, 219 (1949).
6. HOUGHEN, O. A.: Z. Elektrochem., *57*, 479 (1953); Chem. Eng. Progr. Monograph Series Nr. 47 (1951).
7. WICKE, E., AND HEDDEN, K.: Z. Elektrochem., *57*, 636 (1953).
8. HEDDEN, K.: Dissertation Göttingen (1954).
9. MATZ, G.: Dissertation Göttingen (1954).
10. SIHVONEN, V.: Ann. Acad. Sci. Fenn, (A) *33*, part 6 (1930).

11. Meyer, L.: Z. Physikal. Chem., (B) *17*, 385 (1932).
12. Tu, C. M.: Dissertation Mass. Inst. of Technology (1932).
13. Tsuchanova, O. A.: 1947 classe de Sciences techn. Bulletin acad. USSR Iswetija, Akad. Nauk. 375/80.
14. Baetke, F.: Dissertation Göttingen (1951).
15. Kuchta, J. M., Kant, A., and Damon, G. H.: Ind. & Eng. Chem., *44*, 1559 (1952).
16. Clement, J. K., Adams, L. H., and Haskins, C. N.: Bull. Bur. Min. Nr. 7 (1911).
17. Drakeley, T. J.: J. Soc. Chem. Ind., *50*, 319 (1931).
18. Mayers, M. A.: J. Am. Chem. Soc., *56*, 70 (1934).
19. Long, F. J., and Sykes, K. W.: J. Chem. Phys., *47*, 361 (1950).
20. Walker, P. L., Foresti, R. J., and Wright, C. C.: Ind. & Eng. Chem., *45*, 1703 (1953).
21. Tu, C. M., Davies, H., and Hottel, H. C.: Ind. & Eng. Chem., *26*, 749 (1934).
22. Hunt, B. E., Mori, S., Katz, S., and Peck, R. E.: Ind. & Eng. Chem., *45*, 677 (1953).
23. Hadman, G., Thompson, H. W., and Hinshelwood, C. N.: Proc. Roy. Soc. (London), *A137*, 87 (1932).
24. Arthur, J. R., and Bowring, J. R.: J. Chem. Soc., *S1*, (1949); Ind. & Eng. Chem., *43*, 528 (1951).
25. Arthur, J. R.: Trans. Faraday Soc., *47*, 164 (1951).
26. Bridger, G. W. and Appleton, H.: J. Soc. Chem. Ind., *67*, 445 (1948).
27. Arthur, J. R., and Bangham, D. H.: J. Chim. Phys., *47*, 595 (1950).
28. Behrens, H.: Chem.-Ing.-Techn., *24*, 349 (1952).
29. Wicke, E.: Z. Elektrochem., *56*, 414 (1952).

18

COMBUSTION RATE OF PULVERIZED COAL IN A JET STREAM

By KENJIRO SAJI

Introduction

In the combustion of pulverized coal in gas turbines or cement rotary kilns, a so-called fully turbulent flame or combustion rate of the particles in the turbulent field is of interest. This also constitutes a typical example of combustion of a cloud of nonuniform particles in a jet stream. The present paper describes the relationship between the combustion rate of pulverized coal in any cross-section of the flame jet and parameters such as the particle size, and type of coal, the air-fuel ratio, and the nozzle size of the burner. It extends an earlier study entitled *Problems of Turbulent Diffusion and Flame Jet*[1].

The theory takes into account the surface area of the particles; surface gas and ash-films; the type of coal; the particle-size distribution; turbulent diffusion and scale effects; and the superposition of solid and gas combustion. Theoretical conclusions are compared with experimental results obtained by a special quenching and total sampling method.

Formulation of the Problem

Reaction rate of uniform particles in a circular flame jet

In general, for the fixed carbon of a coal particle in a gas stream the specific combustion rate is given by

$$K = k_r C(O_2) \qquad \text{and} \qquad \frac{1}{k_r} = \frac{1}{k_c} + \frac{1}{k_f} + \frac{1}{k_a} \tag{1}$$

The values of k_c, k_f and k_a depend on the surface temperature, the type of coal, the particle size and the relative velocity. As it is impossible to measure the actual surface temperature of the particle, in first approximation we assume that

$$k_r = \frac{A_1 T_f^a}{\delta^{m_1}} \tag{2}$$

Next, we must consider the oxygen concentration of any cross-section of a turbulent flame containing coal particles. For circular flame jets, the author[1] already has proposed the concept of *modified eddy diffusivity for mass transfer* defined as

follows:

$$\bar{\epsilon}_x = 2\bar{k}\bar{u}_x\, d_x = 2.74 \times 10^{-3}\bar{u}_x\, d_x(\mathrm{cm^2/sec}) \quad (3)$$

where $\bar{k}$ is a weighted mean value of k over any cross-section and is constant throughout the fully turbulent range of the jet; $\bar{u}_x$ usually is also a weighted mean; d_x depends on the scale of turbulence. Therefore, we can consider $\bar{\epsilon}_x$ as characteristic of each fluid mass which makes up the turbulent flow, provided that for a given velocity of each fluid mass at the cross-section x, the scale and the velocity gradient are uniform and consequently the intensity of turbulence is the same.

Although this is obviously an approximation $\bar{\epsilon}_x$ is very convenient in treating average phenomena of turbulent diffusion or reaction rate over a given cross-section. In this approximation, the gradient of an intensive transport property such as momentum, heat or mass (generally written as $\partial c/\partial y$) should be replaced by $(c_x/x_1 l_x)$ or $(c_x/x_2 d_x)$. Further, in case of quasicylindrical flow, the diameter d is roughly proportional to d_0. Hence for simplicity, we may assume that the flame is of quasicylindrical form and the nozzle fluid is incombustible except for the coal particles. For an elementary volume of the flame $(\frac{1}{4}\pi\ d_x^2\ dx)$, the amount of oxygen diffused through the surface $(\pi\ d_x\ dx)$ per unit time is:

$$\kappa_3(\pi\ d_x\ dx(\bar{\epsilon}_x)\ \frac{C(\mathrm{O_2})_s}{d_0} \qquad (\mathrm{mol\ O_2/sec}) \quad (4)$$

On the other hand, the amount of decrease of fixed carbons in the portion of the flame per unit time is

$$-\ (\tfrac{1}{4}\pi\ d_x^2\ dx)N\rho\ \frac{\pi\delta^2}{2}\ \frac{d\delta}{dt} \qquad (\mathrm{gram/sec}) \quad (5)$$

Hence, if it is assumed that the amount of residual oxygen either is zero, or depends on the type of coal, the particle size and the amount of oxygen diffused, the following equation can be derived from equations (4) and (5) by analogy with equation (1):

$$-\ (\tfrac{1}{4}\pi\ d_x^2\ dx)N\rho\ \frac{\pi\delta^2}{2}\ \frac{d\delta}{dt} = A_2\ \frac{T_f^b}{\delta^m}\ (\pi\ d_x\ dx)\ (\bar{\epsilon}_x)\ \frac{C(\mathrm{O_2})_s}{d_0}\ N\pi\delta^2$$

and from equation (3) and $\bar{u}_x = dx/dt$:

$$-\delta^m\ d\delta = \frac{A_3 T_f^b C(\mathrm{O_2})_s}{\rho d_0}\ dx \quad (6)$$

If the stagnant surrounding medium is air at constant pressure and in sufficient amount, and since $C(\mathrm{O_2})_s$ is not dependent on x and is inversely proportional to the absolute temperature T_s, we may write:

$$-\ \delta^m\ d\delta = \frac{A T_f^b}{\rho d_0 T_s}\ dx \quad (7)$$

Furthermore, assuming a constant value of m during combustion, we can integrate equation (7) under the following conditions

$$\delta = \delta_0 \text{ for } x = \beta \qquad \text{and} \qquad \delta = \delta \text{ for } x = x,$$

and setting $\delta_0 = \varphi s$, where s is the size of the corresponding sieve opening, i.e., a so-called swelling index, and $\varphi^3\rho = \rho_c$, where ρ_c is the apparent density of the fixed carbon of the original coal dependent on the fixed carbon contents in weight, we obtain

$$\left(\frac{\delta}{\delta_0}\right)^{m+1} = 1 - \frac{(m+1)A\varphi^{2-m}T_f^b}{\rho_c T_s s^{m+1}}\left(\frac{x-\beta}{d_0}\right) \quad (8)$$

The effect of the primary air will be mentioned in the subsequent section.

REACTION RATE OF NONUNIFORM PARTICLES

It is well known that the size distribution of the coal particles ground by technical pulverizers is usually given by the so-called exponential law:

$$R = e^{as^n}$$

We also apply the following weighted mean diameter and dimensionless diameter used by Hottel[2]:

$$s_w = \int_{R=0}^{R=1} s\ dR \qquad \text{and} \qquad s/s_w = S$$

By analogy with the treatment developed by Hottel[2] for the combustion of a cloud of nonuniform carbon particles, the fraction by weight represented by the group of coal particles with diameters between S and $S + dS$ which remain unburned over the distance from β to x is obtained by the equation (8) as follows:

$$du = \left(1 - \frac{L}{S^{m+1}}\right)^{3/m+1} n\left(\frac{1}{n}!\right)^n S^{n-1}e^{-((1/n)!S)^n}\ dS \quad (9)$$

If

$$L = \frac{(m+1)A\varphi^{2-m}T_f^b}{\rho_c T_s s_w^{m+1}}\cdot\left(\frac{x-\beta}{d_0}\right) \quad (10)$$

and the total unburned fraction at $L = S^{m+1}$ is given by

$$u = \int_{S=L^{1/m+1}}^{\infty} \left(1 - \frac{L}{S^{m+1}}\right)^{3/m+1} n\left(\frac{1}{n}!\right)^{n} S^{n-1} e^{-((1/n)!S)^{n}}\, dS \tag{11}$$

for definite values of m and n, we can evaluate a group of curves u vs. ${}_mL_n$ (Figure 1).

SUPERPOSITION OF COMBUSTIONS OF FIXED CARBON AND VOLATILE MATTER WITH PRIMARY AIR

The author has presented earlier an approximate formula for the open turbulent flame length

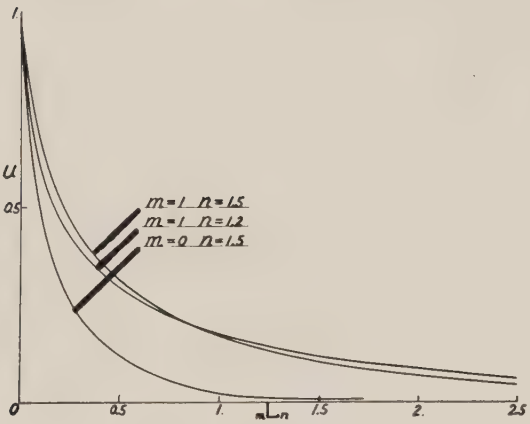

FIG. 1. Graph of u vs. ${}_mL_n$

of pulverized coal neglecting the particle size (1):

$$\frac{L_f - \beta}{d_{\text{II}}} = (10.8)(2 - \log_{10}\gamma)(\rho_{f.g.}/\rho_{n.f.})_n^{1/2} \cdot \{(1.29)(V_0/M_w)(1 - \alpha) + \alpha\} \tag{12}$$

$$\alpha = \frac{1 - (\gamma/100)}{2.3(2 - \log_{10}\gamma)}, \qquad 100 \gg \gamma > 0$$

where $\gamma = 100\ u$ (per cent) (see equation 11). We now expand the application of this formula for given values of the distance x (above certain values) by substituting L_f and (10.8) $(\rho_{f.g.}/\rho_{n.f.})_n^{1/2}$ for x and an unknown factor F respectively. This is possible because the value of $(\rho_{f.g.}/\rho_{n.f.})_n^{1/2}$ is nearly constant except for small values of x. Equation (12) is written as

$$\frac{x - \beta}{d_0} = F(2 - \log_{10}\gamma) \{(1.29)(V_0/M_w)(1 - \alpha) + \alpha\} \tag{13}$$

Equation (12) is based on the assumption that the chemical reaction rate is very large compared with the turbulent mixing rate. In fact, pulverized coal particles used in practice contain considerable amounts of volatile matter and superfine particles which burn like a gaseous fuel, although the size limit is generally unknown. This size limit can be estimated for a specific type of coal from the author's experimental results mentioned later. In general, pulverized coal flames are regarded as complicated phenomena involving the superposition of two combustion processes—that of coarse fixed carbon particles and that of volatile matter and superfine particles. In the case of turbulent flames (equations (10) and (13)) the combustion rate of pulverized coal is given approximately by the following formula:

$$\frac{x - \beta}{d_0} = G({}_w^{m+1}\cdot {}_mL_n)^p [(2 - \log_{10}\gamma)\{(1.29)(V_0/M_w)(1 - \alpha) + \alpha\}]^q$$

$$G = \left\{\frac{\rho_c T_s}{(m+1)A\varphi^{2-m}T_f^b}\right\}^p (F)^q \tag{14}$$

$$\alpha = \frac{1 - (\gamma/100)}{2.3(2 - \log_{10}\gamma)}$$

This formula is applicable not only to open turbulent flames, but also to flames in furnaces where sufficient air is provided.

In conclusion, the author's experimental results indicate that for the case of most technical coal dusts where the original particle size which is usually less than about 25 per cent residual on 170 mesh sieve, probably

$p = 0.5$, $q = 0.5$ and $m = 0 \sim L$ ($m = 1$ for relatively low average flame temperature, from about 900°C to 1000°C).

An exception exists for nonagglomerating coals where

$$p = 0, \qquad q = 1$$

if the average flame temperature is relatively high, as for gaseous fuels.

Experimental Apparatus and Procedure

Figure 2 shows the essential experimental equipment consisting of (A) an air-tight coal bin with two agitators; (B) screw feeder; (C) a diffusion tank; (D) a primary air inlet; (E) a preheater; (F) a secondary air inlet; (G) city gas-to-igniter line; (H) a strainer for secondary air; (I) a firing cylinder jetting numerous small gas flames

towards the center; (J) a series of measuring or sampling holes; (K) mica windows; (L) a narrow chamber for dust; (M) a furnace, 200 cm long, 25 cm inner diameter, 41 cm outer diameter; (N) an exhaust pipe; (O_1 O_2 O_3 O_4), manometers orifices; (P) a conical tip of water-cooled sampling tube with large and small concentric fire-extinguisher rings emitting numerous small CO_2 gas jets; (Q) a narrow mica window; (R) a water-cooled cyclone collector, 25 cm inner diameter; (S) a damper; (T) a suction fan (7.5 hp) and exhaust pipe; (U) a series of liquid CO_2 bombs. Diameters of nozzles used are 1.4 and 1.7 cm.

The sampling tip emitting CO_2 gas is also water-cooled. The sampling apparatus slides along rails into the furnace at a given position, where it collects the total combustion gas and the unburned particles of the flame. Many samples collected in the small cyclone were compared with the samples collected at the same time in a special filter tube with a vacuum pump at the outlet of the water-cooled sampling tube. Having ascertained that these two methods of sampling gave virtually the same results, determination of the burning velocity was based on the ash-analyses of the cyclone samples.

In addition to the amount of coal supplied, various other factors were carefully controlled and checked. These include fineness of grinding of coal, moisture of pulverized coal, hopper condition, and inner pressure of the screw pipe and its outlet to the burner pipe.

Discussion of Results

The properties of the coals used are shown in Table 1. Figures 3 and 4 are graphic representations of equation (14) for the two cases, $p = 0.5$, $q = 0.5$, $n = 1.5$ and $m = 0$ or 1 respectively. The weighted mean diameter of the original coal particles s_w is given by Figure 5[2]. Figure 6 shows combustion rate data for coal A at flame temperatures from 900 $\sim$ 1000°C and compares them with the theoretical curves based on a standard value at E ($x = 160$ cm), i.e., $\gamma = 11$ per cent. The correct value G in equation (14) is determined from the standard value (SV) as $G = 0.96$, for $m = 1$, s_w (u) and V_0 (nm^3/kgm coal). In this case, for $m = 0$, and $G = 11.8$ the calculated values are not in agreement with the experimental results, but for the particle size of 10 per cent residue the curve for $m = 0$ coincides roughly with the curve for $m = 1$ in Figure 6. Figures 7 and 8 show data for coal B and coal C, which are both nonagglomerating; they are compared with curves calculated in a similar way, for $m = 0$ and $G = 6.9$ and 5.9 respectively, for coal B and coal C. Furthermore, in Figure 9 we show some results for coal A and coal B at relatively high

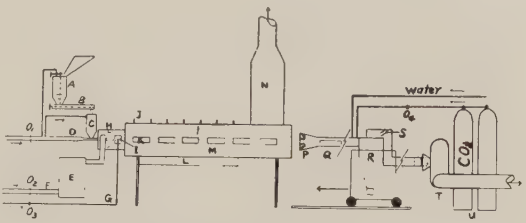

FIG. 2. Experimental apparatus

TABLE 1. PROPERTIES OF COALS TESTED

Coal	Proximate Analysis, per cent				Calorie kcal/kgm	Fuel-Ratio	Property of Agglomerating
	Fixed Carbon	Volatile	Ash	Moisture			
A	47.03	42.35	8.02	2.60	7600	1.11	A (strong)
B	38.09	46.78	9.38	5.75	6630	0.82	NA (non-)
C	38.27	44.10	11.08	6.55	6480	0.87	NA (non-)

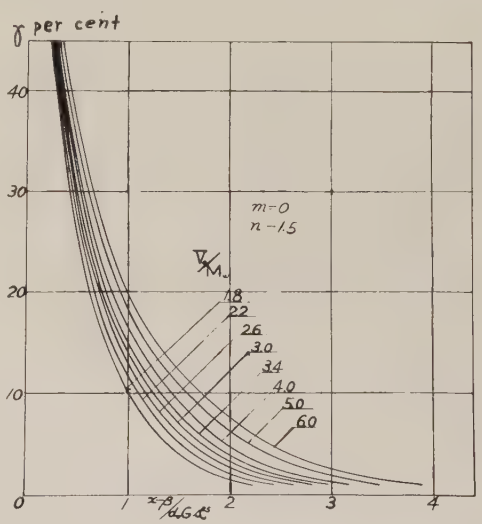

FIG. 3. Graphic representation of equation (14)

flame temperatures (about 1200°C) and secondary air, where $m = 0$ and $G = 11.1$ for coal A, and the burning process is rather similar to gas combustion for coal B. However, setting $m = 0$ for coal B by the same reasoning as above, then $G = 5.2$. Consequently, if we compare coal A with coal B or coal C, with respect to their combustion constant G, it may be said that for

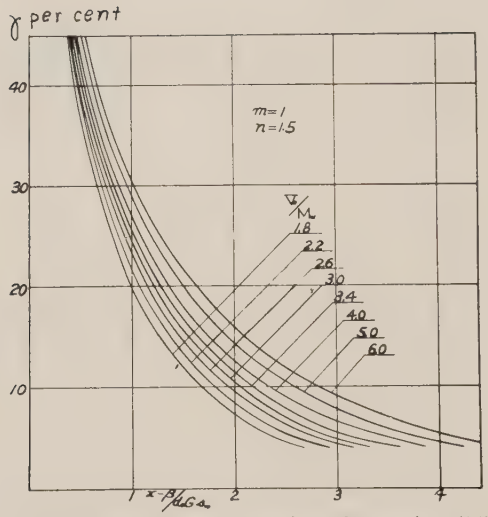

FIG. 4. Graphic representation of equation (14)

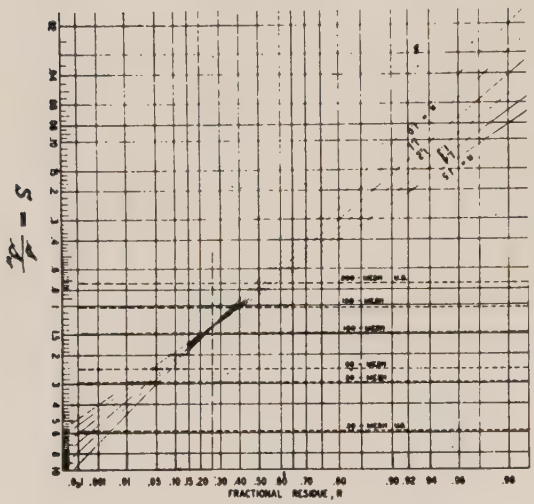

FIG. 5. S vs. R (according to Hottel)

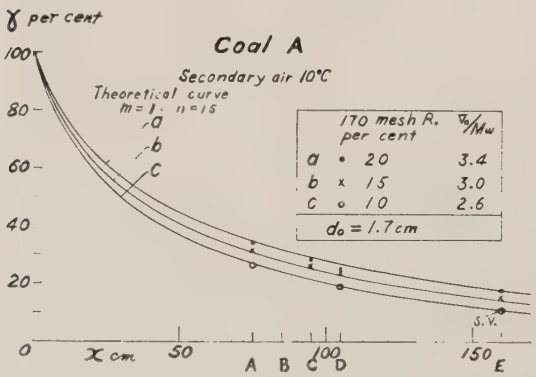

FIG. 6. Combustion rate of coal A at the mean flame temperature 900–1000°C for various particle sizes. Comparison with the calculated curves.

coal A the value of G is about twice as large as for coal B or coal C. At relatively low flame tempera-

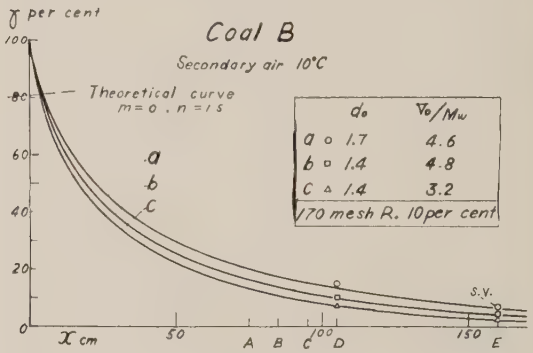

FIG. 7. Combustion rate of coal B at the mean flame temperature 900–1000°C for various nozzle diameters. Comparison with the calculated curves.

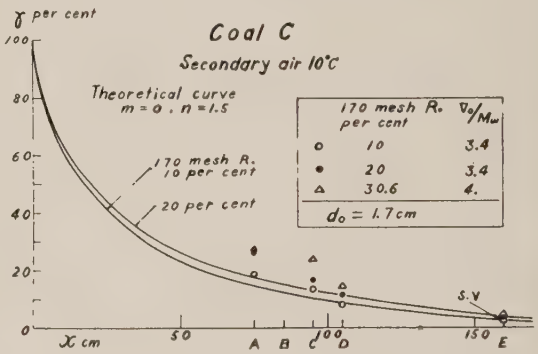

FIG. 8. Combustion rate of coal C at mean flame temperature 900–1000°C for various particle sizes. Comparison with the calculated curves.

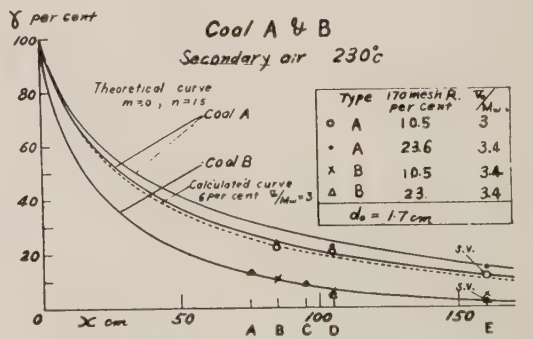

FIG. 9. Combustion rate of coal A and coal B at relatively high flame temperatures (about 1200°C) and secondary air for various particle sizes. Comparison with the calculated curves.

ture, numerous data for coal B and coal C indicate that their burning processes are complicated and vary continuously as $m = 1 \rightarrow 0$ with increase in $(x - \beta/d_o)$.

As mentioned above, although they are all volatile bituminous coals, there is a great difference between coal A and coal B or coal C. However, this difference is evidently explained by the following microscopic observation and by air-elutriation of the unburned and ash particles. Figures 10 and 11 show the results of air-elutriation

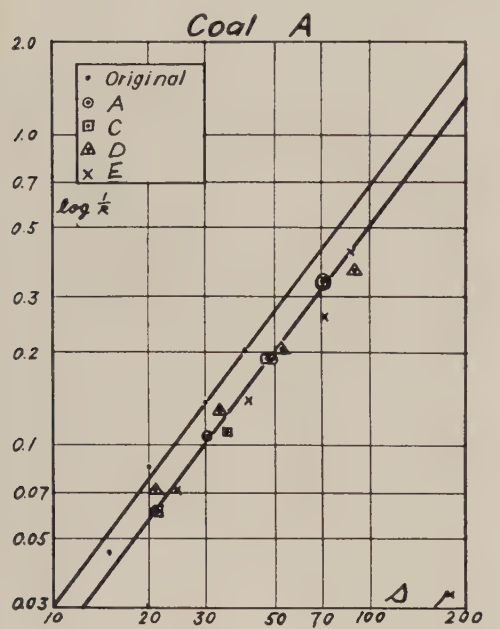

FIG. 10. Air-elutriation of the burning particles (unburned carbon and ash) at each cross-section of the flame of coal A and of the original particles of 20 per cent residue on 170-mesh screen.

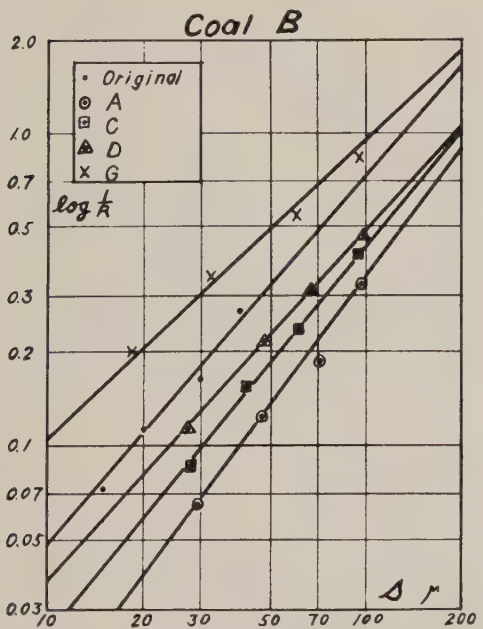

FIG. 11. Air-elutriation of the burning particles at each cross-section of the flame of coal B and of the original particles of 20 per cent residue on 170-mesh screen.

FIG. 12. Microscopic photograph (50 times) of the burning particles of coal A collected at E corresponding to E-line in Figure 10.

FIG. 13. Microscopic photograph (50 times) of the burning particles of coal B collected at E corresponding to E-line in Figure 11.

of the samples collected at positions A, C, D and E (see Fig. 6) and of the original pulverized coal (20 per cent residue on 170 mesh screen for both coals). The particle size was determined microscopically taking the arithmetic mean of length and width of sixty particles in all cases. Photo-

graphs of enlarged (54 times) burning particles of coal A and coal B, both 20 per cent residue, collected at E are shown in Figures 12 and 13, which correspond to the curves in Figures 10 and 11.

FIG. 14. Microscopic photograph (50 times) of the burning particles air-elutriated from the sample shown in Figure 12.

FIGURE 15. Microscopic photograph (50 times) of the burning particles air-elutriated from the sample shown in Figure 13.

Figures 14 and 15 are microscopic photographs (54 times) of the air-elutriated particles (60 $\sim$ 70μ) from the samples corresponding to Figures 12 and 13. There are many spherical particles whose diameter is less than 20 μ in Figure 15. Such small particles are always found in each process of air-elutriation of samples for coal B, but their weight is very small. It is believed that they are mainly ash particles which melt and adhere to the surface of large particles. Figures 16 and 17 show the burning particles at E corresponding to Figure 8 for coal C. Lastly, Table 2 shows the volatile contents of burning particles at each cross-section of the flames of coal A and coal B.

FIG. 16. Microscopic photograph of the burning particles collected at E for coal C of 10 per cent residue (see Fig. 8).

FIG. 17. Microscopic photograph of the burning particles collected at E for coal C of 30.6 per cent residue (see Fig. 8).

In conclusion, the remarkable distinction between coal A and coal B or coal C shown in Figures 6–17 and in Table 2 can be summarized

as follows:

Coal A: spherical, dense and noncrumbling during burning process

Coal B, coal C: angular, porous and crumbling during burning process; combustion rate is very rapid, as for gaseous fuels.

Next, from formula (14) and the value of G under different conditions of temperatures for the same coal and setting $m = 0$, i.e., for $k_r = k_c$, we can approximately deduce that as effect of temperature $b \doteqdot 4$, namely, G is proportional to $T_s^{0.5}$ and T_f^{-2} over a practical range of temperatures. On the other hand, $\rho_c = \rho_0 x$ (fixed carbon per cent/100) and ρ_0 is nearly constant. Furthermore, since the value of coal abruptly heated to a high flame temperature is roughly proportional to (volatile matter and inner moisture per cent)$^{1/3}$,

Table 2. Examples of Volatile Contents of Burning Particles

Coal	Volatile Contents (per cent) of Samples at Several Positions in Flames (see Fig. 6)				Original Size 170 Mesh R, per cent
	A	C	D	E	
A	46.04	44.90	43.90	7.80	20
B	39.60	10.34	8.90	7.20	20
A	39.26	13.60	9.34	6.40	10
B	10.23	9.90	8.70	8.08	10

Secondary air 10°C, average flame temperature 900 ~ 1000°C.

then φ^2 is assumed to be approximately proportional to (volatile matter per cent). Therefore, it may be considered in first approximation that ρ_c/φ^2 in G is proportional to the so-called fuel ratio of coal.

In short,

$$G = A_0 \text{ (fuel-ratio)}^{0.5}(T_s)^{0.5}(T_f)^{-2} \quad (15)$$

except for nonagglomerating coals. However, at present we can give no detail.

Conclusions

(1) Formula (14) is widely applicable to the combustion of nonuniform coal particles in turbulent jet flames either in the case of unconfined combustion or of combustion in a large chamber. It explains many complicated experimental results obtained by researchers in the past.

(2) Of the characteristics of coals, the property of nonagglomeration is especially important.

(3) The so-called economical limits of particle size of coals with respect to combustion are indicated by the author's experimental results.

Nomenclature

K	specific combustion rate (mol C/cm² sec)
$C(O_2)$	oxygen concentration of a fluid mass surrounding a particle (mol O_2/cm)
k_r	resultant reaction rate constant (cm/sec)
k_c	chemical reaction rate constant (cm/sec)
k_f	boundary gas-film constant (cm/sec)
k_a	gas diffusion constant in ash layer (cm/sec)
δ	diameter of a particle (cm) or (μ)
T_f	average flame temperature (°K)
$\bar{\epsilon}_x$	modified mean eddy diffusivity for mass transfer over the cross-section x (cm²/sec)
x	distance along the axis of jet from nozzle mouth (cm)
$\bar{u}_x$	x-component of mean velocity over the cross-section x of jet flow (cm/sec)
d_x	diameter of the cross-section x (cm)
k	empirical constant for momentum transfer of free cold-air jet
$\bar{k}$	weighted mean value of over any cross-section
u_0	nozzle velocity (cm/sec)
d_0	nozzle diameter (cm)
c_x	mean concentration of an intensive property over the cross-section x (intensive property/cm³)
l_x	a scale of turbulence in the cross-section x
$\kappa_1, \kappa_2, \kappa_3$,	empirical constants
$C(O_2)_s$	oxygen concentration of the medium surrounding jet flame (mol O_2 cm³)
N	mean value of number of particles per unit volume of flame gas of interest (number/cm³)
ρ	apparent density of fixed carbon of burning particle (gram/cm³)
b, m	constants in combustion law of particles
A	combustion constant of coal par-

ticles in jet flame dependent on type of coal, b and m

T_s average temperature of the medium surrounding jet flame (°K)

β firing or break-point length (cm)

s size of sieve opening corresponding to original coal particle size δ_0 (cm) or (μ)

φ a swelling index of coal

ρ_c apparent density of fixed carbon of original coal (gram/cm^3)

R fraction by weight of coal remaining on screen of aperture s

n, a constants in size distribution law

L a relative length (dimensionless), equation (10)

${}_mL_n$ value of L corresponding to values of m and n

s_w a weighted mean particle size

S $= s/s_w$

u fraction of fuel unburned

L_f flame length (cm)

γ percentage of fuel unburned, $\gamma = 100\ u$

$\rho_{f\cdot g\cdot}$ flame gas density

$\rho_{n\cdot f\cdot}$ nozzle fluid density

n(suffix) normal state

V_0 theoretical combustion gas volume per unit weight of coal (nm^3/kgm)

M_w primary air-fuel ratio (kgm/kgm)

F a factor dependent on amount of volatile matter and superfine particles, as like as gaseous fuels

G combustion constant dependent on type of coal and temperatures and F, equation (14)

p, q constants in combustion law of superposition of solid and gas burning

ρ_0 density of coal (gram/cm^3)

fuel-ratio (fixed carbon/volatile matter) of dry coal (moisture-free)

Acknowledgments

The author wishes to thank Professor Dr. S. Yagi of the Tokyo University and Mr. J. Hosoi, Director of Laboratory of Nihon Cement Company for advice in the course of this investigation.

REFERENCES

1. Yagi, S., and Saji, K.: *Fourth Symposium (International) on Combustion*, p. 771. Baltimore, The Williams & Wilkins Company, 1952.
2. Hottel, H. C., and Stewart, I. McC.: Ind. & Eng. Chem., *32*, 719 (1940).

19

THE ABSOLUTE THERMAL DECOMPOSITION RATES OF SOLIDS

Part I. The Hot-Plate Pyrolysis of Ammonium Chloride and the Hot-Wire Pyrolysis of Polymethylmethacrylate (Plexiglas IA)[a]

By ROBERT D. SCHULTZ AND ALBERT O. DEKKER

Introduction

Wilfong, Penner and Daniels[1] have proposed that the rate-determining step for solid-propellant burning is a solid-phase unimolecular decomposition of molecules at the burning surface. Even though the decomposition reaction is unimolecular, the overall burning reaction is zero order because the concentration of reactants, i.e., surface molecules, is constant. According to this view, transfer of heat from the gas and solid-phase reactions establishes a steady-state temperature, T_s, of the burning surface. Once this surface temperature is established, the linear burning rate, B, is given by the Arrhenius type equation

$$B = B_0 \exp(-E_s/RT_s) \text{ cm sec}^{-1} \qquad (1)$$

[a] Research utilizing these new techniques is at present being supported under Contract AF18(600)1026 by the United States Air Force through the Office of Scientific Research of the Air Research and Development Command, OSR-TN-54-127.

where E_s is the activation energy for the rate-controlling solid-phase reaction and B_0 is a term which is less strongly dependent on temperature than the exponential term. For practical purposes B_0 is usually considered constant in any given temperature range whose span is less than about 100°K. The burning rate, B, is thus considered equivalent to the linear decomposition rate of the solid at the temperature T_s.

The present paper describes two new techniques of directly measuring the linear decomposition rates of solids as a function of temperature. In each of these methods the solid is pressed against a heated surface maintained at a constant steady-state temperature. The rate of disappearance of the solid in units of cm sec^{-1} is taken as the linear decomposition rate at that temperature. In the hot plate method, the heated surface is a Vycor plate supported over an electric heater or gas flame. In the hot wire method, the heated surface is a small-diameter electrically heated Nichrome or Kanthal wire.

These methods provide not only new experimental techniques for the study of the decomposition rates of solids but they provide also convenient methods for fundamental studies of solid-propellant combustion. An important advantage of these new methods is a closer simulation of conditions that exist during propellant burning. The solid under investigation is brought up from ambient temperature to the temperature of the decomposition interface in a fraction of a second. The temperature of this interface is maintained at a constant steady-state value and fresh solid is automatically supplied to the interface at the same rate at which it is decomposed. Pyrolyses may be performed in an inert nitrogen atmosphere and since evolved gases can be quickly cooled to ambient temperature it should be possible to recover a sample of pyrolysis gas more truly representative of the composition existing at the time of reaction. The hot-plate and hot-wire methods permit measurement of rates at higher temperatures (i.e., above 600°C) than is possible with more conventional apparatus. Moreover, it is possible to measure decomposition rates of solid fuels and solid oxidizers separately. It is anticipated that data so obtained will be useful in explaining the burning rates of composite propellants. The present paper, however, is concerned with the application of these methods in a basic study of the kinetics of solid-phase decomposition of ammonium chloride and polymethyl methacrylate.

Hot-Plate Pyrolysis of Ammonium Chloride

Merck reagent grade ammonium chloride powder, previously dried for six hours at 80°C, was compressed in a preheated mold at 100°C under 9,000 psi pressure for 5 minutes. Pressure was slowly released during a 10-min cooling cycle. The product was a translucent tablet 2 cm diam by 1 cm high. Parallel-sided specimens 4 mm high with a cross-sectional area of roughly 16 mm^2 were cut from the pressed tablet and attached to the lower flat end of a porcelain rod. A small fleck of fluorocarbon or fluorochlorocarbon grease was used as an adhesive. The porcelain rod (about 70 gm in weight) was then placed in a guide permitting free vertical movement and lowered gently until the specimen was in direct contact with a horizontal hot Vycor plate. An electric heater or steady gas flame underneath the Vycor hot-plate maintained constant temperature during the 1 to 6 min duration of a run. After the specimen had been partially decomposed, the rod was quickly raised and the specimen gently lifted from the flat end with a razor blade. The change in the height of the specimen (as measured by a micrometer or optical comparator) divided by the contact time was taken as the decomposition rate. Immediately after each run a flattened thermocouple junction was placed between the rod end and the Vycor plate and the system was permitted to reach equilibrium. The maximum steady state reading (±0.5°C) of the thermocouple was taken as a measure of the temperature of pyrolysis. The hot plate data are plotted in Figure 1 along with data obtained by Spingler[2] and Fehl[3] using an isothermal vacuum-sublimation technique. The latter rate data were converted from mg cm^{-2} min^{-1} units to cm sec^{-1} units by dividing by a factor ($60 \times 1.527 \times 10^3$) where 1.527 is the specific gravity of crystalline ammonium chloride. Because the rates obtained by Spingler and Fehl are in the range 120 to 220°C and those obtained by the hot-plate method are in the range 300°C to 600°C, the data are not directly comparable. However, the temperatures at which the extrapolated Spingler-Fehl data and the hot-plate data yield a linear rate of 2×10^{-4} cm sec^{-1} are 245 and 276°C. It is therefore possible that in this temperature range the ammonium chloride-hot plate interface is about 31°C cooler than the measured temperature of the

ceramic-hot plate interface. The cooling could occur as a result of the endothermic nature of the overall reaction

$$NH_4Cl \text{ (solid)} \rightarrow NH_3 \text{ (gas)} + HCl \text{ (gas)} - 39.4 \text{ kcal} \quad (2)$$

(Note: More recent unpublished data by Bills, Therneau, Mishuck and Schultz show that temperature errors due to this cooling effect can be reduced by interposing a flattened thermocouple between the specimen and the hot-plate during

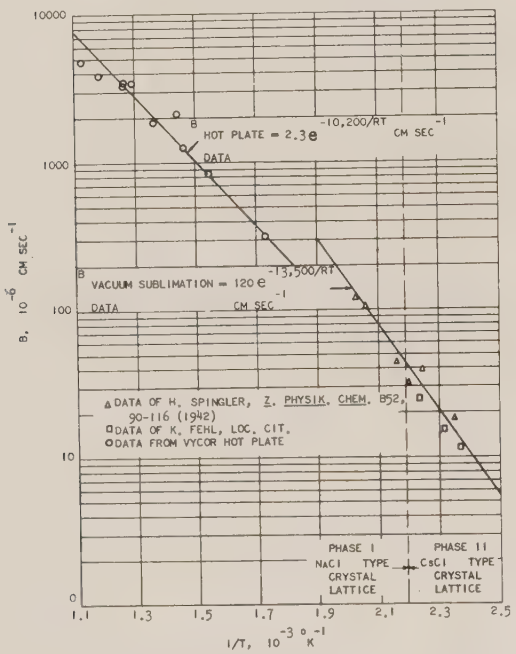
10000
1000
100
10
0
B, 10^{-6} CM SEC^{-1}
B = HOT PLATE = 2.3e$^{-10,200/RT}$ CM SEC^{-1}
DATA
B = VACUUM SUBLIMATION = 120e$^{-13,500/RT}$ CM SEC^{-1}
DATA
△DATA OF H. SPINGLER, Z. PHYSIK. CHEM. B52, 90-116 (1942)
□DATA OF K. FEHL, LOC. CIT.
○DATA FROM VYCOR HOT PLATE
PHASE I NaCl TYPE CRYSTAL LATTICE
PHASE II CsCl TYPE CRYSTAL LATTICE
1.1 1.3 1.5 1.7 1.9 2.1 2.3 2.5
1/T, 10^{-3} °K^{-1}

FIG. 1. Linear decomposition rate of ammonium chloride.

pyrolysis.) The linear vaporization rates correspond to the following Arrhenius type equations

$$B_{NH_4Cl \text{ Vaporization Hot-Plate Method}} = 2.3\, e^{-10,200/RT} \text{ cm sec}^{-1} \quad (3)$$

$$573°K < T < 873°K$$

$$B_{NH_4Cl \text{ Vaporization Spingler-Fehl Vacuum-Sublimation Method}} = 120\, e^{-13,500/RT} \text{ cm sec}^{-1} \quad (4)$$

$$393°K < T < 493°K$$

From these equations it is seen that the experimental activation energy for the pyrolysis of ammonium chloride is 10.2 kcal mole^{-1} by the hot-plate method and 13.5 kcal mole^{-1} by the vacuum-sublimation method. The discrepancy of 3.3 kcal mole^{-1} may be entirely the result of experimental error in the hot-plate method. However, it should be noted that the equilibrium crystal form of ammonium chloride in the temperature range of the hot-plate method corresponds to the NaCl-type cubic lattice, whereas the equilibrium crystal form in the temperature range of the vacuum sublimation method corresponds (except for three points) to the CsCl-type cubic lattice. The phase change occurs at 184.3°C.

It is evident that although the hot-plate method and vacuum-sublimation method at first glance appear to be radically different, the phenomenon measured is the same in both cases, namely the linear vaporization (i.e., decomposition) rate of solid ammonium chloride.

ABSOLUTE RATE EQUATION FOR THE LINEAR DECOMPOSITION OF A SOLID

For the case in which the molecules in a decomposition interface decompose by a unimolecular process, the linear rate of regression of the interface is given by the equation

$$B = n_s \frac{M}{\rho N} k_s \text{ cm sec}^{-1} \quad (5)$$

in which n_s = number of molecules per cm^2 surface
M = molecular weight, g mole^{-1}
ρ = density of solid, g cm^{-3}
N = Avogadro number, molecules mole^{-1}
k_s = unimolecular rate constant, sec^{-1}

However, the number of molecules per cm^2 surface is

$$n_s = \left(\frac{\rho N}{M}\right)^{2/3} \quad (6)$$

and according to absolute reaction rate theory[4]

$$k_s = \frac{kT}{h} \frac{F^*}{F} e^{-E_s/RT} \text{ sec}^{-1} \quad (7)$$

so that equation (5) becomes

$$B = \left(\frac{M}{\rho N}\right)^{1/3} \frac{kT}{h} \frac{F^*}{F} e^{-E_s/RT} \text{ cm sec}^{-1} \quad (8)$$

Note that the term $(M/\rho N)^{1/3}$ is equivalent to the average thickness L of the monomolecular surface layer in which reaction occurs, so that

$$B = L \frac{kT}{h} \frac{F^*}{F} e^{-E_s/RT} \text{ cm sec}^{-1} \quad (9)$$

The above derivation is a generalization of the hypothesis advanced by Wilfong, Penner and Daniels[1] specifically to explain the rate of burning of double base propellants.

It must be emphasized that according to this view the rate-controlling process in a linear solid decomposition occurs in the monomolecular surface layer only, and not below the surface. The possibility of partial decomposition in the subsurface layers is not ruled out, but this partial decomposition is not considered to be rate controlling.

A PROPOSED MECHANISM FOR THE VAPORIZATION OF AMMONIUM CHLORIDE

The surprising fact that the experimental activation energy for the vaporization of ammonium chloride is very much lower (by at least 25.9 kcal mole^{-1}) than the enthalpy of the overall vaporization process rules out reaction (2) as a one-stage rate-controlling process. As Spingler[2] has suggested, the vaporization must involve a multi-stage process. An exact description of these stages or even a count of the number of these stages is beyond our present knowledge of surface processes of crystals. However, as a rough description of the vaporization process consider the reaction sequence

$$\begin{array}{ccccc} \text{Stage I} & & \text{Stage II} & & \text{Stage III} \\ NH_4^+\,Cl^- & \underset{h}{\overset{a}{\rightleftharpoons}} & H_3N{-}H^+\,{}^-Cl & \underset{g}{\overset{b}{\rightleftharpoons}} & H_3N{-}H{-}Cl \\ & & & & c\downarrow\uparrow f \quad d\downarrow\uparrow e \\ & & & & NH_3 \quad HCl \\ & & & & \text{(gas)} \quad \text{(gas)} \end{array} \qquad (10)$$

As depicted above, stage I is intended to represent the normal structure of the surface lattice of the crystal surface. Stage II is intended to represent that orientation of an ion pair in the surface which will result in the lowest activation energy for the overall vaporization process. Stage III is intended to represent a surface state in which an inter-ionic electron transfer has nearly been completed. Stage III is the equivalent of a loosely bound ammonia-hydrogen chloride complex physically adsorbed on the crystal surface. If an activation energy nearly equal to the heat of adsorption is supplied to the complex, it is easy to imagine that the center of gravity of the complex will move away from the surface and facilitate the splitting out of a molecule of gaseous ammonia. This leaves behind a molecule of hydrogen chloride to be desorbed in a subsequent rapid non-rate-controlling step. (Alternatively, the gaseous hydrogen chloride molecule can be imagined as splitting out to leave an ammonia molecule behind or both molecules may be desorbed simultaneously.) If the desorption process is rate controlling, the activation energy, E_s, of the overall reaction is estimated to be nearly equal to the heat of van der Waals adsorption of HCl vapor plus that of NH_3 vapor on a NH_4Cl crystal surface. The average heat of adsorption of a vapor on an ionic crystal is, in turn, estimated to be nearly equal to the heat of sublimation of the vapor. (The validity of this last assumption was tested by the writers for SO_2, NH_3, N_2O and CO_2 by comparing the average heat of absorption ($\overline{\Delta H_c}$) on BaF_2 crystals[5] with the sum of the heat of vaporization and heat of fusion for each of these gases[6]. The deviation of the calculated heat of adsorption from the experimental value was in all cases less than 0.7 kcal g-mole^{-1}.) The activation energy E_s for the linear vaporization of solid NH_4Cl is thus estimated as 11.2 kcal mole^{-1} using heat of transition data on ammonia and hydrogen chloride[6]. This estimated activation energy is in reasonable agreement with the experimental values obtained by the hot-plate and vacuum sublimation techniques (see equations (3) and (4)).

ABSOLUTE RATE THEORY OF THE LINEAR VAPORIZATION OF AMMONIUM CHLORIDE

As a first approximation it will be assumed that the reverse reactions (10) e, f, g, h can be neglected. On this assumption, the absolute-rate expression for the vaporization of ammonium chloride will be written as

$$B = L\left[\nu^* \frac{(kT/h\nu^*)F^*}{F}\, e^{-E_s/RT}\right] \text{cm sec}^{-1} \qquad (11)$$

where L is the average thickness (cm) of a NH_4^* Cl^- ion pair and where the term in brackets is the familiar Eyring expression[4] slightly rewritten in terms of ν^*, the frequency of decomposition in the reaction coordimate of the activated state and the partition function for this frequency, $(kT/h\nu^*)$.

If the previously proposed mechanism is correct, there should be a close resemblence between the activated and initial states for the rate-controlling process, assumed to be either reaction (10c) or (10d) or the simultaneous reactions 10(c + d). It follows that most of the compo-

nent terms of the partition function $(kT/h\nu^*)F^*$ of the activated complex should be nearly equal to the corresponding terms for the initial state partition function. Equation (11) may therefore be approximated as

$$B = L\nu^* \frac{(kT/h\nu^*)f^*(\text{trans.})}{(kT/h\nu_N)(kT/h\nu_{Cl})} e^{-E_s/RT} \qquad (12)$$

where f^*(trans.) is a partition function for a one-dimensional translational motion of the center of gravity of the activated complex in the plane of the crystal surface and where ν_N and ν_{Cl} are normal state frequencies of the nitrogen containing and chlorine containing groups in the initial state corresponding to stage III. Because of the looseness of the complex represented by stage III, the frequencies of the groups may be considered to be nearly those of physically adsorbed molecules of NH_3 and HCl vibrating independently of each other in the plane of the crystal surface. Hill[7] has estimated that for a localized physically adsorbed molecule, the frequencies of such a vibration parallel to the surface are of the order of 3×10^{11} sec^{-1}. In the activated state two degrees of freedom corresponding to ν_N and ν_{Cl} disappear and are replaced by two degrees of freedom corresponding to the decomposition frequency ν^* and to a translational motion of the center of gravity of the activated complex. Since the complex is considered localized, f^*(trans.) will be equated to unity. By making the numerical approximations which have been suggested, it is possible to evaluate B as

$$B_{\substack{NH_4Cl\ \text{Vaporization} \\ \text{Absolute Rate Theory}}} = 300e^{-11,200/RT} \text{ cm sec}^{-1} \qquad (13)$$

$$\text{where} \qquad T_{av} = 550°K$$

In view of the assumptions which have been made, the agreement of equation (13) with experimental equations (3) and (4) is considered adequate. Consideration of reverse reactions (10) e, f, g, h, a space orientation factor, and a transmission coefficient, could bring the frequency factor of equation (12) into complete agreement with the experimental value obtained from the Spingler-Fehl data[2,3].

Hot-Wire Pyrolysis of Plexiglas

A pulley and counterweight system shown in the photograph (Fig. 2) was used to press $\frac{5}{8}$ in wide samples of Rohm and Haas cast Plexiglas IA sheet against an electrically heated No. 22 (B and S gauge) Kanthal wire with a force of 120 gm. The temperature of pyrolysis was measured with a No. 30 gauge Chromel-Alumel thermocouple electrically spot welded to the top center of the hot wire. The maximum steady-state temperature of the thermocouple junction usually obtained when the wire had cut about $\frac{1}{2}$ cm into the sample was recorded as T_s. The heat

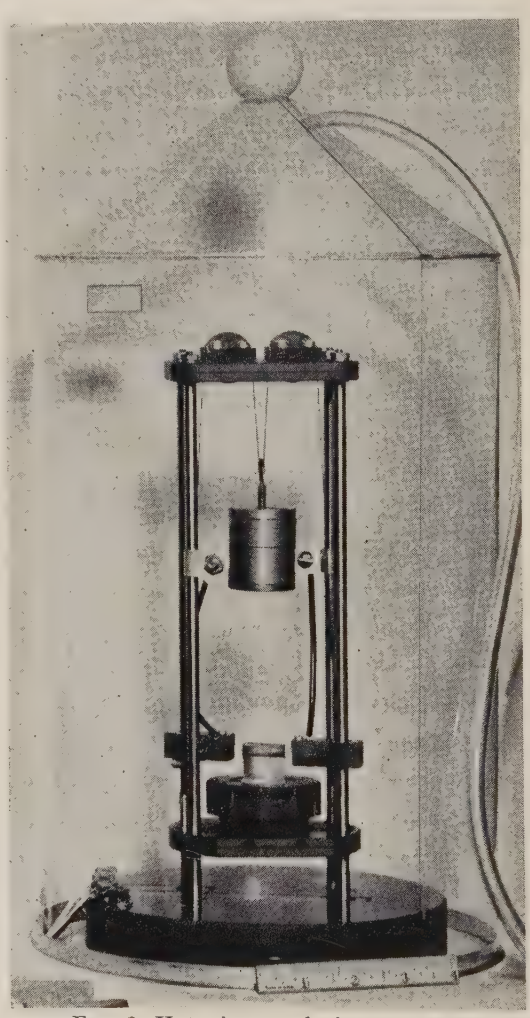

FIG. 2. Hot wire pyrolysis apparatus

conducted away from the hot wire by the thermocouple leads, makes the site beneath the hot-wire junction, the coldest and, therefore, the rate-controlling portion of the hot wire. The linear rate B at which the wire cut through the sample at a given temperature was measured with a cathetometer and stopwatch. The sides of the hot-wire cut were transparent after a run. The use of an inert nitrogen atmosphere had prevented discoloration, charring or inflaming. The

experimental rate data (Fig. 3) correspond to the equation:

$$B_{\substack{\text{Plexiglas 1A}\\ \text{Hot-Wire Pyrolysis}}} = 1.88 \times 10^{6} e^{-27{,}500/RT_s} \text{ cm sec}^{-1} \qquad (14)$$

where $723 < T < 776°\text{K}$

ABSOLUTE RATE THEORY OF THE HOT-WIRE PYROLYSIS OF PLEXIGLAS

In terms of absolute reaction rate theory, the linear rate of cutting or pyrolysis of a polymer by a hot wire should correspond to equation (9) previously discussed

$$B = L \frac{kT}{h} \frac{F^*}{F} e^{-E_s/RT} \text{ cm sec}^{-1} \qquad (9)$$

where L, in this case, is the average thickness (cm) of a polymer chain, approximated as the cube root of the volume occupied by the repeating unit in the chain. Since the activated state should closely resemble the initial state in a depolymerization process, the partition function ratio F^*/F should be close to unity and therefore

$$B = \left(\frac{M}{\rho N}\right)^{1/3} \frac{kT}{h} e^{-E_s/RT} \text{ cm sec}^{-1} \qquad (15)$$

where M is the molecular weight of the repeating unit, g mole^{-1}

ρ is the density of the solid polymer, g cm^{-3}

N is the Avogadro number, molecules mole^{-1}

The absence of any definite knowledge regarding the site of initial splitting in the polymer chain in the high temperature range 450–503°C complicates the choice of a value for the activation energy, E. Absolute rate expressions will, therefore, be calculated for three different proposed mechanisms

(1) *Taylor-Tobolsky Mechanism*[8]*:* Splitting occurs at any place along the chain, followed by an unravelling of the chain by continued splitting of monomer units.

(2) *Grassie-Melville Mechanism*[9, 10]*:* Splitting occurs almost exclusively at end of the polymethyl methacrylate chain. Thereafter the large radical rapidly evolves monomer units until the radical is completely decomposed.

(3) *Madorsky Mechanism*[11]*:* The depolymerization reaction during pyrolysis of polymethylmethacrylate is initiated by the same chemical which served as an initiator in the original polymerization process.

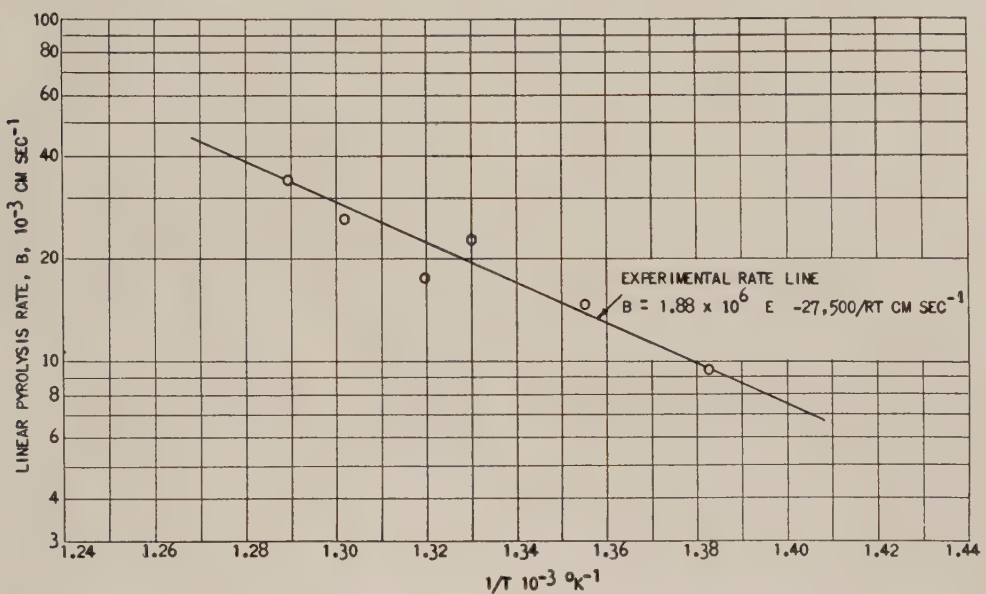

FIG. 3. Hot wire pyrolysis rate of cast polymethylmethacrylate (Plexiglas 1A sheet)

PLEXIGLASS HOT-WIRE PYROLYSIS: TAYLOR-TOBOLSKY MECHANISM

On the basis of the Taylor-Tobolsky mechanism, the activation energy for depolymerization should be equal to the energy of reaction E_r plus the activation energy for chain growth, E_p. The energy of reaction, E_r, is related to ΔH_{gc}, the

enthalpy of depolymerization of condensed polymer to gaseous monomer, by the equation

$$\Delta H_{gc} = E_r + Np_d(v_g - v_f) \qquad (16)$$

since the external work done during the expansion of one mole of monomer from the free volume v_f in the condensed state to the volume per molecule v_g, in the gas state at the decomposition pressure p_d is $Np_d\ (v_g - v_f)$ where N represents the Avogadro number. But v_f is negligibly small compared to v_g, whence $Np_d\ (v_g - v_f) \cong RT$ if the monomer vapor behaves as a perfect gas. Equation (15) may now be approximated as

$$B = e\left(\frac{M}{\rho N}\right)^{1/3} \frac{kT_{av}}{h} e^{-(\Delta H_{gc}+E_p)/RT} \qquad (17)$$

where $T_{av} = 750°\text{K}$ (average of hot wire pyrolysis temperature range)
$M = 100$ g mole^{-1}
$\rho = 1.18$ g cm^{-3}
$\Delta H_{gc} = 21.8$ kcal mole^{-1} (estimated by P. A. Small[12] for temperature range 373–433°K)
$E_p = 5.5$ kcal mole^{-1}

It will be assumed that the above values of ΔH_{gc} and E_p are reasonably correct for the temperature range of the hot-wire pyrolysis. Equation (17) is now evaluated as

$$B_{\substack{\text{Plexiglas Pyrolysis}\\ \text{Taylor-Tobolsky Mechanism}}} = 2.2 \times 10^6 e^{-27{,}300/RT} \text{ cm sec}^{-1} \quad \text{where} \quad T_{av} = 750°\text{K} \qquad (18)$$

PLEXIGLAS HOT-WIRE PYROLYSIS: GRASSIE-MELVILLE MECHANISM

The experimental evidence of Grassie and Melville[9] suggests that the activation energy, E, corresponds to the energy required for the initial fission step involving the end group of the polymethylmethacrylate chain. Rohm and Haas Cast Plexiglas IA is believed to be an unplasticized polymer of methyl methacrylate, possibly containing some ethyl methacrylate to impart resiliency to the final product. Benzoyl peroxide is probably employed as the polymerization initiator. For a benzoyl-peroxide initiated pure polymethylmethacrylate of molecular weight about 179,000, Grassie and Melville[9] obtained an experimental activation energy for depolymerization of 31 ± 1 kcal mole^{-1}. This is in fair agreement with the value of 33 kcal mole^{-1} obtained by Madorsky[11]. Since a photo-initiated polymer gave the same activation energy as the benzoyl-peroxide initiated polymer, Grassie and Melville assumed that in the latter case, the initial fission step occurs at a methacrylate and group rather than a benzoyl end group. Thus most of the discussion of energetics given in connection with the Taylor-Tobolsky depolymerization mechanism may still be applicable, except that E_p now depends on the nature of the end group. If a value of $E_p = 31 - \Delta H_{gc}$ kcal mole^{-1} is now assigned to the activation energy of propagation at the methacrylate end group, equation (17) becomes

$$B_{\substack{\text{Plexiglas Pyrolysis}\\ \text{Grassie-Melville Mechanism}}} = 2.2 \times 10^6 e^{-31{,}000/RT} \text{ cm sec}^{-1} \quad \text{where} \quad T_{av} = 750°\text{K} \qquad (19)$$

which is also in reasonable agreement with the experimental hot-wire result, equation (14). It will be noted in passing that the discussion of the energetics of the polymethylmethacrylate degradation presented by Grassie and Melville (page 38 of reference 9 and page 148 of reference 10) is in error because of failure to credit the contribution of the latent heat of vaporization of liquid monomer, ΔH_{gl}, to the overall heat of depolymerization, ΔH_{gc} of condensed polymer to gaseous monomer. ΔH_{gl} has been estimated by Small[12] to be about 9.1 kcal mole^{-1}.

PLEXIGLAS HOT-WIRE PYROLYSIS: MADORSKY MECHANISM

Madorsky[11] has suggested that benzoyl peroxide, which serves as an initiator in the polymerization process, serves as an initiator also in the depolymerization process during pyrolysis. The experimental activation energy ΔH_{exp} for initiation by benzoyl peroxide in methyl methacrylate is given as 30.0 kcal mole^{-1} by Tobolsky and Baysal[13]. Taking $\Delta H_{exp} = (E + RT)$ equation (15) is evaluated as

$$B_{\substack{\text{Plexiglas Pyrolysis}\\ \text{Madorsky Mechanism}}} = 2.2 \times 10^6 e^{-30{,}000/RT} \text{ cm sec}^{-1} \quad \text{where} \quad T_{av} = 750°\text{K} \qquad (20)$$

which is also in reasonable agreement with the experimental hot-wire result, equation (14).

Conclusion

The good agreement between experiment and theory justifies the conclusion that the two ex-

perimental techniques used are promising methods for the study of the kinetics of solid-phase reactions. Future work will therefore be directed toward a detailed study and reduction of the errors of the methods. A present disadvantage of the hot-plate and hot-wire methods is the difficulty of obtaining precise measurements of the temperature of the decomposition interface. It is recognized that the temperature of even small thermocouple junctions in contact with the heated surfaces may be different from the temperature of the actual decomposition surface, because of the effects of heat convection and heat conduction in the pyrolysis gas film. It is hoped that improvements can be made in the methods which will permit elimination of the uncertainty with respect to temperature or at least permit an estimation of its magnitude. There may also be catalytic effects by the metal of the hot wire and by the material of the hot plate. It will be necessary, therefore, eventually to compare results on apparatus made or coated with different substances. Another point requiring investigation is the effect of varying the force with which the solid specimens are pressed against the heated surfaces. Until these effects are fully explored, the data and many of the conclusions contained in this report must be considered tentative. The agreement between experiment and theory, however, encourages the belief that the rate-controlling process in the hot-plate pyrolysis of ammonium chloride is the desorption of gas molecules from a physically adsorbed ammonia-hydrogen chloride complex and that the rate-controlling process in the hot-wire pyrolysis of Plexiglas is the depolymerization of condensed polymer to gaseous monomer.

Acknowledgments

The authors wish to express their sincere appreciation to Mr. Richard Geckler and Mr. William Campbell of Aerojet-General Corporation for their continued interest and encouragement in this work and to their other colleagues for help and valuable discussions, particularly to Dr. Ralph W. Lawrence.

REFERENCES

1. Wilfong, R., Penner, S., and Daniels, F.: J. Phys. Coll. Chem., *54*, 863–872 (1950).
2. Spingler, K.: Z. physik. Chem., *B52*, 90–116 (1942).
3. Fehl, K.: Loc. cit.
4. Glasstone, S., Laidler, K. J., and Eyring, H.: *The Theory of Rate Processes*. New York, McGraw-Hill Book Company, 1941.
5. Crawford, V. A., and Tompkins, F. C.: Trans. Far. Soc., *44*, 698–708 (1948).
6. U. S. Bureau of Standards Circular 500: *Selected Values of Chemical Thermodynamic Properties*, 1952.
7. Hill, T. L.: J. Chem. Phys., *16*, 181–189 (1948).
8. Taylor, H. S., and Tobolsky, A. V.: J. Am. Chem. Soc., *45*, 2063–2067 (1945).
9. Grassie, N., and Melville, H. W.: Proc. Roy. Soc., *199A*, 1–55 (1949).
10. Grassie, N., and Melville, H. W.: Bull. Soc. Chim. Belg., *57*, 142–153 (1948).
11. Madorsky, S. L.: J. Polymer Science, *XI*, 491–505 (1953).
12. Small, P. A.: Trans. Far. Soc., *49*, 441–447 (1953).
13. Tobolsky, A. V., and Baysal, B.: J. Polymer Science, *XI*, 471–486 (1953).

20

SOME PHYSICAL ASPECTS OF THE COMBUSTION OF MAGNESIUM RIBBONS

By KENNETH P. COFFIN

Introduction

In spite of the expanded efforts on combustion research in recent years, the burning of metallic solids has not received much attention. While solid carbon has been the subject of extensive investigations[1] which have clearly indicated the significance of surface reaction in the utilization on nonvolatile carbon, there is relatively little information of the detailed mechanism of the combustion of metals. A possible reason for this is that previous investigators may have generally

assumed that the burning of metals resembles that of high boiling-point liquids with minor modifications incorporated to accommodate solid combustion products.

Beyond the work directly with carbon, the utilization of solid explosives, primarily as ammunition, has received much attention[2]. A project in the attainment of high temperature by burning various metals has been carried out[3]. Dust explosions in recent years, particularly of metallic powders, have been studied from the aspect of safety[4]. Some work is available on the propagation of flame through dust clouds: the experimental flame speed of aluminum powder dust,

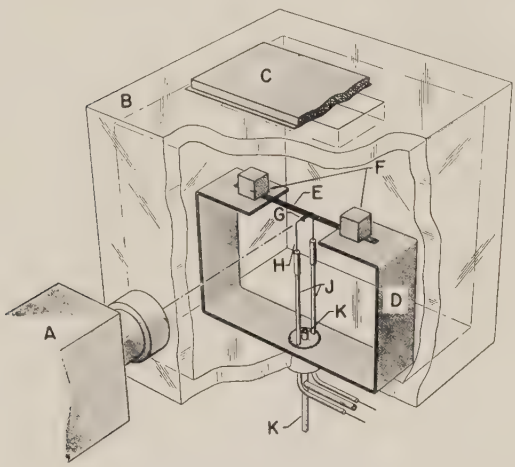

FIG. 1. Magnesium ribbon burning apparatus. A, camera; B, box; C, cover; D, bracket; E, ribbon; F, weights; G, thread; H, heater; J, electrodes; K, filling tube.

together with the effects of concentration and particle size[5], spectral studies of metal dust flames[6], and Bunsen burners employing metal dusts, including the determination of flame temperatures[7, 8].

A considerable volume of work exists on the high-temperature slow oxidation of metals; that is, studies of the growth of oxide films at temperatures below which ignition occurs. These investigations, covering a wide range of metals[9, 10], definitely involve metallic surface phenomena. Studies of the burning of single liquid fuel drops[11, 12, 13] and of liquid fuel from burners of various geometries[14] represent cases where vapor processes are known to occur. Such work has produced successful techniques for the treatment of diffusion flames surrounding single droplets.

A vapor-phase reaction for boiling magnesium is indicated[3], and a mechanism of metal vaporization has been suggested for flaming magnesium.[15] Ignition-temperature studies of magnesium, solid[16] and molten[17], have been carried out. In addition, some of the general references specifically mention magnesium[3, 4, 6, 7, 8, 9, 10]. A summary of the influence of inert gases on homogeneous flame has been prepared[18] (the inerts used in these experiments are included).

The purpose of this investigation was to study the gross physical mechanism of the combustion of relatively small quantities of magnesium metal in order to determine whether a vapor-phase or surface mechanism is involved; further, to examine the effect of the composition of the oxidizing atmosphere, both as a matter of general interest and in the hope that such studies might be informative as to the details of the physical and/or chemical processes involved. In particular, magnesium ribbon was burned in 17 to 100 per cent oxygen mixtures with argon, nitrogen, helium, and argon-water vapor as diluents. Data are presented in terms of burning times for a strip of ribbon about 4.6 cm long; such data bear an approximately inverse relation to average burning rates. The experimental data are compared with average burning times calculated from hypotheses involving diffusion and heat transfer relations; the effects of moisture are less satisfactorily explained. The occurrence of a vapor-phase combustion process is strongly indicated on the basis of the experimental observations and this comparison.

Apparatus

Experiments were carried out in a 7-in, transparent box (Fig. 1), with a gasketed cover which served as an adequate seal under vacuum conditions and as a vent against positive pressures. A rubber stopper in the bottom supported two electrodes and a tube for evacuating and filling the box. The magnesium ribbon was supported by a metal bracket with a gap of about 4.6 cm and held in place by small metal weights. The electrodes supported a Nichrome heater in the form of a squared "U". A bit of magnesium thread wrapped about the heater was ignited electrically; the burning thread then ignited the ribbon.

The magnesium ribbon measured 0.015 by 0.31 cm and weighed 0.0074 gram/cm (about 10 per cent less than the weight calculated from these dimensions). No special precautions were taken to remove oxide film or prevent oxidation, but the

ribbons were kept in closed containers and retained their luster. Mixtures of 17.6, 21.5, 24.1, 34.2, and 43.7 volume per cent oxygen in argon, 34.9, 44.5, and 70.0 per cent oxygen in nitrogen, and compressed air were obtained commercially. 18.2, 32.0, and 70.6 per cent oxygen in argon and 18.0 and 53.0 per cent oxygen in helium were mixed from cylinders of individual gas in a 35-liter tank to a total pressure of 5 atm. Moisture was added to the 21.5 and 43.7 per cent oxygen in argon mixtures by flowing the gas mixture over water in a simple train; the amount of water in the final mixture was controlled by adjusting the fraction of the gas flowing through a dry bypass. The concentration of water in the resulting atmosphere was determined in terms of the dew-point temperature; with adequate conditioning, readings before and after runs of several hours duration checked within about 5 per cent of the amount of water present.

Motion pictures were taken at about 16 frames/sec with spring-driven cameras calibrated for speed and constancy of speed. Detailed still pictures were obtained with a view camera.

Procedure

With the thread and ribbon in position, the box was twice evacuated to 25 to 40 mm and filled with the selected mixture. In addition, for moisture containing mixtures, the box was purged for 8 to 10 min (3 to 4 times the period required to fill the box). The only dependence upon procedure found was in filling with mixtures containing water vapor. While the box was being filled, the external photographic and electrical adjustments were made. With all preparations completed, the heater current was turned on, and then shut off when the thread ignited. The movie camera was started at the first glow of the heater; the still camera was snapped manually while observing through welders' goggles.

All quantitative data contained herein were derived from the motion pictures. Selected and numbered frames are shown in Figure 2 for a run with a burning time of approximately 3 seconds.

BURNING TIME

The time elapsed between the start and the finish of the burning of the magnesium ribbon spanning the 4.6 cm gap in the metal bracket. No corrections were made on the burning time measurements for the action of the igniter or for the quenching effect of the metal bracket (burning approached the bracket somewhat more closely for shorter burning times). The start was taken as the first frame showing a flame which within several frames was observed to be spreading (extending horizontally). Referring to Figure 2, no spreading occurs between the Frames −10, −5, and 0, but by Frame 5 spreading is underway; therefore, 0 is taken as the start (in practice, with

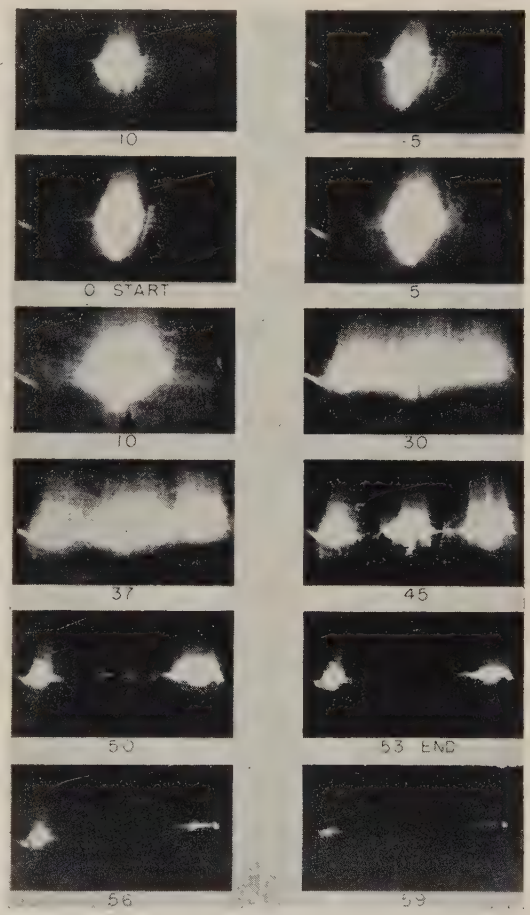

FIG. 2. Selected frames from movie of burning magnesium ribbon.

a viewer, this procedure is capable of finer gradations). Frame 30 shows fully developed combustion. By Frame 37 the flame is starting to subside. An appreciably decreased luminous area is shown in Frame 45, and Frame 50 indicates the final stages of vigorous burning. Frame 53 shows a luminosity which thereafter changes relatively slowly with time (it persists considerably beyond Frame 59). Therefore, Frame 53, as an intermediate condition between vigorous burning and residual luminosity, is taken as the end. On the

whole the reproducibility of this measuring procedure is apparently quite adequate (the spread of the data is shown in Figure 5); the data are of such a nature that a systematic error of a few

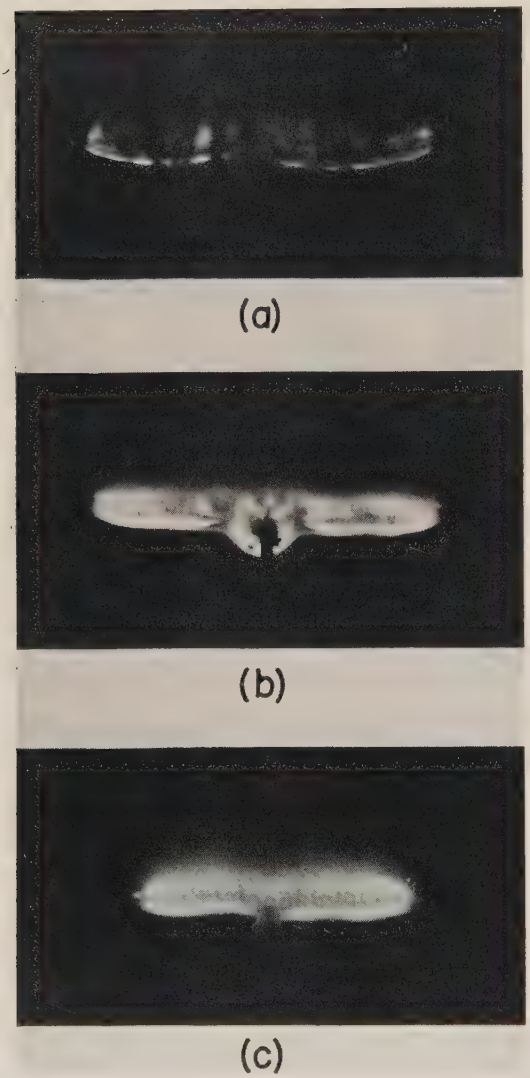

FIG. 3. Three photographs of burning magnesium ribbon, increasing exposures top to bottom.

frames, either as a constant or as a percentage error, will have little effect in the final comparisons.

APPARENT FLAME DIAMETER

The distance from the bottom of the luminous zone to the point above the ribbon where the luminous intensity starts to decrease (Frame 30, Fig. 2); an average over a number of points on each frame and over a number of frames. The numbers are at best relative on a rather indefinite scale because of constant exposure times and differences in energy release rates producing some over-exposure, and because of the difficulties of visually estimating intensities.

Experimental Results

Typical still photographs of burning magnesium ribbons are shown in Figure 3. Figure 3a shows the ribbon twisted horizontally through the flame. Figure 3b is a medium exposure showing the ribbon less clearly than Figure 3a, but giving more emphasis to the flame structure. Figure 3c is a much heavier exposure; the igniter and the unburned ribbon are visible. Magnesium oxide smoke is seen streaming up from the fire, but the structural details of the flame are obliterated. The intense inner regions surrounding the ribbon in both Figures 3a and 3b are surrounded by regions of somewhat lower luminosity which include, although only under the ribbon, a very thin region of high intensity. Figure 4 contains a schematic drawing indicating the various regions and shows microphotometer traces made of photographs across the paths indicated. The microphotometer traces indicate that, while the outer zone (a) line is not an optical illusion, its intensity is not as high as that of the inner zone (c).

The oxide ash left after a fire usually supported itself and spanned the gap. It maintained the general structure of the original ribbon, although it was fluffier for shorter burning times. For combustion in ordinary air about 18 per cent of the original magnesium remained in the ash as the oxide. The ash from the igniter thread also tended to preserve the structure of the original metal.

The experimental burning times are shown in Figure 5. The time decreases with increasing oxygen concentration for all three diluents. The decrease is somewhat less for the nitrogen-inerted case than for the argon case, and is appreciably less for helium than for either argon or nitrogen. An indication of the precision of the data is given by vertical lines indicating the spread of the 2 to 4 individual tests which are included in each average value plotted as a datum point.

The effect of moisture in the surrounding atmosphere on burning time is indicated in Figure 6. Amounts of water vapor, up to saturation at room temperature, were added to the mixtures of 21.5 and 43.7 per cent oxygen in argon. The burning time decreases with increasing amounts of water,

although the decrease in burning time per unit of added moisture is greatest for small quantities of water vapor. The precision of the measurements for low moisture contents is generally poorer than the precision indicated in Figure 5 for equivalent burning times. As a result, the faired curves are somewhat less significant than might be hoped; the qualitative effects are clear.

Discussion

One of the objectives of this investigation was to learn whether a vapor-phase or a surface reaction controls the process under examination. The evidence which indicates that a gaseous reaction occurs includes:

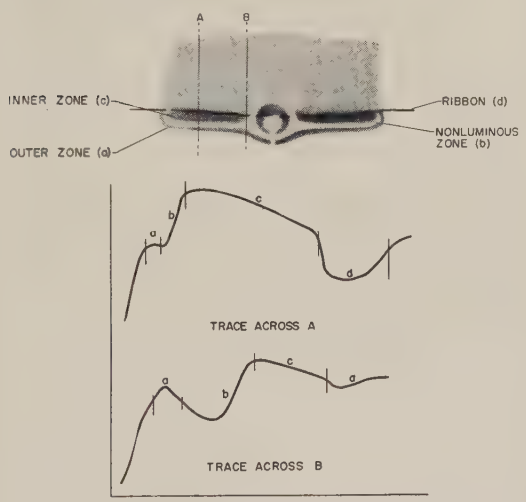

FIG. 4. Schematic drawing of flame; microphotometer traces from photographs.

(1) The distinctive zonal structure visible in the photographs. (The outer luminous zone a, Figure 4, has tentatively been attributed to the recalescence of magnesium oxide.)

(2) The distribution of light intensity away from the ribbon, as indicated on the microphotometer traces (Fig. 4).

(3) The behavior of the ribbon, softening and twisting, but apparently not completely liquifying.

(4) The appearance of the ash, maintaining the general shape of the original ribbon, fluffier for shorter burning times, and apparently not fused.

In view of the evidence suggesting a vapor-phase process in the burning of magnesium, both from these experiments and in the literature, an attempt was made to compute burning rates, and hence burning times, by a method which has proved highly successful for single liquid fuel droplets. The two region "stagnant film" approach of Spalding[11] and later of Graves[13] was adopted. Preliminary calculations (neglecting dissociation) suggested excessive temperatures ($T \cong 5 \times 10^4$ °K times the mole fraction of oxygen); the measurements by Wolfhard and Parker[7] and Scartazzini[8] suggest a flame tempera-

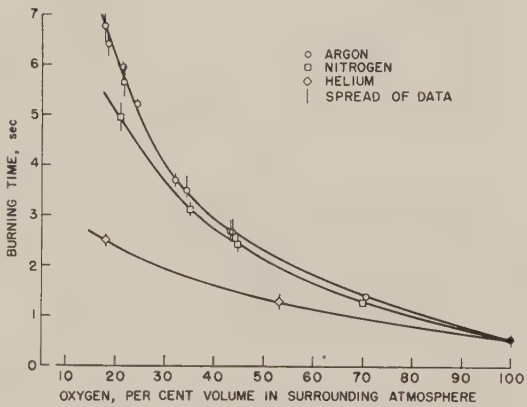

FIG. 5. Variation of burning time with oxygen concentration and diluent.

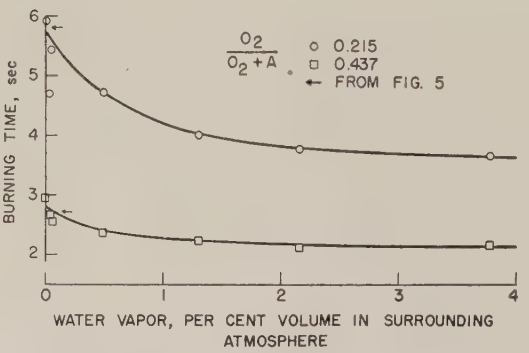

FIG. 6. Variation of burning time with water concentration.

ture of about 3100°K, approximately the boiling point of magnesium oxide. Since the oxide is believed to dissociate almost completely upon vaporization[19], dissociation could not be treated by the technique of Graves. Rather it was decided to abandon the concept of an infinitesimally thin flame front and introduce a finite reaction zone of high temperature diffusion. The model is shown in cross section in Figure 7. It consists of three concentric cylindrical zones, with boundaries designated A, B, B′, and C. The metal is vaporized from the ribbon surface, A, at about

the boiling point of magnesium. Then three zones are established:

(1) A zone, AB, of radially increasing temperature; the metal vapor is heated and heat is conducted to the metal surface to vaporize more metal.

(2) A zone, BB′, a constant temperature reaction zone at the boiling point of magnesium oxide. Interdiffusion of the oxygen and magnesium occurs. The result is a chemical equilibrium between condensed oxide, magnesium vapor, and oxygen all at the boiling point of the magnesium oxide in a stagnant film of inert.

(3) A zone, B′C, of radially decreasing temperature, consisting of a stagnant film of inert with oxygen diffusing inward and being heated and with condensed oxide moving out and being cooled. (In the treatment of the spherical case, a steady state solution is obtained as the radius of the C boundary approaches infinity; however, for the treatment of the cylindrical or flat plate cases, a finite boundary condition is required.)

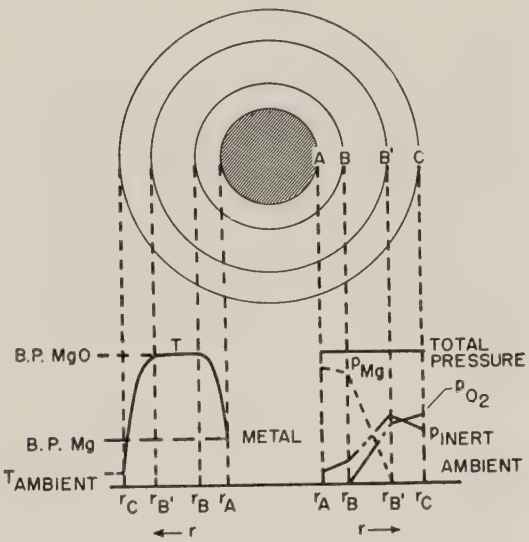

FIG. 7. Cross section of cylindrical stagnant-film model with finite reaction zone.

The general approach and the significant assumptions involved in the calculation will be indicated here. The details of the derivation and the quantities substituted into the working equations will be available[20].

The physical assumptions are:

(1) The metal ribbon can be adequately treated with cylindrical geometry; end effects are neglected.

(2) The temperature does not exceed 3200°K; this follows from the assumption of complete dissociation of magnesium oxide upon vaporization.

(3) The regions of highest luminosity correspond to the reaction zone; specifically, the apparent flame diameter has been taken as the B′ boundary. Some indication of the effect of assuming other boundary conditions will be given.

(4) The effects of free convection are neglected in setting up fuel flow, oxygen diffusion, and heat transfer equations for the steady state process.

(5) The required thermal conductivities and diffusion coefficients may be calculated as no experimental data exist for the high-temperature values required. The thermal conductivity of the gases in the AB zone is taken as that of magnesium vapor (Mg) and in the B′C zone as that of the appropriate inert gas. Diffusion in the BB′ and B′C zones is considered as the diffusion of oxygen into a stagnant film of the appropriate inert[21].

(6) In the B′C zone, as in Spalding[22], the film thicknesses for heat and mass transfer are assumed to be equal.

(7) The pressure throughout the system is at 1 atm.

The calculation of burning time is carried out by computing the average burning rate in terms of the fuel consumed in moles/sec, W_f, for the reaction $Mg + \frac{1}{2} O_2 = MgO$; this requires simultaneous solution of a number of differential equations for the fuel flow rate, oxygen diffusion, and heat transfer. These equations are organized zone by zone and integrated using the boundary conditions indicated in Table 1. Symbols are presented at the end of the paper.

A number of relations may be derived, but the following expressions for burning time are pertinent to the discussion given here

$$t = 4.85 \times 10^{-5} \frac{\ln \frac{r_{B'}}{r_A}}{B + B'} = 4.85 \times 10^{-5} \frac{\ln \frac{r_C}{r_A}}{B + B' + C} = \frac{3.04 \times 10^{-4}}{W_f/l}$$

The constant includes the molecular weight of magnesium and the mass per unit length of the ribbon (0.0074 gram/cm). The definite integrals B and C are small relative to B' for oxygen concentrations above 40 to 50 percent. Since B, B', and C can be evaluated from their defining equations (values are given in Figure 8), the burning

time will be determined by the values assigned to the radii of the boundaries of the zones. The radius r_A is associated with the ribbon, in particular the radius of a cylinder of equal surface area (0.1025 cm) has been adopted; an alternative is the use of the radius of equivalent cross-section (0.0386 cm), and the difference in the result is an increase in t by a factor of about 2. The radius $r_{B'}$ has been taken as one-half the apparent flame diameter; the data are shown in Figure 9. Values have been taken as independent of oxygen concentration; in any case, the error of such an assumption will be insignificant on an absolute basis and of second-order effect on a relative basis. Moreover, it should be noted that while free convection has been neglected in the mathematical derivation, the position of this experimental boundary may be strongly affected by convection.

Figure 10 shows the effects on the computed burning time and zonal structure of the assumption that r_C, rather than $r_{B'}$, is properly represented by a constant diameter. Again, the effect in t on an absolute basis is small, especially for oxygen concentrations above 40 to 50 per cent; relative values of t are decreased to some extent in the lower ranges of oxygen concentration.

It is to be noted that both experimental and computed burning times are averages; further, that the averages are not taken in precisely the same way. There is reason to believe that the burning rate, equivalent to the fuel flow, W_f, may be a function of r, and indeed the expression for burning time shows that it will be, unless the ratios of the diameters of the cylindrical zones remain constant. However, in the experiment a ribbon was used, and, therefore, the assumption of constant surface area and hence constant effective r_A is plausible. In the calculation, the implicit assumption is that the cylinder is ignited over its entire length instantaneously and burns uniformly. In the experiment, the burning time includes time for the flame to spread along the ribbon and takes little account of the fact that some portions are completely burned out in less than the burning time; a rough estimate is that these effects increase the observed times by a factor of about 2 which may also have a second-order dependence on oxygen concentration.

The experimental 100 per cent oxygen value may better be considered as an upper limit than as a true value because of the large calculated effects of traces of inert and/or the possibility that heat transfer processes take control for very short times. The behavior of the computed curve for very high oxygen concentrations is shown by the dotted portion between 90 and 100 per cent in Figure 11.

Figures 11, 12, and 13 show the results of carrying out the calculation outlined previously for each of the inerts, argon, nitrogen, and helium. Each figure gives the appropriate experimental curve from Figure 5, the calculated curve as obtained incorporating the assumptions and boundary conditions specified, and a normalized computed curve for comparison purposes. Normalization consisted of multiplying the computed curve by the ratio (experimental value, 50 per cent O_2)/(computed value, 50 per cent O_2). The values of the ratio used are 2.13 for argon, 2.04 for nitrogen, and 2.72 for helium; the constant for the helium case depends significantly upon the oxygen concentration selected for the normalization procedure. As presented, no physical significance is attached to the ratio; however, factors of the magnitude involved could be obtained by decreasing r_A, by decreasing the high-temperature diffusion coefficient $D_{BB'}$, or by considering the spreading time of the flame.

The correct prediction of the effect of oxygen concentration is the matter of major significance here; that is, the prediction of correct relative rates. In addition, calculation of the proper order of magnitude for the actual time is gratifying; although the absolute agreement within a factor of 2½ for argon and nitrogen must be deemed fortuitous.

The argon curves (Fig. 11) show the best fit

Table 1. Boundary Conditions for Integration

Boundary	Radius	Temperature, °K	Partial Pressure of Oxygen
A	r_A (metal surface)	1393 (b.p. Mg)	
B	r_B (eliminated)	3200 (approx. b.p. MgO)	$p_B = 0$
B′	$r_{B'}$ (luminous surface)	3200 (approx. b.p. MgO)	$p_{B'}$ (calculated)
C	r_C (not used)	300 (ambient)	p_C (ambient)

between experiment and calculation, followed quite closely by the nitrogen case (Fig. 12). The somewhat less satisfactory agreement for nitrogen

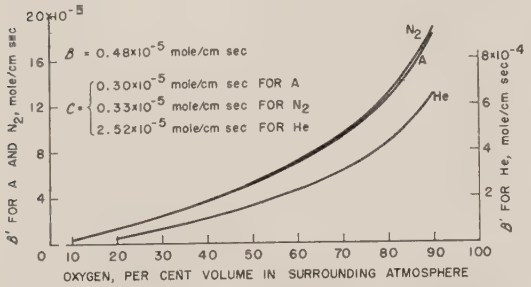
B = 0.48×10^{-5} mole/cm sec
C = 0.30×10^{-5} mole/cm sec FOR A
0.33×10^{-5} mole/cm sec FOR N$_2$
2.52×10^{-5} mole/cm sec FOR He
N$_2$
A
He
β' FOR A AND N$_2$, mole/cm sec
β' FOR He, mole/cm sec
OXYGEN, PER CENT VOLUME IN SURROUNDING ATMOSPHERE

FIG. 8. Values of the definite integrals defined in the Symbol List.

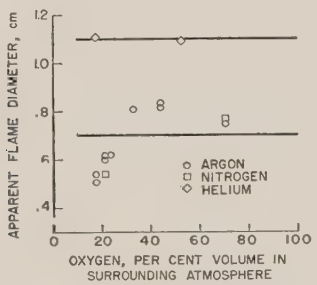

FIG. 9. Variation of apparent flame diameter with oxygen concentration and diluent.

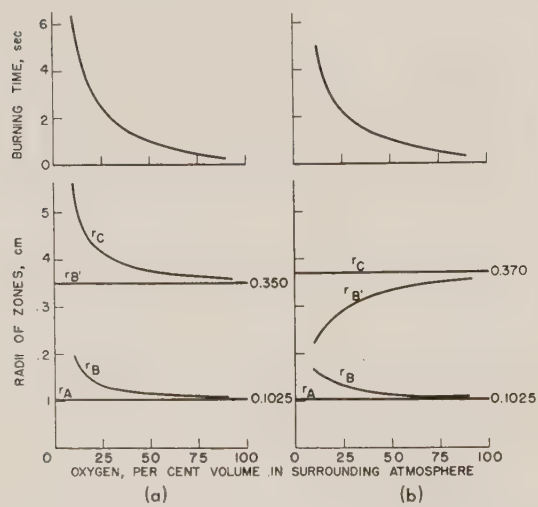

FIG. 10. Effect of boundary conditions on zonal structure and burning time. (a) r_B' held constant; (b) r_C held constant.

is most readily attributed to the fact that nitrogen is not truly an inert in this process. Magnesium nitride is known to form, and traces of ammonia were present after runs. Nitrogen acting as reactant would tend to reduce burning times at low oxygen concentrations as is observed. However, the close agreement between the nitrogen and argon experimental curves shows that here those effects have been eliminated which in high-temperature slow oxidation experiments cause magnesium to oxidize more rapidly in air than in pure oxygen[10, 15]. There is no significant difference in the calculated curves for nitrogen

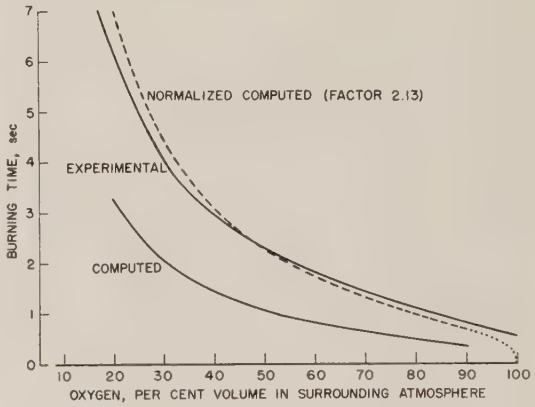

FIG. 11. Variation of burning time with oxygen concentration in argon.

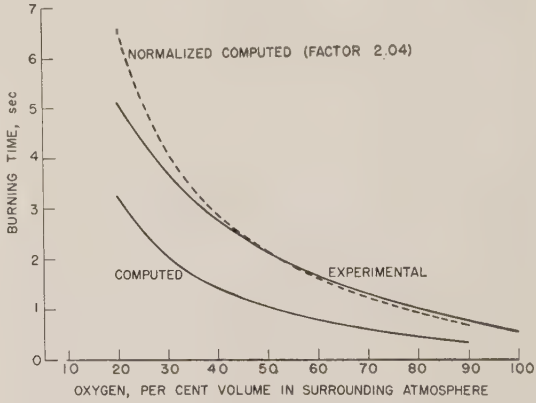

FIG. 12. Variation of burning time with oxygen concentration in nitrogen.

and argon. Although the nitrogen curve is very slightly disposed in the direction indicated by the experiments, the differences are small compared with the assumptions involved, particularly in the calculation of the high temperature diffusion coefficients.

The helium calculation (Fig. 13) shows considerable departure from experiment at low oxygen concentrations (helium mixtures, in contrast to argon and nitrogen mixtures, have an appreciable dependence of density upon oxygen concentra-

tion). A considerable part of this is no doubt due to the difficulties of computing thermal conductivities and diffusion constants for mixtures of constituents varying widely in molecular weight. Efforts to account for the concentration effect on the properties involved are of doubtful validity and, in any case, show little improvement in the final results.

The calculations with the inert gases do predict that helium should show shorter burning times than argon and nitrogen and this prediction is in agreement with the experiments. In comparison, the effect of inerts in reducing the burning velocities of homogeneous hydrocarbon flames appears as $N_2 > A > He$[18]; from this investigation, if there is an analogy between burning velocity and the reciprocal of the burning

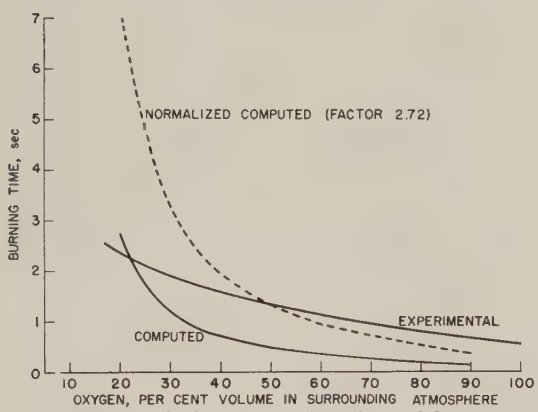

FIG. 13. Variation of burning time with oxygen concentration in helium.

time, $N_2 \cong A > He$. However, here it is known that nitrogen is not completely inert and would tend to produce a shift in the direction observed; from $N_2 > A$ for the hydrocarbon case to $N_2 \cong A$ for the magnesium case. Further in the homogeneous case flame temperatures are not equal as has been assumed here.

The effect of water is less satisfactorily explained in terms of the thermal and diffusional model presented here. It would appear more probable that the moisture affects the chemical or diffusion processes at the B and/or B′ boundaries than that it changes the gross properties within an entire zone. Water vapor produces an increase in the oxidation rate in these experiments as it did in the high-temperature slow oxidation rate studies on magnesium[10].

Nevertheless, in spite of certain anomalies between the experimental data and the computed burning times, the general agreement obtained strongly supports the basic assumption of a vapor-phase reaction.

Summary of Results

Magnesium ribbons were burned in mixtures of oxygen, 17 to 100 per cent by volume, with argon, nitrogen, helium, and argon-water vapor. Experimental burning times were determined and some details of the physical mechanism of the combustion process have been investigated.

(1) The burning time decreases sharply with increasing oxygen concentration.

(2) The burning time in argon-oxygen mixtures decreases in the presence of moisture, with traces of water vapor showing the greatest effect.

(3) A vapor-phase mechanism for the combustion of magnesium ribbons is very strongly indicated.

(4) Stagnant-film concepts involving a reaction zone of finite thickness permit the calculation of relative burning time in terms of the properties of the oxidizing atmosphere.

Symbols

The following symbols are used in this report:

A, B, B′, C — boundaries of zones, Figure 7

AB, BB′, B′C — zones between appropriate boundaries

B — definite integral over temperature in AB zone, moles/cm sec

$$\int_{T_A=1393}^{T_B=3200} \frac{k_{AB}}{[h_{vap} + h_f - h_{fA}]}\, dT \equiv B$$

B' — definite integral over partial pressure of oxygen in BB′ zone, moles/cm sec

$$\frac{-D_{BB'}P}{n_{O_2}RT} \ln (P - p_{B'}) \equiv B'$$

where values of $\ln (P - p_{B'})$ are obtained from

$$\int_{T_C=300}^{T_{B'}=3200} \frac{dT}{[h_{comb} - n_p(h_p - h_{pC}) + n_{O_2}(h_{O_2} - h_{O_2C})]} = \frac{D_{B'C}P}{k_{B'C}n_{O_2}RT} \ln \frac{P - p_{B'}}{P - p_C}$$

C definite integral over temperature in B′C zone, moles/cm sec

$$\int_{T_C=300}^{T_{B'}=3200} \frac{k_{B'C}}{[h_{\text{comb}} - n_p(h_p - h_{pC}) + n_{O_2}(h_{O_2} - h_{O_2C})]}\, dT \equiv C$$

D diffusion coefficient of oxygen, cm²/sec

h_{comb} heat of combustion of fuel at $T_C = 300$°K, cal/mole

h_{vap} heat of vaporization of fuel at $T_A = 1393$°K, cal/mole

h_f, h_p, h_{O_2} enthalpy of fuel, product, oxygen at T, cal/mole

h_{fA} enthalpy of fuel at T_A = 1393°K, cal/mole

h_{pC}, h_{O_2C} enthalpy of product, oxygen at T_C = 300°K, cal/mole

k thermal conductivity, cal/cm² sec(°C/cm)

l length of cylinder, cm

n number of moles per mole of fuel, stoichiometric relation

P total pressure, atm

p partial pressure of oxygen, atm

R universal gas constant, 82.05 cm³atm/°C mole

r radius, cm

T absolute temperature, °K

t computed burning time, sec

W_f fuel flow, moles/sec

SUBSCRIPTS

A, B, B', C boundaries of zones

AB, BB', $B'C$ boundaries of zones

f fuel (magnesium)

O_2 oxygen

p product (magnesium oxide)

REFERENCES

1. Colloque international de la combustion du carbone. J. chim. phys., *47*, 313–378, 523–585 (1950).
2. Muraour, H., and Aunis, G.: Chimie et industrie, *67*, 920 (1952).
3. Grosse, A. V., and Conway, J. B.: First Technical Report, High Temperature Project, Contract N9-onr 87301, Temple Univ. Oct. 15, 1951.
4. Hartmann, I.: Ind. & Eng. Chem., *40*, 752 (1948).
5. Cassel, H. M., Das Gupta, A. K., and Guruswamy, S.: *Third Symposium on Combustion, Flame, and Explosion Phenomena*, p. 185. Baltimore, The Williams & Wilkins Co., 1949.
6. Wolfhard, H. G., and Parker, W. G.: Nature, *162*, 259 (1948).
7. Wolfhard, H. G., and Parker, W. G.: Proc. Phys. Soc. (London), *62B*, 523 (1949).
8. Scartazzini, H.: Comptes rendus, *230*, 97 (1950).
9. Gulbransen, E. A.: Ind. & Eng. Chem., *41*, 1385 (1949).
10. Terem, H. N.: Comptes rendus, *226*, 905 (1948).
11. Spalding, D. B.: Fuel, *30*, 121 (1951).
12. Godsave, G. A. E.: *Fourth Symposium (International) on Combustion*, p. 818. Baltimore, The Williams & Wilkins Co., 1953.
13. Graves, C. C.: Proceedings of the Third Midwestern Conference on Fluid Mechanics, p. 759. Univ. of Minn., 1953.
14. Spalding, D. B.: Fuel, *29*, 25 (1950).
15. Leontis, T. E., and Rhines, F. N.: AIMME, Inst. of Metals Div., Trans., *166*, 265 (1946).
16. Fassell, W. M., Jr., Gulbransen, L. B., Lewis, J. R., and Hamilton, J. H.: AIMME, Metals Trans., *191*, 522 (1951).
17. Bulian, W.: Chem. Abst., *42*, 3302a (1948).
18. Mellish, C. E., and Linnett, J. W.: *Fourth Symposium (International) on Combustion*, p. 407. Baltimore, The Williams & Wilkins Co., 1953.
19. Brewer, L.: Chem. Reviews, *52*, 1 (1953).
20. Coffin, K. P.: NACA TN 3332. Dec., 1954.
21. Sherwood, T. K.: *Absorption and Extraction*. New York, McGraw-Hill Book Co., 1937.
22. Spalding, D. B.: Fuel, *29*, 2 (1950).

21

PRE-IGNITION AND IGNITION REACTIONS OF THE PYROTECHNIC SYSTEM $Zn\text{-}C_6Cl_6\text{-}KClO_4$

By SAUL GORDON AND CLEMENT CAMPBELL

Introduction

Pyrotechnic systems have long been employed for the field production of tactical and simulative military smokes. Zinc dust, chlorinated hydrocarbons and inorganic oxidants have been used for this purpose since World War I[1]. More recently developed pyrotechnic smoke compositions utilize zinc, hexachlorobenzene and potassium perchlorate in various formulations including additives such as aluminum powder to modify the burning characteristics. The chemical reactions involved in the combustion of the basic ternary composition have not been studied with respect to the thermal parameters of ignition, propagative burning, and an elucidation of the reaction mechanisms responsible for these phenomena. In order to investigate the reactions of the above system, binary, ternary, and quaternary mixtures of the three ingredients and carbon (a reduction product of the hexachlorobenzene) were studied by means of (a) differential thermal analysis, (b) determinations of ignition temperatures and the energy of activation for ignition, and (c) determinations of the closed bomb heat of combustion and gas evolution in inert atmospheres. These data have been correlated with the volume and composition of gaseous reaction products, with calculated heats of reaction, and with the thermal behavior of the reactants in order to determine and define the pre-ignition and ignition reactions for the above combustion.

Apparatus and Procedure

Differential thermal analysis (DTA) of a sample consists of measuring the temperature differential between the material under investigation and a thermally inert reference compound (both systems containing series-connected thermocouples), while they are being heated at a constant rate. The DTA curves were obtained by plotting the differential temperature as a function of sample temperature with a Moseley Autograf x-y recorder, at a differential temperature sensitivity of either 0–5 mv or 0–10 mv, and a sample temperature span of 0–10 mv. In order to provide an equivalent sample temperature span of 0–40 mv, the thermocouple is series connected through an external 10,000 Ω precision decade resistor set at 6,000 Ω to the negative input terminal of the recorder. These ranges correspond to temperature spans of ±60°C, ±120°C, and 960°C, respectively, using chromel-alumel thermocouples. The heating apparatus used to contain the sample (ca. 2 gm) and the inert reference material (alumina) are shown in Figure 1. The heating rate employed was 15°C/min. The quantities of single ingredients and mixtures used in the DTA determinations varied from about one to five grams and were chosen so as to produce approxi-

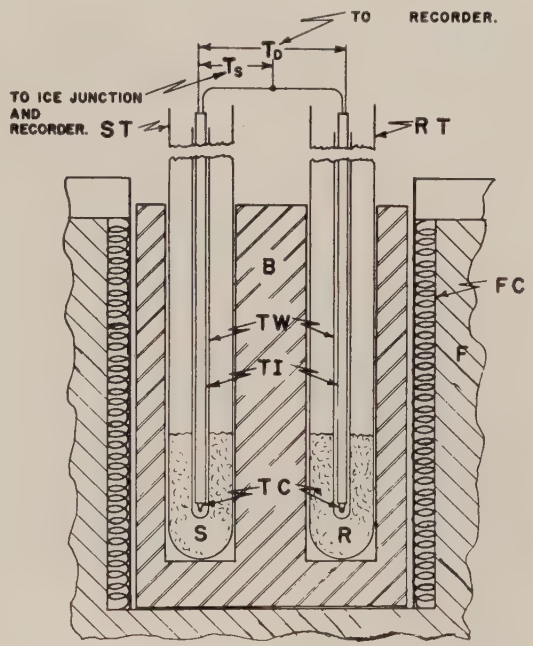

FIG. 1. Differential thermal analysis furnace, block, and sample tube arrangement.

mately full scale differential temperature deflections. Therefore, the relative displacements and band areas are to be qualitatively, rather than quantitatively, interpreted.

The thermal parameters of the propagative ignition and combustion of the pyrotechnic systems were determined by a method similar to that of Henkin and McGill[2]. The apparatus for this technique, shown in Figure 2, consists of a mechanical lever arm used to lower the ignitible sample (ca. 100 mg), contained in a copper blast-

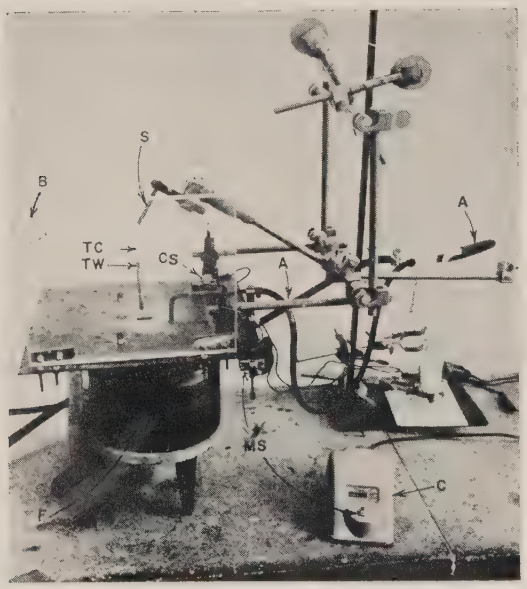

FIG. 2. Ignition temperature apparatus

A–Argon inlet	MS–Manual clock-switch
B–Barricade, plastic	S–Sample tube
C–Clock	TC–Thermocouple
F–Furnace	TW–Thermocouple well
CS–Clock-starting switch	

ing cap (¼ in x 3 in tube, #33 gauge), into the molten metal alloy bath. The bath is maintained at constant predetermined temperatures by means of a Wheelco indicating-controlling pyrometer provided with a Pyrometer Service Company proportioning controller device.

As the sample tube is plunged into the molten metal bath, the lever arm closes a microswitch mounted on the furnace, starting a synchronous motor-driven Veeder-Root tenth-second timer. When the system ignites, as evidenced by a flash of incandescent particles, a series connected switch is manually opened, stopping the clock. Triplicate determinations were made at ten-degree intervals over the temperature range from the lowest temperature at which ignition could be obtained to that temperature at which ignition times were approximately two to three seconds. By plotting the logarithm of the time to ignition (seconds) as a function of the reciprocal of the absolute temperature, it is possible to draw a straight line through the points, the slope of which is a measure of the energy of activation for ignition.

The heats of reaction and volumes of gaseous products were determined by means of a Parr adiabatic calorimeter using a 388 ml two-valve bomb, having a heat equivalent of 2467.3 cal. Three-gram samples, contained in porcelain crucibles (Coors #2), were ignited by means of platinum wire (0.005 in) at twelve volts. The bomb was previously flushed by filling to 10 atm with helium and then exhausting the system to the atmosphere; this was repeated three times before each determination. The gaseous reaction products were collected and measured in a gas buret containing mercury, and the volume corrected to standard conditions. The gases were analyzed for carbon monoxide and carbon dioxide by means of an Orsat apparatus—the carbon dioxide by absorption in alkali solution, the carbon monoxide by cupric oxide oxidation to carbon dioxide and subsequent absorption in alkaline solution.

In order to study the reactions of binary and ternary mixtures containing hexachlorobenzene at or above its boiling point, it was necessary to use sealed pyrex ampoules as reaction tubes. They were prepared by drawing an 18 mm OD test tube so as to provide a reaction volume of approximately 5 ml at the closed end of the tube, and a sharply tapered neck that could be readily sealed off in a flame after filling the bulb end with about one gram of the mixture under investigation.

The ingredients employed in this study consisted of N. J. Zinc Company standard zinc dust-122, (5 μ, 97.8 per cent), J. T. Baker Company potassium perchlorate (A. R., 29 μ), and Wyandotte Chemical Corporation commercial grade hexachlorobenzene, using the fraction through a #60 U. S. S. sieve. Particle size was determined by the air permeability method using the Fisher Sub-Sieve Sizer. The carbon was prepared by refluxing zinc (contained in a porous alundum crucible) with hexachlorobenzene for four hours, and then volatilizing the excess hexachlorobenzene. The resulting carbon, containing some unreacted zinc, zinc chloride, and zinc oxide,

was a very dense and hard mass which was, with difficulty, ground in a mortar and pestle. The fraction used was that passing through a #200 U. S. S. sieve.

All mixtures were prepared by blending the weighed ingredients, with an equal weight of rubber stoppers, in rubber containers on a ball mill for forty-five minutes.

Discussion of Results

A ternary composition containing zinc, potassium perchlorate, and hexachlorobenzene (Composition A, Table 1) was prepared which conformed to a standard military smoke mixture, excluding additives. The differential thermal analysis of the individual ingredients and of this ternary system are shown in Curves 1–5. The DTA of the mixture reveals the melting (230°C) and boiling point (320°C) endotherms of the hexachlorobenzene, and a portion of the crystalline transition (rhombic to cubic, 300°C) of potassium perchlorate. During the descent of the boiling point endotherm, the system ignites and undergoes a highly exothermal propagative combustion. The zinc and cubic potassium perchlorate are in the solid state at this ignition temperature, whereas the hexachlorobenzene is a boiling liquid. Inasmuch as this ternary mixture may undergo any combination of three possible binary reactions it follows that the ingredients must be studied as binary compositions.

The DTA of the binary system containing zinc and potassium perchlorate (Composition B) is shown in Curve 6. The potassium perchlorate transition occurs at 300°C, and the fusion of zinc at about 420°C, followed by an exothermal preignition oxidation reaction. The rate of this reaction progressively increases above the melting point of zinc and very rapidly approaches a point at which the rate of evolution of heat exceeds its rate of dissipation, thus resulting in a propagative burning type of reaction, or ignition, at about 530°C. Consequently, the reaction between these substances must occur between molten zinc and cubic potassium perchlorate, the oxidation starting at the melting point of the metal. Prior to the preignition reaction there is no apparent exothermal reaction between these ingredients, therefore precluding this binary as being responsible for the lower temperature ignition of the ternary mixture. This is also borne out by the lack of chloride in the binary mixture after heating in sealed ampoules for one hour at 320°C, the boiling point of hexachlorobenzene.

The second binary indicated above is hexachlorobenzene and potassium perchlorate (Composition C), shown in DTA Curve 7. The broad endotherms at 220–275°C and 310–500°C correspond to the melting and boiling points of the hexachlorobenzene. The latter endotherm obscures the transition of the potassium perchlorate, part of which is evident as an inflection (290–300°C) during the initial descent of the boiling point endotherm. The endotherms and exotherms between 550° and 650°C are due to the melting and decomposition of the potassium perchlorate. There is no thermal indication of preignition reaction between these ingredients, nor is there any combustion. Consequently, this reaction must not take part in the preignition

TABLE 1. PERCENTAGE COMPOSITIONS OF MIXTURES

	A[a]	B[b]	C[c]	D[d]	E[e]	F[f]	G[g]
Ingredient							
Zinc	61.1	65.4	—	40.8	—	54.5	50.9
Potassium perchlorate	22.2	34.6	57.1	—	74.3	41.2	30.9
Hexachlorobenzene	16.7	—	42.9	59.2	—	—	13.9
Carbon[h]	—	—	—	—	25.7	4.3	4.3

[a] Developmental composition: 55 parts Zn, 20 parts $KClO_4$, 15 parts C_6Cl_6.
[b] Stoichiometric: $4Zn + KClO_4 \rightarrow 4ZnO + KCl$.
[c] 20 parts $KClO_4$, 15 parts C_6Cl_6.
[d] Stoichiometric: $3Zn + C_6Cl_6 \rightarrow 3ZnCl_2 + 6C$.
[e] Stoichiometric: $4C + KClO_4 \rightarrow KCl + 4CO$.
[f] 5 parts "B" + 1 part "E".
[g] 5 parts "A" + 1 part "E".
[h] Prepared by reaction shown in footnote [d].

reaction responsible for combustion of the ternary composition. Additional evidence for the absence of a reaction between these ingredients is provided

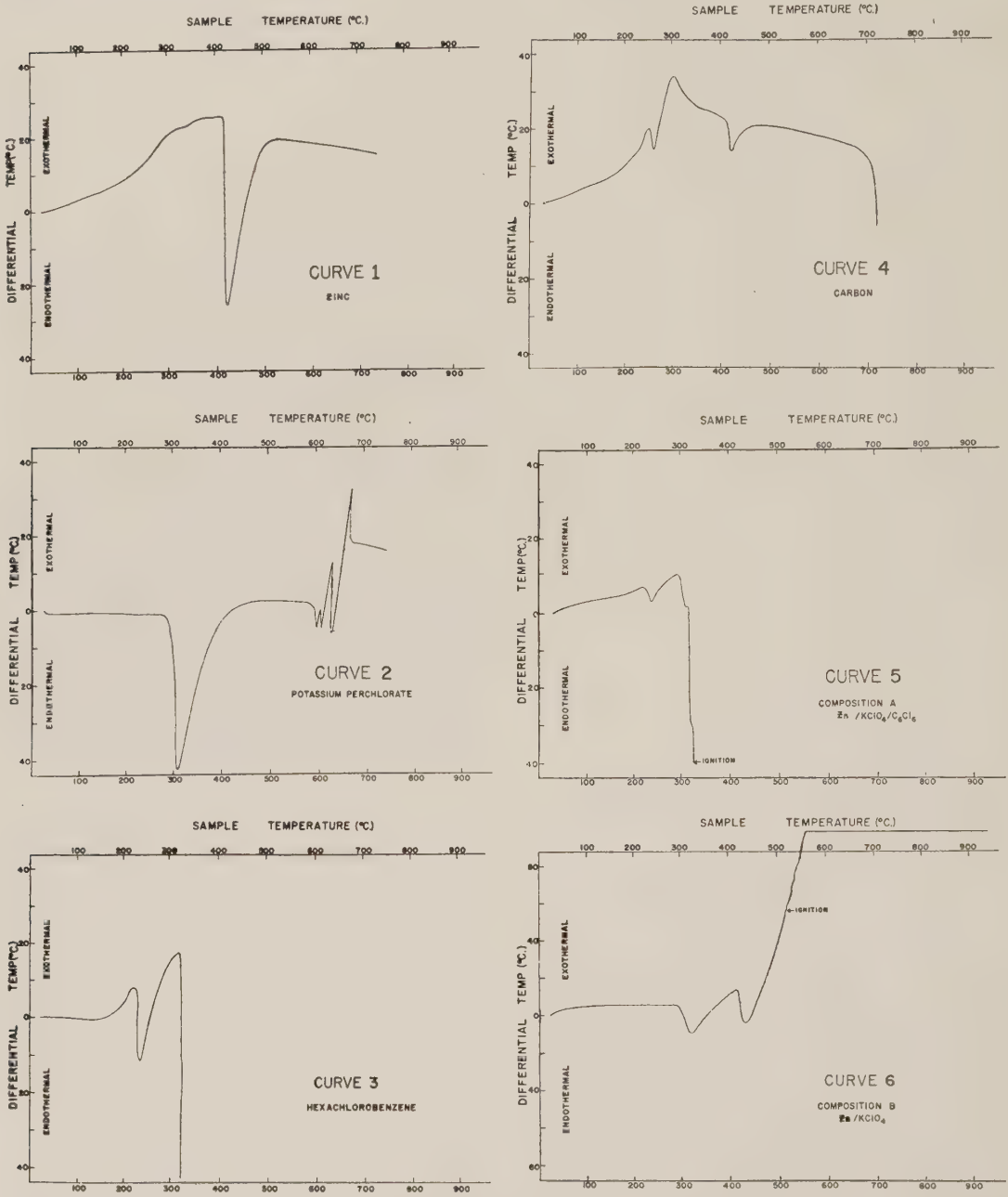

by heating the mixture in a sealed ampoule at 320°C for one hour, at which time there is no chloride ion present.

The remaining binary, zinc and hexachlorobenzene (Composition D), DTA Curve 8, again exhibits endotherms for the melting and boiling of the hexachlorobenzene. However, after the hexachlorobenzene has refluxed for about four minutes, there is a highly exothermal reaction which raises the temperature of the system to about 500°C, well above the melting point of zinc and above the temperature at which zinc and potassium perchlorate undergo exothermal pre-

ignition reaction prior to propagative combustion. This reaction is apparently the oxidation of zinc to zinc chloride and the reduction of hexachlorobenzene to carbon. The blackening of the mass and the copious production of chloride ions substantiate this conclusion, as does the endotherm at 730–750°C, corresponding to the boiling point of zinc chloride. Furthermore, the residue, when cooled to ambient temperatures, exhibits pronounced deliquescence. This is a further indication of the presence of zinc chloride. Heating the mixture in sealed ampoules, below, at, and above the boiling point of hexachlorobenzene produced increasingly larger quantities of chloride ions as measured by a qualitative silver nitrate test. Below the boiling point, reaction is quite slow, but is very rapid above this temperature. It is significant that although the reaction is highly exothermal, it is not propagative and the system does not ignite.

Since carbon, a strong reducing agent, is produced by the reaction between zinc and hexachlorobenzene, it is necessary to consider the possibility that in the ternary mixture it may react with potassium perchlorate, a powerful oxidant[3]. A binary mixture (Composition E) was prepared from the oxidant and carbon obtained by the zinc-hexachlorobenzene reaction. DTA Curve 9, reveals the transition of the potassium perchlorate, rapidly followed by an exothermal pre-ignition reaction which culminates in propagative combustion at about 350°C. Therefore this propagative reaction takes place at a temperature considerably lower than that for the zinc-potassium perchlorate binary system, but slightly higher than that for the zinc-hexachlorobenzene-potassium perchlorate ternary system.

In order to determine the effect of the carbon-potassium perchlorate reaction on the ignition and combustion of the basic ternary system, Compositions F and G were prepared. They consisted of mixtures in the ratio of 5:1, of Compositions A and B, respectively, with E. The results are presented in DTA Curves 10 and 11, in the thermal ignition parameters summarized in Table 2, and in the ignition temperature curves of Figure 4.

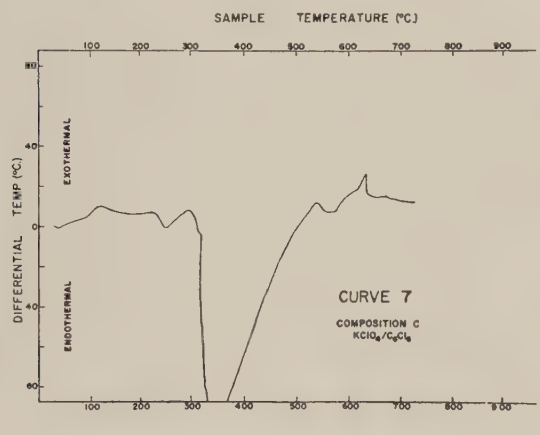

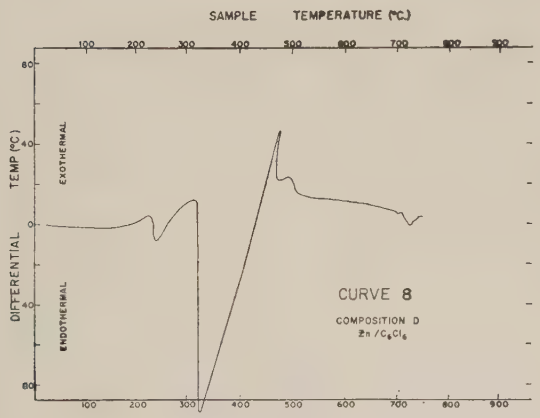

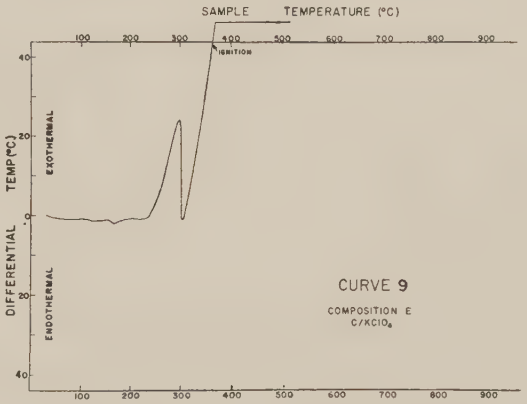

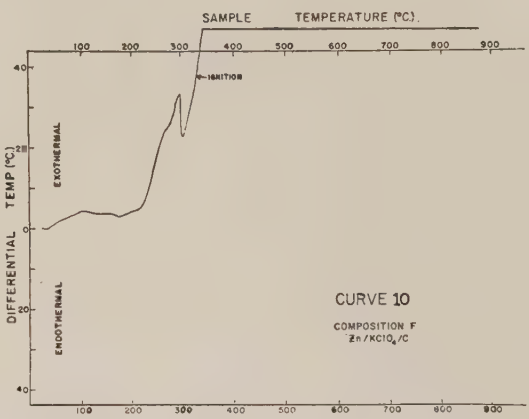

The composition (G), consisting of the ternary mixture and carbon, undergoes an explosive propagation shortly after reaching the boiling point of the hexachlorobenzene, while the ternary alone ignites only after several minutes of hexachlorobenzene refluxing under the DTA conditions. Therefore, the carbon already present has the effect of exothermally reacting with the potassium perchlorate and raising the mass to the ignition temperature in a much shorter period of time by eliminating the need for the carbon produced by the relatively slow reaction between zinc and hexachlorobenzene; the latter reaction being the first stage of the pre-ignition through combustion mechanism for the propagation of the ternary composition.

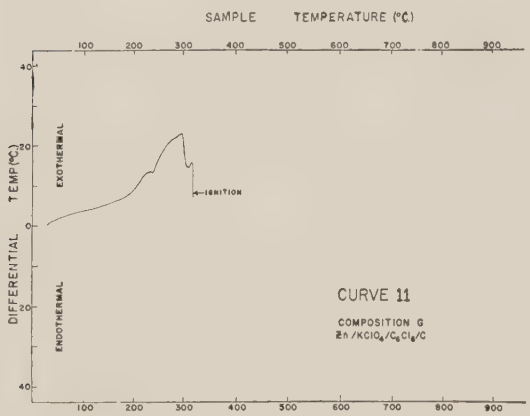

This is further illustrated in Figures 3 and 4 (Curves A and G), and by the data in Table 2. The addition of carbon reduces the energy of activation from 14.9 to 11.8 kcal/mole, and also alters the thermal ignition parameters in that considerably shorter times are required for ignition over the whole temperature range. The latter provides additional evidence for the relatively slow reaction rate constant characteristic of the reduction of hexachlorobenzene to carbon by the zinc.

The addition of carbon to the zinc-potassium perchlorate binary greatly lowers the temperature at which pre-ignition and propagative ignition reactions take place (Curve 10). As in the case of the carbon-potassium perchlorate binary, exothermal reaction leading to combustion occurs after the transition of the potassium perchlorate. This reaction is sufficiently exothermal to, in turn, raise the temperature of the mass to the ignition temperature of the zinc-potassium perchlorate mixture. Consequently, the presence of carbon renders the system much more ignitible.

The energy of activation, ΔE_a, is a measure of the relative ignitibility of the system under study. Since it is the amount of energy required to raise a portion of the system to that point at which it will initiate a propagative ignition reaction, the energy of activation is directly related to the thermal sensitivity of the mixture.

If we assume that the pre-ignition and/or ignition reaction is responsible for the propagation over the temperature range under consideration, then the Arrhenius reaction rate equation should apply as follows:

$$k = Ae^{(-\Delta E_a/RT)} \qquad (1)$$

k = specific reaction rate, A = a constant, ΔE_a

Table 2. Thermal Parameters of the Ignition and Combustion of Zn-$KClO_4$-C_6Cl_6-C Compositions

	Composition	Energy of Activation ΔE_a, Kcal/mole	Ingition Temperature (DTA) °C	Heat of Combustion (ΔH_{rx}) Cal/g	Gas Volume, ml/gram
$Zn/KClO_4/C_6Cl_6$	A	14.9, 29.3	325°	516[a]	76.8[b, c]
$Zn/KClO_4$	B	25.4	520°	815[d]	4.4[e]
$C/KClO_4$	E	13.9	360°	—[f]	—
$Zn/KClO_4/C$	F	9.9	335°	—	—
$Zn/KClO_4/C_6Cl_6/C$	G	11.8	320°	—	—

[a] Calc'd 500 cal/g.
[b] 85.2 percent CO, 10.4 percent CO_2.
[c] Calc'd 78.7 ml/g.
[d] Calc'd 808 cal/g.
[e] Not analyzed.
[f] Not ignitible with electrical system employed.

= energy of activation, R = gas constant, T = absolute temperature.

Assuming that t, the time to ignition, is reciprocally related to the specific reaction rate, we have

$$t = \frac{B}{k} \tag{2}$$

$$t = \frac{B}{A} e^{(\Delta E_a/RT)} \tag{3}$$

$$\ln t = \ln \frac{B}{A} + \frac{\Delta E_a}{RT} \tag{4}$$

$$\log t = \log \frac{B}{A} + \frac{\Delta E_a}{2.30RT} \tag{5}$$

Therefore, a plot of log t vs $1/T_{°K}$ should yield a straight line of slope $\Delta E_a/2.30R$, and intercept log B/A.

Thus, ΔE_a is the energy of activation for thermal ignition of the system.

Those compositions which ignite at relatively low temperatures generally have lower ignition activation energies than systems which ignite at higher temperatures. This may be seen in the data summarized in Table 2.

Furthermore, the effect of additives on ignitibility is readily determined by measuring this thermal energy parameter. Whereas the ternary composition has a ΔE_a of 14.9 kcal/mole over the temperature range of 320–500°C, the value is 29.3 kcal/mole from 500–550°C. This indicates that two reactions are responsible for propagative ignition: one predominating at the lower temperatures and the second over the higher range. An investigation of the two binaries (Figures 3 and 4), namely zinc-potassium perchlorate and carbon-potassium perchlorate, reveals that their respective activation energies and temperature ranges are 25.4 kcal/mole, 520–660°C, and 13.9 kcal/mole, 320–450°C. Furthermore, the previously discussed zinc-hexachlorobenzene system is found to produce carbon at and above the boiling point of hexachlorobenzene. This latter reaction, however, is relatively slow and therefore the ignition times are quite long over the temperature range of 320–500°C. Consequently, the pre-ignition reaction is essentially dependent upon the formation of carbon. This is confirmed by the pronounced decrease in the activation energy for ignition brought about by adding carbon to the zinc-potassium perchlorate binary, and by the slight decrease in the value obtained for the ternary to which carbon has been added. At the higher temperatures, in the absence of carbon, it is the oxidation of zinc by potassium perchlorate which is the predominant pre-ignition and ignition reaction, confirmed by the common slopes of

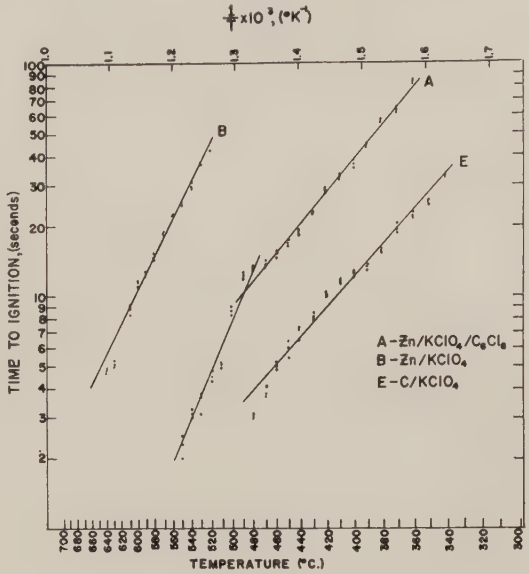

FIG. 3. Time to ignition as a function of temperature.

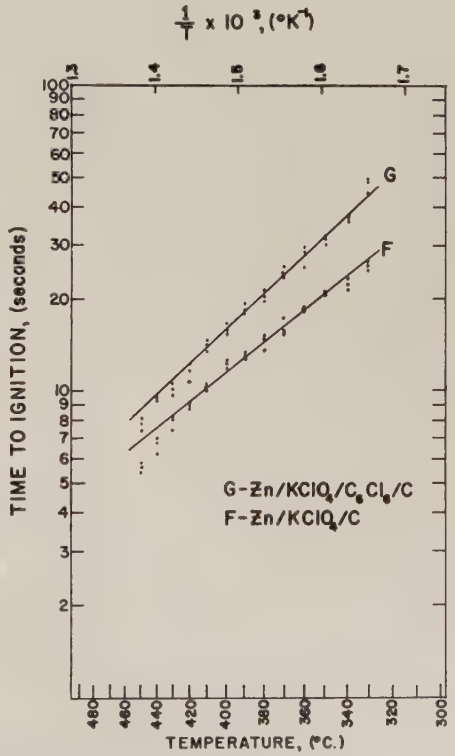

FIG. 4. Time to ignition as a function of temperature.

the ignition temperature curves of this binary and the 500–560°C range of the ternary (Figure 3).

The heats of combustion obtained by closed bomb adiabatic calorimetry in an inert atmosphere at ambient pressures compare very favorably with those calculated on a basis of the following reactions:

(1) $4Zn + KClO_4 \rightarrow 4ZnO + KCl$

(2) $3Zn + C_6Cl_6 \rightarrow 3ZnCl_2 + 6C$

(3) $4C + KClO_4 \rightarrow KCl + 4CO$

(4) $2C + KClO_4 \rightarrow KCl + 2CO_2$

For a zinc-potassium perchlorate system, the experimental and calculated heats of combustion are 815 and 808 cal/gm, respectively. The gas volume, 4 ml/gm, is probably due to traces of carbon oxides or adsorbed gases. The combustion of the ternary system (Composition A) is assumed to be the result of the above reactions; the experimental and calculated heats of combustion being 516 and 500 cal/gm, respectively.

The uncertainty of the heat of formation for hexachlorobenzene and the relative complexity of the combustion reactions preclude the calculation of an exact heat of combustion for this ternary mixture. The value, 30.7 kcal/mole, used for hexachlorobenzene was that obtained from an experimental determination of the heat of combustion. Furthermore, the calculated heat of reaction for the ternary was based upon the gaseous reaction products determined experimentally. The experimental gas volume, 76.8 ml, is in very good agreement with the calculated volume of 78.7 ml, based upon the oxidation of the hexachlorobenzene to carbon monoxide and/or carbon dioxide. Analysis of the gases revealed a composition of 85.2 per cent carbon monoxide and 10.4 per cent carbon dioxide.

Conclusions

The conclusions to be drawn from the above investigations are that there are three chemical reactions responsible for the pre-ignition, ignition, and combustion phases of the propagation of the zinc-hexachlorobenzene-potassium perchlorate system:

(1) $3Zn + C_6Cl_6 \rightarrow 3ZnCl_2 + 6C$

(2) $4C + KClO_4 \rightarrow KCl + 4CO\ (+ CO_2)$

(3) $4Zn + KClO_4 \rightarrow KCl + 4ZnO$

(a) Reaction (1) is a slow exothermal reaction which takes place at, and above, the boiling point of hexachlorobenzene to produce carbon.

(b) Carbon, which is produced at a temperature above the transition point of potassium perchlorate, reacts with the latter at the boiling point of hexachlorobenzene, according to equation (2).

(c) The latter reaction, together with reaction (1) to a limited extent, raises the system to a temperature above 500°C.

(d) At temperatures above the melting point of zinc (419°C), the pre-ignition reaction, equation (3), becomes highly exothermal, and propagation ensues in the range of 520°C.

(e) Therefore, the production of carbon by reaction (1), is an important factor in the sensitivity of this composition to thermal ignition.

Acknowledgments

The authors are indebted to R. W. Velicky and Mrs. L. E. Newman in the Calorimetry Group of the Physico-Chemical Unit for determinations of heats of reaction, gas volumes and gas analyses.

Acknowledgment is made to Garry Weingarten and Charles Knapp, whose applied research efforts led to this basic investigation, and with whom various aspects of the study were discussed.

REFERENCES

1. Berger, E.: Compt. rend., *171*, 29 (1920).
2. Henkin, H., and MacGill, R.: Ind. & Eng. Chem., *44*, 1391 (1952).
3. Patai, S., and Hoffmann, E.: J. Am. Chem. Soc., *72*, 5098 (1950).

Diffusion Flames and Carbon Formation

22

ON THE IONS IN DIFFUSION FLAMES

By TOSIRÔ KINBARA AND JUNJI NAKAMURA

Introduction

It now has been demonstrated beyond all doubt by Lenard[1], Stark[2], and Gold[3] that the negative ion in flames is a pure electron. But the nature of the positive ion has not yet been established although various theories have been suggested. Lusby[4] concluded from his results of mobility measurements that the positive ion in a high-temperature flame containing vaporized salt is a positively charged hydrogen atom. Honda[5] arrived at the same conclusion for the positive ion, using a Bunsen flame without salt vapor.

However, when we consider the mechanism of ion formation it seems inadequate to suppose the ion is a charged atom or molecule, because the ionization potentials of all the atoms and molecules found in the flame are too high (>10 volts). Thus, Bonhoeffer and Haber[6], taking into account the low excitation potentials of the free radicals C_2 and CH (2.4 and 2.85 volts, respectively), suggested that their ionization potentials also might be comparatively low and that these radicals, especially C_2, could ionize positively in the flame. However, it was shown subsequently by Kallmann and Rosen[7] that the ionization potential of C_2 is not less than 11.2 volts, which makes it impossible to accept Haber's theory in its entirety.

Nevertheless, the significant point is that thermal considerations do not account for the large number of ions present, nor can thermodynamic conditions account for the fact that the ion concentration is greater in the reaction zone than in the burned gas. Thus some processes, such as those discussed by Gaydon and Wolfhard[8], and Broida and Gaydon[9] in considering the abnormally high electronic excitation in flames, or those suggested by Behrens[10], must be important. Various studies on the formation or excitation of free radicals, such as those carried out by Wolfhard and Parker[11], Norrish and Porter[12], and Broida and Gaydon[9]; and also the studies on the behavior of ions in the external electric field by Lewis[13], Calcote[14], Pease and Calcote[15], etc., all indicate the mechanism of ion formation, but there seems to be no theory, as far as we know, which offers a convincing explanation of ion formation in the flame.

We have investigated electrically and spectroscopically the diffusion flames of a Bunsen burner supplied with city gas, and with various hydrocarbons. The results of this investigation have established in what part of the diffusion flame and in what stage of the chemical reactions ions are formed, and how they are distributed in the flame. The mechanism of the ion formation and the nature of the positive ion itself remains unsolved and requires further research.

Experimental Procedure and Results

CONDUCTIVITY AND TEMPERATURE DISTRIBUTION IN FLAMES

Observation of ion concentration in the flame was undertaken by means of a probe with two poles mounted in a straight line, 1.2 mm apart. Each pole was made of Pt-wire (diam = 0.2 mm) covered with a fine tube of fused silica (outside diam = 0.7 mm) except for $0.2 \sim 0.3$ mm at one end. This tube kept the Pt-wire rigid and insulated it electrically from the flame. As the distribution of the ion concentration has an axial symmetry, the probe was inserted horizontally in the flame in such a way that both the pole ends were at equal distances from the flame axis. The poles were connected to an electric source of 1.5 v DC, and the current through the flame was read with a galvanometer (sensitivity, 10^{-10} amp).

The current did not vary at all when the pole

ends were separated more widely, showing that the distance 1.2 mm is large enough, and that the observed current is a measure of the conductivity or ion concentration of flame at the pole ends.

In making these measurements precautions were necessary because the insulating power of the fused silica falls off rapidly as the temperature rises and leakage through silica tubes might affect the value measured for the current. To avoid this the experiment was repeated again with the pole ends of the probe covered with fused silica.

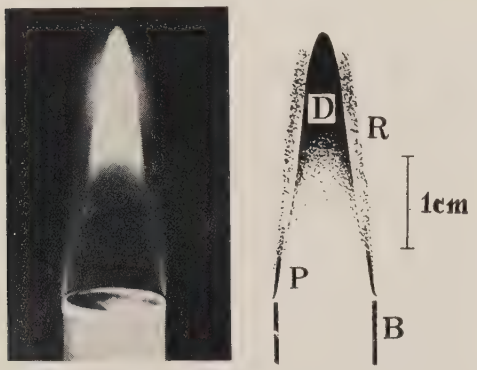

FIG. 1. Diffusion flame of city gas Bunsen burner. D, Diffusion zone; R, Recombination zone; P, Premixed-gas-combustion zone; B, burner port.

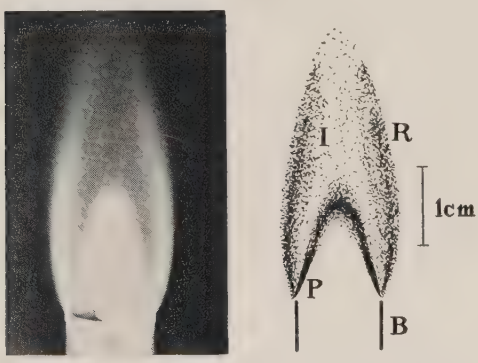

FIG. 2. Premixed-gas flame of city gas Bunsen burner. I, Inner cone; R, Outer cone (recombination zone); P, Inner cone (premixed-gas-combustion zone); B, Burner port.

When this covered probe was inserted in the lower, bluish part of the diffusion flame, the leak did not amount to more than 10^{-10} amp, and the silica proved to be sufficiently resistant in a comparatively low-temperature flame of this type. In the upper non-luminous zone, although the temperature was relatively high, the leak was found to be of the same order of magnitude, indicating a low ion concentration in this zone. When the probe was introduced into the luminous central zone, where both the temperature and ion concentration were high, the leak increased to 10^{-9} amp, which could not be neglected. The leak, therefore, was deducted from the value observed with the uncovered probe to obtain the net current through pole ends.

Further, we had to take into consideration the errors due to thermions emitted by the red-hot probe wires. According to Zachmann[16], it is quite conceivable that the thermions from the Pt-probe might disturb ion distribution in the flame. Fortunately, it was found that the thermions mattered little in the case of our probe, as the flame temperature was comparatively low and the uncovered part of the pole was so small that the number of thermions was small compared to that of the flame ions.

A diffusion flame of city gas is made up largely of zone D (Fig. 1) where combustion takes place by diffusion of air through the fuel gas. Zone D is completely surrounded by the recombination zone R which forms a thin sheath which emits a faint bluish light with continuous spectra. However, close observation always discloses a thin bluish green zone P at the bottom of the flame, the lower part of which assumes especially a bright green color. In the case of premixed-gas flame (Fig. 2), the outer cone R and the inner cone P are found to correspond to the R- and P-zones of the diffusion flame.

Figure 3 shows the distribution of relative conductivity in the diffusion flame in terms of the net current i through the ends of probe pole, at several horizontal sections I, II, III, IV, V and VI. The dotted lines of I and II correspond to the current which could not be observed accurately due to the shortage of ions, while that of IV represents the current without deducting the leak (the leak is maximum in section IV). In Figure 4, the observed current, uncorrected for leakage, is plotted for the premixed-gas flame. The heavy lines in Figure 3 correspond to the region between R and the outer surface of D-zone, while the ones in Figure 4 correspond to the region between the R- and P-zones. It should be pointed out here that when the ends of the poles approach the flame from outside, the flame surface becomes depressed as if it were repulsed by them, and accordingly the extremity of each thick line does not exactly correspond to the margin of the flame.

In any case, it is remarkable that the gases not

yet ignited inside the inner cone (curve III, Fig. 4) might probably have a conductivity. But this point will be discussed later.

Since it might have an intimate connection with the conductivity, the temperature was also measured at several points of the flame, with a thin Pt-PtRh (diam = 0.05 mm) thermocouple. The results are shown in Figures 3 and 4, respectively.

In this case, the thermocouple was not provided with a special device for compensating heat losses, and the results may be less accurate. However, it has become evident that, in general, the conductivity does not depend upon the temperature; which fact suggests, as expected, that the ions are not produced thermally.

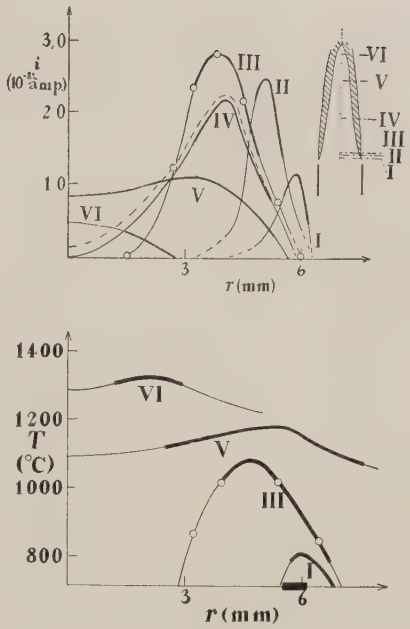

FIG. 3. Electric current (i) and temperature (T) distribution of diffusion flame. Roman numerals correspond to the respective horizontal sections of the right figure, and moreover, thicker parts of curves correspond to the hatched part of the figure which represents the region between R- and D-surfaces.

VOLTAGE DISTRIBUTION IN FLAMES

As electrons are far more mobile than atoms or molecules, the current through the probe poles may be considered as consisting chiefly of negative ions, i.e., electrons. Consequently, the i–r curves in Figures 3 and 4 must represent the electron distribution. If these figures are also to represent the ion distribution, it is necessary that the number of electrons equal the number of ions.

Observation of space-charge density in the flame can tell us whether this condition is satisfied. For this purpose, the electric voltage to the burner port was measured using a potentiometer and half of the two-pole probe, that is, a one-pole probe.

The flame was surrounded with wire netting to exclude effects due to atmospheric electricity; leakage currents and thermions were considered at all times.

With this method, however, the potential at any point can be observed only when there are abundant flame ions at the pole end and the leakage current is negligible. Accordingly, the values for the central part of the flame (curves III and IV, Fig. 5; curves II and III, Fig. 6) must be considered as approximate and it is not reasonable to calculate the charge density ρ in terms of

$$\Delta V = -4\pi\rho \qquad (1)$$

nor to discuss the ρ-distribution in detail on the basis of our present results. Nevertheless, it is certain that the flame is charged negatively to some degree in the inner central zone, and that the charge density is, in general, very small.

Here we can make a rough estimate of the elec-

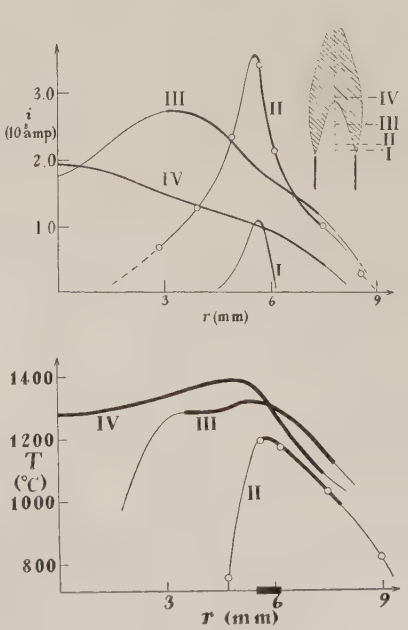

FIG. 4. Electric current (i) and temperature (T) distributions of premixed-gas flame. Thicker part of each curve corresponds to the hatched part of the right figure which represents the region between I-surface and P.

tron concentration n^- at the pole ends from the current through them, assuming that the pole end is a semi-sphere. The resulting value $n^- \simeq 10^{10}$ cm^{-3}, is reasonable compared with the results obtained by Calcote and Pease[14, 15] or by Belcher and Sugden[17].

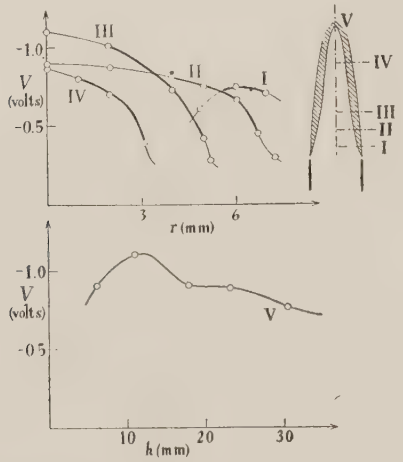

FIG. 5. Horizontal and vertical distributions of electric potential to the burner port in the diffusion flame. The thicker part of each curve has the same meaning as in Fig. 3.

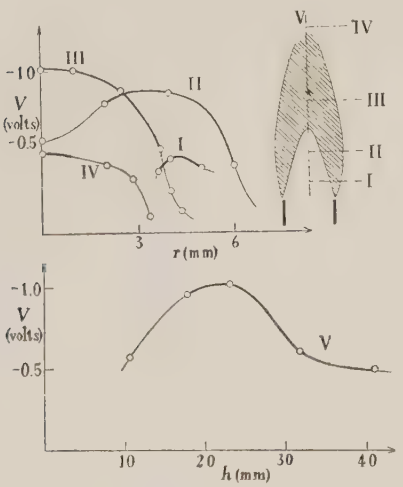

FIG. 6. Electric potential distributions of premixed-gas flame. Thicker parts of the curves have the same meaning as in Fig. 4.

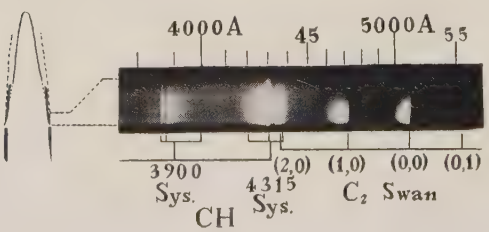

FIG. 7. CH and C_2 bands emitted from P-zone of the diffusion flame of a rectangular burner.

Let the ion concentration and the electronic charge be n^+ and e, respectively, then

$$\rho = e(n^+ - n^-). \tag{2}$$

And since the approximate value of ρ can be obtained by applying equation (1) to the $V - r$ and $V - h$ relations in Figure 5, we finally get the result,

$$\frac{n^-}{n^+} \fallingdotseq (1.01)^{\pm 1}$$

when the difference $| n^- - n^+ |$ is greatest.

Thus, it can be considered that $n^- = n^+$ at any point of the flame, and that the $i - r$ curves in Figures 3 and 4 approximately indicate the $n^+ - r$ relations.

SPECTROSCOPIC INVESTIGATION

Diffusion flames were investigated also with a quartz spectrograph. For this purpose, a burner with a rectangular section (3 cm × 0.4 cm) was used. The two-dimensional flame thus obtained was suited for the investigation of light emitted from any part of the flame.

It was found that the spectra emitted from the lower bright-green region of the P-zone of a diffusion flame (Fig. 1) are very much like those emitted from the inner cone P (Fig. 2) of a premixed-gas flame. All the bands for C_2, CH, OH were present. The C_2 band, as expected, was strongest at the base and became weaker in the upper part, finally disappearing at the top of the green region, whereas the intensity of the CH and OH bands remained virtually unchanged throughout this part (Fig. 7).

It is to be assumed that combustion of premixed gas occurs in the lowest part of the stable diffusion flame. When, for example, N_2 gas was passed around the burner port to obtain a diffusion flame in the absence of premixed-gas combustion, the whole flame went out almost at once. Thus, combustion of premixed gas was found to be indispensable for a steady diffusion flame.

FLAMES OF VARIOUS FUELS

We have also studied the flames of H_2, C_2H_2, C_3H_8; a candle; and various liquid fuels. The liquid-fuel substances used were CH_3OH, C_2H_5OH, C_3H_7OH, C_4H_9OH, $C_8H_{17}OH$, C_6H_6, $C_6H_5CH_3$, $C_2H_5OC_2H_5$, $CH_3COOC_5H_{11}$ and petroleum.

These flames all show D-, R-, and P-zones. Electric conductivity attains its maximum at the top of the green zone, and n^+ is virtually equal to n^-. Thus the flames of these compounds are essentially identical with the diffusion flame of city gas.

As to the relation between ion concentration and fuel, sooty flames such as those of C_6H_6, $C_6H_5CH_3$ or C_2H_2 are, in general, conductive and have high ion concentrations, while the ion concentration in flames of CH_3OH or C_2H_5OH (and of course, H_2) is comparatively low. It follows that both carbon atoms and bond strength are closely related to ion production.

In the alcohol series, CH_3OH, C_2H_5OH, C_3H_7OH, C_4H_9OH and $C_8H_{17}OH$, it was found that the greater the number of carbon atoms present in the fuel molecules, the greater is the ion concentration of the flame.

Discussion

The number N of ions in any horizontal layer of unit thickness can be estimated roughly as

$$N = k \int i 2\pi r \, dr, \qquad (k = \text{const.})$$

and from Figure 3.

It has been deduced from this that N increases rapidly with the height h (practically, $N = \text{const.} \times h^3$) within the bright green region of the P-zone, attaining a maximum at the top of this region, where the C_2 band disappears and N begins to decrease gradually.

Thus, the excited C_2 radical is sure to play an important role in the production of ions, and judging from the N-h relation, it seems probable that most of the ions form at the time of disappearance of the excited C_2 radicals, which after a comparatively long life-time are lost by recombination with electrons. But at present, we can not discuss further the nature of the ion itself.

Ions formed in the green zone ascend with the burnt gas and the electrons, owing to their small mass, diffuse very actively in all directions. The negative charge observed in the central part of the diffusion flame must be attributed to these electrons.

As mentioned previously, the gas in the inner cone of a premixed-gas flame seems to have a slight conductivity at the points near the surrounding cone (curve II, Fig. 4), which is quite incomprehensible, because combustion should not have set in at these points. The investigation was made in the following way.

Two of the one-pole probes previously used were fastened together side by side and the pole ends were kept 1.2 mm apart as before. This probe was inserted in the region within the inner cone through the inside of the burner tube. As the insulating silica tubes did not come in contact with the inner cone, the leak through the silica tubes could be neglected.

The unburned gas was undoubtedly conductive at points comparatively near to the wall of the inner cone. (The i-values corresponding to these points given by curve III, Figure 2, may contain some errors due to vibration of the inner cone.) The conductivity in this case can be explained as due to electron diffusion.

From all these results, we may conclude that the ions in diffusion flames are created at that stage of premixed-gas combustion where the free radicals containing carbon atoms play their own parts. It seems probable that the production of ions is related to the chemical reaction in which C_2 radicals disappear. However, further investigation is required on this point.

REFERENCES

1. Lenard, P.: Ann. d. Phys., *9*, 642 (1902).
2. Stark, J.: Naturw. Rundsch., *17*, 549 (1902).
3. Gold, E.: Proc. Roy. Soc. (London), *A79*, 43 (1907).
4. Lusby, S. G.: Phil. Mag., *22*, 775 (1911).
5. Honda, K.: Bull. Inst. Phys. Chem. Res. (Japan), *6*, 921 (1927).
6. Bonhoeffer, K. F., and Haber, F.: Zeit. f. phys. Chem., *137*, 263 (1928); Haber, F.: Sitz. Preuss. Akad. Wiss., *11*, 162 (1929).
7. Kallmann, H., and Rosen, B.: Zeit. f. Phys., *61*, 332 (1930).
8. Gaydon, A. G., and Wolfhard, W. G.: Proc. Roy. Soc. (London), *A201*, 561, 570 (1950); *A205*, 118 (1951).
9. Broida, H. P., and Gaydon, A. G.: Proc. Roy. Soc. (London), *A218*, 60 (1953).
10. Behrens, H.: Naturwissenschaften, *38*, 187 (1951).
11. Wolfhard, H. G., and Parker, W. G.: Proc. Phys. Soc. *A62*, 722 (1949); *A65*, 2 (1952)
12. Norrish, R. G. W., and Porter, G.: Proc. Roy. Soc. (London), *A216*, 165 (1953).
13. Lewis, B.: J. Am. Chem. Soc., *53*, 1304 (1931).
14. Calcote, H. F.: Third Symposium on Combustion, Flame and Explosion Phenomena. p. 245. Baltimore, The Williams & Wilkins Co., 1949.
15. Calcote, H. F., and Pease, R. N.: Ind. & Eng. Chem., *43*, 2726 (1951).
16. Zachmann, E.: Ann. d. Phys. *74*, 461 (1924).
17. Belcher, H. and Sugden, T. M.: Proc. Roy. Soc. (London), *A201*, 480 (1950).

23

THE HEIGHT OF DIFFUSION FLAMES AND THE RELATIVE IMPORTANCE OF MIXING AND REACTION RATES

By H. N. POWELL

Introduction

Several authors[1, 2, 3, 4, 5, 6] have dealt analytically and experimentally with the gross structure of diffusion flames. The characteristic feature of all these investigations is that the authors, either implicitly or explicitly, were able to consider the reaction zone as negligibly thin in comparison to the dimensions of the fuel and air volumes which it separated. Such flames are essentially mixing rate limited; the purely chemical reaction rate having a negligible influence on the overall combustion rate. A considerable body of inductive reasoning and the absence of any specific reaction rate term in their experimental correlations (partially excepting the treatment by Wohl, et al.[2]) justifies this point of view.

However, in many combustion processes of industrial importance, mechanical dispersion of the fuel, coupled with a high level of turbulence provide a scale of unmixedness which is generally finer than the 2–5 mm thickness of the typical hydrocarbon-air diffusion flame burning zone. For example, the diameter of a vapor pocket from a 100 μ droplet is on the order of 1 mm. For these cases the reaction zones run together and no meaningful reaction zone interface can be defined. This frequently encountered type of combustion lies intermediate between the extreme of mixing rate limited interface combustion on the one hand, and purely reaction kinetics limited premixed combustion on the other. Therefore, in varying proportions, both the mixing and chemical reaction rates share in determining the overall combustion rate.

Except from a largely empirical viewpoint, these intermediate types of combustion have received little attention in the past. In the following paper one phase of the problem is treated analytically, the results of which it is hoped will find application in more general studies of the problem.

In view of the fundamental importance of the mixing processes, a brief review of some elementary considerations is indicated. Since reaction ultimately depends on collisions between individual reactant molecules, the reactants must be mixed with a "grain size" which is commensurate with the molecular mean free path in order for there to be an appreciable overall reaction rate.

But unless the usual concepts of turbulence are stretched to consider individual molecules as eddies, it is apparent that the grain size or scale of unmixedness of a system in which eddy diffusion is the sole mixing mechanism is still very coarse in comparison to that of a true molecular mixture. If the dimension of a typical small eddy, say one 10^{-2} cm in diameter, is compared to a typical molecular mean free path of 10^{-5} cm, the distinction is quite clear.

Molecular diffusion, resulting from the random thermal motions of individual molecules, is effective on all scales of mixing whether turbulence is present or not. The presence of turbulence may therefore greatly accelerate macromixing, i.e., decrease the amount of mixing which molecular diffusion would otherwise have to do, but molecular diffusion is the only mechanism by which the necessary micromixing can be accomplished.

With regard to the chemical kinetic aspects, Gaydon and Wolfhard[7], from spectroscopic analyses of flat, laminar, hydrocarbon-oxygen diffusion flames conclude that the gases are very nearly in a state of chemical equilibrium through the flame zone. They point out that such a situation is a logical consequence of the slow diffusive mixing rates which prevail in such flames. It also follows from the high degree of reversibility which is implicit in this picture, that the overall flame behavior is essentially independent of the nature of the detail chemical kinetic mechanism which occur in it. Although there is some uncertainty about the situation when air is the oxidant, there is little reason to doubt that, in general, slow micromixing rates favor the approach to localized states of chemical equilibrium in the flame zone. The inverse of this line of reasoning leads to the conclusion that as micromixing rates are increased —e.g., through the introduction of turbulence or decreasing the pressure—greater departures from equilibrium and greater irreversibilities are favored. The detail chemical kinetic mechanisms then become increasingly important in determin-

ing the overall flame behavior. At the same time it is observed experimentally that the spectral distribution of the radiation from the flame also changes—good evidence that the detail kinetic mechanisms are shifting. At the hypothetical limit of an infinite micromixing rate, the kinetic mechanisms of a premixed flame prevail and completely dominate the overall flame behavior.

A general quantitative theory of turbulent, inhomogeneous combustion must somehow include the effect of interactions between the micromixing rate, the purely kinetic reaction rate, and their combined effect on the overall combustion. The objective of the development to follow is to treat analytically a limited aspect of the overall problem, namely:

(1) To investigate the functional relationship between the micromixing and reaction rates and how they influence flame height.

(2) To provide equations for determining, from experimental data, how an effective overall reation rate varies with the micromixing rate.

Analytical Development

Because of the considerable experimental difficulties which are associated with the control and measurement of turbulence in flames, a simplified approach involving only laminar flow has been taken. From a physical-chemical standpoint all the essential features of the more complicated turbulent case are retained.

Consider the sandwich burner which is schematically diagrammed in the lower part of Figure 1. It consists of many fuel slots alternating in the horizontal x direction with intervening air slots. No contact between the fuel gas and air streams is permitted until both emerge simultaneously as parallel, vertical and viscously flowing streams. The velocities of the alternating fuel and air layers are maintained approximately equal by adjusting the ratio of the widths of the fuel and air slots to that of the fuel-air volume ratio at stoichiometric. The flame seats on the upper edges of the partitions which initially separate the fuel and air streams. The flame gases are shielded from the external room air by quartz windows on all four sides of the burner. The burner area is made large enough so that wall effects do not disturb a major portion of the flame volume. The center to center distance L, from one fuel passage to the next, is then the wavelength of an x axis periodicity in the fuel and air concentrations, which persists as long as there are inhomogeneities in the flame gases. L is therefore a one dimensional scale of unmixedness, which may be varied from one burner to another.

Let Δl be designated as the nominal thickness of a single, isolated, laminar diffusion flame burning zone. Allowing for two such burning zones to be associated with each fuel slot, it is apparent that when $L \gg 2\Delta l$, the sandwich burner flame consists of a series of essentially independent diffusion flames, which are micromixing rate limited, and basically are similar to those studied by Burke and Schumann and subsequent investigators[1, 2, 3].

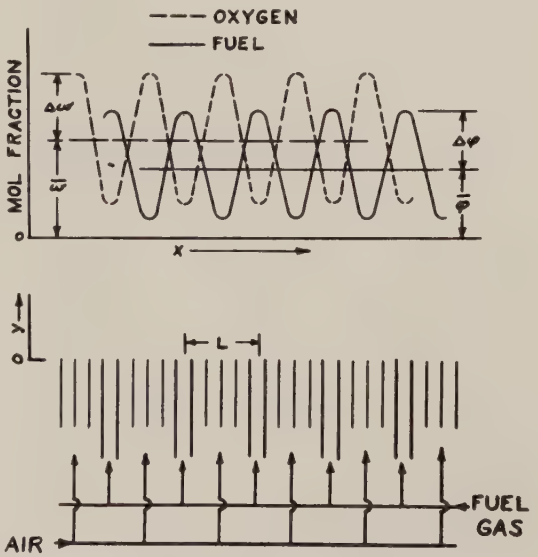

FIG. 1. Schematic diagram of sandwich burner and fuel and oxygen distributions at height y above burner surface.

Conversely, when $L \ll 2\Delta l$, the flame zones blur together and can no longer be regarded as independent, negligibly thin reaction zones. Such sandwich burner flames simulate, with a simple geometry, the essential chemical conditions which prevail in the intermediate type of turbulent combustion. The independent variables for a given burner are the fuel-air ratio and the initial velocity u_0. By varying L from one burner to another, a wide range of scales of unmixedness L, can be achieved, while simultaneously holding all other factors constant. By neglecting the change in total number of mols which accompany the reaction, the concentration variables ω and φ, referring to oxygen and fuel respectively, may be defined as shown below. The origin for both the time t, and the height above the burner y, is at the top surface of the burner.

a = mol fraction of oxygen at point x, y.
b = mol fraction of fuel-equivalent oxygen at point x, y.
$\bar{a}_0$ = x average value of a at $y = 0$.
$\bar{b}_0$ = x average value of b at $y = 0$.
$\omega = a/\bar{b}_0$ and $\varphi = b/\bar{b}_0$ when $\alpha \ll 1$, i.e., the overall mixture is lean
$\omega = a/\bar{a}_0$ and $\varphi = b/\bar{a}_0$ when $\alpha \gg 1$, i.e., the overall mixture is rich
$\alpha = \bar{b}_0/\bar{a}_0 = \bar{\varphi}_0/\bar{\omega}_0$, the overall fuel-air equivalence ratio.

It will later prove convenient to associate $\alpha = 1$ with a true overall fuel-air ratio of 1.06, but for present purposes this latter modification may be neglected. It should be noted that the definitions of ω and φ render them independent of temperature and pressure in the perfect gas law sense.

The four quartz walls of the burner confine the total flow to the vertical direction. The moderately close spacing of the fuel slots in the burner tend to minimize local cross flows; therefore let it be assumed that a local velocity u is entirely in the vertical direction. Consider the factors which change ω and φ in a differential volume which is traveling with a local velocity u. The rate of change of ω or φ with time in this volume is equal to the sum of that caused by unsteady state diffusion from or to adjacent volumes, and that caused by chemical reaction within the volume.

From the geometry of the burner and the considerable height which diffusion flames generally exhibit, it is clear that only x axis diffusion need be considered. Therefore, adopting a common diffusion coefficient, D_T, for all compositions, and neglecting the second degree term $(\partial D/\partial x)(\partial\omega/\partial x)$ we get

$$\frac{\partial\omega}{\partial t} = D_T \frac{\partial^2\omega}{\partial x^2} - \frac{\omega\varphi}{\tau_T} \qquad \text{a}$$

$$\frac{\partial\varphi}{\partial t} = D_T \frac{\partial^2\varphi}{\partial x^2} - \frac{\omega\varphi}{\tau_T} \qquad \text{b} \tag{1}$$

D_T = diffusion coefficient cm^2 − sec^{-1}
$1/\tau_T$ = reaction rate coefficient or time constant, sec^{-1}

using, in the second right hand term, a second order form for the reaction rate expression.

The great complexity of the chemical kinetic mechanism in such flames and the general lack of knowledge concerning them, make it impossible to treat the reaction aspect with much rigor. However, from a general chemical kinetic viewpoint a second order form is most plausible. And indeed, such a form is the simplest which can satisfy the obvious requirements that the reaction rate must approach zero as either, or both, of the reactant concentrations approach zero; certainly a more complex expression is not justified.

The nature of the coefficient $1/\tau_T$ will be discussed later.

Now it is well known that the diffusion coefficient D varies with temperature approximately as $D \sim T^{1.75}$, a circumstance which should be taken into account if possible. The structure of the sandwich burner flames is of considerable help in this connection. The heat thickness of a single diffusion flame front, as detected by schlieren and other methods is considerably greater than the visible flame zone thickness; ratios on the order of four to six have been observed by the author. Therefore, unless L is very large, there is a strong overlapping of the temperature fields from each reaction region, with the result that temperature variations in the x direction are markedly diminished in comparison to those in the y direction. Therefore, let all temperatures and temperature dependent groups be related to an x axis average temperature, which varies only in the y direction.

Therefore, bearing in mind that since the flow is confined essentially to the vertical direction and $u \sim T$, let equations (1a and b) be divided through by $u(T/T_0)^{0.75}$. The result can be expressed as

$$\frac{\partial\omega}{\partial s} = \left(\frac{D}{u}\right)_0 \frac{\partial^2\omega}{\partial x^2} - \frac{\omega\varphi}{\lambda_R} \qquad \text{a}$$

$$\frac{\partial\varphi}{\partial s} = \left(\frac{D}{u}\right)_0 \frac{\partial^2\varphi}{\partial x^2} - \frac{\omega\varphi}{\lambda_R} \qquad \text{b} \tag{2}$$

in which

$$ds = \left(\frac{T}{T_0}\right)^{0.75} dy = \left(\frac{T}{T_0}\right)^{1.75} u_0\, dt \tag{3}$$

and

$$1/\lambda_R = (T/T_0)^{-1.75}/(\tau_T u_0) = 1/(u_0\tau_R) \tag{4}$$

(D/u_0) is a constant, and the new variable s has the dimensions of length. The height y will be recovered from the s at the end of the development.

With regard to the temperature dependence of $1/\tau_T$, $1/\lambda_R$, etc., there is no existing experimental information which is pertinent; indeed, one of the objectives of this analysis is to provide a means of obtaining such data. From a theoretical

standpoint, the enormous number and variety of detailed kinetic mechanisms by which combustion is accomplished in premixed, intermediate, and complete diffusion flames make a general formulation impracticable.

Therefore, since variations of $1/\lambda_R$ with temperature do not alter the *form* of the differential equations, for the purpose of integration it may be held constant, provided that, in the integrated expressions, it is regarded as an effective $1/\lambda_R$ which is associated with a specified temperature rise. For most application purposes such a definition is sufficient. The foregoing considerations do not effect the proportionality $1/\lambda_R \sim 1/u_0$ in which u_0 is the initial velocity. With regard to variations in pressure, the proportionality $1/\lambda_R \sim p$ follows from the second order form.

An exact solution to equations (2a and b) is exceedingly difficult due to the non-linear nature of the equations. Indeed, in view of the inherent physical and chemical approximations, it is questionable whether an exact solution justifies the effort. Instead, a simplified approximate solution will be obtained, care being taken not to simplify away the essential features.

Consider the x axis distribution of ω and φ in the flame at some height y. As long as there are inhomogeneities in the flame gases, ω will have maxima above the air slots and minima above the fuel slots; similarly φ will have maxima and minima above the fuel and air slots, respectively. Due to very rapid diffusive flows which are associated with steep concentration gradients, the $\omega = \omega(x)$ and $\varphi = \varphi(x)$ curves will be of a rounded, smoothly varying nature everywhere except in the immediate vicinity of the burner surface. This type of distribution immediately suggests the formulas:

$$\begin{aligned} \omega &= \bar{\omega} - \Delta\omega \cos(2\pi x/L) && \text{a} \\ \varphi &= \bar{\varphi} + \Delta\varphi \cos(2\pi x/L) && \text{b} \end{aligned} \tag{5}$$

$\bar{\omega}$ and $\bar{\varphi}$ respectively are the x direction average values of ω and φ and vary only with s. $\Delta\omega$ and $\Delta\varphi$ are the amplitudes of the variations in ω and φ, and similarly vary only with s. The latter quantities might be called intensities of unmixedness and carry somewhat the same import as the Hawthorne, Weddell and Hottel[4] unmixedness factor for the turbulent case. The relation of these distribution functions to the geometry of the burner is shown schematically in Figure 1.

Since diffusion alone can in no way alter the average values $\bar{\omega}$ and $\bar{\varphi}$, these quantities can vary only because of reaction. From the original definitions of ω and φ, and the foregoing reasoning concerning their average values, it follows that:

$$\frac{d\bar{\omega}}{ds} - \frac{d\bar{\varphi}}{ds} = 0$$

Upon integration, and placing $s = \infty$, the integration constant is seen to be the excess oxygen $\bar{\omega}_\infty$, or fuel $\bar{\varphi}_\infty$, which remains after complete combustion of an off stoichiometric mixture, i.e.,

$$\bar{\omega} - \bar{\varphi} = \begin{cases} \bar{\omega}_\infty & \text{when } \alpha < 1 \\ & \text{(overall lean)} \quad \text{a} \\ 0 & \text{when } \alpha = 1 \\ & \text{(overall stoich.)} \quad \text{b} \\ -\bar{\varphi}_\infty & \text{when } \alpha > 1 \\ & \text{(overall rich)} \quad \text{c} \end{cases} \tag{6}$$

Now since, by definition either $\bar{\omega}$ or $\bar{\varphi}$ is already normalized with respect to its initial average value; at $s = 0$, we have:

$$\begin{aligned} &\alpha < 1; \quad \bar{\omega}_0 = 1 + \bar{\omega}_\infty, \quad \bar{\varphi}_0 = 1 \\ &\alpha = 1; \quad \bar{\omega}_0 = 1, \quad \bar{\varphi}_0 = 1 \\ &\alpha > 1; \quad \bar{\omega}_0 = 1, \quad \bar{\varphi}_0 = 1 + \bar{\varphi}_\infty \end{aligned}$$

A basic condition on an exact solution of equations (2a and b) is that it satisfy the relation

$$(\omega\varphi)_{s=0} = 0 \text{ at all } x \tag{7}$$

which expresses the fact that at the burner surface, there has as yet been no mixing. In the absence of mixing there can be no reaction, i.e., any physically meaningful solution has to satisfy equation (7) or its equivalent. The same condition which is expressed by $(\omega\varphi)_0 = 0$ may obviously be re-expressed in the equivalent forms:

$$\lim_{w\to\infty} \frac{\int_0^w (\omega\varphi)_0 \, dx}{w} = 0 \tag{8}$$

$$\lim_{w\to\infty} \frac{\int_0^w (\omega\varphi)_0 \cos(2\pi x/L) \, dx}{w} = 0 \tag{9}$$

Considering the form of the assumed approximate distribution relations, equations (5a and b), it is clear that because of their approximate nature, they cannot exactly satisfy equation (7): however, they can be made to satisfy the alternate equations (8) and (9). Therefore, substituting equations (5a and b) into equations (8) and (9) we obtain

$$\Delta\varphi_0\Delta\omega_0 = 2\bar{\omega}_0\bar{\varphi}_0 \quad \text{and} \quad \bar{\omega}_0\Delta\varphi_0 = \bar{\varphi}_0\Delta\omega_0$$

from which there results:

$$\Delta\omega_0 = \sqrt{2}\bar{\omega}_0 \quad \text{a}$$
$$\Delta\varphi_0 = \sqrt{2}\bar{\varphi}_0 \quad \text{b} \qquad (10)$$

To complete the specification of the boundary conditions, it is necessary to stipulate that $(d\bar{\omega}/ds)_0 = (d\bar{\varphi}/ds)_0 = 0$, corresponding to the previously deduced condition that the reaction rate at the origin is zero. It also is apparent that at $s = \infty$ the flame gases will have a uniform composition so that $\Delta\omega_\infty = \Delta\varphi_\infty = 0$. These boundary conditions are conveniently summarized in Table 1.

Now that the boundary conditions are stipulated, we can proceed with a general treatment. Substitute equations (5a and b) into the basic differential equations (2a and b). There results:

$$\frac{d\bar{\omega}}{ds} - \cos(2\pi x/L)\frac{d\Delta\omega}{ds} = \frac{\Delta\omega}{\lambda_D}\cos(2\pi x/L) - \frac{\bar{\omega}\bar{\varphi}}{\lambda_R} + \frac{\bar{\varphi}\Delta\omega}{\lambda_R}\cos(2\pi x/L) \quad \text{a}$$
$$- \frac{\bar{\omega}\Delta\varphi}{\lambda_R}\cos(2\pi x/L) + \frac{\Delta\omega\Delta\varphi}{\lambda_R}\cos^2(2\pi x/L)$$
$$\frac{d\bar{\varphi}}{ds} + \cos(2\pi x/L)\frac{d\Delta\varphi}{ds} = -\frac{\Delta\varphi}{\lambda_D}\cos(2\pi x/L) - \frac{\bar{\omega}\bar{\varphi}}{\lambda_R} + \frac{\bar{\varphi}\Delta\omega}{\lambda_R}\cos(2\pi x/L) \quad \text{b} \qquad (11)$$
$$- \frac{\bar{\omega}\Delta\varphi}{\lambda_R}\cos(2\pi x/L) + \frac{\Delta\omega\Delta\varphi}{\lambda_R}\cos^2(2\pi x/L)$$

in which $1/\lambda_D$ has the units of reciprocal length and is defined by:

$$1/\lambda_D = 1/u_0\tau_D = 4\pi^2 D/L^2 u_0 .$$

The approximate nature of the assumed ω and φ distributions manifests itself in the above equations, since it is seen that an exact equality of the right and left hand members is not maintained for variations in x. However, these equations can be simplified without impairing their general physical import by the following operations:

$$\lim_{w\to\infty}\frac{\int_0^w (\text{eq'n 11a})\,dx}{w} \quad \text{and} \quad \lim_{w\to\infty}\frac{\int_0^w (\text{eq'n 11b})\,dx}{w} \qquad (A)$$

$$\lim_{w\to\infty}\frac{\int_0^w (\text{eq'n 11a})\cos(2\pi x/L)\,dx}{w} \quad \text{and} \quad \lim_{w\to\infty}\frac{\int_0^w (\text{eq'n 11b})\cos(2\pi x/L)\,dx}{w} \qquad (B)$$

Bearing in mind that $\overline{\cos\theta} = 0$, $\overline{\cos^2\theta} = \frac{1}{2}$ and $\overline{\cos^3\theta} = 0$, operations A yield

$$\frac{d\bar{\omega}}{ds} = -\frac{\bar{\omega}\bar{\varphi}}{\lambda_R} + \frac{\Delta\omega\Delta\varphi}{2\lambda_R} \quad \text{a}$$
$$\frac{d\bar{\varphi}}{ds} = -\frac{\bar{\omega}\bar{\varphi}}{\lambda_R} + \frac{\Delta\omega\Delta\varphi}{2\lambda_R} \quad \text{b} \qquad (12)$$

which are consistent with the previously deduced equation (6). Operations (B) yield:

$$\frac{d\Delta\omega}{ds} = -\frac{\Delta\omega}{\lambda_D} - \frac{\bar{\varphi}\Delta\omega}{\lambda_R} + \frac{\bar{\omega}\Delta\varphi}{\lambda_R} \quad \text{a}$$
$$\frac{d\Delta\varphi}{ds} = -\frac{\Delta\varphi}{\lambda_D} + \frac{\bar{\varphi}\Delta\omega}{\lambda_R} - \frac{\bar{\omega}\Delta\varphi}{\lambda_R} \quad \text{b} \qquad (13)$$

By adding the latter two equations, we obtain

$$\frac{d(\Delta\omega + \Delta\varphi)}{ds} = -\frac{(\Delta\omega + \Delta\varphi)}{\lambda_D} \qquad (14)$$

and upon integrating, and applying the previously defined boundary conditions for $\Delta\omega$ and $\Delta\varphi$, there results:

$$\Delta\omega + \Delta\varphi = \sqrt{2}(\bar{\omega}_0 + \bar{\varphi}_0)e^{-s/\lambda_D} \qquad (15)$$

With the use of equations (6a, b and c) and equation (15), it is now possible to eliminate by substitution $\bar{\varphi}$ and $\Delta\varphi$ from equations (12a) and (13a), leaving them completely in terms of $\bar{\omega}$ and $\Delta\omega$; alternatively, a completely equivalent pair of equations in terms of $\bar{\varphi}$ and $\Delta\varphi$ may be obtained from equations (12b) and (13b). The identical nature of these two pairs of equations, suggest the use of a common set of dependent variables ρ and $\Delta\rho$ which are independent of the overall fuel-air ratio. This is most conveniently accomplished if ρ is associated with the more deficient constituent, so that $\rho = 0$ for complete combustion. It is also found expedient for mathematical purposes to replace the independent variable s, by a new one, $\sigma = \exp(-s/\lambda_D)$. These and other appropriate definitions are outlined in the following table of boundary conditions. More boundary conditions are listed than are required to specify the particular solutions.

In addition, let two new constants be defined according to:

$$Q = \lambda_D/\lambda_R = \tau_D/\tau_R = \frac{L^2}{4\pi^2 D\tau_R} \tag{16}$$

and for lean overall mixtures

$$r = 1/\alpha = \frac{\bar{\omega}_0}{\varphi_0}, \qquad \text{from which} \qquad \bar{\omega}_\infty = 1 - r$$

for rich overall mixtures

$$r = \alpha = \frac{\bar{\varphi}_0}{\bar{\omega}_0}, \qquad \text{from which} \qquad \bar{\varphi}_\infty = 1 - r.$$

It should be noted that ρ is always the unaccomplished fraction of the overall reaction. Also Q is a measure of the relative effectiveness of the micromixing and reaction time constants $1/\tau_D$ and $1/\tau_R$, i.e., large values of Q indicate a mixing rate which is slow in comparison to the reaction rate, and small values of Q indicate the inverse. Also r is dependent only on the overall fuel-air ratio.

When the previously indicated substitutions are performed, and the new generalized symbology is adopted, the final form of the differential equations are:

$$-\sigma\frac{d\rho}{d\sigma} = -Q(r-1)\rho + Q(r+1)(\Delta\rho)\sigma - Q\rho^2 - Q(\Delta\rho)^2 \tag{17}$$

$$-\sigma\frac{d\Delta\rho}{d\sigma} = -[1 + Q(r-1)]\Delta\rho + Q(r+1)\rho\sigma - 2Q\rho\Delta\rho \tag{18}$$

It has not been found possible to formulate a general, exact solution to these equations. However, it has been found possible to derive exact solutions for two exactly opposite approximations relating to the coefficient $(1 + Q(r + 1))$ in equation (18), namely, Case I for which $Q(r - 1) \gg 1$ and Case II for which $Q(r - 1) \ll 1$. In the indicated coefficient these conditions permit the 1 to be dropped for Case I and the $Q(r - 1)$ dropped for Case II. It is apparent that the condition $Q(r - 1) = 1$ constitutes a boundary between the region of applicability of the two solutions. Therefore, since the inherent error of approximation is exactly opposite in the two cases, numerical comparisons between the two solutions establishes the maximum error in each case. The Case I and Case II solutions are derived in the Appendix. In Table 2, Case I and Case II solutions are tabulated for the condition $Q = 1$ and $r = 1.428$. It is seen that, except at very small values of σ, the discrepancy between the Case I and II solutions is very small. Therefore, in their respective regions of applicability the Case I and II solutions constitute an effective general solution to equations (17) and (18).

TABLE 1. SUMMARY OF BOUNDARY CONDITIONS

Quantity		Boundary Condition		New Quantity	Boundary Condition	
		$s = 0$	$s = \infty$		$s = 0$	$s = \infty$
Independent variable, s		$s = 0$	$s = \infty$	$\sigma = e^{-s}$ *	$\sigma = 1$	$\sigma = 0$
Lean	$\bar{\omega}$	$1 + \bar{\omega}_\infty$	$\bar{\omega}_\infty$	ρ	1	0
	$\bar{\varphi}$	1	0			
Rich	$\bar{\omega}$	1	0	ρ		
	$\bar{\varphi}$	$1 + \bar{\varphi}_\infty$	$\bar{\varphi}_\infty$			
Lean	$\Delta\omega/\sqrt{2}$	$1 + \bar{\omega}_\infty$	0	$\Delta\rho$	1	0
	$\Delta\varphi/\sqrt{2}$	1	0			
Rich	$\Delta\omega/\sqrt{2}$	1	0	$\Delta\rho$		
	$\Delta\varphi/\sqrt{2}$	$1 + \bar{\varphi}_\infty$	0			
	$\frac{d\bar{\omega}}{ds}$	0	0	$\frac{-\sigma d\rho}{\lambda_D d\sigma}$	0	0
	$\frac{d\bar{\varphi}}{ds}$	0	0			

A large value of Q implies a large reaction to mixing rate ratio, i.e., large values of L and the establishment of the interface type of combustion. The composition parameter $r = 1$ for a stoichiometric overall composition and increases

TABLE 2. VALUES OF ρ AND σ BY THREE METHODS FOR $Q = 1$ AND $r = 1.428$

	Case I $Q(r-1) \gg 1$	Case II $Q(r-1) \leqslant 1$	
σ	ρ by graphical evaluation of equation 7A	ρ by IBM numerical integration of equation 12A	ρ by equation 20
0.1	.234	.254	.245
0.2	.377	.393	.398
0.3	.498	.519	.520
0.4	.621	.626	.636
0.5			
0.6	.820	.817	.812
0.7			
0.8	.942	.952	.933
0.9			
1.0	1.000	1.000	1.000

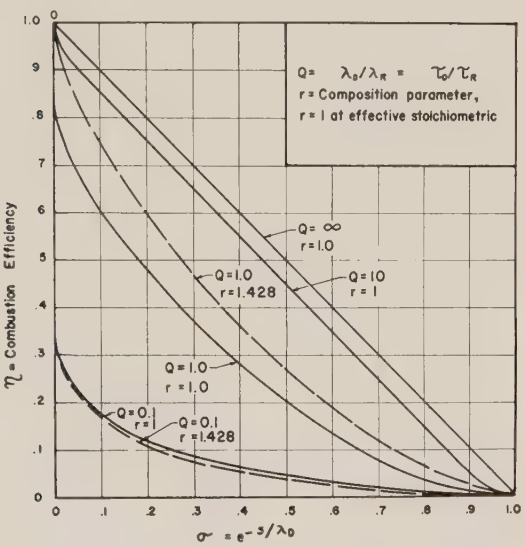
Q = λ_B/λ_R = τ_D/τ_R
r = Composition parameter,
r = 1 at effective stoichiometric
Q = ∞ r = 1.0
Q = 1.0 r = 1.428
Q = 10 r = 1
Q = 1.0 r = 1.0
Q = 0.1 r = 1
Q = 0.1 r = 1.428
η = Combustion Efficiency
σ = e^{-s/λ_D}

FIG. 2. Combustion efficiency as a function of height variable, $\sigma = \exp(s/\lambda_D)$.

for off stoichiometric compositions. A value $r = 1.428$ is approximately consistent with either a 74 or 151 per cent of stoichiometric fuel-air ratio. Therefore, it is seen that the great majority of flames of physical interest fall within the Case II category where $Q(r-1) \leqslant 1$. Consequently, except for the purpose of making the previously outlined numerical comparisons with the Case II solution, the Case I solution is of minor interest and will not be further considered.

The Case II solution (see Appendix for derivation) turns out to be in terms of modified Bessel functions of an irrational order, a circumstance which considerably complicates their numerical evaluation. (The order is rational for the stoichiometric case.)

In order to investigate this situation, D. L. Shell (General Electric Co., Aircraft Gas Turbine Division) with the aid of IBM computing machines, numerically integrated the differential equation (12A) (in the Appendix). Through a fortunate accident it was found that, for use in this equation, approximations of the type $K_{1-\delta}(\theta) \cong K_1(\theta^{1-2\delta})$ are quite adequate; the IBM calculated result was used as the standard of comparison. (See columns 2 and 3 of Table 2). Therefore, for purposes of numerical evaluation, the solution is:

$$\Delta\rho = \sigma \tag{19}$$

$$\rho = \frac{\theta}{Q}\left[\frac{K_1(\psi) - AI_1(\psi)}{K_0(\psi) + AI_0(\psi)}\right]$$

in which

$$A = \frac{\theta_1 K_1(\psi_1) - QK_0(\psi_1)}{\theta_1 I_1(\psi_1) + QK_0(\psi_1)}$$

and

$$\psi = \theta^{1-Q(r-1)} = (Q\sqrt{r\sigma})^{1-Q(r-1)}$$

$$\psi = \psi_1 \qquad \text{when } \sigma = 1.$$

All Case II solutions become exact and identical as $r \to 1$. When $\psi_1 \leqslant 0.15$, equation (20) may be simplified (see Appendix) to:

$$\rho = \frac{1 - \frac{1}{2}A\psi^2}{Q[A - 0.5772 - \ln(\psi/2)]} \tag{21}$$

in which

$$A = \frac{1 + Q[0.5772 + \ln(\psi_1/2)]}{\frac{1}{2}(\psi_1)^2 + Q}$$

Although the principal mathematical problems have been solved, it is still necessary to relate ρ and σ to experimentally significant quantities.

Since ρ has been defined as the unaccomplished fraction of the overall reaction, it follows that:

$$\eta = 1 - \rho \tag{22}$$

in which η is the combustion efficiency. By use of equations (20), (21) and (22) plots of η vs σ are presented in Figure 2 for various values of the parameters Q and r. From this plot, and the relation $-\ln\sigma = s/\lambda_D$, plots of η vs s/λ_D can easily

be made. However, it will be recalled that the s function contains a correction term for the variation of the diffusion coefficient with temperature, and is related to height above the burner surface y, by equation (3). With rearrangement, the latter can be put in the form:

$$y/\lambda_D = -2.303 \int_0^{\log \sigma} \left(\frac{T}{T_0}\right)^{-0.75} d \log \sigma_1 \quad (23)$$

Now since the y axis conductive heat flow is negligible, the temperature rise over any given height above the burner surface is directly related to the combustion efficiency. If an average effective heat capacity is used, they are proportional.

$$\eta = \frac{T - T_0}{T_f - T_0} \quad \begin{aligned} T_0 &= \text{Initial Temperature,} \\ T_f &= \text{Final Temperature} \end{aligned} \quad (24)$$

When this relation is solved for T/T_0 and substituted into equation 23, there results:

$$y/\lambda_D = -2.303 \int_0^{\log \sigma} \left[1 + \eta\left(\frac{T_f}{T_0} - 1\right)\right]^{-0.75} d \log \sigma_1 \quad (25)$$

If the overall heat losses during the course of the reaction are small, T_f can be considered the adiabatic flame temperature corresponding to the specified overall fuel-air ratio. If the adiabatic flame temperatures for a number of hydrocarbon gases (burning with air) are plotted as a function of the fuel-air equivalence ratio, it is found that, percentage-wise on an absolute scale, there are only minor differences in the adiabatic flame temperatures of different fuels for a designated equivalence ratio. Therefore, neglecting these individual variations, a common, average curve for the several fuels can be drawn. Further, it is seen that this average curve shows a very high degree of symmetry about the fuel-air equivalence ratio 1.06, corresponding to the well-known fact that the maximum flame temperatures for hydrocarbon-air systems generally lie somewhat to the rich side of the true stoichiometric. Therefore, defining $r = 1$ as relating to a true fuel-air equivalence ratio of 1.06, the symmetry of the temperature vs r curves can be used to provide a common temperature function for both rich and lean compositions. From the calculated data of Jones, Lewis, Friauf and Perrot,[8] average values of the adiabatic temperature $T_f = f(r)$ relation were estimated and are presented in Table 3.

By introducing appropriate values of T_f/T_o from this table into equation (25) and from the known $\eta = f(\sigma)_{Q,\,r}$, the indicated integral can be evaluated numerically, giving a result of the form $y/\lambda_D = f(\log \sigma)_{Q,\,r}$. From the previously evaluated $\eta = f(\sigma)_{Q,\,r}$ relation, the desired result $\eta_{Q,\,r} = f(y/\lambda_D)$ can be evaluated numerically. Also, since $Q = \lambda_D/\lambda_R$, it follows that $\eta_{Q,\,r} = f(y/\lambda_D) = f(Qy/\lambda_R)$.

Such evaluations have carried out for the cases $Q = \infty$, 10, 1, 0.1, and 0 when $r = 1$. The results are plotted in Figures 3a and 3b which show the rise of combustion efficiency, η, as a function of the dimensionless "reduced diffusion, height, y/λ_D," and the "reduced reaction height, y/λ_R."

Discussion of Results

To be physically meaningful, the final equations should satisfy a number of conditions other than the explicitly applied boundary conditions (see Table 2). Listed below are a number of tests which the equations fulfill and which are based either on already existing knowledge, or on inductive reasoning. Since, in some cases, the formal mathematical proofs that these conditions are indeed fulfilled add no new information, and are involved and tedious, such proofs will be omitted. For several of the tests, however, an inspection of Figures 2, 3a and 3b is adequate.

Table 3. Representative Adiabatic Temperatures for Standard Hydrocarbon-Air Mixtures and the Composition Parameter "r". ($T_0 = 291°$ K)

r	Per Cent True Stoichiometric Fuel Air Ratio		T_f°K	T_f/T_0
	Lean	Rich		
1.000	106		2235	7.68
1.111	95.3	118	2175	7.48
1.250	84.7	132.5	2075	7.14
1.429	74.1	151.3	1700	6.54

(1) at $y = \infty$, the reaction is complete and $\eta = 1$.
(2) at $y = \infty$, the gas is homogeneous, i.e. $\Delta\rho = 0$.
(3) as $1/\lambda_R \to 0$, $\eta \to 0$ at all y.
(4) as $1/\lambda_D \to 0$, mixing is prevented, and $\eta \to 0$ at all y.
(5) as $1/\lambda_R \to \infty$, the overall combustion is mixing rate limited and $\eta = f(y/\lambda_D)$ alone.
(6) as $1/\lambda_D \to \infty$, the overall combustion is reaction rate limited and $\eta = f(y/\lambda_R)$ alone.

(7) Since reaction must always lag mixing, the final stages of combustion must occur in an essentially homogeneous gas and be entirely reaction rate limited i.e., as $y \rightarrow \infty$, $\eta = f(y/\lambda_R)$ in all cases (except of when $1/\lambda_R = \infty$).

In comparing the $r = 1$ and $r = 1.428$ curves for the same Q value in Figure 2, in general, corresponds to the case of an infinite reaction rate and a finite mixing rate, i.e., $1/\lambda_R = \infty$ and $1/\lambda_D$ is finite. On the other hand, the $Q = 0$ curve falls on the abscissa at $\eta = 0$ as is logical if the reaction rate is zero. These two curves then define the boundaries of the region of physical attainment, insofar as variations in the chemical reaction rate are concerned.

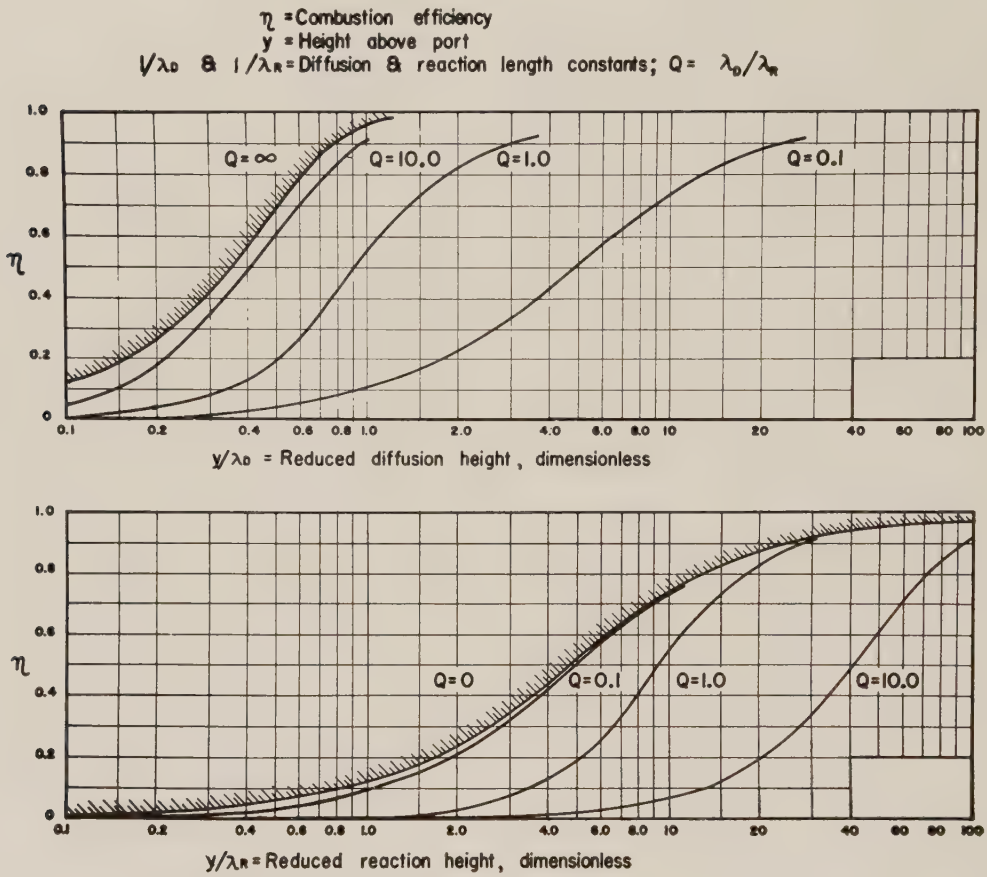

FIG. 3. Combustion efficiency (for overall stoichiometric mixture) as a function of the "reduced diffusion and reaction heights."

variations of η with r for constant values of Q and σ are not large. It is interesting to note that by equation (19), ($\Delta\rho = \exp(-s/\lambda_D)$ the mixing process proceeds independently of the reaction since the foregoing relation is independent of the value of $1/\lambda_R$. In contrast, the corresponding Case I solution is $\Delta\rho = \rho$, showing that for Case I conditions the mixing rate is influenced by reaction.

Figure 3a shows the increase of η as a function of the reduced diffusion height, y/λ_D with several values of Q as a parameter. The $Q = \infty$ curve

Figure 3b is a similar plot of η as a function of the reduced reaction height, y/λ_R. The $Q = 0$ curve here corresponds to the case of an infinite mixing rate and a finite reaction rate, i.e., $1/\lambda_D = \infty$ and $1/\lambda_R$ is finite. On the other hand, the $Q = \infty$ curve falls on the abscissa at $\eta = 0$ as is logical if the mixing rate is zero. These two curves then form the boundaries to the region of physical attainment, insofar as variations in the mixing rate are concerned.

The relationship of the Q, $1/\lambda_D$ and $1/\lambda_R$ parameters in determining combustion efficiency

can be clarified if the flame height is defined as the height above the burner which corresponds to a 90 per cent average combustion efficiency. A plot is given in Figure 4 from which this flame height may be determined for given values of λ_D and λ_R. The lines of constant flame height are all proportional and are in the same length units as λ_D and λ_R. Since $Q = \lambda_D/\lambda_R$, the Q values are given by the rays emanating from the origin.

If the small curvature in the lines of constant flame height is neglected, the flame height, denoted by $h_{90 \text{ per cent}}$, may be expressed simply as:

$$h_{90 \text{ per cent}} = 0.8\lambda_D + 2.5\lambda_R \tag{26}$$

or alternatively,

$$h_{90 \text{ per cent}} = u_0 (0.8\tau_D + 2.5\tau_R) \tag{27}$$

in which u_0 is the initial average gas velocity.

From equation (27) it is obvious that when $0.8\tau_D \gg 2.5\tau_R$, the overall combustion is diffusion controlled, and the interface combustion regime prevails. Conversely when $0.8\lambda_D \ll 2.5\tau_R$, Q is small and homogeneous combustion prevails (see small Q curves of Figures 3a and 3b).

The following relations then hold for the two extreme cases:

$$h_{90 \text{ per cent}} = u_0\, 2.5\tau_R \text{ (complete homogeneous combustion)} \tag{28}$$

$$h_{90 \text{ per cent}} = u_0\, 0.8\tau_D \text{ (complete interface combustion)} \tag{29}$$

It is seen that equation (28) satisfies the basic requirement for an empirical description of premixed combustion. The flame height $h_{90 \text{ per cent}}$ is independent of the volume rate of flow and the burner geometry. It is measured along the same axis as the flow velocity u_0. Therefore, the height $h_{90 \text{ per cent}}$ may be regarded as the thickness of a flame propagation wave traveling with a velocity u_0. Equation (28) may be rearranged to read

$$u_0 = h_{90 \text{ per cent}}/2.5\tau_R \tag{30}$$

in which u_0 is the normal burning velocity.

Turning our attention to the case of complete interface combustion, it would be interesting to make some comparisons between our results and those of other investigations, since this concept has been used explicitly or otherwise in almost all work to date on non-turbulent diffusion flames.

One of the principal consequences of the interface combustion concept, as developed by Burke and Schumann,[1] Wohl, et al.,[2] and Hottel, et al.,[3] is that the flame height of a laminar diffusion flame is proportional to the volumetric rate of fuel flow, and inversely proportional to the diffusion coefficient. Within the limits of experimental error, the results of these authors confirm the validity of this concept for their experimental conditions, except possibly for very high flow

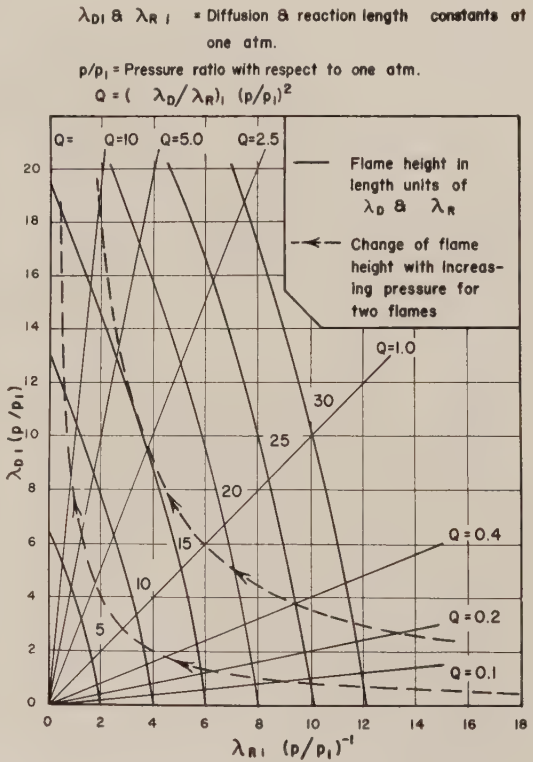
λD & λR = Diffusion & reaction length constants at one atm.
p/p1 = Pressure ratio with respect to one atm.
Q = (λD/λR)1 (p/p1)2
Q= Q=10 Q=5.0 Q=2.5
Flame height in length units of λD & λR
Change of flame height with increasing pressure for two flames
Q=1.0
30
25
20
15
10
5
Q=0.4
Q=0.2
Q=0.1
λD1 (p/p1)
λR1 (p/p1)-1
0 2 4 6 8 10 12 14 16 18
0 2 4 6 8 10 12 14 16 18 20

FIG. 4. Flame height (at 90% combustion efficiency) as determined by the diffusion and reaction parameters λ_D and λ_R.

rates when the transition to turbulent flow begins.

To make a comparison with our result, let the explicit formula for τ_D be substituted into equation (29).

$$h_{90 \text{ per cent}} = 0.8\, u_0 L^2/4\pi^2 D \tag{31}$$

The combined volumetric flow rate at the port of both fuel and air streams is given by $V = u_0 L\, d$ in which d is the depth of the burner. But since in our system the fuel and gas stream velocities are maintained approximately equal, the volume flow rate of fuel, V_f is proportional to the com-

bined flow rate, V. We finally obtain then,

$$h_{90\text{ per cent}} - \frac{V_f}{D}\left(\frac{L}{d}\right) \tag{32}$$

V_f = volume flow rate of fuel $cm^3 - sec^{-1}$
D = diffusion coefficient $cm^2 - sec^{-1}$

The ratio (L/d) constitutes a shape factor which must be held constant if comparisons are to be made to experiments using round tubes. Therefore, the final result is that the height required to achieve a given combustion efficiency is proportional to the volume flow rate of the fuel and inversely proportional to the diffusion coefficient.

It therefore appears that, despite the complex nature of diffusion burning, the mixing and reaction aspects are primarily additive in determining the flame heights. This simple additive nature, as expressed in equations (26) and (27), is quite interesting from the standpoint of possible engineering applications. It will also be realized that the development is a general one which includes formally both the extremes of diffusion and premixed combustion.

Wohl, Gazely and Kapp[2] introduced the effect of chemical reaction by combining the cone height of a premixed flame with the flame height predicted from diffusional considerations alone. Their formula takes the form $1/h = 1/h_D + 1/h_R$. h_R, they relate to the normal burning velocity u_b, by $h_R = \overline{ud}/u_b$ in which $\bar{u}$ is the average gas velocity and d is the tube diameter. If u_b is taken as a measure of the reaction rate, this formula predicts a zero flame height for an infinite reaction rate ($h_R = 0$). When the diffusion rate is made infinite ($h_D = 0$), a zero flame height is also predicted. This formula then does not appear to account for the rate limiting nature of these mechanisms, when one or the other rate is made infinite.

Equation (27) may be put in the more general form

$$h_\eta = u_0(a_{\eta,r}\tau_D + b_{\eta,r}\tau_R) \tag{33}$$

in which a and b are derived coefficients. The subscripts η, r emphasize that the indicated terms are functions of η, r. In general, $\tau_R = f(1/\tau_D, r, \eta)$, but since all these variables can be experimentally specified and controlled, this relationship can be experimentally determined. Once this is accomplished, equation (33) may well find application in turbulent flame studies where L assumes a statistical nature.

On the basis of equation (33) some further predictions may be made. Since $D \sim p^{-1}$ and $1/\tau_R \sim p$, equation (34) may be put in the form:

$$h_\eta = u_0[a\tau_{D1}(p/p_1) + b\tau_{R1}(p/p_1)^{-1}] \tag{34}$$

The effect of pressure on flame height can be seen from the hyperbolic shaped dotted lines of Figure 4. These curves (and the foregoing equation) show that when the reaction rate is controlling, the flame height varies inversely with pressure, approximately in accord with the well known effect of pressure on the thickness of premixed flame burning zones. But as pressure increases, the decreasing diffusive mixing rates cause the latter mechanism to share control, with the result that a minimum flame height is reached. Further increases in pressure cause the flame height to increase and the relations $h_\eta \sim p$ (for constant u_0) and h = constant (for constant mass flow rate) are approached. In thinking in terms of turbulent flames, it should be borne in mind however, that for constant velocities, the Reynolds number is proportional to pressure so that increased turbulence will tend to reduce the scale of unmixedness L, perhaps partially or wholly compensating the effect of pressure on D.

Experimental investigations of several aspects of the general approach which is outlined in this paper are underway.

Appendix

(Equation numbers in the appendix are denoted with an A)

CASE I. INTEGRATION OF EQUATIONS (17) AND (18) FOR THE CONDITION $Q(r - 1) \gg 1$

In accord with the condition that $Q(r - 1) \gg 1$, after dropping the "1" in the coefficient of the first term of equation (18), the two basic equations for this solution are:

$$-\sigma\frac{d\rho}{d\sigma} = -Q(r-1)\rho + Q(r+1)(\Delta\rho)\sigma - Q\rho^2 - Q(\Delta\rho)^2 \tag{17}$$

$$-\sigma\frac{d\Delta\rho}{d\sigma} = -Q(r-1)\Delta\rho + Q(r+1)\rho\sigma - 2Q\rho\Delta\rho \quad \text{(from equation (18))} \tag{1A}$$

If f and g are defined respectively as,

$$f = \rho + \Delta\rho \tag{2A}$$

$$g = \rho - \Delta\rho \tag{3A}$$

the addition and subtraction of equations (17) and (1A) yields equations which are identical in form.

$$-\sigma f' = -Q(r-1)f + Q(r+1)f - Qf^2 \quad (4A)$$

$$-\sigma g' = -Q(r-1)g + Q(r+1)g - Qg^2 \quad (5A)$$

f and g then can only differ in the value of their respective constants of integration.

In accord with the previously derived boundary conditions,

$$\left.\begin{aligned} \rho &= 1 \\ \Delta\rho &= 1 \end{aligned}\right\} \text{ at } \sigma = 1$$

the final particular solutions for $\Delta\rho$ and ρ are:

$$\Delta\rho = \rho \quad (6A)$$

and

$$\rho = \frac{\sigma^{Q(r-1)}e^{-Q(r+1)\sigma}}{e^{-Q(r+1)} + 2Q\int_1^\sigma \left(\sigma^{*Q(r-1)-1}\right)\left(e^{-Q(r+1)\sigma^*}\right)d\sigma^*} \quad (7A)$$

The integral in the denominator cannot be evaluated in a closed form except for the special case $r = 1$.

Numerical evaluations of equation (7A) show that when $Q(r-1) > 1$, the curve of ρ plotted against σ has an elongated "s" shape. For the special case $r = 1$ and the use of the logarithmic integral, $Ei(-x)$, the above equation may be put in the form:

$$\rho = \frac{e^{-2Q\sigma}}{e^{-2Q} + 2Q[Ei(-2Q\sigma) - Ei(-2Q)]} \quad (8A)$$

CASE II. INTEGRATION OF EQUATIONS (17) AND (18) FOR THE CASE $Q(r-1) < 1$

The two equations (17) and (18) become

$$-\sigma\frac{d\rho}{d\sigma} = -Q(r-1)\rho + Q(r+1)\Delta\rho\sigma - Q\rho^2 - Q(\Delta\rho)^2 \quad (17)$$

$$-\sigma\frac{d\Delta\rho}{d\sigma} = -\Delta\rho + Q(r+1)\rho\sigma - 2Q\rho\Delta\rho \quad (9A)$$

after the $Q(r-1)$ term in the coefficient of the first term of equation (18) has been dropped in accord with the condition $Q(r-1) \ll 1$.

The form of equation (15) suggests a possible relationship between $\Delta\rho$ and σ, namely

$$\Delta\rho = K\sigma. \quad (10A)$$

Substitution into equation (9A) shows that if $K = \frac{1}{2}(1+r)$, equation (10A) is a solution. However, at the initial condition when $\sigma = 1$, it is seen that $\Delta\rho \neq 1$ (except when $r = 1$). Equation (10A) then is not consistent with the basic boundary conditions. Also equation (10A) does not permit equation (17) to fulfill the boundary condition that $d\rho/d\sigma = 0$ when $\rho = 1$, $\sigma = 1$. Therefore, let the approximation $\frac{1}{2}(1+r) \cong 1$ be introduced into equation (10A) and these difficulties vanish. (The maximum value of r which is considered in this paper is $r = 1.428$.) Consequently, equation (10A) becomes

$$\Delta\rho = \sigma \quad (11A)$$

A substitution of equation (11A) into the general equation (17) yields

$$-\sigma\frac{d\rho}{d\sigma} = -Q(r-1)\rho + Qr\sigma^2 - Q\rho^2 \quad (12A)$$

This relation satisfies the bouudary condition $(d\rho/d\sigma) = 0$ when $\rho = 1$ and $\sigma = 1$.

For the purpose of mathematical manipulation, it will prove convenient to perform the transformations given by:

$$\rho = y/Q, \qquad \sigma = \frac{x}{Q\sqrt{r}},$$

$$\text{and} \qquad Q(r-1) = 2(1-n)$$

(not to be confused with x and y coordinates in burner.)

The new boundary relations are then:

$$\text{at } x = x_1 = Q\sqrt{r} \begin{cases} y = y_1 = Q \\ \dfrac{dx}{dy} = 0 \end{cases}$$

Let equation (12A) be expressed in the new terminology.

$$-xy' = -2(1-n)y + x^2 - y^2 \quad (13A)$$

Place

$$y = \frac{-uw}{\int^k x\,w\,dx}$$

and the relations: $u = x^{2(1-n)}$

and

$$w' - (x^{2n-1})\int x^{1-2n}\,w\,dx = 0$$

are obtained after placing $k = 1 - 2n$.

Differentiation and resubstitution for w' yields

$$w'' + (1-2n)\frac{w'}{x} - w = 0 \quad (14A)$$

which will be recognized as a form of Bessel's

equation, one form of which may be written as follows:

$$Z'' + (1 - 2n)\frac{Z'}{x} + \left(\beta^2 + \frac{n^2 - p^2}{x^2}\right) Z = 0 \quad (15A)$$

By equating coefficients, we obtain $p = \pm n$ and $\beta = \pm i$. The solution to equation (15A) is

$$w = x^n[aI_n(x) + bK_n(x)] \quad (16A)$$

in which $I_m(x)$ and $K_m(x)$ are modified Bessel functions of the first and second kind, respectively, of the order n. The integration constants are a and b. Rigorously speaking, equation (16A) is a complete solution only when n is a natural whole number. The question will be clarified later.

The complete solution for y now becomes:

$$y = x^{2-n}\left[\frac{K_n(x) - AI_n(x)}{x^{1-n}(K_{n-1}(x) + AI_{n-1}(x)) + B}\right] \quad (17A)$$

in which B is a new constant of integration. A and B must be evaluated so that equation (17A) satisfies the original equation (13A) and its boundary conditions. Let equation (17A) be differentiated. After the differentiated expression is simplified and the Bessel function recurrence formulas are introduced, it is found that $B = 0$.

Therefore, by putting $x = x_1$, $y = y_1$, and $B = 0$ in equation (17A), a determination for A can be made.

The final particular solution therefore is:

$$y = \frac{x[K_n(x) - AI_n(x)]}{K_{n-1}(x) + AI_{n-1}(x)} \quad (18A)$$

in which

$$A = \frac{x_1K_n(x_1) - y_1K_{n-1}(x_1)}{x_1I_n(x_1) + y_1I_{n-1}(x_1)}$$

and $$n = 1\text{-}\tfrac{1}{2}Q(r - 1)$$

It is seen that the modified Bessel functions in the foregoing expressions, in general, will be of an irrational order, but numerical integrations of equation (17A) show that approximations of the type $K_{1-\delta}(x) \cong K_1(x^{1-2\delta})$ are adequate for use in equation (18A) (see Table 2). Since the approximation becomes more accurate as $Q(r - 1)$ diminishes, comparisons of columns 2 and 3 of Table 2 show the maximum error when $Q(r - 1) = 0.428$. The foregoing approximations are incorporated in equation (20) in the main text.

A SIMPLIFIED FORMULATION OF EQUATION (20):

For most cases of physical interest, the condition $Q(r - 1) \leqslant 1$, also implies that $Q\sqrt{r} < 1$. Now since $0 < Q\sigma\sqrt{r} < Q\sqrt{r}$, it follows that the maximum value of the argument of the Bessel functions will always be small in comparison to one for these cases. By an inspection of the expanded equations for the modified Bessel functions it is seen that when the argument $x = Q\sqrt{r\sigma} \leqslant 0.15$, the functions may be approximated to a much simpler form:

$$I_0(x) = 1$$

$$K_0(x) = -0.5772 + \ln\frac{x}{2}$$

$$I_1(x) = \frac{x}{2}$$

$$K_1(x) = \frac{1}{x}$$

When these simplifications are applied to equation (20) it becomes equation (21).

REFERENCES

1. Burke, S. P., and Schumann, T. E. W.: Ind. Eng. & Chem., *20*, 998 (1928).
2. Wohl, K., Gazley, C., and Kapp, N.: *Third Symposium on Combustion, Flame and Explosion Phenomena*, p. 288. Baltimore, The Williams & Wilkins Co., 1949.
3. Hottel, H. C., and Hawthorne, W. R.: *Third Symposium on Combustion, Flame and Explosion Phenomena*, p. 254. Baltimore, The Williams & Wilkins Co., 1949.
4. Hawthorne, W. R., Weddell, D. S., and Hottel, H. C.: *Third Symposium on Combustion, Flame and Explosion Phenomena*, p. 266. Baltimore, The Williams & Wilkins Co., 1949.
5. Yagi, S., and Saji, K.: *Fourth Symposium (International) on Combustion*, p. 771. Baltimore, The Williams & Wilkins Co., 1953.
6. Thring, M. W., and Newby, M. P.: *Fourth Symposium (International) on Combustion*, p. 789. Baltimore, The Williams & Wilkins Co., 1953.
7. Gaydon, A. G., and Wolfhard, H. G.: *Flames, Their Structure, Radiation and Temperature*, Ch. 6. London, Chapman and Hall, Ltd., 1953.
8. Jones, G. W., Lewis, B., Friauf, J. B., and Perrot, G. St. V.: J. Am. Chem. Soc., *53*, 869 (1931).

24

FORMATION OF CARBON AND RELATED MATERIALS IN DIFFUSION FLAMES

By J. R. ARTHUR AND D. H. NAPIER

(1) Introduction

There is considerable interest in this subject at the present time, due not only to its intrinsic scientific appeal, but also in connection with several applied combustion processes, e.g., the smokeless combustion of bituminous coals, the use of flames with high radiant output for steel-making and other purposes, and the preparation of carbon black.

Previous approaches to the problem of carbon formation in flames may be divided into three sections:

(1) Empirical studies of the smoking tendencies of fuels, the aim being to correlate structural features with tendency to carbon formation[1-5].

(2) Thermodynamic and kinetic prediction of the feasibility of various reactions which could produce carbon under flame conditions[6-8].

(3) Spectroscopic studies of flames[9-17].

This work has been reviewed elsewhere[18], and shows that there is as yet no clear and certain picture of the important reactions involved.

In the present work, a rather different experimental approach has been adopted compared with those mentioned above. It is based upon the following simple argument: carbon formation in flames is expected to occur by reactions involving a number of stages, relatively small molecules giving way to large ones. If materials formed in some of the intermediate stages could be isolated and examined, something might be learned of the mechanism of the overall process. This approach therefore resolves into correct choice of combustion and quenching conditions for isolation of intermediates from the reaction zone.

For this purpose two types of diffusion flame have been mainly employed: (1) a reversed (also called inverted) flame and (2) a normal flame working at subatmospheric pressures. The former has been used for the greater part of the work and its suitability appears to arise from its relatively low temperature (see below) and also because it is self-quenching, i.e., the reaction products pass into an atmosphere of cold fuel. There appears to be surprizingly little previous recorded work with reversed flames. They were referred to in a previous communication from this laboratory[19] in relation to an apparent expansion phenomenon arising from the addition of sodium salts to flames. A preliminary publication of their use in carbon formation studies has also been made in collaboration with P. K. Kapur[20].

Much smaller quantities of this type of material have been collected on water-cooled targets using normal flames as follows: (a) sampling above the flame envelope, the flame being vitiated with combustion products; (b) sampling in the luminous envelope.

Table 1. Analysis of Gaseous Fuels Used

Gas	C_2H_4	C_3H_8	CH_4	CO_2	O_2	CO	H_2	N_2	C_2H_6
Ethylene	98.2			0.3	0.1	0.1	0.1	1.2	
Propane		98.4		0.1				1.5	
Methane			90.50	0.2		0.5		6.5	2.3

(2) Experimental

(2.1) fuels

The main fuels used were methane, propane, ethylene and benzene. The analyses of the first three of these are given in Table 1.

(2.2) combustion equipment

Simple Pyrex burners in the open atmosphere were used for the experiments with individual gaseous hydrocarbons at normal pressure and a spirit lamp for liquid hydrocarbons. When hydrocarbons were burnt at reduced pressures, a Pyrex burner of the type used by Parker and Wolfhard[2] was used; the experimental arrangement is shown in Figure 1. Air was drawn into

the burner at a controlled rate by utilizing the reduced pressure in the apparatus. The ignition spiral was of 40 S.W.G. platinum supported by 18 S.W.G. copper leads. Brass targets were mainly used for deposit collection. The glass traps (see Figure 1) were cooled in alcohol/solid CO_2 mixtures held in Dewar vessels. To assist the stabilization of the flame and to avoid explosion risks, the flames were ignited at a higher pressure than was subsequently used. A 10-liter aspirator with controllable leak was inserted in the suction line between the cooled traps and the pump; this assisted flame stability, especially when a rotary oil pump was used. However,

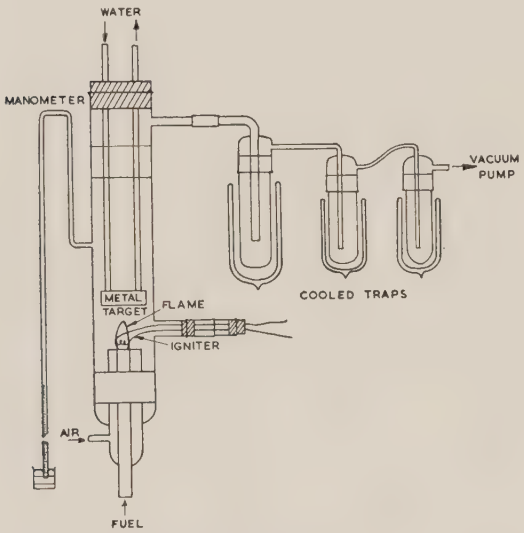

FIG. 1. Apparatus for combustion of gaseous fuels under reduced pressures.

much of the work was carried out with a metal water pump on a high-pressure supply, this giving sufficient pumping capacity.

For studying reversed diffusion flames, Pyrex apparatus was again employed, and is shown diagrammatically in Figure 2. The igniter was similar to that described above. Metal clips were used to hold the copper target in position and were placed on the outside of the tube around *BC*. A rubber gasket was placed between the target and the Pyrex rim at *B* (on the inside). Preliminary experiments showed that the water jacket *A* prevented modification (by heat) of the deposits formed on the walls of the tube. On the outlet from the burner, a side arm allowed collection of gaseous products emitted from the flame and of excess fuel.

For work with reversed diffusion flames of liquid fuels (benzene), the apparatus shown in Figure 3 was used. Commercial oxygen-free nitrogen was employed as carrier gas and was passed through a sintered glass bubbler immersed in benzene, the container for which was in a water-bath maintained at 78–80°C. The nitrogen saturated with benzene passed through vessel *B* packed with glass beads in order to smooth out the flow and thence into the reaction tube. Vessel *B* and the reaction tube were completely and partially immersed respectively in water bath *C* maintained at about 95°C. Oxygen enrichment of air was necessary to maintain a stable flame.

(2.3) TECHNIQUES USED TO INVESTIGATE FLAMES AND THE MATERIALS DEPOSITED FROM THEM

(2.3.1) *Considerations relating to the technique of flame reversal*

Flame reversal is sometimes more complex than might first appear, e.g., in the reversal of a flame supported in air or other mixture of oxygen and inert gas, should the two gas streams consist of fuel + inert/oxygen or fuel/inert + oxygen? In the latter case, the inert gas would be expected to have a rather large influence on the flame. In preliminary work, the first type of flame (fuel + nitrogen/oxygen) was tried, nitrogen being introduced in the proportion (to fuel) of four times the amount of oxygen required for complete combustion of the fuel. On circular burners, these high nitrogen/fuel ratios prevented complete stabilization of the flames. Simple interchange (oxygen + nitrogen/fuel) was concluded to represent the most practical form of reversal.

(2.3.2) *Actual techniques used*

Considerable emphasis was placed on visual properties of the flames, and in particular their shape, length, brightness and stability. In certain cases (where normal flames were diluted with combustion products) semiquantitative measurements by a simple photocell and current indicator were made of the light emission from sections of the flame. Some use has also been made of the point at which hydrocarbon flames may be rendered nonluminous (e.g., by pressure decrease and foreign gas addition). For comparative rather than absolute measurement, flame temperatures were measured by the Kurlbaum method: simple measurements with thermocouples were also attempted.

The carbonaceous deposits collected from the

flames were subjected to the following examinations: (a) appearance (including color, physical state, quantity and smell); (b) apparent solubility in organic solvents; (c) ultimate analyses (crude material, extracts and residues); (d) free-carbon content; (e) ultraviolet absorption spectra; (f) molecular weight determinations; and (g) infrared absorption spectra. An indirect estimate (carried out as a check on the normal gravimetric method) of the composition of the crude deposits from some flames was made by carrying out a material balance on the flames.

(3) Results

(3.1) The shape and other visual properties of diffusion flames

The imposed combustion conditions have a considerable influence on the shape of flames, e.g., when ethylene is burned at a pressure of about 10 cm of Hg, four completely different flame types may be obtained (Fig. 4), the fuel rate being increased on passing from type (a) to type (d). Types (a) to (c) have been previously observed[15]. Type (d) was nonluminous and hollow with an open-topped structure. These same four flame types may also be obtained with methane and propane, though in the former case at a considerably higher pressure.

A comparison of the visual properties of normal and reversed diffusion flames shows that the most striking difference in the two types when hydrocarbon fuels are used is the much stronger luminosity of the normal flame. This large difference is well brought out by comparison of the heights at which the two flames become luminous: with a 4-mm ID burner, a normal diffusion flame of town's gas in air became luminous when its height was greater than 0.5 cm, whereas the reversed flame was nonluminous even when 5 cm long.

There are also other important visual differences between the two types of flame: thus the continuous radiation from the reversed flame comes from a red background whereas the background is yellow in the normal flame. This necessarily implies a difference in temperature (and hence in completeness of reaction) in the two systems (see Section 3.2). An examination of the boundaries of the two flames shows that the outline of the reversed flame is the better defined at the sides of the flames, the reverse being true at the apices: with reversed hydrocarbon flames, there is no well-defined tip, the flame terminating in a diffuse haze, possibly owing to the nature of the material emitted from the flame (see Section 3.5). The poor definition at the tip becomes increasingly noticeable as the flame length is increased, the top of the flame appearing to open up.

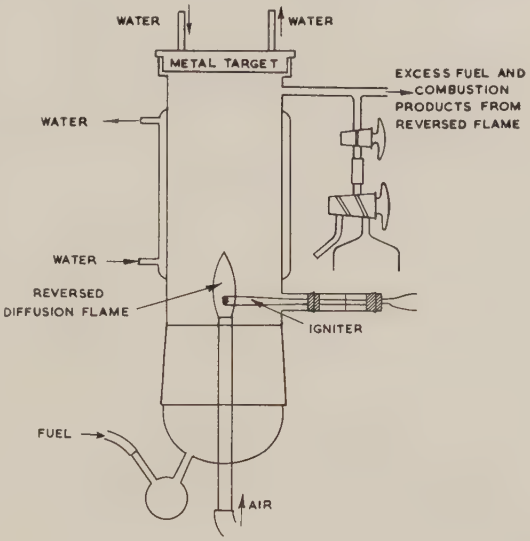

Fig. 2. Apparatus for combustion of hydrocarbon fuels in reversed diffusion flames.

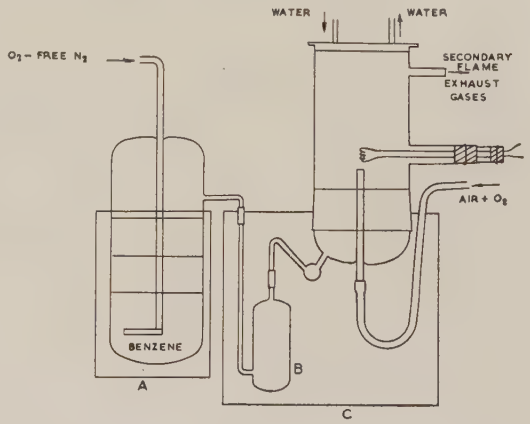

Fig. 3. Apparatus for combustion of liquid fuels in reversed diffusion flames.

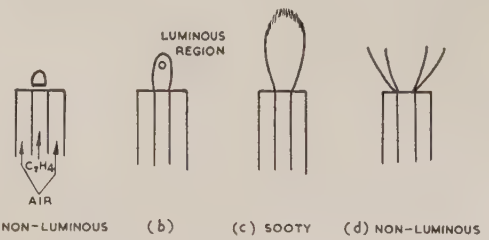

Fig. 4. Types of low-pressure diffusion flame

There is also a marked disparity in the stability and ease of establishment of the two flames, the reversed flame comparing very unfavorably. In the case of methane, the reversed flame using air alone could not be satisfactorily established and oxygen enrichment (to the extent of about 6 per cent) had to be employed. Constrictions at the exit end of the flame tube detract considerably from the stability of reversed flames.

Another property differentiating the normal and reversed flames is the large difference in the extent to which they expand when colored by sodium salts, a difference which has been attributed to the varying survival of atomic hydrogen formed in the flame envelopes[19].

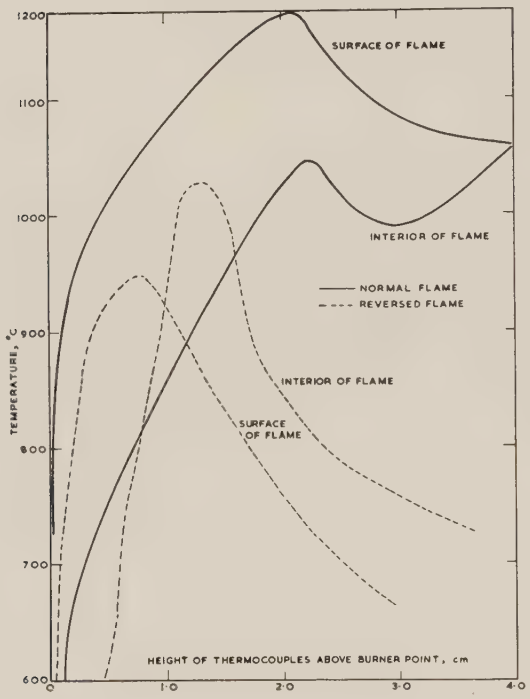

FIG. 5. Flame temperature measurement using simple thermocouple methods.

(3.2) TEMPERATURE DISTRIBUTION MEASUREMENTS

These measurements were made in an attempt to give more quantitative expression to the visual differences in the background radiation from the normal and reversed flames. Owing to the presence of the strong carbon continuum in both flames, the Kurlbaum method was first tried, the fuel being ethylene. For flames about 4 cm high, figures of 1300–1500°C for the normal flame and 800°C for the reversed flame were obtained, but owing to the very low temperature in the latter, the determination was rather unsatisfactory. Resort was therefore made to a thermocouple method which, although suffering from several well-known defects, was thought worthwhile from the point of view of comparative rather than absolute measurement. In Figure 5, temperatures are plotted against distance of the chromel-alumel thermocouple from the burner port. Regions in the center and in the outside surface of the flames were selected. It will be seen that the surface of the normal flame is the hotter region, whereas in the reversed flame the interior is the hotter. This difference is expected from the relative positions of air and fuel. It is concluded that the reversed flame is the colder of the two, a result to be expected from the completeness of the reactions in the two cases (see Section 3.3).

(3.3) COMPOSITION OF THE GASES EVOLVED FROM DIFFUSION FLAMES

The gaseous products from normal diffusion flames burning at atmospheric pressure are almost fully burned (cf. Section 2.3.1), but the position is widely different in reversed flames as Table 2 shows. Samples referred to as I-V were obtained from the following flame systems:

I. Ethylene/air
II. Ethylene/oxygen
III. Nitrogen and ethylene/oxygen
IV. Methane/oxygen and nitrogen
V. Benzene/oxygen and nitrogen.

Acetylene is present in these gases for all fuels used, and considerable quantities of CO and H_2 are also formed. Formaldehyde was shown to be present in the aqueous condensate from ethylene and propane reversed flames, and from methane, propane and ethylene flames burning at reduced pressures.

(3.4) VITIATION OF DIFFUSION FLAMES BY FOREIGN GASES

Combustion in vitiated atmospheres is a subject of considerable technical significance.[21, 22] Observations are reported here which concern not only the addition of flue gas constituents (CO_2, N_2, SO_2, SO_3) to flames, but also other gases (e.g., NO) which might be expected to have a specific catalytic or inhibiting effect.

The most obvious effect of any gas on a luminous flame (normal or reversed) is to reduce its brightness, and large additions will completely

suppress the carbon continuum. The critical rates of CO_2, N_2, SO_2 and CO needed to suppress completely the luminosity of methane flames of various sizes are plotted in Figure 6. Linear relations are observed in all cases. The amounts of additives required to produce these effects are large. A more convincing experiment is to measure the light emission from the flame when gradually increasing quantities of additives (CO_2 and N_2) are added to it (Fig. 7), the light being collected from the central region of the flame. The light yield is drastically reduced by small amounts of additive compared with the amounts needed for a complete suppression of carbon formation. The significance of these results is referred to in the Discussion. Additions of small quantities (ca. ½ per cent) of SO_3 to the fuel and air stream for the flames burning at low pressures produced no obvious visual differences in the flames. Reversed flames are influenced by foreign gas addition in the same way as normal flames. Small additions produced no visual change, except in the case of nitric oxide (ca. 1.25 per cent) added to the air stream supporting an ethylene flame. A bright luminous envelope developed inside the flame in a position approximately between the luminous region due to carbon and the bluish green colored region due to C_2.

Table 2. Composition of Gases from Various Reversed Flames

Sample	CO_2	CnHm	O_2	H_2	CO	C_2H_6	CH_4	N_2
I	5.5	21.3	0.2	6.0	7.9	0.2	0.6	58.3
II	9.1	29.2	0.4	22.2	35.9	0.2	0.9	2.1
III	2.8	4.8	0.7	0.8	1.3	<0.1	<0.1	89.5
IV	7.8	0.8	0.1	3.9	4.7	0.9	16.6	65.2
V	17.7	2.3	0.2	1.5	6.4		0.4	71.5

(3.5) The properties of the carbonaceous deposits from flames

There appears to be very little published information on the chemical and physical properties of soots and their precursors. An exception is the commercial production of carbon black by the incomplete combustion of natural gas, but the examination in that case has usually been restricted to surface area and particle size measurements on the deposited material. The related work by Garner et al.[23] will be referred to in the Discussion.

The solid deposits from the usual type of hydrocarbon diffusion flames are normally regarded as amorphous carbons with a graphite type of crystal lattice. This is satisfactory provided that it is remembered that they are not pure carbons but contain substantial amounts (0.5–1.5 per cent) of hydrogen and 8 per cent or more of oxygen. Such materials are variously described as soots, lamp black or carbon blacks. The chemical structure of these materials is not known and it seems certain that, as they do not have unique ultimate analyses, no one chemical structure could represent them. Nevertheless, in appearance and physical properties they do not show wide variations and the above collective names are justified. To differentiate these materials from other carbonaceous deposits examined in this work, we shall refer to them as usual-type deposits.

Perhaps the main contribution of the present work is to show that by suitable modification of the combustion conditions, changes may be brought about in the type of material deposited from flames. For convenience, this material is referred to as unusual-type deposits. It must be understood, however, that the change-over is not clear-cut, e.g., it is not generally possible to specify a set of combustion conditions where the deposits contain no material which was present under another set of conditions. It is clear from information given later in the paper that there is a lack of adequate means of describing the various materials.

In order to effect the change from a usual- to an unusual-type of deposit, the combustion conditions were changed from a normal diffusion flame burning in air at atmospheric pressure to one of the following: (1) reversal of the flame; (2) combustion of the flame under reduced rather than atmospheric pressure; or (3) vitiation of the flame by added gases.

The first of these brought about the greatest changes in the type of deposit. A description now follows of the deposits according to the various criteria for differentiating between them.

(3.5.1) *Appearance: color, smell, physical state and quantity*

The deposits varied in appearance from the soft, fluffy, voluminous form of soot through sticky, brown, viscous tars to brown oils. Between these extremes was found a range of products of

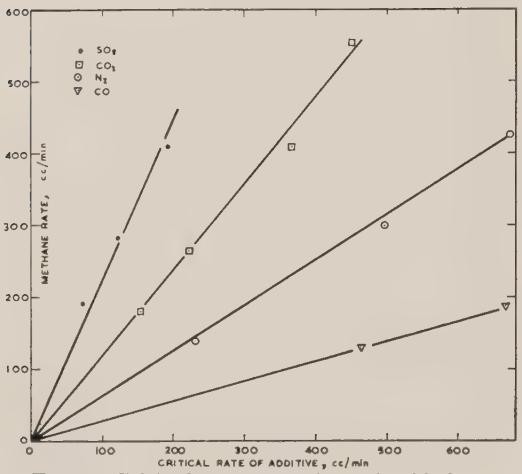

FIG. 6. Critical concentration of added gases to suppress luminosity of methane flames.

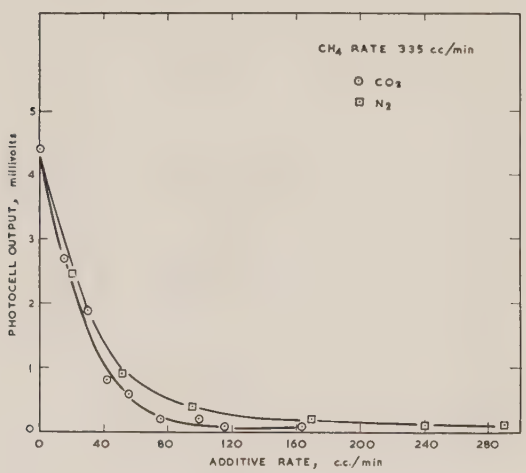

FIG. 7. Light output from a methane flame as a function of added gas concentration.

intermediate color and consistency. The appearance of the crude deposit was not a sensitive method of describing a product: other methods of examination showed differences not visible to the eye. The reversed flame deposits from the paraffins (CH_4, C_3H_8) and ethylene were the most unusual in appearance. The deposit from the reversed benzene flame was fairly usual in appearance; other tests showed, however, that tarry material was present. So also was diphenyl, which was easily detected by its smell and was separated by steam distillation. Of the four types of low-pressure flame (Fig. 4a to d), deposits were obtained from types c and d for methane, propane and ethylene. They were very different in appearance: that from c was sooty, while d gave a brown oil.

The quantities of the various deposits obtained from the different fuels were what would be expected from the known tendencies of flames to deposit carbon. Thus benzene deposited most, followed by propane and ethylene, with methane giving by far the smallest.

(3.5.2) *Apparent solubility of the deposits in organic solvents*

It was found that some of the deposits were partially soluble in organic solvents. This was a valuable property since it enables a convenient examination of some important constitutional properties of the soluble portions to be made (see Sections 3.5.7, 3.5.8, and 3.5.9). Apparent solubility was found, to varying extents, in the following solvents: carbon tetrachloride, acetone, cyclohexane, pyridine and ethylenediamine. In general, the more unusual the deposit, the greater was its apparent solubility. The solubility also increased with the polar nature of the solvents, e.g., pyridine and ethylenediamine were more effective solvents than carbon tetrachloride and cyclohexane. As an illustration of the difference in solubility in CCl_4 of the deposits from normal and reversed flames of ethylene/air, the following figures may be quoted: (1) deposit taken 2.5 cm; above normal flame: 12.9 per cent soluble, and (2) deposit from reversed flame: about 50 per cent soluble.

Both carbon tetrachloride and cyclohexane extracts of the deposits were found to be unstable to light. These solutions were apparently unchanged after six weeks storage in the dark, yet when they were exposed to the light (the containing vessels still being closed and air-free) they became cloudy; the dark brown material which separated floated in the carbon tetrachloride solution but settled in the cyclohexane solution. The color of the solutions, originally dark brown, was simultaneously considerably diminished. The material which separated was readily soluble in pyridine.

This instability is of considerable interest in connection with the nature of the solutions (col-

loidal or molecular), but it complicated the experimental work and necessitated rigid precautions in the storage of solutions.

(3.5.3) *Analyses of the deposits and of materials extracted from them*

(3.5.3.1) *Ultimate analyses.* A number of analyses were made of the carbon and hydrogen contents of the crude deposits and of their soluble portions. The accuracy of some of the determinations is not high, particularly because of the hygroscopic character of these materials. However, the conclusions drawn come from well substantiated results and are reliable. Except where other elements (such as sulfur) were purposely introduced, the analyses allow the indirect estimate of the oxygen content of the deposits. It is unknown how far the oxygen figures obtained are due to chemisorbed oxygen taken up on the sample during its preparation (in the case of normal flames) and its subsequent collection (both types of flame).

Some examples of the analyses obtained are given below to illustrate the effects of certain variables. The carbon and hydrogen figures are expressed on a dry basis. The difference between 100 and the sum of the carbon and hydrogen figures is represented by Δ.

The usual type of crude deposit had a hydrogen content between 0.7 and 1.8 when, as happened in the initial stages of the work, the deposit was dried at 100°C at atmospheric pressure to remove moisture. Examples are given in Table 3. The Δ figures are very large in these cases. The above figures, and particularly those for H_2 and Δ should be compared with the figures in Table 4 which relate to reversed flames of fuel and air. It will be seen that the hydrogen figures are 3–4 times higher and the Δ figures substantially lower than those given in Table 3 for the normal flame deposits.

A comparison has also been made of the ultimate analyses of the soluble and insoluble portions of flame deposits, particularly in the cases of reversed flames. Examples are given in Table 5, the fuel being ethylene in both cases. It should be noted that, although the hydrogen contents of the insoluble are slightly lower than those of the soluble fractions, they are still much higher than the figures obtained for the normal flame deposits (Table 3). The oxygen contents of the soluble fractions are also higher than those of the insoluble fractions; it is noted that the atomic C/H ratio is approximately 2.

The successive extraction (in a Soxhlet) of a crude deposit from a reversed ethylene/air flame with solvents of increasing polarity gave the results shown in Table 6. As the polarity of the solvent increases, the C/H ratio increases and the hydrogen content decreases slowly. The very high H and Δ contents of the residue after extraction with four solvents is particularly interesting.

When CO_2 was added to the fuel or to the air stream feeding a reversed flame, the luminosity of the flame and the yield of deposits were reduced. There was no change in the hydrogen content of the deposits, but the carbon contents were appreciably higher and the Δ values lower.

Table 3. Analyses of Deposits of Usual Type

Type of Flame	Carbon	Hydrogen	Δ	
	per cent	*per cent*		
Normal ethylene/air	92.8	0.7	6.5	Duplicates
	93.0	0.9	6.1	
Normal town's gas/air	86.4	1.5	12.1	Duplicates
	85.3	1.0	13.7	
Normal methane/air	85.9	1.8	12.3	

The use of oxygen instead of air gave a deposit of more sooty appearance and also with a higher carbon and lower hydrogen content, one analysis giving C 96.2 per cent, H 2.1 per cent, Δ 1.7 per cent.

(3.5.3.2) *Analysis by material balance.* Owing to the difficulties of sampling and weighing the deposits from the reversed flames, an analysis was attempted based on a material balance on the flames. Nitrogen was used as a reference between the entering rates of flow and the analyses of the permanent gases evolved. The water formed by combustion was estimated by freezing out with an alcohol/solid CO_2 mixture, and was then displaced by a warm air stream into weighed calcium chloride and anhydrone tubes. Experiments were done with ethylene/oxygen + nitrogen flames. The results showed that the C/H ratios were of the order ½ whereas from the gravimetric ratios they were approximately 2. Also the oxygen contents from the material balance were very much

Table 4. Analyses of Reversed Flame Deposits

Type of Flame	Region of Collection	Carbon	Hydrogen	Δ
		per cent	*per cent*	
Reversed ethylene/air flame	Uncooled Pyrex side wall of burner	92.2	5.1	2.7
Reversed ethylene/air flame	Above (cooled) and at side (uncooled) of burner	91.4 91.6	3.9 3.3	4.7 5.1
Reversed ethylene/air flame, but smaller	Above (cooled)	96.0	3.7	0.3
Reversed ethylene/air flame	Side (uncooled)	93.0 93.1	4.0 3.7	3.0 3.2

lower. Possible reasons for these large discrepancies are: (1) vacuum drying the deposit before ultimate analysis would volatilize low molecular weight material; (2) the tendency of the heated material to hold chemisorbed oxygen could be higher than that of the crude material as deposited.

Table 5. Comparison of Analyses of Soluble and Insoluble Fractions of Ethylene/Air Reversed Flame Deposits

Solvent	Fraction	Carbon	Hydrogen	Δ
		per cent	*per cent*	
Acetone	Soluble	89.9	4.4	5.7
	Insoluble	93.1	3.4	3.5
Carbon tetrachloride	Soluble	88.5	4.2	7.3
	Insoluble	93.1	3.8	3.1

Table 6. Effect of Successive Extractions on Analyses of Residues

Solvent	Carbon	Hydrogen	C/H	Δ
	per cent	*per cent*		
Cyclohexane	92.9	4.4	21.1	2.7
Cyclohexane and carbon tetrachloride	91.5	3.7	24.7	4.8
Cyclohexane, carbon tetrachloride and pyridine	91.1	3.4	26.8	5.5
Cyclohexane, carbon tetrachloride, pyridine and ethylenediamine	88.3	3.1	28.5	8.6

(3.5.4) *Determination of the free carbon content of flame deposits*

It has already been explained that methods of describing flame deposits are limited. Therefore, a determination of the free-carbon content of the deposits was made by a simple empirical method previously used by the Shell Petroleum Company,[24] which depends on the low reactivity of carbon to concentrated nitric acid at 100°C. It is certainly an empirical method only, but appears useful for comparative purposes. The crude deposit was dried under vacuum at room temperature, and an ether extraction was carried out on the distillate which was collected in a trap cooled in alcohol/solid carbon dioxide mixture. The residue was weighed, and to this weight was added that of the material extracted by ether. The residue was then digested with concentrated nitric acid at 100°C for 3 h, and the insoluble material was removed and weighed. Examples of some values obtained are given in Table 7. Free carbon determinations on the crude deposit from an ethylene/air reversed flame gave a figure of 10.1 per cent. The weight of crude deposit in this case included material that was extractable with ether from the material obtained by vacuum distillation. Free carbon determinations were also carried out on the deposits from the systems: (1) reversed ethylene/air flames with 1.25 per cent NO in the air; (2) as for (1), but the NO (1 per cent) included in the ethylene; and (3) reversed ethylene/air flames with 1.25 per cent N_2O in the air. The free-carbon figures obtained were: (1) 12.5; (2) 13.3; and (3) 11.7. Great difficulty was experienced in obtaining agreement between successive determinations in case (2).

The differences between (1), (2) and (3) are considered small.

It should be emphasized that all the above free-carbon determinations related to flames of the same size. Further work, incomplete so far, shows that the free carbon content of a deposit decreases as the flame size decreases.

(3.5.5) *Ultraviolet absorption spectra*

Comparative measurements were made of the ultraviolet absorption spectra of deposits from methane, propane and ethylene flames operated at reduced pressures (about 35 cm Hg). The flames were of type c (Fig. 4). Cyclohexane extracts of the deposits were prepared and the solvent removed under reduced pressure at a maximum temperature of 40°C. These were then redissolved in pure cyclohexane and the ultraviolet absorption spectra measured, the results being shown in Figure 8. There is a marked similarity in the three spectra and the pronounced bands at wavelengths greater than 3100 A correspond to a region where absorption from aromatic compounds is to be expected.

(3.5.6) *Molecular weight determinations*

Measurements of average molecular weights were made on the soluble fractions of certain of the deposits by measuring the lowering of the vapour pressure of the solvent using the differential thermocouple technique. A cyclohexane extract from an ethylene flame gave a value of 250: a vacuum distillation of the extract at 100°C (to remove the more volatile constituents) led to a product with a molecular weight of 600. A carbon tetrachloride extract gave a value of 510, the determination being made in pyridine. This type of result is to be expected: vacuum distillation at 100°C would undoubtedly change some of the material in the cyclohexane extract into a form more akin to that usually extracted in carbon tetrachloride, this being apart from the removal of low boiling fractions.

(3.5.7) *Infrared absorption spectra*

The most outstanding feature of the large number of spectra obtained is undoubtedly their close similarity. This statement applies to the deposits obtained from the following flame systems: (1) normal diffusion flames of methane, propane and ethylene at reduced pressures; (2) normal ethylene flames at atmospheric pressure; and (3) reversed diffusion flames of methane, propane, ethylene and benzene.

The presence of oxygen in form of OH and CO is a result of interest and importance. Examples of the type of spectra obtained are shown in Figure 9 from which the overall similarity is obvious. Variation in intensity of the absorption

Table 7. Free-Carbon Content of Various Flame Deposits

	Nature of Deposit	Free-Carbon Content
1	Deposit after extraction with CCl_4 of crude material from ethylene/air reversed flame	40.9
2	As for 1, but using pyridine instead of CCl_4	56.3
3	Crude deposit from normal flame of ethylene in air, sampling above flame on cooled target	84.1
4	Crude dry deposit from ethylene/air reversed flame, sampled from hot parts of the apparatus	44.1
5	Neospectra carbon black (a commercial product)	104.2

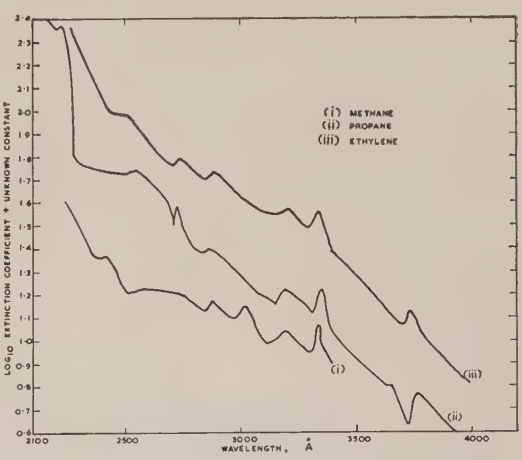

Fig. 8. Ultraviolet absorption spectra of cyclohexane extracts of deposits from low-pressure flames of the following fuels: (i) methane, (ii) propane, (iii) ethylene.

is to be expected when the variation in conditions, fuel and solution for examination purposes, are considered. The continuous line in Fig. 9c represents the spectrum of the deposit from the methane reduced pressure flame after partial extraction with carbon tetrachloride. The dotted line represents the absorption maxima present in the complete deposit. Their high optical density suggests a simple structure and the position could

Table 8. Percentage Absorption by Carbon Tetrachloride Extracts of Flame Deposits at Various Wavelengths

Flame	CH 3300 cm^{-1}	CO 1706 cm^{-1}	$R_1R_2{=}CH_2$ 870 cm^{-1}	$R_1R_2C{=}CHR_3$ 830 cm^{-1}
Reversed ethylene/air	55.8	46.5	71.9	96.2
Normal ethylene/air	39.4	67.9	76.9	99.2

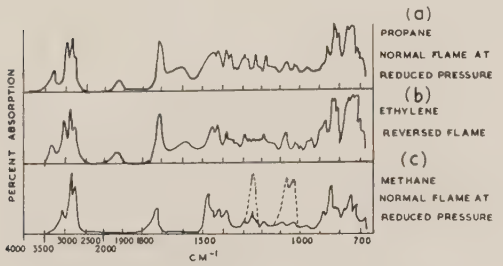

FIG. 9

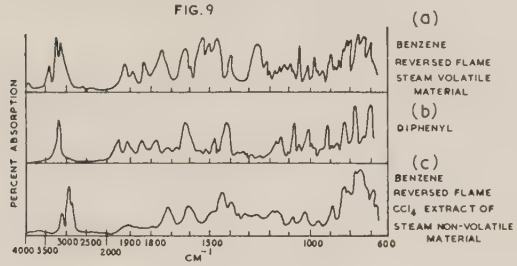

FIG. 10

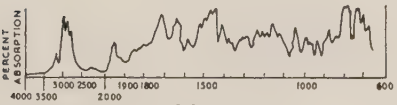

FIG. 11.

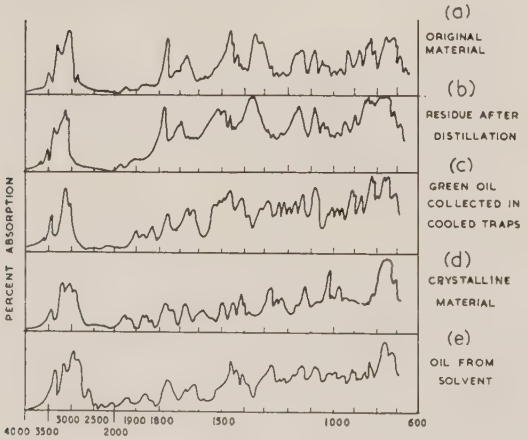

FIG. 12

Figs. 9-12. Infrared absorption spectra of various flame deposits.

indicate

1261 cm^{-1}	C—O,	C unsaturated
1093	C—O—C,	C saturated

with a possible structure of $=\overset{|}{C}-O-\overset{|}{C}-$. Absorption at these values occurs in the other spectra recorded but not to a similar extent, owing, perhaps to the simplicity of the fuel structure.

Mention has already been made of experiments with reversed benzene flames. Spectra are reproduced in Figure 10 of the steam volatile and the carbon tetrachloride extract of the steam nonvolatile material in the deposit. A spectrum determined for diphenyl is also reproduced, from which it can be seen that a large proportion of the steam volatile material is diphenyl. Despite the fact that some contamination with diphenyl of the steam nonvolatile material probably occurred, and that the more complex nature of the fuel allowed a wider range of compounds to form, the resemblance between Figure 10c and Figure 9 is sufficient to justify the conclusion that the major portions of each are identical.

Experiments involving the addition of nitric and of nitrous oxides to the gas streams of reversed ethylene flames have already been discussed from the point of view of carbon determinations. Carbon tetrachloride extracts of the deposits were taken, and, after removal of solvent under reduced pressure, oils remained; in each case the spectra have been obtained, and they resembled those reproduced in Figure 9.

Following experimental work by Garner et al.,[23] a more detailed observation of the type of material obtained from a normal ethylene diffusion flame was made. A very large quantity of soot from such a flame was collected and extracted with carbon tetrachloride. On removal of the solvent, a brown oil remained very similar in appearance and odor to the extracts obtained previously from deposits from reversed flames. The spectrum of the oil is shown in Figure 11 where it will be observed that the main structure is similar to that shown in Figure 9. The difference in absorption intensities between this and the spectrum of the reversed ethylene flame is illustrated by comparing the percentage absorption figures in Table 8. Values for unsaturation are, however, very similar when the difference in conditions is considered. It is somewhat surprizing that such material can survive when emitted from a flame or a hot atmosphere into oxidizing conditions.

In Figure 12 are shown 5 spectra, (a to e), of the products obtained on vacuum distillation at 100°C, of the cyclohexane extract of the deposit from a reversed ethylene flame. In each case, absorption of radiation due to OH (with hydrogen bonding) and to CO occurred. Similarity in this respect is of great importance, especially in the case of the residue, as it shows these bands to be distributed throughout the material and not merely concentrated in the lower boiling fractions. Absorption attributed to $R_1R_2C{=}CH_2$ and $R_1R_2C{=}CHR_3$ occur in all cases situated at 860–875 and 830 cm^{-1} respectively. Possible indication of this same type of grouping occurs in the region due to stretching vibrations (1700–1620 cm^{-1}).

The strong absorption in the region 3000–2500 cm^{-1} is attributable to either unsaturated or aromatic CH. The latter is quite probable, owing to absorption at the other end of the spectrum, namely 830–700 cm^{-1}. Strong absorption, due to methyl, is indicated at 1450 cm^{-1} and is consistently observed.

Apart from these general observations, there is insufficient evidence to enable the allocation of a definite structure at this stage. The outstanding features are the occurrence of oxygen as CO and OH, the unsaturated nature of the extracts, and the probability of the occurrence of aliphatic as well as aromatic structures.

(4) Discussion

The main facts which may be regarded as unequivocably established in the work described are:

(1) The radiation emission from diffusion flames is very dependent on the manner in which the combustion is carried out: reversal of the flame, vitiation of the flame with other gases, and combustion at reduced pressures, all lead to a less luminous flame.

(2) Simultaneously with the diminution in the radiation, there is a marked change in the nature of the carbonaceous deposits from the flames. Many methods of differentiation have been enumerated (see Section 2.3.2).

(3) Several first order differences between normal and reversed diffusion flames have been observed other than those recorded under (1) and (2). These included relative stability, temperature and composition of the product gases. Acetylene is a universal constituent of reversed flame gases.

(4) There is no evidence that fuel type has any influence on the nature of any of the carbonaceous deposits obtained. However, the means available for assessing the deposits are very incomplete.

(5) Oxygen is present in the carbonaceous deposits from all the systems examined by infrared spectroscopy in the form of associated hydroxyl and carbonyl groups. These groupings are not only resident in the highly volatile portions of the deposits. Any theory of carbon formation must therefore account for the fact that oxygen is incorporated in the intermediate products from which the carbon is finally produced.

(6) Absorption attributed to

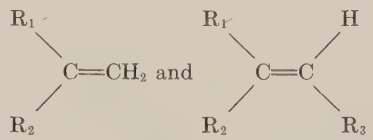

is observed in all cases. Aromatic structures are also present.

(7) Solubility in organic solvents would not appear to be primarily determined by chemical considerations: first-order differences between the ultimate analyses of soluble and insoluble fractions are not observed.

(8) Diphenyl is not a main step in the formation of carbon in flames, but can be a by-product with some fuels.

(9) Additives (such as NO), which are known from work at low temperature to be powerful inhibitors of polymerization reactions, do not produce large differences in the appearance or constitution of the deposits.

(10) The light output from methane flames is drastically reduced by concentrations of additives far less than those required for complete suppression of carbon formation.

These facts are not sufficiently complete to allow a mechanism to be formulated, but it is proposed to examine how far they agree with previously suggested theories.

The expression, formation of carbon in flames, can be easily misinterpreted, and there is evidence from the literature that this has been done. The material which can be formed in flames and which is variously referred to as soot, lamp black and carbon black is composed mainly of carbon, hydrogen, and oxygen. Although this material can be regarded as amorphous carbon with a graphite type of crystal lattice, the presence of covalently bound hydrogen and oxygen is an important feature of its structure and must not be ignored.

Accordingly, it is clear that one of the suggested modes of carbon formation in flames viz

polymerization of C_2, cannot of itself lead to a material with the above constitution or to materials with constitutions shown by the intermediates from reversed flames. Apart therefore from other powerful arguments advanced against this theory (e.g., energy difficulties and evidence for the reverse change: carbon $\rightarrow C_2$), we feel it must be rejected a priori.

An obvious alternative is that carbon can be formed in flames by pyrolysis of the fuel. Pyrolysis is a general term which can cover the widely different processes of hydrogenation, dehydrogenation, cracking, polymerization, etc. Thus Wolfhard and Parker[25] have suggested, as a result of spectroscopic studies with a flat diffusion flame, that "carbon formation in an oxygen diffusion flame occurs in the same way as it does in the pyrolysis of a hydrocarbon." This conclusion is based on the deduction that no molecular oxygen reaches the carbon-producing zone of a diffusion flame. It seems necessary to make some modification to this conclusion in order to bring it into line with the results reported here. We have found oxygen as a universal constituent of all fractions of all the intermediates from all the fuels we have used and we are therefore convinced that oxygen in some form reaches the carbon-forming zone of our diffusion flames. It is true that most of our flames were supported by air whereas Wolfhard and Parker's conclusion refers to a flame supported by oxygen, yet we found identical results in the case (methane) where oxygen enrichment was used. Perhaps the apparent disagreement can be resolved by the suggestion that oxygen is carried to the carbon-producing zone of a diffusion flame other than as molecular oxygen. O and OH are possibilities.

A comparison of our spectra with those of Hadzi[26] from pyrolysis products of some organic compounds, shows basic differences in the complexity of the spectra and in the main regions of interest, and supports the view that pyrolysis alone is at most a minor part of the process of carbon formation in flames.

Porter[8] has recently made some interesting suggestions about carbon formation in flames, basing his remarks mainly on results, obtained from the flash photolysis of ketene and from explosion of acetylene and oxygen sensitized by the photolysis of a small amount of NO_2. From considerations of thermal decomposition of hydrocarbons, Porter first concludes that a probable initial stage in carbon formation is decomposition to acetylene and his main objective is to suggest how acetylene is converted to carbon. To eliminate some of the possibilities he cites two experimental observations: (a) during photolysis of ketene no hydrocarbons higher than C_3 can be detected, although large amounts of carbon can be formed; (b) there is no correlation between C_2 absorption and carbon formation in the acetylene/oxygen explosions. Accordingly, Porter finding no evidence for higher hydrocarbon formation or for dissociation to C_2, suggests that carbon is formed by simultaneous polymerization and dehydrogenation. We find it is difficult to reconcile our results with some of these conclusions. The values for the molecular weight of the soluble portions of the reversed flame deposits certainly suggest that material intermediate in size is involved in the process of carbon formation in flames, and we suspect that carbon formation during the photolysis of ketene is probably occurring by a different mechanism to that existing in flames.

We agree with Porter that a case can be made out for a significant role of acetylene in carbon formation, but we cannot suggest a definite mechanism. We have found acetylene in all cases among the permanent gases emitted from reversed flames, but it is still possible that acetylene is not a main step in the process.

We agree with Garner et al.[23] that diphenyl is not a main step in the formation of carbon in flames, but their infrared spectra show many differences to those we have given in this paper, agreement being mainly restricted to the carbonyl group frequency at 1700 cm^{-1}. They direct particular attention to bands at 1620 and 1570 cm^{-1}: the former was not observed as a main feature in our spectra, and the latter was absent.

One of the authors has previously interpreted[14] the effect of diluent gases on the suppression of the NaD lines and the carbon continuum in flames as due to a reduction in the hydrogen atom concentration in flames, these atoms being necessary both for atomic sodium[27] and carbon formation. The results of the present paper make it clear that dehydrogenation (by atomic hydrogen) and polymerization are themselves insufficient and that the process is probably more complex than this. The data of Figures 6 and 7 are relevant to the influence of foreign gases on carbon formation. The former gives quantitative evidence of the effectiveness of four added gases in suppressing carbon formation. The case of CO is complex in that its combustion will influence the flame temperature, but it is notable that it is

so ineffective compared with the others. The simple thermal view that carbon formation is reduced by additives because of the cooling of the flame seems unlikely because, in addition to the evidence from the CO additions: (a) the critical concentrations are not simply related to their thermal capacities; (b) Figure 7 shows that the light output from methane flames is drastically reduced by amounts of additive much less than those required for suppressing carbon formation.

In conclusion, we suggest that the general approach outlined in this paper is worth further attention and that considerable progress can be made by systematic work on the fractionation of the reversed flame deposits.

Acknowledgments

The authors are grateful to Mr. J. L. Hales of the Chemical Research Laboratory, Teddington, for measurement of the infrared spectra of their materials.

The molecular weight determinations mentioned were carried out through the kind cooperation of Professor W. F. K. Wynne-Jones and Mr. H. E. Blayden.

The details of the method employed for the determination of free-carbon content were made available by the Shell Petroleum Company to whom the authors wish to express their thanks.

The permission of British Coal Utilisation Research Association to publish this paper is gratefully acknowledged.

REFERENCES

1. Minchin, S. T.: J. Inst. Pet. Tech., *17*, 102 (1931).
2. Clark, A. E., Hunter, T. G., and Garner, F. H.: *J. Inst. Pet. 32*, 627, 643 (1946).
3. Coward, H. F., and Woodhead, D. W.: *Third Symposium on Combustion, Flame and Explosion Phenomena*, pp. 518–522. Baltimore, The Williams & Wilkins Co., 1949.
4. Schalla, R. L., and McDonald, G. E.: N.A.C.A. RM E52122 (1952). Alternative reference: 122nd meeting American Chemical Society, Atlantic City, N. J., 1952.
5. Hunt, R. A.: Ind. Eng. & Chem., *45*, 602 (1953).
6. Frazee, J. D., and Anderson, R. C.: 124th Meeting American Chemical Society, Chicago, Ill., 1953.
7. Thomas, N.: J. Chem. Phys., *20*, 899 (1952).
8. Porter, G.: *Fourth Symposium (International) on Combustion*, pp. 248–252. Baltimore, The Williams & Wilkins Co., 1953.
9. Hsieh, M. S., and Townend, D. T. A.: J. Chem. Soc., 332 (1939).
10. Smith, E. C. W.: Proc. Roy. Soc., *A174*, 110 (1940).
11. Gaydon, A. G., and Whittingham, G.: Proc. Roy. Soc., *A189*, 313 (1947).
12. Gaydon, A. G., and Wolfhard, H. G.: Faraday Soc. Disc., No. 2, 161 (1947).
13. Wolfhard, H. G., and Parker, W. G.: Proc. Phys. Soc., *A62*, 722 (1949).
14. Arthur, J. R.: Nature, *165*, 557 (1950).
15. Parker, W. G., and Wolfhard, H. G.: J. Chem. Soc., 2038 (1950).
16. Norrish, R. G. W., Porter, G., and Thrush, B. A.: Nature, *169*, 582, (1952).
17. Durie, R. A.: Proc. Roy. Soc., *A211*, 110 (1952).
18. Gaydon, A. G., and Wolfhard, H. G.: Flames, pp. 162–192. London, Chapman and Hall, 1953.
19. Arthur, J. R., and Littlejohn, R. F.: Nature, *169*, 288 (1952).
20. Arthur, J. R., Kapur, P. K., and Napier, D. H.: Nature, *169*, 372 (1952).
21. Barr, J., and Mullins, B. P.: Fuel, *28*, 181, 225, 228 (1949).
22. Arthur, J. R.: Combustion Eng., *5* (1951); Fuel, *29*, 51 (1950).
23. Garner, F. H., et al., *30*, 266 (1951), *32*, 116 (1953).
24. Private communication of the company to the authors.
25. Wolfhard, H. G., and Parker, W. G.: Proc. Phys. Soc., *A65*, 2 (1952).
26. Hadzi, D.: Fuel, *32*, 112 (1953).
27. Arthur, J. R., Bangham, D. H., Baulk, R. H., and Whittingham, G.: Nature, 358, *166* (1950).

Discussion by Joseph Grumer*

Further evidence that oxidation may precede or be involved in the formation of carbon and related materials in flames (particularly rich premixed flames) may be found in these observations.†

(1) Excluding secondary air, the leanest limit for each of a wide variety of yellow-tipping fuels is roughly 1.4 to 2.0 times the stoichiometric fuel-gas percentage. In most instances, these mixtures have over 80 percent air in the unburned gas. It seems unlikely that purely pyrolytic reactions will proceed in the presence of such concentrations of oxygen or oxygen donors.

---

* Physical chemist, Chief, Flame Section, Explosives and Physical Sciences Division, Bureau of Mines, Pittsburgh, Pa.

† J. Grumer, M. E. Harris, and V. R. Rowe: Study of the Yellow-Tipping Characteristics of Fuel Gases. Interim Research Report No. 2, American Gas Association Project PDC-3, July 1954.

(2) At the yellow-tip limit, yellow appears in the secondary mantle, not in the primary combustion zone or below it. This can be made more apparent in certain instances by inverting the flame with an axially placed rod and a surrounding flow of nitrogen. Inverted yellow-tipped flames of ethylene-air, toluene-air and acetylene-air clearly showed a blue-green combustion zone upstream of the yellow.

25

MECHANISM OF SMOKE FORMATION IN DIFFUSION FLAMES

By ROSE L. SCHALLA AND GLEN E. McDONALD

Introduction

A number of theories have been proposed to explain the mechanism by which smoke is formed in diffusion flames, but at present no definite and completely consistent theory seems to be available. Most of the mechanisms which have been proposed in the past have been partial or generalized mechanisms in that they usually dealt with segments of the over-all process rather than tracing the complete course of the formation of smoke. These generalized mechanisms, such as the polymerization of C_2 or build-up of aromatic ring structures to form smoke, have been subjected to various theoretical and experimental investigation in recent years, and, consequently, information which offers a basis for supporting or rejecting these ideas has become available. With the belief that still more experimental work might be helpful in understanding the over-all mechanism, several experimental projects were undertaken. Smoke formation was investigated in this study from the standpoint of the effect of pressure, fuel type, external air-flow rate, oxygen enrichment, argon substitution in external air, and fuel temperature. The experimental results were interpreted to indicate a possible step involved in the early stages leading to smoke formation. The understanding gained from these experiments, together with information from the literature, has been used to postulate a possible and relatively complete mechanism of smoke formation.

Pressure

The effect of pressure on smoke formation was investigated by burning nine hydrocarbon fuels as diffusion flames from a modified wick lamp in an enclosed chamber. A sketch of the apparatus used to study the effect of pressure on smoke formation is shown in Figure 1. The chamber in which the fuels were burned was approximately 300 mm in diameter and 700 mm high. To obtain pressures above atmospheric, compressed air was admitted at the bottom of the chamber through holes in a perforated circular copper manifold. To remove the combustion products a constant air exhaust of 220 cc/sec was maintained at all pressures. The exhaust rate was measured by a flowmeter connected to the exhaust valve on the lid of the chamber. It was found that appreciable variations could be made in the exhaust rate without changing the smoking tendency of the flame. To obtain pressures below atmospheric, a vacuum line was connected to the exhaust valve and the flowmeter was attached to the air intake line. As a safety precaution and as a means of extinguishing the flame, gaseous carbon dioxide could be admitted to the chamber through a valve in the center of the lid.

The fuels were burned from a wick lamp which consisted of a 15 mm inside diameter glass tube 80 mm high to which was sealed a calibrated side arm. A hydraulic jack, operated from outside the chamber, permitted the raising and lowering of the wick lamp through a supporting collar. The rate of fuel flow needed to attain the smoking point could be controlled by adjusting the height that the wick extended above this support collar. A chimney 180 mm high and 47 mm in diameter was placed with the bottom edge level with the wick tip to keep the flame erect and stable. The smoking point of the diffusion flame was observed

visually through a 25.4 mm Lucite window on the front of the chamber.

The rate at which the fuel could be burned at its incipient smoking point was determined by measuring the time required for the level of the fuel in the side arm of the wick lamp to drop a unit distance. The side arm scale was calibrated against water; the fuel rates in gram/sec could be obtained from this calibration and the specific gravity of the fuel. Reproducibility of the order of ±3 per cent was obtained by this procedure.

In Figure 2a the maximum rate (gm/sec) at which 6 pure hydrocarbon compounds, *n*-octane, 2-methyloctane, octene-1, heptene-1, iso-octane, and cyclohexene, could be burned smoke free is plotted against pressure over a range of about ½ to 4 atm. The pressure range was extended for 2 of the compounds and these results are shown in Figure 2b. In figure 2c the maximum rate for 100 per cent *n*-octane, 2 blends of *n*-octane and toluene, and a JP-4 fuel are plotted against pressure. As can be observed from figures 2a, b, and c, the rate at which the fuels can be burned smoke free consistently decreases with increasing pressure. The JP-4 fuel and the 2 blends of *n*-octane and toluene show the same variation in smoke formation with pressure as do the pure hydrocarbon compounds.

A plot of the smoke-free fuel flow against 1/p is shown in Figure 3. The fairly straight lines obtained in these plots clearly indicates that the smoke-free fuel flow is inversely proportional to the pressure.

Fuel Type

A systematic survey of the smoking tendency of various hydrocarbon fuel types at one atmosphere pressure and room temperature was conducted at the Lewis laboratory[1]. The fuels were burned in still air as diffusion flames from wicks and burner tubes, and the maximum quantity of hydrocarbon which could be burned smoke-free in a given time was used as the criterion of smoking tendency. The maximum smoke-free fuel flow in gm/sec is plotted against the number of carbon atoms in the molecule in Figure 4. The results indicate that the rates at which the hydrocarbons could be burned smoke-free varied as follows: *n*-paraffins > isoparaffins > mono-olefins > alkynes > aromatics.

External Air-Flow Rate

The effects of external air-flow rate on the smoking tendencies of the laminar diffusion flames of eight of the hydrocarbons were investigated. The apparatus used for this purpose is shown in Figure 5. The eight hydrocarbons studied were burned from a stainless steel burner tube 9 mm in diameter (see Fig. 5a). The burner tube was enclosed by a Pyrex glass tube 40 mm in diameter and 760 mm in height. All of the air supplied to the flame was admitted through holes in a perforated cylindrical chamber sealed into the base of the Pyrex tube. Both the fuel and air were metered through flowmeters before entering the tubes. At each selected air flow a

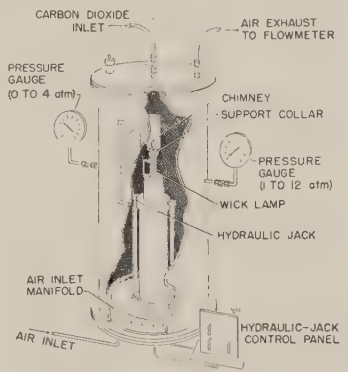

FIG. 1. Diagram of apparatus for determining smoking tendency.

determination was made of the maximum rate of fuel which could be burned without causing the flame to smoke. A visual observation was used to detect the first smoke which issued from the flame.

Since the vapor pressure of pentene-1 was not sufficiently high at room temperature to give the needed fuel flow, a heated bomb was used to hold the vaporized pentene-1 which was then burned in the gas phase in the same manner as the gaseous compounds (Fig. 5b). To determine the fuel flow rate in this case, the bomb plus the sample were weighed before burning the fuel and then reweighed after the fuel had burned at its incipient smoking point for a given interval of time. From the loss in weight over this time interval the maximum smoke-free fuel rate could be obtained.

Figure 6 shows the variation in smoke-free fuel flow with increasing air flow for butene-1,

cyclopropane, propene, pentene-1, neopentene, isobutane, ethylene, and *n*-butane. As the rate of air flow past the flame is increased the rate of flow of fuel which will burn without smoking is at first increased proportionally; however, a limiting fuel flow (F_L) is shortly reached, and additional increases in the air flow do not permit further increase in the fuel flow for smoke-free burning. Of course all of these fuel flows are still in the laminar region and a different maximum limit would be expected if turbulent flames were studied.

Figure 7a is representative of cyclopropane and propene and Figure 7b is representative of the other five hydrocarbons. With the initial increase in the flow rate of a given oxygen enriched mixture, the maximum smoke-free fuel flow also increased. The fuel flow, however, reached a limiting value which is usually greater than that for air although for some fuels the limit fuel flow with oxygen enrichment is actually less than for air. To show the variations of the maximum limit fuel flow with oxygen enrichment a crossplot of the data is shown in Figure 8.

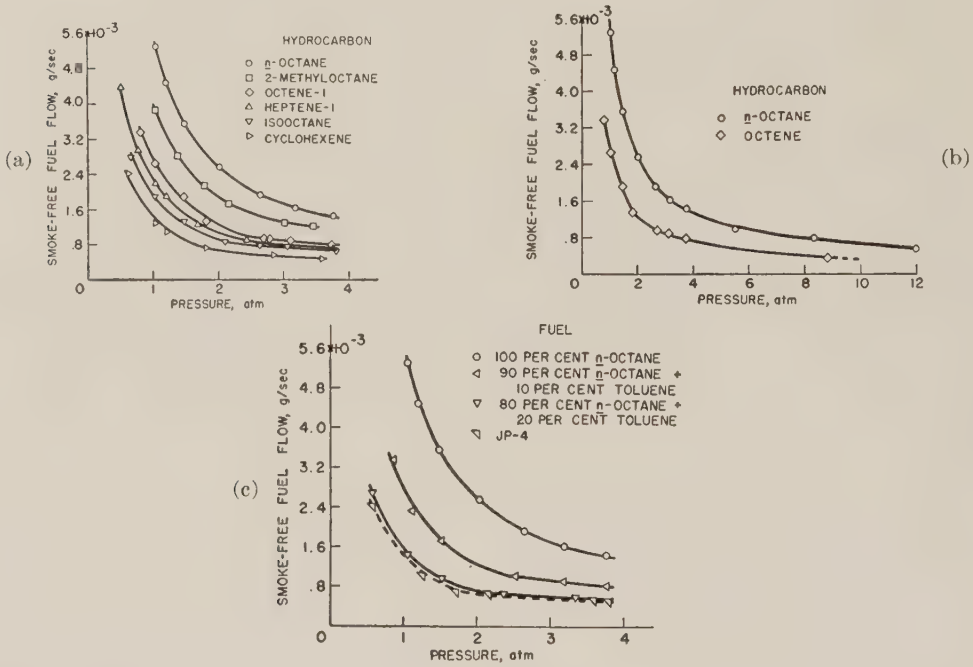

FIG. 2. Variation in smoke-free fuel flow with pressure. (a) Six hydrocarbons at pressures to 4 atmospheres; (b) two hydrocarbons at pressures to 12 atmospheres; (c) various fuels and blends at pressures to 4 atmospheres.

Oxygen Enrichment of External Air

While increasing the rate of air to a diffusion flame will increase the chances for diffusion of oxygen into the flame, a greater quantity of oxygen could enter the flame if enriched oxygen-nitrogen mixtures were used. Consequently oxygen-nitrogen mixtures with oxygen concentrations ranging from 25 to 45 per cent were substituted for air.

The effect on the smoke-free fuel flow obtained by substituting oxygen enriched mixtures of oxygen and nitrogen for air with the same eight hydrocarbons is shown by Figures 7a and b.

For propene, cyclopropane, and butene-1 (Fig. 8a) the limit fuel flow is the same for 21 per cent O_2-79 per cent N_2 and 25 per cent O_2-75 per cent N_2, but decreases for 30 and 35 per cent O_2 mixtures. An increase is again observed for the 45 per cent concentration. For isobutane, neopentane, and pentene-1 (Fig. 8b) the limit fuel flow continually increases with increasing oxygen enrichment. This was also true for ethylene and *n*-butene.

Argon Substition in External Air

The purpose of using argon in place of nitrogen in the external air was to increase the flame tem-

perature without changing the oxygen concentration. An increase in temperature of 250° to 400°C is probably obtained by this method. Substituting argon for nitrogen in the oxygen enriched mixtures caused the smoke-free fuel flow to increase except for butene-1, cyclopropane, and propene, where initial rates were lower than with the corresponding oxygen-nitrogen mixtures. These results are shown in Figures 7 and 8.

Fuel Temperature

To study the effect of preheating a fuel, the apparatus shown in Figure 5c was used. The 9 mm burner tube 700 mm in length, was jacketed by an electric heating coil controlled by a variac transformer. To stabilize the flame a chimney 47 mm in diameter and 300 mm high was placed with the bottom edge level with the port of the burner tube. After the burner tube temperature had reached a constant value with a small air flow passing through it, the maximum rate of fuel which could be burned without smoking was measured. The temperature was then raised until a higher equilibrium value was reached and the smoke-free fuel flow again determined. The results showed that increasing the flame temperature by preheating the fuels over a range of 30° to 190°C had no effect on smoke formation. The change in flame temperature obtained by this method is probably small.

Postulated Mechanisms of Smoke Formation

An attempt to explain the preceding experimental results was undertaken with the hope that an understanding of the factors studied herein would be helpful in postulating a mechanism of smoke formation. While the results did not yield a complete mechanism, they were interpreted to indicate a possible step involved in the early stages leading to smoke formation. The most consistent information which is currently available in the literature was then combined with these findings to complete the mechanism.

The following explanations are proposed to explain the preceding experimental results. The effect that pressure exerts on smoke formation was attributed to the rate of diffusion and mixing of the fuel and air. This explanation is proposed since the smoke-free fuel flow was found to be inversely proportional to pressure and the diffusion coefficient is known to be inversely proportional to pressure.

The effects of the other variables studied are

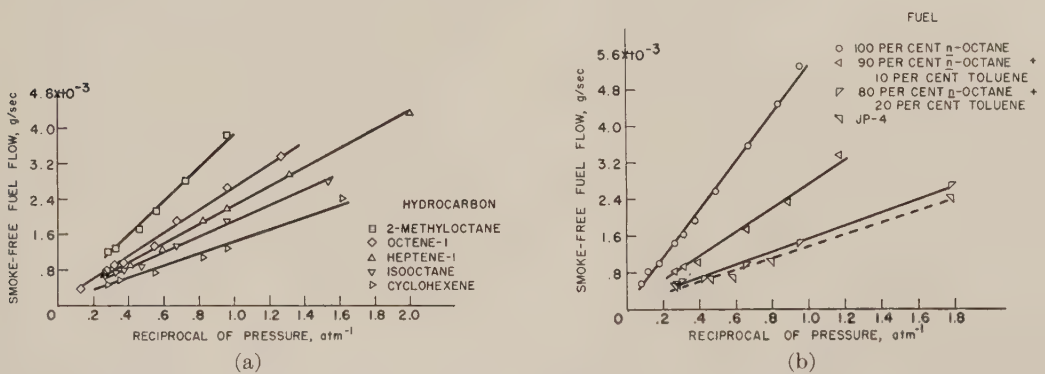

FIG. 3. Smoke-free fuel flow against reciprocal pressure. (a) Five hydrocarbon fuels; (b) various fuels and blends.

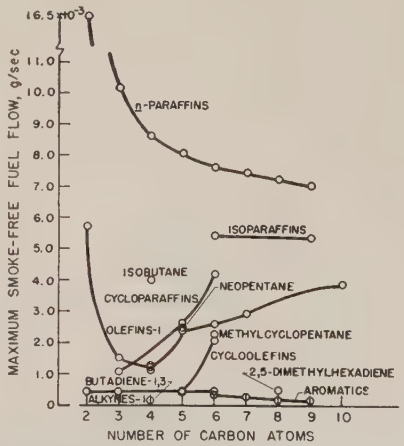

FIG. 4. Variation of maximum smoke-free fuel flow with number of carbon atoms.

too complex to be satisfactorily explained by any one physical process such as diffusion and consequently can have only a chemical interpretation.

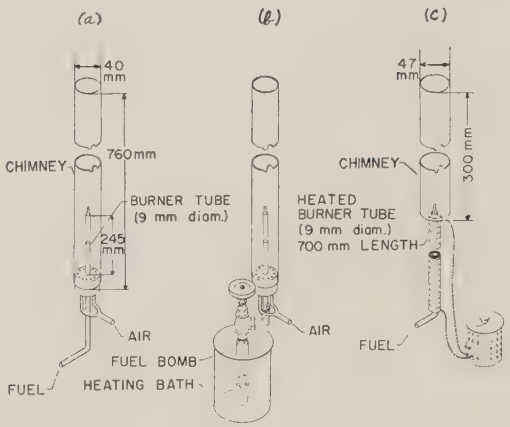

FIG. 5. Diagram of apparatus: (a) burner tube, (b) apparatus modified for vaporized liquid fuels, (c) apparatus modified for preheating fuels.

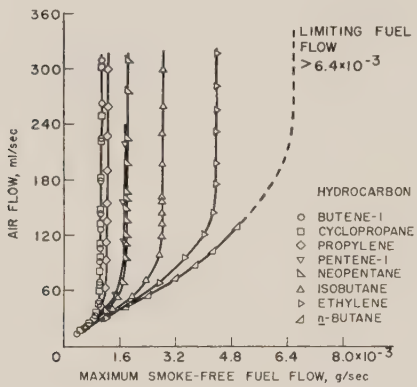

FIG. 6. Variation in smoke-fuel fuel flow with air flow.

From the results of the study on fuel type a correlation was found to exist between the tendency of a fuel to smoke and the stability of the carbon chain or skeleton of the fuel[1] (Fig. 9). Values of the bond strengths are approximately C—C, 80; C—H, 100; C=C, 150; and C≡C, 200 kcal/mole. As the stability of the carbon skeleton is increased the chances of dehydrogenation are increased and it is proposed that this increased ease of removal of hydrogen atoms as compared to the breaking of carbon bonds is responsible for the variations in smoking among different fuel types. These findings would indicate that thermal and oxidative dehydrogenation processes, which would occur very early in the burning process, influence the further course of smoke formation. The thermal dehydrogenation is probably occurring as soon as the fuel enters a laminar diffusion flame because the fuel is heated to temperatures of the order of 800° to 1000°C before coming into contact with oxygen.

The importance of dehydrogenation processes is supported by the results of the oxygen enrichment and argon substitution studies which showed that when fuels of high smoking tendency (butene-1, propene, and cyclopropane) were subjected to oxygen enrichment and consequently increased flame temperatures, or to increased flame temperatures directly through the use of argon, the smoking tendency increased up to a certain point. The higher flame temperatures probably were able to promote dehydrogenation reactions in the case of these compounds possess-

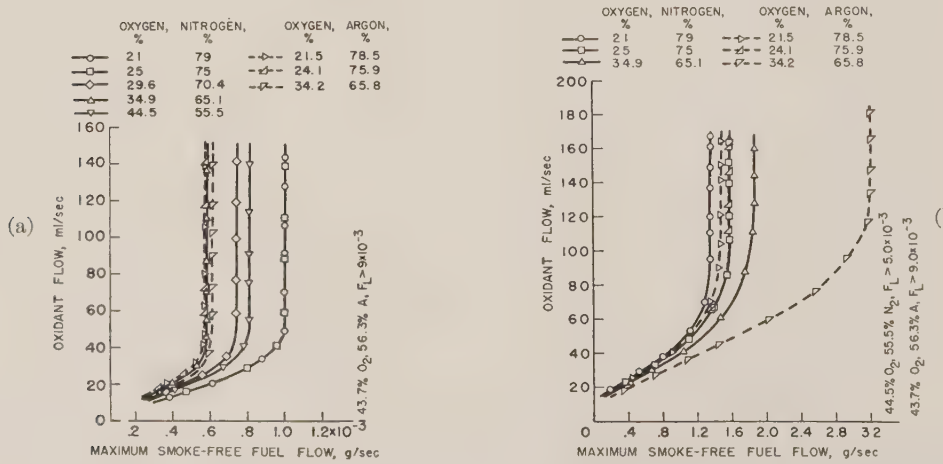

FIG. 7. Variations in maximum smoke-free fuel flow with oxygen-enriched mixtures. (a) butene-1; (b) neopentane.

ing a very stable carbon skeleton. It would appear that once the dehydrogenation process has advanced sufficiently far the increased chances for diffusion of oxygen resulting from oxygen enrichment are no longer effective in reducing smoke formation. However, at the highest oxygen concentration, 44.5 per cent, the temperature may have become so severe that the thermal and oxidative dehydrogenation processes were no longer favored over the breaking of carbon bonds, or at this high oxygen concentration the direct reaction of oxygen with carbon forming intermediates is favored.

hydrogen removal by existing hydrogen atoms or other active particles. These two types of dehydrogenation are of course occurring simultaneously.

Other investigators have considered the importance of dehydrogenation reactions and tend to support these findings. For example, the energy requirements for removal of a hydrogen atom from an acetylene molecule by an existing hydrogen atom,

$$H + C_2H_2 \rightarrow H_2 + C_2H$$

was considered by Frazee and Anderson[2]. This

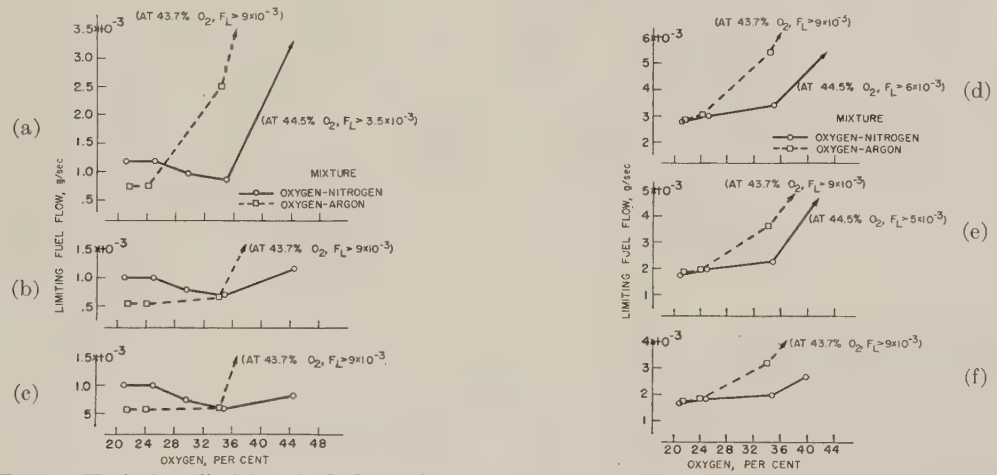

FIG. 8. Variation limiting fuel flow with oxygen enrichment. (a) propane, (b) cyclopropane, (c) butene-1, (d) isobutane, (e) neopentane, (f) pentene-1.

For compounds of lower smoking tendency the smoke-free fuel flow increased with increased oxygen enrichment or increased flame temperature. While these compounds of lower smoking tendency were also undergoing increased thermal decomposition at higher temperatures, the decomposition may have become more evenly distributed among C—C and C—H bond breaking reactions. Actually, the breaking of C—C bonds probably exceeded that of the C—H bonds since, as mentioned above, the bond strengths for C—C and C—H bonds are about 80 and 100 kcal/mole, respectively. Since the carbon bonds in unsaturated molecules are appreciably stronger, such molecules could be more readily dehydrogenated. Compounds possessing very stable carbon skeletons would not only contribute a large concentration of H atoms to the flame as the result of thermal dehydrogenation, but would also be most subject to additional

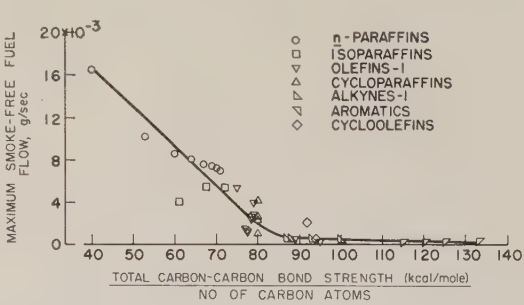

FIG. 9. Variation of maximum smoke-free fuel flow with total carbon-carbon bond strength per number of carbon atoms.

reaction has an activation energy of only 5 kcal/mole which indicates that it could easily be occurring. Activation energies for the reaction of hydrogen atoms with various other hydrocarbon compounds are of similar magnitude[3].

It was observed by Arthur[4] that suppression of the hydrogen atom concentration in flames ac-

companied the suppression of smoke formation. Arthur concluded that smoke formation could be prevented by reactions which consume hydrogen atoms or render them ineffective. It was observed[5] that smoke formation could be suppressed by CO and N_2 which serves as nuclei for the recombination and removal of H atoms.

In addition to H atoms Sachs and Ziebell[6] report that other atoms and radicals such as those found in the pyrolysis of halogen compounds increases smoke formation. All of these active species probably promote polymerization reactions leading to smoke by stripping hydrogen from the fuel molecules. The halogen atoms might be expected to react with and thereby remove existing hydrogen atoms, but the concentration of fuel molecules is probably so much greater than the concentration of the short-lived hydrogen atoms that the halogen probably tends to dehydrogenate the fuel molecules. It is therefore proposed that the removal of H atoms from the fuel molecules both by thermal processes and by the presence of other active atoms is probably the initial process involved in the formation of smoke.

The steps that might occur after total or partial dehydrogenation are very controversial. Since the aromatics are by far the class of compounds having the greatest smoking tendencies and since the graphite structure of carbon particles resembles the molecular structure of benzene's multi-ringed homologues, the formation of smoke by a build-up of aromatic ring structures has been suggested. This theory is not in opposition to the initial step of hydrogen removal since the aromatic fuels would have to lose some hydrogen atoms before a polymerization of the rings might begin. For nonaromatic fuels the hydrogen atoms would have to be removed to permit the formation of unsaturated ring structures. However, absorption spectroscopic examinations in the ultraviolet of a benzene flame by Parker and Wolfhard[7] indicated that benzene is consumed in the lowest portion of the flame and that an appreciable gap exists between the disappearance of benzene and the appearance of smoke particles. No intermediate aromatic products, which absorb very strongly in the ultraviolet, are found in this region. The absence of aromatic intermediates in this gap is evidence against the ring building theory.

Thorp, Long, and Garner[8] analyzed the smoke from a flat benzene flame and found diphenyl to be present, but in later work[9] they did not find diphenyl present in the products of the soots from paraffinic or naphthenic fuels. Consequently Garner, Long and Thorp[9] now consider it unlikely that carbon formation in hydrocarbon diffusion flames occurs through diphenyl, the polyphenyls, or polycyclic aromatics as intermediate compounds.

Parker and Wolfhard have proposed as mechanisms for smoke formation (1) the formation of large molecules which may graphitize from within; or (2) an increase in the concentration of moderately high hydrocarbons until the saturation vapor pressure is reached, at which time condensation occurs to form a mist of droplets that form nuclei and graphitize. Observations on the physical nature of smoke by Grisdale[10] show that the first mechanism of these two proposals is not likely to be occurring. Frazee and Anderson[2] also object to the first mechanism since a prohibitive energy requirement would be expected if large molecules build up and then are dehydrogenated directly to solid carbon. They also propose that similar difficulties arise for a mechanism involving formation of liquid droplets of polymeric hydrocarbons followed by pyrolysis. Porter[11] concludes from considerations based on the time available for polymerization and on the nature of the smoke formed that the droplet formation mechanism or polymerization mechanisms in general do not contribute to any significant extent in ordinary diffusion flames.

After the initial dehydrogenation process it would appear that neither aromatic type compounds nor large polymers are immediately built up, but rather that fuel molecules continually decompose to yield relatively small molecules or fragments of molecules. The findings of Porter[11] would also lead to this conclusion. By rapid adiabatic photolysis Porter was able to simulate in a reaction vessel the rates of liberation of heat and free radicals which occur in flames. A rapid quenching resulted in the retention of a fraction of all stable intermediates. Complete analysis of the products clearly indicated that the series of reactions leading to smoke did not involve the formation of higher hydrocarbons.

Porter's work indicates that fuels in combustion waves decompose thermally and also via intermediate oxidation products to acetylene. A series of reactions proposed by Porter are as follows:

$$C_2H_6 \rightarrow C_2H_4 \rightarrow C_2H_2 \rightarrow \text{carbon}$$

Tropsch and Egloff[12] passed pure hydrocarbons rapidly through a heated tube for various contact times and found in the case of ethane that ethylene, acetylene, and carbon were formed. For methane the results were similar with acetylene again being formed. This experiment simulates the reactions that might occur in the lowest portion of a diffusion flame where the fuel is heated previous to coming into contact with oxygen.

Since acetylene may be the last stable product to appear before smoke formation, the final step in the mechanism of smoke formation would be that leading from acetylene to smoke. If all hydrogen atoms were removed from the C_2H_2 molecule, the mechanism for the final step in the formation of smoke would be that of the polymerization of C_2 radicals.

The polymerization of C_2 to smoke was at one time considered a plausible and promising explanation of smoke formation. The idea initially resulted from limited spectrographic observations[13] which showed increasing C_2 concentration in flames capable of intense smoke formations. The theory of smoke formation via C_2 has now been rejected by numerous authors[2, 7, 11] and will be given no further consideration.

A mechanism based on simultaneous polymerization and dehydrogenation is proposed by Porter to account for the steps between acetylene and smoke. The reaction is exemplified by the following equation:

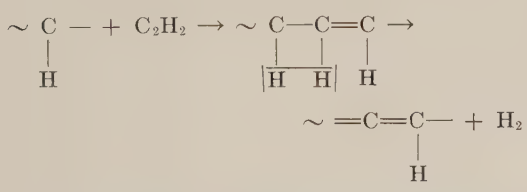

Since no aromatic or high molecular weight hydrocarbons were isolated in Porter's study, it would appear that such compounds do not need to be involved in these final steps leading to smoke. Garner, Long, and Thorp[9] conclude from the work previously discussed that the formation of smoke probably occurs through the production and further reaction of a diene which would only have a transient existence. Porter's mechanism indicates the formation of such transient diene structures. Analogous to the work of Porter is the indication of Frazee and Anderson that a mechanism involving free radicals or atoms is important in the formation of smoke. They considered the energy requirements for such free radical reactions and report the following values:

	E, kcal/mole	
$C_2H + C_2H_2 \rightarrow C_4H_3 \rightarrow C_4H + H_2$	~58	(1)
$C_2H + C_2H_2 \rightarrow C_4H_2 + H$	~29	(2)
$C_2H_2 + C_2H_2 \rightarrow C_4H_3 + H$	~60	(3)

Frazee and Anderson indicate that the first equation is of the type suggested by Porter and propose that, while the reaction is feasible and may occur to some extent, its activation energy is much higher than that for the reaction shown in the second equation. The third equation shows a possibility for the use of the energy of combination in initiating reactions perhaps more effectively than by purely thermal means. At particularly high temperatures, more than one reactive radical or H atom could result from a step such as the second equation, and chain branching might result. They also indicate that steps such as those shown above can occur with molecules containing larger and larger numbers of carbon atoms, leading eventually to formation of carbon nuclei and even to growth of a particle.

Summary

In final summary the general mechanism of smoke formation, based on the information currently available, probably proceeds as follows:

(1) Some hydrogen atoms are removed from the fuel molecule by thermal processes. These hydrogen atoms in turn cause further dehydrogenation of the molecule. The more readily the hydrogen atoms are removed as compared to the breaking of carbon bonds the greater is the probability of smoke formation.

(2) After these initial dehydrogenation steps the fuel molecules probably continue to decompose to smaller molecules and fragments of molecules. Acetylene is reported to be the last stable product to appear before smoke formation. Various authors have shown that a breakdown to smaller products must occur rather than an immediate growth to polymers or aromatic ring structures.

(3) Although a breakdown to small fragments and relatively small molecules takes place, the formation of smoke through polymerization of C_2 radicals has been rejected. It has been proposed that in the final stages the small molecules such as acetylene and hydrocarbon fragments undergo a simultaneous polymerization and dehydrogenation to form smoke.

REFERENCES

1. Schalla, R. L., and McDonald, G. E.: Ind. & Eng. Chem., *45*, 1497 (1953).
2. Frazee, J. D., and Anderson, R. C.: Presented at 124th Meeting of Am. Chem. Soc., Chicago, Ill., Sept. 1953.
3. Steacie, E. W. R.: *Atomic and Free-Radical Reactions*. Reinhold Pub. Corp., New York, 1946.
4. Arthur, J. R.: Nature, *165*, 557 (1950).
5. Iyengar, M. S., Vaidyeswaran, R., and Datar, D. S.: J. Sci. Ind. Res., *11B*, 455 (1952).
6. Sacks, W., and Ziebell, M. T. I.: National Aeronautical Establishment, Lab. Report LR-30, June 1952.
7. Parker, W. G., and Wolfhard, H. G.: J. Chem. Soc. (London), *1950*, 2038 (1950).
8. Thorp, N., Long, R., and Garner, F. H.: Fuel, *30*, 266 (1951).
9. Garner, F. H., Long, R., and Thorp, N.: Fuel, *32*, 116 (1953).
10. Grisdale, R. O.: J. Appl. Physics, *24*, 1082 (1953).
11. Porter, G.: *Fourth Symposium (International) on Combustion*, p. 248. The Williams & Wilkins Co., Baltimore, 1953.
12. Tropsch, H., and Egloff, G.: Ind. & Eng. Chem., *27*, 1063 (1935).
13. Smith, E. C. W.: Proc. Roy. Soc. (London) *174A*, 110 (1940).

26

CARBON FORMATION FROM C_2H_2 AND CO IN DISCHARGE TUBES

By A. G. GAYDON and A. R. FAIRBAIRN

Introduction

Processes of soot formation are far from understood; reviews of possible mechanisms have been given by Gaydon and Wolfhard[1] and Porter[2]. The mechanism may depend on the temperature in the region of the flame in which the formation of free carbon occurs, on whether or not oxygen is present, and on the nature of the fuel. There is good reason to believe that in pyrolysis of pure hydrocarbons and in some diffusion flames there is condensation or polymerization to relatively large molecules of low vapor pressure which may actually condense to liquid droplets, which then graphitize from within. For hot premixed flames, however, there is little actual evidence for the formation of such large molecules. Porter has pointed out that temperature conditions are likely to lead to breaking down rather than to the building up of large molecules, and he has suggested the formation of acetylene as an intermediary. There is certainly plenty of recent evidence for the formation of acetylene from other hydrocarbons, but the mechanism by which relatively large carbon particles are formed from acetylene remains uncertain; Porter suggests reaction of a free radical with acetylene, giving simultaneous polymerization and dehydrogenation. The theory suggested by Smith[3] of polymerization of C_2 radicals (known spectroscopically to be present) has received little support from recent work and it is probably safe to discard it, but it remains possible that the C_2 radicals might act as nuclei for the polymerization-dehydrogenation of acetylene. In flames of burning hydrocarbons there will be some competition between processes of oxidation and of carbon formation by pyrolysis. In some cases even when there is sufficient oxygen for fairly complete oxidation, sufficient carbon is formed to render the flame luminous. For ethylene flames carbon should not, on equilibrium considerations, be formed, provided oxygen is in excess of 34 per cent of the stoichiometric amount, but actually luminosity may be observed up to 52 per cent[1]. Carbon luminosity may even be observed near the weak limit for methane in closed-vessel explosions at high pressure.

During some experiments on atomic flames and afterglows, in collaboration with Broida[4, 5, 6] it was found that carbon monoxide gave a type of bluish afterglow and that when acetylene was introduced into this afterglow a carbonaceous deposit was formed on the walls of the afterglow tube. Since the spectrum of the afterglow showed

bands of C_2, it seemed that there might be some connection between the processes of carbon formation in the afterglow and in flames. The object of this paper is to report our experimental studies on this carbon formation in the afterglow.

The Afterglow of Carbon Monoxide

The afterglow was produced in a fairly wide-bore discharge tube with large aluminum electrodes of the type used for the study of atomic flames[7] or the oxygen afterglow[6]. The discharge was maintained by a 6000-v transformer taking up to 30 amp from the 230-v 50-cycle mains; the current through the discharge tube was up to about 1 amp. The bluish afterglow was obtained best with maximum available current and near the highest pressure at which the discharge would strike, about $3\frac{1}{2}$ mm Hg. For the work on carbon formation in the afterglow an uncondensed discharge was used, but it was found that a condensed discharge, obtained by connecting a 0.1 μF condenser across the discharge tube, gave a much brighter afterglow. The main part of the discharge tube was water-cooled, as in Gaydon and Wolfhard's work[7], and there was some carbon deposition on the hot part of the walls of the discharge tube (not the afterglow tube) above the water-cooling line.

The blue CO afterglow was very unusual in its behavior; its nature and cause remain a mystery. It usually extended from 4 in to 6 in from the main discharge. The distance which it traveled was not appreciably affected by pumping rate, and the glow was obtained quite well with the pump cut off. The afterglow usually took the form of a luminous jet of gas extending from the discharge into any side tube or vessel. With a spherical vessel joined by a short T-piece to the discharge tube, the jet tended to broaden slightly with distance and to end fairly abruptly, but it did not fill the vessel as most afterglows do (e.g., those of N_2 or air). To test whether the afterglow might really be due to fluorescence caused by the light from the discharge, a thin plate of lithium fluoride, known to be transparent to 1070 Å, was placed in the path of the afterglow jet; the jet was deflected around the plate but there was no luminosity behind it; this experiment convinced us that the afterglow was caused by motion of particles, not by radiation. The jet was undeflected by the magnetic field from a strong permanent horseshoe magnet, suggesting that it was not due to a stream of charged particles. The possibility that the afterglow might be associated with gas pulsations excited by the alternating discharge and amplified by resonance with the organ-pipe frequency of the tube was considered; evidence for such effects was obtained in the atomic oxygen/CO flame.[5] However alterations to the design of the discharge tube or the position or design of the afterglow side tube did not obviously alter the character or length of the afterglow, and we conclude that such effects are not the cause of the CO afterglow. On present evidence it seems most likely that the cause of the afterglow excitation is the ejection of fast atoms or molecular fragments from the region of the discharge.

The spectrum of the CO afterglow from the uncondensed discharge showed mainly the high pressure bands of C_2. These are bands of the Swan system having $v' = 6$. Bands of the ordinary Swan system were normally very weak in the afterglow, but when hydrogen or moisture was present as an impurity in the CO the Swan bands were strengthened, and CH bands also appeared. The Swan and CH bands also appeared when a little acetylene was added to the afterglow gases, but an appreciable amount of acetylene quenched the afterglow light altogether. The brighter afterglow from the condensed discharge also showed the line of neutral atomic carbon at 2478 Å (this is the most sensitive line, but is nevertheless due to a transition between highly excited states of C) and some lines of ionized carbon ($\lambda\lambda$3919, 4267 and 6578). The spectrum of the exciting discharge showed the usual band systems of CO (Ångstrom, Third Positive, Fourth Positive) together with the C_2 Swan bands and weak C_2 high pressure bands.

The mechanism by which the C_2 radicals are formed in the vibrational level $v' = 6$ to give the high pressure bands has been discussed by Herzberg[8], who favored recombination of free carbon atoms. Although his detailed mechanism requires a low value for the dissociation energy of C_2 which is difficult to reconcile with other data, it does seem likely that the high pressure bands are associated with the presence of free atomic carbon and that the afterglow gases contain both C_2 molecules and atomic carbon.

The Formation of Carbonaceous Deposits

The design of discharge tube used for most of the work on the introduction of acetylene (and other gases) into the CO afterglow is shown in

Figure 1. Carbon monoxide enters at both electrodes EE, flows through the discharge and up into the afterglow tube to the pump. Acetylene is introduced at a side tube in the afterglow limb. The positions of the afterglow and carbonaceous deposit are indicated. Gas flows were controlled with needle valves and a fast mercury-vapor pump was used[6].

The carbonaceous deposit formed first and was thickest on the walls nearest to the region where the acetylene and afterglow mixed, but it gradually spread some considerable distance towards

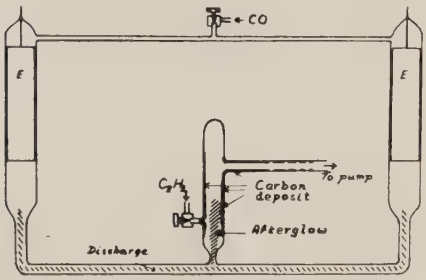

FIG. 1. Diagram of discharge tube

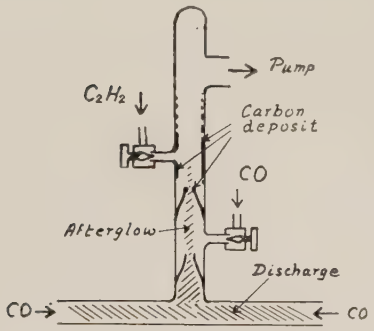

FIG. 2. Diagram of afterglow side tube

the pump. Although the afterglow was never visible for more than about 6 in from the discharge, the deposit was formed for over 2 ft; It thus seems likely that the formation of the carbon may have occurred in the gas phase and settled out on the walls. On the other hand it was of a hard type, quite difficult to remove without hard scratching, so it remains possible that it was actually formed on the surfaces.

With the set-up indicated in Figure 1, there was sometimes a slight tendency for the acetylene to diffuse back into the discharge, as shown by change in the color and spectrum of the discharge in the region near the afterglow tube and by coating of the walls in this region. It is, of course, known that acetylene is decomposed, polymerized, etc., in a discharge. To determine that the effect of carbon formation in the afterglow region was not spurious, resulting from back diffusion, a special form of afterglow side tube was used with a double internal seal and jets and secondary injection of CO designed to reduce back diffusion; this is illustrated in Figure 2. With this design the afterglow in the mixing region was very much weaker and the rate of formation of the carbonaceous deposit was reduced but did still occur. Back diffusion appeared to be completely eliminated.

The carbonaceous deposits were formed freely when either acetylene or benzene were introduced into the afterglow. Ethylene gave a trace of deposit if allowed sufficient time. No deposit at all was observed with methane, ethane or hexane.

The addition of a little hydrogen to the CO supply reduced the rate of formation of the deposit. It may be recalled that this also reduced the intensity of the high pressure C_2 bands in the afterglow spectrum. Using hydrogen instead of CO in the discharge tube to give atomic hydrogen did not lead to any carbon formation at all; indeed deposits of carbon could be burnt off slowly with the atomic hydrogen. With nitrogen in the discharge tube the nitrogen afterglow (active nitrogen) was obtained with moderate strength (this is excited best with a condensed discharge), and when acetylene was added to this there was some deposition on the walls, but the deposit appeared to be of a rather different type from that from the CO afterglow.

The walls of the afterglow tube sometimes became slightly heated, to between 50 and 100°C, and we considered the possibility that the carbon deposition might be due to thermal decomposition of the acetylene. However, external heating of the vessel to the softening point of Pyrex did not cause any deposit on the walls from acetylene at the low gas pressure (3 mm) used.

The Nature of the Deposit

Samples of the carbonaceous deposit from the reaction between acetylene and the CO afterglow were collected by inserting a glass probe into the region of most rapid deposition; this probe was inserted through a ground joint so that it could be removed for examination. Thick deposits appeared black. When thin, the deposit was reddish brown by transmitted light. It was fairly hard, but could be scraped off the glass. When the

deposit was formed slowly using a small flow of acetylene into the afterglow it was relatively hard, whereas a faster flow of acetylene giving a higher rate of deposition led to a softer, more flaky material.

Chemical analyses of small samples (5 mg) of the hard slowly formed and soft rapidly formed material gave empirical formulae roughly $C_{15}H_5O$ and $C_{20}H_4O$.

Electron diffraction examination of a sample deposited on a glass plate, as kindly carried out by H. Wilman, showed three faint diffuse rings consistent with the occurrence of very small graphite crystallites of size probably rather below 20 Å.

The deposit formed from acetylene and the afterglow could be burnt off the walls of the afterglow tube fairly rapidly with atomic oxygen, obtained by flowing oxygen through the discharge. The deposit obtained from active nitrogen and acetylene was removed much more slowly in this way. The brown product obtained on the walls when acetylene was admitted into the discharge tube was very difficult to remove with atomic oxygen, persisting for a long while even on the walls of the discharge tube. It was obviously of a different chemical nature from the mainly carbonaceous material obtained from the afterglow reaction.

The deposit from acetylene in the afterglow was apparently insoluble in all the ordinary solvents tried, alcohol, benzene, carbon tetrachloride, carbon disulphide.

When the deposit from C_2H_2 and the CO afterglow was heated in vacuum in the discharge tube it gave off a little gas, the spectrum of which showed CO bands. The deposit from active nitrogen gave off a little nitrogen, but this was quickly reabsorbed by the deposit in other parts of the tube. When the deposit (from active N_2) was heated in a little oxygen, the spectrum showed strong hydrogen lines, indicating release of hydrogen, probably as water, from the material. Heating of the acetylene/CO-afterglow material in oxygen showed mainly CO bands but with a trace of the hydrogen lines.

Discussion

If we assume that the CO afterglow gases contain either atomic carbon or C_2 molecules (and we know that some at least of the latter are present) and also assume that the carbonaceous deposits are initiated in the gas phase, then the present experiments would be consistent with a polymerization-dehydrogenation of acetylene on C or C_2 as nucleus, such as

$$\begin{aligned} C_2 + C_2H_2 &= C_4 + H_2 \\ C_4 + C_2H_2 &= C_6 + H_2 \end{aligned} \qquad \text{etc.}$$

These reactions are, of course, quite strongly exothermic and the energy released may initially be held at least in part by the growing carbon nucleus so that it remains hot and able to decompose the thermally unstable acetylene. The chemical composition of the carbonaceous deposit containing around 20 to 30 per cent of hydrogen (by numbers of atoms), or perhaps less if the oxygen atom is present as adsorbed water, is not very different from the composition of soot from flames; the composition of soots is rather variable but on the average contains about 12 per cent of hydrogen (by number of atoms).

We know that premixed flames of hydrocarbons contain C_2 molecules and that in many cases it is possible to detect the intermediate formation of acetylene in flames of rich mixtures (including flames of methane). Porter[2] has found that in his flash photolysis work the results for carbon formation are consistent with a mechanism via acetylene. The present afterglow results therefore suggest a possible detailed mechanism for carbon formation in premixed flames. It must, however, be emphasized that this is merely a suggestion, not a proved mechanism. The full tale of carbon formation is probably very complex. In diffusion flames we have strong evidence that solid carbon is formed before the C_2 and that some form of pyrolysis with build-up of large molecules occurs. Even in the afterglow experiments we note that there is also carbon formation from benzene and slightly from ethylene, so that other unsaturated compounds besides acetylene may act as intermediaries.

Acknowledgment

The early part of this work was done in collaboration with Dr. H. P. Broida, to whom we express our sincere thanks.

REFERENCES

1. Gaydon, A. G., and Wolfhard, H. G.: "*Flames, their Structure, Radiation and Temperature,*" Chapman and Hall, London, 1953.
2. Porter, G.: *Fourth Symposium (International)*

on Combustion, p. 248. The Williams & Wilkins Co., Baltimore, 1953.

3. Smith, E. C. W.: Proc. Roy. Soc. A, *174*, 110 (1940).
4. Broida, H. P., and Gaydon, A. G.: Proc. Roy. Soc. A, *218*, 60 (1953).
5. Broida, H. P., and Gaydon, A. G.: Trans. Faraday Soc., *49*, 1190 (1953).
6. Broida, H. P., and Gaydon, A. G.: Proc. Roy. Soc. A, *222*, 181 (1954).
7. Gaydon, A. G., and Wolfhard, H. G.: Proc. Roy. Soc. A, *213*, 266 (1952).
8. Herzberg, G., Astrophys. J. *89*, 290 (1939).

27

THE EFFECT OF HEAT TRANSFER ON THE MAXIMUM REACTION RATES OF A HOMOGENEOUS REACTOR

By E. A. DeZUBAY AND E. C. WOODWARD

Introduction

The beneficial effects that hot surfaces produce in promoting combustion have long been known [1, 2, 3], but the mechanism by which such combustion improvements occur has been in doubt. In this paper these effects will be analyzed with a model consisting of a homogeneous chemical reactor which experiences heat transfer with its boundary. With such a model the dependency of the homogeneous reactor on the wall temperature is predicted. The predicted dependency is then compared with experimental data.

Analysis of Reactor

Let us suppose that the region in which the combustion process occurs is so highly turbulent that this entire region can be considered to be homogeneous. This concept has been used previously in elucidating combustion phenomena[4, 5, 6]. Such a reactor would then behave in accordance with the following reaction equation:

$$rV = my \qquad (1)$$

where

r = reaction rate (moles/volume-time)
V = reactor volume
m = moles of mixture supplied/unit time to reaction zone
y = fraction of supplied mixture converted to products of reaction during residence in the reaction zone

The reaction process of air and fuel in this homogeneous reactor will be approximated by the following assumptions:

(1) There is no change in the total number of moles from the raw mixture to the burned products. This assumption is based on the high nitrogen concentration contained in the air.

(2) The model of the reaction proceeds in the following manner: The total molar flow (m) splits into an infinitesimal number of elemental masses on entering the boundaries of the reactor. A certain fraction (y) of these elemental masses burns to chemical equilibrium composition and attains the adiabatic flame temperature. The remainder ($1 - y$) remains unburned. It is further assumed that all of the constituents of the burned masses act only as diluents and can in no way contribute anything further to the reaction. This would mean that for every mole of fuel consumed per unit time, an amount of oxygen equal to the initial molar oxygen to fuel ratio would be consumed. The reaction rate (r) of the mixture would then be the sum of the reaction rates of the individual constituents undergoing reaction, namely the fuel and the oxidant. Denoting r_f and r_o as the reaction rate of the fuel and oxidant we have that

$$r = r_f + r_o .$$

But

$$r_o = \frac{1}{\eta} \frac{W_a}{M_a} \frac{M_f}{W_f} r_f ,$$

so that

$$r = r_f \left(1 + \frac{1}{\eta} \frac{W_a}{M_a} \frac{M_f}{W_f} \right)$$

where

W_a = weight of air supplied per unit time
W_f = weight of fuel supplied per unit time
M_a = molecular weight of air
M_f = molecular weight of fuel
η = moles of air per mole of oxygen in air = 4.76

(3) The reaction rate of the fuel r_f, is assumed

to be a second order reaction such that

$$r_f = kC_oC_f$$

where

C_f is the fuel concentration $= P_f/RT$
C_o is the oxygen concentration $= P_o/RT$
k is the specific rate of reaction
P_f is the partial pressure of the fuel
P_o is the partial pressure of the oxygen
T is the temperature of the burning zone
R is the universal gas constant.

Then

$$r_f = \frac{k}{(RT)^2} P_oP_f .$$

Since the partial pressure is the product of the mole fraction (n) and total pressure (P),

$$r_f = k\left(\frac{P}{RT}\right)^2 n_on_f$$

Now let γ_i be the molal inlet density P/RT_i, where T_i is the initial temperature of the unburned mixture, then

$$r_f = \gamma_i^2\left(\frac{T_i}{T}\right) n_on_fAe^{-E/RT}$$

where the specific rate of reaction is $k = A$ (exp $- E/RT$) if $T > T_i$ and zero if $T \leqslant T_i$, and E is the activation energy, and A is the frequency factor.

The mole fractions of oxygen and fuel available for reaction can be expressed in accordance with assumptions 1 and 2 as

$$n_o = \frac{1}{\eta}\,\frac{W_a/M_a}{(W_f/M_f + W_a/M_a)}\,(1 - y)$$

and

$$n_f = \frac{W_f/M_f}{(W_f/M_f + W_a/M_a)}\,(1 - y)$$

Hence

$$r_f = \gamma_i^2\left(\frac{T}{T_i}\right)^2\frac{(1 - y)^2}{\eta}\,\frac{(W_a/M_a)\,(W_f/M_f)}{\left(\frac{W_f}{M_f} + \frac{W_a}{M_a}\right)^2}\,A\left\{\exp - \frac{E}{RT}\right\}$$

and since $r = r_o + r_f = r_f\left(1 + \frac{1}{\eta}\,\frac{W_a}{M_a}\cdot\frac{M_f}{W_f}\right)$ as explained in assumption 2, the total reaction rate is

$$r = A\,\{\exp - E/RT\}\,\frac{\gamma_i^2}{\eta}\left(\frac{T_i}{T}\right)^2\frac{(1 - y)^2}{G}$$

where

$$G = \frac{\left(1 + \frac{M_a}{M_f}\cdot\frac{W_f}{W_a}\right)\left(1 + \frac{M_f}{M_a}\cdot\frac{W_f}{W_a}\right)}{\left(1 + \frac{1}{\eta}\cdot\frac{W_aM_f}{W_fM_a}\right)}$$

Then in terms of the molal flow (m) equation (1) yields

$$m = \frac{VA\gamma_i^2}{G\eta}\left(\frac{T_i}{T}\right)^2\frac{(1 - y)^2}{y}\,(\exp - E/RT) \qquad (2)$$

In order to examine equation (2) with respect to any effect the heat transfer may produce, a functional relation between y and T must be defined. Such a relation may be obtained from the energy equation. If the kinetic energy terms are neglected, the increase in enthalpy of the mixture on passing through the reactor must be equal to the chemical energy liberated in addition to any heat added. Expressing the chemical energy added in accordance with assumption 2, the energy equation is

$$(W_a + W_f)c(T - T_i) = yc(W_a + W_f)(T_f - T_i) + hA_s(T_s - T)$$

Then y can be defined as

$$y = \theta(1 + K) - K\varphi \qquad (3)$$

where

T_f = flame temperature if reaction would proceed to maximum possible completion (for example a bunsen flame)
T = reactor temperature
T_i = initial temperature of mixture
T_s = surface temperature of reactor containing walls
c = specific heat at constant pressure
y = fraction of fuel consumed
A_s = surface area of reactor containing walls
θ = $(T - T_i)/(T_f - T_i)$
φ = $(T_s - T_i)/(T_f - T_i)$
K = $hA_s/c(W_f + W_a)$
h = turbulent heat transfer coefficient

Using the above, the reactor temperature (T) may be shown to be

$$T = T_i + \theta(T_f - T_i)$$
$$= T_i(1 + \theta\alpha)$$

where α is the dimensionless flame temperature rise $(T_f - T_i)/T_i$.

Equation (2) combined with equation (3) is now expressible in a more convenient form as

$$\left\{\frac{m}{\gamma_i^2}\frac{\eta}{VA}\right\} = \frac{(1 - \theta(1 + K) + K\varphi)^2}{G(1 + \theta\alpha)^2(\theta(1 + K) - K\varphi)} \exp\{-E'/(1 + \theta\alpha)\} \tag{4}$$

where $E' = E/RT_i$.

For a fixed value of the fuel-air ratio, both G and α are determined. The former is directly dependent on the fuel-air ratio, while the latter is dependent on the adiabatic flame temperature, which in turn is dependent on the fuel-air ratio and the assumed constant ambient temperature. The flow variable $\left(\frac{m}{\gamma_i^2}\frac{\eta}{VA}\right)$ is then only a function of the dimensionless reactor temperature (θ), and the dimensionless wall temperature (φ). The general form of equation (4) is shown on Figure 1 for parametric values of reactor wall temperatures.

The physical significance of Figure 1 can be explained in the following manner. If a combustion reaction is established in the reactor of a fixed wall temperature at a low flow, it will be near the adiabatic value of θ_f where by virtue of equation (4) the concentration of the reactants in the reactor is very small. As the flow is increased the concentration of the reactants increases but the exponential component of the specific reaction rate decreases until a maximum flow is undergoing partial reaction at a temperature corresponding to θ_m. If the flow is further increased, the temperature can no longer accommodate the larger flow. The only region to which the temperature can shift is $\theta = 0$ where any flow is possible with no reaction occurring. Hence, the maximum flow that can pass through the reactor and still maintain combustion would be the maximum value at the temperature θ_m for a given value of the dimensionless reactor wall surface temperature (φ). It is also seen that an increase in the dimensionless reactor wall surface temperature (φ) results in a corresponding increase in the value of θ_m, the maximum reactor temperature attainable just prior to the cessation of burning (or blowout), and an increase in the maximized flow (m/γ_i^2) for a given fuel-air ratio.

This essentially shows that for a given fuel-air ratio the maximum flow which can be passed into the reactor before blowout increases with increasing reactor wall surface temperature. A family of curves similar to that shown in Figure 1 would exist for each fuel-air ratio considered. It is, therefore, possible to obtain another general family of curves connecting the maximum flow conditions $\{(m/\gamma_i^2)\eta/VA\}$ versus the dimensionless reactor wall surface temperature (φ) for a number of fuel-air ratios. An analysis of this family of curves enables one to predict theoretically the limiting fuel-air ratio for a given reactor wall temperature (T_s) for a fixed flow condition $\{(m/\gamma_i^2)\eta/VA\}$.

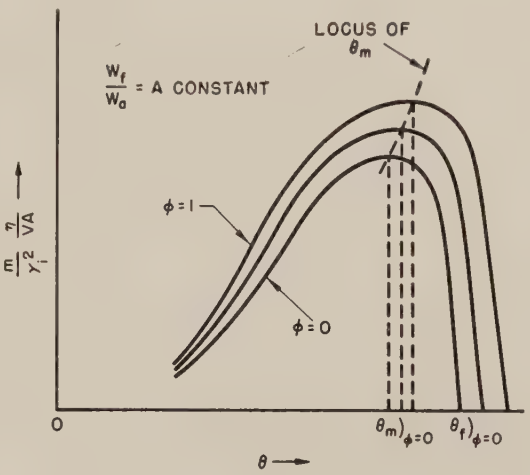

FIG. 1. General shape of equation (4) for constant fuel-air ratio and parametric wall temperatures.

Method of Calculation

The problem of maximizing $\{(m/\gamma_i^2)\eta/VA\}$ to establish the blowout point presents only a tedious task in mathematical manipulation. From equation (4) the flow will be a maximum when

$$\frac{\partial}{\partial\theta}\left\{\left(\frac{m}{\gamma_i^2}\right)\frac{\eta}{VA}\right\} = 0 \text{ for } \phi, \text{ and } \frac{W_f}{W_a} \text{ constant.}$$

Taking the logarithm of both sides of equation (4) and differentiating with respect to θ shows the maximizing equation to be

$$\frac{\alpha}{1 + \alpha\theta}\left(\frac{E'}{1 + \alpha\theta} - 2\right) = (K + 1)\left\{\frac{2}{1 - (K + 1)\theta + K\varphi} + \frac{1}{(K + 1)\theta - K\varphi}\right\} \tag{5}$$

In the process of evaluating the activation energy (E) and the collision factor (A) for use in

equations (4) and (5), recourse was made to the Semenov equation for burning velocity[7] shown below:

$$V_F^2 = \frac{2\lambda_1 c_1^2 AC}{\rho c^3}\left(\frac{T_0}{T_1}\right)^2\left(\frac{N_r}{N_p}\right)^2\left(\frac{\lambda}{\rho c\, d_v}\right)^2 \left(\frac{RT_1^2}{E}\right)^3 \frac{(\exp - E/RT_1)}{(T_1 - T_0)^3}$$

where

λ = thermal conductivity
C = moles of reactants per unit volume (moles oxygen plus moles fuel per unit volume)
d_v = diffusivity
N_r = moles of reactants
N_p = moles of products
T = temperature (absolute)
ρ = density
V_F = flame velocity

Subscripts 0 refer to unburned state while subscripts 1 refer to burned state

The collision factor (A) and the activation energy (E) were obtained by simultaneous application of the Semenov equation at two fuel-air ratios where the values of the flame velocity and flame temperatures were available[8, 9]. The accuracy of this method of obtaining A and E is expected to be fair, since, for good accuracy, the Semenov equation must meet the condition that $E/RT_f \geqslant 10$ and E/RT_F was found to be in the order of 8 for propane.

The values for the constants computed from the above scheme are:

Collision factor $A = 1.44 \times 10^{13}$ ft³/mole-sec

Activation energy $E = 4.27 \times 10^7$ ft lb/lb mole
$= 30.5$ kcal/gm mole

The dimensionless heat transfer factor $K = hA_s/(W_f + W_a)c$ was calculated on the assumption that the heat transfer coefficient (h) for the interior of a cylinder, the anticipated shape of the reactor, could be used if it were suitably modified to include any entrance effect. The value of the turbulent heat transfer coefficient for an annular space was found from the following equation[10]

$$h = 0.023\,\frac{\lambda}{D_e} R_e^{0.8} P_r^{0.4} \qquad (6)$$

where

D_e = equivalent diameter
R_e = Reynolds number
P_r = Prandtl number

The values of P_r and c for air at 2400°R (assumed average film temperature) were taken as 0.65 and 0.285 Btu/lb °F respectively[11]. The available range for the flow rate W_a is from 0.007 to 0.015 lb/sec. With the thought in mind that the calculated results were to be checked by experiment it seemed less time consuming to assume the reactor dimensions comparable to those eventually to be used in the experimental apparatus. On this basis, and for the available range of W_a the equivalent diameter (D_e) and the reactor wall surface area (A_s) were taken to be in the order of 0.11 ft and 0.11 ft² respectively. These values in equation (6) give a value of the turbulent heat transfer coefficient (h) of 7.92 Btu/hr ft² °F where an entrance effect of 2.2 was assumed due to the high turning angle assumed necessary to produce a high degree of turbulence[12]. This, therefore, gives a value of $K = 0.09 \pm 7$ per cent over the flow range $W_a = 0.007$ to 0.015 lb/sec. It is seen that K is relatively insensitive to changes in W_a as it is inversely proportional to the one-fifth power of W_a.

A calculation was made to check the effect of small changes in the dimensionless heat transfer factor K on the predicted family of curves depicting fuel-air ratio versus reactor wall temperature (T_s) for given fixed flow conditions $\{(m/\gamma_i^2)\eta/VA\}$. A change in K by ± 7 per cent failed to produce any significant change in the predicted theoretical results.

The flame temperatures (T_f) were found for a constant inlet temperature (T_i) for various fuel-air ratios[9]. Using these the various values of the dimensionless flame temperature rises (α) were calculated for the fuel-air ratios corresponding to the values of T_f and T_i used.

Knowing the value of T_i assumed in the calculations it is possible to calculate E' based on the activation energy (E) obtained from the Semenov equation.

$$E' = \frac{4.27 \times 10^7}{1545 \times 537} = 51.47$$

where

R = 1545 ft. lb./lb.-mole °R
T_i = 537 °R

The substitution of these values into the maxi-

mizing equation (5) results in the following simplified form

$$\frac{\alpha}{1+\alpha\theta}\left(\frac{51.47}{1+\alpha\theta}-2\right)=\frac{2}{B_1-\theta}+\frac{1}{\theta-B_2} \qquad (7)$$

where

$$B_1=\frac{1}{K+1}+\frac{K\varphi}{K+1}=0.9173+0.0827\varphi$$

$$B_2=\frac{K\varphi}{K+1}=0.0827\varphi$$

The rather tedious task of the trial and error maximization of equation (7) and subsequent maximization of equation (4) was accomplished through the use of the following steps:

(1) Using the constant inlet temperature (T_i), the dimensionless flame temperature rise (α) was calculated for a given fuel-air ratio. The value of the left side of equation (7) was then calculated for assumed values of the dimensionless reactor temperature (θ) and plotted versus θ.

(2) The right side of equation (7) was evaluated using the same assumed values of the dimensionless reactor temperature (θ) for various values of the independent parameter (φ). The values of the right side of equation (7) were plotted versus θ on the same plot mentioned in step 1 above.

(3) The intersection of a curve representing the right side of equation (7) with that representing the left side was recorded as the maximum value of the dimensionless reactor temperature (θ) for a given value of φ and α.

(4) This maximum value of θ is then placed in the right side of equation (4) along with the corresponding values of α, φ, and G. The resulting values of the maximized flow conditions $\{(m/\gamma_i^2)\eta/VA\}$ are then plotted for a given fuel-air ratio versus the reactor wall surface temperature (T_s).

(5) From the plot described in step 4 the values of fuel-air ratio versus reactor wall surface temperature (T_s) for a constant maximized flow condition are plotted. The maximum values of $\{(m/\gamma_i^2)\eta/VA\}$ versus fuel-air ratio are shown for various reactor wall temperatures (T_s) on Figures 2 and 3. Figure 2 represents the lean fuel-air ratios while Figure 3 represents the rich fuel-air ratios.

Description of Experimental Equipment

In order to approach the condition of a homogeneous reactor, the test burner was to be as turbulent as possible. To achieve a highly turbulent condition a reversed flow reaction chamber was desired. The test equipment for conducting these experiments is shown on Figure 4. Basically the reaction chamber consisted of a ceramic cup opening into a mixing chamber. The fuel injector tube extended into the ceramic cup so that the unburned fuel-air mixture must, on emerging from the fuel injector tube, execute a 180° turn in passing through the ceramic cup. Electric heaters and a water jacket surrounding the

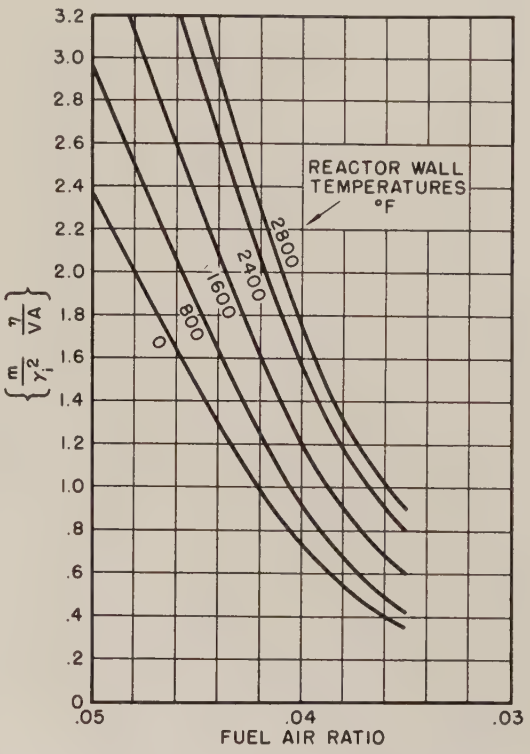

FIG. 2. Maximum flow conditions for lean fuel-air ratios and various reactor wall temperatures.

ceramic cup permitted a relatively large variation in the ceramic wall temperature. The fuel injector tube (0.72 in. diameter) was made of stainless steel and coated with National Bureau of Standards Coating A-418. The end cap in the injector tube contained twenty 0.0700 in.-diameter holes to isolate the burner system from the fuel and air supply system.

The products of combustion on emerging from the ceramic reaction chamber entered the mixing chamber where secondary air was added. Secondary air was introduced by stub tubes thereby diluting and chilling the products of combustion. Complete mixing was obtained by passing the

mixture through the can mixer formed by the downstream section of the flame tube, into the outer annulus, and then into the shielded measuring section which was adequately instrumented with thermocouples.

All fluids were measured by calibrated flow-

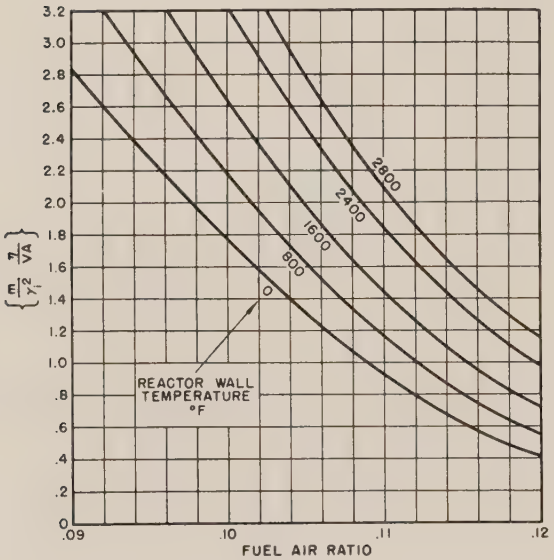

FIG. 3. Maximum flow conditions for rich fuel-air ratios and various reactor wall temperatures.

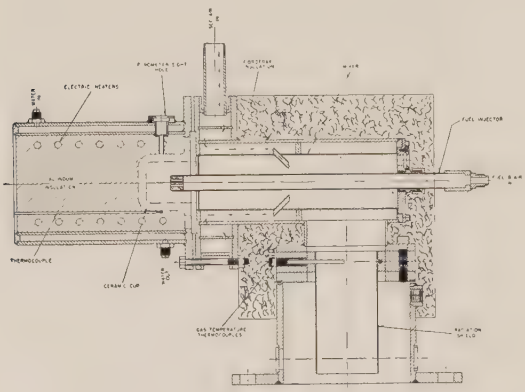

FIG. 4. Ceramic burner.

rators maintained at a constant pressure of 30 psia by pressure regulators. The fuel had a guaranteed composition of a minimum of 95 per cent propane, with the remaining gases being ethane and butane.

Three types of ceramic cups were used in these experiments. These were silicon carbide bonded with silicon nitride, stabilized zirconium oxide, and high strength porcelain. The size of all these cups was the same; namely, 2 in. in diameter and 2 in. deep, inside dimensions.

Description of Test Procedure

To determine the relation between the limits of stable burning and the reactor wall temperature, combustion with fixed flow conditions was established in the test passage, and the fuel rate was increased or decreased until burning ceased in the ceramic cup. Sufficient time always elapsed between fuel rate changes so that equilibrium conditions were attained. When blowout occurred, a lean flame would go out completely in the entire test passage; but on the rich side the flame, after burning ceased in the cup, was still anchored in the annular step formed by the transite ring at the exit of the cup and the start of the mixing section. Both types of blowouts were immediately apparent by the sharp drop in the ceramic surface temperature indicated on a recording potentiometer.

Pressure levels of 5.90 and 8.35 psia were used with primary air flows of 0.007, 0.010 and 0.015 pps. The secondary air flow was maintained at 0.050 pps, after ascertaining that any variation in the secondary air flow had no effect on the blowout point. All three of the previously mentioned ceramic cups were used. In a special test, one of the silicon carbide cups was coated with platinum on the flame exposed surface. This was done to observe any possible catalytic surface effect. This coated cup behaved exactly like any other uncoated cup. The limits of stable burning for all cups tested are shown on Figure 5.

Conclusions

A comparison of the calculated variation of the limiting fuel-air ratio with reactor wall temperature is shown on Figure 6, together with experimentally obtained points. The agreement between the calculated and experimental trends is quite good especially in the rich range. On the lean side the calculated stability limits are somewhat higher than the experimentally obtained ones. However, the agreement is within the range of error expected, if consideration is given to the assumptions made in the calculation of the stability limits. Essentially, the kinetic constants E, the activation energy, and A, the frequency factor, are calculated from experimentally obtained flame velocities, and computed flame temperatures by means of the Semenov equation. Hence these constants would reflect any errors in the

data together with any inaccuracies introduced by the use of Semenov's equation. In the entire

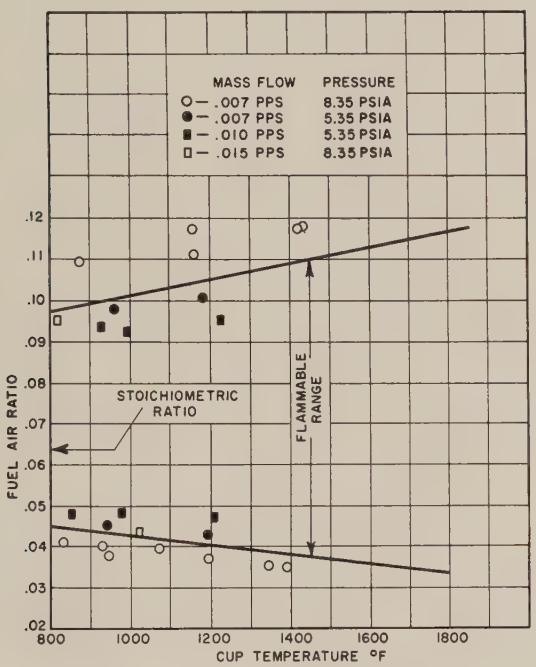

FIG. 5. Stability range of cup burners.

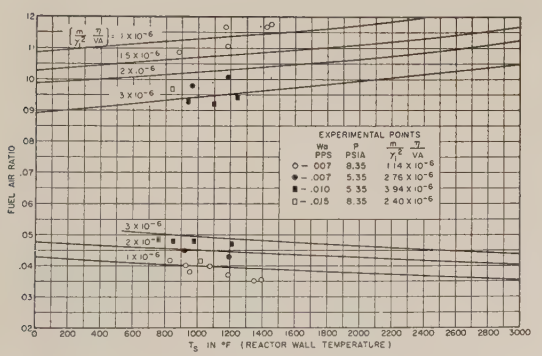

FIG. 6. Comparison of calculated and experimental maximum reaction in a homogeneous reactor with heat transfer.

analysis a second order reaction is assumed which, although a good approximation, may not be entirely accurate. In the light of these assumptions, the agreement between experiment and theory as shown on Figure 6 can certainly be considered more then adequate.

In conclusion then, increasing the temperature of the containing walls of a highly turbulent combustion process widens the limits of stable burning. The widening of these limits can be predicted quite accurately if the containing walls are considered as heat sinks. The amount of heat removed by these surfaces reduces the reacting gas temperature which limits the chemical reaction rate accordingly.

Acknowledgment

The authors wish to express their gratitude to Harrison J. Killian and Gerald H. Farbman, for their assistance in the experimental phase of this program.

REFERENCES

1. BACON, R. F., AND HAMOR, W. A.: *American Fuels*, Chapter XIV, McGraw-Hill Book Co., New York, 1927.
2. BONE, W. A., AND TOWNSEND, D. T.: *Flames and Combustion in Gases*, Chapter XXXVI. Longmans, Green & Co., New York, 1927.
3. WEIR, JR., A.: Ind. & Eng. Chem., *45*, 1637 (1953).
4. DEZUBAY, E. A.: Proceedings of Midwestern Conference on Fluid Mechanics, The Ohio State University Press, 459 (1952).
5. LONGWELL, A. P., FROST, E. E., AND WEISS, M. A.: Ind. & Eng. Chem., *45*, 1653 (1953).
6. AVERY, W. H., AND HART, R. W.: Ind. & Eng. Chem., *45*, 1634 (1953).
7. EVANS, M. W.: Chem. Rev., *51*, No. 3 (1952).
8. JOHNSTON, W. C., Westinghouse Research Laboratories, East Pittsburgh, Pennsylvania (1953): Private communication.
9. SMITH, R. W., EDWARDS, H. E., AND BRINKLEY, JR., S. R.: U. S. Dept. of Interior, Bureau of Mines, Report of Investigations 4938 (1953).
10. MCADAMS, W.: *Heat Transmission*, 2nd edition, p. 168. McGraw-Hill Book Co., New York, 1942.
11. KEENAN, J. H., AND KAYE, J.: *Thermodynamic Properties of Air*. John Wiley & Sons, New York, 1945.
12. BOELTER, L. M. K., YOUNG, G., AND IVENSEN, H. W.: NACA TN No. 1451 (1948).

28

RATIONAL PREDICTION OF COMBUSTION EFFICIENCY FOR BAFFLE-TYPE COMBUSTORS

By GILBERT S. BAHN

Introduction

Considerable success has been attained in prediction of flameholder stability in ramjet engines, having non-uniform profiles of fuel/air ratio and of gas flow parameters, by combination of the treatments of DeZubay and Longwell[1, 2, 3, 4]. Such success affords confidence that fuel distribution patterns can be calculated with reasonable accuracy from combustor geometry, fuel flow rates, and the gas flow parameter profiles. This in turn raises the question of whether the same basic information can be employed to calculate combustion efficiency. Any satisfactory correlation could be employed, along with reasonable assumptions for the gas flow parameter profiles, to allow an estimation of performance for a hypothetical engine before the design ever progressed even to the stage of drawings for development manufacture. Thus manufacture and testing could be restricted to only the most promising designs.

A "blacksmith" or "brute force" calculation scheme has been devised, and has given limited correlation between computed and actual combustion efficiencies when applied to a small number of ramjet engines. The calculation scheme depends upon all of the parameters used for prediction of flameholder stability, and of course is concerned with the stability itself, in assignment of flameholding regions from which flamespreading occurs. In particular the presence of steady-state combustion is assumed, so that the gas flow profiles correspond to the burning condition. The principal techniques of the calculation scheme are: (1) use of Scurlock's graphs which relate burned and unburned gas velocities before and after combustion[5, 6]; and (2) application of the second-order reaction rate equation to the combustion process in order to evaluate reaction times.

To compute a predicted efficiency, it is necessary to estimate the extent of reaction at the engine exhaust, over the flow cross-section. For this estimation there are required: (1) the theoretical reaction time, as a function of local fuel/air ratio; (2) the residence time within the combustor of individual streamtubes; (3) a contour map showing the local (streamtube) fuel/air ratios; (4) the areas of flame stabilization; and (5) the extent of the progress of reaction initiation over the rest of the cross-section. From these factors one can determine which streamtubes have completed reaction at the engine exhaust, and thus predict what temperatures they have attained. The computation of the corresponding combustion efficiency follows directly.

Reaction Time

The second-order reaction rate equation assumed to apply is:

$$\frac{dx}{dt} = ke^{(-\Delta E/RT)}\ (a - x)\ (b - x) \qquad (1)$$

where a, b and x are all in stoichiometric units per pound of mixture, and a represents fuel, b represents air, and x represents the products of reaction. A stoichiometric unit of fuel is 0.0625 lb and a stoichiometric unit of air is 0.9375 lb, for a stoichiometric fuel/air ratio of 0.0667. A stoichiometric unit of combustion products thus consists of the combustion products of one pound of stoichiometric fuel/air mixture. The normal expression for the reaction rate equation is in terms of concentrations per unit volume. To bring equation (1) into agreement, the parameter k accounts not only for the customary collision frequency factor but also for density effects. Both pressure and temperature contributions to density were assumed to be fixed. k would be expected to correlate with a particular static pressure level. Theoretically, of course, assuming maintenance of density equilibrium throughout the course of reaction, k should vary with temperature while the exponential term varies. However, it was convenient to assume that in this regard T remained at the pseudoignition temperature value. This approach accentuated a favorable characteristic of the equation, as discussed below.

Equation (1) implies that there is reaction, however slow, at even very low temperatures. However, the self-accelerating tendency of the reaction then is practically nil. This of course is in agreement with reality, where autoignition does not occur in low temperature mixtures. Thus a source of preheating to a pseudoignition

temperature is required, assuming a steady-state system without continuous external ignition. At the pseudoignition temperature, the temperature rise rate due to reaction greatly exceeds that due to heating by external means.

Time zero is considered to pertain to the achievement of pseudoignition. This is when reaction products are mixed into fresh gas in quantity x_0, as based upon the mixture composition. This is exactly the same as if x_0 reaction products had really been produced in the fresh gas. Therefore $(a - x_0)$ and $(b - x_0)$ are less than a and b, respectively.

For the kerosene-type fuels of interest it was assumed that the pseudoignition temperature was 1800°R. The entering fuel/air mixture temperature was taken as 900°R. It was assumed as a basis of calculation that the entering fuel/air mixture was heated from 900°R to 1800°R by sufficient admixture of recirculating combustion products of the same fuel/air ratio. Accordingly the fuel/air ratios of lowest flame temperatures required the greatest amounts of recirculated products in order to attain mixture temperatures of 1800°R.

When there is incomplete combustion, it follows from the algebra that x and a are related to the fuel/air ratio of the fuel which has burned:

$$(\mathrm{f/a})_{\mathrm{burned}} = \frac{0.0625x}{1 - 0.0625a}$$

$0.0625\ (a - x)$ represents the unburned portion of the fuel. There is, of course, a theoretical temperature rise corresponding to this burned fuel/air ratio. The unburned fuel reduces the actual temperature rise below this value by absorbing heat and rising in temperature to an equilibrium value. A graph was prepared to indicate ΔT for incomplete reaction as a function of both the fresh gas fuel/air ratio, corresponding to a, and the extent of reaction, corresponding to x. This was based upon heat capacities for kerosene-type fuels, estimated without regard for thermal cracking. Thus it was possible to relate T to x, in order to evaluate the exponential term of equation (1).

Now only ΔE was required in order to proceed to the graphical integration:

$$(kt) = \int_0^t k\,dt = \int_{x_0,\,T=1800^\circ\mathrm{R}}^{x,\,T=T_t} e^{(-\Delta E/RT)}\,\frac{dx}{(a - x)(b - x)} \tag{2}$$

Certain data from development testing of baffle-type combustors indicated that for kerosene-type fuels 48,000 cal/gram-mol was a reasonable assumption. This value is subject to verification or modification as more data become available, especially as regards its range of application. A higher value, under the assumptions employed, would have little effect upon the results presented below. A significantly lower value, say below 40,000 cal/gram-mol, would seriously complicate the calculations.

The graphical integration yielded plots of (kt) versus x for the various fixed values of mixture fuel/air ratio. The great bulk of the total reaction time was required to achieve less than 50 per cent completion of reaction for fuel/air ratios richer than about 0.03. The added time required for progression on to about 99 per cent completion was negligible when compared with the time required for the first 50 per cent of reaction. Finally, when the reactant concentrations were almost depleted, the rates did fall off again despite the high temperatures attained. For mixtures around stoichiometric f/a, this eventual decrease in rate became effective only appreciably beyond 99.9 per cent completion. For mixtures leaner than 0.03 f/a, the decrease was rather significant for the last 10 per cent of reaction, approximately, but for convenience this exception was ignored.

The consequence of the very rapid rate of substantial completion of reaction, compared to the relatively slow initial rate, and relatively small initial temperature rise, is this: One can, without outrageous liberty, assume zero reaction (actually, zero temperature rise) in material removed d (f/a) concentration-wise from material which has burned to 99-plus per cent of completion. Thus, instead of a cross-plot of ΔT versus f/a and arbitrary time units of (kt), one can settle for a single plot of f/a (burned) versus (kt) (Fig. 1), and the companion plot of ΔT, corresponding to f/a (burned), versus (kt). This is the fortuitous outcome of the high value of ΔE and the disregard of the effect of temperature upon density, as cited above.

Because of these factors, too, there is no particular significance to the stoichiometric point. When a goes well beyond stoichiometric there is but little diminution of b correspondingly, and per unit volume there is considerably greater quantity of *total* reactants. With the reaction time controlled by the really low temperature rise period corresponding to small values of x, it

is of scant consequence that ΔT for complete reaction of over-rich mixtures is less than the corresponding value for stoichiometric mixtures.

All of the above treatment is concerned with the calculations as a mathematical task, of course. Presumably when mixtures are significantly richer than stoichiometric the simple second-order reaction with $\Delta E = 48{,}000$ cal/gram-mol based upon the first reaction step is no longer valid (see Appendix), and at some point the required reaction time goes through a minimum and then increases with increasing value of f/a. In the light of DeZubay's work it was decided to accept the curve up to the rich blow-out fuel/air ratio given by DeZubay, and to employ the same time value for even richer mixtures.

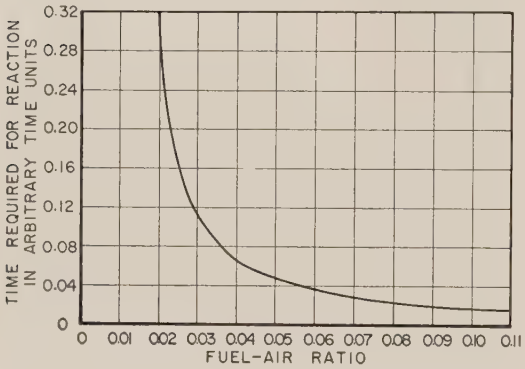

FIG. 1. Theoretical reaction time as a function of fuel/air ratio.

DeZubay's graph of stability limits of f/a is based upon recirculation as a source of steady state combustion in the flameholder protective regions. The lean blowout limit of f/a tends toward 0.038, which apparently cannot be decreased further by any additional improvement of the stability parameter. This is logical because there obviously is some limitingly low value of f/a below which the combustion reaction requires more time than the recirculation time. Let an outside ignition source initiate reaction, after which the igniter is removed. As the material last set off by the igniter completes reaction and is otherwise available to ignite fresh gas, it is too far downstream for recirculation currents to carry it back upstream into the flameholder vortex trails. Thus the flame goes out. Yet flamespreading into so weak and slow burning a mixture has not been precluded. It is noteworthy that rapid increase, with decreasing f/a, of requisite reaction time commences at a value of f/a of about 0.035, corresponding to DeZubay's lower limit of 0.038.

For application of the reaction time calculations it was necessary, obviously, to approximate the value of k. The product (kt) from equation (2) has been labeled in Figure 1 with units of atu (arbitrary time units). k was estimated to be 20 atu/sec, based upon crude data for pressures of 1 atmosphere and greater, so that t in seconds was equal to $\frac{1}{20}$ (kt). Still, this conversion factor was applied to the ramjet data where the pressure was less than 1 atmosphere, and seemed to work out quite well. On this basis a factor of more than 20 atu/sec would seem appropriate for data of tests made at 1 atmosphere pressure or greater.

Fuel/Air Ratio Contour Map

A drawback to the application of the calculation scheme here outlined to studies of purely hypothetical engines is the ignorance in such cases of air flow patterns. However, in general terms it may be considered that no engine with reasonable aerodynamic design is going to have completely unpredictable air flow patterns (unless the combustion process proves unstable). Furthermore, probably the result by which the predicted gas flow pattern for a hypothetical engine deviates from that which the engine would actually produce, if built and tested, is no worse than the deviation between calculation and reality for the ramjet engines examined here.

This study dealt with engines for which fuel distribution calculations had already been made. These calculations were based upon gas flow (i.e., pressure) measurements at two axial stations, made concurrently with procurement of data for the combustion efficiency calculations. What was available to this study, therefore, was the gas flow pattern approaching the flameholder. Also there were several fuel distribution profiles, of f/a versus radial position. These permitted extrapolation into a contour map of f/a (Fig. 2), upon which the flameholder outline was superposed. The difficulty lay in relating the air flow pattern downstream of the flameholder blockage to the measured pattern upstream, so that each given fuel/air profile could be transposed; the contour map had to represent the downstream situation, of course. The relationships applied were thought to be passable; it would be best, if possible, to employ refinements based upon aerodynamic theory in future calculations.

From the flameholder on to the exhaust nozzle it was assumed that there was no further diffusion of fuel. Even the flow past the flameholder was

assumed to affect only the position of streamlines, and not to produce any mixing of one streamline with another. This is probably the most extreme assumption of the whole calculation scheme. However, it is seen that once combustion is initiated, diffusion becomes a very complex problem. Not only are there concentration gradients of the original kind, but also new gradients across the flamefront. The apology for the assumption is thus based upon expedient dealing with this fact, as well as upon the apparent absence of serious consequence to the total method.

The contour lines of fuel/air ratio and the boundary lines of the flameholder elements serve to delineate individual zones of interest on the contour map. Thus, for example, there may be an annular region of fuel/air ratio between 0.040 and 0.045, which may be segmented into zones by intersection with radial flameholder outlines. Each such zone would be considered to have a mean fuel/air ratio of 0.0425, it being assumed that the annulus width is narrow enough to permit linear interpolation.

The easiest situation to deal with is, of course, that where the gas velocity is constant just downstream of the flameholder (but before any combustion). If the flow profile is too uneven, then two or more separate regions must be marked off on the contour map, each of which can be assigned a mean unburned velocity value. Drawing in of the boundaries of such regions will most likely subdivide some of the zones of different fuel/air ratios.

Effect of Combustion Upon Gas Velocity

Obviously all of the material within the combustion duct must speed up as combustion proceeds and the mean density decreases. Scurlock[5] has examined the case of a homogeneous fuel/air mixture burning by flamespreading from a point source of ignition The requirement of homogeneity is not important here and the point source is not an essential requirement in applying Scurlock's data: when a given temperature rise has been obtained in a given fraction of the flow, the particular velocity profile within the burned region is not extremely important. One is concerned with apportioning the available flow area between the burned and unburned gases, and can approximate the actual apportionment by proper interpretation of Scurlock's calculations.

The appropriate graph shows the ratio of flame area to chamber area as a function of fraction burned. There are lines of various density ratios, after and before combustion, for the burned gas. In our case, fraction burned means fraction of flow in which combustion has occurred, and not fractoin of total fuel which has burned. Subscript 1 refers to no combustion and subscript 2 to combustion of part of the material. Subscript burned refers to material which *does burn* between 1 and

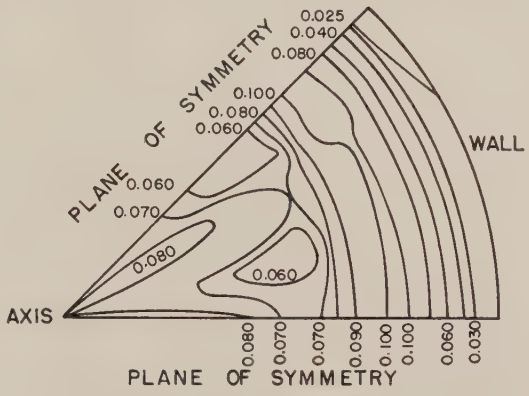

FIG. 2. Sample fuel/air ratio contour map.

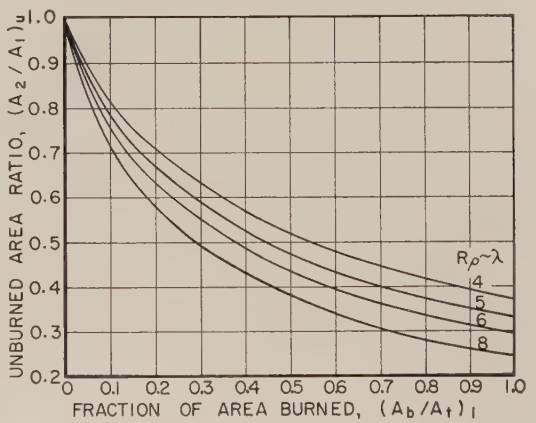

FIG. 3. Relationship between burned and unburned gas cross-sectional areas, before and after combustion, for several density ratios.

2; note that at 1 this material is as yet still unburned, although its area is there designated as $A_{1\text{, burned}}$. The flame area is $A_{2\text{, burned}} \cdot A_{1\text{, unburned}}$ is the complement, out of the total area, of $A_{1\text{, burned}}$ and similarly $A_{2\text{, unburned}}$ is the complement of $A_{2\text{, burned}}$. For convenience Scurlock's data were converted to show $(A_2/A_1)_{\text{unburned}}$ versus $(A_{1\text{, burned}}/A_{1\text{, total}})_1$ (Fig. 3).

Before any combustion occurs, the average Mach number of all the gas in each region is known from its weight flow and total pressure and temperature. In the unburned portion the

total temperature and pressure remain constant (by assumption, and reasonably so in practice), so that the new *unburned gas* Mach number can be established *for each region* on the basis of the over-all area ratio before and after combustion of the burned gas. Now the new velocity can be computed for the unburned gas in each region.

No loss of total pressure through the flamefront was to be allowed for in the calculations, as a simplifying assumption. However, as the combustion approached completion the change in Mach number was to effect a sufficient change in the ratio of total to static density so that this compressibility effect as well as the total temperature ratio was considered. The temperature effect was by far the more important, of course.

On the basis of a broad approximation, the true theoretical temperature rise–fuel/air ratio graph[7] was supplanted by three linear relationships for separate portions of the ideal curve of temperature rise ratio versus fuel/air ratio. This enabled the density ratio to be computed and Scurlock's graphs to be employed conveniently (without repetitive reference to a graph of ΔT versus f/a).

The combustion temperature ratio, $\lambda = (\Delta T + T_{\text{inlet}})/T_{\text{inlet}}$, is taken as the density ratio, R_1. The temperature rise ratio is obviously $(\lambda - 1)$. These relationships were obtained with conversion assumed complete:

$$\text{f/a} \leqslant .050,\ (\lambda - 1) = 3.5\,\frac{\text{f/a}}{.050} = 70\ \text{f/a}$$

$$050 \leqslant \text{f/a} \leqslant .070,\ (\lambda - 1) = 2.25 + \frac{\text{f/a}}{.040}$$

$$= 2.25 + 25\ \text{f/a}$$

$$.070 \leqslant \text{f/a},\ (\lambda - 1) = 5.4 - \frac{\text{f/a}}{.050} = 5.4 - 20\ \text{f/a}$$

The mean fuel/air ratio for each zone under consideration was employed to compute the mean value of $(\lambda - 1)$ for this zone. On the basis of weighting the $(\lambda - 1)$ values according to the size of the zones, the mean value of $(\lambda - 1)$ for all zones burned so far could be computed, and this provided λ_z.

Flameholding and Flamespreading

Combustion was assumed to proceed on the following basis:

(1) For the material in the projected areas of the flameholders which is rich enough to hold flame according to the appropriate value of the DeZubay stability parameter, the combustion reaction commenced at the downstream face of the flameholder.

(2) For the material not in the projected areas of the flameholders (or that too lean to hold flame even though in a flameholder projected area), the combustion reaction commences at the zone boundary when the adjacent flameholder zone completes combustion (actually, when the adjacent region reaches ignition temperature), and spreads through the region with a certain turbulent flamespreading velocity. The latter is hereby defined as the velocity of the spread of reaction *initiation*. For fuel/air mixtures at temperatures of about 900°R this turbulent flamespreading velocity was assumed to be 70 in/sec, based upon observations of flamefront angles. This value was considered applicable to average fuel/air ratios, and probably too high for lean mixtures.

In initiating the actual performance calculations, the stability parameter was evaluated for each flameholder element, and the corresponding rich-limit fuel/air ratio was established. Then the requisite reaction time was ascertained. All zones in the flameholder projected area of rich-limit or greater fuel concentration were considered together. The reaction time divided by the unburned gas velocity established the axial position at which these zones completed combustion. Their fraction of the contour map area and their mean value of temperature rise ratio permitted the modified Scurlock graph to be read, and the new unburned gas velocity to be calculated.

Now it was assumed that the next richest zones moved on downstream at this new velocity until they completed combustion. The additional distance was computed, for the additional time beyond that required by the richest zones. The calculations continued, for succeedingly leaner zones, until all of the material in the flameholder projected area had burned (exclusive of any leaner than the lean stability limit).

It now was necessary to deal with the remaining material, into which flame had to spread from the combustion stabilized by the flameholder. To employ the turbulent flame velocity of 70 in/sec noted above, it was assumed that any increase in this value resulting from heat transfer into the unburned material could do no better than offset any diminution associated with spread into rather lean mixtures.

Analysis was made on the basis of one configuration which exhibited nearly ideal annular

fuel/air ratio zones outside of an annular flameholding element. This afforded the opportunity to examine radial flamespreading very simply. The use of the modified Scurlock graph enabled calculation of the instantaneous radius of the gas which, on the contour map, at time t_0 and axial distance z_0, had been at the edge of the flameholder. Similarly the instantaneous radii of annuli beyond the flameholder edge were also calculated.

Now the flamefront moved into these exterior annuli at the assigned 70 in/sec, initiating reaction in larger and larger fractions of fresh gas per inch of travel as the fresh gas became squeezed into smaller and smaller flow area. After consideration was given to the requisite time for completion of part of this flamespreading combustion, adjustment could be made for its own contribution to area appropriation. Finally, a value was arrived at which denoted the velocity, over the map surface, of the front of reaction initiation. This amounted to 360 in/sec on the original, full-scale contour map, roughly five times the assumed value of the basic flamespreading alone.

Now it was possible to proceed on the contour map with the following steps:

(1) From the time of completion of reaction in each flameholding zone, compute each remaining time of residence of adjacent unburned gas up to some arbitrary reference value of z.

(2) Compute the spread over this remaining time (at 360 in/sec) of the front of reaction initiation into the unburned region from the adjacent flameholding region.

(3) Measure off this spread on the contour map and draw the front of reaction initiation.

(4) Compute the residence time between the reference z and the nozzle exit, and determine the (lean) limiting fuel/air concentration which would burn in this residence time.

(5) For all fuel/air concentrations greater than this limiting value compute a further spread at 360 in/sec until the remaining time was just sufficient to burn the material into which the reaction front had been advanced; similarly, compute backwards from the reference line a diminished spread for concentrations less than the limiting value.

(6) Thus establish a flamefront (of reaction completion) applying to the nozzle exit, with gas within the flamefront assumed to have burned to completion and gas outside assumed to be at the diffuser inlet temperature.

Combustion Efficiency

Now the predicted effective combustion efficiency could be calculated, based upon the concept of non-mixing of stratified temperature streamtubes[1]. Each individual zone of the contour map was assumed to be at the combustion temperature of its representative fuel/air ratio if reaction was complete, and at the inlet gas temperature if reaction was incomplete. The thrust equation was written for the streamtube through each contour map zone. The individual values were summed, and equated to the expression for thrust based upon a single gas stream. Solution of the latter provided the effective over-all combustion temperature, T_c.

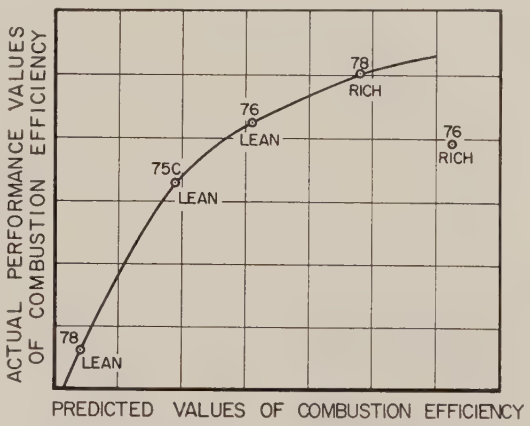

FIG. 4. Comparison of actual and predicted values of combustion efficiency.

Corresponding to the over-all fuel/air ratio there was a theoretical ΔT_e. Thus

$$\eta_c = \frac{T_c - T_{in}}{(\Delta T_e)_{th}}$$

Comparison of these values of η_c with the actual performance values derived from test measurements of thrust is presented in a schematic manner in Figure 4. The numbers shown on the graph are configuration code numbers, and "rich" and "lean" refer to the over-all fuel/air ratio. Four of five points yield a very reasonable graph; the fifth is discussed below. The actual efficiencies were greater than the predicted values, which may be accounted for on the basis of gas stratification.

The major source of hypothetical inefficiency is the *extreme* stratification caused by having unburned zones adjacent to burned zones. This is much more important than simple failure to burn all of the fuel, or the existence after combustion

of stratified temperatures corresponding to stratified fuel/air concentrations. Of the latter two possibilities, one is exemplified by 95 per cent combustion throughout a homogeneous mixture, and the other by complete combustion of adjacent parcels of 0.03 and 0.06 fuel/air ratio. Although both of these cases are detrimental, it is much more severe to have the extreme temperature stratification of complete combustion in 95 per cent of a homogeneous mixture and zero combustion in the adjacent 5 per cent. Of course there is actually considerable destratification downstream of the flameholder. Thus actual combustion efficiencies indeed ought to be greater than the predicted values based upon the contour map made at the flameholder.

It may be postulated that the expected progress of destratification will be influenced by the degree of stratification present. This is, after all, a diffusion process and will proceed more rapidly for a steep concentration gradient than for a moderate gradient. Thus there should be less disagreement between hypothetical and actual values of η_c with a contour map which shows fairly uniform fuel/air concentrations, than with one showing more widely variant concentrations. The one point of the five which does not fall in line may likely be accounted for on this basis; it is nearest to agreement as expected from its fairly uniform fuel/air profiles.

It will be noted that, for security reasons, the coordinates of the data points of Figure 4 have been omitted. The scales are not equal, but both are linear. The figure represents an early stage of correlation development. For the program to which it applies it serves as a bench mark for evaluation of additional "paper" engines. On the basis of there being a minimum acceptable actual combustion efficiency, any "paper" engine yielding a predicted point corresponding to actual performance below this standard would be rejected immediately. In a comparable engine development, a few actual data points would be employed to establish a graph similar to Figure 4, and this graph might then be used in the same way to limit developmental design, manufacture, and test evaluation.

Further work on this analytical tool should be expected to lead eventually to a general correlation. The case for showing the existence of such a correlation has been presented by Godsave[8], in discussing his droplet vaporization data. Once existence of a correlation is demonstrated, there is basis and encouragement for developing it into a completely reasoned and documented scheme having general application.

Appendix

Certain instances have been observed in operation of can-type combustors where rather marked differences in flame appearance occurred upon change of operating conditions. In general, engines exhibit flames of mixed color, partly blue and partly yellow, the degree of yellowness generally increasing with increase of the gross fuel/air ratio. There is considerable evidence that yellow-flame combustion proceeds in one manner (carbonic) and blue-flame combustion in another (aldehydeous). This is discussed in detail by Harvey[9]. Seemingly carbon particles give a much more intense light than do the particles associated with blue-flame reaction, thus producing a fairly strong appearance of carbonic combustion while the aldehydrous combustion is still quite predominant in extent and in control of the reaction rate[10]. The studies made to date on energies of activation and on reaction rates presumably deal with blue-flame combustion; when yellow-flame combustion *actually* predominates, a really different process must be occurring. Thus there can be no major objection to provision for a change in energy of activation (upon the advent of appreciable yellow-flame combustion) at near-stoichiometric proportions.

Nomenclature

A	Cross-sectional gas flow area
a	Fuel concentration
b	Air concentration
ΔE	Energy of activation
f/a	Fuel/air ratio on mass basis
k	Parameter accounting for collison frequency and density
R	Gas constant
R_1	Gas density ratio over reaction distance
T	Temperature
t	Time
x	Combustion products concentration
z	Axial distance from baffle
η_c	Combustion efficiency
λ	Gas temperature ratio over reaction distance

SUBSCRIPTS

$_1$	Before any combustion
$_2$	After some combustion
$_b$	Burned
$_u$	Unburned
$_t$	Total

REFERENCES

1. Friedman, J., Bennet, W. J., and Zwick, E. B.: *Fourth Symposium (International) on Combustion*, pp. 756–764. The Williams & Wilkins Co., Baltimore, 1953.
2. Bjerklie, J. W.: *A Combustor Analysis Method Evolved from Basic Flame Stability and Fuel Distribution Research.* Marquardt Aircraft Co., Preprint, 1954.
3. DeZubay, E. A.: Aero Digest, *61*, 54–56, 102–104 (July 1950).
4. Longwell, J. P., and Weiss, M. A.: Ind. & Eng. Chem., *45*, 667–677 (1953).
5. Scurlock, A. C.: Meteor Report No. 19, Fuels Research Lab., M. I. T. (May 1948).
6. Tsien, H. S.: J. App. Mech., *18*, 188–194 (1951).
7. Mulready, R. C.: Meteor Report UAC-9, United Aircraft Corp. Research Dept. (July 1947).
8. Godsave, G. A. E.: *Fourth Symposium (International) on Combustion*, p. 830. The Williams & Wilkins Co., Baltimore, 1953.
9. Harvey, J. F.: J. Am. Soc. Naval Engrs., *64*, 307–313 (1952).
10. Pavia, R. E.: Commonwealth of Australia Dept. of Supply Aeronautical Research Labs. Engines Note 155 (March 1951), Figures 9 and 13 (ATI No. 160647).

29

MIXING AND COMBUSTION AT HIGH TURBULENCE IN COMBUSTION CHAMBERS

By ERNST H. W. SCHMIDT and FRITZ SCHOPPE

Introduction

Early theories of combustion waves, propagating in a homogeneous mixture of gaseous fuel and air, were based on the concept that the propagation of the flame front is brought about by heat conductivity, the hot combustion gases heating the unburned mixture until it attains ignition temperature. The heat of reaction of this layer in turn heats a new layer of cold gas and so on. Later investigators found that the velocity of the combustion waves is increased by the diffusion of active particles, such as atomic hydrogen or hydroxyl radicals. The well-known cone of a Bunsen flame burning under conditions of laminar flow through a burner tube can be interpreted in this way. A combustion wave burning in the diffusion zone of layers of pure gas and pure air brought into contact in a laminar way offers a similar case. Both these instances have been treated theoretically. However, the calculated values for the rate of the burning velocity are much lower than those observed in many actual combustion processes.

The first experimental and theoretical studies on turbulent flames, based on the Prandtl concept of mixing length, were made by Damköhler[1], in the laboratory of E. H. W. Schmidt at Braunschweig-Völkenrode. Subsequently, various American investigators, especially Karlovitz[2], entered this field. In Germany the recent contributions of Reichardt to the problem of free turbulence have proved equally significant for the problem of combustion.

In contrast to most of the work performed to date on the problem of free turbulence, the present paper deals with turbulence in closed combustion chambers.

Theoretical Considerations

The turbulent dissipation of heat can be treated with the help of Reichardt's inductive theory of turbulence[3]. Introducing two turbulent transmission coefficients A_q and A_τ for the dissipation of heat and momentum, the turbulent shear stress and the density of the turbulent heat flow can be written:

$$\tau = A_\tau \frac{d\bar{u}}{dy} \quad \text{and} \quad q = c_p A_q \frac{d\overline{T}}{dy} \tag{1}$$

where y is the coordinate transverse to the main velocity u, and $\overline{T}$ and $\bar{u}$ are mean values of the fluid temperature T and of the main velocity u of the stream in the direction of the coordinate x.

As momentum is a vector and temperature a

scalar, the transmission coefficients A_q and A_τ have different values. For the wake behind heated rods, Fage and Falkner[4] showed experimentally that $A_q/A_\tau = 2$, in agreement with a theory of G. I. Taylor, whereas Reichardt derived the ratio $A_q/A_\tau = 1.4 \sim 1.5$ from experiments by Elias[5] and by Lorenz[6].

If v is the velocity along the coordinate y and if mean values are indicated by a bar above the letter, the conservation of mass momentum and heat for a medium of constant density, i.e., for small differences of temperature, can be written:

$$\frac{\partial \bar{u}}{\partial x} + \frac{\partial \bar{v}}{\partial y} = 0 \tag{2}$$

$$\frac{\partial \overline{u^2}}{\partial x} + \frac{\partial \overline{uv}}{\partial y} = 0 \tag{3}$$

$$\frac{\partial \overline{Tu}}{\partial x} + \frac{\partial \overline{Tv}}{\partial y} = 0 \tag{4}$$

if the transfer of heat and momentum by heat conductivity and viscosity are neglected by comparison with turbulent transport.

The actual values of velocities u and v, and of temperature T can be expressed as the sum of the mean values $\bar{u}$, $\bar{v}$, $\overline{T}$ and the fluctuations u', v', and T' as follows:

$$u = \bar{u} + u', \qquad v = \bar{v} + v' \quad \text{and} \quad T = \overline{T} + T'. \tag{5}$$

If the fluctuations are small with respect to the mean values, and $\bar{v}$ is small as compared with $\bar{u}$, Reichardt derives from the above relations the equation:

$$\frac{\overline{T}}{\overline{T}_{\max}} = \left(\frac{\bar{u}}{\bar{u}_{\max}}\right)^{A_\tau/A_q} \tag{6}$$

linking the ratio of the transmission coefficients with the shape of the temperature and velocity profiles given by the ratio of $\overline{T}$ and $\bar{u}$ and any point of the profile to their maximum values at the axis of a wake.

In wakes produced by solid bodies, the Reichardt relation is applicable to regions not too near the body, i.e., where the pressure differences are equalized once more, and makes it possible to calculate the temperature profile behind a heat-releasing body, provided the momentum profile behind the same body is known.

As the transport of heat from a solid to a liquid body is analogous to the transport of a gas from a surface to a flowing stream, the temperature profile of a heat-releasing body is the same as the concentration profile behind the same body delivering combustible gas, e.g., by slits, to the stream.

In the case of two streams of different velocities, the rate of heat transport would correspond to the rate of mass transport by mixing if both streams had different compositions, such as gas and air.

The decrease of the maximum concentration $c_{\max}$ of the gas in the wake is given by the condition of continuity in the form

$$\int_{-\infty}^{+\infty} c(u_\infty - u)\, dy = k_1 \tag{7}$$

for the two-dimensional case, and in the form

$$\int_{-\infty}^{+\infty} c(u_\infty - u)\, y dy = k_2 \tag{8}$$

for the rotational case, if c and u are local concentrations and velocities, and u_∞ is the undisturbed velocity of the flow.

The constants k_1 and k_2 are given by the mass flow of gas released through slits or holes in the body to the wake behind it. In practical applications of combustion, the mass flow of gas is small compared with the flow of air.

Experimental observation shows that in turbulent flames the combustion zone coincides with the mixing zone. This means that combustion is completed when the mixing process has produced stoichiometric concentration, and that the flame ends where the maximum concentration of gas in the axis of the wake drops to the stoichiometric value.

In this way flame lengths behind a circular cylinder were calculated from Schlichting's theory[7] of the velocity wake using Reichardt's relation. For a cylinder of diameter d and a resistance coefficient c_r in air flowing at an undisturbed velocity u, and with gas delivered through a slit of width $b \times d$ with a velocity u_g, the length s of the flame is found to be (cf. paper by Miss Swain[8]):

$$s = 1.80 \frac{d}{c^2 c_r} \left(b \frac{u_g}{u_\infty}\right)^2 \tag{9}$$

where c is the stoichiometric concentration (volume ratio of gas to air). For a body of rotational symmetry with a cross-area A normal to the flow, the corresponding equation is

$$s = 1.16 \frac{\sqrt{A}}{c^{3/2} c_r} \left(b \frac{u_g}{u_\infty}\right)^{3/2} \tag{10}$$

The numerical factors 1.80 and 1.16 are of course only rough values due to the fact that the derivation of the equations only holds for distances $> d$ behind the body.

These equations show that the length of a turbulent flame depends on the ratio of the gas velocity and the main stream velocity. Increasing the velocity of the air decreases the length of the flame; adding more gas increases the flame length again to its original value. The flame length is proportional to the characteristic length d or $\sqrt{A}$ of the body; doubling the size of the body doubles the flame length. Finally, the flame length can be reduced by increasing the resistance coefficient c_r of the body. Increasing the mass flow of air and gas by the same factor does not increase the flame length. However, for a given value of the constant c_r, the resistance itself, and therefore the expenditure in flow energy, grows proportional to the square of the mass flow. Similarly, the flame length diminishes if the entering flow has an internal turbulence.

Equations (9) and (10) are valid for values of s/d that are not too small. They can be improved by additional terms taken from the calculation of the velocity wake behind a cylinder. For very high velocities approaching a Mach number of 0.5, mixing and consequently combustion performance begin to decrease, becoming considerably less near sonic velocity.

As a numerical example, let us calculate the lengths of a gas flame behind a cylinder of 1 cm diameter delivering gas through a 0.5 cm slit at its downstream face, at the same velocity as the main stream ($u_g = u$). For $c_r = 1.20$, $b = 0.5$, and $c = 0.25$, equation (9)

$$s = 5.87 \text{ cm}.$$

For a spherical body of the same diameter and a corresponding hole in its leeside, equation (10) gives

$$s = 2.53 \text{ cm}.$$

With these results the heat production per volume, i.e., the so-called heat release rate, can be calculated for a combustion chamber in which one or more resistance bodies deliver gas into the wake behind them. The equation is of the form

$$q = k \times H \times u_\infty \times c, \qquad (11)$$

where H is the caloric value of the gas and c its concentration in a stoichiometric gas-air mixture. The numerical value k depends upon the form of the body and its resistance.

Experimental Results

In order to test these theoretical calculations, experiments were made with two types of combustion chambers using gas from the municipal gas supply of Munich. Gas and air were blown into the combustion chambers with the help of rotational compressors.

One type of combustion chamber, proposed by E. H. W. Schmidt, and shown in Figures 1 and 2, is a spiral similar to the casing of a radial compressor, but the air enters the chamber tangentially and leaves it axially so that the flow has a

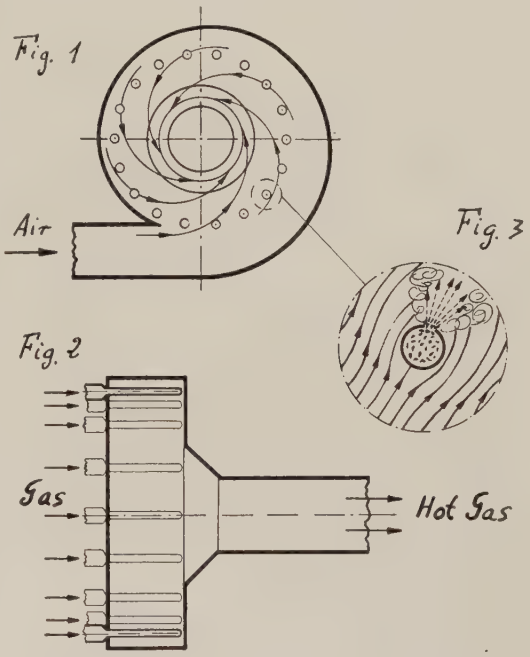

FIGS. 1, 2, and 3. Combustion chamber, proposed by E. H. W. Schmidt.

circumferential and an inward radial velocity. The diameter of the chamber was about 30 cm and its axial length 10 cm. This type of chamber intended for gas turbines and jet-propelled aircraft is especially designed for low pressure loss and a wide control range. Eighteen cylindrical tubes, arranged in the air path in a 24 cm diameter circle, deliver gas on their leeside and provide for mixing and burning of the gas with air as shown in the detail of Figure 3. These tubes are 7 mm in diameter and release the gas through a 0.1 mm slit in their leeside into air which enters the chamber flowing as a flat spiral from the exterior of the casing to the axis and leaving the chamber axially. As the pitch of the spiral was rather small (3°), the hot wake of one tube came

near to the next tube and in this way propagation at the ignition from one tube to the next one was easily obtained. The combustion was visible through two windows in the chamber, one at the perimeter of the spiral casing, the other covering almost the whole front within the circle of the gas-supply tubes. Additional windows of mica and quartz in the gas-outlet pipe made it possible to determine when combustion was completed. Temperature and pressure could be measured at different points of the chamber.

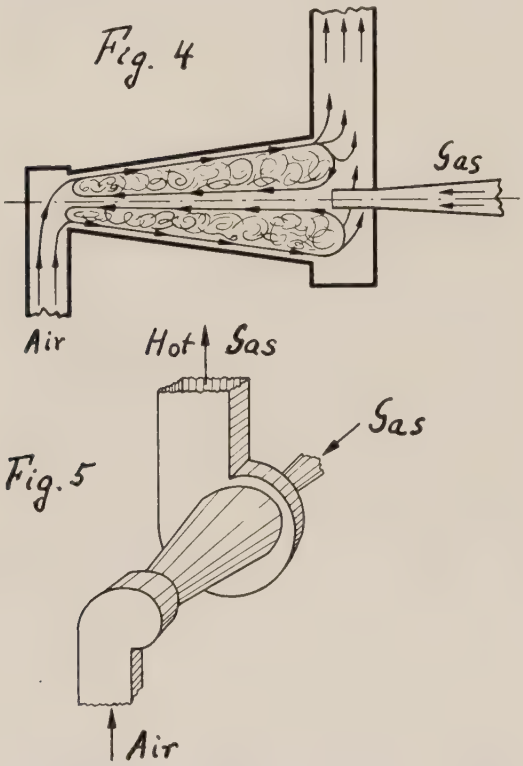

FIGS. 4 and 5. Conical combustion chamber, proposed by Fritz Schoppe.

Observation showed that for small air velocities (Reynolds number <4800 based on the 7 mm diameter of the gas tubes) the flow in the combustion zone was laminar, the flames were yellow and left the tube region in long spiralic strands. The heat output was accordingly rather small.

At higher velocities (Re > 5000) the flow became turbulent, completely changing the appearance of the combustion process. The flame was blue and had a fine curly structure. It made a low hissing sound, its length was small and in the range of the experiments independent of the stream velocity. The heat release at atmospheric pressure in the chamber attained 30×10^6 (kcal/m^{3}h) $= 1.9 \times 10^6$ (BTU/ft^{3}h) and was proportional to the air velocity. The temperature of the gases leaving the chamber could be controlled from 150°C to about 1000°C without extinguishing the flame or blowing it out of the chamber. At the intended normal load corresponding to a heat release rate of about 15×10^6 (kcal/m^{3}h), or 0.9×10^6 (BTU/ft^{3}h) at atmospheric pressure; the pressure loss did not reach 2 per cent of the absolute pressure. The pitch of the spiral way of the hot gas increases with its thermal expansion and it can be arranged that the hot gas hits the rotor blade at the correct angle, thus sparing the nozzle guide vanes. At a gas temperature of about 1000°C, the temperature of the chamber casing swept over by the entering air did not exceed 150°C, whereas the pipe leading off the combustion gases attained red-yellow heat.

Another type of combustion chamber, proposed by Fritz Schoppe, (Figs. 4 and 5) and especially built for high heat release rates made use of the production of turbulence in the mixing zone of two streams flowing at different velocities. The casing of this chamber had the shape of a truncated cone 20 cm long and changing in diameter from 6 cm to 12 cm. The air entered at the smaller end by way of a spiral and the hot gases left the cone at its wider end through a second spiral as shown in Figures 4 and 5. Due to the tangential path of the entering air, a reduction of pressure takes place in the axial region of the chamber and a substantial part of the air sweeping the conical casing returns near the axis. In this way a zone of intensive turbulence is produced around the axis of the cone.

The gas was admitted axially through a tube to this turbulent zone, as shown in Figure 4. There it mixes with air and burns. In this way the flame stands freely in the conical part of the chamber and is held here by turbulence only. The conical wall of the chamber does not reach 100°C even when the flame temperature is above 1500°C, because the air entering tangentially sweeps and cools the casing. The experiments showed also for this type that above a certain Reynolds number characterizing the change from laminar to turbulent motion, the flame length is independent of air velocity. Thus the heat release rate is proportional to the mass flow in agreement with theory.

This combustion chamber attained at atmos-

pheric pressure a heat release rate of more than 120×10^6 (kcal/m^{3}h) or about 7.5×10^6 (BTU/ft^{3}h) at a pressure loss of half an atmosphere. A smaller chamber (half the linear dimensions) of the same type still came to about 450×10^6 (kcal/m^{3}h) with a velocity of about 100 m/s of the air entering it.

REFERENCES

1. Damköhler, G.: Z. f. Elektrochemie, *46*, 601 (1940).
2. Karlovitz, B.: *Fourth Symposium (International) on Combustion*, p. 60. Baltimore, The Williams & Wilkins Co., 1953.
3. Reichardt, H.: *Gesetzmässigkeit der freien Turbulenz*. Berlin, VDI-Forschungsheft 414, 1942.
4. Fage, A., and Falkner, V. M.: Proc. Roy. Soc., *A135*, 685 (1932).
5. Elias, F.: *Die Wärmeübertragung einer geheizten Platte an strömende Luft*, p. 9. Aachener Abhandlungen, 1930.
6. Lorenz, H.: Z. techn. Physik, *15*, 376 (1934).
7. Schlichting: *Grenzschicht-Theorie*. Karlsruhe, 1951.
8. Swain, L. M.: Proc. Roy. Soc. (London), *A125*, 647 (1929).

30

CORRELATION OF AUTOIGNITION PHENOMENA IN INTERNAL COMBUSTION ENGINES AND RAPID COMPRESSION MACHINES

By J. C. LIVENGOOD and P. C. WU

Introduction

The self-ignition of heated and compressed fuel-air mixtures has been the object of much study, particularly in recent years. As a consequence of this wide-spread interest, data have become available from a variety of different kinds of apparatus. It is the purpose of this article to examine some of the possible relationships between these several kinds of results. A successful correlation is demonstrated which is based upon the gross parameters of a hypothetical chemical reaction.

Definitions

The self-ignition of a homogeneous mixture of fuel and air is herein defined as autoignition in order to differentiate this phenomenon from those which involve ignition by spark or from hot surfaces, or self-ignition phenomena involving evaporation and mixing processes. It has been widely demonstrated that the chemical reactions which lead to the eventual ignition of such a fuel-air mixture require a finite time interval. This time interval is, in general, a complex function of the physical state, as defined by the temperature and pressure, of the mixture and of its chemical constitution. For the special case wherein the physical state of the fuel-air mixture can be regarded as constant, this time interval has been called ignition delay, or simply, delay. It has been given the symbol, τ.

Experimental Measurements of Autoignition

RAPID COMPRESSION MACHINES

Special devices[1-6], known as rapid compression machines, have been constructed for the purpose of closely simulating the constant physical state reaction mentioned above. By their use it is possible to elevate quickly the temperature and pressure of a test mixture of fuel and air, and to allow the mixture to remain at this elevated state for the duration of the delay period. For extremely small values of delay (measured from the *end* of the compression process), an appreciable amount of reaction may occur during compression and thus the ideal concept of delay is not strictly applicable. The measurements which have been reported by investigators using these devices are listed in Table 1.

Figure 1 shows a typical pressure-time record from the M. I. T. Rapid Compression Machine. From this figure it can be seen that the physical state (as evidenced by pressure) is constant during the delay period. Some fuels show appreciable departure from this behavior. This problem will be discussed later.

MOTORED ENGINES

While the special rapid compression machine thus permits an evaluation of the autoignition behavior of a fuel-air mixture as a function of its physical state, the application of such devices has been limited by the complexity and special nature of the apparatus, and by the relatively slow rate of production of data which can be obtained. A much simpler procedure for studying autoignition reactions is the use of a motored engine in which the fuel-air charge is compressed (and subsequently expanded) continuously[7-10]. Measurements which have been reported are listed in Table 1. An important disadvantage of this method is that the reactions are carried out in a continuously changing physical environment. This fact causes difficulty in the separation of variables when an analysis of results is undertaken.

FIRING ENGINE

One of the problems which has stimulated much of the activity in the study of autoignition is the phenomenon of knock, or detonation, in the spark ignition internal combustion engine. One widely accepted interpretation of this occurrence is that it results from the autoignition of an unburned part of the fresh charge (end gas). This autoignition of the end gas results from its rapid compression by both the piston and by expansion of the burned portion of the charge behind the flame front.

The various kinds of measurement which have been reported of the autoignition phenomenon in running engines are listed in Table 1.

Temperature Measurements

It is well recognized that the reactions of autoignition are very sensitive to temperature. In the rapid compression machine and in the motored engine the charge is well mixed and is reasonably homogeneous with regard to temperature and pressure. With careful measurements the approximate charge temperature can be estimated, perhaps, within 20°F. However, in a firing engine the temperature of the end gas cannot be accurately estimated from pressure measurements and using the gas law, because of uncertainties in estimating the end gas volume and also because of the relatively large heat-transfer effects. However, recent developments now permit the determination of end-gas temperatures by a technique which measures the velocity of propagation of sound[11, 12].

These measurements have been accomplished in a laboratory engine (Fig. 2) equipped with transducers mounted on opposite sides of the end gas zone. Special instrumentation accomplishes accurate measurement of the transit time of high frequency sound pulses which are projected through the end gas.

When the end-gas composition is known with suitable accuracy (this is usually the case) its temperature can be computed from the classical relationship

$$T = \frac{Mc^2}{\gamma R}$$

Table 1. Reported Measurements in Research on Autoignition in Rapid-Compression Machine, Motored Engine, and Firing Engine

Apparatus	Pressure	Temperature from Gas Law	Temperature of End Gas from Sound Velocity	Temperature of End Gas from Absorption Spectra	Chemical Analysis via Sample	Chemical Analysis via Spectograph	Cool Flame Detection	Time Measurement	Unburned Specific Volume of End Gas	Flame Photograph	Schlieren Photograph
Rapid-compression machine	X	X						X		X	X
Motored engine	X	X			X	X	X	X	X		
Firing engine	X	X	X	X	X	X		X	X	X	X

X = Having reported data.

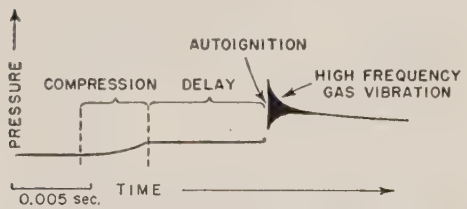

Fig. 1. Typical pressure-time record for rapid compression of stoichiometric mixture of n-heptane and air. (M.I.T. Rapid Compression Machine.)

where T = absolute temperature of the end gas
M = average molecular weight of the end gas
c = average velocity of sound through end gas
γ = average value of specific heat ratio of end gas
R = universal gas constant

In its present state of development this temperature determination can be made within 20°F or better.

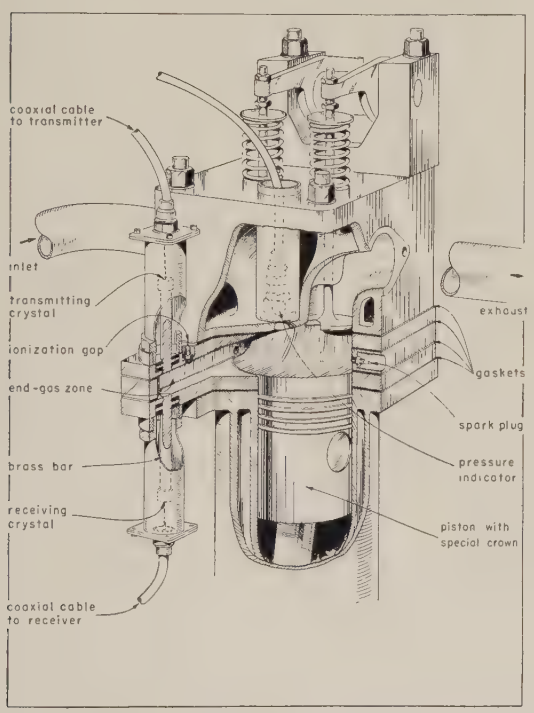

FIG. 2. CFR Engine with special instrumentation for measuring the velocity of sound in the end gas.

Common Features of Autoignition in Different Apparatus

An examination of Table 1 reveals those areas where there is sufficient overlapping of information to support an attempt at a quantitative correlation of the various kinds of results. It is apparent that the best represented data are those which present the autoignition process as a function of pressure, temperature and time. The other measurements serve as aids in estimating the useful limits of assumptions, etc., but until the same techniques have been applied to many kinds of experiment their general utility cannot be appraised.

The Relationship of Delay to Engine Knock

Perhaps the greatest difficulty encountered in attempting a correlation between the results from a rapid compression machine and a firing (or motored) engine is the great difference in state-time history which is produced in the fuel-air mixture. This is, of course, true even when the initial and final states are the same.

Consequently, in order to interpret engine behavior in terms of rapid compression machine results, it is necessary to devise a correlation scheme which accounts for the changing environment to which the fuel-air mixture is subjected in the engine. If the details of the reactions which precede autoignition were known, this might be accomplished. However, as has been suggested[13], it may be practicable to assume that an equivalent aggregate reaction will describe the process insofar as the end result is concerned, provided that it can be further assumed that the reactions are of the same kind in rapid-compression machine, motored engines, and firing engines[a 15, 16]. The gross parameters of such a reaction might have the following general form:

$$\frac{d(x)}{dt} = \phi_1(p, T, t), \qquad (1)$$

$$\phi_2(F, \text{chemical composition, etc.})$$

where (x) = concentration of pertinent reaction products
t = time
p = absolute pressure
T = absolute temperature
ϕ_1, ϕ_2 = empirical functions
F = fuel-air ratio

Equation (1) thus implies that, *for a given fuel-air mixture* there exists a fixed functional relationship between the rate of the aggregate reaction, the instantaneous physical state, and time. It can be assumed further that the ultimate consequence of the gross reaction of equation (1) is a sudden transition to a process which then proceeds to complete the combustion reaction within a time interval which is smaller by orders of magnitude than the preceding delay period. This assumed behavior yields the concept of a critical value for the concentration, $(x)_c$.

This concept of a critical concentration pro-

[a] An analogous procedure has been used by Strickland-Constable[14] to predict the ignition temperature of the gases following the pre-heat zone in a flame.

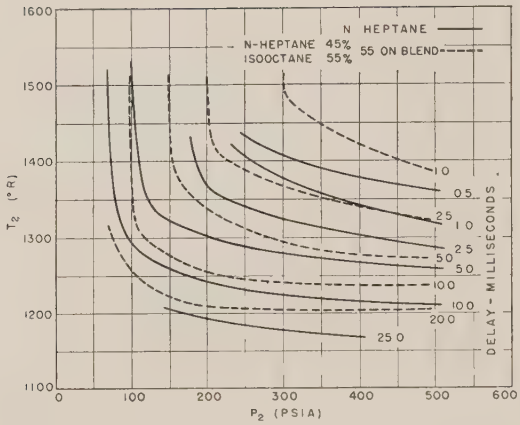

FIG. 3. Ignition delay as a function of temperature and pressure for two fuel-air mixtures.

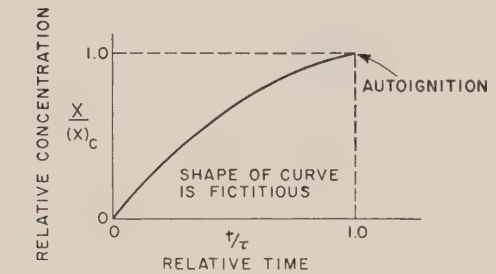

FIG. 4. Hypothetical behavior of preliminary reactions in rapid compression machine processes, each of which is carried out at some particular temperature and pressure. Initial chemical composition of the fuel-air mixture is assumed to be constant.

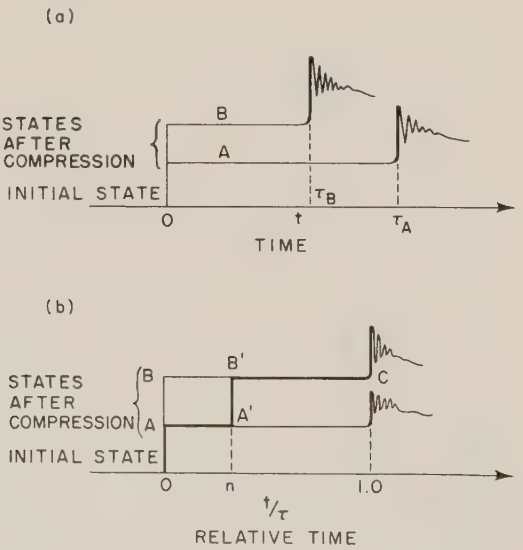

FIG. 5. (a) Hypothetical state-time paths of rapid compression machine processes A and B. (b) Same processes plotted on the t/τ base, with the line OAA'B'C showing a "stepped" process.

vides a limit for an integration process during which the concentration of chain carriers builds up. Hence, once the relationship between physical state and the low speed reaction rate is known, and the critical limit is determined, it should be possible to predict the time of occurrence of the high speed explosion during any state-time process for the fuel-air mixture in question.

This relationship has been studied and reported in the form of ignition delay data for various fuels. Often these data appear as empirical coefficients and exponents in the general form:

$$\tau = ce^{(-b/T)}p^n \qquad (2)$$

where τ = ignition delay
T = mixture temperature
p = mixture pressure
c, b, n = empirical constants

However, for the usual engine fuels, it has been found that this form of equation is adequate only over a limited range of temperature for any particular pressure[17, 18]. For this reason it is convenient to present such data in graphical form.

Two such graphs are shown in Figure 3. The fuels were *n*-heptane and a blend of *n*-heptane and isooctane (2,2,4 trimethylpentane), and they were tested in a stoichiometric mixture with air in the M. I. T. Rapid Compression Machine. The estimated accuracy of the location of the isodelay lines is ±20°F and ±10 psi. The isodelay contours were estimated from Arrhenius plots at various pressures, and the interpolated delay values are within ten per cent. The percentage dispersion of individual test results is of the same order of magnitude except for the very long (25 msec) delay values. In this region occasional test mixtures did not react to completion.

The Relationship between Ignition Delay and Reaction Rate

The reasoning used in the discussion of the reactions in the end gas can be applied with the same approximations to the fixed state process in the rapid compression machine. The assumptions are shown diagrammatically in Figure 4. The curved line implies that the most general assumption is that the reaction rate is not necessarily constant during the delay period. The assumption that there is a functional relationship between the concentration ratio, $(x)/(x)_c$, and the relative time, t/τ, is simply another way of describing the following assumed behavior of a particular fuel-air mixture in the rapid compression machine.

If two experiments were performed at different states, A and B, then the state-time diagrams would appear as shown in Figure 5a. If a third experiment could be performed, employing a stepped compression path, O–A–A'–B' in Figure 5b, then the overall reaction time (delay cannot be used here, since that term has been reserved for constant state reactions) will be:

$$[n\,\tau_A + (1 - n)\,\tau_B]$$

be disallowed, since a shift to a high speed reaction has been reserved as the definition of the end of the delay period. Thus it can be assumed that

$$\frac{d}{dt}\left[\frac{(x)}{(x)_c}\right] = \phi\left(\frac{t}{\tau}\right) \tag{3}$$

From equation (3) it follows that

$$\frac{(x)}{(x)_c} = \int_{t=0}^{t=t_e} \phi(t/\tau)\,dt = 1.0 \tag{4}$$

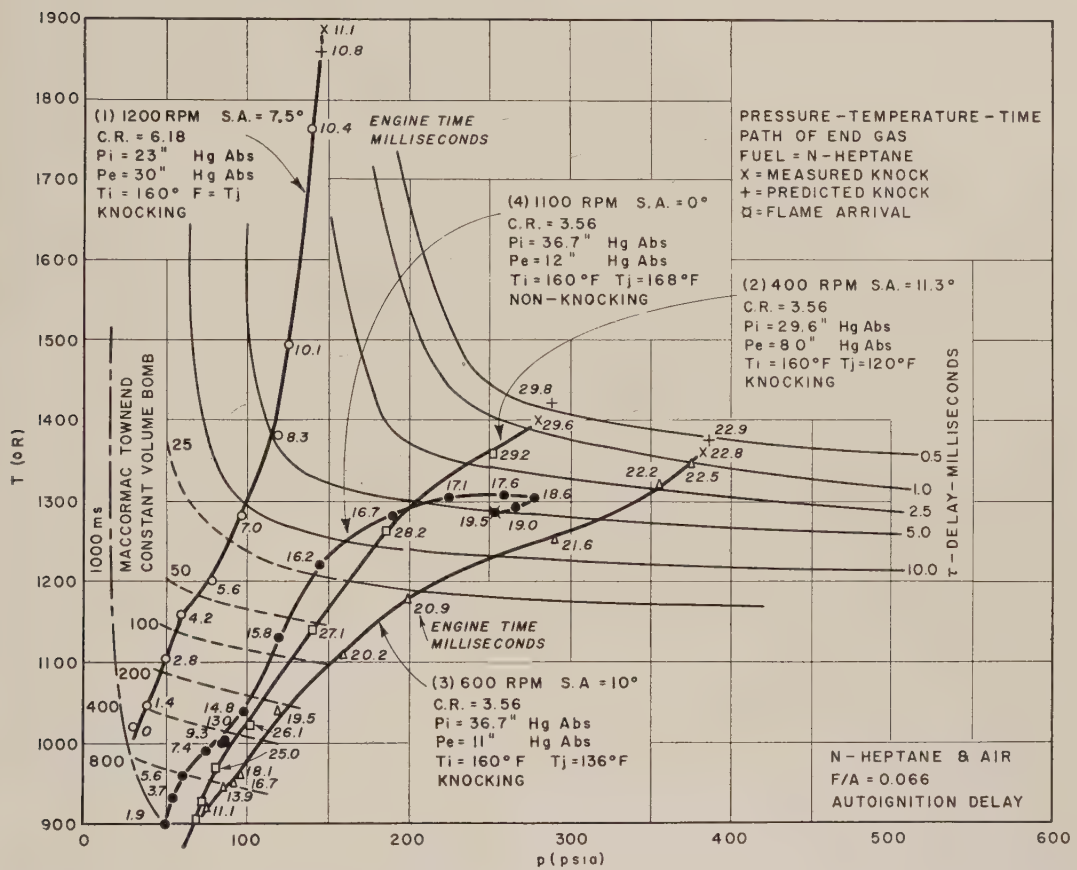

FIG. 6. Temperature-pressure-time paths of the end gas in a firing engine superimposed on auto ignition delay "map" for the same fuel-air mixture. (Dotted lines are extrapolations.)

where n is the time fraction of t/τ which elapsed (at state A) before the next step of the compression to state B. This expression for the reaction time of this stepped process is applicable regardless of the form of the functional relationship between $(x)/(x)_c$ and t/τ. This reasoning also implies that the denominator, $(x)_c$, in the ordinate scale of Figure 4 must be assumed a constant. Otherwise the step from A' to B' in Figure 5b, although completed in zero time, would involve a change in (x). This kind of change must

where t_e is the overall reaction time.

Unfortunately, the function, ϕ, cannot be obtained from ignition delay data. However, if it is assumed that the reaction rate does not change with time during a fixed state process (zero order reaction), $\phi(t/\tau) = 1/\tau$ and we can write

$$\frac{(x)}{(x)_c} = \int_{t=0}^{t=t_e} \frac{1}{\tau}\,dt = 1.0 \tag{5}$$

This equation can be solved with the aid of igni-

tion delay data and a knowledge of the state-time history of the process in question.

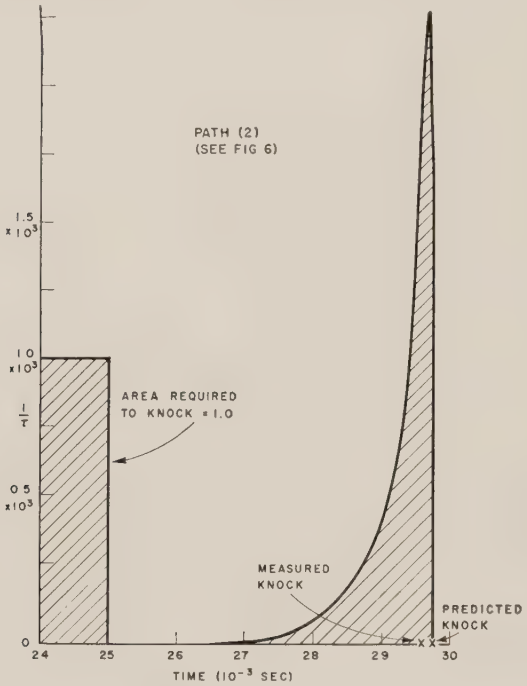

FIG. 7. Graphical integration for the prediction of knock in a firing engine.

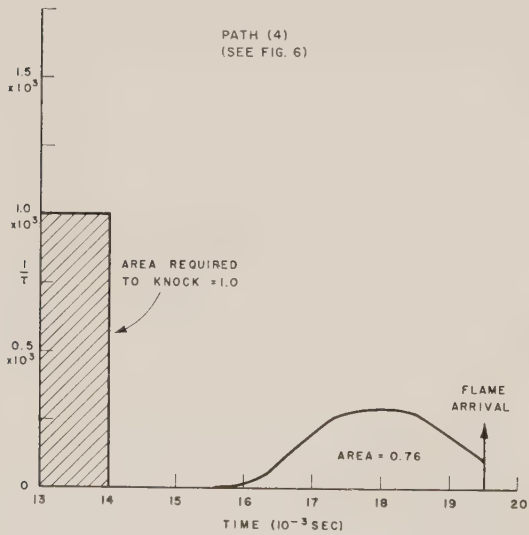

FIG. 8. Graphical integration scheme applied to a knock-free engine cycle.

Application of the Integration to a Firing Engine

As was mentioned earlier, the end gas temperature-time history can now be measured accurately by the velocity of sound technique, and pressure-time records of good precision are also available. From these data it is possible to define the temperature-pressure path followed by the end gas, and along this path to indicate the corresponding time intervals. Several such curves are shown in Figure 6, where the engine temperature-pressure paths have been superimposed on one of the autoignition maps of Figure 3. Shown also is the one second constant delay line obtained in a constant volume bomb[19]. From the intersections of these engine paths with the isodelay contours from the rapid compression machine, the information needed to solve equation (5) can be obtained.

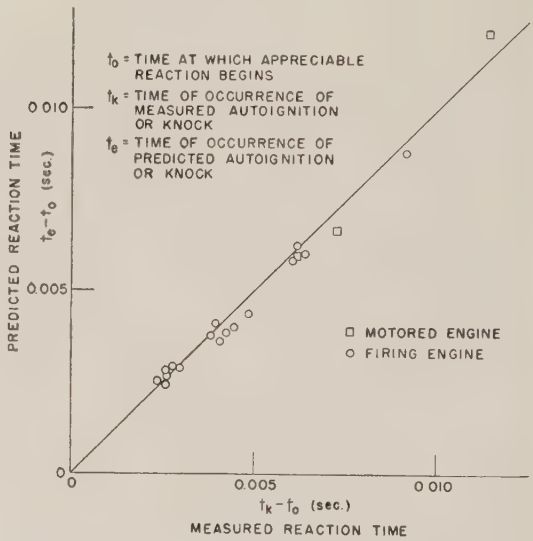

FIG. 9. Correlation between prediction and measurement of the time of autoignition. Plot includes both motored and firing engine cycles.

This integration has been performed graphically, as shown in Figure 7, for example. There is, of course, the problem of choosing the zero for the engine time-scale. This choice is an arbitrary one, but it is not critical provided it is placed at such a low temperature and pressure that the corresponding reaction rates are very low (long delay). In Figure 7, for example, it is apparent that the zero time point for the engine could have been placed 27 msec later in the engine cycle with no effect upon the integration and predicted autoignition. This time, at which appreciable reaction begins, has been called t_0.

Figure 8 shows this kind of integration for an engine cycle which was knock-free. As might be

expected, the normal flame consumed the end gas before autoignition occurred. In this instance the

Similar experiments have been performed over a wide range of conditions, using both *n*-heptane

TABLE 2. PREDICTION OF AUTOIGNITION OR KNOCK IN MOTORED AND FIRING CFR ENGINES

Motored CFR Engine: (Data and computations kindly supplied by E. B. Rifkin and C. Walcutt through courtesy of Ethyl Corporation)

Fuel: *n*-heptane, F/A = 0.066, Mixture Temperature = 150°F

Run	Speed	C.R.	Throttle	Earliest Predicted Significant Reaction			Observed Cool Flame			Observed Autoignition			Predicted Autoignition			Time Difference between Prediction and Measurement, $t_e - t_k$
				t_0	p	T	Time	p	T	t_k	p	T	t_e	p	T	
	rpm			10^{-3} *sec*	*psia*	°*R*	10^{-3} *sec*	*psia*	°*R*	10^{-3} *sec*	*psia*	°*R*	10^{-3} *sec*	*psia*	°*R*	10^{-3} *sec*
1	600	5.54	Open	24	77	1115	30.5	117	1230	35.4	132	1355	35.9	133	1380	+0.5
2	900	5.65	Open	18	95	1202	20.4	123	1265	24.2	134	1450	24.0	133.5	1425	−0.3
3	1200	6.53	Part	7.5	55	1160	11.0	103	1350	14.8	170	>1900	14.1	154	1900	−0.7

Firing CFR Engine: (Sloan Laboratory for Automotive and Aircraft Engines)

Fuel: Run 1–9—*n*-heptane, Run 10–17—*n*-heptane, Iso-octane blend 55 octane number, F/A = 0.0665

Run	Speed	C.R.	T_i	p_i	S.A.	Earliest Predicted Significant Reaction			Observed Knock			Predicted Knock			Time Difference between Prediction and Measurement, $t_e - t_k$
						t_0	p	T	t_k	p	T	t_e	p	T	
	rpm		°*F*	*psia*	°*BTC*	10^{-3} *sec*	*psia*	°*R*	10^{-3} *sec*	*psia*	°*R*	10^{-3} *sec*	*psia*	°*R*	10^{-3} *sec*
1	1200	6.18	160	11.3	7.5	5	70	1180	11.1	150	1900	10.8	147	1870	−0.3
2	400	3.56	160	14.5	11.3	27	135	1130	29.6	280	1390	29.8	286	1415	+0.2
3	600	3.56	160	13.1	10	20	145	1090	22.8	380	1630	22.9	385	1380	+0.1
4	1100	3.56	160	18.0	0	15.5	120	1110				Non-knocking			
5	900	6.18	160	10.3	10	5	60	1090	14.2	260	1900	13.8	205	1800	−0.4
6	600	6.18	160	12.4	5	15	110	1160	21.0	270	1400	21.4	295	1425	+0.4
7	400	3.56	160	14.6	10	23	110	1050	26.2	300	1410	26.3	305	1420	+0.1
8	1200	3.56	160	18.7	15	9	100	1055	11.4	243	1425	11.5	250	1430	+0.1
9	900	3.56	160	19.2	10	13	120	1075	15.6	302	1410	15.4	290	1400	−0.2
10	500	3.56	160	20.9	15	20.3	165	1110	23.3	417	1485	23.2	408	1480	−0.1
11	600	5.08	160	17.5	6	18	143	1120	22.5	420	1750	22.0	370	1620	−0.5
12	1200	5.08	160	12.3	20.5	5.5	70	1120	11.7	268	1750	11.7	268	1750	+0.0
13	600	5.08	160	14.5	13	16.5	115	1100	20.4	355	1900	20.2	340	1750	−0.2
14	400	5.08	200	14.2	20	22	126	1150	26.9	360	1780	26.4	340	1700	−0.5
15	900	5.08	180	14.4	17.5	9	95	1130	13.0	320	1850	13.1	330	1860	+0.1
16	700	5.08	160	20.2	2	14	160	1140	18.1	495	1770	17.6	470	1580	−0.5
17	1200	5.08	160	14.2	25	6	85	1180	10.3	370	1860	9.9	335	1790	−0.4

C.R. = compression ratio; F/A = fuel-air ratio; t_0 = time of earliest predicted significant reaction; t_k = time of occurrence of observed autoignition or knock; t_e = time of occurrence of predicted autoignition or knock (zero of the time axis is arbitrarily set at 300° crank angle); p = cylinder pressure; T = temperature of the end gas; p_i = engine manifold pressure; T_i = engine manifold temperature; S.A. = spark advance.

preliminary reactions were only three-quarters complete.

and a 55 O. N. blend with autoignition characteristics shown in Figure 3. The agreement be-

tween the predicted and measured occurrence of autoignition was similarly good. All of the correlations are summarized in Figure 9 and in Table 2.

Motored Engine Experiments

In addition to the firing engine tests reported above, the results of similar tests obtained in a motored engine were used as a further check on the utility of the integration procedure. The results are also shown in Table 2 and are included in Figure 9. The temperatures shown for the motored engine were obtained from pressure and volume measurements via the perfect gas law.

As was the case for the firing engine, the agreement between the predicted and actual times of occurrence of autoignition is reasonable, particularly in view of the rapidly changing state of the

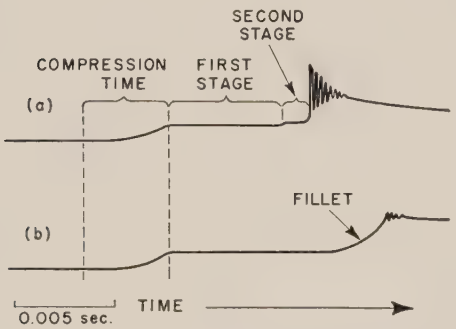

FIG. 10. (a) Two-stage ignition of *n*-heptane/air mixture. (b) Slow reaction, with pressure rise during the delay period, of diisobutylene. (M.I.T. Rapid Compression Machine.)

fuel-air mixture. For example, in the motored engine running at 900 rpm the gas temperature is changing at the rate of 92,000°F/sec at the time of autoignition, and the discrepancy between the measured and predicted temperatures at autoignition is 25°F.

Discussion

The experimental success of the correlations shown is certainly no proof of the validity of the assumptions used for rationalizing the method. Nor is it intended to suggest that a more detailed (and presumably more general) method would not work as well, if such a procedure were available. However, for the two fuel-air mixtures which were tested, over a wide range of values of temperature, pressure and speed, the simple assumptions used yield a correlation which is well within the uncertainties of the experimental measurements.

Nevertheless, under other circumstances, interfering effects may arise. It is felt that these will be of two kinds. First is the question about rapid compression machine processes which do not occur at constant state, as shown in Figure 10. For the two-stage reaction in Figure 10a, it has been suggested that a separate integration be employed for each stage in succession.[b] For this procedure to be successful it will be necessary to have good measurements of the increments in pressure and temperature which occur between the first and second stages. Efforts in this direction are under way.

A more complicated difficulty is anticipated for reactions which behave like Figure 10b. It has been suggested that correction factors[17, 18] be employed to take account of the rising temperature and pressure during the delay period. However, this procedure seems rather like trying to force the definition of delay at constant state onto a reaction to which it obviously does not apply. A more serious objection lies in the photographic evidence[3, 20] that these reactions are extremely non-homogeneous (geometrically speaking, at least). High speed photographs of the fillet region of reactions like that in Figure 10b have always shown the presence of one or more flame fronts. If we speak of delay in such a reaction, to which part of the charge do we refer, the portion which is inflamed or the part which is still unburned? The reasons for this behavior, which occurs with some fuels, are not yet clear.

The second large area of uncertainty lies with the possible behavior of fuel mixtures the components of which have greatly differing functions of reaction rate vs temperature and pressure. A particularly difficult problem is anticipated if the intermediate reaction products of the different fractions should interact[10, 21]. This latter problem comes very close to that of the intricate behavior of additives[22, 23, 24].

Concluding Remarks

(1) Data are becoming increasingly adequate to permit at least exploratory attempts to correlate autoignition phenomena in terms of fundamental concepts.

(2) A hypothetical gross reaction of zero order seems to be adequate for using rapid compression machine data in the prediction of autoignition

[b] Private communications with E. B. Rifkin and C. Walcutt.

(knock) in a motoring engine and in a firing engine. However, only two fuels were tested.

(3) Methods for accurate temperature measurement are required for this work, and recent developments are beginning to provide them.

(4) Additional data from motored engines would greatly augment the presented data. It is hoped that these will be forthcoming.

Acknowledgment

The work herein reported has been made possible by the support of the Ethyl Corporation for the rapid compression machine; the Coordinating Research Council, Inc., the Shell Oil Company, and the Office of Ordnance Research, U. S. Army have generously supported the continuing development of the sound-velocity temperature measurement technique. The motored engine results were contributed by E. B. Rifkin and C. Walcutt, Ethyl Corporation.

REFERENCES

1. Rögener, H.: Zeitschrift für Elektrochemie und angewandte physikalische Chemie, *53*, 389 (1949).
2. Scheuermeyer, M., and Steigerwald, H.: MTZ Motortechnische Zeitschrift, *5*, 229 (1943).
3. Taylor, C. F., et al.: S. A. E. Trans., *4*, No. 2, 232 (1950).
4. Teichmann, H.: Zeitschrift für Elektrochemie und angewandte physikalische Chemie, *47*, Nr. 4, 297, (1941).
5. Jost, W.: *Third Symposium on Combustion, Flame and Explosion Phenomena*, p. 424. Baltimore, The Williams & Wilkins Co., 1949.
6. Tizard, H. T., and Pye, D. R.: Phil. Mag., *1*, Series 7, 1094, (1926).
7. Johnston, R. C.: Thesis, S. M., M. I. T., 1952.
8. Levedahl, W. J., and Howard, F. L.: Ind. & Eng. Chem., *43*, 2805 (1951).
9. Pastell, D. L.: S. A. E. Trans., *4*, 571, (1950).
10. Walcutt, C., Mason, J. M., and Rifkin, E. B.: Ind. & Eng. Chem., *46*, 1029 (1954).
11. Anon.: *Four Methods for Measuring End Gas Temperature*. Coordinating Research Council, Inc., N. Y., 1953.
12. Livengood, J. C., Rona, T. P., and Baruch, J. J.: J. Acous. Soc. Am., *26*, 824, (1954).
13. Macpherson, J. H., Jr.: Thesis, Ph.D., Stanford University, June, 1946.
14. Strickland-Constable, R. F.: *Third Symposium on Combustion, Flame and Explosion Phenomena*, p. 279. Baltimore, The Williams & Wilkins Co., 1949.
15. Davis, W. C., et al.: *A Comparison of the Intermediate Combustion Products in an Engine With and Without Ignition*. To be published in S. A. E. Trans., *63* (1955).
16. Downs, D., Street, J. C., and Wheeler, R. W.: Fuel, *32*, 279, (1953).
17. Beckers, A.: Motortechnische Zeitschrift, *14*, Nr. 12, 345 (1953).
18. Schmidt, F. A. F.: *Verbrennungsmotoren, Thermodynamische und versuchsmässige Grundlagen unter besonderer Berücksichtigung der Flugmotoren*, p. 310. Berlin, Springer-Verlag, 1945.
19. Maccormac, M., and Townend, D. T. A.: J. Chem. Soc. (London), 238 (1938).
20. Livengood, J. C., and Leary, W. A.: Ind. & Eng. Chem., *43*, 2797 (1951).
21. Mason, J. M., Jr., and Hesselberg, H. E.: S. A. E. Trans., *62*, 141 (1954).
22. Street, J. C.: S. A. E. Trans., *61*, 442 (1953).
23. Chamberlain, G. H. N., and Walsh, A. D.: Proc. Roy. Soc., *215*, 175 (1952–53).
24. Hoare, D. E., and Walsh, A. D.: Proc. Roy. Soc., *215*, 454 (1952–53).

Discussion by L. B. Shore*

Messrs. Livengood and Wu offered the following equation to predict the time when knock would occur during the combustion of a fuel-air mixture:

$$1 = \int_{t=0}^{t=t_e} \frac{dt}{\tau}$$

where τ = the delay time at a particular pressure and temperature

t = time

t_e = time of knock

The same equation was derived independently at the Esso Laboratories some time ago as part of an effort to develop a useful and practical tool to aid in the understanding of the various combustion problems in Otto cycle engines. The thinking which led to the equation was quite similar to that of the authors.

An attempt was made to check the equation by a method essentially similar to that employed by the authors. This involved using it to predict the time of knock for two fuels of radically different anti-knock quality, namely, *n*-butane and *n*-heptane when each was being used at its own knock limited compression ratio. The knock limited compression ratio data were obtained from information presented by Campbell et al.† A spark timing of 17°BTC was assumed for both fuels.

* Esso Research and Engineering Company.

† J. M. Campbell, W. G. Lovell, and T. A. Boyd: SAE Journal, *76*, 163 (1930).

Values of delay time were obtained with rapid compression machine data of Roegner.‡ The pressures and temperatures needed were estimated by assuming: (1) a polytropic exponent of 1.3 for air, (2) a linear pressure rise from the time the spark fired to the time of peak pressure development, and (3) perfect mixing and vaporization of the fuel.

In spite of the fact that the two fuels in question differ considerably in octane number and therefore also in knock limited compression ratio (KLCR), the equation predicts the same time of knock for both as shown by the following data:

Fuel	Motor Octane Number	KLCR	Time of Knock Predicted by Equation
n-Butane.....	91	6.4	~10°ATC
n-Heptane....	0	2.8	~10°ATC

This is what might be anticipated with both fuels being burned in engines set at their respective KLCR's. In addition, the time of 10°ATC predicted for knock is quite reasonable with the spark set to fire at 17°BTC.

In view of the relative crudeness of the check method and the simple theories involved in the derivation, it was thought that these surprisingly good results were probably due, in some degree, to compensating errors. It was felt that the equation would probably not be too accurate mainly because its derivation assumes that the critical concentration of the knock producing species is independent of temperature and/or pressure. A priori, this assumption seems rather unlikely. However, in view of the refined experimental work done by the authors, it seems possible that this equation does accurately describe the processes leading to knock, at least for normal paraffins. One reason for this may be the fact that the largest contribution to the integral is made near the pressure and temperature of knock. Thus, the lack of dependence of the critical concentration on pressure and temperature need be true only over a short range of pressure and temperature. Regardless, it is anticipated that the form of the equation is probably right and if rewritten as follows might prove useful in the extrapolation, correlation, and interpretation of experimental results obtained from engines:

$$1 = \int_{t=0}^{t=t_e} \frac{dt}{\phi(T, P)}$$

where ϕ (T, P) = an empirical function of temperature and pressure obtained from engine experiments.

The authors are to be congratulated for their efforts, theoretical as well as experimental, and it is to be hoped that they will continue their work. A numerical attack on the knock problem, even if semi-empirical in nature, could be of great help in understanding many of the everyday problems encountered with Otto cycle engines. Some of the important practical questions which could be approached much more rationally with this analytical treatment as a background are: (1) What is the mechanism by which combustion chamber deposits affect octane requirement and power loss? (2) What are the real differences among fuels of different anti-knock sensitivity? (3) What happens when surface ignition occurs before or after the spark is fired? (4) What causes engine speed to influence the anti-knock rating of fuels? and (5) What are the effects of fuel additives?

‡ H. Roegner: U. S. Govt. Tech. Oil Mission Microfilm Reel 242; Photo Duplication Service, Library of Congress (1945).

31

COMBUSTION OF HYDROGEN AND CARBON MONOXIDE AS RELATED TO KNOCK

By W. F. ANZILOTTI AND V. J. TOMSIC

Introduction

Extensive studies of preknock reactions of hydrocarbon fuels have been conducted by many investigators both in engines and in heated bombs or tubes. These investigations have resulted in advances in the chemistry of hydrocarbon combustion, but also have demonstrated that hydrocarbon-oxygen reactions are extremely complex.

In view of the indications in the literature[1, 2, 3, 4] that hydrogen-oxygen interaction may constitute a very important step common to most hydrocarbon-oxygen reaction mechanisms, and

that carbon monoxide in the presence of water involves the same intermediate products as the hydrogen-oxygen reaction, it seemed plausible that a study of hydrogen and carbon monoxide combustion might shed light on the last key reactions occurring prior to fuel knock. If it could be demonstrated that there is a marked similarity between the behavior of hydrogen, carbon monoxide, and hydrocarbons in an engine, progress in the understanding of the knock reaction might be more rapid. Thus, a portion of the complexities associated with hydrocarbon combustion studies might be circumvented through the use of the relatively simple hydrogen-oxygen, carbon monoxide-oxygen reactions. This approach is strengthened considerably by the recent finding of Downs, Walsh, and Wheeler[5] that hydrogen knocks in an engine and has a tetraethyllead response.

Accordingly, the knock behavior of hydrogen and carbon monoxide was investigated and the results obtained compared with the behavior of selected hydrocarbon fuels, namely, *n*-heptane, isooctane, diisobutylene, cyclohexane, ethylbenzene, and cumene. Moreover, the effect of water content on the engine performance of carbon monoxide, both in the presence and absence of tetraethyllead, was studied with the expectation that the data obtained might shed light on the mechanism through which tetraethyllead exhibits antiknock activity. Finally, laboratory tube experiments were carried out on the H_2-O_2 reaction in the presence and absence of lead and lead oxide in order to observe the inhibiting effect of these materials on the H_2-O_2 explosive reactions.

The experimental information summarized in this paper shows that (1) there is a marked parallelism between hydrogen, carbon monoxide, and the selected hydrocarbon fuels in that they knock in an engine and respond alike to variations in fuel-air ratio, (2) hydrogen responded to the presence of sulfur compounds similarly to a paraffinic fuel, (3) the presence of water vapor decreased the knock resistance of carbon monoxide, (4) the antiknock response of carbon monoxide caused by the addition of tetraethyllead was enhanced by the addition of water vapor, (5) in laboratory tube experiments lead oxide rather than metallic lead inhibits the hydrogen-oxygen explosive reaction.

Engine Experiments

Knock resistance of hydrogen and carbon monoxide was studied in a single cylinder Cooperative Fuel Research (CFR) variable compression ratio engine modified so that gaseous fuel could be metered directly into the carburetor venturi, where it was mixed with air of controlled humidity. Hydrogen and the selected hydrocarbon fuels were rated admixed with air containing 1.4 mole per cent water, whereas with carbon monoxide the water content of the air was varied from 0.01 to 1.4 mole per cent. A schematic diagram of the engine fuel system is presented in Figure 1. Tetraethyllead vapor was added to the gaseous fuels when desired by conducting a portion of the metered hydrogen or carbon monoxide stream through a sintered glass bubbler immersed in liquid tetraethyllead. This tetraethyllead-saturated gas stream joined the main fuel-air mixture at the intake manifold, and the two were intimately mixed by the carburetor venturi effect and swirling action of a shrouded intake valve.

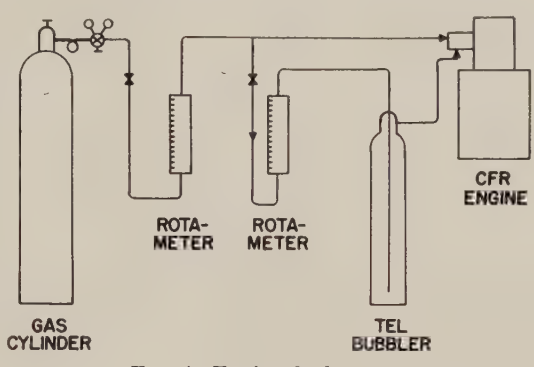

FIG. 1. Engine fuel system.

TABLE 1. ENGINE OPERATING CONDITIONS

Speed, rpm	900
Jacket temperature, °F	212
Inlet mixture temperature, °F	100
Spark advance	Varied
Fuel-air ratio	Varied
Compression ratio	Varied

The engine operating conditions used in this investigation are summarized in Table 1.

A Phillips Model D-1 internal pickup was mounted in the engine cylinder head and the signal fed to a Model 208-B Dumont oscilloscope. The resistance of hydrogen, carbon monoxide, and hydrocarbon fuels to knock was determined by measuring the knock limited compression

ratio, which is defined as that engine compression ratio which gives the first indication of knock on the oscilloscope screen. With hydrogen as the fuel, knock usually was detected audibly at the same time that it was first observed on the oscilloscope screen, whereas a lag of 0.20–0.25 compression ratio units between visible and audible knock occurred with carbon monoxide and the hydrocarbon fuels.

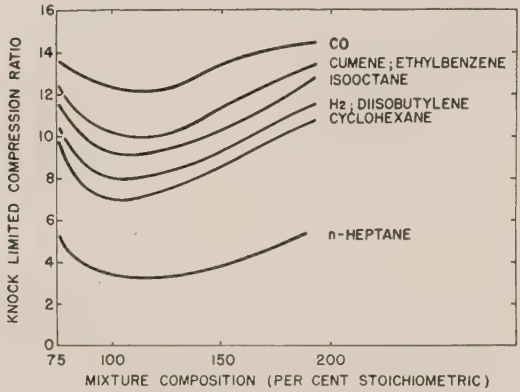

FIG. 2. Knock characteristics of hydrogen, carbon monoxide, and hydrocarbons.

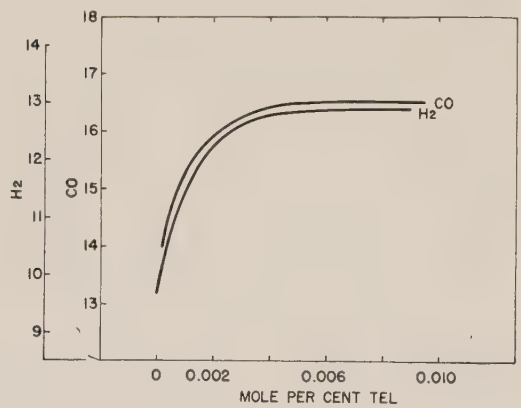

FIG. 3. Tel response of H_2 and CO; 180% stoichiometric.

KNOCK RESISTANCE OF HYDROGEN, CARBON MONOXIDE, AND HYDROCARBONS

A comparison of the engine performance of hydrogen, carbon monoxide, and typical hydrocarbon fuels throughout the mixture range is illustrated in Figure 2. The fuels were rated under identical conditions except for spark advance, which was adjusted to that for maximum power with each fuel. A spark advance of from 28 to 30 degrees before top dead center (BTDC) was used with the hydrocarbon fuels and carbon monoxide, but with hydrogen the spark was at top dead center (TDC) because of its much faster flame speed. The moisture content of the air used in these experiments was controlled at 1.4 mole per cent. These data show that carbon monoxide had by far the greatest resistance to knock. Carbon monoxide, cumene, and ethylbenzene were superior to isooctane in knock resistance, while hydrogen, diisobutylene, cyclohexane, and *n*-heptane were less resistant to knock than isooctane. From the general shape of the curves it is apparent that hydrogen and carbon monoxide respond to variations in mixture strength in much the same manner as do these hydrocarbon fuels.

TETRAETHYLLEAD RESPONSE OF CARBON MONOXIDE AND HYDROGEN

Hydrogen and carbon monoxide resemble the knocking combustion of paraffinic hydrocarbons in another respect—they respond well to tetraethyllead. The marked increase in knock limited compression ratio made possible by the addition of small amounts of tetraethyllead to a mixture of carbon monoxide and air containing 0.65 mole per cent water, based on fuel-air mixture, is illustrated in Figure 3. Although carbon monoxide requires a higher compression ratio than hydrogen for the appearance of knock, the elevation in knock limited compression ratio caused by the addition of an equivalent amount of tetraethyllead is approximately the same in both cases.

PERFORMANCE OF "WET" AND "DRY" CARBON MONOXIDE

Laboratory combustion tube studies have indicated that two separate mechanisms are involved in the oxidation of "wet" and anhydrous carbon monoxide[2]. That the presence and mobility of hydrogen atoms and radicals containing hydrogen are important for flame propagation is shown by Tanford and Pease[3], who calculated the equilibrium concentrations of these components in moist carbon monoxide flames and found a striking correlation between burning velocities and calculated hydrogen atom concentration. In a mixture of 60 mole per cent moist CO, 39.4 mole per cent oxygen and 0.6 mole per cent nitrogen the introduction of 1.5 mole per cent hydrogen increased the burning rate from 68 cm/sec to 93 cm/sec, raising at the same time the equilibrium partial pressure of hydrogen from 2.4×10^{-3} atmospheres to 3.8×10^{-3} atmospheres. It was of interest to observe the difference in knock behavior and

tetraethyllead response of carbon monoxide under "wet" and "dry" conditions in an engine because the results obtained might be utilized in explaining the role radicals containing hydrogen play in promoting preknock reactions as well as indicating whether or not tetraethyllead exhibits antiknock activity by destruction of these atoms or radicals.

Although close mechanical tolerances in the engine were maintained and the fuel induction system was thoroughly dried it was apparent that strictly anhydrous conditions could not be maintained due to trace quantities of crank-case oil gaining access into the combustion chamber and acting as a source of water through combustion. This was confirmed when a water balance over the combustion cycle showed a slight increase in exhaust gas water content above that calculated from the water content of the starting fuel-air mixture. However, in spite of this limitation, definite trends were established in the knock behavior and tetraethyllead response of carbon monoxide-air mixtures by drying the air and carbon monoxide to a water content of 0.01 mole per cent and 0.04 mole per cent, respectively, and then determining knock limited compression ratios at various moisture concentrations by adding a known amount of water vapor to the fuels.

As shown in Table 2 the knock resistance of carbon monoxide is markedly increased by decreasing the water content of the fuel mixture. In a 78 per cent stoichiometric fuel mixture containing 0.012 mole per cent water vapor, knock did not occur until a knock limited compression ratio of 18.3 was reached; the introduction of water vapor to reach a concentration of 0.85 mole per cent lowered the compression ratio at which known occurred 5.1 units to 13.2. This is in accordance with laboratory combustion tube results which show that the presence of water vapor greatly affects carbon monoxide combustion.

The large difference in KLCR at lean mixtures as compared with rich mixtures may be due, in part, to a critical moisture concentration above which additional water plays but a minor role in carbon monoxide combustion. The relationship of KLCR to mixture composition employing a fixed moisture concentration of 0.01 mole per cent for air and 0.04 mole per cent for carbon monoxide indicates that above a water content of 0.016–0.018 mole per cent very little effect on KLCR is noted.

TETRAETHYLLEAD RESPONSE OF "WET" AND "DRY" CARBON MONOXIDE

The presence of water vapor plays an important role in the tetraethyllead response of carbon monoxide since the response decreases as the water content of the fuel is reduced. The decrease in tetraethyllead response as anhydrous conditions are approached is shown schematically in Figure 4. These data are interpreted as indicating that the antiknock activity of tetraethyllead

Table 2. Effect of Moisture Content on the Knock Resistance of Carbon Monoxide

% Stoichiometric	"Dry" Mixtures		"Wet" Mixtures		"Dry"-"Wet" Mixtures, ΔKLCR*
	Mole % H_2O	KLCR*	Mole % H_2O	KLCR	
78	0.012	18.3	0.85	13.2	5.1
100	0.014	15.5	0.79	12.7	2.8
150	0.015	14.1	0.69	13.4	0.7
174	0.016	14.1	0.66	13.8	0.3

* Knock limited compression ratio.

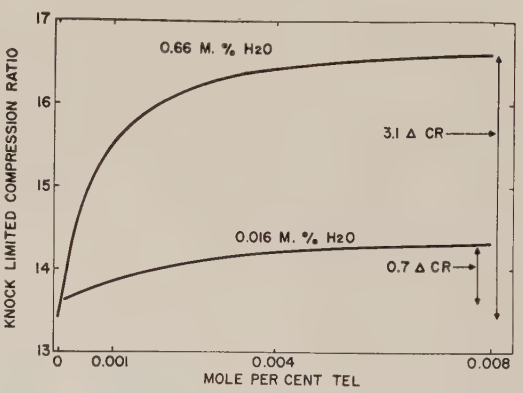

Fig. 4. Tel response of "wet" and "dry" CO; 176% stoichiometric.

is in some manner related to the presence of water vapor or radicals derived from water, such as H˙, OH˙, or HO_2 radicals.

MASS BURNING RATE OF CARBON MONOXIDE, HYDROGEN, AND ISOOCTANE

Because the residence time of the last, knocking portion of a fuel-air mixture in the end gas region of the engine combustion chamber influences the knocking tendency of the fuel, it was of interest to compare the burning rates of hydrogen, carbon monoxide, and isooctane with their tendency to knock in an engine.

Both hydrogen and water increase the burning rate of carbon monoxide as shown in Tables 3 and 4. The indicator card method of Rassweiler and Withrow[6] was used for these calculations. Thus,

Table 3. Effect of Hydrogen on Combustion Time of Carbon Monoxide
(100 per cent Stoichiometric)

	Combustion Time, Crank Angle Degrees		
	7:1 CR		10:1 CR, 30°BTC
	TDC	30°BTC	
Carbon monoxide	46	38	38
Carbon monoxide + 7.5 mole per cent H_2	22	20	20
Hydrogen	12	—	—

Table 4. Effect of Moisture on Combustion Time of Carbon Monoxide
(100 per cent Stoichiometric)

Mole Per Cent H_2O (Based on Total Fuel-Air Mixture)	Combustion Time, Crank Angle Degrees			
	7:1 CR		10:1 CR	
	TDC	30°BTC	TDC	30°BTC
0.08	44	40	42	40
0.82	46	38	39	38
4.65	40	36	34	34

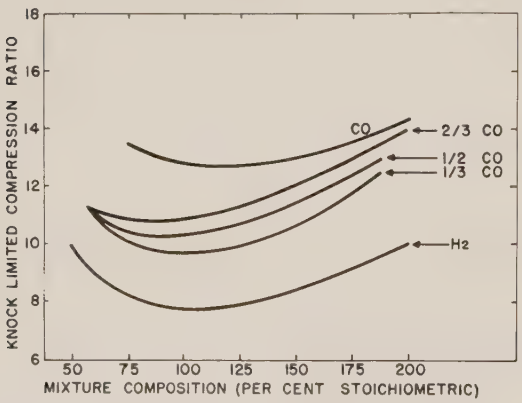

Fig. 5. Knock resistance of H_2-CO mixtures.

in the presence of hydrogen or water the end gas residence time of carbon monoxide is decreased, thereby reducing the knocking tendency of the fuel. However, as shown in Figure 5 and Table 2, the knocking tendency of carbon monoxide is considerably increased by the presence of hydrogen, or water vapor. This suggests that any beneficial effect in the knock resistance of carbon monoxide due to shorter end gas residence time is overshadowed by knock producing species arising from the presence of hydrogen or water.

A comparison of the time necessary for the complete combustion of isooctane, hydrogen, and carbon monoxide in which the air contained 1.4 mole per cent water and carbon monoxide 0.04 mole per cent water is shown in Figure 6. These data show that hydrogen combustion is completed in but 29 per cent of the time necessary for isooctane to burn completely. Carbon monoxide burned slightly faster than did isooctane.

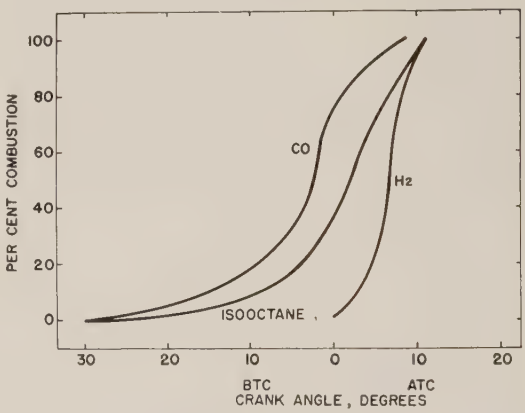

Fig. 6. Burning rates of hydrogen, carbon monoxide, and isooctane.

Effect of Additives Containing Sulfur on Hydrogen Combustion

Additional support for the similarity in knock behavior between hydrogen and paraffinic hydrocarbons is seen in the effect of additives containing sulfur on the engine performance of these fuels. A comparison of the knocking behavior of hydrogen and paraffinic hydrocarbon fuels in the presence of an organic disulfide ($C_2H_5SSC_2H_5$), an oxidized form of sulfur (SO_2), a reduced form of sulfur (H_2S), and a carbon-sulfur compound containing no hydrogen (CS_2) showed that the intensity and order of the proknock effect and sulfur-lead antagonism caused by these additives was similar in these two types of fuels.

PROKNOCK EFFECTS

Certain sulfur compounds act as proknocks and decrease the knock resistance of paraffinic hydrocarbons. Of the sulfur compounds evaluated in

hydrogen, diethyl disulfide showed the greatest proknock effect while sulfur dioxide had no effect. These results, shown schematically in Table 5, are in agreement with the results obtained with a paraffinic fuel.

The fact that hydrogen sulfide exhibits a greater proknock effect than does carbon disulfide may be attributed to the added presence of chain initiating hydroxyl radicals, as shown by Fowler and Vaidya[7].

The thermal stability of sulfur dioxide may account for its inability to influence knock.

SULFUR-LEAD ANTAGONISM

In agreement with paraffinic fuel studies[8], sulfur dioxide caused the greatest deactivation of tetraethyllead in hydrogen—to such an extent that the antiknock effect was completely destroyed and the proknock activity of the ethyl radicals resulting from tetraethyllead decomposition was observed. On the other hand, carbon disulfide showed the least ability to deactivate the antiknock property of tetraethyllead.

SUMMARY OF ENGINE INVESTIGATION

The foregoing discussion has shown that there is a marked parallelism in the engine behavior of hydrogen, carbon monoxide, and paraffinic fuels and that knocking tendency and tetraethyllead response may be related to the presence of H, O, OH, and HO_2. This information is interpreted as indicating that the hydrogen-oxygen reactions may be, at least in part, controlling in the preknock reactions of paraffinic fuels. To assess this concept more fully, additional information on hydrogen-oxygen mixtures was obtained in laboratory combustion tube experiments in which better control of temperature and contact surface was possible.

Laboratory Combustion Tube Experiments

Investigations of the thermal reaction between hydrogen and oxygen have shown the existence of the three definite explosion limits[2] illustrated in Figure 7. Conditions just inside and outside the third explosion limit at a pressure of one atmosphere were selected for our studies. A pressure of one atmosphere is sufficient to hold to a reasonable minimum the effects of diffusivity of reacting atoms and radicals and chain breaking at the wall which play a major part in the reaction kinetics at lower pressure.

The hydrogen-oxygen reaction was investigated in a flowing system either by the method of Pease[9], in which the amount of water and hydrogen peroxide formed was determined, or by observing the temperature at which a hydrogen-oxygen mixture exploded. A schematic flow diagram of the glass combustion train is shown in Figure 8. Hydrogen (99.5 per cent pure, obtained from Paschall) and oxygen (99.5 per cent pure, obtained from Air Reduction) were reduced to 2–3 pounds per square inch gauge and each was passed through a separate, identical series of dry ice traps in order to reduce the likelihood of

TABLE 5. KNOCK RESPONSE OF SULFUR COMPOUNDS IN DECREASING ORDER OF ACTIVITY

Effect	Fuel	
	H_2	Hydrocarbon
Proknock	$(C_2H_5S)_2$ H_2S CS_2 SO_2	$(C_2H_5S)_2$ H_2S CS_2 SO_2
Sulfur-lead antagonism	SO_2 H_2S $(C_2H_5S)_2$ CS_2	SO_2 H_2S $(C_2H_5S)_2$ CS_2

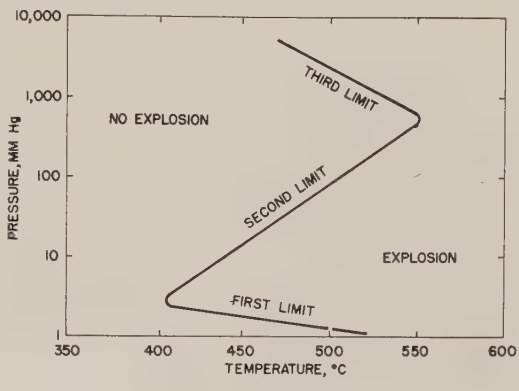

FIG. 7. $H_2 + O_2$ explosion limits; stoichiometric mixture.

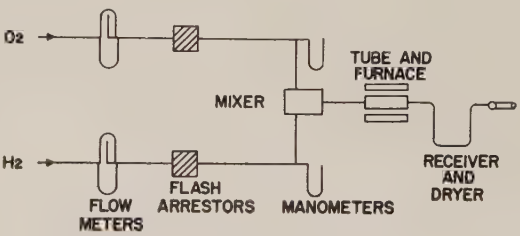

FIG. 8. Combustion train.

explosion flash-back and to eliminate water. The dried gases were brought together in a mixing chamber and then fed into the heated combustion tube, the temperature of which was regulated and maintained within ±1°C by means of a recorder controller. Flow rates were usually such that the residence time of the mixture in the reaction chamber was within the range 30 to 40 seconds.

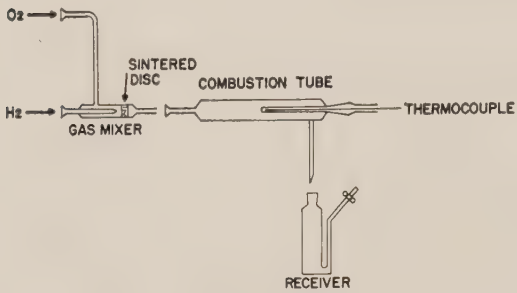

FIG. 9. Combustion tube assembly.

TABLE 6. REPRODUCIBILITY OF THE HYDROGEN-OXYGEN REACTION*

Tube Temperature = 543 ± 3°C
Total Gas Flow = 40 cc/min
Mole per cent H_2 = 66.7 (stoichiometric)

Tube	Gas Residence Time	Mg H_2O_2 Collected	Mg H_2O Collected	Rate of H_2O Formation
	sec			*mg/min*
Quartz	31	0	44–46	1.5–1.5
		0	50–93	1.7–3.1
Pyrex	32	0.4–0.5	98–137	3.3–4.6
brand	38	0.46–0.53	114–135	3.8–4.5
glass		0.20–0.24	54–66	1.8–2.2
		0.24–0.25	44–57	1.5–1.9
	41	1.3–1.4	44–48	1.5–1.6

* The range of values given for each separate set of data represents the degree of variation found in experiments run on a single day. Values within a group represent experiments run on successive days.

The finding of others[9] that the surface of the combustion tube is critical were confirmed and therefore before use each tube was washed two to four times with hot nitric acid and then at least 10 times with distilled water. A typical combustion tube assembly is shown in Figure 9. The reaction chamber is 11 cm in length and 1.8 cm in diameter.

Tetraethyllead was added to the combustion tube by passing the hydrogen stream through a previously calibrated sintered glass tetraethyllead bubbler maintained at constant temperature before introduction into the mixing chamber. Since the tetraethyllead concentration in the effluent gas stream is a function of temperature, the amount being fed into the combustion chamber was varied by altering the bubbler temperature.

THE HYDROGEN-OXYGEN REACTION BELOW THE EXPLOSION TEMPERATURE

A study of the rate of water and hydrogen peroxide formation employing a stoichiometric hydrogen-oxygen mixture revealed that very little reaction took place below 530°C and that the mixture became explosive at 556°C. Accordingly an intermediate temperature range of 540–545°C was selected for initial study of water and hydrogen peroxide formation. Reproducibility and the effects of tube type and residence time are shown in Table 6.

The literature[9] attributes this poor reproducibility, in part, to the extreme sensitivity of the reaction to the combustion tube surface.

The data of Table 6 indicated that hydrogen peroxide was not isolable from experiments conducted with quartz tubes; this has been reported by others[10]. For this reason, Pyrex brand glass reactors were used in place of quartz in the experiments reported in the remainder of this paper.

Since one of the products of tetraethyllead decomposition is lead oxide, it was decided to observe the effects of this latter compound on H_2-O_2 product formation. Measurements were made on the rates of formation of water and hydrogen peroxide from a stoichiometric H_2-O_2 mixture in clean and lead oxide coated tubes. The products formed were totally condensed, weighed, and peroxide determined by permanganate titration. Water was determined by difference. The results, plotted in Figure 10 show that:

(1) In a clean tube water formation increased steadily and appreciably up to the temperature of exploson, and hydrogen peroxide was present in small amounts even just below the explosion temperature.

(2) The PbO coating shifted the curve so that a higher reaction temperature was necessary before water formation took place.

(3) No hydrogen peroxide formation was detected in the lead oxide coated tube.

The similarity of the curves of rate of water formation versus temperature indicates that the PbO may have retarded rather than altered the

oxidation mechanism. The failure to isolate hydrogen peroxide is not unexpected because it is known to decompose readily on contact with a lead oxide surface[10].

EXPLOSION TEMPERATURES OF HYDROGEN-OXYGEN MIXTURES

In contrast with the measurements of products obtained at intermediate temperatures, the data obtained by determining the temperature at which a hydrogen-oxygen mixture exploded were quite reproducible, generally within ±2°C. In as much as most of the variables investigated caused far greater changes in explosion temperatures than ±2°C, this reproducibility was satisfactory.

Measurements of the influence of mixture strength on explosion temperature, presented in Figure 11, showed that in mixtures leaner than 20 mole per cent or richer than 80 mole per cent hydrogen no explosion occurred when the temperature was raised as high as 640°C, which approaches the softening point of Pyrex brand glass. Best checks were obtained with slightly lean mixtures (i.e., approximately 50 mole per cent hydrogen).

As is shown in Figure 12, the addition of very small quantities of tetraethyllead caused a substantial elevation of the explosion temperature of a stoichiometric H_2-O_2 mixture. This marked effect of tetraethyllead correlates with the observation that this compound reduces the knock of hydrogen in engines.

It was of particular interest to find that lead oxide reaction tube coatings increase the explosion temperature while metallic lead coatings have no effect. A lead oxide deposit prepared by decomposing tetraethyllead in an oxygen stream at 350–500°C raised the explosion temperature of hydrogen-oxygen mixtures as shown in Figure 13. When this deposit was reduced to metallic lead by heating in the presence of excess hydrogen, this effect was destroyed completely. It is quite apparent in these experiments that lead oxide rather than metallic lead is the active species causing the elevation of the H_2-O_2 explosion temperature. This is in accordance with the theory that the active antiknock component from tetraethyl-lead in hydrocarbon fuels is lead oxide[11].

EFFECT OF SULFUR DIOXIDE ON H_2-O_2 EXPLOSION TEMPERATURE

Sulfur dioxide had no effect on the hydrogen-oxygen explosion temperature even at a concentration as high as five mole per cent. However, in the presence of tetraethyllead even low concentrations of sulfur dioxide reduced the explosion temperature normally obtained with tetraethyllead. This correlates with the engine studies where sulfur dioxide showed sulfur-lead antagonism but

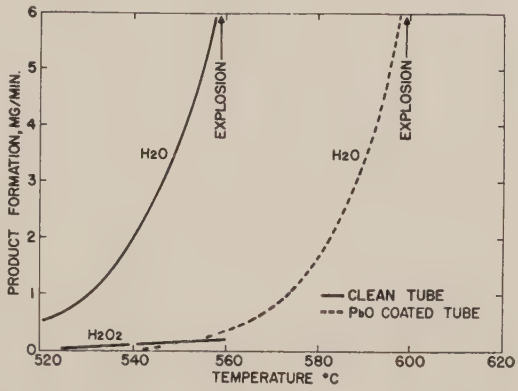

FIG. 10. Pre-explosion reactions; stoichiometric H_2-O_2 mixture.

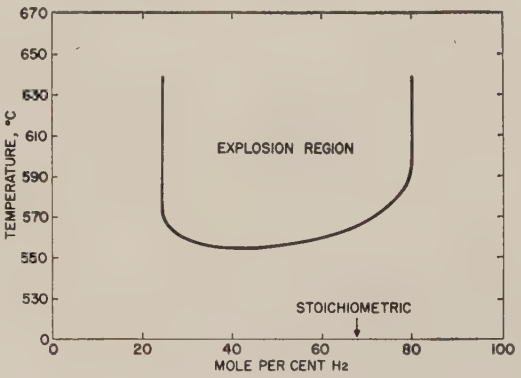

FIG. 11. Explosion temperatures of H_2-O_2 mixtures.

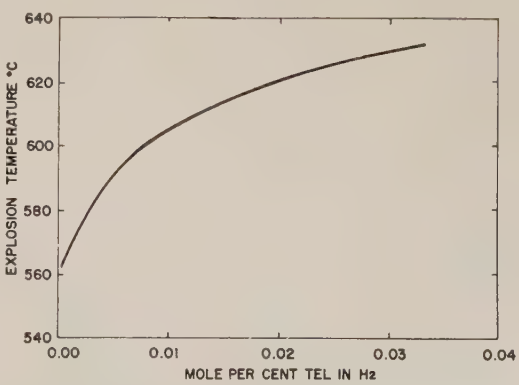

FIG. 12. Effect of tel on explosion temperature, stoichiometric H_2-O_2 mixture.

did not lower the knock resistance of unleaded hydrogen. An example of the effect of sulfur dioxide on hydrogen combustion is shown in Figure 14.

Discussion

The results of the preceding experiments have indicated the following:

(1) The engine behavior of hydrogen, as well as the findings of Geib and Harteck[12] that the introduction of hydrogen atoms causes a very rapid reaction in methane-oxygen mixtures at temperatures as low as −183°C, although ordinarily such mixtures react slowly even at 300°C, indicates that a suppression of hydrogen-oxygen chain branching reactions might result in the elimination of hydrocarbon knock in engines.

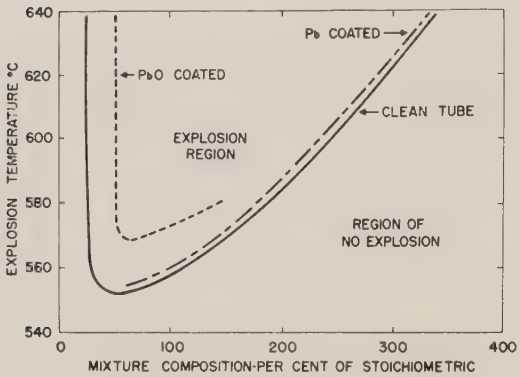

FIG. 13. Effect of Pb and PbO on explosion temperature.

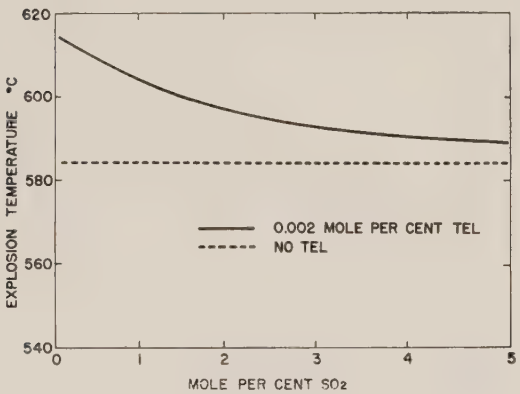

FIG. 14. Effect of SO_2 on H_2 combustion; 80 mole per cent H_2 .

(2) Lead oxide, resulting from tetraethyllead decomposition, suppresses hydrogen-oxygen explosive reactions. This is in agreement with the suggestion advanced by Chamberlain and Walsh[11] that lead oxide is the active antiknock which causes suppression of hydrocarbon preknock reactions.

(3) The presence of water vapor, and hydrogen increased the tendency of carbon monoxide to knock in an engine, presumably due to the presence of those radicals containing hydrogen which initiate chain branching reactions. This view is supported by McDonald[13] and Tanford and Pease[3] who attributed the faster reaction of "wet" carbon monoxide to H· and OH· radicals.

(4) The knock response of carbon monoxide in the presence of tetraethyllead was markedly increased by the addition of water vapor, presumably, the result of lead oxide removing chain carrier and chain initiating radicals containing hydrogen.

An analysis of the differences between steady state and explosive reactions in both H_2-O_2 and CO-O_2 (wet and dry) systems affords a basis whereby the observed results might be rationalized.

STEADY STATE AND EXPLOSIVE REACTIONS

The principal reactions between the second and third explosion limits of hydrogen (Fig. 7) can be summarized in the following equations:

$$\left.\begin{aligned} H + O_2 + M &\rightarrow HO_2^{\cdot} + M \\ HO_2^{\cdot} + H_2 &\rightarrow H_2O_2 + H \end{aligned}\right\} \text{Steady state} \quad (1), (2)$$

$$\left.\begin{aligned} H + O_2 &\rightarrow HO^{\cdot} + O \\ O + H_2 &\rightarrow HO^{\cdot} + H \\ HO^{\cdot} + H_2 &\rightarrow H_2O + H \end{aligned}\right\} \text{Chain branching explosive} \quad (3), (4), (5)$$

According to this mechanism, which is advanced by Lewis and Von Elbe[2], the reaction between H and O_2 in the presence of a third body M forms the postulated and logical $HO_2^{\cdot}$ radical which in turn reacts with H_2 to form H_2O_2 and H. Thus, in the nonexplosive region between the second and third explosion limits a steady state exists as shown in equations (1) and (2). Equation (2) becomes progressively dominant as the temperature and pressure or both are increased until at the third limit the chain branching equations (3), (4), and (5) come into play giving rise to an explosion.

THE ACTION OF LEAD OXIDE

As is evident in the steady state and explosive sequence in the previous equations, the removal of $HO_2^{\cdot}$ radical would be an effective means of indirectly removing chain carrier H. Thus, if HO_2 radicals were reduced to a concentration below

some critical value then as the pressure and temperature were increased the chain carriers resulting from chain branching equations (3) and (4) would not be produced.

As suggested by Chamberlain and Walsh[11], lead oxide may effectively absorb $HO_2^{\cdot}$ radicals and simultaneously promote decomposition of hydrogen peroxide resulting from the combination of these radicals. The latter would prevent desorption of hydrogen peroxide into the gas phase giving rise to chain carriers.

Since lead oxide is presumably one of the active antiknock species resulting from the decomposition of tetraethyllead it seems plausible that the antiknock activity of tetraethyllead may arise from the action of lead oxide on the $HO_2^{\cdot}$ radical.

Additional support for the postulate that tetraethyllead decomposition products are inhibiting explosive reactions by means of interaction with hydrogen-containing radicals is emphasized in the "dry" and" wet" carbon monoxide engine experiments. A trend was established in that the tetraethyllead response of carbon monoxide decreased as the fuel mixture became progressively lower in moisture content presumably due to a reduction in the number of chain carrier radicals. In the presence of water vapor, chain carriers could arise by methods as shown in the following equations[2].

The primary reaction

$$CO + H_2O \rightarrow CO_2 + H_2 \qquad (6)$$

takes place on the surface at low temperature and in the gas phase in the flame giving rise to hydrogen which undergoes chain initiation reactions

$$H_2 + O_2 \rightarrow \text{(Initiation)} \qquad (7)$$

followed by reactions of the chain carrier and branching types

$$H + O_2 + M \rightarrow HO_2^{\cdot} + M \qquad (8)$$

$$HO_2^{\cdot} + CO \rightarrow CO_2 + OH^{\cdot} \qquad (9)$$

$$OH^{\cdot} + CO \rightarrow CO_2 + H \qquad (10)$$

$$H + O_2 \rightarrow OH^{\cdot} + 0 \qquad (11)$$

$$O + H_2 \rightarrow OH^{\cdot} + H \qquad (12)$$

Thus it seems plausible that the active antiknock species arising from tetraethyllead decomposition must destroy in some manner the chain carriers giving rise to chain branching explosive reactions.

From the foregoing discussion it must not be concluded that lead oxide can exhibit an inhibiting effect only in the presence of radicals containing hydrogen. Evidence is provided by the finding of Hoare and Walsh[14] that a lead monoxide coating raises the explosion limit of a dry CO-O_2 mixture in which radicals containing hydrogen are nonexistent. In this instance lead oxide may be acting through another mechanism such as a third body M in the chain breaking reaction shown in the following equations.

$$O + O_2 + M \rightarrow O_3 + M \qquad (13)$$

$$O_3 + CO \rightarrow CO_2 + 20 \text{ (Branching)} \qquad (14)$$

$$O_3 + CO + M \rightarrow CO_2 + O_2 + M \text{ (Breaking)} \qquad (15)$$

However, these particular reactions are merely suggested mechanisms; proof of their validity must await further work.

Conclusions

(1) The knocking behavior of hydrogen and carbon monoxide in engines resemble that of paraffinic fuels suggesting that the relatively simple H_2-O_2 reaction may play a major part in the reactions leading to hydrocarbon knock.

(2) The marked difference in knocking behavior and tetraethyllead response of "wet" and "dry" carbon monoxide-air mixtures is interpreted as meaning that antiknock activity is related to the presence of radicals containing hydrogen, as H, $HO_2^{\cdot}$ and $OH^{\cdot}$.

(3) The ability of tetraethyllead to raise the hydrogen-oxygen explosion temperature apparently arises from the action of lead oxide rather than metallic lead indicating that lead oxide is an inhibitor for H_2-O_2 chain branching explosive reactions.

REFERENCES

1. Anzilotti, W. F., Rogers, J. D., Scott, G. W., and Tomsic, V. J.: In process of publication. Ind. Eng. & Chem., *46*, 1314 (June, 1954.)
2. Lewis, B., and Von Elbe, G.: *Combustion, Flames and Explosions.* Academic Press Inc., New York, 1951.
   Jost, W.: *Explosion and Combustion Processes in Gases.* McGraw-Hill Book Company, New York, 1946.
3. Tanford, C., and Pease, R. N.: J. Chem. Phys., *15*, 431 (1947).
4. Tanford, C.: J. Chem. Phys., *15*, 433 (1947).
5. Downs, D., Walsh, A. D., and Wheeler, R. W.: Trans. Roy. Soc. (London), *243*, #870, 463-524 (July 19, 1951).

6. Rassweiler, G. M., and Withrow, L.: S. A. E. Quart. Trans., *42*, No. 5, 185–204, May, 1938.
7. Fowler, A., and Vaidya, W. M.: Proc. Roy. Soc. (London), *A*, *132*, 310 (1931).
8. Livingstone, H. K.: Oil Gas J., *46*, 80–87 (March 11, 1948).
9. Pease, R. N.: J. Am. Chem. Soc., *52*, 5106 (1930).
Giguere, P. A.: Can. J. Research, *25B*, 135 (1947).
10. Egerton, A. C., and Jain, B. D.: Fuel, *31*, 62–74 (1952).
11. Chamberlain, G. H. N., and Walsh, A. D.: Proc. Roy. Soc. (London), *A*, *215*, 175 (1952).
12. Geib, K. H., and Harteck, P.: Z. physik. Chem. *A*, *170*, 1–19 (1934).
13. McDonald, G. E.: NACA Report No. NACA RME53L08, February 5, 1954, Washington, D. C.
14. Hoare, D. E., and Walsh, A. D.: Proc. Roy. Soc. (London), *215A*, 454–466 (1952).

32

PHOTOGRAPHIC STUDIES OF COOL FLAMES AND KNOCK IN AN ENGINE

By GEORGE A. BALL

Introduction

Among the phenomena of interest in internal combustion engine research are the occurrence of cool flames and knocking combustion. The exact relationship between these two events is still rather obscure although considerable attention has been given in recent years to studying them. One method of investigating the combustion process in an engine has been the use of high-speed photography in which direct, schlieren and streak techniques have been used[1, 2, 3, 4, 5]. The present study confirms many of the photographic results of the authors cited above, and extends the analysis of the films in an attempt to provide a satisfactory basis for explaining the great variation in the physical appearance of knocking combustion.

The previous schlieren studies[3, 4, 5] have not been primarily concerned with the cool flame reaction, and the existence of a cool flame was not at all certain. Before exposing the films presented in this paper, combustion at the stated operating conditions was visually observed through a mechanical stroboscope and the existence of a cool flame was verified. Moreover, the time of occurrence in the cycle was noted so that identification of the cool flame period in the films was positive.

Concurrently with the cool flame studies, a series of films of knocking combustion was obtained. The camera used in this investigation provided a reasonable compromise between image size and definition, while still permitting severa successive cycles to be recorded. Both studies were made in a continuously operating engine as contrasted with the work of other investigators who used a single-explosion technique.

The previously mentioned photographic studies of knocking combustion have recognized the occurrence of autoignition in the end gas, but have not discussed in detail the method by which the autoignition spreads to consume the end gas. Consideration of the propagation of the autoignition reaction leads to a description of knocking combustion which appears to be in agreement with the published photographs of the phenomenon.

Test Apparatus and Methods

The top of the engine piston was ground to a spherical surface, electroplated, polished and used as the schlieren mirror of the coincidence system[6] used in this study. The light from a 40-watt zirconium point source arc lamp was directed by mirrors through a large quartz window in the engine head, into the combustion chamber, to the piston mirror and back out again to the knife edge and camera. The optical path was folded so that the schlieren image could be separated from the direct image which was photographed simultaneously. A separate optical system consisting of a lens and several mirrors projected the timing marks from the flywheel onto the film in the camera. All three events, the direct and schlieren images of the combustion process and the flywheel

timing marks, were photographed simultaneously on Super XX film in a 16 mm Fastax camera operating at about 7200 frames per second. A diagrammatic sketch of the optical system is shown in Figure 1.

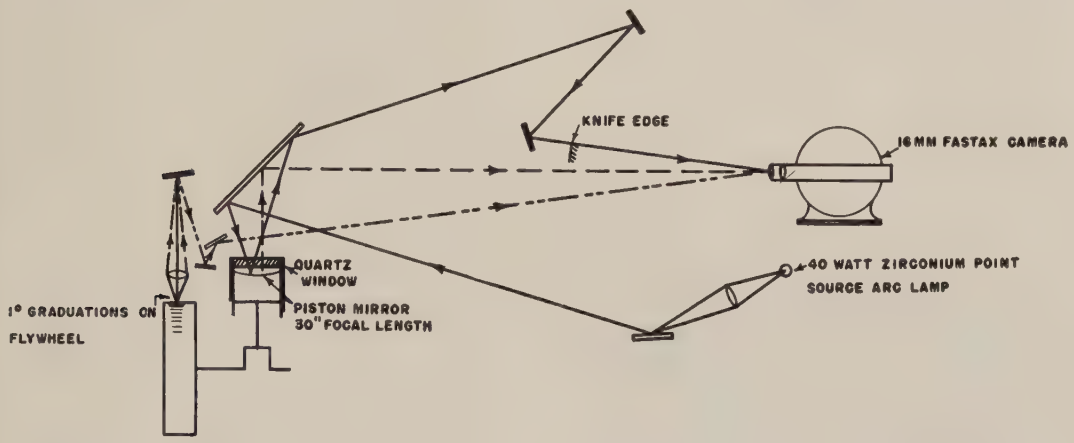

FIG. 1. Arrangement of optical components for photographing combustion process in engine.

The engine used was a CFR unit with an L-head conversion block and a special Invar head containing a quartz window covering virtually the entire combustion chamber (Fig. 2). The piston mirror surface was platinum that had been electroplated onto a copper undersurface. Two methods of obtaining the copper undersurface were tried, electroplating the copper and silver soldering a $\frac{1}{8}$-in slab of 2 per cent beryllium copper to the piston top. Both methods have disadvantages; the electroplates were difficult to polish satisfactorily and the copper slabs produced appreciable distortions which made the use of a schlieren system impractical. As a result the films reproduced in this paper were taken with a piston having the electroplated copper base for the mirror even though the surface contained some imperfections.

The major concern in establishing a test procedure was the problem of preserving the optical properties of the piston mirror. This required that the photographs be exposed as promptly as possible after starting the engine, and also that the oil leakage past the piston rings should be very low. Consequently, prior to making a run, the cylinder jacket cooling water and the intake air heater were preheated, while the engine oil was kept cool. Then, after starting the engine, the alignment of the optical system and the engine operating conditions were briefly checked and the film was exposed, generally within two minutes of starting the engine.

Results

COOL FLAMES

In order to obtain a clear photographic record of a cool flame, it is necessary to isolate the cool

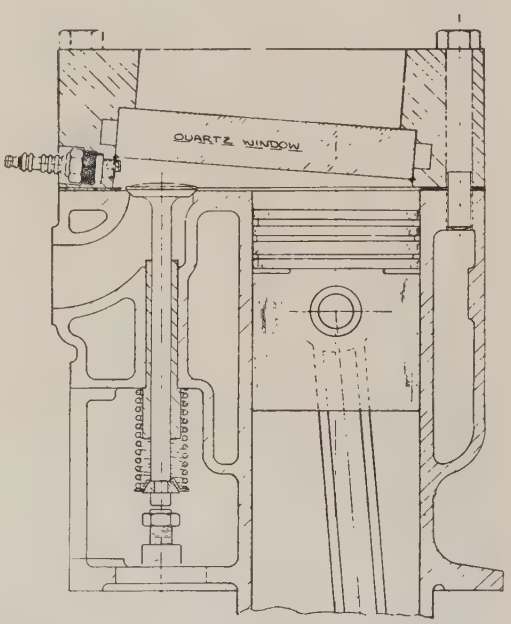

FIG. 2. Arrangement for viewing combustion process in engine.

flame phenomenon from other combustion processes. It was found, in accordance with the data available from Rapid Compression Machines[7, 8], that a motored engine operated at a high peak cycle temperature and a moderate pressure effectively separated the cool flame from the subsequent autoignition of the charge. The engine

conditions used were as follows:

Engine speed	600 rpm
Manifold pressure	29 in Hg
Carburetor air temperature	120°F
Cylinder jacket coolant temperature	190°F
Head coolant temperature	50°F
Oil temperature	<100°F
Ignition	None
Compression ratio	7:1
Fuel	*n*-heptane
Air-fuel ratio	35:1 (approx)

Figure 3 shows a typical sequence of events during the combustion phase of the cycle. Each frame shows a schlieren image of the piston top and a projected image of the flywheel timing marks. A part of the edge of the piston area is obscured by a shoulder which holds the quartz window in the engine head. The background of the schlieren image shows considerable distortion since it is difficult to preserve optical surfaces inside an operating engine.

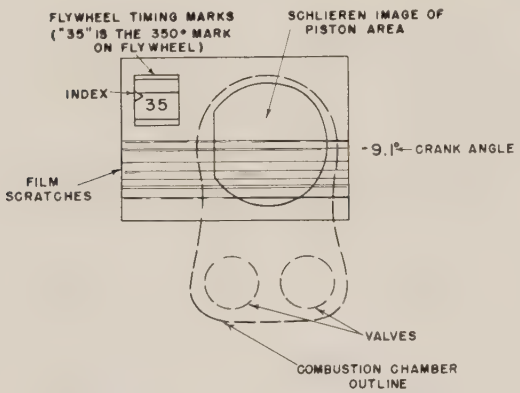

FIG. 3A. Explanation of individual frames of schlieren photograph.

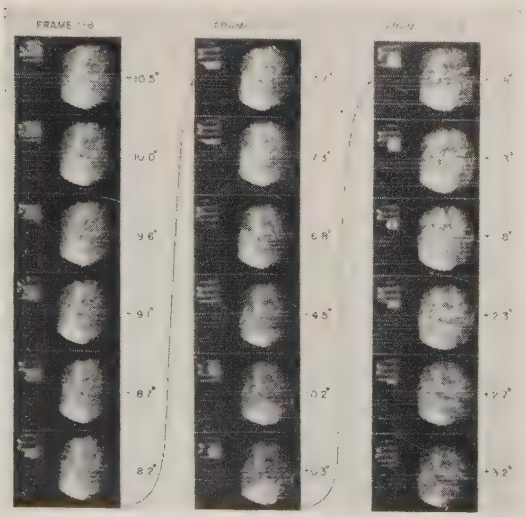

FIG. 3B. Individual frames showing mottling due to cool flame and autoignition.

It is immediately obvious that the reproductions of the individual frames show no clearly defined flame front, particularly of the cool flame reaction. When the films are projected, however, it is possible to detect an indication of an orderly progression of the reaction. Furthermore, if the reaction is viewed directly in the engine through a stroboscopic disc, the existence of a flame front is apparent even though the radiation from the flame is close to the limit of visibility. Consequently the following description of the phenomena represented by Figure 3 is based in part on direct visual observations.

The cool flame reaction initiates at the valve end of the combustion chamber. Since no spark is occurring in the engine, the onset of the cool flame is presumably due to a local source of heat somewhere in the neighborhood of the valves and the spark plug. The reaction passes across the combustion chamber and enters the field of the schlieren image (Frame 2). The reaction travels rather rapidly across the top of the piston, completing its travel by about Frame 8. As the products of the cool flame are exposed to continued compression, a second flame, also originating spontaneously at the valve end of the chamber, follows a path similar to the cool flame. This second flame is seen to enter the field of view in Frame 11 and to complete its travel in Frame 15. The time of transit of each of these flames has been estimated to be about one quarter that of a normal spark-ignited flame. The question of the significance of the speed of flames in an engine is considered in detail later in this paper.

The prominent features, then, of these cool-flame photographs may be summarized as follows:

(1) Confirmation of the existence of the cool-flame reaction in an operating engine.

(2) A demonstration of the possibility of a relatively high rate of propagation for a cool flame.

(3) A demonstration of autoignition occurring subsequent to the cool flame.

KNOCKING COMBUSTION

The engine operating conditions selected for producing knocking combustion are as follows:

Engine speed	600 rpm
Manifold pressure	29 in Hg

Carburetor air temperature	120°F
Cylinder jacket coolant temperature	190°F
Head coolant temperature	50°F
Oil temperature	100°F
Ignition timing	20° BTC (approx)
Air-fuel ratio	14:1 (approx)
Fuel	90 per cent 2,2,4-trimethylpentane + 10 per cent *n*-heptane
Compression ratio	7:1

Figure 4 is a photographic record of simultaneous direct and schlieren images of the combustion process during a typical engine cycle. The bright spot in the direct image is a reflection of the light source from the surface of the quartz window. It so happened that in this exposure the flywheel timing marks were incompletely projected.

The spark-ignited flame is seen to enter the field of view of the schlieren system in Frame 2. Direct light from the flame appears on the edge of the schlieren image and eventually overlaps the direct image. The flame front proceeds normally across the chamber until the appearance of a second flame front (Frame 10). No cool flame reaction is evident in the gases ahead of this second flame. The second flame front consumes the end gas very rapidly, with combustion complete in Frame 16. Rough approximations of the speed of the second flame front indicate a value of several hundred ft/sec, but certainly not as high as a thousand ft/sec. Therefore the end gas is being consumed simultaneously by two subsonic combustion waves. It should also be noted that the primary spark-ignited flame front apparently does not increase in velocity when the secondary flame front sweeps through the end gas. In fact, the gas expansion due to the rapid burning of the secondary flame makes the primary flame appear to stop in its travel. As previously noted, the subject of flame velocities is discussed later

The major features of these photographs can be summarized in this fashion:

(1) When knock occurs under the operating conditions listed with the stated fuel, a well-defined second flame front appears in the end gas, separate from the spark ignited flame.

(2) The secondary flame moves across the end gas with a moderately high velocity.

(3) The primary flame does not seem to accelerate into the end-gas region.

(4) No evidence of a cool flame appears.

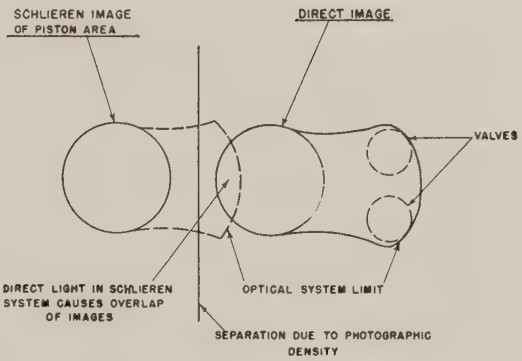
SCHLIEREN IMAGE OF PISTON AREA
DIRECT IMAGE
VALVES
DIRECT LIGHT IN SCHLIEREN SYSTEM CAUSES OVERLAP OF IMAGES
OPTICAL SYSTEM LIMIT
SEPARATION DUE TO PHOTOGRAPHIC DENSITY

FIG. 4A. Explanation of individual frames of simultaneous direct and schlieren images.

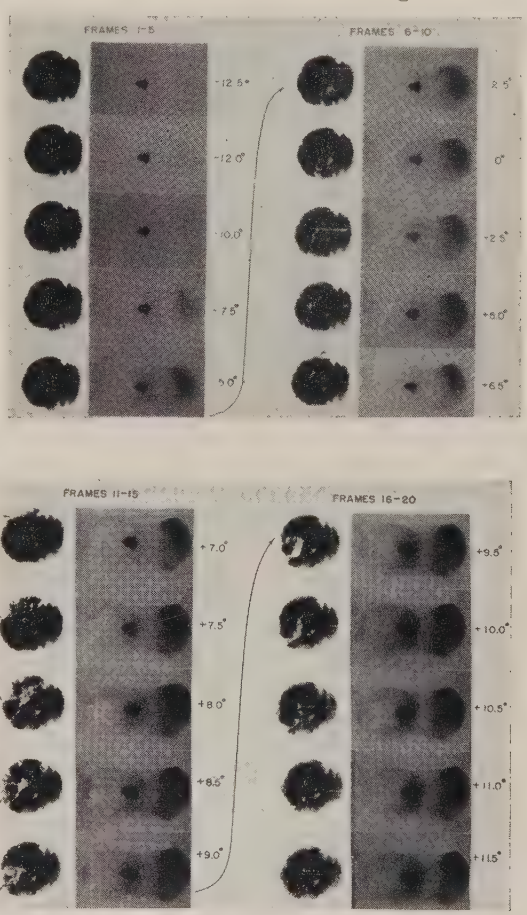

FIG. 4B. Individual frames showing direct and schlieren images of knocking combustion. Dashed lines in direct images emphasize flame front; arrows in schlieren images indicate autoignition flame.

Discussion

There is one feature in particular of these photographs of engine combustion which seems to require critical examination, namely, the co-

existence of two flames consuming a gas mixture at different rates. Neither flame is moving fast enough to be a detonation wave (which must travel at a speed greater than sonic), so that there are two subsonic flames consuming a given mixture at two different rates of combustion. This is in conflict with the usual concept of a single flame speed corresponding to a given state of a mixture. Some additional factor must be present in the case under consideration. One obvious factor concerns the physical boundaries of the gases. Prior to the appearance of the second flame, the unburned gases have been continually heated and compressed by the moving boundary of the combustion chamber, the piston, and also by the spark ignited flame. The unburned gases are already in a state of significant chemical reaction[9], although still at least an order of magnitude less than the maximum rates attainable in a flame. The unburned gases, or end gas, can be said to be in a state of stress. This state of stress makes possible an interaction between the flame and the whole mass of the reactants, extending over a far greater area than is usual for an unstressed mixture. That is, the compression and heating of the end gas by the autoignition flame accelerate the reactions throughout the whole unburned mixture, and not just in a restricted area immediately ahead of the flame. Thus the boundary conditions and previous history of the mixture make it possible for a flame to have a profound effect over a large mass of mixture. Presumably a mixture in a state of appreciable stress should show a schlieren effect, that is, density gradients would be expected to occur in the gases as a result of the chemical reactions in progress. The fact that no cool flame reaction, or other reaction, appears in the films is an indication that the sensitivity of the optical system is too low to show these density gradients.

Now it seems certain that the existence of two flame speeds in a given mixture must imply that there are physical differences in the flames in addition to their respective flame speeds. Moreover it seems reasonable to suppose that a flame in a highly stressed region would be thin, since the so-called preheat zone no longer moves with the flame, but is distributed throughout the end gas. A thin flame, with resulting high thermal gradients, would supply the high rates of energy transport necessary to maintain a high speed flame. We have, then, a stressed mixture being consumed by a thin flame traveling rapidly through the mixture and thus significantly changing the stress distribution. At the same time a thicker flame, moving more slowly and therefore having less effect on the stresses, is simultaneously consuming the same mixture, but because of its smaller gradients cannot build up, in the time available, the driving force needed for a high speed flame. It is suggested that rapid burning in a stressed medium be termed autoignition combustion to differentiate it from normal deflagration.

It seems likely, then, that a wide variety of end-gas inflammations can occur, limited only by the variety of stress distributions possible. Thus hydrocarbons whose normal combustion flames appear virtually identical could exhibit entirely different end-gas combustion due to dissimilar stress distributions. For example, it is characteristic of stoichiometric mixtures of *n*-heptane to autoignite in an engine without producing a clearly defined flame. The stress distributions associated with *n*-heptane are so nearly uniform that a flame cannot become established, but rather many points of ignition occur virtually simultaneously. This produces knocking combustion differing in character from the cycle shown in Figure 4. These differences exhibited by various fuels in their knocking combustion are due to differences in the manner in which an autoignition reaction can spread throughout the mixture. It is not surprising, then, that the cool flame reaction, generally considered as a slowly propagating phenomenon, can pass through a combustion chamber rapidly. The high speed and lack of definition of the cool flame is attributed to a nearly uniform stress which prevents the formation of a sharp boundary while allowing the reaction to spread quickly through the mixture.

The term *stress* has been used to indicate the relative ease with which an element of the mixture will burn. Determining the stress of an element is clearly a problem concerning reaction rates and their variation with pressure and temperature. Also involved is the problem of determining the temperature distribution in the gases so that reaction rates can be determined for each element of the mixture. The solution of these problems, and therefore the solution of the problem of knocking combustion, is extremely complicated since a detailed knowledge of autoignition combustion is essential.

One factor which deserves consideration is the question of the origin of the gas vibrations asso-

ciated with knock. In this connection consider the usual momentum equation for a thin flame,

$$p_1 + \rho_1 q_{1n}^2 = p_2 + \rho_2 q_{2n}^2 \qquad (1)$$

and the continuity equation,

$$\rho_1 q_{1n} = \rho_2 q_{2n} \qquad (2)$$

These may be combined to give:

$$\frac{\Delta p}{p_1}\left(1 - \frac{\Delta p}{p_1}\right) = \gamma_1 M_F^2 \left(\frac{\Delta T}{T_1} + \frac{\Delta p}{p_1}\right) \qquad (3)$$

where p = static pressure
T = static temperature
ρ = density
q = velocity
$\Delta p = p_1 - p_2$
$\Delta T = T_2 - T_1$
γ_1 = ratio of specific heats of reactants
$M_F^2 = q_{1n}^2/\gamma_1 R T_1$
R = gas constant of reactants

Subscript 1 refers to reactants.

Subscript 2 refers to products.

Subscript n refers to a component normal to the flame front.

Consider the magnitude of $(\Delta p/p_1)$ for a flame propagating at $\frac{1}{5}$ the speed of sound with an initial temperature of 1000° R and a final temperature of 4000° R so that $M_F = 0.2$ and $(\Delta T/T_1) = 3$. Assume $\gamma_1 = 1.400$. $(\Delta p/p_1)$ is found to be 0.24, that is, the pressure jump in the thin flame is a considerable fraction of the pressure level in the unburned gases. This suggests the possibility of a large pressure jump associated with the secondary high speed flame sufficient to initiate substantial gas vibrations when it reflects from a boundary. This large pressure effect also indicates the plausibility of suggesting that a high speed flame can appreciably affect the stresses in the end gas. Thus it does not appear necessary to postulate the occurrence of a detonation wave to account for the knocking sound. However, it may be assumed that shock waves can appear in the burned gases as a result of the impact of a high speed flame with the boundary of the chamber.

Conclusions

On the assumption of the existence of autoignition burning, the following tentative conclusions may be drawn.

(1) High velocity combustion waves, which are not detonation waves, can exist in the end gas.

(2) The character of autoignition burning is dependent on the state of stress of the end gas. Whether or not a single combustion wave will occur depends on the stress distribution. For uniform stress the whole end gas would inflame simultaneously.

(3) The state of stress of the end gas, being a point-by-point statement of the chemical character of the mixture, should depend on the type of fuel and the time history of the gases. This explains why the character of knocking combustion changes with fuel type and engine operating conditions.

(4) A mixture undergoing appreciable chemical reaction would usually be expected to contain density gradients and therefore exhibit a schlieren effect. The absence of any indication in the films of preflame reactions is presumed to be due to insufficient sensitivity of the optical system.

(5) The pressure jump in the autoignition burning is sufficient to excite gas vibrations which will produce audible sound, i.e., knock. It is not necessary to postulate a detonation wave to account for knock.

The above conclusions form a picture of knocking combustion in agreement with the films presented here, and not necessarily contradicting previously published photographs. The variation in the physical appearance of combustion during knock reported by the several investigators can be attributed to the different stresses in the end gas. The stress at a point would be characterized by the instantaneous chemical composition at the point and the rate of change of this composition with such factors as pressure, temperature, diffusion rate, etc. Therefore this supports the idea that the study of end-gas combustion and its control is much more concerned with the details of the chemical processes in the reactants than is the study of the usual deflagrations.

REFERENCES

1. Withrow, L., and Rassweiler, G. M.: Automobile Eng., *24*, 281–284 (1934).
2. Withrow, L., and Rassweiler, G. M.: SAE J., *39*, 297–303, 312 (1936).
3. Miller, C. D.: SAE Quarterly Trans., *1*, 98–143 (1947).
4. Osterstrom, E.: NACA TN 1614, June 1948.
5. Male, T.: Third Symposium on Combustion and Flame and Explosion Phenomena, p. 721. Baltimore, The Williams & Wilkins Co. 1949.
6. Liepmann, H. W. and Puckett, A. E.: *Intro-*

duction to Aerodynamics of a Compressible Fluid, Ch. 6. New York, John Wiley & Sons, Inc., 1947.

7. Roegener, H.: Z. Electrochem. *53*, 389–397 (1949).

8. Taylor, C. F., Taylor, E. S., Livengood, J. C., Russell, W. A., and Leary, W. A.: SAE Quaterly Trans., *4*, 232–70 (1950).

9. Walcutt, C., and Rifkin, E. B.: Ind. & Eng. Chem., *43*, 2844–2849 (1951).

33

MULTISTAGE AUTOIGNITION OF ENGINE FUELS

By WILLIAM J. LEVEDAHL

Introduction

In order to clarify the role played by preflame reactions in the autoignition of engine fuels, experimental results obtained from a *continuous-compression* engine were correlated with results obtained from a *rapid-compression machine*. The continuous-compression experiments were conducted in a modified CFR engine at the National Bureau of Standards[a]. This engine compresses a single fuel-air charge until it autoignites, in the absence of residual exhaust gases, cylinder hot spots, and lubricating oil[1, 2]. The rapid compression results were subsequently conducted in a rapid compression machine[b 3, 4]. This machine compresses the mixture suddenly to a preselected temperature and density, and the succeeding combustion processes occur at constant volume.

Data from both apparatuses indicate that the third or hot-flame stage of autoignition reaction in all higher aliphatic hydrocarbons becomes rapid in a temperature region around 1580°R (878°K) for lean mixtures. This temperature is lowered slightly by increased fuel concentrations.

The primary function of the second or cool-flame stage of reaction in promoting autoignition seems to be the heating of the mixture to this temperature region. The function of the first or peroxide stage of reaction is apparently to produce sufficient active particles to promote the exothermic cool-flame reaction. The rates of these reactions determine the autoignition resistance of the mixture. The temperature sensitivity of a fuel is a function of the rate of reaction of the cool-flame stage relative to the rate of the peroxide-forming stage. These rates of reaction during the first two stages increase with the number of secondary carbon-hydrogen bonds in the fuel molecule.

Apparatus

(1) Continuous compression experiments were carried out in a dynamometer-driven engine without spark plug; compression alone was used to autoignite a single premixed charge. Cylinder oil was eliminated from the combustion chamber by use of a cross-head piston and oil seal, and lubrication of the compression piston was furnished by a segmented graphite piston ring. A spring-loaded check valve in the cylinder head opened during the compression stroke, bypassing the gases and preventing reaction from occurring while equilibrium operating conditions were being reached. When a single compression cycle was desired a solenoid-operated mechanism locked the valve closed at the proper time in the cycle. A strain-gage pressure pickup provided a signal used to give pressure and rate of pressure rise, and a photomultiplier tube mounted outside a quartz window measured radiation intensity. These signals were presented as functions of crank-angle (time) on two dual-beam oscillographs and were photographically recorded.

(2) The rapid compression machine consisted essentially of an upright cylinder of 80 mm bore in which a piston mounted on a cylindrical rod was accelerated upward by air pressure against its lower surface, compressing a fuel-air mixture

[a] The experimental work at the National Bureau of Standards, Washington, D. C. was done with the assistance of C. R. Yokley. The project is supported in part by the Department of the Army, Office of the Chief of Ordnance.

[b] Developed under Professor F. A. F. Schmidt at the Institut für Wärmtechnik und Verbrennungsmotoren of the Technische Hochschule Aachen, Germany.

in the upper part of the cylinder. The piston was decelerated from a velocity of about 50 m/sec to zero during the last 35 mm of a 490-mm stroke when the flanged lower end of the piston rod engaged the piston of a hydraulic brake whose orifices were designed to give constant deceleration. Approximately 40 per cent of the pressure rise occurred during the 2 millisecond deceleration period. A strain-gage pressure pickup was used in conjunction with an oscilloscope and drum camera to record pressure as a function of time.

Identification of Phenomena

Autoignition may be considered to occur in three stages which can be named for their distinguishing characteristics. The first or *peroxide* stage, which is not measurably exothermic, has been detected by testing for active oxygen, and is believed to produce alkyl hydroperoxides[5, 6]. The second or *cool-flame* stage is exothermic, produces a blue radiation believed to be from excited formaldehyde[7, 8], and reaches a maximum rate at a moderate temperature. The third or *hot-flame* stage is highly exothermic and generally rapid, produces intense radiation, and is responsible for audible knock vibrations in engines.

The lower temperature limit for peroxide formation in the engine was determined by motoring the engine at progressively increased compression ratios and testing exhaust products for active oxygen. The calculated peak compression temperature corresponding to the first positively-reacting sample was called the *peroxide limit* for that fuel. Whenever active oxygen was found, an aldehydic odor was detected in the exhaust gases.

Cool-flame radiation has been detected at temperatures within about 10°F of the peroxide limit when the radiation detection circuit was used at high gain. Figure 1 shows radiation-time diagrams of four identical combustion cycles; the circuit amplification increases by powers of 10. The cool-flame radiation is detectable progressively earlier as the sensitivity of measurement is increased, and any sharp division of the peroxide and cool-flame stages appears impossible if the start of radiation is used as a criterion. The beginning of the cool-flame reaction is therefore arbitrarily designated as the point at which the rate of pressure rise shows that the reaction has become measurably exothermic.

Pressure, rate of change of pressure, and radiation intensity were usually simultaneously recorded during the cool- and hot-flame reactions in the continuous-compression engine. Figure 2 is a typical oscillogram of *n*-heptane in a 0.5 stoichiometric mixture ($F/A = 0.033$), and the mixture density a top center is 0.0144 lb mol/ft^3.

The upper two traces show the variation in pressure with time in a single cycle; the higher trace was made with a higher amplification factor. The two higher horizontal lines are calibration marks at 314 psia, and the lower horizontal lines represent 14 psia. Time-coordinating marks are represented in degrees of crank angle, with 0° at

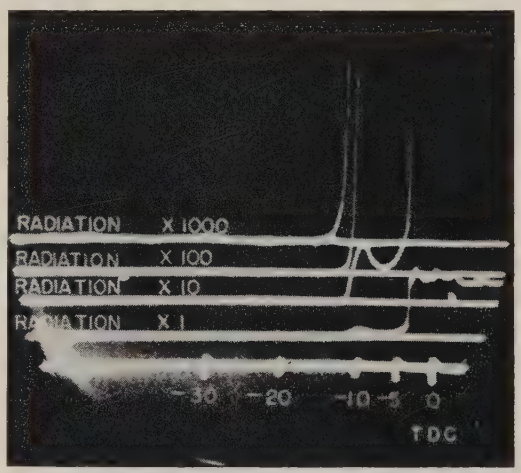

FIG. 1. Radiation intensity vs time of an *n*-heptane autoignition, presented at relative amplification factors of 1, 10, 100, and 1000, showing that cool-flame radiation can be detected progressively earlier with increasing sensitivity of the instrumentation.

top center where combustion chamber volume is at a minimum. One millisec is equivalent to 5.4° crank angle.

The cool flame reaction becomes evident at about 19° before top center where pressure shows a distinct increase over that due to piston motion. The pressure continues to rise at a slower rate up to 6° before top center where the hot flame reaction becomes rapid. The violent pressure vibrations or knock are produced as a result of this reaction and are gradually damped out as the piston descends.

The lower trace in the bottom diagram was made by electronically differentiating the pressure signal, and, when compensated for piston motion, is a measure of the rate of heat release throughout the reaction. Just above the dP/dt line is a radiation-time curve which shows relative emission intensity received by a photomulti-

plier tube. The sharp rise of the dP/dt trace at 19° before top center was selected as the beginning of the exothermic cool-flame reaction. The similarity in shape between the cool-flame radiation trace and dP/dt curves as they reach a peak and then decrease suggests that in this region the rate of heat release and the intensity of cool-flame radiation are closely related. dP/dt reaches a minimum following the cool-flame peak; thereafter the radiation rises sooner than does dP/dt. This earlier rise implies that the hot flame reaction actually begins before the pressure is substantially affected, and that no exact dividing line between stages can be drawn.

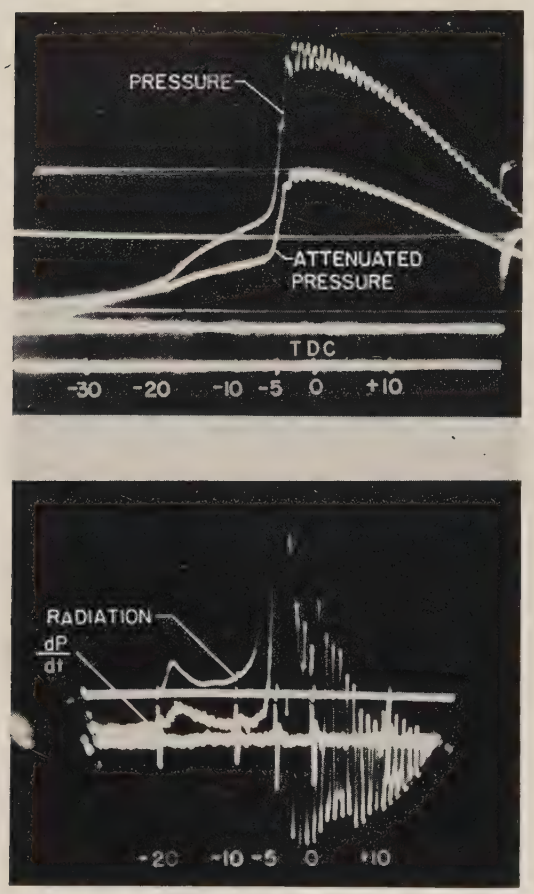

FIG. 2. Typical autoignition oscillogram of a lean, low-density n-heptane mixture in the engine. Pressure, radiation intensity, and rate of change of pressure are shown as functions of crank angle. (5.4° = 1 millisecond.)

FIG. 3. Typical pressure-time trace from rapid compression machine showing two-stage reaction in 2-methylpentane. Calibration mark at left represents 290 psia; pressure before compression is 15 psia.

Studies made in the rapid compression machine gave diagrams typified by Figure 3, which was made with 2-methylpentane at 0.53 stoichiometric, compression density of 0.0210 lb mol/ft^3 and 1215°R compression temperature. The calibration mark at 290 psia is seen at the left; the compression, starting from 15 psia, follows. At the end of compression the pressure remains constant during the peroxide stage or primary delay (τ_1) but rises during the cool-flame reaction or secondary delay (τ_2). τ_2 is terminated by the start of rapid hot-flame reaction.

Temperatures in the engine were computed from the perfect gas law $T = PV/NR$. The pressure was measured from the pressure diagram, and the combustion chamber volume is a known function of crank angle and compression ratio. The number of moles of gas present in the cylinder is the sum of the quantity metered into the chamber plus the quantity of residual unburned charge. Calculations were made with the assumption that no change in number of moles took place during the reaction. Sampling experiments have shown that the maximum increase in number of moles during the cool-flame reaction does not exceed 2 per cent, and the computed temperatures should be high by no more than this amount.

In the rapid compression machine the cylinder volume, gas temperature, and gas pressure before compression were used to compute the number of moles of charge. Temperatures after compression were again computed from the perfect gas law, using the known volume and number of moles in conjunction with oscillographically recorded pressures.

Effect of Fuel Type on Reaction in the Engine

n-Heptane, isooctane, and 40 and 80 octane-number blends were all autoignited with the same top-center density of 0.0288 lb mol/ft^3 and with the same rate of change of density during compression. Higher initial pressure and temperature were necessary to autoignite the less-reactive fuels at the same density. Figure 4 shows a series of radiation-time and pressure-time diagrams for the four fuels at 0.5 stoichiometric. The

rate of cool-flame reaction decreases as the quantity of *n*-heptane in the fuel is reduced; the duration of the reaction is thereby increased.

was substantially affected, the temperatures computed from pressure data would be somewhat high and the error would be greater with

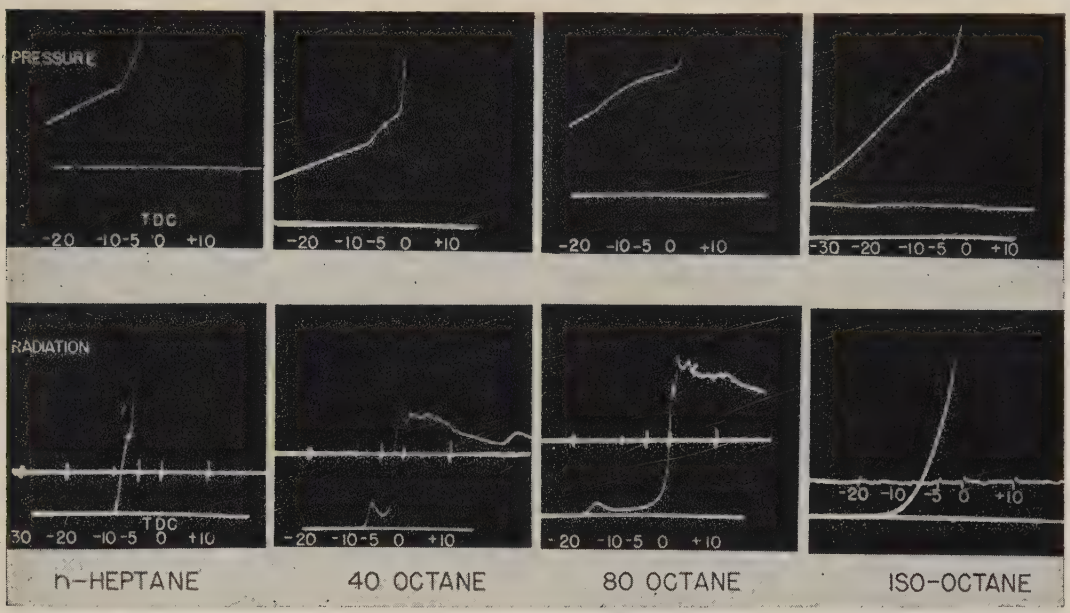

FIG. 4. Pressure- and radiation-time diagrams of 0.5 stoichiometric primary reference fuel blendes. 5.4° = 1 millisecond in the 0, 40, and 80 octane diagrams; 3.6° = 1 millisecond for iso-octan. These diagrams were all taken with identical top center densities and rates of compression.

Figure 5 shows reaction-stage temperature limits of these blends as functions of octane number at fuel-air ratios of 0.5, 0.75, and 1.0 stoichiometric. The temperatures at which peroxides and exothermic cool-flames are first detectable increase substantially as the fraction of isooctane in the blend increases; thus, the higher octane component appears to have an inhibiting effect. A simple diluent effect seems improbable; if an *n*-heptane mixture is diluted with air (i.e., when the mixture becomes leaner), the peroxide and cool-flame reaction stages are comparatively little affected.

The grouping of all hot-flame limit points in the same temperature region is significant. The average temperature for all four fuels at 0.5 stoichiometric is about 1585°R. When the fuel concentration is doubled this temperature decreases to about 1550°R. A slight tendency toward lower temperatures with lower octane number is evident. The inequalities noted may be due to selection of the inflection point in the pressure-time curve as the point at which the hot flame begins. Since the first sign of hot-flame radiation could be found well before the pressure

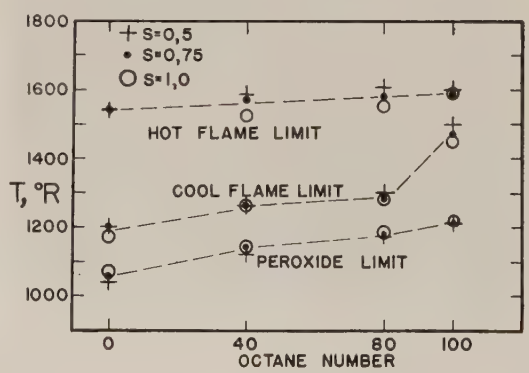

FIG. 5. Temperature limits for first detectable peroxides, measurably exothermic cool-flame, and rapid hot-flame reaction for primary reference fuels reacted with identical rates of compression and TDC densities at fuel-air ratios of 0.5, 0.75 and 1.0 stoichiometric.

the more slowly reacting (leaner and higher octane number) mixtures.

Hot-flame temperature limits were computed from pressure diagrams previously taken[2] on the following fuels: *n*-heptane, *n*-hexane, 2-methylpentane, 3-methylpentane, 2,2-dimethylbutane, 2,3-dimethylbutane, hexene-1, hexene-2, 4-

methyl-2-pentene, cyclohexane, cyclohexene, benzene, *n*-heptaldehyde, 1-hexanol, *n*-heptane + 1 mol per cent ditertiarybutylperoxide. Most fuels showed temperature vs. fuel-air ratio curves similar to those for octane-heptane blends. At 0.5 stoichiometric the average value of the hot-flame limit was about 1580°R, at stoichiometric

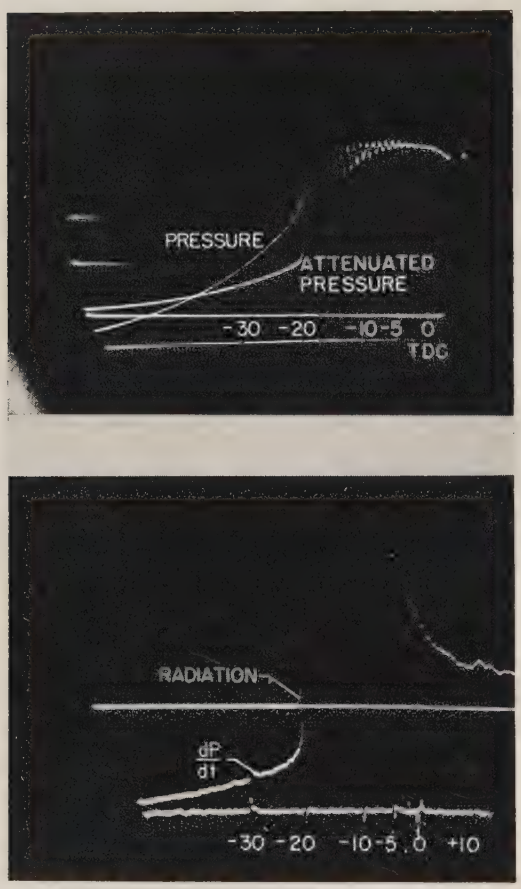

FIG. 6. Autoignition of 0.10 stoichiometric acetylene mixture.

the value was about 1530°R, and at 1.5 stoichiometric the value was about 1500°R.

No consistent trend of temperature with autoignition resistance was noted, and all tests resulted in temperatures within 3 per cent of these values with the following exceptions: benzene showed a very high, inconsistent hot-flame limit; cyclohexane points were irreproducible but low; hexanol temperatures were low at rich mixtures, and 1-hexene showed lower than average temperatures at lean mixtures.

The pressure-time curves for pure aliphatic fuels are similar to those shown in Figure 4 for octane-heptane blends. In the extreme case of acetylene, however, a 0.10 stoichiometric mixture ignites so violently that diagrams like Figure 6 result. No cool-flame reaction could be detected, but the hot-flame reaction sometimes took a two-stage appearance. A rapid hot-flame reaction begins from 1530° to 1560°R, and the violent, almost instantaneous part of the pressure rise begins about 100° higher.

Lean (0.10 stoichiometric) hydrogen-air mixtures ignite with difficulty and burn slowly, like benzene and quite unlike acetylene. When the fuel-air ratio is raised to 0.40 stoichiometric, pressure diagrams like that of Figure 7 are obtained in which the first reaction can be detected at about 1760°R and a more rapid stage at about 2360°R. These temperatures are substantially higher than the temperature at which aliphatics enter the hot-flame reaction.

The hot-flame stage of reaction begins in the same temperature region for aliphatic fuels including paraffins, olefins, acetylene, oxygenated compounds, and blends. The average of the recorded temperatures is about 1580°R for 0.5 stoichiometric mixtures, about 1565°R at 0.75 stoichiometric, about 1540°R at stoichiometric, and about 1500°R at 1.5 stoichiometric. Benzene, hydrogen, and cyclohexane appeared to have no sharply-drawn ignition temperature limits. This characteristic temperature region suggests that some essential reaction common to higher aliphatics (possibly thermal decomposition) becomes predominant and rapid in this range.

The Function of the Cool-Flame Reaction in Autoignition

The primary function of the cool-flame reaction in promoting autoignition is apparently to heat the mixture to the characteristic temperature region. If a mixture which produces little or no cool-flame reaction is to autoignite within a short period of time, it must be compressed directly to a temperature in this region. A mixture which forms a very intense and rapid cool-flame reaction, on the other hand, can be compressed to a substantially lower temperature and will still reach the hot-flame reaction temperature within a short time by virtue of the self-heating effect of the cool-flame reaction.

The rate of heat release at the peak of the cool-flame reaction in *n*-heptane was studied in the engine at several mixture densities and fuel-air ratios. Figure 2 shows a moderate rate of pressure rise during the cool-flame reaction in a

0.5 stoichiometric mixture with peak density of 0.0144 lb mol/ft³ at top center. Figure 8 was made with the same rate of air flow but with twice the fuel flow, so that the mixture was stoichiometric. The peak rate of reaction during the cool flame was approximately doubled, as can be seen from the relative heights of the dP/dt traces. When this higher fuel flow was maintained and the air flow doubled (giving a 0.5 stoichiometric mixture with peak density of 0.0288 lb mol/ft³) the peak rate of reaction during the cool flame was again doubled (Fig. 9). Thus, doubling the total charge density at constant fuel-air ratio quadruples the peak cool-flame reaction rate.

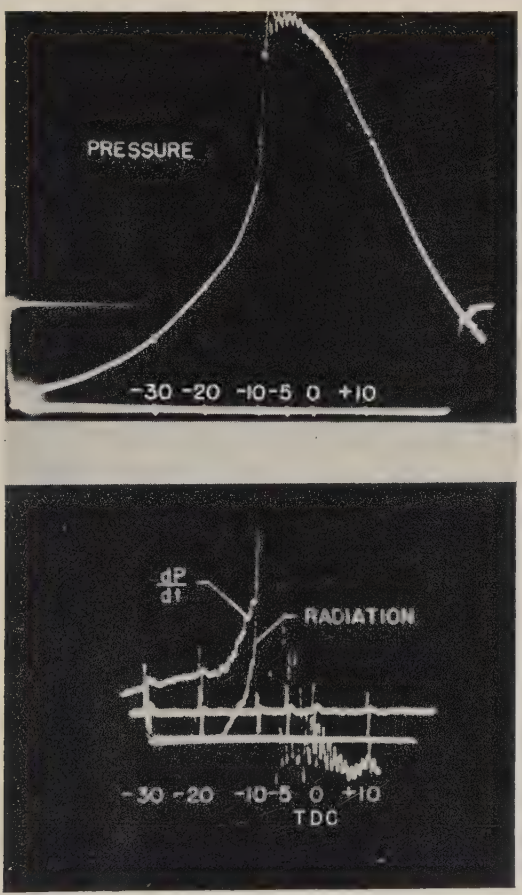

FIG. 7. Autoignition of 0.40 stoichiometric hydrogen mixture.

The maximum rate of cool-flame reaction is therefore proportional to the fuel concentration and to the oxygen concentration. This relation implies that the rate-limiting reaction may be bimolecular. Measurements made with mixtures of three densities and fuel-air ratios ranging from 0.25 to 1.5 stoichiometric show that this relation holds for mixtures which are stoichiometric or leaner (Fig. 10). The addition of fuel above the stoichiometric value apparently produces no additional increase in reaction rate.

The temperature at which the peak rate of reaction was reached increased steadily with the partial pressure of fuel in the combustion chamber. At a density of 0.0288 lb mol/ft³, mixtures which were stoichiometric or richer reached the hot-flame limit before this peak occurred. As the fuel concentration is increased the pressure curve loses its inflection point and progressively approaches the shape of an exponential curve.

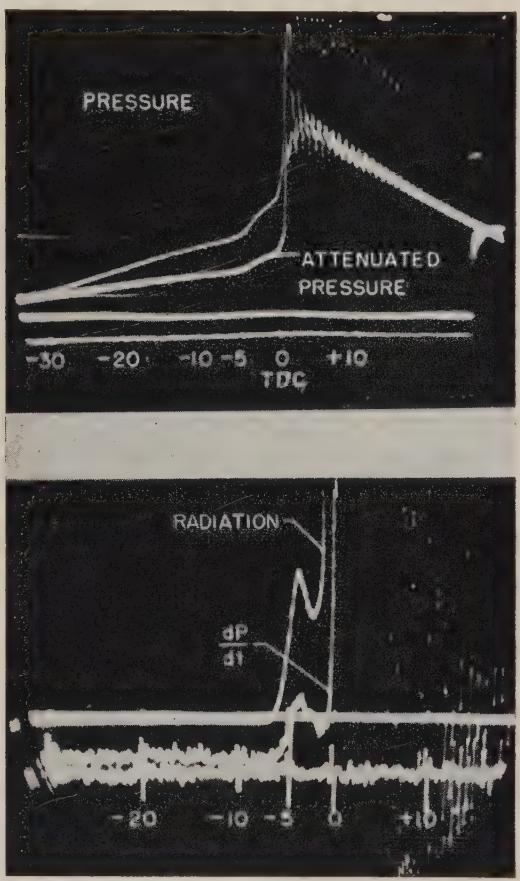

FIG. 8. n-Heptane autoignition under conditions identical to those of Fig. 2 except that the fuel flow was doubled, producing an increased rate of cool-flame reaction.

Since fuel comprised only about 1 to 2 mol per cent of the charge, the total heat capacity of the contents of the combustion chamber is approximately proportional to the air density. Thus,

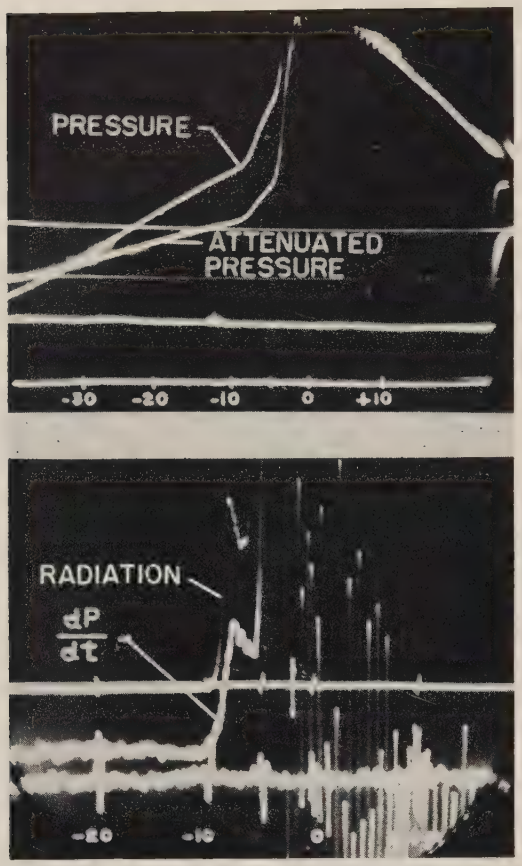

FIG. 9. *n*-Heptane autoignition with lean, high-density mixture. Fuel flow is identical to Fig. 8, airflow is doubled, further increasing the rate of cool-flame reaction.

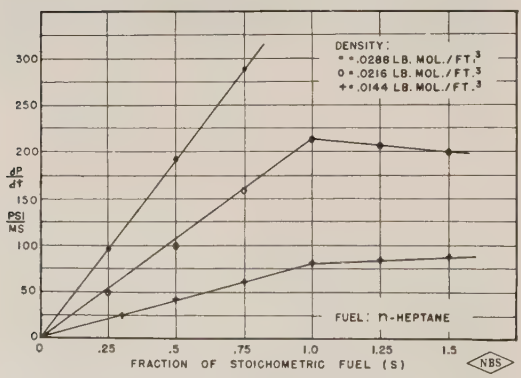

FIG. 10. Maximum rate of pressure rise during the cool-flame as a function of fuel-air ratio at three peak densities. The rate of reaction of lean mixtures is proportional to the fuel density and to the air density, i.e., to the square of the total density at constant F/A.

when the rate of pressure rise is doubled by doubling the air density, the rate of temperature rise should remain nearly constant. The rate at which the temperature rises during the cool-flame reaction is essentially proportional to the concentration of the fuel.

Effect of Fuel Type on Reaction in the Rapid Compression Machine

Thirteen hydrocarbons with 6 to 8 carbon atoms, all alkanes with the exception of cyclohexane and benzene, were investigated in the rapid compression machine. The five aliphatic hexanes, cyclohexane, benzene, iso-octane, and *n*-heptane were all tested under each of the first four conditions listed in Table 1, the dimethylbutanes under the fifth as well, while three iso-heptanes and *n*-octane were tested under condition 2 only.

TABLE 1. CONDITIONS AFTER COMPRESSION IN THE RAPID COMPRESSION MACHINE

Condition	Temperature	Total Density	Fuel/Air (Per cent stoichiometric)	Air Density (Relative)	Fuel Density (Relative)
	°R	*lb mol/ft*³			
1	1140	0.0204	0.375	0.97	0.97
2	1210	0.0210	0.375	1.00	1.00
3	1215	0.0210	0.530	1.00	1.41
4	1219	0.0300	0.375	1.42	1.42
5	1208	0.0216	0.75	1.01	2.02

The values in Table 1 represent average conditions at the end of compression as computed from the initial temperatures, compression ratio (about 9.7), and pressures recorded immediately before compression, and compression pressures measured from the diagrams. Deviations from these values averaged about 2 per cent.

Under the first condition the mixture was lean and temperature and density were low enough so that the most easily reacted hydrocarbon had a fairly long delay period. The second condition differed from the first only by a 70°F increase in compression temperature, while density and fuel-air ratio remained constant within the limits of accuracy to which the preselected condition could be approximated. The third condition differed from the second in that the concentration of fuel (and fuel-air ratio) was increased to $\sqrt{2}$ of its initial value. Condition 4 had the fuel concentration and temperature of condition 3, but the air concentration was increased to $\sqrt{2}$ of

its previous value. The fuel-air ratio was the same as that in condition 2, but the total density was $\sqrt{2}$ times as high. Condition 5, under which only two fuels were tested, had the temperature and density of condition 2, but the fuel concentration was twice as high.

Progression from conditions 1 to 2 therefore showed the effect of temperature, from 2 to 3 and 3 to 5 the effect of fuel concentration, 3 to 4 the effect of air concentration, and 2 to 4 the effect of total density at constant fuel-air ratio.

Figures 11 and 12 show a series of pressure diagrams made under condition 4 with nine fuels. The primary delay is small with the normal paraffins and increases with the amount of branching in the molecule. The secondary delay is short and the cool-flame reaction rapid with the normal paraffins. With the methylpentanes and particularly with 2,2-dimethylbutane the cool-flame reaction rate reaches an early peak, then continues at a slower rate until the hot flame occurs. 2,3-dimethylbutane and cyclohexane do not show distinct peaks in the rate of cool-flame reaction, and benzene shows only a gradual, apparently exponential, one-stage pressure rise which begins after the primary delay. Iso-octane shows a small pressure rise at the beginning of the cool flame, succeeded by a period of slow reaction gradually increasing in rate to the point of hot-flame initiation.

The temperature at which the hot-flame reaction began was calculated from each diagram, and these points are plotted in Figure 13 for each fuel at each of the five conditions described in Table 1. Engine data are also presented for comparison and are designated as condition 6 (0.50 stoichiometric) and condition 7 (0.75 stoichiometric). The temperature averages for the rapid compression machine are presented with the corresponding average deviations in Table 2 and were computed using data from all fuels tested except cyclohexane and benzene. Cyclohexane data, under conditions 1–4, showed an average temperature of 1625°R with average deviation of 113°F.

With aliphatic hydrocarbons at lean mixtures (0.375 and 0.53 stoichiometric) the hot flame became rapid at temperatures averaging 1579°R. Engine data taken at 0.5 stoichiometric averaged 1580°R. The three points at 0.75 stoichiometric averaged 1562°R, which also compares closely with the 1565°R average of the engine data. No consistent trend of hot-flame temperature with compression temperature or charge density was noted. Points for isooctane and 2,3-dimethylbutane were often difficult to select because of the slowness of the hot-flame reaction and consequent lack of a sharp change in slope of the pressure curve. Aside from the points with these two fuels (and with cyclohexane, which was completely inconsistent), no significant trend in temperature with molecular structure was noted. Most of the engine data presented here fall in

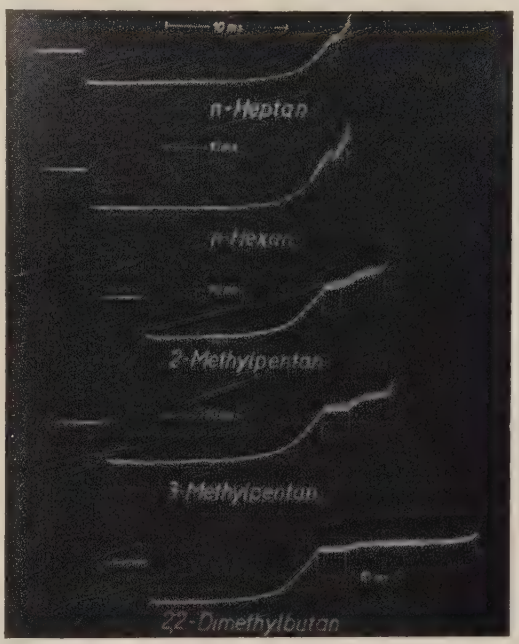

FIG. 11. Autoignition of 5 parafins. F/A = 0.375 stoichiometric, compression temperature = 1219°R, density = 0.0300 lb mol/ft³.

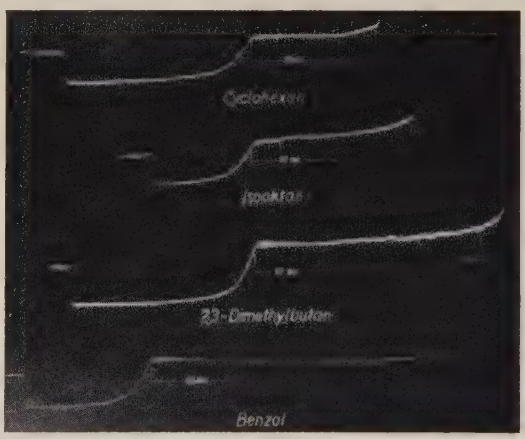

FIG. 12. Autoignition diagram. F/A = 0.375 stoichiometric, compression temperature = 1219°R, density = 0.0300 lb mol/ft³.

the same range as the rapid-compression machine points.

Figures 14, 15, and 16 show respectively the effects of progressing through conditions 1 through 4 on the primary delay, secondary delay, and total delay. An increase of 70°F compression temperature (conditions 1–2) reduced the primary delay of all fuels greatly. The delay decreased in *n*-heptane from 4.1 ms to essentially

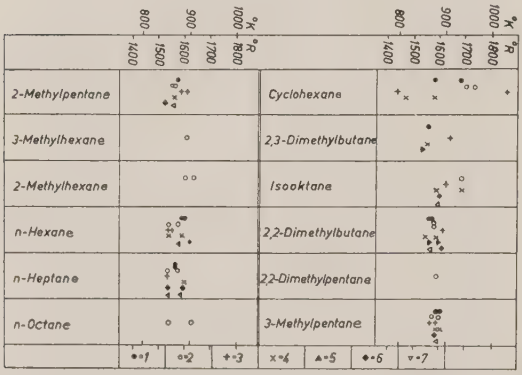

Fig. 13. Hot-flame ignition temperatures with 12 fuels. Conditions 1 through 5 are given in Table 1 for compression machine. Engine conditions 6 and 7 were 0.5 and 0.75 stoichiometric, respectively.

Table 2. Hot-Flame Initiation Temperatures in the Rapid Compression Machine

	Cond. 1	Cond. 2	Cond. 3	Cond. 4	Cond. 5
Number of fuels used	7	11	7	7	2
Number of points used	11	17	12	12	3
Average temperature, °R	1577	1579	1582	1579	1562
Average deviation, °F	26	25	26	29	23

0, in the intermediate branched paraffins about 75 per cent, and in the cyclics and 2,3-dimethylbutane about 17 ms. Increased fuel concentration (conditions 2–3) had a comparatively small effect on all fuels except cyclohexane and 2,3-dimethylbutane. Increasing air concentration (conditions 3–4) was virtually ineffective except with 2,3-dimethylbutane. For most paraffins, the primary delay is an inverse function of temperature. For cyclohexane it is an inverse function of temperature and fuel concentration. For 2,3-dimethylbutane it is decreased by temperature, fuel concentration, and air concentration.

The effects of these three influences on the secondary delay, however, are quite different. Temperature had a substantial effect only on 2,3-dimethylbutane. (Due to the irreproducibility of iso-octane points under condition 1, it is difficult to interpret its apparent decrease in delay. Benzene is not shown since it did not have a cool-

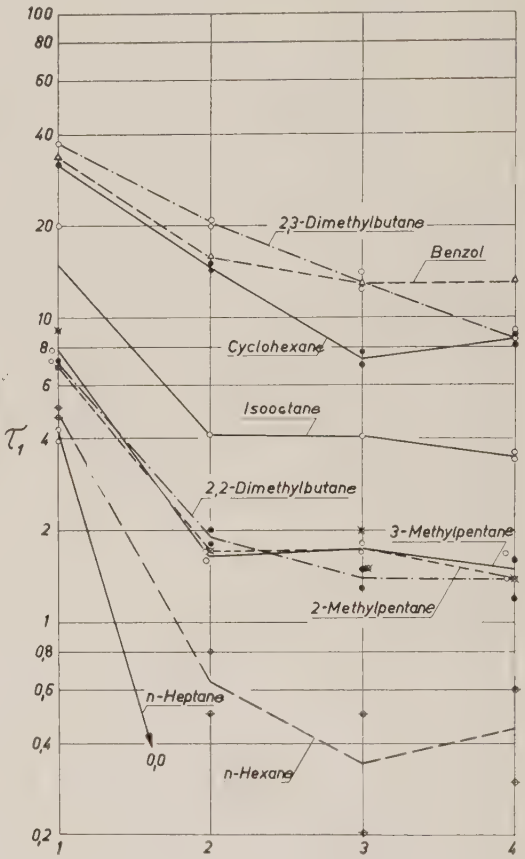

Fig. 14. Primary delay in rapid compression machine. Conditions 1, 2, 3, and 4 are stated in Table 1. From condition 1 to 2, temperature is raised 70°F; from 2 to 3, fuel concentration is raised 41 per cent; from 3 to 4, air concentration is raised 41 per cent.

flame stage.) The secondary delay was nearly halved for each fuel as the fuel concentration was multiplied by $\sqrt{2}$. A corresponding increase in air concentration had small effect on all fuels except 2,3-dimethylbutane, in which delay more than tripled. The secondary delay of most fuels is decreased substantially by increased fuel concentration only; secondary delay of 2,3-dimethylbutane is decreased by increased temperature and fuel concentration but is increased by increased air concentration.

Increased temperature and increased fuel concentration decreased the total delay in every case (Fig. 16). Increased air density had a small effect except in the case of 2,3-dimethylbutane where it increased the total delay substantially.

Significance of Ignition Delay Measurements

During the primary delay the main reaction is believed to be the production of a sufficient concentration of peroxides to initiate the cool-flame reaction[5, 6, 9]. Increased temperature has a strong influence on the rate at which this concentration is reached, but increases in fuel and air densities show little effect. These results agree with those of Rögener[10] who found that the equation for primary delay had a very high apparent activation energy and was uninfluenced by fuel-air ratio for *n*-heptane mixtures between 0.55 and 1.77 stoichiometric.

The cool-flame reaction serves to increase the mixture temperature to the common hot-flame ignition region. The rate of cool-flame reaction usually becomes rapid soon after the beginning of the secondary delay, but is slow during the later part of this stage. An increase in compression temperature decreases the amount of temperature rise which occurs during the rapid part of the reaction, but does not affect the later period. Therefore, increased temperature has little effect on the secondary delay of fuels which have early peaks in the cool-flame reaction rate. 2,3-dimethylbutane shows no peak in the cool-flame reaction rate, and the secondary delay decreases substantially with increased compression temperature.

Engine experiments showed that increased fuel concentration not only caused a proportional increase in maximum cool-flame reaction rate, but also increased the temperature at which the peak rate of reaction occurs. With increasing fuel concentration progressively less of the temperature rise occurs during the period of slow reaction

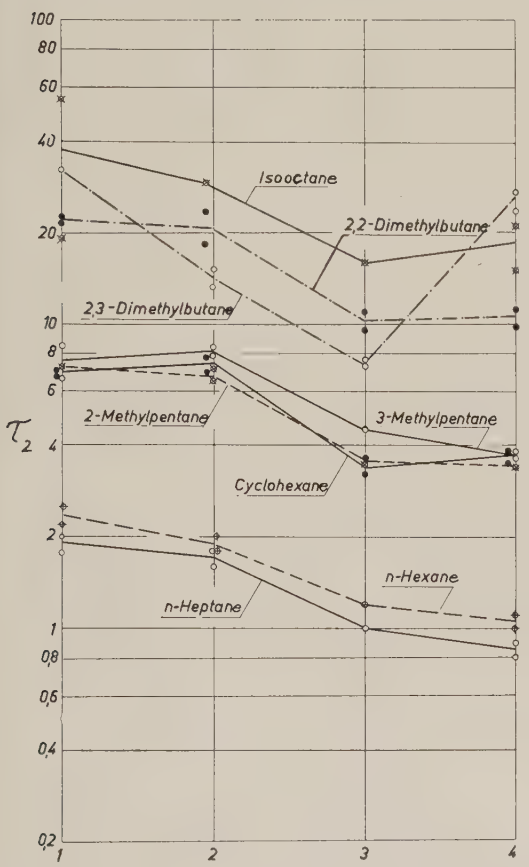

FIG. 15. Secondary delay in rapid compression machine.

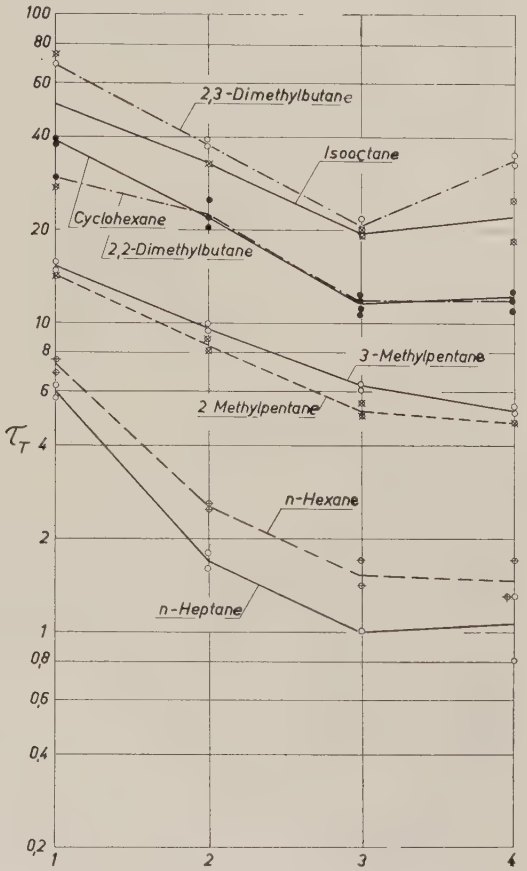

FIG. 16. Total delay in rapid compression machine.

following the peak of the cool flame. Thus the secondary delay decreases more rapidly than the fuel concentration is increased.

Increased air concentration had no sizable effect on the secondary delay of most fuels, thus the average rate of temperature rise remained constant. The total heat capacity of the mixture is approximately proportional to the air concentration, so that rate of exothermic reaction was also proportional to air concentration. This relationship would hold if the average of the reactions throughout the entire stage is bimolecular. Since measurements in the engine indicated that the reaction is bimolecular at its peak, the entire cool-flame reaction can be treated as one of second order.

Table 3. Delay and Sensitivity of Thirteen Fuels

Fuel	Total Delay Condition 2	Absolute Sensitivity Ratio	Octane Number Research Method	Sensitivity (Octane Units)
n-octane	1.5		0	
n-heptane	1.7	47.4	0	0
n-hexane	2.5	33.6	24.8	−1.2
2-methylhexane	3.3		42.4	
3-methylhexane	5.3		52.0	
2-methylpentane	8.5	11.0	73.4	0.1
3-methylpentane	9.7	8.6	74.5	−0.2
Cyclohexane	22.0	12.7	83.0	5.8
2,2-dimethylbutane	22.8	4.2	91.8	−1.6
2,2-dimethylpentane	21.7		92.8	
Isooctane	33.1	12.1	100	0
2,3-dimethylbutane	38.1	50.6	>100	>6.7
Benzene	15.8 (τ_1)	48.4	>100	

Temperature Sensitivity

The temperature sensitivity concept of autoignition has remained obscure because sensitivity data are usually presented in terms of octane units, engine speed, compression ratio, and inlet temperature instead of the more fundamental variables of end-gas temperature, fuel and air densities, and time. Engine knock tests generally determine fuel sensitivity by two tests: one with high density of charge and low compression temperature and one with lower density and higher temperature. The results of such tests are functions of the ratio of temperature sensitivity to density sensitivity instead of direct measurements of temperature sensitivity.

A comparable measurement in the rapid compression machine is the ratio of decrease in delay with increased temperature to decrease in delay with increased density. The following general formulae define dimensionless temperature and density sensitivities and their ratio.

S_{Temp} = Absolute temperature sensitivity

$$= \frac{d\tau_T}{dT}\frac{T}{\tau_T} \tag{1}$$

S_{Density} = Absolute density sensitivity

$$= \frac{d\tau_T}{dD}\frac{D}{\tau_T} \tag{2}$$

S = Absolute sensitivity ratio

$$= \frac{S_T}{S_D} = \frac{\dfrac{d\tau_T}{dT}}{\dfrac{d\tau_T}{dD}}\frac{T}{D} \tag{3}$$

T is compression end temperature, D is compression end density, and τ_T is total delay. Data from the rapid compression machine were substituted in the following formula which is an approximation to the differential equation for absolute sensitivity ratio.

$$S = \frac{(\tau_T)_1 - (\tau_T)_2}{(\tau_T)_2 - (\tau_T)_4}\frac{T_2}{T_2 - T_1}\frac{D_4 - D_2}{D_2} \tag{4}$$

The subscripts refer to conditions 1, 2, and 4 in Table 1.

The 13 fuels tested are listed in Table 3. The total delay under condition 2 and the absolute sensitivity ratio S are listed with comparative data on octane ratings and octane-number sensitivities. The latter were computed by subtracting Motor method from Research method values[11]. The ignition delays follow in the same order as the octane number except for a slight deviation in the case of 2,2-dimethylpentane. Only the primary delay of benzene was measured. Cyclohexane showed a somewhat longer total delay than would be expected from the octane number alone.

Octane-unit sensitivity is actually the difference between the sensitivity of the tested fuel

and the sensitivity of the corresponding isooctane-*n*-heptane blend. *n*-Heptane has a substantially higher absolute sensitivity ratio than isooctane in the rapid compression machine. Thus absolute sensitivity ratios and octane-unit sensitivities of two fuels can be compared directly only when they lie in the same octane-number range. By both methods *n*-hexane is less sensitive than *n*-heptane, 3-methylpentane is less sensitive than 2-methylpentane, 2,2-dimethylbutane is less sensitive than cyclohexane, and isooctane is less sensitive than 2,3-dimethylbutane. Therefore both octane and temperature sensitivity data in engines correlate with rapid compression machine data.

Differences in the progress of reactions during the delay periods in two fuels with comparable total delays but different sensitivities should help clarify the sensitivity concept. The total delay curves for 2,2-dimethylbutane and cyclohexane in Figure 14 show that the two fuels have almost identical total delays under conditions 2, 3, and 4, and thus have equal density sensitivities. However, under lower-temperature condition 1, cyclohexane has a longer delay; its decrease in delay with increased temperature is therefore greater, and both the temperature sensitivity and absolute sensitivity ratio are greater than those of 2,2-dimethylbutane.

An examination of the curves for primary (Fig. 15) and secondary (Fig. 16) delay provides a simple explanation for the differences in sensitivity of the two fuels. The secondary delay in each fuel is temperature insensitive and fuel-concentration sensitive. This temperature insensitive portion of the reaction is, however, about three times as long for 2,2-dimethylbutane as for cyclohexane. In contrast, the temperature sensitive primary delay is several times as long for cyclohexane as for 2,2-dimethylbutane.

These observations, when generalized, provide a simple rule for the variations in absolute sensitivity ratio between fuels: a fuel with a long primary delay and short secondary delay is temperature sensitive and density insensitive; a fuel with short primary delay and long secondary delay is density sensitive and temperature insensitive. The absolute sensitivity ratio increases as the ratio of primary to secondary delay increases.

This general rule is substantiated in principle by some observations made by Jost and Teichmann[12] and Scheuermeyer and Steigerwald[13] in earlier experiments. Jost and Teichmann conducted their experiments at low compression temperatures and concluded that ignition delay is practically uninfluenced by changes in pressure. Under these conditions τ_1 undoubtedly comprised a vast majority of the delay. Scheuermeyer and Steigerwald showed that when the compression temperature was substantially raised, the total delay became pressure sensitive but temperature insensitive. τ_2 would predominate under these circumstances. It can be seen that any measure of absolute sensitivities would hold only in a particular temperature region.

The temperature sensitivity of an engine fuel can be considered primarily as a function of the relative rates of the peroxidation and cool-flame

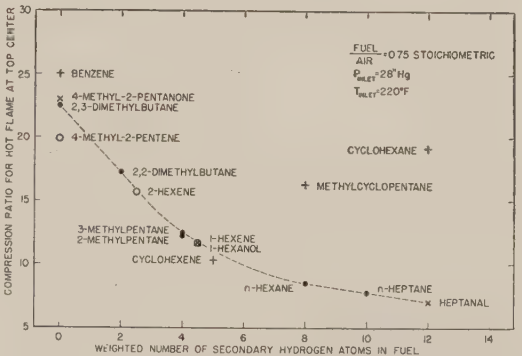

FIG. 17. Autoignition resistance as a function of the number of secondary hydrogen atoms in the fuel molecule. Secondary hydrogen atoms α to a double bond, to an OH group or to a ketone group were arbitrarily assigned a value of $\frac{1}{4}$; an aldehyde group was assigned a value of 4.

reactions. Since changes in fuel-air ratio, temperature and total density affect these two stages differently and in general non-linearly, it would seem improbable that the knock characteristics of a fuel could be adequately described by two tests, as is the current practice. Such data can at best establish trends over a narrow range of operating conditions.

Effect of Fuel Structure on Autoignition Resistance

Malherbe and Walsh[14] have shown that three distinct regions of cool-flame reaction can be observed with various hyrocarbons, and have correlated these regions with the presence of primary, secondary, and tertiary carbon-hydrogen bonds. It is significant that the part of the cool-flame curve associated with secondary bonds extends over the widest range and is the most easily identified.

A plot of the compression ratio required to

cause the hot flame to begin at top center in the continuous compression engine versus the number of secondary hydrogen atoms in the molecule shows a smooth curve for the paraffins (Fig. 17). Olefins and oxygenated compounds will follow the same curve if the secondary hydrogens which are α to a double bond, a ketone carbonyl group, or a hydroxyl group are arbitrarily assigned a relative reactivity of 0.25, and an aldehyde group is assigned a reactivity of 4. Only the cyclic compounds do not conform to this curve. The excellent correlations found for aliphatic fuels on the basis of the reactivity of secondary hydrogens alone give strong support to the theory that attack on these atoms is the primary mode of initiation of the cool-flame reaction.

2,3-Dimethylbutane was the only paraffin tested which contained no secondary hydrogens. It exhibited a long delay. The cool-flame reaction showed no sharp peak and was apparently of less than second order. Cyclohexane, with 12 secondary hydrogens, exhibits characteristics different from those of the alkanes. Its primary ignition delay is comparable to that of benzene. The cool-flame reaction had a rapid, comparatively steady rate; the hot-flame initiation temperature was extremely inconsistent.

All aliphatics from acetylene to the octanes entered the hot-flame stage of reaction at about the same temperature. Benzene and hydrogen did not burn rapidly until substantially higher temperatures had been reached, and showed much more gradual rates of temperature rise, indicating that entirely different mechanisms were rate-controlling in the different types of fuels.

REFERENCES

1. Levedahl, W. J., and Howard, F. L.: Ind. Eng. & Chem., *43*, 2805 (1951).
2. Levedahl, W. J.: Inst. Soc. Am. Paper No. 52-27-3.
3. Schmidt, F. A. F.: Verbrennungskraftmaschinen, 3rd ed. München, Oldenbourg, 1951.
4. Beckers, A.: Motortechnische Zeitschrift, *14*, 12, 345 (1953).
5. Walsh, A. D.: Trans. Far. Soc., *42*, 269 (1946).
6. Downs, D., Walsh, A. D., and Wheeler, R. W.: Phil. Trans. Roy. Soc. London, No. 870, *243*, 465 (1951).
7. Levedahl, W. J., and Broida, H. P.: Anal. Chem., *24*, 1776 (1952).
8. Downs, D., Street, J. C., and Wheeler, R. W.: Fuel, *32*, 3, 279 (1953).
9. Lewis, B., and Von Elbe, G.: *Combustion, Flames and Explosions in Gases*. New York, Academic Press, 1951.
10. Rögener, H.: Z. f. Elektrochem, *53*, H. 6 (1944).
11. API Research Project 45, 12th Annual Report (1950).
12. Jost, W., and Teichmann, H.: Naturwiss., *27* (1939).
13. Scheuermeyer, M., and Steigerwald, H.: Motortechnische Zeitschrift, H. 8/9 (1943).
14. Malherbe, F. E., and Walsh, A. D.: Trans. Faraday Soc., *46*, 835 (1950).

Discussion by J. C. Livengood

The conclusion by Dr. Levedahl that a wide variety of fuel-air mixtures completes a hot-flame autoignition as soon as 1100°F has been reached is interesting, but it is possibly at variance with the results of other experiments.

For example, Figure 3 (Chapter 30, p. 350) shows a range of autoignition temperatures which extends over 350°F, all below 1100°F. Of course these temperatures have been computed for the compressed gas by the gas law relationship for the fuel-air mixtures concerned, and it has been suggested that the exothermic reaction at the end of the first stage results in a temperature higher than shown in Figure 3.

However, in the region in the upper left corner of Figure 3, and bounded below by a line from 100 psia, 1300°R to 300 psia, 1550°R, *n*-heptane (for example) shows no two-stage behavior as far as can be detected by a pressure-time record. Also, preliminary tests using a photomultiplier cool-flame detector have shown no evidence of light emission before the occurrence of the hot flame. There is another single-stage ignition region for *n*-heptane below and to the right (Figure 3) of a line between 300 psia, 1200°R and 500 psia, 1500°R. Between these boundaries lies a region of more or less pronounced two-stage activity. No attempt has been made to estimate the size of the temperature rise which may accompany the completion of the first stage because the demonstrated lack of uniformity of reactions in the M. I. T. Rapid Compression Machine imposes some strain on the necessary assumptions.

The evidence shown in Figure 6 also shows that the final complete autoignition in the end-gas of a firing engine can occur over the appreciable range of temperature of 1400°R–1800°R, depending upon the operating conditions. In this case, although the sound velocity temperature measurements include any exothermic effects of pre-reactions, it might be argued that the time resolution of the measurements was inadequate to separate a very rapid first-stage reaction from an ensuing hot flame process.

It is concluded that the measurements cited here do not indicate that the hot flame occurs at the 1100°F point exclusively unless this point is

traversed so rapidly that present methods fail to distinguish between slow and fast changes in temperature, pressure and light emission.

Author's Reply

In the opinion of the author, his experimental findings and those discussed by Mr. Livengood are not necessarily at variance. At least one possible explanation for the apparent differences in ignition temperature suggests itself when it is understood *what* temperature was measured in each set of experiments.

In the work at NBS and at Aachen, the common temperature region around 1560°R refers to the temperature at which the hot-flame reaction mechanism first became prominent. Under conditions outside the upper pressure limit of Mr. Livengood's 2-stage region, the NBS work has shown that the rate of temperature rise in the cool-flame reaction is very large, and is still increasing when the hot-flame begins. Therefore, no inflection point appears in the pressure- or total-radiation curve at these high pressures, and in order to detect the point at which the hot-flame mechanism becomes important it is necessary to record the first detectable ionization or the first sharp change in water-band emission intensity using a technique recently employed by Mr. C. R. Yokley.

Sound-velocity temperature measurements follow the course of the reaction until the rate of temperature rise becomes so great that irreproducible cyclic variations in the end-gas temperature-time curve cause the measured temperature to vary greatly from cycle to cycle. The last steady temperature is that represented on the M. I. T. charts. This temperature is that at which the rate of temperature rise became unmeasurably great, without regard to chemical mechanism. Temperatures referred to by the author are those at which the *hot-flame* reaction mechanism became detectably rapid, without regard to the overall rate of temperature rise. Under these high-pressure conditions one would expect the sound-velocity ignition temperature to be lower than that at which the mechanism changed.

NBS results obtained in the very-low-pressure region show that the peak rate of cool-flame reaction occurs at a temperature *lower* than the compression-end temperatures used which gave rise to one-stage curves from the M. I. T. rapid compression machine. An inflection point in the pressure- or total-radiation curve is therefore precluded. Under these conditions the rate of hot-flame reaction in the NBS engine was slow until the temperature had risen considerably above the point at which ionization began. It is conceivable that the sound-velocity apparatus was able to follow the temperature reproducibly until well after the hot-flame reaction began, thereby giving ignition temperatures in excess of those at which the hot-flame mechanism became significant.

34

A STUDY OF COOL FLAMES AND ASSOCIATED REACTIONS IN AN ENGINE[a]

By E. W. MALMBERG, M. L. SMITH, J. E. BIGLER, AND J. A. BOBBITT

The existence of faint blue luminescence, called cool flames, under certain conditions during early combustion reactions is well established. These flames have been observed in mixtures undergoing precombustion reactions in glass tubes as well as in engines. Attempts have been made to correlate the cool flame characteristics with various physical phenomena associated with combustion. For example, the compression ratios required to produce cool flames and autoignition for various hydrocarbons and mixture strengths have been reported[1, 2]. Similarly, the effects of other engine variables such as inlet manifold pressure and temperature, engine rpm, etc., on the occurrence of cool flames have been investigated[3]. Other studies have revealed a correlation between the times when cool flames first became evident and the maximum rate of energy release produced in the precombustion reactions, as determined by the rate of pressure change within the cylinder. It is the purpose of this paper to report further evidence from some preliminary attempts to correlate the physical phenomena of cool flames with the chemical characteristics of the intermediate combustion products formed by these early reactions.

[a] This work is part of a fundamental study of the reaction of hydrocarbons directed by Professor Cecil E. Boord under sponsorship of U. S. Air Force Research and Development Command.

Experimental

The precombustion reactions were studied in a modified CFR Type F-4 engine equipped with a pressure transducer, a photomultiplier tube, and a sampling valve. Samples of the precombustion products could be obtained directly from the cylinder during any desired interval covering about 6° of crank rotation when the engine was operated either as a motored or as a fired engine[4]. Samples of the precombustion products from the motored engine also could be obtained from the exhaust manifold. All tests described in this paper were conducted in a motored engine at 900 rpm. The standard induction system of the F-4 engine was used, except that provision was made to throttle the manifold pressures to any desired absolute pressure. Air consumption was measured with a sharp-edged orifice and an inclined draft gage. Fuel consumption was determined volumetrically. The fuel was sprayed continuously through a small orifice into a mixing chamber. The flow rate was controlled by adjusting the pressure on the liquid fuel in the system. Very steady flow rates could thus be established which were reproducible within $\pm\frac{1}{2}$ per cent. To ensure good mixing and evaporation, the fuel was sprayed into a turbulent mixing chamber equal in size to about five displacement volumes of the engine. Air preheat was maintained within ±2°F, with the standard thermostatically controlled heaters. Engine jacket temperature was held close to 150°F. The standard overhead-valve cylinder head having four openings into the clearance volume was used.

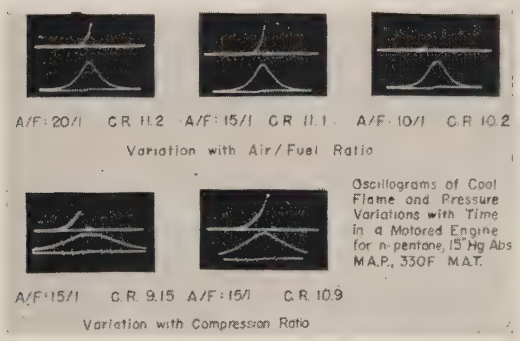
A/F: 20/1 C.R. 11.2
A/F: 15/1 C.R. 11.1
A/F: 10/1 C.R. 10.2
Variation with Air/Fuel Ratio
Oscillograms of Cool Flame and Pressure Variations with Time in a Motored Engine for n-pentane, 15" Hg Abs M.A.P., 330F M.A.T.
A/F: 15/1 C.R. 9.15
A/F: 15/1 C.R. 10.9
Variation with Compression Ratio

FIG. 1. Oscillograms of cool flame and pressure variations with time in a motored engine for *n*-pentane. MAP 15″ Hg abs., MAT 330°F.

Radiations from the cool flames were detected through a quartz window with an RCA 1P22 photomultiplier tube. Constant power input to the tube was maintained and the relative cool flame intensities were measured by comparing the voltages of the input signals at the cathode ray oscilloscope.

The oscillograms shown in Figure 1 are representative of those obtained with numerous fuels and engine operating conditions. In photographing, the record camera reversed the image, so that the portion of the curve representing the compression stroke is on the right. The upper curve indicates the cool flame intensity as a function of time. The lower curve appearing on the screen of the dual beam oscilloscope is the pressure variation with time, as measured with a Li strain-type of pressure transducer. Timing marks at top dead center and 10, 20, and 30° of crank angle rotation on each side of top dead center also appear on the pressure curve. By moving the timing marks close to the cool flame trace, it was possible to measure the timing of the various events of the cool flame rather accurately. Thus, the crank angle positions at the start, point of peak intensity, and end of the cool flame radiations were determined. The values of relative intensity were subject to several known sources of error. Among these, deposits of oil or carbon on the quartz window would cut the intensity measured greatly. Precautions were taken to clean the window prior to making intensity measurements. In addition, with rich mixtures there is considerable cyclic variation of the radiation intensity. Cyclic variation is observed also in mixtures which are compressed to pressures and temperatures considerably less than those associated with borderline autoignition and cause considerable error in intensity measurements. There is little cyclic variation, however, in the crank positions at start, end, and peak of the cool flame radiation for a given fuel-air mixture, manifold air pressure, manifold air temperature, and compression ratio. Data were obtained with the photomultiplier tube aimed at a small cone of the cylinder volume looking toward the center of the piston head. Tests were also conducted with the photo tube located on the side of the cylinder aimed across the entire combustion volume and parallel to the top of the piston. The results observed from both locations were essentially the same except for the relative intensity; the intensity would be proportional to the dimensions of the luminescent volume which was in the line of view of the photo tube. The preceding suggests that the cool flame luminescence is

initiated uniformly in many parts of the charge in the motored engine. At least the cool flame does not form in one section of the cylinder and move relatively slowly across the combustion chamber, as does the normal hot flame.

Cool Flame Characteristics as Affected by Engine Conditions

Figures 2, 3, and 4 show the variations in timing and intensity with air-fuel ratio for isooctane, *n*-heptane, and *n*-pentane, respectively. These particular fuels were chosen for preliminary studies of this nature because considerable chemical data regarding intermediate combustion products sampled from these fuels had already been obtained. With each of these fuels the cool flame persists for some 30 to 40° of crank angle rotation. With the *n*-paraffins reported the cool flame occurs at the same point in the cycle for both lean and stoichiometric mixtures, but each event shifts later in the cycle with rich mixtures. The cool flames in isooctane appear at the same time in the motored engine cycle, regardless of the mixture strength used. With isooctane the peak intensity is greater with rich mixtures and the point of peak intensity occurs earlier in the cycle; whereas for the two *n*-paraffins the peak intensity appears with mixtures which are approximately stoichiometric. In each of these curves the cool flame intensities are plotted in arbitrary units. It will be noted that the peak intensities for the *n*-paraffins are approximately 5 to 10 times as great as for isooctane.

Figure 5 presents the effect of compression ratio on the cool flame occurrence for stoichiometric mixtures of *n*-pentane, *n*-heptane, and isooctane. With each fuel compression ratio was varied until the autoignition limit was reached on the one side or no cool flames could be detected on the other. It is interesting to note the general trends of the curves. The start, end, and point of peak intensity occur earlier in the cycle at the higher compression ratios, and the data for one fuel blends in quite smoothly with the next fuel having different knock resistance. Apparently the point in the cycle at which the cool flame appears is governed more by the pressure and temperature in the cylinder than by the overall structure of the fuel molecule. This observation is borne out by the colinearity of the cool flame start points for *n*-pentane and isooctane over the limited region of compression ratios in which measurements can be made for both fuels.

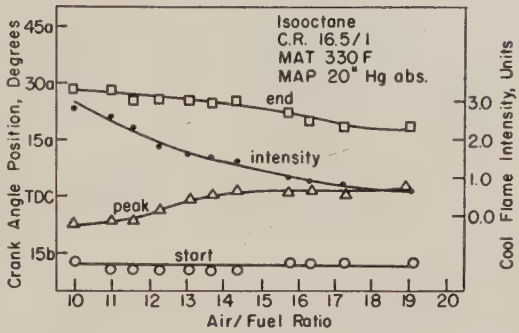

FIG. 2. Variation in cool flame occurrence with air/fuel ratio for isooctane.

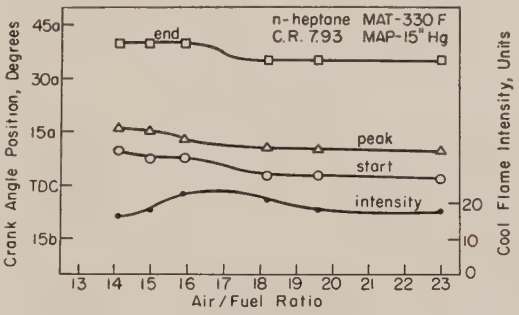

FIG. 3. Variation in cool flame occurrence with air/fuel ratio for *n*-heptane.

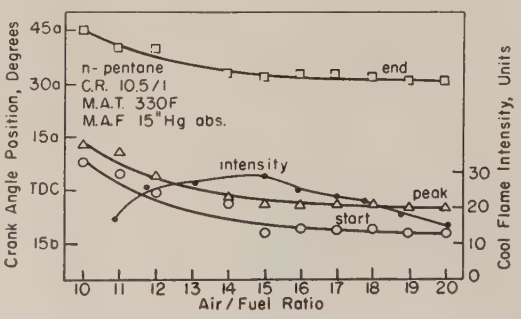

FIG. 4. Variation in cool flame occurrence with air/fuel ratio for *n*-pentane.

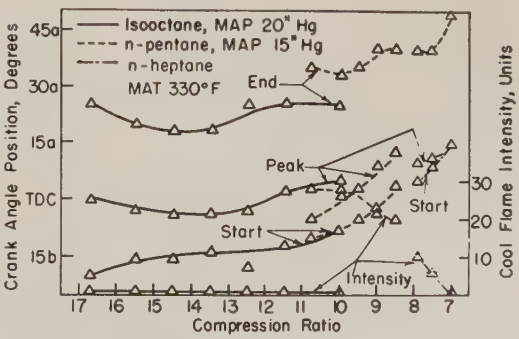

FIG. 5. Variation of cool flame occurrence with compression ratio.

Correlation of Cool Flame Characteristics with Chemical Studies

This study of the timing and intensity of the cool flames is especially interesting because the chemical characteristics of preflame reactions have already been investigated in some detail. The chemical study of the reactions associated with cool flames in engines has been concerned primarily with alkyl hydroperoxides and carbonyl compounds. The carbonyl compounds are of particular interest for two reasons. First, it is well established that excited formaldehyde is the source of the cool flame illumination[5]. Second, the carbonyl products appear to accumulate in cool flame reactions and may possibly be regarded as a measure of the amount of reaction.

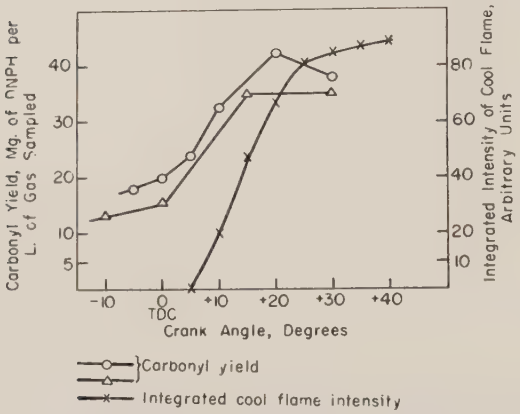
Carbonyl Yield, Mg. of DNPH per L. of Gas Sampled
Integrated Intensity of Cool Flame, Arbitrary Units
Crank Angle, Degrees
TDC
Carbonyl yield
Integrated cool flame intensity

FIG. 6. Carbonyl yield and integrated cool flame intensity; preflame reactions of *n*-heptane.

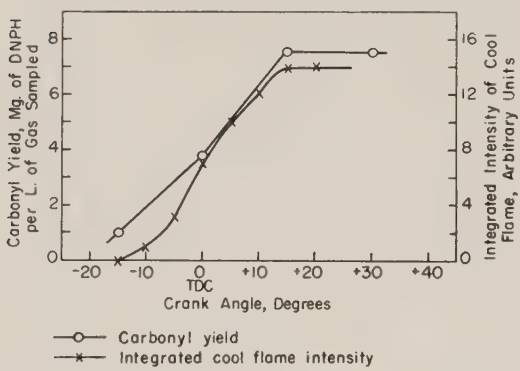
Carbonyl Yield, Mg. of DNPH per L. of Gas Sampled
Integrated Intensity of Cool Flame, Arbitrary Units
Crank Angle, Degrees
TDC
Carbonyl yield
Integrated cool flame intensity

FIG. 7. Carbonyl yield and integrated cool flame intensity; preflame reactions of isooctane.

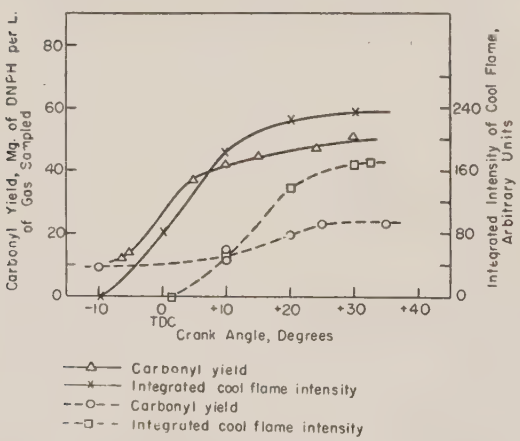
Carbonyl Yield, Mg. of DNPH per L. of Gas Sampled
Integrated Intensity of Cool Flame, Arbitrary Units
Crank Angle, Degrees
TDC
Carbonyl yield
Integrated cool flame intensity
Carbonyl yield
Integrated cool flame intensity

FIG. 8. Carbonyl yield and integrated cool flame intensity; preflame reactions of *n*-pentane. Solid line—high intensity, CR = 11. Broken line—low intensity, CR = 9.

Another measure of the amount of the cool flame reaction is the integrated amount of light produced, the area under the intensity-time curve. This integrated area can also be treated as a function of time; i.e., the total amount of light emitted up to a given time can be plotted as a function of time in the region where the preflame reactions are occurring. This treatment is of interest because the amount of carbonyl compounds which has accumulated in the reaction mixture at a given time can be measured by removing a sample of the gas through the valve which is open only a few degrees of crank rotation[4].

A study was made of the correlation of this integrated area-time curve for the cool flame with the yield-time curve of carbonyl compounds. Some characteristic results are shown in Figures 6, 7, and 8 for *n*-heptane, isooctane, and *n*-pentane. The cool flame luminescence occurs over a period of 30–40° of crank rotation, and in all cases the rise in carbonyl content parallels the integrated intensity curve. This correlation holds even over the greatly different magnitudes of cool flame intensity and carbonyl yield which obtain for these different fuels. In general the integrated cool flame intensity can be duplicated within about 20 per cent with conditions approaching autoignition. As previously mentioned, the error may be considerably greater when the compression ratio is decreased to give lower intensities of radiation (Fig. 8). The appreciable amount of carbonyl compounds present before the cool flame may result from several causes, the most important probably being the incomplete scavenging of the preceding charge in the cylinder.

Before further consideration of the implications of those results, a brief description of some of the chemical characteristics of preflame reactions must be considered.

(1) Chromatographic and polarographic meth-

ods were used in the first experimental proof that alkyl hydroperoxides are indeed present as intermediates in oxidations around 300°C[6]. Further study of peroxides by application of this method to samples taken from the exhaust and at various crank angles in a motored engine has given results shown in Table 1.

Analogous studies of other hydrocarbons such as *n*-pentane and *n*-heptane give the same conclusion: the alkyl hydroperoxides before, during, and after the cool flame are qualitatively the same, they are present in the same relative amounts, and the concentrations of different peroxides at successive points in the cycle are not greatly different. Work is in progress on the determination of the structures of these products.

(2) The qualitative and quantitative study of the carbonyl compounds by chromatographic analysis of the dinitrophenylhydrazones[7] showed the same general characteristics with the difference of course that the carbonyls accumulate during the reaction. Some typical results are shown in Table 2. A quantitative breakdown of Zone 2 can be obtained crudely from an infrared study; the amounts are roughly 4 per cent of acrolein and 2 per cent of crotonal (percentages of individual derivatives in total sample of DNPH precipitate). It has been found that in these samples the polarographic procedure of MacNevin and Urone[8] can be used to determine acrolein and crotonal separately. The results are shown in Table 3.

The same striking feature prevails throughout these results. Regardless of the timing with respect to the cool flame luminescence, the ratios of the individual products among themselves is essentially constant. This same constancy of ratios holds with other fuels such as isooctane, cyclohexane, etc., in which the various components are present in greatly different relative and absolute amounts. The simplest explanation of the results with the peroxides and carbonyl compounds is then that the reactions occurring within wide limits of pressure, temperature, and timing are very closely the same. The one difference, not inconsistent with this interpretation, is that the hydroperoxides set up a steady state concentration which varies little with time, but the yield of carbonyls is integrated over time.

The explanation of the constancy of product ratios provides a reasonably secure basis for discussing some possible chemical backgrounds for the cool flame. Various proposals for the formation of active formaldehyde are discussed by Gaydon[5]; the greatest difficulty probably is to provide the necessary energy of excitation, about 80 kcal. With this requirement, a reasonable assumption might be that among the various paths by which formaldehyde is formed in a cool flame reaction, only one of them yields the activated molecule. A number of fuels of greatly different structure can be chosen so as to vary the proportions of formaldehyde from the various

Table 1. Peroxide Zones Found in Oxidation Products of Isooctane with Standardized Chromatographic Procedures

Sample From			
Valve, TDC		Exhaust	
Position*	Intensity†	Position*	Intensity†
0–10	Deep red	0–12	Very deep red
25–52	Deep red	24–54	Deep red
60–85	Deep red	61–87	Deep red
100–120	Red	102–119	Red
120–130	Very pale red	119–130	Very pale red

* Position of zone shown as mm. from top of column.

† Intensity given by reaction with ferrous thiocyanate reagent.

Table 2. Total Yield of Carbonyl Compounds from Pentane and Quantitative Composition at Various Crank Angles in the Motored Engine

Analysis with 2,4-Dinitrophenylhydrazine

Crank Angle	Yield mg of DNPH per Liter of Gas	Composition* of Carbonyl Fraction			
		FA	AA	Zone 2	Zone 3
−40	3.8	32.4	27.1	12.9	2.4
−30	4.0	34.0	27.2	15.5	2.5
−20	4.9	36.0	31.6	15.0	2.1
−10	10.1	35.2	28.8	15.1	2.4
0†	23.2	34.4	28.0	14.9	1.9
+10	32.7	36.0	31.5	17.1	2.1
+20	30.2	34.2	33.4	16.3	2.7
+30	28.3	29.6	33.6	16.9	2.9
+40	25.8	29.2	32.8	16.4	2.6

* Composition: FA, formaldehyde; AA, acetaldehyde; Zone 2, propionaldehyde, acrolein, and crotonaldehyde; Zone 3, other C_4 carbonyl compounds. Composition is in weight percentage of each derivative in the DNPH precipitate.

† TDC, top dead center.

sources. If the quotient

$$\frac{\text{total cool flame luminescence}}{\text{total yield of formaldehyde}}$$

is compared for the various fuels and a correlation is observed for this value as compared to relative potentialities for the paths of formaldehyde formation, an indication of the source of active formaldehyde may be found. Some results are shown in Table 4.

Consideration of the amounts of various carbonyl products from the first three fuels[9] gave a preliminary indication that the probability of formaldehyde from methyl groups was much higher for ether and isooctane than *n*-pentane; hence the active formaldehyde possibly came from alkoxyl degradation. Cyclohexane was then tested, with the inconclusive result as shown, a ratio intermediate between the two types of test material. This experiment has one decisive result, however, that the active formaldehyde does not arise exclusively from methyl radicals.

Table 3. Polarographic Analysis for Acrolein and Crotonal at Various Crank Angles in the Motored Engine

Crank Angle	Percentage of Total Carbonyls	
	Acrolein	Crotonal
degrees		
−10	4.7	4.3
+10	3.1	4.6
+30	5.5	5.8

Table 4. Ratio of Integrated Cool Flame Intensity to the Total Yield of Formaldehyde

A/F = stoichiometric; C. R. = just below autoignition

Fuel	$\frac{\text{Integrated cool flame intensity}}{\text{Total yield of formaldehyde}}$
n-Pentane	13.1–21.2
Diethyl ether	6.9
Isooctane	5.9
Cyclohexane	10.6

In an experiment in which a solution of *t*-butyl hydroperoxide dissolved in benzene was admitted to a motored engine under conditions which did not produce a cool flame with benzene alone, Sturgis[10] and coworkers found that a cool flame was formed and formaldehyde was produced only when oxygen was present. These results indicate that methyl radicals in the presence of oxygen yield a cool flame. The present work has shown that a cool flame is found when no methyl groups are present in the fuel, hence, the source of active formaldehyde may not be as restricted as was first thought or else is completely different from present ideas.

The results of analysis for the carbonyl products are in agreement with the reactions usually written for the peroxide mechanism, with products of low molecular weight greatly predominating. The preponderance of attack occurs at methylene groups rather than at tertiary carbons. In accordance with this result appreciable quantities of ethylene and propylene are present in a ratio of roughly 10 to 1 from *n*-pentane; their presence is presumably the result of the breakdown of the larger alkyl radicals.

The unsaturated aldehydes present a very interesting problem. We have obtained conclusive evidence that these compounds are not produced by condensation of acetaldehyde with formaldehyde or a second molecule of acetaldehyde. A mechanism of formation is offered which utilizes the intramolecular reaction proposed by Barusch, Neu, Payne, and Thomas[11], but in a way which would yield products which would have a much greater probability of occurrence than the small amounts of acetyl acetone which they found in the pre-cool flame region. One possible formulation of this intramolecular path is:

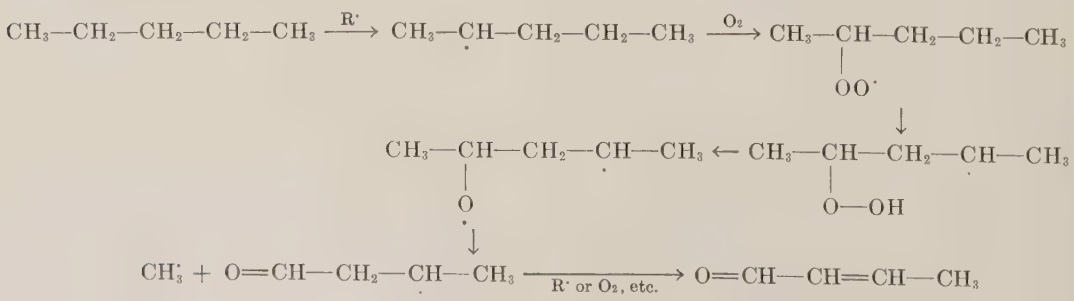

Acrolein would be formed by initial attack at the middle carbon, so the generally slightly greater amount of crotonal as measured polarographically (probably the more accurate measurement) is in better agreement as might be expected.

The steps in this series of reactions can be written in different order which may be of greater or smaller probability. The series in itself is of low probability, although of much greater probability than for the formation of the diketone. These results indicate that the initial intramolecular reaction may be of relatively high probability, but of all the possible subsequent reactions, only a small part may yield products which indicate directly the intramolecular initial step. The intramolecular reaction may therefore be of much greater importance for the degradation of long chains than indicated by the amounts of unsaturated aldehydes.

Conclusions

The effect of fuel-air ratio, compression ratio, and the nature of the fuel on the intensity and duration of cool flame luminescence in a motored engine has been studied.

The yield of carbonyl compounds in the preflame reactions has been shown to be proportional at any time to the integrated intensity of the cool flame up to that time. The proportionality factor may vary from fuel to fuel with no immediately apparent correlation.

The chemical study of preflame reaction product is in agreement with peroxide mechanism of oxidation, with, however, attack occurring predominantly at the secondary hydrogen atoms.

The presence of acrolein and crotonal as primary cool flame products may be explained by means of an intramolecular free radical reaction; this interpretation brings attention to the possible importance of intramolecular attack in oxidation.

Acknowledgment

The interest and support of Professor Cecil E. Boord, director of the project, in this investigation is acknowledged with pleasure. The authors wish to express their appreciation to Mr. Daniel Loughran for aid in the infrared study of olefins; to Mr. Myron Dunton for a number of polarographic analyses; to Mr. William Davis and Mr. David Grant for aid in devising equipment and aiding in the engine studies.

REFERENCES

1. Pastell, D. L.: SAE Quarterly Transactions, *4*, 571 (1950).
2. Downs, D., Street, J. C., and Wheeler, R. W.: Fuel, *32*, p. 279 (1953).
3. Corzilius, M. W., Diggs, D. R., and Pastell, D. L.: SAE Transactions, *61*, 386 (1953).
4. Davis, W. C., Smith, M. L., Malmberg, E. W., Bobbitt, J. A.: *A Comparison of the Intermediate-Combustion Products Formed in an Engine with and without Ignition*, presented at SAE Annual Meeting, Detroit, January, 1954.
5. Gaydon, A. G.: Spectroscopy and Combustion Theory, Ch. V. London, Chapman and Hall, Ltd., 1948.
6. Malmberg, E. W., Fishel, D. L., Smith, M. L., and Davis, W. C.: Meeting, Am. Chem. Soc., Los Angeles, March, 1953.
7. Malmberg, E. W., Bobbitt, J. A., Zamnik, F., Smith, M. L., and Davis, W. C.: Meeting, Am. Chem. Soc., Chicago, September, 1953.
8. MacNevin, W. M., Urone, P. L., *et al.*, Fifth Symposium (International) on Combustion, New York, Reinhold Publishing Corp., 1955.
9. Ref. 7 and later unpublished work on diethyl ether and cyclohexane.
10. Sturgin, B. M.: Preprint, paper presented at SAE National West Coast Meeting, Los Angeles, August, 1954.
11. Barusch, M. R., Neu, J. T., Payne, J. Q., and Thomas, J. R.: Ind. Eng. & Chem., *43*, 2766 (1951).

Discussion by John T. Agnew*

The authors have stated that they have good indications that "the cool flame does not form in one section of the cylinder and move relatively slowly across the combustion chamber, as does the normal hot flame."

Experiments very similar to those of Malmberg et al. have been carried out at Purdue University during the past two years.† These experiments have resulted in a conclusion somewhat different from the above conclusion regarding the propagation of the cool flame.

At Purdue, the problem was approached by using a modified CFR engine of ell-head design with a fused quartz window (4.65 in x 6.59 in x 1 in)

* Professor of Mechanical Engineering, Purdue University.

† *The Time Variation of the Spatial Distribution of Cool Flame Radiation in an Engine Cylinder* by James E. Getz, Ph. D. Thesis, Dept. Mech. Eng., Purdue University, August 1954.

for viewing the entire combustion chamber. A 931-A photomultiplier tube was used as the radiation detector. A steel template containing 52 holes served as a grid for viewing small regions of the combustion chamber. The engine operating conditions consisted of:

Speed	900 rpm
Air-fuel ratio	13:1
Spark timing	20°atdc
Head cooling water	70–85°F
Block cooling water	175°F (ave)
Mixture temperature	variable
Compression ratio	7:1
Manifold pressure	29.5″ Hg abs.
Fuels	30 per cent *n*-heptane, 70 per cent toluene (by volume) 40 per cent *n*-hexane, 60 per cent toluene (by volume) 50 per cent *n*-pentane, 50 per cent toluene (by volume)

Results and conclusions from these experiments included the following:

(1) At low mixture temperatures the cool flame first appeared in the region of the valves and then propagated across the combustion chamber at an average speed of 75 ft/sec which required 27 crankshaft degrees. The word propagation is used in the sense that it is a spreading or enlarging of a flame front in space with respect to the material being consumed and that this self-sustained movement is the result of a transfer of thermal energy and chain carriers.

(2) At high mixture temperatures the cool flame first appeared in the region of the valves, propagated a short distance at ca. 75 ft/sec and then moved across the remaining major portion of the combustion chamber at ca. 500 ft/sec.

(3) At intermediate mixture temperatures a behavior intermediate between the above two phenomena resulted.

(4) As the mixture strength was richened, a point was reached where there was an abrupt decrease (almost may be considered a cutoff) in cool flame intensity.

Considerations of the influence of compression heating (due to piston motion) and heat conduction from the walls of the combustion chamber and other solid surfaces adjacent to the gas have led to the conclusion that in the case of the low mixture temperature of 65°F, there is a true propagation of the cool flame through the fuel-air mixture in the direction from the valves toward the piston at a velocity (relative to the cylinder head) of ca. 75 ft/sec. This propagation is believed to be due to the usual mechanisms of heat conduction and chain carrier diffusion. At the high mixture temperature it is believed that the high rate of propagation of ca. 500 ft/sec is not a true flame propagation. Rather, it is held that the combined effects of the piston compression of this high temperature mixture and heat conduction from solid surfaces result in the progressive formation of the conditions necessary for the spontaneous appearance of a cool flame in a given volume of the mixture. This causes an apparent propagation rate of ca. 500 ft/sec.

Thus the conclusion reached in our studies at Purdue is that neither the appearance nor the time of peak intensity of cool flame radiation are simultaneous over the entire combustion chamber; therefore, caution should be exercised in correlating radiation traces with other variables such as pressure development.

Author's Reply

The authors feel that there is no discrepancy between the findings presented in this paper and the work cited at Purdue. Rather the latter is an extension of the work herein reported. At high inlet temperatures in a fired engine, Mr. Agnew pointed out that the apparent flame propagation rate was about 500 ft/sec, but that it was felt this apparent propagation resulted from different parts of the cylinder reaching a temperature-pressure-time condition conducive to cool flame formation at progressively different times.

All of the work at Ohio State was conducted with high inlet manifold temperatures (250° to 350°F) in a motored engine. Under these conditions it would be expected that all parts of the cylinder would be at more uniform temperature than in a fired engine. Therefore, the conditions which would lead to the apparent cool flame propagation would not be present, or not easily detectable.

It may be true that for lower inlet temperature in a fired engine there may be a true propagation of the cool flame, i.e., a propagation caused by some mechanism other than cool flame reaction occurring spontaneously in succeeding zones of the cylinder. This apparent cool flame velocity of 500 ft/sec is very interesting in that it is more than 10 times as fast as ordinary flame velocities in an engine at these operating conditions. The difference between this behavior and true volume luminescence which is frequently observed in cool flame experiments is an extremely difficult system to analyze either physically or chemically. The authors agree that studies in a motored engine must be applied with caution when making generalizations concerning physical phenomena in the cylinder of a fired engine. So far as chemical phenomena are concerned there is good evidence that there is no difference between cool flame reactions in a motored and fired engine.

Special Techniques

35

A NEW SHOCK TUBE TECHNIQUE FOR THE STUDY OF HIGH TEMPERATURE GAS PHASE REACTIONS[a]

By H. S. GLICK, W. SQUIRE, AND A. HERTZBERG

Introduction

One of the central problems in combustion theory is an understanding of chemical kinetics at high temperatures. While some progress has been made in this field, no adequate theory of homogeneous gas phase reactions has yet been formulated. Experimental studies of reaction kinetics are required both to test present theoretical assumptions and to provide a basis for future theories.

Although experimental kinetics studies of reactions related to combustion are of great importance, the high temperatures and short reaction times introduce major experimental difficulties. Consider a reaction occurring in a few milliseconds at 2000°K. How is the reactant gas to be heated so rapidly that no appreciable reaction will occur until the desired temperature is reached throughout the sample? How is the reaction to be quenched or samples removed rapidly enough for analysis? What structural materials can be used at very high temperatures? Clearly, a technique for subjecting a gas sample to a single, sharply-defined temperature pulse would be very desirable.

Methods utilizing heat transfer across a surface are not satisfactory for uniform, rapid heating of a gas sample, and techniques which operate throughout the gas volume are necessary. A promising line of attack is the use of large amplitude pressure waves which travel at thousands of feet per second and produce high gas temperatures. During the course of theoretical studies of such wave phenomena in tubes, it was recognized that it is possible to devise gasdynamic methods for subjecting a gas sample to a single temperature pulse which seemed sharp enough to provide useful kinetic data. A chemical shock tube which embodied the results of the theoretical analysis was constructed at the Cornell Aeronautical Laboratory. Operation of this facility during the last six months has demonstrated the practicability and usefulness of the chemical shock tube, and the object of this paper is to describe the device and present some preliminary results.

The chemical shock tube is essentially a modification of the conventional shock tube, devised by Vieille[2] in 1899, which since 1940 has come into widespread use as a tool for gasdynamic research[3-6]. The conventional shock tube (Fig. 1) is a straight tube, closed at both ends, containing gas at high pressure (driver) separated by a diaphragm from gas at low pressure (reactant). When the diaphragm is ruptured, the driver gas expands into the low pressure section generating a shock wave that propagates into the low pressure gas, heating and compressing it. The magnitude of the temperature jump across a strong shock wave is not generally appreciated, e.g., temperatures as high as 14,000°K have been produced in argon with relatively simple equipment[3]. While it is harder to heat more complex molecules, real gas temperatures over 5000°K have been obtained in air. The shock wave is then reflected from the closed end increasing the temperature and pressure of the gas still further. Simultaneously, expansion waves, which lower

[a] The work described in this paper was performed under the auspices of Project SQUID, jointly sponsored by the Office of Naval Research (Department of the Navy), Office of Scientific Research (Department of the Air Force), and Office of Ordnance Research (Department of the Army). Some of this work has been presented orally at the 1953 Washington meeting of The American Physical Society[1].

temperature and pressure, travel into the high pressure gas and are reflected from the end of the driver section. Repeated reflections of the pressure waves subject the low pressure reactant gas to a series of temperature pulses of slowly decreasing amplitude (Fig. 2). This complex temperature history limits the value of the conventional shock tube for chemical kinetics investigations.

However, a number of investigations have been carried out using conventional shock tubes as a method of rapid heating. For example, rapid heating of combustible gas samples by shock waves has been used in ignition studies[7-12]. Davidson and co-workers[13, 14] and Greene[15] have utilized the region immediately behind the incident shock

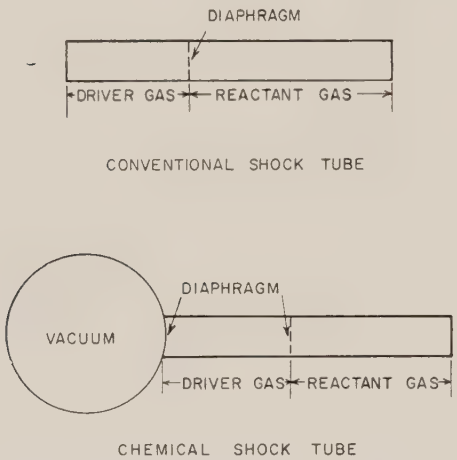

FIG. 1. Simplified diagrams of a conventional and a chemical shock tube.

wave to study reaction kinetics quantitatively. The passage of the first shock is treated as a jump in temperature and the approach to the new equilibrium is followed optically. For example, this method has been used to study such reactions as:

$$N_2O_4 \rightleftharpoons 2NO_2$$

$$I_2 \rightleftharpoons 2I$$

which involve a marked color change.

The novel feature of our method is a modification of the conventional shock tube to produce a single high temperature pulse. The shock tube is modified by adding a large, evacuated tank separated by a second diaphragm from the driver section (Fig. 1). By breaking this diaphragm after the bursting of the first diaphragm, but before the arrival of any pressure waves, sonic flow into the evacuated tank is established, i.e., the local inflow velocity equals the local velocity of sound. Pressure waves which propagate toward the tank are not obstructed by the sonic flow region, and travel into the tank. However, pressure waves which try to travel out of the tank are unable to advance past the sonic flow region, and are therefore trapped in the tank. The sonic flow into the evacuated tank thus serves to prevent any appreciable secondary temperature pulses (Fig. 2).

The bursting of the tank diaphragm also generates a strong expansion wave which cools the

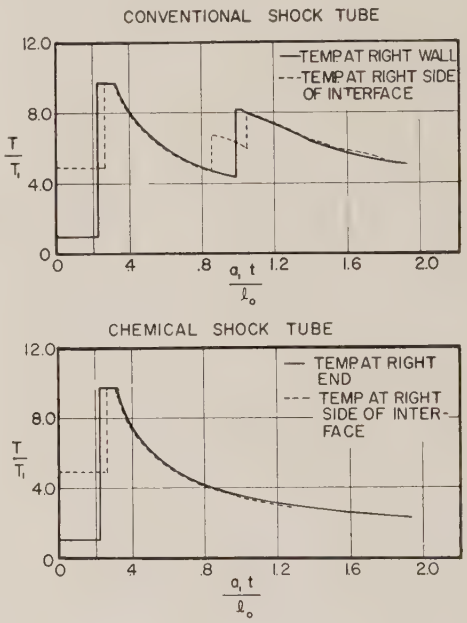

FIG. 2. Temperature history of the reactant gas in a conventional and a chemical shock tube obtained assuming constant heat capacity and a matched impedance gas interface.

reacting gas sample. The cooling rate of this tank-generated expansion wave is greater than the cooling rate of the expansion wave in a conventional shock tube for the same shock tube geometry. An important feature of this method of cooling is that the hot gas is cooled without accelerating it to a high velocity, so that its total energy is reduced. This reduction of total energy is due to the nonsteady wave cooling process. The first passage of the expansion waves accelerates the hot gas back toward the evacuated tank, but after reflection from the end of the reactant section, the acceleration of the reacted gas is reversed. Therefore, the final cold gas has a relatively low velocity and low total energy.

It is therefore possible to process a sample of gas with a single pulse of known temperature and duration. From the analyses of samples subjected to pulses of varying duration, the progress of the reaction can be followed in the case of reactions which can be frozen by quick cooling. Because of the short temperature pulse duration, there is no appreciable heat transfer to the wall and structural difficulties are eliminated.

Design of Chemical Shock Tube

The gasdynamic analysis[16] of phenomena in the chemical shock tube is based on one-dimensional, nonsteady, compressible flow, neglecting viscosity, heat conduction, and relaxation effects. This approximation is justified by the results of numerous shock tube investigations[17, 18]. Since

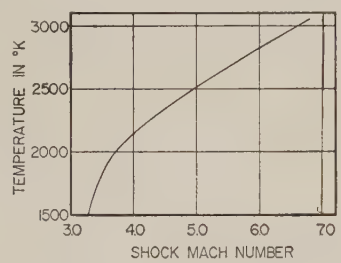

FIG. 3. Equilibrium temperature of air behind the reflected shock wave as a function of the incident shock Mach number when the initial air temperature is 300°K, as computed by the method described in Appendix I.

the temperature behind the incident shock is substantially below the reflected shock temperature (Fig. 2), the amount of reaction occurring before reheating by the reflected shock is very small and has been neglected in this paper. However, since relatively high temperatures occur in the chemical shock tube, the heat capacity of the reactant gas cannot be treated as a constant, and accurate thermodynamic data must be used in the calculation of such physical quantities as temperature, pressure, density, etc. For example, since no satisfactory method was available for measuring the reaction temperature, it was necessary to make a real gas calculation of the temperature behind the reflected shock. The temperature of the gas behind the reflected shock, assuming thermal equilibrium, as a function of the incident shock strength is shown for air in Figure 3, with the details of the calculation given in Appendix I.

The utility of the chemical shock tube, as a tool for kinetics studies, depends on:

(1) The control of the reaction temperature.

(2) The ability to vary accurately the shape and duration of the temperature pulse.

(3) The production of a sufficient cooling rate to freeze the chemical reaction.

(4) The minimizing of secondary temperature pulses.

The reaction temperature depends on the initial temperature and pressure of the reactant gas sample and the strength of the incident shock wave. The shock strength is primarily determined by the pressure ratio across the diaphragm separating the driver and reactant sections, and the

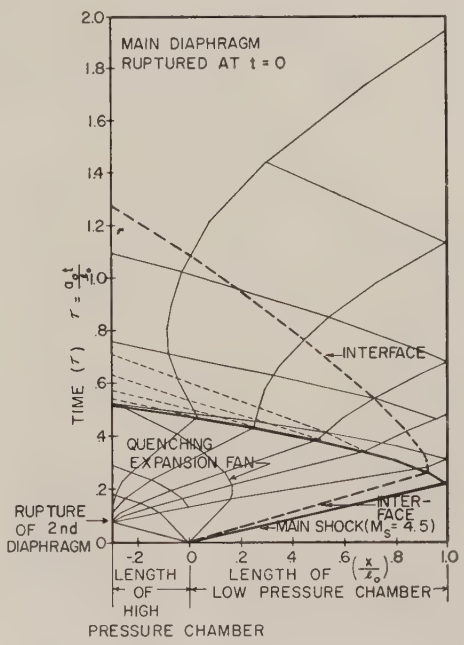

FIG. 4. Typical wave diagram for the chemical shock tube in which the incident shock Mach number is 4.5.

ratio of the speeds of sound of the driver and reactant gases. For reactant gases with complex molecules, greater shock strengths are required to heat the gas samples to high temperatures due to the energy absorbed in the internal degrees of freedom. When strong shocks are required to heat the reactant gas, techniques which may be used include: preheating the driver gas, using low molecular weight driver gases such as hydrogen and helium, diluting the reactant with high molecular weight noble gases such as argon, krypton, and xenon, and the use of combustion drivers[19].

The control of the shape and duration of the temperature pulse depends on the strength of the incident shock wave, the ratio of the lengths of the driver section to the reactant section, the

time delay between the breaking of the two diaphragms, and the absolute length of the reactant section.

The wave phenomena in the chemical shock tube are shown in Figure 4. The diagram is valid only for a restricted range of driver to reactant length ratios. If the driver section is too short, the expansion wave will reach the interface before the reflected shock and cool part of the reactant gas before it has been properly heated. On the other hand, if the driver section is too long, the strong expansion waves from the breaking of the second diaphragm will not overtake the weaker waves from the breaking of the first diaphragm, thus subjecting the reactant gas to a slow initial cooling rate which may not be sufficient to freeze the

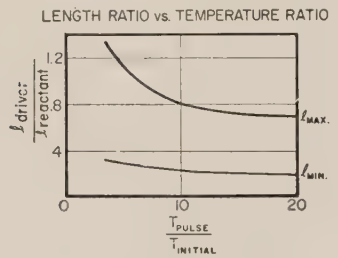

FIG. 5. Maximum and minimum length ratios as a function of the reaction temperature. The temperature is made dimensionless by dividing by the initial reactant gas temperature. The curves were calculated assuming constant specific heat and a matched impedance gas interface.

high temperature composition. A maximum pulse duration and cooling rate for a given shock tube geometry is obtained by breaking the second diaphragm just as the expansion wave generated by breaking the first diaphragm reaches it. The maximum and minimum driver to reactant length ratios and the corresponding heating times with helium as the driver gas and air as the reactant gas are plotted as a function of the reaction temperature in Figures 5 and 6. These curves are calculated assuming that the reacting gas has a constant heat capacity and that the interaction of the reflected shock wave and the gas interface produces no waves that are reflected back into the reaction zone. It is possible to eliminate secondary reflections from the shock-interface interaction by proper adjustment of the acoustic impedance of the driver gas, but these secondary waves are weak even when the impedance match is slightly imperfect.

The importance of a high initial cooling rate can be shown by considering the equation for the amount of products lost during the cooling process:

$$\Delta n = \int_{t_i}^{t_f} \dot{n}(T)\, dt = \int_{T_i}^{T_f} \frac{\dot{n}(T)}{\dot{T}}\, dT$$

where T is the temperature of the reactant sample,

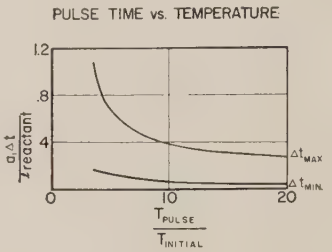

FIG. 6. Heating time of the temperature pulse as a function of the reaction temperature. The heating time and temperature are made dimensionless, and the curves were calculated assuming constant specific heat and a matched impedance gas interface.

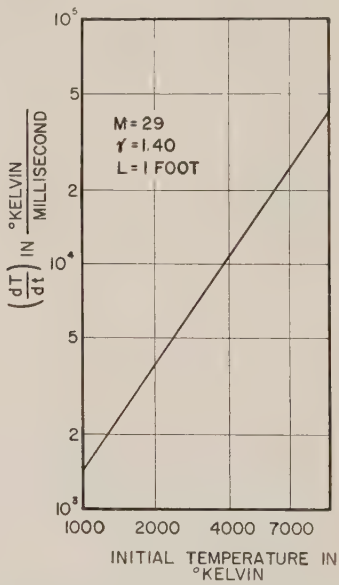

FIG. 7. Estimated initial cooling rate for air in a one-foot chemical shock tube as a function of the equilibrium reaction temperature, computed using Poggi's approximate solution.

$\dot{n}(T)$ is the rate of the reverse reaction, and $\dot{T}$ is the cooling rate. By making $\dot{T}$ sufficiently large, Δn can be made very small. While very little information is available for $\dot{n}(T)$ for various high temperature reactions, the temperature variation is usually taken proportional to $e^{-c/T}$. It is clear from the expression for $\dot{n}(T)$ that the initial cooling rate is extremely important.

The cooling rate for a centered expansion wave

which reflects from a wall can be estimated from an approximate solution given by Poggi[20]. The solution for the cooling rate at the wall is:

$$\dot{T} = -4\left(\frac{\gamma - 1}{\gamma + 1}\right)\frac{a_i T_i}{L}\left(\frac{T}{T_i}\right)^{(\gamma/\gamma-1)}$$

where a_i and T_i are the initial speed of sound and temperature of the undistrubed gas, γ is the ratio of the heat capacities of the undisturbed gas, L is the distance of the origin of the expansion fan from the reflecting wall, and T is the temperature of the gas at time t. Since the state of the gas in the chemical shock tube is not uniform before the initiation of the centered expansion wave, the conditions are more complex than those considered by Poggi, and a pseudo-L value, L', must be estimated. For an order of magnitude calculation, L' may be taken as equal to the sum of the lengths of the driver and reactant sections. For $a_i = (\gamma R T_i/\mu)^{1/2}$, the initial cooling rate is given by:

$$\dot{T}_i = -4\left(\frac{\gamma - 1}{\gamma + 1}\right)\left(\frac{\gamma R}{\mu}\right)^{1/2}\frac{T_i^{3/2}}{L'}$$

where R is the universal gas constant and μ is the molecular weight. The initial cooling rate, assuming constant heat capacity ($\mu = 29$, $\gamma = 1.40$) for a shock tube that is one foot in length is plotted against T_i in Figure 7. The cooling rates compare very favorably with those claimed for modern water-cooled sampling probes[21]. Since the cooling rate increases as $T^{3/2}$ and the rate of the reverse reaction increases as $e^{-\epsilon/T}$, the cooling rate will be inadequate at sufficiently elevated temperatures.

Due to the character of the wave processes, the time scale is proportional to the length of the shock tube proper, i.e., the length of the driver and reactant sections. Therefore, the duration of the temperature pulse can be changed by varying the absolute length of the shock tube. However, the initial cooling rate of the temperature pulse is approximately inversely proportional to the absolute length of the shock tube so that a maximum tube length exists depending on the required cooling rate for the chemical reaction.

The size of the evacuated tank can be conservatively estimated if it is assumed that a state is reached in which the pressure throughout the shock tube and tank is uniform and the reactant and driver gases are unmixed and at different temperatures. The temperature of the reactant gas is then:

$$T = 300\left(\frac{p_d}{p_r}\frac{V_d}{V_t}e^{(\Delta S/R)}\right)^{(\gamma-1/\gamma)}$$

where ΔS is the entropy change experienced by the reactant gas in passing through the incident and reflected shocks, p_d/p_r is the initial pressure ratio of driver to reactant gas, and V_d/V_t is the ratio of driver to tank volume. The volume of the tank, V_t, must be sufficiently large so that the reaction rate is negligible at this final temperature. Since both the pressure ratio and entropy change increase rapidly with shock strength, chemical shock tubes designed for very high reaction temperatures require very large tanks or further design modifications.

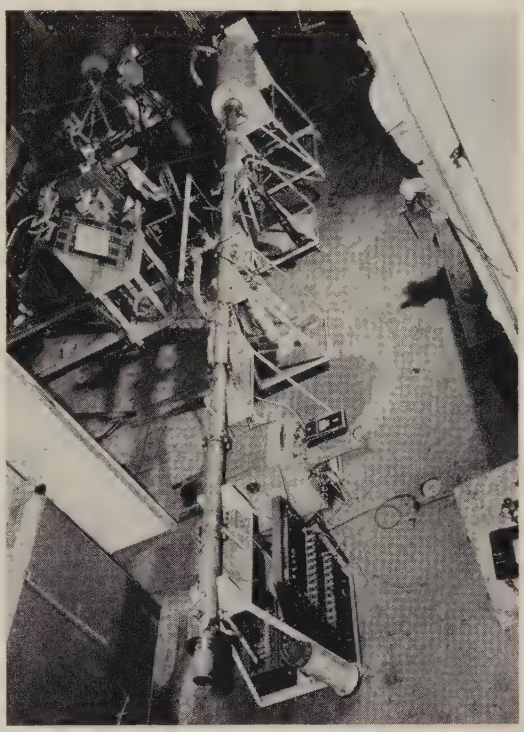

FIG. 8. Photograph of the chemical shock tube showing the overall configuration and the associated instrumentation.

Construction and Operation of the Chemical Shock Tube

The Cornell Aeronautical Laboratory chemical shock tube and the associated instrumentation are shown in Figure 8. The stainless steel evacuated tank is four feet long and eighteen inches in diameter, while the tube proper consists of nine two-foot sections of three-inch stainless steel

pipe, joined together by flanges with O-ring seals. This arrangement allows a large range of ratios of driver length to reactant length to be assembled.

Since the pressure difference across the diaphragms is over 20 atm, metal diaphragms must be used. The diaphragms used in the present work were made of full-hardened, 0.020 in aluminum sheet and were scribed with a cross to vary the bursting pressure. Since accurate control of the time delay between the diaphragm breakings is essential, it is necessary to use powerful, precisely controlled plungers to pierce the strong metal diaphragms. To drive the plungers with the proper time delay, the auxiliary shock tube shown in Figure 9 is used. It consists of a high pressure chamber separated by a diaphragm from a branched line with arms of variable length. The breaking of the diaphragm generates a shock wave which divides and travels through the two branches and then drives the plungers at the end of each branch into the diaphragms with a time delay determined by the difference in length of the two branches. This apparatus gives satisfactory delays which are accurate to 0.1 millisec.

The reaction:

$$^1{}_2N_2 + {}^1{}_2O_2 \underset{k_2}{\overset{k_1}{\rightleftharpoons}} NO,$$

$$\Delta S^\circ_{298.16} = 2.955 \frac{\text{cal}}{\text{mole} - {}^\circ\text{K}},$$

$$\Delta H^\circ_{298.16} = 21.6 \frac{\text{kcal}}{\text{mole}}$$

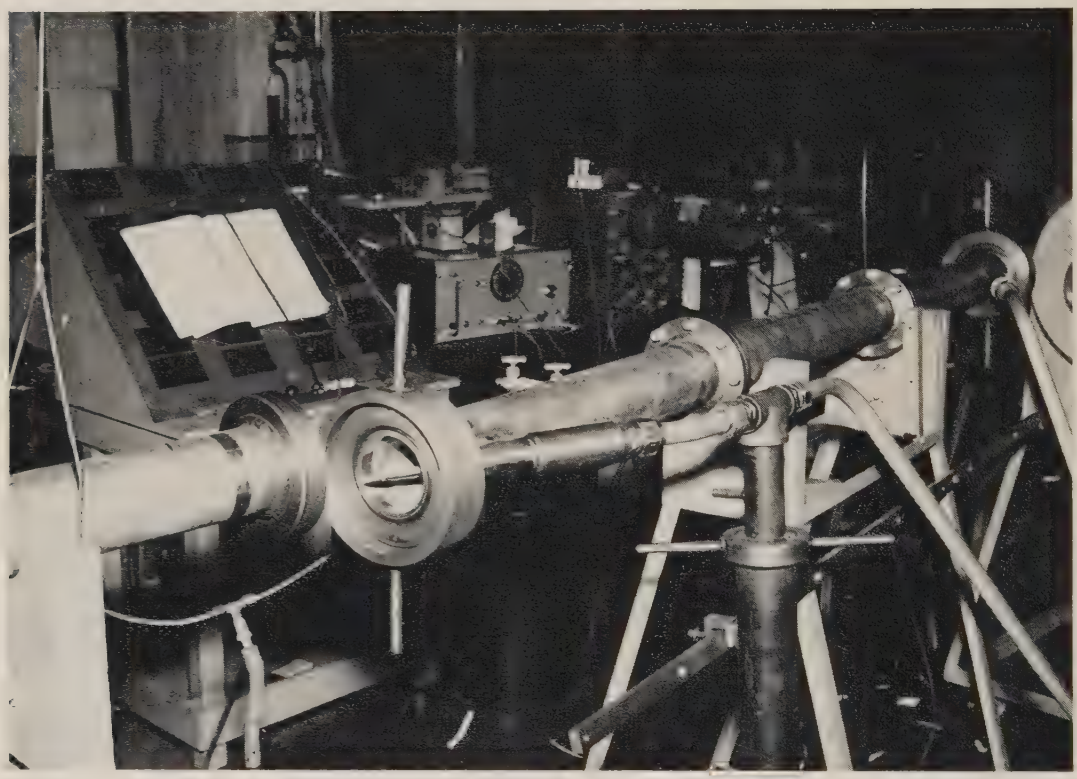

FIG. 9. Closeup photograph showing the diaphragm-breaking apparatus, including the diaphragm-piercing plungers.

was selected for our preliminary work because of the convenience of working with air, the availability of data from other methods, and the importance of the reaction. The experiments were run in a fixed geometry shock tube, with a 6-ft driver section and a 12-ft reaction section. U.S.P. helium at about 300 psia was used as the driver gas, the shock strength being controlled by varying the initial pressure in the reactant section.

A Rutishauser[b] condenser-type pressure transducer was mounted near the closed end to monitor

[b] Rutishauser Corporation, Pasadena, California.

the pressure pulse shape and the shock velocity was measured with ionization gap detectors[3] which performed satisfactorily for shock Mach numbers above 4.

The yield of NO was determined by chemical analysis. It was found that a large sample (about 20 l), withdrawn from a point near the closed end of the reactant section within a few minutes after the run, contained all the reacted gas. This fact was verified by withdrawing additional samples and observing the absence of traces of reactant gas. By adding 20 cc of 10 per cent H_2O_2 and allowing the sample to stand for 12 hours, all the NO was absorbed as HNO_3[c].

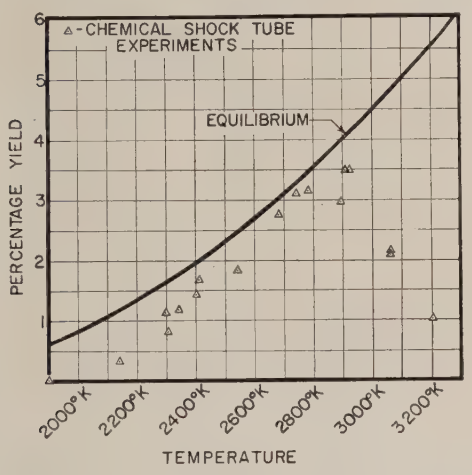

FIG. 10. Percentage of air changed to nitric oxide as a function of the equilibrium reaction temperature behind the reflected shock.

Discussion of Experimental Results

The equilibrium concentration of NO is given by the mass action law:

$$K(T) = \frac{[NO]}{[O_2]^{1/2}[N_2]^{1/2}}$$

where [NO], $[O_2]$, and $[N_2]$ are the equilibrium concentrations at the reaction temperature T. The values of $K(T)$ are known precisely from spectroscopic data[22], and the solid curve in figure 10 is obtained from these values.

The experimental points in Figure 10 show that there is not sufficient time for the equilibrium concentration to form below 2500°K. In the region between 2500–3000°K, the agreement with the theoretical equilibrium concentration is satisfactory considering the preliminary nature of the experiments. The sharp drop at 3000°K is due to the inadequate size of the evacuated tank which causes a reheating of the reacted gas sample and a partial decompostion of the NO formed by the high temperature pulse. With a larger tank or a more efficient driver, the range of these experiments can probably be extended above 3000°K.

From the data obtained below 2500°K, it is possible to obtain an estimate of the reaction rate by assuming some reaction mechanism. However, the mechanism of the NO reaction has not been agreed upon. The pioneer work of Zeldovich[23] and the subsequent studies of Wise and Frech[24] suggest a chain reaction. On the other hand,

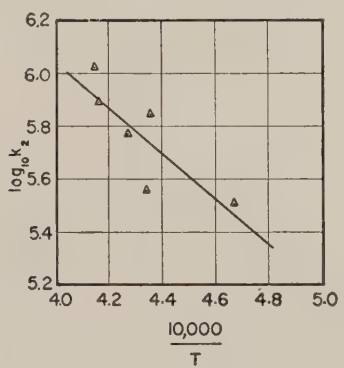

FIG. 11. Plot of the logarithm of the specific reaction rate constant for the decomposition of NO as a function of the reciprocal of the equilibrium reaction temperature. The straight line is obtained by the method of least squares and corresponds to an activation energy of 40 kilocalories/mole.

Daniels[25] has stated the mechanism is bimolecular. Since the data reported in this paper is preliminary, we shall assume the simpler bimolecular hypothesis proposed by Daniels.

For a bimolecular mechanism, the rate of formation of NO is:

$$\frac{d(NO)}{dt} = k_1(O_2)(N_2) - k_2(NO)^2$$

where (NO), (N_2), and (O_2) are the instantaneous concentrations, k_1 is the specific rate constant for the formation of NO, and k_2 the specific rate constant for the decomposition of NO. Assuming that the gas sample is heated to the reaction temperature, T, for a time Δt, which is a space average of the time intervals between the instant the reflected shock wave passes and the time the expansion wave cooling begins, the above rate equation can be integrated. Since in our experi-

[c] This method was suggested by Drs. Daniels and Slaughter of the University of Wisconsin.

ments, $k_1 \ll k_2$ and $(NO) \ll (O_2)$, the result can be simplified to give:

$$(\alpha\beta)^{1/2} K k_2 c_0 \Delta t = \log_e \left(\frac{[NO] + (NO)_{\Delta t}}{[NO] - (NO)_{\Delta t}} \right)$$

where [NO] is the equilibrium concentration of NO at temperature T, $(NO)_{\Delta t}$ is the concentration of NO after time Δt, $K = (k_1/k_2)^{1/2}$ is the equilibrium constant, c_0 is the concentration of air at the reaction conditions, α is the initial mole fraction of N_2, and β is the initial mole fraction of O_2.

The kinetic data obtained below 2500°K is shown in Figure 11 where the logarithm of k_2 is plotted against the reciprocal of the equilibrium reaction temperature. The solid line fitted to the data by the method of least squares gives the following expression for k_2:

$$k_2 = 3.4 \times 10^9 e^{-40{,}000/RT} \left(\frac{\text{liters}}{\text{mole} - \text{sec}} \right)$$

The activation energy of 40 kcal/mole[d] is much lower than those previously reported by Zeldovich (82 ± 10 kcal/mole)[23], Wise and Frech (78.2 kcal/mole)[24], and Daniels (116 kcal/mole)[26]. Since the number of our experimental points is low and the scatter of these points is considerable, the value of 40 kcal/mole is proposed provisionally.

In order to determine accurately the kinetics of the NO reaction, more experimental and theoretical work is necessary. Relaxation effects, reflections of pressure waves from the gas interface, variations of reaction time along the length of the gas sample, and the possibility of secondary reactions occurring during the cooling process require further consideration.

Conclusions

A modified shock tube has been developed at Cornell Aeronautical Laboratory in which a sample of gas can be heated by a single high temperature pulse of known shape and duration. It is believed that useful studies of chemical reactions at high temperatures can be made with this new shock tube technique.

Some preliminary work has been done on the reaction $\frac{1}{2} N_2 + \frac{1}{2} O_2 \rightleftharpoons NO$ In the temperature range from 2500–3000°K, concentrations of NO were found which closely approach the equilibrium values. The high temperature limit in the present experiments was due to the size of the tank in our particular setup and is not an inherent limitation of the method.

From the data obtained below 2500°K, an estimate of the reaction rate was made assuming a bimolecular mechanism. A least square fit of the specific reaction rate constant data gave an activation energy of 40 kcal/mole. This value is much lower than those proposed by previous investigators. Since our kinetic data is meager, the 40 kcal/mole value is reported provisionally.

In this work, only one experiment was made at each temperature. By carrying out a large number of experiments over a wide range of pulse durations, reaction pressures, and initial compositions at each temperature, the scatter of our present data should be substantially reduced. In this way, not only will it be possible to obtain more accurate values of the specific reaction rate constants, but the question of the mechanism of the reaction may also be answered.

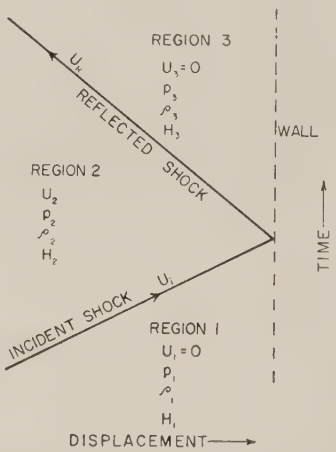

Fig. 12. Schematic sketch to explain the notation used in Appendix I for the calculation of the equilibrium reaction temperature behind the reflected shock.

Acknowledgment

The authors gratefully acknowledge valuable discussions with Professor Simon H. Bauer of Cornell University. Dr. Phillip Campagna of Cornell Aeronautical Laboratory, Inc. assisted in the chemical analyses.

Appendix I

The calculation of the temperature behind a reflected shock is a straightforward application of the laws of conservation of mass, momentum,

[d] The probable error of this value is ± 11 kcal/mole.

and energy, which in a coordinate system fixed in the shock wave are:

$$\rho_a u_a = \rho_b u_b \qquad \text{mass 1a}$$

$$p_a + \rho_a u_a^2 = p_b + \rho_b u_b^2 \qquad \text{momentum 1b}$$

$$H_a + \frac{u_a^2}{2} = H_b + \frac{u_b^2}{2} \qquad \text{energy 1c}$$

where ρ is the density, u the velocity, p the pressure, and H the enthalpy and the subscript a refers to conditions ahead of the shock and b to conditions behind the shock.

Figure 12 shows the conditions of the problem of the reflected shock and the symbols used below. In a coordinate system fixed in the incident shock, the basic equations become:

$$\rho_1 U_i = \rho_2 (U_i - u_2) \qquad 2a$$

$$p_1 + \rho_1 U_i^2 = p_2 + \rho_2 (U_i - u_2)^2 \qquad 2b$$

$$H_1 + \frac{U_i^2}{2} = H_2 + \frac{(U_i - u_2)^2}{2} \qquad 2c$$

while in a coordinate system fixed in the reflected shock, the equations are:

$$\rho_2 (U_R + u_2) = \rho_3 U_R \qquad 3a$$

$$p_2 + \rho_2 (U_R + u_2)^2 = p_3 + \rho_3 U_R^2 \qquad 3b$$

$$H_2 + \frac{(U_R + u_2)^2}{2} = H_3 + \frac{U_R^2}{2} \qquad 3c$$

Eliminating quantities with subscript 2, we have:

$$\rho_1 U_i (U_R + u_2) = \rho_3 U_R (U_i - u_2) \qquad 4a$$

$$p_1 + \rho_1 U_i u_2 = p_3 - \rho_3 U_R u_2 \qquad 4b$$

$$H_1 + U_i u_2 = H_3 - U_R u_2 \qquad 4c$$

Considering the quantities in region 1 (ahead of the incident shock) as known, equations (4a, b, and c) are not sufficient to determine the state of the gas in region 3 (behind the reflected shock). It is necessary to known U_i in terms of U_2 which implies solving equations (2a, b, and c). Fortunately such solutions are already available.

The procedure employed is as follows: Equations (4a, b, and c) may be summarized in the set:

$$\pi = 1 + \frac{\gamma_1 M_i^2}{\left(1 - \frac{\epsilon\varphi}{\varphi - 1}\right)} \qquad 5a$$

$$\epsilon = 1 - \frac{\Omega}{(\pi - 1)} \qquad 5b$$

where

$$\pi = \frac{p_3}{p_1}$$

$$\gamma_1 M_i^2 = \frac{\rho_1 U_i^2}{p_1}$$

$$\varphi = \frac{\rho_3}{\rho_1}$$

$$\epsilon = \frac{u_2}{U_i} = \left(1 - \frac{\rho_1}{\rho_2}\right)$$

$$\Omega = \frac{(H_3 - H_1)}{RT_1}$$

(1) A curve of ϵ versus M_i was prepared (data for such a curve is given in the Hopkins' *Hand book of Supersonic Aerodynamics*[27]).

(2) Curves for Ω and φ versus π for various values of T_3 were prepared assuming the equation of state $p = \rho(R/\mu)T$ and using tables for the enthalpy and molecular weight[27]. It is in this step that the nature of the real gas enters. The assumption of constant heat capacity would give:

$$\Omega = \frac{\gamma}{(\gamma - 1)} \left(\frac{T_3}{T_1} - 1\right)$$

(3) For each value of T_3, assume a number of values of π and determine the corresponding values of ϵ by equation (5b) and the Ω verus π curve. Using these values of ϵ, determine M_i and compute values of π by equation (5a). Then by plotting the computed value versus the assumed value of π, the correct value of π and the corresponding M_i for each temperature are found. The result of this calculation is given in Figure 3. The method would break down at higher temperatures since ϵ approaches a constant limiting value for strong shocks. The above technique, however, is satisfactory for the present range of shock strengths.

REFERENCES

1. Hertzberg, A., and Squire, W.: Bull Am. Phys. Soc., *22*, 45 (1953) (Abstract only).
2. Vieille, P.: Comptes Rendus., *129*, 1228 (1899).
3. Resler, E. L., Lin, S. C., and Kantrowitz, A. R.: J. Appl. Phys., *23*, 1390 (1952).
4. Bleakney, W., Weimer, D. K., and Fletcher, C. H.: Rev. Sci. Instr., *20*, 807 (1949).
5. Bleakney, W., White, D. R., and Griffith, W. C.: J. Appl. Mech., *17*, 439 (1950).

6. Hertzberg, A., and Kantrowitz, A. R.: J. Appl. Phys., *21*, 879 (1950).
7. Payman, W., and Shepherd, W. C. F.: Proc. Roy. Soc., *A158*, 398 (1937).
8. Shepherd, W. C. F.: *Third Symposium on Combustion, Flame and Explosion Phenomena*, p. 301. Baltimore, The Williams & Wilkins Co., 1949.
9. Zeldovich, Y. B., and Chaplintokh, I. Y.: Comptes Rendus (URSS), *65*, 871 (1949). (Available in French as ONERA, Translation 1191.)
10. Gershanik, Y. T. and Zeldovich, Y. B.: J. Phys. Chem. (URSS), *24*, 85 (1950). (Translation available at James Forrestal Research Center.)
11. Berets, D. J., Greene, E. F., and Kistiakowsky, G. B.: J. Am. Chem. Soc., *72*, 1086 (1949).
12. Fay, J.: *Fourth Symposium (International) on Combustion*, p. 501. Baltimore, The Williams & Wilkins Co., 1953.
13. Carrington, T., and Davidson, N.: J. Phys. Chem., *57*, 418 (1953).
14. Marshall, R., and Davidson, N.: J. Chem. Phys., *21*, 659 (1953).
15. Greene, E. F.: J. Am. Chem. Soc., *76*, 2127 (1954).
16. Rudinger, G.: *Wave Diagrams for Nonsteady Flow in Ducts*. New York, Van Nostrand, 1955.
17. Lukasiewicz, J.: National Aeronautical Establishment, Canada, Report No. 15 (1952).
18. Hertzberg, A., et al.: *The Hypersonic Shock Tunnel*. C.A.L. Report (to be published).
19. Hertzberg, A., and Smith, W.: J. Appl. Phys., *25*, 130 (1954).
20. Poggi, L.: J. Aero. Sci., *17*, 813 (1950).
21. Wykoff, W. R., Zelinski, W. H., Davis, S. M., and Reid, W. T.: *Third Symposium on Combustion, Flame and Explosion Phenomena*, p. 674. Baltimore, The Williams & Wilkins Co., 1949.
22. Krieger, F. J., and White, W. B.: Rand Corporation Report R-149, April 1949.
23. Zeldovich, Y. B.: Acta Physicochimica (USSR), *21*, 577 (1946).
24. Wise H., and Frech, M.: J. Chem. Phys., *20*, 22, 1724 (1952).
25. Daniels, F.: Paper given at Symposium on Oxides of Nitrogen at Chicago, September 1953 (to be published).
26. Daniels, F.: Private communication, April 12, 1954.
27. Johns Hopkins University, Applied Physics Laboratory: *Handbook of Supersonic Aerodynamics*, Vol. 5. Washington, 1953.

Discussion by Luigi Crocco*

There exist certain indications, based on controversial experimental evidence, that the passage of a shock wave may produce on chemical reactions effects different from those due to the changes of pressure and temperature alone. I wonder if in the new shock tube technique it would be possible to discriminate these effects, in case they exist, and if efforts are contemplated in that direction.

* Robert H. Goddard Professor of Jet Propulsion, Princeton University.

36

POLAROGRAPHIC STUDY OF COOL-FLAME OXIDATION PRODUCTS OF HYDROCARBONS[a]

By W. M. MacNevin, P. F. Urone, M. L. B. Omietanski, and M. L. Dunton

Introduction

The analysis of the cool-flame oxidation products of hydrocarbons is of interest in the study of the mechanism of combustion. Observations of the kind and the amount of oxidation products and their origin and disappearance in the cool-flame offer a means of elucidating the mechanism.

This paper describes the use of polarography in the study of oxidation products of *n*-hexane, 2-methylpentane, 3-methylpentane and 2,2-dimethylbutane obtained from cool-flame oxidation experiments described elsewhere by Oberdorfer[1].

[a] Investigation carried out as one phase of a research project on the mechanism of combustion, directed by Cecil E. Boord and sponsored by the Air Research and Development Command through a contract with The Ohio State University Research Foundation.

Preliminary work on cool-flame oxidation products taken from the post cool-flame region indicates the presence of one or more of hydrogen peroxide, organic hydroperoxides, crotonaldehyde, formaldehyde and acetaldehyde. Since all of these substances are electroreducible and most of them have been studied polarographically as individuals, the analysis of a mixture of them by polarographic means was attempted.

Polarographic half-wave potentials are known for hydrogen peroxide and for each of the above aldehydes in aqueous solutions[2]. Values for a number of hydroperoxides in aqueous solution are also reported in the literature[3, 4, 5, 6]. Half-wave potentials for a number of other hydroperoxides have been determined by Urone (Thesis, O.S.U., 1954) and occur between 0 and 0.4 v.

Early in this work it appeared that the current voltage curves for hydrogen peroxide and organic hydroperoxides would overlap thus making interpretation difficult or impossible. This difficulty was overcome as described in work already published by MacNevin and Urone[7] by precipitating the hydrogen peroxide with titanium and application of differential polarographic measurement. Certain limitations in the application of polarographic analysis must be realized. It is not conclusive proof of the existence of a compound that a wave having a proper $E_{1/2}$ value is found. Similarly, one may add some of the suspected compound to a sample, obtain an increase in the wave, and still not have proven the presence of that compound in the sample. It is necessary, therefore, to corroborate by other means the qualitative identification at least for each hydrocarbon. This has been done for the individual hydrocarbons reported here by the use of infrared analysis (J. I. Watters, Dan Loughran and Frances Zamnik) and by chromatographic separation and chemical identification (Earl Malmberg and Jane Ann Bobbitt).

It is sometimes not necessary to identify positively every product. For example, the $E_{1/2}$ value for crotonaldehyde is close to that of acrolein in 0.1M potassium chloride solution at pH 7.0 so that polarographically they cannot be determined quantitatively. This is not serious, however, if one is interested in working out a material balance because the carbon contents of the two compounds are similar and the diffusion coefficients of the two are nearly the same. In a material balance calculation the polarographic wave can be attributed entirely to one or the other. When distinctions are important, infrared analysis may be used.

The polarograph may also not distinguish between different organic hydroperoxides. Here again the important matter for the present is the total content of hydroperoxide. However, distinctions can be made by infrared analysis.

The possibility that hydrogen peroxide and aldehydes react and perhaps quickly and that therefore a rapid method of analysis was required was considered as another possible limitation to the use of polarography. No decrease in hydrogen peroxide or aldehyde currents could be detected when mixtures of hydrogen peroxide and aldehyde were prepared and analyzed immediately. These currents were also found to be unaffected up to 2 hours after the sample was taken, but in several cases a noticeable decrease in current occurred after 8 hours. The slowness of the reaction allows time for application of the polarographic method.

The use of the titanium method for distinguishing between hydrogen peroxide and organic hydroperoxide does affect the shape and location of some of the aldehyde waves. This does not, however, constitute a limitation because it is usual practice to run one current-voltage curve covering the voltage range for hydrogen peroxide and all of the aldehydes. This curve is used for estimating the sum of the hydrogen peroxide and organic hydroperoxide and for each of the aldehydes. The same solution is given the titanium treatment to separate hydrogen peroxide and then the peroxide part of the curve is repeated in order to obtain the decrease due to removal of hydrogen peroxide. There has been no evidence in any of this work of interference with the polarographic method used which was caused by addition reactions between hydrogen peroxide and aldehydes. If such addition reactions do occur in the extremely dilute water solutions of the samples, the rate appears to be small.

Apparatus

The current voltage curves obtained in all but the preliminary work were measured with a Leeds-Northrup Electrochemograph, Type E. The polarographic cell was an "H" type cell with sintered glass divider and agar bridge. One half of the cell contained a saturated calomel electrode and all potentials are referred to it. The capillary characteristics in 0.1M potassium chloride and at zero applied voltage were $m = 1.76$ mg mercury/sec, and $t = 4.18$ sec.

All measurements were made at 30 ± 0.1°C. Solutions were outgassed with nitrogen for 10 min. Longer periods of outgassing had no effect on the wave height.

No maxima were encountered in this work. Several maximum suppressors—methyl red, gelatin and dextrin—were added, had no effect on the current and so were omitted in routine measurements.

Experimental

SAMPLING

Three liter samples of combustion gases taken from defined positions in the cool-flame apparatus were bubbled through sintered glass into 50 ml of 0.1*M* potassium chloride solution. Complete absorption of electroreducible products in one absorber was indicated by the absence of more

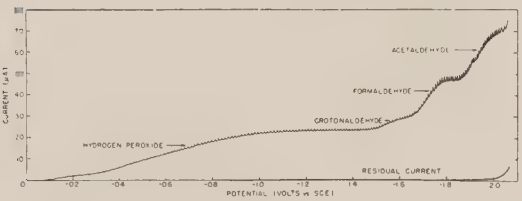

Fig. 1. Current-voltage curve for mixture of hydrogen peroxide, crotonaldehyde, formaldehyde and acetaldehyde.

than a negligible amount in a second absorber. About 10 min was required for the collection of the sample. The absorbate was then adjusted to a pH of 7.0 with potassium hydroxide and diluted to 100 ml with 0.1*M* potassium chloride.

Standardization

In developing the polarographic method, it was found desirable to analyze for all constituents in the same solution, at the same pH, and under the same time, temperature and concentration conditions. Although aldehydes are sensitive to pH in their polarographic behavior, it was found that satisfactory reproducibility could be obtained in a neutral, unbuffered, 0.1*M* potassium chloride solution. When buffered solutions were used, the results were erratic. The use of unbuffered solutions has not created any difficulties as long as the pH was adjusted to 7.0.

Figure 1 shows a polarogram for a synthetic mixture in 0.1*M* potassium chloride containing 3.06 mM hydrogen peroxide, 1.78 mM crotonaldehyde, 18.0 mM formaldehyde and 6.66 mM acetaldehyde. The pH was adjusted to 7.0 with potassium hydroxide. Table 1 summarizes the data for the standard curve. Similar standard curves were prepared for other combinations. Concentrations in samples were considered proportional to the currents obtained.

Analysis of Combustion Products

After the samples were taken, polarograms were run with 10 ml portions of the absorbate. The waves obtained indicated the amounts of the

Table 1. Data for Standard Curve

Compound	Conc. mM/l	$E_{1/2}$ vs SCE	Current* UA
Hydrogen peroxide..	3.06	−0.65	23.3
Crotonaldehyde.....	1.78	−1.53	6.8
Formaldehyde.....	18.0	−1.71	17.0
Acetaldehyde.....	6.66	−1.92	15.2

* $m = 1.76 \times 10^{-3}$ g/sec; $t = 4.18$ sec.

Wave heights and half-wave potentials were measured graphically.

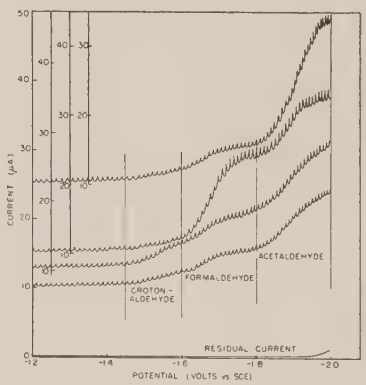

Fig. 2. Current-voltage curves for oxidation products of 2,2-dimethylbutane with added aldehydes.

various aldehydes and the combined amounts of hydrogen peroxide and organic hydroperoxides. The hydrogen peroxide was then precipitated by the method of MacNevin and Urone[7] in which one tenth ml of a titanium solution equivalent to 1 mg of titanium dioxide was added to the polarographic solution, and the titanium and the hydrogen peroxide were precipitated with ammonium hydroxide at the phenol red neutral point. The polarogram was then repeated. The remaining peroxide wave was due to organic hydroperoxide, and the hydrogen peroxide was determined by the difference between the first and second polarograms.

Figure 2 shows the aldehyde portion of several polarograms run from equal aliquots of a sample obtained from the cool-flame combustion of 2,2-dimethyl butane. The first curve is of the sample as received, and the one just above it is of the same solution but with crotonaldehyde added. The third curve is a repeat of the sample with formaldehyde added, and the top curve is another repetition of the sample but with acetaldehyde added. As can be seen the current-voltage curves increase only in the expected positions. Measurement of the wave heights also shows quantitative wave height increases.

Table 2 shows the concentrations of each of the oxidation products obtained from *n*-hexane, 2-methylpentane, 3-methylpentane and 2,2-dimethylbutane at approximately 5 cm beyond the point where the cool-flame was stabilized.

Table 3 is an example of the application of the polarographic method to the analysis of some of the oxidation products of the cool-flame as part of an extensive study of cool-flame mechanisms by Dr. Paul Oberdorfer under the direction of Professor Cecil E. Boord of the Ohio State University[1]. Samples were taken at the points indicated. The concentrations of the substances found are indicated in mM/l. The cool-flame was stabilized at approximately 70 cm.

Conclusion

In conclusion, the polarographic method described here offers a relatively rapid procedure for the measurement of some of the oxidation products of cool-flame combustion studies. It is a sensitive method in that it can measure amounts down to 10^{-5} to 10^{-6} mole of reducible substance. However, it is reliable only in that the identification of the constituents in totally unknown samples should be supplemented with infrared, chromatographic or other chemical identification methods.

Table 2. Estimation of Oxidation Products
(Approx. 5 cm beyond Cool-Flame)

	Observed Concentration in Mol/l of Absorbate				
	H_2O_2	ROOH	C_4H_8O	HCHO	CH_3CHO
n-hexane	0.00177	0.000033	0.00305	0.01035	0.0105
2-methyl-pentane	0.000343	0.000111	0.00021	0.00463	0.00416
3-methyl-pentane	0.00166	0.000036	0.00205	0.00205	0.00706
2,2-dimethyl butane	0.00094	0.000033	0.00128	0.00287	0.00365

Table 3. Estimation of Oxidation Products of 2-Methyl Pentane

CM	ROOH	HOOH	HCHO	CH_3CHO	$CH_3CHCHCHO$
	mM/l	mM/l	mM/l	mM/l	mM/l
30	0.000	0.00	0.00	0.00	0.00
41	0.009	0.00	0.25	0.10	0.00
48	0.039	0.00	0.33	0.29	0.00
60	0.052	0.00	0.00	0.58	0.00
65	0.111	0.34	4.63	4.16	0.00
70	0.080	0.69	7.70	5.95	1.01
80	0.000	1.21	4.52	5.28	1.18
115	0.000	1.52	4.85	5.45	1.23
150	0.000	0.95	4.85	5.50	0.92

REFERENCES

1. Oberdorfer, P. E., The Cool-Flame Combustion of the Isomeric Hexanes. Ph.D. Thesis, The Ohio State University.
2. Kolthoff, I. M., and Lingane, J. J.: Polarography, 2nd Ed. New York, Interscience Publishers, Inc., 1953.
3. Shtern, V., and Pollyak, S.: Acta Physicochim. U. R. S. S., *11*, 797 (1939).
4. Dobrinskaja, A. A., and Neiman, M. B.: Acta Physicochim, U. R. S. S., *10*, 297 (1939).
5. Dobrinskaja, A. A., and Neiman, M. B.: Zhur. Fiz. Khim., *25*, 1169 (1951); C. A., *46*, 5941d.
6. Willits, C. O., Ricciuti, C., Knight, H. B., and Swern, D.: Anal. Chem., *24*, 785 (1952).
7. MacNevin, W. M., and Urone, P. F.: Anal. Chem., *25*, 1760 (1953).

37

MICROWAVE STUDIES IN THE IONIZATION OF ALKALI METALS IN FLAME GASES AND RELATED PHENOMENA

By T. M. SUGDEN

Introduction

This paper is intended to provide a summarized account of measurements made by the author and various collaborators on ionization in flame gases, using the technique of microwave absorption to measure the concentration of free electrons. These electrons have in general been produced by the addition of controlled amounts of alkali metal to the premixed gases before combustion, and it has been shown that their concentration, in the systems which have been studied, are consistent with thermodynamic equilibrium. It is, however, necessary to take into account various side reactions with other constituents of the flame gases, in particular reactions involving hydroxyl radicals, and it is with these that the main chemical interest of the work lies.

The flames used are of hydrogen and air, sometimes further diluted with nitrogen, the premixed gases being burned at atmospheric pressure in a Mèker type of burner. This produces a large number of small cones of primary combustion, in which no thermodynamic equilibrium is expected, and above them a more or less extended zone (interconal gases) which is only faintly luminous, and which is considered to be at or near to equilibrium. It is with this extended zone that this work is concerned. The temperatures have been measured by the sodium D-line reversal method (see, e.g., Griffiths and Awberry[1]), which is expected to be reliable under these conditions. Recent measurements of James and Sugden[2] on flame gases of this type show agreement of measured temperatures within experimental error for both the first and second resonance lines of all the alkali metals, the sodium D-lines being the easiest to read (to within 5°C). The measured temperatures differ from calculated ones on account of two effects, firstly heat losses, mainly to the burner, and secondly the effects of indrawn air, which in a hydrogen-rich flame may give rise to secondary combustion, thereby making the gases non-uniform in temperature cross-section. This latter effect may largely be eliminated by enveloping the flame with nitrogen[3], or, in more recent work[4], by sheathing the flame with a similar flame which contains no added alkali metal. This also reduces boundary self-reversal effects in the temperature determination[5]. The temperatures measured range from 2250°K down to 1800°K, in which range there was no measurable ionization from clean (i.e., without added metal) flames. In this range even the alkali metals are only ionized to a small extent, which greatly simplifies the interpretation of the results. Work at higher temperatures[6], directed towards the ionization of clean flames, meets with very serious difficulties from adventitious traces of alkali metals, and will only become reliable under conditions where the total ionization is considerably larger than that which can be produced from these traces.

The Measurement of Electron Concentration

The presence of free electrons in a gas gives rise to an electrical conductivity σ, which is related to n, the number per cc, by

$$\sigma = \frac{ne^2}{m} \cdot \frac{\omega_1}{\omega^2 + \omega_1^2} \qquad (1)$$

where e and m are the electronic charge and mass respectively, ω is the angular frequency of the applied electric field (microwaves), and ω_1 is the collision frequency of electrons with gas molecules. This equation is based on a very approximate derivation with inaccurate averaging over the collisions, and a more accurate treatment has been given by Margenau[7]. It has, however, been shown to be correct in form by measuring the dependence of σ on ω over a wide range of frequencies[8], and since the quantitative values given by Margenau's much more complicated theory differ very little from those given by equation (1), the simpler expression has been used to derive n from σ. It will be seen that unless there is a very large excess of heavier ions, the small mass of the electrons makes them responsible for effectively all the conduction. It is necessary to work at low microwave powers so that the electrons do not become appreciably hotter than the rest of the gases[7].

Two methods of measurement of σ have been employed; that of direct attenuation of micro-

waves, and that of finding the effect of the flame on the characteristics of a resonant cavity at microwave frequencies. These are shown diagrammatically in Figures 1 and 2 respectively.

The simpler method is that of direct attenuation, in which a beam of monochromatic microwave radiation from a klystron, after suitable attenuation, passes through the flame gases a few cm above the primary cones, between two horns. After further attenuation, the microwaves are rectified by a crystal, and the resultant crystal current passed on to an amplifying and measuring system. It is necessary to have the microwave line carefully tuned with the minimum of standing waves. If the attenuation brought about by introduction of a conducting flame in the gap is β *db*/cm thickness of flame, then σ, and hence n, may be obtained from the equation $\beta = (17.4\pi/c)\sigma$, where c is the velocity of light. This method is suitable for electron concentrations of

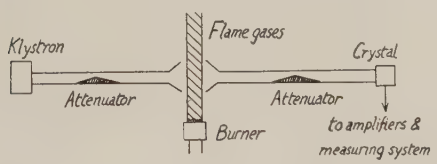

FIG. 1. Direct attenuation apparatus-diagrammatic.

the order of 10^{10}–10^{12}/cc, working with flames of a few cm thick.

Various refinements have been used to extend this to lower concentrations[6], but in Cambridge it has been found more convenient to use the resonant cavity method to achieve this. An account of such an apparatus is given by Sugden and Thrush[9], a rather similar device having been used by Adler[10] to study electrons in discharge tubes.

In this case the microwave power passes through a cylindrical cavity, with apertures to allow ingress and egress of the flame gases axially. The klystron is frequency modulated by a low frequency saw-tooth voltage applied to its reflector plate, and the cavity tuned by a plunger, so that the frequency range used sweeps across the resonance point of the cavity in a suitable mode (TE_{011} is most convenient). By applying the saw-tooth voltage to the X plates of an oscillograph, and the signal transmitted by the cavity to the Y plates, a diagram of the resonance characteristic of the cavity is obtained on the screen. The shape of this is altered when a conducting flame is present in the cavity, the peak becoming less sharp on account of the dielectric losses introduced. From these changes, knowing the geometry of the system, it is possible to deduce the conductivity of the flame gases, and hence the concentration of free electrons. The useful range of this method overlaps with that of the previous one, and extends down to 10^8 electrons per cc. A valuable mode of calibration of this type of apparatus is to use the simple behavior of alkali metals as given by the more straight-forward attenuation method.

The alkali metals are added to the gas stream in the form of finely divided sprays of one of their salts. The maximum added is of the order of 1 part in 10^5 of the total gases, and at this level the corresponding amount of anion plays no effective role, i.e., all salts of a given metal produce the same electron concentration. Thus the amount added can conveniently be controlled by changing the strength of the solution in the

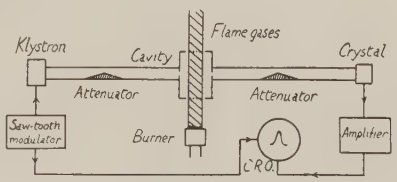

FIG. 2. Resonant cavity method-diagrammatic.

atomizer. The estimation of the total metal picked up can best be made from measurements of loss in the atomizer, coupled with careful estimations of any salt deposited on connecting tubing between the atomizer and the burner. It has been found most convenient to express all concentrations in the flame gases in partial pressures in atmospheres, which will be expressed here by enclosing the appropriate symbol in square brackets—e.g., $[\epsilon]$—for electron concentration.

The Ionization of Alkali Metals and Hydroxyl Effects

When an alkali metal A is added to flame gases in small proportion, the following equilibrium may be supposed to be set up

$$A \rightleftharpoons A^+ + \epsilon; \qquad K_1 = \frac{[A^+][\epsilon]}{[A]} \tag{2}$$

The equilibrium constant K_1 is given by a thermodynamic equation first put forward by Saha[11]:

$$\log_{10} K_1 = -\frac{5050V}{T} + \frac{5}{2}\log_{10} T - 6.50 \tag{3}$$

where V is the ionization potential of the metal in electron volts and T the temperature in °K. Under present conditions the background ionization is negligible so we may put $[A^+] = [\epsilon]$ for charge balance, and the total ionization is small, i.e., $[A^+] \ll [A]$ so we may write $[A] = [A_0]$, where $[A_0]$ represents the total added metal expressed as a partial pressure. In this case equation (2) reduces to

$$[\epsilon]^2 = K_1[A_0] \tag{4}$$

$[A_0]$ will be proportional to the concentration of the salt solution in the atomizer, so that a plot of log $[\epsilon]$ against log (molarity of solution) should be a straight line of slope 0.50. This result is always

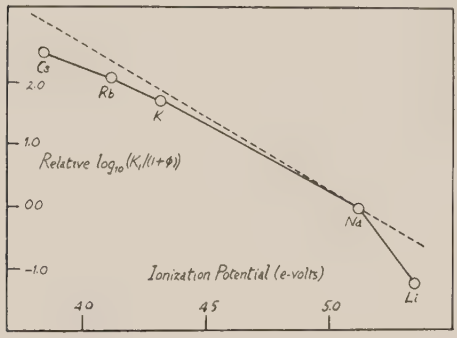

FIG. 3. The relative ionization of the alkali metals in a hydrogen-rich flame of H_2/air (sodium D-line reversal temperature 2245°K). The dotted line through the Na point has a slope corresponding with that predicted by the Saha equation for this temperature.

found to be the case under the conditions used, and is equivalent to the Ostwald dilution law for a not too dilute solution of a weak electrolyte.

This supports the idea of equilibrium, or at least of a steady state of balanced ionization and recombination. The next point is to consider the values of the constant K_1 in the light of the Saha equation (3), but in order to do this it is necessary to examine two possible interactions with the flame gases, which might affect the final equilibrium position. These are the formation of gaseous alkali hydroxide AOH and negative hydroxyl ion OH^-, by reaction with the free hydroxyl of the gases.

$$AOH \rightleftharpoons A + OH; \qquad K_2 = \frac{[A][OH]}{[AOH]} \tag{5}$$

$$OH^- \rightleftharpoons OH + \epsilon; \qquad K_3 = \frac{[OH][\epsilon]}{[OH^-]} \tag{6}$$

If we write $\phi = [OH]/K_2$, and $\phi' = [OH]/K_3$, then ϕ and ϕ' are parameters of the system, the first being characteristic of a given metal and flame, and the latter of a given flame. Since [OH] for the flames under consideration is at least 10 times larger than the amounts of metal added, it will be unaffected by the above two reactions. Assuming balance of charge and of mass:

$$[A^+] = [\epsilon] + [OH^-] = [\epsilon](1 + \phi') \tag{7}$$

$$[A_0] = [A] + [AOH] = [A](1 + \phi) \tag{8}$$

and combining these last four equations with equation (2) the following result is obtained:

$$[\epsilon]^2 = \frac{K_1[A_0]}{(1 + \phi)(1 + \phi')} \tag{9}$$

This equation still gives the observed dilution behavior but with a modified constant. A selection of actual results for various alkali metals in a given flame is shown in Figure 3, and for various hydrogen air flames (i.e., various temperatures) with a given alkali metal in Figure 4. Both of these diagrams show marked deviations from the Saha equation, which would predict straight lines, of slopes $(5050/T)$ and $(5050V)$ respectively in Figures 3 and 4. On the basis of interpretation of deviations from this behavior which has been adopted, then Figure 3 will show up the hydroxide (ϕ) effect only, since the hydroxyl ion (ϕ') effect, if present at all, will influence all metals in a given flame similarly. The extent of the deviations of Figure 3 suggests that LiOH is a very stable compound, followed by CsOH, RbOH, KOH and NaOH in decreasing order of stability.

These molecules should be largely ionic in type, resembling the gaseous alkali fluorides and chlorides, whose heats of formation from atoms are shown in Table 1, and it is interesting to see that the sequence of these is the same as that suggested for the hydroxides, within experimental error. The little thermodynamic evidence which is available[12], suggests that the reaction $K + OH \rightarrow KOH$ is exothermic to the extent of 87 ± 2 kcal, and a statistical calculation of the equilibrium constant of the same reaction for NaOH, assuming a heat of reaction of 5 kcal less than this, shows that NaOH should be so unstable as to be effectively absent under the flame gas conditions used at equilibrium. On this basis that there is no significant hydroxide effect with sodium Smith and Sugden[13] have examined the

deviations shown by LiOH and CsOH, and have shown that they predict a difference of 11 kcal between the heats of formation, LiOH being the more stable, and a similar difference of 5 kcal between CsOH and KOH. These differences closely resemble the halide data of Table 1.

Further, the absolute value of ϕ for Li, on the basis of $\phi = 0$ for Na, taken together with the calculated values of [OH] for the burned gas (based on the composition of the unburned gas and the *measured reversal temperature*) leads to a value of 102 kcal for the reaction Li + OH → LiOH, which with the above measured differences gives 86 kcal for KOH, compared with the value of 87 kcal from independent estimation quoted above.

Thus the evidence on relative ionization of the alkali metals strongly suggests the correctness of the equilibrium hypothesis, when this hydroxide effect is taken into account. This interpretation is also in line with experiments of James and Sugden[14] on the intensity of emission of resonance lines of the various metals in flame gases. In more recent work[4], measurements of the relative ionization of lithium and sodium have been used over a much more extended range of flames than was used to arrive at the above viewpoint, rather to check whether the values of [OH] derived from them agreed with the theoretical ones for the measured temperatures. The results of this, which show good agreement, are shown in Table 2. Additional confirmation of effects involving hydroxyl ion is given by the hook-shaped curves of the type of Figure 4, which show that an oxygen-rich flame always gives less ionization than a hydrogen-rich one of the same temperature—in fact the calculated curve of [OH] against $1/T$ shows an inverted form of this hook-shape. The hook is most marked for lithium but is still present for sodium, even though its hydroxide is so unstable. The explanation of this may lie in the possibility of formation of hydroxyl radicals (ϕ' effect), as may the fact that values of K_1 deduced without allowing for this are always about 5 times lower than those from the Saha equation.

Both of these results are consistent with OH having an electron affinity of 62 ± 6 kcal, but must be treated very cautiously. The use of equation (1) to determine absolute values of electron concentration is much less reliable than in the case of relative ones, and in any case comparison over a series of flames involves the simultaneous change of so many variables that there may be some other explanation for the residual hook in the case of flames containing sodium. A little more evidence is provided by the study of flames containing excess of halogen over the alkali metal.

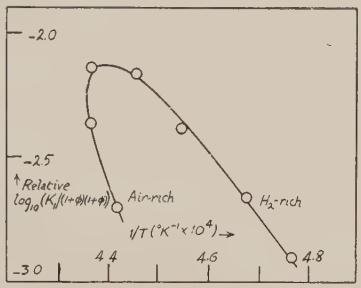

FIG. 4. The relative ionization of lithium in various hydrogen/air flames as a function of the sodium D-line reversal temperature.

TABLE 1. THE HEATS OF FORMATION OF GASEOUS ALKALI FLUORIDES, CHLORIDES AND HYDROXIDES (THE LAST BEING DEDUCED FROM THE PRESENT WORK) FROM ALKALI METAL ATOMS AND HALOGEN ATOMS OR HYDROXYL RADICALS. ALL IN KCAL/MOLE

Alkali Metal	Fluoride	Chloride	Hydroxide
Li	140	116	102
Na	122	96	83
K	126	100	86
Rb	124	104	88
Cs	128	105	91

TABLE 2. COMPARISON OF HYDROXYL RADICAL CONCENTRATIONS OF VARIOUS HYDROGEN/AIR FLAMES ON THE BASIS OF COMPARATIVE IONIZATION OF SODIUM AND LITHIUM AND ON CALCULATION OF FLAME GAS COMPOSITION

Sodium D-Line Reversal Temperature of Flame	[OH] from Relative Ionization of Na and Li	[OH] from Unburned Gas Composition and Na Temp
°K	*atm*	*atm*
2150	4.0×10^{-4}	5.6×10^{-4}
2109	2.1×10^{-4}	3.4×10^{-4}
2063	1.7×10^{-4}	2.1×10^{-4}
2010	9.6×10^{-5}	1.2×10^{-4}
1965	6.3×10^{-5}	7.3×10^{-5}
1907	3.6×10^{-5}	3.7×10^{-5}
1855	2.3×10^{-5}	2.1×10^{-5}

The Effects of Excess Halogen

Although it has been demonstrated that an amount of halogen anion equivalent to 1 part in 10^5 or less of the flame gases has no significant

effect on the ionization of a corresponding amount of alkali metal, it has been found in more recent work by Page and Sugden[15] that if excess halogen is added to the extent of 1 part in 10^4–10^3 parts of

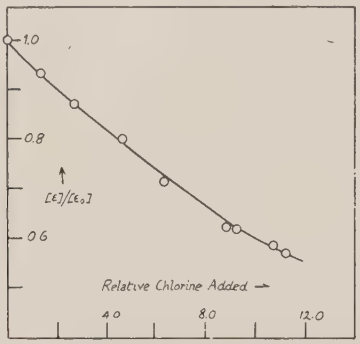

FIG. 5. The effect of the addition of chlorine on the ionization of potassium in a typical hydrogen/air flame.

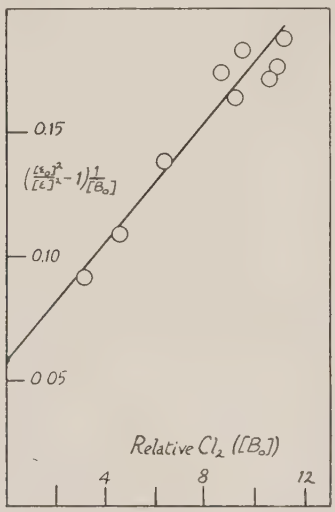

FIG. 6. A plot to test the validity of equation (13) for the effect of chlorine on the ionization of potassium in a hydrogen/air flame.

TABLE 3. A COMPARISON OF a' AS OBTAINED FROM THE EFFECT OF HALOGENS ON ELECTRON CONCENTRATION, AND AS OBTAINED BY THEORETICAL CALCULATION

$a' = (K_5\ (1 + \phi')\ (1 + \theta))^{-1}\ \phi' = 9$ has been taken for the hydrogen/air flame used

Halogen	Electron Affinity	θ	a' (exp)	a' (theor)
	kcal		*atm*	*atm*
Cl	85.8	167	1.8×10^{-3}	3.9×10^{-3}
Br	80.5	2.8	1.1×10^{-3}	0.4×10^{-3}
I	72.4	0.1	2.1×10^{-3}	0.7×10^{-3}

the gases, then a significant reduction in the free electrons from much smaller amounts of alkali metal occurs. This reduction may be the result of one or both of two effects—salt formation and negative ion formation, both of which will be offset by the tendency of the halogen to combine with the hydrogen of the flame gases. These additional equilibria may be expressed as follows:

$$AB \rightleftharpoons A + B; \qquad K_4 = \frac{[A][B]}{[AB]} \tag{10}$$

$$B^- \rightleftharpoons B + \epsilon; \qquad K_5 = \frac{[B][\epsilon]}{[B^-]} \tag{11}$$

$$HB \rightleftharpoons H + B; \qquad K_6 = \frac{[H][B]}{[HB]} \tag{12}$$

Combining these three with the previous three equilibria (B represents an atom of halogen), and introducing the ideas of charge balance, mass balance of metal and halogen, and small ionization of the metal as before, then provided that the total halogen $[B_0]$ is much greater than the total alkali metal $[A_0]$, the addition of the halogen changes the electron concentration from a value $[\epsilon_0]$ (which is that given by equation (9)) to a value $[\epsilon]$ such that

$$\left(\frac{[\epsilon_0]}{[\epsilon]}\right)^2 = \left\{1 + \frac{[B_0]}{K_4(1 + \phi)(1 + \theta)}\right\} \left\{1 + \frac{[B_0]}{K_5(1 + \phi')(1 + \theta)}\right\} \tag{13}$$

where $\theta \equiv [H]/K_6$ is a flame parameter, characteristic of a given flame and halogen. This equation may be written simply

$$([\epsilon_0]/[\epsilon])^2 = (1 + a[B_0])\ (1 + a'[B_0]) \tag{14}$$

where $a = (K_4(1 + \phi)(1 + \theta))^{-1}$, and represents the reduction of electron concentration on account of salt formation (which is offset by the halogen acid (θ) and hydroxide (ϕ) effects). Similarly a' represents the reduction due to negative ion formation (offset by halogen acid (θ) and hydroxyl ion (ϕ') effects.) These overall reductions will be called the salt effect and the halogen ion effect respectively. Equation (14) may be rearranged to

$$\left(\frac{[\epsilon_0]^2}{[\epsilon]^2} - 1\right)\frac{[1]}{[B_0]} = (a + a') + aa'[B_0] \tag{15}$$

which should yield a straight line plot. The effect of chlorine in reducing the electron concentration given by the ionization of potassium in a typical

flame is shown in Figure 5, the maximum chlorine added being about 0.5 per cent of the total flame gases.

A test of equation (15) for the same type of system is shown in Figure 6, which is a fair straight line, with a positive slope, indicating the existence of both salt and halogen ion effects. This is a very sensitive type of plot and better experimental accuracy is desirable.

Values of a and a' may be obtained from graphs of this type, and are distinguished by the fact that, with a given flame, a' is independent of the alkali metal used. The values for the salt effect show reasonable agreement with the predictions of theory (K_4 can be calculated for the salt, θ can be obtained from the stability of the acid and the calculated composition of the flame gases at the reversal temperature, and ϕ from the results of the previous section), but here we shall consider rather a'.

Observed and calculated values of this for three halogens are given in Table 3. The last column was obtained using a value of $\phi' = 9$, and the agreement with the last but one column, although not good, is markedly worsened by omitting this factor in a'. This value is consistent with an electron affinity of 60 ± 5 kcal for the hydroxyl radical. Further work along these lines is proceeding.

Free Electrons from Solid Carbon Particles

The first observations on the free electrons produced by evaporation from carbon particles in acetylene flames by a microwave method were made by Sugden and Thrush[9], more recent data being given by Shuler and Weber[6]. They indicate that the ionization occurring is not inconsistent with thermal ionization of the particles, with values of the work function as for graphite. Although these measurements do not throw any direct light on the mechanism of carbon formation in such flames, it is suggested that examination of the ionization, if any, in metal-free flames in the region of composition just outside that in which luminosity from solid particles appears might provide some extra information. It is well known that even quite small conjugated systems of carbon atoms have quite low ionization potentials, rapidly converging to the work function of graphite. The presence of compounds of this type might be made evident by measurable ionization.

Conclusion

This paper has attempted to demonstrate the uses to which the study of ionization in hot flame gases may be put in some selected problems of high temperature thermodynamics, and has indicated a fairly general consistency with thermal equilibrium under the conditions chosen. The method is not, however, restricted to such systems, and could disclose the absence of equilibrium. The main difficulty is that it only gives information about relatively extended volumes of flame.

REFERENCES

1. Griffiths, E., and Awberry, J. H.: Proc. Roy. Soc. (A), *123*, 401 (1929).
2. James, C. G., and Sugden, T. M.: In course of publication.
3. Smith, H., and Sugden, T. M.: Proc. Roy. Soc. (A), *211*, 31 (1952).
4. Sugden, T. M., and Wheeler, R. C.: In course of publication.
5. Lewis, B., and von Elbe, H.: *Combustion, Flames and Explosions of Gases*. New York, Academic Press, 1951.
6. Shuler, K. E., and Weber, J.: J. Chem. Phys., *22*, 351 (1954).
7. Margenau, H.: Phys. Rev., *69*, 508 (1945).
8. Belcher, H., and Sugden, T. M.: Proc. Roy. Soc. (A), *201*, 480 (1951).
9. Sugden, T. M., and Thrush, B. A.: Nature, *168*, 703 (1951).
10. Adler, F. P.: J. Appl. Phys., *20*, 1125 (1949).
11. Saha, M. N.: Phil. Mag., *40*, 472 (1920).
12. Smith, H., and Sugden, T. M.: Proc. Roy. Soc. (A), *211*, 58 (1952).
13. Smith, H., and Sugden, T. M.: Proc. Roy. Soc. (A), *219*, 204 (1953).
14. James, C. G., and Sugden, T. M.: Nature, *171*, 428 (1953).
15. Page, F. M., and Sugden, T. M.: To be published.

38

TEMPERATURE MEASUREMENTS FROM IODINE ABSORPTION SPECTRUM

By N. J. BECK, SIMON K. CHEN, O. A. UYEHARA, J. G. WINANS, AND P. S. MYERS

Introduction

During the past few years there has been considerable interest in measuring rapidly fluctuating gas temperatures such as occur in internal combustion engines. As a result of this interest a number of temperature-measuring devices have been developed[1, 2, 3]. Almost without exception, however, these devices have required that the gases be at a comparatively high temperature and have sufficient luminosity to use phototubes for measuring intensities. There are conditions, however, when the gas temperature is too low to produce luminosity in the wavelength regions which can be measured by vacuum phototubes and yet the temperature of the gas is varying rapidly so that a detector with rapid response must be used. For example, during the compression stroke previous to ignition in an engine only the faintest luminosity is found and that only when cool flames[4] occur. It was, therefore, of interest to devise and develop an instrument capable of measuring and recording rapidly-fluctuating gas temperatures in the range from room temperature to 1500°F.

An absorption spectrum technique was finally chosen for investigation. This method permitted the use of vacuum phototubes as measuring devices, it did not require luminosity of the gas, and it permitted instantaneous and continuous temperature measurements.

The absorption technique is as follows: light having a continuous spectrum is passed through the gases whose temperature is to be measured. If none of the gases normally present absorb in the wavelength region of interest, it may be necessary to add an absorbing gas to the mixture. At particular wavelengths, depending upon the gas, absorption occurs. The amount of light absorbed in a certain wavelength range depends upon the absorption coefficient of the gas at wavelengths within this range, and also on the number of molecules of the gas in the light path which are able to absorb radiation in this range. The number of absorbing molecules in turn depends upon the temperature of the gas and the total number of molecules of the absorbing gas. By measuring the light transmitted at two different wavelengths the variable of number of molecules may be eliminated and the temperature of the gas may be determined.

Since the absorption technique was to be initially applied to the measurement of compression temperatures in a spark-ignition engine, the following necessary and preferred requirements to be met in the selection of the absorbing gas were set up with this application in mind.

Necessary Requirements

(1) The absorption spectrum of the gas must occur at wavelengths in the range of suitable receivers.

(2) The intensities in the absorption spectrum of the gas must vary a measurable amount with temperature.

(3) The gas should not appreciably affect the combustion reactions.

(4) The gas should have a strong absorption spectrum.

(5) No other gas in the combustion chamber should absorb radiation at the wavelengths used for these measurements.

Since vacuum phototubes were considered to be the only satisfactory receivers, there resulted an automatic limitation to wavelengths below 10,000 Å. The only triatomic gases considered were those normally present in the combustion chamber, i.e., water vapor and carbon dioxide. However, their absorption spectra do not fall in the wavelength region below 10,000 Å.

The diatomic molecules considered were those listed by Herzberg[5]. This list shows vibrational and rotational constants for the electronic states of all known diatomic molecules. The only gases in this table meeting the requirements listed as necessary were the halogens and sulfur. Sulfur was eliminated because it is readily oxidized and not usually found in the diatomic form. This left only the halogens and of these idoine is the most inert.

Iodine seems ideal in every respect except that it may have an effect on the reactions during the compression stroke[6]. It has a strong absorption spectrum at room temperature, and the intensities in its absorption spectrum vary measurably with temperature. It is also comparatively

stable over the temperature range of interest (Fig. 1).

When radiation passes through a uniform absorbing gas the intensity transmitted at wavelength λ is given by

$$I_\lambda = I_{T\lambda} e^{-\alpha_\lambda N_\lambda} \tag{1}$$

where $I_{T\lambda}$ is the intensity of the incident radiation at wavelength λ, N_λ is the number of molecules in the radiation path capable of absorbing radiation at wavelength λ, and α_λ is a constant which changes with wavelength. When intensities are measured by photocells which receive all of the radiation in a certain range of wavelengths, the photocell response D is related to the intensities by

$$D = C \int_{\lambda_1}^{\lambda_2} I_\lambda \, d_\lambda \, . \tag{2}$$

With simplifying assumptions as shown in the appendix the relation between photocell deflections and temperature becomes (equation (19) appendix).

$$\log \frac{\log \dfrac{D_a}{D_T}}{\log \dfrac{D_b}{D_T}} = \text{constant} + \frac{E_b - E_a}{kT} \tag{3}$$

where D_a and D_b are the photocell response for two different ranges of wavelengths in the absorption spectrum of iodine and D_T is the photocell response over these ranges when there is no absorption. (D_T is shown as D_0 in Fig. 2.)

This equation relating photocell deflections and temperature is independent of the concentration (N_0) of the absorbing gas. If the approximations made in the derivation are valid, equation (3) shows that by plotting log (log D_a/D_T/log D_b/D_T against $1/T$, a straight line should result, or, if the temperature is held constant and the concentration of the iodine varied, the left side of equation (3) should have a constant value.

If equation (3) were valid, the instrument could be completely calibrated by one experimental determination of phototube deflections with the absorbing gas at a known temperature.

In order to check the validity of equation (3), experimental data were taken at constant temperature and varying iodine concentration for three wavelength ranges, (a) (5200–5270 Å, (b) (5710–5790 Å) and (c) (6000–6100 Å). These data are presented in Figure 2, where log (log D_a/D_T/logD_b/D_T) is plotted against 1 $-$ (D_a/D_T) which varies when the concentration is varied. Data are shown for three combinations of deflections obtained at the three different wavelength ranges, *a*, *b* and *c*. It appears that the deviations from a constant value exceeds the experimental error when the combination of deflections includes the deflection D_b. This may indicate that the method of averaging the effect of overlapping is not satisfactory.

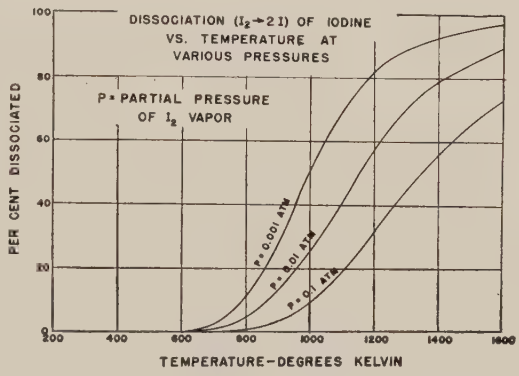
DISSOCIATION ($I_2 \rightarrow 2I$) OF IODINE VS. TEMPERATURE AT VARIOUS PRESSURES
P = PARTIAL PRESSURE OF I_2 VAPOR
P = 0.001 ATM
P = 0.01 ATM
P = 0.1 ATM
PER CENT DISSOCIATED
TEMPERATURE–DEGREES KELVIN

FIG. 1. Percent dissociation of iodine.

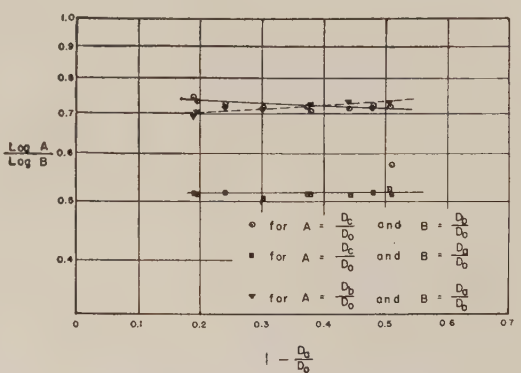

FIG. 2. Experimental data to check equation (3).

Since the maximum obtainable accuracy was desired and since small changes in the term log $\dfrac{\log D_a/D_T}{\log D_b/D_T}$ correspond to comparatively large changes in temperature, it was felt advisable to obtain experimental calibration data showing the effect of overlap and of changes of iodine concentration and to use this experimentally obtained data for determining temperatures in an engine. In this way temperatures which are independent of the concentration of the iodine can be obtained. The procedure used and the calibration data obtained are given in a later section. Work is continuing in an effort to improve the approxi-

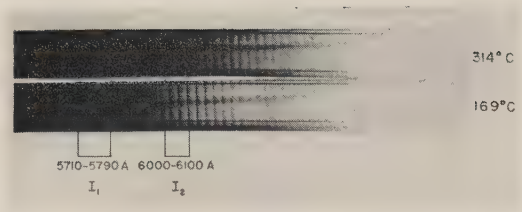

FIG. 3. Iodine absorption at two temperatures.

TABLE 1. IODINE ABSORPTION BANDS[9]

Wavelength in Air in Angstrom Units Å

v'	$v''=0$	$v''=1$	$v''=2$	$v''=3$	$v''=4$
0					
1					
2					
3					
4					
5					6506
6					6456
7			6238	6323	6408
8			6194	6277	6361
9			6153	6233	6316
10			6111	6190	6272
11			6070	6148	6229
12		5954	6030	6108	6187
13		5917	5991	6068	6147
14	5808	5880	5955	6030	6107
15	5773	5845	5918	5995	6070
16	5740	5811	5883		6033
17	5708	5777	5849		
18	5676	5745	5816		
19	5645	5714	5784		
20	5615	5683	5753		
21	5587	5654			
22	5559	5625			
23	5532	5598			
24	5506	5571			
25	5481	5546			
26	5456	5521			
27	5433	5496			
28	5410	5473			
29	5388	5450			
30	5367				
31	5346				
32	5327				
33	5308				
34	5289				
35	5272				
36	5255				
37	5239				
38	5223				
39	5209				
40	5194				
41	5181				

mations and thus to obtain a calibration curve which is independent of concentration.

The absorption spectrum of iodine in the visible region with constant pressure at two temperatures is shown in Figure 3.

The wavelengths for the heads of several of these bands and their vibrational quantum numbers are listed in Table 1. The vibrational energy of the initial levels for these bands can be determined from $E = 213.7\ v'' - 0.592\ v''^2$ cm^{-1}.[7]

To select the most desirable absorption bands for use in temperature measurements, the absorption intensities ΔI of the iodine molecules were compared for several wavelength regions using

$$\Delta I^{v'v''} = K\left[\int \psi_{v'}\psi_{v''}\, dr\right]^2 \tag{4}$$

$\psi_{v'}, \psi_{v''}$ = wave functions (amplitudes) for the vibrational levels v' and v''.

$\Delta I^{v'v''}$ is the absorption intensity for a transition between vibrational states v' and v''.

The wave functions for a harmonic oscillator are

$$\psi_v = N_v e^{-\alpha x^2/2} H_v(\sqrt{a}x) \tag{5}$$

N_v = normalizing factor
a = constant
x = distance from the equilibrium position of the potential energy curve
$H_v(\sqrt{a}x)$ = Hermite Polynomials

For iodine, the wave functions for the vibrational levels of the ground electronic state were taken as the same as those for a harmonic oscillator as plotted in Figure 4.

The wave functions of the upper electronic state were not computed, but two simplifying approximations were made. These were, first, that the upper wave functions are the same for all the vibrational levels considered, and second, that the wave functions differed from zero only at the locus of the maxima for the different levels. The locus was estimated and is represented by the broken line in Figure 4. It is almost parallel to the potential energy curve of the upper electronic state.

Using these approximations it follows that

$$\overline{\Delta I}^{v'v''} = K(\psi)^2_{v''} \tag{6}$$

An approximate intensity distribution for the several bands was calculated using equation (6) and is presented in Figure 5. From this figure

the most desirable spectral region for band absorption intensity measurements can be determined.

The wavelength regions used for the measurement of temperature in this work are shown by the shaded area under the approximate intensity distribution curves of Figure 5. The wavelengths selected were a compromise between the most intense bands and the bands with a minimum of overlap and unabsorbing back-ground. The regions I_1 and I_2 are shown also in Figure 3.

Apparatus and Calibration

The apparatus consisted of a light source, an absorption cell, a spectrograph and the necessary electronic equipment to measure light intensity. A schematic diagram of the absorption pyrometer as arranged for calibration is shown in Figure 6. Since its initial use was to be the measurement of compression temperatures in a spark-ignition engine, the equipment was designed so that it could be used, without modification, on an engine.

In the preliminary measurements a broad-ribbon tungsten-filament lamp was used for the light source because of its ready availability and constant light intensity. However, since considerable light intensity is lost in passing through the engine a 300-watt zirconium-arc lamp operated on direct current was used. The lamp had an apparent temperature of about 6000°F and a brightness 10 times that of a tungsten lamp. It was found experimentally that the location of the luminous spot in the zirconium-arc tended to change in an erratic manner with time, particularly when the lamp was operated below its rated current. It was also found that because of this erratic wandering of the spot, it was necessary to discard lamps long before they showed any other signs of failure.

Two quartz absorption cells inside a heated furnace served as the absorption chamber during calibration of the apparatus, and the engine cylinder served as the absorption chamber when data were being taken on the engine. One of the quartz absorption cells was evacuated and iodine crystals placed in the long stem of the cell. This long stem extended out of the furnace and into an external water bath whose temperature could be controlled. The temperature of the water bath thus determined the partial pressure of the iodine in the absorption cell.

In order to align the absorption cells and to determine the small amount of selective absorption or scattering due to the absorption cell itself, the absorption was measured when the end of the stem of the cell was placed in liquid air to reduce the partial pressure of the iodine vapor to nearly

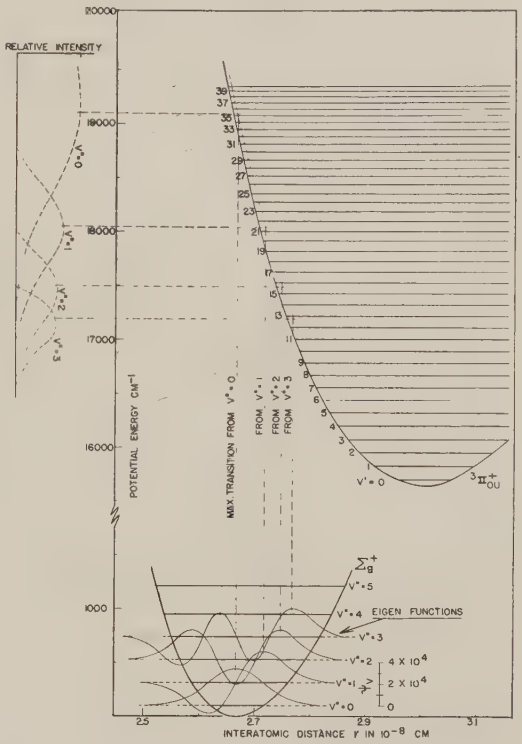

FIG. 4. Iodine potential energy diagram with Eigenfunctions.

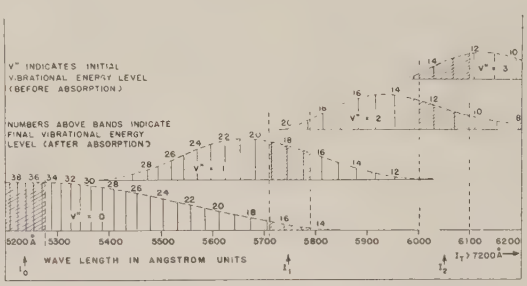
V" INDICATES INITIAL VIBRATIONAL ENERGY LEVEL (BEFORE ABSORPTION)
NUMBERS ABOVE BANDS INDICATE FINAL VIBRATIONAL ENERGY LEVEL (AFTER ABSORPTION)
WAVE LENGTH IN ANGSTROM UNITS

FIG. 5. Absorption spectrum of I_2 gas and approximate intensity distribution for vibrational bands.

zero. In order to compare rapidly the light intensities with and without iodine, the second similar, but empty cell was placed beside the iodine cell and its absorption determined and compared with that of the iodine cell at each of the wavelengths used. By sliding the furnace in which the cells were located, back and forth on a track, either of the two cells could be inserted

into the light path and the difference between iodine and no iodine absorption could be rapidly determined.

The temperature of the cells was measured by three Chromel-Alumel thermocouples inserted beside the quartz cells in the furnace. By controlling the temperature of both the furnace and the water bath any desired iodine concentration and temperature could be obtained.

A special prism spectrograph was constructed

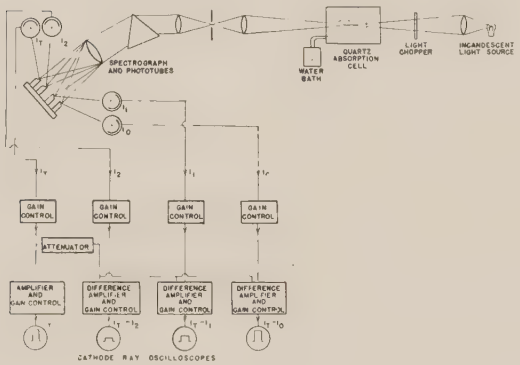

FIG. 6. Schematic diagram of apparatus (as arranged for calibration).

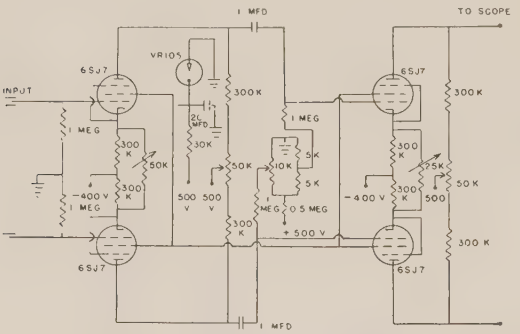

FIG. 7. Difference amplifier.

for this work. A 4-cm, f2 lens was used for the collimating lens. A Gaertner model L161C bilateral spectrograph slit permitted the slit width to be varied without changing the position of the slit image. A 40-in focal length camera lens focused slit images on four movable inconel mirrors. Each of these mirrors reflected light of the desired wavelength range into a multiplier phototube. Three 931A multiplier phototubes experimentally selected for low noise, maximum stability and minimum fatigue were mounted to receive light of wavelength ranges corresponding to the shaded areas of Figure 5. A 1P-22 phototube was placed in the unabsorbing region (7200 Å). In order to minimize any stray radiation, Wratten filters no. 55, 16, 22E and 88 were inserted before the phototubes receiving radiation designated by subscripts 0, 1, 2 and T respectively.

In order to increase the measuring accuracy and to obtain oscillographic signals directly proportional to light absorption at different wavelengths, electronic difference amplifiers were built. These circuits enabled the output voltage from the photomultiplier tubes corresponding to D_0, D_1 and D_2 to be subtracted from the output voltage corresponding to D_T. The voltage signals resulting from this subtraction were amplified and impressed on the vertical deflection plates of an oscilloscope. These deflections are denoted by ΔI_0, ΔI_1, and ΔI_2. Also for the purpose of obtaining correct relative amounts of absorption, a precision attenuator circuit was inserted between the photomultiplier circuit and the amplifier, thus permitting simulation of known amounts of absorption. The circuits used are shown in Figure 7.

The apparatus was developed and calibrated in the steady state using the furnace and quartz absorption cells. The procedure used in obtaining steady state calibration was as follows: With light passing through the empty cell the amplifications of the four photomultiplier tubes were adjusted so that all output voltages were equal. The outputs ΔI_0, ΔI_1, and ΔI_2 were then zero. Experimentally this was accomplished by use of a light chopper and by noting when the deflections ΔI_0, ΔI_1, and ΔI_2 were the same with and without light on the phototube as evidenced by a straight line on the oscilloscope.

When absorption takes place D_0 decreases, D_T remains constant, and one obtains a deflection ΔI_0. This deflection, ΔI_0, is directly proportional to the radiant power absorbed, i.e., $D_T - D_0$. This deflection, ΔI_0, can be expressed in terms of percent radiation absorbed by comparing it with the deflection with no absorption and with the output voltage corresponding to D_T decreased by known percentage by a precision attenuator. When the iodine-filled cell was in the light path, the oscillograph deflections were then proportional to the light absorption at wavelength ranges 0, 1, and 2.

The concentration of the iodine in the absorption cell was determined from vapor pressure versus temperature data, the temperature of the water bath, the temperature of the absorption cell and use of the ideal gas law.

In taking data the furnace was maintained at a constant temperature and the iodine concentration varied. The temperature of the furnace was then changed and the procedure repeated. Typical data obtained when using the zirconium arc lamp are shown in Figure 8. The results of a series of such runs are shown in Figure 9. The data were then cross plotted to give lines of constant percent absorption of I_0 on the plot of absorption ratios against reciprocal temperatures. The resulting curves are shown in Figure 10.

In using Figure 10 to obtain temperature, the three ratios $(\Delta I_2/\Delta I_0)$, $(\Delta I_2/\Delta I_1)$, and $(\Delta I_1/\Delta I_0)$ are obtained from the oscilloscope deflection. Also from ΔI_0 and D_0 the percentage absorption is obtained. Reciprocal temperatures are then obtained using a ratio such as $(\Delta I_2/\Delta I_0)$ and that calibration curve in Figure 10 corresponding to the same percentage absorption. The temperature obtained is thus independent of the percentage absorption, i.e., independent of the concentration of the iodine.

Engine Results

In order to test the operation of the instrument when measuring rapidly varying temperatures, the absorption pyrometer was tested on an operating engine. In addition to the absorption pyrometer, the engine was equipped with a Li pressure indicator to record the pressure in the combustion chamber, an iodine vaporizer to introduce iodine into the intake manifold of the engine when desired, a synchronized light chopper, a magnetic crank-angle-position marker, and a drum camera to record the oscillograph trace and provide a time base.

The engine used was a CFR L-head engine with a compression ratio of 5.6 to 1. Quartz windows were installed to provide a light path through the last portion of the charge to burn.

A typical film as obtained when using the engine is shown in Figure 11. Reading from top to bottom the trace on the film represents:

(1) Total lamp intensity with no absorption, i.e., D_T.

(2) Gas pressure in the engine.

(3) Alignment line produced by a light located between the scopes. This alignment line provides a reference line for measuring deflections.

(4) Light absorption at an effective wavelength 5320 Å, i.e., ΔI_0 which equals $D_T - D_0$. (An increase in absorption gives a downward deflection.)

(5) Crank position markers.

(6) Another alignment line.

(7) Light absorption at an effective wavelength of 6050 Å, i.e., ΔI_2 which equals $D_T - D_2$.

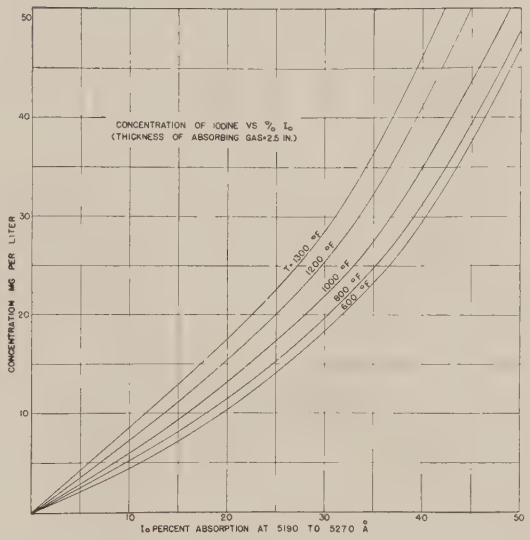

FIG. 8. Concentration of iodine vs. percent I_0 (thickness of absorbing gas = 2.5 in).

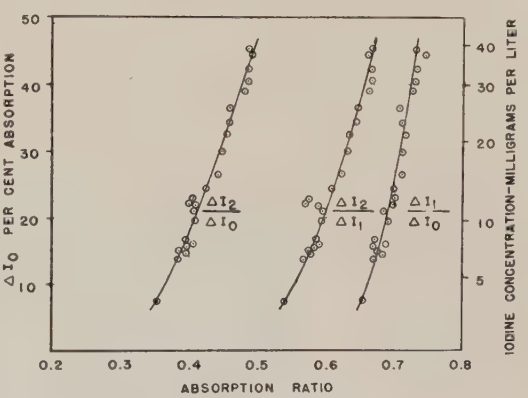

FIG. 9. Zirconium arc source; constant cell temperature 685°F.

(8) Light absorption at an effective wavelength of 5750 Å, i.e., ΔI_1 which equals $D_T - D_1$.

In making temperature determinations from a record such as shown in Figure 11, the zero light absorption point for wavelength ranges 0, 1 and 2 was determined from measurements taken in the exhaust portion of the cycle where the temperature was high and the dissociation of the iodine was probably essentially complete. This procedure compensated for any clouding over of the quartz windows (except for any variation

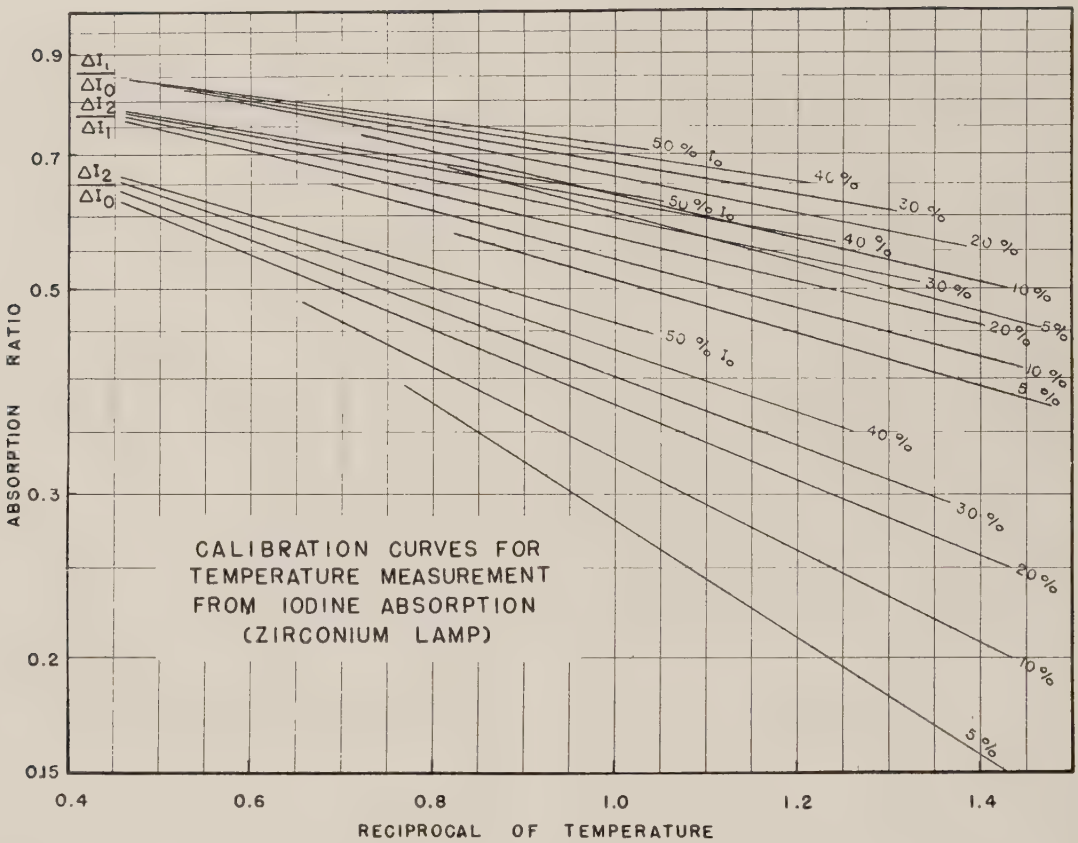

FIG. 10. Calibration curves for temperature measurement from iodine absorption (zirconium lamp). Reciprocal of temperature expressed in °R $\times 10^{-3}$

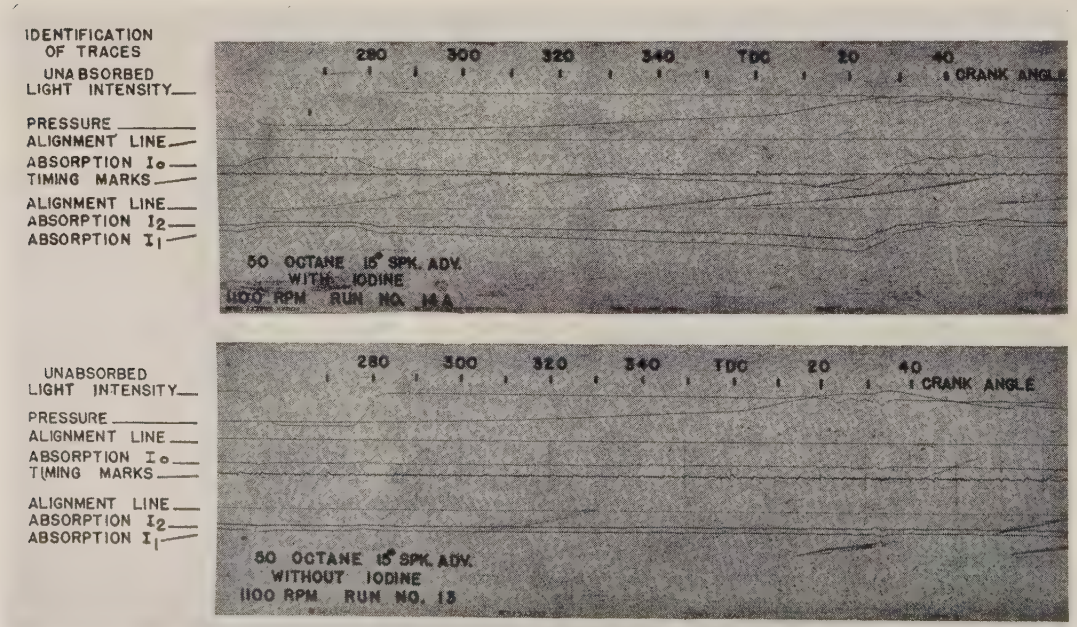

FIG. 11. Typical oscilloscope traces.

during a single cycle) and was considered satisfactory since measurements taken without iodine introduced into the engine established the fact that there was no appreciable absorption anytime during the cycle in the absence of iodine. The chopped light signal shown at the left-hand side of the film was produced by a synchronized light chopper and provided a zero-light reference line enabling measurements of the total lamp intensity to be made. The abrupt deflection at the right-hand side of the pressure trace is a pressure calibration mark.

Data scaled from an oscillogram similar to Figure 11 and translated to pressure and temperature data by means of calibration curves are shown in Figure 12.

Discussion

The temperature determined by the measurement of intensities in the absorption spectrum of iodine is the vibrational temperature of the iodine molecules. This temperature should equal the rotational and vibrational temperature of all of the gases in the absorption region if the pressure is sufficiently high to maintain an essentially equilibrium condition at all times. For rapidly changing temperatures in a region of combustion, there could be a difference between the vibrational temperature and the temperature for rotational and translational molecular motion. Such a difference might be caused by a reaction in the pre-inflammation portion of the cycle in an engine and might introduce error because of difference between vibrational and translational temperatures.

If the temperature determined by this iodine absorption method represents the true temperature of the charge in the cylinder, the temperature determined should be independent of iodine concentration, independent of total pressure, and independent of possible reactions involving iodine.

By comparing absorption intensities for three wavelength regions it was possible to determine the temperature using a procedure which yielded temperature values independent of the concentration of iodine. The temperatures obtained with several different concentrations agreed within experimental error.

For an absorption spectrum such as that of I_2 observed with a relatively wide slit, there is no change in total energy absorbed when the pressure is changed without increasing the number of absorbing molecules. The spectrum is like a continuous spectrum consisting of an infinite number of overlapping lines. An increase in pressure broadens these lines and increases the number overlapping at any one wavelength but does not increase the total absorption coefficient at that wavelength, provided this is not a wavelength at a sharp discontinuity in intensity. At the edges of the slit which determine the wavelength range admitted to the photocell, there would be as much new radiant power brought into this wavelength range by an increase in pressure or temperature as there would be removed from the range provided there is no sharp discontinuity in the spectrum such as a band head located at an edge of the slit. The slit edges in the present experiment did not coincide with any band heads.

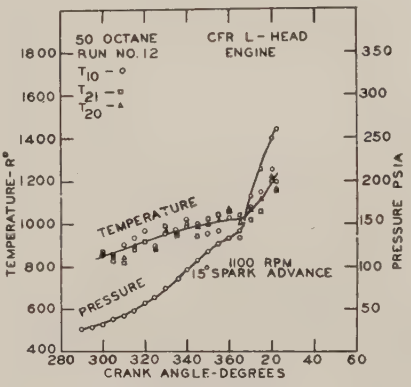

FIG. 12. Measured temperatures and pressures in an operating engine.

The possible effect of chemical reactions on these temperature measurements needs to be considered. It should be noted that measurements are made of the absorption due to iodine molecule and not to other compounds involving iodine. Thus the only chemical reactions of interest are those which affect or produce iodine molecules. Chemical reactions might produce molecules of abnormally high vibrational energy and these molecules might transmit energy to iodine molecules to give them vibrational temperature higher than that of the surrounding gas, also chemical reactions involving iodine might produce iodine molecules with abnormally high vibrational temperatures.

Since iodine is present only in small concentrations, any molecule with abnormally high vibrational energy will on the average make many collisions with other molecules before it collides with an iodine molecule. Any excess vibrational

energy will probably have disappeared before it strikes an iodine molecule. Suppose, however, that some iodine molecules are produced with an excess of vibrational energy over that corresponding to the true temperature either by collision or by chemical reactions involving iodine. These iodine molecules would most likely have a vibrational energy considerably greater than the vibrational energy of states $v'' = 0$ to 3. This would change the intensity of the iodine absorption bands at wavelengths longer than those used in the present measurements but would have no direct effect on the intensity of bands used in these temperature determinations. A slight indirect effect could possibly be produced as these molecules lost vibrational energy until their energy was that to permit absorption in the wavelength range admitted to the photocells. The number of molecules with vibrational energy only slightly higher than that corresponding to the surrounding gas temperature can be considered to be such a small fraction of the total number of iodine molecules that they would not produce a measurable effect on the determinations of temperatures.

The correctness of the above viewpoint is borne out by the statement made by Gaydon[8]: "With low-pressure flames of acetylene burning with oxygen it seems that in the reaction zone the rotational temperature of the OH radicals as determined from a study of the 3064 Å band in emission, is much too high, being around 5000 to 6000°C. Above the reaction zone the rotational temperature is more of the right order of magnitude. The *absorption* bands of OH in the same flame appear to give a reasonable value for the temperature, even in the reaction zone." [Italics by present authors.]

Since three different wavelengths were used, three different but two independent temperature determinations could be made. Thus, three different temperatures are shown in Figure 12. The agreement of these three temperatures should be an indication of the validity of the results. In general, the variation between these three temperatures was less than 100°F. The temperature reading given by the use of D_0 and D_1 has been experimentally found to give the most consistent results. This is not unexpected since their intensity ratio changes the most with a change in temperature.

In closing it might be well to point out that a high order of experimental accuracy and good experimental technique is required in the design and use of this instrument. For example, in determining the amount of absorption, the difference between two large quantities is being taken. Thus, an almost negligible percentage error in either of the two large quantities will produce an appreciable error in their difference. It follows, therefore, that the allowable error or change with time in the photomultiplier tubes and their associated electronic equipment is very small. It also follows that any fictitious absorption of light due to the distortion of the light path must be either eliminated or kept constant. Also, a light source that is constant in intensity and location is required.

Acknowledgment

This work was initiated by the University of Wisconsin, but was later encouraged and in part supported by the Coordinating Research Council. The authors wish to acknowledge their appreciation for the financial aid received from the Coordinating Research Council, from the University of Wisconsin, from the Wisconsin Alumni Research Foundation and from the Research Laboratories of the General Motors Corporation. Acknowledgment is also made of the encouragement received from Professor L. A. Wilson (now retired) and of the assistance of many undergraduate students.

Appendix I

RELATION BETWEEN INTENSITY OF TRANSMITTED RADIATION AND TEMPERATURE FOR MOLECULAR ABSORPTION

The intensity of radiation transmitted at wavelength λ through an absorbing gas is

$$I_\lambda = I_{T\lambda} e^{-\alpha_\lambda N_\lambda} \tag{1}$$

where $I_{T\lambda}$ is the incident intensity at wavelength λ, N_λ is the number of molecules in the light path capable of absorbing radiation at wavelength λ and α_λ is the molecular absorption coefficient at wavelength λ.

For any wavelength there are likely to be molecules of several different initial vibrational and rotational energies capable of absorbing radiation at that wavelength. If the vibrational energies of these molecules are $E_1, E_2, \cdots E_n$, the number of the molecules in each vibrational energy state is given by

$$N_1 \; N_0 e^{-E_1/kT},$$

$$N_2 = N_0 e^{-E_2/kT}, \cdots N_n = N_0 e^{-E_n/kT} \tag{2}$$

where N_0 is the number of molecules in the lowest vibrational energy state. The total number of molecules is

$$N = N_0 + N_1 + N_2 + \cdots N_n = \sum_{v''=0}^{n} N_{v''} \quad (3)$$

where n is the largest possible vibrational quantum number for the molecule (the number when the vibrational energy equals the energy of dissociation).

At any given wavelength the absorption could consist of overlapping lines in P, Q and R branches of several overlapping vibrational bands.

The number of molecules contributing to absorption at wavelength λ can be expressed as

$$N_\lambda = f_{OP\lambda}N_0 + f_{OQ\lambda}N_0 + f_{OR\lambda}N_0 + \cdots f_{v''P\lambda}N_n + f_{v''Q\lambda}N_n + f_{v''R\lambda}N_{v''} \quad (4)$$

Since there may be several overlapping bands with the same value for v'' but different v', $f_{v''}N_{v''}$ should be considered as the sum of molecules of vibrational energy $E_{v''}$ which can absorb energy at wavelength λ. For example $f_{v''Q\lambda}N_{v''}$ is the number of the molecules in the vibrational energy state v'' and with rotational energy such that absorption of radiation at the wavelength λ corresponds to lines in the Q branches. The Maxwell distribution law for molecular rotation gives

$$f_{v''Q\lambda}N_{v''} = N_{v''}\frac{hcB}{kt}(2J_{v''Q\lambda} + 1)e^{-(hcB/kt)J_{v''Q\lambda}(J_{v''Q\lambda}+1)} \quad (5)$$

The expressions for $f_{v''P\lambda}$ and $f_{v''R\lambda}$ are similar to this. In this relationship $J_{v''Q\lambda}$ is the rotational quantum number of the molecules with vibrational energy $E_{v''}$ and rotational energy such that the molecule is capable of absorbing radiation at the wavelength λ as one line in a Q branch. (hcB/k) is a constant containing Planck's constant h, velocity of light c, the molecular rotational constant B and the Boltzmann constant k.

The number $fN_{v''}$ will be small when the rotational energy $E_n = (hcB/kT)\,J(J+1)$ exceeds kT by a factor of two or more.

The molecular absorption coefficient α_λ varies with wavelength and at any one wavelength α_λ will have several values corresponding to absorption as P, R and Q lines.

$\alpha_{v''P\lambda}$ represents the absorption coefficient for wavelength λ for molecules with initial vibrational energy $E_{v''}$ and rotational energy such that absorption at wavelength λ corresponds to a line in the P branch.

Combining these expressions gives

$$\alpha_\lambda N_\lambda = \alpha_{OP\lambda}N_0\frac{hcB}{kT}(2J_{OP\lambda}+1)e^{-(E_0/kT)}e^{-(hcB/kT)J_{OP\lambda}(J_{OP\lambda}+1)} + \cdots \alpha_{1Q\lambda}N_0\frac{hcB}{kT}(2J_{1Q\lambda}+1)e^{-(E_1/kT)}e^{-(hcB/kT)J_{1Q\lambda}(J_{1Q\lambda}+1)} + \cdots \alpha_{v''R\lambda}N_0\frac{hcB}{kT}(2J_{v''R\lambda}+1)e^{-(E_{v''}/kT)}e^{-(hcB/kT)J_{v''R\lambda}(J_{v''R\lambda}+1)} \quad (6)$$

To obtain a mathematical relation between temperature and photocell readings it is first necessary to evaluate

$$\int_{\lambda_1}^{\lambda_2} I_\lambda\,d\lambda = \int_{\lambda_1}^{\lambda_2} I_{T\lambda}e^{-\alpha_\lambda N_\lambda}\,d\lambda \quad (7)$$

where the integration is taken over the range of wavelengths of radiation admitted to the phototube. If no special circuits are used, the phototube signal may be represented by

$$D_a = C_a\int_{\lambda_1}^{\lambda_2} I_\lambda\,d\lambda \quad (8)$$

when there is absorption and

$$D_T = C_a\int_{\lambda_1}^{\lambda_2} I_{T\lambda}\,d\lambda \quad (9)$$

where there is no absorption. The wavelength region λ_2–λ_1 is specified by subscript a. $I_{T\lambda}$ may be assumed constant over the wavelength range λ_1 to λ_2 so that

$$D_T = C_aI_{T\lambda}(\lambda_2 - \lambda_1) \quad (10)$$

Combining equations (1) and (8) gives

$$D_a = C_aI_{T\lambda}\int_{\lambda_1}^{\lambda_2} e^{\alpha_\lambda N_\lambda}\,d\lambda \quad (11)$$

Substitution of $\alpha_\lambda N_\lambda$ from equation (6) would in principle permit analytical determination of D_a if C_a were known. The integration, however is difficult and perhaps impossible except in the simplified case where bands do not overlap and λ_2–λ_1 is the range of wavelengths absorbed by molecules with a single value of v''.

For this simplified case equation (6) becomes

$$\alpha_\lambda N_\lambda = N_0 e^{-(E_{v''}/RT)} \left[\alpha_{v''P\lambda} \frac{hcB}{kT} (2J_{v''P\lambda} + 1) \right.$$
$$e^{-(hcB/kT)J_{v''P\lambda}(J_{v''P\lambda}+1)}$$
$$+ \alpha_{v''Q\lambda} \frac{hcB}{kT} (2J_{v''P\lambda} + 1) \qquad (12)$$
$$e^{-(hcB/kT)J_{v''P\lambda}(J_{v''P\lambda}+1)}$$
$$\left. + \alpha_{v''\lambda R} \frac{hcB}{kT} (2J_{v''R\lambda} + 1) \right.$$
$$\left. e^{-(hcB/kT)J_{v''R\lambda}(J_{v''R\lambda}+1)} \right]$$

Assuming that the average value of the quantities in the brackets in equation (12) between λ_1 and λ_2 is a constant K_a independent of temperature equation (11) becomes

$$D_a = C_a I_{T\lambda} e^{-N_0 K_a e^{-(E_a/kT)}} \int_{\lambda_1}^{\lambda_2} d\lambda \qquad (13)$$

This may be expressed as

$$D_a = D_T e^{-N_0 K_a e^{-(E_a/kT)}} \qquad (14)$$

so that

$$\log \frac{D_a}{D_T} = -N_0 K_a e^{-(E_a/kT)} \qquad (16)$$

For another range of wavelengths λ_3–λ_4

$$\log \frac{D_b}{D_T} = -N_0 K_b e^{-(E_b/kT)} \qquad (17)$$

Dividing gives

$$\frac{\log \dfrac{D_a}{D_T}}{\log \dfrac{D_b}{D_T}} = \frac{K_a}{K_b} e^{E_b - E_a/kT} \qquad (18)$$

or

$$\log \frac{\log \dfrac{D_a}{D_T}}{\log \dfrac{D_b}{D_T}} = \text{Constant} + \frac{E_b - E_a}{kT} \qquad (19)$$

where A is a constant.

Nomenclature

I_λ = Radiant power per unit wavelength range and unit cross sectional area at wavelength λ, which leaves the absorbing region.

$I_{T\lambda}$ = Total radiant power per unit wavelength range and unit cross section area at wavelength λ, which enters the absorbing region.

ΔI_λ = Absorption intensity or $I_{T\lambda}$–I_λ.

K_λ = Absorption coefficient at wavelength λ.

d = The length of the absorption path.

α_λ = Molecular absorption coefficient.

$N_{\lambda v''}$ = Number of molecules in the absorption path and in initial vibrational states v'' permitting absorption at wavelength λ.

$E_{v''}$ = Vibrational energy of the absorbing molecules with vibrational quantum no v''.

$N_{v''}$ = Number of molecules in lower vibrational energy state of v''.

$f_{v''\lambda}$ = Fraction of molecules of vibrational energy $E_{v''}$ which absorbs radiation at wavelength λ.

$J_{v''Q\lambda}$ = Rotational quantum number of the molecules with vibrational energy $E_{v''}$ and rotational energy such that the molecule is capable of absorbing radiation at the wavelength λ as one line in Q branch.

h = Planck's constant.

e = Velocity of light.

B = Rotational constant.

k = Boltzman constant.

T = Temperature.

D = Phototube signal.

C = Phototube and electronic constant

$\Delta I^{v'v''}$ = Absorption intensity for a transition between vibrational states v' and v''.

$\psi_{v'}\psi_{v''}$ = Wave functions (amplitudes) for the vibrational level v' and v''.

N_v = Normalizing factor.

a = Constant.

x = Distance from the equilibrium position of the potential energy curve.

r = Interatomic distance.

$H_v(\sqrt{an})$ = Hermite polynomials

Å = Wavelength unit Å

REFERENCES

1. Uyehara, O. A., Myers, P. S., Watson, K. M. and Wilson, L. A.: A.S.M.E. Transactions, *69*, (January 1946).

2. El Wakil, M. M., Myers, P. S., and Uyehara, O. A.: A. S. M. E. Transactions, *74*, (February 1952).
3. Millar, G. H., Winans, J. G., Uyehara, O. A., and Myers, P. S.: J. Opt. Soc. Am., *43*, 609 (1953).
4. Lewis, B., and Von Elbe, G.: *Combustion, Flames and Explosions of Gases*, p. 116. New York, Academic Press, 1951.
5. Herzberg, G.: *Spectra of Diatomic Molecules*, p. 540. New York, D. Van Nostrand, 1950.
6. Chen, S. K., Beck, N. J., Uyehara, O. A., and Myers, P. S.: *Compression and End Gas Temperatures from Iodine Absorption Spectra*. National Fuel and Lubricants Meeting, S. A. E., Chicago, October 29–30, 1953.
7. International Critical Tables, *5*, 409 (1929).
8. Gaydon, A. G.: *Spectroscopy and Combustion Theory*, p. 173. London, Chapman and Hall, 1948.
9. Mecke, R.: Ann der Phys., *376*, 108 (1923).
10. Mitchell, A. C. G., and Zemansky, M.: *Resonance Radiation and Excited Atoms*, p. 96. New York, The Macmillan Co., 1934.

39

STUDIES OF IONIZATION IN FLAMES BY MEANS OF LANGMUIR PROBES[a]

By H. F. CALCOTE and I. R. KING[b]

Introduction

In previous publications[1, 2] the concentration of positive ions in the combustion zone of a hydrocarbon flame has been estimated to be some 10^{12} ions/cc. This estimate was obtained both by deflection of the flame in an electric field and by the increase in flame pressure when an electric field is applied to the flame. This concentration is considerably greater than can be readily accounted for by thermal ionization of the species which are known to be present. It was therefore proposed that ions are produced, not by thermal processes, but by chemi-ionization or events similar to those causing abnormal electronic excitation in flames. The results have also been taken as evidence that thermal equilibrium does not exist between species in the flame front.

Further investigation of ions in the flame front has been carried out with small electric probes of the type developed by Langmuir[3] to study the properties of the electron plasma in electric discharges. Measurements of the attenuation of electromagnetic waves[4, 5] are inadequate for studies in the combustion zone since the region of reaction is only a fraction of a millimeter thick, whereas the wavelength for short electromagnetic waves is approximately a centimeter. For this reason the probe technique was chosen in spite of the difficulties and limitations involved in placing a small probe into a high-temperature combustion zone.

Were ions due to thermal effects, that is, if they were in thermodynamic equilibrium with their parent species, it should be possible to calculate the ion concentration by means of Saha's relation[6, 7]:

$$\log \frac{N_- N_+}{N_0} = \log K_N = \log G + 15.38 + \tfrac{3}{2} \log T - \frac{5040}{T} V_i \qquad (1)$$

where K_N is the equilibrium constant for $M \rightleftharpoons M^+ + e^-$; N_-, N_+, and N_0 are the concentrations of electrons, positive ions, and neutral molecules per cubic centimeter; $G = g_- g_+ / g_0$, and the g's are the statistical weights; T is the absolute temperature; and V_i is ionization potential in electron volts. The contributions of various species to the thermal ionization in a propane-air flame are presented in Table 1. The equilibrium concentrations of the species at the stoichiometric adiabatic flame temperature, T_b, are tabulated in the third column and were employed as N_0 in

[a] This research was conducted under the auspices of Project SQUID, jointly sponsored by the Office of Naval Research, Department of the Navy, Office of Scientific Research, Department of the Air Force, and Office of Ordnance Research, Department of the Army.

[b] Experiment Incorporated, Richmond, Virginia.

equation (1) to calculate the theoretical ion concentration at 2200°K and at 1400°K. The last column corresponds to a lean flame with a low flame temperature and the same concentrations of neutral species as might exist in a stoichiometric flame. The only real possibilities for ion sources in this set of products are nitric oxide, graphitic carbon[5, 8], and the contaminant sodium[9] or other alkali metal. Actually, in the low-temperature flame graphitic carbon would be the only real contender, and this calculation is based upon the work function for graphite (4.35 ev) instead of that for a small carbon particle with an ionization potential of 8.5 ev as suggested by Shuler[5]. Employing for the equivalent concentration of carbon atoms $N_0 = 4.2 \times 10^{13}$ from Table 1, the ion concentration arising from carbon is 36 ions/cc in the 1400°K flame. Experimental ion concentrations in lean flames where the temperature is low would thus be useful in considering possible sources of ions. Such data have therefore been obtained in the present program.

This paper outlines the probe technique, with typical results, and presents experimental evidence that ionization in the combustion zone is not due to contaminants.

Table 1. Possible Sources of Ions in Flames

Species	Ionization Potential	Equilibrium Concentration at T_b in Stoichiometric Propane-air Flame	Theoretical Contribution to Ionization, ions/cc	
	electron volts	*species/cc*	*2200°K*	*1400°K**
H_2	15.9	8.2×10^{15}	0.89	2.02×10^{-11}
N_2	15.5	2.4×10^{18}	1.2×10^{2}	1.95×10^{-9}
CO	14.1	3.3×10^{16}	2.3×10^{2}	1.02×10^{-7}
CO_2	13.8	3.5×10^{17}	1.5×10^{3}	1.05×10^{-6}
H	13.6	9.2×10^{15}	4.2×10^{2}	3.32×10^{-7}
OH	13.6	7.9×10^{15}	3.9×10^{2}	3.08×10^{-7}
O	13.6	6.6×10^{14}	1.1×10^{2}	8.9×10^{-8}
H_2O	12.6	5.0×10^{17}	4.4×10^{4}	1.77×10^{-4}
O_2	12.2	1.5×10^{16}	2.2×10^{4}	1.55×10^{-4}
C_2	12.0	—	—	—
C (gas)	11.3	—	—	—
CH	11.1	—	—	—
NO	9.5	6.3×10^{15}	1.7×10^{7}	7.06
Na	5.14	1.0×10^{10}†	2.2×10^{9}	6.5×10^{5}
C (graphite)	4.35	4.2×10^{13}‡	(1.0×10^{12})	1.1×10^{9}

At $T_b = 2200$°K, $N_{0(\text{total})} = 3.3 \times 10^{18}$ molecules/cc

* Values calculated with the stoichiometric equilibrium species concentration at 2200°K.

† R. M. Moyerman and K. E. Shuler: Science, *118*, 612 (1953).

‡ This is an equivalent value which was calculated assuming 10^{12} ions/cc at 2200°K.

Absolute Reaction Rate Theory of the Langmuir Probe

If a wire (probe) be placed in an ionized plasma and the current to this probe plotted as a function of the applied voltage, a curve such as that presented in Figure 1 is obtained. When the probe is strongly negative with respect to the plasma, only positive ions will reach it; electrons are repelled as they approach. Only electrons and positive ions are considered because it has been well established that the negative species in flames are mainly electrons[10]. As the probe potential becomes less negative, the fastest electrons will reach the probe, decreasing the total current. The ionic and electronic currents will balance at some negative probe potential because the electrons have a higher mobility than do the positive ions. This probe voltage is called the wall potential. A further increase in probe voltage causes the electron current to exceed the ionic current. The analysis of curves such as Figure 1 by Langmuir Probe Theory permits one to draw a number of conclusions concerning the nature of the plasma.

Although the theory of the Langmuir probe is

described in a number of places[3, 11], it is instructive to derive it by applying the theory of absolute reaction rates[2] to the process. This is a fresh approach and should help to make the phenomena more readily understood. According to the theory of absolute reaction rates, any rate process can be described by the following[12]:

$$\text{Rate} = \kappa N^{\ddagger} \frac{kT}{h} \tag{2}$$

where κ is a transmission coefficient, usually equal to one. The concentration of activated species (or complex) at the top of a potential-energy barrier limiting the rate process is $N^{\ddagger}$. The universal frequency factor kT/h represents the frequency with which the activated species crosses the barrier at a given temperature, T; k is the Boltzmann constant and h is Planck's constant. Applying this relation to the rate at which electrons reach the negative probe, one obtains for the electron current per unit area, j_-,

$$j_- = \kappa e N_-^{\ddagger} \frac{kT_-}{h} \tag{3}$$

The activated electrons, $N_-^{\ddagger}$, which have overcome the probe potential (Fig. 2) are multiplied by e, the electronic charge, to obtain the current. The electron temperature is T_-, assuming a Maxwell-Boltzmann velocity distribution among the electrons. The activated electron concentration, $N_-^{\ddagger}$, can be written in terms of an equilibrium constant between electrons in the plasma and on the probe surface,

$$\frac{N_-^{\ddagger}}{N_-} = K^{\ddagger} = \frac{{}^{\circ}F_-^{\ddagger}}{{}^{\circ}F_-} \tag{4}$$

where ${}^{\circ}F_-$ is the partition function for electrons per unit volume in the plasma, and ${}^{\circ}F_-^{\ddagger}$ is per unit area since only two degrees of freeedom are available for activated electrons on the probe surface. Equation (3) is then written, assuming $\kappa = 1$, as

$$j_- = eN_- \frac{{}^{\circ}F_-^{\ddagger}}{{}^{\circ}F_-} \frac{kT_-}{h}$$

When the energy difference, eV, between electrons in the plasma and on the probe surface is written explicitly, this equation becomes

$$j_- = \frac{kT_-}{h} eN_- \frac{F_-^{\ddagger}}{F_-} e^{-eV/kT_-}$$

Writing out the partition functions, which involve only translational degrees of freedom, the following is obtained:

$$j_- = \frac{kT_-}{h} eN_- \frac{2\pi m_- kT_-/h^2}{(2\pi m_- kT_-/h^2)^{3/2}} e^{-eV/kT_-}$$

where m_- is the mass of an electron. This equation reduces to

$$j_- = eN_- \sqrt{\frac{kT_-}{2\pi m_-}} e^{-eV/kT_-} \tag{5}$$

Equation (5) can be rewritten,

$$\ln j_- = B - \frac{eV}{kT_-} \tag{6}$$

A plot of $\ln j_-$ against V gives a means of evaluating the electron temperature, T_-. The intercept gives the constant B, which can be employed to evaluate N_-.

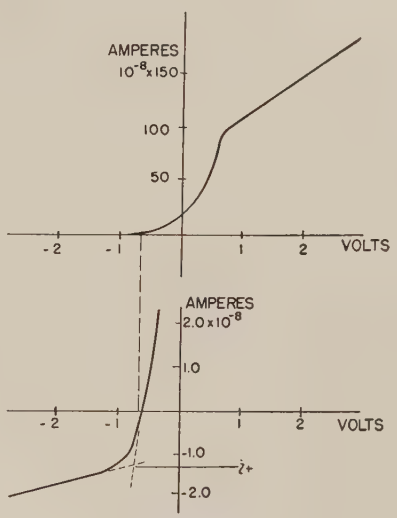

FIG. 1. Typical Langmuir probe curve. Electron current to probe plotted in the positive direction.

For positive ions there will be an equation similar to (5), but with a negative probe the exponent will effectively equal one. A space charge will form around the probe, the thickness of which will vary with the probe voltage. This causes the effective probe area to change. All ions entering the charged region will be captured by the probe, that is, the current will be space-charge limited. Thus,

$$N_+ = \frac{j_+}{e} \sqrt{\frac{2\pi m_+}{kT_+}} \tag{7}$$

The positive-ion temperature, T_+, must be very near the gas temperature, so that if one assumes or knows m_+, equation (7) permits a calculation

of the concentration of positive ions. In an undisturbed plasma $N_+ = N_-$; in a small flame, however, it is possible that the higher diffusion rate of electrons may permit them to diffuse out of the plasma, causing N_+ to exceed N_- .

The wall potential, V_w , can be easily derived

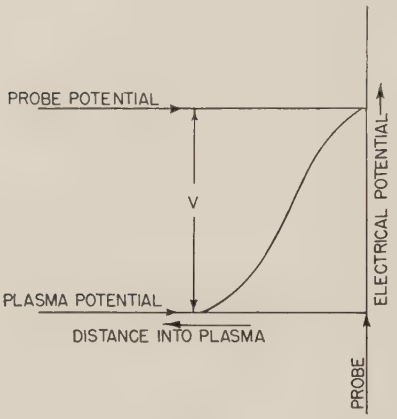

FIG. 2. Potential energy curve for a Langmuir probe.

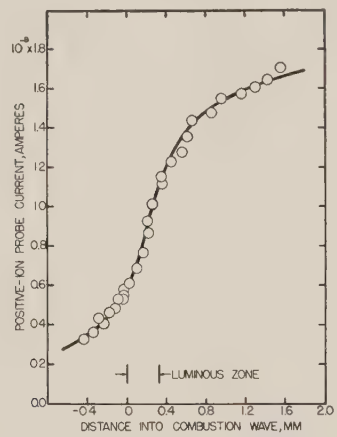

FIG. 3. Typical curve showing positive-ion probe current through the flame front. Inverted propane-air flame at an equivalence ratio of 0.8 and a pressure of 0.3 atm.

since here the probe current $j_p = j_+ - j_- = 0$. Then from equations (5) and (7).

$$V_w = \frac{kT_-}{2e} \ln \frac{T_- m_+}{T_+ m_-} \tag{8}$$

provided N_- be indeed equal to N_+ . This relation should permit a calculation of T_+ or m_+ , depending upon which is known or can be reasonably assumed.

This brief outline of Langmuir Probe Theory will suffice for present purposes. For a more detailed discussion covering difficulties involved in applying the theory and considerations of the thickness of the ion sheath surrounding the probe, the reader is referred to Loeb[11].

Experimental Determination of Ion Concentration

The positive-ion concentration through the combustion wave was obtained by constructing Langmuir probe curves (Fig. 1) at a series of closely spaced points through the flame front. The positive-ion current, i_+ , was then obtained as indicated in Figure 1 and plotted against the probe movement (Fig. 3). The slope of this curve at any given point gave the positive-ion concentration at the given point. From this information curves like Figure 4 were plotted. Distance was measured from the position where the probe first showed a bright red tip.

Considering Figure 3, the total current to the probe will be given by

$$i_+ = 2\pi r \int_0^x j_+ \, dx \tag{9}$$

where r is the probe radius and x is the length of the probe in the ionized region. Differentiation yields

$$j_+ = \frac{1}{2\pi r} \frac{di_+}{dx}$$

The derivative di_+/dx is the slope of the curve in Figure 3. Combining this relation with equation (7) the positive-ion concentration is obtained,

$$N_+ = \frac{di_+/dx}{2\pi e r} \sqrt{\frac{2\pi m_+}{kT_+}}$$

or,

$$N_+ = \text{constant} \frac{(di_+/dx)}{r} \sqrt{\frac{m_+}{T_+}}$$

Thus, if a value be assumed for the mass of the positive ion and the positive-ion temperature be assumed equal to the adiabatic flame temperature, it is possible to determine the positive-ion concentration at any point in the flame. For all of the experiments reported here, except when salts have been added, the mass of the positive ion has been assumed to be 3.3×10^{-23} gram, corresponding to a molecular weight of 20.

The electrical circuitry (Figs. 5 and 6) includes a means of measuring the electrical current to a

sample probe as a function of the applied probe potential. A synchronous motor (3 rpm) is used to drive a variable resistance, thus varying the voltage as a function of time so that the recording current-time meter actually records current-voltage. Since the instrument used for the current measurements must not only be extremely sensitive but must also have a low imput resistance, a Millivac MR-61A micromicroammeter with a Sanborn Recorder was selected. Shielding was used wherever possible to prevent stray pick-up. The probe was connected to the recorder by Teflon-insulated coaxial cable to reduce electrical leakage. The possibility of contact potentials was of course ever present. Thermionic emission has been calculated to be some 1000 times less than the observed current at the probe temperature of 1500°K. A series of preliminary experiments on the effect of probe diameter and of material for nichrome, platinum, and platinum-40-per cent rhodium probes indicated that the experimental results are independent of probe size or material within the experimental error.

The type of flame to be probed was determined by several stringent conditions. First, it was desirable that the probe enter the flame front at right angles and that the exact position of the probe with respect to the flame front be known at all times. Secondly, since the probe itself must be extremely small, it was imperative that the probe enter the flame front from the cool side.

In order to satisfy the above conditions a 3.5-in ID flat-flame burner was constructed (Fig. 6). Fine-mesh screen wire was used to maintain laminar flow. A water jacket was installed around the burner port to maintain a constant temperature. The large flat flame has a great advantage over conventional Bunsen flames in that much leaner mixtures, with lower flame temperatures, can be burned. This permits the use of probes which would deteriorate in a high-temperature flame. The probe entered the burner from the bottom, passed through a ¼-in tapered stainless-steel guide tube, and entered the flame from the cool or upstream side. The probe was driven manually through the flame front by means of a micrometer. Other types of flames were sometimes employed and will be described when referred to.

Ionization in Flames Containing Alkali Chlorides

As a means of examining the probe technique flames were studied into which a known concentration of alkali chlorides had been introduced and the experimental results were compared with the theoretical ion concentrations predicted thermodynamically by Saha's equation.

The burner shown in Figure 7 was used to introduce salt solutions into a Meker-type flame.

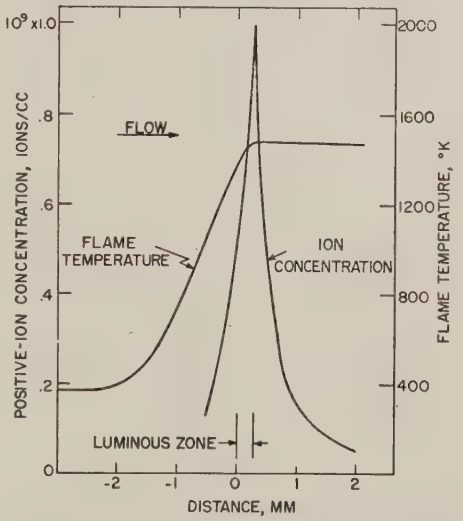

Fig. 4. Typical curves showing positive-ion concentration and temperature through the flame front. Propane-air flame at an equivalence ratio of 0.8. Ion-concentration curve at 0.3 atm using inverted flame. Temperature curve at 0.975 atm on flat-flame burner[13].

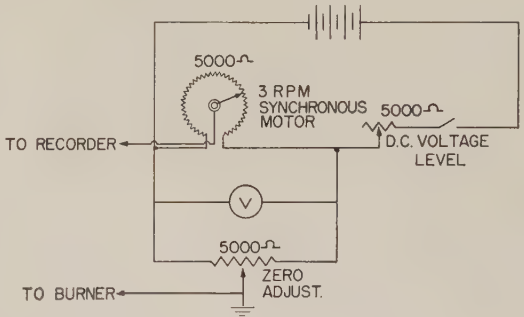

Fig. 5. Variable-voltage supply unit for use with Langmuir probe.

A 500-ml round-bottom flask served as the spray chamber with the neck serving as the solution tube. A 1-in OD glass tube 21 in long served as the burner. The burner tube was made long to allow any of the larger droplets entering the gas stream to fall back before entering the flame. In this way only a very fine mist entered the flame. The salt concentration in the gas stream was determined by measuring the change in solution height with time. No measurements were made

until the burner had been in operation for several minutes so that equilibrium was attained between the salt solution entering the flame and the salt solution condensing on the walls and running

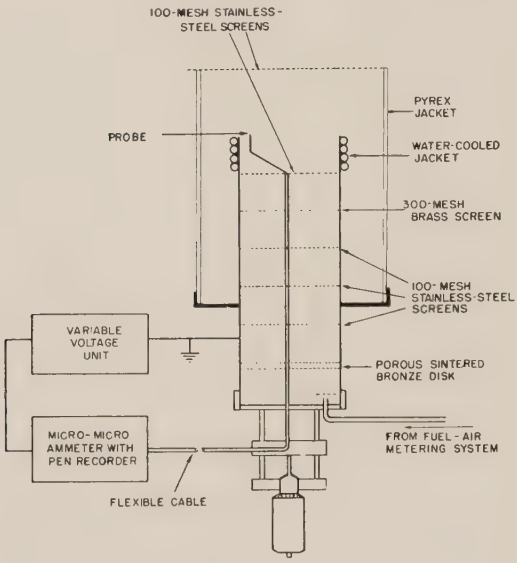

FIG. 6. Flat-flame burner and probe circuits.

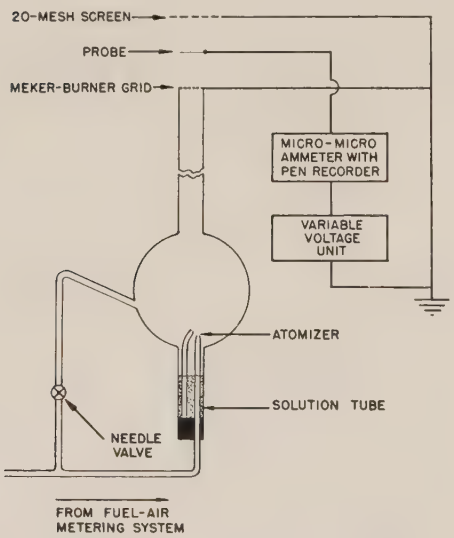

FIG. 7. Apparatus for studying ionization in flames containing alkali chlorides.

back into the solution tube. The measurements were made over a 45-min period. The feed rate was adjusted by regulating the needle valve controlling the quantity of gas passing through the sprayer. Reasonable changes in the liquid feed rate caused insignificant alterations of the theoretical atom concentration; e.g., changing the liquid feed rate from 0.0050 to 0.0060 cc/sec changed the sodium-atom concentration in the flame from 1.32 to 1.58 $\times$ 10^{15} atoms/cc or the thermodynamic sodium-ion concentration from 5.92 to 6.25 $\times$ 10^{10} ions/cc. In computing the positive-ion concentration in the flame the concentration in the unburned gas was corrected for temperature rise but was not corrected for changes in the total number of molecules.

The electrical setup (Fig. 7) was essentially the same as that used in flat-flame measurements with the exception that the probe position was fixed in the flame. A screen was suspended over the flame and grounded to give more consistent results by better fixing the ion plasma potential of the flame. The probe was located 0.7 cm above the burner grid and protruded approximately 1.5 cm into the flame. The actual position of the probe with respect to the burner was held constant in all experiments. Vertical movements up to one cm made no observable changes in current. The probe curve was obtained by averaging more than 5 Langmuir probe curves for each test. The difference between curves was negligible; for example, in experiment no. 7 (9 curves) the standard deviation of the positive-ion current about the arithmetic mean of 5.21 $\times$ 10^{-6} amp was 0.19 $\times$ 10^{-6} amp.

Probe length was determined by holding a vernier caliper near the probe. Half way between the points of a dull color and bright white (<0.2 cm) was taken as the point of entrance of the probe into the flame. Changing the assumed probe length from 1.4 to 1.6 cm for CsCl changed the apparent ion concentration from 2.86 to 2.51 $\times$ 10^{10} ions/cc, an insignificant change.

The day-to-day reproducibility was extremely good; for example, with a 0.10*M* NaCl solution giving 1.96 $\times$ 10^{14} sodium atoms/cc in the flame the experimental ion concentrations were

	Date	Ion Concentration
		ions/cc
Same mixture.....	30 Dec 53	12.2 $\times$ 10^{8}
	7 Jan 54	11.6
New mixture.....	7 Jan 54	11.9

The results of experiments with alkali chlorides added to the flame are summarized in Table 2. The theoretical positive-ion concentration is some 400 times greater than the experimental result. The cause of this discrepancy is probably the cooling effect of the large probe. The

temperature of the probe was determined with an optical pyrometer and found to be approximately 1400°K (column 5, Table 2). If it be assumed that the probe cools the surrounding gas so that the effective temperature is 1500°K, the correlation of experimental and theoretical values is as indicated in Table 2 and Figure 8. Apart from the reasonableness of assuming a temperature slightly in excess of the probe temperature, the value 1500°K receives support from the fact that the agreement between theory and experiment is now reasonably good with respect to to assume that the relative values obtained are comparable and that the absolute concentrations are some 400 times greater than the experimental result. Fortunately this error is on the conservative side for the arguments which are to be formulated from the data presented in the remainder of this paper. None of the results have been corrected except where indicated.

Flames Containing Negligible Ionization

Because the presence of a minute quantity of alkali metal in the atmosphere would give ion

TABLE 2. ION CONCENTRATIONS WITH ALKALI SALTS ADDED TO THE FLAME

Propane-air Flame at Equivalence Ratio of 0.92 (Based on Dry Air)

Total flow velocity = 230.5 cc/sec; water added with salt = 2.6 mole per cent; adiabatic flame temperature = 2190°K; probe: platinum, 0.063-cm diameter.

Expt. No.	Salt	Concentration of Solution	Probe Length	Probe Temp*	Alkali Atom Conc., T = 2190°K	Positive-ion Probe Current, i_+	Ion Concentration, ions/cc			
							T = 2190°K		T = 1500°K	
							Theory	Experiment	Theory	Experiment
		M	*cm*	°K	*atoms/cc*	*amp*				
3	LiCl	0.10	1.5	1390	19.6×10^{13}	6.6×10^{-7}	1.49×10^{11}	2.12×10^{8}	1.99×10^{8}	2.63×10^{8}
9		1.0	1.5	1400	196	13.0	4.7×10^{11}	4.21	6.3	5.23
11	NaCl	0.010	1.5	1410	1.96	6.2	8.99×10^{10}	3.74	1.58	4.64
1, 8, 10		0.10	1.5	1400	19.6	16.5	2.84×10^{11}	9.57	4.98	11.9
12		1.0	1.5	1400	196	55	8.99×10^{11}	32.0	15.8	39.8
6	KCl	0.010	1.4	1395	1.96	20.0	7.4×10^{11}	16.3	35.2	20.2
2		0.10	1.5	1400	19.6	63	2.34×10^{12}	49.3	112	59.8
13	RbCl	0.010	1.5	1410	1.96	30	11.3×10^{11}	33.6	60	41.8
5		0.10	1.5	1400	19.6	120	3.56×10^{12}	133	190	165
7	CaCl	0.010	1.5	1395	1.96	52	2.44×10^{12}	72.4	199	90
4		0.10	1.4	1400	19.6	155	7.71×10^{12}	240	628	286

* Obtained with an optical pyrometer.

changing the alkali metal or the concentration of the salt (Table 2). For sodium the experimental-to-theoretical ion-concentration ratio is greater than for the other alkali metals. A similar discrepancy has also been noted by Wilson[10] using the conductivity method and by Belcher and Sugden[4] using the electromagnetic attenuation method for determining electron concentration. The cause of this discrepancy is unknown.

From Figure 8 and Table 2 it can be concluded, if it is assumed that the ion plasma being sampled has been cooled, that the probe samples the ion concentration fairly well, although the slopes of the experimental and theoretical lines in Figure 8 are somewhat different. It would therefore be reasonable in interpreting probe results in flames concentrations of the order which have been measured, it is necessary to investigate this possibility further. Actually, to obtain 10^9 ions/cc at 2300°K by Saha's equation (see equation (1)) requires only 4.2×10^9 sodium atoms/cc or 1.7×10^{-8} mole-per cent sodium. Since this concentration is well below that which would be amenable to ordinary analytical techniques, the concentration of interfering contaminants will have to be inferred. Thus, if a flame could be found in which the ion concentration were extremely small—where the expected impurities were just as great as in a propane-air flame—it might be argued that the ionization in the propane-air flame is a property of the flame and not due to impurities.

In connection with this line of reasoning it was found that neither a hydrogen sulfide-air flame (flame temperatures up to 2100°K) nor a carbon disulfide-air flame (flame temperature between 1625° and 2265°K) contained ion concentrations within the limits of measurement. For carbon disulfide, stored in glass bottles, it might be expected that sodium would leach out of the glass. The air supply was of course the same as supplied the propane-air flames. In a specific experiment with a carbon disulfide-air flame on a Meker burner at an equivalence ratio (ϕ) of 0.85 (ϕ =

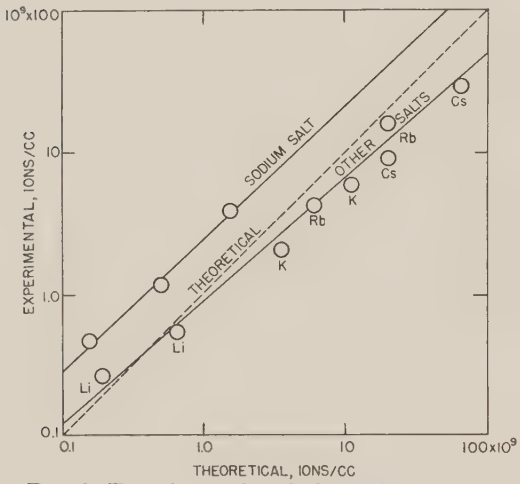

FIG. 8. Experimental and theoretical positive-ion concentrations for propane-air flames containing alkali chlorides at an assumed equilibrium temperature of 1500°K.

stoichiometric air-fuel ratio divided by the actual air-fuel ratio) the following were observed:

Adiabatic flame temperature, T_b	= 2070°K
Probe temperature, T_p	= 1255°K
Probe length = 1.6 cm, diameter	= 0.063 cm
Positive-ion current, i_+	= 0.3 × 10^{-9} amp
Positive-ion concentration, N_+	= 2.2 × 10^5 ions/cc

The result for i_+ and N_+ is only approximate because the sensitivity of the detecting instrument had to be set so high that electrical noise became appreciable.

Since it has been demonstrated that flames exist which possess negligible ionization, it is necessary to inqure as to whether there be some property of these particular flames which prevents ion formation with impurities present. To answer this question both lithium and sodium chloride solutions were sprayed into a carbon disulfide flame in the manner described above and the positive-ion concentration determined. The results from this experiment are recorded in Table 3. Examination of these data indicates that there is no difference in ability of a carbon disulfide-air and a propane-air flame to ionize a salt which is present

Since it has been demonstrated that two flames, those of carbon disulfide and hydrogen sulfide, do not afford ion concentrations comparable to that of propane, and since if ionization were due to contaminants these flames would be expected to have comparable ionization, it can be concluded that ionization in hydrocarbon flames is probably not due to contaminants but is a property of the flame.

Ionization in Very Lean Flames

The ion concentration through the flame front has been determined for very lean propane-air flames burning on the flat-flame burner. Since the stability limits on such burners are very narrow, the equivalence ratio has been altered by the addition of nitrogen to the air. This has in addition made it possible to burn at an equivalence ratio of 0.835 (Table 4) with a flame temperature of only 1535°K compared with the adiabatic flame temperature with undiluted air (at this same equivalence ratio) of 2080°K.

The ion concentrations at different positions in the flame front are presented in Figure 9 for a series of equivalence ratios. The distances are determined relative to the position at which the tip of the probe just becomes red. This plane of reference was chosen rather than the visible cone because it is more definitive. At some future date this plane can be related to the position of the visible cone and to the measurements of temperature or of radical concentrations obtained by others. In general the edge of the visible cone on the unburned side occurs at zero. By means of the flow velocity the distance scale has been converted to time (Fig. 10). This curve is only approximate on the unburned side because in order to correct the flow velocity the temperature profile was approximated from that obtained by Friedman[13]. This profile is shown in Figure 4 of the present paper. On the burned side the flow velocity was corrected for an increase in temperature to the adiabatic flame temperature. The ions are formed in the luminous cone and then disappear very rapidly by recombination. The ion

concentration upstream from the luminous zone (zero) must be due either to diffusion ahead of the flame front or to perturbation of the flame by the probe.

peak in the ionization curves (Figs. 9 and 10) could not arise from contamination because the contaminant concentration would not drop off but would instead remain essentially constant, as

Table 3. Comparison of Ion Concentrations with Salts Added to a Carbon Disulfide Flame and a Propane Flame

Flame Parameters	Carbon Disulfide		Propane	
	LiCl	NaCl	LiCl	NaCl
Equivalence ratio	0.75	0.75	1.14	0.92
Total flow velocity, cc/sec	358	358	276	230
Probe length, cm	1.6	1.65	1.7	1.5
Probe temperature, T_p, °K	1255	1272	1422	1400
Adiabatic flame temperature, T_b, °K	1875	1875	2230	2190
N_0 at T_p	3.78×10^{14}	3.0×10^{14}	4.3×10^{14}	3.07×10^{14}
N_0 at T_b	2.53×10^{14}	2.03×10^{14}	2.75×10^{14}	1.96×10^{14}
N_+ (exp T_p)	6.86×10^{6}	2.79×10^{8}	3.25×10^{8}	12.0×10^{8}
N_+ (exp T_b)	5.65×10^{6}	2.29×10^{8}	2.59×10^{8}	9.57×10^{8}
N_+ (theory T_p)	2.28×10^{6}	5.8×10^{7}	1.56×10^{7}	12.0×10^{7}
N_+ (theory T_b)	2.02×10^{10}	2.25×10^{10}	2.31×10^{11}	2.84×10^{11}
$\frac{N_+ \text{ (theory } T_p)}{N_+ \text{ (exp } T_p)}$	0.332	0.208	0.480	0.100
$\frac{N_+ \text{ (theory } T_b)}{N_+ \text{ (exp } T_b)}$	3.64	98.5	893	297

It is of interest to compare these results with information obtained previously by deflection of a *n*-butane-air flame (equivalence ratio 0.8) in an electric field[1, 2]. From a theory of the deflection based upon an electric wind concept it was deduced that the thickness of the ionization zone was 0.8 mm and the positive-ion concentration about 10^{12} ions/cc. The thickness of the ion zone reported in Figure 12 is about 0.4 mm, and the observed ion concentration corrected to one atmosphere is 1.8×10^{9} ions/cc. Assuming that the ratio of actual to observed ion concentration is here the same as for salts added to the flame—namely, 400—a true ion concentration of 0.73×10^{12} is obtained. The agreement is as good as one could expect and indicates the consistency of the several observations.

This set of probe data negates the possibility that ions result from thermal ionization of impurities in the input feed to the burner, such as atmospheric contamination by alkalies. The

Table 4. Ion Concentration in Lean Flames Diluted with Nitrogen

Flat Propane-air Flame on a 3.5-inch Diameter Burner

Probe: Pt—40 per cent Rh, 0.005-cm diameter.

Equivalence Ratio	Nitrogen added to Air*	Total flow	Probe Temp.	Flame Temp.	Max. Ion Conc.
	mole per cent	*cc/sec*	*°K*	*°K*	*ions/cc*
0.467	0.0	673	1080	1330	3.4×10^{8}
0.521†	0.0	670	—	1520	4.0
0.540	12.7	659	1100	1390	5.3
0.635	31.7	653	1110	1420	6.9
0.765	51.4	626	1155	1490	13.5
0.835	59.6	605	1140	1535	27.0

* Mole per cent of nitrogen added with respect to the air.

† Obtained with a double probe (E. O. Johnson and L. Malter: Phys. Rev., *80*, 56–68 (1950)).

does the temperature (Fig. 4). To explain the peaks as being due to contaminants would require the assumption that ionization is due to a transfer of energy in collisions between chemiacti-

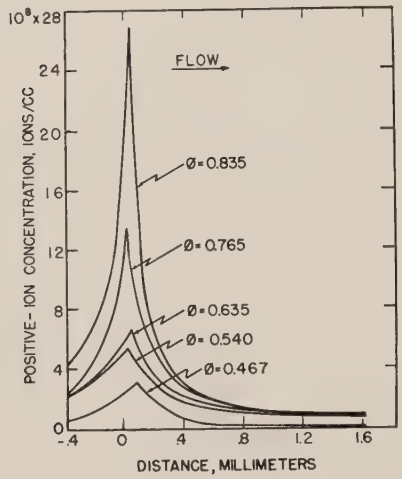

Fig. 9. Positive-ion concentration through the flame front as a function of distance. Equivalence ratio varied by diluting air with nitrogen. Flat-flame burner at one atmosphere.

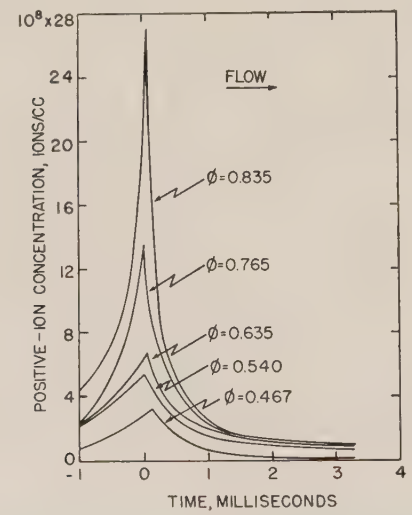

Fig. 10. Positive-ion concentration through the flame front as a function of time. Equivalence ratio varied by diluting air with nitrogen. Flat-flame burner at one atmosphere.

vated species and the impurity. Moreover, to account for 10^9 ions/cc at 1400°K, assuming sodium as the contaminant, would require 9.4×10^{16} atoms of sodium/cc at 25°C. This is 0.3 mole-per cent sodium contaminant in the input gases.

The possibility of nitric oxide as the ion species is also eliminated by these data because the thermodynamic equilibrium concentration of NO^+ for these flames is less than one ion/cc.

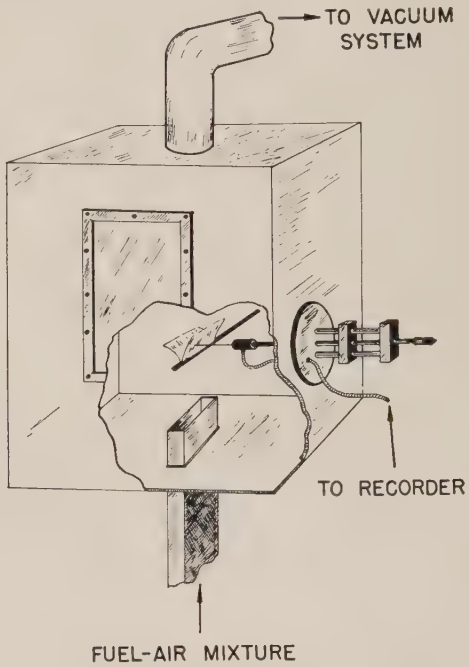

Fig. 11. Inverted flame at subatmospheric pressure.

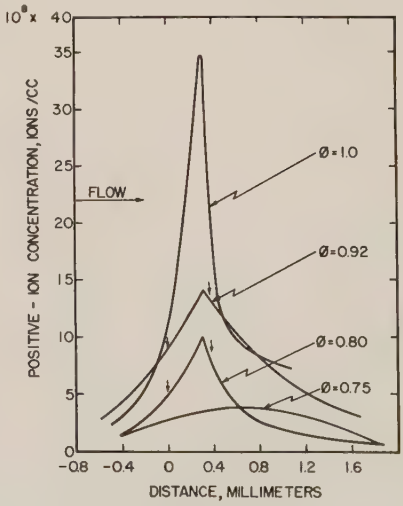

Fig. 12. Positive-ion concentration through the flame front. Inverted propane-air flame at 0.3 atmosphere. Arrows indicate extent of luminous zone.

Effect of Equivalence Ratio on Ion Concentration

The effect on the ion concentration of varying the equivalence ratio was observed by probing

inverted flames at 0.3 atm. Inverted flames were chosen so that the flame could be approached with the probe from the unburned side at various equivalence ratios in the same apparatus. These flames were stabilized on a rod held in a laminar stream emanating from a rectangular duct (Fig. 11). Very stable flames were obtained at 0.3 atm but at other pressures slight oscillations made it difficult to probe the combustion zone. The distance the probe moved into the burning zone was corrected for the angle between the probe and the flame.

The results for lean flames are reported in Figure 12 and for rich flames in Figure 13. The thickness of the ionized region has been increased

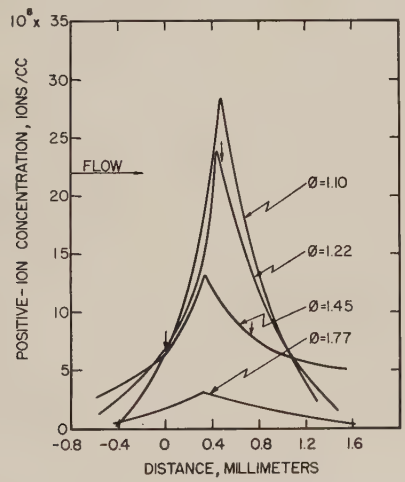

FIG. 13. Positive-ion concentration through the flame front. Inverted propane-air flame at 0.3 atmosphere. Arrows indicate extent of luminous zone.

by a reduction in pressure (cf Fig. 9) just as the thickness of the luminous zone is increased by a reduction in pressure. In Figure 14 the maximum observed positive-ion concentration is plotted against the equivalence ratio along with the adiabatic flame temperature and the burning velocity. All three curves have the same general shape except that the burning velocity drops off considerably faster on the rich side than does the flame temperature or the ion concentration. At any given temperature the ion concentration on the rich side is slightly greater than on the lean side but not sufficiently to make a strong argument for carbon particles as the ion source[5, 8]. Neither does this result eliminate the possibility that the ions are polymerized carbon.

If Saha's equation be rewritten,

$$2 \log N_+ - \tfrac{3}{2} \log T = (\log N_0 + \log G + 15.38) - \frac{5040}{T} V_i$$

it is seen to be possible from a plot of log $(N_+^2/T^{3/2})$ against $1/T$ to calculate the ionization potential, V_i, and the concentration of un-ionized species, provided the species being ionized remains constant throughout the range of composition. This would approximate the situation if the ions were due to contaminants. The results

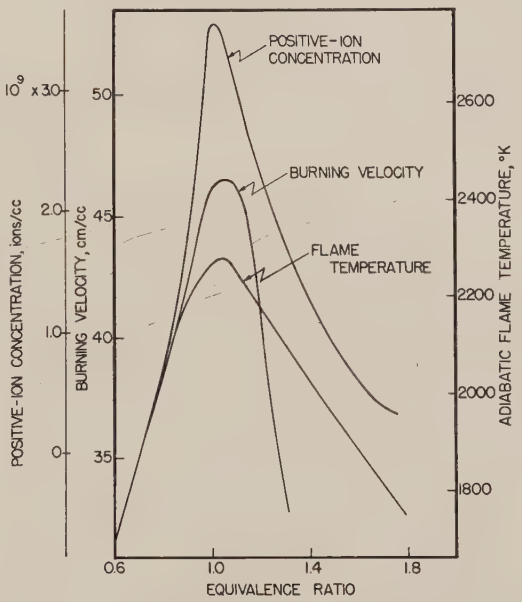

FIG. 14. Positive-ion concentration (0.3 atmosphere), burning velocity (1.0 atmosphere), and flame temperature as functions of equivalence ratio.

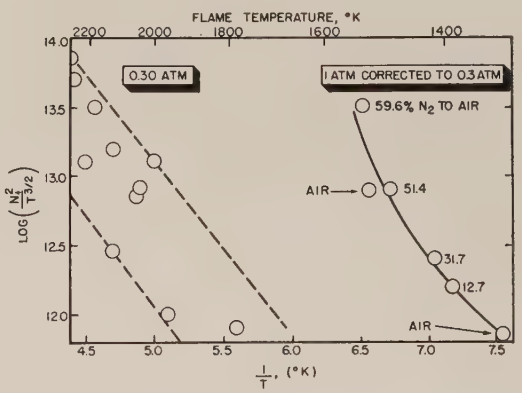

FIG. 15. Reciprocal temperature dependence of ionization assuming contaminants as ion source.

at one atmosphere with nitrogen dilution (Table 4) have been corrected to 0.3 atm, assuming Saha's equation to apply, which gives $N_+(0.3 \text{ atm}) = N_+(1 \text{ atm}) \sqrt{0.3}$.

The function $\log (N_+^2/T^{3/2})$ is plotted against the reciprocal of the adiabatic flame temperature in Figure 15. The points for 0.3 atm, banded by dotted lines, show considerable scatter but are definitely not in the same region as the data obtained at one atm. This is further evidence that the ions are not due to contaminants because the points would then lie on the same curve.

Summary and Conclusions

In addition to an indication of the usefulness within limits of the Langmuir probe for studying ionization in flames, the main conclusion to be drawn from this paper is that ionization in the combustion wave of hydrocarbon flames is not due to thermal ionization of contaminants or nitric oxide. The arguments presented for this conclusion are:

(1) Flames of carbon disulfide and hydrogen sulfide contain very small concentrations of ions. Were contaminants responsible, these flames would be expected to afford ion concentrations comparable to hydrocarbon flames.

(2) Very lean flames at low temperatures have high ion concentrations.
   (a) Close to one mole-per cent sodium impurity in the input gas would be required to account for the observed concentration.
   (b) The thermodynamic concentration of NO^+ in these flames is less than one ion/cc.

(3) The ionization is concentrated in a very thin region comparable in thickness to the reaction zone.

(4) One cannot correlate the results at two pressures by assuming thermal ionization of contaminants.

REFERENCES

1. Calcote, H. F.: *Third Symposium on Combustion, Flame, and Explosion Phenomena*, p. 245. Baltimore, The Williams & Wilkins Company, 1949.
2. Calcote, H. F., and Pease, R. N.: Ind. Eng. Chem., *43*, 2726 (1951).
3. Langmuir, I., and Mott-Smith, H. M.: Gen. Elec. Rev., *26*, 731 (1923); *27*, 449, 583, 616, 726, 810 (1924).
4. Belcher, H., and Sugden, T. M.: Proc. Roy. Soc. London, *201*, 480; *202*, 17 (1950).
5. Shuler, K. E., and Weber, J.: J. Chem. Phys., *22*, 491–502 (1954).
6. Taylor, H. S., and Glasstone, S.: *A Treatise on Physical Chemistry*, p. 388. New York, D. Van Nostrand Co., 1943.
7. Gaydon, A. G., and Wolfhard, H. G.: *Flames, Their Structure, Radiation and Temperature*, Chapter 13. London, Chapman and Hall, 1953.
8. Lewis, B., and Von Elbe, G.: *Combustion, Flames and Explosions of Gases*, p. 206. New York, Academic Press, 1951.
9. Moyerman, R. M., and Shuler, K. E.: Science, *118*, 612–614 (1953).
10. Wilson, H. A.: Rev. Mod. Phys., *3*, 156 (1931).
11. Loeb, L. B.: *Fundamental Processes of Electrical Discharge in Gases*. New York, J. Wiley and Sons, 1939.
12. Glasstone, S., Laidler, K. J., and Eyring, H.: *The Theory of Rate Processes*. New York, McGraw-Hill Book Co., 1941.
13. Friedman, R.: *Fourth Symposium (International) on Combustion*, p. 259. Baltimore, The Williams & Wilkins Company, 1953.

40

KINETICS OF THE GAS-PHASE OXIDATION OF FORMALDEHYDE[a]

By MILTON D. SCHEER

Introduction

The importance of formaldehyde as the rate-determining intermediate in methane oxidation has been conclusively demonstrated[1, 2]. Even in the oxidation of the higher hydrocarbons, formaldehyde has been shown to play an important role[3, 4]. Therefore, in order to be able to solve the general problem of hydrocarbon oxidation, the kinetics of the oxidation of formaldehyde must first be understood.

In the past two decades, many investigators have been engaged in the study of formaldehyde oxidation. Fort and Hinshelwood[5] showed that the rate of pressure rise was independent of oxygen concentration and strongly dependent upon the formaldehyde concentration (F). They also found that $E_{act} = 20$ kcal/mol, as determined from the times of half-reaction at different temperatures. Bone and Gardner[1] studied the reaction rates of 2:1 and 1:1 mixtures of CH_2O—O_2 at pressures ($\sim$1 atm) considerably higher than those employed by other investigators. They found that the rate of pressure rise was retarded by an increase in the surface-to-volume ratio. By an extensive analysis of the reaction products, they found that CO and H_2O were the major products, whereas CO_2, H_2 and HCOOH were formed in smaller amounts. They also found that relatively large quantities of performic acid (PA) and dioxymethyl peroxide ($HOCH_2$—O—O—CH_2OH) were formed during the early stages of reaction. These two peroxidic substances were shown to disappear with time, while the more stable products and the total pressure increased appreciably.

[a] This research is a part of the work by the Bureau of Mines on Order No. CS-670-54-9, supported by Headquarters, Air Research and Development Command, Office of Scientific Research, through Project SQUID.

Spence[6] showed that the oxidation over extensive surfaces of powdered glass occurred slowly and almost exclusively according to the overall reaction: $CH_2O + O_2 = CO_2 + H_2O$. In unpacked Pyrex vessels, he found that the variation of initial rates of pressure rise with temperature yielded an overall activation energy of 17.6 kcal/mol. He suggested a reaction chain analogous to that given by Bäckstrom[7] for the oxidation of aldehydes in the liquid phase. This scheme involved PA, activated CH_2O, and activated HCOOH molecules. The assumption of a steady state for these intermediate species yielded the following equation for the initial rate of disappearance of formaldehyde:

$$\left(-\frac{dF}{dt}\right)_i = k'(F)_i^2 - k''(F)_i + k'''.$$

This equation fits his data well, if his observed $(dp/dt)_i$ are assumed to be proportional to $(-dF/dt)_i$. Snowden and Style[8] made both gas analytical and manometric measurements. In agreement with previous investigators, they found that CO, H_2O, H_2 and CO_2 were the reaction products. From stoichiometric considerations, neglecting peroxide formation, they obtained evidence for the presence of HCOOH. In several experiments they made use of a spectrophotometric method for determining CH_2O (D-band absorption in the near ultraviolet using a hydrogen discharge tube as the source of light). Except for a short initial period of acceleration, they found that their results could be expressed by the rate law: $-dF/dt = KF(F - C)$, where K and C were shown to vary erratically with surface condition. This equation was shown to be a consequence of a modified form of Spence's reaction scheme. Treatment of the reaction-vessel surface with hydrofluoric acid resulted in a

very slow rate of pressure rise after an appreciable induction period. The presence of Hg vapor increased the rate of pressure rise, whereas washing the surface with HNO_3 gave the most reproducible results. Axford and Norrish[9], on the other hand, found, with the exception of a few rare experiments, no convexity toward the time axis in their observed pressure-time curves. Indeed, no observable diameter effect upon the rate of pressure rise was noted in their experiments. From the analytical results of a course-of-reaction series of experiments, they showed that $(-dF/dt)_i = 2(dp/dt)_i$. In addition, the simple rate law, $(-dF/dt)_i = KF_i^2$, was found to fit their data quite well, and an overall activation energy of 21 kcal/mol was observed. They also found that CO and H_2O were the major products, whereas CO_2 and H_2, in almost equal amounts, were minor products. No evidence for the presence of HCOOH or peroxides was found. The addition of N_2 as an inert diluent inhibited the rate of pressure rise. Small quantities of oxygen were found to induce a slow decomposition of formaldehyde at temperatures where it is normally quite stable. These observations were successfully accounted for by these authors by means of a simple reaction scheme involving H atoms as the predominant chain carrier. More recently, Vanpée[10] studied this reaction at considerably higher temperatures (370–550°C) and lower pressures (20–80 mm Hg) than had been done previously. He used a fine tungsten filament (40μ) as a temperature-sensing element in a thermal method for following the rate of reaction. He was able to demonstrate that the reaction followed a $(-dF/dt)_i = KF_i^2$ rate law with an overall activation energy of 29.4 kcal/mol. He showed that an active intermediate, which he assumed to be PA, builds up to a steady state during an initial induction period and is destroyed by a bimolecular process at the vessel wall. The mechanism suggested is a further modification of the Bäckstrom type of scheme first used by Spence. In a recent review of the available literature on formaldehyde oxidation, Lewis and von Elbe[11] came to the conclusion that PA is formed by a chain reaction in which HCO is the predominant chain carrier[b]. The PA thus formed is then assumed to diffuse to the vessel wall and decompose into the products CO, H_2O, CO_2, H_2 and HCOOH. If this process is rapid enough, further gas-phase reactions of the intermediate performic acid with the chain carrier CHO are neglected, and the process becomes a simple steady-state reaction. If the vessel surface, on the other hand, is inactive toward peroxide destruction, gas-phase reactions of the PA then play a role, and the kinetics become more complex. These authors thus attribute the simple kinetics observed by Axford and Norrish to use of a system which rapidly decomposed the intermediate peroxides. In particular, they suggest that the Hg vapor introduced into the Axford and Norrish reaction vessel, as a result of the use of heated mercury cutoffs, could have caused the rapid removal of PA. The more complicated kinetic data obtained by Spence, Snowden and Style, and Bone and Gardner was attributed to the use of systems in which the intermediate PA was not rapidly destroyed.

The purpose of this present investigation is primarily to resolve the difference between the kinetic results obtained by Axford and Norrish on the one hand, and Spence, Snowden and Style, and Bone and Gardner on the other; second, further information is sought concerning the nature of, and the role played by, the intermediate peroxides; and finally, a mechanism is arrived at which is capable of explaining the main features of this reaction as observed to date.

Experimental

MATERIALS

Formaldehyde: Monomeric liquid formaldehyde was prepared by the method of Spence and Wild[15] and stored at −80°C. Alpha-polyoxymethylene was used as the starting material instead of paraformaldehyde, since the former polymer contains less water than the latter.

Oxygen: Oxygen, 99.6 per cent pure, was taken from a cylinder and condensed at liquid-nitrogen temperatures. The middle fraction was evaporated into a large evacuated bulb up to a pressure of about 1000 mm Hg and stored there until ready for use.

APPARATUS

The reaction vessels used were 6-cm and 4-cm silica bulbs. The reaction vessel, wrapped in

[b] They cite the work of Gorin[12, 13] and Style and Summers[14] as evidence for the stability of the HCO radical (i.e., HCO = H + CO—> 26 kcal). The photolysis of CH_2O in the presence of D_2 has been studied recently in this laboratory by Dr. L. J. Schoen. His data provide further independent evidence for the stability of HCO (to be published).

aluminum foil, was immersed in an electrically heated, thermocouple-controlled (±½°C) furnace. A slow stream of air was blown over the reaction vessel to keep the temperature gradient from one side of the bulb to the other within ±½°C. Temperatures were measured with iron-constantan thermocouples, which were calibrated at the ice point and boiling point of water, and the melting points of Sn, Pb, and Zn. Pressures were measured by means of a Bodenstein quartz spiral manometer, which had a galvanometer mirror mounted on it. A conventional projection lamp and scale assembly could then be arranged to give an optical lever which resulted in an instrument sensitivity of 2.5 mm of scale deflection per 1.0 mm Hg pressure differential. The entire system could be evacuated to $<10^{-6}$ mm Hg by means of a suitable combination of diffusion and mechanical pumps. Octoil-S was used as the diffusion-pump fluid. To avoid polymerization of formaldehyde, all lines and stopcocks in contact with formaldehyde were wrapped with nichrome wire and electrically heated to 110°C. Dow-Corning high-vacuum silicone grease was found to be suitable as a stopcock lubricant under these conditions. Figure 1 is a schematic diagram of the apparatus.

PROCEDURE

Mixtures of formaldehyde and oxygen were made up in the thermostated (110°C) mixing vessel. The contents of the mixing vessel was then rapidly shared with the thermostated, thoroughly evacuated, reaction vessel, and the pressure-time dependence was measured with the quartz spiral manometer. At the end of each reaction, or after any period of reaction, the hot gases were quickly shared with, and isolated in, the thermostated (110°C) sampling vessel. The pressure of this sample was quickly measured and then rapidly admitted into the freeze-out trap, which was immersed in liquid nitrogen. The permanent gases were then circulated through the sampling vessel, freezing trap system by means of the Toepler pump, to assure complete removal of the condensable gases. The noncondensable gases were then pumped back into the sampling vessel, and their pressure was measured. An ethyl iodide slurry (−110°C) was then used as a refrigerant in place of the liquid nitrogen. Thus, a rough separation of CO_2 and unreacted formaldehyde was made possible[9]. The CO_2 and traces of formaldehyde were then pumped back into the sampling vessel and the pressure measured once more. The gases now in the sampling vessel were then pumped into the mass spectrometer sample bulb (SB). The sample bulb (SB) was then isolated, removed from the system, and analyzed mass spectrometrically for CO, CO_2, O_2, H_2, and traces of CH_2O. In experiments 10A and 18A, the condensable products were scanned with the mass spectrometer. This was accomplished by opening the stopcock communicating between the freezing trap and the sample bulb (SB), removing the ethyl iodide slurry surrounding freezing trap, and immersing the sample bulb in liquid nitrogen. The sample bulb was again isolated and removed

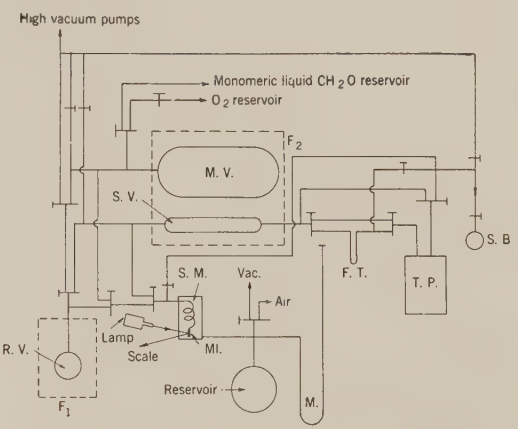

FIG. 1. Schematic diagram of apparatus. R.V., reaction vessel; S.M., quartz spiral manometer; MI., galvanometer mirror; M., mercury manometer; M.V., mixing vessel; S.V., sampling vessel; F_1, main furnace; F_2 secondary furnace thermostatically controlled at 110°C; F.T. freeze-out trap; T.P., toepler pump; S.B., mass spectrometer sample bulb.

from the system, but this time it was kept immersed in the refrigerant until ready to be opened to the evacuated mass-spectrometer inlet manifold and ionization chamber. In this way the possibility of detecting and identifying the unstable peroxides was enhanced.

For those experiments where a fresh, clean silica surface was desired, the reaction vessel was removed from the apparatus, washed with concentrated HNO_3, thoroughly rinsed with distilled H_2O, placed back in the apparatus, and thoroughly evacuated for 24 hr at 350°C. In all other experiments, the vessel was evacuated at 350°C for ½-hr before each run.

To reproduce the experimental conditions of Axford and Norrish, who used heated mercury cutoffs, mercury was added to the mixing vessel.

Since the mixing vessel was thermostated at 110°C, mercury vapor at a partial pressure of ~1 mm Hg was thereby introduced into the reaction vessel with the reaction mixture.

Stoichiometry

With the above apparatus and procedure it was possible to measure the following parameters for this reaction system:

$P_{CH_2O_i}$ = the initial partial pressure of formaldehyde;
Δp = the change in total pressure;
t = time;
$P_{O_{2i}}$ = the initial partial pressure of oxygen;
P_{O_2} = the partial pressure of oxygen at time t; where $\Delta p_{O_2} = P_{O_{2i}} - P_{O_2}$
P_{CO} = the partial pressure of CO at time t;
P_{H_2} = the partial pressure of H_2 at time t;
P_{CO_2} = the partial pressure of CO_2 at time t; and
P_{cond} = the partial pressure of the remaining constituents at time t, which are condensable at −110°C.

The analytical data of Bone and Gardner, as well as the results of this research, indicate that in general the following overall reactions are required to account for the products of this reaction:

$$CH_2O + \tfrac{1}{2}O_2 = CO + H_2O, \quad (a)$$

$$CH_2O + O_2 = CO_2 + H_2O, \quad (b)$$

$$CH_2O = H_2 + CO, \quad (c)$$

$$CH_2O + \tfrac{1}{2}O_2 = HCOOH \text{ (formic acid)}, \quad (d)$$

$$CH_2O + O_2 = HCOOOH \text{ (performic acid or PA)}, \quad (e)$$

and

$$3CH_2O + O_2 = CO + (CH_2OH)_2O_2 \text{ (dioxymethyl peroxide)}. \quad (f)$$

It has been found necessary to assume two types of stoichiometry. The seemingly conflicting results of Axford and Norrish, as opposed to those of Spence, and Snowden and Style, etc., suggest just such a treatment.

Case I: Peroxides are decomposed *rapidly* into CO, H_2O, CO_2, and H_2, and no HCOOH is formed. Reactions (d), (e) and (f) can then be neglected (the conditions of Axford and Norrish).

Case II(a): The peroxides decompose more *slowly* into CO, H_2O, CO_2, H_2 and HCOOH. If the reaction is allowed to go far (90–100 per cent) toward completion, then the quantity of peroxides remaining is very small and (e) and (f) may be neglected.

Case II(b): Same as II(a) above, but where the reaction is stopped sufficiently short of completion, so that the amount of peroxides present cannot be neglected. All of the six overall reactions must then be considered.

From a straightforward stoichiometric consideration of the overall reactions, unmeasured parameters, such as $\Delta p_{CH_2O} = P_{CH_2O_i} - P_{CH_2O}$, P_{H_2O}, P_{HCOOH}, etc., can be calculated from the measured quantities in the following fashion:
Case I:

$$\Delta p_{CH_2O} = P_{CO} + P_{CO_2},$$

and

$$P_{H_2O} = P_{CO} + P_{CO_2} - P_{H_2}.$$

As a check upon the consistency of these results, one can compare the experimentally measured values with those calculated as follows:

$$\Delta p_{calc} = \tfrac{1}{2}(P_{CO} + P_{H_2}),$$

and

$$P_{cond_{calc}} = P_{H_2O} + P_{CH_2O} = P_{CH_2O_i} - P_{H_2}.$$

Case II(a):

$$\Delta p_{CH_2O} = P_{CO} + P_{CO_2} + P_{HCOOH} = P_{H_2} + 2\Delta p_{O_2} - P_{CO_2};$$

$$P_{H_2O} = P_{CO} + P_{CO_2} - P_{H_2};$$

and

$$P_{HCOOH} = P_{H_2} + 2\Delta p_{O_2} - P_{CO} - 2P_{CO_2}.$$

Once more, as a check upon the consistency of the scheme, one can calculate:

$$\Delta p_{calc} = P_{CO} + P_{CO_2} - \Delta p_{O_2},$$

and

$$P_{cond_{calc}} = P_{H_2O} + P_{HCOOH} + P_{CH_2O} = P_{CH_2O_i} - P_{H_2}.$$

Case II(b):

$$\Delta p_{CH_2O} = P_{CO} + P_{CO_2} + P_{HCOOH} + P_{PA} + 2P_{(CH_2OH)_2O_2}$$

$$= \tfrac{1}{2}(3\Delta p_{O_2} + P_{CO} - P_{CO_2} - \Delta p) + P_{H_2} - P_{PA};$$

$$P_{H_2O} = \tfrac{1}{2}(P_{CO} + P_{CO_2} + \Delta p_{O_2} + \Delta p) - P_{H_2};$$

$$P_{(CH_2OH)_2O_2} = \tfrac{1}{2}(P_{CO} + P_{CO_2} - \Delta p_{O_2} - \Delta p);$$

and

$$P_{HCOOH} + 2P_{PA} = \tfrac{1}{2}\,(5\Delta p_{O_2} - 3P_{CO} - 5P_{CO_2} + \Delta p) + P_{H_2};$$

and again, to verify the consistency of the scheme, one can calculate:

$$\begin{aligned} P_{cond_{calc}} &= P_{H_2O} + P_{CH_2O} + P_{HCOOH} + P_{PA} \\ &\quad + P_{(CH_2OH)_2O_2} \\ &= P_{CH_2O_i} + \Delta p_{O_2} + \Delta p - P_{H_2} - P_{CO} \\ &\quad - P_{CO_2}. \end{aligned}$$

lar results were obtained in experiments carried out in the presence of mercury vapor, which was introduced in the manner described above. Curve 2 in Figure 2 is typical of those experiments carried out in a silica vessel after making several successive runs without cleaning (hereafter referred to as an aged vessel). The time interval for the initial convexity toward the time axis tended to increase somewhat with increased vessel aging. This effect is strongly reminiscent of the induction period phenomena encountered so frequently in hydrocarbon oxidation. As will be shown below, this similarity is only superficial in that

TABLE 1

(All Quantities in mm Hg at 337°C)

Experiment No.	7A*	17E*	30†	8B‡
Stoichiometry	I	I	II(a)	II(b)
Vessel and surface condition	6-cm silica bulb, freshly cleaned with HNO_3	4-cm silica bulb, contaminated with Hg vapor	6-cm silica bulb, aged surface	4-cm silica bulb, aged surface
Observed quantities				
Δt (minutes)	32	20	35	3
$P_{CH_2O_i}$	127.4	97.5	93.4	161.6
Δp_{O_2}	50.7	30.3	45.3	34.3
P_{CO}	84.0	56.8	62.1	29.5
P_{CO_2}	23.2	8.0	12.4	26.6
P_{H_2}	13.6	2.8	16.6	38.0
Δp_{obs}	45.8	28.8	29.0	11.9
$P_{cond_{obs}}$	103.0	89.5	76.4	113.7
Calculated quantities				
Δp_{calc}	48.8	29.8	29.2	—
$P_{cond_{calc}}$	113.8	95.6	76.8	113.2
P_{H_2O}	93.6	62.0	57.9	13.1
Δp_{CH_2O}	107.2	64.8	93.4	—
$\Delta p_{CH_2O} + P_{PA}$	—	—	—	85.0
P_{HCOOH}	—	—	20.3	—
$P_{HCOOH} + 2P_{PA}$	—	—	—	18.9
$P_{(CH_2OH)_2O_2}$	—	—	—	5.0

* Exp. 7A, 17E: $(dp/dt)_{max} = (dp/dt)_i$.
† Exp. 3C: $(dp/dt)_{max} = (dp/dt)_t = 3$ minutes.
‡ Exp. 8B: $(dp/dt)_{max} = (dp/dt)_t = 2$ minutes.

Table 1 gives the analytical results of four experiments which are typical of the different stoichiometric conditions described above.

Results

THE PRESSURE-TIME DEPENDENCE

Two types of pressure-time curves have been observed. Curve 1 in Figure 2 gives a typical example of those experiments carried out in a silica vessel freshly cleaned with nitric acid. Similar the rate at which formaldehyde disappears is not slow during this time but is actually greater than in those experiments performed in a clean vessel, or with mixtures contaminated with mercury vapor.

PRODUCTS CONDENSABLE AT −110°C

To obtain specific information about the nature of the products other than CO, CO_2, and H_2, a sample of the products condensable at −110°C

was taken as described above and scanned by the mass spectrometer in the 0–100 mass range. The results for samples taken from an aged vessel and

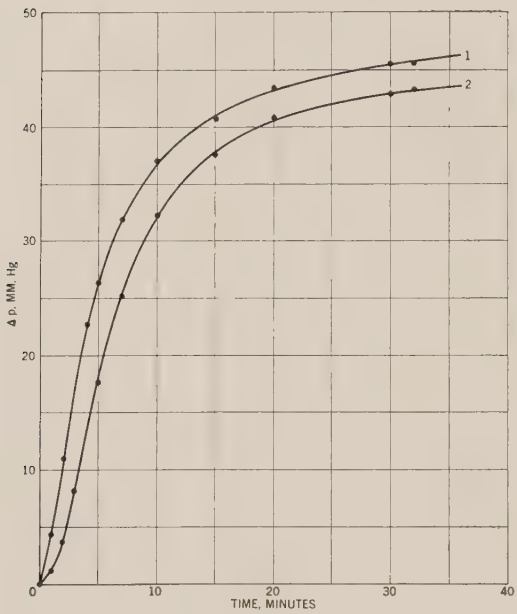

FIG. 2. Curve 1: Exp. #7A; HNO_3 cleaned vessel; $P_{CH_2O_i}$ = 127.4 mm Hg and $P_{O_{2i}}$ = 79.3 mm Hg; T = 337°C; 6-cm silica bulb. Curve 2: Exp. #3A; aged vessel; $P_{CH_2O_i}$ = 127.6 mm Hg and $P_{O_{2i}}$ = 68.6 mm Hg; T = 337°C; 6-cm silica bulb.

TABLE 2

	Aged Vessel	Reaction Mixture Contaminated with Mercury Vapor
Experiment no.	10A	18A
Temperature, °C	337	337
Time, min	5	5
$P_{CH_2O_i}$, mm Hg	175.1	176.0
$P_{O_{2i}}$, mm Hg	80.9	80.7
Analysis, mol per cent		
CH_2O (unreacted)	11.7	5.5
H_2O	61.2	92.1
HCOOH	3.2	Trace (<0.1)
O_2	10.0	0.0
CO_2	1.4	0.0
Unidentified	12.5	2.4

from a reaction mixture contaminated with mercury vapor are given in Table 2.

In agreement with all previous investigators, it is found that H_2O is a major product. The presence of HCOOH in the aged vessel is in complete agreement with the observations of Bone and Gardner[1] and of Snowden and Style[8]. Its comparative absence in the mercury-contaminated system agrees with the results of Axford and Norrish. The presence of O_2 and CO_2 in the sample taken from the aged vessel can probably be attributed to the breakdown of peroxides in the ionization chamber of the mass spectrometer. The unidentified species exhibited a mass spectrum extending over the 30–95 mass range. Small peaks at 62, 61 and 60 were observed and tentatively assigned to PA (with the loss of one and two hydrogen atoms). Since calibrating spectra for peroxides are not available, no particular peroxide species could be positively identified.

The above facts, together with the previous observations of Bone and Gardner[1], Snowden and Style[8], and Axford and Norrish[9], must be taken as strong evidence for the peroxide destroying property of mercury vapor.

COURSE-OF-REACTION EXPERIMENTS

As shown in Table 1, consistent analyses result when Case I stoichiometry is applied to a system with a vessel freshly cleaned with HNO_3 or to a mercury contaminated mixture. Case II stoichiometry, on the other hand, yields consistent results when applied to a system consisting of an aged silica vessel. The significance of these facts is demonstrated by Tables 3 and 4. Table 3 gives the results of a course-of-reaction series of experiments for an aged vessel, whereas Table 4 gives a similar set of data for a vessel contaminated with mercury vapor.

For the vessel contaminated with mercury vapor, dp/dt reaches a maximum at the start of the reaction. Since Case I stoichiometry can be used successfully, peroxides and HCOOH are not present in significant quantities. Also, it is seen that $(dp/dt)_i \approx (\frac{1}{2})(-dF/dt)_i$. These facts are in complete agreement with the data reported by Axford and Norrish.

For the aged vessel, dp/dt does not reach a maximum until about 2.5 minutes after the start of the reaction. Also, note that $(dp/dt)_i \ll (\frac{1}{2})|dF/dt|_i$. Since Case II stoichiometry must be applied to yield consistent results, the presence of HCOOH, PA and $HOCH_2—O—O—CH_2OH$ is strongly indicated and their partial pressures are calculated in the manner described above. These calculations show that during the early stages of reaction the concentration of $(CH_2OH)_2O_2$ builds up faster than either PA or HCOOH. During the first minute of reaction, $(P_{HCOOH} + 2P_{PA})$ is shown to be very small.

Table 3. Vessel: Aged 4 cm Silica Bulb
(All Quantities in mm Hg at 337°C)

Experiment No.	9B	9C	9D	9E	9F
Time, min	1	3	5	10	20
Observed quantities					
Δp_{O_2}	6.7	35.9	51.3	62.0	61.9
P_{CO}	14.2	55.8	73.5	94.1	95.0
P_{CO_2}	2.2	5.3	7.5	14.5	18.2
P_{H_2}	4.4	11.4	15.3	19.1	18.2
Δp_{obs}	.2	5.4	11.7	30.9	41.8
dp/dt, mm Hg/min	.8	3.6	3.6	2.5	.5
$P_{cond_{obs}}$	140.6	124.9	119.9	122.0	129.3
Calculated quantities					
$P_{cond_{calc}}$	140.9	125.2	119.6	122.5	130.0
P_{H_2O}	7.4	34.8	56.7	81.6	90.2
$\Delta p_{CH_2O} + P_{PA}$	25.9	87.8	119.4	136.5	128.6
$P_{HCOOH} + 2P_{PA}$	.0	6.9	20.4	12.1	5.8
$P_{(CH_2OH)_2O_2}$	4.8	9.9	9.0	7.9	4.8

$T = 337$°C.
$P_{CH_2O_i} = 155$ mm Hg.
$P_{O_{2i}} = 75$ mm Hg.
$(dp/dt)_{max} = 3.6$ mm Hg/min (between 2.5 and 8.5 min after the start of the reaction).

Table 4. Vessel: 4 cm Silica Bulb. Reaction Mixture Contaminated with Mercury Vapor at a Partial Pressure of about 1 mm Hg
(All Quantities in mm Hg at 337°C)

Experiment No.	17A	17B	17C	17D	17E
Time, min	1	3		10	20
Observed quantities					
Δp_{O_2}	1.6	9.2	17.0	24.2	30.3
P_{CO}	5.3	19.2	31.7	44.0	56.8
P_{CO_2}	1.5	3.6	4.4	6.6	8.0
P_{H_2}	1.5	2.3	1.8	3.1	2.8
Δp_{obs}	3.3	9.6	16.5	24.0	28.8
dp/dt, mm Hg/min	3.3	3.2	2.4	1.0	.3
$P_{cond_{obs}}$	93.5	90.1	94.0	91.3	89.5
Calculated quantities					
Δp_{calc}	3.4	10.7	16.8	23.6	29.8
$P_{cond_{calc}}$	95.3	94.4	97.0	94.1	95.6
P_{H_2O}	5.3	20.5	34.3	47.5	62.0
Δp_{CH_2O}	6.8	22.8	36.1	50.6	64.8

$T = 337$°C.
$P_{CH_2O_i} = 97.5$ mm Hg.
$P_{O_{2i}} = 100$ mm Hg.
$(dp/dt)_{max} = (dp/dt)_i \approx (1/2)\ (-dF/dt)_i$.

The dependence of $(-dF/dt)_i$ upon $P_{O_{2i}}$ and $P_{CH_2O_i}$

Axford and Norrish[9] have shown that, for a mercury-contaminated system (where PA is rapidly destroyed and never achieves significant concentrations), $(dp/dt)_i$ is independent of $P_{O_{2i}}$ and is proportional to $P^2_{CH_2O_i}$ and $\approx (1/2)\ (-dF/dt)_i$. For an aged vessel, however, it has been shown here that $(dp/dt)_i$ is not simply related to $(-dF/dt)_i$. Consequently, simple manometric measurements do not suffice for a determination of the initial rate. To measure

$(-dF/dt)_i$ in an aged vessel, it has been necessary to resort to the use of analytical data for short-duration experiments. Whereas this technique has several experimental shortcomings, such as the difficulty of obtaining precise determinations of Δt, as well as the inherent inaccuracy of measuring small quantities of products, the data given in Table 5 and Figure 3 do show consistent results.

TABLE 5. VESSEL: AGED 4-CM SILICA BULB

(All quantities in mm Hg at 350°C)

Experiment No.	12B	12C	12D
Observed quantities			
$P_{CH_2O_i}$	112.3	112.2	111.7
$P_{O_{2i}}$	59.7	111.8	169.3
Δp_{O_2}	11.0	11.7	12.5
P_{CO}	17.4	19.4	17.3
P_{CO_2}	2.7	2.3	2.6
P_{H_2}	4.4	7.1	7.0
$P_{cond_{obs}}$	101.0	96.3	99.9
Calculated quantities			
$P_{cond_{calc}}$	101.5	97.0	99.0
P_{H_2O}	9.1	9.9	10.2
$P_{(CH_2OH)_2O_2}$	3.3	4.7	2.7
Δp_{CH_2O}	26.7	30.0	25.2

$T = 350°C$.

Run duration: 1.0 min ($P_{HCOOH} \approx P_{PA} \approx 0$).

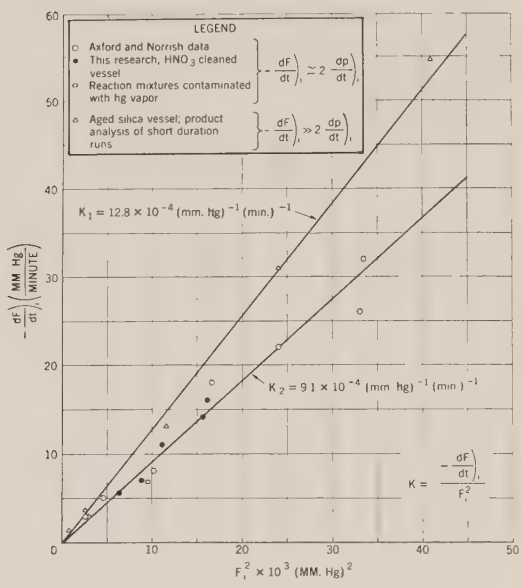
LEGEND
Axford and Norrish data
This research, HNO3 cleaned vessel
Reaction mixtures contaminated with hg vapor
Aged silica vessel; product analysis of short duration runs
K1 = 12.8 × 10⁻⁴ (mm. Hg)⁻¹ (min.)⁻¹
K2 = 9.1 × 10⁻⁴ (mm Hg)⁻¹ (min)⁻¹
K = -(dF/dt)i / Fi²
-(dF/dt)i (MM Hg / MINUTE)
Fi² × 10³ (MM. Hg)²

FIG. 3. Dependence of $-\left(\frac{dF}{dt}\right)_i$ upon $P_{CH_2O_i}$ ($T = 337°C$).

Table 5 indicates that $(-dF/dt)_i$ is independent of $P_{O_{2i}}$ in an aged vessel. Previous investigators, working under various experimental conditions, are in unanimous agreement with this fact. Figure 3 gives the data for the dependence of $(-dF/dt)_i$ upon $P_{CH_2O_i}$. The results of Axford and Norrish[9] and the data obtained in this research for both mercury contaminated and freshly cleaned vessels are shown to be entirely in agreement. The data obtained for aged vessels, on the other hand, definitely show somewhat larger values for $(-dF/dt)_i$ but still exhibit the simple square law dependence upon $P_{CH_2O_i}$, as shown in Figure 3.

THE OVERALL ACTIVATION ENERGY

$(-dF/dt)_i$ in an aged vessel was calculated from analytical data for 1-minute experiments for constant composition mixtures of CH_2O and O_2 in the temperature range 317° to 377°C ($[CH_2O]_i \approx [O_2]_i \approx 2.63 \times 10^{-6}$ mol/cc). An Arrhenius plot of $\ln |dF/dt|_i$ versus $1/T$ is given in Figure 4. The activation energy is 27.4 kcal/mol.

Table 6 gives the activation-energy measurements of previous investigators. Only the Axford and Norrish[9] value of 21 kcal/mol is for the well-defined condition of rapid peroxide destruction. The rather large spread among the other values can probably best be accounted for, at this time, by the use of different types of vessels and surfaces, resulting in different rates of PA destruction and different initial steady-state concentrations of PA.

Mechanism and Discussion

SUMMARY OF THE KINETIC DATA

The results of previous investigations, as well as those of this research, indicate that the following pertinent facts must be taken into account in any final choice of a mechanism for this reaction.

(1) Mercury vapor and surfaces freshly cleaned with HNO_3 result in simple p-t curves where $(dp/dt)_{max} = (dp/dt)_i$. The products are CO, H_2O, CO_2 and H_2, and the available analytical data show that $(dp/dt)_i \approx (\frac{1}{2})(-dF/dt)_i$. The governing rate law is given by $(-dF/dt)_i = K_1 F_i^2$, and the overall activation energy is about 21 kcal/mol. Inert diluents such as N_2 are found to decrease the rate of reaction[9].

(2) For other systems (such as the aged vessel reported in this paper), the p-t curves can show a decided initial convexity toward the time axis, so that $(dp/dt)_{max} \neq (dp/dt)_i$. During this initial

period of small dp/dt, formaldehyde reacts at a rate even faster than that observed in systems where $(dp/dt)_{max} = (dp/dt)_i$. In addition to the products CO, H_2O, CO_2, H_2, significant amounts of HCOOH, PA and $(CH_2OH)_2O_2$ are detected, where $(CH_2OH)_2O_2$ is found in measurable quantities earlier than either HCOOH or PA. The

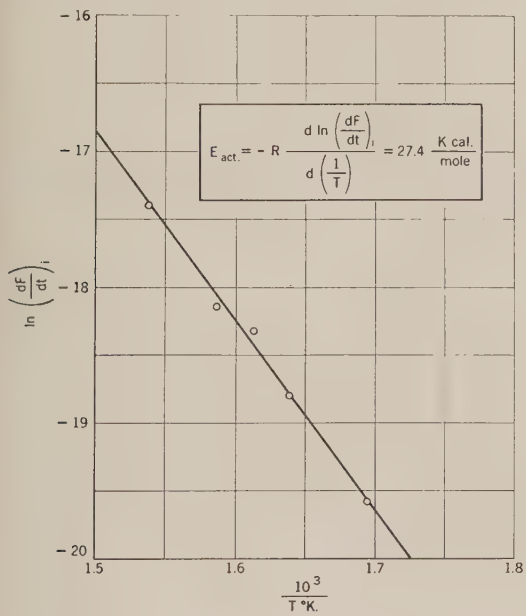

FIG. 4. Overall activation energy measurements, temperature range: 317–377°C.

TABLE 6

Investigators	Activation energy
	kcal/mol
Fort and Hinshelwood	20.0
Spence	17.6
Snowden and Style	25.0
Axford and Norrish	21.0
Vanpée	29.4
This research (for an aged vessel)	27.4

observed rate law is again found to be of the form $(-dF/dt)_i = K_2 F_i^2$ (where $K_2 = 1.4\,K_1$ at 337°C) with an overall activation energy of 27.4 kcal/mol.

These experimental facts are readily interpreted if one assumes that PA is formed by a simple, homogeneous, free radical chain involving CHO and CHO_3 as the major chain carriers. The PA thus formed is then either rapidly destroyed at the wall or by mercury vapor to form the products CO, H_2O, CO_2 and H_2; or it can eventually build up to relatively large concentrations. If the vessel conditions allow the second alternative, the PA initially reacts rapidly with CH_2O to form $(CH_2OH)_2O_2$[c], which can heterogeneously decompose to form HCOOH, CO_2 and $2H_2$ (reactions (8) and (9) below). In either case, however, (PA) is small initially, so that a simple stationary state may be assumed during the early stages of the reaction. The details of such a mechanism are given in the following section.

PROPOSED MECHANISM AND ITS CONSEQUENCES

I. Main chain:

1. $F + O_2 \rightarrow HCO + HO_2$ k_1 chain initiating

2. $HCO + O_2 \rightarrow HCO_3$ k_2
3. $HCO_3 + F \rightarrow PA + HCO$ k_3 } chain continuing

4′. $HCO_3 + O_2 \rightarrow CO + HO_2 + O_2$ $k_{4'}$
4. $HCO_3 + M \rightarrow CO + HO_2 + M$ k_5 } chain terminating

5. $HO_2 \xrightarrow{\text{wall}}$ destruction k_5

II. For the conditions of rapid PA destruction, the main chain is followed by:

6. $2PA \xrightarrow[\text{or Hg vapor}]{\text{active surface}} 2CO + 2H_2O + O_2$ k_6
7. $2PA \xrightarrow{\text{wall}} 2CO_2 + 2H_2 + O_2$ k_7 } where $k_7 < k_6$

III. For the aged vessel condition, the main chain is followed by:

8. $PA + 2F \rightarrow (CH_2OH)_2O_2 + CO$ k_8

9. $(CH_2OH)_2O_2 \xrightarrow{\text{wall}} HCOOH + CO_2 + 2H_2$ k_9

6′. $2PA \xrightarrow[\text{surface}]{\text{inactive}} 2CO + 2H_2O + O_2$ $k_{6'}$
7′. $2PA \xrightarrow{\text{wall}} 2CO_2 + 2H_2 + O_2$ k_7 } where $k_7 < k_{6'} < k_6$

[c] Evidence for the reaction between CH_2O and peroxides to form hydroxyperoxides is given by G. H. N. Chamberlain and A. D. Walsh, *Third Symposium on Combustion, Flame and Explosion Phenomena*, The Williams & Wilkins Co., Baltimore, 1948, pp. 375–382.

For the conditions of rapid destruction of PA (I and II) the rate of disappearance of CH_2O is given by

$$-\frac{dF}{dt} = k_1(F)(O_2) + k_3(HCO_3)(F).$$

Assuming long chains, and since 1 is chain-initiating, $k_1(F)(O_2)$ can be neglected relative to the chain continuing step 3. Therefore,

$$-\frac{dF}{dt} = k_3(HCO_3)(F). \tag{1}$$

Now, with the usual steady-state assumptions for (HCO) and (HCO_3), it is readily shown that

$$(HCO_3) = \frac{k_1(O_2)(F)}{k_{4'}(O_2) + k_4(M)}, \tag{2}$$

and equation (1) becomes

$$-\frac{dF}{dt} = \frac{k_1k_3(O_2)}{k_{4'}(O_2) + k_4(M)}(F)^2 = \frac{k_1k_3}{k_{4'} + k_4\dfrac{(M)}{(O_2)}}(F)^2. \tag{3}$$

For initial rates in the absence of inert diluents, equation (3) becomes

$$\left(-\frac{dF}{dt}\right)_i = \frac{k_1k_3}{k_{4'}}(F)_i^2 \tag{4}$$

which is just the type of rate dependence experimentally observed. Therefore, $E_{act} = E_1 + E_3 - E_4' = 21$ kcal/mol. This activation energy is consistent with an approximate bond energy estimate of $\Delta H_1 + \Delta H_3 - \Delta H_4$; ≈ 10 kcal exothermic[16, 17].

Applying steady-state considerations to (PA), it follows that

$$2(k_6 + k_7)(PA)^2 = k_3(HCO_3)(F). \tag{5}$$

In the absence of inert diluents, the initial rate of pressure rise is given by

$$\left(\frac{dp}{dt}\right)_i = 3(k_6 + k_7)(PA)^2 + k_{4'}(HCO_3)(O_2) - k_2(HCO)(O_2). \tag{6}$$

From the steady-state condition for (HCO_3)

$$k_4(HCO_3)(O_2) - k_2(HCO)(O_2) = -k_3(HCO_3)(F), \tag{7}$$

and from equation (5)

$$3(k_6 + k_7)(PA)^2 = \tfrac{3}{2}\, k_3(HCO_3)(F),$$

equation (6) becomes

$$\left(\frac{dp}{dt}\right)_i = \tfrac{1}{2}k_3(HCO_3)(F)_i = \tfrac{1}{2}\,\frac{k_1k_3}{k_{4'}}(F)_i^2. \tag{8}$$

Comparison of equation (8) with equation (4) yields

$$\left(\frac{dp}{dt}\right)_i = \tfrac{1}{2}\left(-\frac{dF}{dt}\right)_i, \tag{9}$$

which again is seen to be in agreement with the result given by experiment.

For the aged vessel conditions (I and III) the rate of disappearance of CH_2O is given by

$$-\frac{dF}{dt} = k_3(HCO_3)(F) + 2k_8(PA)(F)^2. \tag{10}$$

In the absence of inert diluents, the initial rate is given by using equation (2):

$$\left(-\frac{dF}{dt}\right)_i = \frac{k_1k_3}{k_{4'}}(F)_i^2 + 2k_8(PA)_i(F)_i^2. \tag{11}$$

The stationary state condition for $(PA)_i$ is given by

$$(PA)_i^2 + \frac{k_8(F)_i^2}{2(k_{6'} + k_7)}(PA)_i - \frac{k_1k_3(F)_i^2}{2k_{4'}(k_{6'} + k_7)} = 0. \tag{12}$$

For $(PA)_i$ small, it follows that, to a second-order approximation,

$$2k_8(PA)_i(F)_i^2 = \frac{k_1k_3}{k_{4'}}(F)_i^2\left[2 - \frac{k_1k_3}{k_{4'}}\cdot\frac{4(k_{6'} + k_7)}{k_8^2(F)_i^2} + \cdots\right]. \tag{13}$$

Substituting equation (13) into equation (11), the initial rate for the aged-vessel conditions becomes

$$\left(-\frac{dF}{dt}\right)_i = \frac{k_1k_3}{k_{4'}}(F)_i^2\left[3 - \frac{k_1k_3}{k_{4'}}\cdot\frac{4(k_{6'} + k_7)}{k_8^2(F)_i^2} + \cdots\right]. \tag{14}$$

From the experimental results given in Figure 3, the quantity in the brackets is seen to be approximately equal to 1.4 for the vessel conditions reported here.

DISCUSSION

Whereas the above mechanism provides a satisfactory explanation for most of the observations encountered for this reaction, there are

several results reported by previous investigators which do not fit directly into the scheme. Spence noted that over extensive surfaces of powdered glass, the reaction occurred slowly and almost exclusively to form CO_2 and H_2O. This fact can be understood in light of the suggested mechanism, if one assumes that in the presence of extremely large glass surface to volume ratios, the main chain I is followed predominantly by

$$10. \qquad PA \xrightarrow[\text{surface}]{\text{extensive}} CO_2 + H_2O \qquad k_{10}$$

in lieu of 6 and 7, or 8 and 9. Also, the chain lengths are considerably decreased by the increased likelihood of

$$11. \qquad HCO \xrightarrow{\text{wall}} \text{destruction} \qquad k_{11}$$

or

$$12. \qquad HCO_3 \xrightarrow{\text{wall}} \text{destruction} \qquad k_{12},$$

thereby resulting in a slower rate. Another significant observation that should be amenable to interpretation in the light of the proposed mechanism is that a slow, low-temperature decomposition of CH_2O to CO and H_2 can be induced by traces of oxygen.[9] The following reaction sequence can qualitatively account for this observation:

$$1. \qquad F + O_2 \rightarrow HCO + HO_2 \qquad k_1$$

$$13. \qquad HCO + F \rightarrow CO + H_2 + HCO \qquad k_{13}$$

$$11. \qquad HCO \xrightarrow{\text{wall}} \text{destruction} \qquad k_{11}$$

and

$$5. \qquad HO_2 \xrightarrow{\text{wall}} \text{destruction} \qquad k_5$$

where 13 is assumed to be much slower than 2 but, in the absence of appreciable quantities of oxygen, becomes rate determining.

Thus, the suggested reaction scheme provides a consistent framework from which the diverse and seemingly conflicting observations encountered in the formaldehyde oxidation reaction can be understood. A more complete understanding of the problem, however, must wait upon an accurate knowledge of the heterogeneous decompositions of (PA) and $(CH_2OH)_2O_2$, as well as further information concerning the detailed kinetics of the reaction between PA and CH_2O to form the hydroxyperoxide.

Acknowledgments

The author would like to take this opportunity to thank Drs. B. Lewis and G. von Elbe, first, for suggesting this problem and, second, with Drs. R. Klein and L. Schoen, for participating in the stimulating discussions that provided an ideal atmosphere for this work. Also, the author would like to express his appreciation to A. G. Sharkey and the mass-spectrometer group at the Bureau of Mines, without whose cooperation this research could hardly have been carried out in its present form.

REFERENCES

1. Bone, W. A., and Gardner, J. B.: Proc. Roy. Soc. (London), *A154*, 297 (1936).
2. Norrish, R. G. W., and Foord, S. G.: Ibid , *A157*, 503 (1936).
3. Bone W. A., and Hill, S. G.: Ibid., *A129*, 434 (1930).
4. Pease, R. N.: Chem. Rev., *21*, 279 (1937).
5. Fort, R., and Hinshelwood, C. N.: Proc. Roy. Soc. (London), *A129*, 284 (1930).
6. Spence, R.: J. Chem. Soc. 649 (1936).
7. Bäckstrom, H. L. J.: Z. Physik. Chem., *B25*, 99 (1934).
8. Snowden, F. F., and Style, D. W. G.: Trans. Faraday Soc., *35*, 426 (1939).
9. Axford, D. W. E., and Norrish, R. G. W.: Proc. Roy. Soc. (London), *A192*, 518 (1948).
10. Vanpée, M.: Bull. Soc. Chim. Belg., *62*, 285 (1953).
11. Lewis, B., and von Elbe, G.: *Combustion, Flames and Explosions of Gases*, pp. 94–106. New York, 1951. Academic Press, Inc.
12. Gorin, E.: Acta Physicochim. (U.R.S.S.), *9*, 681 (1938).
13. Gorin, E.: J. Chem. Phys., *7*, 256 (1939).
14. Style, D. W. G., and Summers, D.: Trans. Faraday Soc., *42*, 388 (1946).
15. Spence, R., and Wild, W.: J. Chem. Soc., 338 (1935).
16. Pauling, L.: *Nature of the Chemical Bond.* Cornell Univ. Press, 1945.
17. Glockler, G.: J. Chem. Phys., *19*, 124 (1951).

Discussion by M. Vanpée

In the mechanism proposed by Dr. Scheer, the initiating step is attributed to the reaction:

$$HCHO + O_2 = HO_2 + CHO$$

If this reaction is the only initiating step, then there is no induction period. The author claims that this is the case in the presence of mercury vapor.

However, it will be seen from Figure 1, which represents the combustion of formaldehyde in the presence of mercury vapor, that the use of single pressure-time curves is not sufficient to establish conclusively the absence of an induction period.

It is this which has led us to develop a more sensitive technique* in which the reaction velocity is measured directly by the small temperature rise due to the heat liberated by the reaction. The ΔT curve thus obtained undoubtedly has its origin at zero, $(dP/dt)_0 = 0$, although the ΔP curve shows only a smooth inflexion when ΔT passes through a well characterized maximum.

There is thus no doubt as to the existence of a definite induction period, both in the presence and in the absence of mercury vapor. We must conclude therefore that the reaction is catalyzed by a long-lived intermediate. The obvious compound for this role is performic acid.

The slightly modified symbolic mechanism previously proposed by Snowden and Style:

$$X + F = 2X \quad (1)$$

$$2X = \text{products reaction} \quad (2)$$

is in perfect agreement with this conclusion and we have shown* that it also fits remarkably well all the quantitative kinetic data. For step (1), we proposed the following scheme:

$$PA \rightarrow HCO + HO_2 \quad \text{initiation}$$

$$\left.\begin{aligned} HCO + O_2 &\rightarrow HCO_3 \\ HCO + F &\rightarrow HCO + PA \end{aligned}\right\} \text{propagation}$$

$$HCO_3 \rightarrow \text{wall} \quad \text{termination}$$

With regard to the decomposition of performic acid, it is interesting to consider the combustion of a mixture containing a great excess of formaldehyde (Fig. 2). After all the oxygen is consumed, the formation of performic acid is automatically suppressed and the only possible reaction is the decomposition of the peroxide. The curve representing this decomposition definitely corresponds to a bimolecular process and may thus be considered as direct experimental evidence of step (2). The absence of any vertical fall at point A shows further that the formation of performic acid from formaldehyde and oxygen (step (1)) is thermoneutral, and that the heat generated by the reaction is due only to the decomposition of the peroxide (step (2)).

* M. Vanpée: Bull. Soc. Chim. Belg., *62*, 285, (1953); *62*, 661 (1953).

Author's Reply

The thermal method of following the rate of reaction devised by Dr. Vanpée is a rather interesting approach to the ever present problem of kinetic measurements in complex reaction systems. However, this novel technique is open to question on the following grounds. Using the formaldehyde-oxygen reaction as an example, it has been shown, not only in this research but in the work of Bone and Gardner, Spence, and Snowden and Style, that, in the absence of mercury vapor, spurious surface catalytic effects are always present. Consequently, the use of a fine tungsten wire to follow small local temperature changes, which in turn are interpreted as instantaneous reaction rates, is questionable unless it can be conclusively shown that the tungsten surface contributes no catalytic activity to any phase of the reaction. Evidence in the literature* shows that oxygen is strongly chemisorbed upon tungsten (probably as O atoms). Could not some of the ΔT observed by Dr. Vanpée be attributed to a surface reaction between the adsorbed oxygen atoms and the substrate formaldehyde?

The question of the existence of an induction period for this reaction must ultimately be determined from knowledge of $-\frac{dF}{dt}$ during the initial stages of the reaction. From the analytical measurements given in this manuscript as well as those obtained by Axford and Norrish, no such effect has been observed, either for clean vessels or in the presence of mercury vapor. In the aged vessel, a true induction period may indeed be present (see Table 3), since the PA concentration can build up and react with F by something like reaction (8). In agreement with Dr. Vanpée, it should be emphasized that the S-shape of the Δp-t curve is not conclusive evidence for the existence of an induction period, since it has been shown here not to be simply related to the true course of reaction under conditions inactive to rapid PA destruction (i.e., in an aged vessel).

* I. Langmuir and D. S. Villars: J. Am. Chem. Soc., *53*, 486 (1931).

41

EARLY OXIDATION PRODUCTS OF ACETALDEHYDE AND PROPANE: INTERPRETATION[a]

By JOSEPH GRUMER

Introduction

Several years ago, a broad program was initiated by the Bureau of Mines for studying the kinetics and mechanisms of the basic reactions associated with nonexplosive oxidation of hydrocarbons. One objective was to investigate the mechanism of propane-oxygen reactions. Syntheses were developed for the preparation of end and middle marked C^{13} propane[1]. Special apparatus was designed for experimentation. The basic analytical tool was the mass spectrometer[b]. Experience with unmarked propane soon showed that it was premature to work with marked propane and that information was needed on the oxidation mechanisms of possible intermediate products. Accordingly, a study of the oxidation of acetaldehyde was undertaken.

Apparatus[c]

In observing the early stages of gaseous reactions, short contact times are required, which may be obtained conveniently in a flow system. A novel flow apparatus has been constructed and operated successfully. It offers the following advantages:

(1) No gas is wasted in flushing the apparatus. This is important when the gas is in short supply due to cost or difficulty of preparation.

(2) The pressure can be set at any pressure up to approximately 1000 mm Hg. It remains virtually constant during a run if the mol change due to reaction is negligible. This is the case in the early stages of a reaction, where a flow system is generally necessary. Previously it had been almost impossible to study reactions of gases in limited supply in a flow system at subatmospheric pressures.

(3) The volume of the system can be held constant during a run for values up to 100 cc.

(4) The time spent by the gas in the reaction space can be varied between wide limits.

Figure 1 shows the essential details of the apparatus. At the start of a run, the reactants are mixed in a 100-cc burette (a). The other burette (a′), whose volume and internal diameter are the same as (a), is emptied of gas by displacement with mercury. The leveling reservoirs (b) and (b′) of the burettes are of equal internal diameter, which is many times that of the burettes, so that the flow of mercury in the burettes has a negligible effect on the mercury level in the reservoirs. These reservoirs are set to maintain the desired total pressure in the system during a run by adjusting the lengths of both arms of the steel cord of the motor-driven pulley system (d). This system consists of a constant-speed AC motor coupled to a gear reducer by a belt drive. A gear on the output shaft of the gear reducer drives a fixed gear, which is attached to a threaded drum. The steel cord which moves the mercury reservoirs is wrapped twice around the drum to prevent slippage. The rate of rotation of the drum is determined by the diameters of wheels of the belt drive and the diameter of the gear on the output shaft of the gear box. The rotational direction of the drum is controlled by a reversing switch. The stopcocks of the burettes (a) and (a′) are opened simultaneously to the evacuated reaction train by the lateral motion of a rod (g) which turns the metal lever arm cemented to each stopcock plug. The d.p.d.t. toggle switch (f) is thrown at the same instant, starting an interval timer and the motor of the pulley system (d) which lifts the leveling reservoir (b) of burette (a) at the same uniform rate that it lowers reservoir (b′) of burette (a′). The gear ratio of this system (d) determines the residence time of the gas for a given reaction space (c) and temperature. A sintered-glass baffle disk was attached to the inlet of the reaction space to break up jets of incoming gas. Switch (f) is set so that it is thrown off at the end of the run by the rise of leveling reservoir (b), thus stopping the interval timer and the motor of (d) and activating the electromagnetic pinch clamps (e) and (e′), thereby pre-

[a] This research was conducted at the Bureau of Mines under Contract No. AF 18(600)-156 with the United States Air Force, the sponsoring agency being the Aeronautical Research Laboratory of the Wright Air Development Center, Air Research and Development Command.

[b] Mass spectrometric analyses were carried out by R. A. Friedel and A. G. Sharkey, Jr.

[c] Apparatus designed by the author, A. S. Gordon (presently at Naval Ordnance Test Station, China Lake, California), and P. L. Golden.

venting a surge of mercury at the end of the run. The reaction products are in burette (a′) where they can be collected for analysis.

Oxidation of Propane

The complexity of the stable products observed during the early stages of the oxidation of propane is shown by Table 1. The reaction cylinders for all experiments were around 1.6 cm ID; the hot zone volumes were about 10.5 cc. The major analytical tool was the mass spectrometer which was supplemented by fractionation of products and chemical techniques. Products listed were definitely identified but only the relative order of yields was established. The effect of tube surface

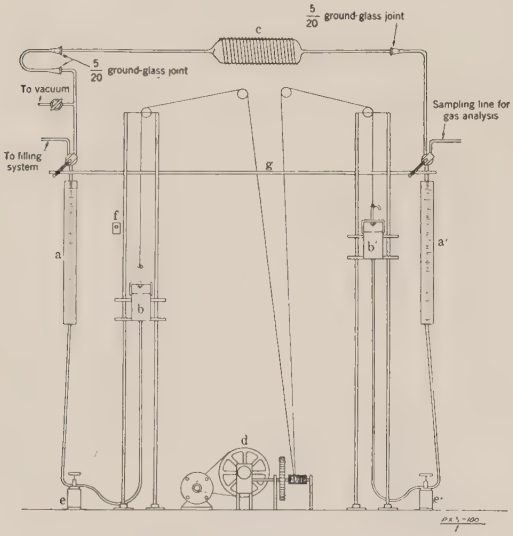

FIG. 1. Constant volume flow apparatus.

was not studied. Surface may have played a role in these reactions.

SUMMARY (PROPANE OXIDATION)

In addition to identifying products, some conclusions may be drawn from these data regarding the early oxidation products of propane:

(1) For $C_3H_8/O_2 > 1$, the temperature coefficient is negative, just as Pease and others[2, 3, 4] have shown to be the case for ratios $\leqslant 1$.

(2) Propylene is a major early product. This agrees with findings of other investigators who report unsaturates as major early products in the oxidation of saturated light hydrocarbons[5, 6]. The yield of propylene increases with temperature and with the original concentration of oxygen, except at high temperatures, where it may begin to oxidize. Very little H_2 is formed, and the temperatures seem too low for rapid hydrogen-oxygen reaction[7]. This indicates that propylene does not form by $C_3H_8 = C_3H_6 + H_2$. On the other hand, $C_3H_7 + O_2 = C_3H_6 + HO_2$ is an entirely feasible reaction.

(3) Methanol, acetaldehyde and formaldehyde are formed. These compounds are logical intermediates in the passage from propane to carbon monoxide, carbon dioxide and water.

(4) Liquid products are found, but the gas phase is not saturated with any of the observed components.

On the basis of the above findings, a study of the oxidation mechanism of acetaldehyde was undertaken on the same apparatus. It is believed that the steps involved in the oxidation of acetaldehyde may be key reactions in the oxidation of hydrocarbons and that information gained from this investigation will throw additional light on the problems raised by the complexity of the propane data.

Mechanisms of the Oxidation of Acetaldehyde

The data given in Table 2 show the reaction products of the oxidation of acetaldehyde at elevated temperatures of the same order as in Table 1. Points of interest are the appearance of methanol as a major product in the oxidation both of propane and acetaldehyde, and the greater ease of oxidation of acetaldehyde, especially at lower temperatures. The rough equivalence between $(CH_4 + 2C_2H_6)$ and CO between 300° and 450°C suggests the occurrence of reactions (1a), (2) and (3). This pyrolysis of acetaldehyde is oxygen-induced (as by reaction (4)). Run 119, in the absence of oxygen, shows no reaction. In addition, the work of Letort[8, 9] strongly supports a chain mechanism for the oxygen-induced pyrolysis of acetaldehyde.

$$CH_3CHO + R = CH_3CO + RH \quad (1)$$

$$CH_3CO = CH_3 + CO \quad (2)$$

$$CH_3CHO + CH_3 = CH_3CO + CH_4 \quad (1a)$$

$$CH_3 + CH_3 = C_2H_6 \quad (3)$$

$$CH_3 + CH_3CO = CH_3COCH_3 . \quad (3a)$$

The formation of CH_3CO in preference to CH_2CHO is shown by data in Table 3. Acetic acid was formed in these experiments in a static system at room temperature. This acid is not likely to form by oxidation of CH_2CHO, but rather from CH_3CO through the intermediate of per-

TABLE 1. MASS SPECTROMETRIC ANALYSIS OF PRODUCTS OF EARLY STAGES OF OXIDATION OF PROPANE

Run	28	31	32	48	46	45	42	50	51	52	56	58	63	59	61	62	66	6
Temperature, °C	375	390	410	345	360	375	390	410	420	450	345	360	375	390	420	450	475	375
Contact time, sec	3.79	3.68	3.60	3.98	4.01*	3.84*	3.81*	3.64*	3.51*	3.38*	3.92	4.11*	3.32*	4.06*	3.70*	3.42	2.75*	3.08
Per cent O_2, orig.	8.3	7.6	7.6	13.1	13.1	13.1	13.1	13.1	13.1	13.1	24.6	24.6	24.6	24.6	24.6	24.6	24.6	51.6
Mol ratio, final/initial	1.00	1.008	1.018	0.99	0.962	0.952	0.952	0.971	1.006	1.023	1.015	0.896	0.90	0.884	0.926	0.995	0.99	0.769
C_3H_8 orig., cc STP	77.8	78.0	78.6	72.6	73.1	73.0	72.6	71.8	73.2	72.6	64.4	64.5	63.0	64.6	63.4	63.8	63.4	39.6
O_2 orig., cc STP	7.04	6.41	6.47	11.1	11.2	11.2	11.1	11.0	11.2	11.2	21.2	21.2	20.7	21.3	20.8	20.9	20.8	42.3
C_3H_8 cons., cc STP	0.6	0.6*	−0.4	1.6	6.1	7.5	6.2	5.2	1.8	1.6	0.0	9.60	9.0	12.5	9.65	4.70	5.90	14.9
O_2 cons., cc STP	0.5	0.1*	0.1	−0.5	10.7	10.7	9.6	5.7	2.3	0.2	−0.4	18.8	16.4	18.8	11.10	2.47	2.55	13.6
Per cent of products in end gas, corrected for mol change																		
C_3H_6	0.4	0.29	0.64	0.0	3.41	4.11	4.72	4.04	2.18	1.71	0.15	5.78	5.52	6.59	6.42	3.39	4.62	3.37
C_2H_6	.1	.47	.16	.0	.08	.08	.0	.0	.13	.0	.0	.0	.0	.0	.0	.0	.0	.0
C_2H_4	.40	.0	.0	.0	.67	.0	.0	.59	.41	.18	.0	1.35	1.29	1.99	1.53	.51	.74	.25
CH_4	.01	.01	.0	.0	.59	.56	.19	.07	.01	.03	.0	.33	.40	.37	.16	.02	.07	.17
CO	.1	.01	.0	.0	5.72	6.59	3.41	1.58	.60	.46	.15	9.46	7.79	9.3	4.67	.92	1.11	4.92
H_2	.02	.01	.0	.0	.44	.34	.21	.10	.02	.03	.0	.44	.41	.32	.27	.04	.16	.17
CO_2	.1	.08	.08	.03	.33	.25	.09	.0	.28	.01	.02	.79	.64	.84	.60	.09	.10	.90
$CH_3CH(OCH_3)_2$	—	—	—	.01	.05	.05	.08	.02	.0	.0	.0	.0	.0	.0	.0	.0	.01	—
$CH_2(OCH_3)_2$	—	—	—	.0	.0	.0	.0	.22	.0	.0	.0	.0	.0	.0	.0	.0	.0	—
C_2H_5CHO	.01	.02	.02	.01	.14	.06	.20	.13	.07	.05	.01	.32	.32	.41	.28	.10	.12	
CH_3CHO	.01	.05	.0	.01	.09	.55	.57	.49	.08	.03	.04	.18	.27	.27	.73	.15	.12	
HCHO	.08	.09	.03	.00	.23	.19	.16	.09	.15	.02	.05	.11	.14	.15	.14	.09	.14	
CH_3COCH_3	.01	—	.01	.0	.0	.0	.0	.0	.0	.0	.0	.01	.0	.0	.0	.0	.0	
$(CH_3)_2CHOH$	.01	.01	.0	.01	.07	.05	.04	.02	.01	.0	.01	.09	.09	.08	.34	.01	.01	About 4.37
CH_3CH_2OH	.01	.01	.01	.01	.08	.08	.18	.03	.02	.02	.01	.14	.09	.17	.06	.02	.03	
CH_3OH	.07	.03	.03	.01	1.67	2.07	1.61	.51	.21	.07	.03	2.63	2.33	2.33	1.04	.18	.20	
H_2O	.31	.34	.46	.11	1.81	1.83	2.64	1.64	1.85	1.77	.26	1.39	1.37	2.12	1.71	2.23	1.80	

* Maximum contact time. Liquid products were obtained but not measured.

TABLE 2. PRODUCTS OF EARLY STAGES OF OXIDATION OF ACETALDEHYDE AT ELEVATED TEMPERATURES

Run	147*	154	153	150*	151	156	161	162	157	101	104	113	160	171	114	163	115	119	166
Temperature, °C	135	150	178	200	226	250	275	300	325	375	375	375	375	375	390	420	420	420	450
Contact time, sec	2.23	2.22	2.09	2.07	1.92	1.79	1.65	1.55	1.41	3.68	3.67	3.01	1.31	1.28	2.87	1.19	2.79	2.68	1.14
Per cent O_2 orig.	3.01	4.07	3.87	3.90	4.00	2.9	2.91	2.36	3.16	2.05	4.07	2.15	3.24	3.33	2.03	2.44	2.31	0.0	2.75
Mol ratio, final/initial	0.980	0.996	0.982	1.01	0.959	0.968	1.014	1.033	1.08	1.11	1.13	1.09	1.10	1.10	1.13	1.15	1.15	1.02	1.23
CH_3CHO orig., cc STP	79.4	84.7	84.5	81.8	83.2	85.0	86.0	84.7	85.0	84.4	88.4	84.8	83.2	84.2	86.6	84.7	85.4	85.5	85.6
O_2 orig., cc STP	2.91	3.62	3.4	3.32	3.47	2.54	2.58	2.05	2.77	1.73	3.76	1.85	2.79	2.90	1.80	2.12	2.02	0.0	2.42
CH_3CHO cons.	0.60	0.9	2.5	0.6	1.55	2.80	—†	7.54	18.6	12.5	19.5	12.3	21.5	15.8	12.2	16.3	14.2	—	20.0
O_2 cons.	2.91	3.62	3.4	3.32	3.47	2.54	—	2.05	2.77	1.73	3.76	1.85	2.79	2.9	1.80	2.12	2.02	—	2.42
Per cent products in end gas, corrected for mol change																			
$CH_3CH(OCH_3)_2$	0.0	0.0	0.0	0.1	0.0	0.0	0.0	0.0	0.0	0.3	0.5	0.3	0.0	0.0	0.2	0.1	0.2	—	0.0
CH_3COCH_3 or CH_3CH_2CHO	.0	.0	.0	.0	.0	.0	.0	.0	.0	—	.2	—	.0	.1	.1	.2	.2	—	.0
CH_3COOH	1.1	3.9	4.0	.1	.1	.0	.0	.1	.3	—	.1	—	.1	.0	—	.0	—	0.1	.0
C_2H_6	.0	.0	.0	.2	.0	.0	—	.3	1.5	.7	.9	.6	1.5	1.3	.7	.9	.8	—	1.6
CH_3OH	.1	.0	.1	.4	.1	.3	.5	.8	2.1	.4	1.2	.3	2.7	2.0	.8	1.4	.8	—	1.23
HCHO	.0	.0	.0	.0	.0	.0	.0	.0	.0	.0	.0	.0	.0	.0	.0	.1	.0	.0	.0
CH_4	.1	.2	.3	1.2	.1	.4	2.1	5.4	12.6	11.7	14.9	9.9	14.0	13.2	10.7	13.8	13.9	—	21.2
CO	.0	.0	.0	3.5	.9	1.5	4.2	6.7	14.7	14.5	18.5	11.1	18.4	17.0	13.5	18.9	17.1	—	24.1
CO_2	.0	.6	.5	.7	.3	.4	—	.9	1.2	—	.8	—	1.1	.8	.6	.6	.5	—	.0
H_2O	.6	.1	.1	.1	.1	.1	.0	.1	.0	.2	.2	3.1	.0	.1	.7	.1	.6	.1	.1
H_2	.0	.0	.0	.0	.1	.0	.1	.0	.0	—	.5	—	.0	.0	—	.0	—	—	.0
CO/CH_3CHO cons.	—	.0	.0	—	.48	.48	—	.77	.69	1.0	.92	.77	.73	—	1.10	1.00	1.04	—	1.06
$(CH_4 + 2\ C_2H_6)/CO$	—	—	—/	—	.11	.25	—	.85	1.06	.90	.90	.99	.92	.94	.89	.78	.91	—	.95
$(CH_4 + 2\ C_2H_6)/CH_3CHO$ cons.	—	.20	.10	—	.05	.12	—	.69	.74	.90	.83	.77	.68	.91	.87	.77	.95	—	1.07
CH_3OH/CH_3CHO cons.	—	.0	.04	—	.05	.09	—	.10	.10	.03	.06	.02	.11	.11	.06	.07	.05	—	.05
Mass balance, final/initial																			
C	—	1.04	1.02	—	0.99	0.98	—	0.99	0.97	1.00	0.99	0.97	0.95	1.00	1.01	1.00	1.01	1.02	1.02
H	—	1.03	1.02	—	.99	.98	—	.98	.97	.99	.98	.99	.94	1.00	1.00	.99	1.00	1.01	1.05
O	—	.99	.99	—	.92	.94	—	.96	.93	.99	1.01	.86	.92	.97	1.03	.98	1.03	1.00	.97

* Liquid products observed.

† (—) = not determined.

acetic acid or the peracetyl radical. The absence of peracetic acid and of peroxy compounds in all mass spectrometric analyses reported here is explained by the demonstrated inability of the analytical procedure to detect added quantities of these compounds.

The existence of peracetic acid as an intermediate finds support in the literature. Swern[10] has reported that peracetic acid has been obtained by reaction of oxygen with both liquid and gaseous acetaldehyde and that under suitable conditions, peracetic acid and acetaldehyde react violently between 90° and 140°C. Reaction (4) is proposed by them and confirmed by their results.

Except for propionaldehyde, whose presence is very uncertain, the data in Tables 2 and 3 show no products that must be derived from CH_2CHO. In particular, there are no products with oxygen on both carbons. Furthermore, Brinton and Blacet[13] have shown by mass spectrometric studies of normal and deuterated acetaldehyde that the aldehyde C—H bond is the weakest C—H in acetaldehyde.

The data in Table 2 show that CH_3COOH

Table 3. Products of the Oxidation of Acetaldehyde at Room Temperature

Run	127	131	128	129	136	130
Per cent O_2, orig	22.9	22.9	22.5	22.3	22.0	22.7
Starting pressure, mm Hg	715	716	729	714	746	713
Pressure, 120 min later, mm Hg	—	614	547	534	742	616
Bulb diameter, cm	3.2	3.2	4.2	6.0	6.0	8.3
Mercury in bulb	—	—	—	—	+	—
Gaseous products, per cent						
$(CH_3CHO)_3$	0.5	1.1	0.0	0.3		
CH_3CHO	51.4	58.2	70.4	44.3		
CH_3COOH	.0	.0	9.8	23.4		
CO_2	2.4	.0	9.8	14.5		
H_2O	3.8	3.0	7.2	15.6		
O_2	41.9	37.7	2.7	1.9		
Liquid products, per cent						
$(CH_3CHO)_3$		18.8	0.3	0.9		
CH_3CHO		66.2	4.8	1.8		
CH_3COOH		.0	74.1	73.4		
H_2O		15.0	20.7	23.8		

to form acetic acid. Bawn and Williamson[11] have shown that the addition of peracetic acid to acetaldehyde-oxygen eliminates the induction period. In our experiments, the presence of peroxy compounds was demonstrated by the liberation by the reacting gases of iodine from potassium iodide, and the ability of mercury to prevent oxidation (Table 3, run 136). This effect of mercury was also observed in a 4.2 cm bulb.

The initiation reaction may well be

$$CH_3CHO + O_2 = CH_3CO + HO_2 . \quad (4)$$

McDowell and Thomas[12] have studied the kinetics of the initiation reaction for the oxidation of acetaldehyde in the gas phase at temperatures (implying CH_3COOOH as a precursor) disappears as an early oxidative product of CH_3CHO, and CH_4 and CO appear around 200°C. This indicates the relative instability of CH_3CO near 200°C and above, in agreement with other observations[14, 15, 16].

At elevated temperature (300° to 450°C approximately), oxidation of acetaldehyde becomes essentially the oxidation of CH_3 to CH_3OH. Raley et al.[17] studied the oxidation of CH_3 radicals produced by the thermal decomposition of di-*t*-butyl peroxide. The oxidation products contained more than 50 per cent CH_3OH and 25 per cent CO, as well as HCOOH, HCHO and CO_2. Raley suggests the following mechanism for the

oxidation of CH_3 to CH_3OH:

$$2CH_3O_2 = 2CH_3O + O_2$$
$$2CH_3O = CH_3OH + HCHO$$
$$CH_3O + HCHO = CH_3OH + HCO$$
$$CH_3O + HCO = CH_3OH + CO.$$

A similar mechanism may be suggested for the oxidation of CH_3 in the presence of excess CH_3CHO:

$$CH_3 + O_2 = CH_3OO \quad (5)$$
$$CH_3OO + CH_3CHO = CH_3OH + CH_3O + CO \quad (6)$$
or
$$= CH_3OOH + CH_3CO \quad (6a)$$
$$CH_3OOH + CH_3CHO = CH_3O + H_2O + CH_3CO \quad (7)$$
$$CH_3O + CH_3CHO = CH_3OH + CH_3CO \quad (8)$$
$$CH_3O + O_2 = CO + H_2O + OH. \quad (9)$$

It is recognized that rate studies in support of reactions (1–9) are lacking and that the reactions listed are not necessarily all-inclusive.

The above mechanism does not explain the liquid products formed during the oxidation of CH_3CHO at elevated temperatures. Mass spectrometric analyses revealed largely CH_3CHO and CH_3OH, but neither of these compounds nor any other gas component was present at 100 per cent saturation. Infrared spectra of this liquid closely match that of a 50/50 mix of liquid CH_3CHO and CH_3OH and differ from those of either compound alone. Heat is evolved on mixing liquid CH_3CHO and CH_3OH. Mixing gaseous CH_3CHO and CH_3OH results in a fairly quick pressure drop and liquid formation. These observations, with the fact that the diacetal of CH_3OH and CH_3CHO is not present in the gas at 100-per cent saturation, indicate that the liquid product is the hemiacetal of CH_3CHO and CH_3OH. The marked pressure drop observed upon mixing alcohol and acetaldehyde justifies reevaluation of the recent initiation rate studies of the oxidation of CH_3CHO by Farmer and McDowell[18]. These studies are based on the inhibition of acetaldehyde oxidation by alcohols but instead may conceivably be a composite observation of oxidation and hemiacetal formation.

SUMMARY (ACETALDEHYDE OXIDATION)

Studies of the early oxidation products of acetaldehyde show that:

(1) Acetaldehyde is very rapidly attacked under conditions where propane was oxidized (compare Tables 1 and 2);

(2) Rapid pyrolysis of acetaldehyde accompanies its oxidation, with product ratio (CH_4 + little C_2H_6)/CO $\sim$ 1;

(3) The attack on the acetaldehyde molecule generally begins at the aldehydic C—H bond;

(4) Methanol is the major stable oxyhydrocarbon product of the oxidation of acetaldehyde and propane;

(5) Liquid hemiacetal of methanol and acetaldehyde is a by-product of the oxidation and forms from gaseous reactants.

Acknowledgments

The author wishes to thank Drs. B. Lewis and G. von Elbe for suggesting the problem and for suggestions received during the course of the work, and Dr. A. S. Gordon for his help and close association with the study of propane oxidation.

REFERENCES

1. Gordon, A. S., and Heimel, S.: J. Am. Chem. Soc., *73*, 2942 (1951).
2. Pease, R. N.: J. Am. Chem. Soc., *51*, 1839 (1929).
3. Pease, R. N.: J. Am. Chem. Soc., *60*, 2244 (1938).
4. Newitt, D. M., and Thornes, L. S.: J. Chem. Soc., 1669 (1937).
5. Steacie, E. W. R., and Plewes, A. C.: Proc. Roy. Soc. (London), *A146*, 583 (1934).
6. Kooijman, P. L.: Rec. des trav. chim., *66*, 5 (1947).
7. Lewis, B., and von Elbe, G.: *Combustion, Flames and Explosions of Gases*, pp. 49, 53. New York, Academic Press, 1951.
8. Letort, M.: Compt. rend., *197*, 1042 (1933).
9. Letort, M.: J. Chem. Phys., *34*, 428 (1937).
10. Swern, D.: Chem. Rev., *45*, 6 (August 1949).
11. Bawn, C. E. H., and Williamson, J. B.: Trans. Faraday Soc., *47*, 735 (1951).
12. McDowell, C. A., and Thomas, J. H.: J. Chem. Soc., 1462 (1950).
13. Brinton, R. K., and Blacet, F. E.: J. Chem. Phys., *17*, 797 (1949).
14. Pitts, J. N., Jr., and Blacet, F. E.: J. Am. Chem. Soc., *74*, 455 (1952).
15. McDowell, C. A., and Thomas, J. H.: J. Chem. Soc., 2217 (1949).
16. Bawn, C. E. H., and McDowell, C. A.: Trans. Faraday Soc., *34*, 608 (1938).
17. Raley, J. H., Porter, L. M., Rust, F. F., and Vaughan, W. E.: J. Am. Chem. Soc., *73*, 15 (1951).
18. Farmer, J. B., and McDowell, C. A.: Trans. Faraday Soc., *48*, 624 (1952).

42

THE KINETICS OF THE THERMAL AND PHOTOCHEMICAL OXIDATION OF ACETALDEHYDE

By C. A. McDOWELL AND J. B. FARMER

Introduction

Acetaldehyde is one of the most easily oxidizable compounds known and it is an important product of the oxidation of many hydrocarbons. The induction periods of some gas phase oxidations have been found to be reduced by the addition of acetaldehyde. A recent example is the observation[1] that the induction period preceding the onset of cool flames in the butanone oxidation is greatly reduced by the addition of a small quantity of acetaldehyde. Furthermore, Norrish[2] has maintained that acetaldehyde and other aldehydes are essential intermediates in the oxidation of hydrocarbons, and that the formaldehyde which is produced during the high temperature oxidation of the higher hydrocarbons arises by the oxidative degradation of other aldehydes. Thus it is obviously important that the mechanism of the oxidation of acetaldehyde be thoroughly understood and in this paper we shall outline the relevant experimental facts known about this reaction, and we shall propose a kinetic mechanism which is in harmony with the facts and which offers some explanation of the various observations.

Early work on the oxidation of acetaldehyde at temperatures between 60° and 90° by Bodenstein[3] was alleged to show that the rate of the oxidation was approximately proportional to the square of the acetaldehyde concentration, and that the reaction was retarded by increasing the oxygen concentration. Later workers have[4, 5, 6], however, all found that the rate in the temperature region up to 120° is approximately proportional to the square of the aldehyde concentration, and independent of the oxygen concentration.

The main product of the oxidation has been shown to be peracetic acid, and it has been shown that in the early stages of the reaction the rate of consumption of oxygen is equal to the rate of production of peroxide. In this region acetic acid is produced but only small amounts of carbon monoxide and carbon dioxide. It also appears that a small quantity of hydrogen peroxide may be formed.

It has been found that the reaction is inhibited by small quantities of nitrogen peroxide[7], by alcohols[4, 8], and by hydrocarbons[9]. Kinetic studies of the nitrogen peroxide inhibition[7] show that the oxidation is initiated by a bimolecular reaction which has been written as;

$$CH_3CHO + O_2 = CH_3CO + HO_2 \quad (1)$$

The kinetics of the alcohol retarded oxidation[8] are most readily understood if it is assumed that the retarding step is

$$CH_3CO_3 + ROH = CH_3CO_3H + R'OH$$

The early stages of the oxidation undoubtedly seem to be;

$$CH_3CHO + O_2 = CH_3CO + HO_2 \quad (1)$$

$$CH_3CO + O_2 = CH_3CO_3 \quad (2)$$

$$CH_3CO_3 + CH_3CHO = CH_3CO_3H + CH_3CO \quad (3)$$

These steps account satisfactorily for the formation of the main product peracetic acid, and it is also easy to explain the occurrence of the other products of the reaction; but so far there has been no satisfactory complete mechanism which besides suggesting feasible routes for the formation of the various products, at the same time yields a resulting kinetic equation which is in agreement with the experimental observations. The difficulty originally seemed to reside in the lack of a satisfactory terminating step which besides being inherently feasible would also yield a correct kinetic expression. The original one suggested, though giving a correct form of the kinetic equation, was an inherently unsatisfactory process.

Some idea of the correct form of the actual termination step can be obtained from a kinetic study of the photochemical gas phase oxidation of acetaldehyde. Many years ago this photochemical reaction was studied by a flow method by Bowen and Tietz[10], and later in a static system by Carruthers and Norrish[11]. Bowen and Tietz found that the rate of reaction at about 20°C was directly proportional to the aldehyde concentration, and independent of the oxygen concentration. The rate was found to be dependent on the square root of the light intensity. More re-

cently we have restudied the photochemical oxidation of acetaldehyde in a static system between 18° and 30°C using modern photochemical techniques with a view to establishing the kinetics of this reaction.

Experimental

Acetaldehyde was prepared by the depolymerization of paraldehyde with phosphoric acid. The freshly generated aldehyde was distilled through a twenty-plate column in an atmosphere of nitrogen, collected at −80°C, and then subjected to bulb to bulb distillation to free it from gas. It was finally distilled into darkened vials and these then sealed. Oxygen was purified by condensing the cylinder product in a trap cooled

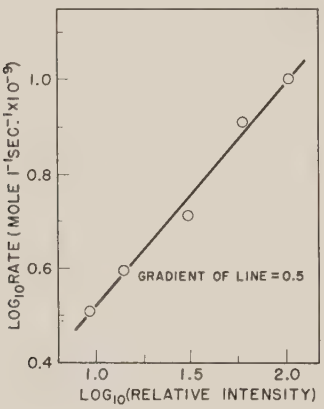

FIG. 1. Variation of rate with intensity.

in liquid nitrogen, and allowing the liquid oxygen to evaporate slowly into the gas reservoir.

The mercury arc was supplied with power from an electronic stabilized power pack similar in design to that described by McCrea and LeRoy[12] although it contained several extra 6L6 valves. The voltage from this power pack had a short term stability of about one part in fifteen thousand.

Liquid filters were used to isolate the 3130 Å line of the mercury spectrum. The amount of radiation absorbed was measured by an electronic photometer unit utilizing a QVA39 quartz photocell as a light detector.

The quartz vessel had optical flat ends and was housed in a block aluminum furnace, the temperature of which could be accurately controlled. The gases were metered into the vessel by means of a very sensitive Pyrex Bourdon gauge. The rate of the reaction was determined by estimating the amount of peracetic acid formed in a known time. The peracetic acid was determined by the ferrous thiocyanate method, a Spekker absorptiometer being used to assess the intensity of the color developed by the various peroxide-ferrous thiocyanate solutions.

Results

Here we shall only give the experimental results in summary as limitations of space prevent their extensive discussion.

(1) The dependency of the rate of oxidation on the light intensity was studied over a tenfold variation of intensity for a mixture of 100 mm Hg of acetaldehyde, and 5 mm Hg of oxygen. It was found that the rate was accurately proportional to the square root of the light intensity (Fig. 1).

(2) The dependency of the rate of oxidation on the aldehyde pressure was studied by maintaining the concentration of oxygen constant at 5 mm Hg and varying the pressure of the acetaldehyde from 25 mm Hg to 200 mm Hg. During these experiments the intensity of the light was maintained constant. As the aldehyde pressure is varied the amount of radiation also varies and this was, of course, taken into consideration in calculating the reaction rate back to a constant rate of light absorption. It was found that over this tenfold variation of the concentration of the acetaldehyde, the rate of oxidation was accurately proportional to the concentration of the aldehyde. A plot of the logarithm of the rate against the logarithm of the acetaldehyde concentration gave a straight line of slope 1.1 (Fig. 2)

(3) The dependency of the rate of oxidation on the oxygen pressure was studied in a system in which the light intensity was maintained constant, and the acetaldehyde pressure kept at 100 mm Hg. The oxygen pressure was varied between 5 mm and 150 mm and it was found that the rate of oxidation was practically constant over this thirty-fold variation of the oxygen pressure (see Table 1).

The above experimental results indicate that the low temperature photochemical gas phase oxidation of acetaldehyde is governed by the kinetic equation;

$$d[CH_3CO_3H]/dt = KI_a^{1/2}[CH_3CHO][O_2]^\circ$$

The Mechanism of the Photochemical Oxidation of Acetaldehyde

It has been shown[13] that when acetaldehyde absorbs radiation of wavelength 3130 Å the main

process occurring is

$$CH_3CHO + h\nu = CH_3 + HCO$$

This primary process is assumed to occur also in acetaldehyde-oxygen mixtures, and the subsequent stages of the oxidation are probably best regarded as occurring by the following steps:

$$\left.\begin{matrix} CH_3 + O_2 = \\ HCO + O_2 = \end{matrix}\right\} R$$

$$R + CH_3CHO = RH + CH_3CO \qquad \phi_2 I_a$$

$$CH_3CO + O_2 = CH_3CO_3 \qquad (2)$$

$$CH_3CO_3 + CH_3CHO = CH_3CO_3H + CH_3CO \qquad (3)$$

$$2CH_3CO = (CH_3CO)_2 \qquad (4)$$

$$CH_3CO + CH_3CO_3 = (CH_3CO)_2O_2 \qquad (5)$$

$$2CH_3CO_3 = (CH_3CO)_2O_2 + O_2 \qquad (6)$$

Since the rate of the photochemical oxidation is proportional to $I_a^{1/2}$ and it is independent of the oxygen pressure, it is probable that reaction (2) is rather fast and it is also likely that reactions (4) and (5) are negligible as compared with reaction (6). It will, therefore, be assumed that the main terminating reaction is that represented by equation (6). Applying the stationary state hypothesis to the above scheme, therefore, leads to the expression;

$$d[CH_3CO_3H]/dt = (k_3/k_6^{1/2})(\phi_2 I_a)^{1/2}[CH_3CHO]$$

which is in agreement with the experimentally determined kinetic law.

The above experimental results and their successful explanation by the given mechanism mean that one must consider a radical-radical interaction process as being the important terminating step in the low temperature oxidation of acetaldehyde.

The Mechanism of the Thermal Oxidation of Acetaldehyde

Earlier in this paper we have outlined experimental evidence which substantiates the view that the early stages in the thermal gas phase oxidation of acetaldehyde are;

$$CH_3CHO + O_2 = CH_3CO + HO_2 \qquad (1)$$

$$CH_3CO + O_2 = CH_3CO_3 \qquad (2)$$

$$CH_3CO_3 + CH_3CHO = CH_3CO_3H + CH_3CO \qquad (3)$$

It has further been pointed out that so far no satisfactory terminating steps have been given. The evidence from the photochemical oxidation studies is that radical-radical interaction is an important terminating step. The photochemical experiments were, however, carried out in the temperature range of 20°–30°C, and the gas phase oxidation results refer to experiments performed at temperatures of about 100°C. The rate of the thermal oxidation is high at about 100°C and it is, therefore, difficult to make accurate photochemical measurements at these temperatures. It has, however, been possible to study the thermal oxidation at temperatures as low as

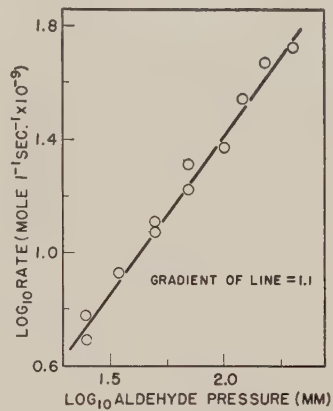

Fig. 2. Variation of rate with aldehyde pressure.

Table 1. Dependence of Rate on Oxygen Pressure

Relative intensity = 100 per cent; Aldehyde pressure = 100 mm

Oxygen Pressure	Time	Peracid × 10^6	Rate × 10^9
mm	*min*	*mole*	*mole* l^{-1} *sec*$^{-1}$
5	25	1.14	14.5
50	30	1.41	14.9
150	25	1.21	15.5

30°C by using a very sensitive Bourdon gauge to follow the progress of the reaction. It has been found that although a mixture of acetaldehyde and oxygen does not appear to undergo any appreciable reaction at about 30°C, it is nevertheless possible to cause them to react by illuminating the mixture for a short time with an intense source of ultraviolet light. There appears to be a certain critical period of illumination for a given intensity, but if the illumination is interrupted after this period the oxidation proceeds.

By studying the effect of varying the concentrations of the two reactants it was found that the rate of this induced thermal oxidation is proportional to the square of the acetaldehyde and

practically independent of the oxygen concentration. Thus it obeys the same kinetic law as that found at higher temperatures, i.e.,

$$-d[O_2]/dt = K[CH_3CHO]^2.$$

It would thus seem that there may be no great change in the mechanism in the two temperature ranges studied.

The fact that the oxidation at low temperatures had long induction periods which could be eliminated by irradiating the mixture with ultraviolet light points to the importance of the building up of some product which itself controls the subsequent oxidation. It would seem that this product is peracetic acid and that it controls the subsequent oxidation by acting as the initiator of chain branching. If this assumption is made and it is further assumed that the main chain terminating process is radical-radical interaction, as is indicated by the photochemical evidence, it then becomes possible to explain many of the features of this oxidation which were previously not completely understood.

The mechanism of the thermal oxidation is then completed by assuming the following two processes to occur:

$$CH_3CO_3H = CH_3CO_2 + OH \qquad (7)$$

$$2CH_3CO_3 = (CH_3CO)_2O_2 + O_2 \qquad (6)$$

Niclause[14] has recently independently outlined a similar scheme as an extension of the Bolland-Gee[15] mechanism in an effort to apply this latter mechanism to the thermal oxidation of acetaldehyde. The equation which he deduced is not in good agreement with the experimental observations. The reasons for this will become clear on reading the following paragraphs.

In equation (7) it is assumed that the peracid is decomposed by a first order mechanism and each of the two new radicals then start off new chains which eventually give CH_3CO_3 and CH_3CO. From the mechanism given above we have:

$$\begin{aligned} d[CH_3CO]/dt = {} & k_1[CH_3CHO][O_2] \\ & - k_2[CH_3CO][O_2] \\ & + k_3[CH_3CO_3][CH_3CHO] \\ & + k_7[CH_3CO_3H] \\ & = 0 \end{aligned} \qquad (8)$$

$$\begin{aligned} d[CH_3CO_3]/dt = {} & k_2[CH_3CO][O_2] \\ & - k_3[CH_3CO_3][CH_3CHO] \\ & - k_6[CH_3CO_3] = 0 \end{aligned} \qquad (9)$$

$$\begin{aligned} d[CH_3CO_3H]/dt = {} & k_3[CH_3CO_3][CH_3CHO] \\ & - k_7[CH_3CO_3H] \end{aligned} \qquad (10)$$

This last equation is not put equal to zero since it is assumed above that the peracid on reaching a critical concentration thenceforth completely determines the course of the subsequent oxidation. On solving equations (8) and (9) for CH_3CO_3 under these conditions and substituting in equation (10) we obtain the result;

$$\begin{aligned} & d[CH_3CO_3H]/dt \\ & = k_3(k_7/k_6)^{1/2}[CH_3CO_3H]^{1/2}[CH_3CHO] \\ & - k_7[CH_3CO_3H] \end{aligned} \qquad (11)$$

In deducing equation (11) it has been assumed in accordance with the statements made above that $k_7[CH_3CO_3H] > k_1[CH_3CHO][O_2]$. This equation on integration gives:

$$\begin{aligned} & [CH_3CO_3H]^{1/2} \\ & = k_3[CH_3CHO][1 - \exp(-k_7t/2)]/(k_7k_6)^{1/2} \end{aligned} \qquad (12)$$

In this reaction the rate of consumption of oxygen equals the rate of formation of peroxide then;

$$-d[O_2]/dt = k_3[CH_3CO_3][CH_3CHO] \qquad (13)$$

When reaction (7) becomes the main initiating step the rate of oxidation will be given by the equation;

$$\begin{aligned} & -d[O_2]/dt \\ & = k_3(k_7/k_6)^{1/2}[CH_3CO_3H]^{1/2}[CH_3CHO]. \end{aligned} \qquad (14)$$

On substituting the value of $[CH_3CO_3H]^{1/2}$ given by equation (12) there results the following expression (15);

$$\begin{aligned} & -d[O_2]/dt \\ & = k_3^2[CH_3CHO]^2[1 - \exp(-k_7t/2)]/k_6. \end{aligned} \qquad (15)$$

Since the critical concentration of peracid is soon established it is readily seen that the maximum rate given by equation (15) is;

$$-d[O_2]/dt = k_3^2[CH_3CHO]^2/k_6. \qquad (16)$$

Other workers[16] have made the same approximation involved in deducing equation (16) from equation (15) for the case of hydrocarbon oxidation and it is not always clear that such assumptions are justified in all cases. For the reaction

under discussion it is possible to satisfy oneself that the approximation is a fairly reasonable one. This can be done by noting that after a certain time the rate of the reaction will tend to a constant value because of the exponential term. It will be convenient to assume that when the exponential term is only about 10 per cent of its original value the rate of the reaction will not increase much with time. Since e^{-2} equals 0.1353, it follows that we can take $k_7 t/2 = 2$. For these conditions to be reached in a time of 10^3 seconds, k_7 must be approximately 4×10^{-3} second^{-1}. This is a reasonable value for the velocity constant for the decomposition of a compound like peracetic acid at 100°C, so in this case it would seem that the approximation used in reducing equation (15) to the form given by equation (16) is justified. It is to be noted that a high rate of initiation by peroxide decomposition such as might be experienced with the above value of k_7 would imply that the chain length may become rather short irrespective of the fact that it might have been long during the initial stages of the oxidation. This could well be the explanation of the fact that the chain length of the thermal oxidation of acetaldehyde has been found to be rather short[7, 8].

Equation (16) is in agreement with the kinetic law established by the experimental results described above. It must, therefore, be acknowledged that the kinetics of the thermal oxidation of acetaldehyde can only be understood if it is admitted that some of the peracid formed can decompose to cause chain branching. It is necessary also to assume, as one must from the photochemical evidence, that the main chain terminating reaction is due to radical-radical interaction.

The conclusions which we have reached are in agreement with those of Semenoff[17]. In discussing the oxidation of acetaldehyde Semenoff mentions that in distinction to all other autoxidations, except that of acetylene, in this case after an initial slow period, the rate of oxidation remains very constant despite the consumption of reactants. He shows that if it is assumed that during the initial stage of the reaction a product is formed which itself can act as a chain branching agent, and if the chains are terminated by mutual interaction, it is then possible that under certain conditions the rate of oxidation may remain constant throughout a large part of the reaction time. This happens because the chain branching process becomes a more efficient way of forming new chains than the original initiating reaction. Also it is readily shown that the equations giving the rate of reaction as a function of time soon approximate to a constant which is the ratio of two terms, one depending on chain branching and the other on chain termination. If both these quantities have the same dependency on the concentration of the reactants then under the experimental conditions then pertaining, the rate of the oxidation will be constant.

A further consequence is that if the critical concentration of the chain branching agent can be rapidly established, say by photochemical means, then on interrupting the irradiation the oxidation should proceed at a constant rate. This we have found to be the case as has been noted above. It is concluded that the present known experimental facts about the thermal oxidation of acetaldehyde can be satisfactorily explained by the mechanism outlined in the present paper.

REFERENCES

1. Bardwell, J., and Hinshelwood, C. N.: Proc. Roy. Soc., *A205*, 375 (1951).
2. Norrish, R. G. W.: Disc. Faraday Soc., *10*, 269 (1951).
3. Bodenstein, M.: Sitzber. preuss. Akad. Phys.-Math. Kl., *3*, 73 (1931).
4. Pease, R. N.: J. Am. Chem. Soc., *60*, 2753 (1933).
5. Hatcher, W. H., Steacie, E. W. R., and Howland, F.: Can. J. Research, *7*, 149 (1932).
6. McDowell, C. A., and Thomas, J. H.: J. Chem. Soc., 2208 (1949).
7. McDowell, C. A., and Thomas, J. H.: J. Chem. Soc., 1462 (1950).
8. McDowell, C. A., and Thomas, J. H.: J. Chem Soc., 2217 (1949); Farmer, J. B., and McDowell, C. A.: Trans. Faraday Soc., *48*, 624 (1952).
9. Small, J., and Ubbelohde, A. R.: J. Chem. Soc., 723 (1950).
10. Bowen, E. J., and Tietz, E. L.: J. Chem. Soc., 234 (1930).
11. Carruthers, J. L., and Norrish, R. G. W.: J. Chem Soc., 1036 (1936).
12. McCrea, J. M., and LeRoy, D. J: Rev. Sci. Inst., *19*, 692 (1948).
13. Blacet, F. E.: J. Phys. Chem., *52*, 534 (1948).
14. Niclause, M.: J. Chimie Physiq., *49*, 157 (1952).
15. Bolland, J. L., and Gee, G.: Trans. Faraday Soc., *42*, 236 (1946).
16. Cullis, C. F., and Hinshelwood, C. N.: Disc. Faraday Soc., *2*, 117 (1947).
17. Semenoff, N.: *Chemical Kinetics and Chain Reactions*. Oxford, 1935.

43

THE OXIDATION OF WEAK METHANE-AIR MIXTURES AT HIGH TEMPERATURES

By J. R. SIMONSON AND N. P. W. MOORE

(1) Introduction

The motored engine technique for studying hydrocarbon combustion processes has been used by Downs, Street, Walsh and Wheeler[1, 2] for investigating cool flame formation, and by Pastell et al.[3, 4] and Levedahl et al.[5] to study precombustion reactions and cool flame limits. Detailed analyses of exhaust products obtained by this method have been made by Pahnke, Cohen and Sturgis[6] and have been discussed in relation to the appearance of cool flames. In addition, Melby[7] has used the method to study the effect of fuel additives on the precombustion reactions of *n*-heptane. The experimental method is to introduce a fuel air mixture to a motored engine and observe the reaction while the compression ratio is slowly increased until auto-ignition occurs. In the present work, however, an engine of fixed compression ratio was used and the induced charge passed through a controlled electric heating system. The initial mixture temperature was therefore the experimental variable, and could be closely controlled during observation of the reactions. Closely related work on the oxidation of methane has been carried out by Burgoyne and Hirsch[8] using a heated tube, the temperature ranges are similar but pressures are very much lower (atmospheric as compared with approximately 30 atm in the present work) and residence time somewhat shorter. The ignition of methane when injected into a high temperature moving air stream has been studied by Mullins[9].

(2) Apparatus and Instrumentation

The work described in the present paper was carried out in a single cylinder engine of 14.7:1 compression ratio coupled directly to a swinging field dynamometer which could be used either as a motor or a generator. Constant engine speed was maintained irrespective of the methane input or charge temperature. Therefore, all results obtained showed the course of reaction for a constant residence time in the engine combustion chamber. Compression of the heated methane air mixture occupied 30 millisec (at 1000 rpm). The reactions occurring in the combustion chamber were due only to the temperature and pressure attained at the end of compression; there was no timed electric spark or injection of fuel oil to initiate the reaction. Pressure at the end of compression was determined from a balanced diaphragm peak pressure indicator, and the charge temperature was calculated from the measured temperature of the mixture in the inlet manifold, using variable specific heat data. An allowance was made for heat loss through the cylinder walls determined from cooling water flow and temperature rise measurements, adapted from a theoretical treatment by Pye[10]. Engine cooling water is pumped in a closed circuit from the jackets to a heat exchanger, and jacket temperatures may be closely controlled. Lubrication is by the dry sump system with accurate control of oil temperature.

During repeated engine cycles of compression and expansion measurements were recorded of cylinder pressure rise and light emission from the combustion reaction by means of cathode ray oscillograph equipment. A variable capacity type pressure pick-up was situated at the end of a short passage leading directly into the combustion chamber. A quartz window was held in a special plug screwed into the top of the combustion chamber and light emission was detected by means of a gas-filled photo cell. A time scale of engine rotation was derived from an electromagnetic pick-up situated close to a brass disc with steel inserts rotating with the engine flywheel. The three separate signals were fed to three cathode-ray tubes and were combined optically to be photographed simultaneously by a rotating drum camera. Calibration of cylinder pressure records was obtained from the independent measurement of peak pressure. Rates of pressure rise were calculated from the photographic traces.

As an alternative fitting to the photo cell, a separate optical system was built to focus an image of the quartz window of the combustion chamber on to the slit of a Hilger small Ramam Spectrograph (E 518) with quartz optics. Spectroscopic studies of the emission spectrum of the reactions have been made. In addition a rotating shutter device with a slit of variable width and

phase in relation to the piston top dead center position enabled spectrographic plates to be obtained of the light emission at different points in the course of the reaction. The cyclic regulárity of the reactions was found to be extremely good, enabling plates to be obtained of up to five hours exposure at one running condition.

A flow diagram of the input gas metering and exhaust analysis systems is shown in Figure 1. Air flow was measured by a sharp edged orifice and pulsations in flow were smoothed out by two flexible ended surge tanks in series. The metered air flow passed to the heater and into the inlet manifold. Gas was introduced at the throat of a mixing venturi arranged to give some 8 inches of the inlet manifold for complete mixing before admission to the combustion chamber. The charge temperature and also the manifold wall temperature were measured by copper-constantan thermocouples. The charge inlet pressure was also measured. The engine exhaust temperature was measured by a Chromel-Alumel thermocouple, and a sampling rake close to the engine was used to draw off exhaust gases for analysis. The gases were passed through infrared analysers for continuous analysis for methane and carbon monoxide or alternatively were compressed into evacuated alloy bottles for subsequent analysis for carbon dioxide. Separate samples were withdrawn close to the engine exhaust port by a water aspirator for formaldehyde analysis, by chemical methods. Commercial methane gas obtained in five hundred cubic foot cylinders was used for the work. The gas contained 86.6 per cent methane and only traces of other hydrocarbons, the remainder being nitrogen, oxygen and carbon dioxide. The gas was fed through two choked nozzles in parallel which could be used together or separately. The pressure and temperature upstream of the nozzle was recorded, and the flow

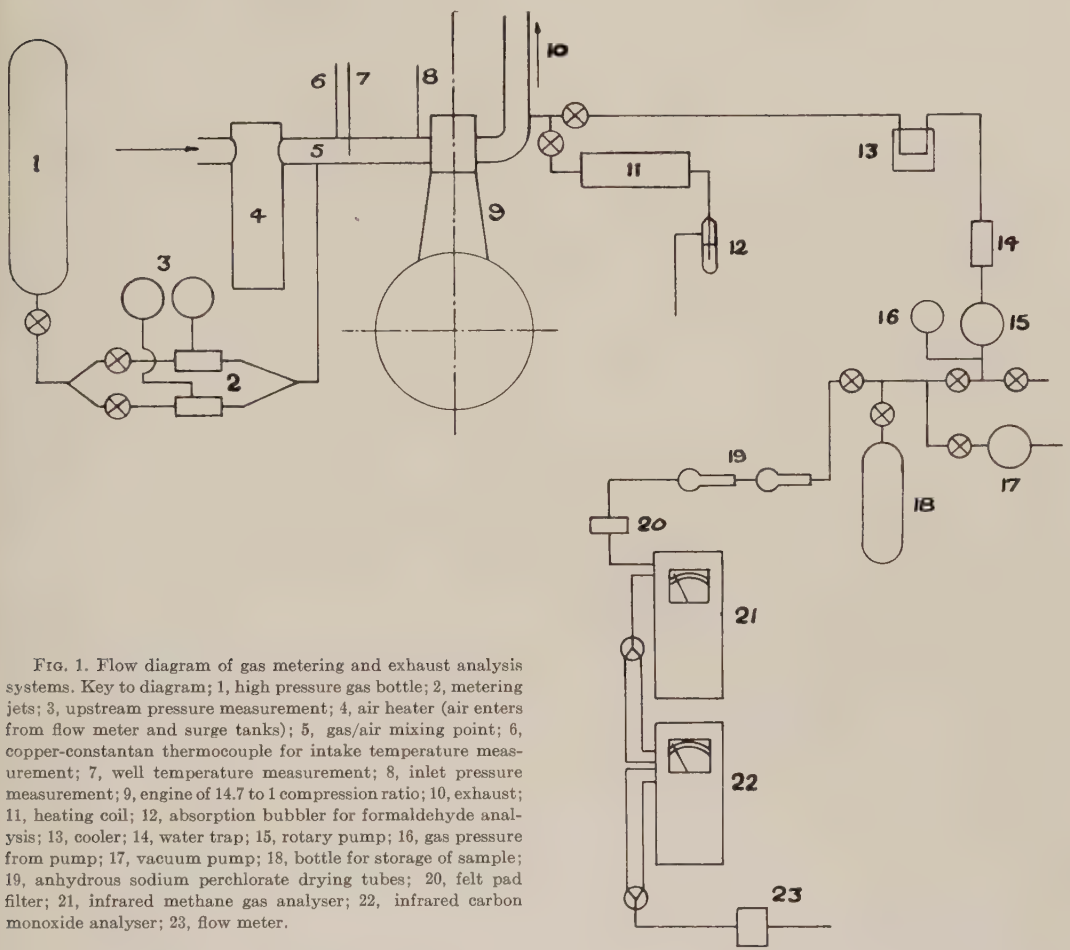

Fig. 1. Flow diagram of gas metering and exhaust analysis systems. Key to diagram; 1, high pressure gas bottle; 2, metering jets; 3, upstream pressure measurement; 4, air heater (air enters from flow meter and surge tanks); 5, gas/air mixing point; 6, copper-constantan thermocouple for intake temperature measurement; 7, well temperature measurement; 8, inlet pressure measurement; 9, engine of 14.7 to 1 compression ratio; 10, exhaust; 11, heating coil; 12, absorption bubbler for formaldehyde analysis; 13, cooler; 14, water trap; 15, rotary pump; 16, gas pressure from pump; 17, vacuum pump; 18, bottle for storage of sample; 19, anhydrous sodium perchlorate drying tubes; 20, felt pad filter; 21, infrared methane gas analyser; 22, infrared carbon monoxide analyser; 23, flow meter.

determined from experimental calibration formulae.

(3) Experimental Results

(3.1) CONSTANT CHARGE TEMPERATURE TESTS

Experiments were carried out at various constant inlet temperatures to give compression temperatures between 600° and 850°C. Methane was introduced into the hot air stream to give mixtures varying between 0.5 and 5.5 per cent

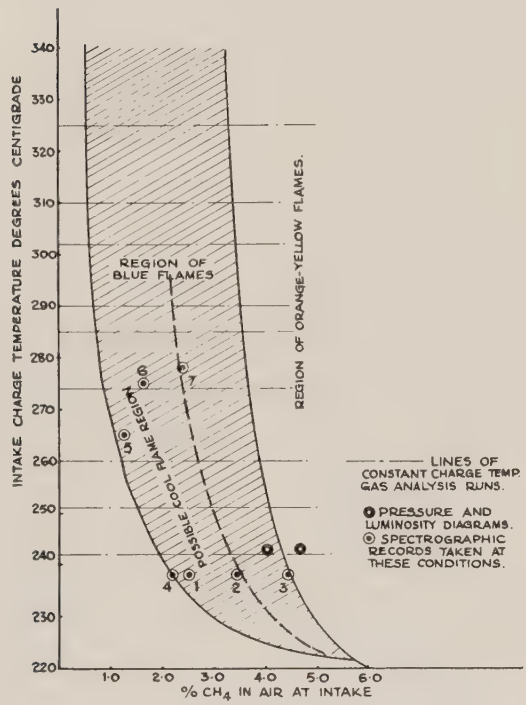

FIG. 2. Ignition boundaries for weak methane—air mixtures.

methane in air. The majority of the work was carried out at mixture strengths below 50 per cent stoichiometric. Engine speed was maintained constant at 1000 rpm, cooling water outlet temperature was 60°C and the oil temperature 40°C.

Pressure measurements were made at five different charge temperatures for variable concentrations of methane. Peak pressures were measured and rates of pressure rise were calculated. Analyses of exhaust gas products for methane and carbon monoxide were obtained for nine different charge temperatures. The appearance of separate blue and yellow flame regions was noted in the course of these experiments and the limits were plotted out in terms of the intake charge temperature and the methane concentration in the intake charge. These visible ignition boundaries are shown in Figure 2, and it can be seen that a blue flame is visible in a mixture of less than one per cent methane, at the highest temperatures. The blue flame region was broader at the higher temperatures, and narrowed off sharply at the lower temperature end, becoming very much less

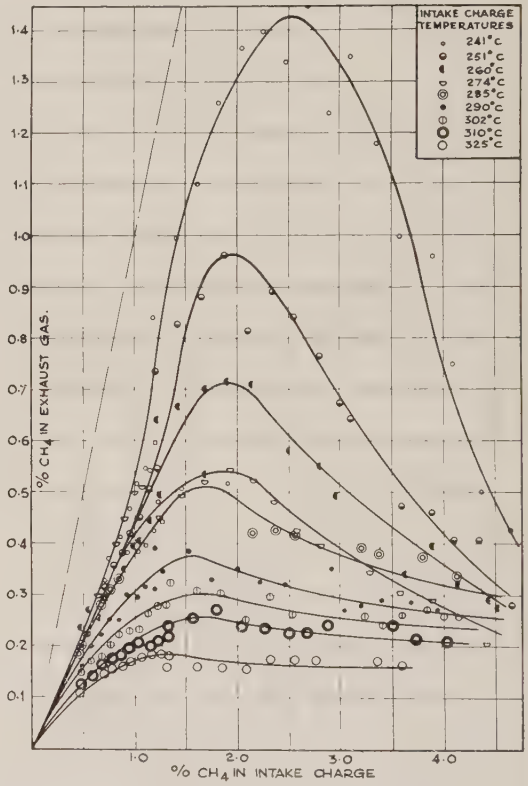

FIG. 3. Percentage methane in exhaust gas products for constant temperature intake conditions.

stable. There appeared to be no blue flame zone at mixture strengths greater than six per cent at the lower temperature conditions and in this region sudden and violent auto-ignition occurred. The inlet temperatures at which exhaust gas analyses have been carried out are shown and curves of percentage methane and carbon monoxide in the exhaust plotted against percentage methane in the inlet are given in Figures 3 and 4. The corresponding values for methane consumed as a percentage obtained from Figures 3 and 4 are plotted in Figure 5. In Figure 3 it can be seen that as the charge temperature increases the peak

in the corresponding methane curve moves towards the weaker end of the mixture strength range and occurs at very much smaller percentages of methane in the exhaust. The chain dotted line represents no methane reaction, i.e., percentage methane in the exhaust equals percentage methane in the intake, and as the charge temperature increases, the methane curves depart further from this line. The peaks in the carbon monoxide concentration in the exhaust also move to the weaker mixture regions as the charge temperature increases and the general width of the peak is much less at these temperatures. On the left hand side of the carbon monoxide peak slow reactions may be said to be predominating, whereas on the right hand side of the peak where carbon monoxide itself is disappearing the reaction is more definitely a true ignition. The range of mixture strength for slow reaction is much less wide at higher temperatures, and the carbon monoxide peaks occur just inside the lower blue flame boundary. The curves of exhaust gas products indicate substantially complete combustion at the yellow flame boundary, the percentage methane consumed increasing steadily at any given charge temperature as the mixture strength moves from the lower blue flame boundary towards the yellow flame boundary.

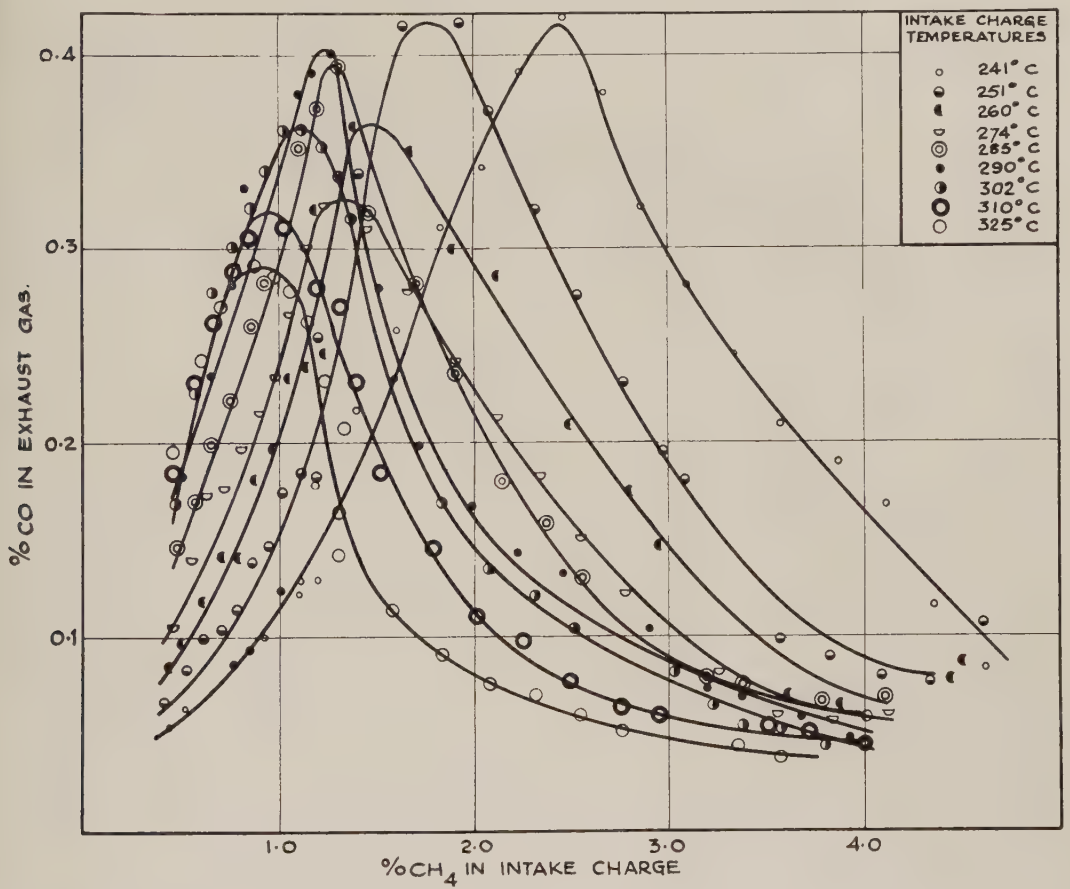

FIG. 4. Percentage carbon monoxide in exhaust gas products for constant temperature intake conditions.

Cylinder peak pressures and rates of pressure rise occurring during auto-ignition are shown plotted at constant charge temperatures for variable methane input concentrations in Figure 6. At the lowest charge temperatures, reaction occurs very late in the cycle and consequently the cylinder peak pressure equals the compression pressure until the mixture strength is sufficient to cause auto-ignition giving a peak pressure greater than the compression pressure. At the same time a measurable rate of pressure rise appears on the oscillograph record. It can be seen

that at 235°C intake temperature this occurs for a 3.5 per cent mixture. At these lower temperatures ignition also occurs very much earlier as the mixture strength is increased. At higher charge temperatures measurable rates of pressure rise and peak pressures greater than the compression occur at leaner methane mixture strengths.

On the ignition boundaries curve (Fig. 2) two points are shown at which typical pressure and luminosity diagrams were recorded. These are discussed in detail elsewhere[11].

Some consideration has been given to the rate of reaction following rapid compression.

In order to provide a basis for correlation it has been assumed that the reaction rate for the oxidation of lean mixtures can be expressed by the following relationship:

$$\frac{d(\mathrm{CH_4})}{dt} = -Ae^{-(E/RT)}\mathrm{O_2CH_4}$$

This assumes the reaction to be first order with respect to both methane concentration ($\mathrm{CH_4}$) and the oxygen concentration ($\mathrm{O_2}$).

Integration of the above expression under the assumption of T approximately constant gives:

$$\log_e \frac{(\mathrm{CH_4})_0}{(\mathrm{CH_4})_t} = +Ae^{-(E/RT)}(\mathrm{O_2})t$$

where $(\mathrm{CH_4})_0$ is the initial methane concentration and $(\mathrm{CH_4})_t$ is the concentration after time t. A is a constant, R the gas constant and E an energy of activation.

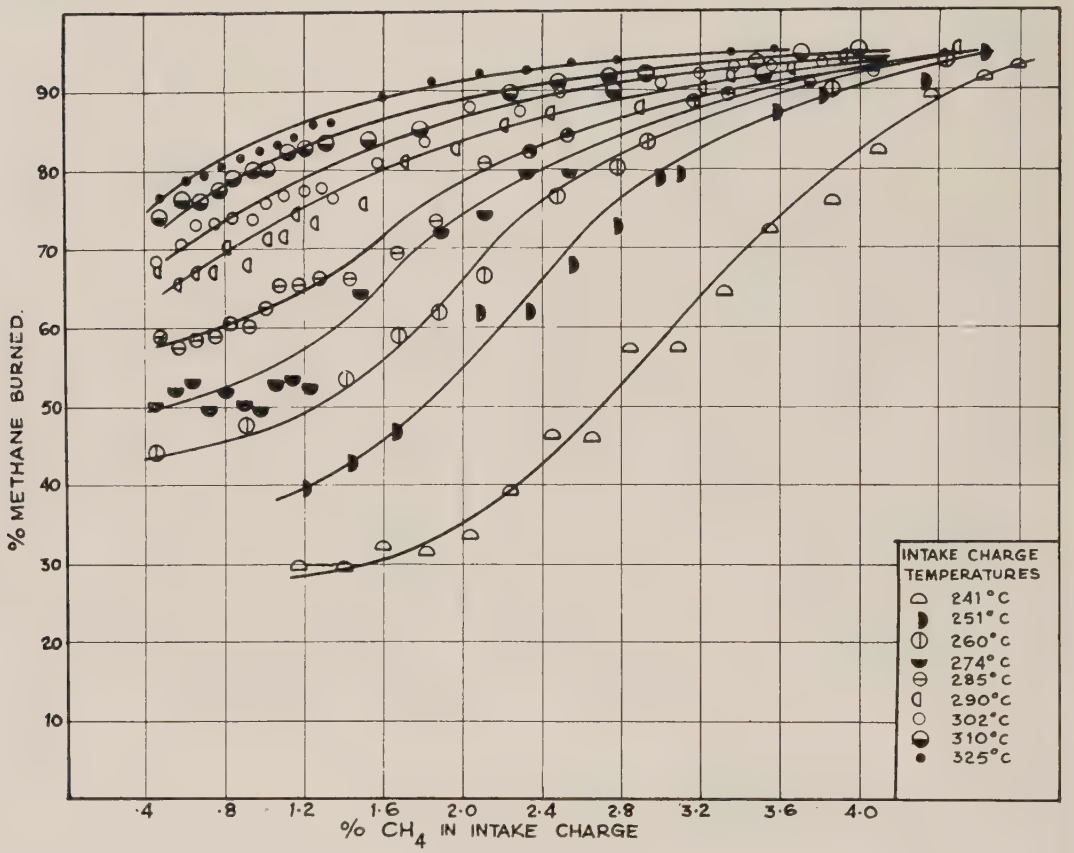

FIG. 5. Percentage methane consumed for constant temperature intake conditions.

The results of applying the above correlation to the present data are shown in Figure 7 in which $\log_{10} \log_e (\mathrm{CH_4})_0/(\mathrm{CH_4})_t$ is plotted to a base of the reciprocal of the absolute temperature at the end of adiabatic compression calculated as mentioned in Section 2. Experiments at 1.2, 2, and 3 per cent methane in air have been included. For comparison data have been included for slow reaction of a lean concentration of methane in air determined in a moving stream within a 10 inch diameter duct[12].

The form of correlation appears to be partially justified, in that over a range of temperature of some 100°C a linear relationship exists between

$1/T$ and $\log_{10} \log_e (CH_4)_0/(CH_4)_t$ indicating a constant value of E.

The possible derivation of activation energy data from a rapid compression experiment has been discussed by Jost[13] for the higher paraffins and benzine.

(3.2) SPECTROSCOPIC INVESTIGATIONS

Spectrographic plates have been obtained at points 1 to 7 shown in Figure 2. These are all in the blue region with the exception of plate 3 which is on the yellow boundary. All plates with the exception of plate 3 show bands of excited formaldehyde, identical with the Emeléus cool flame bands. In addition bands associated with a normal hydrocarbon ignition are present in varying intensity. Cool flame bands are strongest near the blue flame boundary and the HCO and OH bands become stronger as the yellow boundary is approached. In addition to the band systems present a background continuum of burning carbon monoxide is present throughout the blue ignition. A suggested cool flame region within the blue region is shown on the ignition boundary curves; this is suggested by reason of the relative intensities of band systems on the plates obtained. On the other hand no plate except at condition 3 has been obtained without cool flame bands present, but plates at conditions 2 and 7 do show strong band systems of a normal ignition as well as the cool flame bands. A panchromatic plate taken at condition shows a carbon continuum, which is significant in view of the comparatively weak mixture at which it is occurring.

Two check tests were carried out to ensure that the excited formaldehyde band system was in fact due to the methane ignition. In the first, methane of high purity was used in place of commercial methane. This source of 98.8 per cent pure methane is known to be free of other hydrocarbons. A spectrum was obtained at condition 1 which was in every respect similar to previous spectra at this condition. In the second test, the engine lubricating oil was replaced by a special non-oxidizing oil, (Aroclor 1254, a chlorinated diphenyl), as it was considered possible that the normal hydrocarbon lubricating oil could be responsible for the excited formaldehyde emission bands. Essentially pure methane was also used, and the plate obtained, also at condition 1, confirmed that the cool flame bands were due to the methane ignition.

Preliminary experiments with the sectoring

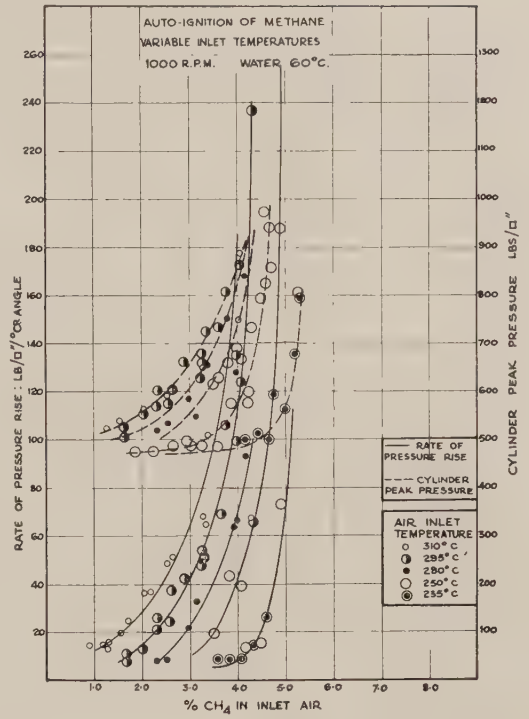

FIG. 6. Peak pressures and rates of pressure rise for constant temperature intake conditions.

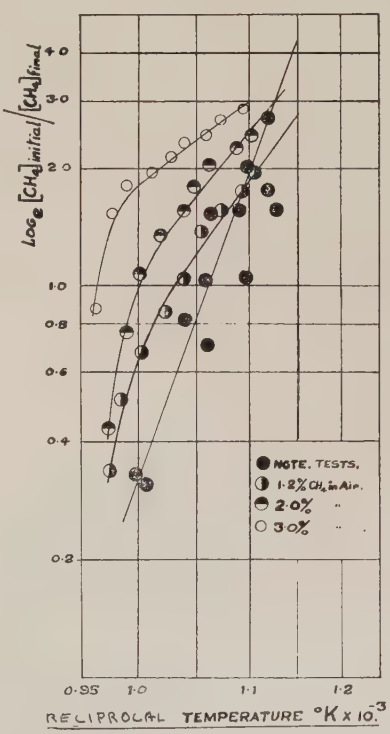

FIG. 7. Correlation of reaction rate with compression temperature at constant percentage methane addition.

shutter have failed to separate the cool flame bands from the hydrocarbon ignition bands. Cool flame bands are present in the first 6° of the reaction, i.e., in the first millesec; in the next 12° or two millesec of the reaction the hydrocarbon ignition bands are present in addition to the cool flame bands; in the next 6° both band systems are much fainter although the cool flame bands are still present; and in the final 6° only the carbon monoxide continuum was visible, which also formed a background to the band systems on the earlier plates, being weakest on the first plate of the set. Thus in a reaction lasting five millesec the cool flame bands are present during the major part of the period of reaction and hydrocarbon emission bands are present in greatest strength in the middle of the reaction. The condition chosen was in the blue region but nearer to the yellow rather than to the blue boundary. A complete account of the spectroscopic work is in preparation.

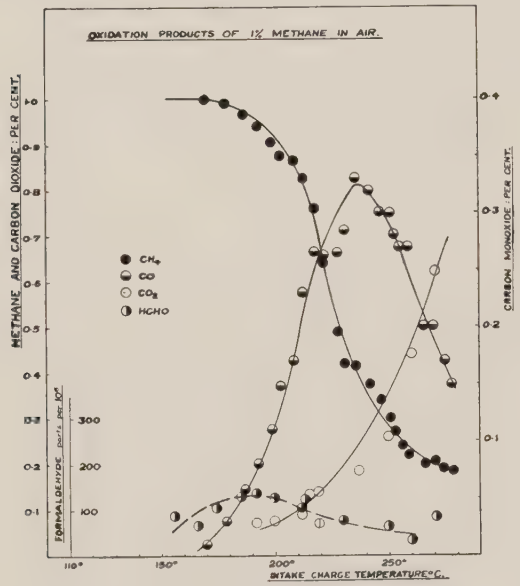

FIG. 8. Reaction products for a 1 per cent methane addition.

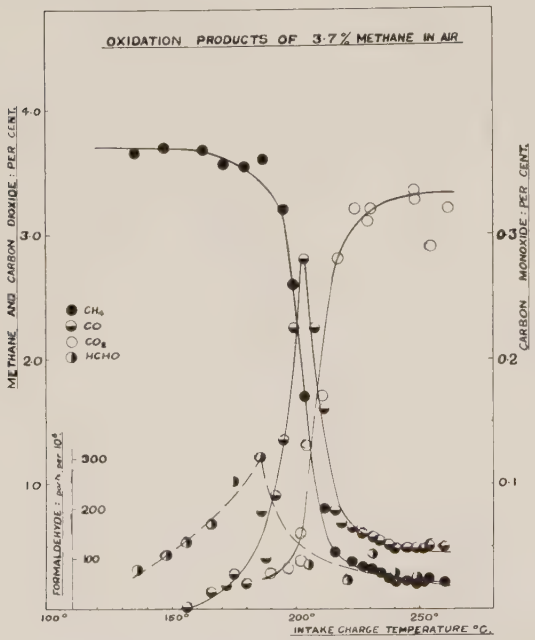

FIG. 9. Reaction products for a 3.7 per cent methane addition.

(3.3) CONSTANT MIXTURE STRENGTH EXPERIMENTS

The mixture strengths of the intake charge was maintained constant and the charge temperature varied so that the temperatures could be determined at which various reaction products appeared. In addition to analysis for methane and carbon monoxide, samples were analyzed for carbon dioxide and formaldehyde. Results obtained for 1 per cent and 3.7 per cent methane in air are shown in Figures 8 and 9 respectively. Percentage methane, carbon monoxide and carbon dioxide, and formaldehyde (expressed as parts per million) are plotted against the intake charge temperature. From the curves for a 1 per cent mixture, Figure 8, it can be seen that the first appearance of carbon monoxide coincides with the first detectable drop in methane concentration, calculated as 670°C compression temperature. The formaldehyde concentration in the exhaust peaks at 700°C and the carbon monoxide concentration peaks at 765°C. Carbon dioxide first appears at 700°C. It should be noted that there is a zero error in the carbon dioxide concentrations due to there being 5.4 per cent CO_2 in the commercial methane and there is also a trace, of course, in the atmospheric air breathed by the engine. The carbon monoxide peak is wider in the one per cent curve than in the 3.7 per cent and the fall in methane concentration is more gradual. In addition there is an absence of the sharp peak in the formaldehyde concentration. This all leads to the conclusion that slow reactions are more predominant in the one per cent methane test compared with the experiment at 3.7 per cent in which there is a sharp drop in methane concentration and a very sharp carbon monoxide peak. It would appear in this case that slow reactions end

with the peak in the formaldehyde concentration and a rapid ignition occurs at that point.

(4) Discussion and Conclusions

In the work of Downs, Street, and Wheeler[2] a blue flame region for methane was reported using the variable compression ratio technique in the motored engine method. But their blue flames were reported at the stoichiometric mixture strength and just below. Cool flames which were detected for other fuels by means of a photomultiplier tube were not observed for methane. Similar bright blue flames for methane, but occurring much later in the cycle compared with normal yellow flames, have also been observed by Egerton, Moore and Lyn[14]. It would appear that the blue flame phenomenon obtained in the reactions of very weak methane air mixtures is different from the more normal cool flame region established for higher hydrocarbon fuels, even though cool flame bands are present in the emission spectrum of this blue flame. In the case of higher hydrocarbon fuels a cool flame is associated with conditions somewhat below the final ignition temperature and when observed is generally followed by the normal hot ignition. In addition, no combustion noise is associated with the passing of a cool flame, and in the present experiments combustion noise is audible in the blue region and normal ignition bands appear in the spectrum in addition to the cool flame bands. It is also interesting that the cool flame bands appear to exist throughout the major part of the combustion period. Spence and Townend[15] and others have reported a second stage ignition following the cool flame giving the same spectrum of excited formaldehyde. This reaction is accompanied by a considerably greater pressure rise than the ordinary cool flame. The basic difference is stated to be that whereas the ordinary cool flame produced large quantities of aldehydes and peroxides, which is confirmed by the results of Panke and others[6], the second stage ignition largely consumes these compounds. This is significant in view of the fact that our results show a sharp drop in formaldehyde concentration as the threshold of the more audible blue reaction is approached.

The importance of the effect of the presence of carbon monoxide on the combustion of methane has now been established. The oxidation of very weak methane air mixtures at atmospheric pressure conditions was found to be greatly influenced by the secondary oxidation of carbon monoxide formed as a product in the work of Burgoyne and Hirsch[8], and similar results are reported by Hoare and Walsh[16]. In view of the fact that work was carried out both by the motored engine method and the heated tube method, there is a striking similarity between the present results and the work of Burgoyne and Hirsch, with the exception that events are occurring at higher pressures, somewhat lower temperatures, and at rather longer reaction times, in the present work.

In view of the importance of the oxidation of carbon monoxide in relation to the oxidation of methane, a detailed study of the carbon monoxide reactions has been made by Hoare and Walsh[16]. Pressure and temperature limits for the onset of a blue glow as well as true explosion limits have been established. This glow was first observed by Prettre and Laffitte[17] who described it as violet, but was later observed by Gaydon[18] who found that the slightest trace of dirt caused Sodium D lines to appear in the emission giving the violet appearance.

Also Prettre[19] has reported some luminescence 40°C below temp. of final ignition with 5.3 and 18.5 per cent CH_4 in air. A preignition glow in methane oxygen mixtures has been reported by Vanpée[20].

In the present work, the more intensive reactions nearer the yellow boundary appeared violet in color; the yellow boundary plotted is a mean boundary in the violet condition between the more definite blue and yellow reactions. There was no definite instantaneous transition from blue to yellow except in the unstable low temperature region, and at higher temperatures the transition became very much more gradual. The spectrographic plates seem to confirm that the yellow flame region does not signify a completely different ignition process to that occurring in the blue region, but in the unstable region the blue flame is much fainter compared to the very bright yellow or white flame. The difference here appears much greater than in the stable regions where spectroscopic investigation is possible.

Acknowledgments

The authors wish to acknowledge support for the present research from the Ministry of Fuel and Power, and particularly to Sir Harold Roxbee Cox, until recently the Chief Scientist, for permission to publish. The authors wish to record

their indebtedness to Dr. A. G. Gaydon for his invaluable assistance and advice with the spectroscopic work.

REFERENCES

1. Downs, D., Street, J. C., and Wheeler, R. W.: Fuel, *32*, 279 (1953).
2. Downs, D., Walsh, A. D., and Wheeler, R. W.: Phil. Trans. *A243*, 463 (1951).
3. Corzilius, M. W., Diggs, D. R., and Pastell, D. L.: S. A. E. Trans., *61*, 386 (1953).
4. Pastell, D. L.: S. A. E. Quart. Trans., *4*, 571 (1950).
5. Levedahl, W. J., Broida, W. P., and Howard, F. L.: Ind. & Eng. Chem., *43*, 2803 (1951).
6. Pahnke, A. J., Cohen, P. M., and Sturgis, B. M.: Am. Chem. Soc., 124th National Meeting, Chicago, Sept. 1953.
7. Melby, A. O.: J. Inst. Petroleum (London), *38*, 348 (Dec. 1952).
8. Burgoyne, J. H., and Hirsch, H.: In course of publication; Hirsch, H.: Ph.D. Thesis, (*The Oxidation of Methane.*) London, 1953; Egerton, A. C.: Fuel, *31*, 385 (1952).
9. Mullins, B. P.: Fuel, *32*, 211 (1953).
10. Pye, D. R.: *The Internal Combustion Engine*, Vol. 1, Art. 62. Oxford University Press, 1935.
11. Moore, N. P. W., and Simonson, J. R.: Nature, *173*, 543 (1954).
12. Cox, H. B., and Moore, N. P. W.: National Gas Turbine Establishment Report No. R.113 (Jan. 1952).
13. Jost, W.: *Third Symposium on Combustion, Flame and Explosion Phenomena*, p. 424. Baltimore, The Williams & Wilkins Co., 1949.
14. Egerton, A. C., Moore, N. P. W., and Lyn, W. T.: Nature, *167*, 191 (1951).
15. Spence, K., Towend, D. T. A.: *Third Symposium on Combustion, Flame and Explosion Phenomena*, p. 404. Baltimore, The Williams & Wilkins Co., 1949.
16. Hoare, D. E., and Walsh, A. D.: Trans. Faraday Soc., *50*, 37 (1954).
17. Prettre, M., and Laffitte, P.: Compt. rend., *189*, 177 (1929).
18. Gaydon, A. G.: *Spectroscopy and Combustion Theory*. London, Chapman and Hall, 1948.
19. Prettre, M.: Ann. Office Nat. des combust. liquides, *6*, 7, 269, 533 (1931).
20. Vanpée, M., and Grard, F.: *Fifth Symposium (International) on Combustion*, p. 484. New York, Reinhold Publishing Corp., 1955.

Discussion by William G. Agnew*

The change in the flame spectrum observed by Simonson and Moore as the lean methane-air mixture was enriched from 1.0 to 6.0 per cent methane in a motored engine was remarkably similar to the change noted by Dr. J. T. Agnew† and myself in a rich two-stage flame of diethyl ether and air. Our two-stage flame was formed in a flat-flame burner and was of the type described in our paper presented at this symposium (see p. 766). Visible spectra of the first stage (cool flame) showed the emission bands of excited formaldehyde superimposed on a rather strong background with some additional unidentified emission in the region from 5200 to 5900 Å. The signal-to-noise ratio and resolution were such that no band structure could be identified with certainty in the 5200 to 5900 Å region. This spectrum remained essentially unchanged as the mixture was leaned from 50 to 30 per cent ether.

The second-stage flame at mixture strengths between 35 and 45 per cent ether showed only the excited formaldehyde bands superimposed on a strong background. However, as the mixture was made leaner than 35 per cent ether, the HCO spectrum and the 4315 Å CH band appeared and gradually grew stronger. At 25 per cent ether the HCO and CH bands were much stronger than the formaldehyde bands. At 15 per cent ether the rich normal flame spectrum of CH, C_2, OH, and weak HCO appeared. During this gradual change of the second-stage flame from a second cool flame to a rich normal flame, the first cool flame became indistinguishable at about 25 to 30 per cent ether. In addition, a yellow luminous column appeared after the second-stage flame in the mixture range from 30 to 15 per cent ether. Thus, for the second-stage burner flame the sequence of formaldehyde to HCO and CH to yellow luminosity and the normal flame spectrum appeared with leaning of the very rich mixture, just as it appeared in enriching the very lean mixture in the engine experiments of Simonson and Moore.

* Research Laboratories Division, General Motors Corporation.

† Purdue University.

44

THE OXIDATION OF METHANE

Part I. Kinetic Laws at ca. 500°C

By D. E. HOARE AND A. D. WALSH

In experimental and theoretical work on the combustion of methane, insufficient attention has been paid to the effect of surfaces. We therefore undertook systematic work to determine how the maximum rate of pressure rise in methane oxidation varies with methane concentration, oxygen concentration, nitrogen addition and temperature when the nature of the reaction vessel surface is changed. The present paper reports results at temperatures in the neighborhood of 500°C. The same silica reaction vessel (diameter, 3.5 cm; capacity 73 cm^3) was used in all experiments, but the surface was pre-treated in four different ways that enable reproducibility to be attained[1]. These pre-treatments yield surfaces that may be labeled HF-treated (or new), aged, heat-treated and PbO-coated; they are detailed below.

Experimental

Cylinder methane and oxygen were purified by successive fractional distillations. Nitrogen was used directly from a cylinder after passage through a liquid nitrogen trap. Comparison with oxygen-free argon, in experiments where inert gases had only a small effect, showed that the oxygen content of the nitrogen was less than 0.5 per cent.

We have expressed the results in terms of the indices in the equation

$$\text{maximum rate of pressure rise} \propto [CH_4]^m[O_2]^x[\text{total pressure}]^t e^{-E/RT}$$

or

$$\text{maximum rate of pressure rise} \propto [CH_4 + O_2 \text{ mixture}]^n e^{-E/RT}$$

although of course there is no suggestion that the true kinetic law is of this form.

By total pressure in the above expression we mean the sum of the partial pressures of methane, oxygen and nitrogen; the value of t being obtained by varying the partial pressure of nitrogen alone. The value of m was obtained by keeping the total pressure and the partial pressure of oxygen constant and varying the partial pressures of methane and nitrogen. The value of x was obtained by varying only the oxygen and nitrogen partial pressures. The value of n was obtained by varying the pressure of a methane-oxygen mixture of fixed proportions. After any series of experiments a check was made to see that the reaction rate under the original conditions was still the same. Further, if experiments A, B, C, D and E were to be performed and a parameter (pressure or temperature) varied monotonically over the series as written above, then the experiments were performed in an order A, D, C, E and B (or some similar irregular order) to eliminate any complicating effect of one reaction upon the succeeding reaction.

By an HF-treated vessel, we mean one that had been washed with aqueous HF and then given several preliminary runs before use. By an aged vessel, we mean one that had been in use for many weeks or months without HF-treatment. Aging is connected with the formation of a devitrified layer of silica on the surface. HF removes this layer. Heating with PbO (which can then be removed with dilute nitric acid) catalyzes the formation of the devitrified layer and so accelerates the process of aging. By a heat-treated vessel, we mean one that had been heated to 950°C *in vacuo* for 10 min between reactions. With such a vessel there was little difference between the reaction rates obtained (after cooling) (a) at once, (b) after treating the vessel with oxygen for 15 min at the temperature to be used for the experiments, followed by evacuation for 10 min. However, procedure (b) gave slightly the better reproducibility and was in fact used for the experiments reported below. A PbO-coating was applied in the manner described by Chamberlain and Walsh[2]. With the PbO-coated vessel, no preliminary runs were necessary to secure reproducibility.

Results

Figure 1 shows typical Δp/time curves for the four vessel surfaces used. It is clear that the four surfaces yield very different rates of pressure rise for otherwise identical conditions and even dif-

ferent shapes for the Δp/time curves. The order of the surfaces as regards the rate yielded is

HF-treated > aged > heat-treated > PbO-coated

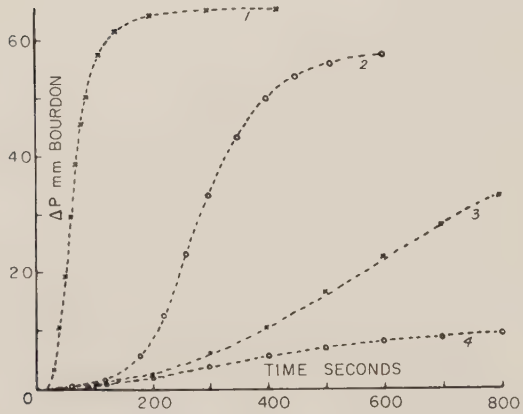

FIG. 1. Comparison of reaction rates with various surfaces. Experiments with $2CH_4:O_2$ at 500°C using (1) 450 mm Hg pressure in the new or HF-treated vessel; (2) 500 mm Hg in the aged vessel; (3) 500 mm Hg in the heat-treated vessel; (4) 500 mm Hg in the PbO-coated vessel. 1 mm Hg = 1.80 mm Bourdon gauge deflection.

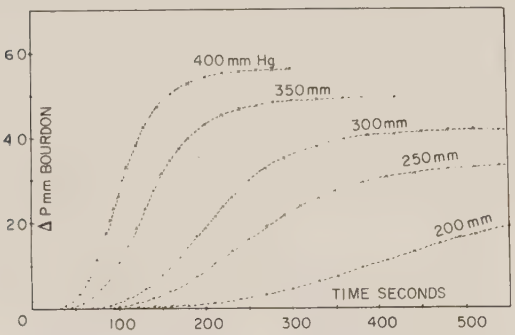

FIG. 2. The effect of varying the total initial pressure of a $2CH_4:O_2$ mixture at 500°C in the HF-treated vessel. 1 mm Hg = 1.80 mm Bourdon.

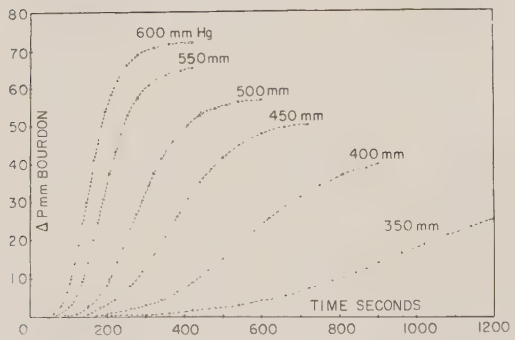

FIG. 3. The effect of varying the total initial pressure of a $2CH_4:O_2$ mixture at 500°C in the aged vessel. 1 mm Hg = 1.80 mm Bourdon.

and the ratio of rates in the HF-treated and PbO-coated vessels may be >100:1.

VALUES OF n

Figures 2, 3, 4 and 5 show the variation in reaction rate with total initial pressure of a mixture of fixed CH_4/O_2 ratio at 500°C using each of the four surfaces in turn. For each surface a plot of log(max rate)/log(initial total pressure) is

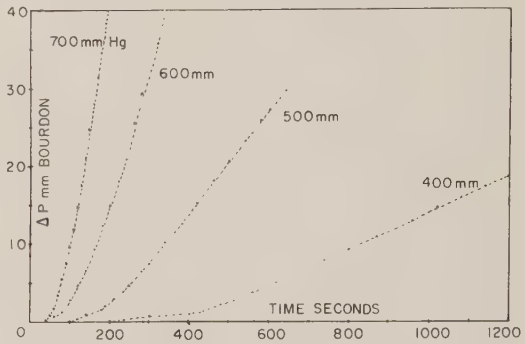

FIG. 4. The effect of varying the total initial pressure of a $2CH_4:O_2$ mixture at 500°C in the heat-treated vessel. 1 mm Hg = 1.80 mm Bourdon.

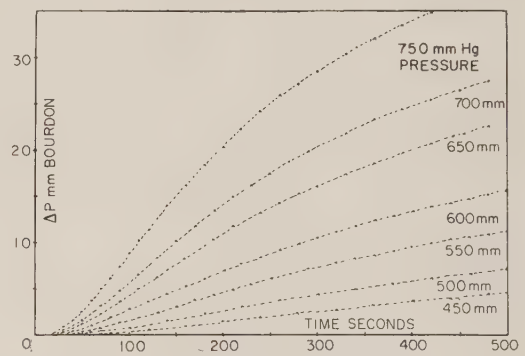

FIG. 5. The effect of varying the total initial pressure of a $2CH_4:O_2$ mixture at 500°C in the PbO-coated vessel. 1 mm Hg = 1.80 mm Bourdon.

a good straight line. The values of n so obtained for the four surfaces are recorded in Table 1; they all refer to a 2/1 CH_4/O_2 ratio. It may be noted that in the aged vessel at 500°C n was rather lower (4.3) with a 1/2 CH_4/O_2 ratio than with a 2/1 ratio (4.8).

VALUES OF m

Figures 6 and 7 show the variation in reaction rate with initial partial pressure of methane in the aged and heat-treated reaction vessels. Similar families of graphs for the HF-treated and PbO-coated vessel have already been published[3].

The values of m obtained for the four vessels are recorded in Table 1. For the aged and PbO-coated vessels, m varied somewhat with CH_4/O_2 ratio; and so beneath the extreme values of m in the corded in Table 1 for the four vessel surfaces. All the values refer to a 2/1 CH_4/O_2 ratio. For the aged vessel at least, the value of t was independent of whether the CH_4/O_2 ratio was 2/1 or 1/2

TABLE 1

Surfaces	HF-treated	Aged	Heat-treated	PbO-coated
n for $2CH_4:1O_2$	3.3	4.8	4.8	4.9
m for	$1CH_4:2O_2$ to $2CH_4:1O_2$ 1.6	$1CH_4:5O_2$ to $5CH_4:1O_2$ 2.3 to 1.9	$1CH_4:2O_2$ to $5CH_4:2O_2$ 2.4	$1CH_4:3O_2$ to $5CH_4:2O_2$ 2.0 to 2.4
x for	$1CH_4:2O_2$ to $2CH_4:1O_2$ 1.2	$1CH_4:3O_2$ to $7CH_4:1O_2$ 1.0 to 2.0	$1CH_4:6O_2$ to $2CH_4:1O_2$ 1.0 to 1.6	$2CH_4:5O_2$ to $4CH_4:1O_2$ 1.55
t for $2CH_4:1O_2$	0.5	0.85	0.9	0.9
E for $2CH_4:1O_2$ for	(300 mm) 475–525°C	(450 mm) 475–525°C	(700 mm) 462.5–500°C	(700 mm) 462.5–525°C
kcal/mole	Decreases from 40 at 475°C to 25 between 500 and 525°C	Decreases from 65 at 475°C to 50 at 525°C	65	58
E for $1CH_4:2O_2$ for	500–525°C (150 mm)	475–525°C (500 mm)		
kcal/mole	Decreases from 32 at 500°C to 25 at 525°C	Decreases from 96 at 475°C to 65 at 525°C		

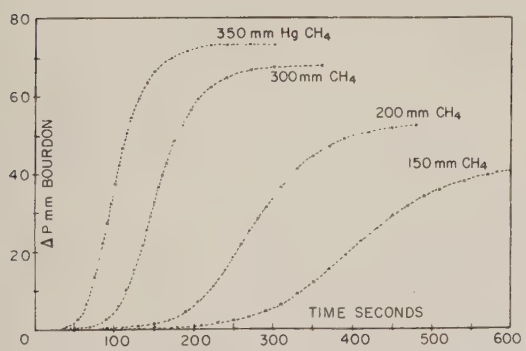

FIG. 6. The effect of varying the initial partial pressure of methane at 500°C in the aged vessel. Constant oxygen partial pressure of 200 mm. Constant total initial pressure ($CH_4 + O_2 + N_2$) of 700 mm. 1 mm Hg = 1.80 mm Bourdon.

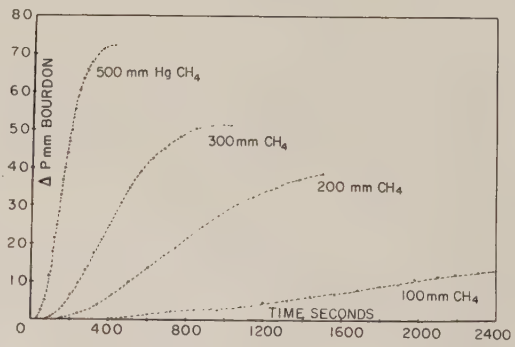

FIG. 7. The effect of varying the initial partial pressure of methane at 500°C in the heat-treated vessel. Constant oxygen partial pressure of 200 mm. Constant total initial pressure ($CH_4 + O_2 + N_2$) of 700 mm. 1 mm Hg = 1.80 mm Bourdon.

Table we have also recorded the relevant ranges of CH_4/O_2 ratio. For a 2/1 CH_4/O_2 ratio, m was 1.6, 2.0, 2.4 and 2.4 for the HF-treated, aged, heat-treated and PbO-coated vessel surfaces respectively.

VALUES OF t

Similar families of graphs for varying partial pressures of nitrogen yielded the values of t re-

VALUES OF x

Similar families of graphs for varying initial partial pressures of oxygen yielded the values of x recorded in Table 1 for the four vessel surfaces. The family obtained for the HF-treated vessel is shown in Figure 8. For the aged and heat-treated vessels, x varied somewhat with CH_4/O_2 ratio. For a 2/1 CH_4/O_2 ratio, x was 1.2, 1.7, 1.6 and

1.55 for the HF-treated, aged, heat-treated and PbO-coated vessels respectively.

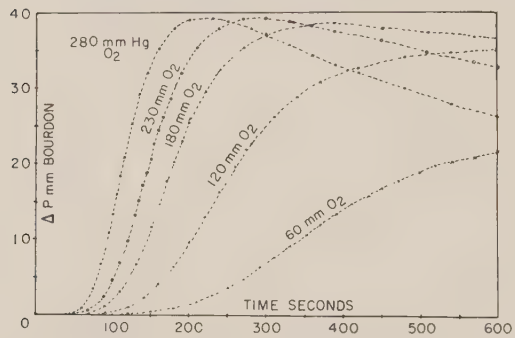

FIG. 8. The effect of varying the initial partial pressure of oxygen in the HF-treated vessel at 500°C. Constant initial methane partial pressure of 120 mm. Constant total initial pressure ($CH_4 + O_2 + N_2$) of 400 mm. 1 mm Hg = 1.80 mm Bourdon.

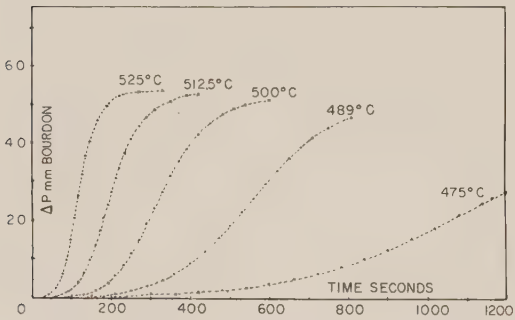

FIG. 9. The effect of varying the temperature, using the aged vessel. Constant initial pressure (at 500°C) of 450 mm. $2CH_4:O_2$. 1 mm Hg = 1.80 mm Bourdon.

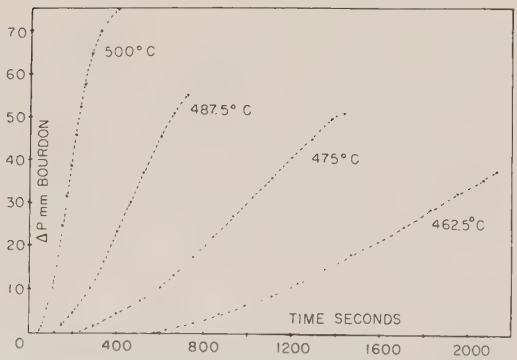

FIG. 10. The effect of varying the temperature, using the heat-treated vessel. Constant initial pressure (at 500°C) of 700 mm. $2CH_4:O_2$. 1 mm Hg = 1.80 mm Bourdon.

It may be seen that for the $2CH_4:O_2$ mixture the relation $n = m + x + t$ is obeyed reasonably well. The figures are:

	m	x	t	$m + x + t$	$n_{observed}$
HF-treated.....	1.6	1.2	0.5	3.3	3.3
Aged.....	2.0	1.7	0.85	4.55	4.8
Heat-treated...	2.4	1.6	0.9	4.9	4.8
PbO-coated....	2.4	1.55	0.9	4.85	4.9

VALUES OF E

Families of graphs showing the variation of reaction rate with temperature in the HF-treated and PbO-coated vessels have already been published[3]. Figures 9 and 10 show the corresponding families for the aged and heat-treated vessels. For the HF-treated and aged vessels, E varies with the temperature; the extreme values and the relevant temperature ranges are recorded in Table 1. For these two vessels, E rose as the temperature fell from 525 to 475°C. E was lower for the HF-treated surface than, under similar conditions, for the other three surfaces. At lower temperatures, E rose still further and reached ca. 80 kcal/mole in a new or HF-treated vessel at ca. 425°C. E was always higher for mixtures weaker in methane; thus, in the HF-treated vessel, E varied from 65 (at 475°C) to 50 (at 525°C) kcal/mole for a $2CH_4:O_2$ mixture but from 96 (at 475°C) to 65 (at 525°C) kcal/mole for a $CH_4:2O_2$ mixture. Consequently, it is easier to follow methane oxidation to low temperatures in (a) mixtures rich rather than weak in methane, (b) the new or HF-treated vessel rather than the other three vessels.

Since E is a function of both mixture composition and temperature, the inadequacy of the equation maximum rate of pressure rise $\alpha[CH_4]^m[O_2]^x[\text{total pressure}]^t e^{-E/RT}$ is apparent. Clearly a much more complex expression is required properly to express the true kinetic law.

Experiments Using Hydrogen Chloride and Carbon Monoxide Additions

Figure 8 shows that in the HF-treated vessel and with initial CH_4/O_2 ratios less than unity a marked pressure drop occurs towards the end of the reaction. No such marked pressure drop was observed with the other three vessel surfaces at 500°C. The pressure drop shows that oxidation of the carbon monoxide formed as a product is occurring; this oxidation being favored by an HF-treated surface and by the presence of excess

oxygen. Addition of carbon monoxide increases the extent of the pressure drop so that the final pressure may fall below the initial value. The induction period to the onset of the pressure drop is the same whether carbon monoxide has been added or not; clearly, therefore, the carbon monoxide oxidation is *induced* by the methane oxidation. There is no evidence that carbon monoxide oxidation occurs in methane oxidation in the aged, heat-treated and PbO-coated vessels at 500°C; indeed there is direct evidence[4] that, in the PbO-coated vessel and in the absence of methane, carbon monoxide oxidation requires a temperature considerably greater than 500°C.

We have recorded elsewhere[4] data on the oxidation of carbon monoxide in the HF-treated vessel; and have shown that it is inhibited by the addition of hydrogen chloride. It was of interest therefore to add hydrogen chloride to the initial CH_4/O_2 mixture in the HF-treated vessel at 500°C. Figure 11 shows that the effect of the addition was to reduce the maximum rate of pressure rise. Either, therefore, hydrogen chloride has a direct inhibiting effect on the methane oxidation or the effect of carbon monoxide oxidation upon the rate of pressure rise (methane oxidation) is an acceleration. In Part II (the following paper) it is shown that when carbon monoxide oxidation occurs during methane oxidation there are two opposing effects on the rate of pressure rise: (a) a decrease which must always be present when conversion of carbon monoxide to dioxide occurs, (b) an increase due to a multiplication of the number of chain centers consequent upon the oxidation of the carbon monoxide. Effect (b) only occurs when the partial pressure of methane is not too high. The effect of additions of hydrogen chloride at 500°C would be consistent with effect (b).

Experiments were also performed to see if additions of hydrogen chloride changed the kinetic law governing the rate of pressure rise in methane oxidation. x was found to be hardly changed (at 1.2), but m was increased from 1.6 to 1.8. At higher temperatures (see Part II, p. 479) larger increases in m and also decreases in x were found to be caused by hydrogen chloride additions. Neglecting any direct effect of hydrogen chloride upon the methane oxidation, we deduce that the effect of carbon monoxide oxidation upon methane oxidation is to decrease the dependence of the rate of pressure rise upon the initial partial pressure of methane and (at any rate at the higher temperatures) to increase the dependence of the rate of pressure rise upon the initial partial pressure of oxygen.

Relation to Other Work

In agreement with our conclusion above, Jorissen and Lebbink[5] noted that an HF-treated silica vessel enabled methane oxidation to occur at much lower temperatures than would otherwise have been the case.

Lewis and von Elbe[6] have also described a change in surface activity after a silica vessel had been in use for some time; a change that could be reversed by treatment with HF.

A glance at the pressure/time curves recorded for methane oxidation by the various earlier

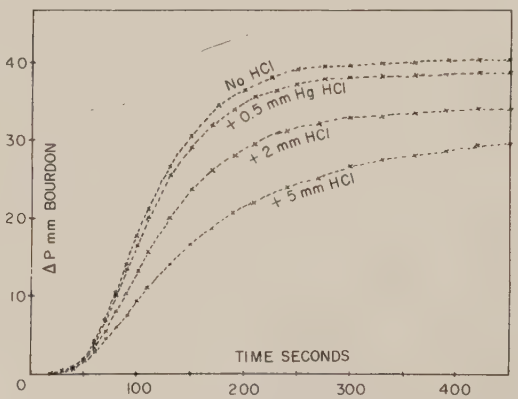

FIG. 11. The effect of adding hydrogen chloride to a $2CH_4:O_2$ mixture in the HF-treated vessel at 500°C. Initial pressure of methane + oxygen = 300 mm. 1 mm Hg = 1.80 mm Bourdon.

workers shows that there are many shapes, varying from an almost symmetrical one in which the maximum rate occurs transiently after ca. 50 per cent of the final Δp has been achieved to one in which the maximum rate is attained almost at the beginning of the pressure rise and the rate continues at the same value for a large fraction of the duration of the oxidation. Bone and Gardner[7], using a silica vessel and a temperature of 390°C, obtained curves of the latter extreme type, although their work is subject to the severe criticism that no experimental points are shown on their graphs. Fort and Hinshelwood[8], using a silica vessel and a temperature of 467°C, obtained curves nearer the former extreme type. Slotin and Style[9], using a silica vessel and a temperature of 430°C, obtained curves wherein the maximum rate of pressure rise occurred after 15 to 30 per cent of the final Δp. Bone and Allum[10], using a temperature of 447°C and a silica vessel obtained

graphs similar in shape to those of Slotin and Style. These differences in shape of the Δp/time plots have not previously been commented upon. Figure 1, however, shows that the symmetrical curves are characteristic of an aged silica vessel, while the Bone and Gardner curves are characteristic of a new (or HF-treated) silica vessel. From what we have said above, one can see that in order to study methane oxidation in a silica vessel at pressures $\leqslant$ atmospheric pressure and at a temperature of 390°C it would probably indeed be necessary to use a new or HF-treated vessel surface. Curves of intermediate shape would be obtained according to the degree of aging of the vessel used.

Norrish and Foord[11], using a soda glass vessel, found that at 480°C the maximum rate of pressure rise varied as the square of the initial methane pressure and the first power of both the initial oxygen and total pressure. These results were far from exact, however, and were based on much more limited data than those reported above. Thus the linear relation between the maximum rate of pressure rise and the total initial pressure (increased by addition of nitrogen) was only true (and then only approximately so) over a limited range of total pressure; over a wider range the curve of maximum rate/total initial pressure showed a marked curvature. Norrish and Foord[11], using Pyrex vessels, also found that at 530°C n varied from 3.7 to 4.2 as the vessel diameter was reduced from 3.75 to 0.75 cm. Comparison of reaction rates shows that their fastest reactions were proceeding at about half the rate observed by us with the HF-treated vessel at 530°C. In all probability, therefore, their vessels corresponded to silica vessels intermediate to our HF-treated and aged ones.

The trend to higher values of E as the temperature is reduced below 500°C is confirmed by various observations scattered through the earlier literature. From the work of Bone and Allum[10], a value of E = ca. 90 kcal/mole between 423 and 447°C may be derived. Fort and Hinshelwood[8] obtained E = 62 kcal/mole between 447 and 487°C. High values of E between 377 and 422°C have been found by Vanpée[12].

Discussion

It is evident from the results given above that not merely the rate of pressure rise observed in a silica vessel but also the kinetic laws governing that rate of pressure rise and the shape of the Δp/time graphs obtained depend markedly upon the pre-treatment accorded to the vessel surface. Thus, in reporting kinetic work, it is not sufficient to specify that the reaction vessel was made of silica; it is important also to specify the immediate history of the vessel.

One sees too that the supposition (made by previous workers) that at ca. 500°C $m = 2$, $x = t = 1$, $n = 4$ is not a very good law for any condition of a silica vessel surface. It is interesting to note, however, that the surfaces used fall into two sharply defined classes. Thus the values of m, x, t and E do not differ greatly for the aged, heat-treated and PbO-coated vessels; but the HF-treated surface yields a markedly different kinetic law to the other three. To a slight extent this is due to the occurrence of carbon monoxide oxidation in the HF-treated vessel and to the effect of this oxidation on the methane oxidation. The experiments using hydrochloric acid, however, enable us to say that, even allowing for the carbon monoxide oxidation, m, t (and therefore n) and E are all markedly less than with the other three surfaces.

The order of decreasing rate for the four surfaces is also the order of increasing ease of reproducibility. Thus several preliminary experiments are necessary to secure reproducibility with the HF-treated vessel; but no such preliminary experiments are necessary with the PbO-coated vessel. It is practically certain therefore that there is an increase in the efficiency of surface chain-ending for one or more particular chain carriers as the surface is changed from HF-treated to aged to heat-treated to PbO-coated. In other words, the surface chain-ending should become more diffusion-controlled in this sequence of surfaces. In accord with this, one notes that t is markedly greater for the aged, heat-treated and PbO-coated vessels than for the HF-treated vessel.

Figure 1 shows that the four surfaces yield much more pronounced differences in the maximum rate of pressure rise than in the early stages of reaction; from which we deduce that they exert their differential effect primarily upon the degenerate branching reaction which must be responsible for the observed slow increase in the rate of pressure rise with time. It appears then that the chain-carrier or-carriers differentially destroyed by the four surfaces may be present solely as a result of the degenerate branching reactions. Now there is a parallel between our results and the effect of surfaces on the hydrogen-oxygen reaction between the second and third explosion

limits. Thus data obtained by Willbourn and Hinshelwood[13] show that two silica vessels of the same diameter may differ enormously in the rates and activation energies they yield for the slow reaction at 510–550°C of hydrogen and oxygen between the second and third explosion limits. A coating of KCl reduces the rate of methane oxidation at 500°C to a value between those yielded by the heat-treated and PbO-coated vessels[1]; a KCl-coating is also an effective inhibitor of the hydrogen-oxygen reaction between the second and third explosion limits. A boric oxide-coated surface resembles an HF-treated silica surface in giving very fast rates of methane oxidation[14]; a boric oxide surface also yields fast rates of the hydrogen-oxygen reaction between the second and third explosion limits. Other coatings have similar effects on the hydrogen-oxygen slow reaction between the second and third explosion limits and on the oxidation of methane at ca. 500°C[14]. Now in the hydrogen-oxygen reaction at pressures between the second and third explosion limits it is generally agreed that chain-ending is by

$$HO_2 \xrightarrow[\text{surface}]{} \text{destruction} \qquad (1)$$

and/or

$$H_2O_2 \xrightarrow[\text{surface}]{} \text{destruction} \qquad (2)$$

It is likely, therefore, that HO_2 and/or H_2O_2 are the entities differentially destroyed by our four surfaces in the methane-oxygen reaction at ca. 500°C. Warren[15] has cited other evidence that a boric oxide surface preserves peroxidic materials; the similarity in effect of boric oxide-coatings and HF-treatments of a silica vessel may then be used to support the suggestion that an HF-treated silica surface is inefficient in bringing about reactions (1) and/or (2). It is established that formaldehyde oxidation is responsible for at least some of the autocatalysis shown by the Δp/time curves of methane oxidation at 500°C. Assuming that degenerate branching in methane oxidation at 500°C is caused solely by formaldehyde oxidation, HO_2 and/or H_2O_2 must be entities which are produced by formaldehyde oxidation under the relevant conditions and which are able directly or ultimately to react with methane molecules. Moreover, as we have argued elsewhere[3], the degenerate branching reactions must *not* produce H, O or OH radicals, or otherwise it would be impossible for a PbO-coating to cut out degenerate branching under the pressure conditions used for methane oxidation. The following reactions would give the simplest interpretation of the degenerate branching consistent with our data on the effect of surfaces:

$$X + HCHO = XH + HCO \qquad (3)$$
$$(X = O_2 \text{ or a free radical})$$

$$HCO + O_2 = HO_2 + CO \qquad (4)$$

$$HO_2 + CH_4 = H_2O_2 + CH_3 \qquad (5)$$

$$HO_2 \xrightarrow[\text{surface}]{} \text{destruction} \qquad (1)$$

although chain steps producing formaldehyde from methane have of course to be added and many more reaction steps (including further reactions of H_2O_2) than these may be involved. Reaction (4) as the fate of HCO radicals under the relevant conditions is also suggested by the fact that formaldehyde inhibits the hydrogen-oxygen reaction at the second pressure limit of explosion[16]; the inhibition almost certainly produces HCO radicals and the most obvious way of explaining why these can be regarded as inert at the second explosion limit is by assuming reaction (4). Evidence for the presence of H_2O_2 during methane combustion at ca. 500°C has been presented by Minkoff and Salooja[17].

The presence of HO_2 and H_2O_2 in the methane combustion chains and the fact that $D(CH_3—H)$ and D(H—H) are almost identical mean that there must be a considerable similarity between many of the reaction steps involved in methane oxidation at ca. 500°C and those involved in the hydrogen-oxygen reaction at ca. 500°C and at pressures between the second and third explosion limits. The full reaction scheme for the latter reaction is undoubtedly complex and is not yet finally established. The full reaction scheme for methane oxidation must be even more complex and attempts to give "complete" schemes seem to us as yet to be premature. We may venture the suggestion, however, that the reason for the abrupt change in kinetic laws on passing from the HF-treated to the other three vessel surfaces is connected with the fact that a boric oxide-coated surface yields kinetic facts in the hydrogen-oxygen reaction at the second explosion limit sharply different to those obtained with, e.g., a KCl-coated surface[18]. We have already mentioned that a boric oxide-coated surface resembles an HF-treated silica surface in giving very fast rates of methane oxidation.

Summary

It has been shown that the kinetic laws governing the rate of pressure rise in methane oxidation at ca. 500°C in a silica vessel are sharply different according to whether on the one hand, the surface has been HF-treated or, on the other hand, the surface has been aged, heat-treated or PbO-coated. One of the reasons for this difference is that the latter three treatments cause the surface to be a much more efficient destroyer of certain chain carriers; in all probability, these chain carriers are HO_2 radicals and/or H_2O_2 molecules. The sharp distinction of the HF-treated surface to the other three surfaces is probably connected with the boric oxide effect noted in the hydrogen-oxygen reaction at pressures $\geqslant$ the second explosion limit. There is a considerable parallel between methane oxidation at ca. 500°C and the hydrogen-oxygen reaction at pressures between the second and third explosion limits. The full reaction scheme for methane oxidation is bound to be complex; the present work reports some of the most systematic work so far carried out to establish the facts which are essential for the complexities of the system to be unravelled.

REFERENCES

1. Hoare, D. E.: Trans. Faraday Soc., *49*, 628 (1953).
2. Chamberlain, G. H. N., and Walsh, A. D.: Proc. Roy. Soc., *A215*, 175 (1952).
3. Hoare, D. E., and Walsh, A. D.: Proc. Roy. Soc., *A215*, 454 (1952).
4. Hoare, D. E., and Walsh, A. D.: Trans Faraday Soc., *50*, 37 (1954).
5. Jorissen, W. P., and Lebbink, H. O.: Rec. trav. chim., *58*, 959 (1939).
6. Lewis, B., and von Elbe, G.: J. Chem. Physics, *10*, 366 (1942).
7. Bone, W. A., and Gardner, J. B.: Proc. Roy. Soc., *A154*, 297 (1936).
8. Fort, R., and Hinshelwood, C. N.: Proc. Roy. Soc., *A129*, 284 (1930).
9. Slotin, L., and Style, D. W. G.: Trans. Faraday Soc., *35*, 420 (1939).
10. Bone, W. A., and Allum, R. E.: Proc. Roy. Soc., *A134*, 578 (1932).
11. Norrish, R. G. W., and Foord, S. G.: Proc. Roy. Soc., *A157*, 503 (1936).
12. Vanpée, M.: Ann. Mines Belg., *47*, 1053 (1948).
13. Willbourn, A. H., and Hinshelwood, C. N.: Proc. Roy. Soc., *A185*, 376 (1946).
14. Cheaney, D. E., and Walsh, A. D.: To be published.
15. Warren, D. R.: Proc. Roy. Soc., *A211*, 86, 96 (1952)
16. Baldwin, R. R.: In press.
17. Minkoff, G. J., and Salooja, K. C.: Fuel, *32*, 516 (1953).
18. Egerton, Sir A., and Warren, D. R.: Proc. Roy. Soc., *A204*, 465 (1951).

44

THE OXIDATION OF METHANE

Part II. Behavior at Temperatures from 500 to 750°C

By D. E. HOARE and A. D. WALSH

The preceding paper has reported systematic work carried out to determine the kinetic laws governing the rate of pressure rise in methane oxidation at ca. 500°C. The present paper reports similar systematic work at temperatures above 500°C and especially around 650 and 750°C.

Experimental

The same reaction vessel, pre-treated in the same ways, has been used as for the work reported in Part I. The quantities m, x, t, n and E have the same definitions as in the preceding paper; it should be particularly noted that they refer to the rate of pressure *rise*.

Results

Between 525 and 600°C, E remained constant for all four vessel surfaces, being 25 kcal/mole for the HF-treated vessel and between 50 and 65 kcal/mole for the other three.

Table 1 shows the values of n, m, x and t obtained for the HF-treated, heat-treated and PbO-

coated vessels at 650°C; and also values of E at ca. 650°C. Comparison with the table in Part I shows that n, m and t fall markedly from 500 to 650°C, while x and E rise.

VALUES OF m AT 650°C

Figure 1 shows the effect of varying the initial partial pressure of methane in the HF-treated vessel at 650°C, keeping constant the initial oxygen and total pressures. It may be seen that with the mixtures containing the smallest initial amounts of methane (i.e., mixtures not richer than $2CH_4:3O_2$) an explosion occurs towards the end of the reaction. The explosion causes a pressure drop and is evidently due to carbon monoxide oxidation. Such oxidation *can* only occur in the weaker mixtures, i.e., when there is sufficient excess oxygen towards the end of the pressure rise. It will be recalled that in Part I we showed that oxidation of the carbon monoxide, formed as a product from the methane oxidation, occurred in the HF-treated vessel at 500°C, though at 500°C the oxidation did not lead to explosion. It may also be seen from Figure 1 that although the Δp/time curves for the two weakest mixtures show the expected slow rate of pressure rise in the early stages, after a while a marked acceleration of the rate of pressure rise occurs before a pressure drop sets in. As a result, the maximum rates of pressure rise exceed those of the richer mixtures; and also the maximum rate occurs nearer the time when the maximum Δp is attained. These phenomena are always associated with methane oxidations in which a carbon monoxide explosion occurs and are therefore to be attributed to a catalysis of the methane oxidation by oxidation of the carbon monoxide. It will be recalled that data presented in Part I for a temperature of 500°C were consistent with such a catalysis.

If the logarithm of the maximum rate of pressure is plotted against the logarithm of the initial partial pressure of methane, it can be seen from Figure 1 that the curve will contain a minimum. This is shown in Figure 2. In other words, the maximum rate of pressure rise in the weaker mixtures *decreases* as the initial amount of methane increases; this is the explanation of the negative values of m recorded in Table 1.

Essentially similar, but less pronounced, effects occur in the heat-treated vessel (see Figs. 3 and 4).

TABLE 1

Surface	HF-treated	Heat-treated	PbO-coated
n for $2CH_4:3O_2$	—	3.4	3.7
n for $2CH_4:O_2$	—	3.6	—
m for	$1CH_4:2O_2$ to $4CH_4:1O_2$	$1CH_4:2O_2$ to $2CH_4:1O_2$	$1CH_4:2O_2$ to $3CH_4:1O_2$
	−1.0 to +0.4	0 to 0.7	0.2 to 1.0
x for	$1CH_4:2O_2$ to $2CH_4:1O_2$	$1CH_4:2O_2$ to $2CH_4:1O_2$	$1CH_4:2O_2$ to $6CH_4:1O_2$
	2.7 to 2.4	2.7 to 2.3	3.0 to 2.0
t for $2CH_4:3O_2$	Negative	0.4	0.3
t for $2CH_4:O_2$	—	0.6	—
E for	$1CH_4:1O_2$, 50 mm and 625–675°C	$2CH_4:3O_2$, 100 mm and 600–675°C	$2CH_4:3O_2$, 300 mm and 575–662.5°C
kcal/mole	43	76	57 to 48
		$2CH_4:O_2$, 150 mm and 600-675°C	$2CH_4:3O_2$, 200 mm and 600–662.5°C
		57	70 to 55

In the PbO-coated vessel, no carbon monoxide explosion occurs (Fig. 5), although the pressure decreases due to carbon monoxide oxidation in the weaker mixtures are clearly visible; and the curvature of the log(maximum rate of pressure rise)/log(initial methane partial pressure) plot (Fig. 6) is an indication that the carbon monoxide oxidation is accelerating the rate of methane oxidation. Clearly, the ease of carbon monoxide oxidation decreases as we pass from the HF-treated to heat-treated to PbO-coated vessel.

VALUES OF x AT 650°C

The values of x obtained for the HF-treated, heat-treated and PbO-coated vessels lie between 2.0 and 3.0, increasing as the acceleration of the

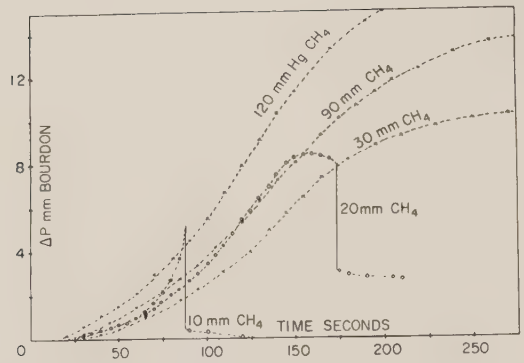

FIG. 1. The effect of varying the initial partial pressure of methane in the HF-treated vessel at 650°C. Constant initial partial pressure of oxygen = 30 mm Hg. Constant initial total pressure $(CH_4 + O_2 + N_2)$ = 150 mm Hg. 1 mm Hg = 1.80 mm Bourdon.

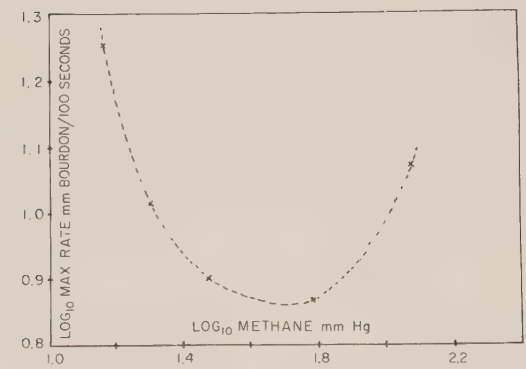

FIG. 2. The effect of varying the initial partial pressure of methane in the HF-treated vessel at 650°C. Constant initial partial pressure of oxygen = 30 mm Hg. Constant initial total pressure $(CH_4 + O_2 + N_2)$ = 150 mm Hg. 1 mm Hg = 1.80 mm Bourdon.

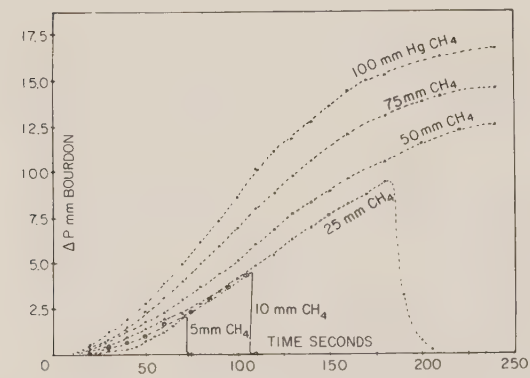

FIG. 3. The effect of varying the initial partial pressure of methane in the heat-treated vessel at 650°C. Constant initial partial pressure of oxygen = 50 mm Hg. Constant initial total pressure $(CH_4 + O_2 + N_2)$ = 200 mm Hg. 1 mm Hg = 1.80 mm Bourdon.

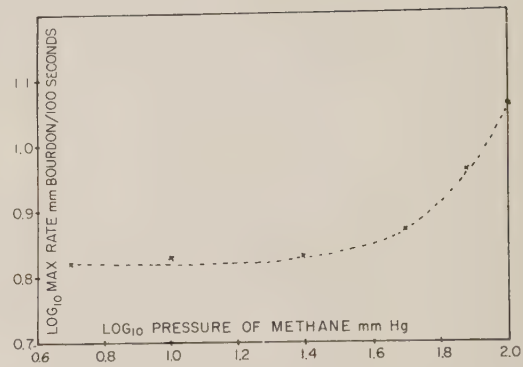

FIG. 4. The effect of varying the initial partial pressure of methane in the heat-treated vessel at 650°C. Constant initial partial pressure of oxygen = 50 mm Hg. Constant initial total pressure $(CH_4 + O_2 + N_2)$ = 200 mm Hg. 1 mm Hg = 1.80 mm Bourdon.

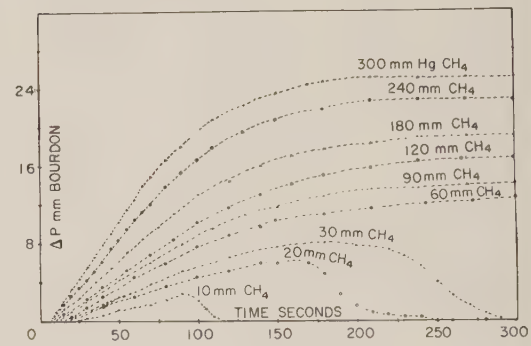

FIG. 5. The effect of varying the initial partial pressure of methane in the PbO-coated vessel at 650°C. Constant initial partial pressure of oxygen = 120 mm Hg. Constant initial total pressure $(CH_4 + O_2 + N_2)$ = 450 mm Hg. 1 mm Hg = 1.80 mm Bourdon.

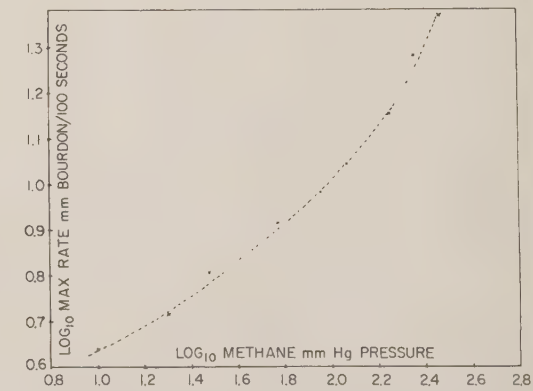

FIG. 6. The effect of varying the initial partial pressure of methane in the PbO-coated vessel at 650°C. Constant initial partial pressure of oxygen = 120 mm Hg. Constant initial total pressure $(CH_4 + O_2 + N_2)$ = 450 mm Hg. 1 mm Hg = 1.80 mm Bourdon.

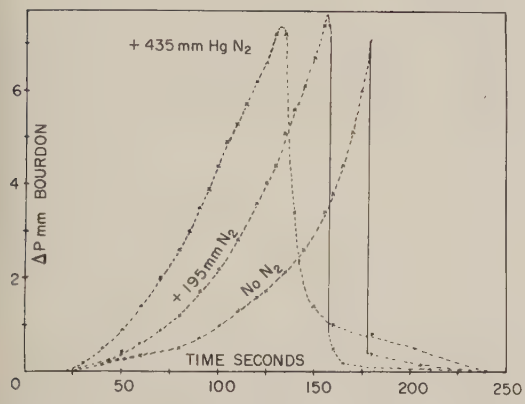

FIG. 7. The effect of adding nitrogen to 45 mm Hg of a CH_4:$2O_2$ mixture at 650°C in the HF-treated vessel. 1 mm Hg = 1.80 mm Bourdon.

ate of pressure rise due to carbon monoxide becomes more marked. In other words, carbon monoxide combustion causes an increase in the value of x; and the value of x tends from 2.0 to 3.0 as the proportion of oxygen in the initial mixture is increased.

VALUES OF t AT 650°C

It is known[1] that the slow oxidation of wet carbon monoxide is inhibited by nitrogen. It is to be expected therefore that values of t will be lower the greater the acceleration of the rate of pressure rise caused by carbon monoxide oxidation. Thus the value of t for a $2CH_4$:$3O_2$ mixture is 0.4 in the heat-treated vessel and negative in the HF-treated vessel. Figure 7 shows the effect of adding nitrogen to a CH_4:$2O_2$ mixture in the HF-treated vessel. The rate of pressure rise in the early stages of reaction is increased, but the acceleration due to oxidation of the carbon monoxide is decreased, so that, as a net effect, the maximum rate of pressure rise is decreased. In other words, with a CH_4:$2O_2$ mixture, t is negative. With a $4CH_4$:O_2 mixture (where carbon monoxide oxidation is less important), t is zero in the HF-treated vessel; with a $2CH_4$:$3O_2$ mixture, it is still negative.

(The inhibiting effect of pressure on the slow oxidation of wet carbon monoxide means that the values of m given in Table 1 for different vessel surfaces are not strictly comparable. The higher pressures used for experiments with the heat-treated and PbO-coated surfaces reinforce the effect of the surfaces themselves in reducing the importance of carbon monoxide oxidation in the heat-treated and PbO-coated vessels relative to the HF-treated vessel.)

VALUES OF E AT CA. 650°C

The values of E at ca. 650°C are similar to those obtained at lower temperatures except that with weak mixtures an increased value of E is obtained because of the increase in carbon monoxide oxidation with temperature. Also, with such weak mixtures, E is higher the lower the initial total pressure because carbon monoxide oxidation is then less inhibited.

TABLE 2

Initial Total Pressure	Initial Partial Pressure of Oxygen	Initial Partial Pressure of Methane	Value Found	Temperature
mm Hg	*mm Hg*	*mm Hg*		°C
100	10 to 30	50	x = 2.0 to 2.4	750
100	20	10 to 80	m = − 0.4 to +0.4	750
40 to 90	$2CH_4$:O_2		n = 3.0	750
60, increased to 480 by addition of N_2	$2CH_4$:O_2		t = 0.3	750
60	$2CH_4$:O_2		E = 66 kcal/mole	725–775

VALUES OF n, m, x, t AND E AT 750°C

Our work at 750°C is confined to the aged vessel. The results, tabulated in Table 2, show that the effect of carbon monoxide oxidation on the oxidation of methane is even more pronounced at 750°C than at 650°C (as would be expected). Figure 8 illustrates experiments with a $2CH_4$:$3O_2$ mixture; abrupt explosions occurred which prevented accurate measurements of the maximum rate of pressure rise (cf. Fig. 1).

EXPERIMENTS WITH ADDITION OF CARBON MONOXIDE AT 650°C (AND 500°C)

The apparent importance of carbon monoxide oxidation in affecting the rate of pressure rise in methane-oxygen mixtures made it of interest to study the effect of initial additions of carbon

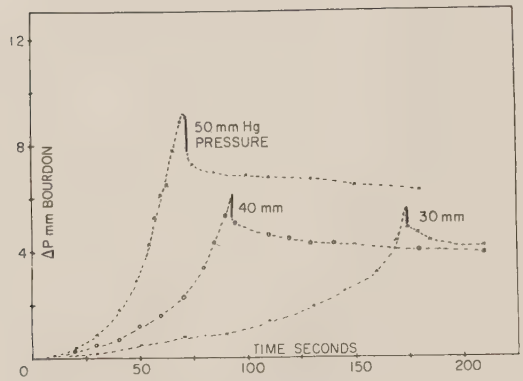

FIG. 8. The effect of varying the pressure of a $2CH_4:3O_2$ mixture in the aged vessel at 750°C. 1 mm Hg = 1.80 mm Bourdon.

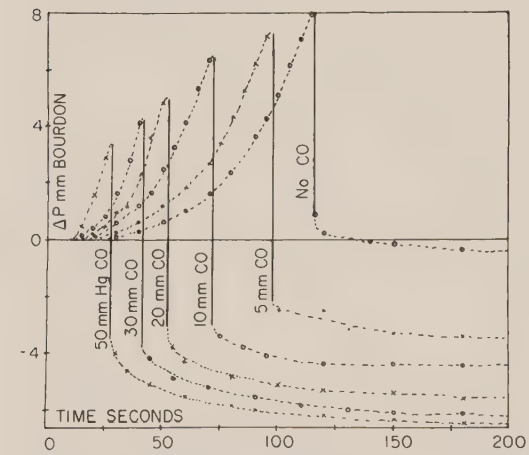

FIG. 9. The effect of varying the initial partial pressure of carbon monoxide added to 100 mm Hg of a $CH_4:2O_2$ mixture in the HF-treated vessel at 650°C. Total initial pressure kept constant at 200 mm Hg by appropriate additions of nitrogen. 1 mm Hg = 1.80 mm Bourdon.

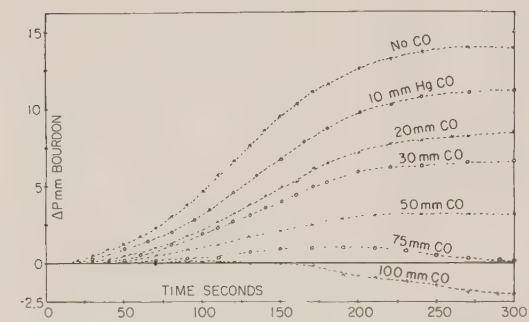

FIG. 10. The effect of varying the initial partial pressure of carbon monoxide added to 100 mm Hg of a $2CH_4:O_2$ mixture in the HF-treated vessel at 650°C. Total initial pressure kept constant at 200 mm Hg by appropriate additions of nitrogen. 1 mm Hg = 1.80 mm Bourdon.

monoxide. Figure 9 shows that such additions increase the rate of pressure rise in a $CH_4:2O_2$ mixture at 650°C, so confirming the deduction above that the occurrence of carbon monoxide oxidation may accelerate the rate of methane oxidation. However, additions of carbon monoxide to a $2CH_4:O_2$ mixture in the HF-treated vessel at 650°C (see Fig. 10) *decrease* the rate of pressure rise.

Similarly, Figure 11 shows that additions of carbon monoxide decrease the rate of pressure rise in a $CH_4:2O_2$ mixture at 500°C in the HF-treated vessel. Evidently, therefore, carbon monoxide oxidation has two opposing effects on the rate of pressure rise in methane oxidation.

With the PbO-coated vessel at 650°C and using $CH_4:2O_2$ mixtures, addition of carbon monoxide caused a small increase in the maximum rate of pressure rise and a larger increase in the subsequent rate of carbon monoxide oxidation.

It was also of interest to see what change, if any, was made in the values of m, x and E when carbon monoxide was initially present at 650°C. Figure 12 shows that, in the presence of fixed initial partial pressures of carbon monoxide and oxygen, and at a fixed initial total pressure, the plot of log (maximum rate of pressure rise)/log (initial partial pressure of methane) resembles that in Figure 2, except that the minimum in the curve occurs with mixtures richer in methane than when carbon monoxide is initially absent. It appears that methane and carbon monoxide compete for some radical or radicals, so that the more carbon monoxide present the more methane must be present to secure positive values of m. The effect is connected with the fact that, in the absence of added carbon monoxide, m is decreased at 650°C from its values at 500°C.

Similarly, since, in the absence of added carbon monoxide, x is increased at 650°C from its values at 500°C, we might expect an increase in x when a fixed initial partial pressure of carbon monoxide is added. Such an increase is indeed found; x = 2.9 in the presence of added carbon monoxide in the HF-treated vessel, (for details, see Table 3), compared with 2.4 to 2.7 for similar methane-oxygen mixtures in the absence of added carbon monoxide.

On the other hand, a value for E of 45 kcal/mole was obtained with 50 mm of a $CH_4:O_2$ mixture in the presence of 8.4 mm added carbon monoxide in the HF-treated vessel; this value

hardly differs from that of 43 kcal/mole obtained in the absence of added carbon monoxide.

EXPERIMENTS WITH ADDITION OF HYDROCHLORIC ACID

Hydrochloric acid inhibits the combustion of carbon monoxide[1]. It was therefore of interest to study the effect of hydrochloric acid additions on the oxidation of methane at 650°C. We have already reported, in Part I, the effect of such additions at 500°C. Figure 13 shows that addition of hydrochloric acid to a CH_4:$2O_2$ mixture at 650°C increases the rate of pressure rise in the early stages of reaction but decreases it in the later stages; it also increases the time before a carbon monoxide explosion occurs. The decrease in the rate of pressure rise in the later stages of reaction confirms the deduction above that carbon monoxide oxidation, occurring towards the end of the reaction, accelerates the rate of methane oxidation. Figure 14 shows that when additions of hydrochloric acid are made to a $2CH_4$:O_2 mixture at 650°C, the only noticeable effect is an increase in the rate of pressure rise in the early stages of reaction; with such a mixture of course the effects of carbon monoxide oxidation would be much less marked.

If we assume that hydrochloric acid additions have no effect on "true" methane oxidation, they may be used to obtain the "true" values of m and x characteristic of methane oxidation at 650°C, by cutting out the effects of the secondary oxidation of carbon monoxide. One would expect addition of hydrogen chloride to have the opposite effect on the values of x and m to the addition of carbon monoxide. This expectation is confirmed. Thus in the presence of a fixed initial partial pressure of hydrochloric acid (for details, see Table 3), x was found to be 1.55 in the HF-treated vessel, which value is much lower than that of 2.4 to 2.7 obtained in the absence of hydrochloric acid. Experiments to determine m show that the minimum in the graph of log(maximum rate of pressure rise)/log(initial methane partial pressure) (see Figs. 2 and 12) is no longer present when hydrochloric acid is added (see Fig. 15). In other words, m is increased from a range including negative values to a range of purely positive values. Table 3 records the values of m and x obtained in the presence of added hydrochloric acid and compares them with the values obtained (a) with added carbon monoxide, (b) in

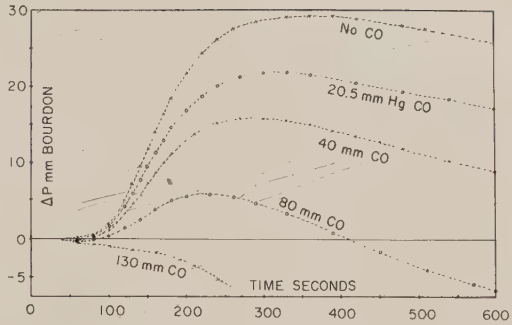

FIG. 11. The effect of varying the initial partial pressure of carbon monoxide added to 270 mm Hg of a CH_4:$2O_2$ mixture in the HF-treated vessel at 500°C. Total initial pressure kept constant at 400 mm Hg by appropriate additions of nitrogen. 1 mm Hg = 1.80 mm Bourdon.

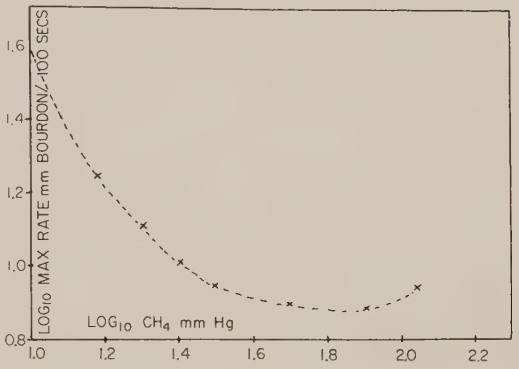

FIG. 12. The effect of varying the initial partial pressure of methane when carbon monoxide is initially present. HF-treated vessel at 650°C. Constant initial partial pressures of oxygen and carbon monoxide = 30 and 10 mm Hg respectively. Total initial pressure kept constant at 150 mm Hg by appropriate additions of nitrogen. 1 mm Hg = 1.80 mm Bourdon.

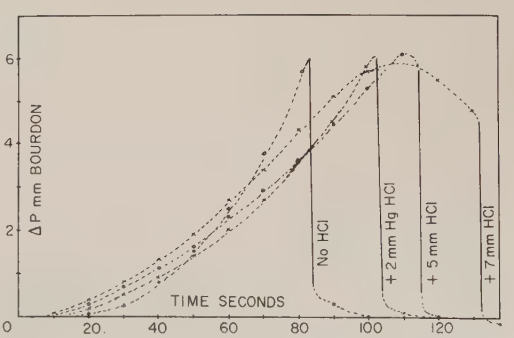

FIG. 13. The effect of adding hydrochloric acid to 34 mm Hg of a CH_4:$2O_2$ mixture at 650°C in the HF-treated vessel. 1 mm Hg = 1.80 mm Bourdon.

the absence of additives. All the data refer to the HF-treated vessel.

RELATION TO OTHER WORK

Earlier workers have noted that n falls as one passes from 500°C to higher temperatures. Thus,

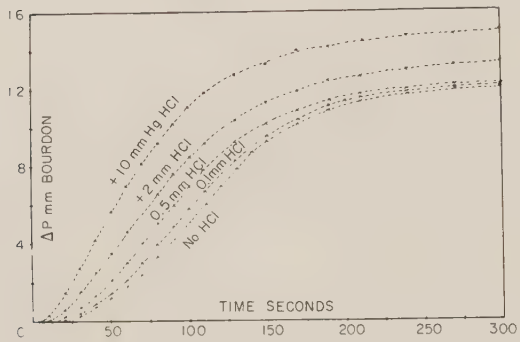

FIG. 14. The effect of adding hydrochloric acid to 75 mm Hg of a $2CH_4:O_2$ mixture at 650°C in the HF-treated vessel. 1 mm Hg = 1.80 mm Bourdon.

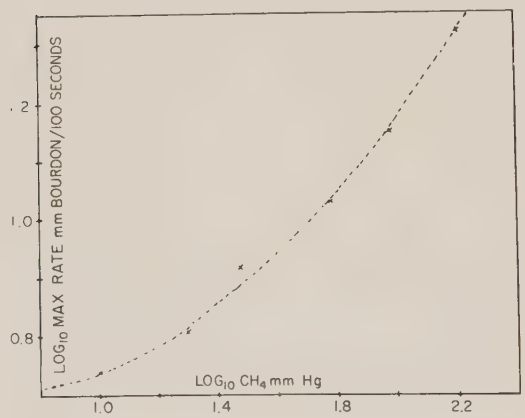

FIG. 15. The effect of varying the initial partial pressure of methane when hydrochloric acid is present. HF-treated vessel at 650°C. Constant initial partial pressures of oxygen and hydrochloric acid = 30 and 10 mm Hg respectively. Total initial pressure kept constant at 200 mm Hg by appropriate additions of nitrogen. 1 mm Hg = 1.80 mm Bourdon.

Frear[2] found $n = 3.5$ at 600°C and Norrish and Foord[3] found $n = 3$ at 620°C, compared with n = ca. 4 at 500°C.

Neumann and Serbinoff[4] found that at ca. 650°C there were three pressure limits of explosion at constant temperature. The three pressure limits of explosion, however, only occur in weak mixtures and explosions between the two lower limits require relatively long induction periods. Dugleux and Freling[5] have shown the explosions between the two lower limits to be due to carbon monoxide formed as a product from the methane. Garner and Ham[6] have also recognized the occurrence of carbon monoxide explosions in the products of methane combustion. Vanpée[7], like us, has recognized the inter-dependence of the oxidations of methane and carbon monoxide; his work is extensive and complementary to the present study.

Medvedev[8] and, later, Norrish and Foord[3] noticed a mild sensitizing effect of hydrogen chloride on methane combustion; evidently this corresponds to our observation of an increase in the rate of pressure rise in the early stages of reaction when hydrogen chloride is added.

TABLE 3

Total Initial Pressure	Initial Partial Pressure of Oxygen	Initial Partial Pressure Methane	Initial Partial Pressure of Additive	Value Found
mm Hg	*mm Hg*	*mm Hg*	*mm Hg*	
100	15 to 60	30	0	$x = 2.4$ to 2.7
100	20 to 50	40	10 mm CO	$x = 2.9$
100	15 to 60	30	10 mm HCl	$x = 1.55$
200	30	30 to 170	0	$m = -0.2$ to $+0.4$
150	30	10 to 120	0	$m = -1.0$ to $+0.4$
150	30	10 to 110	10 mm CO	$m = -2.0$ to $+0.4$
200	30	10 to 160	10 mm HCl	$m = +0.2$ to $+0.8$

Discussion

The work described above has shown that the kinetic laws governing the rate of pressure rise in methane oxidation may be profoundly affected by oxidation of the carbon monoxide formed as a product. Such carbon monoxide oxidation occurs whenever the vessel surface is suitable, whenever the temperature is sufficiently high and of course when there is sufficient oxygen left as the concentration of carbon monoxide becomes appreciable in the later stages of reaction.

The carbon monoxide oxidation occurring during the combustion of methane does not take place by the same mechanism as is involved with pure, dry, carbon monoxide-oxygen mixtures; for the oxidation of carbon monoxide is known[1] to be

profoundly affected by the presence of water vapor, of traces of hydrogen and of formaldehyde (all of which are probably products of methane combustion under the conditions used by us) and also by methane itself. Moreover, since it appears from, e.g., Figure 11, that, in the presence of carbon monoxide additions, no pressure change occurs until oxidation of the methane commences (cf. the evidence in Part I), the carbon monoxide oxidation occurring during methane combustion is not due to a greater ease of initiation of chains from carbon monoxide than from methane, but must be *induced* by the methane oxidation. That this can happen is independently shown by the fact that carbon monoxide oxidation during paraffin oxidation may occur at temperatures far below those at which carbon monoxide spontaneously oxidizes[9]. In other words, either the intermediates or the end products of methane combustion cause the conversion of carbon monoxide to dioxide. Water will be one end product which catalyzes the oxidation of carbon monoxide to dioxide, but in addition it is probable that at least one radical concerned in methane oxidation reacts with carbon monoxide producing the dioxide.

The HF-treated vessel surface particularly favors the rate of the pressure decrease due to carbon monoxide oxidation occurring towards the end of the methane oxidation. Thus only in the HF-treated vessel is there evidence of such a pressure decrease occurring at 500°C; and, while such a pressure decrease occurs in all four vessels used at 650°C, explosive pressure drops are most marked with the HF-treated vessel and have not been observed with the PbO-coated vessel. Carbon monoxide explosions almost certainly involve a branching-chain oxidation. It appears then that the branching-chain is favored by the HF-treated surface and particularly inhibited by the PbO-coated surface. This suggests, from the evidence given in Part I, p. 471, that the branching-chain oxidation of carbon monoxide may involve the HO_2 radical. Possibly the induced oxidation of carbon monoxide includes the step

$$HO_2 + CO = OH + CO_2 \qquad (1)$$

competing with

$$HO_2 \xrightarrow[\text{surface}]{} \text{destruction}$$

The present data show that carbon monoxide oxidation occurring in methane oxidation may cause an acceleration of the rate of pressure rise towards the end of the methane oxidation, and, as confirmed by the work with hydrochloric acid additions, increases the apparent value of x and decreases the apparent value of m. The acceleration is due to the branching-chain reaction which the carbon monoxide oxidation may introduce. Figure 9 may be used to provide direct evidence that additions of carbon monoxide to a $CH_4{:}2O_2$ mixture at 650°C in the HF-treated vessel increase the net branching factor controlling the early stages of the pressure rise in methane combustion.

The effect of additions of methane upon carbon monoxide oxidation has been described elsewhere[1]. There are two opposing effects; small additions catalyze, larger additions inhibit. The catalysis can be explained[2] by the reactions

$$O + CH_4 = OH + CH_3 \qquad (3)$$

$$OH + CO = CO_2 + H \qquad (4)$$

$$H + O_2 = OH + O \qquad (5)$$

i.e., by the production of a H atom (by reaction (4)) followed by the usual branching reaction of the hydrogen-oxygen system. The inhibition can be explained[2] by supposing that, in the presence of considerable quantities of methane, the reaction

$$OH + CH_4 = H_2O + CH_3 \qquad (6)$$

competes with (4); or the reaction

$$H + CH_4 = H_2 + CH_3 \qquad (7)$$

competes with reaction (5); and that the formation of CH_3 leads to partial chain-ending because the further oxidation of CH_3 forms formaldehyde which is known to be an inhibitor.

The work described above shows that additions of carbon monoxide have two opposing effects on the rate of pressure rise in methane combustion. Catalysis occurs in methane-weak mixtures, inhibition in methane-rich mixtures. The inhibition is simply explained; it may be attributed to the fact that carbon monoxide oxidation in itself leads to a pressure decrease which naturally offsets the pressure rise characteristic of methane oxidation. In other words, although reaction (1) may occur when carbon monoxide is added to methane-rich mixtures, it is followed by reaction (6) rather than by reaction (4); or, if reaction (4) occurs, the ensuing reaction is (7) rather than (5). Possibly also, the occurrence of reactions (6) and (7) leads to partial chain-ending (just as in our explanation of the inhibiting effect of large

methane additions upon carbon monoxide oxidation) by ultimate formation of formaldehyde. In either case, the branching reaction (5) is prevented and the effect of carbon monoxide additions to oxidizing methane is simply to offset the rate of pressure rise because of conversion of CO to CO_2.

When carbon monoxide is added to methane-weak mixtures, however, reaction (1) may be followed by reactions (4) and (5). Certainly, the effect of CH_4/O_2 ratio in causing either catalysis or inhibition by added carbon monoxide suggests that the induced oxidation of carbon monoxide to carbon dioxide includes a step

$$X + CO = CO_2 + Y$$

and that Y may then react with O_2 to cause chain-branching or with methane without chain-branching. X = OH and Y = H seem the most plausible identifications for X and Y. The chain-branching step (reaction (5)) causes a multiplication of chain centers and one can thus understand the catalysis caused by the carbon monoxide additions. The pressure decrease due to carbon dioxide formation is masked in methane-weak mixtures by the effects of chain-branching. One can also understand the acceleration of the rate of pressure rise noted when carbon monoxide oxidation occurs in the later stages (i.e., when the initial methane concentration has been greatly reduced) of the oxidation of initially carbon monoxide-free methane-oxygen mixtures; and the apparent inhibiting effect of increasing methane concentration in carbon monoxide-free methane-oxygen mixtures in the HF-treated vessel may be ascribed to reactions (6) and/or (7) competing more and more successfully with reactions (4) and/or (5) respectively. Competition between reactions (5) (causing chain-branching) and (7) may explain why the occurrence of carbon monoxide oxidation in methane oxidation increases the dependence of the maximum rate of pressure rise on oxygen concentration and decreases the dependence on methane concentration. Comparison of Figures 9 and 10 shows that the branching reaction introduced by carbon monoxide is favored by raising the temperature from 500 to 650°C; this is consistent with the branching reaction being (5) and competing with (7), for it is known that reaction (5) requires a considerably greater activation energy (20 ± 1 kcal/mole) than (7) (13 ± 2 kcal/mole[12]). Moreover, reaction (5) will also compete with

$$H + O_2 + M \rightarrow HO_2 + M \qquad (8)$$

so that one may be able to understand the apparent inhibition by inert gases of the rate of pressure rise in the HF-treated vessel at 650°C and why the values of t obtained with the other vessels at 650°C are so small. One cannot understand the intricacies of the data on n, m, x, t and E, especially at temperatures above 500°C, without taking into account the interactions of the oxidations of carbon monoxide and methane.

To identify reaction (5) as the branching reaction introduced by carbon monoxide is also consistent with the belief[1] that additions of small amounts of hydrogen, water vapor and methane all catalyze the oxidation of carbon monoxide essentially by introducing the branching reaction characteristic of the hydrogen-oxygen system. Finally, we may remark that competition at the relevant temperatures between reactions (5), (7) and (8) is compatible with what is known of the absolute rates of these reactions, although the uncertainties in our knowledge of the latter do not permit one to assert with certainty that such competition would occur. (For the rates of reactions (5) and (8) see Baldwin and Walsh[11]. These revise earlier estimates by Lewis and von Elbe. For the activation energy of (7), Steacie[12] gives 13 ± 2 kcal/mole; the steric factor for (7) may plausibly be taken as unity.)

The mild sensitizing action of hydrochloric acid additions in the early stages of methane oxidation may be related to the sensitizing action of hydrobromic acid on paraffin combustion[10].

The marked reduction in the value of m and the marked increase in the values of x and E at 650°C relative to 500°C (even after allowing for the complicating effects of carbon monoxide oxidation) we leave to a future publication for explanation.

This work was intended as a preliminary investigation. It is clear that analytical work is necessary to obtain greater certainty as to the reactions taking place. The reaction steps postulated are intended as an example of the type of reaction scheme needed to explain the qualitative facts; no claim is advanced that the scheme is complete or necessarily correct in all its details.

Summary

Systematic work has been carried out to determine the facts relating to methane oxidation,

at temperatures above 500°C and especially around 650 and 750°C. At these temperatures oxidation of carbon monoxide formed as a product becomes particularly important; and it turns out that much of the work might be alternatively described as a study of the interaction between the oxidations of methane and carbon monoxide. Four different vessel surfaces have been used. Carbon monoxide oxidation occurs particularly in weak mixtures and in the HF-treated vessel, though to some extent at the higher temperatures with all four vessel surfaces used. It causes an increase in the dependence of the maximum rate of pressure rise upon the initial oxygen concentration and a decrease in the dependence of the maximum rate of pressure rise upon the initial methane concentration; and its occurrence catalyzes, particularly when the methane concentration is small, the rate of pressure rise characteristic of methane oxidation. Additions of hydrochloric acid have a mild sensitizing action on the rate of pressure rise in the early stages of methane oxidation, but inhibit the oxidation of carbon monoxide. The effects of such additions have been studied to help elucidate the effects of carbon monoxide oxidation on methane oxidation.

A study has also been made of the effects of carbon monoxide additions to methane-oxygen mixtures; in methane-rich mixtures such additions reduce the rate of pressure rise, in methane-weak mixtures they increase the rate of pressure rise. It appears that a competition occurs between methane and carbon monoxide for at least one chain center. When such centers react with carbon monoxide an induced oxidation of carbon monoxide to carbon dioxide occurs, leading to a pressure decrease offsetting the pressure rise characteristic of methane combustion. If the induced oxidation includes the particular step

$$X + CO = CO_2 + Y$$

and if Y may react with oxygen to cause chain-branching and with methane or formaldehyde without chain-branching, it can be understood why the induced carbon monoxide oxidation catalyzes the rate of methane oxidation in methane-weak mixtures, masking the pressure decrease characteristic of carbon monoxide oxidation. Plausible identifications of X and Y would be X = OH, Y = H.

REFERENCES

1. Hoare, D. E., and Walsh, A. D.: Trans. Faraday Soc., *50*, 37 (1954).
2. Frear, G. L.: J. Am. Chem. Soc., *56*, 305 (1934).
3. Norrish, R. G. W., and Foord, S. G.: Proc. Roy. Soc., *A157*, 503 (1936).
4. Neumann, M. B., and Serbinoff, A. I.: J. Phys. Chem. U.S.S.R., *3*, 75 (1932).
5. Dugleux, P., and Fréling, E.: *Cinétique et Mecanisme . . . de Combustion.* Centre National de la Recherche Scientifique, Paris, 1948.
6. Garner, W. E., and Ham, A. J.: Proc. Roy. Soc., *A170*, 80 (1939).
7. Vanpée, M.: Ann Mines Belg., *47*, 1053 (1948).
8. Medvedev, S. S.: Trans Karpov. Inst. Chem., *4*, 117 (1925).
9. Mardles, E. W. J.: Trans Faraday Soc., *27*, 686 (1931).
10. e.g., Vaughan, W. E., and Rust, F. F.: U. S. Patent 2,395,523 (1946).
11. Baldwin, R. R., and Walsh, A. D.: *Discussions Faraday Soc.*, 1955. In press.
12. Steacie, E. W. R.: *Atomic and Free Radical Reactions* New York, Reinhold Publishing Corp. 1946.

Discussion by Arthur Levy*

The authors comment that small and large concentrations of methane have catalytic and inhibiting effects respectively upon carbon monoxide combustion. These effects offer one of the rarer opportunities of applying our knowledge of relatively low-temperature kinetic phenomena to flame reactions. Walker and Wright† showed a similar effect for both methane and propane on the flame stability of carbon monoxide-air mixtures.

On examining Walker and Wright's data in more detail, it became evident that the effect of adding hydrocarbons to carbon monoxide flames was explained by a consideration of the preflame kinetics of methane oxidation.‡ As pointed out by Hoare and Walsh and others, the oxidation of methane is almost stepwise in that it tends to inhibit its own complete oxidation until the methane first oxidizes to carbon monoxide. Applying this assumption to the hydrocarbon-carbon monoxide flames, the gas mixture passing through the flame zone was considered as a carbon monox-

* Battelle Memorial Institute, Columbus, Ohio.

† P. L. Walker and C. C. Wright: Fuel, *31*, 37 and 45 (1952).

‡ A. Levy and P. F. Kurz: J. Am. Chem. Soc., in press. Presented at the 125th Meeting of the American Chemical Society, Kansas City, Mo., March, 1954.

ide-water vapor mixture obtained by partial oxidation of the original carbon monoxide-hydrocarbon mixture. It was then possible to show that the points of maximum flame stability in carbon-monoxide-hydrocarbon mixtures were related to points of maximum stability in known carbon monoxide-water vapor mixtures. It is of further interest to note that the most stable carbon monoxide-hydrocarbon mixture was equivalent to the most stable carbon monoxide-water vapor mixture, containing approximately seven per cent water vapor.

45

THE KINETICS OF THE SLOW COMBUSTION OF METHANE AT HIGH TEMPERATURE[a]

By M. VANPÉE AND F. GRARD

Although the reaction between methane and oxygen is perhaps the most thoroughly investigated of all chemical changes of the saturated hydrocarbons no systematic kinetic study has been reported for temperatures above 500°C. Recent explosion limits data[1] suggest that the conventional kinetic interpretation, based on experiments performed between 400° to 500°C, no longer applies at higher temperatures.

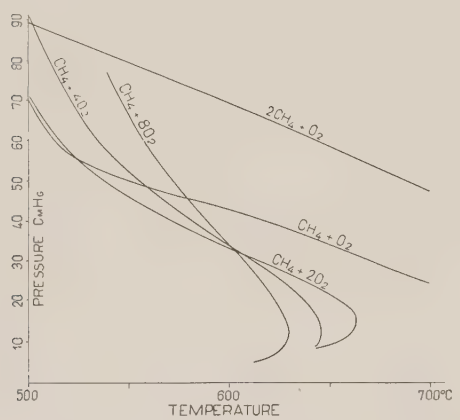

FIG. 1. Explosion limits of CH_4-O_2 mixtures

It will be seen from Figure 1 that the temperature decrement of the upper explosion limit is much larger for rich oxygen mixtures than for rich methane mixtures. Assuming that in this case ignition is a thermal process which sets in at some critical reaction velocity, this behavior indicates that the kinetics of the slow combustion reaction undergo a profound modification when the temperature is raised above 500°C.

The objective of the present work was to investigate this question and to provide a broader experimental basis for the theoretical treatment of this important reaction.

Apparatus and Procedure

Most of the kinetic measurements reported here were made in a cylindrical silica vessel (45 mm internal diameter, 270 cc capacity, 4.7 cc dead space). A few measurements were performed in a larger spherical vessel of the same material (1337 cc capacity, 28 cc dead space). The latter vessel was supported in an electrical furnace formed by adjunction of two movable hemispheres.

Stainless-steel jackets surrounded the reaction vessels and the temperature was maintained constant to within ± 0.2°C by automatic control of the furnace power supply. All connecting tubing was heated above 100°C to prevent the condensation of water produced in the reaction. After the vessels had been aged by a sufficient number of preliminary combustions, satisfactory reproducibility was obtained by rigid standardization of pumping times and other procedures.

Methane and oxygen were mixed to the desired composition and total pressure in a large mixing vessel before introduction into the reaction vessel. The progress of the combustion was followed by a sensitive spoon gauge and recorded on photographic paper[1].

[a] Research supported by l'Institut National de l'Industrie Charbonnière.

Experimental Results

Experimental results are plotted graphically in Figures 2 to 7. Each ΔP curve is marked by a circle giving the mixture composition (straight lines joining the circles) and the initial total pressure in cm Hg (figures in circles). Each diagram refers to a single temperature. Figures 2 to 5 refer to experiments carried out in the small cylindrical vessel, Figures 6 and 7 to experiments carried out in the large spherical vessel.

It will be noted that the initial partial pressures have been chosen from sets of values such that experiments may be gouped in different ways to show the dependence of the reaction on each of the following variables: mixture composition, total pressure, partial pressure of methane, partial pressure of oxygen, temperature, and vessel size.

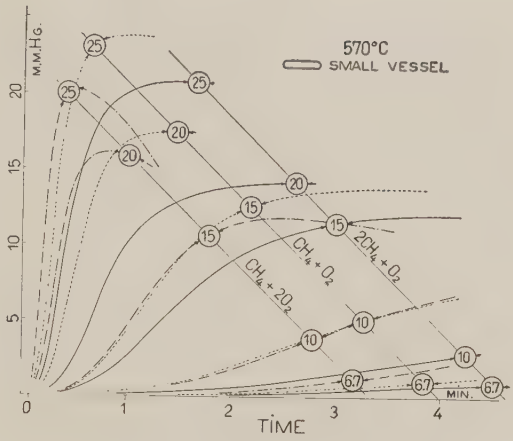

FIG. 2

GENERAL CHARACTERISTICS OF THE COMBUSTION REACTION

All the ΔP curves obtained show the typical course of an autocatalytic process, characterized by an induction period in which little or no pressure rise occurs, followed by acceleration to a maximum rate of pressure rise. It is well known that at temperatures of about 500°C and less, this acceleration is due to the intermediate formation of formaldehyde[2], which gives rise to degenerate branching[3]. It should be noted, however, that the water vapor formed during combustion also accelerates the overall process[4].

Above 600°C, other compounds may play a similar role. They are carbon monoxide and hydrogen which then forms in small amounts during combustion[1].

Although of quite a different type, there is another factor which accentuates the concavity of the curves towards the time axis. It is the inhibitory effect of methane which will be discussed later. This factor operates only above 600°C and is especially noticeable at the end of the combustion of very rich oxygen mixtures. In these combustions, the reaction velocity increases more and more rapidly with the consumption of methane and may culminate in an explosion, presumably of carbon monoxide.

At this point it will be useful to consider briefly the behavior of carbon monoxide in the CH_4-O_2 system. It is well known that the combustion of wet mixtures of carbon monoxide and oxygen becomes perceptible only above 550°C, but can

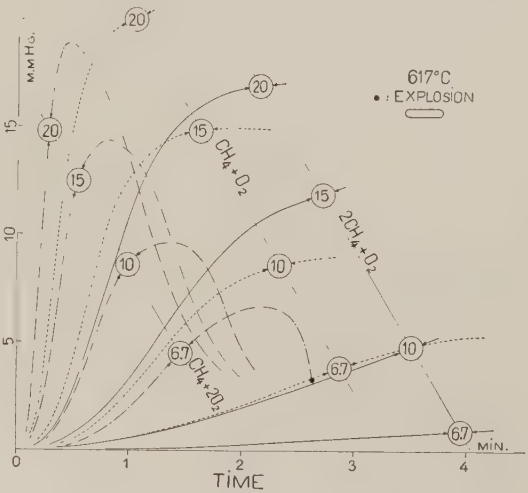

FIG. 3

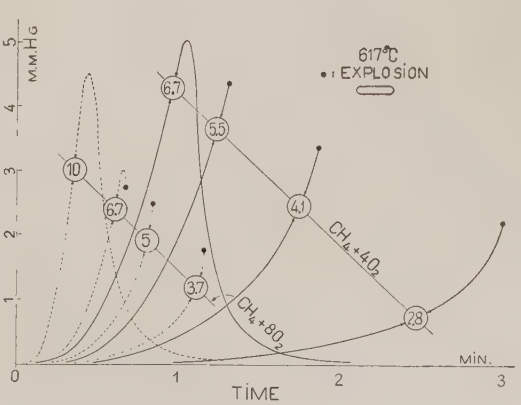

FIG. 4

rapidly become explosive in the neighborhood of 600°C. The presence of methane modifies these properties radically. Slow oxidation starts then at temperatures still lower than 400°C[4] but is, at higher temperatures, retarded by methane[1, 5, 6, 7]. Thus, the latter gas appears to act as a moderator of combustion in the CO-O_2 system.

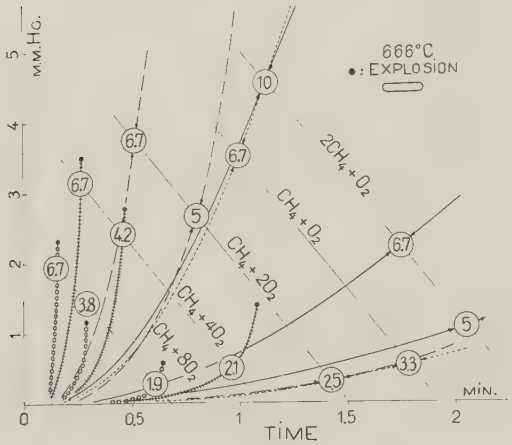

FIG. 5

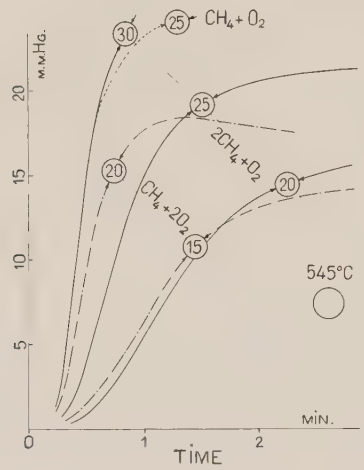

FIG. 6

This, together with the fact that methane also can inhibit its own combustion at high temperature, is the key to the general shape of the ΔP curves for rich oxygen mixtures. In these curves a maximum is reached when the combustion of carbon monoxide ($2CO + O_2 = 2CO_2$ involving a decrease of volume) becomes faster than that of methane ($2CH_4 + 3O_2 = 2CO + 4H_2O$ involving an increase of volume). The reaction culminates in an explosion if the total pressure is less than the second explosion limit of carbon monoxide and if the methane concentration falls below some critical value. However, a maximum is not necessarily reached before the explosion sets in, because the inhibitory effect of methane on its own combustion may be such that the rate of CO consumption never exceeds that of CH_4 consumption during the reaction.

KINETICS OF THE COMBUSTION REACTION

It will be seen from the above discussion that the reaction is very complex. Accordingly, the kinetic laws deduced in this section from the maximum pressure rise data are not to be considered as exact mathematical laws, but rather as being a convenient way to formulate qualitative results.

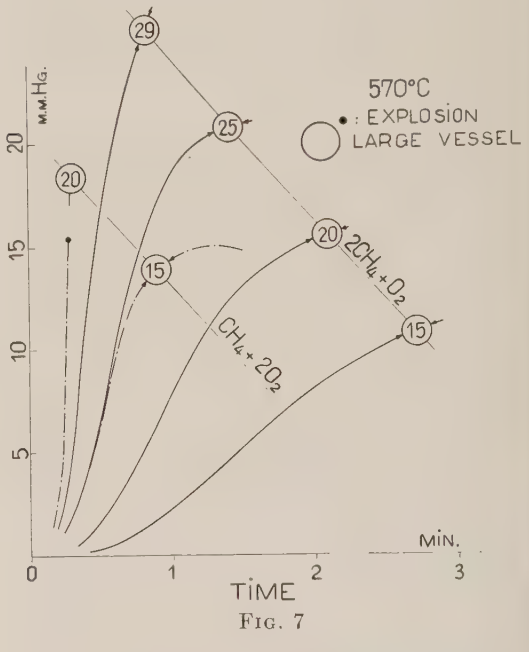

FIG. 7

The dependence of the maximum rate of pressure rise (V_m) on the partial pressures of oxygen, methane, nitrogen (the p_i's) and the total pressure (P) is summarized in Table 1 where the n_i's are exponents defined by the equations

$$V_m = \text{const. } p_i^{n_i} \qquad \text{(I)}$$

It should be noted that no systematic deviation of the exponents with the total pressure could be clearly established, except perhaps that n_p showed some tendency to increase for very small or very high reaction rates. Therefore, this factor has been disregarded as not giving consistent results, and the tabulated values are mean values based

on all the experimental data for each temperature and derived from Figures 2 to 7.

The values of n_{O_2} and n_{CH_4} were obtained by direct comparison of experiments differing only by their partial pressures of methane or of oxygen. If equations (I) are correct, the sum of these values should be equal to the exponent n_p obtained by comparison of experiments performed under different total pressures but referring to the same mixture composition. Our results in this respect show an agreement which is rather surprising in view of the generally qualitative character of our computations and of equations (I). Use was made of this agreement to estimate the value of n_{O_2} in the large spherical vessel at 570°C, where experiments for the direct determination of n_{O_2} unfortunately had not been performed.

As has been suggested above, on the basis of the explosion limit data (Fig. 1), there is a marked change of kinetic behaviour with temperature. As the temperature increases, the reaction becomes more and more sensitive to the oxygen concentration. On the other hand, the dependence on methane decreases, the latter gas showing, as already stated, a definite inhibitory effect when the temperature reaches 666°C.

These conclusions are clearly apparent in the diagrams themselves. Combustions carried out at the same total pressures but with different compositions show that the most reactive mixtures are those of rich oxygen content, a result in contrast with the well-known kinetics of the reaction at 400°C, where the most reactive mixture consists of methane and oxygen in the ratio of 2:1. Nitrogen, as inert gas, has a small accelerating influence which decreases with temperature, indicating a general tendency of chains to break down in the gas phase at high temperature.

When the large vessel is substituted for the small one, the reaction velocities for the $2CH_4 + O_2$ mixture are doubled. Owing to possible variable wall effects, the absolute value of this ratio is not of great significance but the fact that it is much greater for the $CH_4 + 2O_2$ mixture is established. It indicates, as shown in Table 1, that n_{O_2} increases and n_{CH_4} decreases with increasing vessel diameter.

In this respect, the effect of diameter is somewhat similar to that of temperature. The change of kinetics is considered here as a consequence of the overall energy of activation being largely dependent on mixture composition. The energies of activation given in Table 2 are computed, using maximum rate of pressure rise data, as before.

TABLE 1

Vessel Volume	Temp	n_{O_2}	n_{CH_4}	n_p	n_{N_2}*
cc	°C				
270	570	2.40	1.45	3.81	0.43
270	617	2.52	0.11	2.98	0.12
270	666	3.80	−0.14	3.57	0.10
1337	545	3.10	1.18	4.34	
1337	570	2.91 (computed)	0.63	3.54	

* n_{N_2} computed from experiments not recorded in the diagrams.

TABLE 2. OVERALL ENERGIES OF ACTIVATION IN KCAL

Temperature	$2CH_4 + O_2$	$CH_4 + O_2$	$CH_4 + 2O_2$
°C			
	Small vessel		
570–617	27.6	48.6	66.7
617–666	53.6	50.9	57.3
	Large vessel		
545–570	19.2		60.4

TABLE 3

Temperature	Vessel	n_{O_2}	n_{CH_4}	n_{N_2}	E kcal	Authors
°C						
376–400	*	0.5	2.3	1.1	95.5	Vanpée[4]
416	*	0.5	2			Van Meerssche[9]
462–525	†			0.5	25	Hoare and Walsh[10]
	‡			0.9	58	Hoare and Walsh
467	§	1	1.60		61.5	Fort and Hinshelwood[11]
480	¶	1	2	1		Norrish and Foord[12]

* Pyrex, uncoated.
† Quartz, hydrofluoric treated.
‡ Quartz, PbO coating.
§ Soda glass, uncoated.
¶ No information.

E varies considerably with temperature and mixture composition. Very small values are obtained for the $2CH_4 + O_2$ mixture in the neighborhood of 570°C.

RELATION TO OTHER WORK

Our results have been compared with results obtained by other workers at lower temperatures. These are summarized in Table 3, according to increasing temperature.

Although these data were obtained in quite different reaction cells, the general tendency of n_{O_2} to increase and n_{CH_4} to decrease with temperature is clear. The apparent discrepancies are now well understood and are due to a temperature effect. The same is true of the overall energy of activation which, as pointed out by Hoare and Walsh[10], also depends markedly on the nature of the wall.

Discussion

The inhibiting effect that methane exerts on its own combustion sets in around 600°C. It is precisely around this temperature that the combustion of carbon monoxide and hydrogen begins to be inhibited by methane, suggesting that all these retarding influences are due to the same common process. It is generally accepted[4, 6, 7] that inhibition in the latter case is due to removal of hydrogen and oxygen atoms and hydroxyl radicals by methane.

We do not believe, however, that under our experimental condition of high temperature in closed chamber, the removal of H atoms or OH radicals by methane would lead to a chain-breaking process. The resulting methyl radicals:

$$CH_4 + OH = H_2O + CH_3 \qquad (1)$$

may in fact continue chains according to the reaction:

$$CH_3 + O_2 = CH_2O + OH \qquad (2)$$

which will be much faster than the eventual destruction of CH_3 radicals at the walls.

The situation is entirely different for oxygen atoms which may be expected to react with methane according to:

$$CH_4 + O = CH_2 + H_2O \qquad (4)$$

The bivalent CH_2 radical may react further with methane to give rise to a stable ethane molecule:

$$CH_2 + CH_4 = C_2H_6 \qquad (6)$$

Therefore the sequence of reactions (4) and (6) constitutes a gas-phase chain-breaking process in the H_2-O_2 or CO-O_2 system.

If we extend this to the CH_4-O_2 system, we are led to conclude that at high temperatures atomic oxygen also is a chain carrier. This is not a new idea, being supported in the past by Norrish[3] in his well-known mechanism involving the two alternating reactions:

$$O + CH_4 = CH_2 + H_2O \qquad (4)$$

$$CH_2 + O_2 = CH_2O + O \qquad (5)$$

This oxidation scheme is very well supported by the remarkable sensitizing function of nitrogen peroxide, which would act as a chain starter giving rise either to oxygen atoms of CH_2 radicals by reaction with methane.

At low temperature, however, chains (4) and (5) are not likely to be very efficient. As oxygen atoms are the most energy-rich of the radicals considered, their appearance at low temperature is relatively much less probable than the appearance of lower energy radicals, such as OH or CH_3. Accordingly, we shall assume that at low temperature the reaction will be propagated through the gas mainly by chains (1) and (2) proposed earlier by Lewis and Von Elbe[13].

This leads to the concept that the change in kinetic behavior with temperature is due to the gradual replacement of chains (1) and (2) by chains (4) and (5). This may occur if the chain carriers of the high-temperature chain, CH_2 and O, orginate from the chain carriers of the low-temperature chains, CH_3 and OH. On the other hand, the increasing sensitiveness with increasing temperature of the maximum rate towards the oxygen concentration suggests that the vital link between the two different chain processes involves a reaction of CH_3 or OH with oxygen.

A possible reaction of OH with O_2 would be:

$$OH + O_2 = HO_2 + O$$

But this reaction would require a very high energy of activation, (at least 60 kcal). Further, it is not operative in the H_2-O_2 system and therefore will not be considered.

Possible reactions of CH_3 with O_2 are:

$$CH_3 + O_2 = HO_2 + CH_2 \qquad (3)$$

$$CH_3 + O_2 = CH_3O + O \qquad (3')$$

Granted the value of 80 kcal for D (H-CH_2) proposed by Kistiakowsky and Rosenberg[14] and the value of 60 kcal for D (H-O_2), reaction (3) is only endothermic to the extent of 20 kcal. As CH_3 is here present at the very low stationary concentration of a free radical, this makes (3) fast enough to act as an important initiation process above 500°C.

Reaction (3′) in the CH_4-O_2 system is the counterpart of reaction:

$$H + O_2 = OH + O$$

in the H_2-O_2 system. Although it is similar to reaction (3) in its kinetic consequences it will not be considered further here because no evidence has been recorded for the existence of a CH_3O radical.

If it now is assumed that the relatively unreactive HO_2 radical diffuses chiefly to the walls without interfering with the reacting system, the scheme of reactions (1) (2) (3) (4) (5) and (6) leads to the following expression for the rate of consumption of methane:

$$-\frac{d(CH_4)}{dt} = k_1[OH][CH_4]\left[1 + \frac{k_3k_5}{k_6(k_2 + k_3)}\frac{[O_2]}{[CH_4]}\right] \quad (II)$$

It should be noted that the reaction velocity is given here in terms of the steady-state concentration of the hydroxyl radical. The complete solution of the kinetic problem would require the complete specification of the initiating and chain-breaking processes. However, there is considerable uncertainty in this connection and, as the consequences we wish to emphasize are independent of these processes to a first approximation, we prefer for the present to remain indefinite on this point.

Because of this same indeterminacy, equation (II) does not describe explicitly the degenerate branching character of the reaction. The latter is implicitly contained in the term [OH] which is a function of time. This is not discussed here as only the approximate method of comparing maximum rates has been adopted. Therefore emphasis must be placed on trend rather than on exact numerical agreement of equation (II) with experience.

The first term of equation (II) represents the methane consumed by the low-temperature chains and the second term represents the methane consumed by the high-temperature chains. When passing from the first type of oxidation to the second, n_{O_2} and n_{CH_4} respectively, become larger and smaller than unity. The change of kinetics with temperature is thus qualitatively described by equation (II).

Our tentative scheme of oxidation offers furthermore an explanation of the self-inhibiting phenomenon observed in the combustion of rich methane-oxygen mixtures near the upper explosion limit[15].

This phenomenon is depicted by curve II of Figure 8.

It is important to note that the oscillation in curve II is accompanied by a weak blue luminescence[16]. Egerton, Moore and Lyn[17] obtained similar results by adiabatic compression of methane-air mixtures and Moore[18] has recently found that the luminescence shows the spectrum of excited formaldehyde.

According to the views expressed by Lewis and Von Elbe[19], the chemiluminescence of cool flames may be ascribed to the reaction of the

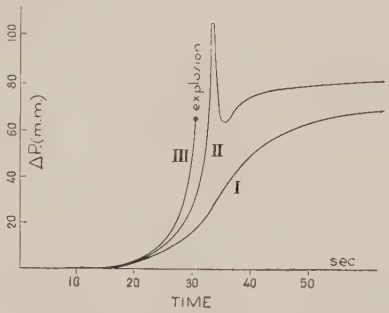

FIG. 8. Pressure pulse in $2CH_4 + O_2$ mixture at 535°C and 780 mm Hg.

comparatively long-lived HO_2 radical with methyl radicals.

$$CH_3 + HO_2 = HCHO + H_2O$$

On this basis, the chemiluminescence would thus be an indication of a rapid removal of free valencies from the reacting system. This agrees well with the experimental fact that the luminescence is concomitant with a sudden decrease of chemical activity.

Our scheme of oxidation contains all the elementary species necessary to explain the methane oscillation on this basis.

The above discussion does not exclude the possibility of a peroxidation mechanism, which could be operative at low temperature as suggested by Everett and Minkoff[22]. Until very recently this type of oxidation, commonly adopted for the higher hydrocarbons, was not thought to be applicable to methane, because no peroxide had been detected in its combustion. However, Minkoff and Salooja[20] now cite evidence for the presence of hydrogen peroxide and methyl hydroperoxide in the slow combustion reaction at 440°C to 520°C. Gray[21] finds similar results for the mercury photo-sensitized oxidation near

room temperature. In Gray's experiments, CH_3OOH appears as a combustion intermediate—a result which becomes understandable if one supposes the existence of the CH_3OO radical.

All these facts lead to the conclusion that even at 400°C CH_3OO is sufficiently stable to permit a chain mechanism of the type:

$$CH_3 + O_2 = CH_3O_2 \qquad (7)$$

$$CH_3O_2 + CH_4 = CH_3OOH + CH_3 \qquad (8)$$

with subsequent oxidation or decomposition of the intermediate methyl hydroperoxide.

The gradual replacement of these new chains by the CH_3-OH chains at higher temperature may lead as before to a marked change in the kinetic behavior. If it is assumed that CH_3OO, like the HO_2 radical, may incur some probability of destruction at the walls, this change only affects the methane exponent, n_{CH_4}, which decreases from unity when passing from the CH_3O_2-CH_3 chains to the CH_3-OH chains.

Finally, it may be noted that in the H_2-O_2 system the combustion properties depend mainly on the reactivity of hydrogen atoms towards oxygen. In the CH_4-O_2 system, CH_3 takes the place of H, and the ultimate reason for the change in the kinetics with temperature lies in the different possibilities of reaction of a CH_3 radical with an O_2 molecule.

$$CH_3 + O_2 = CH_3OO + \simeq 60 \text{ kcal (low temperature)}$$

$$CH_3 + O_2 = CH_2O + OH + 47 \text{ kcal (intermediate temperature)}$$

$$CH_3 + O_2 = CH_2 + HO_2 - 20 \text{ kcal (high temperature)}$$

Acknowledgment

The authors wish to thank M. Fripiat, Director, Institut National des Mines, for his kind interest and for permission to publish this work. Acknowledgment is made also to M. Fourneau, of the Union Chimique Belge, for valuable advice and the construction of the spherical furnace used in this work.

REFERENCES

1. Vanpée, M., and Fally, G.: Bull. Soc. Chim. Belg., *61*, 474 (1952); *61*, 64 (1952).
2. Bone, W. A., and Gardner, J. B.: Proc. Roy. Soc. London, *A154*, 297 (1936).
3. Norrish, R. G. W.: Proc. Roy. Soc. London, *A154*, 297 (1936).
4. Vanpée, M.: Ann. Min. Belg., *47*, 1053 (1948); *48* (1949).
5. Hoare, D. E., and Walsh, A. D.: Nature, *170*, 838 (1952).
6. Dixon-Lewis, G., and Linnett, J. W.: Proc. Roy. Soc. London, *A210*, 48 (1951).
7. Levy, A.: J. Chem. Phys. pp. 566–7 (1953).
8. Baldwin, R. R.: Fuel, *31*, 312 (1952).
9. Van Meerssche, M.: Ann. Min. Belg., 48 (1949).
10. Hoare, D. E., and Walsh, A. D.: Proc. Roy. Soc. London, *A215*, 454 (1952).
11. Fort, R., and Hinshelwood, C. N.: Proc. Roy. Soc. London, *A129*, 284 (1930).
12. Norrish, R. G. W., and Foord, S. G.: Proc. Roy. Soc. London, *A157*, 503 (1936).
13. Lewis, B., and Von Elbe, G.: J. Am. Chem. Soc., *75*, 970 (1935).
14. Kistiakowsky, G. B., and Rosenberg, N. W.: J. Am. Chem. Soc., *72*, 321 (1950).
15. Vanpée, M.: Ann. Min. Belg., *49*, 710 (1950).
16. Vanpée, M., and Grard, F.: Fuel (1954).
17. Egerton, A. C., Moore, N. P. W., and Lyn, W. T.: Nature, *167*, 191 (1951).
18. Moore, N. P. W.: Nature, *173*, 543 (1954).
19. Lewis, B., and Von Elbe, G.: *Combustion, Flames and Explosions of Gases*. New York, Academic Press, Inc., 1951.
20. Minkoff, G. J., and Salooja, K. C.: Fuel, *32*, 516 (1953).
21. Gray, J. A.: J. Chem. Soc., 3150 (1952).
22. Everett, A. J., and Minkoff, G. J.: *Third Symposium on Combustion, Flame, and Explosion Phenomena*, p. 390. Baltimore, The Williams & Wilkins Co., 1949.

46

ON THE COMBUSTION OF PARAFFIN HYDROCARBONS

By P. DUGLEUX AND E. FRELING

Differential Method of Kinetic Study of Oxidation Reactions

In setups commonly used for kinetic studies by the static method[1, 2], recording of the pressure change starts while the gases introduced into the reaction vessel are still being heated. When the inlet stopcock is closed, these gases are not yet in thermal equilibrium with the vessel and at least 5 sec elapse before their heating rate becomes negligible. The course of the heating process depends on the speed of introduction of the gas. As the stopcock is operated manually, it is impossible to determine this speed precisely. This objection prevents the study of short lag phenomena. Moreover, in the case of long recordings, the variations in the furnace temperature, which are negligible for rapid recordings, superimpose their effect on the reaction velocity.

The addition to furnace F of a vessel of suitable volume connected to the outside of the manometer permits thermal compensation and makes possible a totally differential method, whereas in all earlier devices only the manometer was differential. An experimental study having proved that the heating curve depended little on the gas itself, this second vessel was fed from a dry-air tank.

Figure 1 shows the apparatus schematically. Stopcock R_1 is turned mechanically at constant velocity (inlet time, 0.5 sec). It allows simultaneous introduction of the mixture under examination into reaction vessel P_1 and manometer cell J, and of dry air into the compensating vessel P_2 and the second space of the differential manometer M. Stock vessels G_1 and G_2 are at pressures such that, when the inlet stopcock is closed, the pressure is the same in P_1 and P_2. Let V_1 be the volume of P_1 and the portion of the connecting tube inside the furnace; V_1' the volume of the connections outside the furnace and the gage J; V_2 the volume of P_2; and V_2' the volume of the outer tubes and of the second space of manometer M. To realize the compensation, we must have $V_2 = V_1 V_2'/V_1'$. Gage J is of the Bourdon type, made of fused silica. It is placed in a small molded Pyrex recess of the same shape as J, so as to make the ratio V_2'/V_1' as small and as constant as possible. Preliminary tests in which dry air was introduced into P_1 and P_2 show that recordings are useful for times of 1 to 1.5 sec after opening the inlet stopcock. Whenever necessary, connections outside the furnace can be heated.

In the above description, we have stressed thermal compensation. This does not detract, however, from the general applicability of this method which allows the comparison of any mixture (in P_1) with another (in P_2): for instance, comparison of a mixture containing a promoter or an inhibitor with a mixture without promoter or inhibitor; comparison of the pyrolysis of a hydrocarbon with traces of oxygen to that of the pure hydrocarbon; study of the influence of radiation on a reaction; etc. It is necessary, of course,

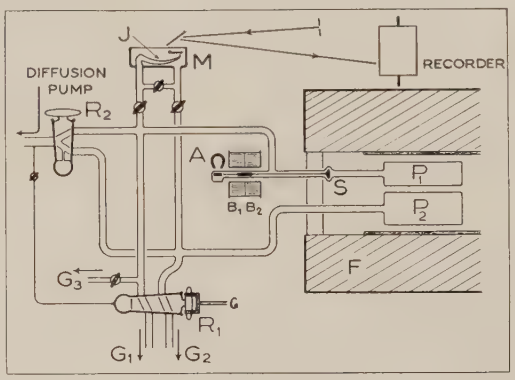

FIG. 1

to have comparable volumes (i.e., $V_2 = 2V_1$, S/V being constant).

Study of Rapid-Burning Mixtures

The apparatus just described can be used for the kinetic study of the slow oxidation and of spontaneous ignition in the presence of an inert gas. When the combuxent is oxygen, the projection of the flame following spontaneous ignition can give rise to an explosive wave inside the tube connecting P_1 to the rest of the apparatus. The propagation of this wave in the connecting tubes almost invariably ruptures them. A systematic study has led us to equip the furnace with a ground silica safety valve S which closes[3, 4] the outlet tube when the temperature gradient reaches a maximum. An electromagnetic device (coil B_1) automatically shuts the valve after the gas has

been introduced. The valve is opened by B_2 and, when not needed, it can be blocked in the open position by a magnet A.

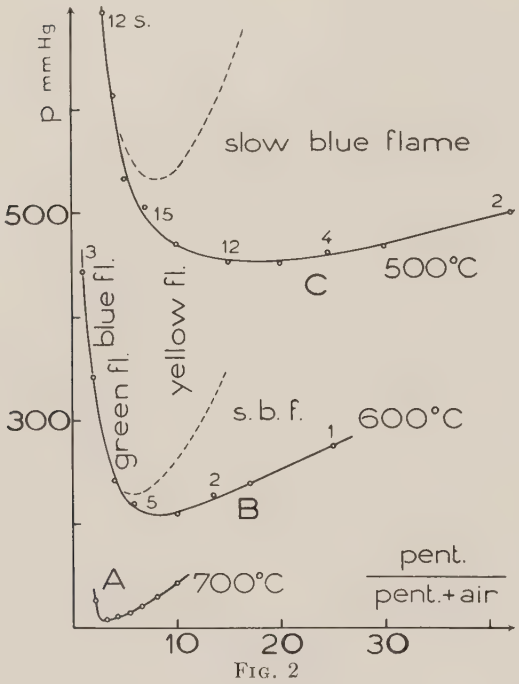

FIG. 2

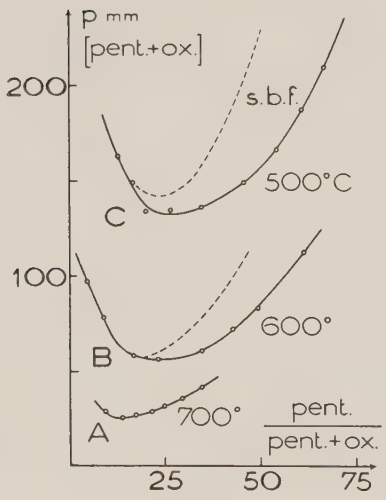

FIG. 3

In addition to isolating the reaction vessel, valve S is used to pump out any mixture remaining in the tubes outside P_1, which is replaced by an inert gas supplied from G_3 at the same pressure. This makes it possible to use the manometer after opening S again without running the risk of having the initial mixture diffuse from the outer tubes, or ignite explosively. The time lag must, of course, be long enough to allow for these operations.

Spontaneous Ignition of Pentane-Air Mixtures

The reaction vessel used is a fused silica cylinder, 28 mm in diameter and 125 mm long. The inlet pressures are less than 1 atm. All explosion regions (pressure against concentration) shown on Figures 2, 3, 4 are for *n*-pentane (Philips Research Grade). They are limited by curves (A, B, C, ··· G) of similar shape inside which the reactions follow an identical evolution. The flames are light blue at low concentrations, and become rapid and bright near the stoichiometric mixture. They are green[5] (C_2 radicals) for concentrations slightly above stoichiometric and take on an orange-yellow tinge for even higher values. As the pressure is reduced, this orange-yellow flame is progressively replaced by a slow, slightly luminous blue flame[6]. The transition is shown on the graphs by the dotted curves. This gradual evolution is independent of temperature. Only the color intensity varies; the green flames, in particular, are clearly visible only at 600°C.

The diagrams in Figures 2 and 3 correspond to the same group of experiments carried out on pentane-air mixtures. Only the coordinates are different. In addition to the variation of the concentration corresponding to the minimum limit, comparison of the two diagrams shows that the study of the oxidation reaction of a combustible-air mixture gives results that are difficult to interpret; the ratio nitrogen/(combustible + oxygen) does not remain constant. In our case this ratio varies from 3.8 to 0.9 when the concentration relative to the air increases from 0 to 40 per cent.

Spontaneous Ignition of Pentane-Oxygen Mixtures. Effect of an Inert Gas

Figure 4 shows the results obtained with oxygen. The explosion limits at 500°C are compared with the limits obtained for mixtures to which enough argon was added to make the ratio argon/(combustible + oxygen) equal to 2. The resulting curve F′ is virtually a translation of F parallel to the pressure axis, showing a promoting effect. The transition from yellow flames to slow, blue flames (*f* and *f*′) is less sharp for high pressures. Comparison of curves A (Fig. 3) and D (Fig. 4)

shows that at 700°C, too, the presence of nitrogen has no effect on the minimum value; in this particular case we can neglect the variation of the nitrogen/(combustible + oxygen) ratio because the minimum is much less flattened and the partial oxygen pressure is relatively high compared to that of the combustible.

As we have stressed above, with or without addition of inert gas and whatever the temperature, the evolution of phenomena remains fundamentally the same. Nevertheless, when mixtures are diluted by an inert gas and the propagation velocity is even lower, confusion between slow, blue flames and cool flames may occur. Mullins[7] and Gray[8], for instance—provided their mixtures were in thermal equilibrium at the time of ignition—were dealing with slow, blue flames rather than cool flames. These are normal flames and their change in color does not correspond to any discontinuity in ignition. Moreover, pressure recordings with time for decreasing inlet pressure along a vertical line intersecting the limit and shown by dotted line (with or without an inert) indicate that the evolution of the phenomenon is the same on both sides of this limit. Recordings obtained are always of type A (Fig. 5); the maximum pressure attained (usually outside the graph) decreasing steadily with the inlet pressure. This regular decrease in pressure leads to recordings of type B near the limit of the explosion range and of type C at this limit whereas farther away there is slow oxidation, D, culminating in a glow. As regards luminous emission, systematic observation shows that the flame front is blue with a yellow nucleus behind. At higher pressures, the brighter orange-yellow emission alone is perceptible to visual observation. As the pressure is reduced, the yellow nucleus becomes less luminous and its diameter becomes less than that of the reaction vessel, bringing into view the blue front around it. At even lower pressures, only the blue front is visible, occupying a progressively smaller cross section of the reaction vessel and propagating more slowly still.

These observations, together with our own experiments on other hydrocarbons, show that this is a general fact. Cool flames occur only at temperatures between 250°C and 450°C. Cool flames are obtained most readily—as we shall see—for a high concentration and the only criterium[9] of their existence is the emission of excited formaldehyde spectra.

Variation of the Concentration Relative to the Easiest Ignited Mixture (Pentane and Other Hydrocarbons)

The regions in Figure 4 together with the qualitative results on Figures 2 and 3 show that the

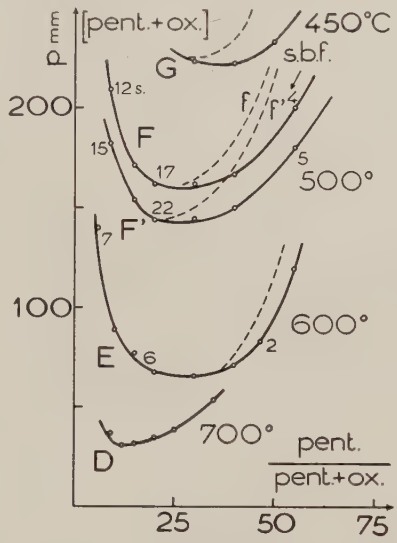

Fig. 4

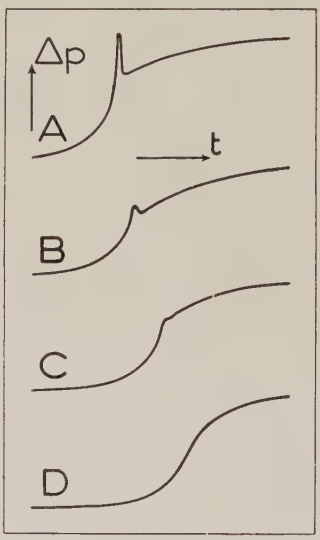

Fig. 5

concentration corresponding to the minimum of the limits of the explosion regions increases when the temperature decreases. (The ignition lags are indicated on the limits.) At 700°C this concentration is virtually equal to the stoichiometric mixture, at 600° and 500°C, its values are of the same order (25 per cent), increasing to 37 per

cent at 450°C. At this last concentration, the time lag is short and the intense glow preceding the flame begins in the admission tube. At lower temperatures we are dealing with another type of ignition which produces cool flames; at higher pressures we have two-stage flames. Between 345° and 317°C, an attempt was made to study passage from cool flames to two-stage flames as a function of the concentration. The passage from the two-stage yellow flame to the blue flame[4]—still in two stages—and then to the cool flame cannot be seen well enough by visual observation to note a change (the transition is sharp only below 30 per cent just where normal flames become intense). Moreover, the phenomenon is too rapid for the manometer to follow the pressure variation and record its value. Accordingly, the manometer was used to observe (light emission being extremely weak) the evolution of the cool flame region at 314°C. Within the limit of experimental error (reproducibility was not satisfactory) the limit is the same (44 mm) for concentrations of 30, 40 and 50 per cent. This leads to a flattened minimum in the (p, c) region. Reproducibility was better at lower temperatures but we had to operate at constant pressure, the cool flame range limit (p, T) being almost vertical in this case. Figure 6 shows the results obtained at 300 mm, a flattened minimum appearing around 50 per cent.

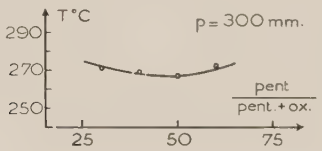

FIG. 6

All that has been said for pentane[10] applies also to the other higher paraffin hydrocarbons. For ethane, Taylor and Ribett[11] obtained a curve (ignition pressure/concentration) with a minimum around 50 per cent for temperatures around 500°C. We repeated these experiments and obtained a minimum around 45 per cent at 486°C. The concentration corresponding to this minimum decreases when the temperature increases. Vanpée and Fally[12] report similar results for methane, although at high temperature the concentration for the minimum of the curve reaches values that are less than the stoichiometric mixture. This is the case for all hydrocarbons if secondary ignition due to carbon monoxide (peninsula) is not eliminated[13, 14]. This elimination which is easy for hydrocarbons above ethane leads to a minimum whose concentration is slightly higher than, or coincides with, the stoichiometric mixture, whereas for methane the separation limit has not yet been determined exactly.

The results can be used to interpret the combustion of hydrocarbons. During slow oxidation, the velocity increases, reaching a maximum before decreasing (Fig. 5d). When this maximum velocity, which for a given reaction vessel is a function of pressure, temperature and concentration, reaches a critical value W_K, ignition takes place. On the other hand, we have just seen that the explosion region (pressure/concentration) is limited by a curve ($W = W_K$) with a minimum corresponding to the most ignitible mixture. For a given pressure, it is for this concentration that the maximum oxidation velocity reaches a maximum value.

Conclusion

For a given temperature above 450°C, the explosion range (pressure-concentration) corresponds to a single type of ignition—normal ignition; only the velocity and emission of the flame vary. The limit of this region is a simple curve with a minimum giving the concentration at which the maximum oxidation velocity reaches a maximum value. This concentration is independent of the presence of an inert gas provided the ratio of the partial pressure of the inert to the total partial pressures of combustible and oxygen remains constant.

The mechanism representing the oxidation of paraffin hydrocarbons must show a series of reaction schemes which explain the change in concentration corresponding to the maximum value of the maximum oxidation velocity. As the temperature increases this concentration varies continually but not uniformly between two extreme values. At low temperature we observe a high value which, in the case of our experiments carried out at reduced pressure, is that of the equimolecular mixture. At high temperature the value is equal to the stoichiometric mixture.

REFERENCES

1. FRELING, E.: Huitième conseil de Chimie (Solvay), Sept. 1950, pp. 126 and 143. (Only devices used by the authors are referred to.)
2. DUGLEUX, P.: Rev. Inst. Fr. Pétrole, *5*, 244 (1950); and Thèse, Paris (1949).

3. Ashmore, P. G., and Norrish, R. G. W.: Nature, *167*, 390 (1951).
4. Freling, E., and Dugleux, P.: Rev. Inst. Fr. Pétrole, *7*, 103 (1952).
5. Hsieh, M. S., and Townend, D. T. A.: J. Chem. Soc., 332, 337, 341 (1939).
6. Newitt, D. M., and Thornes, L. S.: J. Chem. Soc., 1656 (1937).
7. Mullins, B. P.:Fuel, *32*, 327 and 451 (1953).
8. Gray, J. A.: J. Chem. Soc., 741 (1953).
9. Emeleus, H. J.: J. Chem. Soc., 1733 (1929).
10. Dugleux, P., and Freling, E.: C. R. Acad. Sci., *238*, 349 (1954).
11. Taylor, H. A., and Ribbet, E. W.: J. Phys. Chem., *35*, 2667 (1931).
Sagulin, A. B.: Zeit. physik. Chem., *1B*, 275 (1928).
12. Vanpèe, M., and Fally, G.: Bull. Soc. Chim. Belg., *61*, 474 (1952).
13. Freling, E., and Dugleux, P.: C. R. Acad. Sci., *226*, 1985 (1948).
14. Dugleux, P., and Freling, E.: Rev. Inst. Fr. Pétrole, *4*, 459 (1949), [Colloque, Paris 1948].

47

THE FAST AND SLOW REACTIONS OF HYDROGEN-OXYGEN-PROPANE MIXTURES

By ARTHUR LEVY

Introduction

Previous studies of the reaction kinetics of hydrogen-oxygen-methane mixtures[1, 2] showed that methane reduces the pressure at the second explosion limit in hydrogen-oxygen mixtures, and increases the initial rate of combination of hydrogen and oxygen in the slow reaction. It was also shown that the explosion pressure does not decrease continuously to zero pressure with increasing methane concentration but drops abruptly to zero at a critical methane mole fraction. The progressive decrease in explosion pressure has been related to the water vapor formed in the pre-explosion reactions[3]. Complete inhibition of explosion at a critical methane concentration has been attributed to the formation of a critical concentration of formaldehyde, a strong inhibitor.

When propane is added to H_2-O_2 mixtures, there is no break in the concentration-explosion pressure curve. The pressure at the limit drops continuously, and almost linearly, to zero pressure as the propane concentration is increased. It is apparent, therefore, that propane acts differently from methane in these reactions with hydrogen and oxygen.

This report describes more detailed studies of the effect of propane on the H_2-O_2 reactions to determine how propane effects differ from those reported for methane in these reactions.

Kinetic Theory

The effect of hydrocarbons on the accepted mechanism of the hydrogen-oxygen reactions[4] has been discussed by the author[1] and Baldwin[5]. The main kinetic steps for the region of the second explosion limit in the H_2-O_2 reaction are

1. $H_2 + OH = H_2O + H$
2. $H + O_2 = OH + O$
3. $O + H_2 = OH + H$
4. $H + O_2 + M = HO_2 + M$
5. $HO_2 + M \xrightarrow{\text{wall}} H_2O, O_2, M$
6. $H, O, OH \xrightarrow{\text{wall}} H_2, O_2, H_2O.$

To these steps can be added a generalized chain-terminating step representing the interaction of the hydrocarbon, RH,

$$RH + X = \text{termination}$$

where X refers to the atoms and radicals produced in reactions (1–4). Excluding the wall reactions, (5) and (6), which have a minimum effect in the region of the second explosion limit, and applying steady-state treatment to the chain-branching and chain-breaking reactions (2) (3) (4) and (7) the final equation for the reduction of the explo-

sion pressure is

$$P_{RH} = P_0 - \frac{k_7(RH)(X)}{k_4(H)(O_2)} e^{-(E_7-E_4)/RT} \quad (1)$$

In a reduced form for studies at constant temperature and constant H_2/O_2 ratio, this becomes

$$P_{RH} = P_0 - kx_{RH} \quad (2)$$

where x_{RH} is the mole fraction of added hydrocarbon. P_{RH} is the pressure at the second explosion limit for the H_2-O_2-C_3H_8 mixture, and P_0 is the H_2-O_2 explosion pressure with no hydrocarbon present. The explosion pressure P_0 is

$$P_0 = \frac{2k_2}{k_4} e^{-(E_2-E_4)/RT} \quad (3)$$

Although equation (1) indicates a linear relation only when the active species is the hydrogen atom, application of steady-state theory to the chain-propagating and chain-breaking reactions shows that equation (2) is approximately linear for all the active species, H, O, and OH, at the low propane mole fractions used[2].

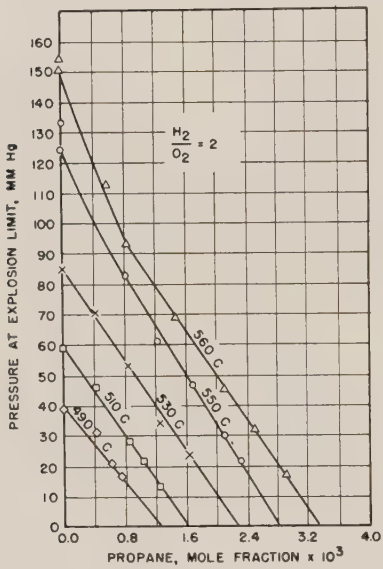

FIG. 1. The effect of added propane on the second explosion limit of 2:1 H_2-O_2 mixtures.

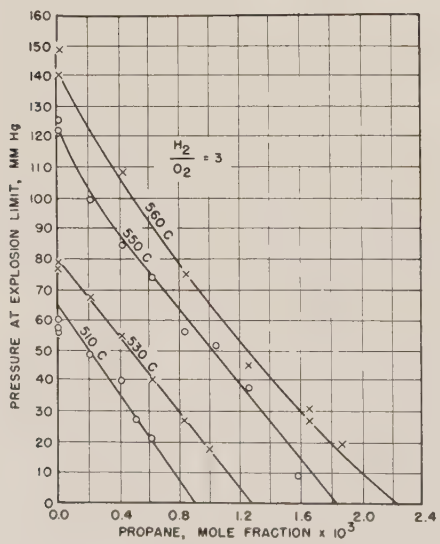

FIG. 2. The effect of added propane on the second explosion limit of 3:1 H_2-O_2 mixtures.

Experimental Procedure

APPARATUS

The studies were preformed in the all-Pyrex vacuum system described previously[1]. The reactions were run in a spherical, 200-cc KCl-coated Pyrex vessel, 7.4 cm in diameter.

MATERIALS

The gases used were Matheson, CP grade. The hydrogen was 99.8 per cent pure, the oxygen 99.6 per cent, and the propane 99.9 per cent. These gases were dried by passing over $CaCl_2$ and P_2O_5. The hydrogen and oxygen were also passed over platinized asbestos at 250°C before drying.

PROCEDURE

The explosion pressures were determined by the withdrawal method[1]. It is interesting to note that the explosion-limit pressures are much lower than those in the methane-inhibition studies, and yet it was still possible to detect the slight pressure changes at the explosion limit for pressures as low as 10 mm Hg.

The slow reactions were followed manometrically, by observing the decrease in total pressure as a function of time.

Experimental Results

EXPLOSION LIMITS

Figures 1, 2, and 3 summarize the explosion studies for 2:1, 3:1, and 1:1 hydrogen-oxygen mixtures, respectively. As seen in the figures, the linearity predicted by Equation 2 is found in rich and stoichiometric H_2:O_2 mixtures at $T \leqslant 530$°C. Above this temperature, and in the lean mixture above 490°C, there is a definite bowing in all the curves. The bowing increases in the leanest H_2-O_2 mixture, suggesting that the kinetic steps as-

sumed in deriving Equations (1) and (2) are oversimplified, and do not represent the complete mechanism.

Baldwin's general conclusion from his studies at 500°C was that only hydrogen-atom reactions could account for a linear decrease in explosion pressure.

Although the author disagreed with this general conclusion[6], it is noteworthy that at the higher temperatures, where the curves become nonlinear, the results conform more closely to the hyperbolic equations derived by Baldwin for the removal of oxygen atoms or hydroxyl radicals, than to the generalized linear equation.

COMPARISON WITH METHANE STUDIES

Figure 4 compares the rate of reduction of the second explosion limit by propane and by methane in stoichiometric hydrogen-oxygen mixtures at 510°C. The propane curve is extrapolated to zero pressure, since, experimentally, the reduction of the explosion limit is continuous. The methane curve drops abruptly at the critical methane mole fraction.

Table 1 is a comparison of the minimum concentrations of propane and of methane (x^*_{RH}) that completely inhibit explosion in stoichiometric hydrogen-oxygen mixtures over the range of temperatures studied. In the range studied the methane/propane ratio remains fairly constant at approximately 32 ± 2.

It was shown in previous studies[3] that equivalent concentrations of methane and of water vapor produced identical reductions in the pressure at the second explosion limit and that the mechanisms of pressure reduction are similar. It might therefore be inferred that the much stronger effect of propane, compared to methane, shown in Table 1 indicates that the interactions of propane with intermediates of the hydrogen-oxygen reaction are quite different from the methane interactions.

There is evidence to support the view that there are major differences and similarities as well. Both the author[1] and Baldwin[5] suggest that the abrupt break in the methane-inhibition curves is probably caused by the formation of a critical concentration of formaldehyde. Since propane is capable of producing formaldehyde more readily under these conditions than methane, it seems probable that formaldehyde contributes to the change in the explosion limit. Furthermore, the linear equations developed above neither predict the observed departure

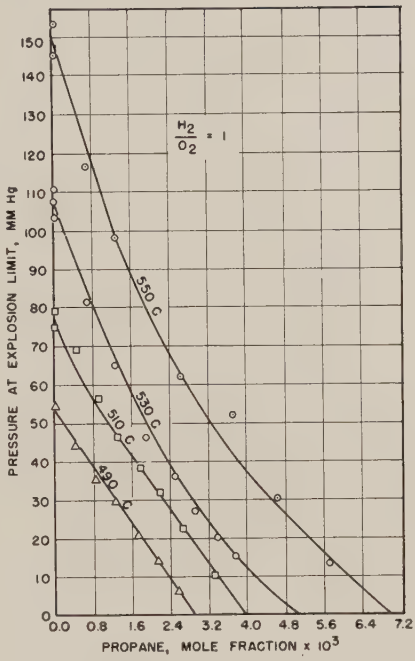

FIG. 3. The effect of added propane on the second explosion limit of 1:1 H_2-O_2 mixtures.

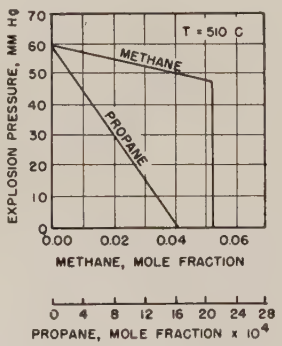

FIG. 4. Reduction of the second explosion limit in stoichiometric H_2-O_2 mixtures by propane and methane.

TABLE 1. COMPARISON OF CRITICAL HYDROCARBON MOLE FRACTIONS CAUSING COMPLETE INHIBITION OF EXPLOSION IN STOICHIOMETRIC HYDROGEN-OXYGEN MIXTURES

Temperature	Critical Mole Fraction	
	Propane	Methane
°C		
490	0.0013	0.043
510	0.0016	0.053
530	0.0023	0.076
550	0.0028	0.086
560	0.0033	—

TABLE 2. SUMMARY OF RATE STUDIES FOR H_2-O_2-C_3H_8 MIXTURES

T = 560°C

P_T = 420 mm Hg

Initial Partial Pressures, mm Hg			Max Rate	t_{max}, min
H_2	O_2	C_3H_8		
			mm Hg/min	
280	140	—	13.0	5.3
276	138	6	15.0	2.8
274	137	9	17.0	1.5
272	136	12	24.0	1.2
170	250	—	8.5	6.0
164	250	6	24	1.25
163	250	7	28	70 sec
162.5	250	7.5	Explosion	40 sec
162	250	8	Explosion	38 sec
200	220	—	11.0	6.0
192	220	8	32.0	1.25
191	220	9	Explosion	40 sec
189	220	11	Explosion	35 sec
240	180	—	11.0	6.5
234	180	6	16.0	3.3
228	180	12	27	1.1
227.5	180	12.5	34	1.0
227	180	13	Explosion	38 sec
226	180	14	Explosion	33 sec
225	180	15	Explosion	20 sec
280	140	—	13.5	5.5
274	140	6	17.0	3.0
268	140	12	24.0	45 sec
265	140	15	31.5	50 sec
263	140	17	33	50 sec
262	140	18	Explosion	30 sec
260	140	20	Explosion	25 sec
310	110	—	10.0	5.8
298	110	12	20.0	1.0
295	110	15	26	1.2
292	110	18	30	1.2
290	110	20	42	40 sec
289	110	21	Explosion	25 sec
288	110	22	Explosion	20 sec
325	95	—	10.0	4.5
305	95	20	54	35 sec
303	95	22	51	30 sec
302	95	23	Explosion*	23 sec
301	95	24	Explosion*	20 sec
300	95	25	Explosion*	25 sec
340	80	—	8.0	3.5
320	80	20	24	40 sec
317	80	23	28	35 sec
313	80	27	36	25 sec
311	80	29	33	25 sec
308	80	32	24	25 sec

* These explosions are rather sluggish.

from linearity in the higher temperature explosion curves, nor do they attempt to account for the possible effect of formaldehyde production. It follows therefore that the departure from linearity may be caused by increased rates of formation of formaldehyde. Propane is probably more effective than methane in inhibiting the explosion reaction because of two supporting effects, (1) its more ready reactions with the O, H, and OH atoms and radical, and (2) a strong inhibiting effect of the increasing amounts of formaldehyde.

The Slow Reaction

GENERAL RESULTS

Table 2 summarizes the slow-reaction studies in lean and rich mixtures in the H_2-O_2-C_3H_8 system. As in previous studies, the reaction rates are expressed as the maximum rate of reaction, in mm Hg/min, and also as the time to reach maximum rate, in min or sec. The maximum rate is the rate of decrease of the total pressure of the system caused by the reaction of hydrogen with oxygen.

Propane causes an increase in both the maximum and the initial rates of reaction of all H_2-O_2-C_3H_8 mixtures. (The initial rate of reaction is inversely proportional to t_{max}.) Th is is somewhat different from the results with methane. Methane increased the maximum rate only when the H_2:O_2 ratio was less than two.

Another difference between the methane- and the propane-H_2-O_2 systems is not apparent in the tabulated results. There occurs a time interval of 10–30 seconds after the start of the slow reaction during which methane systems show no pressure changes, positive or negative. Propane systems however, often show a marked pressure increase before the pressure falls as the hydrogen and oxygen start combining. The observed differences

may be explained by the greater reactivity of C_3H_8-O_2 mixtures at 560°C in comparison with CH_4-O_2 mixtures, and by the greater pressure change in the reaction of propane and oxygen, as shown by comparison of the following induction-period reactions

$$CH_4 + 1.5O_2 = CO + 2H_2O$$

$$C_3H_8 + 2.5O_2 = 3CO + 4H_2O.$$

INDUCED EXPLOSIONS

There is a third difference between the propane and the methane systems in the occurrence of induced explosions that occur outside the H_2-O_2 explosion peninsula. These explosions are not the usual self-ignited, homogeneous explosions. They are instead homogeneously ignited explosions in which the ignition source is a homogeneous propane-oxygen explosion, which releases enough energy to ignite the remaining H_2-O_2 mixtures. Because of the high reactivity of propane at 560°C, the induction period is sometimes characterized by a very rapid pressure increase, followed immediately by a very rapid pressure decrease in the system. In most cases these very rapid reactions, or induced explosions, appear as one sharp explosion reaction. These are, however, two separate reactions as described above. This type of explosion never occurred in H_2-O_2-CH_4 mixtures because methane is not as reactive as propane at this temperature.

It is of interest to note that these induced explosions are not peculiar to the H_2-O_2-C_3H_8 system, but have also been observed in other systems. Badin[7] and others, for example, have used compounds such as zinc dimethyl, boron triethyl, nickel carbonyl, and aluminum borohydride to initiate ignition in hydrocarbons. In such systems it is also the high reactivity of the additive which initiates the subsequent oxidation of hydrocarbon, and causes the hydrocarbon to ignite at rather low temperatures and pressures.

Table 2, besides summarizing the rate results, also illustrates the abrupt transition to the induced-explosion reactions at higher propane concentrations. An interesting feature of the induced-explosion experiments is the abrupt transition from reactions having high, but measurable maximum rates, to the explosions which are too fast to measure by this experimental procedure. The initial rates, however, represented by the reciprocal of t_{max}, increase uniformly, but exponentially, with increasing propane concentrations, even into the induced-explosion regions.

Table 3 summarizes the induced-explosion data to show the dependence of the minimum propane concentration required for such explosions on the initial hydrogen and oxygen partial pressures. Examination of the last column of Table 3, the total pressure drop after explosion, reveals that the data fall into two groups. The first three mixtures show large pressure drops, and the last three mixtures show small pressure drops. Assuming that the induced explosions occur by two reactions in which the propane first explodes homogeneously, and then the remaining hydrogen-oxygen mixture is ignited by the sudden energy release, the existence of two groups of data may be explained qualitatively with reference to the oxygen available to oxidize the hydrogen after the first reaction. Since one volume of propane consumes 3.5–5 volumes of oxygen, the remaining oxygen concentrations in the first three mixtures of Table 3 are still sufficient to form lean and stoichiometric H_2-O_2 mixtures. The last three mixtures, however, are very rich in hydrogen after the propane consumes its share of the oxygen. As a result, the explosive reaction is sluggish and incomplete, and the pressure drop is small.

The assumption of two consecutive reactions is only partially substantiated by the data, however. If the assumption were completely valid, the next to last mixture in Table 3 would be beyond the

Table 3. Minimum Propane Concentrations which Induce Explosion in Hydrogen-Oxygen Mixtures

T = 560°C

P_T = 420 mm Hg

Partial Pressures, mm Hg			ΔP*
H_2	O_2	C_3H_8	
			mm Hg
162.5	250	7.5	81
191	220	9.0	98
227	180	13	70
262	140	18	6.5
289	110	21	4.5
302	95	23	3.5
313†	80	27	—

* ΔP is the pressure difference between P_T = 420 and the final equilibrium pressure after explosion.

† See Table 2. This mixture gave the highest maximum rate, but did not induce explosion.

flammability limit for H_2-O_2 explosions. It was necessary, therefore, to check the general validity of this assumption further. This was done by studying the induced explosions as a function of the total pressure. Since the first step of the induced explosion is postulated to be solely the propane reaction, it should be relatively independent of the hydrogen concentration, and

TABLE 4. EFFECT OF TOTAL PRESSURE ON INDUCED EXPLOSIONS

T = 560°C

Partial Pressures, mm Hg			Total Pressure
H_2	O_2	C_3H_8*	
			mm Hg
146	140	14	300
347	140	13	500
160	190	10	360
229	180	11	420
280	190	10	480

* Minimun propane pressure for induced explosion.

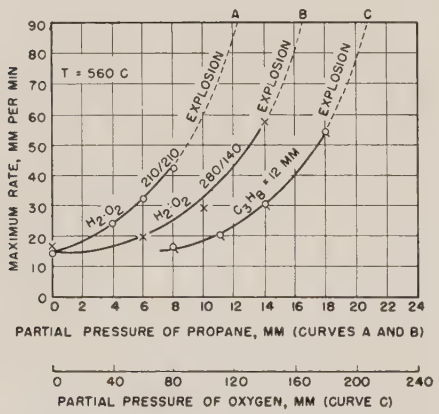

FIG. 5. Variation of maximum rate with partial pressures of propane and oxygen.

should depend primarily on the propane-to-oxygen ratio and pressure.

Table 4 confirms this hypothesis. It represents studies in which the total pressure was varied from 300–500 mm Hg, and the oxygen concentration was set at 140, 180, and 190 mm Hg. In each case the minimum propane concentration for inducing explosion remains relatively constant for a constant oxygen pressure.

The data at P_t = 420 mm Hg do not agree exactly with similar data in Table 3. The difference was caused by surface changes which occurred during the performance of other studies between the two periods when the data were collected for Tables 3 and 4. Changes in surface conditions are a problem in these studies, and have been referred to previously[1].

Figure 5 illustrates the transition from slow reaction to induced explosion on a maximum rate-partial pressure graph. Curves A and B refer to H_2-O_2-C_3H_8 mixtures in which propane is the variable component. Curve C refers to oxygen as the variable gas. In these mixtures the oxygen-to-propane ratio is high and the transition from slow reaction to explosion is abrupt. It was noted, that, as the oxygen-to-propane ratio decreases, the explosions lose their snap. This sluggishness increases with decreasing O_2/C_3H_8 ratio to the point where it is questionable as to whether one has just a fast reaction or a true explosion. The starred explosions in Table 2, where the oxygen-to-propane ratio is less than 4, represent sluggish explosions.

Propane- and Water Vapor-Acceleration of the Rate of Combination of Hydrogen and Oxygen

It was evident in the explosion studies that propane has a much greater effect on the reduction of the second explosion limit of hydrogen and oxygen than methane, and that this increased effect could not be related solely to water vapor produced by propane in the preliminary reactions. Two series of experiments were preformed, as shown in Tables 5 and 6, on H_2-O_2-H_2O and H_2-O_2-C_3H_8 systems to study these effects.

Table 5 compares maximum and initial rates for H_2-O_2-C_3H_8 systems with those for equivalent H_2-O_2-H_2O systems. Equivalence in these mixtures is based on the assumed preliminary reaction

$$C_3H_8 + 3.5O_2 = 3CO + 4H_2O.$$

In making up the H_2-O_2-H_2O mixtures, therefore, each unit of propane concentration is replaced by four units of water vapor, and the oxygen concentration is reduced 3.5 units per propane unit. The results show no quantitative correlation, although qualitatively the increase in rate with increasing concentration of either propane or water vapor suggests that water vapor, either directly or indirectly as a result of propane addition, is the principal rate-accelerating catalyst in these reactions.

Table 6 shows additional measurements of the water-vapor effect in 2:1 H_2:O_2 mixtures. Com-

paring the last two tests in the table in turn with the first test of a dry mixture at 420 mm pressure shows that the water vapor effect on the maximum rate is greater than the total pressure effect by a factor of approximately two. Similarly, the effect of water vapor on the initial rate is 5.5 times the effect of an increase in total pressure alone. The reason for the large influence on the initial rate is that water vapor affects these reactions

TABLE 5. A COMPARISON OF H_2-O_2-C_3H_8 AND EQUIVALENT H_2-O_2-H_2O REACTION RATES

T = 560°C

Partial Pressures, mm Hg				Total Pressure	Max rate	t_{max}, sec
H_2	O_2	C_3H_8	H_2O			
				mm Hg	*mm Hg/min*	
280	140	10	—	430	29	75
280	105	—	40	425	36	40
280	140	14	—	434	57	45
280	90	—	56	426	36	35
280	140	18	—	438	Explosion	25
280	77	—	72	429	57	25

TABLE 6. THE RATE-ACCELERATING EFFECT OF WATER VAPOR ON STOICHIOMETRIC HYDROGEN-OXYGEN MIXTURES

T = 560°C

Partial Pressures, mm Hg			Max Rate	t_{max}, min
H_2	O_2	H_2O		
			mm Hg/min	
280	140	—	17	4.0
280	140	20	31.5	1.5
280	140	40	40	1.0
280	140	60	60	0.6
280	140	80	75	0.5
333	167	—	38	2.75

mostly by reducing the induction period. This may be explained kinetically by the addition of the following step to the H_2-O_2 mechanism

$$H_2O + HO_2 = H_2O_2 + OH.$$

The increase in OH radical concentration in the early stages of the reaction then accounts for the increased initial rate.

COMPARISON WITH METHANE STUDIES

In general the relative effects of propane and methane on the slow reactions are similar to those described earlier for the explosion reactions. The propane effect is always greater than the methane effect. This follows from the greater reactivity of propane at the temperatures and pressures studied. There are two main differences in the slow-reaction results. Propane increases the initial and maximum reaction rates for *all* concentrations studied, whereas methane caused a reduction in the maximum rate for mixtures that were low in oxygen with reference to total oxygen requirements of the methane and hydrogen together. Also, because propane-oxygen mixtures are explosive under the conditions studied, propane induced explosions in hydrogen-oxygen mixtures which were ordinarily in the nonexplosive region.

Although the slow-reaction results show qualitative evidence of the important effect of water vapor on the rate of combination of hydrogen and oxygen, they can not be related quantitatively to propane concentration because of the complex nature of these interactions.

Summary

It has been shown in these studies that propane has a greater effect on both the fast and slow reactions of hydrogen and oxygen than does methane. An unusual induced explosion reaction has also been observed, which, along with the other explosion and slow-reaction studies, is explained in terms of consecutive reactions, whereby propane is oxidized rapidly in the first reaction, and hydrogen and oxygen combine in the second reaction. Induced explosions are attributed to the rapid energy release of the first reaction, and the other explosion and slow-reaction effects are attributed in part to the accelerating effect of water vapor on the H_2-O_2 reaction.

REFERENCES

1. LEVY, A.: *The Inhibition of the Second Explosion Limit of Hydrogen-Oxygen Mixtures by Methane*. Battelle Memorial Institute, Technical Report No. 15036-6 to Wright Air Development Center, Contract No. AF 33(038)-12656, E. O. No. 460-35, S.R.-8, July 1952, 24 pages.
2. LEVY, A.: *Kinetic Studies of Explosion and Slow Reactions in Hydrogen-Methane-Oxygen* Mixtures. Battelle Memorial Institute, Technical Report No. 15036-22 to Wright Air Development Center, Contract No. AF 33(038)-12656, E. O. No. 460-35, S.R.-8, November 1953, 29 pages.
3. LEVY, A.: J. Chem. Phys. *21*, 2132 (1953).
4. LEWIS, B., AND VON ELBE, G.: *Combustion*,

Flames, and Explosions of Gases, Chapter 2. New York, Academic Press, 1951.
5. Baldwin, R. R.: Fuel, *31*, 312 (1952).
6. Levy, A.: Fuel, *32*, 263 (1953).
7. Badin, E. J., Walters, D. R., and Pease, R. N.: J. Am. Chem. Soc., *69*, 2586 (1947).
8. Brokaw, R. S., Badin, E. J., and Pease, R. N.: J. Am. Chem. Soc., *70*, 1921 (1948); *72*, 1793 (1950).

Discussion by R. R. Baldwin

The authors suggest that the inhibiting action of methane arises from water formation, whereas the inhibiting action of propane is due to formaldehyde formation. These suggestions can be eliminated as a result of the following experiments which we have carried out. A mixture of hydrogen-oxygen-nitrogen-methane was prepared containing sufficient methane to suppress explosion completely. The pressure was then reduced to about half the uninhibited limit, so that an inhibiting effect was being obtained due to methane or its oxidation products. The gas was then withdrawn and analyzed, and the amounts of water found were quite insufficient to account for the observed inhibition.

A similar experiment in the case of propane has shown that no formaldehyde can be detected in the gas sample, and that less than 2 per cent of the propane present has oxidized during the mixing, withdrawal and sampling periods. Further, the excellent carbon balance obtained excludes the suggestion that any formaldehyde formed might have been lost by polymerization. These observations, together with the known inhibiting effect of formaldehyde, eliminate the possibility that the inhibiting action of propane arises through formation of formaldehyde.

Author's Reply

The equation for the reduction of the explosion limit pressure refers to conditions *at* the explosion limit boundary. It is therefore the author's opinion that Dr. Baldwin's observations do not necessarily apply to conditions at the boundary since the gases in the experiments outlined must be withdrawn without passing through an explosion limit.

The similarities between methane and water vapor in reducing the explosion limit pressure, have been pointed out by Levy[3] in the following steps,

$$CH_4 + HO_2 = CH_3 + H_2O_2$$

$$CH_3 + O_2 = HCHO + OH = CHO + H_2O$$

and

$$H_2O + HO_2 = OH + H_2O_2$$

On the basis of these steps the HO_2 radical is consumed on a one-to-one basis by methane and/or water vapor.

With regard to the complete inhibition of explosion caused by methane addition, it has been suggested that this is due to the formation of a critical concentration of formaldehyde. As yet, however, no quantitative explanation nor direct experiment has been accomplished to support this suggestion.

48

THE INHIBITION OF THE HYDROGEN-OXYGEN REACTION BY HYDROCARBONS

By R. R. BALDWIN, N. S. CORNEY, and R. F. SIMMONS

The inhibiting effect of hydrocarbons on the hydrogen-oxygen reaction became of particular interest during the course of a war-time study, described elsewhere[1], of the problem of exhaust flames from aero-engines. Preliminary experiments at that time showed that this inhibiting effect was obtained with a range of hydrocarbons from pentane to octane, as well as with the lower alcohols and aldehydes. This investigation has now been extended to the lower paraffins in an attempt to determine the mechanism of the inhibition.

Experimental

The apparatus used in the present investigation has already been described[2]. The second limit was obtained by introducing one gas (usually hydrogen) into the evacuated reaction vessel to a

pressure in excess of the explosion limit, and then admitting the remainder of the pre-mixed gases from the mixing bulb. After allowing one minute for mixing to occur, the mixture was withdrawn through a capillary, and the explosion pressure noted. The first limit was obtained by trial and error determination of the minimum pressure at which a glow or flash could be detected on admission of the pre-mixed gases to the evacuated reaction vessel.

Hydrogen-oxygen-nitrogen mixtures were used to permit the hydrogen and oxygen concentrations to be varied independently. With a constant oxygen concentration (y) of 0.14 mole fraction, the hydrogen concentration (x) was varied from 0.07 to 0.56, and with a constant hydrogen concentration of 0.28, the oxygen concentration was varied over the same range.

Inhibition by Ethane

RESULTS

A systematic study of the inhibition has been made in the case of one of the simplest hydrocarbons, ethane. Preliminary tests showed that the inhibited limit was not affected by variation of the mixing time in the reaction vessel, but the rate of withdrawal had some effect in clean Pyrex vessels under certain conditions. With moderately fast withdrawal rates (>1 mm Hg/sec), a constant normal limit was obtained, but as the withdrawal rate was decreased, a second almost constant limit was reached. This depressed limit could also be obtained by interrupting the evacuation for a period of about five minutes at a pressure just above the normal limit. Figure 1 shows the variation with ethane concentration of the normal limit (in mm Hg), and of the depressed limit obtained by both methods, in a 23 mm diameter clean Pyrex vessel at 500°C. Similar results were obtained in different diameter vessels, and over a range of mixture composition. The simplest explanation of this behavior is that some more efficient inhibitor is formed from the ethane under these conditions, and it is clear that care must be taken to use sufficiently fast withdrawal rates if the normal limit is to be obtained in clean vessels. A similar effect on the uninhibited reaction has already been reported[3].

In potassium chloride coated vessels, the effect of withdrawal rate was much less marked, and to obtain even a slight depression of the limit, it was necessary to use inconveniently slow evacuation rates. Interruption of evacuation just above the normal limit for a period of five minutes gave, however, a depressed limit as in the case of clean vessels.

Most of the results for ethane discussed in this paper were obtained in potassium chloride coated vessels, where no sensitivity to experimental technique exists. In the case of clean vessels, the

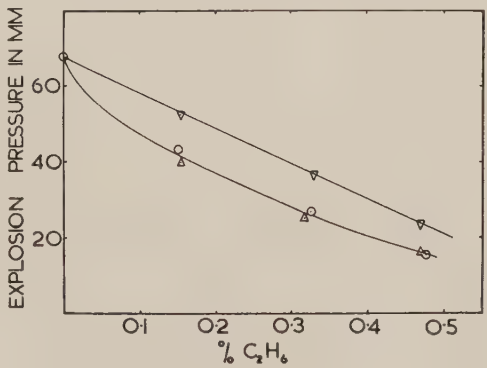

FIG. 1. Variation in explosion pressure with ethane concentration. 23 mm diam. clean Pyrex vessel. Temp. 500°C. $y = 0.14$, $x = 0.80$.
▽ Normal limit. ⊙ Depressed limit by slow withdrawal rate.
△ Depressed limit by interrupting evacuation.

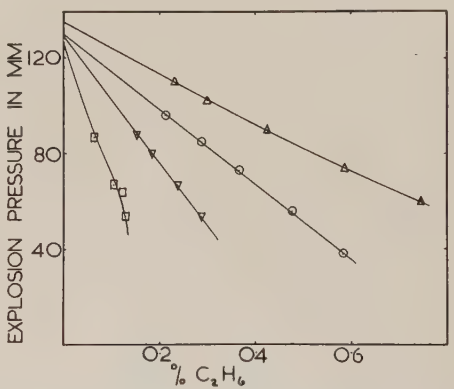

FIG. 2. Variation in second limit inhibition with ethane concentration. 36 mm diam. potassium chloride coated vessel. Temp. 540°C. $x = 0.14$.
△ $y = 0.056$ ⊙ $y = 0.28$ ▽ $y = 0.14$ ⊡ $y = 0.07$

withdrawal rates used were sufficiently high to ensure that the normal limit was obtained.

The inhibiting action of ethane on the second limit has been studied[2] in potassium chloride coated vessels of different diameter over a wide range of mixture composition, and at temperatures between 500 and 550°C. Figure 2 shows some typical plots of the variation of explosion pressure with ethane concentration in a 36 mm diameter vessel at 540°C, and it will be seen that the explosion pressure is reduced in an almost

linear manner. A convenient method, therefore, of assessing the effectiveness of the inhibition is in terms of the quantity of inhibitor ($i_{1/2}$) required to halve the uninhibited limit P_2.

Figure 3 shows that $i_{1/2}$ is approximately proportional to the oxygen concentration (y), but is almost independent of the hydrogen concentra-

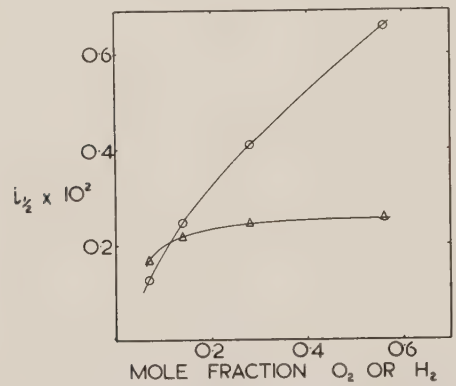

FIG. 3. Variation of $i_{1/2}$ with hydrogen and oxygen concentration. 36 mm diam. potassium chloride coated vessel. Temp. 540°C.
⊙ $x = 0.28$, oxygen varied.
△ $y = 0.14$, hydrogen varied.

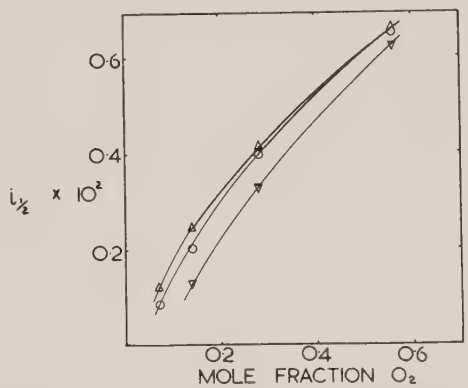

FIG. 4. Variation of $i_{1/2}$ with vessel diameter. Temp. 540°C. $x = 0.28$. Potassium chloride coated vessels.
13 (▽), 23 (⊙), and 36 (△) mm diam.

tion (x). It will be noticed, however, that the oxygen dependence tends to fall off from the linear relationship at high oxygen concentrations, and that some decrease in $i_{1/2}$ is apparent at low hydrogen concentrations.

Figure 4 shows that in potassium chloride coated vessels $i_{1/2}$ is only slightly dependent on vessel diameter, except at low oxygen concentrations, and that no direct diameter dependence is observed at any oxygen concentration. In clean Pyrex vessels at 500°C, the variation of $i_{1/2}$ with vessel diameter is even less marked, and the change in vessel surface only affects slightly the actual value of $i_{1/2}$.

Although $i_{1/2}$ increases uniformly with temperature over the range 500–550°C, the associated activation energy, though varying slightly with mixture composition, is quite small.

To eliminate the possibility that some oxidation product of ethane, such as acetaldehyde, formaldehyde, or ethylene, might be the effective inhibiting agent, a number of analyses were carried out on gas samples which contained sufficient ethane to suppress explosion at all pressures. If any such oxidation product were the effective agent, the known inhibiting efficiency[4] of these compounds would necessitate the occurrence of considerable oxidation of ethane in samples withdrawn from the reaction vessel under such conditions. In actual fact, no significant oxidation was detected, and it may be concluded, therefore, that the inhibition arises through some direct effect of ethane itself.

DISCUSSION

The simplest interpretation of the almost linear increase in $i_{1/2}$ with increasing oxygen concentration is that some chain carrier reacts with ethane giving chain termination in competition with a reaction with oxygen giving chain propagation or chain branching. Since the only chain center in the hydrogen-oxygen reaction that reacts with oxygen is the hydrogen atom, the main primary termination process is thus uniquely defined. Support for this conclusion comes from the low activation energy quoted[5, 6] for reaction (14) compared with reaction (2), and from the difficulty of obtaining a simple alternative explanation.

Addition of the chain termination reaction (14) to the accepted mechanism[7, 8] for the uninhibited reaction gives the following scheme of reactions[a]:

$$H + C_2H_6 = C_2H_5 + H_2 \qquad (14)$$

$$OH + H_2 = H_2O + H \qquad (1)$$

$$H + O_2 = OH + O \qquad (2)$$

$$O + H_2 = OH + H \qquad (3)$$

$$H + O_2 + M = HO_2 + M \qquad (4)$$

[a] A non-consecutive scheme of reaction numbers has been used to maintain uniformity in a series of papers in the process of preparation.

$$HO_2 \xrightarrow{\text{surface}} \tfrac{1}{2}\,H_2O_2 + \tfrac{1}{2}O_2 \qquad (5)$$

$$HO_2 + H_2O_2 = H_2O + O_2 + OH \qquad (6)$$

The explosion condition obtained is:

$$P_2 - P = \frac{3k_{14}i}{2k_4ym} \qquad (i)$$

where P_2, P are the uninhibited and inhibited limits, i, y are the mole fractions of ethane and oxygen, and m is a composite third body term expressing the efficiency of the particular mixture in reaction (4). This equation predicts the linear relation between explosion pressure and inhibitor concentration that is obtained experimentally.

When $P = P_2/2$, equation (i) becomes:

$$i_{1/2} = \frac{k_2y}{k_{14}} \qquad (ii)$$

This relation indicates that $i_{1/2}$ should be proportional to the oxygen concentration, and independent of the hydrogen concentration, vessel diameter, and vessel surface, in agreement with the main experimental facts.

In deducing relations (i) and (ii), it has been assumed that the formation of the ethyl radical automatically results in chain termination. Allowance for this assumption can be made by introducing a factor Q, the fraction of ethyl radicals actually undergoing chain termination, into the numerator of equation (i) and the denominator of equation (ii). Possible reactions of the ethyl radical which should be considered are:

(1) Destruction at the vessel surface (k_s).

(2) Reaction with hydrogen:

$$C_2H_5 + H_2 = C_2H_6 + H \qquad (16)$$

(3) Peroxide radical formation, as in low temperature hydrocarbon oxidation:

$$C_2H_5 + O_2 = C_2H_5O_2 \qquad (17)$$

(4) Aldehyde formation, as suggested for high temperature hydrocarbon oxidation[7, 9]:

$$C_2H_5 + O_2 = CH_3CHO + OH \qquad (19)$$

Complete destruction of all ethyl radicals at the vessel surface ($Q = 1$) can be excluded both from the observations of Moore and Taylor[10] on the increased yields of ethane when mercury diethyl is photolyzed in the presence of hydrogen, and from the low activation energy quoted[5, 11] for reaction[16], which would allow it to compete adequately with surface destruction at the pressures involved. The long chains characterizing both low and high temperature hydrocarbon oxidation also indicate that reactions with oxygen must be much faster than the surface destruction of alkyl radicals.

A partial destruction of alkyl radicals at the surface in competition with propagation reactions involving hydrogen and oxygen would give a fraction Q inversely dependent on the first or second power of the vessel diameter, depending on whether the surface destruction was inefficient or efficient. The results shown in Figure 4 indicate only a minor variation in $i_{1/2}$ with vessel diameter, which is attributed later to secondary factors.

Since it is difficult to conceive a chain termination reaction involving hydrogen, the ethyl radicals must undergo chain termination through reaction with oxygen. Even if the peroxide radical is formed at these temperatures, complete surface destruction can be ruled out, and partial surface destruction can be eliminated from the diameter evidence already quoted. Since reaction (19) leads to chain propagation, a new termination reaction with oxygen is required. This is provided by the reaction:

$$C_2H_5 + O_2 = C_2H_4 + HO_2 \qquad (20)$$

the formation of the HO_2 radical being effectively chain termination. Evidence for this reaction has also been provided recently by the high yields of ethylene obtained in the oxidation of ethane in this temperature range[12].

Competition between the possible reactions of the ethyl radical (excluding the unlikely peroxide radical formation) gives the relation:

$$Q = \frac{k_s + 2k_{20}[O_2]/3}{k_s + k_{16}[H_2] + (k_{19} + k_{20})[O_2]} \qquad (iii)$$

The factor 2/3 arose from the fact that one of every three HO_2 radicals formed in reaction (20) regenerates a chain center by reactions (5) and (6). This expression will not account for the deviations of the experimental results from the simple relationships given by equation (ii). In particular, since k_s can only be of minor importance, the effect of hydrogen in reducing Q and thus increasing $i_{1/2}$ should be most marked at high hydrogen and at low oxygen concentrations. In fact, as shown in Figure 3 and in Figure 6 presented later, the reverse is true, change in hydrogen concentration having most effect at low hydrogen and high oxygen concentrations. This indicates firstly that reaction (16) must be of little importance compared with reactions of the

ethyl radical with oxygen, and secondly that to explain the effects of mixture composition noted in Figures 3 and 6, some other reaction is necessary. Evidence presented later shows that this is a reaction between hydroxyl radicals and ethane.

The relatively minor diameter effects noted in Figure 4 could be attributed either to the k_s term in equation (iii), or to surface destruction of atoms and radicals present in the uninhibited reaction. Since the former explanation would require the fraction Q to become markedly dependent on pressure at low pressures, the inhibition of the first limit by ethane has been studied.

FIRST LIMIT INHIBITION

A simple expression for the effect of ethane on the first limit can be obtained if the following assumptions are made:

(1) Gas phase termination by reaction (4) is negligible.

(2) Hydrogen atoms are destroyed efficiently by a potassium chloride coated surface (k_H).

(3) Destruction of oxygen atoms and hydroxyl radicals at the surface can be neglected.

(4) Chain termination through reaction of oxygen atoms and hydroxyl radicals with ethane is negligible.

The explosion condition then obtained by equating the chain branching and chain breaking rates is:

$$2k_2[O_2] = k_H + k_{14}[C_2H_6]Q' \qquad \text{(iv)}$$

where Q' is the fraction of ethyl radicals undergoing chain termination. Since k_H is inversely proportional to pressure, equation (iv) becomes:

$$2k_2y = k_{14}iQ' + A/P^2 \qquad \text{(v)}$$

If Q' is approximately constant, a plot of $1/P^2 - i$ should give a straight line of intercept $2k_2y/k_{14}Q'$. Further, if Q has the same value at first and second limit pressures ($Q = Q'$), the intercept should be twice the value of $i_{1/2}$ for the relevant mixture.

The results shown in Figure 5, and summarized in Table 1, confirm these predictions. A more rigorous treatment[13], in which allowance is made for all four assumptions involved in the simple treatment, confirms the conclusion that the fraction of ethyl radicals undergoing chain termination is constant over the pressure range 5–100 mm. This conclusion eliminates the possibility that the diameter dependence shown in Figure 4 arises from the surface destruction of ethyl radicals, or any other radical formed from ethane. During the course of the detailed analysis it became apparent, from the values obtained for k_H/k_2 and k_{OH}/k_1, that surface destruction of hydrogen atoms and hydroxyl radicals could affect significantly the values of $i_{1/2}$, particularly at low oxygen concentrations and in the smallest vessels. A simple treatment using the values of k_H/k_2 and k_{OH}/k_1 obtained from measurements of the uninhibited first limit for different mixtures permits the correction of the experimental values of $i_{1/2}$ for such surface termination. Application of this correction confirms that the diameter dependence arises solely from surface destruction of radicals present in the uninhibited reaction.

As the terms k_s and $k_{16}[H_2]$ have been eliminated from equation (iii), the fraction Q is thus determined by the two reactions with oxygen according to the relation:

$$Q = \frac{2/3k_{20}}{k_{19} + k_{20}} = 2/3R \qquad \text{(vi)}$$

where $R = k_{20}/(k_{19} + k_{20})$.

REACTION OF HYDROXYL RADICALS WITH ETHANE

The experimental evidence indicates that the fraction Q of ethyl radicals destroyed is independent of pressure and vessel diameter, and that the effect of mixture composition cannot be explained by the occurrence of reaction (16). Introduction of the additional but less important chain termination reaction (15) provides an alternative method of obtaining a hydrogen dependence[b]

$$OH + C_2H_6 = C_2H_5 + H_2O \qquad (15)$$

Competition of this reaction with the chain propagation reaction (1) will become most marked at low hydrogen concentrations, and thus reduce the value of $i_{1/2}$, in agreement with the results shown in Figure 3. Confirmation of this explanation comes from the more marked variation in $i_{1/2}$ with hydrogen concentration than is obtained at higher oxygen concentrations, as shown in Figure 6; this behavior is consistent with the increased importance of reaction (15) at high $[O_2]/[H_2]$ ratios.

If reactions (15) and (20) are added to the scheme given on page 504 and if it is assumed

[b] Chain termination through reaction of oxygen atoms with ethane cannot be excluded, as it gives kinetic expressions similar to (vii) and (viii), but is considered less likely owing to the ease with which reaction (3) occurs.

that R is unity, $i_{1/2}$ is given by:

$$\frac{1}{i_{1/2}} = \frac{2k_{14}}{3k_2y} + \frac{4k_{15}(1 + 1/4 + k_{14}i_{1/2}/6k_2y)}{3k_1(x + 2k_{15}i_{1/2}/3k_1)} \quad \text{(vii)}$$

If the terms $k_{14}i_{1/2}/6k_2y$ and $2k_{15}i_{1/2}/3k_1$ are neglected, this reduces to:

$$\frac{1}{i_{1/2}} = \frac{2k_{14}}{3k_2y} + \frac{5k_{15}}{3k_1x} \quad \text{(viii)}$$

The linear plots of $l/i_{1/2}$ against l/y (at constant x) and against l/x (at constant y) shown in Figures 7 and 8 provide further confirmation that this explanation of the effect of mixture composition is correct.

Accurate values of the rate constant ratios k_{14}/k_2 and k_{15}/k_1 cannot be obtained from these plots, as the terms $2k_{15}i_{1/2}/3k_1$ and $k_{14}i_{1/2}/6k_2y$ (the latter approaching a maximum value of 1/4 when reaction (15) becomes negligible) must be taken into account. The most accurate values for these rate constant ratios are obtained by using various combinations of these ratios in equation (vii) to calculate the values of $i_{1/2}$ for all the mixtures studied, and selecting the pair giving best agreement. The correctness of the proposed mechanism is indicated by the fact that the best combination enables $i_{1/2}$ to be predicted with a root mean square deviation within 2 per cent for the eleven mixtures investigated[13].

If R is not unity, relation (vii) is modified to:

$$\frac{1}{i_{1/2}} = \frac{2k_{14}R}{3k_2y} + \frac{4k_{15}R(1 + 1/4 + [3k_{14}i_{1/2} - 2k_{14}i_{1/2}R]/6k_2y)}{3k_1(x + 2k_{15}i_{1/2}R/3)} \quad \text{(ix)}$$

Evidence that R is close to unity comes first from the yields of olefin up to 80 per cent obtained by Gray[12] in the oxidation of ethane, and secondly from the fact that a value of R less than 0.5 would result in the term $(3k_{14}i_{1/2} - 2k_{14}i_{1/2}R)/6k_2y$ becoming sufficiently important for its effect to be detected under certain conditions. While, therefore, the value of R is sufficiently close to unity for the effect of this term in equation (ix) to be calculated on the basis of $R = 1$, the comparison of observed and calculated values of $i_{1/2}$ actually gives the best values of $k_{14}R/k_2$ and $k_{15}R/k_1$. The actual rate constant ratios, therefore, are uncertain to the extent to which R may differ from unity.

If it is assumed that $R = 1$, the best value[c] for k_{14}/k_2 at 520° is 68. Taking the expression for k_{14} given by Berlie and LeRoy[6]:

$$k_{14} = 3.4 \times 10^{12} e^{-6800/RT} \text{ cm}^3\text{mole}^{-1}\text{sec}^{-1} \quad \text{(x)}$$

the value obtained for k_2 at 520°C is 1.1×10^{-15} cm³ molecules⁻¹ sec⁻¹. If the collision yields obtained by Berlie and LeRoy[6] are expressed by a combination of higher pre-exponential factor, and higher activation energy, as favored by earlier workers, the value of k_{14} is increased at 520°C. This uncertainty might be sufficient to cause a

[c] This value is based on a preliminary estimate of surface correction factors, and may be in error by a few per cent.

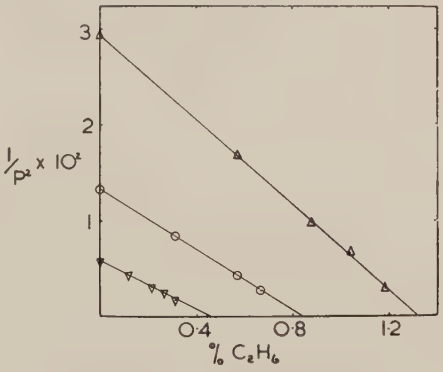

FIG. 5. Variation in first limit inhibition with oxygen concentration. 36 mm diam. potassium chloride coated vessel. Temp. 540°C. $x = 0.28$. △ $y = 0.56$ ⊙ $y = 0.28$ ▽ $y = 0.14$.

TABLE 1. COMPARISON OF FIRST AND SECOND LIMIT INHIBITION BY ETHANE

Mole Fraction		$i^*_{1/2} \times 10^2$*	Intercept $(I) \times 10^2$	$\frac{I}{2i_{1/2}} = \frac{Q}{Q'}$
H_2	O_2			
0.28	0.14	0.265	0.46	0.87
0.28	0.28	0.428	0.84	0.98
0.28	0.56	0.672	1.32	0.98

* Corrected for surface termination of hydrogen atoms and hydroxyl radicals.

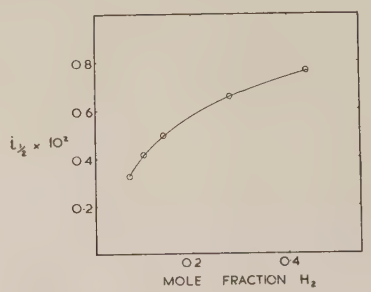

FIG. 6. Variation of $i_{1/2}$ with hydrogen concentration at high oxygen concentration. 36 mm diam. potassium chloride coated vessel. Temp. 540°C. $y = 0.565$.

fivefold increase in the estimated value of k_2. The use of first limit measurements[4], together with the calculated diffusion constant for hydrogen atoms, gives a preliminary value for k_2 of 5×10^{-15}. These values are in reasonable agreement with the value of 1.12×10^{-14} obtained by Semenoff[14], but are significantly higher than the value of 0.87×10^{-17} quoted by Lewis and von Elbe[7].

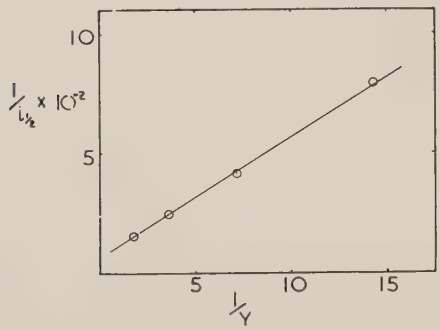

FIG. 7. Variation of $1/i_{1/2}$ with $1/y$. 36 mm diam. potassium chloride coated vessel. Temp. 540°C. $x = 0.28$.

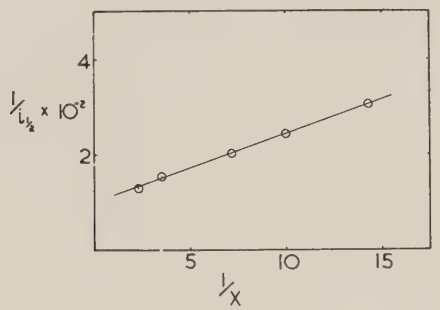

FIG. 8. Variation of $1/i_{1/2}$ with $1/x$. 36 mm diam. potassium chloride coated vessel. Temp. 540°C. $y = 0.56$.

CONCLUSIONS

The main conclusions from the above work may be summarized as follows:

(1) The proposed mechanism, incorporating reactions (1–6), (14) (15) (19) and (20), and surface destruction of hydrogen atoms and hydroxyl radicals, accounts satisfactorily for all the observed facts.

(2) It seems probable that reaction (20) is not the sole reaction of ethyl radicals with oxygen, as otherwise the oxidation of ethane would consist of conversion to ethylene, followed by oxidation of the ethylene, and the products of both oxidations would thus be identical. Evidence that reaction (20) is the predominating reaction comes from the high ethylene yields obtained in ethane oxidation, and from the fact that a ratio for $k_{20}/(k_{19} + k_{20})$ less than 0.5 would give a kinetic expression not consistent with the observed results.

(3) The failure to detect any evidence for the occurrence of reaction (16) indicates that reaction of ethyl radicals with oxygen must be at least ten times faster than reaction with hydrogen. Wijnen and Steacie[11] conclude that the activation energy of reaction (16) is 11.5 kcal, and if the steric factor of 10^{-3} they find for reaction with deuterium is considered to apply also to reaction with hydrogen, the collision yield of reaction (16) at 540° is obtained as 8×10^{-7}. This gives a lower limit of 8×10^{-6} for the collision yield of the reaction between ethyl radicals and oxygen.

(4) Since ethylene has been found[4] to be a more powerful inhibitor than ethane, the formation of ethylene in the termination reaction (20) accounts for the depressed limits that can be obtained if the explosion boundary is crossed slowly.

Inhibition by Other Compounds

PROPANE

The main features of the inhibition of the second limit by propane[15] are essentially similar to those obtained with ethane. In particular, a preliminary analysis of the results indicates the occurrence of the two primary inhibition reactions (14a) and (15a), together with the effective termination reaction (20a). As in the case of ethane, some competition of the aldehyde forming reaction (19a) cannot be excluded.

$$H + C_3H_8 = C_3H_7 + H_2 \qquad (14a)$$

$$OH + C_3H_8 = C_3H_7 + H_2O \qquad (15a)$$

$$C_3H_7 + O_2 = C_3H_6 + HO_2 \qquad (20a)$$

$$C_3H_7 + O_2 = C_2H_5CHO + OH \qquad (19a)$$

The instability of the higher alkyl radicals, shown by the failure to detect their presence in the pyrolysis of the higher lead alkyls[16], suggests that decomposition reactions such as (21) and (22) should be taken into account.

$$C_3H_7 = C_2H_4 + CH_3 \qquad (21)$$

$$C_3H_7 = C_3H_6 + H \qquad (22)$$

A significant competition of either of these reactions with reaction (20a) would give the fraction

Q of propyl radicals destroyed as[d]:

$$Q = \frac{2/3k_{20a}[O_2]}{k_{21} + k_{22} + (k_{19a} + k_{20a})[O_2]} \qquad \text{(xi)}$$

and the oxygen dependence in equation (ii) would thus be almost neutralized. Although a detailed study of the results is still being completed, there appears no evidence for this effect at second limit pressures.

Further evidence that reactions (21) and (22) cannot predominate comes from the ratio of the inhibiting efficiencies of propane and ethane which, at low oxygen concentrations where the primary process (14) predominates, is about 2.0:1. This agrees closely with the ratio $k_{14a}/k_{14} = 2$, estimated from the data of Darwent and Roberts[17], suggesting that the fraction Q is not very different for ethane and propane. Since the work with ethane indicates that the majority of ethyl radicals undergo reaction (20), a significant contribution of the propagation reactions (21) and (22) is thus excluded.

This contrast with the work of Paneth[16] indicates that under these experimental conditions, reactions of the propyl radical with oxygen must be much faster than its decomposition. The presence of ethylene and propylene in the products from the slow oxidation of propane has usually been attributed to the occurrence of the radical cracking reactions (21) and (22). While some of the olefins formed in propane rich mixtures may arise in this manner, it seems more likely that the majority of the propylene results from reaction (20a). This conclusion is supported by the analyses of Newitt and Thornes[18], who find that at 400°C, the maximum propylene concentration is reached well before all the oxygen is consumed. An alternative mode of formation of ethylene could be through the reaction sequence:

$$C_3H_7 + O_2 = C_2H_5CHO + OH$$

$$C_2H_5CHO + \text{radical} = C_2H_5CO$$

$$C_2H_5CO = C_2H_5 + CO$$

$$C_2H_5 + O_2 = C_2H_4 + HO_2$$

A similar suggestion has recently been made by Knox and Norrish[19].

[d] As pointed out later, the methyl radical produced in (21) will continue the chain by reacting with oxygen to give an hydroxyl radical.

FORMALDEHYDE

Study of the inhibition by formaldehyde is complicated by the significant oxidation that occurs in the mixing and evacuation processes. Preliminary observations (20), however, suggest that $i_{1/2}$ is approximately proportional to the oxygen concentration and approximately independent of the hydrogen concentration and vessel diameter. If the primary inhibition process is considered to be:

$$H + HCHO = H_2 + HCO \qquad \text{(14b)}$$

possible reactions of the formyl radical are:

$$HCO = H + CO \qquad \text{(22b)}$$

$$HCO + O_2 = CO + HO_2 \qquad \text{(20b)}$$

$$HCO + O_2 = HCO_3 \qquad \text{(17b)}$$

the performyl radical in (17b) being eventually destroyed at the wall. Since the propagation reaction (22b) is of a different order with respect to oxygen concentration, it cannot predominate over the termination reactions (17b) and (20b) without removing the oxygen dependence introduced by reaction (14b). Confirmation comes from the fact that the ratio of the inhibiting efficiencies of formaldehyde and propane is about 3:1, while estimation of the probable value of the rate constant ratio k_{14b}/k_{14a} from the data of Calvert and Steacie[21] gives a value of about 4:1. Since, as pointed out, most propyl radicals must undergo chain termination, the agreement of these ratios indicates that reaction (22b) cannot predominate. Further work to determine the relative importance of these reactions is in progress.

METHANE

In contrast to the behavior of ethane and propane, increasing concentrations of methane have only a slight effect on the second limit until a critical concentration is reached when explosion is suddenly suppressed[15]. The experimental facts[15, 22] suggest that a new type of inhibition is involved, due to the intermediate formation of formaldehyde by reactions which develop when the net branching factor first becomes positive. If insufficient formaldehyde is formed, the concentration of centers will continue to rise as a result of branching until explosion occurs just below the uninhibited limit. If, however, sufficient formaldehyde is formed to reduce the net branching factor below zero, the concentration of centers, after rising to a maximum, will begin to decrease.

If this maximum concentration of centers is insufficient to produce explosion, and if the equilibrium concentration of formaldehyde finally obtained is sufficiently high, explosion will never occur. This suggestion gains support from the fact that considerable oxidation of the methane was found to have taken place in samples which contained sufficient methane to suppress explosion, and which had been maintained within the uninhibited explosion peninsula. No such oxidation was found in samples maintained outside the explosion peninsula.

The absence of a simple isothermal mechanism in the case of methane can be attributed to the absence of a direct termination reaction between methyl radicals and oxygen. The corresponding reaction to that proposed for ethane and propane is:

$$CH_3 + O_2 = CH_2 + HO_2$$

There is no evidence that this reaction occurs, and in any case, owing to the reactivity of the methylene radical, it is unlikely to result in chain termination.

Summary

The inhibiting effects of methane, ethane, propane and formaldehyde on the hydrogen-oxygen reaction have been described, and mechanisms suggested to account for the observed results.

Acknowledgment

The authors wish to thank the Royal Society and the Imperial Chemical Industry for their generous grants towards the provision of apparatus, the Surrey Education Committee for a grant to Mr. R. F. Simmons, and the Department of Scientific and Industrial Research for a grant to Mr. N. S. Corney.

REFERENCES

1. Baldwin, R. R.: Fuel, *31*, 312 (1952).
2. Baldwin, R. R., and Simmons, R. F.: Submitted for publication.
3. Baldwin, R. R., and Precious, R. M.: Nature, *169*, 290 (1952).
4. Baldwin, R. R., and Simmons, R. F.: Unpublished work.
5. Steacie, E. W. R.: *Atomic and Free Radical Reactions*. New York, Reinhold Publishing Corp., 1946.
6. Berlie, M. R., and LeRoy, D. J.: Faraday Soc. Disc., *14*, 50 (1953).
7. Lewis, B., and von Elbe, G.: *Combustion, Flames and Explosion of Gases*. New York, Academic Press, 1951.
8. Warren, D. R.: Proc. Roy. Soc., *A211*, 86, 96 (1952).
9. Walsh, A. D.: Trans. Faraday Soc., *43*, 297 (1947).
10. Moore, W. J., and Taylor, H. S.: J. Chem. Phys., *8*, 396 (1940).
11. Wijnen, M. H. J., and Steacie, E. W. R.: J. Chem. Phys., *20*, 205 (1952).
12. Gray, J. A.: J. Chem. Soc., 741 (1953).
13. Baldwin, R. R., and Simmons, R. F.: In preparation for publication.
14. Semenoff, N.: Acta Physicochim., *20*, 290 (1945).
15. Baldwin, R. R., Corney, N. S., and Precious, R. M.: Nature, *169*, 201 (1952).
16. Paneth, F., and Lautsch, W.: Ber., *64*, 2702, 2708 (1931).
17. Darwent, B. de B., and Roberts, R.: Faraday Soc. Disc., *14*, 55 (1953).
18. Newitt, D. M., and Thornes, L. S.: J. Chem. Soc., 1656 (1937).
19. Knox, J. H., and Norrish, R. G. W.: Proc. Roy. Soc., *A221*, 151 (1954).
20. Baldwin, R. R.: Unpublished work.
21. Calvert, J. G., and Steacie, E. W. R.: J. Chem. Phys., *19*, 176 (1951).
22. Baldwin, R. R., and Corney, N. S.: In preparation for publication.

49

THE ROLE OF PROPYLENE IN THE PARTIAL OXIDATION OF PROPANE

By CHARLES N. SATTERFIELD AND ROBERT C. REID

Introduction

The partial oxidation of propane and of mixtures of propane and propylene was studied in order to elucidate the role of propylene in the mechanism of propane oxidation and to aid in the evaluation of the industrial potentialities of such an oxidation process for producing hydrogen peroxide. In these experiments substantial quantities of the following intermediate products of the oxidation were isolated: formaldehyde, acetaldehyde, methanol, hydrogen peroxide, carbon monoxide, and the olefins, propylene and ethylene. The theoretical significance of such studies proceeds from the fact that propylene is itself formed in the reaction and it has been found in general to inhibit free radical reactions. In practical operations, the propane feed gas for an industrial plant, whether obtained from the petroleum refinery or from recycling the unreacted propane in a partial oxidation process, may contain some propylene. The knowledge of how this diluent affects the yields of hydrogen peroxide and other products would indicate whether the propylene must first be separated from the propane feed gas.

The literature indicates that the oxidation of propane has been more extensively investigated than that of any other hydrocarbon. A recent paper[17] gives references to the previous work. The rate and products of the oxidation are greatly influenced by the reaction temperature. At pressures of 1 to 2 atmospheres and with a high ratio of propane to oxygen, the important effects of temperature may be summarized as follows[16]:

(1) At temperatures below 375°C, the products of the reaction are mainly formaldehyde, acetaldehyde, and methanol although some propylene is also formed.

(2) As the temperature is raised above 375°C, a range is reached in which the rate of oxidation decreases with increasing temperature. The exact range of this negative temperature coefficient can vary with the partial pressure of reactants and surface conditions but is usually observed between 400–425°C. With further increase in temperature the rate passes through a minimum and then increases.

(3) In the range of the negative temperature coefficient, as the temperature is raised the proportion of oxygenated products decreases and that of the olefins increases.

(4) As the reaction rate increases after passing through the minimum, the proportion of reacted propane going to oxygenated organic products continues to decrease and the proportion going to olefins increases. Ethylene production increases very rapidly, and above about 500–550°C, the reaction becomes essentially an oxygen-sensitized cracking of propane.

Hydrogen peroxide is reported as a product at temperatures between 300–500°C, but the quantities isolated depend to a great extent on the type of reactor surface used in the experiments as well as the temperature and reactant ratio. When soft glass or salt-coated glass reactors are used, very little hydrogen peroxide is found but when Pyrex or silica glass reactors are substituted, the yields of hydrogen peroxide increase. The amounts of hydrogen peroxide appear to increase with temperature, but often the increased decomposition rate of this species at the higher temperatures leads to lower overall yields.

The effect of propylene addition was noted by two previous investigators with conflicting results; Chernyak and Shtern[5] reported that the addition of propylene had no effect on either the rate or the product distribution; the propylene which was added reportedly passed through unchanged. Harris and Egerton[8] found that propylene addition decreased the induction period in propane oxidation but did not change the final amount of propylene isolated. Neither attempted any explanation of their results.

Experimental

The experimental apparatus consisted of a tubular Pyrex flow reactor, 1 in in diameter and 3 ft long, preceded by separate, electrically heated hydrocarbon (propane and propylene) and oxygen preheaters and followed by a tubular surface condenser cooled with circulating ice-water. The arrangement is shown on Figure 1. Since backmixing would confuse kinetic interpretation of results, a long cylindrical reactor shape was chosen in order to make the flow characteristics of the reacting gases approach slug flow as nearly

as possible. Propylene and propane of 99 per cent purity and oxygen of 99.5 per cent purity were used as the reactants. The propylene was metered separately and added to the propane stream just prior to the hydrocarbon preheater. The residence time was varied by changing the inlet gas flow rates; this in turn controlled the amount of reaction occurring. The first 24 in of the reactor was maintained isothermal by insulation and electrical heaters. Either electrical heating or cooling by forced air convection could be externally applied to the last 12 in of the reactor, the cooling being necessary to maintain isothermal conditions in runs in which a large amount of reaction took place. Temperatures of the hydrocarbon and oxygen gases were measured before they were mixed at the reactor inlet, and of the reacting gases at every 12 in along the reactor.

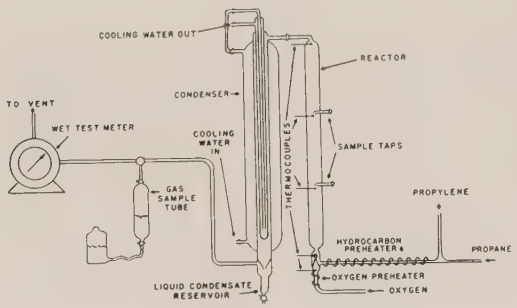

FIG. 1. Apparatus used

In each run, the oxidation was allowed to reach steady state, after which liquid and gas flow rates were measured and samples of both streams collected. The gas samples were analyzed volumetrically by selective chemical absorption for carbon dioxide, acetylene, propylene, ethylene, oxygen, and carbon monoxide[2]; hydrogen was selectively oxidized by copper oxide; and methane was determined by infrared absorption. Propane was determined by difference. Acetylene was never detected in the exit gas by this chemical absorption technique except in a few runs where pure propylene was oxidized. Previous work[17] has shown that small amounts of ethane are also present in the product gas but essentially no olefins higher than propylene nor saturated hydrocarbons higher than propane are found. This latter result suggests that polymerization reactions of hydrocarbon radicals here are negligible.

The liquid condensate was analyzed as follows: total peroxide was determined iodimetrically using 56 per cent hydriodic acid in glacial acetic acid solvent; total aldehyde was determined by measuring the amount of acid liberated using hydroxylamine hydrochloride; formaldehyde was determined colorimetrically with acidified Schiff's reagent; methanol was determined colorimetrically with ceric ammonium nitrate after separation of the methanol from the aldehydes and peroxides. Acetaldehyde was calculated as the difference between the total aldehyde and formaldehyde.

The intensity of the purple color developed when Schiff's reagent reacts with formaldehyde is decreased when the formaldehyde solution also contains hydrogen peroxide. The hydrogen peroxide reacts with the formaldehyde to form organic peroxides which are apparently incompletely reconverted to formaldehyde in the analytical procedure. Correction factors were therefore established by determining the effect on the reported value of (1) the time that the formaldehyde and hydrogen peroxide were in contact with one another before analysis, (2) the temperature, and (3) the initial concentration of formaldehyde and hydrogen peroxide. By this means it was possible to determine formaldehyde concentrations to within ± 10 per cent of the true value.

A check on the overall accuracy was obtained by calculating material balances from the analytical results for the gas and liquid samples, combined with the flow rate measurements. The quantity of the liquid condensate, as measured by direct weighing of a sample taken over a known time interval, was corrected for the amounts of the liquid components left uncondensed in the gas phase. The gas stream left the condenser at a temperature between 5–10°C and presumably was in equilibrium with the liquid condensate. The results of some experiments by Cooper[6] were used to calculate the equilibrium partial pressures of the liquid components in the exit gas stream and these data, combined with a knowledge of the total gas flow from the condenser, made it possible to calculate the amount of the various liquid components carried out of the condenser by the exit gas. This correction affects particularly the amount of methanol reported since it is quite volatile in dilute aqueous solutions. Studies were made at three different temperatures; 375°C, representative of the so-called low-temperature oxidation region; 425°C, which is in the temperature region where the rate of reaction has a negative temperature coefficient; and 475°C, representative of the high-temperature region.

In all studies the molar ratio of propane to

oxygen was kept constant at 5.5:1. Each series of experiments consisted of three runs. In the first, propane and oxygen were reacted with no propylene added. In the second, a concentration of propylene equal to 5 per cent of the total entering gases was used; in the third 15 per cent propylene was added. All three runs were carried out at the same contact time, achieved by reducing the propane and oxygen flow rates as propylene was added. The residence times reported were calculated by dividing the reactor volume by the entering gas volumetric flow rate, corrected to the temperature prevailing in the reactor. This method of calculating residence times, of course, gives only an approximation to the true contact time because there is an increase in the number of moles during the reaction, and slug flow is not completely achieved. By varying the residence time in successive studies, the progress of the reaction was followed from the early stages up to the point where essentially all of the inlet oxygen had reacted. A total of 48 runs were made.

Results

A large number of figures would be required to bring out the full significance of the results[a]. For the present there are given only a few plots to illustrate the most important effects of reaction temperature, inlet propylene concentration, and extent of reaction on the product distribution. The general effect of these variables may be briefly summarized as follows:

REACTION TEMPERATURE

The effect of temperature was similar to that noted by previous investigators. At the low temperature, 375°C, the products consisted largely of oxygenated organic species in addition to some propylene. At 425°C, in the negative reaction rate zone, the quantities of oxygenated organic compounds decreased and some ethylene and methane were found. The yield of propylene and hydrogen peroxide isolated per mole of propane reacted reached a maximum at 425°C, as shown in Figures 2 and 3. At 475°C, the amount of oxygenated organics formed per quantity of propane reacting had further decreased, the amount of propylene began to decrease, and the amount of ethylene and methane increased. The products are primarily water and olefins.

[a] Two tables giving the tabulated experimental results of all runs have been prepared by the authors and copies are available from them without charge. These give for each run the quantities of each species formed, per cent of inlet oxygen reacted, material balances, and other information.

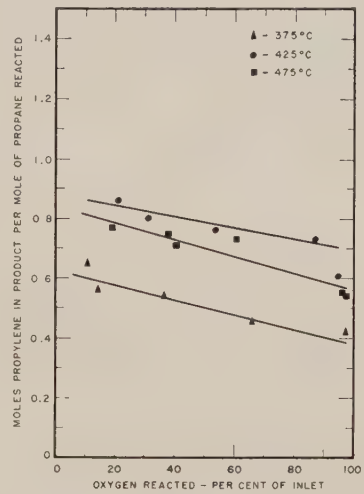

FIG. 2. Yield of propylene in absence of added propylene. (Data taken in runs where no propylene was added.)

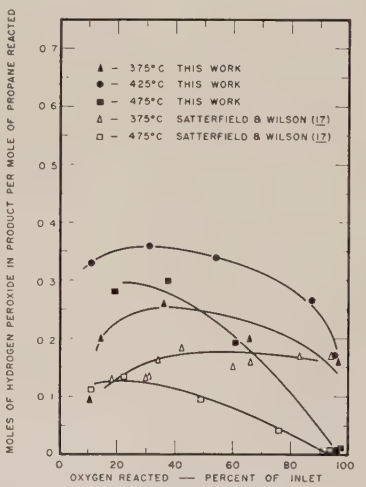

FIG. 3. Yield of hydrogen peroxide in absence of added propylene.

INLET PROPYLENE CONCENTRATION

At all temperatures investigated, when the inlet propylene concentration was increased, the induction period of the reaction decreased although the overall rate of oxygen consumption was not significantly changed. Figures 4, 5, and 6 show the extent of reaction as a function of residence time at 375°, 425°, and 475°C for different inlet propylene concentrations. The figure given as per cent of the inlet oxygen reacted was calculated by

dividing the total of the oxygen atoms found in the product less the unreacted oxygen atoms in the oxygen gas as such in the product, by the total

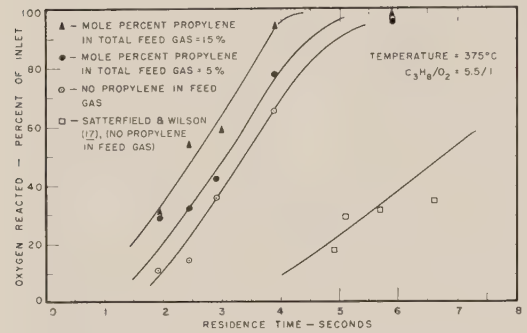
▲ – MOLE PERCENT PROPYLENE IN TOTAL FEED GAS = 15%
● – MOLE PERCENT PROPYLENE IN TOTAL FEED GAS = 5%
○ – NO PROPYLENE IN FEED GAS
□ – SATTERFIELD & WILSON (17), (NO PROPYLENE IN FEED GAS)
TEMPERATURE = 375°C
C_3H_8/O_2 = 5.5/1
OXYGEN REACTED – PERCENT OF INLET
RESIDENCE TIME – SECONDS

FIG. 4. Effect of added propylene on the rate of reaction—375°C.

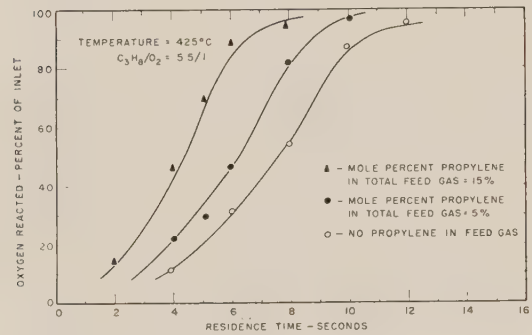
TEMPERATURE = 425°C
C_3H_8/O_2 = 5.5/1
▲ – MOLE PERCENT PROPYLENE IN TOTAL FEED GAS = 15%
● – MOLE PERCENT PROPYLENE IN TOTAL FEED GAS = 5%
○ – NO PROPYLENE IN FEED GAS
OXYGEN REACTED – PERCENT OF INLET
RESIDENCE TIME – SECONDS

FIG. 5. Effect of added propylene on the rate of reaction—425°C.

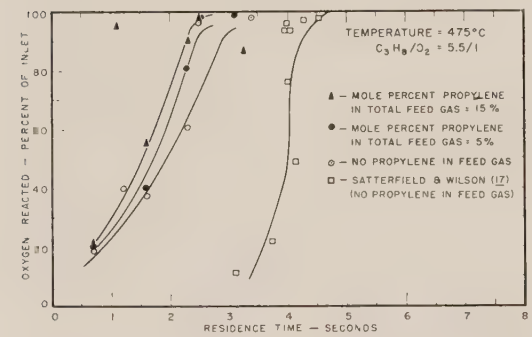
TEMPERATURE = 475°C
C_3H_8/O_2 = 5.5/1
▲ – MOLE PERCENT PROPYLENE IN TOTAL FEED GAS = 15%
● – MOLE PERCENT PROPYLENE IN TOTAL FEED GAS = 5%
○ – NO PROPYLENE IN FEED GAS
□ – SATTERFIELD & WILSON (17) (NO PROPYLENE IN FEED GAS)
OXYGEN REACTED – PERCENT OF INLET
RESIDENCE TIME – SECONDS

FIG. 6. Effect of added propylene on the rate of reaction—475°C.

of the oxygen atoms found in the product. The resulting number was multiplied by 100.

The quantities of acetaldehyde, formaldehyde, methanol, and water found per mole of oxygen reacted increased somewhat when propylene was added. Except for methanol the effect is more pronounced at 475°C than at 375°C. Three typical plots are presented in Figures 7, 8, and 9, showing the effect of inlet propylene concentration on the amounts of acetaldehyde, formaldehyde, and methanol isolated per mole of oxygen reacted. The quantity of hydrogen peroxide isolated per mole of oxygen reacted decreased as the inlet

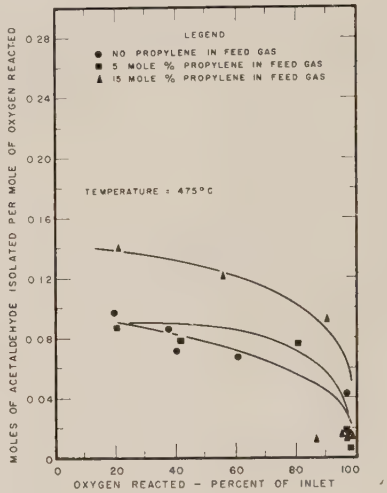
LEGEND
● NO PROPYLENE IN FEED GAS
■ 5 MOLE % PROPYLENE IN FEED GAS
▲ 15 MOLE % PROPYLENE IN FEED GAS
TEMPERATURE = 475°C
MOLES OF ACETALDEHYDE ISOLATED PER MOLE OF OXYGEN REACTED
OXYGEN REACTED – PERCENT OF INLET

FIG. 7. Effect of propylene on the amount of acetaldehyde isolated—475°C.

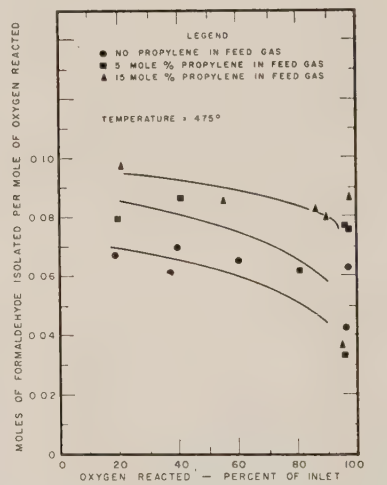
LEGEND
● NO PROPYLENE IN FEED GAS
■ 5 MOLE % PROPYLENE IN FEED GAS
▲ 15 MOLE % PROPYLENE IN FEED GAS
TEMPERATURE = 475°
MOLES OF FORMALDEHYDE ISOLATED PER MOLE OF OXYGEN REACTED
OXYGEN REACTED – PERCENT OF INLET

FIG. 8. Effect of propylene on the amount of formaldehyde isolated—475°C.

propylene concentration was increased. This is clearly shown in Figure 10 for the reaction temperature of 425°C. The effect is again more pronounced at 475°C and 425°C than at 375°C. The sum of the water plus hydrogen peroxide isolated per mole of oxygen reacted was not significantly affected by propylene addition.

Some of the diluent propylene may have reacted at 375°C since the amount of propylene isolated at this temperature was much lower than

that predicted from the total of the propylene added and the propylene which would be expected to be formed from the propane-oxygen reaction.

In each group of three runs, as more propylene was added, the propane-oxygen flow rates were reduced. This, in effect, gave a higher total hydrocarbon-to-oxygen mole ratio. It has been reported[16] that such an increase in the hydrocarbon-to-oxygen mole ratio of itself increases the oxidation rate, even at very high ratios. This is not the case here, as shown by the results of two additional runs in which additional propane was added instead of propylene. Compared to runs with a lower propane-oxygen ratio, the additional propane was found to give only a slightly increased degree of reaction, much less than the effect of propylene. It was therefore concluded that increased amount of reaction occurring when propylene was added was due to a specific chemical effect and not to the increased hydrocarbon-to-oxygen ratio as such.

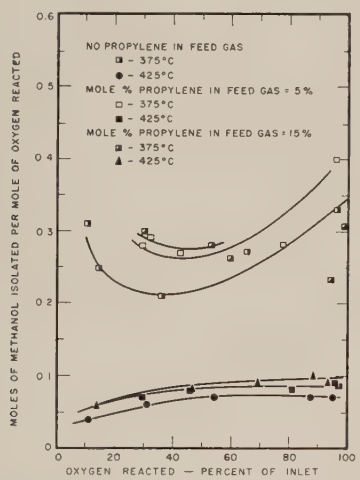
NO PROPYLENE IN FEED GAS
□ - 375°C
● - 425°C
MOLE % PROPYLENE IN FEED GAS = 5%
□ - 375°C
■ - 425°C
MOLE % PROPYLENE IN FEED GAS = 15%
▲ - 375°C
▲ - 425°C
MOLES OF METHANOL ISOLATED PER MOLE OF OXYGEN REACTED
OXYGEN REACTED — PERCENT OF INLET

FIG. 9. Effect of propylene on the amount of methanol isolated.

EXTENT OF REACTION

The quantities of methanol, the carbon oxides, ethylene, water, and methane found in the products per mole of oxygen reacted generally increased as the per cent of the inlet oxygen reacted increased. The effect is particularly striking for methane, as shown in Figure 11 for 475°C. The yields of acetaldehyde, formaldehyde, and hydrogen peroxide per mole of oxygen reacted sometimes increased to a maximum as the reaction progressed but always rapidly decreased as the per cent oxygen reacted approached 100 per cent.

The maximum yield of hydrogen peroxide expressed as moles isolated per mole of oxygen reacted was found to be 0.42 at 425°C with 11 per cent of the inlet oxygen reacted; the maximum concentration of hydrogen peroxide in the exit gas was found to be 3.3 mole per cent at 425°C with 87 per cent of the inlet oxygen reacted.

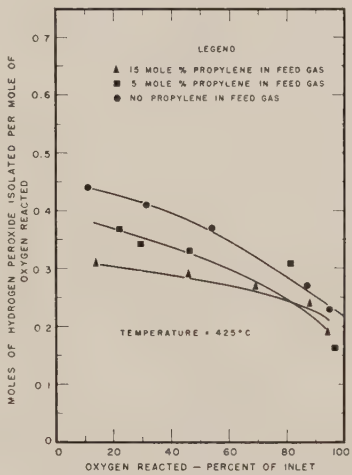
LEGEND
▲ 15 MOLE % PROPYLENE IN FEED GAS
■ 5 MOLE % PROPYLENE IN FEED GAS
● NO PROPYLENE IN FEED GAS
TEMPERATURE = 425°C
MOLES OF HYDROGEN PEROXIDE ISOLATED PER MOLE OF OXYGEN REACTED
OXYGEN REACTED — PERCENT OF INLET

FIG. 10. Effect of propylene on the amount of hydrogen peroxide isolated—425°C.

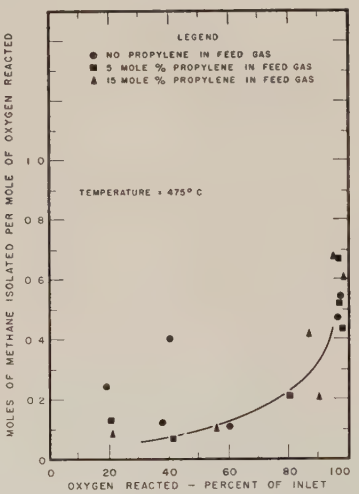
LEGEND
● NO PROPYLENE IN FEED GAS
■ 5 MOLE % PROPYLENE IN FEED GAS
▲ 15 MOLE % PROPYLENE IN FEED GAS
TEMPERATURE = 475° C
MOLES OF METHANE ISOLATED PER MOLE OF OXYGEN REACTED
OXYGEN REACTED — PERCENT OF INLET

FIG. 11. Effect of oxygen concentration on the amount of methane isolated.

A 5.5:1 molar mixture of pure propylene and oxygen was also allowed to react in two runs, one at 375°C and one at 475°C. The same qualitative distribution of products was found as in the oxidation of propane alone. In addition to the

aqueous condensate produced, a yellow-brown oil layer was formed which was undoubtedly a propylene polymer. Material balances indicated that at 375°C about 6 per cent, and at 475°C, about 28 per cent of the carbon in the propylene reacting appeared as this polymer. A significant fact was that much longer contact times were required to consume a given fraction of the inlet oxygen when it was reacting with pure propylene than with pure propane. However, mixtures of propane and propylene reacted faster than either species alone.

help to orient the reader in the following discussion.

INITIATING REACTIONS

In a propane and oxygen mixture at high temperature, the initial fission of the propane molecule can occur either by thermal cracking or by attack from an oxygen molecule. Thermal cracking is not considered to be important for the following reasons. Experimentally, when propane and nitrogen (instead of oxygen) were preheated and passed through the reactor, no products of

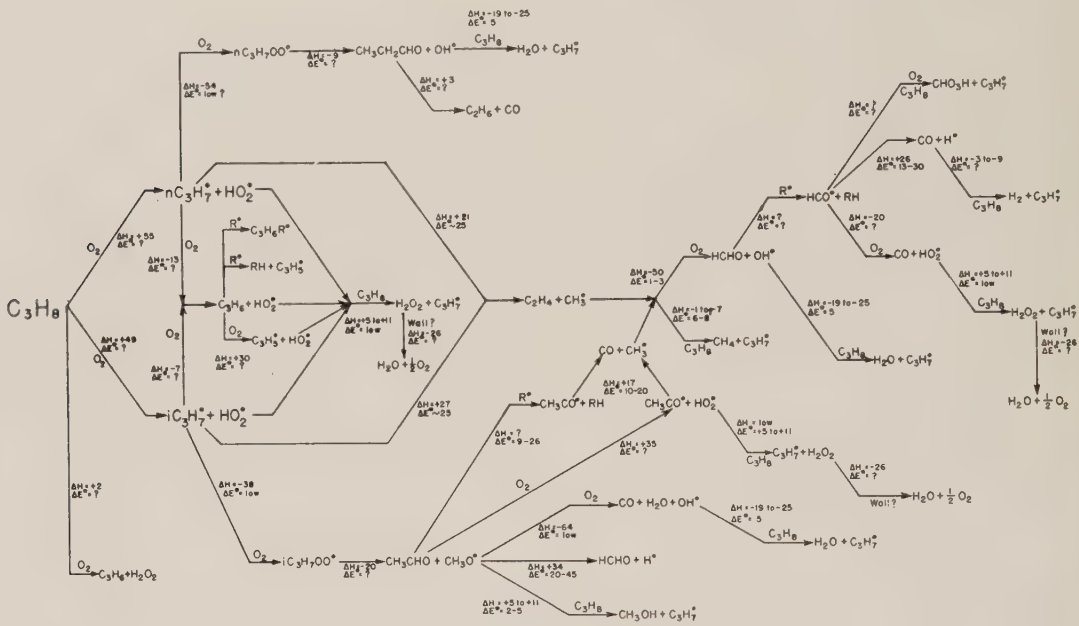

FIG. 12. An outline of reaction steps in propane oxidation.

Discussion of Results

When propane alone is oxidized, propylene is a major product. Since this propylene acts similarly to any added propylene, the experimental results must be interpreted on a relative basis, i.e., the effect of added propylene on the induction period, reaction rate, and product distribution will only magnify any effects which may be due to propylene in the undiluted case. The discussion presented here will attempt to outline a mechanism of propane oxidation emphasizing the reactions in which propylene plays an important role. Various reaction steps which may be involved in propane oxidation are presented in Figure 12. Many of those shown do not occur in the particular circumstances discussed here and other paths not shown are also possible, but the scheme may

cracking were detected until a temperature of 475°C was reached. At this temperature, only about 0.1 to 0.2 per cent of the inlet propane was found to decompose, forming predominantly hydrogen and propylene. This small amount of cracking has of itself a negligible effect on the product distribution obtained. The free radicals produced in the cracking reaction are not important in initiating the reaction since it is known that propylene inhibits the thermal decomposition of propane[15]; yet propylene added to a propane-oxygen mixture was found to decrease the induction period of the oxidation. If thermal cracking were a significant initiating step, the addition of propylene to the propane feed gas should instead increase the induction period of the hydrocarbon oxidation reaction. It

is therefore clear that the free radicals produced by propane cracking are not important in initiating the propane-oxygen reaction.

A second possibility for the initiating reaction is that with oxygen,

$$C_3H_8 + O_2 \rightarrow C_3H_7\cdot + HO_2\cdot \qquad (1)$$

This reaction is quite endothermic and is believed to have a low reaction rate. The products are, however, reactive free radicals which are capable of autocatalyzing the oxidation.

The addition of propylene to a propane-oxygen mixture was found to decrease the induction period of the reaction although it did not greatly affect the subsequent reaction rate, as is shown in Figures 4, 5, and 6. The induction period may be considered as the time necessary to attain the straight-line section of the curve, and the rate of the reaction as the slope of the straight line section of the plot. Propylene addition causes displacement of the curves to the left but has little effect on their slopes. An explanation of this acceleration effect proceeds from a closer examination of the properties of the propylene molecule.

Propylene, although thermally stable, is highly reactive in most free-radical reactions since a hydrogen may be easily extracted by a free radical.

$$C_3H_6 + R\cdot \rightarrow C_3H_5\cdot + RH \qquad (2)$$

Taylor and Smith[22] experimentally bombarded various hydrocarbons with free methyl radicals and determined the relative rates of hydrogen abstraction. Their results showed that the average C—H bond strength in propylene was about 5.2 kcal less than the C—H bond strength in ethane, 2.4 kcal less than the bond strength of the secondary bond in *n*-butane, and 1.1 kcal less than the bond strength of the tertiary C—H bond in isobutane. Thus the inhibiting action of propylene in free-radical reactions is attributable to its reaction with reactive free radicals as in equation (2) producing a resonance-stabilized inactive allyl radical. This long lived radical may, in fact, combine with another to produce diallyl, the net result of which is the removal of two chain carriers per molecule of diallyl formed.

When propylene is added initially to the propane and oxygen mixture, the oxygen will preferentially attack the propylene since it has the weakest carbon-hydrogen bond.

$$C_3H_6 + O_2 \rightarrow C_3H_5\cdot + HO_2\cdot \qquad (3)$$

The products of reaction (3) should be able to attack propane with more ease than oxygen.

$$C_3H_8 + HO_2\cdot \rightarrow C_3H_7\cdot + H_2O_2 \qquad (4)$$

$$C_3H_8 + C_3H_5\cdot \rightarrow C_3H_7\cdot + C_3H_6 \qquad (5)$$

The initiating steps in the reaction are summarized thus: if no propylene is present, the initiating reaction is presumably reaction (1) which is slow and explains the induction period found experimentally; if propylene is added to the reacting mixture of propane and oxygen, reactions (3), (4), and (5) eclipse reaction (1) as the initial reaction steps, thereby decreasing the induction period. Propylene, whether produced as a product of the reaction between propane and oxygen or added as a diluent, would act similarly in the initiating steps.

REACTIONS OF THE PROPYL RADICAL

The various reactions of the propyl radical have been thoroughly discussed in a recent paper[17] and will be but briefly reviewed here.

It is postulated that essentially all the products isolated from propane oxidation are formed by reactions of the propyl radical which may proceed by three paths, the predominating reaction being determined by the temperature.

(1) The propyl radicals may thermally decompose to ethylene and methyl radicals.

$$C_3H_7\cdot \rightarrow C_2H_4 + CH_3\cdot \qquad (6)$$

From a consideration of the bond dissociation energies of the carbon-carbon and carbon-hydrogen bonds in the propyl radical[21], plus the fact that very little hydrogen was found here, it is concluded that only a negligible fraction of the propyl radicals thermally decomposed to form propylene and hydrogen atoms. This conclusion is supported by experimental data on the products of cracking of the propyl radical[20].

(2) Propyl radicals may react with oxygen according to reaction (7):

$$C_3H_7\cdot + O_2 \rightarrow C_3H_6 + HO_2\cdot \qquad (7)$$

(3) The propyl radical may react with oxygen to form the propyl peroxide radical which in turn can lead to the formation of the oxygenated organic species, acetaldehyde, formaldehyde, and methanol.

$$C_3H_7\cdot + O_2 \rightarrow \text{oxygenated species} \qquad (8)$$

Reaction (6) becomes important at very high temperatures, i.e., over 500°C. At lower tempera-

tures reaction (7) predominates; the maximum yield of propylene per mole of propane reacting was found at 425°C. Further decrease in temperature increases the importance of reaction (8) and decreases that of reaction (7); thus increased quantities of oxygenated organic species and decreased quantities of propylene are found.

It may be shown that the ratio (moles of propylene/moles of propane forming oxygenated organics) is almost constant at any one temperature for varying degrees of completion of reaction. The constancy of this ratio implies that little or no propylene, once formed in the reaction, reacts further. This ratio does decrease somewhat at 375°C indicating that at this temperature propylene reacts further forming some of the oxygenated organic products. Any reaction involving propylene probably proceeds through the allyl radical which is resonance stabilized and reacts more slowly than the other free radicals participating in the oxidation.

There is no general agreement as to the subsequent reactions of the propyl peroxide radicals formed in reaction (7), and the results obtained here do not contribute further evidence. The mechanism postulated by Lewis and von Elbe[9] is used in Figure 12, but alternately the peroxide radicals may react with the alkyl radical or another peroxy radical to form an alkoxy radical, as postulated by Bell et al.[1].

FORMATION OF METHANOL

The methanol formed in the reaction is attributed to the reaction of the methoxy radical, $CH_3O\cdot$, with propane or propylene.

$$CH_3O\cdot + C_3H_8 \rightarrow CH_3OH + C_3H_7\cdot \qquad (9)$$

The methoxy radical may also react with oxygen in a competing reaction.

$$CH_3O\cdot + O_2 \rightarrow CO + H_2O + OH\cdot \qquad (10)$$

Experimental evidence for the existence here of this pair of competing reactions comes from noting that the yield of methanol per mole of oxygen reacted increased as the reaction progressed, i.e., as the concentration of oxygen decreased. Adding propylene to the propane-oxygen mixture increased the methanol isolated per mole of oxygen reacted. This is consistent with the hypothesis that propylene, possessing an easily extractable hydrogen, should increase the amount of reaction (9) relative to reaction (10), thus leading to the higher yields of methanol.

REACTIONS OF ACETALDEHYDE

Acetaldehyde is not a stable intermediate; only a fraction of the total amount presumably formed from the decomposition of the isopropyl peroxide radical is found in the products. One way it may disappear is by reaction with free radicals.

$$CH_3CHO + R\cdot \rightarrow CH_3CO\cdot + RH \qquad (11)$$

The acetyl radical is unstable[7, 19] and readily decomposes.

$$CH_3CO\cdot \rightarrow CH_3\cdot + CO \qquad (12)$$

It has been realized for some time that oxygen catalyzes the free-radical decomposition of acetaldehyde[10, 11, 12, 13, 23], so it appears plausible to insert a competing oxidation reaction with the straight free-radical decomposition reaction.

$$CH_3CHO + O_2 \rightarrow CH_3CO\cdot + HO_2\cdot \qquad (13)$$

In reaction (13) the hydrogen atom attached to the carbonyl carbon is considered more labile, but this view has been disputed[4, 5]. The principal difference between reactions (11) and (13) is that the former is a straight chain-continuing reaction while the latter is chain-branching. The branching-chain characteristics of reaction (13) predict that the higher the concentration of acetaldehyde and oxygen in a propane-oxygen system, the more rapid the reaction. Until recently the effect noted when acetaldehyde was added to the original propane-oxygen system at low temperatures was one of decreasing the induction period and increasing the rate of the oxidation[8, 14]. This agrees well with prediction. However, recent work[18] has indicated that this rate-accelerating effect of acetaldehyde is not present at the higher temperatures. The tentative conclusion may be drawn that at the low temperatures, the branching reaction of acetaldehyde predominates, but as the temperature is increased the free-radical non-branching reaction increases in importance. This view leads one to postulate that the change in mechanism is the cause of the decreasing rate region noted between 400 and 425°C. In the same temperature region there is also a decreasing amount of acetaldehyde formed with increased temperature, as discussed previously, which likewise decreases the effect of the oxidation reaction.

The effect of propylene on these two reactions would be to increase the amount of acetaldehyde found in the products by (1) decreasing the active free-radical concentration (reaction (2)),

and (2) by reaction with the acetyl radical to reform acetaldehyde. The experimental data indicate that the yield of acetaldehyde per mole of oxygen reacted does indeed increase with the addition of more propylene as shown at 475°C in Figure 7.

REACTIONS OF THE METHYL RADICAL

The methyl radicals, formed from the decomposition of the acetyl and propyl radicals, may react in two ways.

$$CH_3\cdot + C_3H_8 \rightarrow CH_4 + C_3H_7\cdot \quad (14)$$

$$CH_3\cdot + O_2 \rightarrow HCHO + OH\cdot \quad (15)$$

There is some question about the exact mechanism of reaction (15)[11, 20], as no spectroscopic OH bands have been noted in oxidation studies of the methyl radical[3].

Figure 11 shows that the methane yield per mole of oxygen reacting increases as the concentration of oxygen decreases, as would be predicted. However, the effect of propylene on the methane yield is not as pronounced as might have been expected from the analogous case involving the methoxy radical. Undoubtedly propylene does provide a readily extractable source of hydrogen in reaction (14) which should increase the rate of this reaction; however, propylene may also react with methyl radicals in an addition reaction[22].

$$CH_3\cdot + C_3H_6 \rightarrow C_4H_9\cdot \quad (16)$$

The net effect of propylene is thus small as the reactions tend to counterbalance each other.

REACTIONS OF FORMALDEHYDE

Formaldehyde decomposes primarily by a free-radical mechanism similar to that proposed for acetaldehyde.

$$HCHO + R\cdot \rightarrow CHO\cdot + RH \quad (17)$$

The experimental data show that propylene addition increases the amounts of formaldehyde found in the products, as shown, for example, at 475°C in Figure 8. Propylene presumably inhibits the decomposition of formaldehyde by regeneration of formaldehyde from the peroxyformyl radical and by decreasing the free-radical concentration. The fate of the radical HCO· has been thoroughly discussed elsewhere[9].

FORMATION OF WATER, HYDROGEN PEROXIDE, AND HYDROGEN

The formation reactions are believed to be:

$$H\cdot + C_3H_8 \rightarrow H_2 + C_3H_7\cdot \quad (18)$$

$$OH\cdot + C_3H_8 \rightarrow H_2O + C_3H_7\cdot \quad (19)$$

$$HO_2\cdot + C_3H_8 \rightarrow H_2O_2 + C_3H_7\cdot \quad (20)$$

The hydrogen peroxide which is formed may decompose or react further. Hydrogen peroxide vapor is known to decompose heterogeneously at high temperatures to form water and oxygen even on relatively highly inert surfaces such as glass. Here it may also decompose homogeneously or react further with the other products of the oxidation.

The highest yield of hydrogen peroxide was 0.27 mole/mole of propane reacting at 425°C. Coating the surface with alkali halides or boric anhydride decreased the yield. The addition of propylene to the reaction mixture led to decreased amounts of hydrogen peroxide found per mole of oxygen reacted and this is shown at 425°C in Figure 10. However this propylene addition did not greatly affect the yield of water plus hydrogen peroxide. Propylene may be adsorbed on the surfaces of the reactor rendering them more active in converting hydrogen peroxide to water.

HETEROGENEOUS EFFECTS

Previous studies of hydrocarbon oxidation in glass vessels have shown that the results may vary as the reactor surface ages. Such an aging process was very slow and relatively insignificant here. However, it is interesting to compare the present results with earlier results[17] which were obtained in the same laboratory under the same conditions and in the same type of reactor. After several hundred hours of operation, a brownish-red film was found deposited throughout the propane preheater and the internal surface of the lower section of the reactor used for the previous studies. Some film may also have been present throughout the remainder of the reactor, although it was not visible to the eye. The film dissolved in nitric acid and was combustible in oxygen. Presumably it was a polymeric substance resulting from polymerization of propylene and possibly also ethylene. The previous rate-of-reaction results are compared to the present ones in Figures 4 and 6, and it is seen that the induction period in the present studies was much shorter.

Figure 3 shows that the hydrogen peroxide yield per mole of propane reacted obtained in the previous studies was also much smaller than that obtained in the present work. It may be concluded that the propylene polymer forms a more active surface for the destruction of free radicals and hydrogen peroxide. Cleaning the previous reactor with nitric acid caused an increase in the reaction rate, an increase in the hydrogen peroxide yield, and also an increase in the ratio of acetaldehyde to formaldehyde in the products, the total aldehyde remaining essentially constant. This latter result suggests that at least some of the reactions of acetaldehyde leading to formaldehyde are heterogeneous in nature.

Summary

The role of propylene in the partial oxidation of propane is seen to derive primarily from its relatively weak carbon-hydrogen bond compared to most other hydrocarbons. However, once the initial hydrogen has been removed from propylene, a relatively stable allyl radical results. This accounts for the acceleration effect of propylene in the initial stages of the propane oxidation, as well as its inhibiting effect under most other conditions.

Acknowledgment

The authors wish to acknowledge the financial support of the Office of Naval Research under Contract No. N5ori-07819, NR-092,008.

REFERENCES

1. Bell, E. R., Raley, J. H., Rust, F. F., Seubold, F. H., Jr., and Vaughan, W. E.: Disc. Faraday Soc., *10*, 242 (1951).
2. Burke, O. W., Starr, C. E., and Tuemmler, F. D.: *Light Hydrocarbon Analysis*, pp. 134, 223–231. New York, Reinhold Publishing Corp., 1951.
3. Blaedel, W. J., Ogg, R. A., and Leighton, P. A.: J. Am. Chem. Soc., *64*, 2499 (1942).
4. Chamberlain, G. H. N., and Walsh, A. D.: *Cinétique et mécanisme des reactions d'inflammation et de combustion en phase gazeuse*, p. 29. Paris, Centre National de la Recherche Scientifique, 1948.
5. Chernyak, N., and Shtern, V.: Doklady Akad. Nauk. S.S.S.R., *78*, 91 (1951).
6. Cooper, D. O.: S. M. Thesis, Department of Chemical Engineering, Mass. Inst. of Tech., 1952.
7. Glazebrook, H. H., and Pearson, T. G.: J. Chem. Soc., 567 (1937).
8. Harris, E. J., and Egerton, A.: Chem. Rev., *21*, 287 (1937).
9. Lewis, B., and von Elbe, G.: *Combustion, Flames and Explosions of Gases*. New York, Academic Press, Inc., 1951.
10. Letort, M.: J. chim. Phys., *34*, 265, 355, 428 (1937).
11. Letort, M., and Niclause, M.: Rev. inst. franc. pétrole, *4*, 319 (1939).
12. Morris, J. C.: J. Am. Chem. Soc., *63*, 2535 (1941).
13. Morris, J. C.: J. Am. Chem. Soc., *66*, 584 (1944).
14. Pease, R. N.: Chem. Rev., *21*, 279 (1937).
15. Rice, F. O., and Polly, O. L.: J. Chem. Phys., *6*, 273 (1938).
16. Robertson, N. C: *The Partial Oxidation of the Simple Paraffinic Hydrocarbons*, in B. T. Brooks, et al.: *The Chemistry of Petroleum Hydrocarbons*, Vol. II, p. 365, New York, Reinhold Publishing Corp., 1955.
17. Satterfield, C. N., and Wilson, R. E.: Ind. & Eng. Chem., *46*, 1001 (1954). See also Satterfield, C. N., and Reid, R. C.: *J. Phys. Chem.*, in press.
18. Shtern, V., and Antonovski, V.: Doklady Akad. Nauk S.S.S.R., *78*, 303 (1951).
19. Spence, R., and Wild, W.: J. Chem. Soc., 352 (1937).
20. Steacie, E. W. R.: *Atomic and Free Radical Reactions.*, Second Edition A.C.S. Monograph No. 125. New York, Reinhold Publishing Corp., 1954.
21. Szwarc, M.: Disc. Faraday Soc., *10*, 143 (1951).
22. Taylor, H. S., and Smith, J. O.: J. Chem. Phys., *8*, 543 (1940).
23. Yagi, S.: Rev. Phys. Chem. (Japan), *19*, 106 (1945).

Query by A. R. Ubbelohde*

Do any of the yields of hydrogen peroxide indicate that the oxidation of propane might become a useful commercial source of hydrogen peroxide?

Authors' Reply

A critical problem industrially is the separation of hydrogen peroxide from oxygenated organic species which are condensed out with it, particularly aldehydes. No satisfactory low cost method has yet been developed for this. The cost of producing the impure condensate itself, per mole of peroxygen contained therein, appears to be relatively low compared to present costs for hydrogen peroxide. There may be industrial uses for such a mixture without further purification, i.e., in bleaching.

* Imperial College of Science and Technology.

50

THE OXIDATION OF OLEFINS

By C. E. H. BAWN AND G. SKIRROW

Systematic investigation[1] of the autoxidation of hydrocarbons and aldehydes in solution at low temperatures has shown that the chemistry of the reaction is relatively simple and that the course of the oxidation conforms kinetically to a general mechanism. These studies have established the free radical character of the oxidative reaction which has been shown to occur in two well-defined stages: (1) The addition of oxygen to the initially formed free radical—the O—O linkage being maintained intact—with the formation of a hydroperoxide ROOH; (2) the decomposition and reaction of the hydroperoxide with the formation of the many diverse substances—alcohols, aldehydes, ketones, acids, etc. —which usually appear as the end products of the overall oxidation. By far the larger amount of information has been obtained from the study of the liquid or solution phase oxidation of olefins, aldehydes, side chain aromatic and hydro-aromatic hydrocarbons, mainly because these substances oxidize much more readily at low temperatures. This work substantiates the view that the primary oxidation process is a chain reaction of the following general type

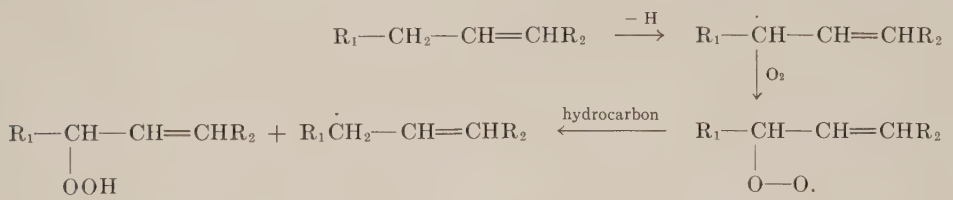

The close similarity between autoxidation of the hydrocarbons and aldehydes in liquid state and the low temperature gaseous oxidation has been frequently stressed by workers in the field[2]. A considerable body of evidence points to the conclusion that: (1) peroxides are the first molecular products of the slow combustion; (2) the point of oxygen attack is determined by the condition of minimum energy expenditure and is as a rule at the weakest C—H linkage. The present work which is part of a systematic study being made by the authors of both the low temperature gaseous combustion and the solution catalyzed oxidation of olefins in solution is in general agreement with these conclusions. This paper summarizes some of the results obtained for the gaseous oxidation of some of the simplest olefins. A full account of this work will shortly be submitted for publication in the Proceedings of the Royal Society and in this short survey no experimental details are included, attention being confined largely to the more general character and mechanism of the processes occurring.

Oxidation of Propylene, Butene-2 and Hexene-1

Little work has been carried out on the gas phase oxidation of olefins containing three or more carbon atoms, and other than the determination of the cool flame and second ignition limit, no detailed investigations have been reported except for propylene. Lenher[4] using a flow system observed that the condensable products of the oxidation of an 85/15 mixture of propylene and oxygen at 315°C contained propylene oxide, propylene glycol, acetic acid, formaldehyde, acetaldehyde, propionaldehyde, formic acid and a peroxide. Stern and Polyak[5] report that CO, CO_2 and water were formed in the cool flame region but outside this aldehydes and peroxides were found. A detailed study of the products formed during the induction period at 290°C has been reported by Mulcahy and Ridge[6]. Like Stern and Polyak they conclude that degenerate branching is brought about by aldehydes higher than formaldehyde.

PRESSURE-TIME MEASUREMENTS AND THE EFFECT OF REACTANT CONCENTRATION

A characteristic feature of the oxidation of the saturated hydrocarbons is that the pressure-time curves of the reaction show a well-defined induction period followed by a pressure rise to a maximum rate. The relative rates of oxidisability in this series have been compared by measurement

of the maximum rate of reaction attained after the end of the induction period[7], and this procedure is justifiable because there is a strict correlation between the pressure change and the analytical measurements of the consumptions of the hydrocarbon and the oxygen. This condition is also obeyed with ethylene[11] but is not generally true with olefins (q.v.).

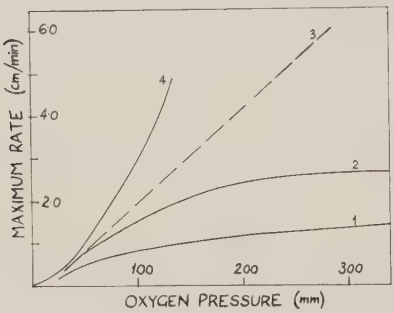

FIG. 1. Variation of maximum rate of oxidation with pressure of the reacting gases. Pressure of propylene: Curve (1) 40 mm; (2) 50 mm; (3) 60 mm and (4) 70 mm. Temp. = 340°C.

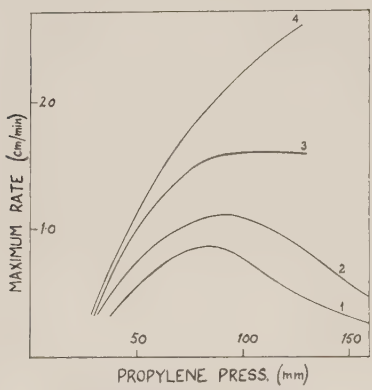

FIG. 2. Variation of maximum rate of oxidation with pressure of reacting gases. Pressure of oxygen: Curve (1) 40 mm; (2) 50 mm; (3) 60 mm; (4) 70 mm. Temp. = 340°C.

In the slow combustion of propylene the pressure-time curves combined with analytical measurements show that little chemical change occurs during the induction period and that the subsequent pressure change is a measure of the rate of consumption of the reactants. The oxygen-time and pressure-time curves were similar in form and the maximum slopes occurred at the same time. In contrast with propylene, the results obtained with hexene-1 and butene-2 establish that except when the oxygen is in great excess the maximum rate of oxygen uptake occurs at an appreciable time before the maximum rate of pressure change (see Figs. 4 and 5). In fact, with hexene-1 at 263°C and butene-2 at 290°C the measurements show that after a period of inappreciable pressure change, the pressure actually decreases to a minimum, after which it rapidly increases to its final value. This is very pronounced with butene-2 and before any appreciable pressure rise occurs almost all the oxygen has been consumed. The pressure increase must be associated with the decomposition and reaction of intermediates formed during the induction period. Only with propylene was it possible therefore to use pressure changes in deriving kinetic information and with the other two hydrocarbons it was necessary to employ the much more laborious procedures of detailed analysis of the rate of consumption or reactants.

The dependence of the maximum rate on oxygen pressure varies with the initial amount of hydrocarbon in the reaction mixture and with the temperature. Thus at high propylene pressures the rate rapidly increases with increase in oxygen pressure at ca. 340°C and in a manner which indicates that the order of the dependence on oxygen pressure is greater than unity (Fig. 1). At lower propylene pressure the rate tends to a limiting value with oxygen pressure (Fig. 1). The maximum rate is also independent of oxygen pressure at high oxygen pressures for both hexene-1 at 230–270°C and butene-2 at ca. 290°C within certain limits of olefin pressures. The effect of propylene pressure on the maximum rate at constant oxygen pressure shows that at the lower oxygen pressures the curves pass through a well-defined maximum indicating that propylene inhibits the reaction (Fig. 2). Similar results were obtained with butene-2 and hexene-1 and may be ascribed to the formation of resonance stabilized radicals of the allylic type. This type of inhibition appears to be a general feature of the oxidation of olefins containing reactive C—H bonds in the alpha position to the double bond. It is proposed to investigate olefins which do not conform to this structure in order to obtain further information on this point.

Induction period

The induction period has been variously defined by different workers and in the present investigations it was taken as the interval between the time of admittance to the reaction vessel and the commencement of the rapid pressure increase or

decrease. With propylene this was a period in which little reaction had occurred (Fig. 3). At 340°C and 398°C the reciprocal of the induction period varied linearly with oxygen pressure at constant propylene, and with the propylene pressure at constant oxygen pressure. Mulcahy and Ridge[6] have observed a similar result at 292°C and have concluded that the induction period was terminated when sufficient amounts of aldehydes were produced. Butene-2 simulates propylene in that the reciprocal of the induction period is a linear function of the oxygen pressure. In this case the length of induction period was taken as the time at which a pressure decrease commenced.

Influence of added gases

The addition of hydrogen, nitrogen and carbon monoxide at pressures from 20–200 mm to propylene-oxygen mixture was without influence on the maximum rate or the final pressure but each decreased the induction period up to about 30 per cent. The results are similar to those obtained by Hinshelwood and Cullis for pentane at 227° [8] and by Pease for propane at 270° [9]. Added water vapor up to 16 mm had only a minor influence on the above factors. With butene-2 and hexene-1 progressive additions of nitrogen up to 140 mm pressure did not modify the course of the reaction.

The role of aldehydes in hydrocarbon oxidation has been extensively studied in view of the powerful and often controlling influences they exert on chain branching. In the oxidation of propane, pentane and hexane[10] added formaldehyde exerts an inhibiting effect while in ethylene-oxygen mixtures at 400°C[11] formaldehyde decreased the induction period and if added in slight excess of the corresponding amount formed in the reaction, eliminated the induction period without affecting the maximum rate. Harding and Norrish[11] showed that in the oxidation of ethylene the rate was closely dependent upon the development of formaldehyde and concluded that it was the important degenerate branching agent for this reaction. The effects of the addition of small amounts of formaldehyde and acetaldehyde to the propylene-oxygen and butene-2 oxygen reactions are shown in Tables 1 and 2. Acetaldehyde which is an important intermediate in the oxidation in both hydrocarbons eliminated the induction period when added in concentrations of approximately the maximum amount observed analytically during the oxidation. It also increased the maximum rate and the total pressure change. Formaldehyde was not nearly so effective and reduced the induction period without eliminating it entirely. Large amounts added

Table 1. Effect of Formaldehyde on Induction Period

Temp. = 340°C; I = induction period; θ = maximum rate; ΔP_∞ = total pressure change

HCHO	C_3H_6	O_2	I	θ	Δp_∞
mm	*mm*	*mm*	*min*	*cm/min*	*cm*
0.0	51.0	70.5	15.0	1.1	1.76
2.0	49.0	70.0	6.6	1.0	1.76
4.5	51.0	69.0	4.0	1.0	1.75
8.0	51.5	71.0	3.0	1.0	1.76
20.0	50.0	70.0	—	0.6	2.4

Table 2. Effect of Acetaldehyde on Induction Period

Temp. = 340°C; I = induction period; θ = maximum rate; ΔP_∞ = total pressure change

CH_3CHO	C_3H_6	O_2	I	θ	Δp_∞
mm	*mm*	*mm*	*min*	*cm/min*	*cm*
0	51.0	70.5	15.0	1.1	1.76
1.5	49.0	71.0	3.3	1.2	1.80
3.0	48.5	70.0	0.0	1.3	1.82
4.0	51.5	71.0	—	1.6	1.85

Table 3. Effect of Acrolein on Induction Period

Temp. = 340°C; I = induction period; θ = maximum rate; ΔP_∞ = total pressure change

CH_2CHCHO	C_3H_6	O_2	I	θ	Δp_∞
mm	*mm*	*mm*	*min*	*cm/min*	*cm*
0	51.0	69.0	15.5	1.1	1.85
2.0	49.5	69.5	11.0	1.2	1.90
3.0	50.0	70.5	6.5	1.2	1.85
7.0	52.0	70.0	0	1.2	1.95

altered the general character of the oxidation. The effects of other aldehydic products were also investigated; thus acrolein (Table 3) eliminated the induction period for propylene without influencing the maximum rate and unsaturated aldehydes reduced the induction period for the oxidation of butene-2.

Detailed analyses

As already stated, the pressure-time curve, although the most useful means of following the reaction, does not always lead to significant results. In such instances much reliance has been placed on information obtained by detailed analysis of the consumption of the reactants and formation of the products. The results for each of the hydrocarbons will be summarized separately. Typical sets of analytical data for propylene oxidation are shown in Figure 3. Both oxygen and propylene decrease in a parallel manner, the

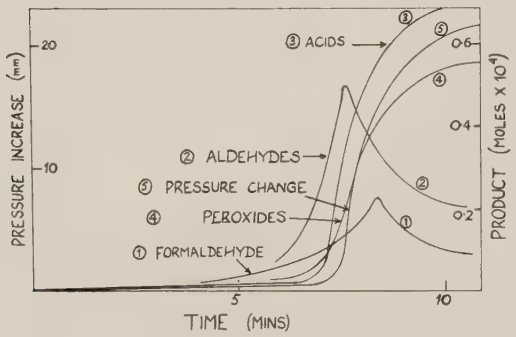

Fig. 3. Analysis of products from oxidation of propylene at 340°C. Propylene 50 mm; oxygen 140 mm.

Table 4

Temperature = 340°C.
Initial peroxide = 1.6×10^{-5} g mol
Undecomposed peroxide recovered = 0.2×10^{-5} g mol
Carbon monoxide = 0.4×10^{-5} g mol
Acetaldehyde = 1.1×10^{-5} g mol
Formaldehyde = 0.6×10^{-5} g mol
Methane or hydrogen = 0.2×10^{-5} g mol

maximum rate of consumption occurring in the vicinity of the maximum rate of pressure increase. In the above experiments in which initial concentrations of O_2 and C_3H_6 were 3.35×10^{-4} and 2.25×10^{-4} g mol the concentration at the end of the induction period had decreased to 2.87×10^{-4} and 1.90×10^{-4} g/mol respectively. Analyses during the induction period of the oxidation of propylene at 290°C have been carried out by Mulcahy and Ridge[6] who find: (1) The formaldehyde concentration becomes appreciable about half way through the induction period and rises progressively. (2) The concentrations of higher aldehydes and peroxides remain very small until the end of the induction period and increase rapidly as the reaction accelerates. (3) The length of the induction period depends on the rates of production of formaldehyde and higher aldehydes. (4) Throughout the induction period the magnitudes of the concentrations are in the order formaldehyde > higher aldehydes > peroxides. Although no detailed analyses were made during the induction period our results obtained at much higher temperatures are in agreement with those of Mulcahy and Ridge as regards the relative concentrations of the intermediates. At the end of the induction period and under the experimental conditions of Figure 3 the relative concentration of formaldehyde, total aldehyde and peroxide were 0.03×10^{-4}, 0.25×10^{-4} and 0.05×10^{-4} respectively. No curve was obtained for the rate of production of acetaldehyde but analyses at the end of the run showed that this aldehyde accounted almost entirely for the difference between total aldehyde and formaldehyde, acrolein being also present in amounts of about 10 per cent of the acetaldehyde concentration. Small amounts of methane, ethane and a primary or secondary alcohol were also present in the end products but ethylene was shown to be absent. The material balance of the reaction under conditions of Figure 3 showed that the analysis accounted for 80 per cent of the carbon and 84 per cent of hydrogen and all the oxygen in the initial reactants. In the presence of a greater excess of oxygen, 90 per cent carbon was recovered as product. The loss of carbon was probably due to polymerization (qv) and also alcohol and propylene oxide previously observed as products by Lenher were not included in the analysis.

The occurrence of a peak in the peroxide-time curves implies that the formation and decomposition reactions are proceeding simultaneously. An attempt was made to investigate the chemistry of the decomposition of the peroxides by isolating the peroxides from several identical experiments and decomposing in the reaction vessel under normal reaction conditions. The results are summarized in Table 4. These results indicate that the aldehydes formed in the oxidation of propylene are produced, at least in part, as decomposition products of the peroxide. The carbon monoxide and hydrogen (or methane) are doubtless formed by subsequent decomposition and oxidation of the aldehydes.

The analytical data illustrating the course and nature of the products of the butene-2 oxidation are shown in Figure 4. The outstanding feature

of these curves is that the minimum in the pressure-time curve corresponds almost exactly to the maximum in both the curve of peroxide production and the maximum rate of oxygen consumption. This seems to be unequivocal evidence that the pressure drop is associated with hydroperoxide formation and the stoichiometric equation for peroxide formation

$$RH + O_2 \rightarrow ROOH$$

would require a decrease in the number of molecules. The maximum in the total aldehyde curve also occurs at approximately the same time as that of the peroxide. The aldehydes consisted of formaldehyde (shown separately), acetaldehyde and acrolein. The formaldehyde was produced in relatively small amounts compared with the higher aldehydes and the ratio of acetaldehyde:acrolein varied from 2 to 3 according to the composition of the original mixture and the temperature. Although the peroxides formed have not been completely characterized, analysis showed that at least two different peroxides were formed. Investigation showed that the peroxides isolated from a run decompose under the experimental conditions to give high yields of acetaldehyde. In addition to the products shown in Figure 5 the following hydrocarbons were formed: methane, ethane, ethylene and propylene. No hydrogen was produced. A similar set of curves showing the progressive formation of products of the oxidation of hexene-1 is given in Figure 5 for the mixture initially at a pressure of 59.5 mm of both hexene and oxygen and at 265°C. In addition to the products shown small amounts of hydrogen and methane were formed.

As with butene-2 the initial decrease in pressure observed can be most satisfactorily explained in terms of the formation of hydroperoxide. Since no evidence was obtained for radical induced polymerization of the olefin the subsequent pressure increase and the ultimate acceleration of the rate must be associated with the decomposition of the peroxide and further reaction of the products so formed. The exact nature and structure of the peroxides and aldehydes formed from hexene-1 have not yet been determined.

Influence of surface

The effect of changing the nature of the surface throws further light on the reaction occurring in the early stages of the oxidation. Coating the reaction vessel by potassium chloride by rinsing with a 20 per cent solution produced a very marked retardation of the oxidation of propylene and no reaction occurred within an hour with a reaction mixture of 50 mm C_3H_6 and 70 mm O_2 at 340°C, whereas with the same mixture in the untreated vessel reaction was complete within 25–30 mins. With the mixture 50 mm C_3H_6 and

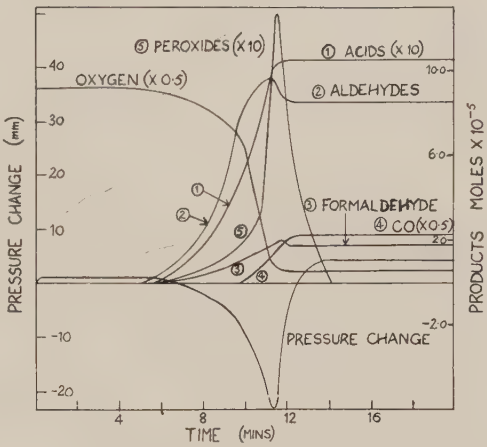

FIG. 4. Analysis of products from oxidation of butene-2 at 290°C. Butene-2 46.5 mm; oxygen 36 mm.

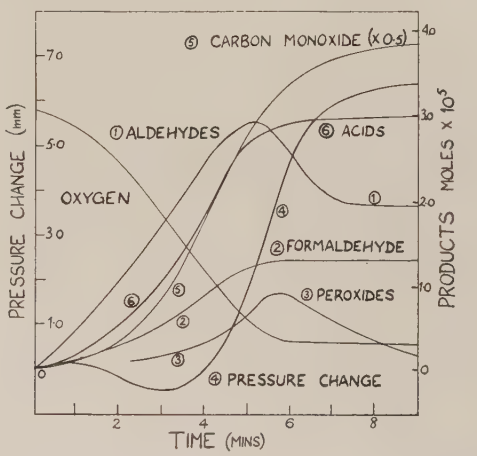

FIG. 5. Analysis of products from oxidation of hexene-1 at 263°C. Hexene-1 59.5 mm; oxygen 59.5 mm.

270 mm O_2 reaction occurred at a much decreased rate, no sharp demarcation of the induction period was observed, no peroxide and only small amounts of aldehydes were formed. Peroxide formed in an untreated vessel when admitted to the coated vessel was found to decompose at the normal rate and thus it may be concluded that the coated vessel inhibits the formation of peroxide.

Mechanism of Oxidation

The oxidation of propylene and the higher olefins in common with the oxidation of paraffinic hydrocarbons, in general shows the characteristics of a degenerately branching chain. The intermediates responsible for branching have been variously postulated as peroxides or aldehydes. The decision between these alternatives is not always clear-cut but the experimental facts establish the formation of peroxides in the early stages of the oxidation of both propylene and butene-2 and that acetaldehyde must in part, at least, be responsible for chain branching.

The initial attack of radicals (including oxygen) will be expected to occur by analogy with the mechanism of the lower temperature liquid phase oxidation, predominantly at the α position to the double bond since this is energetically favorable, viz.: Radical X (or O_2) + $R_1—CH_2—CH{=}CH_2$ → XH (or HO_2) + $R_1CH—CH{=}CH_2$ which by direct oxygen addition will lead to

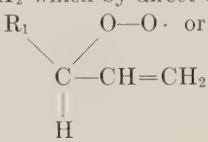

or the hydroperoxide

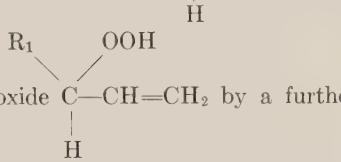

by a further hydrogen abstraction reaction. Either of these types of products (written RCH_2OO, RCH_2OOH or

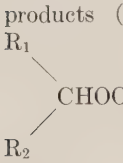

for generality) can give rise to aldehydes, alcohols, etc. by the following well-established reactions.

$$RCH_2OOH \rightarrow RCH_2O\cdot + OH \qquad (1)$$

$$2RCH_2OOH \rightarrow RCH_2O\cdot + RCH_2OO\cdot + H_2O \qquad (2)$$

$$RCH_2O\cdot \rightarrow R\cdot + CH_2O \qquad (3)$$

$$\text{(4)}$$

$$RCH_2O\cdot + RH \rightarrow RCH_2OH + R\cdot \qquad (5)$$

$$R\cdot + ROOH \rightarrow ROH + RO\cdot \qquad (6)$$

or by inter-radical reaction

$$RCH_2O\cdot + R\cdot \rightarrow RH + RCHO \qquad (7)$$

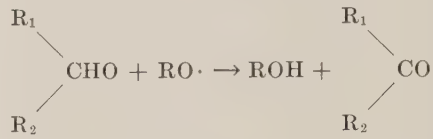

$$\text{(8)}$$

It is most probable that the aldehydes formed are products of the decomposition or reaction of RO_2 radical or the hydroperoxide, and no satisfactory mechanism can be put forward in which an aldehyde can be formed in a single reaction by a direct attack of oxygen on the hydrocarbon. Degenerate branching can be postulated as arising from the reaction of aldehyde with oxygen, viz.

$$RCHO + O_2 \rightarrow RCO + HO_2 \qquad (9)$$

or alternatively via the typical aldehyde oxidation reaction chain

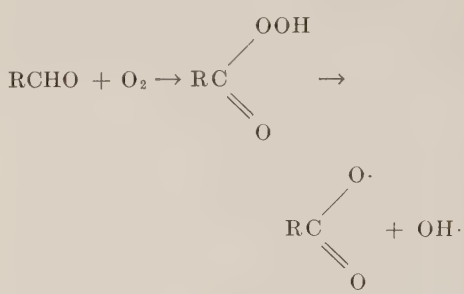

$$\text{(10)}$$

the intermediate peracids being so unstable at temperatures of 300°C or higher that they can have only a fleeting existence. For the latter reason it is fairly certain that the peroxidic products isolated from the oxidation ca 300°C are hydrocarbon hydroperoxides and not peracids formed via aldehydic intermediates.

Reactions (1–3) and (9–10) may be postulated as an alternative chain branching reactions and any decision between these reactions is not possible on experimental grounds because of the ease with which the peroxides give rise to aldehydes. It is likely that both play their part but the rapidity of the aldehyde-oxygen chain at high temperatures together with the specific action of acetaldehyde in the propylene and butene-2 reactions leads to the conception that this aldehyde exerts the predominating influence in determining branching.

With the higher olefins the additional possibility of isomerization of the initially formed

radical may occur; for example

$$R\cdot\dot{C}H{-}CH{=}CH_2 \leftrightharpoons RCH{=}CH{-}\dot{C}H_2$$

and as a consequence more than one type of peroxy radical or hydroperoxide may be formed. The detection of the formation of at least two peroxides in the oxidation of each of the three olefins studied may be ascribed to this cause, and this is supported by the variety of products formed.

Based on the above broad generalization the following detailed mechanisms are proposed for the particular oxidation reactions and these explain in a reasonably satisfactory manner the kinetic and analytical results.

The primary initiation reaction may well be mainly heterogeneous and although reaction (a) is highly probable any other initiation process giving the hydrocarbon radical would be equally satisfactory.

Propylene

$$CH_3CH{=}CH_2 + R \text{ or } O_2 \rightarrow \qquad (a)$$
$$CH_2{=}CH{-}\dot{C}H_2 + R \quad \text{or} \quad HO_2\cdot$$

$$CH_2{=}CH{-}\dot{C}H_2 + O_2 \rightarrow \qquad (b)$$
$$CH_2{=}CH{-}CH_2OO\cdot$$

$$CH_2{=}CH{-}CH_2OO\cdot + RH \rightarrow \qquad (c)$$
$$CH_2{=}CH{-}CH_2OOH + R\cdot$$

$$CH_2{=}CH{-}CH_2OOH \rightarrow$$
$$CH_2O + CH_2{=}CH\cdot + OH \qquad (d)$$
or
$$CH_2O + CH_3CHO$$

$$CH_2{-}CH{-}CH_2OOH \rightarrow \qquad (e)$$
$$CH_2{=}CH{-}CHO + OH\cdot$$

This mechanism alone, although it accounts for the aldehydic products predicts a ratio of formaldehyde:acetaldehyde of unity which is not in agreement with experiment. Furthermore, acetaldehyde is the more readily oxidized and thus the observed ratio of less than unity cannot be explained as arising from loss of formaldehyde by oxidation. The allyl radical formed in (a) may be so stable that peroxidation to $CH_2{=}CH{-}CH_2OO\cdot$ would be a relatively slow process. This non-reactivity is in keeping with the inhibiting effect of excess propylene and once reaction has started propylene can function as a chain breaking agent. It is this inhibition by the formation of stabilized olefinic radicals which accounts for the ready oxidizability of the paraffins compared with that of the corresponding olefins. It appears, therefore, that besides α methylenic initiation a second chain mechanism occurs which results from direct addition of radicals or oxygen to the double bond. The latter type of reaction has been suggested by Paquot[12] to account for the different classes of decomposition products actually found. The most probable addition reaction is that of the initially formed $HO_2\cdot$ radical, viz.

$$HO_2 + CH_3CH{=}CH_2 \rightarrow CH_3\cdot\underset{\displaystyle OOH}{\underset{|}{C}}H{-}CH_2\cdot$$

when the following chain will be set up

$$CH_3{-}\underset{\displaystyle OOH}{\underset{|}{C}}H{-}CH_2\cdot + CH_3CH{=}CH_2 \rightarrow$$

$$CH_3\underset{\displaystyle OOH}{\underset{|}{C}}H{-}CH_3 + \cdot CH_2{-}CH{=}CH_2$$

$$CH_3{-}\underset{\displaystyle OOH}{\underset{|}{C}}H{-}CH_3 \rightarrow CH_3CHO + OH + CH_3\cdot$$

This accounts for the higher acetaldehyde yield. The deficiency of carbon in the analytical balance at high propylene pressure is also explained by the inactivity of the allyl radical and its slow disappearance by dimerization rather than oxidative reaction. The secondary reactions, in addition to the main scheme above, which give rise to acids, carbon monoxide and dioxide, etc., may be explained in terms of the accepted mechanism of the oxidation of aldehydes.

Butene-2

It is known from the solution studies of Bolland[1] that increase in the double bond substitution increases the efficiency of the reaction $RO_2\cdot + RH \rightarrow ROOH + R\cdot$ and in general leads to an increase in methylenic activity. The greater ease of oxidation of butene-2 compared to propylene may be ascribed to this cause and also to the effect of the methyl group in increasing the reactivity of the double bond. The following scheme, analogous to that of propylene, accounts for the observed behavior of butene-2:

$$CH_3CH{=}CH{-}CH_3 + O_2 \rightarrow CH_3CH{=}CHCH_2\cdot + HO_2$$

$$CH_3CH{=}CHCH_2\cdot \rightarrow CH_3{-}\dot{C}H{-}CH{=}CH_2$$

$$CH_3CH{=}CH{-}CH_2\cdot$$

$$\text{or } CH_3\dot{C}H{-}CH{=}CH_2 \xrightarrow{O_2}$$

$$CH_3CH{=}CHCH_2OO\cdot \text{ or } CH_3CH(OO\cdot)CH{=}CH_2$$

$$CH_3CH{=}CH{-}CH_2OO\cdot$$

$$\text{or } CH_3{-}CH(OO\cdot){-}CH{=}CH_2 \xrightarrow{RH}$$

$$CH_3CH{=}CH{-}CH_2OOH \text{ or } CH_3CH(OO\cdot){-}CH{=}CH_2$$

$$CH_3{-}CH{=}CH{-}CH_2OOH \rightarrow$$

$$CH_3{-}CH{=}CH\cdot(\cdot CH_2{-}CH{=}CH_2) + HCHO + OH\cdot$$

$$CH_3CH(OOH){-}CH{=}CH_2 \rightarrow$$

$$CH_3CHO + OH + \cdot CH{=}CH_2 \text{ or } \rightarrow$$

$$CH_3OH + CH_2{-}CH{-}CHO \rightarrow$$

$$CH_3CHO + HO{-}CH{=}CH_2 (CH_3CHO)$$

If the $RO_2\cdot$ type radical decomposes directly rather than forming the hydroperoxide similar products would result. The allyl and $\cdot CH{=}CH_2$ radicals may either form propylene and ethylene or be further oxidized to aldehydes.

Although this scheme accounts for the major products the allylic type radicals, as with propylene, may not be sufficiently reactive to maintain a high rate of oxidation and hence reactions involving direct addition to the double bond may play an active part in the overall reaction. For example, the addition of HO_2 produced in the initiation reaction, viz.

$$CH_3{-}CH{=}CH{-}CH_3 + HO_2 \rightarrow CH_3{-}CH(OOH){-}\dot{C}H{-}CH_3\cdot$$

$$CH_3{-}CH(OOH){-}\dot{C}H{-}CH_3\cdot \rightarrow$$

$$CH_3CHO + HO\dot{C}H{-}CH_3 \text{ (or } C_2H_4 + OH)$$

$$CH_3CH(OOH){-}\dot{C}H{-}CH_3 + RH \rightarrow$$

$$CH_3CH(OOH){-}CH_2{-}CH_3 \rightarrow CH_3CHO + C_2H_5OH$$

$$CH_3CH(OOH){-}CH_2{-}CH_3 \rightarrow CH_3OH + CH_3CH_2CHO \text{ or } CH_3COCH_3$$

It is difficult to see how acrolein may be produced unless the double bond in the olefin is maintained intact and this provides support for direct reaction of the radicals produced by α methylenic reaction.

Acknowledgment

We wish to record our indebtedness to Messrs. J. D. Mullen and A. Blundell who carried out most of the experimental work.

REFERENCES

1. Bolland, J. L.: Quart. Rev., *3*, 1 (1949).
2. Mulcahy, M. F. R.: Faraday Soc. Discussions, No. 10, 259 (1951); Walsh, A. D.: Trans. Faraday Soc., *42*, 269 (1946); Bailey, H. C., and Norrish, R. G. W.: Proc. Roy. Soc., *A212*, 311 (1952); Harris, E. J., and Egerton, A. G.: Proc. Roy. Soc., *A168*, 1 (1938).
3. Farmer, E. H.: Trans. Faraday Soc., *42*, 228 (1946); ref. 1.
4. Lenher, S. J.: Am. Chem. Soc., *53*, 3737 (1931).
5. Stern, V. Ya., and Polyak, S. S.: Compt. rend. (U.R.S.S.), *65*, 311 (1949); *66*, 235 (1949).
6. Mulcahy, M. R. R., and Ridge, M. J.: Trans. Faraday Soc., *49:* 206, 1297 (1953).
7. Cullis, C. F., and Hinshelwood, C. N.: Disc. Faraday Soc., No. 2, 117 (1947).
8. Cullis, C. F., and Hinshelwood, C. N.: Ibid., p. 124.

9. Pease, R. N.: J. Am. Chem. Soc., *60:* 2244 (1938).
10. Chamberlain, G. H. N., and Walsh, A. D.: *Third Symposium on Combustion, Flame and Explosion Phenomena*, p. 368. The Williams & Wilkins Co., Baltimore (1949); also ref. 7.
11. Harding, A. J., and Norrish, R. G. W.: Proc. Roy. Soc., *A212*, 291 (1952).
12. Paquot, C.: Bull. Soc. chim., *12*, 120 (1945).

51

COOL FLAMES IN BUTANE OXIDATION

By J. BARDWELL

Introduction

A common feature of the combustion of many gaseous fuels is the occurrence of cool flames. Such flames are recognizable by their pale luminescence, their low velocity, and their tendency to recur in the same reaction mixture. Studies of cool flames have included investigations of their range of occurrence[1], spectroscopic and photoelectric study of the luminescence[2, 3] and analysis for chemical products and intermediates[4, 5]. Considerable speculation has arisen about the chemical processes responsible for cool flames but no general agreement has yet been reached[6, 7].

In the gas-phase oxidation of *n*-butane, cool flames appear at convenient pressures, and permit systematic investigation of their kinetics. In this paper the relationship of the cool flame to other types of combustion will be considered and the phenomenon of multiple cool flames discussed.

Experimental

APPARATUS

The apparatus consisted of a silica vessel connected to a manometer and to an appropriate vacuum system. The reaction vessel was cylindrical in shape, 6 cm in diameter and 9 cm long, and was supported vertically in a furnace in a region where the temperature was uniform to within $\pm 1°C$. The reactant gases were admitted separately to the vessel and the combustion followed by pressure measurements, by visual observation through a window, and by chemical analysis. The *n*-butane used was supplied by the Matheson Co. and was 99 per cent pure.

ANALYSIS FOR PEROXIDES

The combustion was interrupted at appropriate stages by the rapid withdrawal of the gases into an evacuated pipette. Peroxides were determined iodimetrically by a method similar to that suggested by Wagner, Smith and Peters[8]. The sample was shaken with a mixture of isopropanol (25 cc) and glacial acetic acid (1 cc) and transferred to a 250 cc Erlenmeyer flask. A saturated solution of sodium iodide in isopropanol (5 cc) was then added and the solution refluxed gently for five minutes. The solution was cooled, 5 cc of water was added and the liberated iodine was titrated with $0.01N$ sodium thiosulfate. The result was expressed as the partial pressure of peroxides in the combustion gases at the moment of sampling.

ANALYSIS FOR ALDEHYDES

For this analysis the sample of combustion gases was shaken with water. A small aliquot was used for analysis of formaldehyde by the chromotropic acid method of Bricker and Johnson[9]. The remainder was analyzed for total aldehyde by a bisulfite method similar to that of Goldman and Yagoda[10]. Analysis of mixtures of formaldehyde and higher aldehydes by this method was successful only when the final pH was adjusted to about 9.7, prior to titration with iodine. When the pH was lower than this figure the rate of dissociation of the bisulfite-formaldehyde complex was too small; when the pH was higher, interference was encountered because of formation of iodoform. The optimum pH was obtained by addition of a carbonate-bicarbonate buffer.

Results

IGNITION DIAGRAMS

Experiments with butane-oxygen mixtures at different temperatures and pressures revealed at least six different types of combustion.

(1) Slow combustion: In this type, no luminescence was observed, nor was there any sudden increase of pressure.

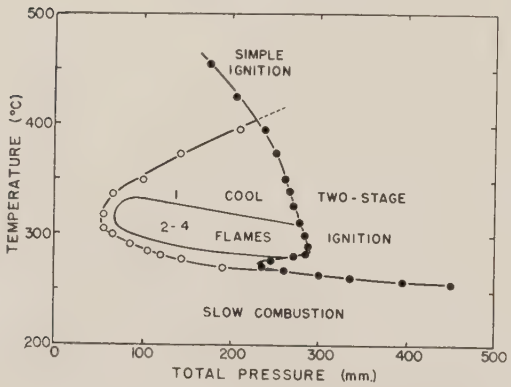

FIG. 1. Conditions of temperature and pressure for combustion in butane-oxygen mixtures containing 50 per cent butane. The numbers shown indicate the number of cool flames observed.

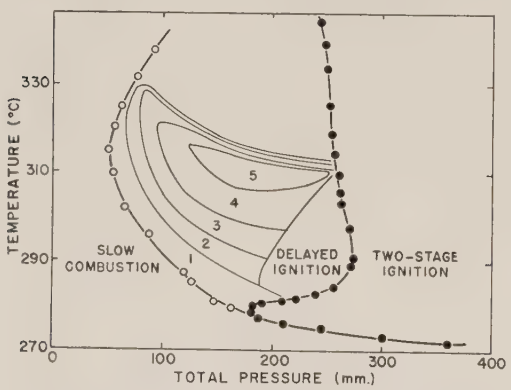

FIG. 2. Conditions of temperature and pressure for combustion in butane-oxygen mixtures containing 33 per cent butane. The numbers shown indicate the number of cool flames observed.

(2) Single cool flame: After an appreciable induction period, a flicker of bluish light was observed in the reaction vessel. At the same time a moderate pressure-pulse occurred. This was usually followed by a period of slow combustion.

(3) Multiple cool flames: Pale flames up to five in number passed in succession through the reaction mixture. The time intervals between flames ranged from about one second up to one hundred seconds, depending on the temperature and pressure.

(4) Simple ignition: A single bright flame passed through the mixture and was accompanied by a large pressure increase.

(5) Two-stage ignition: The hot flame was similar in appearance to that found with simple ignition, but was preceded by a cool flame. The interval between flames was usually about one second.

(6) Ignition at second cool flame (delayed ignition): Ignition was delayed until the passage of the second cool flame, usually a minute or more after the first cool flame. The inflammation was usually accompanied by an audible click.

The conditions of temperature and pressure that gave rise to each type of combustion when an equimolecular mixture of butane and oxygen was used are shown in Figure 1. The corresponding ignition diagram for mixtures containing 33 per cent butane is shown in Figure 2. The main features of these diagrams are similar to those found with other hydrocarbon fuels[1, 7], e.g., there is a low-temperature ignition peninsula at about 275°C and a large cool-flame region between 275°C and 400°C. The principal difference between the diagrams for 50 per cent butane and 33 per cent butane is the occurrence in the latter of a second peninsula for delayed ignition.

The effect of mixture composition on the ignition limits and cool-flame limits at 287°C is shown in Figure 3. Of particular interest here is the manner in which the different types of ignition intervene as the partial pressure of each reactant is changed.

FACTORS INFLUENCING THE COOL-FLAME FREQUENCY

When multiple cool flames occurred there was an appreciable time-lag between successive flames. The symbol θ_2 will be used for the time-lag between the first and second cool flames and its reciprocal will be called the cool-flame frequency. The induction period, i.e., the time-lag between the admission of the reactants to the vessel and the occurrence of the first cool flame, will be called θ_1. Its reciprocal is a measure of the rate of the chemical reactions in the early stages of oxidation.

The effect of temperature on the cool-flame frequency and on the reciprocal induction period in the range where multiple cool flames are found is shown in Figure 4. The dependence of fre-

quency on temperature is large and approximately exponential in form; for each ten-degree rise of temperature the frequency increases by a factor of about 3.2. The plot shown in Figure 4 yields an activation energy of approximately 73,000 calories. It is interesting to note that the reciprocal induction period shows a similar dependence on temperature in this region.

The cool-flame frequency also varies with reactant pressure. The variation with the initial partial pressure of each reactant, the other being held constant is shown in Figure 5. The reciprocal induction period is also shown and its increase with each partial pressure resembles that of the cool-flame frequency.

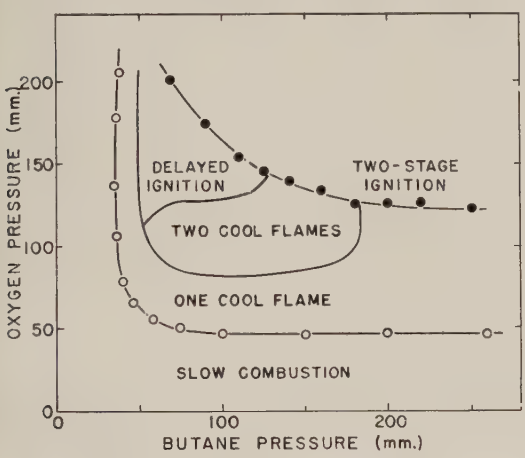

FIG. 3. Effect of mixture composition on inflammation limits at 287°C.

THE FORMATION OF PEROXIDES

The combustion gases were analyzed for peroxides during a typical oxidation giving rise to two cool flames. The vessel temperature was 284°C and the reaction mixture was: butane, 120 mm; oxygen, 120 mm. Under these conditions the induction period was about 90 seconds and the interval between flames 50 sec. The results, including the pressure-time record, are shown in Figure 6. The most striking feature of the variation of peroxide concentration with time is the sharp drop accompanying the *second* cool flame.

THE FORMATION OF ALDEHYDES

The corresponding variation of aldehyde concentration with time is shown in Figure 7. It is evident that formaldehyde is the principal aldehyde formed, making up approximately 80 per cent of the total aldehyde. It is also clear that the

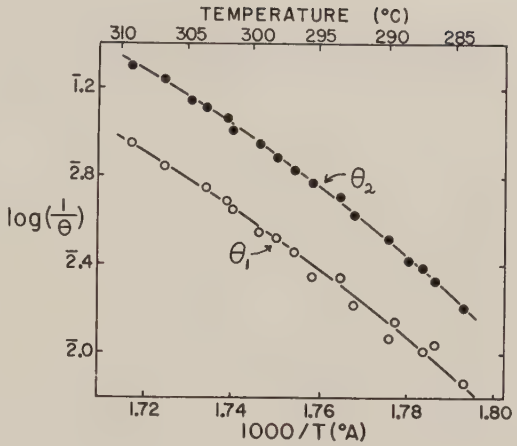

FIG. 4. Effect of temperature on the reciprocal induction period and cool-flame frequency. Butane: 100 mm, oxygen: 100 mm.

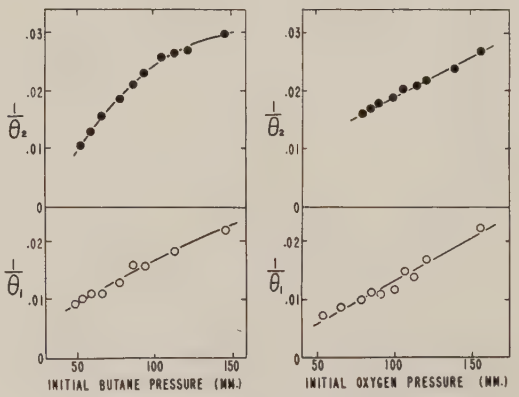

FIG. 5. Effect of reactant pressure on the reciprocal induction period and cool-flame frequency at 287°C. (a) Diagram at left: oxygen pressure, 110 mm. (b) Diagram at right: butane pressure 80 mm.

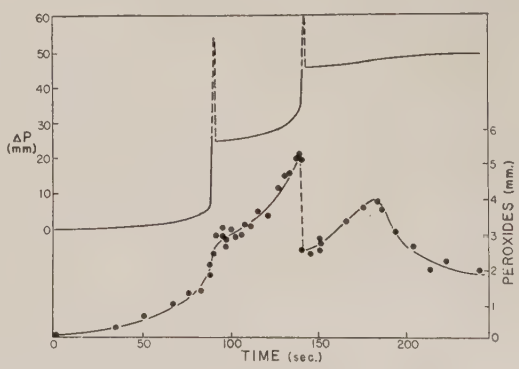

FIG. 6. Pressure-time record and variation of peroxide concentration during cool-flame oxidation of butane at 284°C. Butane pressure: 120 mm; oxygen pressure: 120 mm.

most favorable period for aldehyde formation is immediately prior to and during the first cool flame. At no stage in cool-flame oxidation does aldehyde concentration undergo a *decrease* comparable to that of peroxides at the second cool flame.

A few measurements were made to assess the effect of a two-stage ignition on the concentration of peroxides and aldehydes. The temperature was 284°C and the pressure of butane and oxygen 140 mm each. Under these conditions the first cool flame gave rise, after an interval of 1.3 sec to a hot flame. The hot flame reduced the peroxide partial pressure from 2.7 mm to less than 0.2 mm. The total aldehyde pressure fell from 14 mm to 8 mm.

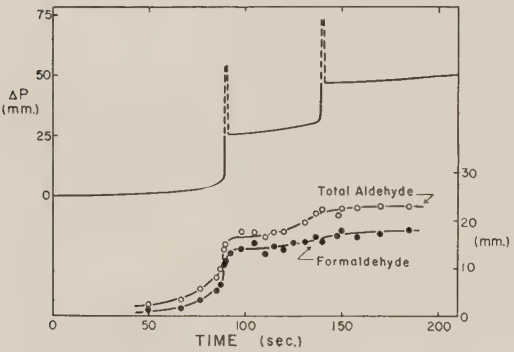

FIG. 7. Pressure-time record and variation of concentrations of formaldehyde and total aldehyde during cool-flame oxidation of butane at 284°C. Butane pressure: 120 mm.; oxygen pressure; 120 mm.

EFFECT OF ADDED ALDEHYDES

When a small amount of acetaldehyde was added along with the butane and oxygen the induction period was considerably reduced. The subsequent course of the reaction was, however, unaffected by the initial addition of acetaldehyde. When formaldehyde was used as an additive, the effect was more complex. The induction period was lengthened but the subsequent reaction was made more vigorous. For example, at 284°C, when 10 mm of formaldehyde was added, the pressure limit for a two-stage ignition was lowered from 280 mm to 240 mm.

EFFECT OF INERT GAS

The influence of inert gas at 284°C was tested by adding various amounts of argon, nitrogen and water vapor along with a reaction mixture composed of 120 mm each of butane and oxygen. Without inert gas, two cool flames were observed, but when sufficient inert gas was added the second cool flame was eliminated. The partial pressures of argon, nitrogen and water vapor required to just suppress the second cool flame were approximately 250, 150, and 90 mm respectively. The induction period, however, was unaffected by the presence of inert gas.

A similar inhibitory effect was observed when nitrogen was added to mixtures that gave rise to delayed ignitions, i.e., oxidation where the *second* cool flame ignited the fuel-oxygen mixture. At 284°C with a butane pressure of 100 mm such delayed ignitions occurred when the oxygen pressure was in the range, 130 to 150 mm. In the presence of 180 mm of nitrogen, however, the ignition was suppressed, two cool flames only being observed.

Nitrogen was found to have a small effect on the limiting pressure of reactants for the occurrence of a single cool flame and for the onset of two-stage ignitions. In the presence of 180 mm of nitrogen each of these limits at 284°C was increased by about 10 mm.

Discussion

IGNITION LIMITS

The relation of the cool flame to other types of combustion may conveniently be considered with reference to Figures 1, 2 and 3 which show the range of occurrence of each type of oxidation. The ignition diagram for mixtures containing 50 per cent butane (Fig. 1) shows many points of resemblance to those for propane[11] and butanone[12] but the pressure limits are lower, as might be expected from the greater ease of oxidation of butane[13]. The pressure-limit for ignition varies comparatively little between 300°C and 400°C but rises sharply as the temperature falls below 270°C. As with propane[14] there is a well defined peninsula in the ignition curve at about 275°C.

Although this paper is concerned primarily with the characteristics of oxidation in the cool-flame zone, attention should be called to the peculiarities of ignition in the low-temperature range, i.e., below about 400°C. Unlike the simple inflammation that occurs at higher temperatures, ignition here is a two-stage process, the hot flame occurring a second or two after a cool flame.

A still more complicated type of ignition occurs when the proportion of fuel in the mixture is reduced. Figures 2 and 3 show that in certain regions of temperature and pressure where multi-

ple cool flames might be anticipated, there occurs a delayed ignition. Here the first cool flame is normal, in the sense that immediately after it the reaction rate falls to a very low value. There follows a period of autocatalytic reaction (characteristic of multiple cool flames) at the end of which a true ignition occurs. Experimentally such delayed ignitions are easily distinguished from two-stage ignitions by the much longer quiescent period after the first cool flame, this interval amounting to as much as 100 sec in some instances. Figures 2 and 3 show that the conditions required for such ignitions are a temperature between 280°C and 310°C, less than 50 per cent butane in the mixture, and a total reactant pressure somewhat below the limit for two-stage ignition.

The exact reactions responsible for such delayed ignitions are not yet clear, nor is it obvious why the second cool flame should succeed in igniting the mixture when the first flame has failed to do so. A clue to this anomaly may, however, be contained in the analytical results for peroxides and aldehydes during multiple cool-flame oxidation. Figures 6 and 7 show that substantial quantities of both peroxides and aldehydes are present immediately prior to the second cool flame and it is possible that these substances are induced to participate in some highly exothermic reaction by the flame. The favorable effect of excess oxygen and the unfavorable influence of inert gas support the view that the chemical processes in delayed ignitions are rather different from those responsible for two-stage ignitions.

COOL-FLAME LIMITS

To the left of the curves for ignition in Figures 1 and 2 is the boundary between the areas of cool flames and slow combustion. On the low-temperature side this curve appears as an extension of the ignition boundary; on the high-temperature side, however, it intersects the ignition boundary at almost a right angle.

Malherbe and Walsh[15] have examined the form of the cool-flame boundary with several fuels and have concluded that it is of a composite nature, occasionally showing two lobes instead of a single lobe as in Figures 1 and 2. Careful study during the present investigation of the pressure-temperature limits for mixtures containing 33 per cent and 50 per cent butane failed to uncover any such inflections in the cool-flame boundary.

For equimolecular mixtures of butane and oxygen the areas of single and multiple cool flames are also distinguished in Figure 1, the maximum number of flames being four. Figure 2 shows in greater detail the behavior in the low-temperature region with a mixture containing 33 per cent butane. Here the maximum number of flames is five, this number being attained at temperatures in the vicinity of 310°C. The number of flames, and their frequency diminish with decrease of either temperature or reactant pressure. As the temperature is increased the frequency increases to such an extent that the individual flames can no longer be distinguished, the multiple flames being replaced by a single glow lasting for several seconds.

PERIODICITY OF COOL FLAMES

The periodic nature of the cool-flame reaction has aroused the curiosity of many investigators. Salnikov[16] related the waxing and waning of reaction rate to the accumulation and decomposition of a combustion intermediate. If the combustion is represented by:

$$A \rightarrow X \rightarrow B$$

chemical periodicity may result if both of the following conditions are satisfied:

(1) The temperature coefficient of the second step is greater than that of the first.

(2) The second step is highly exothermic.

In these circumstances, the concentration of X and its rate of decomposition may rise to such values that isothermal conditions can no longer be maintained. In the ensuing self-heating however, the concentration of X may be considerably reduced if the postulated relation of temperature coefficients holds. A repetition of the cycle then becomes possible, provided, of course, that true ignition does not intervene.

By an extension of Salnikov's theory, Bardwell and Hinshelwood[12] were able to account for many of the properties of the cool flame in the oxidation of butanone. Application of similar ideas to the foregoing results for butane leads to the following conclusions:

(1) The theory accounts satisfactorily for the general form of the pressure-time curve in Figure 6. The pressure-pulse is ascribable to moderate self-heating in the cool flame. The low rate of reaction immediately after each flame is consistent with the partial destruction of a combustion intermediate.

(2) The effect of temperature on the cool-flame frequency and the parallel effect on the reciprocal induction period (Fig. 4) suggest that the chemical processes occurring between flames are similar to those preceding the first flame.

(3) The similarity of the effect of reactant pressure on the cool flame frequency, to its effect on the reciprocal induction period (Fig. 5) supports the conclusion in (2).

The chemical structure of the intermediate, X, cannot, however, be conclusively deduced from the results presented in this paper. Several investigators have postulated peroxides as the essential oxidation intermediates at low temperatures[17, 18]; others have suggested aldehydes[19]. The Salnikov theory predicts an appreciable reduction in the concentration of intermediate with the passing of the cool flame. Figure 6 shows that with peroxides such a reduction does occur with the passing of the *second* cool flame in butane oxidation. No similar reduction occurs with the first flame, however. The same conclusion has been drawn from experiments with diethyl ether[20]. From the standpoint of the Salnikov theory, the postulate of intermediate aldehydes is still less satisfactory since their concentration does not decrease significantly at any stage in the reaction (Fig. 7).

An alternative interpretation of the periodicity of cool flames has been proposed by Frank-Kamenetzki[21] and elaborated by Walsh[22]. In this theory *two* intermediates are postulated, the second being formed autocatalytically from the first, but capable of destroying it. It can be shown that such interplay of intermediates may result in a sinusoidal variation in the concentration of each. Walsh suggests that the two combustion intermediates are peroxide and formaldehyde. The analytical results in Figures 6 and 7 fail to provide any support for this interpretation.

Summary

The ranges of temperature and pressure in which slow combustion, ignition, and cool flames occur in the oxidation of *n*-butane have been determined. When multiple cool flames occur their frequency is an exponential function of temperature and varies with the pressure of each reactant.

Peroxides and aldehydes are formed, the concentration of peroxides increasing sharply prior to and during the first cool flame, but suffering a sharp reduction in the second flame. Aldehydes accumulate throughout the reaction.

Acknowledgments

The author is indebted to the National Research Council of Canada for a grant in aid of this research, and to Muriel Finlayson, Nan Shu, and B. Sokalski for assistance with the experimental work.

REFERENCES

1. Townend, D. T. A : Chem. Rev., *21*, 259 (1937).
2. Ubbelohde, A. R.: Proc. Roy. Soc., *A152*, 354, 378 (1935).
3. Ouellet, L., Leger, E., and Ouellet, C.: J. Chem. Phys., *18*, 383 (1950).
4. Leger, E., and Ouellet, C.: J. Chem. Phys., *21*, 1310 (1953).
5. Bailey, H. C., and Norrish, R. G. W.: Proc. Roy. Soc., *A212*, 311 (1952).
6. Lewis, B., and von Elbe, G.: *Combustion, Flames, and Explosions of Gases*. New York, Academic Press, 1951.
7. Jost, W.: *Explosion and Combustion Processes in Gases*. New York, McGraw-Hill Book Co., 1946.
8. Wagner, C. D., Smith, R. H., and Peters, E. D.: Ind. & Eng. Chem. (Anal. Ed.), *19*, 976 (1947).
9. Bricker, C. E., and Johnson, H. R.: Ind. & Eng. Chem. (Anal. Ed.), *17*, 400 (1945).
10. Goldman, F. H., and Yagoda, H.: Ind. & Eng. Chem. (Anal. Ed.), *15*, 377 (1943).
11. Newitt, D. M., and Thornes, L. S.: J. Chem. Soc., 1656 (1937).
12. Bardwell, J., and Hinshelwood, C.: Proc. Roy. Soc., *A205*, 375 (1951).
13. Bardwell, J.: Proc. Roy. Soc., *A207*, 470 (1951).
14. Day, R. A., and Pease, R. N.: J. Am. Chem. Soc., *62*, 2234 (1940).
15. Malherbe, F. E., and Walsh, A. D.: Trans. Faraday Soc., *46*, 835 (1950).
16. Salnikov, I. E.: C. R. Acad. Sci. (U.R.S.S), *60*, 405 (1948).
17. Walsh, A. D.: Trans. Faraday Soc., *43*, 297 (1947).
18. Egerton, A. C.: Nature, *121*, 10 (1928).
19. Norrish, R. G. W.: Disc. Faraday Soc., *10*, 269 (1951).
20. Eastwood, T. A., and Hinshelwood, C.: J. Chem. Soc., 733 (1952).
21. Frank-Kamenetzki, D. A.: C. R. Acad. Sci. (U.R.S.S.), *25*, 671 (1939).
22. Walsh, A. D.: Trans. Faraday Soc., *43*, 305 (1947).

52

FREE RADICALS IN COMBUSTION PROCESSES: THERMOCHEMISTRY OF THE ALKOXY RADICALS RO

By PETER GRAY

Introduction

The mechanism of combustion reactions has been discussed for many years[1, 2, 3]. Their behavior has been interpreted in terms of transient intermediate compounds varying in stability and complexity; prominent among them are the aldehyde and peroxide molecules, hydroxyl and hydrocarbon radicals and hydrogen atoms. Lately, increasing attention has been paid to the importance in combustion (especially in the early stages of reaction and in cold flames) of peroxides and hydroperoxides. Work on the properties of individual peroxides has in turn focused attention on the alkoxy radicals RO($R{=}C_nH_{2n+1}$) in combustion, and various suggestions have been made about the part played by RO[4, 5].

It is a commonplace that often more than one detailed reaction mechanism is concordant with the experimental data. As thermochemistry has advanced, to the well-known heats of formation of molecules have been added the heats of formation of numerous atoms and radicals. These data have already been of the greatest value both in making the choice between alternative kinetic schemes and in enabling values of enthalpy changes, activation energies, and bond dissociation energies in radical reactions to be assigned. For the role of the alkoxy radicals RO to be understood it is equally desirable for their thermochemistry to be put on a sound basis.

Accordingly this paper deals with experimental evidence for establishing values of heats of formation of the lower alkoxy radicals: methoxy; ethoxy; *n*- and *sec*-propoxy; *n*-, *iso*-, *sec*- and *tert*-butoxy.

Theoretical Basis

Because of their labile nature, free radicals often cannot be examined directly. Thus their enthalpies of formation must be derived indirectly by measurements on a reaction in which they take part. A reversible reaction is sought, of the general form:

$$\mathrm{ROX} \underset{E_2}{\overset{E_1}{\rightleftharpoons}} \mathrm{RO} + \mathrm{X}$$

Enthalpy of formation ΔH_1 ΔH_2 ΔH_3

Then since $\Delta H = E_1 - E_2$

$$\Delta H_2 = (E_1 - E_2) + \Delta H_1 - \Delta H_3 \qquad (1)$$

If the various quantities on the right-hand side of (1) can be measured ΔH_2 may be found. (Although values of activation energies at one temperature are combined with enthalpies at another, errors introduced in this manner are considerably smaller than experimental errors in the individual terms.) One especially favorable case exists. When X is itself a free radical there is considerable support for setting $E_2 = 0$ and writing:

$$\Delta H_2 = E_1 + \Delta H_1 - \Delta H_2 \qquad (2)$$

reducing the number of unknowns from four to three.

Method

In practice the steps are as follows:

(1) Choose a compound ROX.

(2) Show that the decomposition ROX→RO + X occurs and is accessible to measurement. Determine the energy of activation of this step.

(3) Measure the enthalpy of formation of ROX.

(4) Measure the enthalpy of formation of X.

Numerous compounds of general formula ROX exist—alcohols, hydroperoxides, ethers, acetals, peroxides, esters, alcoholates. Some fail to satisfy the condition in paragraph 2 because the RO–X link in them is not weak enough to be studied easily in isolation. Classes which remain as possibilities are the nitrite and nitrate esters and the peroxides. These are especially favorable systems because in each no new experiments are needed to determine the enthalpy of formation of X. For the nitrites and nitrates X is NO or NO_2 and its enthalpy of formation is known; for the peroxides, X is another RO radical and equation (2) reduces to $\Delta H_2 = \frac{1}{2}(E_1 + \Delta H_1)$. It is still necessary, of course, to prove that conditions in paragraphs (2) and (3) are satisfied.

THE NATURE OF THE DECOMPOSITION OF NITRITES RONO AND NITRATES $RONO_2$

The interpretation of the behavior of the organic nitrites in decomposition has been based[6]

on the initial step:

$$RONO \rightarrow RO + NO \qquad (3)$$

The evidence has, of necessity, been indirect; it may be summarized as the first order kinetics in decomposition of the nitrites and the approximate constancy of activation energy within the nitrite series. The organic nitrates[7] appear to share both these properties and by analogy with

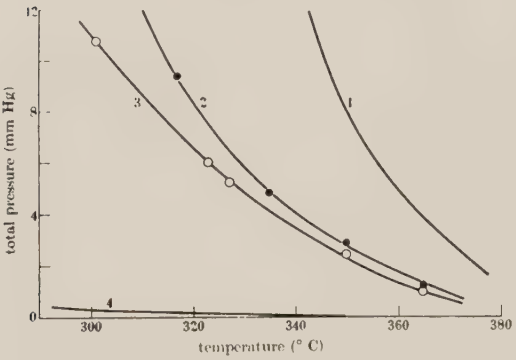

FIG. 1a. Pressure limits for chemiluminescence of stoichiometrically similar mixtures ($CH_3ONO + NO_2$ and $CH_3ONO_2 + NO$). 1, pure nitrate; 2, methyl nitrite + nitrogen dioxide; 3, methyl nitrate + nitric oxide; 4, pure nitrate.

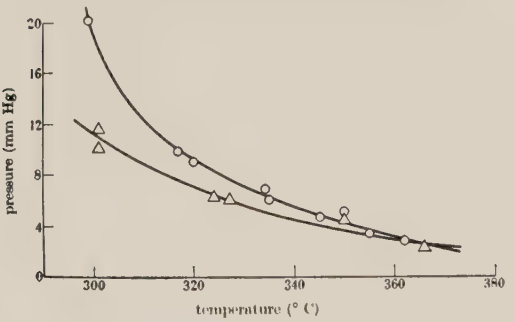

FIG. 1b. Pressure limits for explosion of stoichiometrically similar mixtures.
○, $CH_3ONO + NO_2$; △, $CH_3ONO_2 + NO$.

the nitrites the same initial step has been postulated[7, 8]:

$$RONO_2 \rightarrow RO + NO_2 \qquad (4)$$

New evidence has recently been found[9] to support these steps in equations (3) and (4). Experiments have been made on the stoichiometrically identical mixtures (methyl nitrite + nitrogen dioxide) and (methyl nitrate + nitric oxide). These mixtures do not react in the cold, but ignite at elevated temperatures[9, 10, 11] and each mixture may then display two distinct modes of inflammation, both bright explosion and a feeble luminescence. The conditions for the occurrence in the two separate mixtures of these phenomena have been determined and in Figure 1 they are mapped on the pressure-temperature diagram. The behavior of the two mixtures shows the most striking resemblance; the pressure limits of luminescence are almost superimposed, though far apart from the corresponding limits for *pure* nitrite or *pure* nitrate[9, 11], while the explosion limits actually coalesce. The simplest inference is that at these temperatures the two mixtures are in fact the same. A way in which this can be so which is in accord with all the other evidence is that they should react initially according to the equations:

$$CH_3ONO_2 + NO \rightarrow CH_3O + NO_2 + NO$$

$$CH_3ONO + NO_2 \rightarrow CH_3O + NO + NO_2$$

The comparison of the two mixtures thus provides elegant confirmation of the initial fission at the O—N bond in the thermal decomposition of the nitrates and nitrites.

Other workers[12] have presented evidence strongly supporting O—O bond fission as the initial step in di-alkyl-peroxide pyrolysis:

$$ROOR' \rightarrow RO + OR'$$

For the hydroperoxides, decomposition is often complicated[13] by heterogeneous and inter-molecular changes. The homogeneous fission:

$$ROOH \rightarrow RO + OH$$

has been isolated for *tert*-butyl hydroperoxide[12] but has not been similarly studied in isolation for the methyl, ethyl or *n*-propyl compounds.

ENTHALPIES OF FORMATION OF NITRITES, NITRATES, PEROXIDES AND RELATED COMPOUNDS

The enthalpies of formation adopted are listed in Table 1; they are in kcal and refer to the gaseous state at 25°C and 1 atm. Reference is made to all the sources used and it is believed that the data assembled for the nitrates and nitrites is complete. Other values come mainly from the International Critical Tables[14] and the circulars of the National Bureau of Standards[15]; values for hydrocarbon radicals are given by Szwarc[16]. The values for the radicals and for some of the molecules may be in error by several kcal. However they appear to be the best available at present.

BOND-DISSOCIATION ENERGIES IN NITRITES, NITRATES AND PEROXIDES

Activation energies which have been measured and identified with the enthalpy change in the initial step

$$RO—X \rightarrow RO + X$$

in some ROX compounds are listed in Table 2. These experimental values are used to derive the independent experimental values of the enthalpies of formation of the various alkoxy radicals in the gaseous state. The values are listed in Table 3.

The accuracy of the values derived for the enthalpies of formation of the alkoxy radicals is limited by the accuracy of the heats of formation and activation energies of decompostiion of the reference compounds. In the list in Table 3 the enthalpy of formation of the ethoxy radical, based on three entirely separate sets of experimental data, is the least uncertain. Methoxy and *tert*-butoxy are each derived from two sets of experiments and *n*-propoxy from one. When these values are compared with the enthalpies of formation in the gaseous state of the corresponding alcohols and hydrocarbon radicals (see Table

Table 1. Enthalpies of Formation (kcal mole^{-1}) in Gaseous State at 25°C

Atoms and Radicals	References	Value Adopted
H	15	52.1
O	15	59.2
OH	15	10
NO	15	21.6
NO_2	15	8.0
CH_3	16	31.5
C_2H_5	16	24.5
n-C_3H_7	16	22
sec-C_3H_7	16	17
n-C_4H_9	16	19
tert-C_4H_9	16	4.5
Nitrites, nitrates and peroxides		
CH_3ONO	9, 17	−16.7
C_2H_5ONO	9, 18	−25.9
CH_3ONO_2	19, 20	−29.4
$C_2H_5ONO_2$	18, 19, 21	−36.6
n-$C_3H_7ONO_2$	19	−41.6
$(C_2H_5O\text{-})_2$	22	−47.8
(*tert*-$C_4H_9O\text{-})_2$	23	−84.7
tert-C_4H_9OOH	24	−52.3
Alcohols, ethers, carbonyl compounds		
CH_3OH	25	−48.1
C_2H_5OH	25	−56.3
n-C_3H_7OH	25	−62.2
sec-C_3H_7OH	26	−65.9
n-C_4H_9OH	25	−67.8
iso-C_4H_9OH	14, 27	−69.4
sec-C_4H_9OH	27	−71.5
tert-C_4H_9OH	23	−77.0
CH_3OCH_3	14	−45.3
$CH_3OC_2H_5$	14	−53.2
$C_2H_5OC_2H_5$	14	−61.5
CH_2O	15	−27.7
CH_3CHO	15	−39.8
$(CH_3)_2CO$	14	−53.0
$CH_3COC_2H_5$	14	−59.7
C_2H_5CHO	14	−46.1

Table 2. Activation Energies (kcal/mole) in Decomposition Reactions

Compound	References	Value Adopted
Nitrites		
CH_3ONO	6	36.4
C_2H_5ONO	6	37.7
n-C_3H_7ONO	6	37.6
sec-C_3H_7ONO	6	37.0
n-C_4H_9ONO	6	37.0
Nitrates		
CH_3ONO_2	8, 9	38.4
$C_2H_5ONO_2$	7, 9, 28	36.4
n-$C_3H_7ONO_2$	7	37.6
Hydroperoxides		
tert-C_4H_9OOH	12	39
Peroxides		
$C_2H_5OOC_2H_5$	29, 30	31.6
n-($C_3H_7OOC_3H_7$)	31	36.5
tert-($C_4H_9OOC_4H_9$)	12, 32, 33	37
tert-($C_5H_{11}OOC_5H_{11}$)	12	37

Table 3. Enthalpies of Formation in Gaseous State at 25°C ΔH_f in kcal mole^{-1}

Radical	Enthalpy of Formation
HO	+10
CH_3O	−0.5
C_2H_5O	−8.5
n-C_3H_7O	−13
sec-C_3H_7O	*−18*
n-C_4H_9O	*−17*
iso-C_4H_9O	*−18*
sec-C_4H_9O	*−20*
tert-C_4H_9O	−25
tert-$C_5H_{11}O$	*−30*

1) similar variations from member to member are observed in the three series. This parallelism has been used as a guide to interpolate values for structural isomers. Such indirect figures are shown in italics in Table 3.

(1) Hydrogen–oxygen link in alcohols.

$$ROH \rightarrow RO + H$$

Molecule → Radical + Atom ··· D

R	H	CH_3	C_2H_5	*n*-C_3H_7	*sec*-C_3H_7	*n*-C_4H_9	*iso*-C_4H_9	*sec*-C_4H_9	*tert*-C_4H_9
D...	120	100	99	101	100	103	103	103	104

The hydrogen–oxygen link in the alcohols thus has a value of about 100 kcal, markedly less than its value in water.

(2) Carbon–oxygen link in alkoxy radical.

$$RO \rightarrow R + O$$

Radical → Radical + Atom ··· D_1

Analogous to this process is the fission of the carbon-oxygen link in the alcohols.

$$ROH \rightarrow R + OH$$

Molecule → Radical + Radical ··· D_2

R	H	CH_3	C_2H_5	*n*-C_3H_7	*sec*-C_3H_7	*n*-C_4H_9	*tert*-C_4H_9
D_1...	101	91	92	94	94	95	89
D_2...	120	89.5	90.5	94	93	97.5	91.5

(3) Carbon–oxygen link in ethers.

Original Molecule	R_1	R_2	ΔH
CH_3OCH_3	CH_3	CH_3	77.3
$CH_3OC_2H_5$	CH_3	C_2H_5	75.7
$CH_3OC_2H_5$	C_2H_5	CH_3	77.2
$C_2H_5OC_2H_5$	C_2H_5	C_2H_5	77.0

The heats of formation of the ethers are themselves consistent only to within about ± 2 kcal; the bond dissociation energy is thus about 77 kcal.

(4) Hydrogen-α-carbon links.

$$R_1R_2CHO \rightarrow R_1R_2CO + H$$

Radical → Molecule + Atom

Original Radical	R_1	R_2	Molecule Formed	ΔH
Methoxy...	H	H	Formaldehyde	25
Ethoxy....	CH_3	H	Acetaldehyde	21
n-Propoxy..	C_2H_5	H	Propionaldehyde	19
sec-Propoxy.....	CH_3	CH_3	Acetone	17
n-Butoxy...	*n*-C_3H_7	H	*n*-Butyraldehyde	—
iso-Butoxy.	*sec*-C_3H_7	H	*iso*-Butyraldehyde	—
sec-Butoxy.	C_2H_5	CH_3	Methyl ethyl ketone	12

(5) Carbon-α-carbon links.

$$R_1R_2R_3CO \rightarrow R_1R_2CO + R_3$$

Radical → Molecule + Radical

Original Radical	R_1	R_2	R_3	Molecule Formed	ΔH
Ethoxy	H	H	CH_3	Formaldehyde	13
n-Propoxy	H	H	C_2H_5	Formaldehyde	10
n-Butoxy	H	H	*n*-C_3H_7	Formaldehyde	11
sec-Butoxy	H	H	*iso*-C_3H_7	Formaldehyde	9
sec-Propoxy	H	CH_3	CH_3	Acetaldehyde	12
sec-Butoxy	H	CH_3	C_2H_5	Acetaldehyde	5
sec-Butoxy	H	C_2H_5	CH_3	Propionaldehyde	5
tert-Butoxy	CH_3	CH_3	CH_3	Acetone	3

$$R_1OR_2 \rightarrow R_1 + OR_2$$

Molecule → Radical + Radical

Accurate combustion data is relatively limited and estimates are made for the three lower ethers only viz. dimethyl, diethyl, and methyl ethyl ether.

(6) Disproportionation reaction.

$$R_1O + R_2R_3CHO \rightarrow R_1OH + R_2R_3CO$$

Radical + Radical → Molecule + Molecule

For pairs of identical radicals the exchange is markedly exothermic. Thus:

$$\begin{array}{lr} & \Delta H \\ 2CH_3O \rightarrow CH_3OH + CH_2O & -75 \\ 2C_2H_5O \rightarrow C_2H_5OH + CH_3CHO & -79 \\ 2\ sec\text{-}C_3H_7O \rightarrow sec\text{-}C_3H_7OH + (CH_3)_2CO & -83 \end{array}$$

Discussion

Various general properties of the alkoxy radicals and the bonds which they form may be inferred from the numerical data presented.

The hydrogen–oxygen link in the alcohols does not appear to vary significantly from one alcohol to another but lies always near to 100 kcal. The same constancy of bond energy in RO–X is of course observed in the reference compounds studied, the nitrites, nitrates and peroxides. In mercury-photosensitized decomposition of methanol it seems that the H–CH_2OH link and not the CH_3O–H link is broken, suggesting a rather lower bond dissociation energy for hydrogen attached to carbon in the alcohols.

Fission of the carbon–oxygen link in the alcohols requires 90 to 95 kcal and the same energy is needed to break the carbon–oxygen link in the alkoxy radicals. (This similarity is the reason why the erroneous[32] calculation made by Vaughan et al.[23] of the bond dissociation energy in di-*tert*-butyl peroxide gives a numerically satisfactory answer.) The same bond, carbon to oxygen, is broken in ether pyrolyses[34] and, just as separating H from OR in the alcohols requires 20 kcal less than separating H from OH in water so also separating R for OR in the ethers needs 77 instead of the 90 to 95 kcal needed to separate R from OH in the alcohols.

The alkoxy radicals may also decompose either by splitting off an α-hydrogen atom to leave an aldehyde or ketone, a process requiring an enthalpy increase of between 25 and 12 kcal, or by splitting a carbon–carbon link to form a hydrocarbon radical and an aldehyde or ketone, with an enthalpy increase of between 13 and 2.5 kcal. Both these processes are relatively favorable compared with carbon–oxygen bond fission and when alkoxy radicals decompose it is by one of these paths. When alkoxy radicals are liberated in hydrocarbon solution another reaction is important; hydrogen extraction from the solvent to form alcohol. As we have seen, for a series of alkoxy radicals in a given solvent, the enthalpy change in forming an RO—H bond at the expense of the solvent is substantially the same.

Vaughan and his collaborators[12] used the frequencies of decomposition reactions, types 4 and 5, relative to this hydrogen abstraction to compare the stabilities in cyclohexene solution of a number of alkoxy radicals. They deduced the series below, of diminishing stability from left to right:

$$CH_3O > C_2H_5O > n\text{-}C_4H_9O > sec\text{-}C_3H_7O \begin{cases} > iso\text{-}C_4H_9O \\ > tert\text{-}C_4H_9O \end{cases}$$

Apart from the position of the n-C_4H_9O radical, which they themselves suggested to be an anomalous result, the stability obviously diminishes with increasing size.

In the absence of adequate data on activation energies, the series may be compared with that obtained by placing the radicals in order of diminishing enthalpy requirements for decomposition. Since the enthalpy requirements of hydrogen abstraction are the same for all the radicals, the only magnitudes varying from radical to radical are the minimum enthalpy requirements for decomposition. These are the numbers below the radicals in the series below:

Radical	CH_3O	C_2H_5O	sec-C_3H_7O	n-C_4H_9O	n-C_3H_7O	iso-C_4H_9O	sec-C_4H_9O	$tert$-C_4H_9O
Minimum enthalpy for decomposition	25	13	12	11	10	7	5	3

The general agreement between the two series is striking. When the concentration of alkoxy radicals is high, the disproportionation reaction (6) may be expected to be important. It is a highly exothermic step with $\Delta H = -75$ to -80 kcal, and disproportionation of methoxy radicals has been suggested as the reaction giving rise to the emission of light in cool flames by acting as a source of excited formaldehyde:

$$2CH_3O = CH_2O^* + CH_3OH \quad \Delta H = -75 \text{ kcal}$$

It may however be objected that the total enthalpy change is scarcely enough to account for the light emitted and that, even if it is enough, it is also necessary that the formaldehyde has the whole of the excess energy and the alcohol none. An alternative proposal and one more favorable from an energetic standpoint is hydrogen ab-

straction from methoxy by a hydroxyl radical[35,36]:

$$CH_3O + OH = CH_2O^* + H_2O \quad \Delta H = -96 \text{ kcal}$$

This reaction involves identical structural changes to disproportionation, but is 20 kcal more exothermic.

Summary

Values have been deduced for the heats of formation of the lower alkoxy radicals RO (R = methyl to butyl) and these values have been used to derive previously unknown bond-dissociation energies in compounds containing the alkoxy groups. These include the oxygen–carbon bond in the alkoxy radicals themselves, D (R—O) = 92 kcal; the oxygen–carbon bond in the ethers, D (RO—R) = 77 kcal; and the oxygen–hydrogen bond in the alcohols, D (RO—H) = 100 kcal.

REFERENCES

1. Lewis, B., and von Elbe, G.: *Combustion, Flames and Explosions of Gases*. New York, Academic Press, 1951.
2. Jost, W.: *Explosion and Combustion Processes in Gases*, (translation). New York, McGraw-Hill Book Co., 1946.
3. Gaydon, A. G., and Wolfhard, H. G.: Flames. London, Chapman and Hall, 1953.
4. Gray, P., and Yoffe, A. D:. Proc. Roy. Soc., *A200*, 114 (1949).
5. Gray, P., and Yoffe, A. D.: J. Chem. Soc., 3180 (1950).
6. Steacie, E. W. R.: *Atomic and Free Radical Reactions*. New York, Reinhold Publishing Corp., 1946; and references quoted therein.
7. Phillips, L.: Ph.D. Thesis, London, 1946.
8. Appin, A., Chariton, J. B., and Todes, O. M.: Acta Physicochem, (U.R.S.S.), *5*, 655 (1936).
9. Gray, P.: Proc. Roy. Soc., *A221*, 462 (1954).
10. Gray, P., and Rogers, G. T.: Trans. Faraday Soc., *50*, 28 (1954).
11. Gray, P., and Yoffe, A. D.: J. Chem. Soc., 1412, (1951).
12. Bell, E. R., Raley, J. H., Rust, F. F., Seubold, F. H., and Vaughan, W. E.: Disc. Faraday Soc., *10*, 242 (1951).
13. Bateman, L.: Private communication.
14. *International Critical Tables*, *V*, 169. New York, McGraw-Hill Book Co., 1927.
15. Selected Values Chemical Thermodynamic Properties. U. S. Bureau of Standards Circular No. 500 (1950).
16. Szwarc, M.: Disc. Faraday Soc., *10*, 336 (1951).
17. Leermakers, J. A., and Ramsperger, H. C.: J. Am. Chem. Soc., *54*, 1837 (1932).
18. Thomsen, J.: Quoted by Bichowsky and Rossini: *Thermochemistry of Chemical Substances*. New York, Reinhold Publishing Corp., 1936.
19. Wheeler, W. H., Whittaker, H., and Pike, H. H. M.: J. Inst. Fuel, *20*, 137 (1947).
20. Gray, P., and Smith, P. L.: J. Chem. Soc., 2380 (1953).
21. Gray, P. and Smith, P. L.: J. Chem. Soc., 4580, (1954).
22. Zihlman, F. A.: Quoted by Leermakers and Ramsperger[17].
23. Raley, J. H., Rust, F. F., and Vaughan, W. E.: J. Am. Chem. Soc., *70*, 88 (1948).
24. Bell, E. R., Dickey, F., Raley, J. H., Rust, F. F., and Vaughan, W. E.: Ind. & Eng. Chem., *41*, 2597 (1949).
25. Rossini, F. D.: Bur. Stand. J. Res., *13*, 189 (1934).
26. Parks and Moore: J. Chem. Phys., *7*, 1066 (1939).
27. Landolt-Börnstein: Tabellen.
28. Adams, G. K., and Bawn, C. E. H.: Trans. Faraday Soc., *45*, 494 (1949).
29. Harris, E. J., and Egerton, A. C. G.: Proc. Roy. Soc. *A168*, 1 (1938).
30. Rebbert, R. E., and Laidler, K. J.: J. Chem. Phys., *20*, 574 (1952).
31. Harris, E. J., and Egerton, A. C. G.: Proc. Roy. Soc., *A173*, 126 (1939).
32. Murawski, J., Roberts, J. S., and Szwarc, M.: J. Chem. Phys., *19*, 698 (1951).
33. Brinton, R. K., and Volman, D. H.: J. Chem. Phys., *20*, 25 (1952).
34. Rice, F. O., and Herzfeld, K. F.: J. Am. Chem. Soc., *56*, 284 (1934).
35. Walsh, A. D.: Trans. Faraday Soc., *43*, 297, (1947).
36. Knox, J. H., and Norrish, R. G. W.: Proc. Roy. Soc., *A221*, 151 (1954).

Author's Replies

(*In reply to a question by Professor Matsen*) I agree that appearance potential data will be of great value in evaluating radical thermochemistry but at present the measurements available and relevant to establishing the thermochemistry of the alkoxy radicals are meager and unfortunately all require for their application good thermodynamic data for other free radicals.

(*In reply to a question by Professor Ubbelohde*) All the data presented refer to the gas phase and only experimental values of latent heats have been used. Within the accuracy of the experimental data, the heats of formation of members beyond methoxy of the homologous series of alkoxy radicals do seem to show the familiar constant increment of about 5 kcal per CH_2 group.

53

THE VAPOR PHASE OXIDATION OF 2,4,4-TRIMETHYLPENTENE-1 (α-DI-ISOBUTYLENE) AND MIXTURES OF THIS WITH *n*-HEPTANE

By F. H. GARNER, R. LONG AND G. A. WEBSTER

Introduction

The oxidation of hydrocarbons in the vapor phase may take place by both a low temperature and a high temperature mechanism. The work of Townend[1] and his school showed that the pressure-temperature ignition diagrams for most paraffin hydrocarbons comprise two main regions, the so-called "low" and "high" temperature regions. This work, together with that of Walsh, has revealed that at low pressures the low temperature region lies below 450°C for paraffins and that ignition in this region is by a two-stage process involving cool flames and the formation of peroxides.

Downs, Walsh and Wheeler[2] have produced much experimental evidence showing that, in the end gas of a spark-ignition engine, the reactions which lead to knock correspond to those involved in the "low" rather than the "high" temperature oxidation with most normal fuels.

Previous communications from this laboratory have dealt with the vapor phase oxidation of *n*-heptane and of methycyclohexane by a flow method, the liquid and gaseous products being analyzed for various functional groups[3] and in other papers[4, 5] the amounts of the individual aldehydes and acids in the products of oxidation have been reported, and some of the ketones present have been identified. It has also been shown[5] that the low temperature oxidation of *n*-heptane below (about 450°C) is itself a composite process. Three distinct maxima and minima have been found in the curves obtained by plotting peroxide concentration against temperature of oxidation. These experimental observations have been related to the results of slow-oxidation studies by other workers.

In the present investigation it was considered that it would be interesting to study the oxidation of di-isobutylene (2,4,4-trimethylpentene-1) both by itself and in admixture with *n*-heptane, and in particular to study the effect of additions of di-isobutylene upon the composite nature of the peroxide concentration vs. temperature curve for *n*-heptane and upon the concentrations of the other reaction products. The oxidation of di-isobutylene is of interest since it is said to have an unusually high blending octane number and not to give rise to cool flames on oxidation[7]. The octane number (research method API) of di-isobutylene is about 103, (compared with 28.7 for octene-1), and this itself suggests that this hydrocarbon is resistant to preflame oxidation.

Experimental

MATERIALS USED

The *n*-heptane was supplied by Westvaco Chlorine Products, Ltd., and had a refractive index n_D^{20} of 1.3877 and a boiling point (760 mm Hg) of 98.43°C.

The 2,4,4-trimethylpentene-1 was freed from peroxides present in the material by refluxing with sodium for several hours afterwards, distilling off the di-isobutylene from fresh sodium. The fraction boiling between 101°C–102°C was collected and had a refractive index n_D^{20} of 1.4090.

APPARATUS

The apparatus was of the continuous flow type and has already been described in an earlier paper[6]. The stainless steel reaction vessel used in this work had been designed to give a short residence time (ca. 0.3 sec) in order that the results obtained should bear some relationship to the preflame reactions in engines. The analytical methods employed have also been described in the above paper.

RESULTS AND DISCUSSION

The investigation of the oxidation of di-isobutylene alone, comprised 25 separate experiments over a temperature range of 276°C to 660°C. In each experiment the products of oxidation were analyzed for peroxides, carbonyl compounds, acids, and formaldehyde. The results are illustrated in Figure 1.

The three peaks in the plot of peroxide concentration vs. temperature of oxidation are distinctly clearer for *n*-heptane (which was studied for purposes of comparison) in Figure 1 than in earlier work reported[6]. The temperatures corresponding to the peroxide peaks appear to be much lower also. This is probably because considerable care

was taken to exclude mercury vapor from the system, after the inhibiting effect of this upon

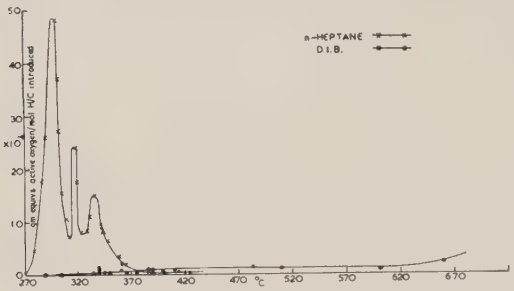

(a) Total active oxygen (peroxides)

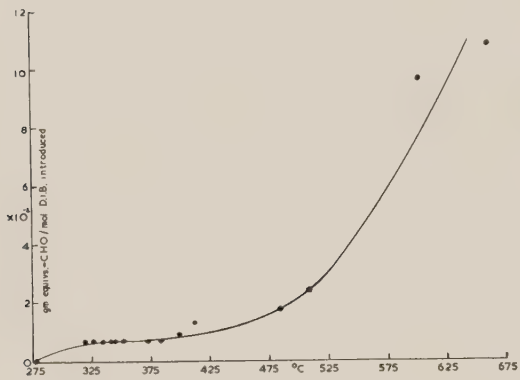

(b) D.I.B. total carbonyl compounds

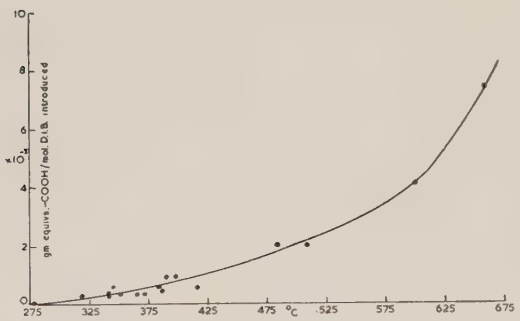

(c) D.I.B. total acids

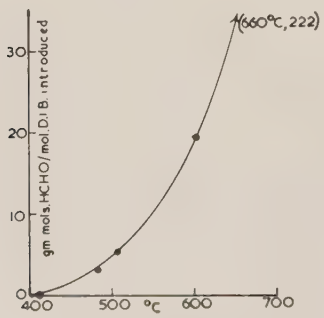

(d) D.I.B. formaldehyde

FIG. 1

hydrocarbon oxidation had been described by Small and Ubbelohde[8].

The interesting feature of these results for the oxidation of di-isobutylene is that there appears to be no low temperature region, the concentration of oxidation products remaining very small up to a temperature of about 450°C. Above this temperature there is a steep upward trend in the curves of carbonyl compound, acid and formaldehyde concentrations respectively vs. temperature. No formaldehyde could be detected below 400°C nor was an aqueous phase recognizable in the products of oxidation below about 600°C.

The conclusion that no low temperature mode of oxidation exists substantiates earlier investigations upon the preflame reactions in motored engines. By this technique, Downs, Walsh and Wheeler[2] could observe no blue glow which they usually detected when cool flames were occurring, nor did they detect any falling off in the motoring torque required (which would have given an indication of the occurrence of preflame reactions).

Experiments by Pahnke, Cohen and Sturgis[7], also involving the use of a motored engine, showed that the oxidation of di-isobutylene proceeds very slowly with increase in temperature and the results observed were said to explain the excellent blending characteristics of this hydrocarbon. These authors suggested that it is reasonable to suppose that the di-isobutylene not only inhibits its own oxidation but also the oxidation of any hydrocarbon with which it is blended.

Earlier work by Jost, Müffling and Rohrmann[9] in which the oxygen consumption was measured during the oxidation of stoichiometric mixtures of various hydrocarbons at different temperatures also indicated that the oxidation of di-isobutylene does not occur rapidly until the temperature exceeds 450°C.

In a recent paper Downs, Street and Wheeler[10] report the detection of a rudimentary cool-flame with di-isobutylene in a motored engine, employing a wide range of mixture strengths. They point out, however, that the intensity of this cool flame is only $\frac{1}{50}$th of that of iso-octane which is itself only faint. They have prepared a table of cool-flame intensities for various fuels and this shows that the cool-flame of di-isobutylene is the least intense; the hydrocarbons benzene and methane giving no cool flames. It has also been pointed out[11] that for equal concentrations in *n*-heptane, di-isobutylene is more effective in suppressing the reactivity of *n*-heptane (measured

in terms of knocking tendency in an engine) than is iso-octane.

MIXTURES OF DI-ISOBUTYLENE WITH *n*-HEPTANE

Two mixtures were studied, namely, 5 per cent di-isobutylene with 95 per cent *n*-heptane (by volume) and 25 per cent di-isobutylene with 75 per cent *n*-heptane (by volume).

The study of the first mixture comprised thirty-one separate experiments over a temperature range of 283°–565°C while that of the second mixture comprised thirty-nine experiments over approximately the same temperature range.

The results obtained are illustrated in Figure 2. This shows the concentrations of peroxides, carbonyl compounds, acids and water respectively, in the products of oxidation, compared with the corresponding figures obtained in the oxidation of *n*-heptane alone.

It can be seen that no oxidation can be detected until the temperature is about 10°C higher (in the case of the 5 per cent di-isobutylene mixture) or about 20–30°C higher, (in the case of the 25 per cent di-isobutylene mixture) than is necessary for the commencement of oxidation of *n*-heptane alone. In this respect there is an inhibition of the initiation of the *n*-heptane oxidation. Once oxidation has commenced, however, the curves are rather similar to those for *n*-heptane alone.

The curves for carbonyl compound formation and water formation are remarkably similar, supporting the view that both of these come from the same source, probably by surface dehydration of alkyl hydroperoxide[12] $RCH_2O—OH \rightarrow R \cdot CHO + H_2O$.

There appears to be evidence that the concentration of acids is higher at the temperature of 350°C (corresponding with the peak in the curve for the 5 per cent di-isobutylene mixture) than for pure *n*-heptane.

It is interesting to note the effect of admixture of di-isobutylene on the total peroxide concentration in the products. The effect is to reduce this quite noticeably although with the 5 per cent mixture the three distinct peroxide peaks are still visible, the effect on the first peak, however, being more pronounced than on the other two. In the case of the 25 per cent mixture the first two peaks disappear altogether.

These three peaks (following Malherbe and Walsh[13]) have been attributed to attack of oxygen in a chain-branching mechanism, upon the tertiary, secondary and primary C—H bonds of the alkyl hydroperoxide most readily formed by the hydrocarbon[6].

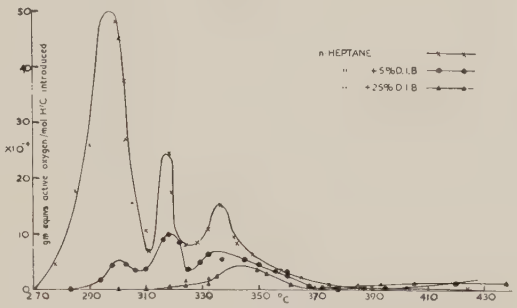

(a) Total active oxygen (peroxides)

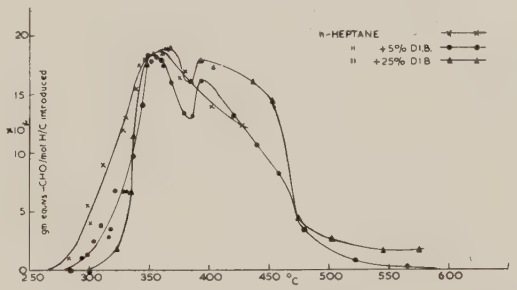

(b) Total carbonyl compounds

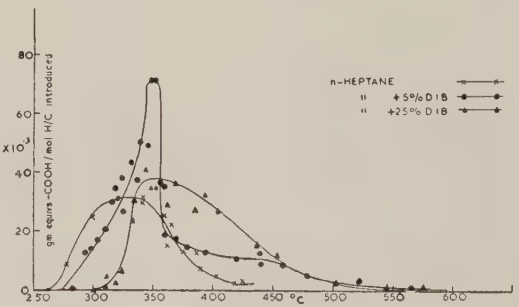

(c) Total acids

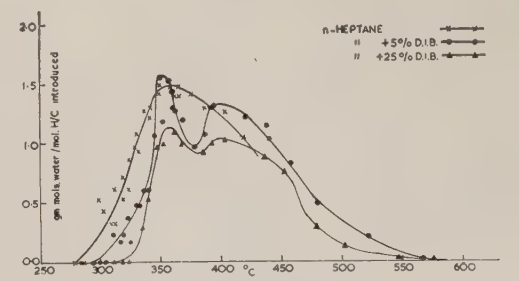

(d) Aqueous phase

FIG. 2

It can be seen that there is a considerable reduction in peroxide concentration at temperatures below 350°C. There is no reduction in the concen-

trations of the other oxidation products such as carbonyl compounds and water at higher temperatures than 350°C. It is difficult to distinguish between alkyl hydroperoxides and hydrogen peroxide in the analysis of the oxidation products and in the present work only total peroxides have been extimated. Many workers[7, 14, 19], have estimated hydrogen peroxide by a colorimetric method using titanium reagent but this reagent is unreliable in the presence of formaldehyde[15], as has been confirmed in this laboratory[16]. The development of improved methods of distinguishing between alkyl hydroperoxides and hydrogen peroxide is necessary and some preliminary work has been reported upon this problem[17].

It is impossible to decide in the present work, therefore, whether the amount of alkyl hydroperoxide is reduced or whether it is the reactions giving rise to hydrogen peroxide which are inhibited. It has been suggested that in low temperature oxidation the greater part of the total peroxide is hydrogen peroxide[18].

Kahler, Bearse and Stoner[19] have shown that the precool flame oxidation of *n*-hexane produces organic peroxides, whereas cool flame oxidation leads mainly to the formation of low molecular weight substances including hydrogen peroxide. (These workers, however, used the colorimetric method based upon the use of the titanium reagent.) Harris[20] has shown that hydrogen peroxide can exist in the vapor state at temperatures up to 500°C and that it may therefore accumulate during the slow combustion of hydrocarbons. However, it seems clear that the effect of admixture of di-isobutylene is to inhibit the initiation of *n*-heptane oxidation, particularly below temperatures of approximately 325°C. This is the reason for the high blending octane number of di-isobutylene.

It seems surprising that, while the peroxide concentration and the concentrations of the other products are reduced below 350°C, the concentrations of carbonyl compounds, water and acids above this temperature should be so little changed on admixture of di-isobutylene with *n*-heptane. A plausible reaction scheme for the vapor phase oxidation of hydrocarbons in the low temperature region (below about 320°C) is that originally put forward by Ubbelohde[21]. This involves the following processes:

Initiation.

$$RH + X \rightarrow R\cdot + XH$$

where, X is some hydrogen acceptor which may be an atom or free radical.

The *Main Reaction Chain* is then:

$$R\cdot + O_2 \rightarrow RO_2\cdot$$

$$RO_2\cdot + RH \rightarrow RO\cdot OH + R\cdot$$

It is clear from the experimental results described above that di-isobutylene inhibits the oxidation of *n*-heptane, particularly at low temperatures. This suggests that the radicals produced by removal of a hydrogen atom from di-isobutylene are incapable of continuing the chain.

Thus, we can write:

$$RO_2\cdot + R'H \rightarrow RO\cdot OH + R'\cdot$$

(di-isobutylene) (inactive)

This inhibiting effect, which is most pronounced where oxidation is just being initiated, can be compensated for by an increase in temperature. Small and Ubbelohde[22] have shown a rather similar state of affairs to occur during the oxidation of acetaldehyde where hydrocarbons exert an inhibiting effect, this being greatest in the case of an unsaturated hydrocarbon. They have suggested that this is related to the smaller activation energy required to remove hydrogen atoms from the α-position relative to a double-bond in an olefin compared with that in the case of a paraffin.

This is probably one reason for the effectiveness of di-isobutylene in inhibiting the oxidation of *n*-heptane. Further work will include a similar study of the effect of octene-1 on the oxidation of *n*-heptane for purposes of comparison.

As shown by Small and Ubbelohde in a later paper[8], it is the initial build up of reaction chains or the transition from the induction period to the onset of rapid oxidation which is important with regard to these inhibition phenomena. The effect of mercury vapor (mentioned earlier) is suggested by these workers as being due to a reaction such as

$$RO_2\cdot + Hg \rightarrow HgO + \text{decomposition products}$$

In this connection it is interesting to note that the present work shows that the effect of added di-isobutylene is greatest on the first peroxide peak, suggesting that it is in the early initiation of oxidation, by the most favorable mode of attack upon the *n*-heptane, that the inhibition is most significant.

Finally the difference between liquid and vapor phase oxidation of di-isobutylene is of considerable importance. It will be noted that we found it necessary to treat the di-isobutylene in order to eliminate peroxides, and work done on the liquid phase oxidation of di-isobutylene shows

that it is easily attacked producing epoxides[23]. This would suggest that there is a marked difference in the mechanism of oxidation in the liquid and gaseous phases.

Similar inhibition of normal heptane oxidation was caused by the presence of benzene which is accompanied by oxidation of benzene itself at a temperature at which it would not normally be oxidized[24], suggesting that in this way benzene oxidation chains can be started at lower temperatures than usual. Phenol was detected in the liquid products from this vapor phase oxidation of benzene and heptane.

It has been suggested that the promotion of benzene oxidation by cycloparaffins and paraffins might be used commercially in the high pressure oxidation of benzene to phenol[25]. The oxidation of mixtures of *n*-heptane and benzene at atmospheric pressure is being studied in this laboratory at the present time.

REFERENCES

1. Townend, D. T. A.: Chem. Rev., *21*, 259 (1937).
2. Downs, D., Walsh, A. D., and Wheeler, R. W.: Phil. Trans. Roy. Soc., *A243*, 463 (1951).
3. Garner, F. H., and Petty, D. S.: Trans. Faraday Soc., *47*, 877, 884 (1951).
4. Garner, F. H., and Raine, T. L.: Trans. Faraday Soc., *47*, 896 (1951).
5. Garner, F. H., Long, R., and Temple, R. G.: Trans. Faraday Soc., *49*, 1193 (1953).
6. Fallah, A., Long, R., and Garner, F. H.: Fuel, *31*, 4, 403 (1952).
7. Pahnke, A. P., Cohen, A. M., and Sturgis, B. M.: Paper presented before the Division of Petroleum Chemistry, Am. Chem. Soc., Chicago Meeting, September 1953.
8. Small, N. J. H., and Ubbelohde, A. R.: J. Chem. Soc., 4619 (1952).
9. Jost, W., von Müffling, L., and Rohrmann, W.: Z. Elektrochem, *42*, 488 (1936).
10. Downs, D., Street, J. C., and Wheeler, R. W.: Fuel, *32*, 279 (1953).
11. Walcutt, C., Mason, J. M., and Rifkin, E. B.: Paper presented before the Division of Petroleum Chemistry, Am. Chem. Soc., Chicago Meeting, September, 1953.
12. Harris, E. J.: Proc. Roy. Soc., *A173*, 126 (1939).
13. Malherbe, F. E., and Walsh, A. D.: Trans. Faraday Soc., *46*, 835 (1950).
14. Franck, C. E., and Blackham, A. U.: Ind. & Eng. Chem., *46*, 212 (1954).
15. Wheeler, R. W., Downs, D., and Walsh, A. D.: Nature, *162*, 893 (1948); see also reference 2.
16. Unpublished work in this laboratory.
17. Bruschweiler, H., Minkoff, G. J., and Salooja, K. C.: Nature, *172*, 909 (1953).
18. Norrish, R. G. W.: Disc. Faraday Soc., *10*, April, 1951.
19. Kahler, E. J., Bearse, A. E., and Stoner, G. G.: Ind. & Eng. Chem., *43*, 2777 (1951).
20. Harris, E. J.: Trans. Faraday Soc., *44*, 764 (1948).
21. Ubbelohde, A. R.: Proc. Roy. Soc., *A152*, 354 (1935).
22. Small, N. J. H., and Ubbelohde, A. R.: J. Chem. Soc., 723 (1950).
23. Gasson, E. J., Millidge, A. F., Primavesi, G. R., and Webster, W.: J. Chem. Soc. 2161 (1954).
24. Mardles, E. W. J.: J. Chem. Soc., 872 (1928).
25. Denton, W. I., Doherty, H. G., and Krieble, R. H.: Ind. & Eng. Chem. *42*, 777 (1950).

54

THE KINETICS OF THE OXIDATION OF SOME TERTIARY ALIPHATIC AMINES

By C. F. CULLIS and D. J. WADDINGTON

The ideal antiknock additive, besides having high activity, should burn away completely and not leave harmful deposits as the metal alkyls do. Among purely organic compounds, amines are the best antiknocks, although they are much less effective than organometallic compounds. Aliphatic amines of low molecular weight have, however, recently found considerable use as fuel additives[1]. After a gasoline has been loaded to capacity with lead tetraethyl, it is sometimes desirable to increase further the knock rating and hence the power output of an engine, especially

during short periods of increased load. This can be done by introduction of certain primary and secondary amines, and their addition can cause a considerable increase in power. Of the compounds investigated, dimethylamine has the highest antiknock activity, while trimethylamine is a proknock.

A more fundamental understanding of the oxidation of the amines should facilitate their technical application as fuel additives. Boyd[2] investigated the antiknock properties of a number of amines and found that their effect is dependent on the nature of the alkyl or aryl groups in the molecule. The most active compounds contain at least one aryl group, and secondary amines are more effective than primary or tertiary compounds. Chamberlain and Walsh[3] studied the inhibiting effect of aromatic amines and other compounds on the vapor-phase oxidation of ethers, and Walsh[4] has discussed their mode of action. A striking correlation exists between antiknock effect and the influence of the side chain on the electron properties of the aromatic ring; the activity increases with decreased binding of the π-electrons in the benzene ring. The amines fall into line with other aromatic compounds. Their effect is primarily due to the ring system, and the nitrogen group in the side chain serves to modify the properties of the ring. With the aliphatic amines, the activity must be more directly related to the presence of nitrogen since other aliphatic compounds do not show a comparable antiknock influence.

Recent studies of the combustion of the paraffins and their simple derivatives have increased understanding of the factors which control the ease of oxidation of organic compounds[5]. If a hydrocarbon has hydrogen replaced by a group X, a change in ease of oxidation occurs. The initial fate of a molecule undergoing vapor-phase oxidation is generally believed to involve abstraction of a hydrogen atom. When the group X itself contains hydrogen, attack may occur preferentially at this point, in which case the oxidation mechanism may be radically altered. If X is not susceptible to direct attack, oxidation will continue to take place on the hydrocarbon chain without fundamental change in mechanism. With primary and secondary amines, oxidation may occur either at the amino or imino group or on the hydrocarbon chain. Kinetic studies[6, 7] have shown that the oxidation of primary and secondary amines resembles that of the paraffins in many respects. Analysis of the products of the slow oxidation of methylamine[8, 9] suggests that attack occurs at the methyl group in preference to the amino group. On combustion, therefore, these amines behave as substituted hydrocarbons in which the substituent is relatively inert. Recent work on the oxidation of trimethylamine[10] has revealed differences between its behavior and that of the corresponding primary and secondary amines. This work is being continued, and in this paper the results of a preliminary study of the combustion of trimethylamine and triethylamine are presented.

Experimental

The apparatus was similar to that already described[6]. Separate cylindrical Pyrex reaction vessels, 8.5 cm in length and 6.1 cm in diameter, were used for the oxidation of each compound.

The gaseous amines and ammonia were prepared by dry distillation of their hydrochlorides with lime or by dropping strong aqueous solutions on solid potassium hydroxide. They were dried by passage through calcium oxide and the middle fractions of the condensates were distilled into storage globes. Compounds which are liquids at room temperature were carefully fractionated before use, and after introduction into the apparatus were freed from dissolved air by repeated freezing followed by evacuation. The purified amines were tested for the presence of related compounds, which were invariably found to be absent. Formaldehyde was prepared by gentle heating of paraformaldehyde.

The course of the reaction was followed by measurements of pressure change and by periodic analysis. In order to form a qualitative picture of the main reactions which occur, attention was paid to intermediate reaction products. Spot tests were found to be useful for this preliminary investigation because of their simplicity and quickness. The tests are semiquantitative and give the order of magnitude of the products formed.

For analysis, the products found at various stages of reaction together with unchanged reactants were withdrawn from the reaction vessel and extracted into aqueous solution. Each test was applied to a few drops of this solution. A strictly comparative method was adopted, each test solution being treated in the same way as a series of freshly prepared standards. In order to avoid spurious interference from other substances present in the reaction mixture, a standard addition technique was used. In general the concen-

tration of intermediates varied within the range 5–500 μg in one drop of aqueous solution. These tion mixtures examined. For comparison, column S gives the limiting sensitivity of the test, which

TABLE I

A. For Detection of Functional Groups

Functional Group	Reaction Involved	Standard Added	R	S	Remarks
Aldehydes	Reaction with azobenzene phenylhydrazine sulfonic acid in sulfuric acid gives red color, which is extracted into chloroform	Acetaldehyde	0–500	5	Ketones react much less readily. Amines do not interfere
Secondary amines	Soluble violet-blue compound on reaction with sodium nitroprusside and acetaldehyde in sodium carbonate solution	Diethylamine Dimethylamine	0–75 0–10	5 5	Primary and tertiary amines do not react. Tests showed other reaction products do not interfere
Primary amines	Reaction with sodium nitroprusside and acetone in neutral solution gives red color[12]	Ethylamine Methylamine	0–150 0	4 2	Color develops slowly. Free amine only is detected

B. For Detection of Particular Compounds

Substance	Reaction Involved	R	S	Remarks
Formaldehyde	Reaction with chromotropic acid in strong sulfuric acid gives violet-pink color	0–75	1	Other simple aldehydes do not react.
Acetaldehyde	Reaction with mercuric oxide in sodium sulfite solution gives white precipitate[13]	—	—	Used to confirm presence of acetaldehyde in triethylamine reaction mixtures
Hydrogen cyanide	Conversion to thiocyanate which is detected with ferric ion	0	5	
Ammonia	Reaction with phenol and sodium hypochlorite yields blue color[14]	0–7	1	Amines do not interfere. Nessler's reagent cannot be used in presence of amines or formaldehyde
Hydroxylamine	Reaction with salicylaldehyde and copper acetate gives a yellow precipitate	0	5	
Nitrous acid	Griess test with sulfanilic acid and α-naphthylamine	0	0.1	
Nitric acid	Red color with brucine in sulfuric acid	0	1	

concentrations may readily be related to the number of moles present in the reaction vessel.

The spot tests used are summarized in Table 1. References are given only when the test is not described by Feigl[11]. Column R shows the concentration range detected in the different reac- was found by addition of standards to typical reaction mixtures. Concentrations are expressed in μg detected in one drop of aqueous solution.

The concentrations of total free base were also measured. The reaction products, together with unchanged reactants, were extracted into a known

excess of hydrochloric acid, and the free acid was back-titrated against sodium hydroxide with bromo phenol blue as indicator. In the early stages of reaction, the base concentration provides a measure of free amines (and ammonia) in the system.

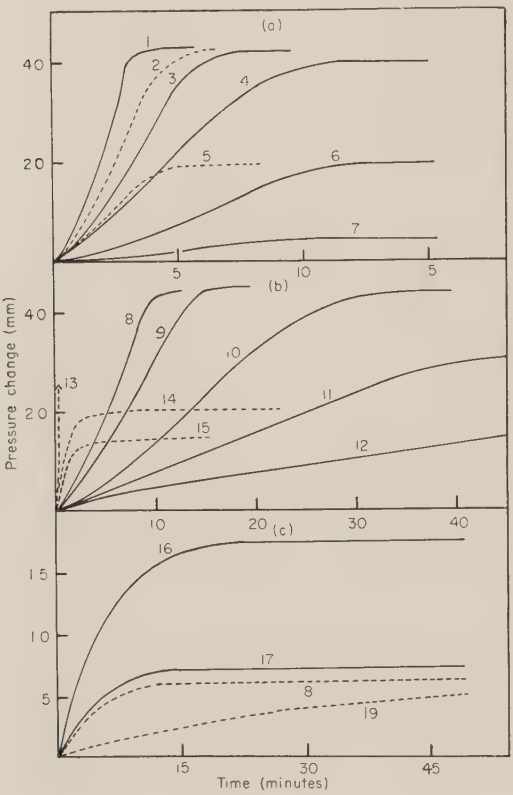

FIG. 1. The oxidation of triethylamine and tri methylamine. See table below for explanation of curves.

Graph	Curve	Amine Pressure (mm)		Oxigen Pressure (mm)
		Triethalamine	Trimethylamine	
	1	41	—	100
	2†	21	—	100
1 (a)	3	21	—	100
	4	18	—	100
264°C	5‡	10	—	100
	6	10	—	100
	7	3	—	100
	8	50	—	499
	9	50	—	250
1 (b)	10*	50	—	250
	11	50	—	79
211°C	12*	50	—	80
	13	—	50	70
	14	—	50	52
	15	—	50	34
1 (c)	16	—	100	100
	17	—	50	250
170°C	18*	—	100	100
	19*	—	50	250

* Packed vessel (5 × surface); † 140 mm nitrogen added; ‡ 200 mm nitrogen added.

Results

TRIETHYLAMINE

General kinetic characteristics

Triethylamine starts to oxidize at about 200°C, whereas thermal decomposition does not occur below 450°C[15]. The course of the reaction is shown by pressure-time curves given in Figure 1. There is no induction period, and at low temperatures (Fig. 1b) the initial rate remains almost constant until a considerable proportion of the reaction is complete. At a higher temperature (Fig. 1a) the autocatalytic character is more pronounced, but a gradual increase of rate from a low to a high value is not observed. The oxidation rate is strongly dependent on the initial reactant pressures, but the organic compound exerts a greater influence than oxygen. At 264°C, acceleration is observed on addition of nitrogen (Fig. 2a), but at 211°C such additions have no influence. Reaction is retarded by a 5-fold increase in surface (Fig. 1b).

The influence of temperature is shown in Figure 2. Above 278°C, an explosive region is encountered in which cool flames are sometimes observed. Between 360°C and 400°C, slow combustion again takes place, but at still higher temperatures, true ignition finally intervenes.

Analytical results

The products at various stages during reaction of different amine: oxygen mixtures at 211°C are shown in Figure 3. With an equimolar mixture (Fig. 3a), a constant concentration of free base is maintained until reaction is more than half complete. This implies smooth conversion of triethylamine to other basic compounds of a similar nature. Ethylamine is formed at a greater rate than diethylamine. Copious amounts of an aldehyde are produced; this is assumed to be exclusively acetaldehyde, since formaldehyde is absent and specific tests for acetaldehyde[13] give strongly positive results. No other products tested for could be detected.

With more oxygen (Figs. 3b and 3c), secondary interactions occur to an increased extent, and less of the reactants can be accounted for as simple products. Smaller amounts of primary and sec-

ondary amines are formed and this is reflected in a greater decrease in free base concentration.

Analysis of the products of complete reaction with varying amounts of oxygen (Figure 4) shows that the accompanying pressure changes increase until the amine:oxygen ratio is about 1:3. The concentrations of primary and secondary amines and of total aldehydes pass through a maximum as the oxygen concentration is increased. With excess oxygen, small amounts of ammonia and formaldehyde are formed.

At 372°C, the general picture is qualitatively unchanged. More free base is consumed, and the amounts of diethylamine, ethylamine, and acetaldehyde are much less than at 211°C. This is

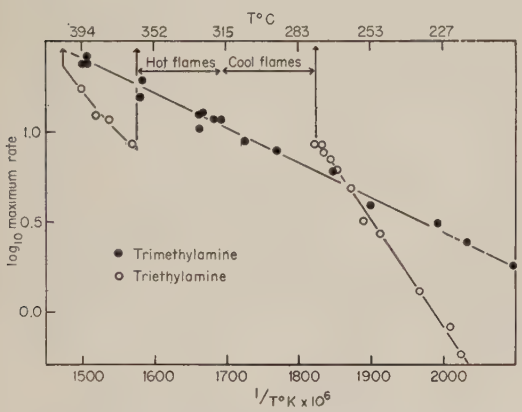

FIG. 2. The influence of temperature on the oxidation of triethylamine and trimethylamine. Amine pressure 10 mm; oxygen pressure 100 mm.

no doubt due to secondary reactions of these products at elevated temperatures.

Secondary reactions

Interaction of diethylamine and ethylamine with acetaldehyde occurs only to a very small extent at 211°C, and these products can readily be detected in presence of one another.

The combustion of acetaldehyde at this temperature is, however, found to be inhibited by triethylamine. Small amounts of the amine cause an induction period and decrease the subsequent rate of oxidation; larger amounts completely inhibit oxidation. Ethylamine has a definite, although less pronounced, inhibiting influence. This probably explains why large amounts of acetaldehyde are detectable under conditions where its oxidation is normally rapid[16, 17]. Inhibition of acetaldehyde oxidation by alcohols[18] and by hydrocarbons[19] has also been observed and is ascribed to transfer of hydrogen from the inhibitor to a peracetyl radical.

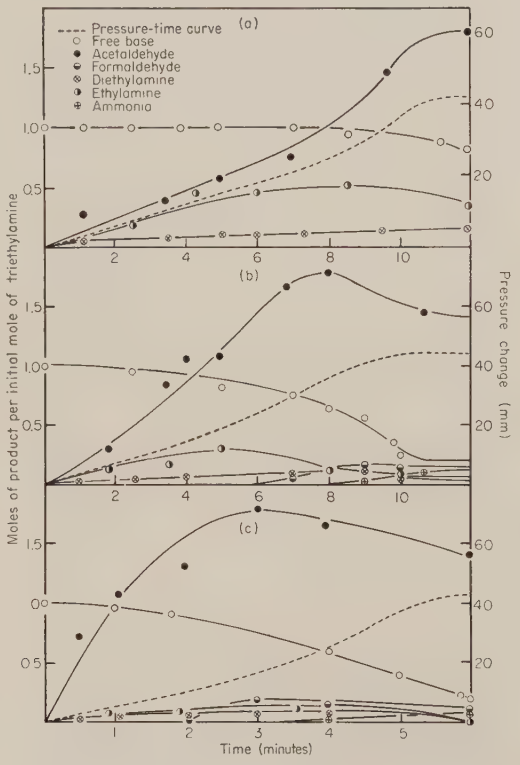

FIG. 3. The products of the oxidation of triethylamine at 211°C. (a) Amine pressure mm, oxygen pressure 100 mm. (b) Amine pressure 50 mm, oxygen pressure 250 mm. (c) Amine pressure 50 mm, oxygen pressure 500 mm.

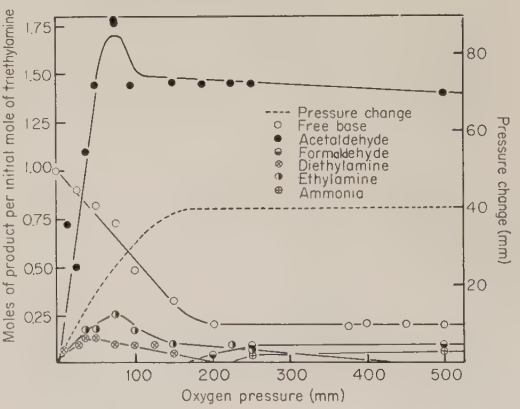

FIG. 4. The products of the complete oxidation of 50 mm triethylamine at 211°C.

TRIMETHYLAMINE

General kinetic characteristics

Trimethylamine starts to oxidize at a measurable rate above 150°C; pyrolysis does not occur

below about 400°C[20]. Some typical pressure-time curves are shown in Figure 1; these reveal little or no autocatalytic character. Reaction is accompanied by a relatively small pressure increase, and the sharp fall-off in rate as reaction proceeds is characteristic of the behavior of this compound.

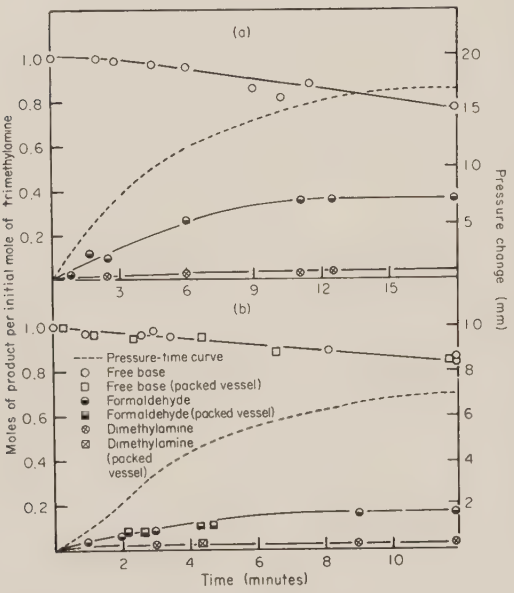

FIG. 5. The products of the oxidation of trimethylamine at 170°C. (a) Amine pressure 100 mm, oxygen pressure 100 mm. (b) Amine pressure 50 mm, oxygen pressure 250 mm.

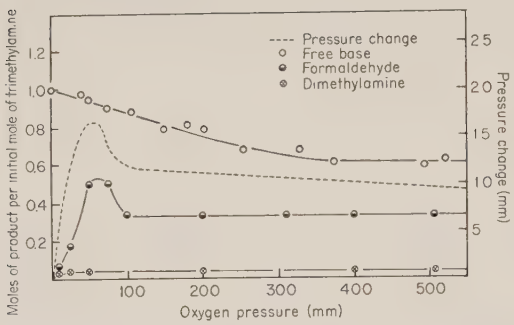

FIG. 6. The products of the complete oxidation of 100 mm trimethylamine at 170°C.

Added nitrogen has no influence, but in a packed vessel the rate of oxidation and the overall pressure change are reduced (Fig. 1c). The rate increases linearly with oxygen concentration until the reactants are in equimolar quantities; thereafter, oxygen pressure has little influence. The reaction is very sensitive to the concentration of trimethylamine. Above a critical pressure of the combustible, explosion occurs; below this pressure, very high rates can be measured without ignition intervening. The explosions are exceptionally violent, even at comparatively low pressures, and on several occasions the reaction vessel was shattered. The temperature coefficient is considerably smaller than with triethylamine (Fig. 2), and under similar concentration conditions, no explosion region is encountered up to temperatures at which thermal decomposition sets in.

Analytical results

Figure 5 shows some results obtained during the slow combustion of 1:1 and 1:5 amine:oxygen mixtures at 170°C. A striking feature is the small consumption of free base. That the residual base is mainly unchanged trimethylamine is suggested by the failure to find significant quantities of other basic compounds. Formaldehyde together with dimethylamine in much smaller amounts are the only detectable products. Analyses in a packed vessel yield similar results (Fig. 5b). Further measurements which confirm these findings are shown in Figure 6. The fact that, even with excess oxygen, not more than 40 per cent of the base is used up suggests that further oxidation may become inhibited as reaction proceeds. The amount of base consumed increases with temperature.

Secondary reactions

In the oxidation of trimethylamine, formaldehyde and basic nitrogen compounds are not found in comparable amounts. This may be partly due to the fact that condensation reactions of amines occur more readily with formaldehyde[21] than with other aliphatic aldehydes. It was shown that at 170°C, formaldehyde reacts rapidly with dimethylamine, methylamine and ammonia, although no reaction occurs with the tertiary base. Analysis of the products showed that the amount of formaldehyde detected is largely unaltered by the presence of the amines and ammonia. In contrast, the concentration of dimethylamine is considerably reduced and neither methylamine nor ammonia can be detected in presence of formaldehyde after reaction at these temperatures. The free basic content of the products is reduced in each case to between one half and one third of the original amount present.

Neither formaldehyde, dimethylamine, methylamine or ammonia inhibit the oxidation of trimethylamine; nor do the products of reaction of formaldehyde with the three bases.

Discussion

Molecules which contain only methyl groups as potential points of attack are often resistant to oxidation. Ethane, for example, is much less readily oxidized than the higher paraffins[22, 23], and acetone in its behavior on oxidation differs markedly from the higher ketones[24]. Methylamine and dimethylamine, on the other hand, show no sharp differences from their higher homologues[6, 7]. This preliminary investigation suggests that the modes of oxidation of trimethylamine and triethylamine are different. Lengthening of the carbon chain generally increases suceptibility to oxidation[25, 26]. Trimethylamine, despite its structure, begins to oxidize at lower temperatures than triethylamine. Quantitative comparisons, based only on pressure measurements, are of doubtful significance, but the differences are too marked (Fig. 2) to allow any doubt as to the order of reactivity of the two compounds.

TRIETHYLAMINE

The kinetic and analytical results obtained suggest that the mechanism of oxidation is analogous to that occurring with primary and secondary amines. The principal products are acetaldehyde, ethylamine and diethylamine, which in the early stages account for the major part of the combined carbon and nitrogen. This suggests that reaction consists essentially of oxidation of the alkyl groups, initial attack occurring at CH_2, and C—N bonds subsequently being broken.

The main overall changes appear to be:

$$(C_2H_5)_3N + \tfrac{1}{2}O_2 = (C_2H_5)_2NH + CH_3CHO \quad (1)$$

$$(C_2H_5)_3N + O_2 = C_2H_5NH_2 + 2CH_3CHO \quad (2)$$

The large quantities of acetaldehyde formed (more than one mole per initial mole of triethylamine) and the detection of larger amounts of ethylamine than diethylamine suggest that (2) occurs in preference to (1). Ethylamine does not arise from further oxidation of diethylamine, since the latter is not appreciably oxidized under the conditions used and increases in concentration throughout reaction. Since combustion of triethylamine probably involves stepwise attack of the alkyl groups, oxidation of the first group would yield initially the radical $(C_2H_5)_2N$-. The small amounts of secondary base found thus suggest that these radicals react to form ethylamine before they can stabilize themselves by hydrogen abstraction to form diethylamine.

TRIMETHYLAMINE

The combustion of trimethylamine shows little similarity in its kinetic characteristics to the oxidation of triethylamine and other amines. A surprising feature is the apparently small extent of reaction at low temperatures. Analysis is complicated by secondary reactions and low results are obtained for nitrogen compounds, although these must presumably be formed in quantities equivalent to the formaldehyde present. Detection of formaldehyde in presence of amines is quite reliable. This is probably due to hydrolysis of condensation products with regeneration of formaldehyde under the strongly acid conditions used to detect its presence; such products are generally stable in neutral or alkaline solution so that the amines are not readily detected[21]. Reaction of the amines with formaldehyde is accompanied by a sharp fall in basic strength. The high value of the final free base concentration and the small amounts of formaldehyde formed suggest that at 170°C a large proportion of the tertiary amine remains unchanged even in presence of excess oxygen.

Inhibition of further reaction may be due to the poisoning of a wall reaction or to the breaking of chains in the gas phase. The suggestion that a surface reaction may be the rate-controlling step, although consistent with the low temperature coefficient observed, is not supported by the results in a packed vessel where a marked lowering of oxidation rate occurs.

Small quantities of the probable simple reaction products do not retard combustion of trimethylamine, so that the cause remains unknown. It must be concluded that either the reactants themselves or some unidentified product are responsible for the observed inhibition.

More reliable analytical data must be obtained and a fuller kinetic investigation undertaken before further conclusions can be reached. It is, however, of interest that the difference in behavior of trimethylamine and triethylamine reported here is reflected in their effects as fuel additives, for triethylamine is, like other amines, an antiknock[2], whereas trimethylamine has a proknock influence.

Acknowledgments

The authors would like to express their gratitude to the Shell Petroleum Company for generous financial assistance which has made this work possible. It is also a pleasure to thank Mr. J. A.

W. Dalziel for his advice with the microanalytical procedures used, and for many helpful discussions.

REFERENCES

1. British Patents Specification. 592, 966.
2. Boyd, T. A.: Ind. & Eng. Chem., *16*, 893 (1924).
3. Chamberlain, G. H. N., and Walsh, A. D.: Trans. Faraday Soc., *45*, 1032 (1949).
4. Walsh, A. D.: Trans. Faraday Soc., *45*, 1043 (1949).
5. Hinshelwood, C. N.: Disc. Faraday Soc., *10*, 266 (1951).
6. Cullis, C. F., and Smith, L. S. A.: Trans. Faraday Soc., *46*, 42 (1950).
7. Cullis, C. F., and Isaac, I.: Trans. Faraday Soc., *48*, 1023 (1952).
8. Jolley, L. J.: J. Chem. Soc., 1957 (1934).
9. Cullis, C. F., and Willsher, J. P.: Proc. Roy. Soc., *A209*, 218 (1951).
10. Cullis, C. F., and Isaac, I.: Unpublished results.
11. Feigl, F.: *Spot Tests*. New York, Elsevier Publishing Co., Inc., 1947.
12. Rimini, E.: L'Orosi, *22*, 40 (1899).
13. Leys, A.: J. pharm. chim. [6], *22*, 107 (1897).
14. Cuny, L : J. pharm chim. [8], *3*, 150 (1926).
15. Taylor H. A., and Juterbock, E. E.: J. Phys Chem., *39*, 1103 (1935).
16. Pease,. R. N.: J. Am. Chem. Soc., *55*, 2753 (1933).
17. McDowell, C. A., and Thomas, J. H.: J. Chem. Soc., 2208, 2217 (1949).
18. Farmer, J. B., and McDowell, C. A.: Trans. Faraday Soc., *48*, 624 (1952).
19. Small, M. J. H., and Ubbelohde, A. R.: J. Chem. Soc., 723 (1950); 637 (1953).
20. Carter, A. G., Bosanquet, P. A., Silcocks, C. G., Travers, M. W., and Wilshire, A. F.: J. Chem. Soc., 495 (1939).
21. Walker, J. F.: *Formaldehyde*. New York, Reinhold Publishing Corp., 1953.
22. Prettre, M.: Acta Physicochim. (U.R.S.S.), *9*, 581 (1938).
23. Mulcahy, M. F. R.: Disc. Faraday Soc., *2*, 128 (1947).
24. Bardwell, J.: Proc. Roy. Soc. *A207*, 470 (1951).
25. Cullis, C. F., and Hinshelwood, C. N.: Disc. Faraday Soc., *2*, 117 (1947).
26. Cullis, C. F., Hinshelwood, C. N., and Mulcahy, M. F. R.: Proc. Roy. Soc., *A196*, 160 (1949).

Earl W. Malmberg*

In the oxidation of triethylamine, the analytical results show the presence of a large amount of ethylamine with considerably smaller amounts of diethylamine and ammonia. The separate experiments by Cullis and Waddington on reaction of oxygen with diethylamine show that the secondary amine is not an intermediate in the formation of the primary amine. The necessity arises then of showing how the two ethyl groups can be removed in one step to give the large amount of ethylamine.

My suggestion is that the intramolecular attack first described by Borusch and coworkers† and extended in our paper in this Symposium‡ may be the explanation of these results, as shown.

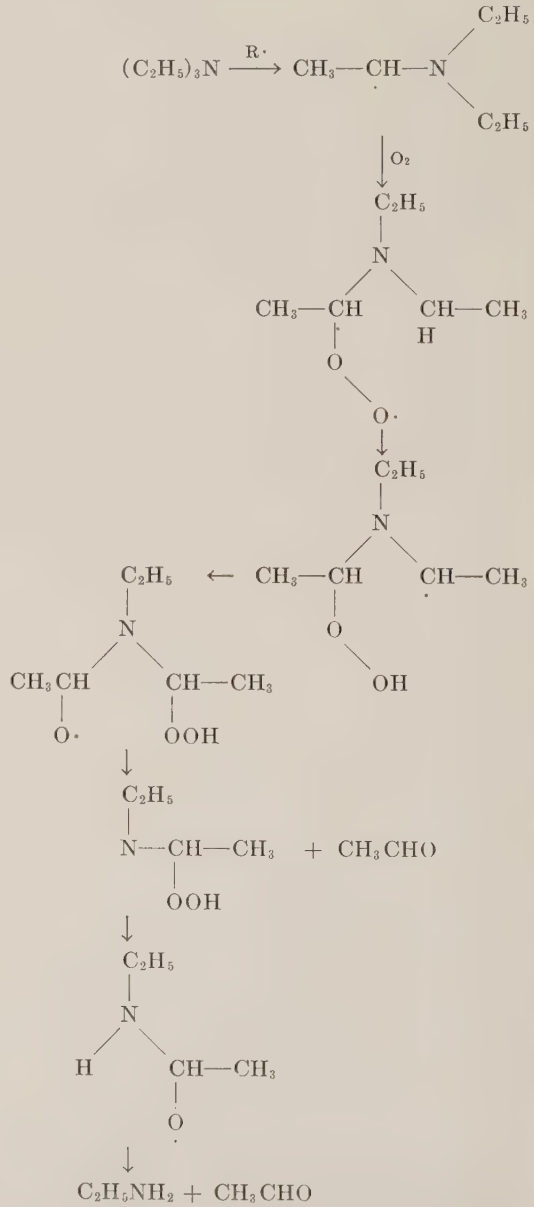

* Ohio State University.

† M. R. Borusch, J. T. Neu, J. Q. Payne, and J. R. Thomas: Ind. & Eng. Chem., *43*, 2766 (1951).

‡ Chapter 34, page 385.

All the reactions aside from the intramolecular step are as usually written. The order in which the reactions are written is arbitrary; a number of possibilities suggest themselves. The formation of diethylamine and ammonia fit into this picture as well.

AUTHORS' REPLY

The suggestion that ethylamine is formed by a process involving intramolecular oxidative attack is an interesting one, and tests with scaled molecular models show that on steric grounds such a reaction may well be feasible. In absence of further experimental evidence, however, the possibility remains that production of ethylamine occurs as the result of step-wise intermolecular oxidation of the alkyl groups in the tertiary amine. The fact that diethylamine is not further oxidized by gaseous oxygen under the experimental conditions used does not invalidate such a mechanism, for consecutive attack of the alkyl groups in triethylamine could occur without the intermediate production of the dialkylamine.

Further experimental evidence is clearly needed before a decision can be made as to the nature of the reactions leading to the formation of the monoalkylamine.

55

A KINETIC COMPARISON OF THE COMBUSTION OF METHYL ALCOHOL AND METHANE

By WENDELL H. WISER AND GEORGE RICHARD HILL

The problem of an a priori prediction of the relative velocities of flames in CH_4 and CH_3OH involves estimating or measuring (1) the temperatures of burning, (2) the mechanisms of reaction and (3) the elementary reaction rates. Since methane combustion is more exothermal than that of methyl alcohol and since the average heat capacity of equimolar mixtures of methane in air is less than of methanol in air, one would expect its flame temperature to be higher. If the activation energies were the same methane should burn faster than methanol. Research in this laboratory has shown this not to be the case.

The expression for the rate of a chemical reaction is

$$k' = \kappa \frac{kT}{h} e^{-\Delta H\ddagger/RT} e^{\Delta S\ddagger/R} \qquad (1)$$

where k' can be the rate for the single slowest step in the net reaction or an average value when several different chain carrying steps occur simultaneously.

Since the elementary processes in the chain reactions occurring in the combustion of methanol are very probably the same, the entropies of activation should be almost identical. The temperatures, calculated from heats of reaction and heat capacity data differ by about 140° which would mean that the term $\kappa kT/h$ for methane would be 7 per cent larger than the corresponding term for methane. This means that the difference in the observed rates of combustion of methane and methanol will be accounted for in the exponential ratio $\Delta H\ddagger/RT$. Since it has been shown that the burning velocity $U_f = C(k')^{1/2}$ [1], a comparison of the squares of the fundamental burning velocities and of flame temperatures for the two compounds will establish whether the difference is kinetic or thermodynamic in character.

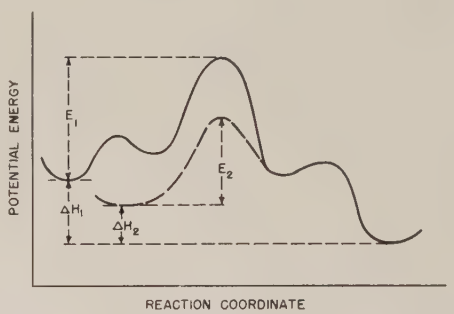

FIG. 1. Potential energy curves for methane and methanol combustion.

Figure 1 is a schematic representation of potential energy curves for the reactions (1) $CH_4 + 2O_2 \rightarrow CO_2 + 2H_2O$, and (2) $CH_3OH + \frac{3}{2} O_2 \rightarrow CO_2 + 2H_2O$. ΔH_1, the heat of combustion of methane is 210.8 kcal. Methanol, on burning to the same products, $CO_2 + H_2O$, has a heat of reaction ΔH_2 of 170.9 kcal.

The overall activation energies for the two reactions are denoted by E_1 and E_2, respectively. If $E_2 < E_1$ the flame velocity for methanol may well be greater than that of methane in spite of the fact that $\Delta H_1 > \Delta H_2$.

Data were not available on the flame velocity for methyl alcohol so a determination of the velocity of burning and of combustion limits was undertaken.

Experimental

A horizontal tube, like that described by Gerstein, Levine, and Wong[3] was used for the flame velocity determinations. The combustion chamber consisted of a 3.0 cm Pyrex tube 57 cm between orifices. A 35/25 ball joint was attached to each end of the tube for connection to the vacuum apparatus. During the combustion both ends were opened to the atmosphere. At the end of the tube at which ignition was effected an 0.8 mm orifice was placed. An orifice 1.7 mm in diameter was placed in the end of the tube toward which the flame advanced. These orifices decreased the turbulence and net gas translation (measured) during combustion.

Preparation of Combustible Mixture

The entire system, including mixing vessel and combustion tube, was evacuated to a pressure of less than 50 μ. The mixing chamber, a 3-l vessel equipped with a magnetic stirrer, was closed off from the rest of the system, and methyl alcohol vapor was admitted to the mixing chamber until the desired, predetermined pressure was reached. This was measured by a mercury manometer. The air, or the oxygen-nitrogen mixture, properly cleaned and dried, was then admitted to the chamber until the desired total pressure (greater than atmospheric) was reached.

The mixture of gases was stirred for five minutes to ensure uniform mixing of the gases. Following this the combustion tube portion of the system was filled. The pressure in this part of the system before influx of the mixture was less than 5 μ.

Prior to ignition of the combustible mixture, the ends of the combustion tube were opened to the atmosphere. Ignition was effected with a methanol-air flame; this prevented the introduction of any foreign atoms or molecules into the system.

A pair of photomultiplier tubes with collimating slits were used to determine the velocity of the flame front. These were located far enough down the tube from the ignition end that constant velocity and flame shape had been attained. The impulse from each photocell caused a spark discharge to burn a hole in a waxed tracing paper which was mounted on an aluminum disc rotated by a synchronous motor. The velocity of the flame as it traveled the 15.2 cm between the photocells was calculated from the total revolutions between sparks as recorded on the tracing paper.

Photographs were taken of the flame front in the region of the photocells for the purpose of calculating their areas.

The expansion due to combustion caused a slight movement of the gases in front of the flame. The velocity of the unburned gas was measured by photographing an expanding soap bubble at 64 frames/sec. The soap bubble was silhouetted against a cathode ray oscillograph screen which made it possible to determine (by connection to the photomultiplier tube circuit) the portion of the bubble expansion which occurred as the flame passed between the photocells. The volume increase during this interval enabled calculation of the velocity of the unburned gas.

Results and Discussion

The limits of combustion of methyl alcohol-air mixtures in the horizontal tube were found to be 7.9 $\pm$ 0.2 per cent and 25.0 $\pm$ 0.6 per cent. The pressure for the experiments was 65 cm of mercury, (atmospheric pressure in Salt Lake City) and the initial temperature in all cases was 24–27°C.

The fundamental flame velocity was calculated from the following equation used by Gerstein, Levine, and Wong[3].

$$U_f = (U_0 - U_g)A_t/A_f \qquad (1)$$

where U_f is the fundamental flame velocity, U_0 is the observed velocity of the flame travelling down the tube, U_g is the velocity of travel of unburned gas in front of the flame, A_t is the cross-sectional area of the tube, and A_f is the area of the flame front.

The flame front was considered to be a semi-ellipsoid, the axes of which were equal to (1) a line joining the points where the flame touched the top and bottom of the tube, (2) twice the perpendicular distance between that line and the point most remote from it on the photograph

of the flame front, and (3) the diameter of the tube. The area of the half-surface of the ellipsoid was calculated from the following equation derived from the integral form given by Jellét[4]:

$$A = \pi b(a^2 - c^2)^{1/2} \cdot E(k, \phi) + \pi bc^2(a^2 - c^2)^{1/2} \cdot F(k, \phi) + \pi c^2$$

where a, b, and c are the semi-axes of the ellipsoid, $a > b > c$; $k = e'/e$; $\phi = \sin^{-1} e$; e and e' are the eccentricities of the ellipses in the plane of the axes a and c, and b and c, respectively. The values of $E(k, \phi)$ and $F(k, \phi)$, the elliptic functions of the second and first kind, respectively, were obtained from a table of elliptic functions[5]. In using this table,

$$\alpha = \sin^{-1} k.$$

Table 1. Flame Velocity, Composition Data for Methanol, Air Mixtures

CH_3OH	U_0	Area of Flame	U_f
per cent	*cm/sec*	*cm²*	*cm/sec*
8.3	29.9	13.3 ± 0.2	13.1
9.1	40.9	11.3 ± 0.2	21.2
10.0	53.6	11.2 ± 0.1	28.0
11.1	70.6	10.8 ± 0.2	38.2
12.5	85.3	11.4 ± 0.2	43.2
13.9	90.0	11.7	44.5
14.3	91.2	11.8 ± 0.1	44.7
14.7	89.0	11.6	44.4
16.7	74.2	12.1 ± 0.04	36.0
20.0	38.0	19.2 ± 0.5	11.7

The eccentricities were calculated in the normal manner for ellipses; i.e., define a distance $m = (a^2 - c^2)^{1/2}$ where a and c are half the major and minor axes of the ellipse, respectively. Then the eccentricity, $e = m/a$. Similarly, $n = (b^2 - c^2)^{1/2}$ and $e' = n/b$.

Table 1 lists the measured flame velocities, calculated flame front areas, and fundamental flame velocities as a function of per cent methanol in methanol-air mixtures. The initial temperature of the combustion mixtures was 27°C, the total pressure being 65 cm of mercury.

Figure 2 is a plot of translation velocity of unburned gas, U_g, versus the observed flame velocity; unmeasured values of U_g were obtained from this plot.

Figure 3 is a plot of the fundamental flame velocity versus composition. As is true with hydrocarbon flames, the maximum flame velocity occurs on the fuel rich side of stoichiometric composition.

Figure 4 illustrates an interesting phenomenon with regard to the area of the burning front as the concentration of methanol was changed. It would be expected that the minimum flame front would

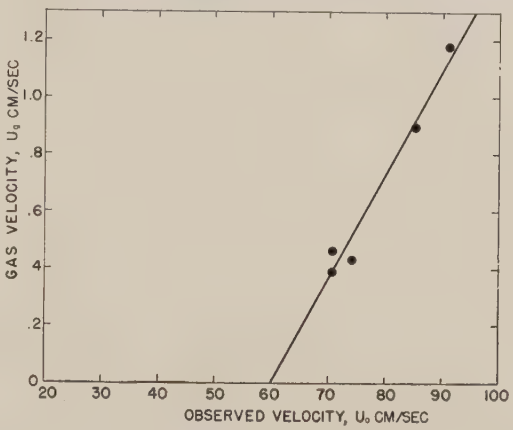

Fig. 2. Gas velocity (translational) vs. observed velocity.

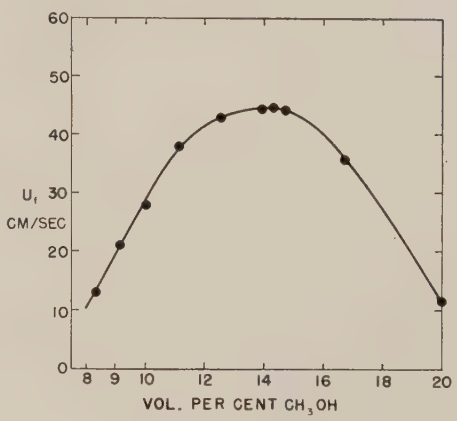

Fig. 3. Fundamental flame velocity vs. composition for methanol-air mixtures.

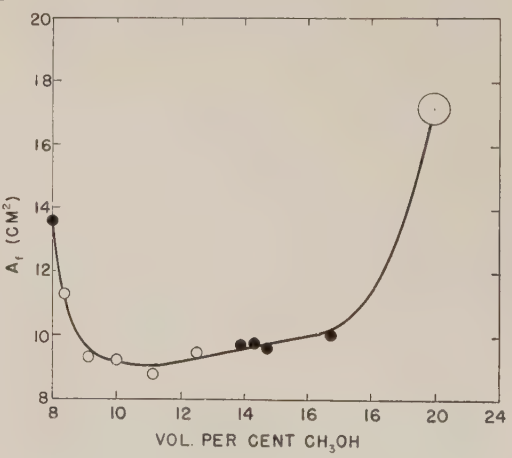

Fig. 4. Plot of A_f vs. composition

be associated with the maximum velocity flame. The minimum area, however, occurs at 11.1 mole per cent methanol, while the maximum velocity occurs at 14 mole per cent. Since the shape of the

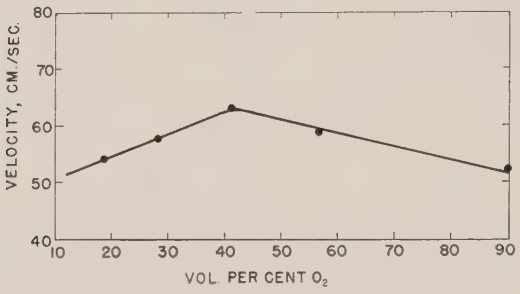

FIG. 5. Plot of U_0 vs. % O_2 at 10% CH_3OH

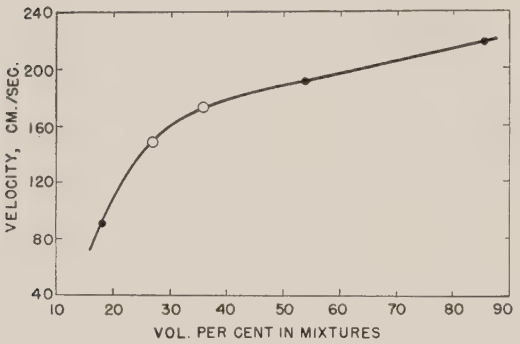

FIG. 6. Plot of U_0 vs. % O_2 at 14.3% CH_3OH

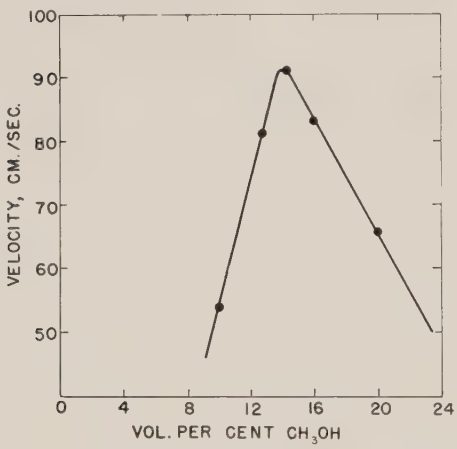

FIG. 7. Plot of U_0 vs. % CH_3OH at 18.0% O_2

flame is largely a function of the buoyancy of the hot gases (and cooling by the walls) it would be expected that the smaller flame front would be associated with a lower temperature of the gases. Average molecular weights for the gaseous mixture associated with each flame front were calculated. Temperatures were determined from heat of combustion and heat capacity data. Relative average molecular velocities of the gases were then calulated. Assuming that the flame front area would increase as the square of the average velocity of the gas molecules it was found that the maximum velocity mixture should have an area 16 per cent larger than the 11.1 per cent mixture. Experimentally, the difference in area was +13.5 per cent.

In an effort to determine the dependence of the velocity of combustion upon the concentrations of methyl alcohol and oxygen, runs were made holding one of these variables constant and varying the other over a wide range. Two points on the composition vs. U_0 curve were chosen, at ten per cent methyl alcohol, well on the lean side,

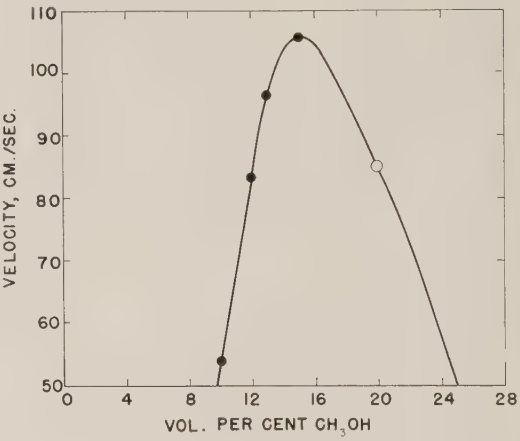

FIG. 8. Plot of U_0 vs. % CH_3OH at 18.9% O_2

and at 14.3 per cent methyl alcohol, the point of maximum velocity in methyl alcohol-air mixtures. Figures 5–8 are the results of these experiments.

The stoichiometric mixture in Figure 5 would occur at 15 per cent O_2. An essentially linear dependence on oxygen concentration is noted up to ca 3× stoichiometric.

In Figure 6 the velocity of the flame doubled as the oxygen pressure doubled in the concentration range around stoichiometric. The decrease in velocity at higher oxygen concentrations did not occur at this concentration of methyl alcohol. Figures 7 and 8 illustrate the large effect of methyl alcohol concentration variation on the flame velocity. Stoichiometric mixtures were at 12 per cent and 12.6 per cent methyl alcohol in the two curves. The inhibitory effect of excess methanol became great enough to decrease flame velocity

at 14 per cent and 15 per cent methanol in each system. In each case this is 17 per cent over the stoichiometric concentration. The large inhibitory effect is very probably due to the large heat capacity of the alcohol molecules and to their effectiveness as third bodies in chain terminating collisions.

In Table 2 the maximum flame velocities for methyl alcohol and methane and its homologs are compared. The first value listed for methane was determined in the same tube as the value for methyl alcohol.

Calculations were made to determine maximum adiabatic flame temperatures of mixtures of each gas with air for maximum velocity compositions

TABLE 2. COMPARISON OF U_f OF METHYL ALCOHOL WITH SOME HYDROCARBONS

Fuel	Max. U_f
	cm/sec
Methyl alcohol*	44.7
Methane*	36.3
Methane†	33.8
Methane‡	37.0
Ethane†	40.1
Propane†	39.0
Butane†	37.9
Pentane†	38.5
Ethylene†	68.3

* This research.
† Gerstein, Levine, and Wong[3].
‡ Jost and Croft[9].

using heats of combustion of 210.8 kcal for methane and 170.9 for methanol and heat capacity data from the literature[6, 7, 8]. The temperatures calculated were 1890°C and 1750°C respectively.

Using the experimental values $U_{0_{CH_3OH}} = 44.7$ cm/sec and $U_{0_{CH_4}} = 36.3$ cm/sec, calculation of the relative heats of activation gives the following results.

	T	U_f	ck'
	°K	*cm/sec*	
CH_4	2163	36.3	1317
CH_3OH	2023	44.7	2000

$$\Delta H^{\ddagger}_{CH_4} - 1.07\Delta H^{\ddagger}_{CH_3OH} = 2.067 \text{ kcal}$$

For $\Delta H^{\ddagger}_{CH_4} = 5$ kcal, $\Delta H^{\ddagger}_{CH_3OH} = 2.79$ kcal
For $\Delta H^{\ddagger}_{CH_4} = 10$ kcal, $\Delta H^{\ddagger}_{CH_3OH} = 7.4$ kcal
For $\Delta H^{\ddagger}_{CH_4} = 30$ kcal, $\Delta H^{\ddagger}_{CH_3OH} = 26$ kcal

Spectroscopic Data and Reaction Mechanism

Guenault[10] reported in 1937 that the methyl alcohol flame showed Emeleus' cool flame bands which are known to be emitted by formaldehyde. The formaldehyde bands were difficult to identify because of their being masked in many cases by the stronger CO flame bands. Gaydon and Wolfhard[11] in 1949 carried out spectroscopic studies on methyl alcohol flames at reduced pressures. Their technique involved scanning the flame systematically to identify the regions where certain radicals and compounds were most prominent. They found that the base of the flame showed the cool flame bands, indicating the early formation of excited formaldehyde molecules. These bands occurred well below the CH bands and slightly below the OH bands. It would appear reasonable from these observations that formaldehyde may well be an important intermediate in the early phases of the combustion of methanol.

Two of the possible reaction sequences which methanol might follow in its oxidation are:

$$CH_3OH + O_2 \rightarrow CH_3O + OH$$

$$CH_3O + M \rightarrow HCHO + OH + M$$

and

$$CH_3OH + OH \rightarrow CH_2OH + H_2O,$$

$$CH_2OH + O_2 \rightarrow HCHO + HO_2 .$$

It is not possible to determine which of these (or other) reaction sequences account for the lower heat of activation for the methanol combustion from the data presented in this research. The remainder of the steps in the reaction would likely be those discussed by Lewis and von Elbe for the oxidation of formaldehyde[12].

Acknowledgment

This research was supported by the United States Air Force under Contract Number AF 33(038)-20839, monitored by the Office of Scientific Research and Development Command.

REFERENCES

1. GLASSTONE, S., LAIDLER, K. J., AND EYRING, H.: *The Theory of Rate Processes.* McGraw-Hill Book Company, Inc., 1941.
2. EVANS, N. W.: Chem. Rev., *51*, 363 (1952).
3. GERSTEIN, M., LEVINE, O., AND WONG, E. L.: J. Am. Chem. Soc., *73*, 418 (1951).

4. Williamson, B.: *An Elementary Treatise on Integral Calculus*, p. 283. London, Longman-Green, 1891.
5. Jahnke, E., and Ende, F.: Tables of Functions, p. 62–72. New York, Dover Publications, 1945.
6. *International Critical Tables, V*, pp. 80, 81–84.
7. Eucken, A., and Franck, E. V.: Zeit. Elektrochem., *52*, 195–204 (1948).
8. Hougen, O. A., and Watson, K. M.: *Chemical Process Principles*, p. 212. New York, John Wiley and Sons, 1947.
9. Jost, W.: *Explosion and Combustion Processes in Gases*, p. 122. New York, McGraw-Hill Book Co., 1946.
10. Guenault, E. M.: Ann. Rep. Safety in Mines Res. Bd., *16*, 64 (1937).
11. Gaydon, A. G., and Wolfhard, H. G.: *Third Symposium on Combustion, Flame, and Explosion Phenomena*, p. 504. Baltimore, The Williams & Wilkins Co. (1949).
12. Lewis, B., and von Elbe, G.: *Combustion, Flames, and Explosions*, pp. 99–114. New York, Academic Press, Inc., 1951.

56

THE SLOW OXIDATION OF SOME ALIPHATIC ALCOHOLS

By E. J. NEWITT

The vapor phase oxidation of the paraffins and their derivatives has been much studied during the past twenty-five years. The combustion of the aliphatic alcohols has, however, received remarkably little attention, despite the technical importance of alcohols as fuels in internal combustion engines[1] and in certain types of jet engine[2]. Furthermore, alcohols have been postulated as intermediates in hydrocarbon oxidation[3], and are present in the products of combustion, especially at high pressures[4].

The oxidation of methanol has been studied by several workers, particularly in relation to the oxidation of methane[5]. Although methanol oxidizes more readily than methane[5, 7], its behavior is generally similar. Oxidation becomes appreciable above 380°C and it is usually agreed that the combustion of both compounds proceeds solely by a high-temperature mechanism.

Much less information is available concerning the higher alcohols. Layng and Youker[6] studied the slow combustion of heptanol and commented on its marked resistance to oxidation. Kane, Chamberlain and Townend[8] determined the pressure-temperature limits of ignition in air for ethanol, propanol, butanol and pentanol, and concluded that, while the alcohols show the same sequence of oxidizability as the corresponding paraffins, the higher alcohols become relatively less reactive. Thus, although methanol, ethanol and propanol are more readily oxidized than methane, ethane and propane, the situation is reversed with butanol and the higher homologue Other combustion studies in which alcohols hav received attention are those of Mardles[9], Pettre[10] Mulcahy[11], and Farmer and McDowell[12].

A comprehensive investigation into the vapor-phase oxidation of the aliphatic alcohols is in progress in these laboratories, and some preliminary results are here presented.

Experimental

A static apparatus was used. It consisted essentially of a cylindrical Pyrex reaction vessel of length 9.5 cm and diameter 6.0 cm, suspended vertically in an electric furnace whose temperature could be controlled[13] to ±0.5°C in the temperature range 200° to 500°C. The reaction vessel was connected to an electrically heated bulb of 250 ml capacity containing alcohol vapor, and to storage globes containing permanent gases. Pressures were measured on a mercury manometer. A column of gold foil between the reaction vessel and the manometer prevented diffusion of mercury vapor. The manometer and all connecting capillary leads to the reaction vessel were electrically heated to avoid condensation.

Oxygen from a cylinder was passed over magnesium perchlorate and through two traps cooled to −80°C; it was used without further purification. The ethanol was B.D.H. absolute alcohol for spectroscopy. Pure commercial samples of propanol, butanol and pentanol were further purified as follows: (1) fractional distillation over

sodium hydroxide at atmospheric pressure; (2) drying over sodium metal; (3) vacuum distillation in the apparatus. The final fraction in each case was distilled into the vertical stem of the vaporizing bulb.

Reproducible results could only be obtained by rigorously observing a standard procedure with every run, and by carrying out a given series of experiments in the shortest possible time. The reaction vessel was evacuated after each run for 3 min by an oil pump and then for 7 min by a mercury diffusion pump; it was kept at 300°C overnight.

Results

The development of the slow reaction with time, as measured by pressure change, is generally similar to that of the parent hydrocarbons, showing the familiar features associated with degenerate branching[14]. Two parameters of the rate of reaction were calculated from the pressure-time records: (1) the maximum rate developed, (ρ_{max}); (2) the reciprocal induction period, ($1/\theta$). The induction period (θ) is defined as the time between admission of the reactants and the attainment of the maximum rate.

THE FORM OF THE PRESSURE-TIME CURVES

For a reaction involving non-stationary chains the increase in pressure is given by an equation of the form:

$$\Delta P = \frac{C}{\phi^2}(e^{\phi t} - 1)$$

If the growth of rate during the period of autocatalysis is characterized by chains of this type, a plot of log ΔP against time should be linear as soon as $e^{\phi t}$ appreciably exceeds unity. Figure 1 shows some typical plots, together with the corresponding pressure-time curves. The curves in Figure 1a refer to low temperatures, while those in Figure 1b were obtained at intermediate temperatures with ethanol and propanol, and at the temperature-threshold of the cool-flame region with pentanol. With all the alcohols, an exponential law is obeyed only at low temperatures; at intermediate temperatures log ΔP shows greater than first-order dependence on time well below the maximum rate, indicating a more marked acceleration than is predicted by the simple theory of non-stationary chains. It is found that, with butanol and pentanol, the upward curvature becomes exaggerated as the cool-flame region is entered. Self-heating may become significant at these temperatures.

The variation of the net branching factor ϕ could not be studied owing to the non-linear nature of the plots of log ΔP against time.

INFLUENCE OF TEMPERATURE

Oxidation of the four alcohols becomes appreciable at temperatures above 270°C. Figure 2 shows the effect of temperature on the maximum rate developed and on the reciprocal induction period.

A slackening of the temperature coefficient of ρ_{max}, very weakly developed with ethanol, becomes more pronounced with propanol. Butanol and pentanol give rise to single and multiple cool-flames (as indicated by pressure pulses of 2–10 cm) between 303°C and 340°C; as the temperature is further increased, the cool-flame region is superseded by a high-temperature region in which exceptionally high maximum rates are sustained without ignition occurring. With propanol and the higher alcohols, oxidation can evidently occur by both low and high temperature mechanisms; the region of transition is characterized by a negative temperature coefficient which may, as in the case of butanol and pentanol, be obscured by cool-flames. With ethanol, the position seems uncertain, but evidence of two-stage ignition at higher pressures[8] indicates that this alcohol can also oxidize by two mechanisms.

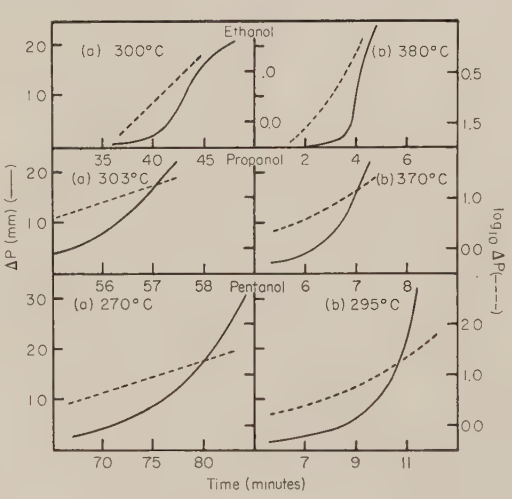

FIG. 1. Typical plots of ΔP (full line) and of $\log_{10}\Delta P$ (broken line) against time. Reactant concentrations correspond to: alcohol pressure, 40 mm; oxygen pressure, 200 mm at 323°C.

With ethanol and propanol the logarithm of

the reciprocal induction period is proportional to $1/T°K$ (Fig. 2b) over the entire temperature range, while the corresponding plots for the two higher alcohols show a fairly sharp break at

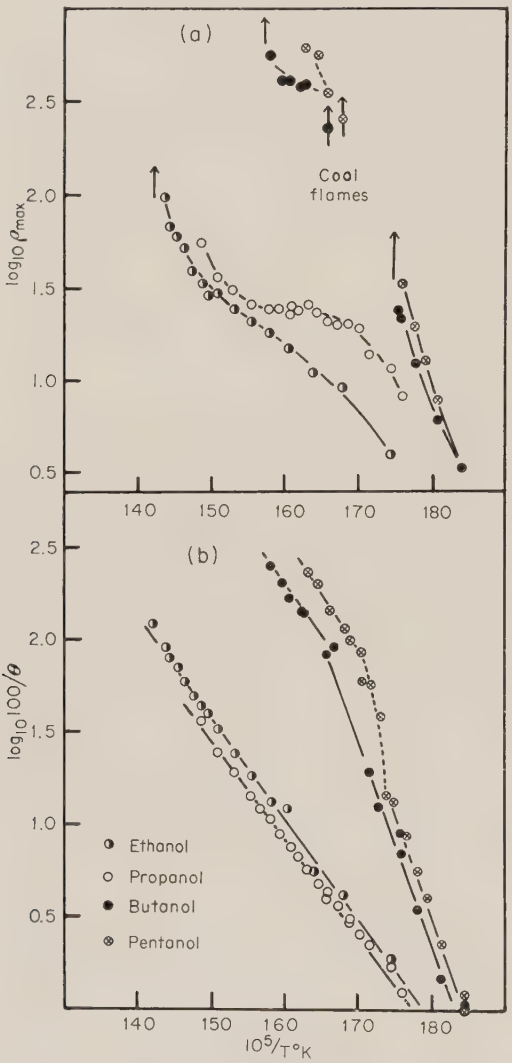

FIG. 2. The effect of temperature on (a) the maximum rate of oxidation; (b) the reciprocal induction perriod. Reactant concentrations correspond to: alcohol pressure, 40 mm; oxygen pressure, 200 mm at 323°C.

temperatures approaching the upper cool-flame limit, i.e., in the region where the high-temperature mechanism predominates. All four plots become approximately parallel in this region. The slight upward shift of the log $1/\theta$ plot for pentanol in the cool-flame region may well be due to self-heating effects.

INFLUENCE OF STRUCTURE

An important feature of the low-temperature oxidation of hydrocarbons is the large influence of structure on reactivity as the series is ascended[15], and this behavior appears to be closely paralleled with certain other aliphatic compounds[16]. The maximum rates of pressure increase were used as the basis of comparison, but it was found necessary to compare these compounds in pairs at different temperatures in order to make a complete survey. This method of comparison is open to the objection that no account is taken of differences in the temperature coefficients of reaction rate.

Figure 2a shows that for the four normal alcohols, the influence of carbon chain length on ρ_{max} is much less marked. While the sequence of ease of oxidation is maintained with the lower members of the series, the higher alcohols become relatively more resistant to oxidation. These results are in broad agreement with those of other workers[6, 8].

In comparisons of reactivity calculated from rates of pressure increase (Fig. 1a), allowance must be made for the number of carbon atoms which tends to weight the results in favor of the higher members of the series[17]. An examination of the pressure-time curves shows that, while the total pressure change (ΔP_∞) accompanying oxidation of the four alcohols increases with temperature, the pressure change at which the maximum rate is reached ($\Delta P\rho_{max}$) remains sensibly independent of temperature (Table 1). This suggests that the period of autocatalysis is not appreciably affected by secondary oxidations which appear to increase in importance with temperature. Hence $\Delta P\rho_{max}$ provides a measure of the relative increase in the number of molecules occurring during the induction period as a direct result of alcohol consumption. Values of $(\rho_{max}/\Delta P\rho_{max})$, which are independent of carbon chain-length, may then be derived as shown in Table 2. The effect of the correction is to reduce further the apparent influence of structure on ρ_{max} at low temperatures, although the sequence of ease of oxidation is retained.

The reciprocal induction period as a criterion of oxidizability shows both similarities to and striking differences from the maximum rate (Fig. 2b). The same sequence is maintained except with propanol, which appears to be slightly less reactive than ethanol. A singular feature of the plots shown in Figure 2b is their

separation into pairs. This tendency appears to be paralleled by the maximum rate plots (Fig. 2a) in the high-temperature region.

TABLE 1. THE EFFECT OF TEMPERATURE ON ΔP_∞ AND $\Delta P_{\rho max}$

Reactant concentrations correspond to: alcohol pressure, 40 mm; oxygen pressure, 200 mm at 323°C

Alcohol	Temp.	ΔP_∞	$\Delta P_{\rho max}$
	°C	*mm*	*mm*
Ethanol	300	30	10
	340	38	10
	380	61	10
	410	68	10
Propanol	303	46	17
	330	52	18
	360	65	17
	390	95	17
Butanol	270	58	25
	282	65	25
	296	75	25
	310	82	25*
Pentanol	270	70	33
	285	81	35
	295	87	35
	300	95	35*

* Pressure increase prior to passage of a cool-flame.

TABLE 2. TEMPERATURE: 295°C

Alcohol	ρ_{max}	$\Delta P_{\rho max}$ (relative to ethanol)	$\frac{\rho_{max}}{\Delta P_{\rho max}}$
	mm min^{-1}	*mm*	*min*$^{-1}$
Ethanol	3.2	(1.0)	3.2
Propanol	8.3	1.7	4.9
Butanol	20.0	2.5	8.0
Pentanol	32.7	3.5	9.35

INFLUENCE OF REACTANT CONCENTRATIONS

The effect of reactant pressures on ρ_{max} and $1/\theta$ has been examined for ethanol and butanol at a single temperature in the low-temperature region.

Both ρ_{max} and $1/\theta$ increase rapidly with alcohol concentration. Comparative results are shown in Figures 3 and 4. Linear dependence of $1/\theta$ on the pressure of combustible is exhibited.

ρ_{max} shows approximately first-order dependence on oxygen concentration at low oxygen pressures but becomes independent at higher

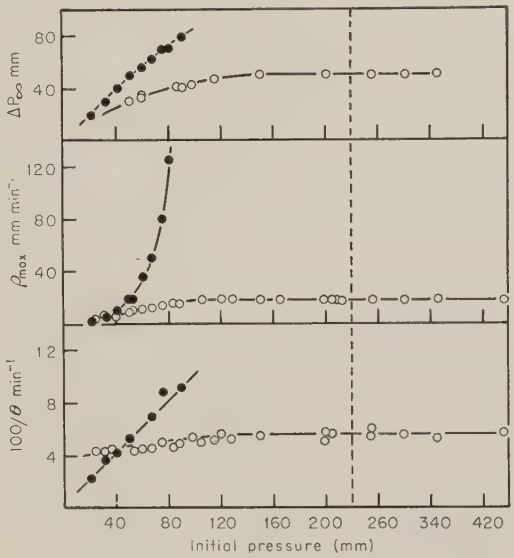

FIG. 3. Ethanol-oxygen mixtures (323°). The influence of reactant concentrations on the total pressure increase (ΔP_∞), the maximum rate of oxidation (ρ_{max}) and the reciprocal induction period ($1/\theta$).
○ oxygen varied; ethanol, 50 mm.
● ethanol varied; oxygen, 200 mm.

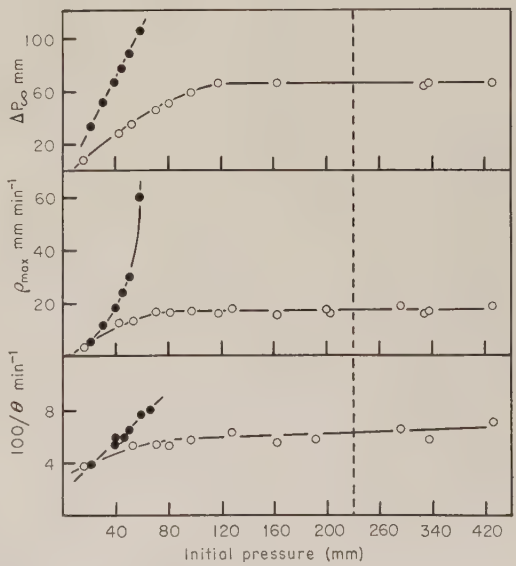

FIG. 4. Butanol-oxygen mixtures (295°C). The influence of reactant concentrations on ΔP_∞, ρ_{max} and $1/\theta$.
○ oxygen varied; butanol, 40 mm.
● butanol varied; oxygen, 200 mm.

pressures; the change-over occurs somewhat below the stoichiometric ratio, as measured by

ΔP_∞. The reciprocal induction period appears to be sensibly independent of oxygen concentration with both alcohols over the whole experimental range.

Discussion

The main facts established in the present work are:

(1) The dependence of log ΔP on time during the period of autocatalysis ceases to be linear as intermediate temperatures are reached.

(2) Sharp differences exist between the behavior of ρ_{max} and $1/\theta$ as functions of temperature and reactant concentrations. The dependence of $1/\theta$ is simple in both cases.

(3) At low temperatures, ρ_{max} shows the influence of alcohol structure on reactivity to be very small and to diminish further as the series is ascended. In contrast, $1/\theta$ does not show a well-graded variation and indicates a negative structural influence between ethanol and propanol

(4) Ethanol and butanol show closely similar kinetic behavior in the low-temperature region.

In their oxidation, the four alcohols have many features in common with the praffins above ethane, although the influence of structure is much less marked. The greatest contrast occurs between ethanol and ethane. If the temperature-dependence of ρ_{max} is adopted as the criterion, ethanol does not appear to oxidize solely by a high-temperature mechanism as is generally assumed for ethane, nor does it show a distinct transition region. In its kinetics, ethanol resembles the higher hydrocarbons, known to oxidize by a low-temperature mechanism.

The observation that the dependence of log ΔP on time becomes more complex at intermediate temperatures during periods of autocatalysis has been reported elsewhere[18], but has been little discussed. The simplest explanation of the cessation of linear chain-branching is that isothermal conditions are not maintained. This view is consistent with those of other workers concerning the origin of cool-flame phenomena[19, 18].

A significant feature of alcohol oxidation is the simple temperature dependence of the reciprocal induction periods which, with ethanol and propanol, is maintained throughout both low and high temperature regions. $1/\theta$ also shows first-order dependence on alcohol pressure at lower temperatures. Similar behavior is shown by the low-temperature oxidation of butane and propylene[20]. However, the insensitivity to oxygen, except at very low pressures, of the induction periods observed with the alcohols, contrasts with the linear dependence of $1/\theta$ on oxygen found with the hydrocarbons. With the latter it was suggested[20] that, whereas ρ_{max} depends upon the rate of delayed chain-branching, $1/\theta$ is proportional to the rate of chain initiation; the initiating process was considered to be a bimolecular reaction between oxygen and hydrocarbon. The present results indicate that a simple chain-initiating mechanism operates over a considerable temperature range, but that higher pressures of oxygen do not favor development of the chains.

The different structural effects indicated by the two parameters, ρ_{max} and $1/\theta$, may be significant. For example, the initiating reaction will be influenced by the alcohol structure; a branching chain reaction involving decomposition of an intermediate is likely to depend also upon the concentration of intermediate attained, and hence upon its stability. While in principle it follows that $1/\theta$ provides a more fundamental measure of structural influence, experimentally this parameter is so sensitive to the nature and extent of the surface and to traces of impurity that its quantitative significance is often a matter of doubt.

The introduction of an —OH group into ethane increases markedly its susceptibility to oxidation. This effect is similar to that of chlorine substitution[16], and has been attributed to the influence of such substitution on the inductive effect and symmetry of the methyl group. However, with the straight-chain alcohols, the increasing resistance to oxidation points to the development of special stability as the carbon-chain is lengthened.

Acknowledgment

The author wishes to express his gratitude to Dr. C. F. Cullis for much helpful advice and discussion, and also for making available apparatus provided through the generosity of the Shell Petroleum Company.

REFERENCES

1. Ross, J. D., and Ormandy, W. R.: J. Soc. Chem. Ind., *45*, 273 (1926).
2. Spalding, D. B.: *Fourth (International) Symposium on Combustion*, p. 847. Baltimore, The Williams & Wilkins Co., 1953.
3. Bone, W. A.: Proc. Roy. Soc., *A137*, 243 (1932).
4. Newitt, D. M., and Haffner, A. E.: Proc. Roy. Soc., *A134*, 591 (1932); Newitt, D. M., and Szego, P.: Proc. Roy. Soc., *A147*. 555 (1934).

5. Fort, R., and Hinshelwood, C. N.: Proc. Roy. Soc., *A129*, 284 (1930); Bone, W. A., and Gardner, J. B.: Proc. Roy. Soc., *A154*, 297 (1936).
6. Layng, T. E., and Youker, M. A.: Ind. & Eng. Chem., *20*, 1048 (1928).
7. Fort, R., and Hinshelwood, C. N.: Proc. Roy. Soc., *A129*, 284 (1930); Bone, W. A., and Gardner, J. B.: Proc. Roy. Soc., *A154*, 297 (1936); Kane, G. P., Chamberlain, E. A. C., and Townend, D. T. A.: J. Chem. Soc., 436 (1937).
8. Kane, G. P., Chamberlain, E. A. C., and Townend, D. T. A.: J. Chem. Soc., 436 (1937).
9. Mardles, E. W. J.: J. Chem. Soc., 872 (1928); Trans. Faraday Soc., *27*, 681 (1931).
10. See, for example, Prettre, M.: Bull. Soc. Chim. Fr., *51*, 1132 (1932).
11. Mulcahy, M. F. R.: Trans. Faraday Soc., *45*, 537 (1949).
12. Farmer, J. B., and McDowell, C. A.: Trans. Faraday Soc., *48*, 624 (1952).
13. Roberts, M. H.: Electronic Engineering, *23*, 51 (1951).
14. Semenov, N.: *Chemical Kinetics and Chain Reactions*. Oxford, 1935.
15. Cullis, C. F., and Hinshelwood, C. N.: Disc. Faraday Soc., *2*, 117 (1947).
16. Cullis, C. F., Mulcahy, M. F. R., and Hinshelwood, C. N.: Proc. Roy. Soc., *A196*, 160 (1949).
17. Norrish, R. G. W.: Disc. Faraday Soc., *10*, 327 (1951).
18. Bardwell, J., and Hinshelwood, C. N.: Proc. Roy. Soc., *A207*, 461 (1951).
19. See, for example, Pease, R. N.: J. Am. Chem. Soc., *60*, 2244 (1938); Salnikov, I. E.: C. R. Acad. Sci. (U.R.S.S.), *60*, 405 (1948); Bardwell, J., and Hinshelwood, C. N.: Proc. Roy. Soc., *A205*, 375 (1951); Knox, J. H., and Norrish, R. G. W.: Proc. Roy. Soc., *A221*, 151 (1954).
20. Mulcahy, M. F. R.: Trans. Faraday Soc., *45*, 575 (1949); Mulcahy, M. F. R., and Ridge, M. J.: Trans. Faraday Soc., *49*, 1297 (1953).

57

EFFECT OF TEMPERATURE, PRESSURE, AND COMPOSITION ON IGNITION DELAYS FOR PROPANE FLAMES

By RICHARD S. BROKAW and JOSEPH L. JACKSON

Although conditions which may lead to the spontaneous ignition of fuels have been a subject of investigation for many years, the results of various researchers are in most instances not directly comparable, since the experimental conditions at the point of ignition may vary; in some cases these conditions are not completely defined.

In particular, the composition of the fuel-air mixture in the zone in which ignition occurs is frequently not known. This is the case, for example, in the A. S. T. M. standard test method for autogeneous ignition temperature[1], which determines the lowest temperature of an air-filled cavity that will cause ignition when drops of liquid fuel are introduced into it. Here a fuel concentration gradient exists from the bottom of the vessel, where evaporation takes place, to the opening at the top, where dilution with the ambient air occurs.

Ignition delays have been studied in flow systems which allow reactants to be preheated separately to the desired temperature. For very lean mixtures, Mullins[2] reports no effect of fuel concentration on ignition lag when kerosene was injected from a small port into the center of a large duct of heated air. This method does not seem well suited to the study of concentration effects, since all mixtures from pure fuel to pure air may be present in the duct. Indeed, in the work of Olsen[3], where an attempt at rapid mixing was made, a definite shortening of ignition lag with increasing heptane concentration was noted.

Constant volume static systems, where premixed gases are admitted into a heated vessel, are suitable only at temperatures where ignition delays are quite long. Adiabatic compression machines are applicable principally to high pressure conditions.

Accordingly, a program has been undertaken at the NACA Lewis laboratory to clarify in particular the effects of such parameters as fuel and oxygen concentration, pressure, temperature, and

inert diluents, on ignition delay. Furthermore such data may help to elucidate the chemistry of the ignition reactions. A flow apparatus has been employed, since it permits control of temperature, pressure, and composition from the time of mixture preparation until ignition occurs. Reactants were mixed at the desired temperature in a time much shorter than the ignition lag. The results on propane flames presented here were made over a wide range of fuel percentages at atmospheric pressure and temperatures from 520°–740°C. A few results obtained at reduced pressure are also included.

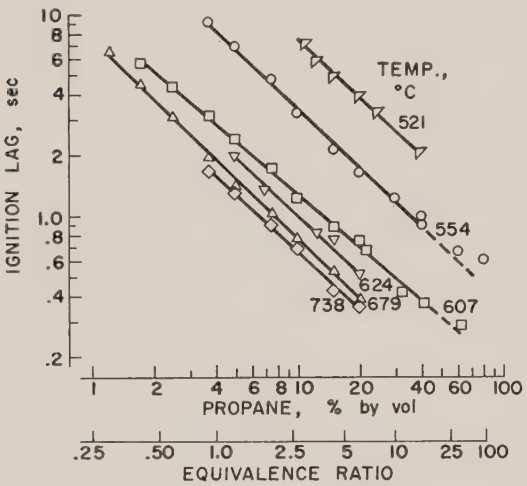

FIG. 1. Variation of ignition lag with propane concentration. Tube diameter, 50 mm.

Experimental

The flow apparatus employed in this research has been described in detail elsewhere[4], so that only its essential features will be mentioned here. The ignition section of the apparatus consisted of a Vycor tube three ft in length and either 25 or 50 mm in diameter, maintained at a constant temperature and pressure. Fuel and air (metered through critical flow orifices) were preheated separately to the tube temperature and mixed rapidly in a tangential jet mixer (volume about one cc). The residence time in the mixing cup was in the range of 0.05–2 per cent of the ignition delay. The ignition lag was determined as the time between the introduction of combustible into the mixer and the appearance of a sudden pressure increase, as indicated by a strain gauge type pressure pickup located at the downstream end of the tube.

The customary procedure was to adjust the air flow through the apparatus while by-passing fuel to the exhaust. A solenoid valve on the fuel line was then energized which diverted the fuel flow into the mixer and started the time indicator. When the pressure pulse appeared, the fuel valve was de-energized and the ignition delay recorded. Four or five runs were made for each fuel-air ratio. A constant total flow rate was usually maintained for all determinations at a given temperature, unless a change in flow was required to keep ignition within the central two-thirds of the tube length (as calculated from flow rate and ignition delay).

Experiments in which a flow of nitrogen preceded fuel and air into the mixer have been fully discussed heretofore[4]. Delays determined in this manner were the same as those obtained with air as the leading gas, indicating that the presence of leaner fuel-air mixtures in the interfacial region between leading air and following combustible mixture was not affecting the results.

Results

When only fuel-air ratio was varied, ignition delays decreased with increasing propane concentration. Figure 1 shows typical logarithmic plots of ignition lag versus volume per cent propane at various temperatures in a 50-mm Vycor tube at one atm; similar results were obtained in a 25 mm tube. In general, these plots are linear, so that the dependence of ignition delay on propane concentration may be expressed by an equation of the type

$$\frac{1}{\tau} = \text{const } [C_3H_8]^n \qquad (1)$$

where

τ = the ignition delay, sec

$[C_3H_8]$ = propane concentration

n = a constant

The slopes of the straight lines (as given by n in equation (1)) lie between the extremes of 0.74 and 1.0, with an average of 0.93. For half of the results, unit slopes were observed, and there did not seem to be any trend in the slope variations, although most of the low slopes were observed on data obtained in the 25 mm tube.

The results on propane-air mixtures show principally the effect of fuel concentration on ignition delay with only a slight resultant variation in oxygen concentration. In order to determine the

dependence of ignition lag on oxygen concentration, delays were obtained for mixtures in which the volume per cent of propane was held constant, while oxygen-nitrogen mixtures containing 9.5, 20.9 (air), and 39.5 per cent oxygen were employed. In Figure 2 the logarithm of ignition delay is plotted against the logarithm of $[O_2]/([O_2] + [N_2])$ for four different propane concentrations at 666°C in the 25 mm tube. These results are typical of others obtained in the larger tube, and at a variety of temperatures from 554°–738°C. It is seen that the dependence of delay on oxygen concentration is slight, being somewhat more pronounced at higher propane percentages. The dependence at constant fuel concentration is given approximately by

$$\frac{1}{\tau} \cong \text{const } [O_2]^{1/4} \tag{2}$$

where $[O_2]$ is the mole fraction of oxygen in the total mixture, although an equation of the form

$$\frac{1}{\tau} = \frac{\text{const } [O_2]}{(1 + k[O_2])^2} \tag{2a}$$

where k is a constant describes the results somewhat better, by implying a greater dependence of lag on oxygen concentration in richer mixtures. The constant k has a value of approximately four when concentrations are expressed as mole fractions.

Combining equations (1) and (2) results in

$$\frac{1}{\tau} = \text{const } [C_3H_8]^n[O_2]^{1/4} \tag{3}$$

which applies for variations of both fuel and oxygen concentration.

Decreases in total pressure were found to increase ignition delays. Results of a series of determinations on propane-air mixtures at 615°C in the 50 mm tube are presented in Figure 3, in which the logarithm of the pressure is plotted against reciprocal ignition delay for mixtures containing 5, 10, 20, and 40 per cent propane. An empirical equation of the form

$$\frac{1}{\tau} = \text{const} \log \frac{p}{p_0} \tag{4}$$

in which p is the pressure and p_0 a limiting pressure, describes the results, when composition is held constant. The limiting pressure does not seem to be greatly affected by changes in propane concentration. For experiments on a mixture containing 20 per cent propane in air at a higher temperature (675°C) equation (4) again fits the data well, although with a lower limit pressure (see 675°C air curve of Figure 5).

The effect of oxygen concentration on ignition

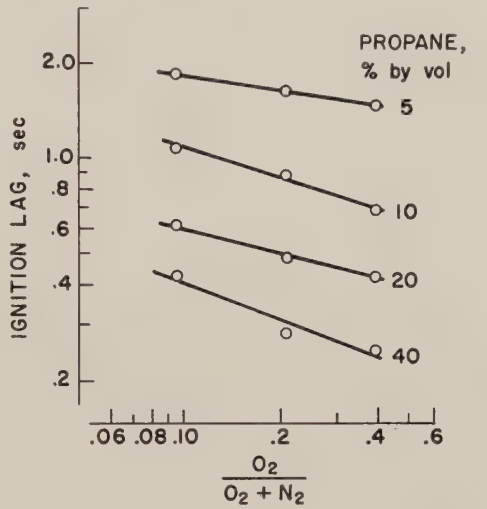

FIG. 2. Variation of ignition lag with oxygen concentration in 25-mm tube. Temperature, 666°C.

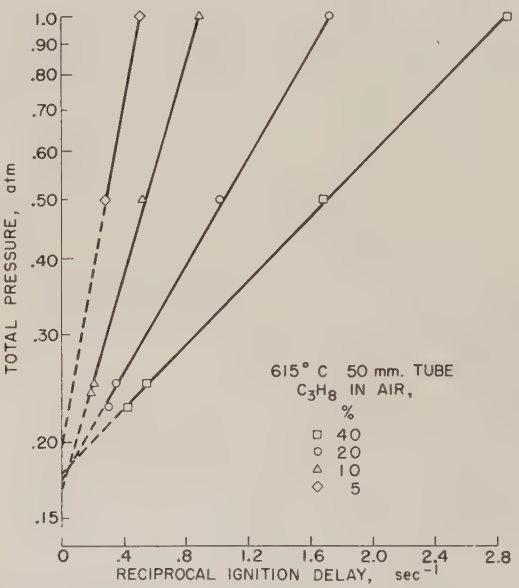

FIG. 3. Variation of reciprocal ignition delay with pressure for various fuel concentrations. (50-mm tube, 615°C).

delay, while slight at atmospheric pressure, appears to be more pronounced at reduced pressures, as may be seen from Figure 4. The limiting pressure appears to be considerably raised for low oxygen concentration.

Experiments were performed with helium-oxy-

gen and argon-oxygen mixtures (oxygen content approximately 21 per cent by volume) substituted for air. Delays at atmospheric pressure were but slightly affected by changing inert gas (Fig. 5). However, at reduced pressures, helium mixtures gave longer delays, while lags for argon mixtures remained essentially the same as those observed for air.

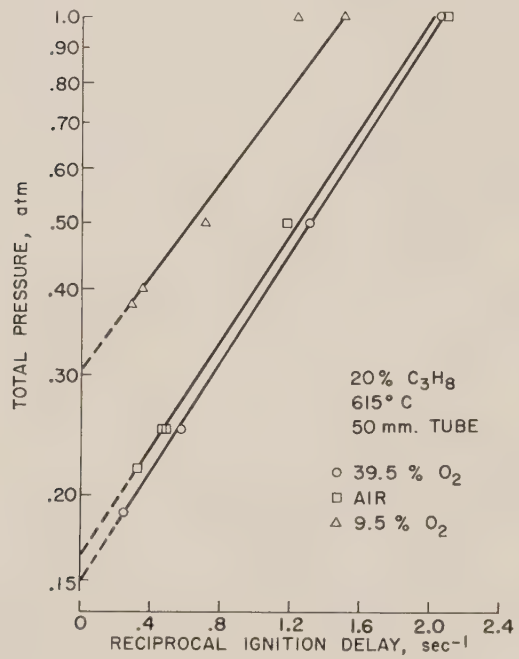

FIG. 4. Variation of reciprocal ignition delay with pressure for various oxygen-nitrogen ratios. (20 per cent propane, 50-mm tube, 615°C).

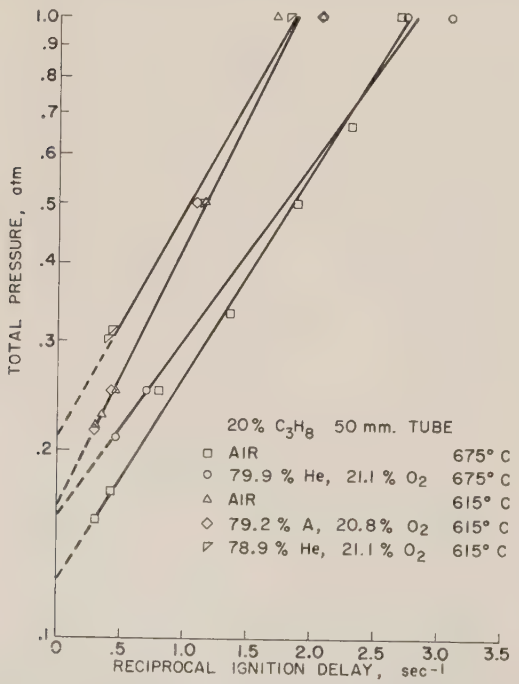
TOTAL PRESSURE, atm
RECIPROCAL IGNITION DELAY, sec⁻¹
20% C3H8 50 mm. TUBE
□ AIR 675° C
○ 79.9 % He, 21.1 % O2 675° C
△ AIR 615° C
◇ 79.2 % A, 20.8% O2 615° C
▽ 78.9 % He, 21.1 % O2 615° C

FIG. 5. Variation of reciprocal ignition delay with pressure for various inert diluents. (20 per cent propane, 50-mm tube, 615° and 675°C).

Under comparable conditions of volumetric flow rate, fuel concentration and temperature, lags observed at one atmosphere pressure in the 25-mm Vycor tube were on the average very slightly higher than in the 50-mm tube[4]. This difference was in general within experimental error. However, a few determinations in the 25 mm tube at 615°C indicate that at reduced pressure delays are definitely longer in the smaller tube. Furthermore, the lowest pressure at which ignition was observed was 0.39 atm, as compared with 0.22 atm for the corresponding mixture in the 50-mm tube at the same temperature. The nature of the tube surface did not influence ignition delays at atmospheric pressure. At 607°C, 50-mm tubes of Vycor, stainless steel, and Vycor coated with potassium chloride all gave the same results.

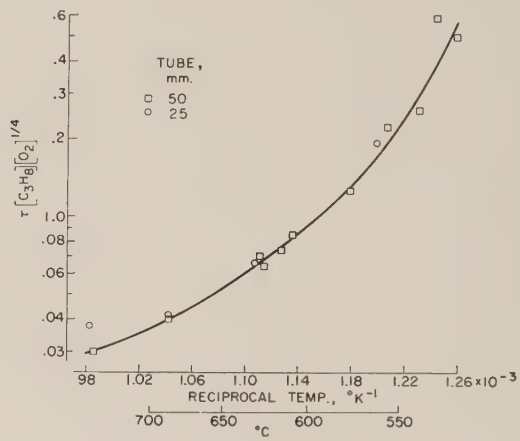

FIG. 6. Variation of the parameter $\tau[C_3H_8][O_2]^{1/4}$ with reciprocal temperature.

Ignition lags decreased with increasing temperature (Fig. 1). Data at constant temperature could be fairly well represented by equation (3) with the exponent n taken as unity. The effect of temperature on lag is illustrated in Figure 6 in which the quantity $\tau[C_3H_8][O_2]^{1/4}$ for runs at one atm is plotted against reciprocal temperature on semilogarithmic paper. Much of the data obtained in the 25 mm tube is not included in Figure 6, since optimum flow rates were not used, and delays were somewhat long[4]. The nonlinearity of

the plot illustrates the fact that the temperature dependence of ignition delay is not of the simple Arrhenius type with a constant activation energy.

Discussion

While the slow oxidation of propane has been the subject of considerable research[5, 6, 7, 8], most of this work has been concerned with reaction rates and product analysis. The induction period prior to the onset of rapid reaction has not been closely scrutinized; indeed, in many instances it has been deliberately altered either by the addition of aldehydes or by treatment of vessel walls. The ignition delay measurements described in this report have been carried out at higher temperatures (525°–740°C) than have been employed in slow oxidation (280°–475°C) studies. Kinetic measurements have not been made in the higher temperature regime since the induction period is followed by explosion in which the reaction proceeds to completion with a considerable temperature rise. Rates are by present methods immeasurably high and analysis of final products cannot be expected to yield information on reaction intermediates and thereby the chain of reactions involved in the explosion.

In considering the events leading to the thermal ignition of propane-oxygen-nitrogen mixtures we must therefore examine the reactions proposed to explain the products in the partial oxidation of propane-oxygen mixtures at the highest temperature for which measurements have been carried out. Satterfield and Wilson[9] suggest a scheme involving some twenty reactions in order to indicate the origin of all reaction products. The propyl radical is a key intermediate, and may react with oxygen in two ways: (1) to form propylene and HO_2, and (2) to form oxygenated organic products. At 375°C, it is suggested that approximately 60 per cent of the propyl radical-oxygen reaction proceeds by the first path; at 475°C this increases to ninety per cent. For simplicity, then, we shall not consider the second mode of reaction to be significant at the higher temperatures at which ignition lag measurements have been made.

In general, kinetic analysis of explosion phenomena has been concerned with the existence or nonexistence of a finite reaction rate (the steady state). Such considerations serve to define the conditions of temperature, pressure, etc., under which explosion may occur; that is to say, the limits for spontaneous inflammation.

The ignition lag on the other hand is a measure of the time required to achieve the unsteady state (explosion). The kinetic scheme adopted must therefore be one in which no steady state solution exists. The following reactions, selected from Satterfield and Wilson[9], can serve to explain, at least qualitatively, the ignition lags of this report.

$$C_3H_8 + O_2 \xrightarrow{k_1} C_3H_7 + HO_2 \qquad \text{(i)}$$

$$C_3H_7 \xrightarrow{k_2} C_2H_4 + CH_3 \qquad \text{(ii)}$$

$$C_3H_7 + O_2 \xrightarrow{k_3} C_3H_6 + HO_2 \qquad \text{(iii)}$$

$$C_3H_8 + HO_2 \xrightarrow{k_4} C_3H_7 + H_2O_2 \qquad \text{(iv)}$$

$$C_3H_8 + CH_3 \xrightarrow{k_5} C_3H_7 + CH_4 \qquad \text{(v)}$$

In this scheme, the initiating reaction is the only chain branching step. The propyl and methyl radicals are highly reactive, so that a steady state in these species is assumed, (that is to say, the rate of production is equal to the rate of destruction). On the other hand, it will be assumed that the HO_2 radical is comparatively long-lived, as suggested by Lewis and von Elbe[10], so that its concentration builds up during the induction period. These considerations lead to the following expressions for the rates of change of propane and HO_2 concentration:

$$-\frac{d[C_3H_8]}{dt} = \left(1 + \frac{k_2}{k_3[O_2]}\right)(k_1[C_3H_8][O_2] + k_4[C_3H_8][HO_2]) \qquad (5)$$

$$\frac{d[HO_2]}{dt} = 2k_1[C_3H_8][O_2] \qquad (6)$$

Equation (6) is easily integrated if we assume that during the preignition period the propane and oxygen concentrations are substantially constant. The expression obtained for HO_2 concentration as a function of time may then be substituted in equation (5), which leads to the relationship:

$$-\frac{1}{[C_3H_8]}\frac{d[C_3H_8]}{dt} = k_1\left(\frac{k_2}{k_3} + [O_2]\right)(1 + 2k_4[C_3H_8]t) \qquad (7)$$

This equation describes the observed lags if it is assumed that $k_4[C_3H_8] \gg 1$ and that ignition occurs when the fractional rate of propane consumption reaches a critical value characteristic for a given temperature and pressure. If this is

so then

$$\left(\frac{k_2}{k_3} + [O_2]\right)[C_3H_8]\,\tau = \text{const} \qquad (8)$$

The first assumption is reasonable since reaction (iv) is an exothermic radical reaction and therefore probably has a large rate constant. The ad hoc postulate that a critical fractional rate of propane consumption is attained at the time of ignition is not so easily justified. However, if the explosion is thermal in origin (that is to say, heat is generated by the slow reaction more quickly than it is dissipated by conduction to the surroundings so that temperature rises, and, with it, reaction rates) we might expect that more propane should be required to prereact in rich mixtures for the following reasons: (1) In richer mixtures, initial reaction of propane to give cracked products (methane and ethylene) will occur more frequently relative to partial oxidation (to propylene and hydrogen peroxide). This may result in less heat generated per molecule of propane consumed. (2) For a given heat evolution, the resultant temperature rise will be lower at higher propane concentrations due to the higher heat capacity and thermal conductivity of rich mixtures.

The dependence of ignition lag on oxygen concentration as given by equation (8) is qualitatively correct if k_2/k_3 is of the order of unity. (E.g., if $k_2/k_3 = 1$ and $[O_2] \cong 0.2$, the variation would be as $[O_2]^{1/6}$.) However, experimentally the effect of oxygen concentration was more pronounced for mixtures of low oxygen-nitrogen ratio (best described by equation (2a)) while equation (8) predicts the opposite.

The variation of ignition lag with temperature should involve principally the energies of activation of reactions (i) and (ii). Reaction (i) is endothermic by roughly 50 kcal, so its activation energy must be at least that large. However, the observed variation of ignition delay with temperature is not compatible with such a high energy of activation, unless nonkinetic factors are playing a dominant role in the temperature effect.

The experiments on the effect of pressure cannot be explained by these reactions alone, for while equation (8) predicts increased delays at lower pressures, experimentally there appears to be a limiting pressure below which ignition will not occur.

Finally, experiments in which the inert gas was varied suggest that the explosion is not primarily thermal in origin, since large changes in thermal conductivity do not cause corresponding changes in ignition delay at atmospheric pressure. (The substitution of helium for nitrogen in the fuel-oxidant-inert mixture probably increases the thermal conductivity three- or fourfold[11].)

Alternatively, the effect of propane and oxygen concentration on ignition delay might be explained in terms of initiation by means of a bimolecular surface reaction between propane and oxygen. If the induction period varies inversely with the initiation rate, then

$$\frac{1}{\tau} \propto \text{initiation rate} = k'\theta_{O_2}\theta_{C_3H_8} \qquad (9)$$

where θ_{O_2} and $\theta_{C_3H_8}$ are the fractions of the surface covered by oxygen and propane respectively, and represent surface concentrations; k' is a constant. For monolayer chemisorption on a homogeneous surface, with oxygen moderately adsorbed, θ_{O_2} is given by

$$\theta_{O_2} = \frac{k''p_{O_2}}{1 + k''p_{O_2}} = \frac{k[O_2]}{1 + k[O_2]} \qquad (10)$$

where p_{O_2} is the partial pressure of oxygen[12]. When the mole-fraction of oxygen is used as a concentration unit then the constant of equation (10) is pressure dependent. If propane is weakly adsorbed, its surface concentration will be proportional to its gas phase partial pressure and to the bare surface $(1 - \theta_{O_2})$.

$$\theta_{C_3H_8} = a(1 - \theta_{O_2})[C_3H_8] = \frac{a[C_3H_8]}{1 + k[O_2]} \qquad (11)$$

Substitution of (10) and (11) into equation (9) yields an expression for the ignition delay:

$$\frac{1}{\tau} \propto \frac{[O_2]\,[C_3H_8]}{(1 + k[O_2])^2} \qquad (12)$$

Note that the dependence of lag on propane and oxygen concentration is as given in equations (1) and (2a) respectively.

However, if a surface reaction is involved, it is surprising that delays at one atmosphere were unaffected by changes in the reaction tube surface and surface-volume ratio. The latter observation might be explained by the fact that while the smaller tube (with a larger surface-volume ratio) gives greater surface concentrations of reactants per unit volume of gas, the smaller tube also offers more surface per unit volume for the

removal of heat or the destruction of chain carriers.

Neither of the suggested mechanisms serves to explain all of the observed ignition delays. However, the experimental results do yield qualitative information as to the reaction processes which lead to ignition. The ignition delay may be characteristic of the time required to build up, via chain branching reactions, a critical concentration of some active intermediate. The existence of low pressure limits which appear to be affected by tube size, and an inert gas effect at low pressures, suggests that the intermediate may be destroyed after diffusion to the walls.

Summary of Results

The variation of spontaneous ignition delays of propane with temperature, pressure and composition has been studied in a flow system. The reactants were mixed in a time much shorter than the ignition lag at the temperature of the reaction chamber. Ignition delays were measured with a pressure recorder.

Ignition lags were found to be:

(1) Inversely proportional to the 0.74–1.0 power of the propane concentration.

(2) Inversely proportional to approximately the 0.25 power of the oxygen concentration.

(3) Increased by decreasing pressure.

(4) Increased by substitution of helium for nitrogen at low pressure, but unchanged when nitrogen was replaced by argon.

(5) Unaffected by changes in tube surface, and by changes in tube size under comparable flow conditions at atmospheric pressure; at reduced pressures delays were longer in a smaller tube.

(6) Decreased by increasing temperature.

Specific reaction mechanisms proposed do not fully explain observed ignition delays. However, the experimental results suggest that the ignition delay is determined by gas phase chain branching reactions, with destruction of chain carriers occurring at the walls.

REFERENCES

1. A. S. T. M. Standards on Petroleum Products and Lubricants, Test D286-30.
2. Mullins, B. P.: Fuel, *32*, 234 (1953).
3. Olsen, D. P.: *Spontaneous Ignition Time for Mixtures of Heptane Vapor in Air.* Yale University Doctoral Dissertation, 1951.
4. Jackson, J. L., and Brokaw, R. S.: Ind. & Eng. Chem., *46*, 2547 (1954).
5. Pease, R. N.: Chem. Rev., *21*, 279 (1937); J. Am. Chem. Soc., *60*, 2244 (1938).
6. Pease, R. N., and Munro, W. P.: J. Am. Chem. Soc., *56*, 2034 (1934).
7. Newitt, D. M., and Thornes, L. S.: J. Chem. Soc., 1656 (1937).
8. Harris, E. J., and Egerton, A. C.: Chem. Rev., *21*, 287 (1937).
9. Satterfield, C. N., and Wilson, R. E.: Division of Industrial Cooperation, M. I. T. Report D. I. C. 6552, April 1953.
10. Lewis, B., and von Elbe, G.: *Combustion, Flame and Explosions of Gases*, p. 154. New York, Academic Press, 1951.
11. Clingman, W. H., Brokaw, R. S., and Pease, R. N.: *Fourth Symposium on Combustion*, pp. 310–313. Baltimore, The Williams & Wilkins Co., 1953.
12. Taylor, Hugh S., and Taylor, H. Austin: *Elementary Physical Chemistry*, p. 443. New York, D. Van Nostrand Co., Inc., 1942.

58

EFFECT OF ATOMIC RADIATION ON THE COMBUSTION OF HYDROCARBON AIR MIXTURES[a]

By ROBERT E. CULLEN and MARTIN E. GLUCKSTEIN

The effect of nuclear radiation on combustion of hydrocarbon-air flames has been experimentally investigated from a phenomenological standpoint. No attempt was made to obtain kinetic data, but it will be shown that the results obtained are consistent with proposed mechanisms for flame propagation and the interaction of radiation and matter. It was demonstrated

[a] This work was performed under grants from the United States Atomic Energy Commission under Contract AT(11-1)-162 and the University of Michigan Memorial Phoenix Project.

that accelerated combustion effectiveness results from a strong source of radiation in the vicinity of the radiation zone.

Introduction

Soon after the discovery, in the early twentieth century, of the nature of the radiation from radioactive material, considerable interest was shown in the effect such radiation would have on various chemical systems. Lind, in 1921, published the first edition of a monograph entitled *The Chemical Effects of Alpha Particles and Electrons* (American Chemical Society Monograph Number 2), in which he discusses theoretical and experimental contributions to this field[1]. In particular, it is shown that gaseous hydrocarbons may be altered by the absorption of energy from radioactive materials.

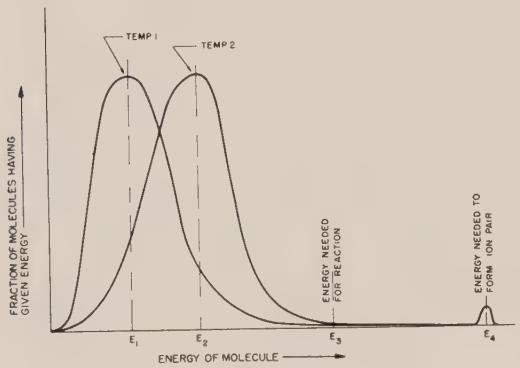

FIG. 1. Energy distribution for system under the influence of nuclear radiation.

The possibility of utilizing radioactive materials to increase reaction rates was not seriously considered until more recent years.

As a result of the operation of this nation's atomic energy program, quantities of radioactive materials, called fission products, accumulated. These isotopes are essentially the ashes resulting from the fission of uranium fuel in nuclear reactors. In an attempt to find uses for these materials, the United States Atomic Energy Commission has sponsored research to survey aspects of fission product utilization.

The possible improvement of power plant operation by the introduction of radioactive sources into the combustion phase is one such possible use. In view of these possible improvements, the effect of beta emitting radioactive sources on Bunsen and drag stabilized flames has been investigated[2, 3, 4].

Theory

The process of the absorption of beta radiation by a medium surrounding the radiation source has been treated from a theoretical standpoint. Spring[5] offers a review of some of the proposed mechanism of these interactions, but calculations necessary to evaluate quantitatively the effect of the electrons on a chemical system are not readily performed. Lind[1] has offered several working equations specifically derived for application to reacting systems, and suitable modifications of these relationships will be employed.

The process of absorption of beta radiation may be described if one knows the energy of the particles and characteristics of the absorbing medium. Complicating factors which prevent an exact description are secondary radiation, reflection and the distribution of the energy of beta radiation.

For particles of average energy of 10^5–10^6 electron volts, attenuation takes place at a rate which is roughly inversely proportional to the density of the medium. As the electron passes through, it causes ionization of the attenuating medium along the electron's path. The resultant ions are formed in pairs and consist of relatively large fragments of the original molecules. The average potential for the formation of such a pair is approximately 33 electron volts[6]. This value is in excess of usual values for activation energies. Existence of the pairs has been confirmed by cloud chamber and similar techniques[5]. As the energy from the incident electrons is absorbed, the overall energy of the system is changed by adding to the original energy spectrum an additional distribution of about 33 electron volts. This is shown schematically in Figure 1. It should be noted that this process does not cause significant alteration in the mean energy.

If E_T is the activation energy, the net effect of the radiation is to increase the number of molecules of energy greater than E_T. It should be noted that some molecules may absorb energy without undergoing ionization.

A simple kinetic model may be devised by considering a reaction rate given by the equation

$$-\frac{dN_A}{dt} = kN_A^{\alpha} \tag{1}$$

where k is determined by the Arrhenius equation

$$k = A \exp(-E_T/RT) \tag{2}$$

and $\exp(-E_T/RT)$ is the fraction of molecules

of energy equal to or greater than E_T[7]. However, for the case being considered an additional fraction of molecules possesses energy greater than E_T by virtue of the radiation absorption.

Let $y(\beta)$ be this additional fraction. The rate constant equation may then be modified to (approximately)

$$k' = A\,[\exp\,(-E_T/RT) + y(\beta)] \qquad (3)$$

The value of $y(\beta)$ depends on source strength, source energy, the average life of the specie formed, absorption factors and geometry. Dividing equation (3) by equation (2), one obtains the ratio of reaction rate constants as

$$k'/k = 1 + y(\beta)\,\exp\,(E_T/RT) \qquad (4)$$

To calculate $y(\beta)$ it is necessary to calculate the number of ion pairs formed. If N is the number of ion pairs formed, then

$$N = \frac{E\beta}{33} \times 3.7 \times 10^{16}\ \text{ion pair/sec} \qquad (5)$$

where E is the source strength in million electron volts, and β the activity in curies. The specific ionization is given by

$$N' = \frac{E\beta}{33R} \times 3.7 \times 10^{16}\ \text{ion pair/sec/cm} \qquad (6)$$

where R is the range of the electron in centimeters.

For a system of principal dimension, L, less than R, with the source located within the boundaries of the system, equation (6) must be modified to account for losses of radiation through the boundaries. A simple system of this type is a hollow cylinder. If electrons are emitted from points in the wall and travel along diameters to opposite points, the ionization induced will be

$$N_i = 3.7 \times 10^{16}\,\frac{E\beta L}{33R}\ \text{ion pair/sec} \qquad (7)$$

Upon reaching the opposite points, the electrons will be either absorbed or reflected. Those which are reflected will go through a similar process after being reflected. The maximum number of times any electron may be reflected is R/L. If F is the fraction of electrons reradiated, the total pair formation for a source of this type is

$$N_T = 3.7 \times 10^{16}\,\frac{E\beta L}{33R}\,S_n \qquad (8)$$

where S_n is the sum of the finite series:

$$1 + F + F^2 + \cdots + F^n, \qquad F < 1$$

and n is the nearest integer less than R/L. The value of L is not a simple function of the physical dimensions of the system, but is an average length which may be approximated from consideration of the spatial distribution of the emitted electrons.

In the event several energies are associated with the particular decay process, it is necessary to evaluate the ionic contribution of each energy separately and then add the individual values. The effect of secondary radiation is evaluated by similar techniques.

The value of $y(\beta)$ for a flow system is obtained from equation (8) by the equation

$$y(\beta) = 2\theta N_T/AM \qquad (9a)$$

or

$$y(\beta) = \frac{2\theta E\beta LS_n}{33AMR} \times 3.7 \times 10^{16} \qquad (9b)$$

where M is the molal flow rate (moles/sec); A is the Avogadro number; θ is the ratio of the average life of an ion to the residence time in the system; and the factor 2 is a proportionality factor for converting ion pairs to molecules. This equation applies to a single step process. For radiation induced chain reactions, $y(\beta)$ must be multiplied by the average chain length. These equations serve as a guide for experimental design and are correct only to orders of magnitude.

The type of reactions induced by radiation are in many respects similar to combustion processes. Ozone has been identified in irradiated oxygen[1] and may be formed by reaction schemes similar to the following:

$$O_2 \xrightarrow{\beta^-} 2O \qquad (a)$$

$$O + O_2 \longrightarrow O_3 \qquad (b)$$

or

$$O_2 \xrightarrow{\beta^-} O_2^* \qquad (c)$$

$$O_2 + O_2^* \longrightarrow O_3 + O \qquad (d)$$

$$O + O_2 \longrightarrow O_3 \qquad (e)$$

Organic fuels are subjected to a series of reactions which include bond splitting, dehydrogenation, and other rearrangements[1].

For a saturated hydrocarbon

$$2RH \xrightarrow{\beta^-} RR + H_2 \qquad (f)$$

$$2R \xrightarrow{\beta^-} R_1 + R_2 \qquad (g)$$

are two possible reactions. In particular for pro-

pane one may have propyl, ethyl and methyl radicals, free hydrogen and charged particles. Unsaturated hydrocarbons are even more reactive under radiation. Combination of the products of

Table 1. Characteristics of Radioactive Isotopes

Isotope	Half life	Energy, million electron volts			Maximum activity, curies
		β^-	β^+	γ	
	hrs				
Cu^{64}*	12.9	.55	.60	1.35	1300
Au^{198}	65	.96	None	.41	2100
Pd^{109}	14	.95	None	None	100

* Cu^{64} served as bond for Au^{198}

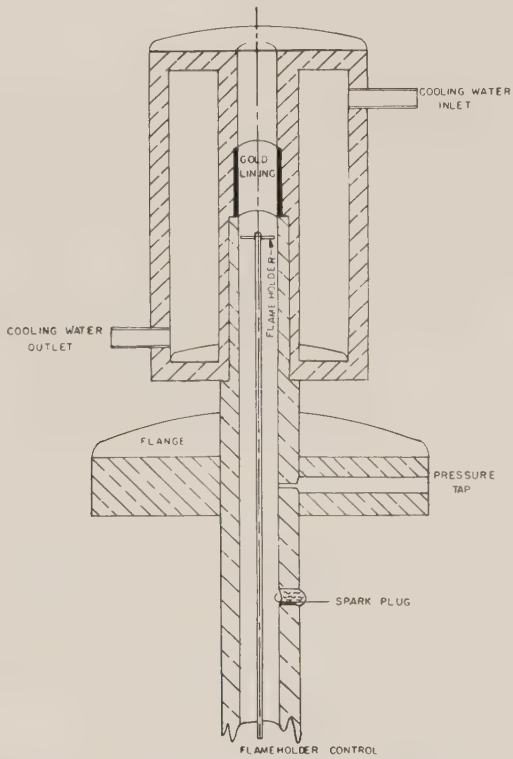

Fig. 2. Schematic diagram of constant area combustor.

reaction (f) and (g) with those of reaction (a) to (e) will give various oxidation products of the hydrocarbons[1].

Examination of equation (4) shows that the radiation induced reactions should be more pronounced in the preflame zone and that the overall effect is to introduce into the reaction volume additional active species.

The isotopes used in these studies were palladium 109, gold 198 and copper 64. Table 1 gives the characteristics of these materials (8).

Equipment

The equipment used in this work consisted of a Bunsen burner, the flame of which could be surrounded by radioactive foil, a radioactive spherical flameholder placed at the exit of a convergent nozzle, and a constant area combustion chamber of circular cross section with a flameholder (Fig. 2), the radioactive material being inserted in the walls.

In the first two series of runs (the Bunsen burner and spherical flameholder) Pd^{109}, at low levels of activity, was the source material. Since this isotope is a pure beta emitter, it was only necessary to use light shielding to protect the investigators. Handling was readily accomplished with tongs and other tools, 3 ft long. A vacuum chamber, fabricated of $\frac{3}{8}$-in. steel, in which the burner was located, provided adequate shielding. For the final series of runs, utilizing the constant area combustor, high activity sources of Cu^{64} and Au^{198} were utilized. Due to the rather high gamma radiation level, it was necessary to design the equipment so that all assembly and data taking operations could be performed remotely. Figure 3 is a line diagram of the instrument and control lines. Approximately 5 ft of water or 30 in. of sand were necessary to provide adequate shielding[b].

The burner tube was attached to the bottom of a 6-ft vertical tank and the tank was filled with water. It was then possible to assemble the burner components under water by means of long tongs.

Additional safety precautions included the installation of a filter in the exhaust line from the plenum chamber, a blow-out diaphragm in tee on the exhaust line and water cooling in the burner head.

The flameholder used was a cross baffle of approximately 30 per cent blockage. Provision was made for the adjustment of the flameholder with respect to the burner exit and source position.

[b] Calculation of shielding requirements were performed by Mr. J. V. Nehemias of the University of Michigan's Fission Products Laboratory, and Mr. A. H. Emmons of the University's Radiological Safety Department. Their assistance in the design of the equipment is gratefully acknowledged.

This adjustment was accomplished by means of a micrometer screw located outside the sandbagged area. Two burner heads, which differed only in their length, were provided. The difference in length of the two heads was the length of the source ($1\frac{3}{16}$ in.). Prior to the isolation of the system, the flameholder was adjusted to a position 3 in. from the exit of the longer head (i.e., at the upper edge of the source). By adjustment of the lead screw it was then possible to vary the flameholder-exit position to any desired value. The diameter of the burner was $\frac{1}{2}$ in. and the source a hollow cylinder fabricated from gold tubing $\frac{1}{2}$ in. in diameter and 0.006 in. thick. Copper was plated on the outside to increase its strength.

Procedure

To obtain data to show possible changes in combustion processes due to radiation, simple experimental techniques were utilized. These consisted of the measurement of flame speeds in the Bunsen burner, blow off velocities from a spherical flameholder, and pressure drop due to combustion in the constant area combustor.

The various burners were ignited by means of a spark discharge from an induction coil. Flow rates were then adjusted to the lowest values for which the flame remained stable and the measurements taken. The flow rates were increased until the flame blew out, with data being recorded as the flow rates increased.

Generally the flow rates, fuel-air ratio, ambient pressure and source activity were recorded. In addition, for the Bunsen flame a photograph was taken, and for the constant area combustor, the pressure drop due to burning was measured.

Results

Comparison of the flame speed and the blow off velocities from a spherical flameholder for propane-air flames showed no significant changes due to radiation at low source intensity. Some of these data are presented in Figures 4 and 5.

In the constant area combustor, the effect of the high levels of radiation tended to increase the pressure drop due to burning as a function of fuel-air ratio above the pressure drop when no radiation was present. These results are shown in Figures 6 through 16. For propane-air these results are expressed in terms of the air specific impulse which is defined as

$$S_a = \frac{F_2}{W_A \phi(M)} \qquad (10)$$

where F_2 is the force on the burned gas, W_A is the air flow rate and $\phi(M)$ is a function of the Mach number of the exit gases. This equation is a

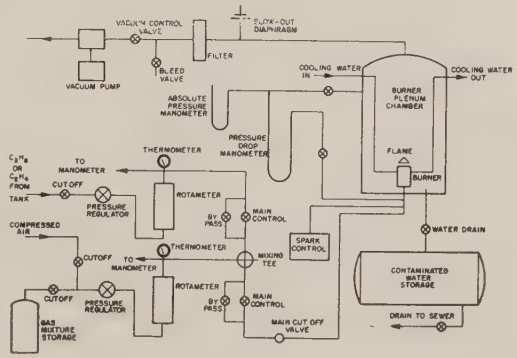

FIG. 3. Line diagram of experimental equipment

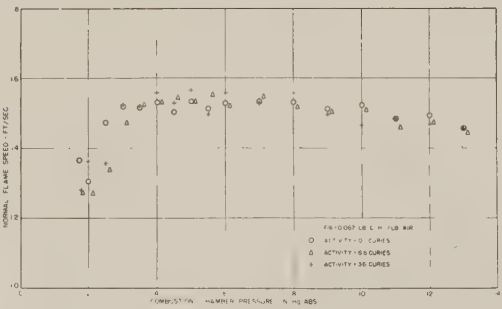
NORMAL FLAME SPEED - FT/SEC
COMBUSTION CHAMBER PRESSURE - IN HG ABS
F/A=0.067 LB C3H8 /LB AIR
ACTIVITY = 0 CURIES
ACTIVITY = 66 CURIES
ACTIVITY = 36 CURIES

FIG. 4. Results for propane-air Bunsen flame

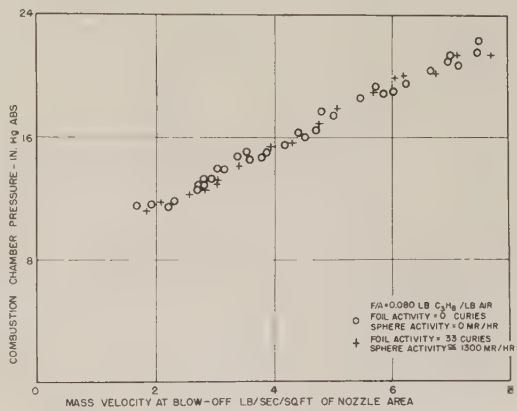
COMBUSTION CHAMBER PRESSURE - IN Hg ABS
MASS VELOCITY AT BLOW-OFF LB/SEC/SQFT OF NOZZLE AREA
F/A=0.080 LB C3H8 /LB AIR
FOIL ACTIVITY = 0 CURIES
SPHERE ACTIVITY = 0 MR/HR
FOIL ACTIVITY = 33 CURIES
SPHERE ACTIVITY = 1300 MR/HR

FIG. 5. Results for spherically stablized propane-air flame.

measure of the overall effectiveness of heat addition to a moving stream[9, 10].

These data (constant area combustor) are for one atm exit pressure and source activities of 2050–8 curies. Mass velocity is a parameter for each curve. The flameholder position for activities

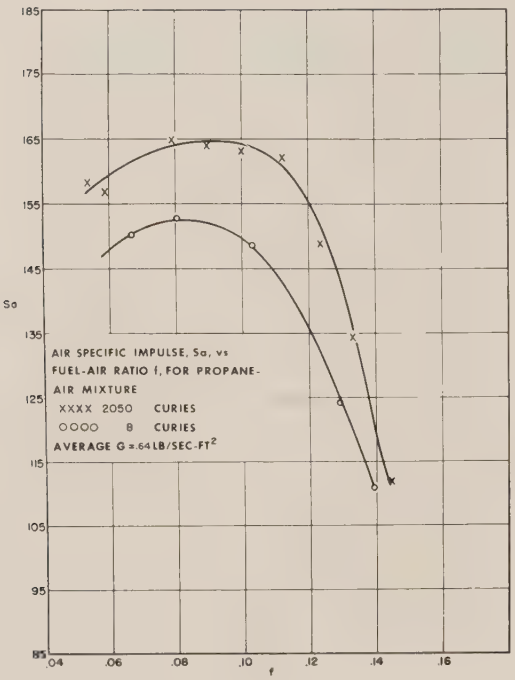

FIG. 6. Results for constant area combustor: propane-air.

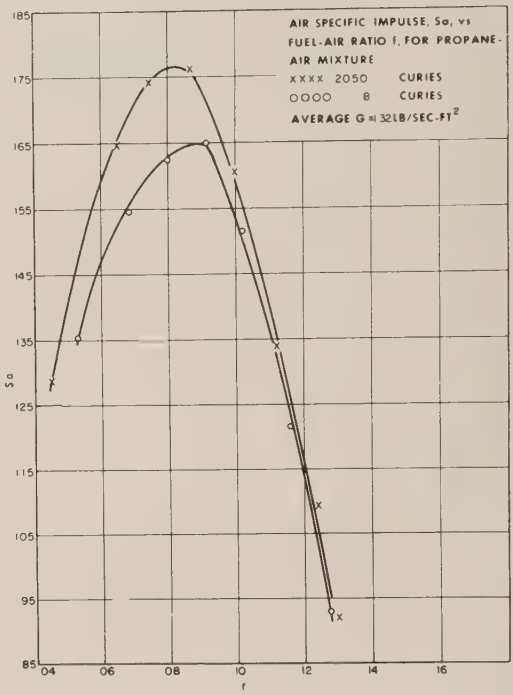

FIG. 8. Results for constant area combustor: propane-air.

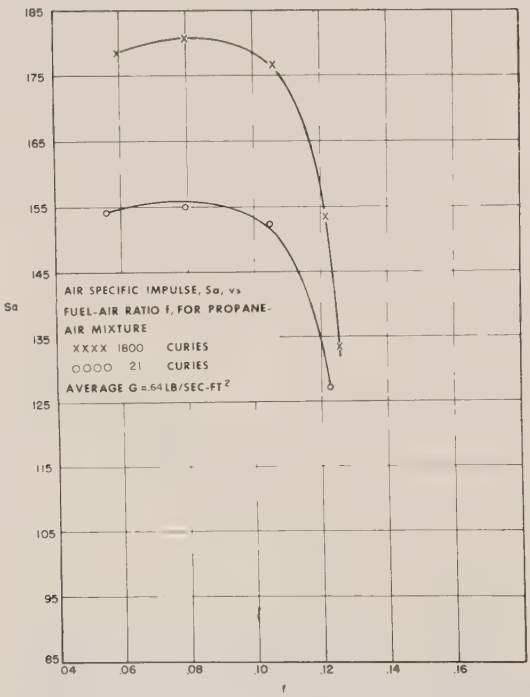

FIG. 7. Results for constant area combustor: propane-air.

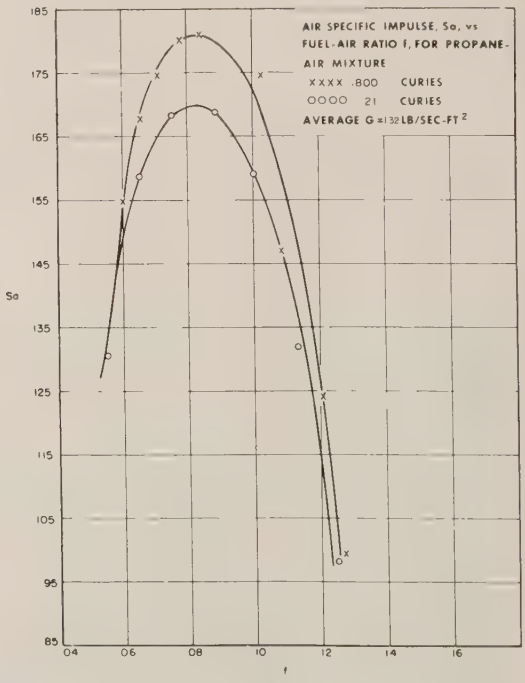

FIG. 9. Results for constant area combustor: propane-air.

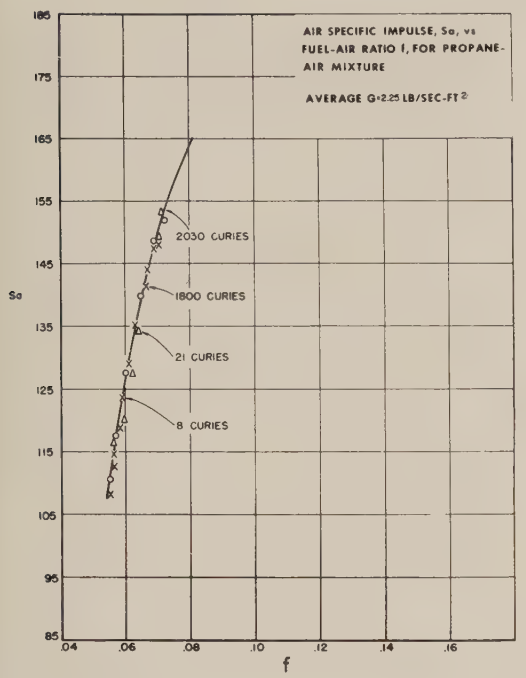

FIG. 10. Results for constant area combustor: propane-air.

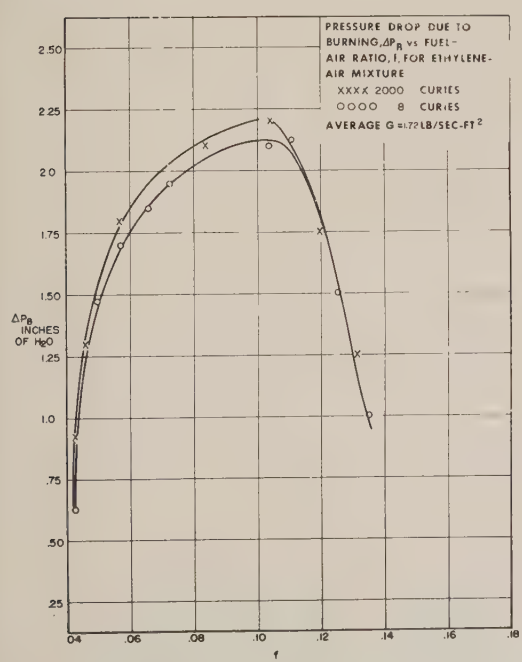

FIG. 11. Results for constant area combustor: ethylene-air.

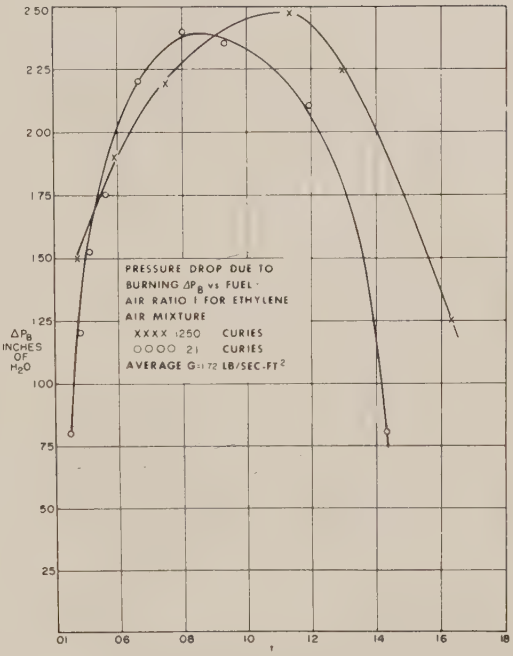

FIG. 12. Results for constant area combustor: ethylene-air.

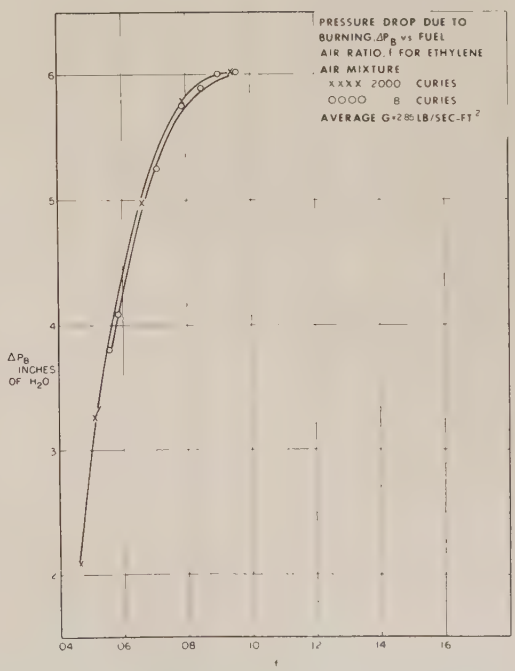

FIG. 13. Results for constant area combustor: ethylene-air.

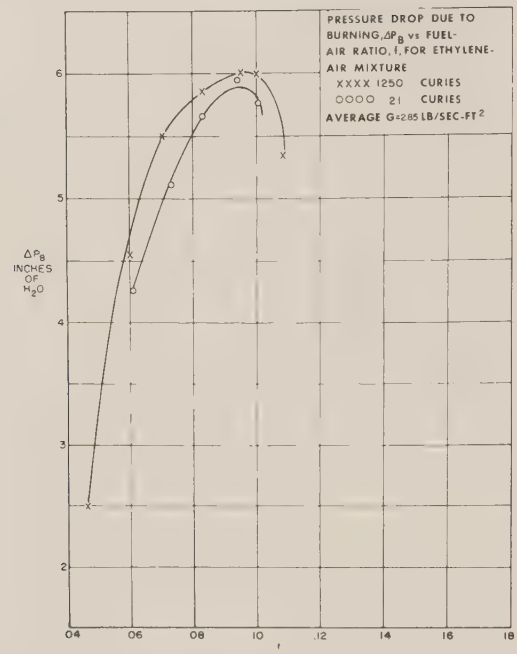
PRESSURE DROP DUE TO BURNING, ΔP_B vs FUEL-AIR RATIO, f, FOR ETHYLENE-AIR MIXTURE
XXXX 1250 CURIES
0000 21 CURIES
AVERAGE G=285 LB/SEC-FT^2
ΔP_B INCHES OF H_2O
f

FIG. 14. Results for constant area combustor: ethylene-air.

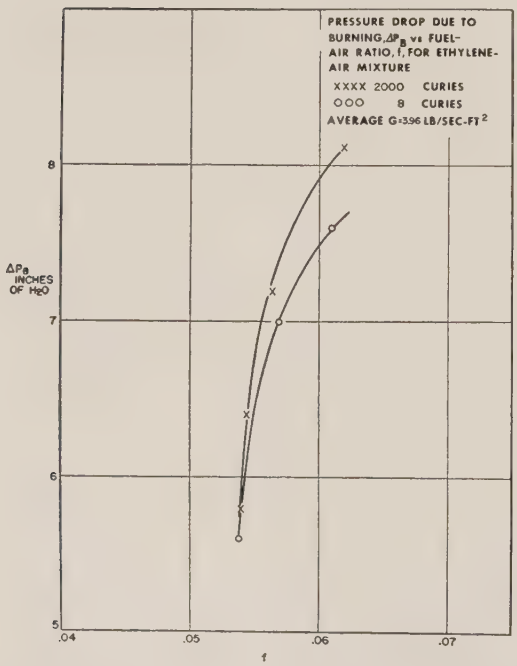
PRESSURE DROP DUE TO BURNING, ΔP_B vs FUEL-AIR RATIO, f, FOR ETHYLENE-AIR MIXTURE
XXXX 2000 CURIES
000 8 CURIES
AVERAGE G=396 LB/SEC-FT^2
ΔP_B INCHES OF H_2O
f

FIG. 15. Results for constant-area combustor: ethylene-air.

of 2050 and 2000 curies was at the downstream end of the source and for 1800 and 1250 curies at the upstream end of the source.

Quantitatively, there appeared to be slight variations in the rich and lean blow-off limits.

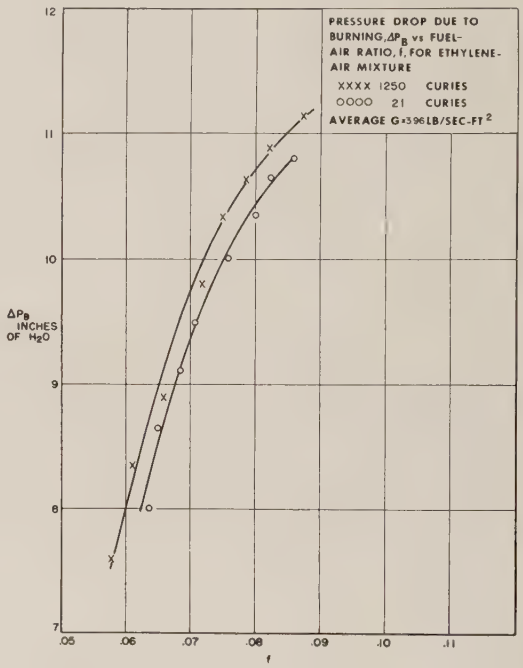
PRESSURE DROP DUE TO BURNING, ΔP_B vs FUEL-AIR RATIO, f, FOR ETHYLENE-AIR MIXTURE
XXXX 1250 CURIES
0000 21 CURIES
AVERAGE G=396 LB/SEC-FT^2
ΔP_B INCHES OF H_2O
f

FIG. 16. Results for constant area combustor: ethylene-air.

TABLE 2

Type	$y(\beta)$	β(curies)	$y(\beta)/\beta$	k'/k
Bunsen flame*.....	10^{-3}	100	10^{-5}	1.001
Spherically stabilized flame.....	10^{-4}	100	10^{-6}	Negligible
Constant area combustor†.....	10^{-1}	2000	10^{-4}	1.1

* For primary radiation only.

† Includes factor for secondary radiation.

No attempts were made to measure ignition limits.

Discussion

The results of this experimental work are readily analyzed from consideration of the ratio of reaction rate constants given by equation (4) and the active fraction given by equation (9a) or (9b).

The molal flow rate for most of this work was in the range of 10^{-3}–10^{-4} mols per second and the value of θ is about 10^{-2} for Bunsen flames and 10^{-1} for the spherically stabilized flame and ram jet type combustor. Substituting these values in equation (9b) gives an order of magnitude of $y(\beta)/\beta$ of 10^{-4}–10^{-6} active molecules per molecule per curie of activity. Since the activity for the spherically stabilized flame and the Bunsen flame never exceeded 100 curies and for the constant area combustor was in excess of 1,000 curies, $y(\beta)$ is therefore in the range 10^{-4}–10^{-1}. These values are tabulated in Table 2. The very low values for the spherically stabilized flame are due to the low value of L/R in equation (9b).

The temperatures of about 500°K $\exp(E_T/RT)$ would have values in the range of 1–10 (i.e., $E_T \cong 1\text{–}10\,K$ cal) (11) and k'/k have values of from 1 to about 2. It is therefore concluded that the radiation causes increased reaction rates in the combustor. This analysis is predicated on the mechanism of reaction remaining fixed. It is possible that the active species introduced may alter the course of the reaction and initiate other reactions. The actual course of the observed effect is more likely to be a combination of increased reaction rates and modified mechanisms.

It is interesting to note that the rate of energy addition into the system due to radiation is very small, being approximately to 10 joules per hour.

Conclusion

Beta radiation will increase the pressure drop due to combustion in a constant area chamber. The data should be considered as applicable only to the experimental systems considered and no quantitative conclusions should be drawn for other systems.

Acknowledgment

Dr. Richard B. Morrison's experience in this field and his assistance greatly facilitated the completion of this work.

The United States Air Force provided an airlift for transporting the radioactive material.

REFERENCES

1. Lind, S. C.: *The Chemical Effects of Alpha Particles and Electrons*, 2nd Ed. New York Chemical Catalog Co., 1928.
2. Brownell, L. E. et al.: Progress Report 3, Engineering Research Institute Project M943, University of Michigan, Ann Arbor, Michigan, 1952.
3. Brownell, L. E. et al.: Progress Report 4, Engineering Research Institute Project M943, University of Michigan, Ann Arbor, Michigan, 1953.
4. Brownell, L. E. et al.: Progress Report 5, Engineering Research Institute Project M943, University of Michigan, Ann Arbor, Michigan, 1953.
5. Spring, K. H.: *Photons and Electrons*. New York, John Wiley, 1950.
6. Pollard, E. C., and Davidson, W. L.: *Applied Nuclear Physics*, New York, John Wiley, 1951.
7. Kennard, E. H.: *Kinetic Theory of Gases*. New York, McGraw-Hill Book Co., 1938.
8. Nuclear Data. National Bureau of Standards, Circular 499.
9. Rudnick, P.: J. Aeronautical Sci., *14*, 540 (1947).
10. Sellars, J., and Davis, T.: JHU/APL, Project Bumblebee, Report 32, March, 1946.
11. Steacie, E. W. R.: *Atomic and Free Radical Reactions*, New York, Reinhold Publishing Company, 1946.

59

THE COMBINATION OF HYDROGEN ISOTOPES AND OXYGEN INITIATED BY TRITIUM BETA-RADIATION[a]

By LEON M. DORFMAN

Introduction

The combination of hydrogen and oxygen under various types of initiation and activation to form water and, under certain conditions, hydrogen peroxide, has been the subject of very extensive investigations over a period of years. The mechanism of the thermal reaction, which has received the greatest part of this attention, is reasonably well established[1, 2]. A considerable amount of work has been done on the synthesis of water in various types of electric discharge[3, 4] and reaction rates have also been determined for the combination of hydrogen and oxygen induced by alpha particles[5]. In an investigation of this latter effect Lind[5] found a water yield of 3.92 molecules per ion-pair. Marshall[4] in his work on the hydrogen-oxygen combination under the effect of cathode rays reported yields similar to to those of Lind. He found, also, that in a flow system substantial amounts of hydrogen peroxide were obtained. Photochemical investigations[6] have been made both by absorption in the Schumann region and by mercury photosensitization. In the latter type of studies, quantum yields on the order of 2 have been obtained.

The isotopic hydrogen-oxygen system consisting of tritium and oxygen presents a rather interesting study since it has a self-contained source of ionizing radiation, the nuclear beta-particles from the tritium decay, and will therefore undergo reaction at room temperature in the absence of any external excitation energy. The intensity of ionizing radiation is readily determinable from the tritium concentration since the radioactive half-life and the average energy of the beta-spectrum are accurately known. In order to determine reaction yields, therefore, the rate of the beta-particle induced reaction

$$HT + \tfrac{1}{2}O_2 = HTO \qquad (1)$$

has been investigated at 25°C, in the absence of mercury vapor, by using a sensitive glass Bourdon gauge as the manometric device.

[a] The work reported here was carried out under Contract No. W-31-109 Eng. 52 with the Atomic Energy Commission.

Experimental Methods

Pure reactants were obtained in the following manner: Oxygen was prepared by thermally decomposing potassium permanganate which had previously been warmed and degassed repeatedly in the vacuum system. The oxygen liberated was passed through a coil immersed in liquid nitrogen then into a storage bulb closed off by a Fugassi valve. Hydrogen was purified by sorption, pumping and subsequent desorption on a uranium bed. The hydrogen was stored in a Pyrex bulb connected to a Fugassi valve. The tritium was stored on a uranium bed and desorbed as required for each run. Krypton gas, used in one run, was degassed for a short time at −195°C and then pumped into the reaction cell through a trap immersed in a dry ice-acetone bath.

The H_2-T_2 mixtures used in the runs were analyzed on the General Electric analytical mass spectrometer in use here. Previous calibrations[7] had shown that the two isotopes have equal mass spectrometric sensitivities.

Preliminary runs using a mercury manometer to follow the course of the reaction showed clearly that there was a substantial oxidation of the mercury. Material balance, according to equation (1) could not be obtained. All subsequent runs were therefore carried out in a mercury-free reaction cell. To this end a modified glass Bourdon gauge with a tilting mirror attachment was used to follow the pressure drop during the run. The arrangement employed a lamp and translucent scale at a distance of 50 from the tilting mirror. The Bourdon gauge with reaction vessel attached is shown in Figure 1. The tilting mirror M is suspended in a glass stirrup T and has a connection to the tip of the spoon gauge S, by means of the glass hook H. W is a plane window and J a ground glass joint. In the event of breakage of the spoon a replacement could be made without removing the whole assembly from the hot laboratory.

Reproducible calibrations showed a gauge sensitivity of 27.9 mm scale deflection per mm pressure differential. The response was linear over a pressure difference of at least 10 mm, and the

gauge could therefore be used either as a direct reading or a null instrument. The outside envelope of the Bourdon gauge was connected to a mercury bulb for sensitive pressure adjustment, and to a mercury manometer on which the pressure was read with a cathetometer. The inside of the gauge was connected to the reaction cell C.

The reaction vessel was a spherical Pyrex bulb to which was connected a very small U-tube for freezing out the water product at the end of a run. The actual bulb volume was 212 cc, the total reaction volume 248 cc. The reaction cell was closed by a 2 mm vacuum stopcock, V, lubricated with Apiezon-N grease. The outlet arm of this stopcock was connected to a U-tube and hence to the vacuum system. This outside U-tube was kept in a dry ice-acetone bath to remove mercury vapour from the cell during degassing and to prevent its reentry during filling of the cell. At no time during the series of eleven runs was there any discoloration or deposit on the walls of the cell, which would have resulted from oxidation of the mercury.

The reactants were mixed in a separate bulb, transferred to the reaction cell by means of a Toepler pump and the pressure readings were started. The reaction cell was immersed in a water bath, which although not thermostated, maintained a temperature of 25.0 ± 2.0°C. Precise temperature readings, using a thermometer with 0.02°C graduations, were taken at the time of each pressure reading. The pressure was read intermittently for a period of 20–40 hr over a total pressure change of at least 3 mm and in no case more than 8 mm. The pressure of the water product was thus always below its equilibrium vapor pressure to ensure that the tritium would remain in the gas phase.

If, at the end of a run, material balance measurements were desired the condensible product was frozen inside the cell using liquid nitrogen, and the remaining tritium-oxygen mixture removed. The pressure of condensible product could then be read. The tritium-oxygen mixture, and later the water product, were processed over a magnesium bed at 600°C to remove the oxygen and to permit the tritium to be taken up again on a uranium bed.

In the single run which contained krypton, the krypton was frozen in the cell at −195°C and the reactant gases were then added in the normal manner to start the run.

Results and Discussion

A series of eleven runs was carried out involving varying amounts of the two hydrogen isotopes and oxygen. To avoid any confusion in nomenclature the normal stable isotope will be referred to as protium, and a mixture of the two isotopes, protium and tritium, will be referred to as hydrogen.

The tritium pressure covered a range of 30 to 104 mm, the oxygen pressure ranged from 69 to 218 mm. The mole fraction of protium in the hydrogen reactant ranged from 0.055, the purest tritium used, to 0.831. The details of these experimental conditions are listed in Table 1. The results of material balance measurements for six of the runs are listed in column 5. They show that the overall reaction may, indeed, be almost completely represented by equation (1). If water is the only condensible product, complete material balance in equation (1) will be represented by $P_w/2\Delta P = 1$. This ratio attains values as high as 0.97 and 0.98, indicating that if any hydrogen peroxide is formed it must, in the static system involved here, have only a transitory existence, ultimately amounting to less than 2 to 3 per cent of the condensible product.

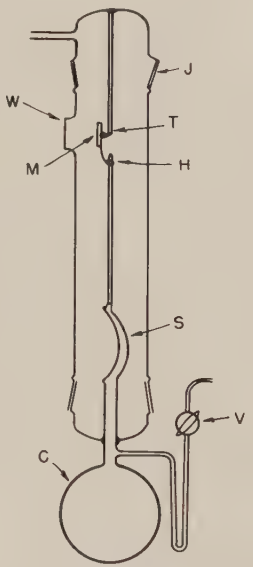

FIG. 1. Bourdon gauge

The rate curves for two of the runs are shown in Figure 2 in which the pressure, on a greatly expanded scale, is plotted against the time in minutes. It may be seen that the rate is not independ-

ent of time, but shows a slight continual decrease as the reaction proceeds. The most definitive rate to be used in a correlation of the data is the initial rate, obtained from the slope of the rate

TABLE 1

Run no.	Pressure of reactants (mm)			Material balance $P_w/2\Delta P$	$\left(-\frac{dP}{dt}\right)_{t=0}$	$k = \frac{R_0}{C_{T_2}(1+0.3m_H)}$
	Tritium	Protium	Oxygen			
					$mm/min \times 10^3$	$min^{-1} \times 10^4$
7	104.4	7.4	69.4	0.94	6.16	1.16
1	95.8	16.9	115.5	0.97	6.57	1.31
2	92.6	10.5	218.3	0.97	5.03	1.06
8	73.8	4.4	138.0	0.96	4.53	1.21
10*	56.9	3.3	93.7	—	2.90	1.00
9	45.2	127.3	99.9	—	3.26	1.18
4	42.2	16.4	106.8	0.98	2.62	1.14
11	39.8	195.9	68.9	—	2.80	1.13
6	37.5	72.2	90.2	—	2.94	1.31
5	32.4	82.1	103.0	—	2.12	1.08
3	30.2	18.5	184.0	0.96	2.24	1.30
Mean*						1.19

* Run 10 contains, in addition to the reactants shown, krypton at a pressure of 85.6 mm. It has been omitted in averaging the values for k.

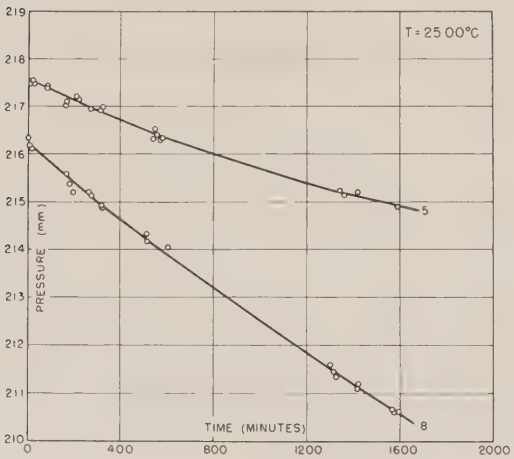

FIG. 2. Rate curves for runs No. 5 and No. 8

curves at the ordinate axis. These initial slopes have been calculated for each run by fitting the third degree polynomial:

$$y = a + bx + cx^2 + dx^3 \qquad (2)$$

to each set of points. The limiting slope was obtained as the coefficient of the first degree term. These calculations were carried out by the machine calculations group. The results are listed in column 6 of Table 1, which shows the initial rate of pressure decrease in mm/min. The initial reaction rate, in terms of hydrogen disappearance, or water formation, will be twice the rate of pressure decrease.

The intensity of beta-radiation may be calculated directly from the tritium concentration. The tritium beta-spectrum has an end-point energy of 18 kev[8, 9] and an average energy of 5.69 kev[10]. The range [11] for these nuclear beta-particles is 0.7 mgm/cm^2. From the results of a recent determination[12] of the absorption curves for tritium beta-particles in hydrogen and oxygen it can be shown that in the present investigation, with a reaction cell 73 mm in diameter, the gas density is sufficiently high in all runs so that practically all the beta-particle energy is absorbed in the gas phase. For the series of runs shown in Table 1, therefore, the absorbed beta-intensity is proportional to the tritium pressure.

It may be seen from the data that the reaction rate increases with increasing tritium pressure, or, in other words with increasing intensity of the initiating beta-radiation. It can be shown that the initial rate is directly proportional to the tritium pressure. There is, however, a small secondary effect which must be taken into account in this correlation. The reaction rate shows a slight dependence on the isotopic composition of the hydrogen reactant, tending to rise with increase in the mole fraction of protium. This may be seen from Figure 3 in which the initial rate divided by the tritium pressure is plotted against the mole fraction of protium in the hydrogen. The ratio on the ordinate is proportional to the initial ion-pair yield. As an approximation this isotope effect has been represented as a linear trend. Evidence of such an effect was obtained in the preliminary experiments in which mass spectrometric analyses showed an isotopic fractionation in the reaction, with protium concentrating in the water product.

The initial reaction rate, for the conditions of this investigation, may be represented by the equation:

$$R_0 = kC_{T_2}(1 + bm_H) \qquad (3)$$

where R_0 is the initial reaction rate, with units determined by the units in which C_{T_2} is expressed, C_{T_2} is the tritium concentration in m/l or other absolute concentration units, k is the rate con-

stant in min^{-1}, b, the isotope effect correction, has the value 0.3, and m_H is the mole fraction of protium in the hydrogen reactant.

The validity of equation (3) may be seen from Figure 4, in which $R_0/(1 + 0.3\ m_H)$ is plotted against the tritium pressure. A straight line through the origin fits the data reasonably well over a 3½-fold variation in tritium pressure. The values of k for each run are listed in column 7 of Table 1; k has a mean value of 1.19×10^{-4} min^{-1}, with an average deviation from the mean of 0.076 or 6.4 per cent.

Since the initial rate is directly proportional to the tritium pressure, and hence to the absorbed beta-energy, the initial ion-pair yield $(M/N)_0$, for hydrogen disappearance will be independent of the tritium pressure. On the basis of an energy requirement[13] of 33 ev per ion-pair in the reactant mixture equation (3) gives an initial yield of $(M/N)_0^T = 3.25$ molecules/ion-pair for the reaction of pure tritium with oxygen. On the basis of the observed isotope effect the initial yield for the beta-particle induced reaction of pure protium with oxygen is $(M/N)_0^H = 4.2$ molecules/ion-pair. This latter value compares very closely with the value 3.92 obtained by Lind[5] for the alpha-particle induced reaction. Lind's value is obtained directly from the measurement of a finite pressure change, and may be expected to be somewhat lower than the initial yield. The experimental yield values above correspond to G values of 9.8 and 12.7 molecules/100 ev respectively.

An extensive discussion of the reaction mechanism does not seem to be warranted, since it must be stated that examination of a number of mechanisms fails to meet the test of uniqueness. Several different reaction schemes lead to a rate equation of the form $R = f$ (intensity), with R independent of the reactant pressures as long as the total pressure is high enough for complete absorption of the beta-radiation. Several significant factors pertaining to mechanism may however be pointed out.

It is clear from the values for the ion-pair yield that the reaction involves very short chains, but that branched chains do not occur. This is probably due, as in the case of the thermal reaction, to the fact that the reaction:

$$H + O_2 = OH + O \qquad (4)$$

does not occur at room temperature, having an activation energy[14] of 17 kcal. in the case of protium. The fate of the hydrogen atoms is then:

$$H + O_2 = HO_2 \qquad (5)$$

Although little or no hydrogen peroxide appears in the product, it must be formed in the reaction, subsequently disappearing by reaction with atoms and radicals. This conclusion is a necessary consequence of the requirement for a chain terminat-

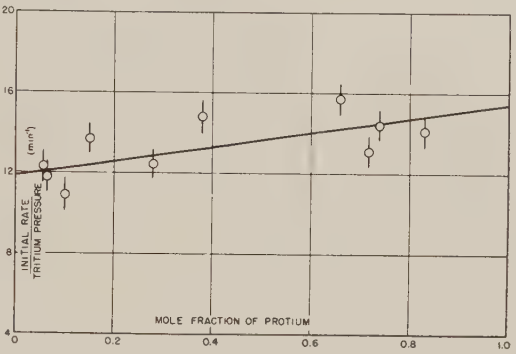

FIG. 3. Dependence of rate on the isotopic composition of the hydrogen. Temperature 25°C. A quantity proportional to the yield is plotted against the mole fraction of protium.

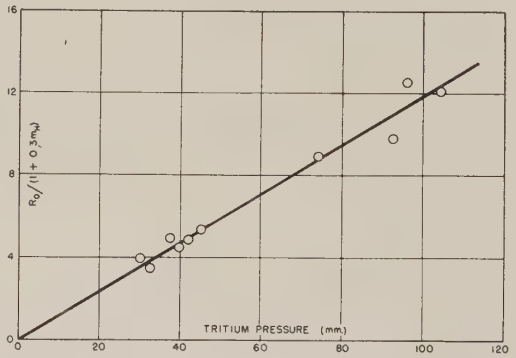

FIG. 4. Plot of equation (3). Temperature 25°C

ing step of the type:

$$HO_2 + HO_2 = H_2O_2 + O_2 \qquad (6)$$

Chain breaking steps which re-form reactants, for example:

$$H + H = H_2 \qquad (7)$$

lead to a rate equation of the form $R = f(I_0)^{1/2} + f'(I_0)$ where I_0 is the beta-intensity, and are therefore excluded.

A kinetic analysis of the data will not differentiate between the role of oxygen atoms or ozone in the reaction with hydrogen molecules. The possible role of excited ozone molecules is suggested

in view of the high energy of the initiating radiation. And finally, the occurrence of an efficient energy transfer process is suggested by the fact that the presence of krypton seems to have little or no effect on the yield. The krypton would however, markedly affect the primary absorption process.

Acknowledgment

The author is indebted to Miss C. J. Hibbert and personnel of the Machine Calculations Unit and to Dr. W. S. Horton of the Chemistry and Chemical Engineering Section for their assistance in the curve-fitting computations.

REFERENCES

1. von Elbe, G., and Lewis, B.: J. Chem. Phys., *10*, 366 (1942).
2. Lewis, B., and von Elbe, G.: *Third Symposium on Combustion, Flame and Explosion Phenomena*, p. 484. Baltimore, The Williams & Wilkins Co., 1949.
3. Kirkby, P. J.: Proc. Roy. Soc., *A85*, 151 (1911).
4. Marshall, A. L.: J. Am. Chem. Soc., *50*, 3197 (1928).
5. Lind, S. C.: J. Am. Chem. Soc., *41*, 531 (1919).
6. Noyes, Jr., W. A., and Leighton, P. A.: *The Photochemistry of Gases*, p. 236 f and p. 250 f. New York, Reinhold Publishing Corp., 1941.
7. Mattraw, H. C., Pachucki, C. F., and Dorfman, L. M.: J. Chem. Phys., *20*, 926 (1952).
8. Curran, S. C., Angus, J., and Cockroft, A. L.: Phil. Mag., *40*, 53 (1949).
9. Hanna, G. C., and Pontecorvo, B.: Phys. Rev., *75*, 983 (1949).
10. Jenks, G. H., Gohrmley, J. A., and Sweeton, F. H.: Phys. Rev., *75*, 701 (1949).
11. Glendenin, L. E.: Nucleonics, *2* (No. 1), 12 (1948).
12. Dorfman, L. M.: Phys. Rev., *95*, 393 (1954).
13. Valentine, J. M., and Curran, S. C.: Phil. Mag., *43*, 964 (1952).
14. Lewis, B. and von Elbe, G.: *Combustion, Flames and Explosions of Gases*, p. 28. New York, Academic Press Inc., 1951.

60

STABILIZATION AND TEMPERATURE MEASUREMENT OF FLAT COOL FLAMES[a]

By ROY J. FORESTI

Introduction

Thorough comprehension of the formation, stabilization, and mechanism of cool flames should be of great help in understanding the analogous properties of the higher temperature reactions. Indeed, it seems likely now that cool flames might play an important role in the initiation and propagation of hot flames. It has already been shown[1] that cool flames occur in the cylinders of internal combustion engines, and numerous investigators have associated this with engine knock.

Most of the investigators in the past have studied this phenomenon in a static type of system. This, in general, tends to make measurements and observation difficult as well as inaccurate due to wall effect. Maccormac and Townend[2] described a technique for stabilizing cool flames in conical quartz tubes, which, although an improvement over the static type of system, still had many of its inherent disadvantages. Powling[3] described a burner tube that would produce a flat, horizontal, hot flame in a vertically flowing gas stream and mentioned that cool flames had also been produced. It was felt that a system such as this would be ideally suited to cool flame studies, since it would permit observation and measurement of a stationary phenomenon. Accordingly, a burner similar to that of Powling[3] was constructed and modified in such a manner that low-temperature flames could be stabilized. Preliminary studies have been carried out on this burner in which the requirements for stabilization were observed, temperature measurements through the flame recorded, and several gas samples collected and analyzed.

[a] This research is a part of the work by the Bureau of Mines on Project No. NA onr 25-47, NR 098 117, supported by the Office of Naval Research, through Project SQUID.

Apparatus

The burner used in this work is shown in Figure 1. This burner is essentially the same as that used by Powling[3] but with some modification. The cylindrical burner tube was packed with two plugs of rolled, corrugated, 0.003-in, chrome-plated brass strips with a stainless steel, 200-mesh screen between them. Since the burner tube was so short, it was necessary to insert the screen in order to make the velocity profile uniform. The end of the $\frac{3}{8}$-in entry tube was plugged, and small holes were drilled near the end around its periphery to distribute better the gas flow in the burner tube. A resistance wire wound around the top portion of the burner for a distance of approximately 1 cm permitted the burner tube and grid to be heated to temperatures as high as 300°C. Another single loop of resistance wire rested on the tip of the burner tube and was held in position by several small dots of refractory cement. This wire was so positioned that the reactant gases leaving the burner tube contacted the inner edge of the hot wire and were ignited by it.

The entire burner tube was enclosed by a square brass jacket as shown. This eliminated the disturbing influence of room air currents. Two Pyrex plate-glass windows permitted undistorted visual and photographic observation. The $\frac{3}{8}$-in tube was held in the base of the jacket by a collet-type clamp which permitted the burner tube to be moved up or down in the jacket. A 100-mesh brass screen on the top of the jacket kept out room air currents and also helped to stabilize the secondary flame.

The diethyl ether used was of 99.98 per cent purity by the manufacturer's analysis. The ether flowed as a liquid through a small rotameter, then to the throat of a small venturi mounted beneath the burner tube. The ether was vaporized in the venturi and passed directly into the burner tube. The air was dried by passing it through anhydrous magnesium perchlorate and was metered by means of a rotameter.

The thermocouple used to measure temperature in the flame reaction zone was made of platinum and platinum-10 per cent rhodium wire 0.001 in in diameter. This wire was mounted on platinum and platinum-10 per cent rhodium prongs in such a manner that only the wire was in the flowing gas stream and at least 1 cm of the wire on either side of the junction was in a constant-temperature zone. The thermocouple wire was covered with N.B.S. A-418 ceramic coating to eliminate catalytic effects on the surface of the wire. The thermocouple supporting prongs were connected to a traversing mechanism which permitted graduated movement of the junction in both vertical and horizontal positions. Thermocouple temperatures were read on a self-balancing potentiometer. This entire temperature-measuring system was then calibrated against a standardized thermocouple connected to a precision potentiometer.

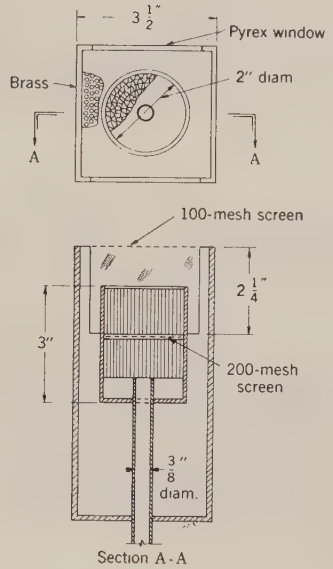

FIG. 1. Cool-flame burner

Experiments

Since most of the cool-flame data available in the literature were obtained for diethyl ether, this fuel was selected as the first to be used in studying the characteristics of the burner. The ether was vaporized directly beneath the burner tube, and considerable turbulence was created in the bottom of the tube to create a uniform fuel-air mixture. All studies were carried out at atmospheric pressure.

To start a cool flame, a very rich ether-air mixture was passed through the burner, and the resistance wire igniter on the rim of the burner was heated by an electric current. If the ether-air mixture were correct, a cool flame was formed having a very low light intensity. As the mixture was made leaner, a secondary flame was formed above the cool flame and the light intensity of the cool flame increased slightly. Figure 2 is a photo-

graph of a horizontal cool and secondary flame stabilized in a vertical flowing gas stream. The thin lower flame is the cool flame and has two

FIG. 2. Cool and secondary flames in vertical gas flow.

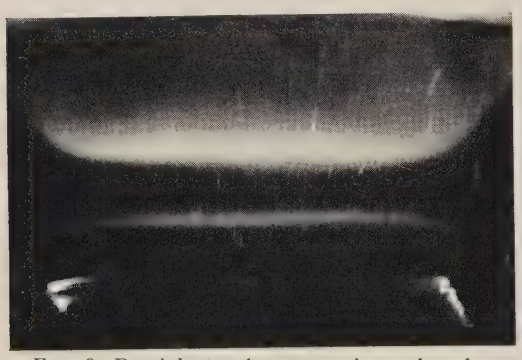

FIG. 3. Particle track pattern in cool and secondary flames.

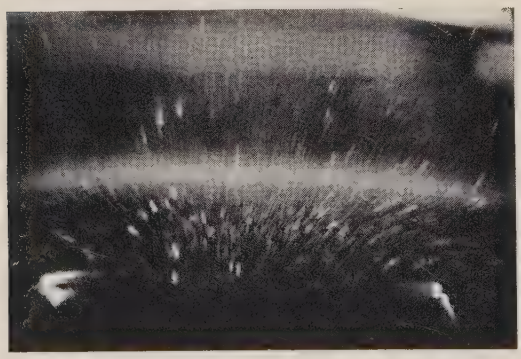

FIG. 4. Particle track pattern in coalesced cool and secondary flames.

faint, curved sections on the sides which nearly touch the tip of the burner tube. Above the cool flame is the secondary flame. Its reaction zone is thicker and its light intensity greater than those of the cool flame. The region of low light intensity extends up to the stabilizer screen on top of the jacket surrounding the burner. The path of gases through such a two-stage flame is clearly shown by the particle-track patterns in Figure 3. Upon further decrease of fuel-air ratio, the secondary flame moved closer to the primary cool flame and finally coalesced with it. When the two flames coalesced, the intense, white, luminous radiation from carbon particles was very pronounced. Figure 4 is a photograph of particle tracks through a coalesced cool and secondary flame just before luminous carbon particles appeared. The divergence of the gas stream preceding the flame front is due to the higher pressure differential, which in turn is due to the increased temperature gradient across the flame front. By making the mixture still leaner, the flame became cellular, with the number of cells inversely proportional to the fuel concentration. As the number of cells increased, the burning velocity also increased to such an extent that the flame flashed back in the burner tube.

Using ether as a fuel, it was not necessary to maintain the ignition wire at a high temperature after the flame had been stabilized for a period of time. Enough heat was transferred back to the burner rim from the flame to ignite the emerging gases.

Stabilized cool flames were also produced in *n*-heptane-air mixtures and *n*-hexane-air mixtures under the same conditions as the ether flames, except that it was necessary to preheat the reactants before they emerged from the burner tip. This was accomplished by means of the resistance wire wound around the top portion of the burner tube. The amount of preheating depended on the fuel. *n*-Heptane had to be preheated to approximately 200°C, while *n*-hexane had to be heated to 250°C. It was not possible to preheat the gases to a higher temperature, so it was not determined whether or not cool flames could be stabilized in this manner using *n*-pentane or *n*-butane.

The appearance of the hydrocarbon flames was very similar to that of the ether flames, the only difference being that the secondary flames of hydrocarbon fuels were very bright green along the edge. The ether flames were always intensely blue, except for the white carbon particle emission described before.

Stabilized flat cool flames were produced in ether mixtures of 28–44 per cent ether flowing at a rate of ca. 10 cm/sec. Cool flames were produced in richer mixtures but were not flat or stable. Two-stage flames, that is, cool plus secondary

flames were produced in mixtures of 13 to 28 per cent ether flowing at 7 to 13 cm/sec. Cellular and coalesced flames were produced in mixtures of 7 to 13 per cent ether and flow rates of 11 to 16 cm/sec.

Only a few preliminary sample analyses have been made, but since they do indicate a trend, they will be presented here. Samples from the various regions of the reaction zone were drawn at sonic velocities through a quartz probe 0.005 in in diameter at the tip. This probe entered the flame from the side of the burner, so that it did not pierce either of the flames. As a result of this, the disturbance to the flames was kept at a minimum. The samples were collected at 10 mm Hg pressure in 100-ml containers, which were first evacuated to less than 2 μ pressure at 200°C. These containers were then taken to the mass spectograph and their contents analyzed.

Table 1 lists the mol percentages of three samples taken at different positions in a two-stage ether-air flame. Sample 1 was taken immediately preceding the visible flame front of the cool flame and consists mainly of unreacted ether and air, plus methyl alcohol and very small quantities of hydrogen and water vapor. The second sample was taken from between the cool and secondary flames and shows evidence of considerable reaction. The third sample was taken from above the secondary flame. At this point, practically all of the reactants had been consumed, and most of the products were the result of pyrolysis reactions.

Similar analyses were carried out using *n*-heptane as a fuel in place of ether. Analysis of gases preceding and immediately following the cool flame showed only air and *n*-heptane. A sample taken from the secondary flame showed only pyrolysis products and a very small quantity of CO_2. However, these samples were taken following the particle-track measurement, and it was found later that some of the TiO_2 particles were still in the system. Since the oxygen-nitrogen ratio in all of the samples was much lower than in the entering air, it may be that the TiO_2 adsorbed the oxygenated compounds.

The flame-temperature profiles were obtained by stabilizing a flame on the burner tube, then passing the thermocouple vertically through the flame front and reading the temperatures at measured distances from the rim. Figure 5 shows the profiles obtained from the various types of flames mentioned earlier. Curve A is the profile for a cool and secondary flame. As the gas emerges from the burner tip, the temperature remains constant for a distance. As the gas approaches the flame front, its temperature is slowly raised by the conduction of heat upstream and the heat released as a result of the reaction. In the region of the visible cool flame, there is a very rapid rise in temperature, followed by a distance of relatively constant temperature at approximately 520°C. There is no visible emission in this region. There is another sharp rise in temperature in the region of the visible secondary flame; however, the slope is not so great as in the case of the cool flame. Curves B, C, and D were obtained from flames of successively lower fuel to air ratios. It will be noted that all of the curves exhibit the same general trend, but as the reactants become leaner, the two flames move closer to one another and the secondary flame temperature increases. When they coalesce, the luminosity increases; and finally, when the fuel concentration is further decreased, the white emission of carbon is visible. This occurs at a secondary flame temperature of 1000°C.

Table 1. Gas Composition at Three Positions Relative to Ether-Air Cool and Secondary Flames

Compound	Initial mixture	1	2	3
Diethyl ether	14.7	12.8	7.8	0.1
Acetaldehyde		.6	6.0	1.2
Methyl alcohol		5.5	5.1	.6
O_2	17.9	13.8	8.0	1.0
N_2	66.5	65.9	64.9	48.8
Argon	.9	.8	.7	.6
H_2		.4	2.0	8.3
H_2O		.2	2.6	7.5
CO			2.2	17.7
CO_2				1.0
Ethane of formaldehyde			.8	1.7
Methane				6.5
Ethylene				4.8

Figure 6 shows the effect of the preflame temperature of the reactant gases. These flames were produced in a 13.2-per cent ether-air mixture flowing at a rate of 16.5 cm/sec, but in each case the reactant gases were preheated to a different temperature. It will be noted that the distance between the two flames (or secondary induction period) increases with preflame gas temperature; however, neither the cool flame nor the secondary flame temperatures are affected. The secondary flame temperature might possibly be controlled

by the stabilizing grid above it; however, in light of the curves of Figure 5 it seems unlikely that it would hold the secondary flame temperature

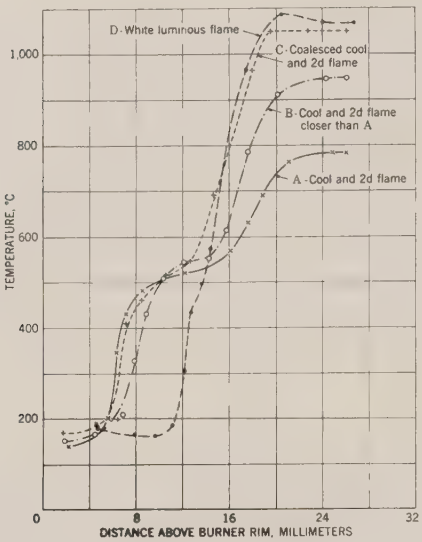

FIG. 5. Flame temperature distribution at various ether-air ratios.

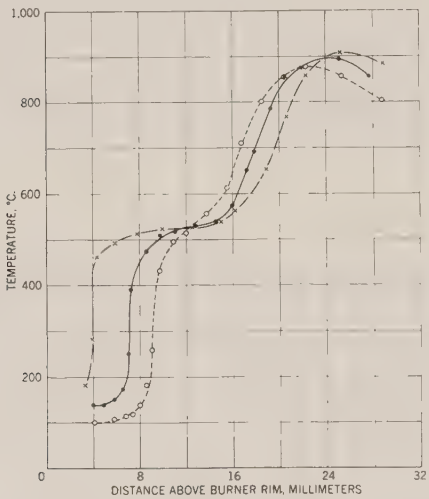

FIG. 6. Temperature distribution resulting from different preflame temperatures in ether-air flames.

constant. It was not possible to obtain temperature profiles for cool flames at preheat temperatures above approximately 180°C. If the reactant gases were heated above this temperature, the cool flame moved very close to the burner tip, and the lowest temperature measurable was about 450°C.

A comparison of temperature profiles for *n*-hexane and *n*-heptane is shown in Figure 7. Only a few measurements have been made for these fuels, so it is not possible to say very much about these flames. The temperature rises are not as sharp as in the case of the ether flames. One very interesting feature of these curves is that the temperature immediately following the cool flame is still in the region of 520°C.

As a result of fluctuations of the flame and various other slight inaccuracies in the experimental techniques, the temperature measurements are probably accurate to ±10°C. Since the calculated error due to radiation was considerably less than

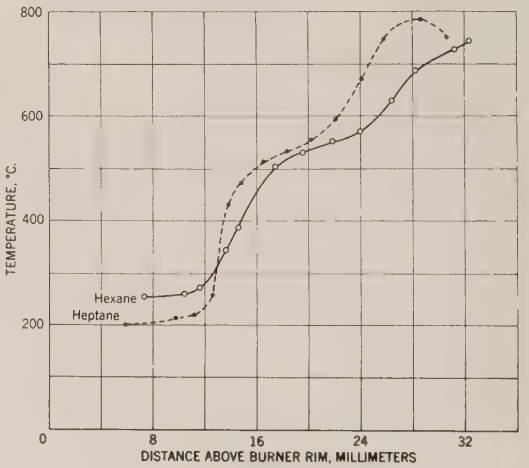

FIG. 7. Flame temperature distribution for hexane-air and heptane-air mixtures.

this, no corrective was made for this in the reported values.

Discussion

Analysis of the temperature profiles yields some very interesting information concerning cool flames. It was noted at first that all of the profiles obtained from ether-air flames had a similar shape at the lower end of the curve. Nearly all these curves were horizontal for a short distance at the very beginning. The curves then gradually rose until a temperature somewhere between 150° and 200°C. was attained, at which point the curves rose very sharply. It was also noted that cool flames could not be stabilized if the reactant-gas temperature exceeded ca. 180°C. At temperatures higher than this, the cool flame entered the burner tube and disappeared. This all agreed very well with the spontaneous ignition temperature re-

ported by Grove and Walsh[4]. An attempt was then made to fit this lower portion of the curve to the equation for heat transfer upstream by conduction. In all cases it was found that the experimental points were considerably above the values predicted by the equation. This appears indicative that a very slow reaction is taking place well before 180°C, and hence this is not a specific ignition temperature. Sample 1 in Table 1 was taken slightly upstream of the 180°C location of the flame and very definitely shows evidence of reaction. Unfortunately, it is not clear whether data are available that would prove that these reaction products were produced immediately preceding the flame or at some point further upstream.

The temperature of the gas leaving the burner tube is quite important, since it determines whether or not a stabilized flame can be produced. The total energy (either from diffusing radicals or transfer of heat) traveling upstream from the cool-flame front is exceedingly small, so, for ignition to take place, the reactants must already have an amount of energy close to that required for initiating reaction. For this reason, the hydrocarbons had to be preheated before they could be ignited.

The most interesting portion of the temperature profiles is the region immediately after the cool flame, where the temperature rise decreases and in some cases completely stops. Two features of this zone are of particular interest. The first of these is the temperature, and the second is the length, which can be described as the distance between the two flames or the second induction time t_2. It was found that this temperature was 520°C under all conditions of ether-air flow and composition. The same appeared to be the case for *n*-hexane and *n*-heptane, although too few data are available to be conclusive on this point. This temperature appears to be quite important and should be of considerable aid in understanding the reaction that predominates at this point. Since it is the same for two different types of compounds, this would indicate that the dominant reaction here must involve the reaction of one of the decomposition products that is common to both of these compounds.

The distance between the flames was found to be quite variable. This increased with increase of precool flame temperatures and of fuel-air ratio. Visual observations indicated that this distance also decreased when the TiO_2 was added for the particle-track measurements. The increase of distance as a function of preflame temperature was similarly reported by Andreev[5], who derived an equation expressing secondary induction time as a function of temperature. The decrease in the distance between the flames as the mixture became leaner probably was not due to increase in burning velocity of the secondary flame. The particle-track patterns indicate that the flow pattern is only very slightly divergent, so that any increase in secondary flame burning velocity would have resulted in more drastic changes than were observed. Therefore the increased oxygen must partially remove the intermediate which is responsible for the secondary induction period.

The data available for the effect of TiO_2 particles on the flames are still too limited for any conclusions to be drawn. Chamberlain, et al.[6] found that colloidal PbO had no effect on cool flames but did inhibit secondary reactions. The TiO_2 also did not seem to affect the cool flames, yet appeared to accelerate the secondary reaction. However, since this was only a visual observation, an examination of its significance should await more quantitative information. The complete absence of any oxygenated compounds in any part of the *n*-heptane flame containing TiO_2 particles is particularly striking and worthy of further investigation.

Acknowledgment

The author wishes to express his appreciation to B. Karlovitz and J. M. Singer for countless suggestions and contributions throughout the progress of this work. He would also like to acknowledge the help of Drs. B. Lewis and G. von Elbe and members of the Bureau of Mines Explosives and Physical Sciences Division.

REFERENCES

1. Downs, D., Street, J. C., and Wheeler, R. W.: Fuel, *32*, 279 (1953).
2. Maccormac, M., and Townend, D. T. A.: J. Chem. Soc., *143*, 151 (1940).
3. Powling, J.: Fuel, *28*, 25 (1949).
4. Grove, J. R. and Walsh, A. D.: *Fourth Symposium (International) on Combustion*, p. 429. Baltimore, The Williams & Wilkins Co., 1953.
5. Andreev, E. A.: Acta Physicochim (U.R.S.S.), *6:* 57 (1937).
6. Chamberlain, G. H. N., Hoare, D. E., and Walsh, A. D.: Disc. Faraday Soc., *14*, 89 (1953).

Discussion By Joseph M. Singer*

At a later date, and with the same apparatus, additional experimental temperature traverses were taken† with ether-air mixtures. In two separate experiments, 4 per cent (by volume) of CCl_4 and PbO particles were added to 14 per cent ether-air mixtures. Neither addition affected the shape of the temperature traverse curve, the cool flame temperature again being approximately 520°C.

Discussion by Russell Donovan‡

I would like to point out the correlation between Dr. Foresti's work and some somewhat similar work we have been doing in our laboratory, which will be published shortly. We have been studying the infrared emission and absorption of a two-stage diethyl ether flame in a burner similar to that described in this paper. We have identified the following components in the spectrum; CO_2 , CO, H_2O, HCHO, CH_3OH, C_2H_4 . These components all appear near the first flame and increase somewhat in the second flame. We have shown that there are carbonyl compounds formed in the first flame which are consumed in the second flame.

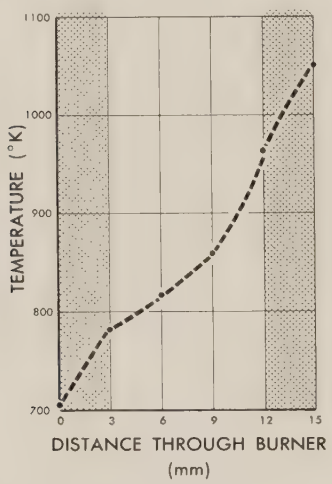

Fig. 1. (Of discussion).

We have made some temperature calculations using the infrared monochromator method at the following wavelengths; the C—H stretching and bending vibrations at 3.4 and 7.3 μ, the C═O band at 5.65 μ, the C—O band at 8.9 μ, CO_2 at 4.3 μ and C_2H_4 at 10.5 μ. The average of these calculations are shown in Figure 1. The temperatures here are averaged over a region of about 3 to 4 mm by our beam width which is somewhat larger than that of Dr. Foresti's thermocouple, so we cannot pinpoint small temperature variations, but the general temperature range is very closely correlated, and there was no large deviation in the individual calculations at the various wavelengths for any position, which indicates that the infrared radiation from these chemiluminescent flames is of thermal origin.

Discussion by Kenneth Wark*

The first comment is with regard to the fuel-air limits presented for three types of flames in the flat flame burner. Data collected with diethyl ether as the fuel at Purdue University indicate significantly different limits. For the cellular, two-stage, and single cool flame we have determined limits of 6–8, 8–25, and 25–32 per cent by volume respectively (14–18, 18–45, and 45–55 per cent by weight). Comparable data given in the Foresti paper were 7–13, 13–28, and 28–44 per cent. If these data are per cent by volume, it would appear that the upper cool flame limit exceeds the commonly accepted flammability limit of ca. 36.5 per cent. On the other hand, if the data are per cent by weight, the lower cellular flame limit would lie below the stoichiometric value for ether-air mixtures. While agreement is fairly good on the lower limit for cellular flames and the upper limit for two-stage flames based on volume per cent, there appears to be a rather wide discrepancy in the other limits.

Secondly, an interesting comparison may be made of approximate flame speeds based on the flow area. Foresti gives data for the three types of flames mentioned previously as 11–16, 7–13, and 10 cm/sec respectively. Comparable data obtained at Purdue are 5–7, 3–4.5, and 2–3 cm/sec. Not only is there a two- to five-fold variation in results, but our values decrease progressively with an increase in fuel-air ratio, as might be expected when the mixture is enriched to higher fuel-air ratios away from stoichiometric.

Finally, it seems worth mentioning that on many occasions it has been observed in our laboratory that considerable visible luminosity was in evidence in the region between the cool flame and the second stage flame. This radiation can become quite intense (with diethyl ether as the fuel) and has been confirmed by long exposure Kodachrome photographs. Optimum conditions for the highest

* Physical chemist, Flame Research Section, Explosives and Physical Sciences Division, Bureau of Mines, Pittsburgh, Pa.

† This research is also a part of the work carried out at the Bureau of Mines on Project NA onr 25-47, NR 098 117, supported by the Office of Naval Research through Project SQUID.

‡ Research Laboratories Division, General Motors Corporation.

* Research Fellow, Department of Mechanical Engineering, Purdue University.

intensity luminosity in the region between the cool and second stage flame has not yet been established.

AUTHOR'S REPLY

All gas percentages were reported on a volume basis.

The flammability and burning velocity values were presented only to give order of magnitude and were never intended as fundamental data. Flammability limits of these flames are very difficult to determine by such a method since they are affected by both the temperature of the system and the flow velocity of the gas.

The divergence of the particle tracks leaving the burner rim (see Figure 4) clearly shows that the gas flow velocity is not an accurate measure of the burning velocity. Burning velocities would not be affected by system design and thus should be reproducible. The values presented were gas flow velocities and these would vary somewhat as a function of burner design.

61

EFFECT OF PREFLAME REACTION ON FLAME VELOCITY OF PROPANE-AIR MIXTURES

By GORDON L. DUGGER, ROBERT C. WEAST, AND SHELDON HEIMEL

Introduction

With the growing interest in high speed combustion systems in which the attainment of greater heat release rates per unit volume is demanded, it becomes more important to know how faster-burning fuel-air mixtures can be obtained. Avery and Hart[1] have pointed out that under ram-jet conditions of maximum heat release rate the flame kinetics, rather than mixing, may be the controlling factor. It has long been known that one way to increase the burning rate of a gaseous mixture is to preheat it. In 1930, Passauer[2] demonstrated that for a number of fuels the mass burned per unit area of flame front per unit time was approximately proportional to the absolute initial temperature of the fuel-air mixture, or the flame velocity (volume burned per unit area per unit time) was proportional to the square of the absolute initial temperature. A more recent investigation[3] showed that for propane and air the maximum flame velocity (with respect to fuel concentration) was related to temperature according to the empirical equation

$$u_{f(\max)} = 10 + 0.000342\ T_0^{2.00} \qquad (1)$$

where $u_{f(\max)}$ is the maximum flame velocity in cm/sec and T_0 is the absolute initial mixture temperature in the range 200° to 617°K. This observed temperature dependence of flame velocity was found to be in agreement with the temperature dependence predicted by approximate theoretical equations based on either a thermal or an active-particle-diffusion mechanism of flame propagation. Thus it is both observed experimentally and predicted theoretically that the heat release rate per unit volume of combustion space is approximately proportional to the initial temperature of a homogeneous mixture. (Actually the temperature dependence is even greater when the decrease in thickness of the flame reaction zone is taken into account.)

The question arises as to how far this process of increasing the flame velocity by increasing the initial temperature can be carried. How important is the time required to preheat the mixture? If the time is sufficiently great that some oxidation occurs before the mixture reaches the flame, will the flame velocity be reduced?

The present investigation was undertaken at the Lewis Flight Propulsion Laboratory of the NACA (1) to determine experimentally whether the flame velocity is affected by contact time between fuel and air at the temperatures previously studied (617°K and below[3]); (2) to extend propane-air flame velocity data to higher temperatures; (3) to increase contact times and temperatures until appreciable effects of slow oxidation on flame velocity were observed, and (4) to obtain information on the major products of the slow oxidation in near-stoichiometric propane-air mixtures as determined under steady-

state flow conditions. Contact times (½ to 15 sec) and temperatures (617° to 906°K) were varied by injecting heated propane into heated air at different points in an air-to-gas heat exchanger, hereinafter called the soaking chamber. The equivalence ratios (fuel-oxygen ratio/stoichiometric fuel-oxygen ratio) studied fell in the range of 1.0–1.53. Flame velocities were determined, oxygen consumption was followed, and in some cases qualitative gas analyses of the preflame mixtures were made.

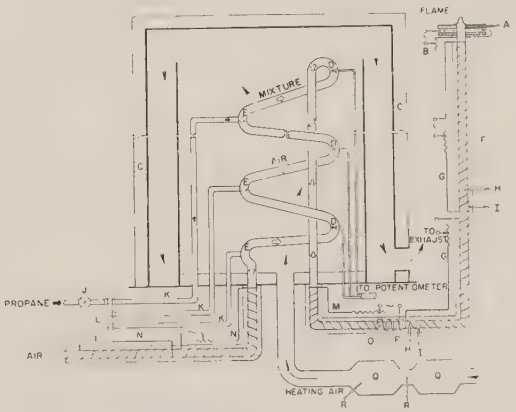

FIG. 1. Schematic diagram of contact-time apparatus. A, thermocouple for burner lip temperature; B, lip heater; C, soaking chamber; D, well-type thermocouple (18 in all); E, fuel injector (15 in all); F, burner tube; G, burner-tube heater; H, bare thermocouple for gas temperature; I, thermal couple for wall temperature; J, shut-off valve; K, fuel injector tube; L, cap on fuel injector not in use; M, connecting-tube heater; N, air preheater; O, flash-back arrestor; P, silver-soldered tube coupling; Q, electric heater; R, controlling thermocouple.

Apparatus and Procedure

The soaking apparatus and burner are sketched in Figure 1. The combustion air and propane were metered by critical flow orifices (not shown; see Anderson and Friedman[4]) and admitted to the soaking equipment as shown. The combustion air (approximately 0.4 mole per cent water) was preheated by heating elements N before passing into the helical soaking coil inside the soaking chamber C. Propane (99 mole per cent pure) was injected into the constant temperature air stream inside the coil at one of fifteen injection stations E. The propane was partially heated as it passed through the injection tube K prior to injection into the coil, so that, once inside the coil, it rapidly attained the air temperature. After passing through the remainder of the constant temperature coil, the hot mixture passed through a connecting length of tubing and a flash-back arrestor O and into a burner tube F, all of which were maintained at the desired temperature by means of heating elements G and M. The mixture was then burned at the port for a flame velocity measurement and/or sampled to determine the preflame oxygen consumption and in some cases the water, carbon dioxide, carbon monoxide, hydrogen and hydrocarbon contents.

SOAKING CHAMBER AND BURNER

The soaking chamber C was a simple air-to-gas heat exchanger which consisted of an insulated double-walled steel chamber constructed so that the heating air coming from the electric heater Q passed up over the coil, back down between the walls and out to the exhaust. The coil, which actually had thirty complete turns and an overall length of 49 m, is represented schematically in Figure 1 by three turns. It was made of 12.8-mm-inside-diameter by 1.6-mm-wall stainless-steel tubing and was bent into a helix of 48.6-cm diameter, so that each turn contained 153 cm of tubing. The series of fifteen fuel injection stations is schematically represented by three stations. The injectors were made from 4.8-mm-inside-diameter by 0.8-mm-wall stainless-steel tubing K. The ends of these injector tubes E were sealed and nine 0.4-mm holes were drilled on the upstream side of each tube. These holes were drilled on a square pattern of 1.6-mm spacing which began 1.6 mm from the sealed end. The injection tubes were brazed into the coil perpendicular to the coil tube wall in a position such that the center of the above hole pattern was located at the tube axis and was facing upstream. The resulting propane distribution, together with the turbulence caused by the presence of the injector in the coil, caused rapid mixing. The burner tubes were made from stainless-steel tubing of 0.96- or 1.28-cm inside diameter. Each burner tube had a vertical straight section of approximately 1.6 m.

Temperatures inside the soaker were indicated by iron-constantan thermocouples in well-type installations. There were 18 thermocouples in all, distributed in three vertical banks of six each, spaced 120 degrees apart, so that in each vertical bank there was a thermocouple in every fifth turn of the coil. The 18 thermocouples are schematically illustrated by one vertical bank of three couples D in Figure 1. It was found that

the temperatures indicated by the three vertical banks were very nearly equal (differences of 1° to 5°C). Temperatures indicated by the upper five couples within a vertical bank were also within 5°C of a common value, but the lowest couple in each bank showed that there was a 10° to 15°C temperature drop in the first few turns of the coil at the bottom of the chamber (due primarily to heating-air channeling and poorer insulation on the chamber bottom). Consequently, injection stations 14 and 15 (longest contact times), which were located in this region, were seldom used. In the higher temperature runs it was frequently observed that when the fuel flow was started through an injector there was a sudden rise in temperature in the immediate downstream portion of the soaking coil. In such cases, no data were taken until the temperature dropped back to within 10°C of the desired temperature level. In some of the later runs this problem was avoided by increasing the fuel flow by gradual steps until the desired flow was reached. The indicated temperatures inside the burner and the connecting tube were maintained within approximately 5°C of the mean value shown for the upper five-sixths of the soaking chamber. To this 5°C variation another 5° to 10°C should be added as the probable order of magnitude of the instrumentation errors.

FLAME VELOCITY MEASUREMENT

Flame velocity was measured by the total area method

$$u_f = V/A \qquad (2)$$

where V is the volumetric flow rate of the unburned gas at the conditions of the test, and where the total surface area of the flame A is calculated by the method previously described[3] from measurements based on the outside edge of the schlieren image of the flame cone. The schlieren image was obtained with a two-mirror Z-type system[5] in which a horizontal knife-edge was advanced from above.

GAS ANALYSIS

In early stages of the work, oxygen analyses of the soaked mixtures were obtained by diverting approximately 4 cc/sec (at room conditions) of the flow from the port of the burner to an oxygen analyzer through a water-cooled probe. The end of the probe was tapered so that the desired flow could be obtained by adjusting the position of the probe in the burner port, thus changing the ram pressure of the gas, and allowing the analyzer to exhaust to the atmosphere. This scheme was refined to permit simultaneous flame velocity determination and gas analysis by taking the sample from the side of the burner at a point 75 cm upstream of the port. In the latter case a water-cooled tube was flush-mounted in the burner wall and the sample was drawn through the analyzer by exhausting it through a critical flow orifice, the downstream side of which was kept at 300 mm Hg absolute pressure. When more complete analyses were to be made, the necessary absorbers and traps were placed downstream of the orifice.

The oxygen analyzer (Beckmann, model G-2) was of the magnetic susceptibility type[6] which depends on the fact that oxygen is strongly paramagnetic, while the other common gases are with few exceptions slightly diamagnetic. Further analysis of the soaked mixture, which was intended only to provide qualitative information regarding the major products of preflame reaction and general trends in concentrations, was carried out as follows. Anhydrone and Ascarite absorption bulbs were placed in the line to permit the gravimetric determination of water and carbon dioxide. The absorption bulbs were followed by a liquid nitrogen trap for the removal of less volatile components. Since the trap was operated at 300 mm Hg pressure, it was assumed that the quantities of ethylene and ethane passing it were negligible. A Baird infrared recording spectrophotometer with a 5-cm path length was used to analyze the trapped components at sample pressures of ½ to ⅔ atm. In tests in which the Anhydrone and Ascarite bulbs were removed from the line, no evidence of compounds containing hydroxyl or carbonyl groups was found in the infrared analyses, hence the concentrations of any oxygenated compounds must have been very small. The wavelengths used for determinations of propane, propylene, and ethylene were 7.22, 6.02, and 10.55 μ, respectively. The gas which passed the liquid nitrogen trap was collected and passed through a primary catalytic oxidation stage at 150°C in which the hydrogen and carbon monoxide were converted to water and CO_2, respectively, and absorbed in Anhydrone and Ascarite for gravimetric determinations. The remaining gas, assumed to be methane, was oxidized by a second catalytic stage at 500°C to

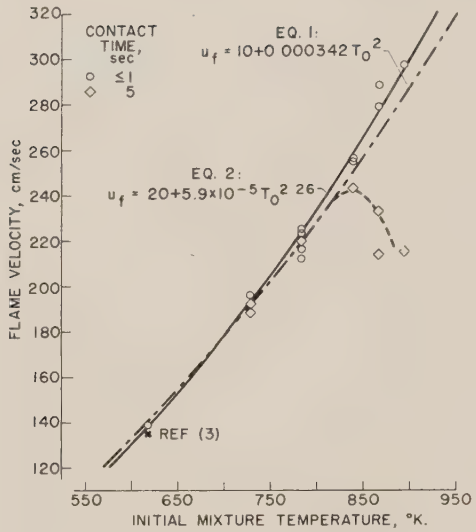

FIG. 2. Flame velocity vs. initial mixture temperature at an equivalence ratio of 1.15.

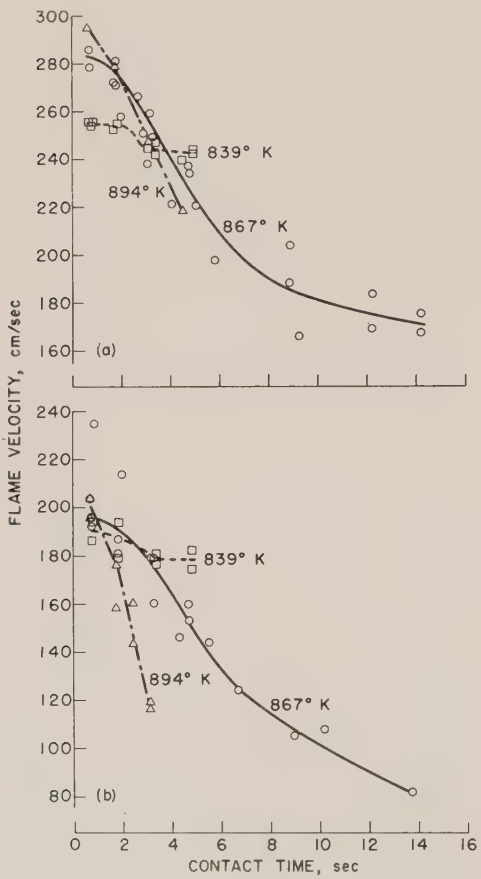

FIG. 3. Effect of contact time on flame velocity at three temperatures and two equivalence ratios. (a) Equivalence ratio 1.15; (b) equivalence ratio 1.43.

water and CO_2, which were again absorbed and weighed.

Results and Discussion

The results obtained during the first few months of exploratory operation seemed to show greater effects of preflame reaction than data obtained later, but the early results were rather erratic. It is believed that this was due in part to a surface aging process. For this reason, only the data obtained after several months of intermittent high-temperature operation are discussed herein.

FLAME VELOCITY RESULTS

Typical results with respect to the objectives (1), (2), and (3) listed in the introduction are illustrated by Figure 2, which shows flame velocity versus initial mixture temperature for an equivalence ratio of 1.15 and temperatures ranging from 617° to 894°K. The solid curve in Figure 2 is a plot of the equation

$$u_f = 20 + 5.9 \times 10^{-5}\ T_0^{2.26} \qquad (2)$$

This equation was obtained from a log-log plot of the data obtained at the shortest contact times studied ($\leq$ 1 sec; circles) and points taken from the faired curves of flame velocity versus equivalence ratio in Dugger[3]. Equation 2 represents the present data for the range 617° to 894°K with an average deviation of 2.1 per cent, and it represents the previous results for the same equivalence ratio, 1.15, with an average deviation of 1.8 per cent. The somewhat simpler equation reported for maximum flame velocities in the lower temperature range has been shown by a dash-dot curve; the average deviation of the present higher-temperature data from the latter curve is 3.3 per cent. Results obtained at a contact time of approximately 5 sec are shown by the diamonds and the dashed curve, which does not deviate appreciably from the 1-sec solid curve until temperatures greater than 783°K are reached. Therefore, Dugger's[3] results were not affected by preflame reaction. At temperatures of 867°K and above, there was a marked decrease in flame velocity after a residence time of five seconds.

The effect of contact time, and hence of the extent of preflame reaction, on flame velocity is more clearly shown by Figure 3. In Figure 3a curves of flame velocity versus contact time are presented for initial mixture temperatures of 839°, 867°, and 894°K for a mixture having an

equivalence ratio of 1.15; in Figure 3b, curves for the same three temperatures are presented for an equivalence ratio of 1.43. It is not surprising that there is so much scatter in the data points, which for each curve represent several runs, when it is remembered that the experimental precision in the measurement of flame velocity is of the order of ±3 per cent under the best conditions, and that the preflame reactions which affect the flame velocity are very dependent on temperature, thus being very sensitive to temperature variations within the isothermal system. Moreover, the way in which the curves are drawn through the data is a matter of the interpretation of the authors, since some of the regions represented by curves might equally well be represented by straight lines in the absence of any attempted interpretation. However, the authors believe that these data are not inconsistent with the pattern which might result from a two-stage ignition mechanism. (See, for example, the literature review on the mechanism of propane oxidation given by one of the authors[7].) That is, if the curves, particularly the 839° and 867°K curves, are drawn as shown, the first step in the pattern of flame velocity decrease seems to be a period of comparatively slow decrease, which may correspond to the induction period for the first stage of ignition. The first stage of ignition, in which chain-branching may be important, is perhaps represented by a period of more rapid decrease. This may be followed by a period of slower decrease corresponding to the induction period for the second stage, or explosion. At the contact times of Figure 3, the second stage did not occur in the coil. However, when attempts were made to determine flame velocities at temperatures slightly above 894°K, it was found that no flames could be obtained on the port. In these cases the gas leaving the port contained visible amounts of soot.

In considering the reasons for the observed decrease in flame velocity with increasing contact time, it must be remembered that the preflame reaction occurred under essentially isothermal conditions and that the heat evolved by the reaction was lost to the apparatus. The products of preflame reaction which entered the flame served as either combustible additives or inert diluents at the test temperature. The over-all stoichiometry with respect to the total combustible and oxygen (equivalence ratio) would remain unchanged. Thus the flame velocity decrease would have to be explained by (1) the formation of combustible intermediate products which had lower flame velocities than propane or (2) the formation of water and carbon dioxide. The former is improbable because most of the expected intermediate products[7] have higher flame velocities than propane; for example, olefins, alcohols, aldehydes, carbon monoxide, and hydrogen[8]. On the other hand, the formation of water and carbon dioxide is a doubly effective diluting process, because not only is the concentration of inert gases in the total mixture increased, but the fuel and oxygen concentrations are simultaneously decreased by the conversion. Inasmuch as carbon dioxide is more effective in reducing the flame velocity of a hydrocarbon than an equal quantity of nitrogen[9] but water is probably less effective than nitrogen[10], the importance of these dilution effects may be approximately illustrated

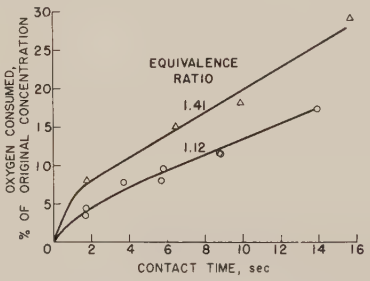

FIG. 4. Variation of oxygen consumption with contact time at 867°K for two equivalence ratios.

by an example of the effect of nitrogen dilution at constant equivalence ratio. The data of Dugger and Graab[11] show that an increase in nitrogen corresponding to only 2 per cent of the total mixture would be required to decrease the flame velocity of a propane-air mixture ($\varphi = 1.06$) by 25 per cent. Thus the formation of the order of 2 per cent of water plus carbon dioxide could explain the flame velocity decrease caused by the first 6 seconds of preflame reaction at 867°K and an equivalence ratio of 1.15 if all other factors were constant. Actually, the decrease due to water and carbon dioxide might be partially counterbalanced by an increase due to higher flame-velocity intermediates as mentioned above.

OXYGEN CONSUMPTION RESULTS

Figure 4 shows the effect of contact time on oxygen consumption for equivalence ratios of 1.12 and 1.41 and an initial temperature of 867°K. The oxygen consumption was computed as percentage of the original oxygen partial pres-

sure, that is 100 × (original-final)/(original). No correction to the final partial pressure reading was made to take into account the increase in the number of moles due to reaction; such a correction would be bigger for greater contact times or more reaction, but it would never be greater than the probable experimental error. In connection with the previous discussion of the reasons for the flame velocity decrease with contact time, the rapid early increase in oxygen consumption may indicate the formation of combustion intermediates having flame velocities comparable to or greater than that of propane, with little CO_2 and water being formed. Subsequently, the rate of oxygen consumption remains fairly constant, presumably as intermediates or products of the first stage of ignition are converted to CO_2 and water. It might be expected that these oxygen consumption curves should

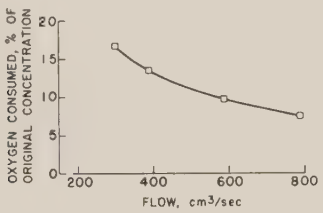

FIG. 5. Oxygen consumed vs. flow rate. Equivalence ratio, 1.12; temperature 867°K; contact time, 6.9 sec.

tend to level off during the period which was interpreted as the induction period for second-stage ignition from the flame velocity curves; the fact that they did not weakens that interpretation.

An effect of flow rate (either volumetric flow rate or linear flow velocity; only one soaking-coil diameter was used) on the extent of preflame reaction was indicated by oxygen consumption data (Fig. 5). As the flow rate was increased from 300 to 800 cc/sec, the oxygen consumption was halved for a contact time of 6.9 seconds at 867°K. This effect may be considered consistent with a surface inhibition of the preflame reactions, because at higher flows there would be more turbulence and eddy diffusion, which would increase the number of collisions between chain carriers and the inhibiting surface per unit time. The 867°K flame velocity curves in figure 3 and the 867°K oxygen consumption curves of Figure 4 were obtained at comparable flow rates (~400 cc/sec). However, the 839° and 894°K flame velocity curves were obtained at much higher flow rates (~1200 cc/sec). As a result, the effect of contact time on flame velocity shown by these latter curves is smaller than it would have been had they been determined at the same flow rate as the 867°K curve, but it is believed that they would still cross over the 867°K curve in the same relative order, so that at some contact time of the order of 3–5 sec the flame velocity would decrease with increasing temperature.

MAJOR PRODUCTS OF SLOW OXIDATION

The approximate gas analysis scheme described heretofore was used to indicate the major products of the preflame reactions. After four seconds at 867°K the major products were, in the following decreasing order of mole percentages, hydrogen > water ≅ carbon monoxide > carbon dioxide > propylene ≅ ethylene. In some cases methane was found in the overhead from the liquid nitrogen trap, but other analyses indicated no methane. In all cases a carbon deficiency was noted when a carbon mass balance was attempted. At 867°K, for equivalence ratios from 1 to 1.5 at a contact time of approximately 4 sec, this deficiency amounted to approximately 10–15 per cent of the total carbon input and of the order of 50 per cent of the carbon represented by the number of moles of propane reacting. It is believed that a large part of the carbon deficiency in the samples was due to formation and deposition of carbon. Hydrogen deficiencies calculated in a similar manner were smaller, and oxygen balances came out fairly well, with even a slight excess calculated in some cases.

COMPARISON OF RESULTS WITH IGNITION DELAY LITERATURE

There are few data in the literature to which these results can be compared. There are some figures on ignition temperatures and ignition delays which appear to correspond approximately to the first stage temperatures and times quoted herein. For example, Jackson[12] reported the spontaneous ignition temperature of propane to be 778°K with an ignition lag of 0.1 min when determined by a liquid drop test. Brokaw and Jackson[13] recently determined ignition delays for propane-air mixtures by an improved flow method. Ignition delays for an equivalence ratio of 1.15 were estimated from their general correlation plot to be as follows: 800°K, 14 sec; 850°K, 4 sec; and 900°K, 2 sec. The fact that ethylene and propylene were among the major products of

slow oxidation might be considered to be consistent with the kinetic mechanism suggested by Brokaw and Jackson[13] in connection with their findings on the effects of fuel and oxygen concentration and temperature on the observed ignition delay.

Summary of Results

The results of an investigation of the effects of contact time of propane and air in an isothermal soaking coil on the flame velocity and oxygen consumption for the mixture were as follows:

(1) There was no effect of contact time in the range 1 to 5 sec until temperatures greater than 783°K were reached, hence the flame velocities previously reported[3] for contact times less than two seconds at temperatures up to 617°K were not affected by preflame reactions. The flame velocities which were determined for contact times of less than one second at an equivalence ratio of 1.15 smoothly extended the curve of flame velocity against initial temperature plotted from previous data curves[3].

(2) Marked effects of preflame reactions on flame velocities for equivalence ratios of 1.15 and 1.43 were noted at temperatures of 867°K and above. Flame velocity decreased with contact time in a manner which was not inconsistent with a possible two-stage ignition process such as has been frequently reported for the oxidation of hydrocarbons. The decrease in flame velocity with contact time was attributed mainly to the diluting effects of water and carbon dioxide formed by preflame reaction.

(3) At 867°K, the oxygen consumption due to preflame reactions increased with contact time in a manner which seemed compatible with the changes in flame velocity, except that in the period presumed to correspond to the induction period for the second stage of ignition, the rate of oxygen consumption remained essentially constant. An effect of flow rate (either volumetric rate or linear flow velocity, only one soaking coil diameter was used) was shown by oxygen consumption data; the oxygen consumption progressively decreased as the flow rate was increased at constant contact time. This effect might be explained by the surface destruction of chain carriers for the preflame reactions, because the greater turbulence at higher flow rates would give greater exposure to the surface through eddy diffusion.

(4) The major products of the preflame reactions after four seconds at 867°K (period of maximum rate of flame velocity decrease) were, in the following decreasing order of mole percentages, hydrogen > water $\cong$ carbon monoxide > carbon dioxide > propylene $\cong$ ethylene. A carbon deficiency amounting to about one-half of the carbon content of the propane reacting was attributed largely to carbon formation.

In closing it must be pointed out that the deleterious effect of contact time on flame velocity would be less important in a non-isothermal system where the heat evolved in preflame reaction could be made available to the combustion cycle.

Acknowledgment

The authors are indebted to Marianne Buddie and Albert Evans, Jr. of the NACA Lewis laboratory for aid in the gas analyses made.

REFERENCES

1. Avery, W. H., and Hart, R. W.: Ind. & Eng. Chem., *45*, 1634 (1953).
2. Passauer, H.: Gas- u. Wasserfach, *73*, 343, 369, 392 (1930).
3. Dugger, G. L.: NACA Report 1061 (1952).
4. Andersen, J. W., and Friedman, R.: Rev. Sci Instruments, *20*, 61 (1949).
5. Lewis, B., and von Elbe, G.: *Combustion, Flames, and Explosions of Gases*, p. 212. New York, Academic Press, Inc., 1951.
6. Pauling, L., Wood, R. E., and Sturdivant, J. H.: J. Am. Chem. Soc., *68*, 795 (1946).
7. Dugger, G. L.: Ph. D. Thesis, Case Inst. Tech. (1953).
8. Calcote, H. F., Barnett, C. N., and Irby, M. R.: Paper presented at 116th meeting Am. Chem. Soc., Atlantic City, Sept. 18–23, 1949.
9. Linnett, J. W., and Hoare, M. F.: Trans. Faraday Soc., *47*, 179 (1951).
10. Kapp, N. M., Snow, B., and Wohl, K.: Project METEOR Report UAC-30, United Aircraft Corp. Research Dept. (1948).
11. Dugger, G. L., and Graab, D. D.: *Fourth Symposium (International) on Combustion*, p. 302. Baltimore, The Williams & Wilkins Co., 1953.
12. Jackson, J. L.: Ind. & Eng. Chem., *43*, 2869 (1951).
13. Brokaw, R. S., and Jackson, J. L.: *Fifth Symposium (International on Combustion*, p. 563. New York, Reinhold Publishing Corp., 1955.

62

A STUDY OF THE ETHYLENE OXIDE DECOMPOSITION FLAME

RAYMOND FRIEDMAN AND EDWARD BURKE[a]

1. Introduction

There are only a few gaseous systems capable of deflagration for which knowledge of the chemical kinetic parameters is available. In general it is necessary to extrapolate the parameters from the relatively low temperature conditions of an isothermal kinetic study in a closed system to the much higher temperatures of a flame. Furthermore the intermingling of reactants, intermediates, and products occurs differently in a homogeneous reactor than in a flame, because of diffusion, and hence reactions which are negligible in one case may become important in the other. For these reasons, thorough kinetic studies of both the slow isothermal reaction and the flame are needed before any system may be said to be understood.

The thermal decomposition rate of ethylene oxide vapor at about 400°C has been studied by a number of workers, the most recent being Mueller and Walters[1]. They find the overall process to be first-order, with an activation energy of 52.7 kcal and a frequency factor of 1.5×10^{13} per sec. However, quite a variety of reaction products are obtained, and certain additives inhibit the reaction, so the detailed mechanism may not be simple. Lossing, Ingold, and Tickner[2] have studied the reaction in a flow system with helium as a carrier at 800–1000°C, following the decomposition by mass spectrometry. They also find a variety of products, including an abundance of CH_3 radicals. They report a first-order process, but with an activation energy of 42 kcal, and a rate at 850°C which we have calculated to be only $\frac{1}{16}$ as great as the value extrapolated from Mueller and Walters' work near 400°C. According to a published discussion of this work between J. C. Polanyi and Lossing et al.[3], the presence of a non-uniform temperature in the reactor could readily account for the discrepancy in rate parameters.

Burden and Burgoyne[4], in 1949, were the first to show that a decomposition flame could propagate through pure ethylene oxide. Gerstein, McDonald, and Schalla[5] made the first burning velocity measurements, in 1952, for such a flame propagating upward through a tube. They found their burning velocity to agree quite well with the value which they predicted from the Mueller-Walters kinetic parameters. Later in 1952 the present writers[6] succeeded in stabilizing an ethylene oxide decomposition flame on a flat-flame burner. This made possible for the first time an accurate study of the flame properties. The first results with the stabilized flame[6] showed the burning velocity to be less than one-fourth as great as the value reported by Gerstein et al.[5]; this stimulated a rather complete investigation of the flame, which is described in this paper. The measurements include burning velocity as a function of pressure and temperature, product gas analysis, final gas temperature, and temperature profile through the flame. The kinetic significance of these results is discussed throughout the report, and in a general discussion at the end.

Mention may be made of the possibility that ethylene oxide will find important applications as a monopropellant, so this study may have practical as well as theoretical significance.

2. Burning Velocity

(2.1) EXPERIMENTAL

The flat-flame burner technique, previously described by Powling[7], by Egerton et al.[8, 9], and by the present writers[10, 11], was chosen for this investigation, since it is particularly suitable for slow-burning flames such as ethylene oxide.

The ethylene oxide, specified to be 99.5 per cent pure, was supplied in cylinders by the Matheson Company, East Rutherford, New Jersey. The vapor pressure was found to be in agreement with published values. The liquid was colorless. No further tests of purity were made.

The essential elements of the flow system will be described. The ethylene oxide cylinder was maintained in an inverted position at 50°C. The liquid was evaporated by passage through a heat exchanger the wall temperature of which never exceeded 70°C. The vapor then flowed through an insulated surge tank and line to a Moore Nullmatic pressure regulator with a Neoprene diaphragm. The vapor left the regulator at a reduced, constant pressure, was metered by a Fischer and Porter "Flowrator" with a special magnesium

[a] Mr. Burke terminated his participation in this research program in September, 1953.

float, and then passed through a needle valve the setting of which controlled the flow rate. Next, the vapor flowed through an electric pre-heater (used only in certain tests) and into the burner, which was housed in a vacuum chamber of 38 cm diameter and 81 cm height, with windows. This apparatus has been described in detail in an earlier publication[11]. Some of the tests were made with a burner of 10 cm inside diameter and others (at the lower pressures) with a burner of 25 cm inside diameter. The 10-cm burner was similar to that used by one of the present authors[10] for lean propane-air, except that the screen below the flame (5 cm below the burner rim) was made of platinum wire, the low absorptivity of which minimized radiative pre-heating of the gas. The upper screen was 2.5 cm above the burner rim.

The geometry of the 25-cm burner is shown in Figure 1. The conical baffle was found to be necessary to obtain a satisfactory flame shape. Presumably, it acted to minimize convective eddies at the periphery of the flame.

Ignition was obtained for both burners by a hydrogen-air torch, itself spark-ignited, which threw a flame down through the stainless steel screen above the burner. A continuous flow of nitrogen was maintained through the exhaust line, as a precaution against ethylene oxide-air explosions and to help in stabilizing the vacuum chamber pressure. However, no gas was introduced into the annular space immediately surrounding the burner.

The pressure level in the vacuum chamber was controlled manually by the setting of the valve in the exhaust line to the pumping system. In the pre-heating experiments, kerosene at the same temperature as the pre-heated ethylene oxide was circulated through coils around the burner. The temperature of the gas issuing from the burner was measured with a low-emissivity thermocouple of 0.012-mm wire. Because of the fineness of the wire, the calculated radiation correction was only 3°C. Cold water was circulated at all times in the vacuum chamber coils.

The Flowrator was calibrated by: (1) measuring the volume of the vacuum chamber, (2) evacuating this chamber to a low pressure, (3) letting ethylene oxide flow into the chamber for a measured time-interval, with the exhaust valve closed, and observing the pressure rise, and (4) calculating the flow rate, with a correction for the gas imperfection, obtained from the P-V-T data of Walters and Smith[12]. The overall error in flow metering is believed to be somewhat less than one per cent.

For each condition of pressure and initial temperature, the burning velocity was measured by adjusting the flow so that the flame was as flat as possible and roughly a centimeter above the rim of the burner. The edge of the flame would overhang the burner slightly, and would sometimes turn downward at the extremity, and sometimes upward. Each flame was photographed; the flame area was calculated from measurements of the photographs; and the burning velocity

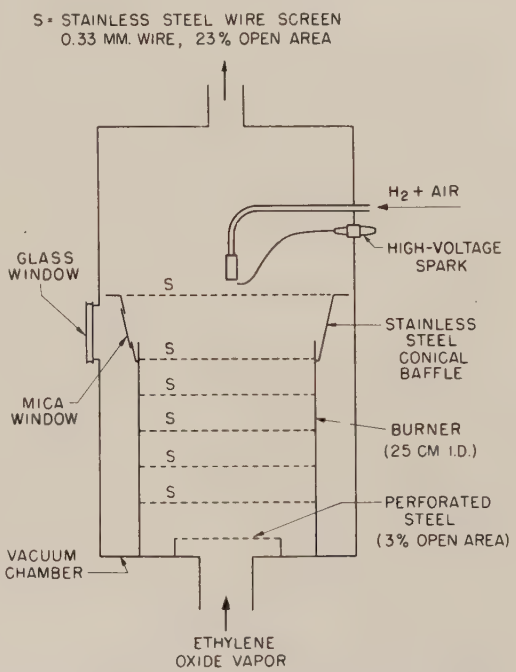

FIG. 1. Schematic representation of 25-cm burner.

taken to be the volumetric flow divided by the flame area. The validity of the procedure appeared to be justified by tests which showed that a five per cent increase or decrease in volumetric flow caused a proportionate increase or decrease in flame area. Also, from a consideration of the geometry of the flame and the burner, it is hard to imagine how an absolute error of more than a few per cent is possible. A final confirmation of the method is the excellent agreement between the results obtained with the 10-cm burner and those of the 25-cm burner. These burners are of sufficiently large size to minimize the quenching effect of the burner on the flame.

(2.2) RESULTS

Figure 2 shows the burning velocity of ethylene oxide initially at 70°C as a function of pressure. The initial temperature, which varied somewhat from run to run, was always appreciably higher than room temperature because of radiative preheating, believed to be mainly due to radiative transfer from the hot screen above the flame to the cold screen below the flame, although radiation from the burned gases to the cold screen makes a certain contribution. All data shown in Figure 2 were corrected to 70°C by means of the burning velocity vs. temperature curve for ethylene oxide previously published by the present authors[6].

The solid points (10-cm burner) and the open points (25-cm burner) in Figure 2 are seen to be mutually consistent. The data show a slight decrease in burning velocity with increasing pressure, the effect being greater at higher pressures. From the theory of flame propagation, it may be shown quite rigorously that, for a simple flame of ideal gases governed by a first-order decomposition, the burning velocity must be inversely proportional to the square root of pressure. Comparison of the broken and solid curves of Figure 2 shows that the data differ significantly from an inverse square-root law.

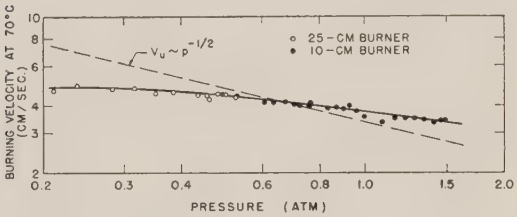

FIG. 2. Burning velocity of ethylene oxide decomposition flame vs. pressure (log-log plot).

It remains to discuss the magnitude of the burning velocity, which, when corrected to room temperature, is less than one-fourth as great as that reported by Gerstein et al.[5], and, incidentally, is the lowest burning velocity ever reported, to the best of the authors' knowledge. The discrepancy between these results and those of Gerstein, which are based on upward propagation through a tube, may quite possibly be due to convective currents which influence this slow-moving flame as it progresses through the tube. This hypothesis is supported by the failure of Burden and Burgoyne[4] as well as Gerstein et al.[5] to obtain downward propagation with tubes in which upward propagation could be readily obtained. Since the validity of the tube method has never been demonstrated for such slow-burning flames, the writers feel that the flat-flame burner method must be considered the more reliable of the two.

The burning velocity at one atmosphere and 25°C was found by the writers to be 2.7 cm/sec, while the calculations of Gerstein et al.[5], based on Mueller and Walters'[1] kinetic parameters, led to a burning velocity of 9.6 cm/sec. An explanation of this difference is to be found in the incorrect assumption of flame temperature in the above calculations. Gerstein et al.[5] assumed that the only reaction was $C_2H_4O \rightarrow CH_4 + CO$, and accordingly calculated a flame temperature of 1460–1600°K. However, as Burgoyne[13] has pointed out, gas analysis shows that substantial proportions of H_2 and C_2H_4 are to be found in the product gases; these components correspond to a much less exothermic overall process, and according to Burgoyne, a calculated flame temperature of 1220°K. Product gas analyses made in the present investigation, to be described in Section 4, lead to a calculated flame temperature of 1217°K, in good agreement with Burgoyne. Furthermore, direct measurements of flame temperature with a thermocouple, described in Section 5, give a value of 1182°K, when corrected to 25°C initial temperature.

Reference to Figure 2 of Gerstein et al.[5] shows that burning velocity is strongly dependent on flame temperature. According to this figure, reduction of the flame temperature from 1500 to 1250°K would reduce the theoretical burning velocity from 15 to 2.4 cm/sec. Thus, if the flame temperature is taken to be 1200°K, our measured burning velocity would be somewhat higher than the theory calls for, while the measured burning velocity of Gerstein et al.[5], being more than four times our value, would differ greatly from the theory. We shall refrain from making more exact comparison of our result with theoretical prediction, since the theory requires knowledge not only of the precise flame temperature but also of the thermal conductivity of the rather complex gas mixture. Product gas analysis reveals about 20 per cent of hydrogen, which would have an important effect on the conductivity. In view of the uncertainty of any calculation which would attempt to take such effects into account, we shall satisfy ourselves with the order-of-magnitude agreement between our result and Figure 2 of Gerstein et al.

3. Description of Flame

In the course of the burning velocity studies described above, a number of interesting observations of the appearance of the flame were made, which will now be described.

The flame was sufficiently faint so that it could only be properly observed when the room was completely darkened, so all tests were made under this condition. An idea of the intensity of luminosity may be obtained from photographic exposure times. With a f/1.8 lens, Tri-X Panchromatic film, and Eastman D-23 developer, exposure times of 10 to 30 sec were required, depending somewhat on the flame pressure.

The color of the luminous zone appeared to be very pale blue, perhaps blue-gray. This luminosity did not stop abruptly above the flame, but appeared to decrease gradually to a low residual value. The most intense part of the luminous zone was about one-half mm thick at atmospheric pressure, and was thicker and less luminous at lower pressures. No information was gained in an attempted spectroscopic examination of the flame, because of insufficient light.

A powdery carbonaceous deposit, insoluble in hot carbon tetrachloride, was observed to build up on the stainless steel screen above the flame. Some of this came from the interaction of the ignitor flame with the ethylene oxide, but a substantial portion came from the decomposition flame. This was demonstrated by an experiment in which an electrically heated wire was used as an ignitor. No deposit was seen on the screen immediately after ignition, but, after an hour of burning at atmospheric pressure, 0.07 gm of carbonaceous material was found on the screen. During this period, about 860 gm of ethylene oxide had been burned, so the proportion of carbonaceous material formed is extremely small. However, it is of interest to consider whether this material forms in the reaction zone itself, in the burned gases, or at the solid surface.

If one considers the thermodynamic stability of the combustion products (see Section 4), one finds from the free energies that the products obtained are less stable than solid carbon, H_2 and CO, at 1000–1200°K. Therefore, if the kinetics are favorable, it is quite possible for the CH_4 and C_2H_4 in the combustion products to be slowly decomposing to form carbon. Kassel[14] has studied the kinetics of the pyrolysis of CH_4 at about 1000°C in a closed vessel; he finds an initially first-order rate of $10^{12}\exp(-79{,}400/RT)$ per second, and states that "the only products of importance" are carbon and hydrogen. Gordon[15], who studied the same process in a flow system, analyzed the product gases. A study of his reported analyses shows the overall atomic H/C ratio in the product gases to be of the order of 10 (rather than 4); this clearly shows that carbon, or a material of very low H/C ratio, was depositing on the wall of his tubular reactor. Indeed, he mentions that he periodically burned off such deposits.

Let us make an order-of-magnitude calculation of the amount of carbon that would be expected to form in our burner between the flame and the screen, on the assumption that Kassel's kinetic equation[14] for pyrolysis of CH_4 is applicable. From the flow velocity of the hot gases, the "residence time" before the gases reach the screen is found to be about $\frac{1}{8}$ second. According to Kassel's kinetics[14], if the gas temperature is (1) 1100°K, (2) 1200°K, then (1) $\frac{1}{5800}$, (2) $\frac{1}{270}$ of the CH_4 should have decomposed during this time. The 0.07-gm deposit of carbonaceous material mentioned previously corresponds to decomposition of about $\frac{1}{2400}$ of the CH_4 known to be present. If the measured flame temperature of 1182°K is taken to be correct, the agreement between the calculated and the actual carbon deposition is seen to be acceptable. Hence it is reasonable to conclude that the carbon forms by slow pyrolysis of the product gases, and not in the intense reaction zone of the flame.

4. Product Gas Analysis

(4.1) EXPERIMENTAL

Gas samples were withdrawn from the flame gases by a copper tube, 0.62 cm outside diameter, the mouth of which just protruded through a hole in the center of the screen above the 10-cm burner. The flame was about a centimeter below the mouth of the tube, the samples being withdrawn sufficiently slowly so as not to change the flame shape. The tube was not water-cooled. Sampling was done only with the flame at atmospheric pressure. Gas analysis was carried out with a modified Orsat apparatus.

The average result of analysis of four samples was as follows:

CO	44.3 per cent
CH_4	25.9 per cent
H_2	19.6 per cent
unsaturates	10.2 per cent

The unsaturates were assumed to consist entirely

of C_2H_4; on this basis, the analysis gives an atomic C/H ratio of 0.494, to be compared with a theoretical value of 0.500. The atomic C/O ratio is 2.045 instead of 2.000.

(4.2) CALCULATION OF FLAME TEMPERATURE FROM GAS ANALYSIS

First, we must normalize the above gas analysis to be in perfect agreement with the C/H and C/O ratios of the fuel. We then obtain:

CO	44.9 per cent
CH_4	24.2 per cent
H_2	20.6 per cent
C_2H_4	10.3 per cent

This corresponds to 54 per cent of the fuel decomposing according to $C_2H_4O \rightarrow CO + CH_4$ and 46 per cent according to $C_2H_4O \rightarrow CO + H_2 + \frac{1}{2} C_2H_4$. Using the National Bureau of Standards values[16] for heats of formation, we obtain $\Delta H^\circ_{298} = -32.11$ kcal/mole for the first reaction and -7.98 kcal/mole for the second reaction. Then, from a knowledge of the enthalpies of the product gases, we may readily calculate that, for C_2H_4O vapor initially at 25°C, the adiabatic flame temperature is 1217°K. The close agreement between this result and the value obtained in a similar way by Burgoyne is to some extent fortuitous, since both the heats of reaction and the gas composition used by Burgoyne in his computation differed moderately from our values.

Calculations based on specific heats show that, for each degree the initial temperature is increased above 25°C, the flame temperature is increased 0.44°, as long as the product gas composition does not change.

5. Temperature Measurements

(5.1) EXPERIMENTAL

In order to make accurate measurements of the temperature of a hot, slow-moving gas by means of a thermocouple which is free to radiate to cold surroundings, an extremely small thermocouple must be used. If sufficiently small, its temperature will be very close to the gas temperature, because the heat transfer coefficient between the gas and the thermocouple increases with decreasing size.

The use of a thermocouple of very fine wire is also advantageous in that aerodynamic perturbation of the flame by the thermocouple is minimized, so that a detailed investigation of the temperature profile becomes possible.

Thermocouples of platinum and platinum-10-per cent-rhodium wire, of 0.0012-cm diameter, were used in this investigation. The wires were gas-welded to form a bead the thickness of which was roughly twice the wire diameter. The thermocouple was supported and moved through the flame as described in a previous study[11]. In the first tests, the wires were provided with a thin ceramic coating, to insure absence of catalytic effects. However, the emf of such thermocouples was found to decrease with time while exposed to the flame gases, at a rate of roughly 10 per cent per hour. This was attributed to the chemically reducing action of the flame gases on the oxides, such as SiO_2, in the ceramic composition. Therefore, the study was continued with uncoated thermocouples, which were found to be much more stable with time. Since the temperature traverses with coated and uncoated thermocouples qualitatively resembled each other, it appears that no catalytic effects occur at the platinum surface with this flame, although such effects are certainly present in the lean propane-air flame[10].

The possibility of making a very accurate measurement of the temperature distribution, so as to obtain the heat release pattern, was limited by the flickering of the flame, which was considerably worse than that encountered with lean propane-air[11]. The flicker had an approximate "frequency" of one cycle/sec, with erratically varying amplitude, which seldom exceeded a millimeter (for flames near atmospheric pressure). We are speaking here of the residual flicker which remained after substantial improvements in the flame had been achieved by changes in burner geometry. It seems likely that the flicker is due to convective gas motions at the flame-edge, the perturbation of the flame being greater for lower burning velocities. Incidentally, this effect may determine the measured limit of inflammability of a mixture on a burner, when the burner is large enough so that quenching is not limiting.

(5.2) RESULTS

The temperature distribution was obtained by the same technique as has been described earlier[11], except that the flame flicker caused more scatter of points in the zone of steep temperature gradient. A typical traverse obtained with an uncoated thermocouple at 0.90 atmospheres is shown in Figure 3. The general shape of the curve is just what would be expected from theoretical considerations; this strengthens the

argument that no strong catalytic effects are occurring on the thermocouple.

The maximum temperature reading, which was in or at the termination of the zone of intense luminosity, was 1197°K. This value was corrected for the radiation error of the thermocouple by making heat transfer calculations, based on microscopic measurement of the bead size and an assumption of 0.15 for the emissivity. The correction came out to be 14°K, giving a corrected flame temperature of 1211°K. This value was then corrected from an initial temperature of 92°C to an initial temperature of 25°C, by the procedure mentioned in the last paragraph in Section 4.2. This reduced the value from 1211 to 1182°K.

It is of interest to know whether the flame temperature varies with pressure. A traverse at 0.66 atm showed the maximum temperature to be just one per cent lower than at 0.90 atm.

Returning to Figure 3, we see that the temperature of the burned gases is dropping steadily at 53°/cm, as the gases flow upward. Order-of-magnitude calculations show that this is consistent with the expected heat loss from the gases by infra-red radiation.

The traverse is not determined precisely enough to say anything very definite about the temperature at which heat release begins. However, it would appear that this temperature must be much closer to the maximum temperature than to the initial temperature. This is what one would expect from the high activation energy of the low-temperature decomposition.

The overall thickness of the flame, including the pre-heating zone, is seen from Figure 3 to be of the order of a cm at 0.90 atm. It is interesting to consider how this distance is related to Burden and Burgoyne's observation[4] that upward propagation of the flame in a tube of 5-cm diameter is not possible at pressures below 0.83 atm. From their observation, we may compute the quenching distance at 0.90 atm, if (1) we define quenching distance as half the distance between parallel plates which will just quench the flame, (2) we use the quenching relation of Simon, Belles, and Spakowski[17]:

$$\frac{\text{critical distance between parallel plates}}{\text{critical tube diameter}} = \sqrt{\frac{3}{8}},$$

and (3) we extrapolate from 0.83 to 0.90 atm by taking the quenching distance to vary inversely with pressure. We then obtain 1.4 cm for the quenching distance, which is not too different from the flame thickness of Figure 3.

6. General Discussion

We have found that the magnitude of the burning velocity is in reasonable agreement with the value to be expected from first-order kinetic parameters determined from decomposition studies at around 400°C, even though the flame temperature is more than 900°C. However, the pressure dependence of burning velocity differs significantly from the inverse square-root law to be expected for a flame governed by a first-order process. An attempt at reconciliation of these two findings is therefore in order.

Let us suppose that in the flame the rate of the decomposition is limited by a slow first-order

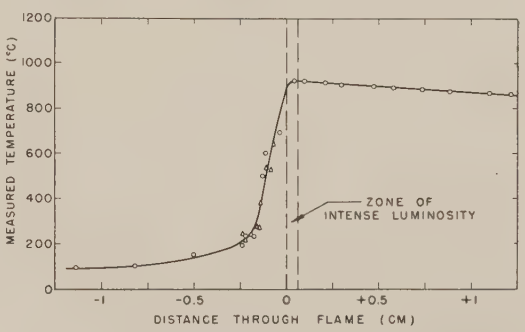

FIG. 3. Temperature distribution in ethylene oxide decomposition flame at 0.90 atmospheres.

step, but the product distribution, and therefore the net heat evolved, is influenced by second-order as well as first-order steps, these being all rapid relative to the rate-limiting step. Further, let us postulate that these effects operate so as to favor $CH_4 + CO$ (+32 kcal) as products at higher pressures, and $\frac{1}{2}\ C_2H_4 + H_2 + CO$ (+8 kcal) at lower pressures. An obvious consequence of this model is an increase of flame temperature with increasing pressure; this would tend to make the burning velocity decrease less rapidly with increasing pressure than the inverse square-root law would demand. Hence, if this effect were of the proper magnitude, the anomaly of the previous paragraph would be resolved.

The thermocouple measurements of flame temperature (Section 5.2) showed a one per cent increase in flame temperature when the pressure was increased by 27.5 per cent. This is in the right direction to be consistent with the foregoing proposal; however, a computation must be performed to see if it is large enough to account for the ob-

served change of burning velocity over this pressure range.

To make the computation, we shall use the burning velocity equation of Zeldovich and Frank-Kamenetsky[18] for a first-order reaction. We shall assume that the ratio of the thermal conductivity of the burned gases to the effective heat capacity is directly proportional to the absolute burned-gas temperature T_b. The equation then reduces to the following proportionality:

$$\text{burning velocity} \sim \frac{T_u T_b^2}{(T_b - T_u)} \exp(-E/2RT_b)$$

If we let T_b be 1200°K, T_u (the unburned gas temperature) be 343°K, and E (the activation energy) be 52,700 cal/mole (Mueller and Walters' value[1]), then we find that a one per cent increase in T_b gives a 13 per cent increase in burning velocity. For the pressure range in question (0.66 to 0.90 atm) the inverse square-root law for pressure dependence of burning velocity calls for a 14.4 per cent decrease in burning velocity. Thus, the net effect would be a small decrease in burning velocity with increasing pressure, which is what is observed (Fig. 2). The accuracy of the temperature measurements (perhaps ±0.2 per cent) is not sufficient to justify a more detailed comparison.

Further support may be found for the model being proposed in this section from consideration of the effect of pre-heating on the burning velocity. From Figure 2 of the writers' earlier paper on ethylene oxide[6], it is seen that the burning velocity for an initial temperature of 373°K is 1.17 times as great as for an initial temperature of 343°K. Let us take the corresponding values of T_b as 1202°K and 1202 + 13 = 1215°K (cf. Section 4.2). Then, by means of the proportionality based on the equation of Zeldovich and Frank-Kamenetsky[18], we may solve for the activation energy. We obtain 14 kcal/mole, which disagrees drastically with the value of activation energy which was successfully used in predicting the magnitude of the burning velocity, namely 52.7 kcal/mole. This anomaly, which otherwise would be quite difficult to account for, can be readily explained on the basis of the proposed model. We must assume that the effect of preheating is to change the product distribution so as to favor the products corresponding to the less exothermic of the two reaction paths. It would follow that the effect of pre-heating would be to increase the flame temperature by a smaller amount than the 13° calculated naively from the heat capacities of the unburned and burned gases. If the flame temperature increase were sufficiently small, the results would be consistent with an activation energy of 52.7 kcal.

There is yet another viewpoint from which we may consider the problem, namely the relation between the activation energy and the temperature at which reaction begins. If the activation energy is really as low as 14 kcal/mole, the reaction would begin at a quite low temperature. Let us define an "ignition temperature" T_i as the temperature at which the reaction rate constant is $1/100$ as great as it is at T_b. Then, the following relation is readily obtained from the Arrhenius law:

$$\frac{T_i}{T_b} = \frac{1}{[RT_b(\ln 100)/E] + 1}$$

We let T_b be 1211°K (cf. Section 5.2). Then, when E is 52.7 kcal/mole, T_i comes out to be 730°C. On the other hand, if E is taken to be 14 kcal/mole, T_i is then 400°C. The temperature profile of the flame, shown in Figure 3, has not been determined with sufficient precision to permit an unambiguous choice between these two values, even if the effect of the varying thermal conductivity of the complex gas mixture were known. However, the location of the beginning of luminosity on the temperature profile suggests that the higher value for T_i, and hence the higher activation energy, is more likely to be correct.

7. Summary

For the first time, a technique has been developed for stabilizing a decomposition flame of ethylene oxide. The burning velocity has been measured over the pressure range from 0.2 to 1.5 atm; the dependence of burning velocity on initial temperature has also been determined. Observations concerning flame appearance and carbon formation are described, and an explanation of the carbon formation is proposed. The combustion products were analyzed, and were found to consist of 44.9 per cent CO, 24.2 per cent CH_4, 20.6 per cent H_2, and 10.3 per cent C_2H_4. The flame temperature, measured with a thermocouple, was found to be 1182°K (based on an initial temperature of 25°C). This is in good agreement with a thermodynamically calculated value of 1217°K. The temperature distribution through the flame was also measured, and the result discussed.

The magnitude of the burning velocity is found to be in agreement with theoretical relations based on kinetic parameters obtained from studies of the first-order decomposition at much lower temperatures. However, neither the pressure dependence nor the temperature dependence of the burning velocity is consistent with this first-order theory. If the assumption is made that the burning rate is governed by the same first-order reaction as that which governs the low-temperature decomposition, but subsequent flame reactions governing distribution of products, and therefore the final flame temperature, depend upon the pressure and initial temperature, it then becomes possible to account for all of the results.

REFERENCES

1. Mueller, K. H., and Walters, W. D.: J. Am. Chem. Soc., *73*, 1458 (1951).
2. Lossing, F. P., Ingold, K. U., and Tickner, A. W.: Disc. Faraday Soc., *14*, 34–44 (1953).
3. Polanyi, J. C., and Lossing, F. P. et al.: Disc. Faraday Soc., *14*, 115 (1953).
4. Burden, F. A., and Burgoyne, J. H.: Proc. Roy. Soc., *A199*, 328 (1949).
5. Gerstein, M., McDonald, G. E., and Schalla, R. L.: *Fourth Symposium (International) on Combustion*, pp. 375–383. Baltimore, The Williams & Wilkins Co., 1953.
6. Friedman, R. and Burke, E.: J. Chem. Phys., *21*, 165 (1953).
7. Powling, J.: Fuel, *28*, 25 (1949).
8. Egerton, A. and Thabet, S. K.: Proc. Roy. Soc., *A211*, 445 (1952).
9. Egerton, A., and Sen, D.: *Fourth Symposium (International) on Combustion*, pp. 321–328. Baltimore, The Williams & Wilkins Co., 1953.
10. Friedman, R.: *Fourth Symposium (International) on Combustion*, pp. 259–263. Baltimore, The Williams & Wilkins Co., 1953.
11. Friedman, R., and Burke, E.: J. Chem. Phys., *22*, 824 (1954).
12. Walters, C. J., and Smith, J. M.: Chem. Eng. Prog., *48*, 337 (1952).
13. Burgoyne, J. H.: *Fourth Symposium (International) on Combustion*, p. 383. Baltimore, The Williams & Wilkins Co., 1953.
14. Kassel, L. S.: J. Am. Chem. Soc., *54*, 3949 (1932); *57*, 833 (1935).
15. Gordon, A. S.: J. Am. Chem. Soc., *70*, 395 (1948).
16. Rossini, F. D., et al.: *Selected Values of Chemical Thermodynamic Properties*. Washington, National Bureau of Standards, 1952.
17. Simon, D. M., Belles, F. E., and Spakowski, A. E.: *Fourth Symposium (International) on Combustion*, pp. 126–138. Baltimore, The Williams & Wilkins Co., 1953.
18. Zeldovich, Y. B., and Frank-Kamenetsky, D. A.: Zhur. Fis. Khimii, *12*, 100 (1938); Acta Physico-chimica (URSS), *9*, 341 (1938). cf. also NACA Tech. Memoranda 1026 and 1084.

63

SECOND LIMITS IN MIXTURES OF HYDROGEN, CARBON MONOXIDE AND OXYGEN

By G. DIXON-LEWIS

Dixon-Lewis and Linnett[1] have recently reported an investigation of the second limits of hydrogen + carbon monoxide + oxygen mixtures in a potassium chloride-coated vessel of 4 cm diameter and 6 cm length at temperatures between 510 and 580°C. In mixtures having a fixed ratio of combustible gas (H_2 + CO) to oxygen, the effect of varying the ratio of hydrogen to carbon monoxide was found to be twofold. Until about 90 per cent of the hydrogen in a hydrogen + oxygen mixture is replaced by carbon monoxide the limit is raised towards higher pressures and the carbon monoxide behaves approximately as an inert gas like nitrogen. Further replacement of hydrogen by carbon monoxide, however, causes the limit to fall off more and more rapidly towards lower pressures, and some new chain breaking process becomes important. Since Buckler and Norrish[2] had previously found that the second limits for 2CO + O_2 mixtures containing small amounts of hydrogen were not much affected by vessel diameter, it was assumed that this chain

breaking occurred in the gas phase. However, in some of the mixtures studied by Dixon-Lewis and Linnett[1] the hydrogen pressure was as little as 0.05 mm Hg, and it would seem very likely that in such mixtures chain destruction may occur by diffusion of oxygen atoms to the vessel wall. The influence of vessel diameter on the limits has therefore been reinvestigated.

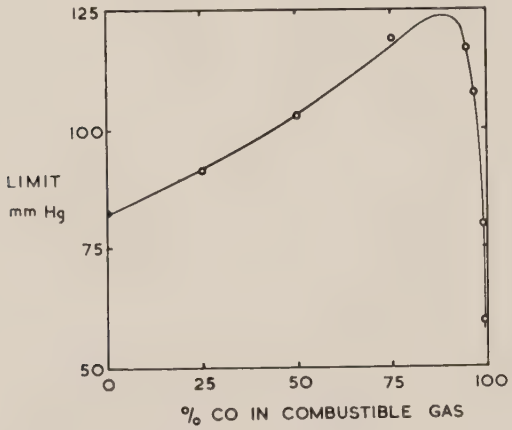

FIG. 1. Second limits for mixtures $2X + O_2$ at 529.9°C in 4 cm diameter KCl coated vessel.

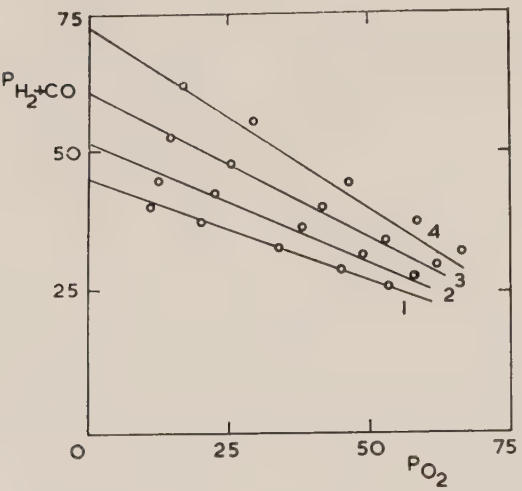

FIG. 2. Second limits for $H_2 + CO + O_2$ mixtures at 510.1°C (4 cm diameter vessel). Curve 1. $[CO]/[H_2] = 0$. Curve 2. $[CO]/[H_2] = 0.33$. Curve 3. $[CO]/[H_2] = 1$. Curve 4. $[CO]/[H_2] = 3$.

Experimental

Limits were determined by the withdrawal method. The silica reaction vessels used were heated by means of an electric furnace. Their surfaces were coated with a thick layer of potassium chloride. The gases were admitted to the vessel separately, their partial pressures being controlled to produce the desired composition, and the oxygen being admitted last from a calibrated vessel. A calibrated gas pipette was used for the measurement of small quantities of hydrogen. After a very rapid evacuation to a pressure somewhat above the estimated explosion limit, withdrawal was carried out fairly rapidly (ca. 40 mm sec^{-1}) until the limit was observed. If evacuation of mixtures containing only small amounts of hydrogen was carried out much more slowly than this, lower values were obtained for the limits due probably to inhibition by products formed immediately before reaching the limit (von Elbe and Lewis[3]). On the other hand, Broida and Oldenberg[4] have found that the limit in hydrogen + oxygen mixtures is also lowered by a too rapid rate of withdrawal, since there must be an induction period while the explosion builds up. The results obtained in this work were reproducible and independent of small variations in withdrawal rate. They are therefore regarded as sufficiently satisfactory for an analysis of the main effect of the carbon monoxide.

Cylinder hydrogen and oxygen were used, both gases being dried by calcium chloride and phosphorus pentoxide. Carbon monoxide was prepared by dropping 98 per cent formic acid on to sulphuric acid at 100°C in an all-glass apparatus. It was passed over soda-lime to remove acids, and was dried by calcium chloride and phosphorus pentoxide.

Results

THE EFFECT ON THE SECOND LIMITS OF REPLACING HYDROGEN BY CARBON MONOXIDE

In order to give a qualitative picture of the order of magnitude of the two effects of carbon monoxide mentioned above, the limits in the 4 cm-diameter vessel at 529.9°C for the mixture $2X + O_2$, where X represents the $H_2 + CO$ mixture, are shown in Figure 1. It is clear that the chain breaking effect of the carbon monoxide does not become appreciable until the amounts of hydrogen in the mixture have become quite small.

THE EFFECT OF VARYING THE RATIO OF COMBUSTIBLE GAS TO OXYGEN

This effect is best shown by plotting the partial pressure of combustible against the partial pressure of oxygen. Figures 2–5 show the curves obtained at 510.1 and 539.7°C from the previous work in the 4 cm vessel. As would be expected,

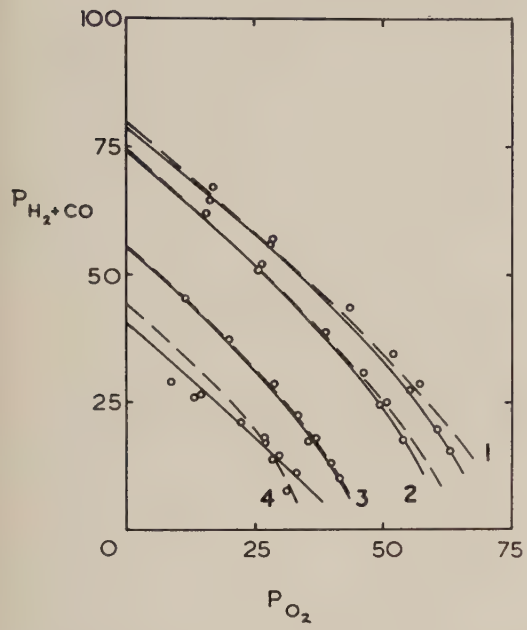

FIG. 3. Second limits for $H_2 + CO + O_2$ mixtures at 510.1°C (4 cm diameter vessel). Curve 1. $[CO]/[H_2] = 19$. Curve 2. $[CO]/[H_2] = 32.3$. Curve 3. $[CO]/[H_2] = 99$. Curve 4. $[CO]/[H_2] = 199$.

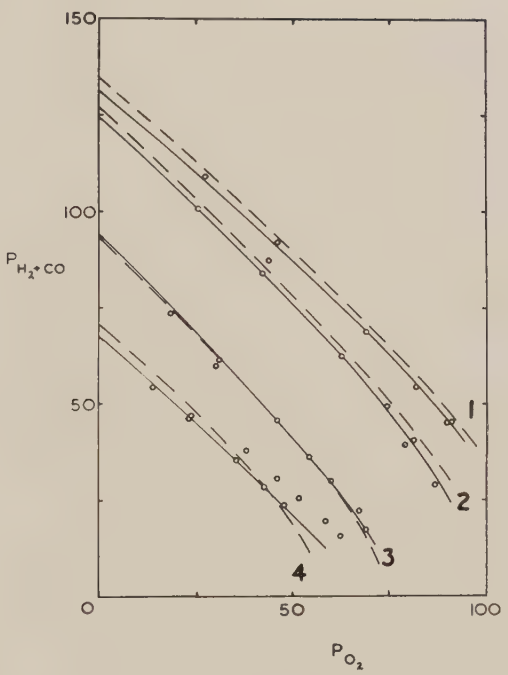

FIG. 5. Second limits for $H_2 + CO + O_2$ mixtures at 539.7°C (4 cm diameter vessel). Curve 1. $[CO]/[H_2] = 19$. Curve 2. $[CO]/[H_2] = 32.3$. Curve 3. $[CO]/[H_2] = 99$. Curve 4. $[CO]/[H_2] = 199$.

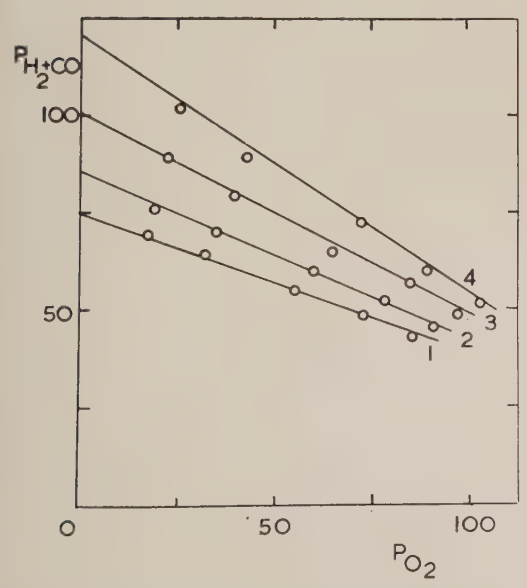

FIG. 4. Second limits for $H_2 + CO + O_2$ mixtures at 539.7°C (4 cm diameter vessel). Curve 1. $[CO]/[H_2] = 0$. Curve 2. $[CO]/[H_2] = 0.33$. Curve 3. $[CO]/[H_2] = 1$. Curve 4. $[CO]/[H_2] = 3$.

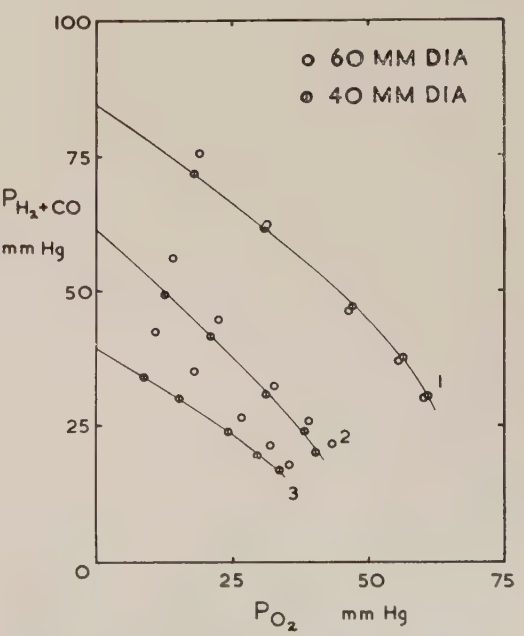

FIG. 6. Effect of vessel diameter at 515.5°C. Curve 1. $[CO]/[H_2] = 19$. Curve 2. $[CO]/[H_2] = 99$. Curve 3. $[CO]/[H_2] = 199$.

the slopes of the lines increase as the proportion of carbon monoxide in the combustible is increased. The lines for mixtures having $[CO]/[H_2] = 199$ are, however, shallower than those for mixtures with $[CO]/[H_2] = 99$.

THE EFFECT OF VESSEL DIAMETER

Limits were measured at 515.5°C and 534.3°C in a cylindrical KCl coated vessel of 8 cm length and 60 mm diameter, and at the latter temperature in a vessel of 8 cm length and 22 mm diameter. The results, together with those obtained by interpolation from the results of the previous work in a vessel of 40 mm diameter, are shown in Figures 6–8. They will be discussed below.

Discussion

(1) In the previous paper[1] the following were considered as possible reactions controlling the second limits in hydrogen + carbon monoxide + oxygen mixtures:

initiation $\rightarrow OH$

(i) $OH + H_2 = H_2O + H$

(ii) $H + O_2 = OH + O$

(iii) $O + H_2 = OH + H$

(iv) $H + O_2 + M = HO_2 + M$

(v) $HO_2 \rightarrow$ destr. at KCl wall

(vi) $H + CO + M' = HCO + M'$

(vii) $HCO \rightarrow$ destr. at KCl wall

(viii) $HCO + O_2 = HO_2 + CO$

(ix) $O + O_2 + M'' = O_3 + M''$

(x) $O + CO + M''' = CO_2^* + M'''$

(xi) $O + CO = CO_2^*$

In addition, it may be necessary to consider diffusion of hydrogen or oxygen atoms to the vessel wall with subsequent destruction of chain centers. Thus, Warren[5] has argued that wall destruction principally of hydrogen atoms may explain the effect of vessel surface and diameter on the hydrogen + oxygen second limits. In the present case, at the limits where the chain breaking action of the carbon monoxide is apparent, the hydrogen is in very short supply. It may therefore be particularly necessary to consider wall destruction of oxygen atoms. Reactions

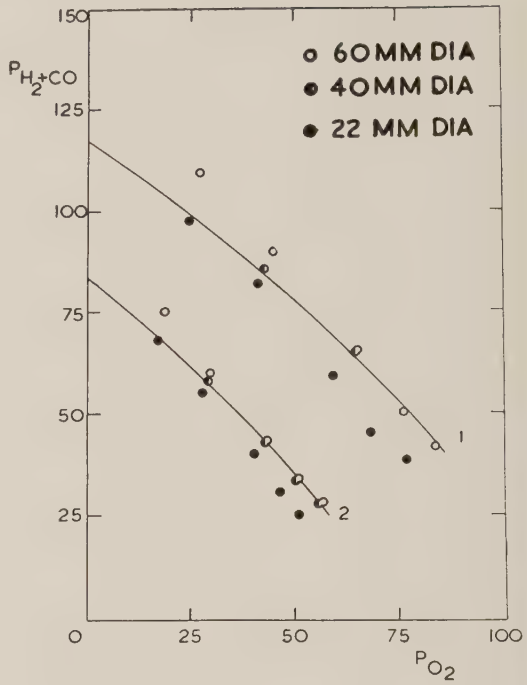

FIG. 7. Effect of vessel diameter at 534.3°C. Curve 1. $[CO]/[H_2] = 19$. Curve 2. $[CO]/[H_2] = 99$.

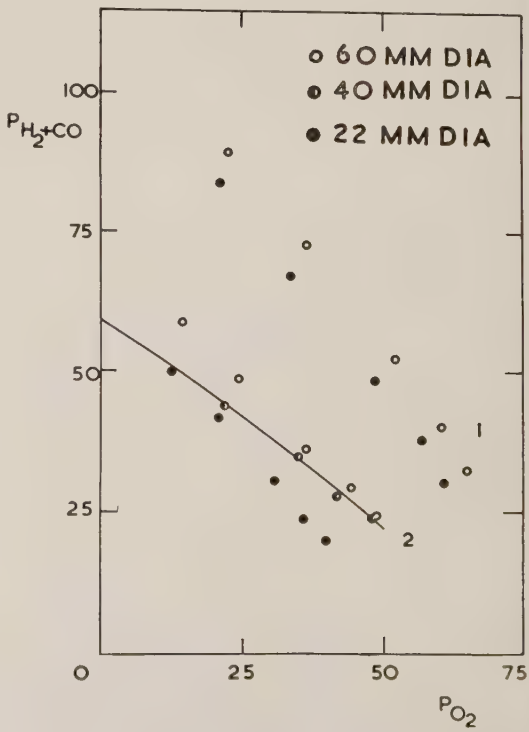

FIG. 8. Effect of vessel diameter at 534.3°C. Curve 1. $[CO]/[H_2] = 49$. Curve 2. $[CO]/[H_2] = 199$.

(xii) and (xiii) should therefore also be considered:

(xii) $H \rightarrow$ destr. at wall

(xiii) $O \rightarrow$ destr. at wall.

If now it is assumed that O_3 formation by reaction (ix) leads entirely to chain termination, reactions (i) to (xiii) lead to equation (1) for the limits:

$$\begin{aligned} 2k_2 = \{&\Sigma k_4[M] + k_6\Sigma[M'][CO]/[O_2] \\ &+ k_{12}/[O_2]\} \times \{k_9\Sigma[M'']/[O_2]/k_3[H_2] \\ &+ k_{10}\Sigma[M''']/[CO]/k_3[H_2] \\ &+ k_{11}[CO]/k_3[H_2] + k_{13}/k_3[H_2] + 1\} \end{aligned} \tag{1}$$

where

$$\Sigma[M] = [H_2] + k_{O_2}[O_2] + k_{CO}[CO]$$

$$\Sigma[M'] = [H_2] + k'_{O_2}[O_2] + k'_{CO}[CO] \quad \text{etc.}$$

k_{O_2}, k_{CO} etc. being the third body coefficients of the respective molecules in reactions (iv), (vi), (ix) and (x). By multiplying out, equation (1) can be shown to be of the correct general form for describing the limits. The first four terms in the second bracket represent the various chain breaking reactions which may compete with the branching reaction $O + H_2 = OH + H$ for the oxygen atoms in the system. The combination of reactions (vi) and (ix) also produces an effect which depends on the $[CO]/[H_2]$ ratio, but this is coupled with a further effect which depends only on the $[CO]/[O_2]$ ratio, and which should be apparent at small values of $[CO]/[H_2]$. The points in Figures 2 and 4 show the experimental limits obtained by Dixon-Lewis and Linnett[1] for low values of $[CO]/[H_2]$. Their approximate linearity indicates that the CO is here behaving quite closely as an inert gas. Reaction (vi) can therefore be ruled out as a major chain breaking reaction.

(2) Figures 6–8 show the effect of vessel diameter to be small, thus confirming the previous result of Buckler and Norrish[2] for $2CO + O_2$ mixtures containing small quantities of hydrogen. However, referring again to equation (1), it is clear that even if the whole of the chain breaking effect when $[CO]/[H_2]$ is large depends on diffusion of O atoms, the overall effect of vessel diameter on the limit need not be great, since it depends on the magnitude of the term $k_{13}/k_3[H_2]$ relative to 1. From Figures 6–8 it would appear that the magnitude of the diameter effect is not very closely related to $1/[H_2]$. Further, Figure 1 shows that, assuming the third body coefficient k_{CO} to be in the neighborhood of 0.5 (collision theory gives a value of 0.45), then for the 4 cm vessel the term $k_{13}/k_3[H_2]$ would need to have a value of rather more than 1 when $[CO]/[H_2] = 199$. For these mixtures the effect on the limits at 534.3°C of changing the vessel diameter from 22 mm to 60 mm (Fig. 8) is not nearly large enough for a diffusion mechanism to provide the main chain terminating step. It must be concluded therefore that the main chain breaking action occurs in the gas phase.

(3) The possibilities now remaining are that the chain breaking is due to a reaction of CO with either O atoms or OH. However, a terminating reaction of OH with CO would have to compete not only with reaction (i) $OH + H_2 = H_2O + H$, but also with reaction (xiv) $OH + CO = CO_2 + H$, which may be quite a rapid reaction. Of the possibilities considered, the most likely terminating reaction would therefore seem to be the association $O(^3P) + CO(^1\Sigma) \rightarrow CO_2^*$ which produces CO_2 molecules in an excited triplet state.

(4) Dixon-Lewis and Linnett[1] found the limits in the 4 cm diameter vessel to be closely described by equation (2). The second term in the bracket on the left-hand side of equation (2) merely allows for a proportion of the ozone formed in reaction (ix) re-entering the reaction cycle by way of (xv) $O_3 + H_2 = OH + HO_2$. If this term is neglected,

$$\begin{aligned} K_1\{1 + \tfrac{1}{2}K_4K_3\Sigma[M'']/[O_2]/[H_2]\} \\ = \Sigma[M]\{K_3\Sigma[M'']/[O_2]/[H_2] \\ + K_2[CO]/[H_2] + 1\} \end{aligned} \tag{2}$$

equation (2) is identical with equation (1) if $K_1 = 2k_2/k_4$, $K_2 = k_{11}/k_3$, $K_3 = k_9/k_3$, and k_6, k_{10}, k_{12} and $k_{13} = 0$.

In establishing the form of equation (2) describing the limits, the values used for K_1 and k_{O_2} were obtained from experiments with hydrogen + oxygen mixtures. The value used for k_{CO} was 0.45, obtained by assuming the physical effect of carbon monoxide as a third body in reaction (iv) to be identical with the effect of nitrogen which was determined separately. However, in studying the effect of carbon monoxide on the hydrogen + oxygen limits we are in fact studying two opposing effects of the same substance, a physical effect which tends to raise the limit pressure and a chemical effect which tends to lower it. The apparent form of the

chemical effect may well be quite sensitive to the value assumed for k_{CO}. On the other hand, due to the existence of the chemical effect it may be difficult to determine the physical effect directly with any certainty. At 539.7°C the best value for k_{CO} appeared to be 0.48. Limits calculated from equation (2) using $k_{CO} = k''_{CO} = 0.48$, $k_{O_2} = k''_{O_2} = 0.36$, $K_1 = 75.0$ mm. $K_2 = 6.44 \times 10^{-3}$, $K_3 = 1.78 \times 10^{-4}$ mm^{-1}, $K_4 = 0.641$ are shown as the full lines in Figures 4 and 5. The agreement with experiment is very good. At 510.1°C using the same values of the third body coefficients, together with $K_1 = 45.0$ mm, $K_2 = 6.56 \times 10^{-3}$, $K_3 = 2.60 \times 10^{-4}$ mm^{-1}, $K_4 = 0.656$, the agreement (full lines in Figures 2 and 3) is not quite so good for mixtures containing excess oxygen and having small values of $[CO]/[H_2]$.

(5) In interpreting results, equation (2) requires that the association reaction assumed to occur between O and CO should follow a second order rate law. On the other hand, associations between simple species such as O and CO can only occur when one of two conditions is satisfied. Either (1) a three-body collision is necessary in order to stabilize the product, or (2) stabilization occurs by emission of radiation.

In the second case the reaction (xi) $O + CO = CO_2 + h\nu$ may be responsible for the continuous emission of the CO flame. Such an assumption is not, however, without difficulty. Firstly, due to the greater likelihood at the limit pressures of collisional deactivation of an attractive state of CO_2^* if this can be formed in the association, it would be required that the O and CO should approach along a repulsive potential energy curve. Using the revised values of k_{CO}, the value of $K_2 (= k_{11}/k_3)$ has been found to be about 6×10^{-3} at 539.7°C. If reaction (iii) is assumed to have an activation energy of 6 kcal mol^{-1} [6] and a steric factor of about one (as Semenov's figures[7] indicate for the similar type of reaction (ii) $H + O_2 = OH + O$) this value of K_2 is higher than would be expected for a repulsive state even assuming a fully allowed transition. Secondly, the continuum is more characteristic of the hot flames of CO. At the lower temperatures with which we are dealing, the glow of $CO + O_2$ mixtures exhibits the band spectrum much more strongly, and this is thought by Gaydon[8] and by Walsh[9] to be probably due to CO_2. Although reaction (xi) cannot be ruled out, it seems to be less probable as a limit controlling process than the corresponding termolecular reaction

$$\text{(x)} \qquad O + CO + M''' = CO_2^* + M'''.$$

The second possibility to be considered is that reaction (x) occurs, but that the life of the vibrationally activated CO_2^* formed in the first stage of the association is sufficiently long for (x) to give second order kinetics. At the lowest measured pressures of 40 mm Hg the complex would undergo about 3×10^8 collisions sec^{-1}, so that its average life would need to be at least of the order of 10^{-7} sec. The probable life of a *symmetrical* triatomic molecule of this type which, although it contains sufficient energy to dissociate, may disperse this energy between like bonds is not known. Alternatively we could consider the equilibrium (x) and reaction (xvi). If $k_{10b} \gg k_{16}$ these too lead to second order kinetics for the association. Here, an average life

$$\text{(x)} \quad O + CO + M''' \underset{b}{\overset{a}{\rightleftharpoons}} CO_2^* + M'''$$

$$\text{(xvi)} \qquad CO_2^* = CO_2^{**} + h\nu \text{ (banded)}$$

of the newly formed, vibrationally activated CO_2^* of the order of 10^{-12} to 10^{-11} sec would probably be sufficient to explain the rates of association at 510.1°C. Assuming this set of reactions with k_{16} independent of temperature, the ratio of second order rate constants K_2 would be expected to decrease with increasing temperature due to the shift of the equilibrium (x) and the activation energy of reaction (iii). It is difficult to be certain of the dependence of K_2 on temperature because of its marked dependence on the value assumed for k_{CO}.

Lastly, assuming reaction (x) to be third order, we may consider the following as contributing to produce results in conformity with equation (2): (1) wall destruction reactions, and (2) further reactions of CO_2^*. The effect of vessel diameter is not inconsistent with a minor contribution from wall destruction terms, but it seems that the effects to be explained are rather large to be accounted for solely in this way. Detailed examination is not justified. For (2) we could consider reaction (x) to be followed by (xvi), (xvii) and (xviii). When $[O_2]$ is zero, a competition between reactions such as (xvi) and (xvii) is possible if (xvi) represents a transition of high probability. Walsh[9] has recently made a new analysis of the CO flame bands, and has concluded that the emission is probably from an upper, linear triplet state of CO_2 to a lower, strongly bent triplet

state (not the ground state). Such a transition may have quite a high probability.

$$\text{(x)} \quad O + CO + M''' = CO_2^* + M'''$$

$$\text{(xvi)} \quad CO_2^* = CO_2^{**} + h\nu \text{ (banded)}$$

$$\text{(xvii)} \quad CO_2^* + H_2 = CO_2 + H + H$$

$$\text{(xviii)} \quad CO_2^* + O_2 + M = CO_2 + O_2 + M$$

Using reactions (x) and (xvi)–(xviii) to describe the action of the CO, the intercepts of the partial pressure curves on the p_{H_2+CO} axis ($[O_2]$ zero) are given by equation (3).

$$K_1\left\{1 + \frac{k_{17}[H_2]}{k_{16} + k_{17}[H_2]} \frac{k_{10}[CO]}{k_3[H_2]} \Sigma[M'''']\right\} = \Sigma[M]\left\{1 + \frac{k_{10}[CO]}{k_3[H_2]} \Sigma[M'''']\right\} \quad (3)$$

The intercepts of the broken lines in Figures 3 and 5 are calculated from equation (3) using the following new constants:

at 510.1°C, $k_{10}/k_3 = 2.9 \times 10^{-4}\text{mm}^{-1}$,

$k_{16}/k_{17} = 4.65$ mm;

at 539.7°C, $k_{10}/k_3 = 2.1 \times 10^{-4}\text{mm}^{-1}$,

$k_{16}/k_{17} = 4.28$ mm.

The third body coefficients in reaction (x) were assumed to be the same as in reaction (iv), and the other constants had the same values as previously. The lines themselves were obtained assuming reaction (xvii) to be negligible when $[O_2]$ is large, together with a contribution from the ozone forming reaction (ix). The values used for k_9/k_3 were: at 510.1°C, 8.9×10^{-5} mm^{-1}; at 539.7°C, 4.5×10^{-5} mm^{-1}, but they have little significance.

It is seen that a series of reactions such as (x) and (xvi)–(xviii) is capable of explaining some of the observed effects, and the values which must be assumed for the constants k_{10}/k_3 and k_{16}/k_{17} are not unreasonable. It must be concluded that although an association between O atoms and CO is likely to be largely responsible for the observed chemical effect of CO on the hydrogen + oxygen second limits, the simplest assumption which fits the observed kinetics, namely that of a bimolecular association, presents certain difficulties. The alternative is that if such an association does play a part in controlling the limits it occurs termolecularly, and that other factors contribute to give the association either true or apparent second order kinetics.

Acknowledgment

The author is indebted to Professor A. L. Roberts and to the Joint Research Committee of the Gas Council and the University of Leeds for their encouragement during the course of this work, and to Dr. A. D. Walsh for helpful comments.

REFERENCES

1. Dixon-Lewis, G., and Linnett, J. W.: Trans. Faraday Soc., *49*, 756, (1953).
2. Buckler, E. J., and Norrish, R. G. W.: Proc. Roy. Soc., *A167*, 292, 318 (1938).
3. von Elbe, G., and Lewis, B.: J. Chem. Phys., *9*, 194, (1941).
4. Broida, H. P., and Oldenberg, O.: J. Chem. Phys., *19*, 196 (1951).
5. Warren, D. R.: Proc. Roy. Soc. *A211*, 86, 96 (1952).
6. Harteck, P., and Kopsch, U.: Z. physikal. Chem., *B12*, 327, (1931).
7. Semenov, N.: Acta Physicochim. (U.R.S.S.), *20*, 291 (1945).
8. Gaydon, A. G.: *Spectroscopy and Combustion Theory*. London, Chapman and Hall, 1948.
9. Walsh, A. D.: J. Chem. Soc., 2266 (1953).

64

THE PROBLEM OF THE SECOND EXPLOSION LIMIT IN THE CARBON MONOXIDE-OXYGEN SYSTEM[a]

By GUENTHER VON ELBE, BERNARD LEWIS AND WALTER ROTH

Introduction

It has been discovered independently by Kopp, Kowalsky, Sagulin and Semenoff[1] and by Hadman, Thompson and Hinshelwood[2] that the pressures and temperatures at which a carbon monoxide-oxygen mixture explodes occupy a peninsula-shaped region in a pressure-temperature diagram. Along the lower bound of this region—the first explosion limit—the pressure decreases with increasing temperature, whereas along the upper bound—the second explosion limit—the pressure increases with increasing temperature. The existence of such peninsulas may be taken as evidence[3] that a branched-chain reaction occurs which is competing with two chain-breaking reactions, one predominating at low pressure and the other at high pressure. Because the three reactions are competitive, they are necessarily of equal order with respect to the concentration of chain carriers[4]; hence, if that order is known for one reaction, it is likewise known for the other two reactions. In the experiments of Hadman, Thompson and Hinshelwood[2] the first explosion limit was found to be raised, and the area of the explosion peninsula correspondingly reduced, when the surface-to-volume ratio of the reaction vessel was increased; this shows that chain-branching occurs in the gas phase and chain-breaking at the vessel surface. The latter process, being controlled by diffusion from the interior of the vessel to the wall, constitutes, in effect, a first-order reaction with respect to the chain-carrier concentration. It follows that the branching reaction and the high-pressure breaking reaction are also of first order with respect to the chain-carrier concentration. Furthermore, considering that the branching reaction occurs in the gas phase and that kinetically significant reactions are unlikely to involve collisions of more than three species, it seems reasonable to suppose that the branching reaction is a binary reaction involving collision between a chain carrier and a reactant molecule, and the high-pressure breaking reaction is a ternary reaction involving collision between a chain carrier, a reactant molecule, and a third molecule.

The presence of water vapor in the experiments of Kopp, Kowalsky, Sagulin and Semenoff[1] raises the question whether their data may have been affected by reactions involving H_2O. However, the experiments of Hadman, Thompson and Hinshelwood[2] were performed with gases dried over P_2O_5 ; in addition, the second explosion limit was found to be substantially higher for oxygen-rich than for oxygen-lean mixtures, indicating that oxygen promotes the explosive reaction, whereas the water-catalyzed CO-O_2 reaction is, on the contrary, inhibited by oxygen[5]. One may therefore conclude that the explosion limits observed by these authors were unaffected by traces of water vapor, so that the branching and breaking reactions involve only CO, O_2, and species derived from these molecules.

Speculation concerning these species is restricted by the requirement that the postulated reactions must be consistent with present theoretical knowledge of rate processes. This has been discussed by Griffing and Laidler[6] and by Gaydon, Walsh, Hoare and Dixon-Lewis[7], and will be considered later in this paper. Additional restrictions are imposed by the observable changes of the limit pressures that result from changes of experimental variables. These variables comprise the mixture composition, which provides information on the chemical identity of the species participating in the mechanism, and the temperature, which provides information on the difference of activation energies between the branching and breaking reactions.

The relation between limit pressures and mixture composition becomes enormously complicated when surface chain-breaking occurs simultaneously with gas-phase chain-breaking. It is therefore necessary to confine the observations to second-limit pressures and to eliminate any significant effect of the vessel surface on the experimental data—in other words, to make the

[a] This research is a part of work by the Bureau of Mines under Contract AF 18(600)-156, supported by the Flight Research Laboratory, Wright Air Development Center.

first-limit pressure as small as possible in relation to the second-limit pressure. This requires establishment of very low chain-breaking efficiency of the surface by selection of a suitable vessel material, or by suitable treatment of the surface, or both. The condition of negligible surface effect is obtained if it can be shown that the second-limit pressures do not change when the vessel diameter is changed. Inasmuch as such data have not been reported previously, the present experimental work has been directed toward this aim.

Apparatus and Experimental Procedure

The apparatus was in most respects similar to that used by Gordon[8] in experiments previously reported. In this preliminary work conditions for independence of second-limit pressures on vessel diameter were not found.

Oxygen was prepared by passing tank oxygen through a KOH trap to a trap cooled by liquid N_2, where it was liquefied. The trap was connected to a vacuum line until one-third of the liquid had boiled away. Another third was evaporated into a previously evacuated storage vessel to a pressure of about 1 atm. A mass-spectrometric analysis of the gas prepared in this manner indicated that it contained 99.0 per cent O_2, 0.6 per cent N_2 and 0.4 per cent A.

Carbon monoxide was prepared by the action of orthophosphoric acid on formic acid in the temperature range 140°–160°C. The gas was passed through a series of traps in the following order: Water ice, dry ice, KOH, dry ice. Following the last dry-ice trap, the gas was liquefied in a trap cooled by liquid N_2. The trap was connected to a vacuum line until about one-third of the liquid CO had boiled away. Another third was evaporated into a storage vessel to a pressure of about 1 atm. The gas prepared in this manner was found to be 100 per cent pure by mass-spectrometric analysis.

Carbon dioxide was prepared from tank carbon dioxide by first allowing a considerable quantity of the gas to escape from the tank to the atmosphere, then freezing some of the gas in a trap cooled by liquid N_2, pumping on the solid for 15 minutes, distilling to another liquid N_2 trap and evaporating to storage.

Nitrogen was prepared from tank nitrogen by passing the gas through two liquid-N_2 traps and directly to storage.

A scheme of the apparatus is shown in Figure 1. Mixtures were prepared on a pressure basis and stored in the mixture vessel for further use.

Before a run was made, the furnace was raised about the quartz reaction vessel, which was pumped down to $<10^{-6}$ mm. Thereafter, pumping was continued for two hours while the temperature was maintained at 800°–900°C. Following the bake-out, the furnace was lowered and the vessel cooled to about 70°C by blowing a stream of air upon it. The quartz-spiral-gage manometer was set for any desired pressure and the reaction vessel filled with mixture to the desired pressure by bringing the spiral gage to a null point. The spiral gage was then reset to a pressure approximating the expected explosion pressure and the furnace was raised about the vessel. The air stream was maintained and the

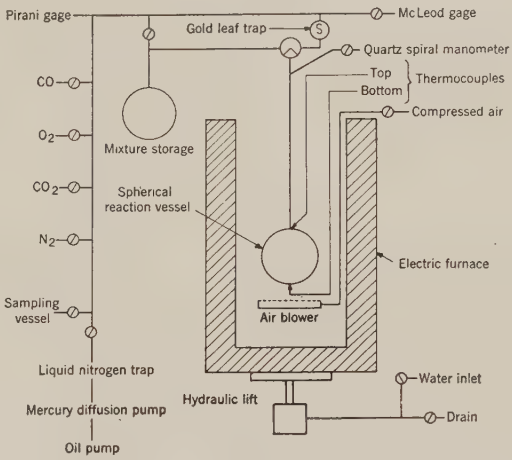

FIG. 1. Apparatus used for measurement of second explosion limits of CO-O_2 mixtures.

temperature indicated by the thermocouples at the top and bottom of the vessel were periodically observed as the vessel temperature increased. When the top thermocouple indicated a temperature 5°–10°C higher than the bottom thermocouple, the air stream was shut off. The spiral-gage scale was observed until a sharp decrease in pressure, indicating explosion, was noted. The pressure just before explosion and the temperature of the bottom thermocouple at the instant of explosion were recorded. In addition, the pressure just after explosion and the time from raising the furnace to explosion were recorded. The former value was used to calculate the fraction of the mixture that had reacted. Immediately after the temperature was read from the bottom thermocouple, the temperature of the top thermocouple was checked to determine the magnitude of any gradient that existed. If the gradient exceeded 10°C, if the heating time ex-

ceeded 2½ min, or if there was a large amount of slow reaction preceding explosion, the run was rejected. In this connection, it was observed that unless the furnace temperature was at least 100°C above the expected explosion temperature, heating was too slow and considerable slow reaction took place before explosion, sometimes enough to inhibit explosion entirely.

The bottom thermocouple was calibrated against a standard couple in the range of interest each day and the millivoltmeter was checked with a potentiometer.

On a number of occasions, the reaction vessel was observed visually by use of a mirror or by use of a sensitive photomultiplier tube. In every case, a brilliant flash of light was observed to occur simultaneously with the sharp pressure decrease that indicated explosion. A preexplosion glow was never noted, even where slow reaction preceded explosion.

In those experiments involving nitrogen addition, the nitrogen was added directly to the mixture in the reaction vessel using the spiral gage to indicate the partial pressure of N_2 in the final mixture. This procedure allowed one CO-O_2 mixture to be used for experiments with varying percentages of N_2.

In the course of this study, considerable time was spent to determine experimental conditions that would yield results that were reproducible and independent of vessel diameter over a range of variables. To achieve this, it was found necessary to adhere to the following rules:

The bake-out procedure previously described had to be followed before each run.

Gases had to be absolutely dry. The effect observed when small amounts of water vapor were present is described below. If the system was opened to the atmosphere for any reason, a prolonged period of pumping had to follow to insure the removal of water vapor. Flaming of the tubing as an aid to outgassing was not permissible.

If glassblowing was necessary to repair or modify the system, glassware had to be thoroughly cleaned for several inches on either side of the repair site before a flame was applied. It was found that a film of grease spread throughout the system from the stopcocks. If this film was not removed before glassblowing, its pyrolysis led to adverse effects described below. In this connection, silicone grease is to be preferred to apiezon grease because of its higher temperature stability.

The vessel had to be absolutely free of foreign material. On one occasion, a new silica reaction vessel was being prepared to be sealed to the system and the capillary tube leading to the vessel, having a rough edge, was smoothed by scraping with a wire gauze. Apparently several minute particles of iron oxide were scraped from the gauze and accidentally introduced into the vessel. Subsequent use of this contaminated vessel resulted in slow reactions only. After

Table 1. Data on Second Explosion Limit in Carbon Monoxide-Oxygen Mixtures Without Inert Gas

$CO:O_2$ = molar ratio; d = vessel diameter in cm;
T = temperature in °C; P = pressure in mm Hg

$CO:O_2$	1:4		1:4		1:2		1:2		4:1		4:1		1:1		2:1	
d	4		6		4		6		4		6		6		6	
	T	P	T	P	T	P	T	P	T	P	T	P	T	P	T	P
	717	389	676	314	639	172	642	166	704	100	713	157	690	92	687	53
	728	435	685	364	645	183	644	192	722	124	701	161	699	110	689	66
	729	500	697	434	652	221	673	300	725	164	719	181	695	138	703	87
	739	507	703	438	657	239	670	303	761	218	761	268	706	174	707	98
	748	571	710	555	665	280	706	368			749	273	736	206	707	101
			728	619	686	331	704	384					731	208	737	207
			735	637	686	335	714	412					739	211	739	212
			742	735	712	381	738	482					757	308	740	213
			739	738	742	492	735	486					765	336	771	306
					738	500	766	552					764	344	771	308
					752	526	768	571								
					753	533										

thorough cleaning the effect disappeared and explosion data could again be obtained.

RESULTS

Table 1 and Figures 2 and 3 indicate the effect on the second limit of varying the mixture ratio and the diameter of the reaction vessel. Table 1 and Figures 2 and 3 were used to construct Figure 4, which shows the effect of variation of mixture composition in a 6-cm-diameter vessel. Table 2 and Figure 5 indicate the effect of the addition of 20, 40 and 60 per cent of nitrogen to mixtures of $CO + 2O_2$ and $2CO + O_2$ in a 6-cm-diameter vessel.

If the bake-out procedure previously described was omitted and the reaction vessel was merely pumped down at room temperature between runs, results were erratic but always indicated a higher temperature for explosion at any given pressure than did explosions in a baked-out vessel. Since the only reaction product was CO_2, it was thought that this was being strongly adsorbed on the wall of the vessel and, in some manner, making the wall an efficient chain breaker. This theory was tested by admitting about ½ atm of CO_2 to a previously baked-out vessel and then pumping away the CO_2 at room temperature. Results were then equivalent to those obtained with unbaked vessels[b].

Accidental pyrolysis of grease in the system resulted in a very large decrease in the pressure limit and the appearance of a large-diameter effect. It is noted that Mardles[10] found a strong inhibitory effect when adding 10 per cent of CH_4 to the reaction mixture. These seemingly allied effects could result from the rapid production of CO_2 in the gas phase.

If the mixture was not completely dry, the pressure limit was found to increase considerably. This has also been pointed out by Hoare and Walsh[11]. If glassblowing repairs necessitated opening the system to the atmosphere, pumping for 1 or 2 days was required to sufficiently remove water vapor without having to flame the glass.

Discussion

An increase of the second explosion limit with increasing O_2:CO ratio has already been reported by Hadman, Thompson and Hinshelwood[2]. In the experiments of Kopp, Kowalsky, Sagulin and Semenoff[1] it was found that addition of N_2 to a CO-O_2 mixture did not change the limit pressure, a result which has been confirmed in the present experiments with dry mixtures. To explain these facts, Lewis and von Elbe[12] suggested that the explosion limit is essentially controlled by the

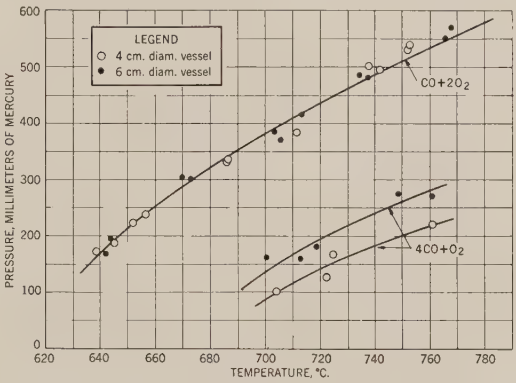

FIG. 2. Second explosion limit for $CO + 2O_2$ and $4CO + O_2$.

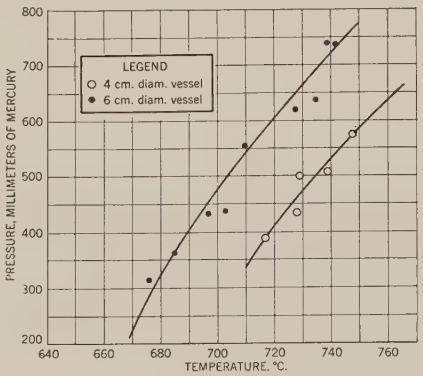

FIG. 3. Second explosion limit for $CO + 4O_2$.

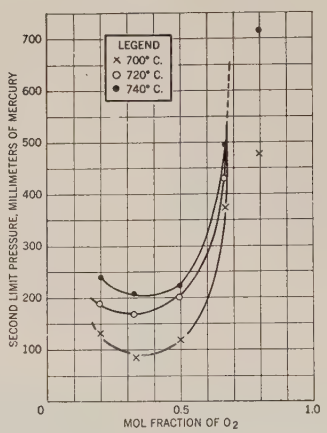

FIG. 4. Effect of variation of mixture composition on second explosion limit of CO-O_2 system. 6-cm (diameter) silica vessel.

[b] A. F. Benton[9] reports that powdered silica adsorbs CO_2 tenfold over CO or O_2 at temperatures up to 184°C.

reactions

$$O + O_2 + M = O_3 + M \quad \text{(i)}$$

$$O + CO + M = CO_2 + M \quad \text{(ii)}$$

$$O_3 + CO = CO_2 + 2O \quad \text{(iii)}$$

$$O_3 + CO + M = CO_2 + O_2 + M \quad \text{(iv)}$$

and that the molecules N_2, O_2 and CO are about equally effective third bodies M in the ternary ratio and to be independent of the mole fraction of N_2. This is due to the introduction of the competitive reactions I and II into the scheme, coupled with the assumption that the third-body efficiencies of N_2, O_2 and CO are equal. It is important to note that no other set of assumptions seems discoverable that would serve the purpose of qualitatively explaining the O_2- and N_2-effects; on the other hand, equation (1) is inconsistent

Table 2. Effect of Addition of Nitrogen to the Reaction Mixture
(6-cm vessel)

$CO:O_2$.....	1:2		1:2		1:2		2:1		2:1		2:1	
Per cent N_2...	20		40		60		20		40		60	
	T	P	T	P	T	P	T	P	T	P	T	P
	680	299	688	322	663	313	716	104	684	98	699	99
	679	318	704	388	697	344	736	160	725	160	735	163
	725	421	709	433	733	436	741	166	743	212	750	217
	731	441	726	501	765	524	748	212	759	303	773	306
							775	291				

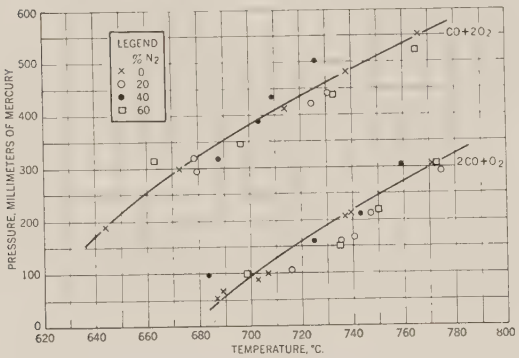

Fig. 5. The effect of the addition of nitrogen on the second explosion limit. (6-cm vessel.)

reactions (i), (ii) and (iv). On this basis the explosion condition becomes

$$[M]_e = \frac{\frac{k_1}{k_2}\frac{f_{O_2}}{f_{CO}} - 1}{\frac{k_3}{k_4}\frac{k_1}{k_2}\frac{f_{O_2}}{f_{CO}} + 1}, \quad (1)$$

where $[M]_e$ denotes the total concentration of molecules CO, O_2 and N_2 at the explosion limit; k_1, etc., the rate coefficients of the various reactions, and f_{O_2} and f_{CO} the mole fractions of O_2 and CO, respectively. As may be seen from equation (1), the scheme shows the second-limit pressure to increase with increasing O_2:CO ratio and to be independent of the mole fraction of N_2. This is due to the introduction of the competitive reactions I and II into the scheme, coupled with the assumption that the third-body efficiencies of N_2, O_2 and CO are equal. It is important to note that no other set of assumptions seems discoverable that would serve the purpose of qualitatively explaining the O_2- and N_2-effects; on the other hand, equation (1) is inconsistent with the trend of the data in Figure 4 inasmuch as it predicts that the limit pressure vanishes as the O_2:CO ratio is decreased, which is certainly not borne out by the curves in Figure 4.

The answer to this problem seems to be provided by the fact[6, 7] that the CO_2 molecule formed in reaction (ii) is in an electronically excited (3π) state which is quenched in collisions with oxygen, as for example,

$$CO_2^* + O_2 = CO_2 + 2O. \quad \text{(v)}$$

Thus, another chain carrier is introduced into the mechanism and the reaction possibilities are correspondingly increased. However, before discussing this subject further, it is in order to discuss another aspect of the present theory and the experimental data.

If the chain-breaking reaction (iv) were omitted from the scheme, there would be no second-limit pressure, and the reaction would always be explosive. Now, the data of Figure 4 suggest that this is actually the case above a critical O_2:CO-ratio situated somewhere between 2:1 and 4:1. This view is based on the fact that at the 4:1-ratio the limit pressures are dependent upon vessel diameter[c] (see Figure 3), and that

[c] The bake-out treatment did not provide vessel-diameter independence of the limit under these conditions.

therefore the points in Figure 4 at $f_{O_2} = 0.8$ would probably shift to much higher values if the vessel diameter were increased beyond 6 cm, which was the largest diameter in the present experiments. The diameter effect signifies either that the chain-breaking efficiency of the wall is substantially larger for such mixtures, which would remain unexplained at present, or that the branching reaction is arrested by second-order reactions such as $O + O_3 = 2O_2$, and that in consequence the process shifts from isothermal branched-chain explosion to thermal explosion. This is because a second order chain-carrier reaction limits the growth of chain-carrier concentration; however, the reaction rate may become fast enough to unbalance the thermal equilibrium. In either case it appears that gas-phase chain-breaking loses control at such mixture ratios, and this in turn means that reaction (iv) has no place in the mechanism.

To explain the existence of a limit pressure at lower O_2:CO-ratios, it is necessary to introduce the additional CO_2^*-quenching reaction

$$CO_2^* + O_2 + M = CO_2 + O_2 + M. \quad \text{(vi)}$$

This yields the explosion condition

$$[M]_e = \frac{k_5}{k_6} \frac{1 + \frac{k_1}{k_2}\frac{f_{O_2}}{f_{CO}}}{1 - \frac{k_1}{k_2}\frac{f_{O_2}}{f_{CO}}}. \quad (2)$$

According to this equation, the limit is infinite at a critical value of the O_2:CO-ratio and decreases to a finite value as the O_2:CO ratio is decreased. While the scheme accounts for the sharp upturn of the limit at large O_2:CO-ratios, it does not describe the upturn shown in the curves of Figure 4 on the CO-rich side. However, it is not certain whether the curves are sufficiently accurate to establish this latter upturn as an experimental fact.

Perhaps the most important uncertainty arises from the fact that, in order to obtain finite limits below the critical O_2:CO-ratio mentioned earlier, the equation demands the ratio k_1/k_2 to be somewhat smaller than unity, whereas other evidence[13] suggests that this ratio is much larger than unity. It may be proposed that the reaction

$$O_3 + CO = CO_2 + O_2 \quad \text{(vii)}$$

occurs with a frequency slightly smaller than the frequency of the reaction III; in this case, the factor k_1/k_2 is replaced by the factor $(k_1/k_2)(k_3 - k_7)/(k_3 + k_7)$ which is conceivably as small as demanded by equation (2).

With regard to the now discarded reaction (iv), it is noted that the introduction of a third-body molecule M was an *ad hoc* assumption necessitated by the requirement that, in order to obtain a limit pressure at all, the chain-breaking reaction be of higher order with respect to pressure than the chain-branching reaction. A similar situation exists perhaps with regard to reaction (vi), inasmuch as the branching reaction (v) is supposed to require a high activation energy (about 35 kcal) and quenching is not supposed to occur in ordinary binary O_2–CO_2^* collisions. Hoare[7] has suggested that $CO_2(^3\pi)$ reacts with O_2 in the ground state to form excited $(^3\Sigma_g)$ O_2, viz.,

$$CO_2^* + O_2 = CO_2 + O_2^*, \quad \text{(viii)}$$

which is followed either by

$$O_2^* = 2O \quad \text{(ix)}$$

or by

$$O_2^* + M = O_2 + M. \quad \text{(x)}$$

A scheme comprising reactions (viii), (ix) and (x) in place of reactions (v) and (vi) leads to an explosion condition substantially as in equation (2). Thus, a fourth chain carrier O_2^* has been introduced and the reaction possibilities are correspondingly enlarged. However, it does not seem possible to devise an explanation for the O_2- and N_2-effects other than the explanation given previously which is based on reactions I and II and equal third-body efficiencies of O_2, CO and N_2.

In contrast to the hydrogen-oxygen system, the problem of the second limit in carbon monoxide-oxygen mixtures is thus found to be very complex. The problem has reached a point where further progress can only be expected from careful selection of the kinds of experiments to be performed.

REFERENCES

1. Kopp, D., Kowalsky, A., Sagulin, A., and Semenoff, N.: Z. physik. Chem., *B6*, 307 (1930).
2. Hadman, G., Thompson, H. W., and Hinshelwood, C. N.: Proc. Roy. Soc. (London), *A138*, 297 (1932).
3. Cf. Kassel, L. S.: *The Kinetics of Homogeneous Gas Reactions*. Am. Chem Soc. Monograph, 1932.

4. Cf. Kassel, L. S., and Storch, H. H.: J. Am. Chem. Soc., *57*, 672 (1935).
5. Hadman, G., Thompson, H. W., and Hinshelwood, C. N.: Proc. Roy. Soc. (London), *A137*, 87 (1932).
6. Griffing, V., and Laidler, K. J.: *Third Symposium on Combustion, Flame and Explosion Phenomena*, p. 432. Baltimore, The Williams & Wilkins Co., 1949.
7. Anon.: *Symposium on Carbon Monoxide*. Dept. Chem. Eng. and Applied Chem., Imperial College, London, England, March 27, 1953.
8. Gordon, A. S.: J. Chem. Phys., *20*, 340 (1952).
9. Benton, A. F.: J. Am. Chem. Soc., *45*, 887 (1923).
10. Mardles, E. W.: Trans. Faraday Soc., *27*, 688 (1931).
11. Hoare, D. E., and Walsh, A. D.: Nature, *170*, 838 (1952).
12. Lewis, B., and von Elbe, G.: J. Am. Chem. Soc., *59*, 2025 (1937); *Combustion, Flames and Explosions of Gases*, pp. 78–83. New York, Academic Press, 1951.
13. Garvin, D.: J. Am. Chem. Soc., *76*, 1523 (1954).

65

THE INFLUENCE OF INERT GASES ON THE EXPLOSION LIMITS OF CYANOGEN

By P. LAFFITTE and H. JAMES

The explosion limits of gaseous mixtures of dry cyanogen and air have been studied at reduced pressure by the static method. The reaction vessel used is a tube of transparent silica, 125 mm long and 25 mm in diameter[1]. The precision and reproducibility observed in the determination of these limits has led us to compare the influence of nitrogen, argon and helium on the cyanogen-oxygen reaction.

To establish the greatest number of experimental parameters, the following experimental method was used. Having determined one explosion limit for a given cyanogen-air mixture, we determined the limits of two other mixtures differing only from the first mixture by the fact that nitrogen (considered with oxygen as the sole constituent of air) was replaced by equal quantities of argon or helium. These mixtures of identical concentration and stoichiometry are called equivalent.

Experimental Results

For the cyanogen-oxygen system, the stoichiometric mixture corresponding to the complete combustion of cyanogen to carbon dioxide and nitrogen is one volume of cyanogen for two volumes of oxygen, making the stoichiometric cyanogen-air mixture one volume of cyanogen to almost ten of air. This mixture is referred to as mixture 1 S. By analogy, any mixture xS contains x volumes of cyanogen for ten volumes of air. Based on these conditions, a systematic study was made of the following equivalent mixtures:

1 S or 9.1 per cent cyanogen
1.5 S or 13 per cent cyanogen
2 S or 16.7 per cent cyanogen
5 S or 33.3 per cent cyanogen
10 S or 50 per cent cyanogen

Generally speaking, the explosion limits obtained for equivalent mixtures and with increasing pressures fall in the following order:

Limit of cyanogen-oxygen-argon mixture,
Limit of cyanogen-oxygen-nitrogen mixture,
Limit of cyanogen-oxygen-helium mixture.

It should be noted that for decreasing cyanogen concentrations, the interval between the corresponding curves increases. To simplify the graphs, Figure 1 shows only the explosion limits of equivalent mixtures 2 S (16.7 per cent) and 10 S (50 per cent cyanogen).

Observation of flames for limit mixtures and examination of explosion limit curves lead to the following remarks: (1) As a rule, near the explosion limits, time lags are short and become nil at higher temperatures; (2) Semenoff's equation

$$\log P = \frac{A}{T} + B$$

in which P is the pressure at the limit, T the

absolute temperature, A and B are constants, can be applied for equivalent mixtures.

Figure 2 shows the corresponding curves (straight lines) for mixtures 2 S and 10 S.

The parallel character of these curves is striking, especially at high temperatures. The slope A of these lines being equal (to within a constant approximation) to $E/_n$ (ratio of the global activation energy to the overall order of reaction), it seems probable that the reaction process would be the same for equivalent mixtures. This assumes that the role of the inert gases added is primarily physical.

Theoretical interpretation of the experimental results

The physical influence of inert gases on the explosion limits, together with the variations in these limits with the nature and amount of inert gas added, has led us to consider the cyanogen-oxygen reaction from the thermal standpoint.

At the explosion limit, the classic thermal relation is:

$$vQ = K(T - T_0) \qquad (1)$$

where v is the reaction velocity,

Q the reaction heat corresponding to the reaction mechanism,

T_0 the temperature of the reaction vessel,

T the mean temperature of the reaction medium,

K a constant.

According to relation (1) this constant K has the form of a thermal conductivity. The aim of our study has been to find a relation between this resulting thermal conductivity of a mixture and the thermal conductivities of its components. It was proposed also to relate the reaction velocity at the explosion limit to the resulting thermal conductivity of the mixture considered.

Relation (1) can be written:

$$k\left(\exp - \frac{E}{RT}\right) P^n Q = \lambda_r (T - T_0)$$

where k (exp $-$ (E/RT)) is the overall velocity constant,

P the critical explosion pressure,

n the overall order of reaction,

λ_r the resulting thermal conductivity of the mixture considered.

As noted in the experimental part of this paper, (see under Remarks (2)) a single reaction mechanism can be ascribed to equivalent mixtures. Therefore:

Q can be considered constant,

k (exp $-$ (E/RT)) can be considered constant for a given temperature.

n can be considered constant.

The constancy of this last term will be verified for each group of equivalent mixtures. The

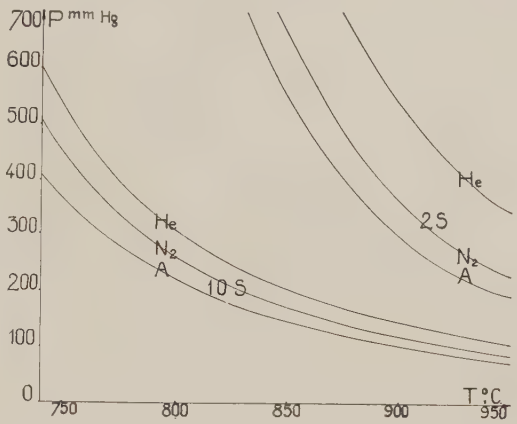

FIG. 1. Influence of inert gases on cyanogen explosion limits. Mixtures 2S and 10S.

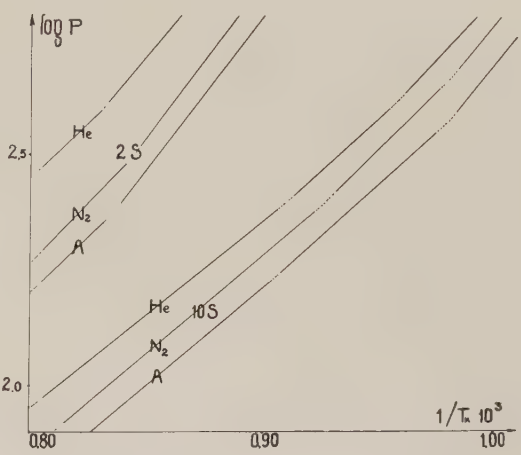

FIG. 2. Application of relation $\log P = \frac{A}{T} + B$. Mixtures 2S and 10S.

temperature T of the reaction medium is a function of P, but practically T is always very close to T_0. Therefore, $(T - T_0)$ may be considered constant for each temperature. This will be verified within the limits of experimental error.

As a result of the above simplification, relation (1) now becomes:

$$P^n = \lambda_r$$

and can be used to compare equivalent mixtures.

DETERMINATION OF THE RESULTING THERMAL CONDUCTIVITY

The thermal conductivity of a gaseous mixture is, in general, a complex function of the concentration of its components and of their respective thermal conductivity. Moreover, the law governing variations of thermal conductivity with temperature is not well known, especially within our temperature range (750–950°C). It is possible, however, to account for our experimental results by a simple relation involving only physical constants of the constituents of the mixture studied for their respective concentrations.

Two preliminary hypotheses, however, are necessary:

(1) Considering that the explosion of cyanogen-oxygen-inert mixtures has a very short ignition lag (generally less than one second), the resulting thermal conductivity at the explosion limit of this mixture can be considered as unaffected by the reaction products and, therefore, related only to the constituents of the fresh mixture.

(2) The law governing the variation of the resulting thermal conductivity with temperature is the same for equivalent mixtures. This hypothesis seems verified in the course of this study.

Based on these conditions, the following ponderal relation of the mixtures rule has been applied to the calculation of the resulting thermal conductivity:

$$\lambda_r = \frac{\sum C_i \rho_i \lambda_i}{\sum C_i \rho_i}$$

where C_i, ρ_i and λ_i are respectively the concentration, the specific mass and the thermal conductivity of the constituent i under normal conditions of temperature and pressure.

Table 1. Numerical Data

Gas	Cyanogen	Oxygen	Nitrogen	Argon	Helium
ρ	2.34	1.43	1.25	1.78	0.179
$\lambda.10^5$	3.45	5.83	5.81	3.89	34.30

Mixtures in stoichiometry	Concentrations (in per cent)			Resulting thermal conductivity, 10^5		
	Cyanogen	Oxygen	Inert	Argon	Nitrogen	Helium
1	9.09	19.10	71.81	4.14	5.46	10.96
1.5	13.05	18.30	68.65	4.10	5.31	9.84
2	16.66	17.50	65.84	4.06	5.18	9.02
5	33.33	14	52.67	3.91	4.69	6.59
10	50	10.5	39.5	3.78	4.29	5.27

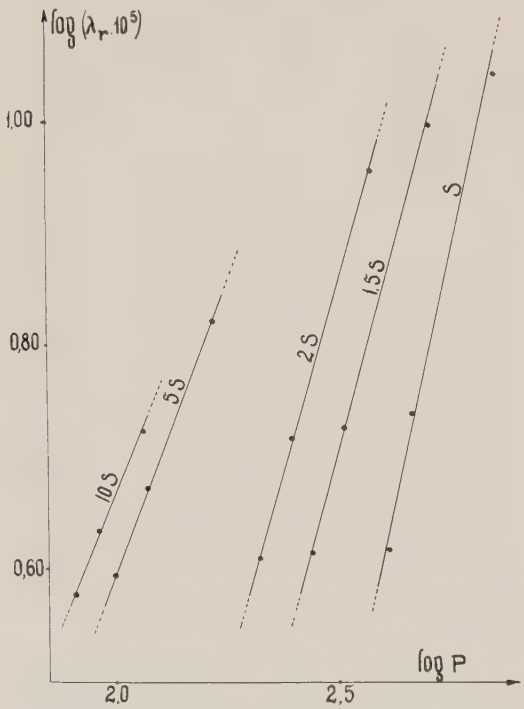

Fig. 3. Application of relation $n \log P = \log \lambda_r$ (940°C).

NUMERICAL DATA

Table 1 shows the physical constants considered together with the resulting thermal conductivity for each mixture at N.T.P. The thermal conductivity of cyanogen has recently been determined[2]. Thermal conductivities are expressed in cal. cm^{-1} sec^{-1}.

STUDY OF THE COMPARISON RELATION. EXPERIMENTAL CHECK

Considering the hypothesis formulated above, the comparison relation takes the form:

$$P^n = \lambda_r .$$

This relation has been verified under the form:

$$n \log P = \log \lambda_r .$$

Figure 3 shows the application of this relation: $\log_{10}$ of the resulting thermal conductivity 10^5 are plotted against $\log_{10}$ of total pressures expressed in mm Hg at the explosion limit. Over all the temperature range studied, a family of straight

lines of almost equal slope was obtained for each series of equivalent mixtures. To avoid overloading the graph, curves are shown for only one temperature, 940°C.

Table 2 shows the mean values of n corresponding to each family of straight lines together with the mean relative differences of n observed in the temperature range studied. A very acceptable verification of the proposed thermal relation is observed.

Conclusion

This study shows that, under certain conditions, a simple explanation for the variations of the explosion limits of cyanogen gas mixtures may be found in the variation of what might be called the "thermal constant of the mixture". We have in this way shown the purely diluting effect of inert gases on the cyanogen-oxygen reaction. This implies a predominatingly thermal character.

Remarks

(1) The resulting thermal conductivities as *calculated* by us do not claim to express the thermal conductivities of the mixtures considered as *determined* by classic methods. They are merely comparison terms here.

(2) In the course of this study, we have been able to define the exponent n of the pressure in the classical velocity relation. In first approximation, this exponent seems to be a function only of the concentration of the gaseous mixture considered. If related to the overall reaction order of the cyanogen-oxygen reaction, we again find the complex character of the reaction which can be considered as the sum of two consecutive and competitive reactions: namely the oxidation of cyanogen in carbon monoxide and the oxidation of the carbon monoxide formed into carbon dioxide. Both reactions are effective in the reaction medium[3]. Evidently according to the concentration of the constituents, these two reactions will go on with different velocities and overall apparent reaction orders, showing that the respective contribution of each of the two reactions must be an important function of the concentrations of the constituents.

The relation that might be given for the calculation of n must show the competitive character of the two reactions above, without excluding the possibility of other reactions such as a recombination of radicals.

Table 2. Experimental Values

Mixtures in stoichiometry	1	1.5	2	5	10
$\bar{n}$	1.75	1.51	1.39	1.06	0.95
$\overline{dn}/\bar{n}$	—	2.3%	2.4%	1.9%	3.8%
Temperature ranges (°C)	930–950	900–950	870–950	770–950	720–950

REFERENCES

1. James, H., and Laffitte, P.: C. R., *236*, 811, (1953).
2. Von Leonid, A.: Z. Elektrochem., *56*, 54, (1952).
3. Hadow, H. J., and Hinshelwood, C. N.: Proc. Roy. Soc., *A132*, 375, (1931).

66

REGIONS OF FLAMMABILITY OF BINARY MIXTURES OF HYDROCARBONS WITH NITROUS OXIDE: ACTION OF NITROUS OXIDE AS OXIDANT

By GUY PANNETIER AND ADRIEN SICARD

Introduction

A mixture of combustible and fuel is flammable only over a well-defined range of temperature, pressure and concentration. It is interesting to determine this region for two reasons: first, for the practical purpose of eliminating the industrial hazards which the flammable gas mixture may present and, second, for the purely theoretical purpose of studying the combustion reaction and kinetics.

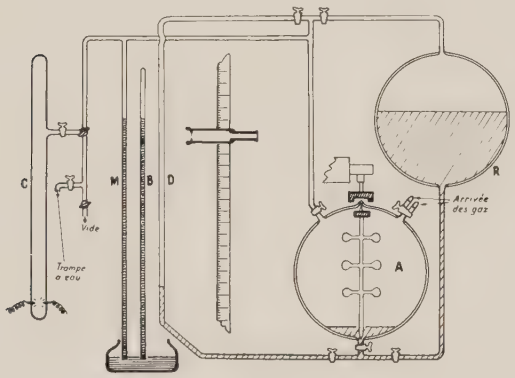

FIG. 1. Diagram of apparatus: R—Mercury reservoir; A—Mixing vessel; D—Differential manometer; B—Barometer; M—Manometer; C—Combustion tube.

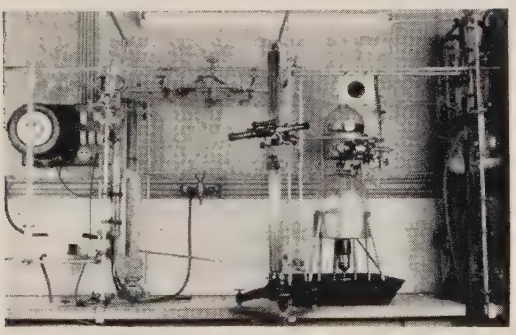

FIG. 2. Photograph of apparatus.

Combustion in nitrous oxide has not been studied extensively to date[1, 2, 3]. It is to fill this gap that we have undertaken the study of the flammability of binary mixtures of various fuels with nitrous oxide at pressures equal to, or less than, atmospheric pressure. We have investigated the action of nitrous oxide as an oxidant by observing first its general behavior in this region, and second the effect of various diluents on the form of the diagrams obtained.

The few measurements made previously were carried out at atmospheric pressure. Moreover, there is some doubt as to the homogeneity of the mixtures, as the experiments were performed without the precautions which we ourselves have taken.

Experimental Method

APPARATUS

All our measurements were made on flames that propagated upwards in a 25-mm tube, 1 m long, and closed at both ends. Ignition was obtained by a series of high frequency sparks and high voltage sparking between two tungsten electrodes 5 mm apart, and located 2.5 cm from the end of the tube. The spark was formed by an induction coil which produced the same amount of energy in a given time in each run by action of a revolving contact plate in the primary circuit.

The general setup was similar to that used by one of us to prepare gaseous mixtures by the classic method of partial pressure (Figs. 1 and 2). However a marked improvement was effected in the mixer[5] by replacing the mechanical drive situated between the axle of the motor and that of the stirrer with a magnetic drive which eliminates all spaces that could not be cleaned thoroughly or could not be reached at the time of homogenization.

To eliminate traces of water, the gases were stored in 5-liter flasks over phosphorus pentoxide. These flasks were fitted with manometers which made it easy to exert a certain measurable pressure, and eliminated the possibility of air entering the flasks. The manometers also indicated the pressure at which the gases were introduced into the mixer.

The fuel was a commercial liquefied product delivered in a bottle labeled "except when otherwise indicated 98 per cent $\pm$ 0.3 pure nitrous oxide", the remainder being nitrogen. The dosage was carried out with a Claude burette. (The gas was dissolved in alcohol at 95° [6].)

The source and purity of the various combustibles will be indicated as their investigation is described.

ACCURACY OF RESULTS

With this apparatus we were able to measure concentrations with relative errors of 1/100 for low combustible concentrations and 1/500 for high concentrations.

Furthermore, the errors in the determination of the limiting pressures for ignition at various concentrations are essentially due to uncertainty regarding the reproducibility of the results. These pressures are given with an accuracy of 2 mm, except for the parts of the diagrams where the tangent is practically vertical and where the addition of errors may cause the pressure to vary a few cm Hg from one measurement to the next without modifying the general slope of the curve.

We shall first give a simple description of the different regions and the observations made in them. We then shall draw the conclusions indicated by these results.

Experimental Results

COMBUSTION OF VARIOUS SATURATED HYDROCARBONS

Butane-nitrous oxide (Fig. 3)

The only previous measurements are those made by Van der Wal[2] at atmospheric pressure which give 2.5 per cent for the lower and 20 per cent for the upper limit in a tube of 18 mm diameter.

We have reinvestigated and completed this work at all pressures below or equal to atmospheric pressure. The combustible used for this purpose was a mixture of practically equal parts of butane and isobutane of 99 per cent or greater purity. The fuel used in these experiments titrated to 99.5 per cent of nitrous oxide in the Claude burette. The main experimental results are given in Table 1.

The curve enclosing this region shows two points of inflection, *A* and *B* (Fig. 3). The flame is always very fast and occupies the whole of the combustion tube. At very low concentrations (less than 5 per cent butane), the flame is white, it becomes bluish up to *A*, then white between *A* and *B*, and finally a sooty yellow beyond *B*. At low concentrations, up to about 3.5 per cent butane, we observed considerable formation of nitrous vapors. At high butane concentrations (greater than 17 per cent of butane), a heavy deposit of carbon formed on the walls of the tube corresponding to the appearance of the yellow, sooty flames. This deposit must be removed regularly with chromic-sulfuric acid, which

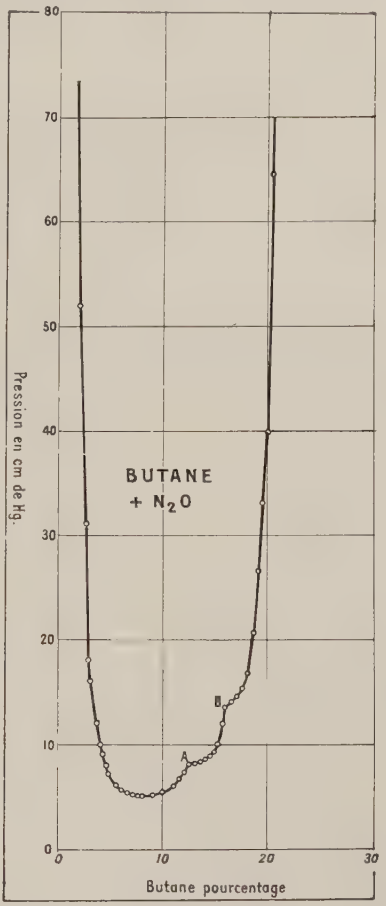

FIG. 3. Region of flammability of butane-N_2O mixtures.

TABLE 1. BUTANE-N_2O

Pressure	Concentration butane	Pressure	Concentration butane	Pressure	Concentration butane
mm Hg	*per cent*	*mm Hg*	*per cent*	*mm Hg*	*per cent*
700	1.80	52	8.0	120	15.8
520	2.00	54	10.0	136	16.0
320	2.50	60	11.0	138	16.5
180	3.0	68	12.0	146	17.0
120	3.5	75	12.3	166	18.0
100	4.0	80	12.5 (A)	270	19.0
80	4.5	82	13.0	496	20.0
68	5.0	84	14.0	700	21.0
60	5.5	92	15.0		
56	6.0	110	15.5		

however does not influence the reproducibility of the results. On the other hand, if this cleaning is not carried out and the carbon deposits are allowed to remain on the walls, the gaseous mixture becomes flammable in an unpredictable manner and the limits observed in no case fit a regular curve. This confirms the experiments undertaken by one of us[7] on the influence of the state of the tube at the time of inflammation of the gas mixture.

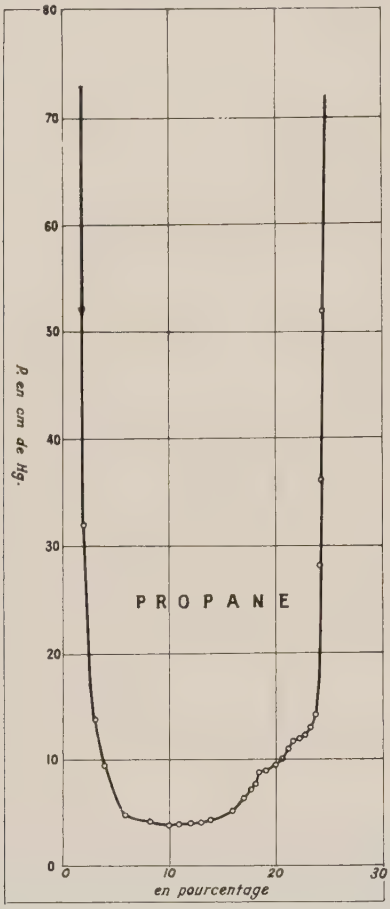

FIG. 4. Region of flammability of propane-N_2O mixtures.

TABLE 2. PROPANE-N_2O

Pressure	Concentration propane	Pressure	Concentration propane	Pressure	Concentration propane
mm Hg	*per cent*	*mm Hg*	*per cent*	*mm Hg*	*per cent*
700	2.10	46	14.0	108	21.0
520	2.15	54	16.0	118	21.5
320	2.20	66	17.0	119	22.0
140	3.0	72	17.5	121	22.5
94	4.0	78	18.0	128	23.0
50	6.0	88	18.5	142	23.5
42	8.8	89	19.0	280	24.0
40	10.0	92	20.0	520	24.5
44	12.0	100	20.5	700	24.8

Propane-nitrous oxide (Fig. 4)

We have found no reference in the literature to work done on the combustion of propane in nitrous oxide. The only combustible commercially available was a mixture of equal amounts of propane and propylene. The propylene was eliminated by bubbling the gas mixture through concentrated sulfuric acid where it combines with the acid, which becomes brownish and viscous and must be replaced. Regular bubbling of the gas through a 3 per cent aqueous solution of potassium permanganate provides information on the purity of the gas and the extent of purification. The numerical results obtained with these mixtures are given in Table 2.

The curve of limiting flammability (Fig. 4) varying from 2.4 to 24.8 per cent propane has a form similar to that observed for butane with two points of inflection, *A* and *B*. As in the previous case, the flame which is always very fast is white at low combustible concentrations then bluish-mauve until it becomes white again between *A* and *B* and finally sooty yellow beyond *B*. As in the case of butane, there are nitrous vapors at low concentrations, and carbon deposits at high propane concentration (above 22 per cent).

Methane-nitrous oxide (Fig. 5)

The fuel used was high grade methane (more than 99.5 per cent pure) obtained by fractional distillation. The results reported previously for the lower and upper limits were respectively 2.2 and 36.6 per cent[1] and 3.9 and 36.9 per cent[2], whereas we obtained 4 and 40.2 per cent in the present series of experiments. Table 3 gives the results of our measurements. The limiting flammability curve has the same general form as the two previous curves with two points of inflection, *A* and *B* (Fig. 5).

Observations on the speed (very rapid propagation of the flame front) and the color of the flame (white at low concentrations, then clear blue to *A*, white between *A* and *B*, to become sooty at high combustible concentrations) are similar to those made in the case of propane and

butane. The production of nitrous vapors at low concentrations also is observed.

However, it is to be noted that above B, the flame does not become yellow for some time. The carbon deposit appears only immediately before the upper limit. Prior to this, a white sooty flame forms which leaves behind a large amount of condensed water vapor. This is easily explained if one considers that the relative hydrogen content

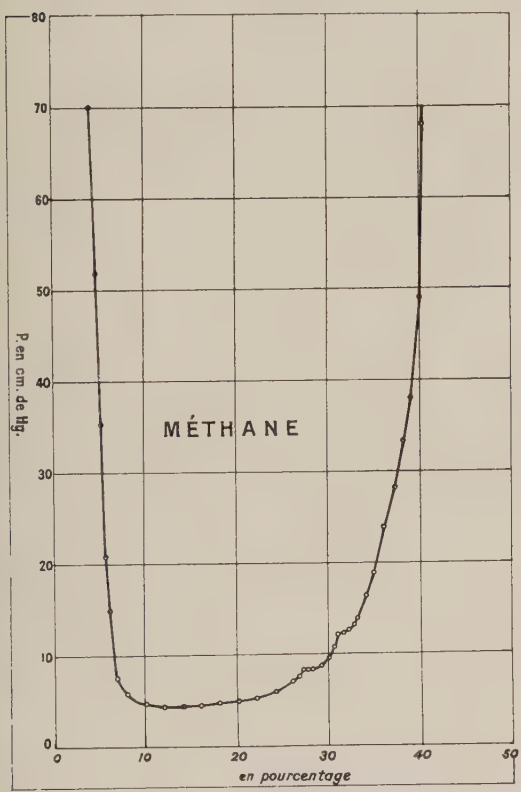

FIG. 5. Region of flammability of methane-N_2O mixtures.

of methane is much higher than that of other saturated hydrocarbons.

COMPARISON OF THE REGIONS OF THE VARIOUS HYDROCARBONS

In order to compare the characteristic values (upper and lower flammability limits, concentration at maximum pressure) of the different saturated hydrocarbons, the values given above as per cent of combustible in the total mixture have been converted to the proportion of combustible based on the stoichiometric mixture, this proportion being by definition equal to 1. The reaction:

$$C_nH_{2n+2} + (3n + 1)\,N_2O \rightarrow n\,CO_2 + (n + 1)\,H_2O + (3n + 1)N_2$$

serves as the basis for all the hydrocarbons considered.

This leads to the results shown in Table 4. The values for propane and butane are virtually identical. On the other hand, those for methane although of the same order of magnitude are appreciably different, due no doubt to the higher hydrogen concentration of methane.

TABLE 3. METHANE-N_2O

Pressure	Concentration methane	Pressure	Concentration methane	Pressure	Concentration methane
mm Hg	*per cent*	*mm Hg*	*per cent*	*mm Hg*	*per cent*
700	4.0	50	20.0	121	31.0
520	4.5	54	22.0	123	31.5
356	5.0	60	24.0	126	32.0
210	5.5	72	26.0	132	32.5
151	6.0	71	26.5	140	33.0
78	7.0	84	27.0	188	35.0
59	8.0	84	27.5	238	36.0
50	10.0	84	28.0	336	38.0
46	12.0	88	29.0	380	39.0
46	16.0	97	30.0	488	40.0
48	18.0	108	30.5	700	40.2

TABLE 4

	Lower limit	Upper limit	Concentration at the minimum pressure
Butane.....	0.25	2.73	1.1
Propane....	0.24	2.72	1.09
Methane....	0.2	2.01	0.75

The slope of the various curves as well as the speed and colors of the flames are similar for all the saturated hydrocarbons, and in all cases nitrous vapors form at low concentration of combustible and carbon deposits, producing sooty flames at high concentration.

The above observations indicate that:

(1) The different saturated hydrocarbons burn in nitrous oxide following the same combustion kinetics.

(2) Each diagram is made up of three parts, each of which corresponds to a different reaction process.

COMBUSTION OF BUTANE IN A MIXTURE OF $N_2 + \frac{1}{2} O_2$ (FIG. 6)

It might be thought that nitrous oxide behaves like a mixture of nitrogen and oxygen, the first stage in its combustion being decomposition according to $N_2O \rightarrow N_2 + \frac{1}{2} O_2$.

If this were the case, the flammability region of any saturated hydrocarbon burning in a mixture of $N + \frac{1}{2} O_2$ corresponding to this reaction would be very similar to the region of this same hydrocarbon burning in nitrous oxide. We undertook to investigate this point for butane, using a mixture of butane and isobutane. The oxygen and nitrogen used were both titrated at a purity greater than 99 per cent in the Claude burette, using a hydrosulfite solution as a reducing mixture (150 gr hydrosulfite).

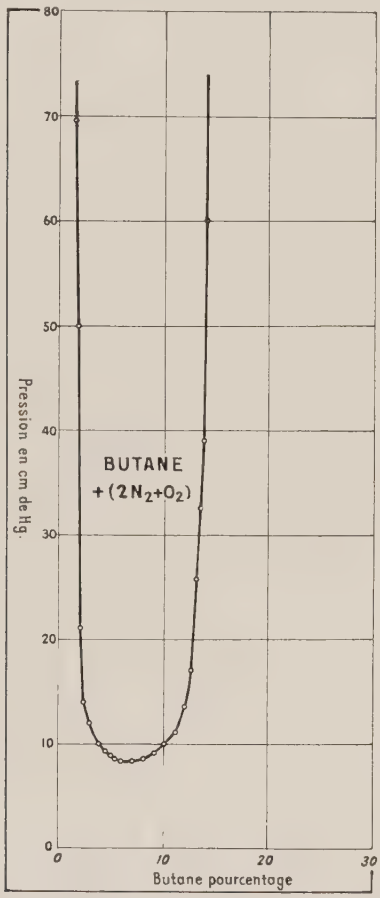

FIG. 6. Region of flammability of butane-$(2N_2 + O)$ mixtures.

As there is no reference in the literature to numerical data concerning the combustion of butane in superoxygenated air corresponding to the above conditions, the principal values corresponding to this diagram (Fig. 6) are given in Table 5. The region extends from 1.6 to 14.6 per cent butane. The flame is always very rapid, and passes from violet at low concentrations to blue at 5 per cent, becomes green at 10 per cent, and finally orange-yellow near the upper limit. As before, there was an abundant carbon deposit near the upper limit. However there was no formation of nitrous vapors at low butane concentrations.

The flammability region is completely different from that found for butane in nitrous oxide, both as to its general slope, the color of the flames, and the products of combustion. This eliminates completely the possibility that the kinetic mechanism of nitrous oxide consists in a rupture of the molecule into its two constituents. This is confirmed by the following investigation.

TABLE 5. BUTANE-$N_2 + \frac{1}{2}O_2$

Pressure	Concentration butane	Pressure	Concentration butane	Pressure	Concentration butane
mm Hg	*per cent*	*mm Hg*	*per cent*	*mm Hg*	*per cent*
700	1.60	88	5.0	100	10.0
208	2.00	96	6.0	110	11.0
140	2.50	86	7.0	138	12.0
120	3.0	87	8.0	235	13.0
100	4.0	92	9.0	700	14.6

EFFECT OF SMALL QUANTITIES OF NITROGEN AND OXYGEN ON THE REGION OF FLAMMABILITY OF BUTANE AND NITROUS OXIDE

If the first stage of combustion were a total dissociation of the nitrogen compound, the addition of increasing amounts of nitrogen or oxygen should deform the diagram in a regular manner without changing its general form.

Action of nitrogen (Fig. 7)

A small amount of nitrogen (5 per cent of total fuel) maintains the upper limit of flammability, but diminishes the lower limit of butane from 1.8 to 0.95 per cent. The points of inflection *A* and *B* although less well defined are still perceptible.

A larger amount of nitrogen (8 per cent) maintains the lower limit at 0.95 per cent, but reduces the upper limit of butane from 21 to 20 per cent and, in this case, the points *A* and *B* are com-

pletely absent. The experimental results are explicit enough in the accompanying diagram to make it unnecessary to give the main numerical values.

Action of oxygen (Fig. 8)

For a low oxygen concentration (5 per cent of total fuel), the upper limit remains unchanged, but the lower limit is reduced from 1.8 to 0.84 per cent butane. The two points of inflection *A*

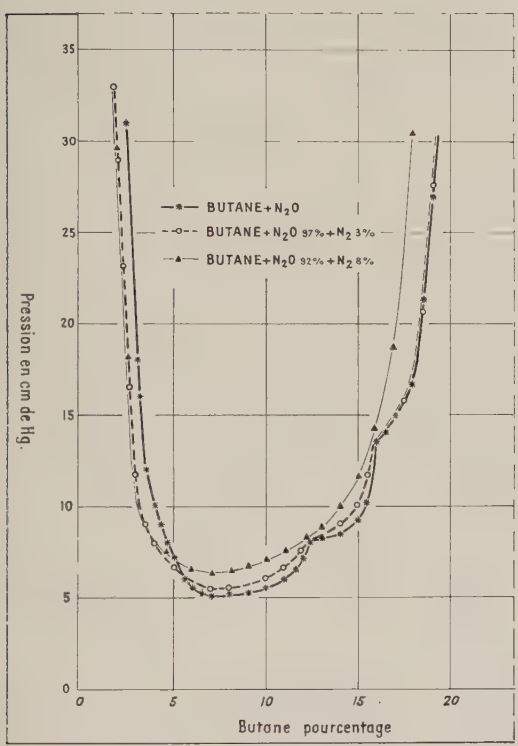

FIG. 7. Effect of addition of small amounts of N_2 on the flammability region of butane-N_2O mixtures.

and *B* are still visible although less marked, and a third point *C* appears as shown in the diagram.

If the amount of oxygen in the fuel is increased (10 per cent of total fuel), the lower limit remains at 0.84 per cent whereas the upper limit rises from 21 to 22 per cent, points *A* and *B* disappear, leaving only point *C*.

Thus, in both cases, points *A* and *B* disappear due to the mechanism of combustion of nitrous oxide. Furthermore, with oxygen a new point of inflection *C* appears.

The action of the latter fuel is superimposed on that of nitrous oxide and finally supplants the latter as the concentration increases.

The observations regarding color and speed of flame, production of nitrous vapors and deposit of carbon, made for the combustion of butane in pure nitrous oxide, are still valid.

The previous observations on (1) the general form of the curves for limits of flammability, (2) action of oxygen and nitrogen as diluents, (3) the production of nitrous vapors at low concentrations, and (4) the fact that the spectra of saturated hydrocarbon flames in N_2O show bands due to the NO molecule at all concentrations,

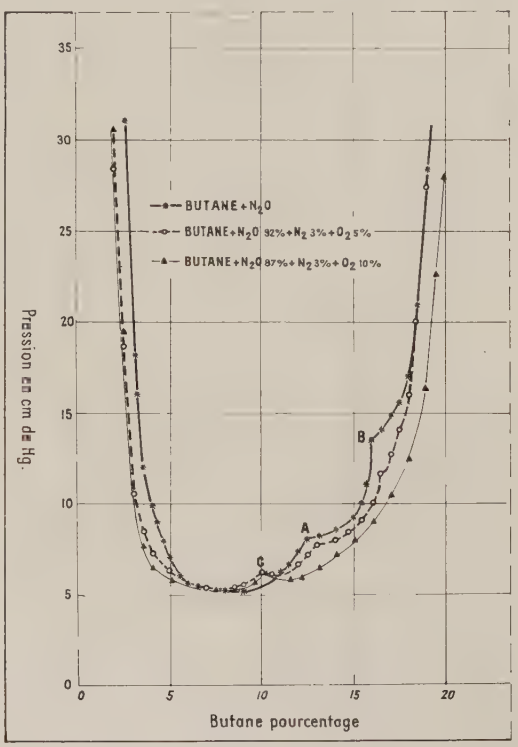

FIG. 8. Effect of addition of small amounts of O_2 on the flammability region of butane-N_2O mixtures.

lead us to conclude that nitrous oxide functions as a fuel according to the initial reaction $N_2O \rightarrow NO + \cdots$.

COMBUSTION OF UNSATURATED HYDROCARBON (PROPYLENE) IN NITROUS OXIDE

It appeared interesting to determine the slope of the combustion diagram for an unsaturated hydrocarbon. No previous measurements had been made with this system. As an example, we took commercially available propylene at a purity greater than 99.5 per cent. The main results obtained are given in Table 6.

The diagram plotting the limits of flammability (Fig. 9) as a function of pressure shows only one

TABLE 6. PROPYLENE-N_2O

Pressure	Concentration propylene	Pressure	Concentration propylene	Pressure	Concentration propylene
mm Hg	*per cent*	*mm Hg*	*per cent*	*mm Hg*	*per cent*
700	1.80	40	14.0	146	25.5
560	1.90	42	16.0	330	26.0
336	2.00	46	18.0	580	26.4
198	2.50	58	20.0	700	26.8
126	3.0	84	22.0		
90	4.0	100	22.5		
48	6.0	126	23.0		
40	8.0	124	23.5		
39	10.0	124	24.0		

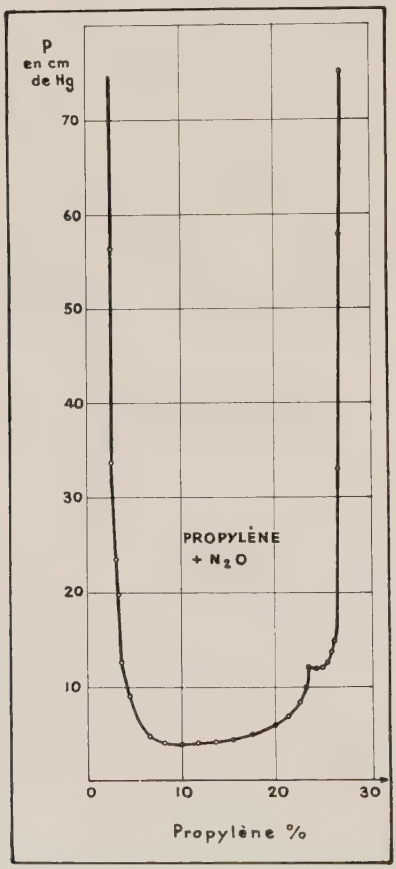

FIG. 9. Region of flammability of propylene-N_2O mixtures.

point of inflection instead of the two found for propane. Its general form, however, is virtually the same as that of the latter gas. The flame remains rapid and in the neighborhood of A passes from white to yellow-orange. The appearance of nitrous vapors at low concentrations and the carbon deposit near the upper limit are the same as for the saturated hydrocarbons.

The apparatus which we used did not allow us to construct this diagram for pressures above atmospheric and thus it was not possible to find the second point of inflection above atmospheric pressure. However, observations show that there is a difference in the combustion mechanism for this unsaturated hydrocarbon, as compared to the saturated hydrocarbons. The other conditions of flammability are actually the same, in particular, the hydrodynamic conditions linked to

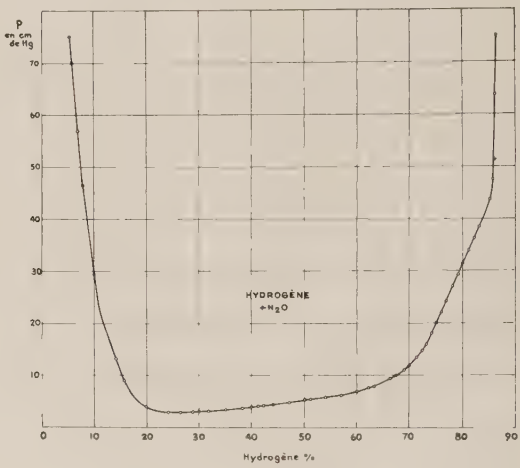

FIG. 10. Region of flammability of hydrogen-N_2O mixtures.

the geometric parameters of the vessel in which the inflammation occurs.

COMBUSTION OF HYDROGEN IN NITROUS OXIDE

The results obtained with hydrogen are even more important as this is the only simple fuel which is not a hydrocarbon and does not contain carbon. Very pure commercial hydrogen was used.

The only values found in the literature are those of the lower (5.2 per cent) and upper (76.2 per cent) limits at atmospheric pressure[3]. Our values are virtually the same for the lower limit at atmospheric pressure (5.8 per cent), but they are much higher for the upper limit (86.2 per cent).

The data in Table 7 interpret Figure 10. The shape of the curve is entirely different from the previous ones. The flame which is still very fast passes from a reddish yellow at low hydrogen

concentrations to white at 50 per cent, then to bluish white at the upper limit.

As before, there was an abundant production of nitrous vapors at low combustible concentrations, but there was no longer any point of inflection. These latter are not due to certain hydrodynamic conditions related to the geometry of the tube, but are the consequence of the combustion mechanism. This confirms the validity of the reasoning concerning the displacement of the points of inflection observed for the hydrocarbon upon addition of small quantities of oxygen or nitrogen.

The appearance of nitrous vapors at low hydrogen concentrations, which excludes intervention of hydrocarbon products, corroborates

Table 7. Hydrogen-N_2O

Pressure	Concentration hydrogen	Pressure	Concentration hydrogen	Pressure	Concentration hydrogen
mm Hg	*per cent*	*mm Hg*	*per cent*	*mm Hg*	*per cent*
700	5.8	32	35.0	122	70.0
568	7.0	36	38.0	160	73.0
462	8.0	42	42.0	220	76.0
294	10.0	48	47.0	310	80.0
130	12.0	52	50.0	356	82.0
88	16.0	60	54.0	400	84.0
40	20.0	66	57.0	436	85.0
30	24.0	72	60.0	464	85.5
28	26.0	87	64.0	638	86.0
28	30.0	100	70.0	700	86.2

the viewpoint already expressed on the functioning of nitrous oxide as a fuel.

All these results appear to be perfectly compatible with a rupture of the molecule N_2O at the moment of oxidation:

$$N_2O \rightarrow NO + \cdots .$$

Conclusions

Apart from the physico-chemical constants of flammability of mixtures of nitrous oxide with various fuels which we have determined, and which were not previously known, the work as a whole leads to the following conclusions:

(1) The almost complete numerical identity of the different diagrams representing the flammability limits as a function of the pressure for the various saturated hydrocarbons studied and the difference which these diagrams show with respect to that of an unsaturated hydrocarbon or hydrogen, seem to prove that the combustion mechanism of the saturated hydrocarbons is identical and differs, in all cases, from that of hydrogen.

Three types of hypotheses have been advanced to interpret these combustions and have been applied to the case where oxygen is used as a fuel. As they do not involve the nature of the fuel, we assume that they are still valid when N_2O is employed as oxidant.

According to the first hypothesis, the hydrogen atoms of the hydrocarbons are removed one after the other. This mechanism was suggested by the experiments of Bonhoeffer and Harteck[8], and was later disputed by Hsieh and Townend[9].

In this case it would seem that as the hydrocarbons studied do not possess the same number of hydrogen atoms, points A and B of the diagram would vary more and the similarity between the hydrocarbon diagrams and that of hydrogen would be greater. Furthermore, there is no reason why the difference between saturated and unsaturated hydrocarbons should be so great.

The second hypothesis postulates the intermediate formation of peroxides which decompose again[10].

Finally a third mechanism proposed by Gaydon and Wolfhard assumes condensation or polymerisation of the hydrocarbon to give a large unsaturated molecule which breaks up into smaller fragments[11].

Although the similarity in the diagram obtained for the same group of hydrocarbons would incline one towards the third hypothesis, as the big fuel molecule formed would be practically the same in each case, it unfortunately does not appear as though our investigation would allow us to decide between the two theories. On the contrary, both are compatible with our experimental results, which may throw doubt on the validity of the first hypothesis but do not help us to choose between the latter two hypothesis.

(2) Finally, the production of nitrous vapors at high fuel concentrations necessarily involves NO and O_2 as possible intermediates in the decomposition of N_2O.

It may be assumed that the exothermal nature of the reaction at the flame front is sufficient to dissociate N_2O into other products, such as nitrogen dioxide, which would intervene in one of the stages of the kinetics of N_2O as a fuel. This is also apparent from spectroscopic observation of flames fed with N_2O as fuel over as wide as possible a range of mixture concentra-

tions. It also follows from our investigations on the variation of the limits of the range of flammability as a function of the addition of small quantities of nitrogen and oxygen.

REFERENCES

1. Jorissen, W. P., and Van Der Dussen, A. A.: Rec. Travaux Chim. Pays Bas, *52*, 327–332 (1933).
2. Van Der Wal: Rec. Travaux Chim. Pays Bas, *53*, 97 (1934).
3. Posthumus, K.: Rec. Travaux Chim. Pays Bas, *49*, 309–347 (1930).
4. Pannetier, G.: Paris, Thèse, 1948.
5. Sicard, A., and Goux, D.: Bull. Soc. Chim., in press.
6. Air Liquide: Private communication.
7. Pannetier, G., and Laffitte, P.: C. R. Acad. des Sc., *221*, 553 (1945).
8. Bonhoeffer, K. F., and Harteck, P.: Z. Phys. Chim., *A1396*, 64, (1928).
9. Hsieh, M. S., and Townend, D. T. A.: J. Chem. Soc., 332 (1939).
10. Hornbeck, G. A., and Herman, R. C.: Ind. & Eng. Chem., *43*, 2739 (1951).
11. Gaydon, A. G., and Wolfhard, H. G.: Proc. Roy. Soc. *A201*, 570, (1950).

67

SELF-COMBUSTION OF ACETYLENE. I. PRE-IGNITION KINETICS[a]

By W. W. ROBERTSON, E. M. MAGEE, JANICE FAIN, and F. A. MATSEN

Introduction

Pure acetylene, in the absence of oxygen, can support a flame. The flame can be initiated by passing the gas through a heated tube, by bringing it in contact with a glowing wire and possibly by the introduction of free radicals. A great deal

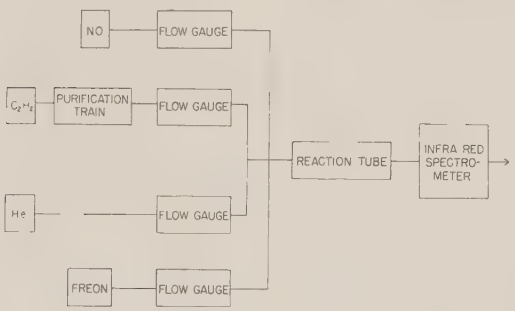

Fig. 1. Block diagram of reaction system.

of chemical reaction occurs at temperatures below the ignition temperature. In this paper are presented data on the rates of some of these reactions at temperatures up to and including the ignition temperature.

The research on the thermal reactions of acetylene through 1944 has been summarized by Steacie[1]. Kinetic studies have been made by Pease[2], Taylor and van Hook[3], Frank-Kamenetzky[4], Blumberg and Frank-Kamenetsky[5], and Kuri[6]. All report that extensive polymerization occurs. Pease and Burnham[7] report inhibition by nitric oxide. A number of primary steps have been suggested. Pease[2] suggests the formation of $(C_2H_2)_4$, Zelinsky[8] diacetylene, Frank-Kamenetsky[4, 5] polygen (C_4H_4), and Kuri[6] cyclooctatetrene.

Experimental

All experiments were performed on the flow system shown in Figure 1. The reactor was of vycor, was electrically heated, and its temperature was measured by a thermocouple placed on the exterior wall. The temperature profile inside the tube was also determined. The product gas was passed through a Perkin Elmer 12C infrared spectrometer. The acetylene was determined from the intensity of a band at 3.05 μ, freon (see below) at 8.62 μ, benzene 3.28 μ and ethylene 10.51 μ. Occasional samples were taken for mass spectrometer analysis.

Capillary flow meters were used. The helium meter was calibrated against the conventional wet flow meter. The acetylene and freon meters were calibrated by mixing each of the gases with metered amounts of helium and determining the infrared absorption. The flow rate in the nitric

[a] This research was supported by the U. S. Air Force, through the Office of Scientific Research of the Air Research and Development Command.

oxide flow meter, which contained eighty feet of capillary tubing was calculated from the viscosity of nitric oxide.

The volume change in the course of the reaction was determined by the change in freon pressure as measured by the intensity [optical density = OD] of its infrared absorption

$$1 - \frac{OD}{OD_0} = -\frac{\Delta V}{V} \qquad (1)$$

The sources of the chemicals used are as follows:

Helium: Bureau of Mines, Amarillo, Texas

Nitric Oxide: Matheson Co., East Rutherford, N. J.

Freon: Dupont Co., Wilmington, Delaware

Acetylene: Houston Oxygen Co., Houston, Texas

For infrared calibration

Ethylene: Houston Oxygen Co., Houston, Texas

Benzene: Eastman Kodak Co., Rochester, N. Y.

Several purification processes for the acetylene were employed. The simplest, water, $NaHSO_3$ solution, $CaCl_2$ appeared sufficient.

Results

The principal gaseous products were found to be benzene, ethylene, hydrogen, and methane. Only the first two can be determined by infrared analysis; it is for these that the most data is available. A set of typical results is presented in Figure 2. It will be noted that benzene increases exponentially with temperature, that ethylene comes in at higher temperatures than benzene but has a larger temperature coefficient, and that the volume decrease parallels ethylene formation. When the ethylene concentration and the volume change are large, a white cloud appears in the reactor.

Dilution with helium raises the ignition temperature and displaces the curves a proportionate amount toward higher temperatures. Dilution affects some changes: the temperature coefficients are reduced and the white cloud appears farther below the ignition temperature.

The addition of small amounts of nitric oxide (1 per cent) raises the ignition temperature considerably. See Figure 3. It has an inhibitory effect on both benzene and ethylene formation, and on volume changes.

A rather complete study of the effect of nitric oxide on benzene formation has been made. In the temperature region appropriate to observing benzene the ethylene concentration is very low and a small amount of NO reduces the ethylene concentration to zero. Consequently it was not possible to study the effect of nitric oxide on ethylene at the same time. It is planned to make ethylene the subject of a future study.

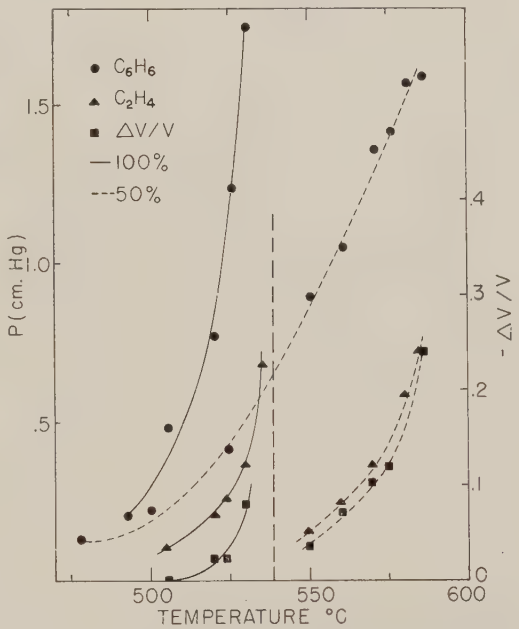

FIG. 2. Fractional volume change, benzene and ethylene pressure as a function of temperature and acetylene concentration; the vertical dotted line indicates the ignition temperature for 100% acetylene.

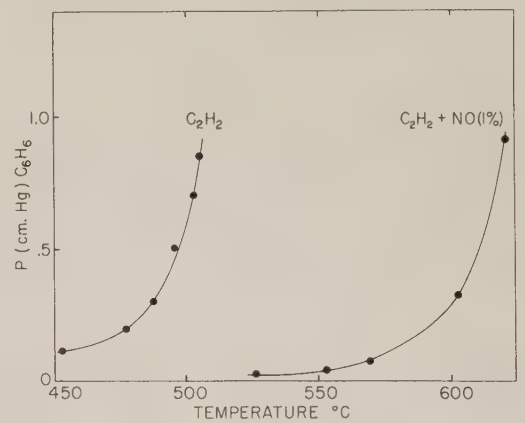

FIG. 3. Effect of NO on benzene pressure-temperature curve.

In Figure 4 is plotted a typical benzene vs. nitric oxide curve. The plot resembles that obtained from the thermal decomposition of a num-

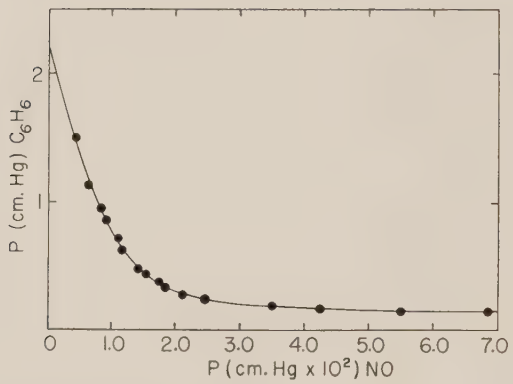

FIG. 4. Benzene pressure vs. NO pressure at 518°C and 100% acetylene.

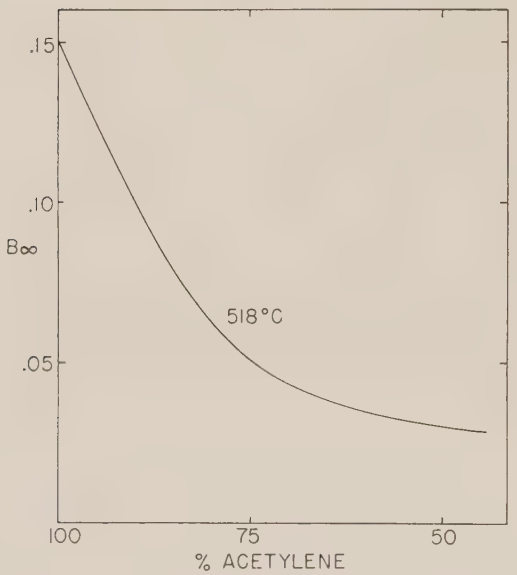

FIG. 5. Dependence of rate of non free-radical process upon acetylene concentration at 518°C.

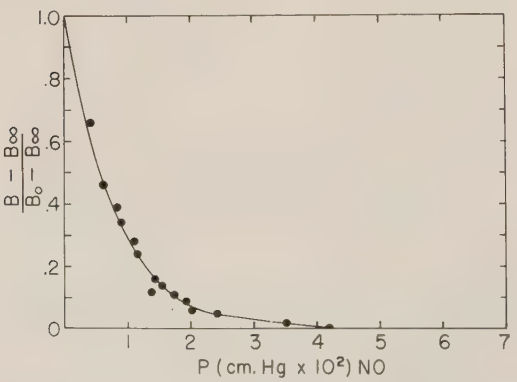

FIG. 6. Benzene inhibition curve at 518°C and 100% acetylene.

ber of organic compounds. It will be noted that nitric oxide does not completely inhibit benzene formation.

Discussion

The benzene-inhibition experiments were all carried out at constant flow rate and low acetylene conversion. Under these conditions it is a fair approximation to take the partial pressure of benzene as proportional to the rate of its formation.

It was noted above that a portion of the benzene, B_∞, was not inhibited by nitric oxide. This formation must then take place by a non-free-radical process. In Figure 5 is given a plot of B_∞ against acetylene concentration. The large dependence of B_∞ upon the acetylene concentration suggests a stepwise polymerization in which the helium collisions are deactivating. Such a process might be written

$$\begin{aligned} A + A &\rightarrow A_2 && k_1[A]^2 \\ A_2 + M &\rightarrow 2A && k_2[A_2][M] \\ A_2 + A &\rightarrow A_3 && k_3[A_2][A] \\ A_3 + A &\rightarrow B + A && k_4[A_3][A] \end{aligned}$$

then assuming steady states for intermediates A_2 and A_3

$$B = \frac{k_1 k_3 [A]^3}{k_3[A] + k_2[M]}$$

and since the total pressure is constant.

$$B = \frac{k_1 k_3 [A]^3}{k_3[A] + k_2(1 - [A])} \qquad (2)$$

This formulation fits the data reasonably well.

The free radical process for the formation of benzene follows the pattern obtained in the nitric oxide inhibition of the thermal decomposition of a number of organic compounds; e.g., ethane[9]. A typical inhibition curve, $(B - B_\infty)/(B_0 - B_\infty)$ vs. NO, is given in Figure 6.

A possible formulation for the free radical production of benzene is as follows:

$$\begin{aligned} A + A &\rightarrow A + A^* \rightarrow nR \\ 2R + N &\rightarrow \text{recombination} \\ R + A &\rightarrow AR \\ AR + A &\rightarrow A_2R \\ A_2R + A &\rightarrow B + R. \end{aligned}$$

The inhibition reactions would then be

$$NO + R \rightarrow RNO$$

$$NO + AR \rightarrow ARNO$$

$$NO + A_2R \rightarrow A_2RNO.$$

Assuming steady state, an expression for B can be developed. This is not simple and further contains enough different combinations of the eight rate constants to make possible the fitting of any data. The curves can be fitted fairly well with the

TABLE 1

Temperature	Acetylene concentration	B_0	B_∞	C(eq. 3)
°C	*per cent*	*cm*	*cm*	cm^{-2}
495	75	.11	.03	7
495	100	.29	.08	2
518	75	.34	.03	10
518	90	1.45	.05	3
518	100	2.20	.15	2.3

empirical formula

$$\frac{B - B_\infty}{B_0 - B_\infty} = \frac{1}{1 + C[NO]^2} \qquad (3)$$

the B_0, and B_∞ and C for the various conditions studied are listed in Table 1.

It is clear that benzene forms by two mechanisms and it is also clear that both the molecular and free radical reactions occur at temperatures below the ignition temperature. Further, these reactions occur before any appreciable ethylene is formed or high-order polymerization occurs. The question may then be raised as to how the free radicals are formed at these rather low temperatures. We would like to propose that free radicals are formed in the course of the molecular production of benzene. In particular, step 4

$$A_3 + A \rightarrow B + A^*$$

is exothermic by ~120 kcal, so that a reaction such as

$$A^* \rightarrow H + C_2H$$

could occur. These free radicals might then initiate the free radical process for benzene. At higher temperatures other free radical processes come in giving ethylene and polymer. Finally the strong dependence of the molecular process on acetylene concentrations explains qualitatively the results of the dilution experiments.

It is planned to make a similar analysis of the products, ethylene, hydrogen, methane and high polymer.

REFERENCES

1. STEACIE, E. W. R.: *Atomic and Free Radical Reactions*. New York, Reinhold Publishing Co., 1946.
2. PEASE R. N.: J. Am. Chem. Soc., *51*, 3470 (1929).
3. TAYLOR, H. A., AND VAN HOOK, A.: J. Phys. Chem., *39*, 811 (1935).
4. FRANK-KAMENETSKY, D. A.: Acta Physicochemica (USSR), *18*, 148 (1943).
5. BLUMBERG, E. A., AND KAMENETSKY, D. A.: J. Phys. Chem. (USSR), *20*, 1301 (1946).
6. KURI: Bull. Chem. Soc. (Japan), *26*, 280 (1953).
7. BURNHAM, H. P. AND PEASE, R. N.: J. Am. Chem. Soc., *64*, 1404 (1942).
8. ZELINSKI, N. D.: Ber., *57*, 264 (1924).
9. HOBBS, J. E. AND HINSHELWOOD, C. N.: Proc. Roy. Soc., *A167*, 447 (1938).

68

SELF-COMBUSTION OF ACETYLENE. II. REACTIONS IN FLAME PROPAGATION[a]

By E. A. WESTBROOK, KATHERINE HELLWIG, AND ROBBIN C. ANDERSON

Introduction

The study of reactions in the self-combustion of acetylene, i.e., where flame propagation occurs in acetylene alone, without oxygen present, is of interest because they are associated with a system of flame propagation involving hydrocarbons only. It also offers a possible source of additional information about processes which are of practical importance in work with acetylene at high

[a] This research was supported by the U. S. Air Force, through the Office of Scientific Research of the Air Research and Development Command.

pressures and temperatures and in oxyacetylene systems where excess acetylene is present.

Thermal polymerization and decomposition reactions in acetylene have been well-known for years[1, 2]. Numerous investigators have noted that flashes or flame could be observed in acetylene on occasion, and extensive measurements have been made of the conditions for ignition or explosion, but relatively little attention has been given to the flame propagation. Alexejew made a study of effects of pressure, temperature, tube diameter, and various additives on ignition and flame propagation, but the work is available only in an abstract[3].

Prout and Anderson have reported similar experiments on flame propagation in tubes[4, 5], using moving-pictures to determine flame velocities. At initial temperatures in the neighborhood of 300°C and pressures of 1–2 atm, there was an increase of pressure during actual flame propagation, but a net decrease in pressure for the overall process. Velocities increased with increased pressure and were sensitive to the type of tube used, in the general order of decreasing flame velocity: brass > aluminum > lead > glass > carbon-coated glass. Temperature effects on the flames were fairly small, indicating apparent energies of activation for the over-all reaction of 4–20 kcal/mole. The main reaction was decomposition to carbon and hydrogen, with small amounts of methane and benzene also appearing.

Frazee and Anderson[6] have studied carbon formation and growth in acetylene. Their results indicate that surface reaction with hot acetylene is a reaction of importance as well as the pyrolysis reactions usually considered. Observations of ultraviolet emission and absorption spectra under pre-ignition conditions and in flames by Robertson, Humphrey, and Anderson[7] showed no evidence of radicals such as C_2 or CH. The spectra showed a continium which might result from excited molecules or free radicals or from the presence of polyacetylenic hydrocarbons. Studies of the ignition reactions, using infrared spectra, by Robertson, Magee, Fain and Matsen[8], show that formation of benzene and ethylene start under similar conditions. Addition of nitric oxide inhibits the formation of ethylene completely. The rate of formation of benzene is decreased, but there is some residual reaction unaffected by the nitric oxide.

In this paper further results on flame propagation are reported, in addition to other experiments which, while not made in actual flames, do give information on the reactions occurring there.

Experimental Methods

The apparatus and procedure for observations of flame velocities have been described earlier[4, 5]. The apparatus consisted essentially of a straight tube of borosilicate glass, of internal diameter one in. and fitted with a heating-jacket and manometer so that the temperature could be controlled and the pressure determined. A small wire coil at one end was used as igniter. For the experiments reported here, the gases were at an initial temperature of 300°C.

The additive was introduced as gas or vapor in each case, the acetylene then added, and the mixture allowed time to mix and to come to the desired temperature. Mole percentages were calculated from the initial partial pressures of the gases.

Flame velocities were determined by photographing the flame over 75–100 cm of its course, using a Bell and Howell 16 mm camera, at 32 or 64 frames/sec, and Super XX Pan film. A scale below the tube was also photographed so that graphs of flame position at various times could be made from the films.

The data reported here are for flame velocities rather than true burning velocities. Correction for the shapes of the flames and gas-flow factors for the flames in acetylene alone[5] indicate that the burning velocities for the conditions used here would be about 0.7–0.8 of the observed flame velocities. However, since there are some variations in shape of flames and pressure changes with the various additives, it was impracticable to determine the burning velocities for a variety of mixtures. The flame velocities are useful for comparisons in a given system, but due caution must be observed in comparing values for different substances.

The mass spectrographic measurements were made with a Westinghouse instrument which employs a conventional 90° momentum filter. Its resolution is at least 1 mass unit in 120. An operating pressure of about 10^{-5} mm is maintained by a mechanical pump and two mercury diffusion pumps.

In some instances mass-spectrographic analyses were made of samples taken from a simple reaction train in which acetylene or acetylene-helium mixtures are passed through a heated reaction zone and then through a dry ice-acetone trap.

Both the gases passing through the cold trap and the liquids condensed out were checked. In other experiments, particularly for acetylene-deuterium mixtures, samples of gas were heated in a closed system.

The experiments on the ultraviolet absorption spectra were made using the heated absorption cell described earlier[7]. This could be used in a flow system. It could also be used for measurements of static mixtures, in which case pressure changes could be followed by a manometer attached.

The materials used were obtained as or prepared from reagent grade chemicals. The acetylene was stripped of acetone as already noted[5].

Results

FLAME PROPAGATION

The measurements of flame speeds have been extended to observe the effects of various chemical additives. Nitrogen and propane decreased flame velocities somewhat until quenching occurred (at 14 per cent for nitrogen, 11 per cent for propane) as would be expected with diluents. Oxygen and acetone, on the other hand, showed maxima (Figs.1 and 2). Hydrogen up to 0.5 per cent tends to increase flame speeds, but in larger proportions causes a decrease. Hydrogen bromide and bromine cause marked decreases. Water vapor increased the time lag on ignition but had no marked effect on flame speed. Nitric oxide also made ignition more difficult but gave erratic effects on flame velocity. Addition of benzene slowed down the flames and caused them to flicker badly.

As noted before, the observed flame speeds are not highly precise on an absolute basis, but they do show clearly that the flame reactions are sensitive to small amounts of additives which might be expected to affect a free-radical system.

PRESSURE EFFECTS AND ABSORPTION SPECTRA

In the investigations of ultraviolet spectra it was found that mixtures of acetylene and helium could be heated to temperatures well above the ordinary ignition-point for acetylene. For each mixture a temperature is eventually reached at which a cloud of particles appears, though no actual ignition of flames occurs in the more dilute mixtures. Table 1 indicates the maximum temperatures attainable.

The pressure changes occurring in such mixtures have been checked also. Figure 3 shows a typical set of pressure curves. For other mixtures similar curves are obtained but for different temperatures. Figure 4 shows a comparison of the pressure effects with the variations in absorption limit and the extent of absorption.

There are many difficulties apparent for interpretation of these spectra, but it is significant that there is no change in the basic pattern as acetylene is heated past its ordinary ignition temperature and even up to temperatures comparable to those which must exist in the flames. There are also strong indications that combination reactions occur even in conditions where decomposition is a final result.

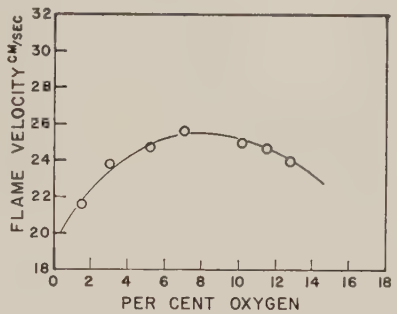

FIG. 1. Effect of oxygen on flame.

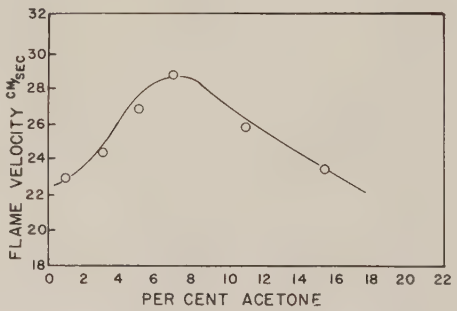

FIG. 2. Effect of acetone on flame.

REACTION PRODUCTS

In samples of liquid polymer frozen out after heating acetylene to temperatures below its ignition-point, benzene tends to obscure any other products. As the temperature is increased the liquid deposit becomes yellow and orange. Just before ignition it becomes murky and gray. In this region, ion peaks at masses 104, 103, and 102 were observable. Similar results were obtained with mixtures of acetylene and helium, which could be heated to temperatures above the ignition temperature of acetylene.

These results and the color effects noted above are in accord with the report of Kuri[9] that cyclooctatraene is an intermediate in the thermal reactions of acetylene and the suggestion of Garner, Long, and Thorp[10] that fulvenic-type compounds

Table 1. Temperatures for Particle Formation

Mole per cent		Temperature
C_2H_2	He	
		°C
100	0	500
40	60	600
20	80	680
15	85	730
10	90	800
7	93	850

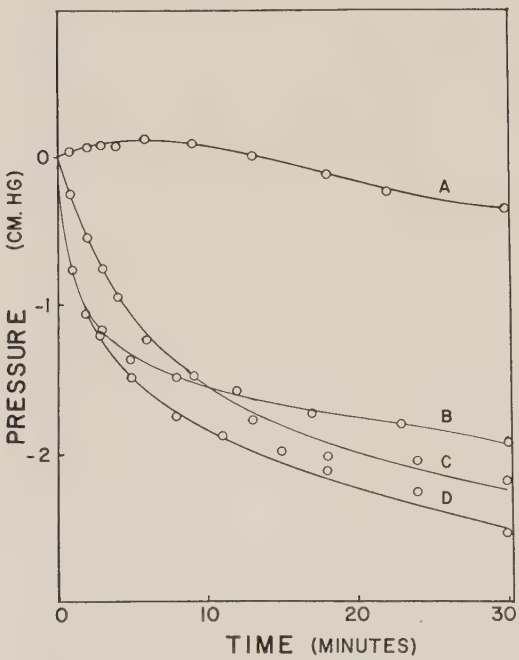

Fig. 3. Pressure drop vs. time after stopping flow for 10% C_2H_2–90% He. A—at 535°C; B—at 800°C; C—at 660°C; D—at 735°C.

may be precursors of carbon. Additions of small amounts of nitric oxide or propylene were found to inhibit formation of the colored polymers and of carbon as well as of benzene.

The carbon formed in the flames contains appreciable amounts of liquid polymers in which benzene is readily detectable. Extraction with hexane gives yellow, yellow-orange, or red solutions, the amount of colored material extracted being less for flame propagation at higher pressures.

Qualitative tests with these colored polymers showed that, on heating above 600° in N_2, they react to give carbonaceous deposits. They react even more readily in the presence of acetylene.

In the gases escaping from the cold trap, some faint peaks were detected for masses 52, 51, and 50, corresponding to intermediates having four carbon atoms, but these are not conclusive. All

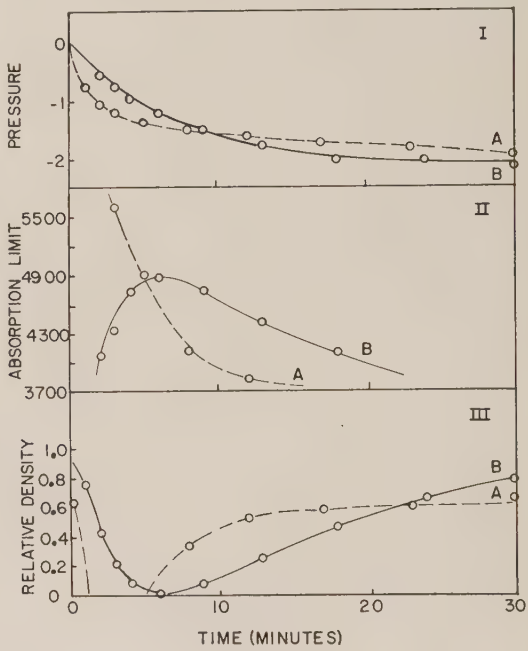

Fig. 4.
Graph I: Pressure drop vs. time after stopping flow. A—10% C_2H_2–90% He at 800°C; B—10% C_2H_2–90% He at 660°C.
Graph II: Long wavelength absorption limit vs. time after stopping flow. A—10% C_2H_2–90% He at 800°C; B—10% C_2H_2–90% He at 660°C.
Graph III: Density vs. time after stopping flow. A—10% C_2H_2–90% He at 800°C; B—10% C_2H_2–90% He at 660°C.

results on acetylenic systems indicate the four-carbon intermediates must be highly reactive and transitory.

Qualitative analyses of mixtures of acetylene and deuterium which were heated up to as high as 550°C showed formation of mono-deuterated acetylene and benzene in particular (plus some di- and tri-substituted products) to an extent well beyond the exchange which could be obtained by reaction of either benzene or ethylene under the conditions used. Both were markedly reduced by addition of nitric oxide.

ENTHALPY AND FREE ENERGY OF REACTION

Approximate calculations of energy relations for various types of reactions which might be important in the flames were also made.

For many of the compounds and reactions which may be involved in propagation of these flames, thermodynamic data are not available. However, the method of group contributions developed by Franklin[11] and modified by van Krevelen and Chermin[12] makes it possible to get reasonable estimates of enthalpies and free energies of these reactions. Results of such calculations are summarized in Table 2.

The group contributions were not corrected for the possible effects of conjugation, since these are relatively small and in most cases the magnitude would be doubtful. Comparisons made of calculated values with data such as those of Stamm, Halverson and Whalen[13] for vinyl acetylene and of Ferigle and Weber[14] for biacetylenes indicate that variations of as much as 5–6 kcal/mole might be expected if such corrections were made, but these would not affect the comparisons made here.

The group contributions for the free radicals were evaluated by starting with reactions such as

$C_2H_2 = C_2H + H$ and $HC_2 - C_2H = 2C_2H$

and using values for the C—H (104 kcal) and C—C (59 kcal) bond energies to estimate the heats of reaction. The former gives 106 kcal and the latter 83 kcal for the heat of formation of C_2H, as contrasted to 120 kcal from kinetic data[2]. Other values could be obtained by using, for example, the value of 85 kcal for the C—C bond (based on L(C) = 170 kcal). The value of 83 kcal was used here because it gives more conservative estimates for the reactions being investigated, though it is quite evidently a minimum value. The entropy contributions were taken from those for closely similar compounds.

Two points of interest in the values of Table 2 are the indications of favorable energy conditions for formation of non-aromatic polymers and for formation of H_2, either by decomposition or by reaction of free radicals or hydrogen atoms.

ENERGIES OF ACTIVATION

In certain cases, as indicated in the discussion below, energies of activation for certain steps have been estimated on the basis of the Hirschfelder approximations[15]. These are only estimates, but again no attempt is being made to make detailed and quantitative comparisons. Comparisons with kinetic data on polymerization experiments and on the reactions of various active particles indicate that the values used are reasonable[2].

Table 2. Enthalpy and Free Energy of Reaction

	ΔH_{298}	ΔG_{300}	ΔG_{800}	ΔG_{1500}
$C_2H_2 + C_2H_2 = C_4H_4$	−40	−31	−17	4
$C_2H_2 + C_2H_2 = C_4H_2 + H_2$	0	1	−17	−43
$C_4H_2 = C_4 + H_2$	58			
$C_4H_4 + C_2H_2 = C_6H_6$ (straight-chain)	−40	−30	−14	9
$C_4H_4 + C_2H_2 = C_6H_6$ (aromatic)	−78	−61	−31	12
$C_2H_2 = C_2H + H$	81	78	72	63
$C_2H + C_2H_2 = C_4H_3$	−27	−17	1	24
$C_2H + C_2H_2 = C_4H_2 + H$	23	20	13	5
$C_2H + C_2H_2 = C_4H + H_2$	0	1	−16	−43
$H + C_2H_2 = C_2H + H_2$	−23	−19	−30	−48
$H + C_4H_3 = C_4H_2 + H_2$	−54	−60	−90	−130
$H + C_2H = C_2 + H_2$	98	102	91	73

Discussion

The data reported here for absorption spectra, pressure changes, mass spectra, etc., were not taken from direct observations on burning gases (in which the formation of carbon obscures most other effects). They were, however, taken under conditions which approximate closely in many respects those which must exist in the flames, and the types of reaction products, etc., can be shown to parallel the flame reactions. The results furnish, therefore, a useful indication of reactions which can occur in the flames. Consideration of these, plus the energy relations involved, can give a

fair picture of the chemical changes which must be occurring in flame propagation.

The pressure effects and the polymeric products obtained show that combination occurs at least partially, even at high temperatures, though the major products are carbon and hydrogen. Attempts to detect specific free radicals such as C_2 and CH were unsuccessful, but the general behavior both in flames and in high-temperature reactions is characteristic of a free-radical mechanism. The tests with deuterium indicate that C_2H, in particular, is important in the high-temperature reactions.

The general resemblance of the flame reactions to thermal reactions of acetylene at high temperature would suggest as a first possible mechanism of flame propagation a thermal one involving reactions such as

$$C_2H_2 + C_2H_2 = C_4H_4 \qquad E \sim 40 \text{ kcal/mole} \quad (1)$$

or

$$nC_2H_2 = (C_2H_2)_n \quad (2)$$

Carbon might be formed as a secondary process by dehydrogenation reactions of the type

$$C_4H_4 = C_4H_2 + H_2 \qquad E \sim 50 \quad (3)$$

$$C_4H_2 = C_4 + H_2 \quad (4)$$

However, this involves a sequence of reactions of relatively high activation energies and it offers no explanation for the effects of surfaces or of additives on the flames.

A simple chain mechanism is no more satisfactory. It would have to follow a sequence such as:

$$C_2H_2 = C_2H + H \qquad E \sim 104 \text{ kcal/mole} \quad (5)$$

$$H + C_2H_2 = H_2 + C_2H \qquad E \sim 6 \quad (6)$$

$$C_2H = C_2 + H \qquad E \sim 80\text{–}100 \quad (7)$$

or occasionally

$$H + C_2H = C_2 + H_2 \qquad E \sim 80\text{–}100 \quad (8)$$

and

$$nC_2 = C(s)$$

Reactions (5), (7), and (8) are highly endothermic, and no appreciable energy is released until the last step, which is unlikely to occur rapidly enough for a self-propagating reaction.

For the flames in acetylene a major question is that of a mechanism of pyrolysis by which the energy inherent in the condensation of carbon can in effect be used in advance. Some combination of decomposition or dehydrogenation with combination or polymerization steps is, therefore indicated both by the energy requirements and the experimental results at high temperatures. Such a process can be started by step (5) on a hot-wire igniter, or by free radicals from some other molecule:

$$R + C_2H_2 = RH + \cdot C_2H \qquad E \sim 6 \text{ (for } CH_3) \quad (9)$$

Combination steps can then occur readily:

$$C_2H + C_2H_2 = C_4H_3 \qquad E \sim 3 \quad (10)$$

The energy of this combination may also activate molecules so that on occasion

$$C_2H + C_2H_2 = C_4H_2 + H \qquad E \leqslant 26 \quad (11)$$

The hydrogen atoms can react in a sequence of steps such as reaction (6) or:

$$H + C_4H_3 = H_2 + C_4H_2 \quad (12)$$

$$H + C_4H_2 = H_2 + C_4H \quad (13)$$

$$H + C_4H = C_4 + H_2 \quad (14)$$

even down to

$$H + C_nH(s) = C_n(s) + H$$

All of these should have low energies of activation and favorable enthalpy values and give highly reactive products. This is similar to the mechanism of photochemical polymerization suggested by Lind and Livingston[16] but they considered only the possible combination steps, such as reaction (10).

A second possibility in lieu of reaction (5) which might be considered[17] is that of breaking of the second pi bond of acetylene:

$$C_2H_2 = \cdot CH{=}CH \cdot \quad (15)$$

This could involve only some 50–60 kcal. It might react readily in such steps as

$$\cdot CH{=}CH \cdot + C_2H_2 = \cdot CH{=}CH_2 + C_2H \quad (16)$$

This is of interest because of the appearance of ethylene along with benzene in the preignition reactions and its suppression by nitric oxide[8].

The equations above are written for only the simplest molecules or particles. In the real reaction system highly unsaturated molecules containing many carbon atoms must be built up quickly. However, comparison of reaction (14) with reaction (6) and of reactions (10) and (11) with (1) or (2) indicates that it would be possible to follow a series of steps, which could lead even-

tually to formation of extensive carbon skeletons, virtually stripped of hydrogen. These steps would include unsaturated intermediates, both aromatic and alicyclic. The energy requirements would not be high in any single step, and the activation energies would be compatible with observed temperature effects.

The system of reactions should include polymerization reactions occurring and serving as an energy source; but flame propagation would not be dependent on these thermal effects alone. Dehydrogenation as in step (3) probably occurs also. Many further questions can be raised about the reaction mechanisms, but the results so far do indicate that the self-combustion of acetylene does not occur as a simple decomposition flame. It seems clearly to involve a complex mixture of molecular and free-radical reactions, with polymerization and dehydrogenation occurring simultaneously, rather than in sequence.

Additional experiments are being carried out to obtain further information about bond strengths and reactivity of some of the acetylenic compounds and about the nature of products appearing at various stages in different reaction mixtures.

Acknowledgment

The authors wish to acknowledge the assistance of K. E. Clonts and Don Oakes and of W. W. Robertson and Wm. Fain in some of the experiments.

REFERENCES

1. Ellis, C.: *Chemistry of Petroleum Derivatives*, p. 81. New York, Chem. Catalog Co., 1934.
2. Steacie, E. W. R., *Atomic and Free Radical Reactions*, p. 164. New York, Reinhold Publishing Corp., 1946.
3. Alexejew, D.: Chem. Zentralblatt, *2*, 1588 (1925).
4. Prout, W. E., and Anderson, R. C.: Texas J. Sci., *4*, 521 (1952).
5. Prout, W. E., and Anderson, R. C.: Fuel, *33*, 125 (1954).
6. Frazee, J. D., and Anderson, R. C.: *Carbon Formation and Reaction in Flames in Acetylene*. Paper presented at Am. Chem. Soc. Meeting, Chicago, Ill., Sept., 1953.
7. Robertson, W. W., Humphrey, N. B., and Anderson, R. C.: J. Chem. Phys. *21*, 2093 (1953).
8. Robertson, W. W., Magee, E. M., Fain, J., and Matsen, F. A.: *Fifth Symposium (International) on Combustion*, p. 628. New York, Reinhold Publishing Corp., 1955.
9. Kuri, Z.: Bull. Chem. Soc. (Japan), *25*, 116 (1952); *26*, 280 (1953).
10. Garner, F. H., Long, R., and Thorp, N.: Fuel, *32*, 116 (1953).
11. Franklin, J. L.: Ind. & Eng. Chem., *41*, 1070 (1949).
12. van Krevelen, D. W., and Chermin, H. A. G.: Chem. Eng. Sci., *1*, 66 (1951).
13. Stamm, R. J., Halverson, R., and Whalen, J. J.: J. Chem. Phys., *17*, 104 (1949).
14. Ferigle, S. M., and Weber, A.: J. Chem. Phys., *20*, 1657 (1952).
15. Hirschfelder, J. O.: J. Chem. Phys., *9*, 645 (1941).
16. Lind, S. C. and Livingston, R.: J. Am. Chem. Soc., *56*, 1550 (1934).
17. Franklin, J. L.: Humble Oil and Ref. Co., private communication.

69

CHAIN-BRANCHING ACTIVATION ENERGY IN ACETYLENE-OXYGEN FLAMES

By J. VAN WONTERGHEM and A. VAN TIGGELEN

Introduction

According to the theory proposed by one of us[1], the burning velocity of a flammable mixture depends markedly on the activation energy of the branching reaction to be considered in the development of the chain mechanism of the overall reaction. If this is the case, it is important to determine this activation energy for different fuels and oxidants and to compare it with values derived from burning velocity measurements.

The quantitative spectral investigation of premixed acetylene-oxygen flames[2], and especially the investigation of OH emission has afforded us an opportunity to calculate an activa-

tion energy of 30 kcal for the formation of the OH radical, which may reasonably be considered as one of the active centers that propagate the chain reaction in the combustion of acetylene. Since the replacement of active centers lost by chain-breaking reactions proceeds from a branching rather than from a primary reaction because of the larger activation energy of the latter, we concluded that the activation energy of 30 kcal corresponds really to the branching reaction itself.

The experimental procedure[2] consisted in measuring the change in OH emission with increasing dilution of a mixture with a constant acetylene-oxygen ratio. A chemiluminescent excitation was assumed for the OH radical.

The purpose of the present work was to establish whether the same value can be derived from

Table 1

$\frac{C_2H_2}{C_2H_2 + O_2}$	$\frac{N_2}{C_2H_2 + N_2 + O_2}$	V_0	T_f	$T = T_0 + 0.74(T_f - T_0)$	Y	E_f'
		$cm\ sec^{-1}$				
0.2	0.71	113.5	2150	1665	0.29	34.3
0.2	0.73	102	2095	1628	0.27	
0.2	0.76	75	2010	1558	0.24	
0.233	0.71	140.5	2275	1768	0.29	32.4
0.233	0.73	122.5	2200	1700	0.27	
0.233	0.76	92.5	2135	1655	0.24	
0.233	0.79	67	2015	1565	0.21	
0.263	0.71	153	2362	1818	0.29	30
0.263	0.73	133	2290	1770	0.27	
0.263	0.76	108.5	2215	1713	0.24	
0.263	0.79	81	2100	1625	0.21	
0.294	0.71	165	2442	1886	0.29	31
0.294	0.73	146.5	2360	1818	0.27	
0.294	0.76	113.7	2255	1745	0.24	
0.294	0.79	82.8	2140	1657	0.21	
0.294	0.81	63.2	2040	1580	0.19	
0.313	0.71	162	2460	1895	0.29	31.2
0.313	0.73	143.5	2370	1830	0.27	
0.313	0.76	111	2270	1735	0.24	
0.313	0.79	80.8	2155	1668	0.21	
0.313	0.81	59.5	2055	1543	0.19	
0.333	0.71	159	2480	1912	0.29	33
0.333	0.73	137	2385	1841	0.27	
0.333	0.76	106	2270	1750	0.24	
0.333	0.79	75	2165	1675	0.21	
0.333	0.81	53.5	2060	5195	0.19	
0.337	0.71	147	2491	1922	0.29	33
0.337	0.73	122	2399	1847	0.27	
0.357	0.76	92.2	2290	1770	0.24	
0.357	0.79	57	2147	1652	0.21	
0.385	0.71	123	2489	1921	0.29	33.2
0.385	0.73	90.5	2380	1837	0.27	
0.385	0.76	58	2270	1750	0.24	

the burning velocities of the corresponding mixtures. Our deductions are based on the following relation for burning velocity[1]:

$$V_0 = \frac{4T_0}{\pi}\sqrt{\frac{2R(\partial - \beta)}{3MT}}$$

where ∂ and β represent the chain-branching and chain-breaking probabilities in any collision,

M is the mean molecular weight of the active centers, (taking into account the alternative formation of two or more different radicals);

T is the mean temperature of the flame front (reaction zone) equal approximately to:

$$T = T_0 + 0.74\ (T_f - T_0)$$

where T_0 and T_f are the initial and the flame temperatures.

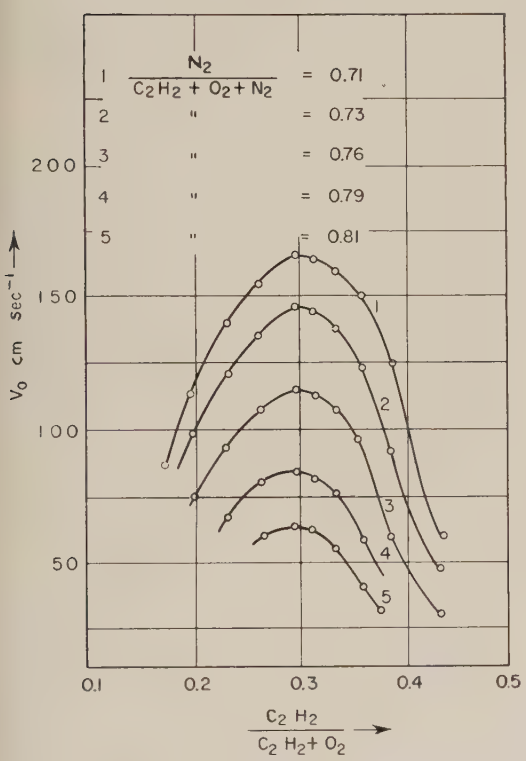

FIG. 1. Flame propagation velocity; C_2H_2-O_2-N_2 flame.

For a given fuel-oxidant system, and when the flammable mixture is not near the ignition limits, β may be neglected as compared to ∂ and all the constants may be combined. This leads to the very simple relation:

$$V_0 = K\sqrt{\frac{\partial}{T}}$$

The probability ∂ of branching in any collision is given by a kinetic equation which must be first-order with respect to the initial constituents:

$$\partial = f(C_2H_2\ ,\ O_2)\cdot e^{-(E'_r/RT)}$$

This relation states the dependence on the acetylene-oxygen ratio and on the temperature. We shall assume that for each series of mixtures with a constant acetylene-oxygen ratio and increasing dilution, the function $f(C_2H_2\ ,\ O_2)$ varies proportionally with the concentration of the undiluted flammable mixture:

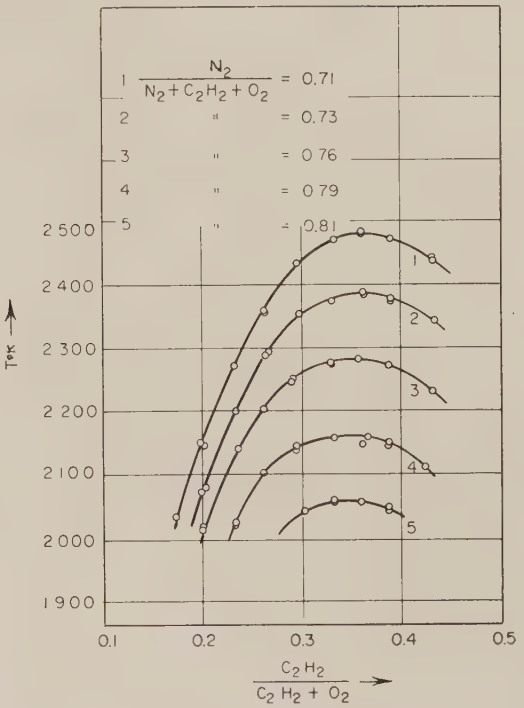

FIG. 2. Flame temperature (sodium-line-reversal method); C_2H_2-O_2-N_2 flame.

$$Y = \frac{100 - \text{per cent inert.}}{100}$$

Thus for each set of values:

$$V_0 = K'\sqrt{\frac{Y}{T}}\cdot e^{-(E'_r/RT)}.$$

Taking the logarithm, the expression becomes:

$$\log V_0 - \tfrac{1}{2}\log Y + \tfrac{1}{2}\log T = K'' - \frac{E'_r\cdot 0.4343}{2RT}.$$

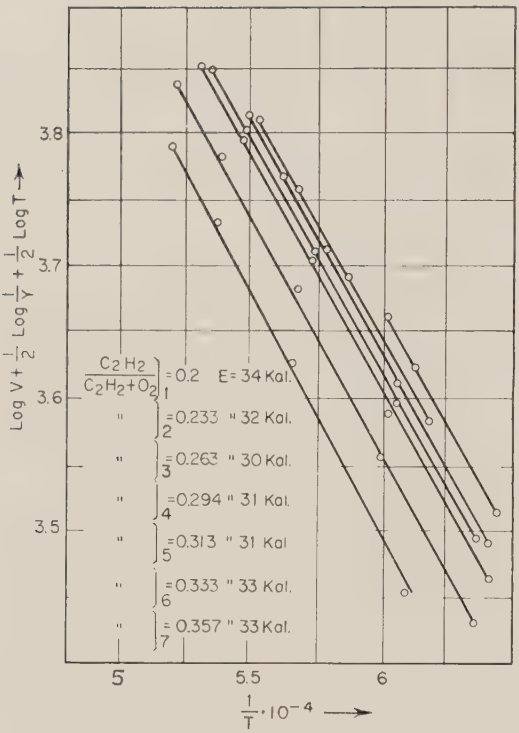

FIG. 3. Activation energy; C_2H_2-O_2-N_2 flame.

tion energy E'_r from the slope of the curves obtained by plotting (log V_0 − ½(log γ) + ½ log T) in terms of $1/T$.

Experimental Method

DETERMINATION OF THE BURNING VELOCITY

Burning velocities were determined by the total area method, applied to the schlieren cone. The surface of the cone was calculated on a tenfold enlargement of the photographic image. Each result is the average of two to five measurements and is reproducible to within ±2 per cent.

Conical burners with diameters between 0.5 and 0.8 cm were used. The independence of burning velocity on burner diameter was checked.

DETERMINATION OF THE FLAME TEMPERATURE

The sodium-line-reversal method was used on flames that were completely colored by an NaCl aerosol obtained by electric discharge between an electrode and moist NaCl in the nitrogen stream. The optical system was free from optical aberrations and the usual corrections were made for brightness temperature and light absorption by the lenses. The results were reproducible to within

TABLE 2

$\frac{C_2H_2}{C_2H_2 + O_2}$	$\frac{\text{Inert}}{\text{In.} + C_2H_2 + O_2}$	V_0 (cm sec^{-1})	T_f	$T = T_0 + 0.74(T_f - T_0)$	Y	E'_r
		Inert = argon				
0.286	0.792	151.5	2505	1923	0.203	31.9
0.286	0.855	73.2	2130	1653	0.145	
0.286	0.877	48	1990	1550	0.123	
		Inert = helium				
0.286	0.75	297.5	2490	1918	0.25	32.9
0.286	0.804	273	2340	1810	0.196	
0.286	0.85	134	2090	1623	0.15	
0.286	0.88	74.5	1890	1475	0.12	
		Inert = nitrogen				
0.286	0.7	188	2480	1913	0.3	31.5
0.286	0.8	86	2100	1633	0.2	
0.286	0.8	78	2100	1633	0.2	
0.286	0.85	40	1850	1440	0.15	

The only difference between the equations for each series lies in the constant K''. It is now possible to calculate the value of the apparent activa-

±10°. The values obtained are 80° to 140° lower than the calculated temperatures. The tungsten-strip lamp was carefully calibrated.

GASES AND FLOW MEASUREMENT

Commercial acetylene was used and passed through a CO_2 ice trap to remove acteone. The oxygen was 99 per cent pure. Rotameters used to measure the flow of the different gases were calibrated at frequent intervals against a standard gas meter.

Experimental Results

All results are given in Table 1 and represented graphically in Figure 1 for burning velocities, in Figure 2 for flame temperatures and in Figure 3 for the calculated activation energy E'_r.

Discussion

The value of E'_r derived from our results is compared in Table 2 with V_0 and T_f values reported by Morgan and Kane[3]. These results also were used to calculate the value of E'_r by the same graphic method. As shown in the last column of Table 2, the same value was obtained with three different diluents. We may therefore compare the value of 30 kcal derived quite independently from OH-band intensities with varying dilution[2] and the values ranging from 30 to 34 kcal in Tables 1 and 2.

This agreement may be taken as an argument in favor of the important role played by the OH radical in the chain reaction. We believe that the acetylene molecule is attacked by the radical and that this reaction constitutes one of the links of the chain. Furthermore, the formation of new OH radicals to compensate losses by chain breaking in the reaction zone occurs by a reaction whose real activation energy must be close to 30 kcal. This value can only be explained by a branching reaction, such as the reaction between an oxygen molecule and some fragment of the acetylene molecule.

It should be noted that the exact nature of the reaction need not be known in making *a priori* calculations of the burning velocity when diluting with more inert gas.

Acknowledgments

The authors express their thanks to the "Fonds National de la Recherche Scientifique" for financial support in this research. One of them (J. Van Wonterghem) also is indebted to the I.R.S.I.A. for a postgraduate fellowship.

REFERENCES

1. Van Tiggelen, A.: Mem. Acad. Roy. Belge, (Cl. Sc.), *27*, 1 (1952).
2. Ausloos, P., and Van Tiggelen, A.: Bull. Soc. Chim. Belge., *62*, 223 (1953).
3. Morgan, G., and Kane, W.: *Fourth Symposium (International) on Combustion*, p. 313. Baltimore, The Williams & Wilkins Co., 1953.

70

THE EFFECT OF LEAD OXIDE AND COPPER SURFACES ON THE THERMAL DECOMPOSITION OF ETHYL NITRATE VAPOR[a]

By W. R. ELLIS, B. M. SMYTHE, and E. D. TREHARNE

1. Introduction

Although the homogeneous decomposition of ethyl nitrate vapor has been extensively investigated[1, 2, 3] there has been little previous work published on the effect of various solid surfaces on this decomposition.

Adams and Bawn[1] have shown that an increase of surface in a Pyrex reaction vessel has no influence on the rate of reaction of ethyl nitrate, the decomposition being homogenous. Gray and Yoffe[4] have studied the effect of surfaces on the explosion limits of methyl and ethyl nitrates. The fact that a decrease in volume surface ratio and coating the Pyrex surface with KCl and KI increases the explosion limits suggests a radical chain mechanism for the explosion of these nitrates. Lead tetraethyl was shown to have no effect, contrary to what would have been expected in view of the effect of potassium salts. Walsh[5] suggests that $Pb(Et)_4$ exerts an influence on hy-

[a] Publication of this paper has been approved by the Chief Scientist, Department of Supply, Australia.

drocarbon combustion by virtue of forming PbO which is an inhibitor because it causes a surface destruction of chains. He has shown that in the presence of oxygen, $Pb(Et)_4$ can form PbO at a temperature of 360°C. In the case of Gray and Yoffe's work[4], it is unlikely that PbO would be formed due to the low temperature and absence of oxygen in its free state. This could explain the absence of any effect by $Pb(Et)_4$ on the explosion limits of methyl nitrate and ethyl nitrate. PbO has been shown by Walsh[5] to inhibit generally the slow oxidation of hydrocarbons. It is well known that copper and other metallic surfaces accelerate the oxidation of hydrocarbons. In view of these facts it was thought that it would be of interest to observe the effect of these two types of surface on the thermal decomposition of ethyl nitrate.

2. Experimental

The apparatus was similar to that used by Adams and Bawn[1]. The rate of reaction was measured in the conventional manner by allowing the ethyl nitrate vapor to decompose at constant volume and temperature and following the pressure increase by means of a glass spiral gauge.

The reaction vessel was situated in an electrically heated furnace of large heat capacity; its temperature did not vary by more than ±2°C over several hours.

Liquid ethyl nitrate stored in a small container attached to the apparatus, which had previously been thoroughly evacuated, was warmed, and the vapor admitted to a heated storage flask of 1-liter capacity until the desired pressure had been reached.

A known pressure of air was admitted to the outside of the Bourdon gauge, then the tap connecting the ethyl nitrate vapor storage flask to the reaction vessel was opened and vapor allowed to flow into the reaction vessel until the Bourdon gauge again returned to its position. The reaction vessel was then isolated from the storage vessel. By this means, after some practice, a known pressure of ethyl nitrate vapor would be rapidly and accurately admitted to the reaction vessel.

Subsequent pressure readings were then taken at convenient time intervals. This procedure was repeated at various temperatures.

Experiments were carried out in three types of reaction vessel: (1) A plain Pyrex flask; (2) A Pyrex flask coated internally with lead oxide; (3) A Pyrex flask containing chopped copper foil.

The PbO coating was prepared[5] by adding crushed Pyrex glass to the flask, then a few grams of solid PbO, evacuating and heating to 300°C for half an hour. This produced a film of PbO on the walls of the flask. Adams and Bawn[1] had found that packing their reaction vessel with Pyrex tubing had no effect on the rate of the reaction. Hence any change in rate produced in this case would be due to the lead oxide.

All experiments were carried out at an initial ethyl nitrate pressure of 50 mm.

3. Materials

Ethyl nitrate was prepared by the nitration of ethyl alcohol[6]. The product was washed with water, sodium carbonate solution and water, dried over calcium chloride and distilled. The fraction boiling at 85–85.5°C was collected and used throughout this work.

Copper was AR foil. Lead Oxide was AR quality.

4. Results

Curves of pressure increase vs. time for the Pyrex flask, PbO-coated flask and copper-filled flask are shown in Figures 1 to 4. From these curves maximum rates of pressure increase were determined. It is interesting to note that in the case of the lower temperatures with copper (Fig. 4) there is a slight and varying period of induction, before the rate of pressure increase reaches its maximum value.

The log of maximum rate of pressure increase was then plotted against reciprocal temperature (Fig. 5) and, from the resulting straight line, a value for the activation energy for the initial stages of the reaction was determined.

Following the method adopted by Adams and Bawn[1], the results were also plotted as if the reaction were first order, i.e., log $(p_\infty - p_t)$ was plotted against time. Here p_t is the pressure of the system at time t, and p_∞ is the final pressure, i.e., the pressure attained by the system when equilibrium has been established. Adams and Bawn[1] found that the final pressure varied between 185 and 212 per cent of the initial pressure, but, in this work the final pressure in each case was taken to be twice the initial pressure, i.e., for an ititial pressure (p_σ) of 50 mm, the final pressure (p_∞) was taken to be 100 mm.

For the plain Pyrex vessel the temperature range covered was 182–219°C. The plot of log $(p_\infty - p_t)$ vs. time was essentially linear for four

of the five temperatures, although at two temperatures (200 and 210°C) a change of slope occurred.

At the highest temperature used (219°C) the graph deviated slightly from linearity.

For the lead oxide-coated vessel the temperature range was 189–227°C. The plot of log $(p_\infty - p_t)$ vs. time was linear at 189°C, but deviated from

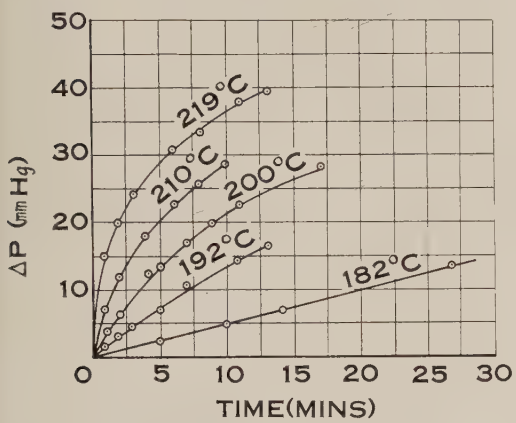

Fig. 1. Pressure-time curves for decomposition in Pyrex vessel.

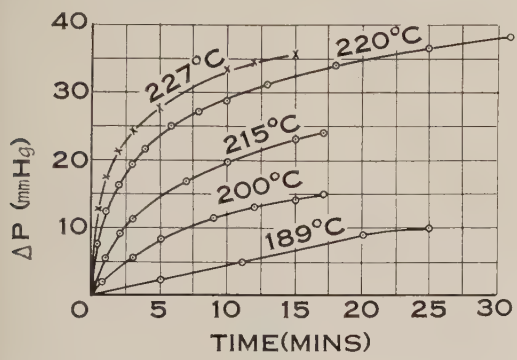

Fig. 2. Pressure-time curves for decomposition in PbO-treated vessel.

linearity at higher temperatures during the later stages of the reaction.

In the case of the copper-filled vessel, experiments were carried out at temperatures between 147°C and 200°C. For temperatures up to 167°C the plot of log $(p_\infty - p_t)$ vs. time was linear throughout a large part of the reaction, but at the higher temperatures the curve deviated markedly from linearity at an early stage of the reaction.

The values of maximum rate of pressure increase and rate constants obtained for each of the three types of reaction vessel are summarized in Table 1. From the slopes of the initial linear portions of these curves, rate constants, k, were determined for each temperature for each of the

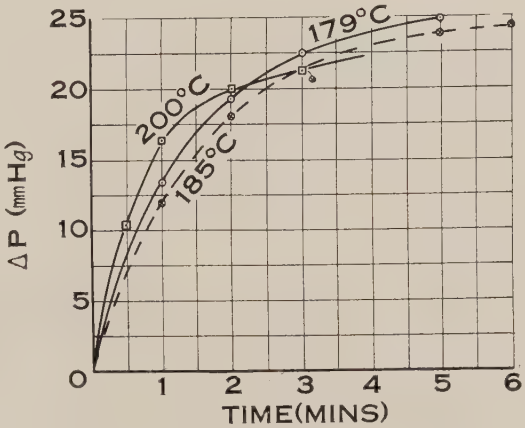

Fig. 3. Pressure-time curves for decomposition in vessel containing copper.

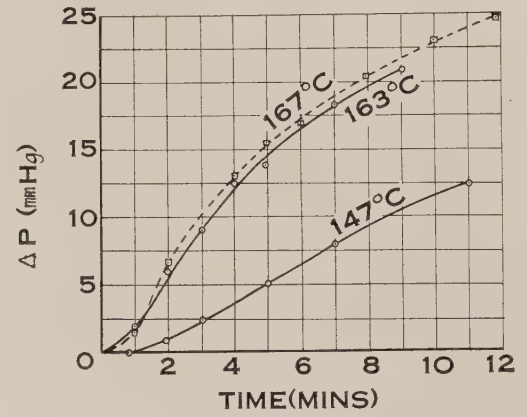

Fig. 4. Pressure-time curves for decomposition in vessel containing copper.

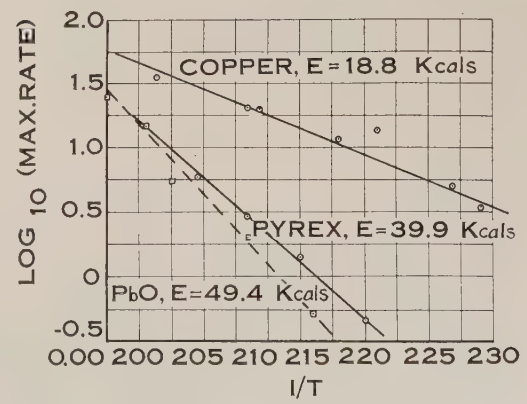

Fig. 5. Activation energies for ethyl nitrate decomposition calculated from initial rate of pressure increase.

three types of reaction vessel, and, by plotting log k vs. reciprocal of the absolute temperature, activation energies were determined for the initial reaction in each of the three types of reaction vessel.

Frequency factors were also determined from the log k, $1/T$ plots.

Table 2 shows the frequency factors obtained and a comparison between the activation energies obtained by the two methods outlined above.

Table 1. Maximum Rate and k for Reaction under Various Conditions

Temp	Max Rate	$k(\times 10^4)(sec^{-1})$
°C	*mm/min*	
Pyrex Vessel		
182	0.5	1.84
192	1.5	5.16
200	2.9	11.7
210	6.2	22.2
219	15.0	43.0
PbO-coated Vessel		
189	0.53	1.64
200	2.0	6.30
215	5.5	16.4
220	15	47.7
227	24	—
Copper-filled Vessel		
147	1.4	4.32
163	3.5	10.3
167	4.9	10.3
179	14	51.2
185	12	38.2
200	21	69.8

Initial pressure ethyl nitrate in all cases = 50 mm. Assumed final pressure = 100 mm.

Table 2. Activation Energies and Frequency Factors for Decomposition of Ethyl Nitrate

	E (kcal/mole) (initial pressure increase)	E (kcal/mole) (initial rate constant)	Frequency factor
Pyrex flask.	39.9	38.3	14.7
PbO-coated flask.....	49.4	46.6	20.4
Cu-filled flask.....	18.8	21.4	7.7

When the copper-filled flask was in use, care was taken to reduce thoroughly the copper between each run to ensure a reproducible copper surface and constancy of results. This was done by evacuating the flask (at say 200°C) then filling it with hydrogen to one atm pressure and leaving for about 10 min.

Table 3 illustrates the marked decrease in the catalytic efficiency of the copper at 198°C if this precaution is omitted. It is typical of many similar cases encountered.

The minimum temperature of explosion for ethyl nitrate vapor at a pressure of 50 mm in the Pyrex vessel was about 225°C, while for the PbO-coated vessel the explosion limit at the same pressure appeared slightly higher at 227–230°C. No attempt was made to determine the limit with the copper-filled vessel, but a run was successfully carried out at 218°C without any sign of explosion.

Table 3. Decrease in Activity of Copper

	Pressure increase during 1st minute
	mm
1st run	16.5
2nd run	12.5
3rd run	7.5
4th run	6.5

After the experiments with the copper-filled flask had been completed and the flask removed from the furnace, without reduction of the copper, it was noticed that the copper was covered with a reddish brown material (presumably cuprous oxide) with a few black patches (possibly cupric oxide).

5. Discussion

The activation energies for the reactions carried out under the three conditions were obtained from both the maximum rate of pressure increase and from the initial rate constants. The difference between the two methods illustrates the variation in activation energy (E), that would be expected in considering the reaction rate over different periods of time. Hence values usually quoted for activation energy and frequency factor (A) for the decomposition of alkyl nitrates should not be regarded as those for the overall reaction. For the sake of comparison both within themselves and with the results of other workers,

we will consider the rate expressions derived from the initial rate constants. In the case of the plain Pyrex reaction vessel the rate equation

$$k = 10^{14.7}\, e^{(-38.3/RT)}\ \text{sec}^{-1}$$

agrees favorably with that quoted by Adams and Bawn[1]. The presence of a copper surface exerts a catalytic effect on the decomposition of ethyl nitrate, considerably reducing the apparent activation energy and frequency factor. If the rate controlling step in the homogeneous decomposition of ethyl nitrate is the endothermic rupture of the O—NO_2 bond with which an activation energy of the order of 39 kcal is usually associated, it is obvious that in the presence of a copper surface this step is no longer rate controlling. The activation energy of ca. 21 kcal may be associated with some subsequent step in the reaction or with a process connected with the initial breakdown of chemisorbed ethyl nitrate on the copper surface. It is interesting that Thomas[7] obtained a rate equation

$$k = 10^{8.9}\, e^{(-19.8/RT)} 1.\ \text{mole}^{-1}\ \text{sec}^{-1}$$

for the reaction between glyoxal and NO_2 between 160°–210°C.

Pollard and Wyatt[8] have reported a rate equation of

$$k = 10^{7.1}\, e^{(-15.1/RT)} 1.\ \text{mole}^{-1}\ \text{sec}^{-1}$$

for the reaction between formaldehyde and NO_2 below 160°C. Above this temperature the equation becomes approximately

$$k = 10^{9}\, e^{(-19/RT)} 1.\ \text{mole}^{-1}\ \text{sec}^{-1}$$

This agrees remarkably with that for the reaction between glyoxal and NO_2 (above). Moreover, both the activation energy and frequency factor are the same order as those obtained in the present work for the decomposition of ethyl nitrate in the presence of copper, i.e.,

$$k = 10^{7.7}\, e^{(-21.4/RT)}\ \text{sec}^{-1}$$

A large number of reactions involving NO_2 have frequency factors of the order of 10^7–10^9, and activation energies of ca. 20 kcal. It is therefore possible that in the thermal decomposition of ethyl nitrate on a copper surface the rate controlling step is one involving NO_2. Further information on this possibility should be obtained from the proposed investigation of the reaction between NO_2 and formaldehyde in the presence of a copper surface.

In the presence of a PbO surface the rate equation for the thermal decomposition of ethyl nitrate becomes

$$k = 10^{20.4}\, e^{(-46.6/RT)}\ \text{sec}^{-1}$$

At a temperature of ca. 200°C the rate is reduced to about half the rate without lead oxide present. As the temperature increases, however, as can be seen from Fig. 6, the retarding effect is not as great, and above about 220°C the rate would be expected to be greater in the presence of a lead oxide surface if the explosion limit was not reached. This is to be expected considering the abnormally high frequency factor, and a difference in activation energy of some 8 kcal.

It is interesting to note that a lead oxide surface causes the rate equation for the decomposition of ethyl nitrate to approach those obtained for some of the higher nitric esters. Phillips[2] has reported the initial rate equation for the decomposition of erythritol tetranitrate, in the liquid phase, to be

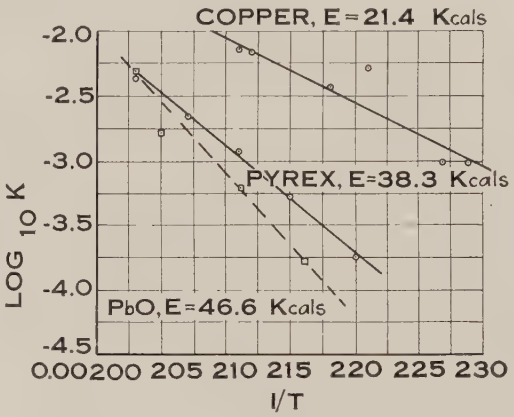

FIG. 6. Activation energies for ethyl nitrate decomposition calculated from initial rate of pressure constants.

$$k = 10^{20.2}\, e^{(-46.3/RT)}\ \text{sec}^{-1}$$

for the temperature range 144–169°C.

Several other nitric esters, including nitroglycerine, show rate equations with abnormally high frequency factors and activation energies in excess of 40 kcal. Phillips[2] has suggested that the high frequency factors may be due to high positive entropies of activation which might arise from restricted rotation about C—C bonds in the initial state, due to dipolar repulsion.

These high values for A and E seem to be connected with the possibility that the radical formed

from the initial rupture of the O—NO_2 bond can undergo decomposition as well as reacting with further unchanged nitric ester molecules.

The possibility of the radical, formed from a nitric ester such as nitroglycerine, undergoing decomposition to form smaller fragments before reacting further with other molecules, would be expected to be greater than in the case of a simpler radical such as the ethoxy radical formed when ethyl nitrate decomposes.

It is possible that two parallel mechanisms may be operative, the one with the higher A and E becoming more important at the higher temperature. A possible mechanism would be

$$RO\ NO_2 \rightarrow RO + NO_2 \quad (1)$$

$$RO \rightarrow \text{fission into fragments} \quad (2)$$

The radical RO can undergo unimolecular decomposition rather than attack the RO NO_2 molecule with the abstraction of a hydrogen atom.

$$RO + RO\ NO_2 \rightarrow RO\ H + R\ CH_2O + NO_2 \quad (3)$$

This suggested mechanism is supported by the present work. It has been shown by Walsh[5] that PbO is a very efficient surface for the destruction of radicals. Lead oxide is not generally regarded as an efficient catalyst for molecular decomposition. It seems likely that if ethoxy radicals are formed in the decomposition of ethyl nitrate the presence of a lead oxide surface would favor the occurrence of reaction (2) in competition with reaction (3), the fission of the radical being very much more efficient on the lead oxide surface. If the normal course of decomposition of ethyl nitrate at these temperatures and pressures is through reaction (3), the occurrence of reaction (2) would tend to retard the rate of the overall reaction, as in fact the presence of PbO has been shown to do. The fragments produced by the unimolecular decomposition of the ethoxy radical are capable of further reaction with NO_2, etc. e.g.

$$CH_3\ CH_2O \rightarrow CH_3\cdot + CH_2O \quad (4)$$

$$CH_3\cdot + NO_2 \rightarrow CH_3{\cdot}NO_2 \quad (5)$$

$$CH_2O + NO_2 \rightarrow CO + H_2O + NO \quad (6)$$

It is therefore possible that this could become an alternative path in the overall decomposition of ethyl nitrate to CO, NO, H_2O, etc. It could become more favorable than the normal course at high temperatures. This is indicated by the rate equation obtained for a PbO surface, the path with the higher E and A values becoming more important at high temperatures.

Study of the decomposition of a higher nitrate in the gas phase in the presence of a lead oxide surface is proposed. If the decomposition of such a nitrate normally displays a high frequency factor and an activation energy in excess of 40 kcal, it would be expected that the presence of a lead oxide surface would cause an acceleration in the rate of decomposition.

It is of interest to consider the effect of lead tetramethyl on the combustion of ethyl nitrate reported by Adams et al.[9] The addition of up to 1 per cent of lead tetramethyl causes a reduction in the rate of burning by a factor of about 3, whereas more than 1 per cent of this substance causes an acceleration in the rate of burning. The active agent is presumably PbO (which can be formed from the lead tetramethyl) since mercury dimethyl and methyl iodide do not show the same effect.

The presence of a small amount of PbO surface could produce a retardation of the rate of burning by a process similar to that postulated above for the thermal decomposition of ethyl nitrate. However, when a large amount of PbO is present, the conditions could be altered so that the alternative reaction path through the unimolecular decomposition of radicals could become the more favorable.

6. Conclusions and Further Work

The presence of a copper surface accelerates the thermal decomposition of ethyl nitrate. Under these conditions the rate controlling step appears to involve the NO_2 molecule.

The presence of a lead oxide surface retards the thermal decomposition of ethyl nitrate in the temperature range studied. It is suggested that this is due to the destruction of radicals through which the reaction normally proceeds under these conditions.

To obtain further information it is intended to carry out the following investigations:

(1) Gas analysis to determine if different products are formed when the reaction takes place on a PbO and copper surface.

(2) Detailed investigation of the effect of PbO and Cu surfaces on the kinetics of the NO_2-formaldehyde reaction. This work is now in progress and the results will be published when the work is completed.

(3) A more detailed study of the radical reac-

tions involved in the thermal decomposition of nitric esters. The technique of flash photolysis developed by Porter[10] will be used to obtain this information.

(4) The effect of PbO and copper surfaces on the thermal decomposition of those higher nitric esters which have a high activation energy and frequency factor.

REFERENCES

1. Adams, and Bawn: Trans. Faraday Soc., *45*, 494, (1949).
2. Phillips: Nature, *160*, 753, (1947); Thesis, University of London (1949).
3. Pollard, Marshall, and Pedler: Nature, *171*, 1154 (1953).
4. Gray, and Yoffe, J. Chem. Soc. 3180, (1950).
5. Walsh: Proc. Roy. Soc., *A215*, 175, 454 (1952); Disc. Faraday Soc., *24*, 48 (1953).
6. Gatterman: *Laboratory Methods of Organic Chemistry*, p. 148. New York, The Macmillan Co., 1938
7. Thomas: Trans. Faraday Soc., *49*, 630, (1953).
8. Pollard, and Wyatt: Trans. Faraday Soc., *45*, 760, (1949).
9. Adams, Parker, and Wolfhard: Disc. Faraday Soc., *14*, 97, (1953).
10. Porter: Disc. Faraday Soc., *14*, 23, (1953).

Discussion by Peter Gray

The work emphasizes the need for satisfactory product analyses. Without them it is not possible to interpret pressure-time curves in such a system, as has been shown most clearly by the excellent work of Levy. It seems likely that the nitrate or its decomposition products will react readily both with copper and with lead monoxide at 200°C. Is copper oxide found after reaction? Flash photolysis might yield some more detailed information, although we have made such measurements ourselves so far without success.

Author's Reply

A number of the investigations we have carried out in this laboratory on the decomposition and combustion reactions of nitric esters have shown us the striking similarity between these radical reactions and those involved in the combustion of hydrocarbons. The present work was undertaken to observe the general effect on the decomposition of ethyl nitrate, of two substances whose action in hydrocarbon combustion is relatively well known. No attempt was made to interpret pressure-time curves beyond using the rate of pressure increase in the same manner as Adams and Bawn[1] as a comparison with their work. Product analyses under such circumstances would not have been of great assistance. In the study of such complex radical reactions as those of the nitric esters, the end products often give little indication of the course of the reaction. Accordingly, we have neglected such analyses in favor of obtaining more direct information by the technique of flash photolysis with which we have had considerable success. This technique has illustrated the important role of formaldehyde in the decomposition of ethyl nitrate (a further analogy with hydrocarbon combustion). This suggests that PbO plays a similar role in the radical reactions of ethyl nitrate as Walsh[5] has shown in hydrocarbon combustion.

The copper surface exhibits the usual effect that it normally does where it functions as an oxidation catalyst; there is evidence of the surface having been oxidized and subsequently reduced but no large amount of the oxides of copper remain after the reaction.

71

THE EFFECT OF METHYL BROMIDE ON THE COMBUSTION OF SOME FUEL-AIR MIXTURES

By M. C. BURDON, J. H. BURGOYNE and F. J. WEINBERG

Many detailed determinations have been made of the effect of incombustible materials upon limits of flammability of combustible gases and vapors in air[1]. Seldom, however, have such determinations included any study of the chemical nature of the flame products in the presence of the added material. The present work is concerned with that aspect in the particular case of methyl bromide added to hydrogen/air and carbon monoxide/air so as to form near-limit mixtures. It is a continuation of the work on methyl bromide already published by Burgoyne and Wil-

liams-Leir[2], and by Coleman and Gaydon[3], in which effects of methyl bromide upon limits and upon flame spectra respectively were studied.

Experimental

Near-limit mixtures were exploded in a closed vertical Pyrex tube 60 cm long, 7.5 cm diameter and having a wall thickness of 3 mm. The source of ignition was an induction coil spark between glass-sheathed tungsten electrodes at the lower end of the tube.

Mixtures were made up in the evacuated explosion vessel by partial pressures, a calibrated metering vessel being employed to introduce constituents at less than 10 per cent concentration. Thorough mixing was effected by means of a Topler circulating pump and the pressure was adjusted to atmospheric before firing.

The explosion products were pumped out at a controlled rate through an analytical train consisting of a tarred anhydrone tube (for water), a solid carbon dioxide/acetone trap, a potassium hydroxide tube and a liquid oxygen trap. The uncondensed gases were sampled and analyzed in a Bone-Newitt apparatus for hydrogen, carbon monoxide, methane, oxygen and (by difference) nitrogen.

The condensate from the carbon dioxide/acetone trap was analyzed for bromine (iodometrically) and for hydrogen bromide (by titration with alkali after fixation of bromine with mercury). Qualitative tests on this condensate for aldehydes, alcohols, acids and organic halogen compounds gave negative results throughout the investigation.

The contents of the potassium hydroxide tube were dissolved in water and a portion made slightly acid with nitric acid, the temperature being kept below 30°C. The solution was neutralized with sodium carbonate and titrated for bromide with silver nitrate solution (potassium chromate indicator).

Table 1. Explosion Products of Near-Limit Hydrogen-Air-Methyl Bromide Mixtures

Run no.	Reactants (moles per cent)				Products (moles from 100 moles total reactants)												Type of flame	Calc. flame temp.
	CH_3Br	H_2	Air		H_2O	Br_2	HBr	CH_3Br	CO	CO_2	O_2	N_2	C_2H_2	C_2H_4	CH_4	H_2	C_2H_6	
			O_2	N_2														°C
SH2	4.02	6.5	18.8	70.6	12.0	1.14	1.70	—	.69	3.26	9.6	70.6	—	—	—	—	—	C	1280
SH2(rep)	3.99	6.47	18.8	70.7	12.4	1.13	1.74	—	.72	3.30	9.5	70.7	—	—	—	—	—	C	1305
SH3	8.00	4.50	18.4	69.1	14.5	2.48	3.02	—	.89	7.1	3.54	69.1	.102	—	—	22	—	C	1580
SH4	8.66	23.7	14.2	53.4	16.0	—	8.47	0.164	3.8	3.58	1.22	53.4	.003	.036	1.23	11.4	—	A	1640
SH5	13.5	5.27	17.0	64.2	14.1	.50	12.5	0.17	3.72	7.1	.44	64.2	.014	.051	2.58	.31	.015	C	1880
SH6	3.98	36.6	12.5	47.0	19.7	—	3.87	0.165	1.35	1.17	.83	47.0	.0055	.106	1.51	17.9	.0065	A	1530
SH7	—	72.4	5.7	21.9	11.6	—	—	—	—	—	—	21.9	—	—	—	61.0	—	C	980
SH9	—	5.55	19.8	74.8	3.03	—	—	—	—	—	17.7	74.8	—	—	—	2.5	—	D	420
SH8	—	10.4	17.9	71.5	10.3	—	—	—	—	—	12.7	71.5	—	—	—	—	—	D	860

Table 2. Explosion Products of Near-Limit Carbon Monoxide-Air-Methyl Bromide Mixtures

Run no.	Reactants (moles per cent)				Products (moles from 100 moles total reactants)								Type of flame	Flame calc. temp.
	CH_3Br	CO	O_2	N_2	H_2O	Br_2	HBr	CH_3Br	CO	CO_2	O_2	N_2		
														°C
SCM1	3.99	34.7	12.9	48.4	6.63	.24	3.48	.044	18.0	18.1	0.18	48.4	A	2000
SCM2	6.05	21.2	15.2	57.5	6.3	.51	5.1	.073	7.12	18.9	3.82	57.5	A	1980
SCM3	6.01	15.7	16.5	61.8	5.9	.33	5.3	.065	1.95	19.4	3.15	61.8	A	2140
SCM5	2.00	17.3	17.0	63.7	2.98	.45	1.06	—	2.32	16.9	6.27	63.7	A	1850
SCM6	—	15.3	17.8	66.9	—	—	—	—	1.7	13.7	11.1	66.9	B	1180
SCM7	1.01	15.1	17.7	67.0	1.45	.278	.444	—	1.78	14.0	9.3	67.0	C	1300
SCM8	—	67.4	6.85	25.7	—	—	—	—	53.5	11.7	1.01	25.7	B	1060

A second portion of the potassium hydroxide solution was treated with sodium sulfate and orthophosphoric acid in a calibrated closed apparatus and the carbon dioxide evolved was measured manometrically.

The liquid oxygen condensate was fractionated at low pressure to separate methyl bromide which was expanded into a calibrated vessel and measured manometrically. The more volatile gases were analyzed, in a Bone-Newitt apparatus, for the higher paraffins, olefines and acetylene.

After calculating the quantities of the various products formed, carbon, hydrogen and oxygen balances were drawn up between reactants and products. In general the agreement was satisfactory. Finally, the adiabatic flame temperature was calculated for each mixture exploded, making use of the analytical data obtained, and employing the method of successive approximation and graphical interpolation[4]. Equilibrium constants, etc., were obtained from Justi[5] or Lewis and von Elbe[6], except in the case of bromine and hydrogen bromide, when the data of Gordon and Barnes[7] were employed. All the heats of formation were taken from Bichowsky and Rossini[8].

The mixtures exploded were chosen to be as near as possible to the limit compositions determined by Burgoyne and Williams-Leir[2] and to cover the limit mixtures in a representative manner. The complete results for hydrogen-air-methyl bromide and carbon monoxide-air-methyl bromide mixtures are summarized in Tables 1 and 2 respectively. The reactants and products are shown on a basis of 100 moles of initial mixture. The apperance of each explosion flame is indicated according to the following system:

A = pale yellow
B = pale blue
C = orange
D = invisible under experimental conditions

The mixture containing only 5.55 per cent of hydrogen (Table 1, Run SH9) did not of course propagate a continuous flame and the adiabatic flame temperature therefore has no real significance in this case. The 10.4 per cent mixture (SH8) was near to the lower limit for a coherent flame-front in hydrogen/air mixtures.

Discussion

A striking feature of the results, both for the hydrogen and carbon monoxide mixtures, is that the limit flame temperature is substantially and progressively raised by the increasing additions of methyl bromide both on the lower and upper limit sides. This is in contrast with the effect of inert diluents such as nitrogen, carbon dioxide, argon and helium (see, for example, Egerton and Powling[9]) and it may be attributed to the chemical intervention of methyl bromide in the flame reactions.

It therefore becomes necessary to regard limits in the light of such chemical interventions and accordingly it has been assumed that a limit occurs when the rate of chain breaking (β) becomes equal to the rate of chain branching (δ). The limit curve is then the locus $\beta = \delta$. In general, let the branching rate be proportional to the mth power of the concentration of a species M, and the breaking rate to the bth power of the concentration of another species B. Then at the limit

$$K_M[\mathrm{M}]^m e^{-(E_M/RT)} = K_B[\mathrm{B}]^b e^{-(E_B/RT)} \qquad (1)$$

where E denotes activation energy, K includes steric factors and rate constants and T is a temperature near to the maximum flame temperature, T_f. From equation (1)

$$\ln \frac{K_B}{K_M} + \frac{E_M - E_B}{RT} = \ln \frac{[\mathrm{M}]^m}{[\mathrm{B}]^b} \qquad (2)$$

If, therefore, $\ln [\mathrm{M}]^m/[\mathrm{B}]^b$ is plotted against $1/T_f$ a straight line will result if the species M and B and the indices b and m have been selected correctly.

Furthermore, the slope of the line will give the difference in the activation energies of the processes controlling chain branching and breaking. When these activation energies are known, it is possible to calculate burning velocities of non-limit mixtures on the basis of a flame propagation theory such as that of van Tiggelen[10], but in the present discussion the analysis is not carried to that point. Multiplication of equation (2) by -1 shows that the chain branching and breaking agents are liable to be interchanged unless it is known which of the activation energies is the greater. Since, however, the limits of flammability are widened with increasing temperature,

$$\left[\frac{\partial \delta}{\partial T}\right]_M > \left[\frac{\partial \beta}{\partial T}\right]_B$$

Now,

$$\left[\frac{\partial \delta}{\partial T}\right]_M = \frac{E_M}{RT_f^2} \cdot \delta \quad \text{and} \quad \left[\frac{\partial \beta}{\partial T}\right]_B = \frac{E_B}{RT_f^2} \cdot \beta$$

Moreover, as the limit condition demands $\delta = \beta$, it follows that $E_M > E_B$ so that if the gradient of the straight line is positive, M and B have been assigned their respective roles correctly.

Both $[M]^m$ and $[B]^b$ may be the products of several of the reactant concentrations each raised to any reasonable power and the number of possibilities is obviously too great for each to be tried individually. In general, if $[R_j]$ is the jth reactant, r_j its correct exponent which may be positive, negative or zero, $\theta = 1/T_f$ and K and K' constants,

$$\ln ([R_1]^{r_1}[R_2]^{r_2}[R_3]^{r_3}\cdots) = K\theta + K' \qquad (3)$$

should give a straight line of positive slope, for the correct choice of the R^s and $r^s \cdot r_j > 0$ then labels chain branching agents, $r_j < 0$ chain breaking agent and $r_j = 0$ denotes non-participation of the particular reactant. Differentiation with respect to θ gives

$$\sum_j r_j \cdot \frac{d \ln [R_j]}{d\theta} = K = \text{constant} \qquad (4)$$

The procedure of selecting the correct chain branching and chain breaking processes can therefore be made systematic by plotting the logarithms of each of the reactants against $1/T_f$, evaluating the gradients of these curves at a number of points and substituting these into equation (4). Solution of the simultaneous equations yields the correct values of the exponents.

The general theory outlined above was applied to the experimental results presented for the hydrogen and carbon monoxide air systems in the presence of methyl bromide.

HYDROGEN-AIR-METHYL BROMIDE MIXTURES

Inspection of the results shows that as (O_2) decreases T_f rises to a maximum and then falls. Accordingly log $[M]^m/[B]^b$ must vary reciprocally. The only reactant that shows a stationary concentration is methyl bromide and since this stationary value is a maximum, methyl bromide is immediately identified with B, the chain breaking agent. It was found that the results were well-satisfied when $M = O_2$ and $m = b = 1$. From the slope of the straight line thus obtained $E_M - E_B$ was evaluated as about 14.0 kcal.

Since the branching probability is proportional to $[O_2]$, the controlling reaction is presumably $H + O_2 = OH + O$, which has an activation energy of 17.0 kcal.

The breaking probability is proportional to $[CH_3Br]$ and an activation energy for the controlling step of 3.0 kcal is indicated. The most likely step is $H + CH_3Br = CH_3 + HBr$, the activation energy of which, according to Steacie, is 3–7 kcal.

CARBON MONOXIDE-AIR-METHYL BROMIDE MIXTURES

Application of equation (4) showed that equation (2) could not be satisfied with any allocation of CO, O_2 or CH_3Br, alone or in combination, to the roles of B and M. It was therefore concluded that either the agent controlling chain breaking or that controlling chain branching, or both, were not among the three reactants.

The possibility was considered that chain branching might be controlled by moisture vapor, but unless this varied (and steps were taken by drying to avoid this) it should be possible to find a linear relation between $\ln (1/[B]^b)$ and $1/T_f$. This could not be done with either of the reactants in the role of B.

The alternative was therefore considered that chain breaking might occur predominantly at the walls. Their area remains constant and their temperature is invariably low. Thus in equation (2)

$$\frac{E_M - E_B}{RT_f} \quad \text{is replaced by} \quad \frac{E_M}{RT_f} - \frac{E_B}{RT_B},$$

but since $T_f \gg T_B$, this is approximately equal to $-E_B/RT_B$, which is constant. Thus, it follows from equation (2) that $\ln [M]^m$ should be approximately constant.

Use of equation (4) then indicated that $\ln [O_2]^2[CO]$ satisfies this condition whether methyl bromide is present or not. The branching step may therefore involve two molecules of oxygen with one of carbon monixide, whilst chain termination occurs predominantly at the surface. Methyl bromide does not participate in this scheme and it must be concluded that its role is, in this case, chiefly that of a second fuel, competing for oxygen with the carbon monoxide, and having no specific inhibiting action.

The conclusion is consistent with the view that the branching reaction is of the kind

$$CO + O_3 = CO_2 + 2O$$

followed by

$$2(O + O_2 + M = O_3 + M).$$

and not of the kind

$$CO_2^* + O_2 = CO_2 + 2O$$

followed by

$$2(O + CO = CO_2^*)$$

which would give a branching rate dependence on $[CO]^2[O_2]$.

Acknowledgment

The work described was carried out in the Department of Chemical Engineering and Applied Chemistry, Imperial College, London, S.W.7, as part of the extra-mural research program of the Department of Scientific and Industrial Research and Fire Offices Committee Joint Fire Research Organization, and is published by permission of the Director.

REFERENCES

1. Burgoyne, J. H., and Williams-Leir, G.: Fuel, *27*, 118 (1948).
2. Burgoyne, J. H., and Williams-Leir, G.: Proc. Roy. Soc., *A193*, 525 (1948).
3. Coleman, E. H., and Gaydon, A. G.: Disc. Faraday Soc., *2*, 166 (1947).
4. Garrison, H. R., Lasater, J. A., and Anderson, R. C.: *Third Symposium on Combustion, Flame and Explosion Phenomena*, p. 158. Baltimore, The Williams & Wilkins Co., 1949.
5. Justi, E.: *Spezifische Wärme, Enthalpie und Dissoziation Technischer Gase*, Berlin, Julius Springer, 1938.
6. Lewis, B., and von Elbe, A.: *Combustion, Flames and Explosions of Gases*. New York, Academic Press, 1951.
7. Gordon, A. R. and Barnes, C.: J. Chem. Phys., *1*, 692 (1933).
8. Bichowsky, F. R., and Rossini, F. D.: *The Thermochemistry of Chemical Substances*. New York, Reinhold Publishing Corp., 1938.
9. Egerton, A. and Powling, J.: Proc. Roy. Soc., *A193*, 190 (1948).
10. Van Tiggelen, A.: Bull. Soc. Chim. Belge., *58*, 258 (1949).

72

KINETIC STUDIES OF GASEOUS EXPLOSIONS

By R. G. W. NORRISH, G. PORTER and B. A. THRUSH

Kinetic data concerning combustion are derived mainly from the investigation of two systems, the slow isothermal reaction in a closed vessel and the laminar flame. The former can be followed directly in time and is experimentally and theoretically attractive, but it is only one aspect of the process of explosive combustion. The latter presents a flow system in which rate processes of diffusion, thermal conduction and chemical reaction are all involved. Neither has proved capable of furnishing even the most qualitative data about the kinetic mechanism of combustion at high temperatures.

Such information will probably be eventually obtained from direct measurements on a homogeneous closed system undergoing explosive and approximately adiabatic conversion, i.e., one which proceeds by the same mechanism as the premixed flame without its attendant complexities of inhomogeneity. The kinetic study of such a system is experimentally more difficult and its analysis is apparently less straightforward than that of the laminar flame, although this is mainly due to the numerous unknown quantities which appear in the latter treatment. We describe here some attempts to produce homogeneous explosions in gaseous mixtures in closed vessels and to study them as a function of time.

Homogeneous Initiation

If the kinetics of chemical change are to be studied, then the change itself, and not its propagation through space, must be rate determining. It follows that the change must be initiated in such a way that, after initiation, the rate of chemical change is equal in all parts of the volume investigated. Such a state is not attained by the usual methods of initiation, such as sparks or admission to a heated vessel, and the method which we have used, that of flash photolysis[1], seems to be the only suitable one at present, with the possible exception of rapid adiabatic compression. Probably no real process is ideally homogeneous; the important criterion is that any

phase difference between reaction in different parts of the vessel should be small compared with the duration of the reaction to be investigated.

Investigations by Flash Spectroscopy

The second requirement for this type of investigation is the recording of some significant parameter of the change as a function of time. Absorption spectroscopy has been mainly used and our early results, using a flash photographic technique are described elsewhere[2, 3]. The minimum time resolution of this method was 30 μsec and it was established that, within this time interval, flash photolysis produced homogeneous initiation throughout a 50 cm long reaction vessel. It was also found that explosion was produced by flash energies above a certain critical value, and that below this value no measurable reaction occurred, apart from the primary photochemical change. Thirdly, it was found that there was an initial period after the flash before any observable reaction occurred, and it was this fact which made the method of flash initiation particularly convenient, since no interference was experienced between the initiating flash and measurements of the explosion itself.

Application of Photoelectric Techniques

While the above method was suitable for the study of reaction times of 200 μsec or more, it soon became clear that the study of the development of chain branching and other rapid changes would require better time resolution, the main limiting factor being that a different explosion was used to obtain each point and the initial period showed a scatter of the order of 50 μsec. By photoelectric methods a time resolution of 1 μsec has now been obtained, and both emission and absorption spectra have been used to follow the kinetics of the change.

The combination of emission and absorption intensities has been used to obtain a value of the temperature as a function of time during the explosion from both the diatomic radical and continuous spectra. The rapidity of the changes and the high temperatures encountered during the explosions preclude temperature measurements with probes or by pressure changes. Of the possible optical methods, one involving the spectral variation rather than the absolute intensity of the light emitted or absorbed by the system was considered less desirable, since the former, which gives a temperature based on the vibrational, rotational or translational energy distribution of the system, involves a relatively high spectroscopic resolution which limits the rapidity of measurement. For this reason and because of its applicability to both discrete and continuous spectra, a modification of Schmidt's method[4] has been used. The light emission or absorption of a small wavelength range by successive explosions under identical conditions have been recorded photoelectrically using a calibrated background source, and it has thus been possible to obtain a value of the effective electronic excitation temperature of the system with a time resolution of better than 10^{-5} sec. Considerable changes were found in the populations of the upper electronic states of the radicals even within this time resolution.

Experimental

A Siemens E2DC xenon arc was used for absorption measurements, the stability needed being obtained by operating it from a 120 v bank of accumulators through a variable resistance. The optical arrangement is shown in Figure 1. A magnified image of the arc was formed in the center of the reaction vessel by a lens and a plane aluminized mirror and the light from this image was focused accurately on the spectrograph slit (Hilger E478), quartz optics being used throughout. An electromagnetic shutter was provided to protect the reactants from decomposition by the arc until immediately before initiation. The photocell unit, which was interchangeable with the plateholder, carried two movable photomultiplier cell mountings arranged so that the adjustable slits in front of the cells (RCA type 1P28) were always in the focal surface of the spectrograph.

The outputs from the photocells were fed into direct-coupled balanced amplifiers having a gain of 750 and a rise-time of less than 1 μsec. The two light intensity against time curves were displayed on a Cossor double-beam cathode ray tube, the final anode and beam splitting electrode of which were supplied from a dummy amplifier which minimized drift and eliminated trace interaction. An automatic trace-brightener was incorporated to improve the recording of the fastest transients. The scattered light from the initiating flash was sufficient to prevent measurements during the first 500 μsec after initiation, this signal being used to trigger the oscillograph time-base.

Measurement of Temperatures

The light received from the explosion alone, and also from the xenon arc observed through the exploding gases, was recorded by photographing the oscillograph traces on stationary 35 mm film. From these traces deflections, which were proportional to the light received from the arc alone (L_1), from the arc and explosion together (L_2), and from the explosion alone (L_3) were measured. It can be shown that, for a wavelength range λ_1 to λ_2

$$\frac{L_3}{L_1 - L_2 + L_3} = \frac{\int_{\lambda_1}^{\lambda_2} B''_\lambda \epsilon_\lambda \, d\lambda}{\int_{\lambda_1}^{\lambda_2} B'_\lambda \epsilon_\lambda \, d\lambda}$$

where B'_λ = brightness of the xenon arc at wavelength λ.

B''_λ = brightness of the explosion gases at wavelength λ for infinite path length.

ϵ_λ = emissivity of the explosion gases at wavelength λ.

The temperature determinations were made in two regions of 30A near 3900A, one on the CN (O,O) sequence, the other away from any diatomic radical spectra. The spectrograph slit was 0.4 mm long and 0.25 mm wide to ensure even illumination by the cathode bright-spot of the arc, the brightness of which was determined photographically with the optical arrangement described by replacing it with a standard tungsten strip-filament lamp, corrections being applied for reciprocity law failure and for light losses at the appropriate interfaces. The optics were arranged to satisfy all the requirements for accurate temperature measurements and the arc gave a constant value of B'_λ in the regions chosen.

If it is assumed that B''_λ is independent of wavelength over the range used, a value of the effective electronic excitation temperature of the system can be obtained for all stages of the explosion for which the quantities $(L_1 - L_2)$ and L_3 can be measured. For band spectra showing purely thermal excitation, and for continuous spectra, B''_λ should be constant over the ranges studied. For band spectra which show a non-equilibrium energy distribution, both B''_λ and ϵ_λ will vary over the range studied, and the measured temperature will indicate roughly an average electronic excitation temperature. The absolute accuracy of the temperature determination given is about $\pm 300°K$, the reproducibility is of the order of 50°K near the peak temperature; this was determined by the signal-to-noise ratio, which was about 20:1 at full band width with no absorption. For studying the light emission alone the signal-to-noise ratio was improved by opening the slit to 5 x 1 mm.

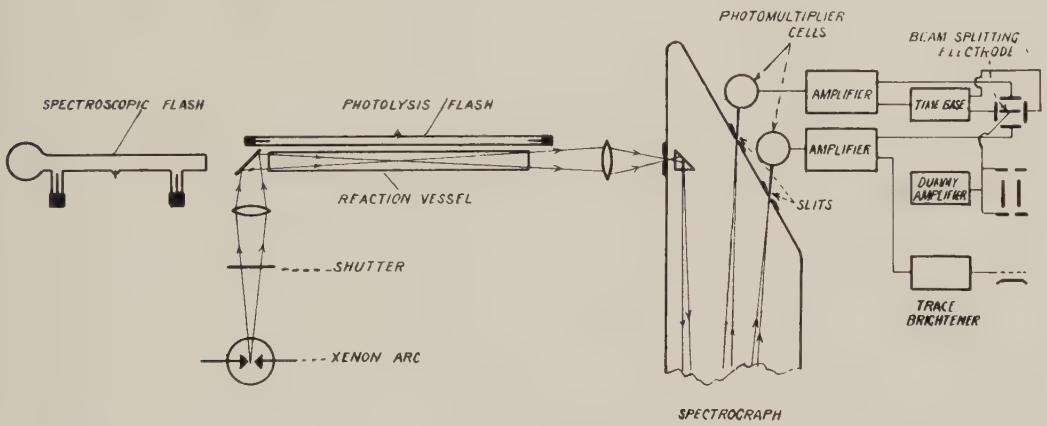

FIG. 1. Experimental arrangement.

Results

WAVELENGTH DEPENDENCE OF THE EMITTED RADIATION

While the light emitted by the explosions is many times too small to be recorded photographically, it can be observed photoelectrically, providing the duration of the initial period is sufficient to eliminate the scattered light from the initiating flash. The relative emission of the various species present in acetylene/oxygen mixtures of different composition photosensitized by nitrogen dioxide were determined by measuring

the total light emission over a series of wavelength ranges chosen to give either the highest or lowest ratio of continuous to diatomic radical spectra. The logarithm of this emission in ergs

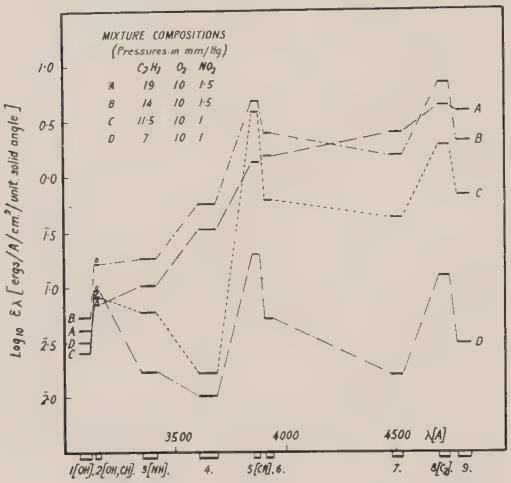

FIG. 2. Logarithm of total emission as a function of wavelength and mixture ratio.

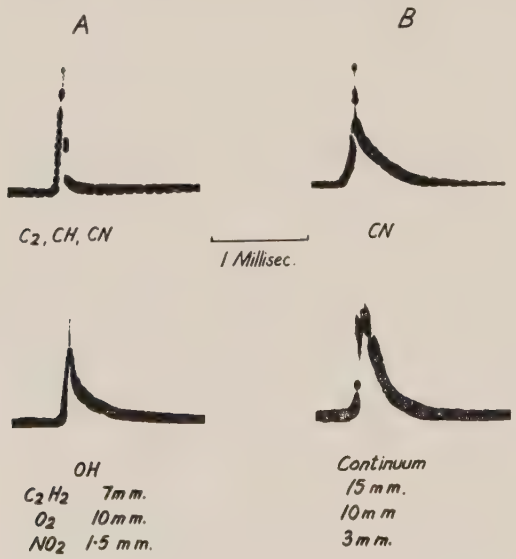

FIG. 3. Traces of light emission against time.

per Angstrom for a 50 cm path length is plotted against wavelength in Figure 2. The absolute intensities were obtained by graphical integration of the emission-time curves using the calibration of the xenon arc at 3900A. They therefore depend on the published spectral response curve of the photomultiplier cell (1P28), but any error arising from this is likely to be small compared with the large range of intensities studied.

The most fuel-rich mixture studied (A) has a smooth variation of light output with wavelength, and the emission observed is probably to be identified with the intense continuum measured photographically in absorption[3]. As the amount of acetylene present is reduced, however, the level of the continuous emission falls, and it is possible to distinguish the C_2 and CN radiation from the continuous background in all the other mixtures. The OH radiation can only be separated from the continuum in mixtures C and D, as the bands lack a sharp head which would increase the sensitivity of detection. The CH ($^2\Sigma^+ - {}^2\Pi$) band at 3143A is so weak compared with the continuum or OH in fuel-rich and oxygen-rich mixtures respectively that none of the radiation observed in this region of the spectrum can be attributed to CH. The radiation of the CH ($^2\Delta - {}^2\Pi$) band at 4315A was not studied in mixtures of all compositions, and is therefore not plotted in Figure 2, but in oxygen-rich systems it was found to be strong compared with the continuum. None of the radiation in the neighborhood of 3360A can definitely be attributed to NH. If allowance is made for the considerable decrease in radiation intensity which is to be expected at shorter wavelengths, it can be seen that the general form of this emission curve is in close agreement with that to be expected on the basis of the concentrations previously observed in absorption[2, 3].

TIME DEPENDENCE OF LIGHT EMISSION

The form of the light emission curve is much more strongly affected by the inhomogeneity of the explosion than is the total light output. The most homogeneous explosions are presumably those having the highest peak light outputs and shortest durations. Typical emission curves of this type for an oxygen-rich mixture are given in Figure 3a and for a fuel-rich mixture in Figure 3b. The OH radiation in oxygen-rich mixtures and the CN, C_2 and continuous radiation in fuel-rich systems show relatively slow decays corresponding to those observed photographically in absorption, although the emission is governed by the temperature and the excitation conditions, as well as by the concentration of the substance responsible.

Apart from the sharp emission peaks of short duration which will be discussed later, the traces obtained from CN, C_2 and CH in oxygen-rich mixtures show an unexpected feature which was not revealed in our earlier work, owing to the

limited time resolution. In complete contrast to the emission curves in rich mixtures, the rate of decay is very much greater than the apparent rate of formation. Furthermore, the rise is not exponential as might perhaps have been expected for the development of an explosion, but it shows a fairly accurate linear dependence on time. The total rise time is about 40 μsec and the decay is complete in less than 2 μsec. In these mixtures, the rise of OH is also approximately linear, and it seems likely that the rise of the carbon radicals is governed by the difference between the rates of formation and removal, and that the rapid decay corresponds to this rate of removal alone, the reactions forming the radicals being complete at this stage. On this basis, it seems likely that the OH emission in fuel-rich mixtures is probably similar in form although it cannot be distinguished from the continuous emission which overlies it.

The traces shown in Figure 3 have certain irregularities which are presumably due to inhomogeneity, since they varied from trace to trace. The main form of these curves is, however, representative of the great majority of those obtained under identical conditions and therefore is, in our opinion, a fundamental property of the exploding system.

ABSORPTION AND TEMPERATURE MEASUREMENTS

Figure 4 shows tracings of the light emission and absorption curves for a region including the CN violet (O,O) band head obtained with a fuel-rich mixture containing 14 mm acetylene, 10 mm oxygen and 1.5 mm nitrogen dioxide together with the temperature curve derived from them by the method described. It will be seen that the continuous absorption falls slightly during the initial period, after which both the emission and absorption increase rapidly together as the radicals appear, and then decay more slowly. A sharp emission peak of duration 2–4 μsec appears superimposed on both traces, and it is not appreciably reduced in height when observed against the xenon arc, which has an effective brightness temperature of 4070°K under these conditions. The main curve maximum, on the other hand, gives a value for the temperature which agrees well with the calculated maximum adiabatic explosion temperature, providing allowance is made for the energy absorbed from the initiating flash. The magnitude of this energy is somewhat uncertain, but its effect on the peak temperature is relatively small, owing to the high degree of dissociation of the explosion products at this temperature. Further evidence for the mainly thermal nature of the emission is provided by the temperatures measured in the continuum beyond the CN (O,O) band sequence,

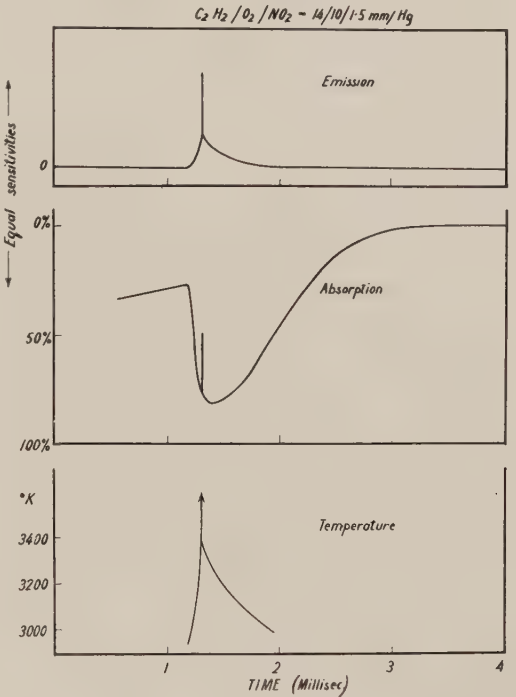

FIG. 4. Emission, absorption and reversal temperatures.

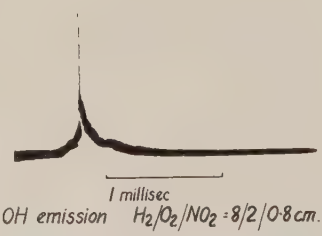

FIG. 5. Hydrogen-oxygen explosion, OH emission against time.

which agree with those given to within 50°K, except for the absence of the sharp emission peak.

By combining the measured rate of cooling with the exponential decay of the CN radical which has been observed photographically for this mixture, a reasonable value for the heat of appearance of CN is obtained, assuming that the concentration of this radical is close to the thermal equilibrium value in the decay. While

the energy value obtained is very approximate, all the evidence available indicates that the rate of decay of the carbon radicals and the continuum under these conditions is governed mainly by cooling and not by chemical reaction.

The absorption measurements clearly show that the sharp emission peak mentioned previously represents a considerable increase in the population of the excited state of the radical for a period of less than 5 μsec, without a corresponding increase in the number in the ground state. Emission peaks of this type have been observed from C_2, CH and CN but not from the continuum in fuel-rich mixtures. With oxygen-rich systems, similar emission has been observed from C_2, CH, CN and OH just before the point where the sudden drop in carbon radical emission occurs. This phenomenon has also been observed in OH emission from hydrogen/oxygen explosions photosensitized by nitrogen dioxide (Fig. 5). Unfortunately, it has not been possible to make temperature determinations in any of the other systems mentioned, since the continuum and the CN (O,O) head in fuel-rich mixtures are the only spectra which are sufficiently intense over a wide enough range for absorption measurements with the present noise level.

The total light emitted in this peak by the CN violet sequence for the mixture containing 14 mm acetylene, 10 mm oxygen and 1.5 mm nitrogen dioxide is of the order of 10^{-5} quanta per molecule of nitrogen dioxide originally present. It is tempting to attribute this radiation to chemiluminescence similar to that observed in emission from flames[5], but the possibility that the effect is a result of some inhomogeneity of the system, such as might arise from the meeting of two shock waves, cannot at present be eliminated. Further work is at present in progress, and we hope that this may lead to a better understanding of the extent to which our explosions are truly homogeneous.

REFERENCES

1. Norrish, R. G. W., and Porter, G.: Proc. Roy. Soc., *A210*, 439 (1952).
2. Norrish, R. G. W., Porter, G., and Thrush, B. A.: Proc. Roy. Soc., *A216*, 165 (1953).
3. Norrish, R. G. W., Porter, G., and Thrush, B. A.: Proc. Roy. Soc., *A227*, 423 (1955).
4. Schmidt, H.: Ann Physik. *29*, 1027 (1909).
5. Gaydon, A. G., and Wolfhard, H. G.: Flames. London, Chapman and Hall, 1953.

73

FLAME PROPAGATION IN METHYL AND ETHYL NITRATE VAPORS

By G. K. ADAMS and J. SCRIVENER

(1) Introduction

The propagation of flame in alkyl nitrate vapors is of interest for a number of reasons. Methyl and ethyl nitrates are the simplest members of a series of organic nitric esters extensively used as constituents of explosives and propellants. As combustion systems they differ from those commonly studied in being combustible in the absence of air or oxygen; the thermal energy required for combustion is released by chemical reaction between the oxygen of the nitrate group and the carbon and hydrogen of the organic part of the molecule.

The kinetics of thermal decomposition of nitrous and nitric esters have been reported by a number of workers and, although unpublished work by Levy in the United States and by Pollard and Marshall in Great Britain has shown the overall reaction to be complex, it is commonly assumed that the primary step is the breaking of the RO—NO_2 bond. The energies of activation found by various workers differ but are significantly similar to the energy of this bond, ~35 kcal/mole. It is possible that the rate-controlling process in the propagation of flame in nitric esters is a decomposition process, the breaking of this bond. Gray and Yoffe[1] studied the thermal ignition limits of methyl and ethyl nitrate vapors and concluded that the influence of inert gases indicates that the initiation is chain-thermal in character.

The results of some measurements of the speed of flame propagation at low pressures in methyl and ethyl nitrate vapors, in mixtures of the two esters and in mixtures with inert gases, are presented. These results are examined to decide whether any conclusions can be drawn as to the nature of the rate-controlling reaction.

(2) Experimental

(2.1) measurement of flame speeds

Because of the explosive nature of the nitric esters and their low vapor pressure at ambient temperatures, a closed vessel method was used. The combustible was admitted to an evacuated cylindrical glass vessel fitted with plane windows and ignited at the center by a spark passed across tungsten electrodes. The spark was produced by the discharge of a condenser, charged to 6 kV, through a three electrode gap in series with the igniter gap.

The flame is not sufficiently luminous for direct photography so a schlieren technique was used to record the position of the flame front. Repetitive spark photographs showed that, except in the immediate vicinity of the electrodes, the flame front was spherical. It was necessary to use a vessel 25 cm in diameter to eliminate the effects of flame front curvature and the initial asymmetry of the flame. These effects are most apparent at low flame speeds. Distortion or lifting of the flame by thermal convection did not occur to a degree sufficient to impede the measurement of flame speed, even at the lowest flame speeds. These were measured by recording the horizontal diameter of the flame front as a function of time with a rotating drum camera. In soapbubble experiments, lifting of the flame by convection is observed at much higher flame speeds than those given in this paper. The absence of a convectional effect in these experiments is attributable to the low pressure employed.

At low spark energies the flame traces show an initial acceleration of the flame speed extending over the first 1–3 cm of the flame diameter. The extent increases with decrease in flame speed of the combustible mixture. The effect is due to the curvature of the flame front. When the radius is small and of the same order as the flame thickness the flame speed is reduced. Since the flame thickness is inversely proportional to the flame speed the effect is more marked at low flame speeds.

As the spark energy is increased the size of the spark kernel increases and the flame speed, initially high, decreases until at 3 cm diameter it assumes a constant value which extends up to about 50 per cent of the vessel diameter. The velocity in this region is independent of the spark energy. At flame diameters greater than 50 per cent of vessel diameter the flame speed decreases owing to the compression of the products of combustion by the pressure rise.

Fiock and Marvin[2] deduced the following relations between the linear velocities of flame propagation and the pressure in the vessel at any position of the flame front:

$$S_u = S - [(R^3 - r^3)/3\gamma_u r^2 P]\, dP/dt \qquad (1)$$

$$S_b = [S + (r/3\gamma_b P)\, dP/dt \qquad (2)$$

where S, r, P and dP/dt are the observed flame speed, flame radius, pressure and rate of pressure rise respectively at a time t. R is the radius of the vessel.

The adiabatic exponents, γ_u and γ_b, and the flame velocities, S_u and S_b, refer to the unburned and burned gases respectively. Eliminating $dP/P\ dt$ and writing ϵ for the expansion ratio at constant pressure, S_b/S_u:

$$S_b = S\epsilon\ (1 + \alpha)/(1 + \alpha\epsilon) \qquad (3)$$

where

$$\alpha = \gamma_b(R^3 - r^3)/\gamma_u r^3$$

Thus as r increases from zero to R, S decreases from S_b to S_u. The flame speed falls appreciably only in the region, $r/R > 0.5$. A simulated flame trace was constructed by replacing S by dr/dt and integrating to give r as a function of t. It was assumed that ϵ and γ_b/γ_u were constant. With these parameters taking values of 10 and 1, respectively, the curve of r against t is linear (within the accuracy of measurement of the average flame trace) between values of r/R of 0.2 and 0.5. The measured mean slope is equal to $0.95\ S_b$. The constant is insensitive to large variations in expansion ratio.

The observed flame speed, measured by taking the best tangents to the trace at a radius 40 per cent of the equivalent spherical vessel radius, is therefore a fair approximation to the velocity of flame propagation with respect to the combustion products for expansion ratios of five or greater.

This flame velocity is commonly assumed to lack the fundamental character of that measured with respect to the reactant, the burning velocity

derived from burner measurements. There appears to be no justification for this view.

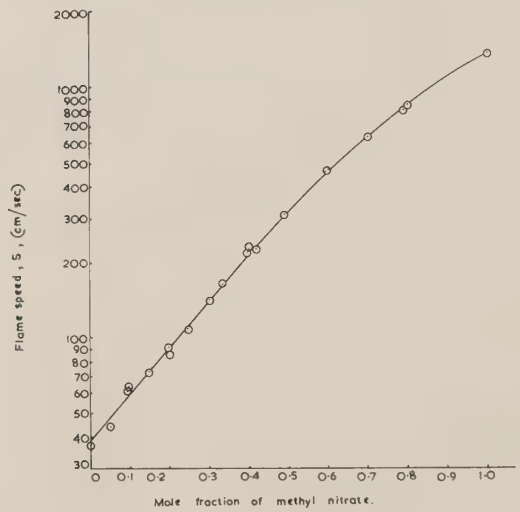

FIG. 1. Flame speeds in methyl nitrate/ethyl nitrate mixtures.

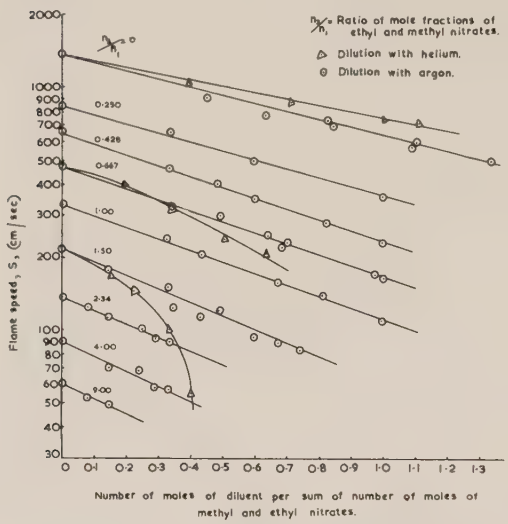

FIG. 2. Effect of dilution on flame speeds in methyl nitrate/ethyl nitrate mixtures.

(2.2) FLAME SPEEDS IN METHYL NITRATE/ETHYL NITRATE MIXTURES

Measurements were made on compositions varying from pure methyl nitrate (S = 1345 cm/sec) to pure ethyl nitrate (S = 37 cm/sec). The former and a number of mixtures were studied at total pressures of 17 and 35 mm Hg. No significant difference in flame speed at these two pressures could be observed. Pure ethyl nitrate vapor requires a high spark energy for ignition (a 5 mm gap between point electrodes required a capacity 0.05 μF, charged to 6 kV, at 30 mm Hg and 0.1 μF at 25 mm Hg). The flame front was ill-defined and the speed was of poor reproducibility. Seven experiments gave a mean square deviation of ± 4 cm/sec. The mean value lies close to the extrapolated curve for the methyl/ethyl nitrate mixtures, Figure 1. This diagram shows the flame velocity plotted logarithmically against the molar composition.

(2.3) THE INFLUENCE OF INERT DILUENTS ON FLAME SPEEDS

An earlier paper[3] showed that flame speeds in methyl nitrate vapor were reduced by the addition of argon, nitrogen, carbon dioxide and water vapor roughly in proportion to the molar heat capacity of the added diluent. The effect of argon and helium on flame speeds has been determined for compositions containing up to 90 per cent ethyl nitrate. The addition of as little as 10 per cent of diluent to pure ethyl nitrate prevented ignition. The argon and helium were commercial products and were used without further purification. The flame speeds of mixtures at a total pressure of 35 mm Hg are shown in Figure 2 as a function of the number of moles of diluent divided by the sum of the number of moles of methyl and ethyl nitrates. The flame speeds of ternary mixtures were less reproducible on account of difficulties in making up the mixtures.

In mixtures diluted with argon the curves corresponding to constant ratios of methyl to ethyl nitrate are approximately linear, although some deviation from linearity can be detected in the composition containing only methyl nitrate and diluent. The slope of the curves increases as the proportion of ethyl to methyl nitrate increased. For the helium mixtures with methyl nitrate the curve is linear and has a smaller slope than the argon curve. With compositions containing ethyl nitrate the helium curve is non-linear and intersects the corresponding argon curve. In mixtures containing ethyl nitrate and considerable amounts of helium the flame speeds are apparently lower than in argon mixtures.

A comparison of the flame traces for corresponding mixtures with argon and with helium, Figure 3, shows that this result is a function of the method of measurement. To measure the flame speed under constant pressure conditions the slope of the trace was evaluated at a flame

diameter of 40 per cent of the vessel diameter. On the argon flame trace of Figure 3 the slope is constant in this region, but for the helium mixture the slope is increasing at this point and reaches a maximum at a diameter of about 70 per cent of the vessel diameter. It is evident that in mixtures containing helium the flame speed increases with diameter. The effect increases with increase in ethyl nitrate content and with increase in the concentration of helium. Experiments in which the flame speed of the mixture was diminished by addition of argon in place of ethyl nitrate showed that flame speed was the determining factor rather than the presence of ethyl nitrate. Hydrogen in place of helium gave a similar type of flame trace.

The addition of low molecular weight diluents appears to enhance the effect of flame curvature on the flame speed. This is consistent with the view advanced in Section 2.1 that the effect of curvature in reducing the flame speed is determined by the flame thickness, since this is directly proportional to the thermal diffusivity and inversely proportional to the flame speed. The addition of diluents of low molecular weight will cause a considerable increase in the mean thermal diffusivity in the flame. No adequate theory of the effect of curvature on flame speed exists whereby the quantitative effect of thermal conductivity can be checked.

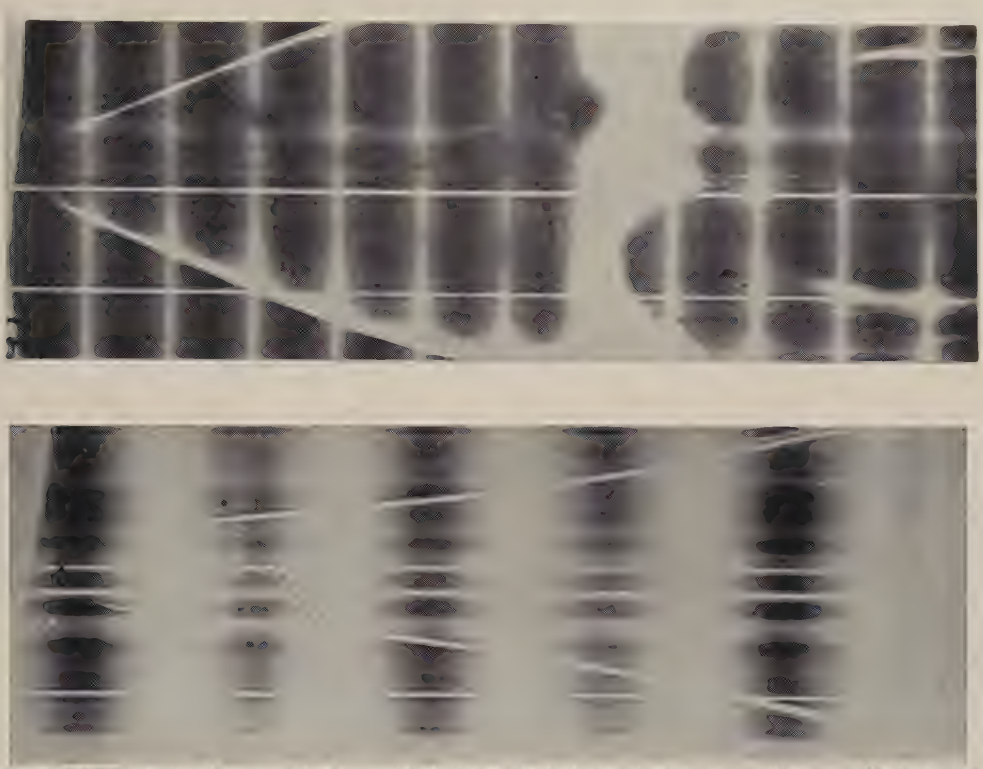

FIG. 3. Flame trace photographs for methyl nitrate/ethyl nitrate/inert gas mixtures. Mole fractions: (a) Methyl nitrate, 0.354; ethyl nitrate, 0.239; argon, 0.407. (b) Methyl nitrate, 0.367; ethyl nitrate, 0.243; helium, 0.390. The time scales are different in (a) and (b) and are indicated by millisecond time marks.

(2.4) ANALYSIS OF THE PRODUCTS OF COMBUSTION

Under constant volume conditions the combustion products of pure methyl nitrate may contain nitrogen together with a little nitric oxide, or nitric oxide with a little nitrogen and nitrous oxide, depending upon the initial pressure and the diameter of the vessel. Cinephotographs show that the products of the primary nonluminous flame are reignited in a diffuse region at the center of the vessel at the time when the primary flame reaches the walls of the vessel. The bright whitish-blue secondary flame corresponds to the reduction of nitric oxide and the ignition is

thought to be due to the adiabatic compression of the initial products. To determine these products it is necessary to perform the combustion at constant pressure. This was done by containing the nitric ester vapor in a thin latex balloon placed in an evacuated vessel. The gaseous products were determined by chemical analysis. The only other products present in significant amounts (as determined by infrared spectra) were water and aldehydes. The amounts of these were calculated from element balances. The composition of the products was fairly reproducible. The following reaction equations fit the analytical data:

$$CH_3ONO_2\ (g) \rightarrow 0.88\ NO + 0.04\ N_2 + 0.02\ N_2O + 0.60\ CO + 0.05\ CO_2 + 0.35\ CH_2O + 0.10\ H_2 + 1.05\ H_2O + 44\ \text{kcal}$$

$$C_2H_5ONO_2\ (g) \rightarrow 0.90\ NO + 0.04\ N_2 + 0.01\ N_2O + 0.31\ CO + 0.01\ CO_2 + 0.035\ CH_4 + 0.02\ C_2H_4 + 0.345\ CH_2O + 0.63\ C_2H_4O + 0.785\ H_2O + 37\ \text{kcal}$$

The heats of reaction are calculated from thermodynamic data for gaseous products at 300°K. The values used for the heats of formation of methyl and ethyl nitrates were 28.0 and 33.4 kcal/mole respectively.

Since the components diffused through rubber at different rates it was not possible to analyze the products of mixtures of the alkyl nitrates and inert gases by this method.

(3) Discussion

(3.1) THE INFLUENCE OF ADDED GASES ON FLAME VELOCITIES IN METHYL NITRATE VAPOR

The experimental results quoted in this and in a previous paper[3] show that the influence of gaseous diluents on the flame velocity can be expressed by the empirical equation:

$$\log S = \log S_1 - B\, n_3/n_1 \qquad (4)$$

S and S_1 being the velocities of flame propagation in the mixtures and in pure methyl nitrate respectively, n_1 and n_3 being the partial pressure or, since the pressures are low enough for the ideal gas law to hold, the mole fractions of methyl nitrate and diluent respectively.

The values of the constant B are: He, 0.26; A, 0.33; N_2, 0.58; CO_2, 0.79. These are roughly in proportion to the molar heat capacities of the diluent. The small difference between the two rare gases suggests that thermal conductivity is also relevant.

The proportionality to heat capacity indicates that flame temperature is the most important factor in determining the flame velocity. The flame temperature is a function of the heat of reaction, the initial temperature and the total heat capacity of the product gases. Thus if;

$$H = \int_0^T C dT = \bar{C}T \qquad (5)$$

where C is the heat capacity of the products referred to one mole of methyl nitrate and $\bar{C}$ is the mean value between 0°K and the final temperature T°K, then

$$T = H/(\bar{C}_1 + \bar{C}_3 n_3/n_1) \qquad (6)$$

The form of equation (4) suggests that the flame velocity is an exponential function of the reciprocal flame temperature, since, if

$$S \propto \exp(-A/T), \quad \text{from (6) } \log S = \log S_1 - \bar{C}_3\, An_3/2.303\, Hn_1 \qquad (7)$$

which is of similar form to equation (4), the constant B being identified with $\bar{C}_3 A/2.303H$. This is very nearly constant over a limited range of composition since both $\bar{C}_3$ and $H = -\Delta H_0 + \int_0^{300} C_r dT$ (C_r being the heat capacity of the reactants referred to one mole of methyl nitrate) vary only slowly with n_3/n_1.

A better demonstration that flame temperature is the main factor determining the flame velocity in mixtures of methyl nitrate diluted with other gases can be made by comparing velocities at a constant flame temperature. This requires some knowledge of the heat of the reaction (although it is not very sensitive to the actual value taken) and the assumption that the nature of the reaction is unchanged by dilution. Some analyses of the products of constant volume combustion in the presence of diluents previously reported[3] support this assumption.

The mixtures having a flame temperature of 1600°K were calculated assuming a heat of reaction corresponding to the products estimated at constant pressure:

$$CH_3ONO_2\ (g) \rightarrow 0.88\ NO + 0.04\ N_2 + 0.2\ N_2O + 0.60\ CO + 0.05\ CO_2 + 0.35\ CH_2O + 0.1\ H_2 + 1.05\ H_2O + 44\ \text{kcal at } 300°K$$

This gives a temperature of 1800°K for the combustion products of pure methyl nitrate vapor at 300°K. The compositions and flame velocities corresponding to mixtures with a temperature of 1600°K are given in Table 1.

The deviations from a mean value are small and of the sign to be expected if thermal conductivity was also a factor determining the flame velocity.

In a theory of flame propagation depending upon thermal activation, the relevant conductivity value approximates to that of the products of the reaction at the maximum flame temperature[4]. There is no information in the literature on the conductivities of poly-component mixtures at low or at high temperatures. However, the work of Hirschfelder and his coworkers[5] has made it a relatively simple matter to calculate the viscosity of pure gases at high temperatures. It seems probable that the Eucken equation will hold better at high than at low temperature, so that the thermal conductivity can be calculated from the viscosity by the relation:

$$\lambda = (C_v + 9R/4)\mu/m \qquad (8)$$

Although there is no adequate theory of the thermal conductivity of mixtures of polyatomic gases, some semi-empirical expressions based on simple kinetic theory exist, which give good results for binary mixtures at normal temperatures. They should be better approximations at high temperatures. The relation derived by Lindsay and Bromley[6] is the simplest to evaluate and it will be assumed to apply to poly-component mixtures. The necessary data were taken from Hirschfelder et al.[5] except that for formaldehyde for which values of the energy and molecular radius were estimated from the boiling point and the parachor respectively.

The calculated values of the thermal conductivities of the products are tabulated in Table 1 together with the values of $S/\lambda^{1/2}$. The latter are more nearly constant than the values of S, although the value for the mixture with helium is significantly low. This exception may be due to (1) inaccuracy of the calculated value of the conductivity (the method used is likely to be subject to a bigger error in the case of diluents of small molecular weight), (2) the effect of other transport properties not considered, such as mass diffusivity, varying with composition in a different degree to the conductivity, (3) the effect of helium on the influence of flame curvature on flame velocity described in an earlier section. A comparison of the flame traces for methyl nitrate diluted with equal amounts of argon and of helium shows that although no acceleration of the flame is measurable in the case of helium (as is the case for low flame velocities), the radius at which the flame velocity begins to decrease is greater than for the argon trace. This decrease in flame velocity is ascribed to the compression of the burned gases and should be identical for both diluents if the flame velocity is in both cases independent of flame curvature.

It appears that even at high flame velocities the addition of helium introduces a dependence of flame velocity on flame radius which could cause the measured values to be as much as 5 per cent low.

The values listed in Table 1 show that the flame velocities in mixtures with gaseous diluents at constant total pressure depend upon the flame

Table 1

Diluent	S	$\lambda \times 10^6$	$S/\lambda^{1/2} \times 10^{-2}$
moles/mole of ester	*cm/sec*	*cal/cm sec degree*	
1.045 A	610	283	362
1.045 He	720	437	344
0.675 N_2	645	313	364
0.420 CO_2	650	313	368

temperature (and to a small extent on the thermal conductivity in the flame) and are independent of the partial pressure of methyl nitrate vapor at a constant flame temperature. Thus the change in flame velocity on adding a diluent gas can be used to calculate the dependence of flame velocity on flame temperature.

On the assumption that the mechanism of flame propagation is the thermal activation of chemical reaction the temperature coefficient of the flame velocity should be related to that of the rate-controlling chemical reaction. The value of this latter quantity may be useful in identifying this reaction. The non-dependence of flame velocity on partial pressure of methyl nitrate shows that this reaction is second order with respect to the concentration of reactants. Numerous expressions have been derived for the flame velocity in the case of a second order reaction but the simplest is that due to Semenov[4].

$$S(k/\lambda c^2)^{1/2}(E/RT^2)^{3/2}(w_1^2 m_1 H_1^3/B)^{1/2} = \exp -(E/2RT) \qquad (9)$$

where λ and c are the thermal conductivity and heat capacity per unit weight for the products; $B \exp -(E/RT)$ is the rate of reaction in cc/mole-sec, m_1 the molecular weight, w_1 the weight fraction, H_1 the heat of reaction per unit weight of combustible and k is a numerical constant of the order of unity.

Although this relation is only accurate for large values of E/RT and a ratio of mass to thermal diffusivity equal to unity, it is adequate for the approximate calculation of B and E. Plotting the LHS as a logarithmic function of $1/T$ we should obtain a straight line with a slope of $-E/2R$. The value of B is calculated by inserting E/R into equation (9) and evaluating for the appropriate values of the other parameters.

The value of B is rather sensitive to the choice of the final combustion temperature. This has been calculated for the products of the reaction as determined by analysis. In a previous paper[3] the reaction was assumed to be simply:

$$CH_3ONO_2 \rightarrow NO + CO + H_2O + \tfrac{1}{2}H_2$$

It was thought that the small amounts of nitrogen and nitrous oxide found in the products of a constant volume explosion were the results of decomposition of nitric oxide in the products subsequent to the passage of the flame and during the period when they are heated to a much higher temperature by adiabatic compression. However, this cannot be true since the amount of nitric oxide reduced is the same when the experiment is carried out at constant pressure. The reduction must be the result of side reactions occurring within the combustion wave.

This increases the temperature by about 250°C over that of the simple reaction and the uncertainty in the flame temperature due to possible errors in analysis is of the order of ±50°C. Errors in the temperature resulting from errors in the estimation of other products are relatively small.

The derived rate constant is:

$$K = 10^{15} \exp(-22 \times 10^3/RT) \text{ cc/mole sec.}$$

in the flame temperature range, 1600–1800°K. The collision number is about normal for a second order process at high temperature. The activation energy is far too low for the rate-controlling reaction to be identified with the reaction:

$$CH_3ONO_2 \rightarrow CH_3O + NO_2 \qquad \Delta H \sim 35 \text{ kcal/mole.}$$

A reaction involving reduction of nitrogen dioxide, assuming this to be the primary product, seems more probable. The measured activation energies of this type of reaction vary between 19 and 25 kcal/mole at lower temperatures.

(3.2) FLAME PROPAGATION IN METHYL/ETHYL NITRATE MIXTURES

An examination of the curve relating flame velocity to the mole fractions of the two nitric esters and the amount of added diluent, Figure 2, shows that the slopes of the diluent curves increase as the mixture of nitric esters is made richer in ethyl nitrate. If it is assumed that these slopes vary approximately as $\bar{C}_3 A/\bar{H}$ as in the case of a single nitric ester, then either A increases or $\bar{H}$ (a mean value referred to one mole of ester) decreases. Assuming that the heats of reaction of the esters in a mixture are the same as those calculated from the products of each burning separately, the mean value will not decrease sufficiently to account for the change in slope and it appears that the temperature coefficient, A, must increase from methyl to ethyl nitrate.

When, as in Figure 4, the values of the flame speed are plotted against the calculated flame temperature, they lie fairly close to a single curve, irrespective of composition. However, the thermal conductivities of the products must vary considerably with composition and the flame speeds must be corrected for this. To get a rough correction it is assumed that the Prandtl number and the viscosity are constant, so that the flame speed can be corrected for the effect of thermal conductivity by dividing by the square root of the heat capacity per unit weight of the product. The exact calculations of thermal conductivity and viscosity for the products of mixtures of methyl nitrate and argon indicate this to be a fair approximation for this diluent. When this correction is made, Figure 4b, the result indicates that both the temperature coefficient and the flame speed are functions of the ratio of methyl to ethyl nitrate.

In order to discuss this result one needs to know the variation of flame speed with composition in a mixture of combustibles reacting at unequal rates. In the special case of two simultaneous reactions of dissimilar rates but with similar energies of activation the differential equations of flame propagation can be solved to give an analytical solution for the flame speed. The method of solution follows Boys and Corner[7]. A full account will be given elsewhere. Here it is sufficient to indicate that equation (9) will hold

to the same degree of approximation for a mixture containing two reactive components if the group $(w_1^2 m_1 H_1^3/B)^{1/2}$ is replaced by:

$$(w_1^2 m_1 H_1^3/B_1)^{1/2}$$

$$[1 + (m_2/m_1)^{1/3}(H_2/H_1)(B_1/B_2)^{1/3}(w_2/w_1)^{2/3}]^{3/2} \quad (10)$$

the suffixes 1 and 2 referring to the two combustible components. The other parameters in equation (9) are evaluated for the combustion products of the mixture.

The result is in the nature of a mixing rule for flame velocities. It should hold good so long as the rates of heat production by the pure components differ by not more than a few powers of ten (otherwise the substance reacting more slowly will act as an inert diluent).

If it is assumed that the modes of decomposition of ethyl and methyl nitrate are independent, so that the flame temperature and other properties of the combustion products of a mixture can be calculated from the reaction equations for the pure components, then one can calculate the apparent activation energy of the mixture from the argon dilution curves in the same way as for a pure compound. When this is done for the data in Figure 2 the activation energy does not remain approximately constant but increases threefold as the mixtures become richer in ethyl nitrate. Furthermore, the behavior of the undiluted nitric ester mixtures suggests that while at the lower end of the temperature range ethyl nitrate reacts more slowly than the methyl ester, at the high temperature end (corresponding to mixtures containing a small fraction of ethyl nitrate) it reacts faster than methyl nitrate.

Thus one or more of the initial assumptions must be incorrect. If the reactions can be assumed to be independent, then the energy of activation of the rate controlling reaction for ethyl nitrate is not similar to that for methyl nitrate but must considerably exceed it. A variation of the temperature independent factor in the reaction rate equation would not, by equation (10), account for the observed result. Since equation (9) modified according to equation (10) holds only if the activation energies are similar, the value obtained for ethyl nitrate by its application is not necessarily correct. It is not possible to obtain a simple solution to the problem involving unequal energies of activation but some numerical approximate solutions indicate that the apparent energy of activation of the rate-controlling reaction for ethyl nitrate is in the region of 70 kcal/mole. However, the equation derived for equal activation energies, (9) modified by (10), can be used to give a semi-empirical solution for the general case. It can be written in the simple form:

$$1/S^{2/3} = (w_1/S_1)^{2/3} + (w_2/S_2)^{2/3} \quad (11)$$

where S is the flame velocity in a mixture of two combustibles, the weight fractions being w_1 and

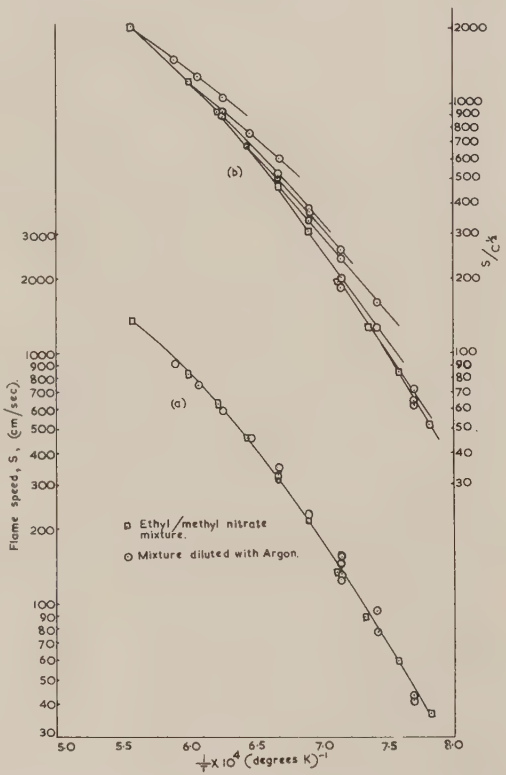

FIG. 4. (a) Flame speed in mixtures with inert gases as a function of flame temperature. (b) Ratio of flame speed to the square root of the heat capacity per unit weight of product gases as a function of flame temperature.

w_2. S_1 and S_2 are the flame velocities which the pure components would exhibit if their products had flame temperatures, heat capacities and thermal conductivities identical with those of the mixture. If it is assumed that equation (11) holds also for a mixture of two components with dissimilar activation energies then S_1 can be calculated from the equation:

$$S_1 = S_{1,0}(T_{1,0}/T)^3(c_{1,0}/c)^{3/2}[\exp(E_1/2RT)/\exp(E_1/2RT_{1,0})] \quad (12)$$

where the parameters with zero subscripts are calculated for the pure component and the others

for the mixture; S_2 can be calculated from a similar equation with activation energy E_2. For simplicity in deriving equation (12) it has been assumed that thermal conductivity is proportional to the heat capacity.

The data on ethyl nitrate/methyl nitrate mixtures in Figure 1 can be represented with a maximum error of about 5 per cent and that on mixtures with argon in Figure 2 with an error of about 10 per cent. The value of the activation energy used for ethyl nitrate was 73 kcal/mole. This figure requires an effective collision number of the order of 10^{26} cc/mole sec and implies a complex reaction scheme. It does not seem worth speculating on the significance of these figures until the ethyl nitrate system has been studied by more direct methods.

Acknowledgments

The authors are pleased to record the assistance of Mr. M. P. Osen in the experimental work reported in this paper and of Miss Shelia Bennett in the numerical calculations. This paper is published by permission of the Chief Scientist, British Ministry of Supply.

REFERENCES

1. Gray, P., and Yoffe, A. D.: J. Chem. Soc., 3180 (1950); 1412 (1951).
2. Fiock, E. F., and Marvin, C. F.: Chem. Rev., *21*, 380 (1937).
3. Adams, G. K., Stocks, G. W., and Wyatt, R. M. H.: Compte Rendu des Conference sur les problem de la combustion, la detonation, les ondes de choc. Memoire 14m/51, Laboratoire de Recherches Techniques de Saint Louis.
4. Semenov, N.: Progress of Physical Science (U.S.S.R.), *24*, 423, 1940, NACA Tech. Memo. No. 1026.
5. Hirschfelder, Curtiss, Bird, and Spotz: *The Propreties of Gases*, Mark II, Ch. 8. University of Wisconsin Naval Research Laboratory, 1952.
6. Lindsay, A. L., and Bromley L. A.: Ind. & Eng. Chem., *42*, 1508 (1950).
7. Boys, S. F., and Corner, J.: Proc. Roy. Soc., *A197*, 90 (1949); Corner, J.: Proc. Roy. Soc., *A198*, 388 (1949).

Discussion by F. Schultz-Grunow*

A dimensional analysis as shown at the last symposium would enable more general conclusions of these important results.

Discussion by Peter Gray

The authors are to be congratulated both on this ingenious approach to flame propagation problems in nitrate esters and on the realistic attitude that rate-controlling steps may more readily be derived from measured flame speeds than vice versa. The difficulty of ascribing a rate constant $k = 10^{15} \exp(-22000/RT)$ cc mole^{-1} sec^{-1} to an NO_2 oxidation seems to me to be the high pre-exponential factor; most known NO_2 oxidations have much lower values than 10^{15}.

* Technische Hochschule, Aachen, Germany.

74

THE IGNITION OF COMBUSTIBLE MIXTURES BY SHOCK WAVES

By M. STEINBERG and W. E. KASKAN

Introduction

Previously reported results on the ignition of combustible mixtures by shock waves have indicated that with shocks, ignition may take place at temperatures lower than those required by other means. Thus, Fay[1] has reported that a $2H_2 + O_2$ mixture was ignited by a shock that raised the temperature of the gas to only 400°K, whereas the temperature required for thermal ignition at the pressure behind this shock is 790°K[2]. Shepherd[3] reports similarly low ignition temperatures obtained by shocks. Berets, Greene, and Kistiakowsky[4], and Mooradian and Gordon[5] have investigated the ignition of combustible mixtures by shocks produced by detonations. In these cases the shocks, unlike those produced in a shock tube, are followed almost immediately by a rarefaction, so that their results are not entirely comparable with those of the first two authors. Even so, Berets, Greene, and Kistiakowsky[4] re-

port a minimum temperature for ignition of $6H_2 + O_2$ between 658°K and 867°K. According to Dixon and Crofts[6] the ignition temperature by adiabatic compression for this mixture is 860°K.

As Fay[1] has pointed out, anomalously low ignition temperatures by shocks might be ascribed to non-equilibrium conditions known to exist behind shocks[7]. Deviation from thermal equilibrium is generally most pronounced when associated with lag in vibrational equilibration. This would appear to be a possibility in the case of a hydrocarbon containing combustible mixture. For $2H_2 + O_2$, however, this explanation would be difficult since even at the reported ignition temperature of 400°K, neither molecule should be appreciably vibrationally excited. Furthermore, as Fay points out, there is not much reason to expect rotational lag to be important in this case either.

On the other hand there is reason to suspect that the reported results are not anomalous and are instead to be attributed to the existence of non-one-dimensional effects, such as are associated with the formation of the shock after diaphragm rupture[8] and with shock reflections at discontinuities on the walls of the shock tube.

In the work of both Fay[1] and Shepherd[3], the lowest ignition temperatures were observed when combustible mixture was placed next to a diaphragm which was burst. These temperatures, however, were computed from standard one-dimensional shock tube theory for the gases behind completely formed flat shocks. When by some means or another the combustible was removed from this location, higher ignition temperatures were observed. It has been shown that a plane shock is not formed immediately after rupture of the diaphragm[8]. Instead a rather complicated situation arises, with more than one shock or pressure wave, not necessarily flat or perpendicular to the tube axis, in evidence. Thus, if ignition occurs in the region near the bursting diaphragm, it does not appear possible at present to describe accurately the state of the gas in which the ignition has occurred.

The purpose of the work reported here was to try to establish conclusively whether shock ignition was in fact anomalous. For this purpose a shock tube was designed in a way such that it was reasonably certain that the shock waves which impinged on the combustible mixture were flat and normal to the tube axis. Only under these conditions can the state of the gas behind the shock be described with reasonable certainty.

Experimental

APPARATUS

The shock tube used in this work had a 2-in square inside cross section and consisted of three chambers, illustrated diagrammatically in Figure 1. The three chambers were the compression chamber CC (2 or 3.5 ft), the buffer chamber BC (2 ft), and the expansion chamber EC (4 ft). CC and BC were held together by a pair of toggle clamps which could be quickly opened and closed to provide for rapid changes of diaphragms. BC and EC were separated by a sliding shutter with a 2 in square hole in it so that when open it was continuous with the walls within about $\frac{1}{32}$ in, and when closed it separated the combustible gas in EC from an inert gas in BC. EC was closed by

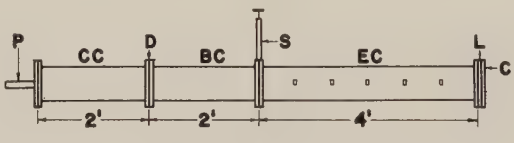

FIG. 1. Schematic diagram of shock tube. CC = compression chamber, BC = buffer chamber, EC = expansion chamber, P = plunger housing, D = diaphragm, S = shutter, L = Lucite window plate, C = window cover plate.

a flat Lucite plate supported by a steel plate with a hole in it so that observations could be made looking up the tube from the end.

BC and CC were of welded steel, $\frac{1}{2}$ in thick. CC was equipped with a solenoid actuated steel needle plunger for breaking diaphragms. EC was of bolted and pinned stainless steel construction and when assembled had a cross section which was $2.005 \pm .003$ in wide for the full length of the tube. The inside height of the section tapered uniformly from 2.050 to 2.035 in from one end to the other. It was rendered gas tight by appropriate gasketing. The inside surface of the chamber had a polished finish. EC was provided with five pairs of plate glass windows, 1 in square and $\frac{1}{2}$ in thick, equally spaced along the tube. The windows were mounted by clamping the glass in holes in the walls of EC so that they were flush with the inside surface of the shock tube wall and then filling the space between the glass and metal with an epoxy resin. When polymerized, this resin could be shaved off so that the entire window assembly was smooth to within about

0.005 in. However, after continued operation during which the tube was at reduced pressure much of the time, some of the windows tended to creep inward, necessitating an occasional remounting.

In assembly, EC, the shutter, and BC were bolted together permanently and were mounted on wheels so that they could be moved from CC as a group when changing diaphragms. The mismatch is surfaces at the shutter were as much as $\frac{1}{32}$ in. How difficulties caused by this mismatch were avoided will be described later.

The observed quantity in these studies was the shock velocity. Four schlieren activated photomultiplier tubes sensed the passage of the shock along the tube. A fifth photocell looked up the end of the tube so as to record ignition if it occurred any where in the tube. The output of the photocell furthest upstream was used to trigger the beam of a CRO, and the outputs of the other four photocells were tied together in parallel and fed, together with timing marks from a crystal controlled oscillator, into the Y axis of the CRO. The schlieren light beams were about 2 mm wide and traversed at an angle of about 3° from the normal. They were spaced at intervals of 254 mm and shock velocities were determined to within 2 per cent. There was no observable attenuation of shock velocity in the 500 mm of the tube under observation. When ignition occurred, the light emitted was sufficient to send the beam of the CRO off scale.

Each of the chambers of the shock tube required its own gas supply. Hydrogen was used as a driver gas and was fed directly into CC from a compressed gas bottle. BC was filled with an inert gas whose average molecular weight was the same and whose ratio of specific heats was nearly the same as that of the combustible gas. For the $2H_2 + O_2$ experiments the buffer gas was hydrogen and nitrogen in the proper proportions, and for the stoichiometric propane-air experiments the buffer gas was propane and nitrogen in the proper proportions. Buffer gas was prepared by filling a storage tank with the gases at the proper partial pressures and mixing by internal agitation. Explosive mixture was prepared continuously by metering the gases separately through critical flow orifices, and then mixing. The critical flow orifices were calibrated in place by a displacement technique. The gases were brought into the shock tube through $\frac{1}{4}$-in taps. The tap into BC was located 2 in down-stream of the diaphragm and the one into EC was 3 in downstream of the shutter.

PROCEDURE

The procedure adopted was designed to allow flat shocks, whose surface was normal to the tube axis, to propagate into the explosive mixture with a minimum of other disturbances. Diaphragm material (Dow Ethocell Sheet) which would withstand a little more than the required pressure difference was clamped into place and all three chambers evacuated. Due presumably to the evolution of water adsorbed on the metal walls, the pressure in the tube could not be reduced below about two mm. When the desired vacuum was reached CC was filled to a safe pressure somewhat below that to be employed and EC and BC were filled simultaneously to $\frac{3}{4}$ of the firing pressure with combustible and buffer gas respectively. The shutter was tight enough so that no appreciable leakage took place as long as the pressure difference across it was only a few cm of mercury. In order to avoid contamination due to leakage, the pressure in EC was maintained a little higher than in BC while filling the tube, and after filling the pressure was equilibrated by opening a valve which by-passed the shutter. During equilibration some combustible entered the buffer chamber, but since it was a relatively small amount and was diluted it caused no difficulty. After all valves were closed CC was filled to the firing pressure with driver gas. Then as quickly as possible the shutter was opened, buffer gas was admitted to BC to the desired pressure, valves closed and the diaphragm ruptured. On the average less than thirty seconds elapsed between the opening of the shutter, which allowed the buffer and combustible gases to meet, and the puncturing of the diaphragm. Calculation of the extent of diffusion to be expected in this time indicated that at distances of 6 in from the position of the interface between the gases the dilution of combustible with buffer should have been less than 1 per cent, negligible for our purposes. The procedure of adding the last quarter of the gas in the form of buffer gas pushed the original interface 12 in downstream of the shutter, thus tending to isolate the explosive mixture from the reflections which undoubtedly occurred in the vicinity of the shutter. Under these conditions the shocks did not encounter combustible mix until a distance

of about 6 in downstream of the diaphragm. Bleakney has found that shock fronts are usually well formed a few diameters downstream from the diaphragm[9].

In another expansion chamber of the same cross section, but having windows which allowed the entire height of the shock tube to be viewed, schlieren photographs of shock waves in air having velocities up to 1100 m/sec were found to be flat and perpendicular to the tube axis at a distance of 2 ft from the diaphragm.

As the shock passed the first schlieren station the CRO beam was triggered and the progress of the shock down the tube as seen on the CRO screen was recorded photographically. At the same time a visual observation of the shock tube was made since the light from the ignition could be easily seen. If ignition took place with a time delay such that it was not recorded on the CRO, the experiment was repeated with a longer sweep time.

Shock Properties

Properties of the gases behind the incident and reflected shocks in both stoichiometric hydrogen-oxygen and propane-air were calculated as a function of incident shock velocity for the initial temperature of $T_1 = 298°K$. The calculations were made according to steady state shock wave theory with the usual assumption that the perfect gas law was valid over the range of temperatures and pressures encountered, but without any simplifying assumptions as to the dependence of heat content on temperature. Instead, properties of the gases behind the incident and reflected shock waves were calculated exactly through the use of tabulated values of heat content as a function of temperature[10], thereby taking full account of heat capacity variations over the temperature range of interest. A tabulation of the shock wave properties for the propane-air system is given in Table 1 over the range of temperatures for which heat content-temperature data is available. In the Table, T_1 and p_1, T_2 and p_2, and T_3 and p_3 are the temperature and pressure of the test gas in front of the incident shock, behind the incident shock, and behind the reflected shock, respectively, D_1 and D_2 are the shock velocities of the incident and reflected shocks relative to the gases through which they travel, and w is the velocity of the gases behind the incident shock front relative to the laboratory coordinates.

Results

HYDROGEN-OXYGEN

Shock ignition studies were carried out on stoichiometric hydrogen-oxygen mixtures with initial pressures, p_1, in the test and buffer sections of approximately 200 and 300 mm Hg. With initial pressures of 100 mm Hg the schlieren outputs were so low compared to photo-cell noise, that it was difficult to trigger the CRO or measure velocities. To produce shock waves of varying strength in the test gas, diaphragms were ruptured at pressures up to 370 psia with hydrogen as the driver gas.

It was found that ignition phenomena were more reproducible behind shocks reflected from the end plate than behind incident shocks. Hence,

Table 1. Shock Waves in Stoichiometric Propane-Air Mixtures ($T_1 = 298°K$)

T_2	p_2/p_1	D_1	w	T_3	p_3/p_1	D_2
°K		m/sec	m/sec	°K		m/sec
400	2.72	534	271	508	6.53	576
500	4.87	703	461	713	17.3	771
600	7.19	849	611	914	31.5	937
700	9.65	979	740	1111	48.9	1079
800	12.22	1098	858	1308	68.4	1212
900	15.17	1208	968	1507	93.1	1331
1000	17.61	1312	1062			
1100	20.71	1410	1159			
1200	23.31	1506	1246			
1300	26.22	1595	1330			
1400	29.21	1680	1411			
1500	32.24	1763	1488			

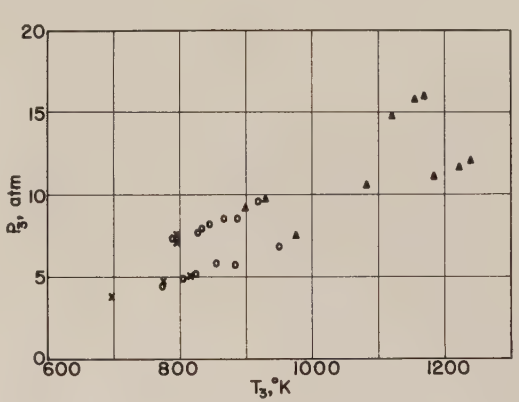

Fig. 2. Ignition of $2H_2 + O_2$ mixtures by reflected shock waves. p_3 and T_3 are temperature and pressure behind reflected shocks, X = no ignition, O = ignition after observable time delay, ▲ = ignition immediately after reflection.

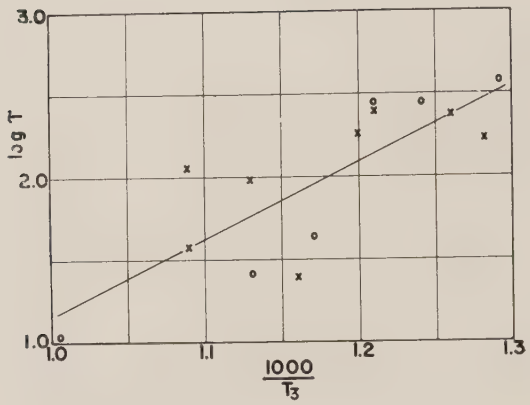

FIG. 3. Ignition delays in $2H_2 + O_2$ after reflection. τ in μsec; X, p_1 = 200 mm Hg; O, p_1 = 300 mm Hg.

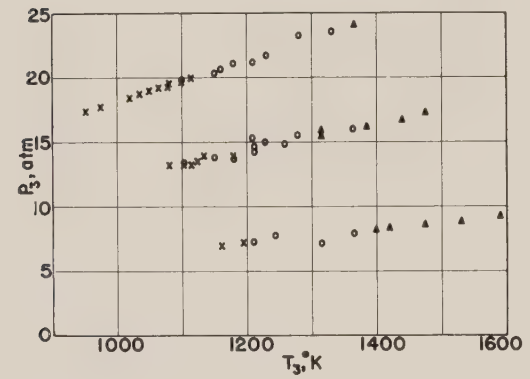

FIG. 4. Ignition of stoichiometric propane-air mixture by reflected shock waves. p_3 and T_3 are pressure and temperature behind reflected shocks, X = no ignition, O = ignition after observable time delay, ▲ = ignition immediately after reflection.

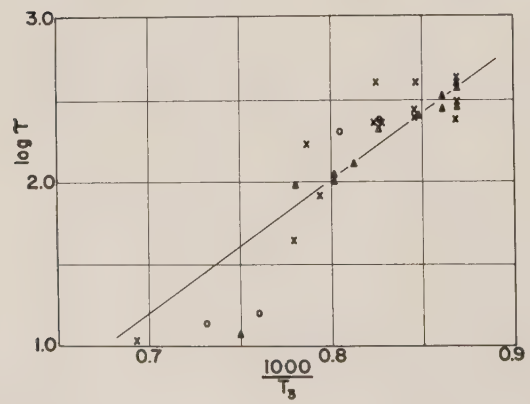

FIG. 5. Ignition delays for stoichiometric propane-air after reflection. τ in μsec; O, p_1 = 100 mm; X, p_1 = 200 mm; ▲, p_1 = 300 mm.

extensive data was collected only for ignition upon reflection from the end of the tube.

Data obtained for the hydrogen-oxygen mixtures are presented in Figure 2. The various points in the Figure indicate the conditions of temperature and pressure behind the reflected shocks, both calculated from incident shock velocities, for no ignition, ignition at some time after reflection from the end cover plate, and ignition at or very shortly after reflection. The lower and upper series of points are for mixtures initially at approximately 200 and 300 mm Hg, respectively. From Figure 2 it can be seen that the lowest temperatures at which ignition was observed behind the reflected shock wave was in the range of 775°K to 825°K. There appeared to be no pressure effect on the ignition limit over the range studied. One shock having a velocity of 1660 m/sec, which corresponds to T_2 = 815°K and p_2 = 2.90 for p_1 = 203 mm Hg, ignited the mixture about 50 μsec before the shock struck the end of the tube.

It is interesting to consider the time delays to ignition in those tests in which ignition occurred some time after reflection. Unlike the diffuse boundary between buffer gas and test gas, the boundary conditions at the end of the tube are well defined and the time delays for ignition can be related to the temperature, T_3, behind the reflected shocks. A plot of the logarithm of the ignition delay, τ (expressed in μsec), is given against the reciprocal of the reflected temperature, T_3, in Figure 3. In most cases ignition was quite abrupt and the time could be determined within about ten μsec. In some cases, however, ignition was not sharply defined but was noted by a gradual increase in light output detected by the photomultiplier which looked up the end of the tube. Such data were not used in the time delay tabulation. The observed ignition delays varied from essentially 0 to 380 μsec. The best straight line through the data when represented in the usual exponential form is

$$\tau = 3.4 \times 10^{-4} \exp (11000/T_3). \qquad (1)$$

An analysis of the positions of the shock front, contact surface, and rarefaction wave as a function of time in the system used (conventional x-t plot) indicated that the volume element of gas which first experiences the passage of the reflected shock may exist under the conditions (T_3, p_3) for as long as 350 to 400 μsec before a rarefaction makes its presence felt. This time is

approximately the longest ignition delay observed for the hydrogen-oxygen system. It is reasonable to expect that lower ignition temperatures might be observed if a longer test section were used which would allow longer induction times before the arrival of a rarefaction at the reflecting surface.

PROPANE-AIR

Studies were made at initial pressures of approximately 100, 200, and 300 mm Hg in the test gas. Ignition data are presented in the same manner as for the hydrogen-oxygen system in Figure 4. The three series of test points represent conditions resulting from the three initial pressure conditions. In order to investigate the effect of time allowed at the conditions of temperature and pressure T_3 and p_3, tests were made with compression chambers 2 ft and 3.5 ft long so as to vary the arrival time of the rarefaction wave at the reflecting surface.

Variations in the length of the compression chamber appeared to have little effect on the ignition properties of the system and, therefore, data obtained with the two compression chambers were not differentiated in the figure. Although the ignition limits are not too clearly defined in Figure 4, there appears to be a small dependence on pressure. The ignition limits are approximately 1200°K at 7 atm, 1150°K at 14 atm, and 1100°K at 20 atm.

The time delays for ignition after reflection in the propane-air systems are given as the logarithm of the time delay, τ, versus the reciprocal of the reflected temperature in Figure 5. The best straight line through the data expressed in the exponential form is

$$\tau = 2.8 \times 10^{-5} \exp (19000/T_3). \qquad (2)$$

The longest ignition delays which were observed were 470 μsec with the long compression chamber and about 350 μsec with the short chamber. The times are in accord with the values of about 600 and 300 μsec for the long and short chambers as calculated from the x-t plot.

Efforts to establish the shock strength required for ignition by the primary shock produced some peculiar behavior. Incident shocks through the propane-air mixtures at 100 mm Hg, which raised the temperature to about 1175°K to 1300°K at 2.6 to 3.3 atm, yielded CRO traces which had humps on them immediately after the shock front passed the schlieren velocity stations. These shocks would produce ignition in the usual fashion upon striking the reflecting end of the test section. This light emission zone closely followed the shock front, and its intensity was orders of magnitude less than that observed during the usual ignition. This emission was presumably due to chemical reaction. If this was the case, the heat release in the zone behind the shock front was insufficient to increase the velocity over what would be expected in the absence of any reaction. Further increase of shock strength did produce ignition before reflection at shock temperatures of 1290°K to 1320°K. Since the conditions under which the shock passes from buffer gas to the test gas are poorly defined, little can be said of the time delay for ignition in this case.

Discussion

The data reported here are best considered as evidence that shock ignition is a thermal process and that the anomalously low ignition temperatures previously reported must be attributed to some other phenomena. The evidence for the two fuel-oxidant systems will be considered separately below.

HYDROGEN-OXYGEN

The lowest ignition temperatures observed were approximately 800°K for final pressures of approximately 5 and 7.5 atm. These ignitions occurred under conditions where the gas mixture remained at the maximum temperature and pressure for only 300–400 μsec.

From the thermal explosion limit data for $2H_2 + O_2$, at pressures of 5 and 7.5 atm, the ignition temperatures are 760°K and 740°K, respectively[2]. This data can be considered as that for an essentially infinite time delay. From the trend shown in Figure 3 one might expect that if longer times were available for reaction the experimental ignition temperatures might be in closer accord with the thermal explosion data. Furthermore, our experimental error is at least as large as the small difference of 20°K between the ignition temperatures at 5 and 7.5 atm, so that it is not surprising that no pressure effect was detected.

For ignition by adiabatic compression, ignition temperatures of 820°K[11] and 800°K[6] for $2H_2 + O_2$ have been reported. These are in excellent agreement with our lowest ignition temperature, corresponding to the longest time delay.

The only other data on the ignition of $2H_2 + O_2$ by flat topped shock waves appears to be that of Fay[1]. In this work several ignition temperatures ranging from 400°K to 650°K were reported depending on the experimental arrangement. The lowest ignition temperature was observed when combustible gas was placed next to a diaphragm which was burst. From the observations reported it appears that ignition took place near the bursting diaphragm. As has been stated previously in this paper, it does not seem possible to accurately describe the state of the gas which is ignited in this case.

In some of our early experiments, ignitions were obtained with shock strengths considerably below those reported here. These were observed when the buffer-explosive interface was allowed to remain at the shutter, where there were discontinuities in the shock tube wall. Under these conditions there was also a considerable lack of reproducibility in results. With the adoption of the technique of displacing the explosive-buffer interface well downstream of these known surface irregularities, erratic ignition before reflection was eliminated, and considerably stronger shocks were required to initiate explosion.

The only explanation of this behavior seems to be that reflected waves from surface irregularities near the shutter were subjecting certain portions of the gas already heated by the initial shock to still higher temperatures and pressures, sufficient to cause ignition. The act of removing the gas interface from the source of disturbance should, according to shock tube experience, improve the situation with regard to the ability to accurately describe shock conditions.

Of the several set ups used by Fay[1], his arrangement D most closely resembled that described here. Arrangement D had a 3 ft compression chamber, 2 ft buffer chamber, and an expansion chamber presumably 6.25 ft long. It differed mainly in that the buffer-combustible interface was not moved downstream as in our case, but the tube was opened at this point for a short time so that probably some dilution with air took place in this region. With this arrangement Fay reported ignition temperatures of about 650°K for both initial and reflected shocks. Since Fay's initial pressure was 1 atm, the final pressures reached in his experiments at the limits of ignition were about 7.5 and 12 atm for the initial and reflected shocks respectively. For these two pressures, thermal ignition limits are 740°K and 720°K respectively, a difference negligible for our purposes.

The fact that the ignition temperatures observed with arrangement D were the highest Fay observed agrees with our experience concerning the necessity of avoiding extraneous disturbance. The longer shock tube used by Fay would be expected, in the light of our data on time delays, to allow him to observe somewhat lower ignition temperatures than have been reported here. This difference should be small, however, perhaps 30°K. The rather sizable discrepancy which remains between Fay's results and those reported here remains unexplained.

PROPANE-AIR

The data presented here on this system are in a region of higher temperature and shorter ignition delay than are generally available for hydrocarbon-air systems. Data on ignition delays of propane-air mixtures shorter than about 1 sec do not appear to be available. For heptane-air, at pressures of 9–20 atm ignition delay has been shown to decrease from about 1 sec to milliseconds with increase of temperature from 600°K to 750°K, in a manner described by an equation of the form of equation (2)[12]. From 750°K to almost 900°K the delay at 9 atm appears to increase whereas that at 15 and 20 atm remains about constant. Our data for propane-air indicate a rapidly decreasing time delay, from approximately 0.5 msec at 1150°K to essentially zero at 1300°K. Although these delays are order of magnitude what one could obtain by extrapolation of the heptane data, the temperature dependence is considerably stronger.

It is interesting to note that the time delays required for ignition at the reflected shock temperatures are in the same range of time and temperature that an element of gas is subjected to on passage through the zone of rising temperature ahead of the reaction zone in a flame front. Using a thermal model for flame propagation, Strickland-Constable has suggested that the temperature at which appreciable heat release begins in a flame front is dependent on the time-temperature history of the gases passing through the flame front and the ignition delay properties of the fuel-oxidant systems[13]. He proposed that the criterion for ignition be given by:

$$\int_{T_u}^{T_i} \frac{dt}{\tau} = 1 \qquad (3)$$

T_u and T_i are the initial unburned gas temperature and the "ignition temperature" in the flame front, respectively, t is the time and τ is the ignition delay time which can be expressed as a function of temperature. According to this expression during a time dt at a temperature T the system undergoes a fraction dt/τ of its total required ignition delay, and when the sum of these fractions become unity, ignition (i.e. heat release) occurs. Since our data for τ show very little pressure dependence they would seem to be directly applicable in equation 3.

Fristrom, et al. in a study of flame structure reported temperature profiles of some propane-air flames[14]. The time-temperature relation determined from Fristrom's curve for the region ahead of reaction zone in a near stoichiometric mixture ($\phi = 1.04$, see ref. 14) was substituted in Strickland-Constable's equation along with the expression for ignition delay given in equation (2). Equation 2 refers to a stoichiometric mixture but a few experiments with our shock tube have shown that ignition delays are insensitive to composition changes in this region of composition. By graphical integration it was found that a value of $T_i = 1550°K$ satisfied equation 3. The point at which the experimentally determined temperature profile indicated heat release due to reaction was about 1400°K. It is not intended here that these two figures should agree. Firstly, the uncertainty in the ignition delay data could introduce sizeable errors into the calculation of an "ignition temperature" in a flame front. Secondly, the Strickland-Constable criterion is based on a thermal model in which thermal conduction is the only mode of flame propagation. There is probably a contribution to the flame propagation from the diffusion of active radicals upstream from the reaction zone into the unreacted gases. In fact, Avery reported appreciable diffusion of combustion products back into preheat zone in the unburned gas[15]. Any contribution of diffusion to flame propagation would tend to make the so-called ignition temperature in a flame front lower than that calculated on the basis of Strickland-Constable's model. However, the relatively good agreement shown above suggests that this technique of determining these very short ignition delays in the range of temperatures at which appreciable reaction begins in a flame front may be of value in ascertaining the relative contributions of radical diffusion and thermal conduction to flame propagation.

Acknowledgment

In conclusion, the authors wish to acknowledge the aid of Mr. J. F. McDevitt, who assisted in the experimental work.

REFERENCES

1. Fay, J. A.: *Fourth Symposium (International) on Combustion*, p. 501. Baltimore, The Williams & Wilkins Co., 1953.
2. Lewis, B., and von Elbe, G.: *Combustion, Flames and Explosions*, p. 29. New York, The Academic Press, 1951.
3. Shepherd, W. C. F.: *Third Symposium on Combustion, Flame and Explosion Phenomena*, p. 301. Baltimore, The Williams & Wilkins Co., 1949.
4. Berets, D. J., Greene, E. F., and Kistiakowsky, G. B.: J. Am. Chem. Soc., *72*, 1080 (1950).
5. Mooradian, A. J., and Gordon, W. E.: J. Chem. Phys., *19*, 1166 (1951).
6. Dixon, H. B., and Crofts, J. M.: J. Chem. Soc., *105*, 2036 (1914).
7. Bethe, H. A., and Teller, E.: Deviations from Thermal Equilibrium in Shock Waves, Aberdeen Proving Ground X-117. Reprinted by the University of Michigan, Ann Arbor.
8. Geiger, F. W., and Mautz, C. W.: The Shock Tube as an Instrument for the Investigation of Transonic and Supersonic Flow Patterns, Engineering Research Institute, University of Michigan, Ann Arbor, 1949.
9. Bleakney, W., Weimer, D. K., and Fletcher, C. H.: Rev. Sci. Inst., *20*, 207 (1949).
10. American Petroleum Institute Research Project 44, Carnegie Institute of Technology, Pittsburgh, Pa., June 30, 1949, and Dec. 31, 1952.
11. Falk, K. G.: J. Am. Chem. Soc., *28*, 1517 (1906).
12. Scheuermeyer, M., and Steigerwald, H.: Motortech. Zeitschrift, Stuttgart, *8–9* (1943); cf. Ref. 2, p. 151.
13. Strickland-Constable, R. F. *Third Symposium on Combustion, Flame and Explosion Phenomena*, p. 229. Baltimore, The Williams & Wilkins Co., 1949.
14. Fristrom, R. M., Prescott, R., Neumann, R. K., and Avery, W. H.: *Fourth Symposium (International) on Combustion*, p. 267. Baltimore, The Williams & Wilkins Co., 1953.
15. Avery, W. H. *Fifth Symposium (International) on Combustion*, p. 86. New York, Reinhold Publishing Corp., (1955).

Discussion by J. A. Fay and W. J. Hooker*

We have recently repeated the earlier experiments on $2H_2$-O_2 ignition (Reported in the Fourth

* Cornell University, Ithaca, New York.

Combustion Symposium) with an apparatus similar to that of the authors, with substantially the same results as they have obtained, namely, an ignition temperature after reflection between 510 and 600°C. It was found that the low ignition temperatures previously reported were due to a gas dynamic effect produced by the existence of a small clearance volume at the reflecting end of the shock tube. A simple one-dimensional theory gave good quantitative correlation of tests involving the use of an artificial clearance space.

In the original shock tube, due to a slight eccentricity of the test chamber, there existed a clearance space about $\frac{1}{32}$ in wide and $\frac{1}{4}$ in deep along a portion of the circumference at the reflecting plate. It appeared possible that the stagnant gas behind the reflected shock wave could expand into this space, thereby generating a shock wave in this miniature shock tube. A simple one-dimensional calculation showed that an incident shock wave of Mach number 1.9 would generate a shock of Mach number 2.25 in the narrower channel, the latter being sufficiently strong to produce the normal ignition temperature upon reflection.

Upon eliminating the clearance space, the shock ignition temperature was found to be not substantially different from that measured by the adiabatic compression method.

To demonstrate more clearly this effect, a hole $\frac{1}{16}$ in in diameter and $\frac{1}{4}$ in deep was drilled in the center of the end plate. The Mach number of the incident shock wave which produced ignition was the same as that of the early experiments, and the ignition temperature calculated on the basis of the shock wave generated in the small hole was between 530 and 580°C.

Since there are thus no anomalous effects, there seems little doubt that, with sufficient attention given to refinements of construction, the shock tube would be very useful in ignition studies in the range of ignition delays of the order of several milliseconds or less.

The research referred to above was supported in part by the United States Air Force through the Office of Scientific Research of the Air Research and Development Command.

75

THE STRUCTURE OF THE REACTION ZONE IN A DETONATING EXPLOSIVE

By S. PATERSON

(1) Introduction

When a column of explosive detonates, a wave of reaction passes through it at high and in general steady speed. According to the accepted view, this wave consists of (1) a leading *shock* or region of extremely rapid pressure rise, (2) a *steady zone*, in which conditions though not constant in space remain unaltered in time from the standpoint of an observer accompanying the wave, and (3) a non-steady *wake*, where gradients of temperature, pressure, etc., become continually less steep.

In Figure 1, X_s is part of the section of the shock front at any instant. The region to the right of X_s is occupied by undetonated explosive which flows into the wave-front with constant velocity D. We shall use the subscript 0 to indicate conditions in this region. X_sX_1 is the steady zone: the unqualified symbols p, T, etc., denote values at an arbitrary section X in X_sX_1. Conditions at the rear surface of X_s itself are distinguished by a subscript s and those at X_1 by subscript 1. Beyond X_1, the motion is non-steady.

In the undetonated explosive, reaction is restrained by the low temperature and substantial activation energy, until arrival of the shock front X_s. The abrupt compression at X_s initiates rapid reaction, which proceeds through a series of non-equilibrium states until equilibrium is reached in a plane Y, say, some distance behind X_s. We call X_sY the *reaction zone*. Beyond Y the material is in thermodynamic equilibrium. Of course, if the reaction is of first or higher order, equilibrium will not theoretically be established within any definite time. However, the state of the products will approach closely to equilibrium in a rather well-defined time, and the corresponding distance X_sY may be regarded as the effective reaction zone thickness. In any event, X_sY must greatly exceed the shock front thickness, within which no significant chemical change will take place[1, 2].

In general, the steady zone must fall entirely within the reaction zone, since a non-reactive rarefaction cannot be steady. There is no guaran-

tee that reaction is complete within the steady zone; and, in fact, it will probably not be so when lateral confinement is imperfect[2, 3, 4]. However, it appears that in a steady plane wave Y normally coincides with X_1, so that the reaction and steady zones also coincide. The detonation wave as a whole then consists of (1) a non-reactive shock X_s followed by (2) a steady region X_sX_1 in which the material reacts and therefore passes through non-equilibrium states, and finally (3) a non-steady region beyond X_1 comprising equilibrium states. In (2) the conservation laws apply in integral form, but the material does not follow a single adiabatic; in (3) the flow is adiabatic, but the differential equations of motion must be used.

The following analysis of the steady zone is that of Zeldovich[3], Neumann[5], and Döring[1]. If p, v, W, E are the pressure, specific volume, streaming velocity and internal energy per unit mass at any section in X_sX_1, and p_0, etc., the corresponding quantities in the undetonated explosive, while D is the steady wave speed, conservation of mass, momentum and energy implies

$$D = v_0\sqrt{(p - p_0)/(v_0 - v)} \qquad (1)$$

$$W = \sqrt{(p - p_0)(v_0 - v)} \qquad (2)$$

$$E - E_0 = \tfrac{1}{2}(p + p_0)(v_0 - v) \qquad (3)$$

If p, v, W, E are given the suffix 1, these equations apply at the section X_1. By use of the equilibrium conditions, equation (3) can be reduced to an equation in p_1 and v_1 alone, defining a curve in the (v, p)-plane. This equilibrium Rankine-Hugoniot curve is of the shape shown at CIG in Figure 2. Its elementary properties have been fully discussed by various writers[6, 7, 8], who conclude that in a stable wave, the state at X_1 corresponds to the point of contact I of the upward tangent from A. At this point,

$$a_1 + W_1 = D \qquad (4)$$

where a_1 denotes the velocity of sound.

With suffix s, equation (3) defines a Rankine-Hugoniot curve on which (v_s, p_s) must lie. Since the shock is non-reactive, this curve, represented by LNA in Figure 2, passes through A, and may in general be assumed to lie entirely below the equilibrium curve CIG. Now, if I defines the state (v_1, p_1) at X_1, it is clear from equation (1) that every intermediate state (v, p) including (v_s, p_s) must lie on AIL. The state-point is thus carried discontinuously from A to L in the leading shock, and thereafter subsides along LI to I as reaction proceeds. Assume that the chemical composition at any stage during reaction can be defined by a single parameter Z. This will be the case if the process involves only one elementary reaction, or alternatively if all other parallel reactions proceed at a speed relatively much faster, so that they reach effective equilibrium at each stage of the process. The state-variables, including those defining the composition, can then be expressed in terms of v, p and Z, and the RH-equation determines a one-parameter family of curves with parameter Z. If Z represents the fraction of an initial reactant decomposed, then the RH-curve $Z = 0$ coincides with LNA. If we further assume that the concentration of this reactant is negligibly small in any practicable equilibrium state, the curve $Z = 1$ coincides with CIG. Between these two extreme curves will lie

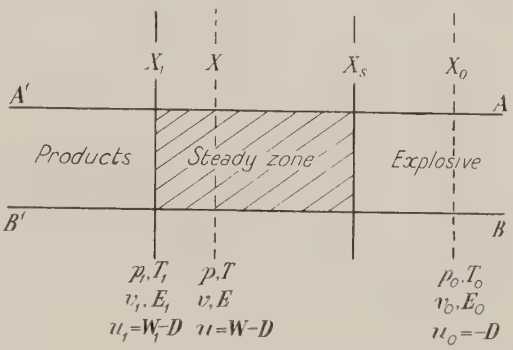

FIG. 1. Sectional diagram of the steady plane detonation wave from the standpoint of an observer accompanying the wave.

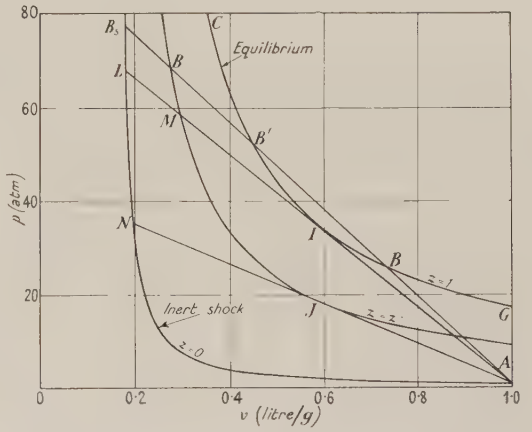

FIG. 2. Extended RH-diagram for detonation. The numerical values apply to an explosive for which $\triangle = 1$ g/litre, $p_0 = 1$ atm, $T_0 = 300°$K, $Q_1 = 1000$ cal/g, $\gamma = 1.4$ and $c_1 = 0.33$ cal/g. B^*MJ corresponds to $Z^* = \frac{1}{2}$.

the rest of the RH-family, corresponding to values of Z between 0 and 1.

By means of such constructions, the authors cited have shown that in a well-confined cartridge steady waves cannot normally arise with velocities smaller than that corresponding to AIL, and at the same time have confirmed that the end of the steady zone must coincide with the plane in which chemical equilibrium is established. The discussion is rather idealized. However, it is not unreasonable to assume that the reaction rate in a condensed explosive is determined principally by the initial decomposition of the explosive molecule, and in many cases even by a heterogeneous process confined to the surface of grains (see Sections 3, 6 below), and that the subsequent reorganization of the gaseous decomposition products is achieved at a much more rapid rate. Again, the assumption that the RH-family do not intersect or have an envelope is probably well justified in practice.

The general nature of the variation in pressure, density, etc., throughout the steady zone is made clear by Figure 2. Pressure, density, streaming velocity and temperature increase abruptly in the leading non-reactive shock. During the subsequent reaction, the pressure and density decrease again towards p_1 and $\rho_1 \equiv 1/v_1$. The flow velocity W by equations (1) and (2) satisfies

$$DW = v_0(p - p_0) \tag{5}$$

and must therefore also decrease. The temperature, on the other hand, is determined, at least for a homogeneous explosive of low or moderate density, principally by release of chemical energy, and should therefore continue to rise beyond T_s as reaction proceeds. As we shall see, this may not apply in high density or granular explosives.

(2) Ideal Gaseous Explosives

On the same assumption as before, that the composition is determined by one parameter Z only in addition to v and p, Döring[1] has found the distribution of pressure, etc., through the steady zone in terms of this parameter for an ideal gaseous explosive, whose products are constant along $Z = 1$, and have a constant ratio of specific heats γ throughout the (v, p) plane. In fact, ZQ_1 $(0 \leq Z \leq 1)$ denotes the chemical energy released at any stage, the RH-equation is $(p \gg p_0)$

$$pv/(\gamma - 1) = ZQ_1 + \tfrac{1}{2}p(v_0 - v) \tag{6}$$

and the following relations are easily deduced

$$v/v_1 = (\gamma - f)/\gamma \tag{7}$$

$$p/p_1 = W/W_1 = 1 + f \tag{8}$$

$$(a/a_1)^2 = T/T_1 = (\gamma - f)(1 + f)/\gamma \tag{9}$$

where $f^2 \equiv 1 - Z$. The pressure and flow velocity are therefore just twice as high in the shock-front as at the CJ-plane. The temperature is perhaps one-third as high. The density falls by a ratio of six to one from X_s to X_1 if $\gamma = 1.2$.

If we make some plausible assumption regarding the reaction rate, we can complete the solution by evaluating Z as a function of time or distance. For example, a bimolecular reaction can be represented by

$$d\mu/dt = -B\mu^2\sqrt{T}\, e^{-A/RT} \tag{10}$$

where B is a constant factor, A is the activation energy per mole and

$$\mu \equiv (1 - Z)/v \equiv f^2/v \tag{11}$$

Equations (7), (9) and (11) then allow (10) to be reduced to

$$X\, dt = -\frac{2\gamma - f}{f^3\sqrt{\{(\gamma - f)(1 + f)\}}}\, e^{Y/(\gamma - f)(1+f)}\, df \tag{12}$$

where $X \equiv B\rho_1\sqrt{\gamma T_1}$ and $Y \equiv A\gamma/RT_1$. This provides the history of reaction in any chosen element of gas. The space-distribution at any instant is obtained from

$$\frac{df}{dx} = \frac{df}{dt}\bigg| (D - W) \tag{13}$$

x being a space-co-ordinate measured from the shock-front towards the reaction products. Consequently,

$$\frac{X}{W_1}\, dx = (\gamma - f)\left(X\frac{dt}{df}\right) df \tag{14}$$

Plausible numerical values are $A = 35{,}000$ cal/mol, $T_1 = 3500°\text{K}$, $\gamma = 1.2$, whereupon $Y = 6$. The results of integrating equations (12) and (14) with these values are shown in Figures 3 and 4. They should be regarded merely as illustrations of the theory. The presence of an appreciable induction time is a consequence of the particular values of γ, A and T_1 used. In the case examined, if $X \sim 10^{11}\ \text{sec}^{-1}$, the reaction time is of the order of a μsec, and the reaction zone thickness is a few tenths of a millimeter.

(3) Granular Explosives

Analysis of the reaction zone structure for a condensed explosive presents much greater difficulties. Even if we simplify the problem by assuming perfect homogeneity at every stage, it is a formidable task to supply an equation of state which will describe the reacting material as it passes continuously from the original liquid or solid explosive to the appropriate equilibrium products. Equations parallel to (7), (8) and (9) can indeed be deduced[2] on the basis of the Abel equation of state

$$p(v - \alpha) = nRT \qquad (15)$$

with constant covolume α, and the resultant wave structure is, broadly speaking, very similar to that for ideal gases. However, most condensed explosives have a granular structure, and the marked effects of grain size upon the behavior of the detonation wave make it appear probable that reaction frequently consists in surface burning of the grains[2, 9, 10, 11, 12]. Even apparently homogeneous liquids like nitroglycerine may decompose heterogeneously from reaction nuclei provided by minute discontinuities of one kind or another, for example gas bubbles[2]. In such cases, the partially reacted material will consist of solid or liquid fragments burning in a gaseous atmosphere which is constantly augmented by the products of their decomposition. The temperatures of the two phases at any stage will certainly differ, and it is not even certain that they share the same translational velocity. Compression of the unreacted particles also requires to be taken into account. Under such circumstances, the assumption of a homogeneous process is evidently a poor approximation.

We shall rather assume that, at any intermediate stage in the reaction of a typical element of explosive, part of the element has been transformed into gaseous products in effective chemical equilibrium, while the remainder is still in its original condensed state. It will further be assumed that this unreacted portion has not been significantly heated by thermal diffusion from the hot gases[2]. This is consistent with earlier studies on mixtures of explosive and inert material[10, 13]. Finally, in keeping with the asumptions made at the CJ-plane, we shall regard the condensed and gaseous phases in any cross-section as sharing a common velocity W, so that conservation of mass momentum and energy may be expressed by the usual equations (1), (2) and (3).

When a fraction Z of the explosive has reacted, a fraction $m = m_0 + Z(1 - m_0)$ by mass is gaseous, where m_0 is the mass of gas (air) present in unit mass of the undetonated materal. Except when Z is very small, m is indistinguishable from Z, but the use of m allows the equations to be applied up to the shock-front. We also assume,

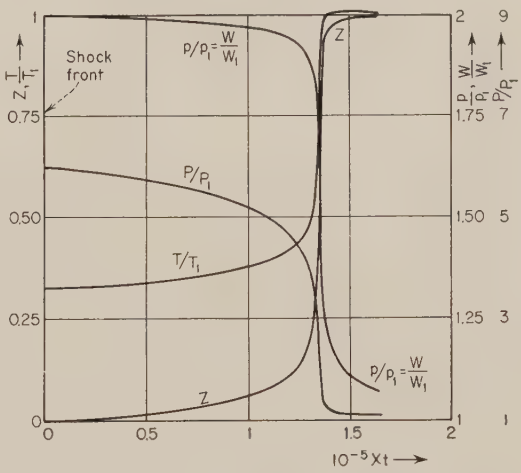

FIG. 3. Timewise reaction zone profiles for an ideal gaseous explosive with $A = 35{,}000$ cal/mole $T_1 = 3{,}500°K$, $\gamma = 1.2$.

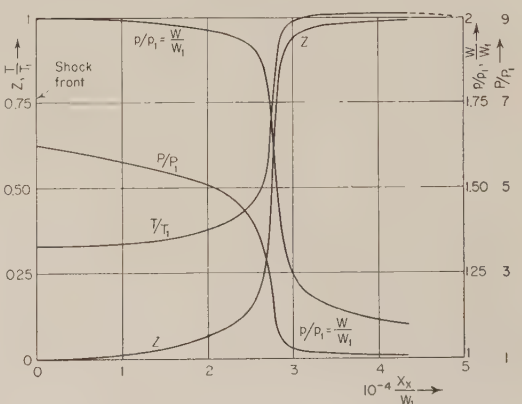

FIG. 4. Spacewise reaction zone profiles for the explosive of Fig. 3.

for simplicity, that the composition of the reacted phase is independent of Z: this will not, of course, in general be true, but the simplification should not seriously affect the results. Then, if accented symbols refer to properties of the gas phase, reckoned per unit mass of that phase, and ϵ, φ are the internal energy and specific volume of the condensed phase, the RH-family is

$$m(E' - E'_{\mathrm{NTP}}) + (1 - m)(\epsilon - \epsilon_{\mathrm{NTP}}) = ZQ_1 + \tfrac{1}{2}(p + p_0)(v_0 - v) \qquad (16)$$

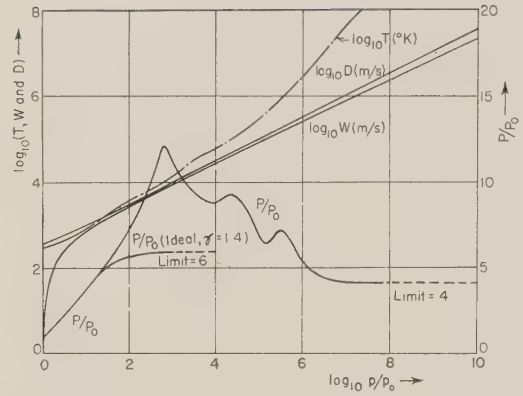

FIG. 5. Shock wave properties of air: $p_0 = 1$ atm, $T_0 = 273°K$.

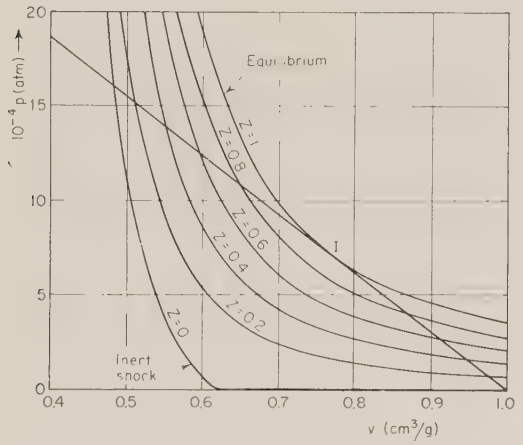

FIG. 6. Family of RH-curves for PETN cartridged at 1.0 g/cm³.

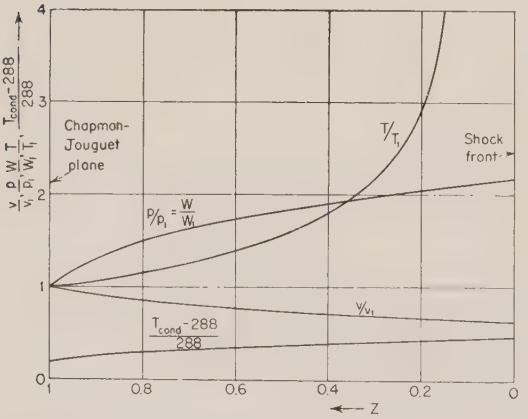

FIG. 7. Reaction zone structure for PETN cartridged at 1.0 g/cm³.

If we now regard the unreacted material as having traversed a simple shock from p_0 to p, then

$$\epsilon - \epsilon_{NTP} = \tfrac{1}{2}(p + p_0)(\varphi_0 - \varphi) \tag{17}$$

In view of the small compressibility of liquids and solids, and the assumption of negligible heat transfer, this term will in any case be a minor one, except perhaps at small Z, and the above rough formulation simplifies equation (16), which with the relations

$$v_0 = m_0 v_0' + (1 - m_0)\varphi_0 \tag{18}$$

$$v = mv' + (1 - m)\varphi \tag{19}$$

becomes

$$m(E' - E'_{NTP}) = ZQ_1 + \tfrac{1}{2}(p + p_0)[m_0 v_0' - mv' + (m - m_0)\varphi_0] \tag{20}$$

By means of the equations of state for the gas phase, equation (20) can now be expressed in terms of p and v', whereupon the intermediate RH-equation relating p, v follows from equation (19) provided $\varphi(p)$ is known.

Equation (20) can be simplified when $Z = 0$ or when m is not small. In the former case, which corresponds to conditions immediately behind the leading non-reactive shock, we set $m = m_0$, whereupon

$$E_s' - E'_{NTP} = \tfrac{1}{2}(p_s + p_0)(v_0' - v_s') \tag{21}$$

This is identical with the RH-equation for shocks in the gas (air) originally present. If this gas behaves ideally, with constant specific heat ratio γ, then equation (21) becomes[14, 15]

$$v_s'/v_0' = \frac{p_s/p_0 + \lambda}{\lambda p_s/p_0 + 1} \tag{22}$$

where $\lambda \equiv (\gamma + 1)/(\gamma - 1)$. When $p_s/p_0 \gg 1$, (22) reduces to

$$v_s' = v_0'/\lambda \tag{23}$$

According to the present assumptions, therefore, the gas pockets suffer only a moderate compression in the shock-front, and must therefore reach extremely high temperatures.

Again, when m is not very small, $m \doteq Z$, and m_0/m is negligible, whence

$$E' - E'_{NTP} = Q_1 + \frac{1}{2Z}(p + p_0)[v_0 - \varphi_0 - Z(v' - \varphi_0)] \tag{24}$$

In particular, when $Z = 1$ and so $v' = v_1$, this becomes

$$E_1 - (E_1)_{NTP} = Q_1 + \tfrac{1}{2}(p_1 + p_0)(v_0 - v_1), \quad (25)$$

which is the usual RH-equation for equilibrium.

When the RH-family of curves has been drawn by means of equations (21) and (24), the pressure, density and streaming velocity are obtained as functions of Z by intersecting the family with the tangent to the final curve $Z = 1$. The gas phase temperature is determined from p, v' and the equation of state. The temperature reached by shock-wave compression, according to equation (17), in the partially reacted explosive particles can be estimated from p, if an equation of state is assumed for the condensed explosive material.

(4) Application to PETN

The above analysis has been applied to PETN (pentaerythritol tetranitrate, $C_5H_8(NO_3)_4$). The equation of state used for the gaseous phase in the reacting material was one due to Hirschfelder, Stevenson and Eyring[16], and applied in previous work[13, 17], namely

$$pv' = n' RT\sigma(b/v'), \quad (26)$$

where n' is the number of gaseous moles per g of gas, and

$$\sigma(x) \equiv 1 + x + 0.625x^2 + 0.287x^3 + 0.193x^4 \quad (27)$$

$b = \Sigma n_i B_i$ was compounded linearly from the high temperature second virial coefficients B_i of the various gaseous species present.

$E' - E'_{NTP}$ could then be represented for PETN products between 2000 and 6000°K by

$$E' = E'_{273} = 0.371\ T - 279 \text{ cal/g} \quad (28)$$

The RH(v', p)-equation was then obtained from equation (24) with $Q_1 = 1412$ cal/g and $\varphi_0 = 0.565$ cm³/g; and the RH(v, p)-equation deduced from equation (19). To estimate φ, the compression as regarded as isothermal and in the absence of relevant data PETN was assumed to compress like NaCl. This approximation is, of course, crude, but it probably introduces only minor errors.

The RH-curves were drawn for $Z = 0.2$, 0.4, 0.6, 0.8, 1.0 at each of three loading densities 0.5 0.75 and 1.0 g/cm³. To complete each family it was still necessary to trace the curve $Z = 0$, defined by equation (21), or by equation (22) if the gas (air) originally present could be taken as ideal. However, the temperatures in the air pockets at the shock front turned out to be so extreme that the ideal gas equation was quite inadequate, and account had even to be taken of dissociation and ionization. Fortunately, shock wave characteristics for air up to very high pressures and temperatures have been published by several independent workers[6, 18, 19, 20, 21]. There is remarkably close general agreement between these, and a mean (p, ρ)-curve can be drawn which is probably close to the truth over the entire range. This is shown in Figure 5, together with the corresponding (p, T)-, (p, W)- and (p, D)-curves. The RH-curve $Z = 0$ may then be drawn with the aid of equation (18). The entire family for a loading density of 1.0 g/cm³ is shown for illustration in Figure 6, and the corresponding variation

Table 1. Reaction Zone Structure in PETN at 0.5, 0.75, 1.0 g/cm³

	v/v_1				$p/p_1 = W/W_1$				T/T_1				$T_{cond.} - 288(°)$		
C \ Δ	0.5	0.75	1.0	*	0.5	0.75	1.0	*	0.5	0.75	1.0	*	0.5	0.75	1.0
0	0.48	0.58	0.63	0.67	2.13	2.10	2.18	2	34.6	61.6	110.7	1.333	56	135	332
0.2	0.52	0.61	0.66	0.70	2.01	1.98	2.06	1.90	2.69	2.87	2.90	1.33	51	125	307
0.4	0.59	0.66	0.71	0.74	1.88	1.84	1.91	1.78	1.70	1.74	1.80	1.32	46	112	266
0.6	0.66	0.73	0.77	0.79	1.71	1.67	1.73	1.63	1.35	1.36	1.40	1.29	42	98	232
0.8	0.76	0.83	0.84	0.85	1.48	1.45	1.50	1.45	1.12	1.15	1.15	1.23	34	82	190
1.0	1.00	1.00	1.00	1.00	1.00	1.00	1.00	1.00	1.00	1.00	1.00	1.00	(23)	(50)	(105)

* Calculated from equations (7), (8), and (9) with $\gamma = 3$. The CJ-values are as follows:

Δ	0.5	0.75	1.0 g/cm³
v_1	1.36	0.97	0.76 cm³/g
p_1	21,300	41,900	73,800 atm
T_1	5,000	5,060	5,150 °K
W_1	1,175	1,240	1,340 m/s

of p, v, etc., with Z in Figure 7. The other loading densities give similar curves. Numerical values are collected in Table 1. For comparison, the Table also includes values calculated from equations (7), (8) and (9) with $\gamma = 3$, an order of value for the adiabatic index—$(d \log p/d \log v)_s$ suggested by various workers[22, 23, 24, 25]. It can be seen that the behavior of v, p and W at the higher loading densities approaches that of the idealized homogeneous material with $\gamma = 3$. The temperature in the gas phase, however, behaves in quite a different manner, falling continuously from a very high level in the shock-front to the equilibrium value T_1 at the CJ-plane. In fact, according to the present theory, the gaseous temperature is determined principally by compression and only to a minor extent and in the rear of the reaction zone by release of chemical energy.

(5) Discussion

The enormous shock-front air pocket temperatures shown in Table 2 must naturally be treated with reserve. In formulating the present theory we have taken account of the heterogeneous nature of the explosive only in one sense. From a hydrodynamic point of view the material is treated as homogeneous, although with the equation of state prescribed by its actual heterogeneous structure. Thus in the first place, the finite size of the elementary unit of each phase—the solid particle or gas pocket—is disregarded: the equations cannot, therefore, be expected to give a reliable description of events which take place within distances of the order of the grain size. However, such experimental estimates as have been made of the reaction zone length suggest an order of magnitude many times greater than the grain diameter. More serious objection may perhaps be raised to the fact that we have assumed both phases to share a common velocity at each stage. A treatment by Eyring and coworkers[2] is indeed based on just the opposite assumption. In this theory, the solid fragments remain at rest and only the products of their surface reaction are entrained by the wave. The extremely high shock-front air pocket temperatures shown in Table 2 are a direct consequence of our assumption regarding entrainment, and the values derived by Eyring et al.[2] are very much lower, though still somewhat above the CJ-level.

No doubt, the truth may lie somewhere between these two extremes. However, there seems, in fact, no reason to doubt that the picture which we have presented above is qualitatively correct. In particular there are good grounds for believing that exceedingly high temperatures will arise in the air pockets. Thus, both theory and experi-

Table 2. Conditions at the Shock-Front (Suffix s) and at the CJ-Plane (Suffix 1) in PETN

Δ	0.50	0.75	1.00	1.25	1.50
g/cm^3					
D (m/s)	3,670	4,520	5,560	6,800	8,150
T_s (°K)	173,000	312,000	570,000	850,000	1,160,000
$(T_{cond.})_s$ (°K)	344	423	620	1,070	1,935
T_c (°K)	16,900	27,800	41,700	82,200	120,000
T_1 (°K)	5,000	5,060	5,150	5,220	5,340
p_s (atm)	45,400	88,000	160,900	275,000	427,000
p_1 (atm)	21,300	41,900	73,800	121,000	188,000
W_s (m/s)	2,500	2,600	2,920	3,250	3,520
W_1 (m/s)	1,175	1,240	1,340	1,430	1,550

Conditions in the shock-front have also been calculated for 1.25 and 1.5 g/cm³. Table 2 summarizes the shock-front variables over the range of density considered and shows how they compare with the CJ-values.

An estimate of the temperatures produced by compression in the condensed phase can be made by following the line of thought which led to equation (17). The temperature of the explosive fragments at any section where the pressure is p will then be the shock temperature corresponding to p. Of course, we do not have requisite physical data for PETN to enable such temperatures to be properly calculated. However, they have been roughly assessed by comparison with values already derived for NaCl, and are included in Tables 1 and 2. They cannot be expected to have more than a qualitative significance, but they certainly suggest only a slight compressive heating, except at the highest loading densities.

ment agree in attributing temperatures of the order of 30,000°K to the luminous air waves produced beyond the end of a detonating cartridge[26, 27, 28, 29]. It is difficult to avoid the conclusion that air pockets, in which repeated reflexions must occur, will reach considerably higher temperatures. This in turn suggests that when a granular explosive is detonated under water (to eliminate external luminous shocks) a significant part of the light emitted may arise from compression of the internal air pockets. Experiments which were designed to test this view and which provide considerable support for it have been described elsewhere[30]. In these experiments zebra charges consisting of alternate layers of common salt and a smooth-textured plastic explosive were fired in water in front of a wave-speed camera. Practically no light was recorded from the reaction wave in the plastic explosive; but intense light was emitted by the salt layers. When air pockets were artificially introduced into the explosive it became luminous on detonation. *Granular* explosives, themselves less powerful than the plastic, emitted copious light. Further confirmatory experiments have been made more recently by Cumming[31]. It was found that evacuation of a granular cartridge reduced the detonation luminosity; a similar effect was produced by replacing the air with butane, a gas of high specific heat, while replacement with argon (low specific heat) enhanced the luminosity. Flooding a common salt target with glycerine reduced the light emitted by the target to a very low level.

It would appear from this evidence that, when atmospheric effects are eliminated, the light emitted by a granular detonating explosive is largely due to compression of the air pockets between the solid particles. This supports the present theory, and also suggests that the duration of luminosity is an unreliable index of reaction time.

(6) The Mechanism of Propagation

As already indicated in Section 3, the view is commonly held, with regard at least to granular explosives, that reaction is initiated by some means on the surface of the explosive grains and thereafter spreads inward at a rate determined by temperature and pressure. In detail, the process then resembles the burning of a propellant, although from a large-scale viewpoint this process must be regarded as taking place within some such wave-structure as has been described above.

With regard to the precise means whereby the explosive grain is initiated, Eyring et al.[2] quote evidence for the view that reaction commences at hot-spots produced by compression or grinding at the points of contact between grains. On this theory, the reaction time will depend, not only on the average grain size, but also on the efficiency of initiation of each grain, as represented by the number of contact points. Such a variation of reaction time with efficiency of initiation may be postulated in general, whether the mechanism depends on contact effects or not. For example, the two alternative velocities observed with gelatinous explosives based on nitroglycerine and recently also with hydrogen peroxide-fuel mixtures and granular explosives can be explained if we assume that reaction may be initiated in two different ways, one of which requires a higher energy input than the other but leads to a more rapid reaction. Thus, let us suppose that in a detonation wave of low velocity and therefore also low shock pressure, initiation of each explosive element takes place on its surface, either by friction and impact, or by thermal conduction from pockets of gas heated in the leading shock. The reaction is then heterogeneous, and proceeds at a relatively low rate determined largely by the process of heat diffusion into the explosive element. In moderate cartridge diameter, therefore, we may expect only part of the heat of reaction to be set free in advance of the CJ-plane, and the detonation velocity to be locked at a low level. As the cartridge diameter is increased, this low velocity may be expected to rise and, in the absence of any alternative mechanism of initiation, should continue to do so in a smooth manner until the full hydrodynamic velocity is almost attained. However, we can presume that small shock waves will pass through the individual grains of explosive and that the intensity of these microshocks will depend naturally on that of the wave as a whole. Then, in addition to the localized surface heating produced by impact, friction and contact with hot gas, each element of explosive will now suffer a more or less homogeneous energy increase due to the passage of these microshocks. If, as the cartridge diameter is increased, the velocity and so the pressure at the wave-front rise to such a level that this homogeneous energy absorption is sufficient to initiate reaction, the element may be expected to decompose in a much shorter time than before. A small advance beyond the diameter at which this pro-

cess first becomes operative should then lead to an abrupt shortening of the reaction zone thickness, and a consequent exploitation by the wave of the reaction energy to a much fuller degree than would otherwise be possible in such diameters. An immediate consequence of this will be a sudden rise in velocity to a value probably little short of the theoretical limit. At greater diameters only the higher velocity will be stable, the lower value even if temporarily established changing spontaneously into the higher as a consequence of the change of mechanism suggested.

The above theory of the two-velocity effect was advanced by the writer some years ago[32]. It is

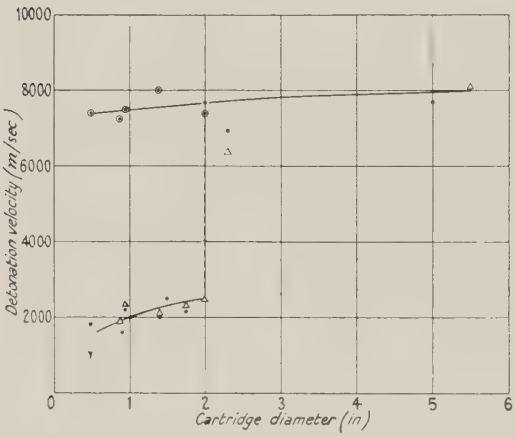

FIG. 8. Detonation velocity as a function of cartridge diameter in blasting gelatin. ● small detonator (No. 1 fulminate); △ intermediate detonator (No. 6 fulminate); ⊙ powerful detonator (No. 8 Briska).

not claimed that this theory is necessarily the correct one; but it does appear consistent with the available evidence. Thus Figure 8 summarizes the results of an unpublished investigation carried out in 1947 by the writer[33] on the effect of cartridge diameter and initiator on the detonation velocity of blasting gelatine (92 per cent nitroglycerine, 8 per cent nitrocotton). The cartridges, which were fired without wrapper, on wooden slats, had been stored for three weeks after manufacture, since the explosive was known to be unusually sensitive to high-velocity initiation when freshly made. The conclusions were as follows.

(1) At ½ inch diameter, a steady low velocity (~2000 m/s) could not be obtained. Attempts in this direction resulted either in a rise to high velocity (~7000 m/s) or more usually in failure. Steady high velocity was consistently produced by a powerful detonator.

(2) From ⅞ to 2 in, inclusive, a steady low or high velocity could be obtained, according to the detonator used.

(3) Above 2 in diameter, only the high velocity was stable.

(4) Both low and high velocity increased with diameter, but the proportional increase in high velocity was very slight.

Further investigation showed that in 2 5/16-in cartridges initiated by a detonator of intermediate strength (No. 6 fulminate/chlorate) the wave travelled at low velocity, 2500 m/s, for 4 in from the detonator and then changed speed abruptly to the high level, 7800 m/s. In 1½ in diameter, however, a steady low velocity of 2350 ± 40 m/s was maintained over the entire length of an 18-ft cartridge.

With regard to the likelihood that the proposed mechanisms operate in practice, we have now some theoretical evidence. Thus Ratner[34] concluded that temperatures sufficiently high to ensure rapid reaction should be expected from shock waves travelling in liquid explosives with the high velocity of detonation (~7000–8000 m/s); but this conclusion would not apply if the velocity were of the order of 2000 m/s. Again, in granular explosives, our calculations (Table 2) of the temperatures produced by compression in the explosive grains make it appear rather unlikely that initiation is effected in this way, except perhaps at the higher loading densities. On the other hand, if the air pockets are in fact raised to transient temperatures T_s of the order of 10^4 to 10^6 degrees in the shock-front, they may well serve as reaction nuclei or hot-spots. The work of Bowden[35] and his school[36, 37, 38, 39, 40, 41, 42, 43, 44, 45, 46] has given abundant proof of the important part played by compressed gas pockets in the initiation of explosion by relatively small blows; and Bowden and Gurton[42] have suggested that compression of gas bubbles is often the means by which low velocity detonation is maintained. The possibility that high velocity waves are propagated by direct shock compression of the explosive material is also explicitly considered by Bowden and Gurton[42], Bowden[35], and Taylor[47].

Of course, although the temperatures T_s shown in Table 2 are extremely high, the heat capacity of the air pockets is small, so that a relatively much lower compromise temperature (T_c) will be instantly established at the air-explosive interface. Reliable calculation of this temperature is out of the question in our case, but by making what seem fair assumptions regarding the mean

thermal parameters we have deduced for PETN the values of T_c shown in Table 2. They are about one-tenth of T_s, but still very high. Little significance can be attached to their absolute values, which in any case would tend rapidly to fall in consequence of the cooling of the gas phase by expansion, as indicated in Figure 7. But they certainly do not discourage the view that gas pockets may serve as reaction nuclei in the wave-front.

Rather striking experimental evidence on this question has recently been reported by Gurton[48] and by Bowden and Williams[44, 45]. These workers find that low velocity detonation in certain explosives is inhibited by subjecting them to hydrostatic air pressures of less than 100 atm. It can be foreseen that pressures of this low order will have little effect upon the Chapman-Jouguet variables in a condensed explosive where the pressures involved are enormously greater. Neither, we may suspect, will the energy input into the explosive grains themselves in the shock-front be appreciably altered. As Gurton points out, the only part of the system likely to be affected is the gas pockets. In the next section, we present a detailed analysis which extends the approximate theory put forward by Gurton[48] and by Bowden and Williams[44, 45], and which confirms these expectations.

(7) Effect of Variation in the Initial Hydrostatic Pressure

We consider a granular explosive, occupying a fixed cartridge volume, part of which is taken up by the grains of explosive themselves, and the remainder by pockets of gas between the grains. We are concerned with the effect of varying the hydrostatic pressure of this gas, without changing the overall cartridge volume, as when the cartridge is enclosed in a porous wrapper and the surrounding gas pressure is either raised or lowered.

Assume, in the first place, that the products of detonation form an ideal gas with constant γ and composition independent of temperature and pressure. The gas initially present is supposedly also ideal, with the same γ. Then if 1 cm³ of the undetonated cartridge contains $m\Delta$ g of explosive and $(1 - m)\Delta$ g of air, and Q_1 is the heat liberated by 1 g of explosive, the terminal RH-equation is, when $p_0/p_1 \ll 1$,

$$\frac{p_1 v_1}{\gamma - 1} = \tfrac{1}{2} p_1 (v_0 - v_1) + H \qquad (29)$$

where $v_0 \equiv 1/\Delta$ and $H \equiv mQ_1 + cT_0$, c being the specific heat of the products. The CJ-condition is

$$\frac{v_1}{v_0} = \frac{\gamma}{\gamma + 1} . \qquad (30)$$

Eliminating v_1, we have

$$p_1 = 2\Delta H(\gamma - 1) \qquad (31)$$

This includes gaseous detonations ($m = 1$). For such a case, $\Delta \propto p_0$ if p_0 is not too high, so that

$$p_1 \propto p_0 , \qquad (32)$$

justifying neglect of p_0 in equations (29) and (30). It follows at once that W_1 and D are almost independent of p_0 in an ideal gaseous explosive. This conclusion, together with equation (32), are well confirmed by Manson's detailed calculations[49] for various gases.

In the granular explosive, let the superscript ^{0} refer to conditions when $p_0 = 1$ atm. Thus Δ^0 is the cartridge density at 1 atm. Then at p_0 atm,

$$\Delta = m^0 \Delta^0 + (1 - \varphi m^0 \Delta^0)\delta \qquad (33)$$

where δ is the density of the interstitial gas, and φ is the specific volume of the explosive component alone, in each case at p_0. The explosive is negligibly compressed at the level of p_0 considered (say 1–100 atm), so that φ is a constant. If the gas remains ideal up to p_0, we have also

$$\delta = p_0 \delta^0 \qquad (34)$$

Finally, if $\Delta^0 \ll 0.05$ g/cm³, we may set $m^0 \fallingdotseq 1$. Then equation (31) gives

$$p_1/p_1^0 = 1 + (1 - \varphi\Delta^0)\frac{\delta^0}{\Delta^0} p_0 \qquad (35)$$

which is the required relation. It may be expected to apply rather closely to an explosive cartridged at $\Delta^0 \sim 0.1$ g/cm³ and subjected to pressures not exceeding 100 atm.

As an example, take $\Delta^0 = 0.06$ g/cm³, $\varphi = 0.6$ cm³/g, $\delta_0 = 1.293 \times 10^{-3}$ g/cm³, $p_0 = 80$ atm. These values correspond to a case of low density guncotton in air investigated by Gurton[48]. Then $p_1/p_1^0 = 2.66$; it appears that the effect of raising p_0 by a factor of 80 is to raise p_1 by a factor of about 2½ only. Since $p_1^0 \sim 1450$ atm, p_0/p_1 is still negligible, justifying equations (29) and (30). This will remain true even when p_0 is large, for then, by equation (35),

$$p_1/p_0 \sim (1 - \varphi\Delta^0)\frac{\delta^0}{\Delta^0} p_1^0 \sim 30$$

Of course, the solution cannot apply rigorously when p_0 is too large, because of the failure of equation (34).

As to D and W_1, they are still independent of p_0, to the same approximation.

The above idealized theory was confirmed by detailed calculations for the guncotton used by Gurton[48]. The general conclusions may then be summarized as follows. In an explosive whose density does not exceed 0.1 g/cm³, W_1 and D are almost unaffected by varying p_0 between 0 and 100 atm. At gaseous densities, p_1 varies in proportion to p_0; at 0.1 g/cm³ much more slowly. These conclusions give no grounds for expecting p_0 to have any marked effect upon the propagation. However, when we transfer attention from the CJ-layer to the shock-front, a very different picture emerges. Since $p_s > p_1 \gg p_0$, equation (8) shows that for gaseous explosives and condensed explosives of low density the shock pressure varies in the same ratio as the CJ-pressure when p_0 is altered. This means, of course, that p_s/p_0 is independent of p_0 for gases, but depends markedly on p_0 for granular explosives at 0.1 g/cm³. In fact, in the latter case, from equations (8) and (35),

$$p_s/p_o \doteqdot 2p_1^0\left[\frac{1}{p_0} + (1 - \varphi\Delta^0)\frac{\delta^0}{\Delta^0}\right] \qquad (36)$$

Now, according to equation (23), the compression ratio of the gas pockets in an intense shock-front is $1/\lambda$, irrespective of p_0. Consequently,

$$T_s/T_0 \doteqdot p_s/\lambda p_0 \qquad (37)$$

$$T_s/T_s^0 \doteqdot \frac{1}{p_0} + (1 - \varphi\Delta^0)\frac{\delta^0}{\Delta^0} \qquad (38)$$

With the same values as before, $T_s \sim T_s^0/30$. The shock-front temperature is thus reduced in a ratio somewhat less than, but of the same order as, that through which p_0 is raised.

The assumption that air behaves as an ideal gas with constant γ involves major errors at high shock intensities. The shock-front variables have, therefore, been recalculated using the data of Figure 5. Nitrocotton was assumed to compress like starch for which an isotherm was available[50].

Table 3. Nitrocotton (13.45 per cent N_2) Cartridged at 0.06 g/cm³ and Detonated at Various Air Pressures

A: *Detailed calculation*
B: *Idealized theory*

Initial p_0	CJ-plane		D	Shock-front			$T_c - T_0$
	p_1	W_1		p_s	W_s	T_s	
atm	*atm*	*m/s*	*m/s*	*atm*	*m/s*	*°K*	*°C*
1 A	1450	1020	2390	2975	2090	29700	378
B				2900	2040	150,000	
5 A						6550	184
B	1600	1020	2390	3200	2040	33000	
10 A						3580	141
B	1750	1020	2390	3500	2040	18000	
20 A						2100	114
B	2050	1020	2390	4100	2040	10600	
50 A						1210	101
B	2920	1020		5840	2040	6120	
80 A	3420	910	2370			989	100
B	3900	1020	2390	7800	2040	4990	
100 A						912	100
B	4470	1020	2390	8940	2040	4160	

Table 4. PETN Cartridged at 0.75 g/cm³ and Detonated at Various Air Pressures

A: *Detailed calculations*
B: *Idealized theory*

Initial p_0	CJ-plane		D	Shock-front			$T_c - T_0$
	p_1	W_1		p_s	W_s	T_s	
atm	*atm*	*m/s*	*m/s*	*atm*	*m/s*	*°K*	*°C*
1 A	41,900	1240	4520	89,400	2650	317,000	3460
B				83,800	2480	3,800,000	
5 A						63,300	1380
B	42,100	1240	4520	84,200	2480	760,000	
10 A						32,000	900
B	42,300	1240	4520	84,600	2480	384,000	
20 A						16,200	548
B	42,700	1240	4520	85,400	2480	194,000	
50 A						6650	245
B	44,000	1240	4520	88,000	2480	79,800	
80 A	47,600	1250	4730			4280	139
B	45,200	1240	4520	90,400	2480	51,300	
100 A						3480	99
B	46,100	1240	4520	92,200	2480	41,800	

Unfortunately, the data of Figure 5 apply only when $p_0 = 1$ atm. In order to make a comparison, we have assumed that T_s will be reduced in the same ratio at any higher pressure p_0 as it is at $p_0 = 1$ atm. Finally, a tentative estimate has been made of the compromise temperatures T_c produced at the surface of the nitrocotton fibers. The results are shown in Table 3, together with those of the idealized theory: p_s and W_s are almost unchanged, but T_s is greatly reduced.

At high loading densities, p_1 is no longer profactory explanation of the fact that detonation may be inhibited in granular explosives of moderate or low density by applying an initial hydrostatic air pressure of 50–100 atm. The CJ-variables are relatively little affected by such pressures unless indeed the cartridge density is extremely low; but the pressure ratio across the shock-front and the consequent temperature rise in the air pockets depend critically upon p_0.

In conclusion, it will be appreciated that the "high" velocity of detonation, if propagated by a

Table 5. PETN Cartridged at 1.5 g/cm³ and Detonated at Various Air Pressures

A: *Detailed calculations*
B: *Idealized theory*

Initial p_0	CJ-plane		D	Shock-front			
	p_1	W_1		p_s	W_s	T_s	$T_c - T_0$
atm	*atm*	*m/s*	*m/s*	*atm*	*m/s*	*°K*	*°C*
1 A	188,000	1550	8150	426,000	3510	1,160,000	13,400
B				376,000	3100	17,107,000	
5 A						232,000	5770
B	188,100	1550	8150	376,200	3100	3,424,000	
10 A						116,000	3950
B	188,200	1550	8150	376,400	3100	1,712,000	
20 A						58,100	2680
B	188,500	1550	8150	377,000	3100	857,600	
50 A						23,400	1550
B	189,200	1550	8150	378,400	3100	344,400	
80 A	191,100	1535	8260			14,700	1140
B	190,000	1550	8150	380,000	3100	216,100	
100 A						11,800	982
B	190,600	1550	8150	381,200	3100	173,300	

portional to Δ, and equation (35) can hardly be expected to apply accurately. On the other hand, since δ^0/Δ^0 is now small, p_1/p_1^0 approaches unity for moderate values of p_0, so that the error in equation (35) is unlikely to be serious. This was confirmed by making detailed calculations for PETN at 0.75 and 1.5 g/cm³ (Δ^0) with $p_0 = 1$ atm and 80 atm. The CJ-variables are shown in Tables 4 and 5, together with values predicted by equation (35). The shock-front variables were also estimated, first with air as an ideal gas with constant γ and then by means of the accurate air shock characteristics. Tables 4 and 5 summarize these calculations also.

The above study appears to provide a satishomogeneous mechanism, should be independent of initial hydrostatic pressure. Gurton[48] finds that this is in fact the case.

Acknowledgments

The writer is greatly indebted to Miss J. M. Davidson, M. A., who carried out all the computational work. The material of this paper formed part of a study of the theory of detonation undertaken by the Nobel Division of I.C.I. and the writer wishes to thank Dr. J. Taylor, then Research Director, for encouragement in this as in previous work.

Thanks are also due to the Oxford University

Press for permission to reproduce Figures 1, 2 and 8 from a book recently published by them[12].

REFERENCES

1. Döring, W.: Ann. Physik, *43*, 421 (1943).
2. Eyring, H., Powell, R. E., Duffey, G. H., and Parlin, R. B.: Chem. Rev., *45*, 69 (1949).
3. Zeldovich, Y. B.: J. Exptl. Theoret. Phys., *10*, 542 (1940).
4. Devonshire, A. F.: 1943. Quoted by Eyring, Powell, Duffey and Parlin[2].
5. von Neumann, J.: Quoted by Eyring, Powell, Duffey and Parlin[2].
6. Becker, R.: Z. Physik, *8*, 321 (1922).
7. Lewis, B., and von Elbe, G.: *Combustion, Flames and Explosions of Gases*. New York, Academic Press, 1951.
8. Jost, W.: *Explosion and Cumbustion Processes in Gases*. New York, McGraw-Hill Book Co., 1946.
9. Belyaev, A. F.: Acta Physicochim. (U.R.S.S.), *8*, 763 (1938).
10. Copp, J. L., and Ubbelohde, A. R.: Trans. Faraday Soc., *44*, 646, 658 (1948).
11. Kistiakowsky, G. B.: *Third Symposium on Combustion, Flame and Explosion Phenomena*. Baltimore, The Williams & Wilkins Co., 1949.
12. Taylor, J.: *Detonation in Condensed Explosives*. Oxford University Press, 1952.
13. Paterson, S.: Research, *1*, 221 (1948).
14. Rankine, W. J. M.: Phil. Trans. Roy. Soc., *160*, 277 (1870).
15. Hugoniot, A.: J. école polyt., *57*, 3 (1887); *58*, 1 (1889).
16. Hirschfelder, J. O., Stevenson, D. F., and Eyring, H.: J. Chem. Phys., *5*, 896 (1937).
17. Morris, G., and Thomas, H.: Research, *1*, 132 (1947).
18. Bethe, H. A., and Teller, E.: Quoted by Fuchs, Kynch, and Peierls[19].
19. Fuchs, K., Kynch, G. J., and Peierls, R.: Atomic Report MS 61, 1942.
20. Burkhardt, G.: See Döring[29].
21. Davies, D. R.: Proc. Phys. Soc., *61*, 105 (1948).
22. Landau, L., and Staniukovich, K.: Compt. rend. (*U.R.S.S.*), *46*, 362 (1945).
23. Pokrovsky, G. I., and Staniukovich, K. P.: Compt. rend. (U.R.S.S.), *53*, 33 (1946).
24. Jones, H.: Proc. Roy. Soc., *A189*, 415 (1947).
25. Jones, H., and Miller, A. R.: Proc. Roy. Soc., *A194*, 480 (1948).
26. Jouguet, E.: Compt. rend., *202*, 796, 1225, 1320 (1936).
27. Jouguet, E.: Mém. Artill. franc, *21*, 235 (1947).
28. Muraour, H.: Chimie et Industrie, *47*, 3 (1942). (Contains complete bibliography of earlier papers.)
29. Döring, W., and Burkhardt, G.: *Beiträge zur Theorie der Detonation*. Berlin-Gatow, 1944.
30. Paterson, S.: Nature, *167*, 479 (1951).
31. Cumming, I. G.: Private communication (1951).
32. Paterson, S.: Proc. Phys. Soc., *59*, 50 (1947).
33. Paterson, S.: Unpublished I. C. I. report (1947).
34. Ratner, S.: Compt. rend. (U.R.S.S.), *22*, 357 (1947).
35. Bowden, F. P.: Proc. Roy. Soc., *A204*, 20 (1950).
36. Bowden, F. P., Eirich, F., Ferguson, A. E., and Yoffe, A. D.: Council Sci. Indust. Res (Austr.) Bulletin 167 (1943).
37. Bowden, F. P., Eirich, F., Mulcahy, M. F. R., Vines, R. G., and Yoffe, A. D.: Council Sci. Indust. Res. (Austr.) Bulletin 173 (1943).
38. Bowden, F. P., Mulcahy, M. F. R., Vines, R. G., and Yoffe, A. D.: Nature, *157*, 105 (1946).
39. Bowden, F. P., Mulcahy, M. F. R., Vines, R. G., and Yoffe, A. D.: Proc. Roy. Soc., *A188*, 291, 311 (1947).
40. Vines, R. G., and Mulcahy, M. F. R.: Nature, *157*, 626 (1946).
41. Mulcahy, M. F. R.: Phil. Mag., *39*, 547 (1948).
42. Bowden, F. P., and Gurton, O. A.: Proc. Roy. Soc., *A198*, 337, 350 (1949).
43. Yoffe, A.: Proc. Roy. Soc., *A198*, 373 (1949).
44. Bowden, F. P., and Williams, H. T.: Proc. Roy. Soc., *A208*, 176 (1951).
45. Bowden, F. P., and Williams, H. T.: Research, *4*, 339 (1951).
46. Blackwood, J. D., and Bowden, F. P.: Proc. Roy. Soc., *A213*, 285 (1952).
47. Taylor, J.: Proc. Roy. Soc., *A204*, 20 (1950).
48. Gurton, O. A.: Unpublished I. C. I. report, 1949.
49. Manson, N.: Compt. rend., *218*, 29 (1944).
50. Bridgman, P. W.: Proc. Am. Acad. Arts Sci., *76*, 9 (1945).
51. Chapman, D. L.: Phil. Mag., *47*, 90 (1899).
52. Cole, R. H.: *Underwater Explosions*. Princeton University Press, 1948.
53. Muraour, H., Michel-Lévy, A., and Vassy, A.: Rev. d'Optique, 55 (1941).
54. Thomas, L. H.: J. Chem. Physics, *12*, 449 (1944).

76

RECOMBINATION OF OXYGEN ATOMS ON SURFACES

By D. G. H. MARSDEN AND J. W. LINNETT

This paper describes a preliminary investigation of the variation of several catalysts' efficiencies for oxygen atom recombination over a range of temperatures. Such measurements are of interest in connection with surface effects in reaction kinetics, which may decide the importance of a given radical or atom in a reaction scheme.

For hydrogen atoms, many qualitative measurements of catalytic efficiencies, chiefly for metals, have been made[1]; all, except those of Smith[2] have consisted of a comparison of temperature rises produced by placing the various catalysts in the atomized gases flowing from the discharge tube. Until the work of Smith, no attempts had been made to compare various catalysts at the *same* temperature, or to study the variation of a single catalyst with temperature.

If the results for catalytic activity are to be of use in kinetics, the catalysts must be tested under the same conditions in which they are used as surface coatings in reaction vessels. Thus, it is of no value to measure the temperature rise of a metal thermocouple covered with a necessarily imperfect coating of KCl if the results are to be compared with the effect of a KCl coating on a glass or quartz vessel.

For these reasons, it was decided to apply the catalysts to a glass-sleeved platinum wire, with no part of the bare platinum exposed to the atomized gas; the wire was electrically heated and its temperature determined from its resistance. The efficiencies of the catalyst were estimated from the difference in power required to heat the filament to a particular temperature with and without the passage of a discharge. An advantage of this method is that the electrical measuring system is entirely isolated from the effects of stray discharges. A similar method has been suggested by Steacie[3] for the estimation of hydrogen atoms, and has been used by Roginskii and Shekhter[4] for various bare metal wires.

The method has several defects. In the first place, unless the wire is sufficiently long, there will be end temperature corrections; the true surface of the glass sleeve, unless it is very thin, and fits the wire closely, will be at a sensibly lower temperature than the wire. Secondly, Busch[5] has shown that under certain conditions (namely low pressures, high thermal conductivity of the gas, and a high resistance-temperature coefficient of the wire) the temperature gradient along an electrically heated wire may become unstable. However, our experimental results seem to indicate that none of the conditions for this effect occurred. Finally, unless the pressure is very low, the effect produced by active catalysts will be partially masked by the rate of diffusion of atoms, due to the concentration gradient set up in the vicinity of the catalyst. However, it was hoped that in spite of these defects, these preliminary measurements would give some idea of the various efficiencies.

Species Produced from An Oxygen Discharge

The production of oxygen atoms by a Wood's tube was first observed in 1912 by Strutt[6], but the atoms were not recognized as such until after Wood's discovery of the production of hydrogen atoms in a discharge tube, when Bonhoeffer, Wrede, and Harteck[7], among others, demonstrated the production of oxygen atoms and investigated their reactions on surfaces and in the gas phase.

In the case of oxygen, there is the possibility of several species: oxygen atoms, in ground or excited states, atomic and molecular ions, ozone, and excited molecules. The evidence that ground state oxygen atoms are the only important species in the flow from a discharge tube is summarized as follows:

(1) The oxygen atoms produced by a discharge do not react appreciably at room temperature with hydrogen[8], whereas it has been shown that

$$NO_2 + h\nu \rightarrow NO + O\ ^3P\ \lambda = 3500\ \text{Å}$$

$$NO_2 + h\nu \rightarrow NO + O\ ^1D\ \lambda < 2450\ \text{Å}$$

and that with hydrogen present, O ^{1}D will react, but O ^{3}P will not.

Similarly, photochemical oxidation of hydrogen only occurs if light of a wavelength sufficiently short to dissociate the oxygen into O ^{3}P + O ^{1}D is used[10]; the reaction between O and H_2 is exothermic for O ^{1}D, but is endothermic for O ^{3}P. The fact that atoms from a discharge tube do not

react appreciably with H_2 at room temperature argues that O ^3P is the main species produced.

Kurt and Phipps[11] measured the Stern-Gerlach splitting of a beam of oxygen atoms produced from a discharge and found it to correspond with that to be expected from the ground state. More recently, Beringer[12] has observed some of the transitions in the triplet levels of the ground state by paramagnetic resonance. This does not prove conclusively that the ground state is the only one present, as other states may not exhibit a paramagnetic spectrum, may be present in such low amounts as to be undetectable, or may not yet have been discovered. The argument of Harteck and Kopsch[7] that oxygen atoms may be detected for perhaps 10^{-2} and 10^{-1} second after the discharge tube, and therefore must be in a ground state, is not conclusive as metastable states may have a comparatively long life, which may be determined by the chance of a collision or reaction with O_2 molecules or the walls rather than by the transition probability. Finally, the measured heat of recombination of oxygen atoms from a discharge[13], though of poor accuracy, agrees well with the spectroscopic value for the ground state. The sum of the evidence, seems to suggest that ground state atoms are probably the only important species.

(2) Harteck and Kopsch[8] showed that ions were probably absent, by placing an ionization gauge beyond the discharge. No increase in ion current beyond that expected was observed when the discharge was switched on.

(3) Ozone, if present, would result from the reaction of atoms and undissociated molecules. Harteck and Kopsch[8] showed that ozone was absent, and advanced arguments to show why this was so.

(a) Ozone is detectable in very small amounts by its strong ultraviolet absorption band. It was found impossible to detect it in the stream beyond the discharge tube, although preliminary experiments passing ozonized oxygen through the discharge tube showed that 0.005 mm O_3 in 1 mm total pressure would be detectable.

(b) For the formation of ozone, a three-body collision is almost certainly necessary;

$$O + O_2 + M \rightarrow O_3 + M$$

but its destruction occurs by a two-body collision

$$O_3 + O \rightarrow O_2 + O_2 .$$

The former probably occurs at every collision, while the latter has an efficiency of probably 1 in 2000 collisions. As it is a two-body reaction, at room temperature and pressures of the order of 1 mm the removal reaction is far more efficient than the formation reaction. The stationary concentration of ozone is therefore extremely small, and decreases as the pressure is lowered. If the temperature is lowered, the stationary concentration of ozone increases, as the rate of the removal reaction is lowered markedly, due to its activation energy.

Thus, it is found that at a sufficient distance away from the discharge tube, no ozone is formed in a liquid air trap; at closer distances large amounts of ozone are formed as oxygen atoms have not all recombined.

(4) Excited molecules must be present in the discharge itself, as the energy required for formation of the $^3\sum_u^-$ and lower excited states is less than that required for formation of O_2^+ ions. Kaplan and Branscombe[14] have shown that at lower pressures an after-glow spectrum due to $^1\sum_g^+ \rightarrow {}^3\sum_g^-$ transition is obtainable after long exposures, and more recently, Broida and Gaydon[15], using very fast flow rates at pressures from 1–4 mm, have obtained an after-glow due to Herzberg bands in emission ($^3\sum_u^+ \rightarrow {}^3\sum_g^-$). They suggest that these result from recombination of oxygen atoms to form the excited rather than the ground state.

It is difficult to estimate what amount of the activity of the oxygen from a discharge tube is really due to excited molecules, but from the measured heat of recombination it would appear that they cannot be of great importance.

Apparatus

GENERAL

The apparatus is shown in block diagram in Figure 1. The oxygen was generated in a water-cooled U-tube electrolytic cell with nickel electrodes, which was capable of passing 10 amps; the electrolyte was 15 per cent NaOH saturated with baryta. Hydrogen in the oxygen was removed by platinized asbestos at 400°C, and a constant water vapor content ensured by passage through a trap at 0°C. The gas was allowed to leak into the vacuum through a detachable capillary, protected from dust by a sintered disc, and thermostated at 25°C. The pressure of oxygen on the high pressure side was kept to a constant value with a Toricellian manometer by adjusting the levels of oxygen and hydrogen blow-off to atmosphere. The pressure on the vacuum side

was measured on a McLeod gauge; an oil manometer was used for a quick check on its constancy.

The discharge tube and pumping lines were of 20–25 mm tubing. The discharge tube itself was 300 cm long and U-shaped; oxygen entered at one end and left at the middle. Two electrodes were of aluminium and were contained in attached electrode chambers with tungsten seals. A third electrode in a small side tube was grounded, and served to remove any stray discharges.

The atomized oxygen leaving the discharge tube passed a side arm 15 cm away containing the probe which projected into the flow. Beyond this a furnace heated to 300°C served to remove any ozone and oxygen atoms before they should reach the liquid air traps and form liquid ozone.

The pump used was an Edwards' Speedivac of 150 liter/min displacement. A two-stage mercury pump was used for initial evacuation. All detachable vacuum joints were cone and sockets greased with Apiezon L.

THE PROBE

The probe was made (Fig. 2) in the form of a U about 6 mm long and 3 mm wide from 0.05 mm platinum wire. The glass covering was made by drawing a Pyrex tube down to a thin-walled capillary of the size used for melting point determinations. This was then drawn down to a capillary in which the platinum wire was just a sliding fit; one of the wider ends from the first drawing down was left on to facilitate the inserting of the wire. The U shape was formed by bending the glass-sleeved wire over an electrically heated silica tube, platinized to prevent the glass from sticking. Finally, enough glass was removed to leave 5 mm of bare platinum at each end.

The mounting for the U was made from 6 mm tubing internally sealed to a cone fitting in the side arm beyond the discharge tube. Two thin legs, 5 mm long, 2 mm internal diameter, were attached to the bottom and drawn down at the ends, so that the glass sleeved ends of the wire would just slide inside. The legs were then collapsed on to the sleeve and wire, using a needle flame. It is essential that the flame not be allowed to play on the sleeved wire outside the leg, as otherwise the sleeving melts and retracts into small beads, leaving the wire uncovered. The probe was annealed at 400°C. Current and potential wires were attached to the bare platinum wires inside the legs with soft solder, this being first melted in the legs with a fine flame and the leads pushed in while it was molten.

The probe was calibrated on a Callendar-Griffiths bridge rather than by a potentiometer as it was felt that for a calibration of the same accuracy, less current would be required (resulting in less heating of the wire) if the bridge were used. The calibration points were 0°C, 100°C and the boiling point of aniline (fractionated twice over sodium), the temperature being adjusted for atmospheric pressure.

The values of resistance in all cases corres-

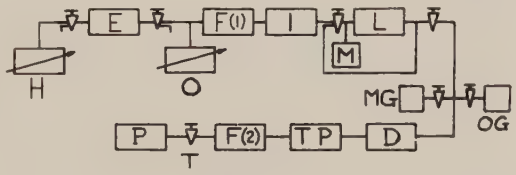

FIG. 1. Block diagram showing layout of apparatus. E, electrolytic cell; H, variable hydrogen blow-off; O, variable oxygen blow-off; F(1), furnace to remove hydrogen; F(2), furnace to destroy ozone; I, ice trap; L, leak to provide pressure drop; M, manometer; MG, McLeod gauge; OG, oil pressure gauge; D, discharge tube; TP, test probe; P, pumps.

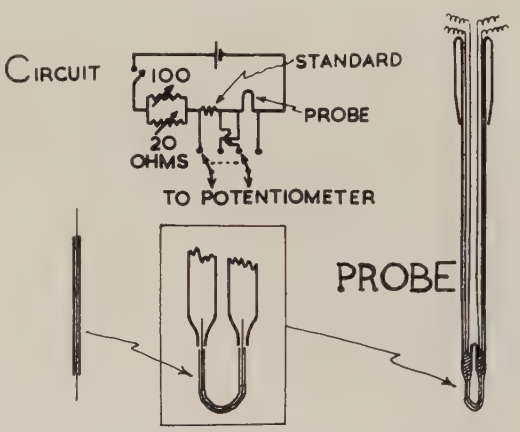

FIG. 2. Diagram of test probe consisting of a fine platinum wire in a glass sleeve, showing also the method of construction.

ponded to a value of α°_{100} lower than that defined for a platinum resistance thermometer. This may have been due to strain at the seal, or, more probably to the use of a non-thermopure grade of platinum, as the calibrations of the various probes made were consistent. Further, it was necessary to assume that the temperature scale held up to 400°C, as it was impossible to calibrate above 200°C, because of the melting and possible contamination of the solder used to connect the current and potential leads. (It should be possible to avoid these difficulties by gold-soldering the

leads before the glass seal is made, and by leaving the glass sleeves expanded at the ends, to avoid sealing on to the wire itself; any strain due to a Pyrex platinum seal would thus be avoided.)

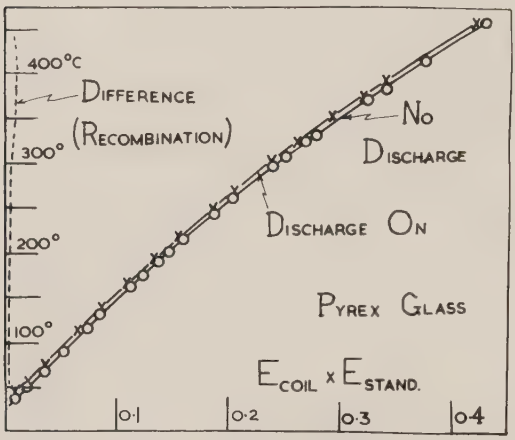

FIG. 3. Graph of temperature attained by platinum wire against power input (in arbitrary units) with uncoated Pyrex glass sheath. Curves are shown with no discharge, with the discharge on, and also (dotted line) the difference between these.

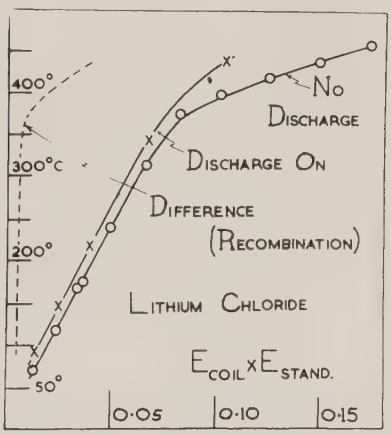

FIG. 4. Graph of temperature attained by platinum wire against power input (in arbitrary units) with Pyrex glass sheath coated with lithium chloride. Curves are shown with no discharge, with the discharge on, and also (dotted line) the difference between these.

The current passing through the probe was measured by the potential across a manganin resistance in series with it, calibrated by a potentiometer against a standard.

The probe was coated by immersion in saturated solutions of salts, special care being taken to avoid contamination of the salts and the surface of the probe and containers of the solutions. It was dried quickly with hot air, placed in position, and the apparatus evacuated as soon as possible. The platinum was applied as a 1 per cent solution of $PtCl_4$ in alcohol, and burned to the metal by passing a sufficient current through the probe wire.

EXPERIMENTAL PROCEDURE

The oxygen was allowed to flow through the discharge tube for at least one hour for the pressure to become steady; small alterations to the flow rate could be made by adjusting the setting of tap (T). During this time the accumulator supplying the probe was also discharged through auxiliary resistance, to stabilize the EMF.

The temperature of the probe was now raised in steps of about 50°C up to 450°C, enough time being allowed at each temperature for the potential differences across the probe and standard resistance to become constant; readings at intermediate points were then taken while the temperature was lowered. Similar readings were taken with the discharge switched on, the current in the discharge being kept constant manually, a few check points being taken with the discharge switched off as the temperature was lowered.

Results and Discussion

The results in this section will be presented in the following form. The power, as measured by the product of the potential across the platinum filament and the potential across the standard series resistance, is plotted against the filament temperature both with the discharge on and with it off. On each graph is also plotted the difference between them, which is a measure of the extent to which oxygen atoms are recombining on the surface.

SILVER

It had been decided to test silver, as Strutt[6] had found that nearly every collision was effective in recombination. However, it proved impossible to use. A silver coating produced by chemical silvering turned black as soon as the discharge was switched on, and flaked off. The black product oxidized the manganous ion in solution to permanganate and must therefore have been argentic oxide; it reverted slowly to the normal oxide.

PYREX GLASS

The results for Pyrex glass are shown in Figure 3. From this it is seen that the curve with the dis-

charge on is practically coincident with that with it off, implying a small efficiency which varies very little with temperature.

LITHIUM CHLORIDE

In the first experiment with the discharge on very little difference from the blank was noticeable at low temperatures, but, as the temperature was raised, a diffuse red glow suddenly appeared immediately around the probe. The lithium chloride appeared to melt and became red hot. This phenomenon could not be repeated with the same specimen of lithium chloride; using the same surface after this phenomenon had occurred, the results shown in Figure 4 were obtained. It will be seen that up to about 350°C this lithium chloride surface showed very little activity, though it was slightly greater than that of the glass. However, above 350°C there was a considerable increase in the activity. When this lithium chloride was removed from the probe and replaced by a fresh coating the same sudden appearance of the diffuse red glow was observed on raising the temperature.

It seems probable that the interesting behavior of lithium chloride, which is different from that of potassium chloride (see below), may be related to the low melting point of lithium chloride and to the fact that it is both hydrated and hygroscopic. The sudden onset of activity could then be ascribed to the loss of water from the solid resulting in a honey-comb structure which exposes a surface with a large effective area. The high activity of this surface would then result in the lithium chloride's being raised to a high temperature so that it would melt with a consequent reduction in the effective surface area. As a result a subsequent test with the same sample would not show any repetition of this phenomenon. However this surface shows an increase in activity above about 350°C. This might be due to the onset of a new process possessing an activation energy or possibly to the further loss of some last trace of water, perhaps from the surface of the lithium chloride.

POTASSIUM CHLORIDE

The results for this substance are shown in Figure 5. It had an activity about 8 times that of glass; this activity did not vary greatly with temperature. With potassium chloride there was no sudden increase in activity on raising the temperature such as had been observed with lithium chloride. It seems probable that this difference may be due to the fact that potassium chloride is not hygroscopic, and that it melts at a considerably higher temperature than lithium chloride. Consequently, the nature of the surface would be expected to remain unchanged over the whole temperature range studied. The slight rise with temperature might indicate a process with a very small activation energy, but it is so small that it may not be real. The behavior of the potassium chloride was also different from that of the fused lithium chloride, for, although the latter was less effective below 350°C, it showed a marked increase in efficiency above 350°C, whereas KCl showed no analagous effect up to the highest temperature studied (450°C).

PLATINUM

This was so much more active than the salts that the discharge had to be reduced to 40 per cent of its original value to obtain reasonable measurements of heat input to the probe. Even then the rate of heat liberation by oxygen atom recombination on the surface of the probe was 40—100 times that on the surface of the glass. The results obtained using platinum are shown in Figure 6. The minimum heat input to the probe was sufficient to raise the temperature to 120°C when the discharge was on. As the power input was increased the temperature rose to nearly 300°C. However, a further increase in the power input then caused a fall in temperature of the filament of the probe so that, at this temperature, there must have been a decrease in the catalytic effectiveness of the platinum surface. Further increases in the power input resulted in further rises in temperature.

There are several possible explanations of the break at about 250–300°C. The possibility of the occurrence of anomalous temperature gradients along the wire by the Busch[5] effect is not likely, as no instability was noticed in this region. Secondly the high efficiency of the platinum might have caused a local deficiency of oxygen atoms in the vicinity of the probe, resulting in an apparent loss of act'vity. Voevodskii and Lavroskaya[16] have described experiments in which a sudden rise in the temperature of the catalyst is ascribed to this cause, but we have been unable to confirm this in some more recent experiments. The most likely cause is a change in the characteristics of the platinum surface by sintering or shrinking

from the surface of the Pyrex glass because of different thermal coefficients of expansion. As several experiments showed that there was no precise temperature at which this effect occurred (225°–275°C) it is thought that one of these was more probably the explanation.

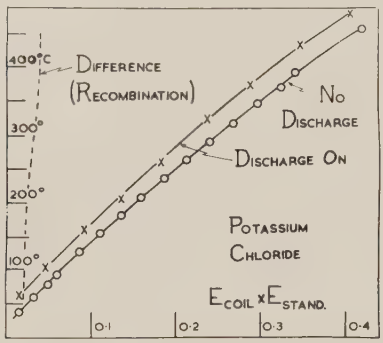

Fig. 5. Graph of temperature attained by platinum wire against power input (in arbitrary units) with Pyrex glass sheath coated with potassium chloride. Curves are shown with no discharge, with the discharge on, and also (dotted line) the difference between these.

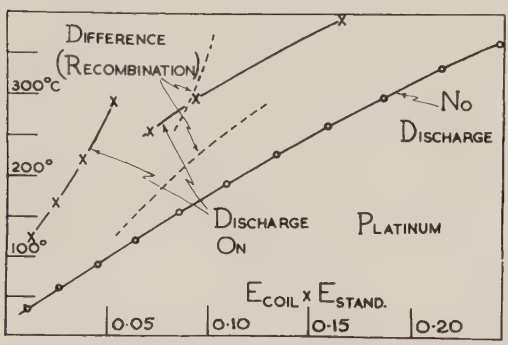

Fig. 6. Graph of temperature attained by platinum wire against power input (in arbitrary units) with Pyrex glass sheath coated with platinum. Curves are shown with no discharge, with the discharge on, and also (dotted line) the difference between these.

Conclusion

In this section two general topics will be considered: (1) The relation of the present results to those obtained from kinetic studies; (2) Some tentative comments on the mechanism of the recombination process.

(1) Warren[17] has recently studied the hydrogen-oxygen reaction in such a way as to determine the relative efficiencies of different surfaces in catalyzing the recombination of hydrogen atoms. Unfortunately, he was not able to obtain detailed results for the effect of different surfaces on the recombination of oxygen atoms. For hydrogen atoms he states that silver is probably highly active, the alkali metal chlorides of medium activity, and Pyrex, cleaned with acid (as was done in the present experiments), of low activity. This is the same order of activity as is found in our experiments on oxygen atom recombination. Lewis and von Elbe[18] list the efficiencies of different surfaces in removing and destroying HO_2 and H_2O_2. Again silver and clean Pyrex are of high and low efficiency respectively while the alkali metal chlorides show an intermediate activity. It is perhaps surprising that, for all the above catalytic processes, the order of efficiency of the different surfaces is the same. However, it should be remembered that it is only possible to ascribe the action of the surface to a particular removal process after making certain assumptions regarding the mechanism for the reaction in the gas phase.

(2) All recombinations of atoms and free radicals on surfaces have been found to be first order over a wide range of temperature[19]. Smith[2] found that hydrogen atoms obeyed the first order law over the temperature range $-183°$ to $+250°$C, on both efficient and inefficient surfaces, wet or dry. It is also well known that metals are good catalysts for hydrogen and oxygen atom recombination, while glass and silica are poor. The two simplest possible mechanisms which would account for a first order recombination are:

(a) A slow adsorption stage; in this case the adsorbed atoms would have to be mobile so that, once adsorbed, the atoms eventually meet on the surface and recombine.

(b) An approximately complete and immobile layer of adsorbed atoms, the slow stage of the recombination being the reaction between one of the adsorbed atoms and a gas phase atom colliding with an adsorbed atom.

Shuler and Laidler[20] have discussed Smith's[2] results for hydrogen in terms of absolute rate theory, and consider that (b) is more likely on energetic grounds. The main experimental reasons for preferring this mechanism are the results obtained by Langmuir[21]. He showed that hydrogen atoms, dissociated at a tungsten filament, could migrate to the glass walls of the vessel at liquid air temperatures, and exhibit reducing powers. Clean-up of gaseous hydrogen in this manner was limited, and corresponded to the formation of a monolayer (10^{15} atoms per sq cm). Similarly, Johnson[22] found that the clean-up, at room tem-

perature, of hydrogen in an electrodeless discharge, and of hydrogen admixed with mercury vapor and illuminated with a mercury vapor lamp, could be explained only by the formation of a stable monolayer of hydrogen atoms. The heat of adsorption of this layer was calculated from the desorption temperature and found to be about 11 kcals/gm atom. However, other workers[23] have suggested that the clean-up of hydrogen in discharges may be due to the formation of water or of silicon hydrides, which would show abnormal reducing properties, and consequently be confused with atomic hydrogen. It is known that hydrogen *molecules* are adsorbed on metals with dissociation to form a monolayer of atoms, so that, on metals, process (b) is probable.

From the value of the heat of adsorption of atomic hydrogen on glass, Shuler and Laidler[20] derive absolute rate expressions for the rate of reaction and the efficiency of recombination γ, using Hirschfelder's[24] approximation for the activation of an exothermic reaction.

$$A + BC = AB + C, \qquad E_{act} = 0.055\ D_{BC}$$

where D_{BC} is the dissociation energy of the molecule BC, or in this case:

$$S{-}H + H = S + H_2$$

for dry surfaces, where S represents the surface atom. The values obtained for γ agree with Smith's[2] results, using 10^{15} for the number of atoms per sq cm of surface.

The greater activity of metals is understandable from Trapnell's[25] experiments on the variation of the heat of adsorption of molecular hydrogen. On tungsten, it is found that the heat falls from 45 kcals at $\theta = 0$ to 2.4 kcals at $\theta = 1$ (where θ is the fraction of the surface covered) so that the energy of activation, from Hirschfelder's[24] approximation may easily be much less than for glass, assuming that coverage is nearly complete at the pressures used in Smith's[2] experiments.

With oxygen, there appears to be little evidence that the clean-up of gas by filaments or from discharges gives a stable atomic layer on glass. Langmuir[21] showed that, by evaporating the layer of atomic oxygen produced on tungsten at very low pressures, a substance possessing abnormal oxidizing powers could be condensed onto a glass surface at the temperature of liquid air. However, this evidence is difficult to interpret with certainty as no mention was made of the stability of the layer or whether it persisted at higher temperatures. The electron impact experiments of Glockler[26] appear to indicate that no clean-up of oxygen occurs on clean glass at room temperature when electrons of energies definitely sufficient to dissociate oxygen are used. It would also seem perhaps less likely that oxygen atoms would be bonded to a glass or silica surface than would hydrogen atoms, for it is probable that such a surface consists largely of bonded oxygen atoms. Consequently, if the recombination of oxygen atoms on glass is of the first order, as seems likely as a result of more recent experiments we have made, the mechanism may be of type (a).

The high efficiency of metals for oxygen atom recombination would, at first sight, seem to be explicable in the same way as for hydrogen atoms. However, the measurements on the heat of adsorption of molecular oxygen on metals shows that, in at least one case[27], the heat of adsorption does not fall off with increasing coverage nearly as much as for molecular hydrogen, so that the energy of activation would still be expected to be high.

From the effect on silver, which is oxidized in bulk to a higher oxide, it may be that, in general, the effect of atomic oxygen on metals is not merely to cover the metal with a layer of atoms, as does molecular oxygen, and as do, it seems, both atomic and molecular hydrogen, but rather that they form a surface oxide layer, or, in some cases, a bulk oxide, on which the atoms would be sufficiently weakly adsorbed for recombination with gas phase atoms to be efficient.

REFERENCES

1. Bonhoeffer, K.: Z. phys. Chem., *113*, 199 (1924); Taylor, H. S., and Lavin, G.: J. Am. Chem. Soc., *52*, 1910 (1930); Katz, S., Kistiakowski, G. B., and Steiner R. F.,: J. Am. Chem. Soc., *71*, 2258 (1949).
2. Smith, W. V.: J. Chem. Phys., *11*, 110 (1943).
3. Steacie, E. W. R.: *Atomic and Free Radical Reactions*, p. 67. New York, Reinhold Publ. Corp., 1946.
4. Roginskii, S., and Shekhter, A.: Act. Phys. Chem. (U.R.S.S.), *1*, 318, 473 (1934); *10*, 371 (1939).
5. Busch, H.: Ann. Physik, *64*, 401 (1921).
6. Strutt, R. J.: Proc. Phys. Soc. (London), *23*, 66, 147 (1910).
7. Wrede, E.: Z. Physik, *54*, 53, 71 (1929); Harteck, P.: Naturwiss, *17*, 727 (1929).
8. Harteck, P., and Kopsch, U.: Z. phys. Chem., *B12*, 327 (1931).

9. Schumacher, H. J.: J. Am. Chem. Soc., *52*, 2584 (1930).
10. Neujmin, N., and Popov, B.: Z. phys. Chem., *B27*, 15 (1934).
11. Kurt, E., and Phipps, T.: Phys. Rev., *34*, 1357 (1929).
12. Beringer, R.: Phys. Rev., *88*, 677 (1952).
13. Bichowski, F., and Copeland, L.: Phys. Rev., *36*, 1221 (1929).
14. Kaplan, J.: Nature, *159*, 673 (1947); Branscombe, L.: Phys. Rev., *86*, 258 (1952).
15. Broida, H., and Gaydon, A. G.: Proc. Roy. Soc., *A222*, 181 (1954).
16. Voevodskii, V., and Lavrovskaya, G.: Zhur. Fiz. Khim., *25*, 1050, (1951)
17. Warren, D.: Proc. Roy. Soc., *A204*, 465 (1951); *A211*, 86, 96 (1952).
18. Lewis, B., and von Elbe, G.: *Combustion, Flames and Explosions of Gases*. New York, Academic Press, 1951.
19. von Muffling, L.: In *Handbuch der Katalyse* by Schwab, G. M.: Vol. VI, p. 94. Berlin, Verlag Julius Springer, 1943.
20. Shuler, K. E., and Laidler, K. J.: J. Chem. Phys., *17*, 1212 (1949); Laidler, K. J.: J. Phys. Chem., *53*, 712 (1949).
21. Langmuir, I.: J. Chem. Soc., 518 (1940); J. Am. Chem. Soc., *37*, 1162 (1915).
22. Johnson, M. C.: Trans. Faraday Soc., *28*, 162 (1932).
23. Taylor, J.: Nature, *122*, 347 (1928); Mierdel, G.: Ann. Physik, *85*, 612 (1928); Heidemann, E.: Z. phys. Chem., *A153*, 210 (1931); *A164*, 20 (1933).
24. Hirschfelder, J.: J. Chem. Phys., *9*, 645 (1941).
25. Trapnell, B. M. W.: Proc. Roy. Soc., *A206*, 39 (1951).
26. Glockler, G., and Wilson, J.: J. Am. Chem. Soc., *54*, 4544 (1932).
27. Trapnell, B. M. W., and Rideal, E. K.: Proc. Roy. Soc., *A205*, 409 (1951).

77

EXPLOSIVE DECOMPOSITION AND COMBUSTION OF HYDRAZINE

By PETER GRAY and J. C. LEE

Introduction

Hydrazine is an unstable compound and even in decomposition to nitrogen, ammonia and hydrogen it can support a flame. Self-supporting decomposition stoichiometrically must lie between the two extremes:

$$N_2H_4 = N_2 + 2H_2$$

$$N_2H_4 = \tfrac{1}{3}N_2 + \tfrac{4}{3}NH_3$$

It has been studied as a gas-burner flame[1], as a decomposition flame of the pure liquid[2] and in spark-ignited explosion in a closed vessel[3]. In oxidation, when reaction goes to completion and nitrogen plus water are the final products, still more vigorous reaction is possible:

$$N_2H_4 + O_2 = N_2 + 2H_2O$$

Slow thermal oxidation[4, 5], oxygenated flames[1] and spark ignition in air[6] have been reported. Experiments have now been made on the spontaneous ignition of pure hydrazine and its mixtures with oxygen[7] and on the propagation of the decomposition flame[8]. This paper deals with the spontaneous ignition of hydrazine-oxygen mixtures.

In work on the complex spontaneous inflammation of the alkyl nitrates, Gray[9-11], used measurements of spontaneous ignition limits to interpret the mechanism of decomposition. Similarly, for the combustion of hydrazine, the conditions of temperature, pressure and composition for the spontaneous ignition may be measured and the influence of the extent and nature of the vessel surface, and the effect of added inert gases may be investigated to supply similar information. An examination of the heterogeneous decomposition of hydrazine, reported by other workers has been made to discover whether it interferes with the explosive oxidation. The extent to which self-heating is able to account quantitatively for the spontaneous ignition in oxidation and in decomposition is discussed.

A second mode of combustion has been observed. In oxygen-rich mixtures, under conditions too mild for explosion, a feeble, delayed ignition

occurs. This delayed ignition has been examined and experiments are described which reproduce it artificially. Since at any instant the composition of the partially reacted m'xture initially containing $N_2H_4 + 2O_2$ lies between the 4 extremes

(1)	$N_2H_4 + 2O_2$	Corresponding to no reaction
(2)	$N_2 + 2H_2O + O_2$	Corresponding to complete oxidation
(3)	$N_2 + 2H_2 + 2O_2$	Corresponding to complete decomposition without oxidation,
(4)	$\frac{1}{3}N_2 + \frac{4}{3}NH_3 + 2O_2$	

experiments with these artificial mixtures may be used to assist in identifying the ignition and to reveal the processes responsible for the induction period.

Experimental

MATERIALS

Concentrated hydrazine, containing approximately 98 per cent N_2H_4 by weight, is dehydrated by refluxing for 2–3 hours over fused caustic soda in an atmosphere of nitrogen at 120–150 mm Hg, followed by distillation under similar conditions. Iodate analysis[12] shows 99.9–100.2 per cent N_2H_4.

Oxygen, nitrogen, hydrogen, argon, and helium are taken from cylinders and dried by freezing out the water at −180°C. Ammonia is obtained by dehydrating the 0.880 solution or from a cylinder.

METHOD

Critical pressure limits of spontaneous ignition are determined by measuring the total pressure of the mixture necessary for ignition on admission to a hot vessel. The apparatus used is described by Gray[11]. The reaction vessel is maintained at a steady, uniform temperature in a furnace. A window in the side of the furnace permits the whole length of the vessel to be observed. Two cylindrical Pyrex reaction vessels are used; one 4.6 cm internal diameter, 420 cm^3 volume, 405 cm^2 surface area, the other 2.6 cm internal diameter, 140 cm^3 volume, 220 cm^2 surface area. They are cleaned with hot nitric acid and washed with distilled water before use. The vacuum line and mixing vessels are heated electrically to prevent condensation of hydrazine. The apparatus may also be used to follow changes of pressure in a reacting system, although it is not suitable for accurate determination of rate constants because the dead space is not negligible.

Results

HETEROGENEOUS DECOMPOSITION OF PURE HYDRAZINE

It is necessary to determine whether heterogeneous decomposition is likely to interfere in later experiments.

Values for the half life of the heterogeneous decomposition have been obtained under conditions similar to the ignition experiments. Known initial pressures of hydrazine vapor are admitted to the reaction vessel and isolated. After a measured interval the pressure is measured. The results show a wide scatter. The half lives were always much greater than the induction periods before explosion: at 420°C 11 min; at 492°C 1 min; at 536°C 30 secs. The products of the decomposition were analyzed for ammonia and hydrogen; nitrogen was determined by difference. The results are shown in Table 1. The satisfactory element balances show the accuracy of the analyses. Product analyses and measured pressure increases during reaction are in accord.

Table 1. Products of Heterogeneous Decomposition of Pure Hydrazine at a Pyrex Surface

Initial pressure 17.5 mm Hg

Temperature	Decomposition time	Composition			Element balance, H/N ratio
		H_2	NH_3	N_2	
°C	min	per cent	per cent	per cent	
478	35	5.9	72.8	21.3	1.99
536	29	11.0	67.0	22.0	2.01
536	34	10.9	66.5	22.6	1.98

THE DELAYED IGNITION OF HYDRAZINE-OXYGEN

This new mode of ignition was first observed during measurements of the explosion limits at 536°C. In mixtures containing more oxygen than the stoichiometric proportion ($1N_2H_4:1O_2$), at pressures below the limit for the bright explosion (see Figure 1), a yellowish glow appears after 5–10 sec. This is much less intense than, and quite distinct from, the explosion. In mixtures containing 5–20 per cent hydrazine, this distinction is rather less marked, but rarely presents any difficulty. For these mixtures, the delayed ignition,

like the explosion, is itself less intense and more blue in color. The delayed ignition cannot be found in mixtures containing more than 50 per cent hydrazine.

TABLE 2. COMPOSITION OF GASEOUS PRODUCTS BEFORE AND AFTER DELAYED IGNITION

Original composition $N_2H_4 + 2O_2$

	H_2	NH_3	N_2	O_2
	per cent	*per cent*	*per cent*	*per cent*
Before ignition	18.3	13.1	32.5	36.1
Before igintion	19.0	12.5	29.8	38.7
After ignition	1.6	12.8	44.7	40.9

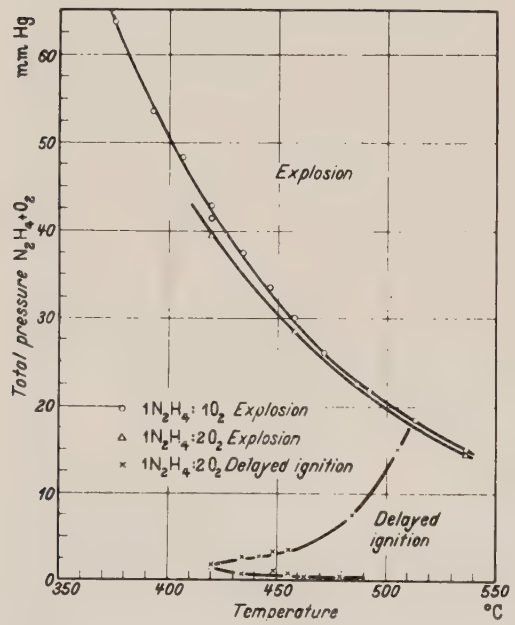

FIG. 1. Spontaneous explosion and delayed ignition of hydrazine-oxygen mixtures. Dependence of pressure limits on temperature. ○ $1N_2H_4 + 1O_2$, explosion; △ $1N_2H_4 + 2O_2$, explosion; × $1N_2H_4 + 2O_2$, delayed ignition.

Pressure changes during delayed ignition

The pressure change accompanying the delayed ignition in $N_2H_4 + 2O_2$ was followed on a glass Bourdon gauge. After the mixture is admitted to the vessel, reaction causes a gradual increase to an apparently steady value. Then ignition occurs and there is a sudden drop in pressure of 3.5 per cent.

By 536°C, although the process is too rapid to follow continuously, the fall in pressure on ignition is again 3.5 per cent.

Chemical changes during delayed ignition

It was decided to attempt analyses of the mixture immediately before and after the ignition. At high temperatures where appeciable pressures could be used, the induction period was too short to permit sampling. Hence the temperature chosen was 478°C, with an induction period of about 80 sec, although the initial pressure was only 3 mm Hg. The products were expanded into a cold vessel, dried over caustic soda or calcium oxide, and ana'yzed for hydrogen, ammonia, oxygen and nitrogen. Table 2 shows these results. The analyses show a striking decrease in the hydrogen present after ignition has occurred.

Conditions for occurrence of delayed ignition

Upper and lower pressure limits for the delayed ignition exist. They are not easy to measure because of the feeble illumination and they are sensitive to the treatment of the vessel surface. The range of conditions (pressure and temperature) for the delayed ignition of $1N_2H_4 + 2O_2$ (4.6 cm Pyrex vessel) are shown in Figure 1. They lie, on the pressure temperature diagram, in a promontory running out from the explosion area to 420°C. From 420°C, along the lower limit, induction periods lengthen; along the upper limit they decrease as the pressure rises until at about 510°C the spontaneous explosion limit is reached. The induction periods throughout the delayed ignition region, like the pressure limits of the process, are somewhat variable, but at a given temperature, between the upper and lower limit they appear to pass through a minimum.

In the 2.6 cm diameter Pyrex vessel at 536°C, the delayed ignition in a mixture $N_2H_4 + 2O_2$ is not seen at a pressure of 18.2 mm, but appears at pressures of 9.0, 5.1 and 2.3 mm; it is less intense than in the 4.6 cm vessel. In a silica vessel, and in the small vessel coated with KCl the delayed ignition is not found.

Delayed ignition and artificial mixtures

The following mixtures were prepared:

(1) $N_2H_4 + 2O_2$ — corresponding to no reaction

(2) $N_2 + 2H_2 + 2O_2$ — corresponding to complete decomposition but no oxidation

(3) $\frac{1}{3}N_2 + \frac{4}{3}NH_3 + 2O_2$ — corresponding to complete decomposition but no oxidation

(4) $N_2 + 2H_2O + O_2$ — corresponding to complete oxidation.

The composition of any partially reacted system initially containing $N_2H_4 + 2O_2$ may be simulated by an appropriate combination of these mixtures.

Preliminary experiments at 536°C showed that while no ignition is obtained with the ammonia mixture C alone, an immediate bright flash is seen when the hydrogen mixture B is admitted to the hot vessel. This result, the 3.5 per cent pressure fall in ignition, and the analyses confirm that the delayed ignition involves the oxidation of hydrogen, present to the extent of about 9 per cent in the reacting mixture.

Table 3. Delayed Ignition of Hydrazine + Oxygen Simulated by Artificial Mixtures

A = $N_2H_4 + 2O_2$; B = $N_2 + 2H_2 + 2O_2$; C = $\frac{1}{3} N_2 + \frac{4}{3} NH_3 + 2O_2$; D = $N_2 + 2H_2O + O_2$

Mixture no.	Composition, per cent				Observation	Induction period	Comments
	A	B	C	D			
						sec	
1	100	—	—	—	Delayed ignition	9	I.e. original mixture. Pressure fall 0.3 mm
2	—	15	—	85	Immediate ignition	0	Intensity and pressure fall similar to (1)
3	—	15	4	81	Immediate ignition	0	Intensity and pressure fall similar to (1)
4	—	15	7	78	—	—	Immediate ignition *below* an upper pressure limit
5	—	15	15	70	—	—	Slow fall in pressure only
6	85	15	—	—	Delayed ignition	7	Pressure fall 0.5 mm; ignition more intense than (1)
7	93	—	7	—	—	—	Pressure rises slowly then falls by 0.3 mm
8	91	—	9	—	—	—	Delayed ignition below an upper pressure limit

Various combinations of these mixtures A, B, C and D have been examined, and their behavior is presented in tabular form in Table 3. The principles on which combinations 2 through 6 have been chosen is the need for an artificial mixture to contain the same amount of hydrogen before ignition as did the original mixture; its percentage composition may be specified in terms of the equivalent amount of A required to produce the amounts of B, C and D actually present. It is found that, though added ammonia may narrow the range of conditions under which the hydrogen-oxygen ignition occurs (mixtures 3, 4, 5) and may suppress the delayed ignition of hydrazine itself (mixtures 7, 8), it never introduces an induction period. Induction periods before ignition are not found in systems from which hydrazine is absent (mixtures 2, 3). When hydrazine is present (mixtures 1, 6, 8) ignition is delayed.

THE EXPLOSIVE COMBUSTION OF OXYGEN-HYDRAZINE MIXTURES

Induction periods of about 1 sec separated the admission of the mixtures and audible explosion. Explosion limits were readily reproducible at low pressures.

Effect of temperature on explosive combustion

The explosion of the stoichiometric mixture was examined from 370–450°C. Figure 1 shows the variation of the limiting total pressure with temperature for this mixture and for $N_2H_4 + 2O_2$. After the explosive combustion of the stoichiometric mixture the measured pressure increase is about 53 per cent, indicating complete oxidation:

$$N_2H_4 + O_2 = N_2 + 2H_2O$$

Effect of extent and nature of surface on explosive combustion

Alteration of the extent and nature of the vessel surface affects the explosion limit. Explosion is more difficult in the smaller vessel where the surface/volume ratio is greater. When the surface of the smaller vessel is coated with KCl, the explosion limit is further increased slightly. Both

these effects in the $1N_2H_4 + 1O_2$ mixture are shown in Figure 2.

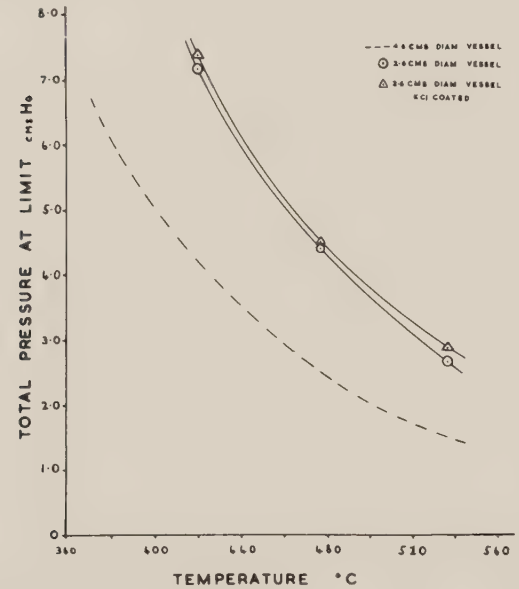

FIG. 2. Spontaneous explosion of $1N_2H_4 + 1O_2$. Influence of extent and nature of vessel surface. ----- 4.6 cm vessel, clean Pyrex; ⊙ 2.6 cm vessel, cean Pyrex; △ 2.6 cm vessel, KCl.

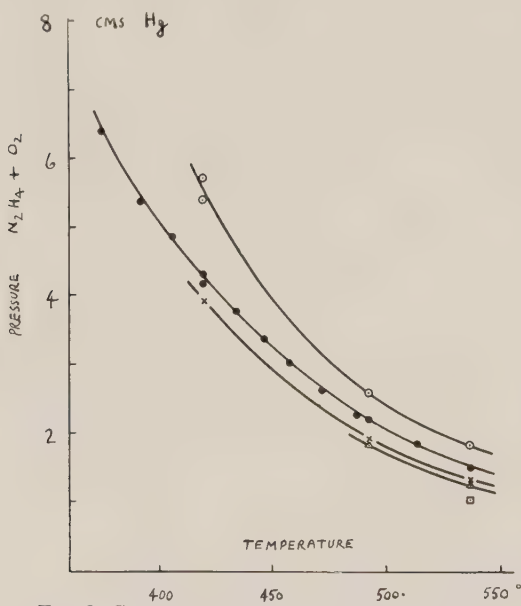

FIG. 3. Spontaneous explosion of $1N_2H_4 + 1O_2$. Influence of inert gases. ● $1N_2H_4 + 1O_2$; △ $1N_2H_4 + 1O_2 + 2A$; ⊙ $1N_2H_4 + 1O_2 + 2He$; X $1N_2H_4 + 1O_2 + 2N_2$; ⊡ $1N_2H_4 + 1O_2 + 10N_2$.

Effect of added inert gases on explosive combustion

The addition of inert gases also alters the explosion limit. Figure 3 shows the variation with temperature of the explosion limit for mixtures of the composition $N_2H_4 + O_2 + 2X$ where X is He, A, N_2. Argon and nitrogen aid the explosion, even in 5-fold diluted mixtures, e.g., $(N_2H_4 + O_2 + 10N_2)$, the explosion limit is reduced by 20 per cent. Helium makes explosion more difficult.

Effect of oxygen-hydrazine ratio on explosive combustion

Oxygen-rich mixtures are somewhat more readily ignited than the stoichiometric; the color of the explosion was bright yellow in hydrazine-

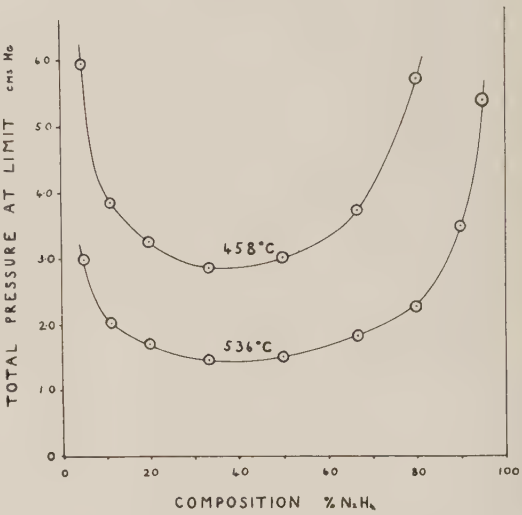

FIG. 4. Spontaneous explosion of hydrazine-oxygen mixtures. Dependence of pressure limit on composition.

rich mixtures and blue in the oxygen-rich case. Figure 4 shows the variation with composition of the pressure limit of spontaneous ignition at 458° and 536°C.

Artificial mixtures and explosive combustion

In contrast to their marked effects on the delayed ignition small additions of the hydrogen and ammonia mixtures B, and C produced little change in the pressure limit for the bright explosion. The critical pressure limit $P(N_2H_4 + 2O_2)$ in a mixture 91 per cent $(N_2H_4 + 2O_2) + 9$ per cent B and 14.8 mm; in a mixture 91 per cent $(N_2H_4 + 2O_2) + 9$ per cent C it was 13.8 mm. The differences between these figures and the value of 14.6 mm for the unadulterated $(N_2H_4 + 2O_2)$ mixture are small.

EXPLOSIVE DECOMPOSITION OF PURE HYDRAZINE

The use of a silica vessel extends the temperature range above 550°C. The spontaneous ignition in decomposition of pure gaseous hydrazine is seen as a bright yellow flash. The pressures required are approximately 80 mm at 620°C and 10 mm at 720°C: the induction periods were too short to measure.

Discussion

Despite its apparent simplicity, hydrazine can behave in a variety of different ways. The experiments fall into two groups; decomposition processes and oxidation or combustion processes.

DECOMPOSITION PROCESSES

All decomposition processes must lie between the two extremes

$$N_2H_4 = N_2 + 2H_2$$

$$N_2H_4 = \tfrac{1}{3}N_2 + \tfrac{4}{3}NH_3$$

and correspondingly the enthalpy change of any observed mode of decomposition lies between 22,750 cal and 37,470 cal.

Heterogeneous decomposition of pure hydrazine

The heterogeneous decomposition of pure hydrazine has been reported by various workers[13, 14, 15]. Its rate is markedly sensitive to the treatment of the surface; the reaction appears not to involve free radicals[15, 16]. On a Pyrex glass surface we find the proportion of hydrogen produced increases as the temperature rises; the overall equations for decomposition may be written

At 478°C: $N_2H_4 = 0.37\ N_2 + 0.10\ H_2 + 1.26\ NH_3$

At 536°C: $N_2H_4 = 0.40\ N_2 + 0.20\ H_2 + 1.20\ NH_3$

It is interesting to note that these analyses show that more hydrogen is formed from decomposition at a glass surface than at silica[13].

Spontaneous ignition of pure hydrazine

It is interesting to compare the predictions of the simple theory of thermal explosions developed by Frank-Kamenetzky[17] with the observed result that pure hydrazine is able to undergo spontaneous ignition under the experimental conditions. The familiar expesssion for critical conditions

$$\frac{Q}{\sigma}\frac{E}{RT_0^2}r^2w = \delta$$

leads in this instance to

$$p(\text{mm Hg}) = 10^{-21}\,T^3 \exp(30000/T)$$

where Q = exothermicity of reaction
E = activation energy
r = radius of cylindrical vessel
w = speed of reaction per unit volume
δ = 2.00 for a cylinder
σ = thermal conductivity of reactant
R = gas constant
$T_0 = T$ = temperature of vessel (°K)
p = critical explosion pressure in mm Hg

Thus, theory suggests that hydrazine at a pressure of 80 mm will require a temperature of 660°C for explosion; and at a pressure of 10 mm will require a temperature of 720°C. The temperatures measured were in fact 620°C and 720°C. If the same theory is employed to estimate minimum induction periods τ the formula below results

$$\tau\ (\text{seconds}) = 5.7 \times 10^{-21}\,T^2 \exp(30{,}000/T)$$

At 720°C this gives $\tau = 0.1$ sec in agreement with the absence of noticeable induction periods.

OXIDATION PROCESSES

Delayed ignition in oxidation

The delayed ignition has been found in a range of reactant compositions from $N_2H_4 + O_2$ to $N_2H_4 + 19O_2$. It is not found in oxygen deficient mixtures and it does not occur at temperatures below 420°C or outside critical upper and lower pressure limits. The induction periods vary from 6 sec at 536°C at the upper limit where delayed ignition passes over into bright explosion, to 320 sec at the tip of the delayed ignition peninsular and 475 sec near the lower pressure limit at 478°C. Analyses made on the samples taken from the reacting mixture confirm the presence during oxidation of decomposition products, hydrogen and ammonia. The observed pressure fall (3.5 per cent) on ignition at 478°C corresponds to a hydrogen consumption of about 10 per cent of the *total* reacting mixture. In accord with this, in the *condensable* fraction of the reactants, the hydrogen content drops from about 18 per cent to less than 2 per cent. These results identify the process responsible for the delayed ignition; it is the oxidation of hydrogen.

The induction periods are too long for the hydrazine decomposition to be neglected. However, even if all the ammonia present (Table 2) comes from the heterogeneous decomposition, the

amount of hydrogen concurrently produced by this mode is less than that actually found (Table 1). Hence, as well as reacting with the oxygen to yield water and nitrogen, the hydrazine must also give rise in the presence of oxygen to more hydrogen than can be explained by its normal heterogeneous decomposition.

The artificial mixtures provide further information. Hydrogen and oxygen explode alone or in the appropriate mixtures with nitrogen immediately on admission to the vessel. The ignition is unaltered in character by added oxidation products (nitrogen or water); the range of explosion (separation of upper and lower pressure limits) is very wide. When the decomposition product, ammonia, is added instead of an oxidation product, the pressure limits of inflammation are affected. The upper limit of spontaneous ignition is decreased although when ignition occurs it is immediate and not delayed. Thus ammonia cannot account for the variable but ever present induction periods. When instead of either decomposition or oxidation products, pure reactants $N_2H_4 + 2O_2$ are added, the effect is striking. The immediate explosion of pure hydrogen and oxygen is replaced by a delayed ignition and hydrazine is revealed as an agent which can delay the hydrogen-oxygen reaction in a way in which ammonia cannot.

Thus, the delayed ignition in hydrazine oxidation is due to the ignition of hydrogen produced in a side reaction. The ignition is inhibited by the hydrazine. Hydrogen accumulates until the hydrazine has gone; when it has gone, ignition occurs.

Explosive combustion in oxidation

The explosive combustion is preceded by induction periods much shorter than the values determined for the half-life of the heterogeneous decomposition; heterogeneous decomposition is therefore unlikely to interfere with explosion. Further, if hydrogen or ammonia from the decomposition were necessary for explosive combustion, added hydrogen or ammonia might be expected to affect the spontaneous explosion limit. This is not found. Thus, it is the primary oxidation reaction of hydrazine which leads to explosion, and not secondary reactions of its decomposition products. This behavior is the same as that of the slow oxidation reported by Bowen and Birley[4]. The pressure increase after the explosion corresponds to the reaction

$$N_2H_4(g) + O_2(g) = N_2(g) + 2H_2O(g)$$
$$\Delta H = -138{,}000 \text{ cal}$$

Murray and Hall[1] suggested that the combustion of hydrazine occurring in the premixed flame was a two stage process: first, decomposition of the hydrazine; then, oxidation of the products. However, from the ease of the homogeneous oxidation relative to the homogeneous decomposition[15], the primary reaction occurring in the premixed flame is more probably the direct oxidation. Murray and Hall's[1] scheme is true of the diffusion flame, where two flame zones corresponding to decomposition and oxidation, respectively, are clearly marked[1, 2].

Bowen and Birley[4] concluded that the slow thermal oxidation was a homogeneous reaction, approximately first order with respect to each component, involving short radical chains and a similar interpretation may be made of the explosion. In hydrazine oxidation there is no abrupt transition to explosion from almost negligibly slow reaction such as occurs, for example, in the branched-chain explosion of hydrogen oxidation. Now, explosion is possible even in the absence of long, branching chains if marked self-heating occurs. The great exothermicity of the oxidation (138 kcal) favors this. The simple theory[17] of thermal explosion assumes that the heat generated by reaction is lost by conduction only. The addition of helium, of high thermal conductivity, raises the pressure limit, showing that self-heating is in fact occurring. The theory of thermal explosion may be applied to hydrazine combustion if it is assumed that (1) The rate of reaction is first order with respect to hydrazine and oxygen; (2) The rate of reaction obeys Arrhenius' law; (3) Heat is lost only by conduction; (4) A negligible amount of reaction occurs in induction period before ignition.

These assumptions lead to a relation between the vessel temperature T and the partial pressures (mm Hg) $P_{N_2H_4}$ and P_{O_2} at the spontaneous ignition limit:

$$\ln P_{N_2H_4} \times P_{O_2}/T^4 = E/(RT) + \ln 2R\sigma/QEkr^2 \quad (1)$$

R is the gas constant, σ the thermal conductivity (cal cm^{-1} sec^{-1} deg^{-1}) of the mixture[18], Q the heat of the reaction, E the activation energy, r the radius of the vessel and k the proportionality

constant in the equation:

$$\text{Rate of reaction (moles cc}^{-1}\text{ sec}^{-1}) = k(P_{N_2H_4}P_{O_2}/T^2)\exp(-E/RT)$$

In this thermal theory all the magnitudes are in principle experimental quantities; here, thermal conductivities of 2- and 3-component mixtures have been calculated[18].

From equation (1) two deductions may be made:

(*1*) *Effect of inert gases: constant temperature and hydrazine/oxygen ratio.* If $P = P_{N_2H_4} + P_{O_2}$, the equation (1) may be written

$$\ln P/T^2 = B + E/2RT + \tfrac{1}{2}\ln 2\sigma R/QEkY^2 \quad (2)$$

where B depends only on the hydrazine-oxygen ratio ($P_{N_2H_4}/P_{O_2}$). Hence with a given proportion of hydrazine to oxygen $P/\sigma^{1/2}$ should be constant for the addition of an inert gas. This is very closely true. At 492°C for example $P/\sigma^{1/2}$ takes the values:

No inert gas added	1.84×10^3
Helium added	1.76×10^3
Nitrogen added	1.66×10^3
Argon added	1.72×10^3

(*2*) *Effect of hydrazine/oxygen ratio: constant temperature.* From equation (1), at constant temperature $(P_{N_2H_4} \times P_{O_2})/\sigma$ should be constant. However, it varies somewhat; at 458°C from 1.3×10^6 to 3.6×10^6; at 536°C from 0.29×10^6 to 0.83×10^6.

The thermal theory is thus reasonably satisfactory and is able to explain the influence of added inert gases on explosion. Much remains to be done before a detailed kinetic interpretation can be successful. The sensitiveness of ignition to the nature of the surface indicates the presence of free radicals and their presence may be the cause of such discrepancies from the simple thermal theory as the superior explosiveness of oxygen-rich mixtures.

Acknowledgments

We thank Professor T. R. C. Fox of Cambridge for his interest in this work. We are also grateful to the Royal Society for a Research Grant for equipment and to Dr. F. P. Bowden, F.R.S. for a generous gift of apparatus.

REFERENCES

1. Murray, R. C., and Hall, A. R.: Trans. Faraday Soc., *47*, 743 (1951).
2. Adams, G. K., and Stocks, G. W.: *Fourth Symposium on Combustion*, p. 239. Baltimore, The Williams & Wilkins Co., 1953.
3. Bamford, C. H.: Trans. Faraday Soc., *35*, 1239 (1939).
4. Bowen, E. J., and Birley, A. W.: Trans. Faraday Soc., *47*, 580 (1951).
5. Winning, I. H.: J. Chem. Soc., 926 (1954).
6. Scott, F. E., Burns, J. J., and Lewis, B.: U. S. Bur. Mines R. I., 4460, (1949). ,
7. Gray, P., and Lee, J. C.: Research, *7*, S2 (1954).
8. Gray, P., and Kay, J. C.: Unpublished (1954).
9. Gray, P., and Yoffe, A. D.: Proc. Roy. Soc., *A200*, 114 (1949).
10. Gray, P., and Yoffe, A. D.: J. Chem. Soc., 3180 (1950).
11. Gray, P.: Proc. Roy. Soc., *A221*, 462 (1954).
12. Penneman, R. A., and Audrieth, L. F.: Ind. & Eng. Chem. (Anal.), 20, 1058 (1948).
13. Hanratty, T. J., Pattison, J. N., Clegg, J. W., and Lemmon, A. W.: Ind. & Eng. Chem., *43*, 1113 (1951).
14. Askey, P. J.: J. Am. Chem. Soc., *52*, 970 (1930).
15. Szwarc, M.: Proc. Roy. Soc., *A198*, 267 (1949).
16. Birse, E., and Melville, H. W.: Proc. Roy. Soc., *A175*, 164 (1940).
17. Frank-Kamenetzky, D. A.: Acta Physicochim. (U.R.S.S.), *10*, 365 (1939).
18. Lee, J. C.: Unpublished (1954).

Discussion by Cyrus G. Dunkle*

It was said that (delayed) ignition takes place when the hydrazine content reaches zero. Must it really reach zero, or just decrease to a small critical value?

Peter Gray:

Our experiments show that it is the presence of hydrazine which gives rise to the induction period and we suppose that delayed ignition occurs when there is not enough hydrazine left to prevent the hydrogen-oxygen explosion any longer. That is to say, we assume that the hydrazine content decreases to a critical value. Now, the induction periods are so long that heterogeneous decomposition alone could account for the disappearance of almost all the hydrazine, so the critical value is very small.

Authors' Reply

In reply to a question by Professor Pannetier, we ensured that no difficulties were arising from

* Picatinny Arsenal, Dover, New Jersey.

inadequate mixing by admitting the constituents of a reactant mixture to the mixing vessel in different orders, e.g., sometimes hydrazine first, sometimes oxygen first. We were able to obtain with a mixture of given proportions an explosion limit quite independent of the method of mixing and felt safe, therefore, in assuming that mixing was perfectly satisfactory.

78

SENSITIZED IGNITIONS IN MIXTURES OF HYDROGEN AND CHLORINE

By P. G. ASHMORE

Introduction

It is generally accepted that the thermal reaction between hydrogen and chlorine, like the photochemical, proceeds by a non-branching chain mechanism. Above 300°C, the reaction is sufficiently rapid for inflammation to occur with reactant pressures less than one atmosphere[1]. There is a minimum pressure (P) for ignition at each temperature (T), and P increases as T decreases; the locus of the points gives a lower ignition boundary such as ZZ' in Figure 1. This boundary can be expressed by the equation $\ln (P/T) = A/T + B$ where B varies with the vessel diameter and the proportions of the reactants used, but A is independent of these factors. This kind of relation is often found for thermal explosions, and in agreement with this, the rate of reaction between hydrogen and chlorine is appreciable some distance below the boundary, and increases steadily as the boundary is approached. Above the boundary, combination is complete during the hot, bright ignition which occurs as the premixed gases flow into the reaction vessel.

In the presence of small percentages of certain substances, the ignition boundary takes quite different shapes. Some of these are shown in Figure 1. Nitrogen trichloride, long recognized[2] as an inhibitor of the photochemical reaction between hydrogen and chlorine, actually produces[3] a low temperature, low pressure ignition peninsula Y. Chloropicrin produces[4] an ignition region X similar in shape to the region of cool flames observed during many oxidations, with an upper temperature boundary. One of the decomposition products of chloropicrin, nitrosyl chloride, twists the normal ignition boundary ZZ' into position WW', while its own decomposition product, nitric oxide, moves[5] the boundary to VV'. In each case it seems that the parent substance and any decomposition products play some part in controlling the chlorine atom concentration, which in turn regulates the rate of formation of hydrogen chloride by the familiar reactions.

$$Cl + H_2 \rightarrow HCl + H \qquad (1)$$

$$H + Cl_2 \rightarrow HCl + Cl \qquad (2)$$

Within each of the ignition regions, the combination of the hydrogen and chlorine is complete. The phenomena observed just outside the regions differ widely, however, and throw light on the reactions which lead to ignition; in particular, they give information about the mechanism of the thermal decomposition of each added substance. These decompositions proceed according to the stoichiometric equations.

$$CCl_3NO_2 \rightarrow NOCl + COCl_2 \qquad (3)$$

$$2NOCl \rightarrow 2NO + Cl_2 \qquad (4)$$

$$2NCl_3 \rightarrow N_2 + 3Cl_2 \qquad (5)$$

This review summarizes the information which has been obtained from studies of these ignition boundaries and of the reactions just outside them. It is hoped that the review will draw attention to the fact that marked sensitization of ignitions can occur even when the main reaction proceeds by a non-branching chain mechanism, and emphasize that it is not always necessary to invoke branched chain mechanisms to account for ignitions at comparatively low temperatures.

The Ignitions in the Presence of Nitrosyl Chloride and Nitric Oxide

It will be convenient to indicate first the principal facts emerging from the investigations[4, 5, 6]

of the system containing hydrogen, chlorine, nitric oxide, and nitrosyl chloride.

(1) The delineation of the ignition boundaries showed that the nitrosyl chloride slightly lowers the boundary of ignition below 390°C, but slightly raises it above 390°C. There is a short induction period before ignition, and with increasing initial concentration of nitrosyl chloride the ignition boundary rapidly becomes independent of the nitrosyl chloride concentration. In contrast, nitric oxide lowers the boundary considerably at all temperatures; ignitions occur immediately the premixed gases enter the reaction vessel; the boundary falls as the concentration of nitric oxide is increased, but eventually rises again due to the formation of nitrosyl chloride in the mixing vessel at a rate proportional to p_{NO}^2.

(2) Measurements of the rate of formation of hydrogen chloride below the ignition region show that there is a real induction period in which virtually no hydrogen chloride is formed, then a rapid acceleration to a maximum rate which proves to be independent of the concentration of nitrosyl chloride used, but less than the initial rate in the absence of nitrosyl chloride. The induction periods can be considerably shortened by adding nitric oxide, and then the maximum rate of reaction is substantially increased.

(3) Measurement of the rate of decomposition of nitrosyl chloride in the presence of the hydrogen and chlorine shows that it is extensively decomposed during the induction period. The rate is much faster than would be predicted from the accurate work of Waddington and Tolman at lower temperatures, and points to a mode of decomposition additional to the bimolecular process (4). The initial rate of decomposition is increased by the presence of chlorine, in spite of the opposing back reaction

$$2NO + Cl_2 \rightarrow 2NOCl.$$

These facts can best be explained as follows. While nitrosyl chloride is present, the chlorine atom concentration is reduced by the well-established reaction

$$Cl + NOCl \rightarrow NO + Cl_2 \qquad (6)$$

The rate of formation of hydrogen chloride is therefore low, depending as it does on reaction (1) followed by (2). As the nitrosyl chloride decomposes thermally, the chlorine atom concentration is increased because reaction (6) becomes slower, and also because the back reaction becomes increasingly important as an initiating mechanism

$$NO + Cl_2 \rightarrow NOCl + Cl \qquad (7)$$

It is this initiating mechanism which causes the rate of formation of hydrogen chloride to increase more than twenty-fold when the concentration of nitrosyl chloride has halved, and which causes the increased rate upon addition of nitric oxide.

The usual stationary state treatment, applied to this system of reactions, leads to an expression for the rate of reaction

$$\frac{d[HCl]}{dt} = \frac{2k_7k_1[NO]}{k_6[NOCl]}[H_2][Cl_2]$$

This fitted the results well at 250°C, and because

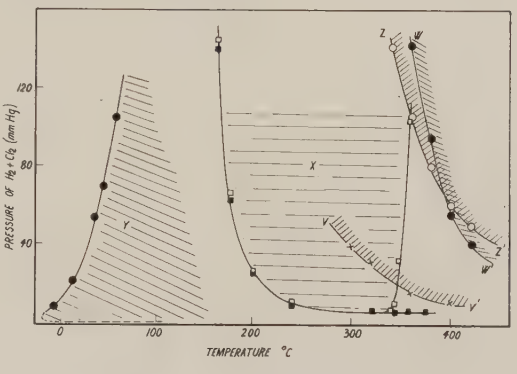

FIG. 1. Regions of ignition for equimolar $H_2 + Cl_2$. (a) alone, above ZZ'. (b) with 0.5 mm NOCl, above WW'. (c) with 0.5 mm NO, above VV'. (d) with 0.5 mm CCl_3NO_2, within X. Short entry tube; □ long entry tube. (e) with 0.5% $NaCl_3$, within Y.

the ratio k_7/k_6 is the equilibrium constant of the reversible reaction

$$NO + Cl_2 \rightleftharpoons NOCl + Cl$$

it can readily be calculated from known equilibrium data. Hence a value for the velocity constant k_1 can be calculated. At 250°C it is $(4.8 \pm 0.4) \times 10^8$ 1 mole^{-1} sec^{-1}. A combination of this value with those of other investigators at about 25°C and at about 727°C gives an activation energy of 5500 ± 200 cal for reaction (1).

At higher temperatures, other initiating reactions must be allowed for. In particular, the reactions

$$NOCl \rightarrow NO + Cl \qquad (8)$$

$$Cl_2 \rightarrow Cl + Cl \qquad (9)$$

whose precise site is not yet established, probably

become important around 300°C. The first of these provides, with reaction (6), an alternative mode of decomposition of nitrosyl chloride. It has a higher activation energy ($\geq$ 38 kcal for the gas phase dissociation) than that of the bimolecular process $2NOCl \rightarrow 2NO + Cl_2$ (24 kcal) so that its relative importance will increase rapidly with increasing temperature, and calculations[6] show that it is quite capable of accounting for the enhanced rate of decomposition of nitrosyl chloride mentioned in paragraph (3) above. Similar calculations show that the effect of chlorine in increasing the rate of decomposition of nitrosyl chloride can be accounted for by reaction (9) followed by reaction (6). It appears that further work on these enhanced rates of decomposition might give information about the site of the reactions (8) and (9) and about their velocity constants.

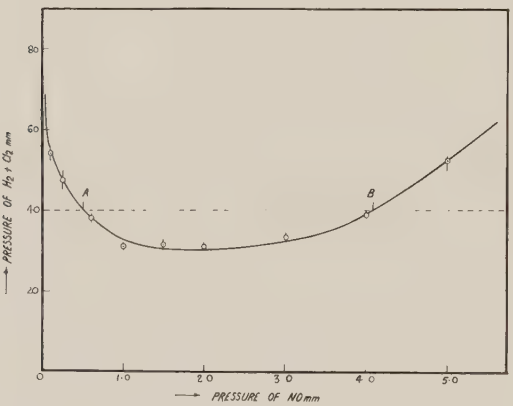

FIG. 2. Lower boundary of ignition of 300°C, for various pressures of NO. With 40 mm of reactants, A would be a lower and B an upper sensitizer limit of ignition.

The expression for the rate of reaction also successfully predicts that the maximum rate will be independent of the initial pressure of nitrosyl chloride. For the value of the ratio [NO]/[NOCl] rapidly approaches the equilibrium value, which in the presence of excess chlorine is nearly independent of the initial pressure of nitrosyl chloride. Now the ignitions are almost certainly thermal in origin and occur when the rate of reaction exceeds some critical value; because the maximum rate with nitrosyl chloride present is less than the initial rate of reaction of pure hydrogen-chlorine mixtures, it will be necessary to go to higher pressures to achieve ignition in the presence of nitrosyl chloride. Thus the limit of ignition is raised by nitrosyl chloride, and because the maximum rate is independent of the initial nitrosyl chloride concentration, the limit of ignition similarly becomes independent of the nitrosyl chloride concentration. The induction period is the time taken to reach the maximum rate. The principal experimental results at temperatures below the crossover point of the curves ZZ' and WW' can thus be explained by the mechanism proposed.

It seems likely that, at temperatures near the crossover, reaction (8) is becoming more important as an initiating reaction than is (4) followed by (7). If, however, reaction (6) remains the predominant chain terminating reaction, the maximum rate of reaction and hence the limit of ignition would remain independent of the nitrosyl chloride concentration, as observed experimentally.

One experimental observation[7] deserves further emphasis. In paragraph (1) above it was mentioned that when mixtures of nitric oxide, chlorine, and hydrogen are made up, allowed to mix, and admitted to the reaction vessel, the pressure required for ignition at a fixed temperature decreases as the nitric oxide is increased, up to a point. When the concentration gets above a certain value, which depends upon the time of mixing, the rate of formation of nitrosyl chloride ($2NO + Cl_2 \rightarrow 2NOCl$) is fast enough to give sufficient nitrosyl chloride to inhibit the reaction. Hence above this particular concentration of nitric oxide, the limit rises again. Therefore, by working at a fixed temperature, with a fixed total pressure of chlorine and hydrogen, and increasing the concentration of nitric oxide, a lower and an upper sensitizer limit of ignition can be obtained (for example at A and B in Figure 2) in a system which almost certainly does not involve branching chains. Here the double action of the sensitizer—sensitization at low concentration and inhibition at higher—is clearly due to reactions involving the disappearance of one chemical and the formation of another.

The Ignitions in the Presence of Chloropicrin

Since chloropicrin decomposes so readily[8] to yield nitrosyl chloride, it might be expected to inhibit the hydrogen-chlorine reaction. However, a study[9] of the effect of chloropicrin upon the ignition of hydrogen and oxygen mixtures had suggested that a copious supply of chlorine atoms

was produced at an early stage of the decomposition. This supposition received considerable support from the experimental observation that small quantities of chloropicrin lower the ignition boundary of hydrogen and chlorine by over 200°C. The boundary of the region X (Fig. 1) on the low temperature side is clear and reproducible, and independent of the way the premixed gases flow into the vessel, for it occurs a few seconds after admission. Above 300°C, however, ignitions occur as the gases flow into the vessel, and some extraord nary effects of the flow were observed. These effects can be summarized as follows:

(1) The boundary remains very low at temperatures above 320°C if the narrow entry tube is short (full squares in Figure 1). It rises steeply, however, if there is a long entry tube inside the furnace, especially if the flow is delayed by a capillary constriction (open squares in Figure 1).

(2) This high temperature boundary is raised if the concentration of the chloropicrin is increased.

(3) With a long heated entry tube, there is a remarkable backfire phenomenon observed at pressures just below the boundary of ignition in the region of 360°C. Here, a flame begins in the entry tube and propagates back into the cold mixing vessel, but not into the hot reaction vessel. It is evident that some substance formed by the decomposition of the chloropicrin during the brief time of flow through the heated entry tube inhibits the ignition. All the evidence points to nitrosyl chloride as the inhibitor, and deliberate addition of nitrosyl chloride does in fact wipe out the region of ignition X.

It was inferred from these effects that there is an atom or radical, capable of initiating the hydrogen-chlorine chains, produced early in the decomposition of the chloropicrin, and that the nitrosyl chloride produced in parallel removes this atom. In all probability it is a chlorine atom, produced in one step from the chloropicrin

$$CCl_3NO_2 \rightarrow NO + Cl + COCl_2 \qquad (10)$$

The nitrosyl chloride produced in a parallel reaction

$$CCl_3NO_2 \rightarrow NOCl + COCl_2 \qquad (11)$$

then removes the chlorine atom by the familiar reaction

$$Cl + NOCl \rightarrow NO + Cl_2 \qquad (6)$$

This means that the equilibrium $NOCl \rightleftharpoons NO + \frac{1}{2}Cl_2$ is very rapidly established in the decomposition of chloropicrin, as was observed by Smith and Steacie.[8] The detailed analysis suggests that a further reaction

$$Cl + CCl_3NO_2 \rightarrow NO + Cl_2 + COCl_2 \qquad (12)$$

ought to be considered, but that the striking effect of nitrosyl chloride in eliminating the ignition region X showed that reaction (12) was slow compared with (6).

This set of reactions makes an interesting kinetic scheme[10]. It leads to equations which have been solved numerically to show how the relative value of the chlorine atom concentration varies with time at different temperatures with different initial pressures of chloropicrin. The chlorine atom concentration passes through a maximum value, which at temperatures above 340°C is reached within one msec. It occurs earlier, and is greater in magnitude, the higher the chloropicrin pressure at a given temperature, or the higher the temperature for a fixed concentration of chloropicrin (Fig. 3).

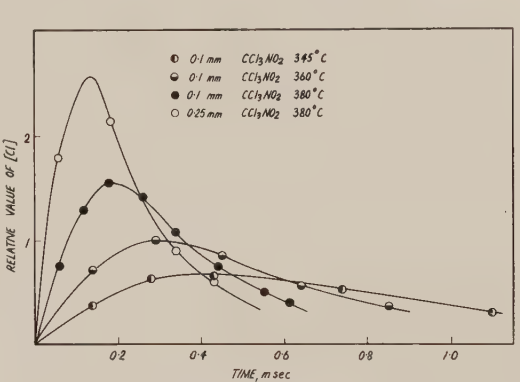

FIG. 3. Relative values of chlorine atom concentration during the decomposition of chloropicrin.

These conclusions are in complete agreement with the experimental observations. With a short entry tube, the gases reach the vessel before the maximum chlorine atom concentration is passed, and ignition occurs. With a long entry tube, the maximum is reached in the narrow entry tube, where, (as observed by Sagulin[1]) a much higher pressure of gases would be required for ignition; by the time the gases reach the vessel, the chlorine atom concentration has sunk to a low value, so that ignition occurs only with higher reactant pressures; moreover, as Figure 3 shows, the atom concentration in the later stages is lower the higher the temperature, so that the ignition boundary must rise with temperature. Evidently,

when the backfire phenomenon is observed, conditions are ripe for explosion in the entry tube, but the increasing nitrosyl chloride concentration nearer the reaction vessel prevents the flame propagating towards it. In the mixing vessel, however, there is no nitrosyl chloride to prevent the flame from striking back, and it is probably assisted by the early stages of the decomposition of the chloropicrin just ahead of the flame front.

The Ignitions in the Presence of Nitrogen Trichloride

Although traces of nitrogen trichloride are known to inhibit the photochemical reaction between hydrogen and chlorine at about atmospheric pressures, at sufficiently low total pressures they can cause explosive combinations of those reactants[3]. The ignitions are preceded by an induction period. The region of pressure and temperature in which they occur (Y in Figure 1) is quite different in shape from those regions which have just been discussed. This is because the decomposition of chloropicrin and of nitrosyl chloride, though fast under the conditions of the experiments, are not explosive; the ignition regions are extensions or contractions of the primary region bounded by ZZ'; and the reactions introduced are simple initiating or terminating reactions for the primary chains. On the other hand, nitrogen trichloride vapor decomposes spontaneously at room temperature, and under certain conditions this decomposition is explosive[11]. Explosions occur when the total pressure falls below an upper limit, the value of which depends upon the precise gases present. Thus, the upper limit can be made up almost entirely of nitrogen, or other inert gas. If a mixture is made up of hydrogen, chlorine, and a trace of nitrogen trichloride, at a pressure below the appropriate upper limit, the explosive decomposition of the nitrogen trichloride acts as a detonator for the hydrogen-chlorine reaction; hence such mixtures ignite after an induction period which may last several minutes.

The principal results of a comparison of the system hydrogen, chlorine, and nitrogen trichloride, with the system nitrogen, chlorine, and nitrogen trichloride, have been reported[3]. The upper limits of explosion vary with temperature in a similar manner, and each is independent of the pressure of nitrogen trichloride when this is between 0.1 and 2 per cent of the total. The induction periods increase rapidly with increasing pressure at a fixed temperature, in each system. Above the upper limit, the rate of decomposition of the nitrogen trichloride follows an S-shaped curve, and it seems that the induction period before explosion in each system is the time taken for the rate to reach its maximum value. Above the limit, there appears to be very little combination of the hydrogen and chlorine, whereas below it, combination is complete. The addition of a trace of nitrosyl chloride eliminates the explosions in each system.

These results can be explained in terms of a branched chain decomposition of the nitrosyl trichloride, which causes a rapid multiplication of some chain center for the hydrogen-chlorine chains. A reaction scheme was proposed by Griffiths and Norrish[2] which accounted very satsifactorily for the results of the chlorine-photosensitized decomposition of nitrogen trichloride, and this scheme can be modified to allow for the branching which becomes important at low pressures. In the thermal decomposition, the initiating reaction may be

$$NCl_3 \rightarrow NCl_2 + Cl \qquad (13)$$

and this will be followed by the propagating steps

$$Cl + NCl_3 \rightarrow NCl_2 + Cl_2 \qquad (14)$$

$$NCl_2 + NCl_3 \rightarrow N_2 + 2Cl_2 + Cl \qquad (15)$$

The second step is highly exothermic, and might occasionally take the course

$$NCl_2 + NCl_3 \rightarrow N_2 + Cl_2 + 3Cl \qquad (16)$$

The terminating step proposed by Griffiths and Norrish[2] was

$$M + NCl_3 + Cl \rightarrow NCl_4 + M \text{ (end chains)} \qquad (17)$$

The competition between the branching step (16) and the terminating step (17) leads to an upper limit P_U given by the expression

$$P_U(k'_{17}f'_{17} + k''_{17}f''_{17} + \cdots) = k_{16}\frac{k_{14}}{k_{15}}$$

where f', etc., are the mole fractions of the gases present and k', etc., are the corresponding constants for the terminating reaction (17). This scheme suggests that the upper limit will vary with the composition of the gas mixture, but will be independent of the pressure of nitrogen trichloride provided that this pressure is not high enough to make a significant contribution to the term within the bracket. The experimental results are in keeping with these suggestions, but it is

possible that other intermediates could successfully explain these results. It would appear that there is room for further work in identifying the true intermediates.

Conclusions

It has been seen that the ignitions of mixtures of hydrogen and chlorine are affected by the addition of small proportions of chloropicrin, nitrosyl chloride, and nitric oxide in ways which can be ascribed to the introduction of fresh initiating reactions which supply chlorine atoms for the main chain reaction, or terminating reactions which remove them. Studies of the ignition regions, and of the reactions just outside them, have given information upon the mechanism of decomposition of these additives. Nitrogen trichloride behaves differently from the other additives, and the region of ignition which it yields is closely connected with the region of explosive decomposition of the nitrogen trichloride vapor itself. Although a mechanism of decomposition can be suggested, further identification of the intermediates is required.

REFERENCES

1. Sagulin, A. B.: Z. Phys. Chem., *B1*, 275 (1928).
2. Griffiths, J. G. A., and Norrish, R. G. W.: Proc. Roy. Soc., *A130*, 591 (1931).
3. Ashmore, P. G.: Nature, 172, 449 (1953).
4. Ashmore, P. G., and Norrish, R. G. W.: Proc. Roy. Soc., *A203*, 472 (1950).
5. Ashmore, P. G., and Chanmugam, J.: Trans. Faraday Soc., *49*, 254 (1953).
6. Ashmore, P. G., and Chanmugam, J.: Trans. Faraday Soc., *49*, 265 (1953).
7. Chanmugam, J.: Thesis, University of Cambridge (1952).
8. Smith, W. McF., and Steacie, E. W. R.: J. Chem. Phys., *6*, 145 (1938).
9. Ashmore, P. G., and Norrish, R. G. W.: Proc. Roy. Soc., *A203*, 454 (1950).
10. Ashmore, P. G., and Norrish, R. G. W.: Proc. Roy. Soc., *A204*, 34 (1950).
11. Apin, A. J.: Acta Physicochim. (U.R.S.S.), *12*, 406 (1940).

79

COMBUSTION STUDIES OF ALKYLSILANES

By ROSE L. SCHALLA, GLEN E. McDONALD, and MELVIN GERSTEIN

Introduction

The spontaneous flammability of certain metal hydrides and organo-metallic compounds[1] suggests that metal-to-hydrogen and metal-to-carbon bonds are more susceptible to oxidation than carbon-to-hydrogen or carbon-to-carbon bonds. Much work has been done on the relative ease of oxidation of hydrocarbons, but the similarity in susceptibility to oxidation of the different bonds within the hydrocarbon molecule makes it difficult to isolate the separate steps in the reaction. The introduction of a metal atom into a molecule may add certain bonds which are more easily attacked by oxygen than the remainder of the molecule, and hence it may be possible to follow more readily the initial attack on the molecule by oxygen. Because of its similarity to carbon, silicon is a reasonable metal atom to use in such a study. Consequently, several alkylsilanes were prepared at the NACA Lewis laboratory[2], and a study of the oxidation properties of these fuels was conducted.

The temperature required for the rapid oxidation or explosion of alkylsilane-air mixtures at one atmosphere pressure were determined. Methylsilane, dimethylsilane, trimethylsilane, tetramethylsilane and vinylsilane were studied. In addition, the initial rate of oxidation of a 50 per cent mixture of trimethylsilane and air was studied by measurements of pressure and concentration changes at a temperature slightly below the explosion temperature.

Experimental

FUELS

The method of preparing the alkylsilanes used in this study is described by Tannenbaum et al.[2] The tetramethylsilane had been purified from

a commercially available product while the methyl-, dimethyl-, trimethyl-, and vinylsilanes had been prepared by reduction of a proper alkylchlorosilane with lithium aluminum hydride in anhydrous ethyl ether or dioxane. Some of the physical properties of the fuels are listed in Table 1.

admitted very slowly to determine the presence of cool flames. Occurrence of an explosion was indicated by a strong surge of the mercury in the manometer, and occasionally a flame was seen to travel up the tube leading from the reaction vessel. Although such flames usually did not travel very far, they did on several occasions

Table 1. Physical Properties of Alkysilanes[2]

Compound	Boiling point* (760 mm)	Freezing point	Density,† g/ml	
			A	B
	°C	°C		
CH_3SiH_3	−57.5	−156.81	0.001282	0.5540
$(CH_3)_2SiH_2$	−19.6	−150.22	0.001143	0.6149
$(CH_3)_3SiH$	6.7	−135.89	0.001085	0.6448
$(CH_3)_4Si$	26.2	α = −101.7 β = −99.5	0.001042	0.6634
$(CH_2{=}CH)SiH_3$	−22.8	α = −179.08 β = −171.61	0.001187	0.6393

* Determined by extrapolation of vapor pressure data.
† Constants for equation: Density = $-At + B$; t = °C.

REACTION SYSTEM

A diagram of the apparatus used in this study is shown in Figure 1. Fuel and filtered air were admitted at the positions indicated and mixed in

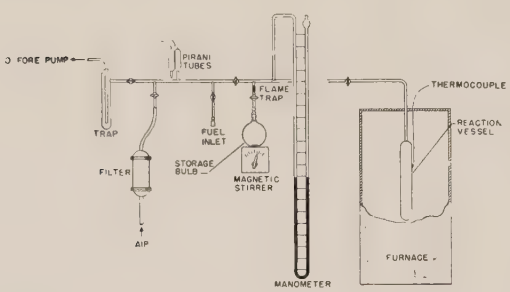

Fig. 1. Apparatus for determining explosion limits.

a 1-liter storage bulb by means of a magnetic stirrer. The pressure of the mixture in the storage bulb was such that, when opened to the heated, evacuated reaction vessel, the resulting pressure in the system was 1 atm. The temperature of the Pyrex reaction vessel, 1½ in in diameter and 10½ in long, was measured by a thermocouple attached to the outside of the vessel.

Admission of the mixture to the reaction vessel was usually made as rapidly as possible although, as described later, the mixture was sometimes flash back into the mixing bulb and cause an explosion. Consequently, a roll of wire gauze was placed between the mixing bulb and the reaction vessel to serve as a flame trap. After this flame arrestor was installed, no further trouble from flash-back was encountered.

In the reaction rate study, trimethylsilane and air in equal proportion by volume were admitted to the reaction vessel at 220°C. The initial pressure in the reaction vessel, prior to reaction, was 940 mm in most of the tests, but pressure was varied in some of the experiments. The manometer, shown in Figure 1 was read at regular intervals to determine the pressure change. In order to determine changes in oxygen concentration, the reaction was stopped at different stages in different runs. Oxygen was determined by conventional gas analysis techniques. The nature of some of the other components of the reaction mixture was determined from the infrared absorption spectrum of the products of reaction.

Results

EXPLOSION LIMITS

Tetramethyl- and trimethylsilanes

Two distinctly different types of explosion limits were encountered in this study. The first type, typical of those reported for hydrocarbons

at a pressure of 1 atm was found for tetramethyl- and trimethylsilanes. For both of these compounds, the fuel-air mixture was admitted rapidly to the evacuated reaction vessel to a pressure of 1 atm, and at a sufficiently high temperature an explosion occurred. Usually, if no rapid reaction took place within 30 sec, only a very slow increase in pressure was observed and no explosion was detected even after time intervals of one hour. It was observed for trimethylsilane that at certain temperatures below the explosion region, there was an initial pressure decrease immediately after introduction of the fuel-air mixture.

The temperature-composition curves separating the explosion from the non-explosion region for tetramethyl- and trimethylsilane are shown in Figure 2. Determinations were made of both the temperature at which explosion occurred within 15 sec and the temperature below which no explosion took place after long standing. As shown in Figure 2, these two temperatures do not differ by more than 15°C; and, consequently, the minimum explosion temperature under the conditions of the test lies within this 15°C temperature range. Rich mixtures of tetramethylsilane and air ignited at a temperature as low as 450°C, while rich trimethylsilane-air mixtures required a temperature of only 310°C. The explosion limit curves for these silanes resemble those for hydrocarbons[3, 6] except that the silanes ignite at appreciably lower temperatures. Some typical curves for hydrocarbons are given in Figure 3.

Dimethyl-, methyl-, and vinylsilanes

The second type of explosion limit was encountered with the dimethyl-, methyl-, and vinylsilanes; and the temperature-composition curves for these compounds could not be obtained by the technique used for the previous two compounds, tetramethyl- and trimethylsilane. The temperatures below which no explosion occurred, shown in Figure 4, could be determined unambiguously. Above these temperatures, however, the observed phenomena depended upon the rate of admission of the fuel-air mixture to the reaction vessel. In those cases where the mixture was introduced rapidly, an explosion took place before the pressure in the reaction tube reached atmospheric pressure. Mixtures were therefore admitted very slowly to observe the pressure at which reaction was first indicated. By this procedure it was observed that a series of minor explosions, probably cool flames, occurred over a pressure range of 50–100 mm Hg.

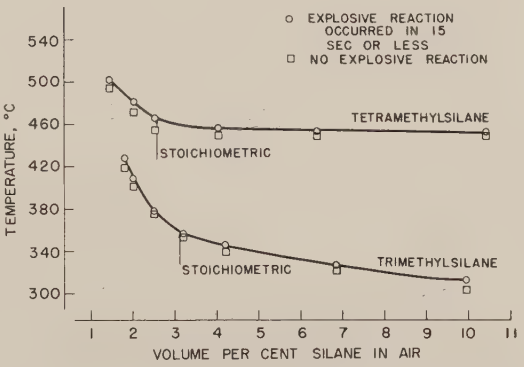

FIG. 2. Temperature-composition explosion curves for tetramethyl- and trimethylsilane at pressure of 1 atmosphere.

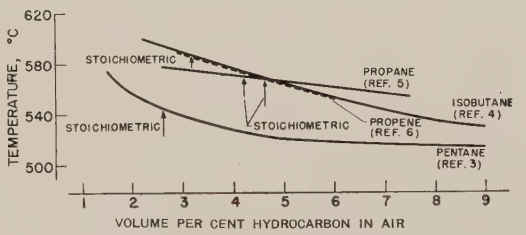

FIG. 3. Temperature-composition explosion curves for hydrocarbons at pressure of 1 atmosphere.

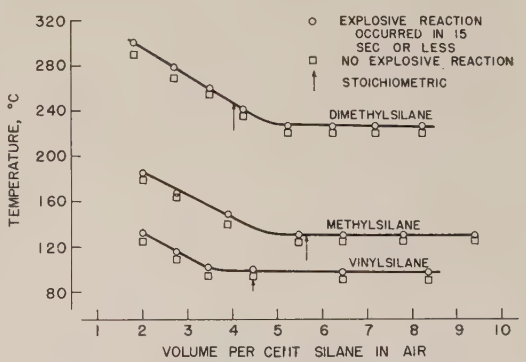

FIG. 4. Temperature-composition explosion curves for dimethyl-, methyl-, and vinylsilane at pressure of 1 atmosphere.

After this pressure range was exceeded, no further reaction took place when the mixture was slowly admitted to a pressure of 1 atm at temperatures just above the nonexplosion temperature.

Since a very vigorous reaction took place when the mixture was rapidly admitted, it is believed

that the cool flame reaction occurring at a pressure of 50–100 mm set off an explosive reaction

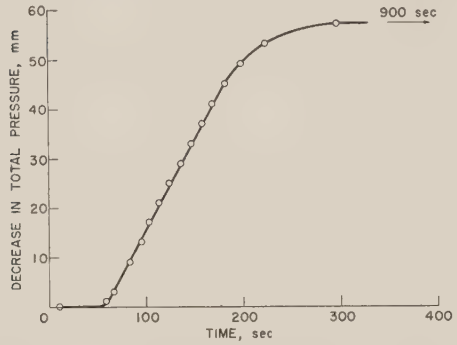

FIG. 5. Decrease in total pressure with time for a mixture containing 50 per cent trimethylsilane and 50 per cent air; temperature, 250°C; initial pressure, 760 mm.

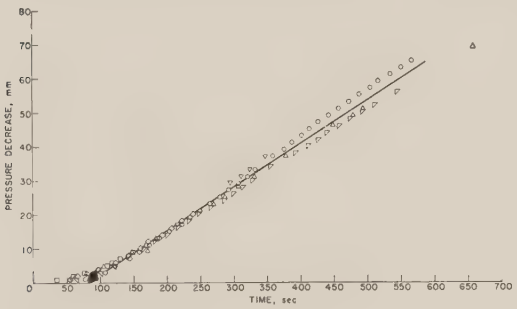

FIG. 6. Variation of pressure decrease with time for a mixture containing 50 per cent trimethylsilane and 50 per cent air; initial pressure, 940 mm; temperature, 220°C. Data from 7 separate runs.

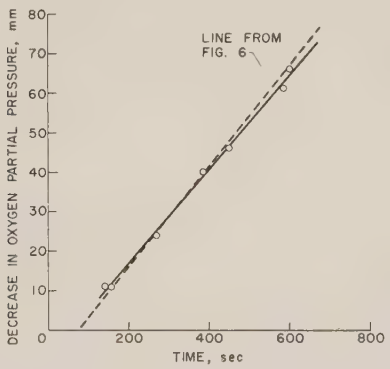

FIG. 7. Decrease in the partial pressure of oxygen with time for mixtures containing 50 per cent trimethylsilane and 50 per cent air; initial total pressure, 940 mm; temperature, 220°C.

when additional fuel-air mixture was being supplied at a sufficiently rapid rate. The temperature-composition explosion curves for dimethyl-, methyl-, and vinylsilane (Fig. 4) actually represent the appearance of cool flames. The cool flames are capable of causing a more complete explosion if additional fuel-air mixture is immediately available to react. If cool flames did not occur, the explosion temperature for an air mixture of these fuels at an initial pressure of 1 atm would be expected to be higher than the temperature recorded in figure 4 for the occurrence of the cool flames.

RATE OF OXIDATION OF TRIMETHYLSILANE

The rapid decrease in explosion temperature as the number of silicon-to-hydrogen bonds in the alkylsilane molecule is increased suggests that this bond may be considerably more reactive than the remaining bonds in the molecule. Further, the decrease in pressure noted earlier, when air and trimethylsilane are first added to the reaction vessel suggests an initial reaction which may involve the absorption of oxygen by the silane molecule and/or the condensation of the reaction product. The rate of oxidation of a mixture containing 50 per cent trimethylsilane and 50 per cent air was studied. While leaner mixtures showed similar trends to those reported below, the fuel rich mixture was used to simplify identification of some of the products of the reaction.

A typical curve of pressure decrease against time is shown in Figure 5, for a mixture containing 50 per cent trimethylsilane, 50 per cent air at 250°C and an initial pressure of 1 atm. After a short induction period, there is a linear decrease of pressure with time until a point is reached at which the rate of pressure decrease becomes quite slow. In an effort to relate the pressure decrease to the change in concentration of the reactants, a series of experiments was performed with the 50 per cent trimethylsilane mixture at 220°C and an initial pressure of 940 mm; each of the runs was stopped at a different stage and the oxygen content of the mixture determined by gas analysis. The pressure changes for seven of the tests are shown in Figure 6. A mean line has been drawn through the data. The corresponding changes in the partial pressure of oxygen with time are shown in Figure 7. The line from Figure 6 for the changes in total pressure with time has been included to show that the changes in total pressure and changes in oxygen partial pressure are almost equal in the interval shown. Further analyses showed that approximately two molecules of trimethylsilane were consumed for each molecule of oxygen used. Thus, for the change

in total pressure to equal the change in oxygen partial pressure, the series of reactions which involve one oxygen molecule and two trimethylsilane molecules must result in two product molecules.

Several other observations were made to assist in studying the trimethylsilane oxidation. The major product of the oxidation was a substance which existed in the gas phase at 220°C and condensed to an oily liquid on cooling. An infrared spectrograph of the condensed material was similar to that of a silicone oil. Further examination of the gaseous and liquid products of the reaction indicated less than one per cent of the following: methyl alcohol, water, carbon monoxide, and carbon dioxide. Analysis of the gas phase indicated the absence of hydrogen in the reaction products.

In addition to the trimethylsilane-air reaction, two other possible reactions were examined. It was found that tetramethylsilane does not react with air under the conditions of the test and that under these same conditions a mixture containing equal volumes of water and trimethylsilane shows no reaction.

Discussion

While the data obtained are insufficient to formulate a mechanism for the oxidation of trimethylsilane, some reasonable postulates can be made. The lower explosion temperatures of alkylsilanes containing silicon-to-hydrogen bonds and the reactivity of trimethylsilane under conditions where tetramethylsilane does not react with air, strongly suggests that the initial attack on the trimethylsilane occurs at the silicon-to-hydrogen bond. The formation of a product having an infrared spectrum like that of a silicone oil also suggests that subsequent attack of the trimethylsilane must invole either the carbon-to-hydrogen bonds or the silicon-to-carbon bonds or both. If only the silicon-to-hydrogen bond were involved in the oxidation, only a dimer could form. The dimer should have resulted in the formation of water which was not observed; hence such a simple reaction seems unlikely. There is insufficient information to establish a probable mechanism for the reaction.

A possible reaction scheme for the initial phases of the oxidation may involve the formation of peroxides in a manner similar to that suggested for hydrocarbons[7]

$$RH + O_2 \rightarrow R + HO_2 \qquad \text{(initiation)} \quad (1)$$

$$R + O_2 \rightarrow ROO \qquad (2)$$

$$ROO + RH \rightarrow ROOH + R$$

where R = $(CH_3)_3$ Si

The initiation step during which the free radical R, which may be $(CH_3)_3$ Si, is being formed may be sufficiently slow to account for the induction period (Fig. 5). In order to explain the formation of the silicone oils found experimentally, subsequent reactions must involve the breaking of carbon-to-hydrogen or silicon-to-carbon bonds. In hydrocarbon oxidation it has been suggested that the radical ROOH decomposes as follows[7]

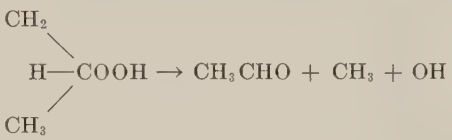

In a similar manner, a reaction of the type:

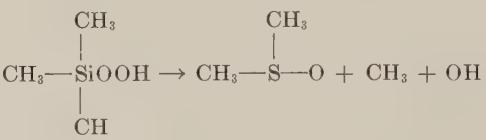

may occur, followed by condensation of the $(CH_3)_2$ Si O radicals to form silicone oils, and possibly also account for the occurrence of some methyl alcohol in the reaction products. This is, of course, only one of many reactions which could be written to account for the observed products.

Summary

Explosion limits of a series of alkylsilanes have been determined at 1 atm pressure. The explosion temperature decreases in the order: tetramethylsilane > trimethylsilane > dimethylsilane > methylsilane > vinylsilane. It is suggested that the initial attack of the silane molecule by oxygen occurs at the silicon-to-hydrogen bond, and is followed by further oxidation of the molecule to form groups which can condense to silicone oils. Oxidation of trimethylsilane at a temperature below its explosion temperature results in a regular pressure decrease. The rate of pressure

decrease follows closely the rate of oxygen consumption.

REFERENCES

1. Krause, E., and von Grosse, A.: Die Chemie Der Metall-Organische Verbindungen. Berlin, Gebrüder Bornträger, 1937.
2. Tannenbaum, S., Kay, S., and Lewenz, G. F.: J. Am. Chem. Soc., *75*, 3753 (1953).
3. Townend, D. T. A., and Mandlekar, M. R.: Proc. Roy. Soc. (London), *A143*, 168 (1934).
4. Townend, D. T. A., Cohen, L. L., and Mandlekar, M. R.: Proc. Roy. Soc. (London), *A146*, 113 (1934).
5. Townend, D. T. A., and Chamberlain, E. A. C.: Proc. Roy. Soc. (London), *A154*, 95 (1936).
6. Kane, G. P., and Townend, D. T. A.: Proc. Roy Soc. (London), *A160*, 174 (1937).
7. Walsh, A. D.: Trans. Faraday Soc., *42*, 269 (1946); *43*, 297 (1917).

80

COMBUSTION OF DIBORANE-OXYGEN MIXTURES AT THE SECOND EXPLOSION LIMIT[a]

By WALTER ROTH and WALTER H. BAUER

Introduction

Thermochemical calculations indicate that the oxidation of a boron hydride should release approximately twice as much energy per pound as the oxidation of an equal weight of a hydrocarbon. This high energy release makes the boron hydrides interesting as potential rocket fuels[1]. In this respect, pentaborane, B_5H_9, has a combination of desirable properties which make it of particular interest. However, in order to first obtain greater insight into the general mechanism of boron hydride combustion, a study was made of the kinetics of the oxidation of the simplest of the boron hydrides, diborane.

Price[2] found that diborane oxidation exhibits upper and lower pressure limits of explosion. Whatley[3] studied the composition limits of this explosive reaction. The results of the two investigations were not in agreement. This may have been a function of the different experimental procedures used by Price[2] and Whatley[3] for determining the limits. It was decided, therefore, to repeat and extend the work using a third procedure designed to eliminate some of the shortcomings of the other two. In addition, Price's[2] results indicate that the lower explosion limit results from chain branching and breaking at the vessel wall while the upper limit is determined by gas phase branching and breaking. To avoid wall effects, in this investigation the work at the second explosion limit has been initially emphasized.

[a] This paper is based on a portion of a thesis submitted by Walter Roth to the faculty of Rensselaer Polytechnic Institute, in partial fulfillment of the requirements for the degree of Doctor of Philosophy, June, 1954.

Materials and Procedure

DIBORANE

Diborane was prepared by reaction of BF_3 etherate with $LiAlH_4$ according to the method of Shapiro et al.[4]. It was stored in stainless steel cylinders in a freezer at −20°C until used. When required, the diborane was transferred from the steel cylinders to a glass storage vessel attached to the vacuum system. Purification during the transfer was effected by pumping on the frozen diborane at liquid nitrogen temperature and by distilling between two liquid nitrogen traps. Infrared analysis revealed no higher hydride impurities. The storage vessel was never allowed to warm up above dry ice temperature.

OXYGEN

Matheson Company extra dry oxygen (99.6 per cent purity) was liquefied at liquid nitrogen temperature. One third of the resulting liquid was pumped away. A second third was distilled to another liquid nitrogen trap, pumped upon and finally distilled to a glass storage vessel.

MIXTURES

Diborane-oxygen mixtures were prepared on a pressure basis. Generally, fresh mixtures were prepared daily and kept in a glass storage vessel. In several cases, however, mixtures having low diborane concentrations were used for two successive days. In none of these cases did the longer storage period cause any significant change in results.

In order to exclude mercury vapor from the system, pure gas and mixture storage vessels were equipped with metal diaphragm type pressure gages. In making mixtures, a metal bellows pressure gage, described below, was used to measure partial pressures of the components.

Just prior to making a mixture, the diborane was subjected to two cycles of freezing, pumping and thawing in order to remove any hydrogen which may have been produced.

TEMPERATURE MEASUREMENT

Explosion temperatures were measured with a copper-constantan thermocouple connected to a Brown, Model No. 153X18P-X-66, Electronik High-Speed Recording Potentiometer calibrated 0–300°C and having a 1-second full-scale pen speed. Tests of the accuracy of measurement of the temperature within the reaction vessel were made by heating the vessel filled with nitrogen. Calculations of the temperature of the nitrogen at intervals during the heating process were made from pressure measurements assuming ideal gas behavior. The thermocouple was deliberately provided with a large junction in contact with the outside vessel surface. It was found to closely represent the nitrogen temperature after heating had proceeded for a few seconds. Experience gained during explosion experiments has verified the accuracy of temperature measurement.

PRESSURE MEASUREMENT

Pressures were measured with a metal bellows differential manometer, schematically represented in Figure 1. A brass bellows having one end closed and eight corrugations was connected to the reaction system with copper tubing.

A dial gage, calibrated in 0.0001 in and having a total range of 0.03 in was mounted so that its stem touched the closed end of the bellows. The whole was enclosed in a brass container provided with a window for viewing the dial gage face. A mercury manometer was connected to the brass container and was used to adjust the pressure on the outside surface of the bellows. Pressure measurements could be made directly or by a null-point method. The sensitivity was 0.54 mm Hg per dial gage division. Pressure changes of 0.1 mm Hg could easily be estimated. To improve the reproducibility of pressure measurements an electrical vibrator was mounted on the side of the brass container. A system of valves was provided for connection of the metal manometer to the reaction vessel or the mixture storage vessel. The apparatus had the advantage of excluding mercury vapor from the reaction system.

VACUUM SYSTEM AND REACTION SYSTEM

In view of the solubility of diborane in stopcock grease, metal valves of the bellows and of the diaphragm type were used in all portions of the system involved in diborane transfer. Valve

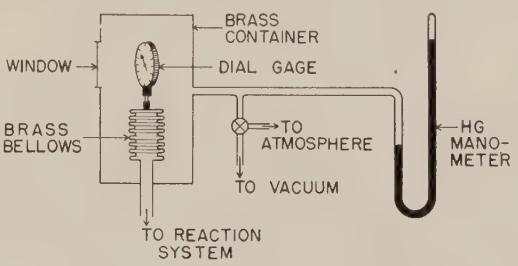

FIG. 1. Bellows differential manometer.

seats were of Teflon or Kel-F. In addition, a large portion of the vacuum train was constructed of ⅜-inch outside diameter copper tubing. Connections to glass parts of the system were made with Kovar to Pyrex seals. All joints were made with silver solder. To eliminate oxide formation, soldering was done with a stream of nitrogen flowing through the tubing, where possible. When construction was completed, the apparatus was filled with hydrogen and flamed to remove any oxide which may have formed. Reaction vessels were Pyrex spheres and had 1 mm inside diameter capillary tube inlets. To further insure exclusion of mercury vapor from the reaction system, a gold-leaf trap was installed at the upper end of the reaction vessel inlet tube. Prior to a run, the vessel was suspended above a bath of silicone oil, General Electric Type SF-96 (40). The bath temperature could be kept constant to ±0.5°C in the region of 150–200°C.

PROCEDURE

The vessel was evacuated to about 10^{-5} mm Hg at bath temperature and filled with diborane-

Table 1. The Explosion Limits as a Function of Surface Condition and Vessel Diameter

(Vessels evacuated at bath temperature except where otherwise noted)

$(O_2)/(B_2H_6)$	Vessel diam = 4.6 cm		Vessel diam = 5.8 cm	
	Pressure	Temperature	Pressure	Temperature
	mm Hg	*°C*	*mm Hg*	*°C*
4	13.6	186	14.3	182
	14.1	181	15.1	165
	15.2	180	17.4	182
	15.8	178	17.7	163
	16.0	173	19.4	183
	16.2	172	23.3	192
	16.3	164	28.3	190
	16.3	177	33.3	193.5
	17.2	163.5	51.6	183
	17.2	176		
	18.8	180		
	18.9	188		
	19.0	186		
	19.1	187		
	20.4	181.5		
	21.2	186		
	25.3	185		
	30.9	183		
	38.8	176		
	46.3	172		
	53.6	165		
3	13.9	177	16.7	171
	15.1	172.5	18.9	169
	15.6	168	20.6	175
	16.2	185	21.9	177.5
	16.7	157	22.6	171
	17.1	163	24.2	176.5
	17.1	181*	27.0	187
	17.7	178†	28.5	186
	18.7	164	35.7	187
	19.1	168.5	43.2	187.5
	19.4	171	51.4	188
	19.5	193*		
	20.0	168		
	20.3	184*		
	21.1	174		
	21.4	173.5		
	23.3	179		
	27.3	180		
	27.5	173		
	28.6	172.5		
	29.8	173		
	32.4	173.5		
	36.9	171		
	37.4	156		

* Vessel evacuated at room temperature.

† Diborane decomposed in vessel prior to experiment.

oxygen mixture to the desired pressure. The hot silicone oil bath was raised with a motor-driven automobile jack until the vessel was entirely immersed. Explosion was indicated by a bright green flash of light and a sharp pressure change. For stoichiometric and lean mixtures, the pressure decreased upon explosion. For rich mixtures, explosion resulted in an initial pressure increase which was followed by a pressure decrease. The pressure at the time of explosion was observed. The explosion temperature was recorded. For a given mixture, a series of different initial pressures gave results which defined the explosion limits very well.

Since a solid product was deposited on the vessel wall, periodic cleaning of the vessel was necessary. This was done by successive rinses with methanol and hot cleaning solution followed by treatment with steam and several rinses with distilled water.

Results

EFFECT OF SURFACE CONDITION

Explosion temperatures at various pressures are listed in Table 1. It has been found that explosion limits depend somewhat on the condition of the vessel surface. This is illustrated in Figure 2 in which explosion limits are shown for the stoichiometric mixture. Price's[2] results have been included in the figure for comparison purposes. His procedure involved evacuation of the vessel with a mechanical pump only at room temperature. His second limit was determined by a withdrawal method. In the present work, vessels were evacuated at bath temperature and a mercury diffusion pump was used to insure thorough outgassing of the vessel. With this method, the first limit is seen to agree very well with that reported by Price but the second limit is shifted toward lower temperatures and higher pressures. It is interesting to note that if the vessel was evacuated at room temperature following an explosion, then isolated from the pump and immersed in the bath, the pressure was seen to rise rapidly to a point where the ionization gage was off scale. The upper pressure limit for the gage is two microns. This indicated a large amount of outgassing from the vessel surface. Furthermore, when Price's evacuation procedure was duplicated and the explosion bulb was evacuated at room temperature, the results of this work and those of Price were in very good agreement, as shown in Figure 2. In a further attempt to find the causes of the discrepancy in results, a vessel which had

previously been outgassed at bath temperature was filled with B_2H_6 to a pressure of 30 mm Hg, and then heated for 8 min at bath temperature in order to decompose the B_2H_6. It was finally evacuated at room temperature. A subsequent experiment in this vessel resulted in an explosion at a point very close to Price's second limit curve, as may be seen in Figure 2.

Another observation was made which illustrates the strong adsorption on the vessel wall. On several occasions, the bath temperature was too low to cause an explosion of the mixture in the vessel. When this was evident, the bath was lowered, the vessel was allowed to cool and the reactants initially evacuated with the mechanical pump only. Pumping was continued for a few minutes after the bellows manometer had returned to its zero setting. The bath was then raised until the explosion vessel was immersed. Several seconds later, a blue-green glow was seen to fill the vessel, often lasting for as long as 15 sec. It is evident that this glow was being produced by reaction of some substances which were being outgassed from the wall. As the number of explosions which had taken place in a given vessel increased, the solid products of the reaction caused an increasingly heavy coating to be formed on the wall and a consequent increase in the time necessary for evacuation. The vessel was cleaned when reproducible results could not be readily obtained. The result of the first experiment in a clean vessel was not significantly different from subsequent results. The coating produced on a vessel wall was observed to be heavier at the bottom of the vessel indicating that the solid products were being formed in the gas phase and were settling to the bottom. Coatings were generally white but appeared slightly tan or yellowish when rich mixtures were ignited. X-ray analysis of the coating indicated only H_3BO_3.

DIAMETER EFFECT

Experiments on mixtures of $B_2H_6 + 3O_2$ and $B_2H_6 + 4O_2$ were made in 4.6 cm and 5.8 cm diameter vessels. The results are given in Table 1. It may be seen that the second limit, (Fig. 3) is virtually independent of vessel diameter in this diameter range. Preliminary work seems to indicate that the first limit is also independent of vessel diameter. On the other hand, the position of a third limit, existing at pressures above the second limit, is seen to be strongly dependent on the vessel diameter.

THE EFFECT OF VARIATION OF DIBORANE-OXYGEN CONCENTRATION RATIO ON THE SECOND EXPLOSION LIMIT

The explosion temperatures at various pressures for additional mixtures of diborane and oxygen in a 5.8 cm diameter vessel are given in Table 2. The results obtained with five mixtures whose mole ratio, $f_{O_2}/f_{B_2H_6}$, varies from 1 to 4 are shown in Figure 4. As the mole ratio $f_{O_2}/f_{B_2H_6}$ approaches unity, the explosion limit curves increase in slope, becoming almost vertical when $f_{O_2}/f_{B_2H_6}$ equals one. The radically different shape of the limit curve for the mole ration of unity indicates that a previously negligible factor has

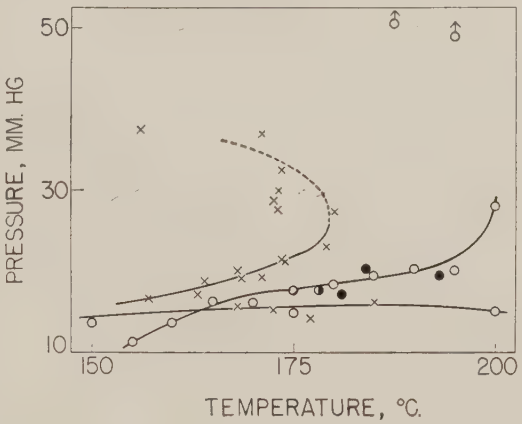

FIG. 2. Explosion limits for the stoichiometric mixture of diborane and oxygen. ○, Price (averaged results); ♂, indicates explosion immediately upon opening stopcock; x, this work, 4.6 cm spherical, Pyrex vessel, evacuated at bath temperature; ●, vessel evacuated at room temperature; ◑, diborane decomposed in vessel prior to experiment.

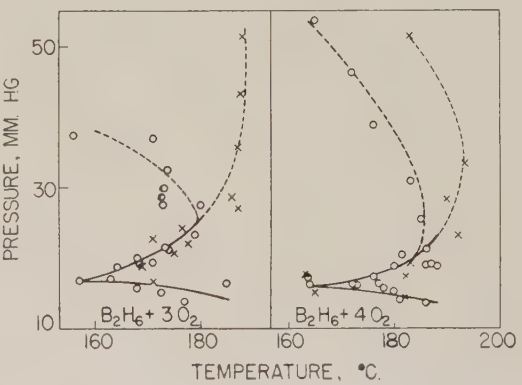

FIG. 3. The effect of vessel diameter on the explosion limits of diborane-oxygen mixtures; ○, 4.6 cm diameter; x, 5.8 cm diameter.

become important. When this became apparent, a mixture of mole ratio 2.5 was studied in order to provide data from four different mixtures all of which exhibited typical second explosion limits.

Table 2. The Second Explosion Limit for Various Mixture Compositions

(*Vessel diameter 5.8 cm*)

$[O_2]/[B_2H_6] = 2.5$		$[O_2]/[B_2H_6] = 1$	
Pressure	Temperature	Pressure	Temperature
mm Hg	°C	*mm Hg*	°C
19.7	160	8.4	147
22.5	163	14.3	149
25.1	166	16.4	150
25.7	166	17.1	148.5
28.5	168	19.8	147.5
		20.7	146
$[O_2]/[B_2H_6] = 2$		23.2	148.5
		24.8	147
18.6	153	32.4	147
20.9	155	37.4	142
24.3	159	40.3	127
24.9	161		
32.0	167.5		

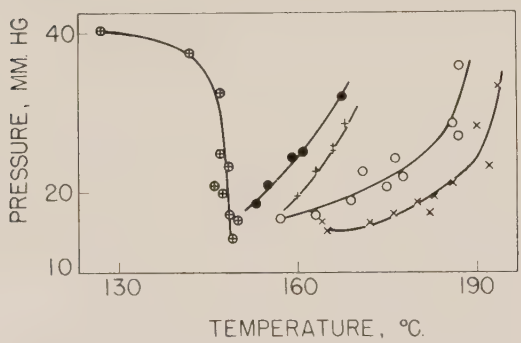

Fig. 4. Second explosion limits for various mixtures of diborane and oxygen. $(B_2H_6)/(O_2)$, X, 1:4; ○, 1:3; +, 1:2.5; ●, 1:2; ⊕, 1:1.

Discussion

The existence of an equilibrium between diborane and borine, $B_2H_6 \rightleftarrows 2BH_3$, is well established and the mechanisms of several reactions have included this equilibrium as a primary step[5, a, b, c, d]. Indeed, the equilibrium constant has been estimated from thermodynamic data[6]. Therefore, in developing a mechanism for the oxidation of diborane at the second explosion limit, it is plausible to assume the initial presence of borine. If BH_3 enters into the reaction there is an interesting parallel between this reaction and the hydrogen-oxygen reaction. The introduction of H-atoms into hydrogen-oxygen mixtures at room temperature does not cause the mixtures to ignite[7]. Similarly diborane-oxygen mixtures are stable at room temperature despite the presence of BH_3. A simplified mechanism, analogous to that for hydrogen oxidation at the second limits, may be written as follows:

$$BH_3 + O_2 = BH_2OH + O \quad (1)$$

$$O + B_2H_6 = BH_2OH + BH_3 \quad (2)$$

$$BH_2OH + B_2H_6 = BH_3 + B_2H_5OH \quad (3)$$

$$BH_3 + O_2 + M = HBO_2 + H_2 + M \quad (4)$$

$$BH_3 + B_2H_6 = B_3H_7 + H_2 \quad (5)$$

$$B_3H_7 \rightarrow \text{higher hydrides} \quad (6)$$

B_2H_5OH disproportionates to $B(OH)_3$

$$+ B_2H_6 \quad (7)$$

where M, in equation (4), is any third body.

The analogy to the H_2-O_2 reaction extends only to reactions (1) through (4), above.

If, at the second explosion limit, steady state concentrations of the reactive species, O, BH_3, and BH_2OH are assumed, then,

$$\frac{d[BH_3]}{dt} = -k_1[BH_3][O_2] + k_2[O][B_2H_6] + k_3[BH_2OH][B_2H_6] - k_4[BH_3][O_2][M] - k_5[BH_3][B_2H_6] = 0 \quad (8)$$

$$\frac{d[O]}{dt} = k_1[BH_3][O_2] - k_2[O][B_2H_6] = 0 \quad (9)$$

$$\frac{d[BH_2OH]}{dt} = k_1[BH_3][O_2] + k_2[O][B_2H_6] - k_3[BH_2OH][B_2H_6] = 0 \quad (10)$$

Solution of these simultaneous equations results in the expression

$$[M] = (2k_1/k_4) - k_5[B_2H_6]/k_4[O_2] \quad (11)$$

Bauer[8] estimated the rate constant for the self-deuteration reaction investigated by Maybury and Koski[5a],

$$BH_3 + B_2D_6 \rightarrow B_2H_3D_3 + BD_3$$

as

$$k_d = 2.8 \times 10^{13}\, e^{-7800/RT} \text{ moles}^{-1} \text{ cc sec}^{-1}$$

In addition, he estimated the rate constant for the reaction,

$$BH_3 + B_2H_6 \rightarrow B_3H_7 + H_2 ,$$

which had been proposed by Clarke and Pease as[5b] a step in the pyrolysis of diborane. This latter estimate was

$$k = 1.14 \times 10^{11} e^{-11500/RT} \text{ moles}^{-1} \text{ cc sec}^{-1}$$

Assuming, then, that any isotope effect is small enough to be neglected, the ratio of these two rate constants indicates that, at temperatures in the region of the second limit, only one in about 10^4 collisions between BH_3 and B_2H_6 results in reaction (5). In addition, in this work, $[B_2H_6]$ was always less than or equal to $[O_2]$. Therefore, the second term on the right-hand side of equation (11) may be neglected. Possibly, at high B_2H_6 concentration, this term becomes important. Of course, once the explosion flame has developed temperatures are high enough so that higher hydride production via reaction (5) is probably appreciable. Omission of this term leads to the modified expression,

$$[M] = 2 k_1/k_4 \qquad (12)$$

k_4 is actually a composite rate constant the value of which depends on the composition of the mixture. Thus,

$$k_4 = \Sigma k_{4,M} f_M \qquad (13)$$

where the f_M are mole fractions. In this work only the effect of varying the $(B_2H_6)/(O_2)$ ratio was studied. Therefore, M represents either B_2H_6 or O_2. Furthermore, since (M) is the total concentration at the explosion limit, it may be represented by P_2/RT_2 where P_2 and T_2 are the pressure and temperature of the second limit explosion, respectively. Substitution in equation (12) gives

$$P_2/RT_2 = 2k_1/(k_{4,O_2} f_{O_2} + k_{4,B_2H_6} f_{B_2H_6}) \qquad (14)$$

Equation (14) may be rearranged to

$$f_{O_2}/f_{B_2H_6} = (2RT_2/P_2 f_{B_2H_6})(k_1/k_{4,O_2}) - (k_{4,B_2H_6}/k_{4,O_2}) \qquad (15)$$

Now, ordinarily, it would be convenient to plot $f_{O_2}/f_{B_2H_6}$ against the reciprocals of the pressures on an isotherm in Figure 4. The intercept of such a plot would be the negative of the ratio of rate constants, $k_{4,B_2H_6}/k_{4,O_2}$. However, it can be seen from the figure that an isotherm cannot be drawn which intersects all of the second limits represented at points sufficiently removed from the first and third limits. Indeed, when this is attempted, negative, and, therefore, impossible, values are obtained for the ratio $k_{4,B_2H_6}/k_{4,O_2}$. All of the second limits, however, occur in approximately the same pressure range. It is therefore possible to draw an isobar which intersects the central portions of each of the second limits represented. Explosion temperatures may then be compared at constant pressure. For this to be useful, however, equation (15) must be further modified. Thus,

$$k_1/k_{4,O_2} = C \exp - (\Delta E/RT_2)$$

where C is a constant and ΔE is the difference in activation energies for branching reaction (1)

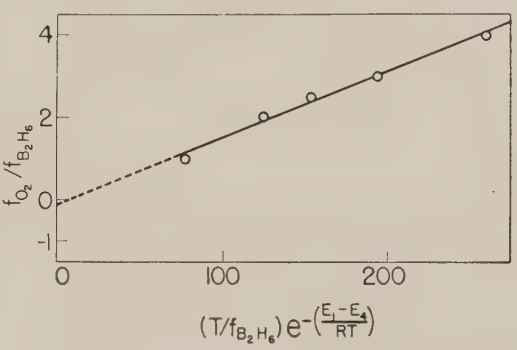

FIG. 5. The effect of mixture composition on a function of the second limit explosion temperature at a pressure of 23 mm Hg. $E_1 - E_4 = 2000$ cal/mole.

and breaking reaction (4). Substitution in equation (15) gives

$$f_{O_2}/f_{B_2H_6} = C'(T_2/f_{B_2H_6}) \exp (- \Delta E/RT_2) - (k_{4,B_2H_6}/k_{4,O_2}) \qquad (16)$$

Now, it is highly probable that the activation energy for the trimolecular reaction (4) is independent of the nature of the third body. Therefore, the ratio, $k_{4,B_2H_6}/k_{4,O_2}$, is temperature independent. Plots of $f_{O_2}/f_{B_2H_6}$ against $(T_2/f_{B_2H_6})$ exp $(-\Delta E/RT_2)$, assuming a different value of ΔE for each plot, should give a family of straight lines. This is in fact observed when small values are chosen for ΔE. Now, since $k_{4,B_2H_6}/k_{4,O_2}$ must be positive, only straight lines having negative intercepts are meaningful. It is found that the intercept is $\leqslant$ zero only when $\Delta E \leqslant 2$ kcal/mole. The line for which it is assumed that $\Delta E = 2$

kcal/mole is given in Figure 5. It can be seen that the intercept is approximately zero. The data for this plot are given in Table 3 for a constant pressure of 23 mm Hg. It is interesting to note that Harteck[9] has estimated a maximum activation energy of 4 kcal/mole from work on the O-atom-diborane reaction. Modification of equation (16)

Table 3. The Effect of Mixture Composition on the Second Limit Explosion Temperature at 23 mm Hg

$f_{O_2}/f_{B_2H_6}$	Temperature	$T/f_{B_2H_6}$	$(T/f_{B_2H_6})$ exp $(-2000/RT)$
	°K		
4	461.5	2307.5	260.7
3	451	1804	194.8
2.5	437	1529	152.9
2	431.5	1294.5	125.6
1	421	842	77.5

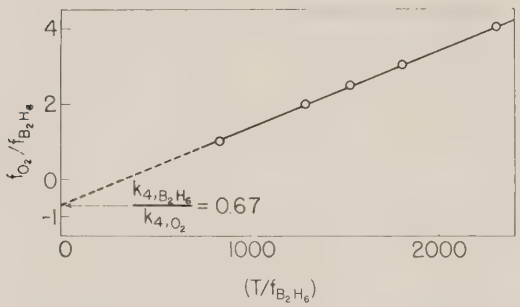

Fig. 6. The variation of a function of the second limit explosion temperature at 23 mm Hg with mixture composition. The intercept indicates the maximum relative third body efficiencies of B_2H_6 and O_2.

by assuming $\Delta E = 0$ gives

$$f_{O_2}/f_{B_2H_6} = C''(T_2/f_{B_2H_6}) - (k_{4,B_2H_6}/k_{4,O_2}) \quad (17)$$

When $f_{O_2}/f_{B_2H_6}$ is plotted against $T_2/f_{B_2H_6}$, a straight line is obtained, whose intercept is a maximum value for the relative three body efficiencies of B_2H_6 and O_2. The best straight line, determined by the method of least squares, is shown in Figure 6 and indicates that O_2 is at least 1.5 times as efficient a third body as B_2H_6. Using estimates of molecular diameters based upon liquid densities, it can be shown that B_2H_6 should be about 1.3 times as efficient as O_2 as a third body.

It should be noted that the result for the 1:1 mixture falls on the straight lines in Figures 5 and 6 despite the fact that this mixture exhibits a limit curve which indicates a change in relative importance of factors affecting the mechanism.

Undoubtedly, the presence of O-atoms leads to the formation of ozone by the reaction

$$O + O_2 + M = O_3 + M \quad (18)$$

Presumably, O_3 could then act like an O-atom in attacking diborane. Thus,

$$O_3 + B_2H_6 = BH_2OH + BH_3 + O_2 \quad (19)$$

However, decomposition of ozone must be considered as a competing reaction. Thus, at the low pressures of the second limit,

$$O_3 + M = O + O_2 + M \quad (20)$$

If M were O_2, reaction (20) would certainly occur provided the activation energy requirement were satisfied. If M were B_2H_6, then, from the relative complexity of reaction (19) as compared to equation (20), one may assume that $k_{20} \gg k_{19}$. Inclusion of reactions (18) and (20) in the reaction scheme produces no change in the final result.

In reactions (1) and (2) the formation of BH_2OH has been postulated. Actually, this product could not be formed in either reaction without internal rearrangement of the collision complex. However, this rearrangement may occur rapidly. The formation of BH_2OH has been shown to be the primary step in the rapid hydrolysis of diborane. In addition, when B_2H_6 is adsorbed on ice at −80°C, the amount of hydrogen evolved suggests a partial hydrolysis to $BH(OH)_2$. On silica gel at −23°C, there is evidence for replacement of only one hydrogen in BH_3 [5b].

There is no evidence in the literature for the existence of B_2H_5OH, the product of reaction (3). However, the halides, B_2H_5X, have been prepared. The disproportionation of B_2H_5OH to B_2H_6 and $B(OH)_3$ via reaction (7) is proposed by analogy with the disproportionation of the halides[1].

From reaction (4), it would appear that the product of the overall reaction is metaboric acid. Although analysis of the solid reaction product indicates that it is ortho-boric acid, it is probable that the latter is formed by hydrolysis of HBO_2 after the reaction vessel has been cooled. Ortho-boric acid is unstable above about 70°C, decomposing, by loss of water, to HBO_2[10]. At the second limit temperatures, therefore, H_3BO_3 should not exist.

Price[2] has reported a crossing of first and second explosion limits for the stoichiometric mixture,

$B_2H_6 + 3O_2$, so that, in the neighborhood of the tip of the explosion peninsula, the second limit pressure was lower than the first limit pressures. His withdrawal method for determination of second limit pressure, however, allowed for some thermal decomposition of B_2H_6. His procedure for determination of first limit pressures could result in very little, if any, decomposition of B_2H_6. The results of this work have clearly shown that thermal decomposition of B_2H_6 leads to a second limit which is in agreement with that reported by Price[2]. In addition, Price reported a third explosion limit but was unable to determine its position. Figure 3 indicates that this limit is pressure independent over a wide pressure range. Again, Price's procedure was not applicable to the determination of a pressure independent limit. The strong diameter effect at this limit would add to the difficulty. It should be pointed out that, where comparable, the results of this work agree very well with those obtained by Price, despite the fact that Hg vapor and stopcock grease were present in Price's experiments.

It should be emphasized that no induction periods were observed in these experiments and in those by Price[2]. Whatley[3] has observed induction periods sometimes greater than 1000 sec. He attributes this to the necessity for diborane to decompose to a higher hydride, possibly pentaborane, before an explosive reaction can develop. A comparison of his results with those of Price[2] or with this work indicates that the highest temperature at which he worked barely corresponds to the lowest second limit explosion temperature reported here or by Price[2]. Pyrolysis of diborane may indeed have taken place to produce some reaction sensitizer. The second limits reported by Whatley[3] cannot then be regarded as the explosion limits for pure diborane-oxygen mixtures.

Acknowledgments

The authors are indebted to Mr. G. Stridde and Mr. J. Fisher, both of Rensselaer Polytechnic Institute, for preparation of diborane and x-ray analysis.

REFERENCES

1. Hurd, D. T.: *Chemistry of the Hydrides*, pp. 82–83, 93–94. New York, John Wiley and Sons, Inc., 1952.
2. Price, F. P.: J. Am. Chem. Soc., *72*, 5361 (1950).
3. Whatley, A. T.: Ph.D. Thesis, Princeton Univ. (1952); Whatley, A. T., and Pease, R. N.: J. Am. Chem. Soc., *76*, 1997 (1954).
4. Shapiro, I., Weiss, H. G., Schmich, M., Skolnik, S., and Smith, G. B. L.: J. Am. Chem. Soc., *74*, 901 (1952).
5. (a) Maybury, P. C., and Koski, W. S.: J. Chem. Phys., *21*, 742 (1953). (b) Weiss, H. G., and Shapiro, I.: J. Am. Chem. Soc , *75*, 1221 (1953); (c) Clarke, R. P., and Pease, R. N.: J. Am. Chem. Soc., *73*, 2132 (1951). (d) Bragg, J. K., McCarty, L. V., and Norton, F. J.: J. Am. Chem. Soc., *73*, 2134 (1951).
6. Bauer, S. H., Shepp, A., and McCoy, R. E.: J. Am. Chem. Soc., *75*, 1003 (1953).
7. Lewis, B., and von Elbe, G.: *Combustion, Flames and Explosions of Gases*, pp. 27–30. New York, Academic Press, 1951.
8. Bauer, S. H.: Private Communication, Chemistry Department, Cornell Univ.
9. Harteck, P.: Private Communication, Chemistry Department, Rensselaer Polytechnic Inst.
10. Thorne, P. C. L., and Ward, A. M.: *Ephraim, Inorganic Chemistry*, p. 827. New York, Nordeman Publishing Company, 1939.

81

SPECTRA AND COMBUSTION MECHANISM OF FLAMES SUPPORTED BY THE OXIDES OF NITROGEN

By H. G. WOLFHARD AND W. G. PARKER

Introduction

In a paper presented at the Fourth Symposium on Combustion[1] the authors described some premixed gas flames in which various fuels including hydrogen, carbon monoxide, ammonia and hydrocarbons were burned with nitric oxide and with nitrogen dioxide. Burning velocities and quenching diameters were reported which showed that the characteristics of these flames differed widely from those of the more familiar oxygen and air flames. It was suggested elsewhere[2] that one of the reasons for these differences lay in the fact that nitric oxide can react in two ways. It can react with radicals such as NH or NH_2 in steps which require only a small activation energy or it can decompose thermally by a process which requires a high activation energy and which will not proceed unless the temperature approaches about 2800°C. In many flames both mechanisms are operative, but do not occur at the same temperature level. The combustion then takes place in two or more stages separated in space and the flame exhibits two or even three reaction zones.

A detailed spectroscopic examination has been made of these flames and the results which are reported strongly support and amplify the views expressed by Adams et al.[2]. The extension of spectroscopy to flames burning with oxidants other than oxygen has also produced a good deal of fresh evidence of the existence of non-equilibrium conditions in the combustion zone. This phenomenon is discussed at the end of the chapter.

Experimental

For spectroscopic examination of a premixed gas flame the reaction zone should be flat and of sufficient optical depth for the application of absorption spectroscopy. To obtain a flame of this kind which was nonturbulent and did not strike back a rectangular burner was used having a length along the optical path of about 1 cm and a width of around 0.1 cm depending on the quenching distance of the flame. The reaction zone on this burner was nearly flat as shown in Figure 1 (top right). The optical arrangement for absorption work is shown diagrammatically in Figure 1 (bottom) and it should be emphasized that quartz fluorite achromatic lenses are essential. The ones used by us had a focal length of 30 cm and a diameter of 2 cm although the actual aperture employed was smaller than this and much less than that shown in the diagram. The light source was either the anode of a carbon arc, a medium pressure mercury vapor lamp or a hydrogen discharge tube and the spectrograph was either a Hilger medium quartz instrument or a Hilger-Littrow type instrument with a quartz or glass set. The type of photographic plates used are indicated in the descriptions to Figures 2 and 3.

Experimental Results

NITROUS OXIDE FLAMES

The spectra of these flames burning at atmospheric pressure are similar to those obtained previously at reduced pressure[4]. Thus the reaction zone of a hydrogen-nitrous oxide flame emits ammonia α-bands, NH, OH and NO bands, and these bands are strongest for mixtures near to stoichiometric proportions. The burned gases emit only OH bands and even these are much weaker than in the reaction zone.

The reaction zone of an ethylene flame supported by nitrous oxide is typical of all hydrocarbon fuels and emits C_2, CH, CN, OH and NO bands with the maximum intensity in slightly fuel rich mixtures. The burned gases again emit only OH bands which are weaker than those in the reaction zone (Fig. 2A). Mixtures which are very fuel rich burn with a halo above the reaction zone. This halo, in which CN and C_2 bands appear, is also shown by flames supported by NO and NO_2 and occurs when there is not sufficient oxygen in the mixture to convert all the carbon to carbon monoxide. Under these extremely reducing conditions C_2 and CN molecules formed in the reaction zone have an unusually long lifetime and persist in the burned gases. In an ethylene flame a halo appears in mixtures richer than $C_2H_4 + 2N_2O$.

The absorption spectra of the nitrous oxide flames were examined and revealed several inter-

esting differences. In the hydrogen flame the OH absorption bands unlike the emission bands showed no enhanced strength in the reaction zone. The NO bands behaved similarly although some NO absorption was present in the burned gases whatever the mixture strength, which in the case of fuel rich flames indicates a small degree of incomplete combustion. In lean flames the Schumann-Runge oxygen bands could be seen in absorption. In an ethylene flame the NO bands are emitted so strongly in the reaction zone that reversal cannot be achieved even with the continuum of a powerful hydrogen lamp. In this flame NH absorption bands occur at a position in the reaction zone where the OH absorption bands are still weak.

NITRIC OXIDE FLAMES

Emission spectra

In the NO decomposition flame which was obtained by the authors[1] Schumann-Runge oxygen bands were observed in emission from the visible region down to a wavelength of 2200Å (Fig. 2B). This was the only emission apart from some OH bands which may be attributed to the presence of moisture. When hydrogen was burned with nitric oxide, OH and O_2 bands were the principal emitters and appeared in both the reaction zone and in the burned gas. Weak NO bands may have been present in the reaction zone. Very weak NH bands were also observed but these may have been caused by the presence of N_2O as impurity. The NH bands disappeared when the hydrogen-nitric oxide mixture was preheated to 1000°C presumably because the N_2O was decomposed at this temperature.

The reaction zone of a methane-nitric oxide flame emits very weak ammonia-α and C_2 bands and strong CH, CN, NH, OH and NO bands. Other hydrocarbon flames give a similar spectrum except that the ammonia α-bands are missing and the C_2 bands are much stronger. Oxygen bands are always strongly emitted from the reaction zone and from the burned gas when the mixture is fuel lean. Contrary to their behavior in the nitrous oxide flames the OH bands have no enhanced strength in the reaction zone, and indeed in fuel lean flames OH emission is actually weaker in the reaction zone (Fig. 2C). Acetylene is an exception however. All fuel rich hydrocarbon-nitric oxide flames show the halo above the reaction zone which was discussed for the nitrous-oxide flames (Fig. 2D). Fuel lean flames possess a second reaction zone above the first. This coincides with an increase in the strength of the OH radiation brought about by an increase in the flame temperature as the excess nitric oxide decomposes. This is accompanied by a greyish continuous radiation in the visible region.

Two other flames were examined. The first of these was a moist carbon-monoxide-nitric oxide flame which has a yellowish reaction zone. The emissions from the reaction zone and the burned gases were similar and consisted of the CO-flame bands and weak OH bands. Oxygen bands were prominent in lean flames but there were no NH bands emitted at any mixture strength. In the other flame examined, ammonia was burned and NH_2, NH, OH and NO bands were observed in the flame front. The OH bands in the reaction zone were a little enhanced compared with the emission in the burned gas immediately above but the strength of these bands increased again a few millimeters higher up which seems to indicate a small temperature rise brought about by further reaction in the burned gas.

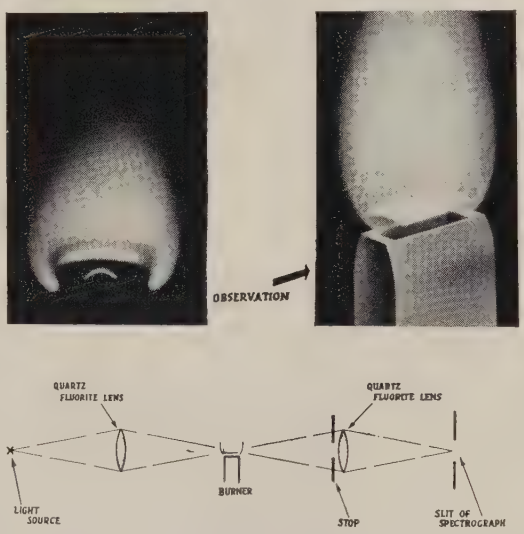

FIG. 1. Flat flame supported on rectangular burner, and scheme of optical system.

Absorption spectra

In the hydrogen-nitric oxide flame there are no intermediate radicals except OH which can be detected in absorption but it is possible to follow the NO γ bands through the flame. It was found that whatever the mixture strength the nitric oxide was decomposed in the reaction zone and

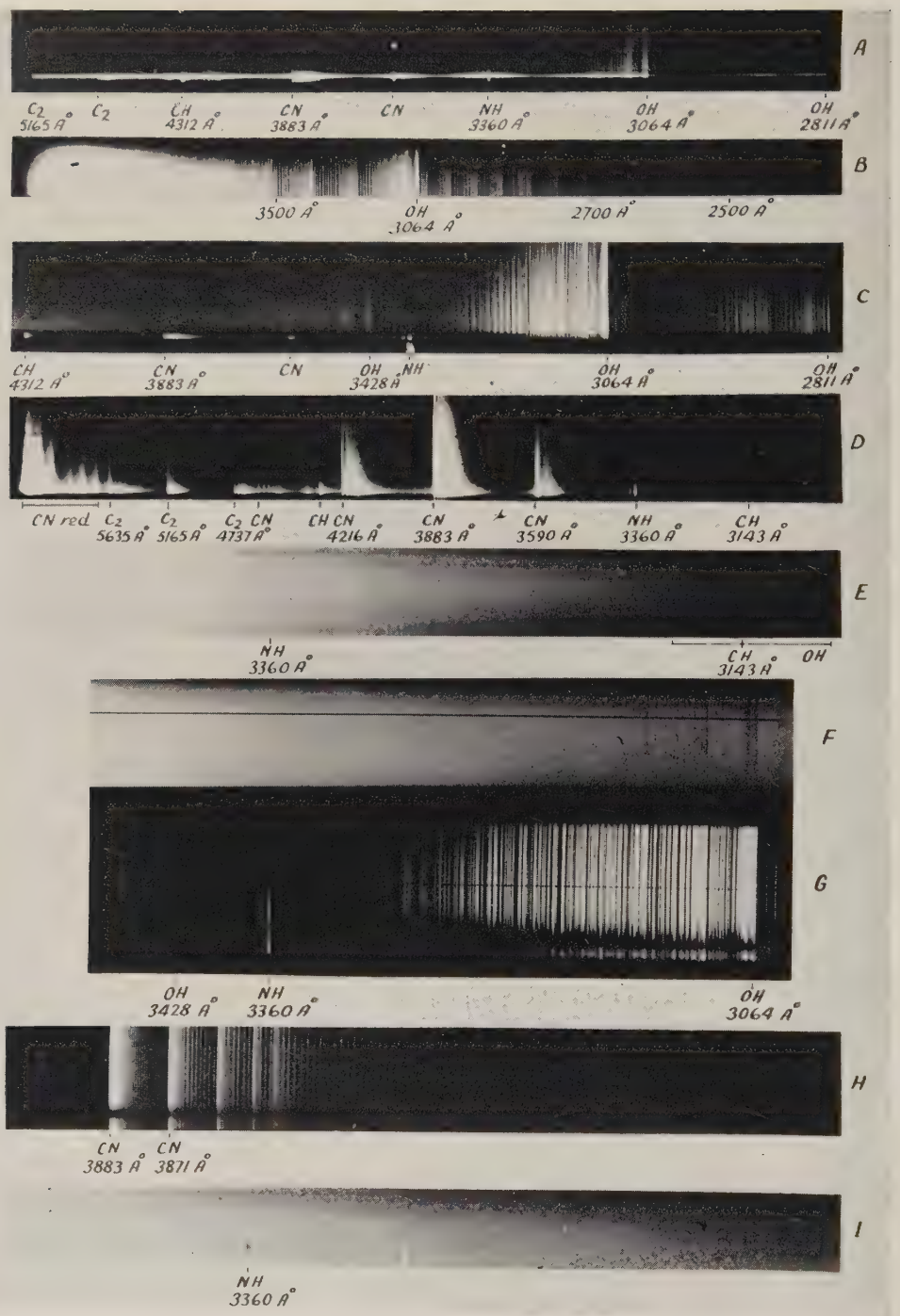

FIG. 2

NOTE: All the spectra shown with the exception of 2B and 3H were taken from flat flames supported on the rectangular burner illustrated in Fig. 1. The reaction zone can usually be identified and located in emission and absorption by the band systems of C_2, CN, NH etc. The radiation above this zone is emitted by the burnt gases. All the spectra were taken with a medium Hilger quartz spectrograph unless otherwise stated.

only very small concentrations corresponding to the equilibrium amounts appeared in the burned gas. In fuel weak mixtures the excess nitric oxide is decomposed and the oxygen can be detected by the Schumann-Runge bands in absorption (Fig. 3B).

Nitric oxide behaves differently in the ammonia-nitric oxide flame, however, and can be readily detected in absorption in the burned gas of nitric oxide rich flames. Decomposition of the excess nitric oxide does not take place and no oxygen bands can be detected (Figs. 3C and 3D).

The behavior of the hydrocarbon-nitric oxide flames is again shown to be more complex and depends on the nature of the hydrocarbon. Acetylene behaves rather like hydrogen and any excess nitric oxide is decomposed in the reaction zone. Contrary to other hydrocarbons acetylene shows an excess radiation in the reaction zone which is especially visible in the (0, 1) band of NO (Fig. 3A). Lower hydrocarbons such as ethane convert all the excess NO of weak mixtures into oxygen but it is noticeable that the resulting oxygen bands only begin a short distance above the reaction zone and this position corresponds to the second reaction zone mentioned above.

CN radicals have been detected in absorption in these flames by a line absorption method. The positive column of a carbon arc which emits CN at a temperature of about 6000°C was focused into the flame and the CN emission lines of the arc were absorbed by the CN radicals in the flame. This results in an interruption of the CN emission lines at the position of the reaction zone (Fig. 2H). In an acetylene-nitric oxide flame the concentration of CN radicals is sufficiently large for this effect to be very marked, and in an ethylene flame it can just be detected but it was not observed in an ethane flame. Thus the CN radical concentration in the reaction zone seems to depend on either the reaction velocity or on the temperature of the flame.

Absorption bands of NH radicals have been observed in a variety of flames. In an ammonia-oxygen flame these bands were very strong in the reaction zone and were not greatly affected by the mixture strength (Fig. 2I). In the ammonia-nitrous oxide flame the bands were almost as strong as those in the oxygen flame and in both cases the radicals are probably formed by the decomposition of the ammonia. In the ammonia-nitric oxide flame, however, the NH absorption is very weak and only just visible in fuel rich flames. This is an interesting difference, because the burning velocity of the nitric oxide flame is about the same as that of the nitrous oxide flame and the reaction velocities are presumably similar, also.

In hydrocarbon-nitric oxide flames the NH bands could not be observed in absorption. In the acetylene flame NH bands were in emission against the radiation of the anode of a carbon arc and the same was true for the CH band at 3143Å. These observations coupled with the fact that the neighboring bands of OH were obtained in absorption demonstrate the existence of non-equilibrium conditions in the acetylene flame (Fig. 2E).

NITROGEN DIOXIDE FLAMES

Emission spectra

In all hydrocarbon flames supported by nitrogen dioxide there are two visible reaction zones

FIG. 2

FIG. 2A. *Ethylene-nitrous oxide flame in emission.* Zenith plate. OH radiation stronger in reaction zone than in burnt gas.

FIG. 2B. *Nitric oxide decomposition flame in emission.* Flame supported in a 3 cm diameter quartz tube in a furnace at approx. 1000°C. Schumann-Runge bands of oxygen and OH bands can be seen.

FIG. 2C. *Ethane-nitric oxide flame (fuel lean) in emission.* Zenith plate. OH radiation weaker in reaction zone than in burnt gas.

FIG. 2D. *Acetylene-nitric oxide flame (very fuel rich) in emission.* HP_3 plate. C_2 and CN bands extend into hole above the reaction zone.

FIG. 2E. *Acetylene-nitric oxide flame in absorption.* Carbon arc light source and Hilger Littrow type spectrograph used with quartz set. Process plate. Bands of NH (3360) and CH (3143) stand out in emission whereas the OH band at 3064 appears only in absorption in the burnt gas.

FIG. 2F. *Hydrogen burning with a mixture of nitrous and nitric oxides.* Absorption spectrum. Carbon arc light source and Littrow type spectrograph. Zenith plate. OH bands alone seen in absorption.

FIG. 2G. *Hydrogen flame as in 2F seen in emission on the same plate.* Two reaction zones can be distinguished. The strength of the OH emission in the first reaction zone is not matched by a corresponding strength in absorption.

FIG. 2H. *Acetylene-nitric oxide flame in absorption* against the positive column of a carbon arc. Littrow type spectrograph with glass set. Panchromatic plate. The CN bands of the light source are absorbed in the reaction zone of the flame.

FIG. 2I. *Ammonia-oxygen flame in absorption.* Continuous radiation of the anode of the carbon arc used as light source. Littrow type spectrograph with quartz set. Process plate. NH bands seen in absorption in the reaction zone.

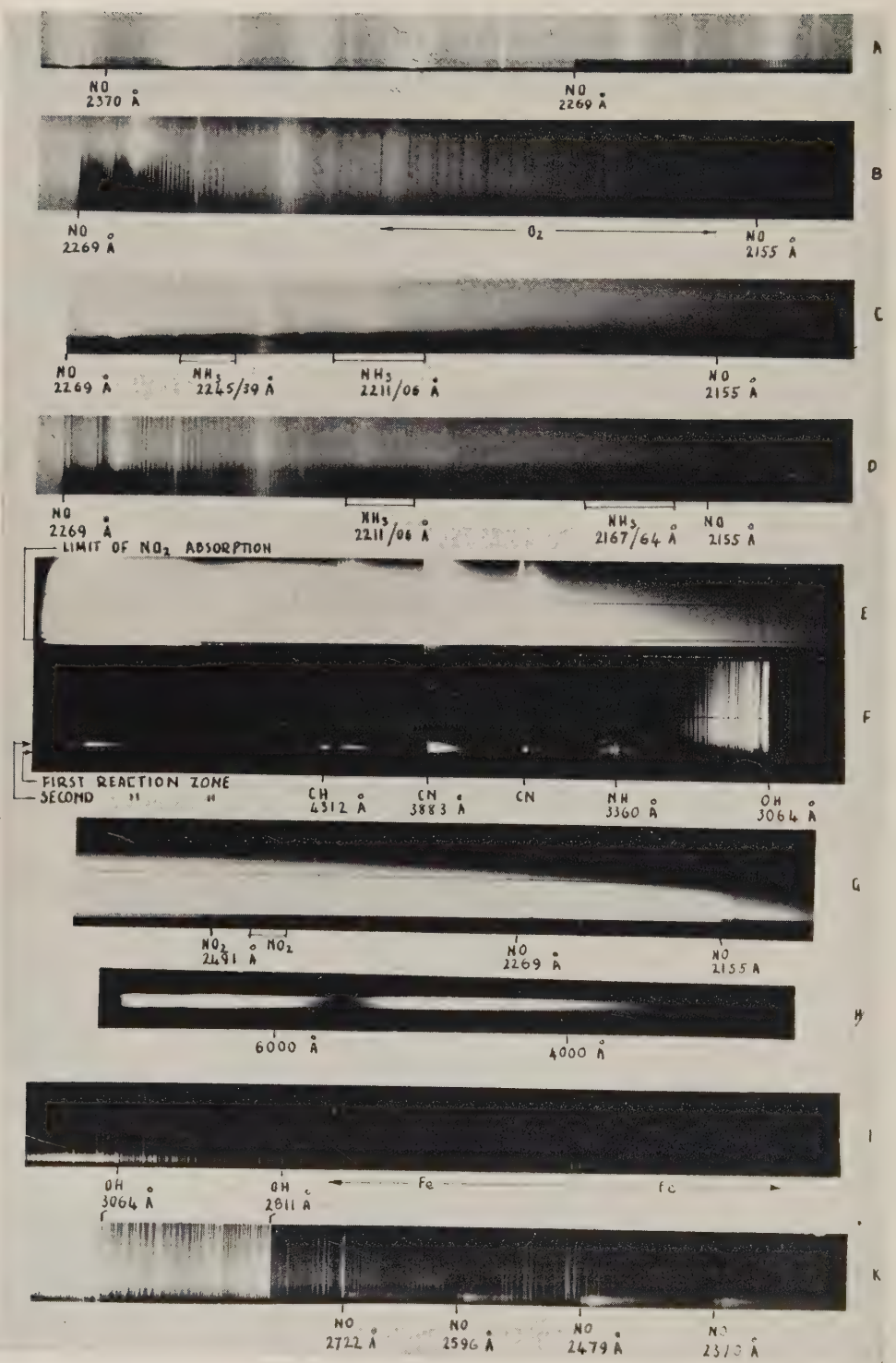

FIG. 3

(*See note on p. 720*)

and although the separation between these zones is small in fuel lean flames it increases to as much as 2 mm for very fuel rich mixtures (Fig. 1). The spectra of the two zones can be separately identified as shown in Figure 3F, but the emission of the second zone is usually much the stronger which makes identification difficult at times.

The emission of the second reaction zone is similar to that of a nitric oxide flame burning with the same fuel, and a halo may be observed as with the nitric oxide flame. Furthermore, the OH emission of flames of the lower hydrocarbons is weak in the second reaction zone but increases in strength in the gases above. This effect is particularly marked in fuel lean mixtures, as was the case with the nitric oxide flames, and in very lean flames three reaction zones appear, the last being the decomposition region of the excess nitric oxide formed in the flame. In fuel rich flames on the other hand, a carbon zone sometimes forms between the first and second zone. Its presence in this region is not surprising, since thermal cracking of the hydrocarbon must occur at the elevated temperature and oxygen is very deficient until the nitric oxide reacts in the second zone.

The emission of the first reaction zone was investigated more easily by quenching the second in a special burner. In this device the flame was allowed to strike back in a small quartz tube and settle on a smaller burner inside. The diameters of the tube and burner were such that only the first reaction zone remained on the burner with the tube acting as a sort of Smithells separator. The intensity of this reaction zone is not great and a Hilger-Raman type spectrograph with a glass prism was used to examine the flame. The spectrum was found to be completely continuous and stretched from the red into the blue region giving the overall impression of yellow light. Absorption bands of nitrogen dioxide were superimposed on the continuum because the reaction zone was conical and part of the light traveled through unburned gases.

Hydrogen and carbon monoxide flames supported by nitrogen dioxide have only one reaction zone and the spectrum of this is identical with that of the first reaction zone of the hydrocarbon flames (Fig. 3H). The three minima which appear in the spectrum are caused by the three sensitivity gaps in the Ilford long-range spectrum plates used.

If nitrogen dioxide is present in excess, the hydrogen and carbon monoxide flames show an after-glow which is caused by slow reaction in the burned gas. The after-glow has a grey color and its spectrum is again mainly continuous. In the hydrogen flame strong bands of NO and OH and weak bands of NH are superimposed on the continuum, and in the after-glow of the carbon monoxide flame OH and NO bands are visible. The first reaction zone of a separated hydrocarbon flame also shows an after-glow when NO_2 is in excess. This is not a proper second reaction zone although in a methane flame for example very

FIG. 3

FIG. 3A. *Acetylene-nitric oxide flame in absorption.* Continuous radiation from medium pressure Hg-vapour lamp used as light source. Littrow type spectrograph with quartz set. Schumann plate. Nitric oxide bands end abruptly in reaction zone where emission occurs.

FIG. 3B. *Hydrogen-nitric oxide flame (fuel lean) in absorption.* Reaction zone not quite flat. Hg vapour lamp used as light source. Littrow type spectrograph with quartz set. Schumann plate. Excess nitric oxide is decomposed and oxygen bands appear.

FIG. 3C. *Ammonia-nitric oxide flame (fuel rich) in absorption.* Hg-vapour lamp used as light source. Littrow type spectrograph with quartz set. Schumann plate. Absorption bands of ammonia and nitric oxide end in the reaction zone.

FIG. 3D. *Ammonia-nitric oxide flame (fuel lean) in absorption.* Conditions as in Fig. 3C. Ammonia absorption bands end in the reaction zone but those of nitric oxide go partially through. No oxygen bands are observed.

FIG. 3E. *Methane-nitrogen dioxide flame in absorption.* Carbon arc used as light source. Panchromatic plate. The limit of the NO_2 absorption marks the beginning of the first reaction zone.

FIG. 3F. *Methane flame as in 3E seen in emission on the same plate.* Position of absorption and emission can be correlated relative to the hair lines.

FIG. 3G. *Methane-nitrogen dioxide flame in absorption.* Hydrogen discharge lamp used as light source. Schumann plate. NO_2 absorption can be seen together with the appearance and disappearance of NO bands.

FIG. 3H. *Carbon monoxide-nitrogen dioxide flame in emission.* Raman spectrograph with glass set. Long range spectrum plate. Only one reaction zone is observed corresponding to the first reaction zone of a hydrocarbon-nitrogen dioxide flame.

FIG. 3I. *Ethane-oxygen flame in emission.* Zenith plate. Small quantity of iron penta-carbonyl added. Fe lines seen to be highly excited in the reaction zone.

FIG. 3K. *Ethane-nitric oxide flame in emission.* Zenith plate. Small quantity of iron penta carbonyl carbonyl added. Fe lines of equal strength in reaction zone and burnt gas. Reaction zone indicated by the emission of the NO bands.

weak NH and CN bands are visible together with the bands of NO and OH.

Absorption spectra

Absorption experiments were particularly interesting because nitrogen dioxide and the nitric oxide derived from it in the flame could be detected. Figures 3E and 3F show an absorption and an emission spectrum respectively of a flame under the same conditions. The lower hairline seen in the spectra was located just under the second reaction zone and it may be seen that the NO_2 absorption ceases at the beginning of the first reaction zone and that the OH absorption bands which are an indication of the temperature level in this part of the flame begin just after the second reaction zone. Absorption by NO bands begins where the NO_2 disappears but it does not persist far into the second reaction zone (Fig. 3G). Some indication of the progress of the fuel molecules was obtained by mixing benzene with methane and observing the disappearance of the benzene bands in absorption. These bands disappeared when the NO_2 bands disappeared at the beginning of the first reaction zone.

Table 1

Composition of combustible	Theoretical flame temperature	Experimental flame temperature
	°C	°C
$H_2 + \frac{1}{2}O_2$	2810	—
$H_2 + NO$	2840	2820
$H_2 + \frac{1}{2}NO_2$	2660	1550
$NH_3 + \frac{3}{4}O_2$	2560	—
$NH_3 + 1\frac{1}{2}NO$	2675	2640
$C_2H_2 + 2\frac{1}{2}O_2$	3055	—
$C_2H_2 + 5NO$	3090	3095
$C_2H_2 + 7NO$	2855	—
$C_2H_6 + 7NO$	—	2865

Hydrogen and carbon monoxide flames show strong nitric oxide bands in absorption in their burned gas above the single reaction zone. This fact holds for fuel rich and lean flames, and shows that NO does not play a major part in the reaction. In hydrocarbon flames the absorption in the burned gas is analogous to that of the NO flame.

Flame Temperatures

The temperature of a flame is the best indication of the completeness of the combustion and measurements were therefore made using the line-reversal method. For flames of moderate temperature sodium was introduced locally as sodium chloride; in high temperature flames, however, it was more convenient to use the OH radicals already contained in the flame.

The experimental results for various flames are shown in Table 1 in comparison with the theoretical adiabatic flame temperature assuming complete combustion.

In most cases the agreement is good and within the experimental error. In a fuel lean ammonia-nitric oxide flame which is not quoted in Table 1 the flame temperature seemed to depend very much on the flame size because the NO which escaped decomposition in the reaction zone decomposed slowly in the burned gas and the resulting temperature rise was dependent on cooling by the surrounding air. Hydrocarbons supported by nitric oxide burn completely as shown in Table 1 and it is fairly certain that the same is true when these fuels burn with NO_2. The only striking exceptions are the hydrogen-NO_2 flame and probably the carbon monoxide-NO_2 flame in which the nitric oxide formed does not react, and the combustion does not go to completion.

Relative Intensities of the OH Bands

The emissions of many bands and especially the OH bands differ very much in strength in the reaction zones of various flames. Comparisons can only be made for flames having the same optical depth and burning at the same pressure. At a pressure of 20 mm Hg and with a light path of 2 cm the following relative intensities of the OH bands in various flames were estimated assuming the strength of these bands in the hydrogen-oxygen flame to be unity.

Nature of flame	Relative intensity of OH bands
NH_3-O_2	5
H_2-NO_2	$\frac{1}{100}$
H_2-N_2O	180

These flames were burning stoichiometric mixtures, and theoretically the temperature of the H_2-N_2O flame is close to that of the H_2-NO_2 flame, but the strength of the OH emission in the reaction zone is nearly 20,000 times as great. This indicates that the reaction mechanism is quite different in the two flames. It may be mentioned here also that the radiation of OH radicals is usually stronger in the reaction zone than in the burned gas which means that either the concen-

tration is higher in the reaction zone or the mode of excitation is not thermal.

Flames with Double Reaction Zones

The formation of more than one reaction zone in a flame is linked with the fact that different reactions begin at different temperature levels in the combustion wave. In several of the flames studied two principal reactions began at nearly the same temperature level and no clear separation occurred. An example of this is a hydrocarbon burning with a mixture of nitric oxide and air in which the reaction zone was more complex than that of a flame supported by either air or nitric oxide alone but did not separate into two distinct luminous zones. On the other hand a flame of hydrogen burning with a mixture of nitrous and nitric oxides has two separate reaction zones because the H_2/N_2O reaction and the H_2/NO reaction are very different and begin at very different temperature levels. In a single combustion wave reactions of this kind, although separate, must be interrelated and the resulting spectrum depends very much on variables such as the N_2O/NO ratio and the mixture strength. A complete analysis of this and similar flames has not yet been attempted on account of the experimental difficulties. Evidence of excess excitation of the OH bands in part of the flame has been obtained however and in Figure 2G it may be seen that very strong OH bands are emitted by the H_2/N_2O reaction in the first zone, while the OH radiation from the H_2/NO reaction on the second zone is not excessive compared with that in the burned gas. The second reaction zone in this spectrum can be distinguished by a continuum in the visible region. From the absorption spectrum of the same flame (Fig. 2F) it may be inferred that there is no excess OH concentration in the first reaction zone because the OH absorption is clearly much weaker in this part of the flame.

Abnormal Excitation in Flames

A method of distinguishing between thermal and non-thermal radiation in flames has been described[5] which depends on the relative intensities of lines in the iron emission spectrum, the iron being introduced by adding traces of iron penta-carbonyl to the unburned gases. Figure 3I shows an example of this technique applied to a fuel rich acetylene-oxygen flame. The iron lines are preferentially excited in the reaction zone and this can be readily seen from the Fe lines in the ultraviolet region.

We have applied the technique to flames supported by the oxides of nitrogen, and Figure 3K shows the spectra of an ethane nitric oxide flame where the iron lines are if anything a little weaker in the reaction zone and there is evidently no excess excitation in this flame.

In a faster burning flame such as acetylene and nitric oxide a slight amount of excess excitation is observed, however. NO_2 flames behave in all respects like the NO flames as regards the second reaction zone. The first reaction zone is not hot enough to give an Fe emission spectrum. In ammonia flames there is some excess excitation when oxygen is used and only slight evidence of it when oxygen is replaced by nitric oxide.

All flames burning with nitrous oxide show the effect quite strongly.

Diffusion Flames

Either NO or NO_2 can replace air or oxygen in a diffusion type flame. A nitric oxide-hydrocarbon diffusion flame is similar in appearance to an oxygen flame and with the help of absorption spectroscopy it may be seen that most of the NO decomposes into oxygen (and nitrogen) in the high temperature zone. A little of the NO diffuses into the carbon zone and is responsible for rather weak CN and NH emission bands which occur in the position occupied by the C_2 and CH bands of an oxygen flame[3].

A hydrocarbon-NO_2 diffusion flame is difficult to keep steady but in this flame also it seems that the oxidizer has sufficient time to decompose before reacting with the fuel. The zone in which the NO_2 decomposes to NO radiates a yellow continuum which is presumably identical with that observed in the premixed H_2-NO_2 flame, and the cause of the emission is probably a reverse reaction such as $NO + O \rightarrow NO_2$ rather than a reaction involving the fuel.

Discussion of Results

We believe that the results obtained in the spectroscopic study of these flames have helped to clarify our knowledge of the reactions involved and have also provided valuable information on the mode of excitation of molecules in the reaction zone.

There can be little doubt now that two mechanisms exist whereby nitric oxide is decomposed in flames. At high temperatures and in the absence

of suitable radicals such as NH, NH_2 and possibly C_2, CH and CN, nitric oxide decomposes thermally. Thus it is decomposed in a hydrogen-nitric oxide flame irrespective of the mixture strength because the temperature of such flames is always sufficiently high. In an ammonia-nitric oxide flame, on the other hand, the temperature is lower and the rate of thermal decomposition is too small to be significant. Decomposition in this flame depends on a radical mechanism and is not always complete. In fuel lean flames, for example, the concentration of radicals is limited by the lower concentration of the fuel and the lower temperature so that only a portion of the nitric oxide is decomposed, the rest is present in the burned gas.

The hydrogen-nitrogen dioxide flame is interesting and shows the remarkable stability of nitric oxide. In this flame there is no second reaction zone as in a lean hydrocarbon-nitric oxide flame and the nitric oxide formed in the first reaction zone does not seem able to react for two reasons: (1) because the final temperature is probably below the threshold required for thermal decomposition, and (2) because the initial stage in the reaction between hydrogen and nitrogen dioxide has too high a burning velocity for the subsequent slow reaction between hydrogen and nitric oxide to follow. The second zone even if it could exist would not be stationary.

This general picture of the role of nitric oxide in flames is confirmed by a number of the detailed spectroscopic observations. It is in accord with the temperature measurements and the absorption experiments which show the presence or absence of nitric oxide and oxygen in the burned gases. The purely thermal mode of decomposition does not seem to involve radicals such as NH or NH_2 and these are not detected in the decomposition flame or in the hydrogen-nitric oxide flame. In the ammonia flame, however, reaction occurs at a lower temperature and it seems fairly certain that NH and NH_2 radicals known to be present in the flame provide an alternative mechanism for

Table 2

Flame	Condition of flame	Remarks	Reference
Hydrocarbon-oxygen	Premixed	High excitation	5
Hydrocarbon-air	Premixed	High excitation (very pronounced)	5
Hydrogen-O_2 and carbon monoxide-O_2	Premixed	Mainly thermal with slightly high excitation	Unpublished results
Hydrogen-air and carbon monoxide-air	Premixed	Slight indication of high excitation	Unpublished results
Hydrogen-nitrous oxide and carbon monoxide-nitrous oxide	Premixed	High excitation (moderate)	5
Ammonia-oxygen and ammonia-nitrous oxide	Premixed	High excitation	5
Cyanogen-oxygen	Premixed	High excitation	5
Carbon disulfide-oxygen	Premixed	Thermal radiation	5
Methane, ethane and ethylene-nitric oxide	Premixed	Thermal	
Acetylene-nitric oxide	Premixed	Very slight indication of high excitation	
Ammonia-nitric oxide	Premixed	Moderate amount of high excitation	
Ethane-nitrogen dioxide	Premixed	Thermal	
Acetylene-nitrogen dioxide	Premixed	Very slight high excitation (in second reaction zone)	
Hydrocarbon-oxygen	Diffusion, high pressure	Thermal	3
Hydrocarbon-oxygen	Diffusion, very low pressure	High excitation very pronounced	3
Hydrocarbon-air or very diluted hydrocarbon with oxygen	Diffusion, any pressure	High excitation	Unpublished results

the decomposition of the nitric oxide. It is probably significant that the NH concentration in the reaction zone of the ammonia-nitric oxide flame is smaller than that in the ammonia-oxygen or the ammonia-nitrous oxide flames since the NH is rapidly removed by reaction with nitric oxide. Whether radicals such as C_2, CH and CN play a similar role in the hydrocarbon-nitric oxide flame is uncertain, but it seems probable, although the concentration of CN is found to be high, indicating a low rate of removal.

All the spectroscopic evidence shows that the second reaction zone of hydrocarbon-nitrogen dioxide flames is identical with a hydrocarbon-nitric oxide flame. The hydrocarbon is not completely decomposed into hydrogen and carbon monoxide in the first reaction zone, however, because subsequent reaction of these gases with nitric oxide would not yield the C_2, CH, CN and NH radicals which are the principal characteristics of the second reaction zone. It is, however, likely that complicated hydrocarbons such as benzene break down to simpler ones which cannot be detected by absorption. The first reaction zone of the hydrocarbon-nitrogen dioxide flame is difficult to understand since the radiation is identical with that of a pure NO_2 decomposition into NO and O_2 in a diffusion flame, and does not show any characteristics which help to unravel the reactions concerned. It is strange that the oxygen produced in the decomposition of the nitrogen dioxide does not react with the hydrocarbon in the usual way to give rise to radiation of C_2, CH and OH. The explanation may be that the reactions in the first reaction zone go at very low temperatures[1] and are analogous to those in a cool flame, where the emission by these radicals is also missing.

In most flames OH radiation is much stronger in the reaction zone than in the burned gas but there is no corresponding enhancement of the absorption of the OH bands in the reaction zone which clearly indicates nonthermal excitation. This phenomenon is absent, however, in hydrocarbon-nitric oxide and nitrogen dioxide flames, except for acetylene. In a similar way, iron atoms show excess radiation in the reaction zone of many flames, but appear to be thermally excited in the very hot nitric oxide and nitrogen dioxide. The behavior of iron atoms introduced as traces of iron carbonyl has been used as a basis of assessing the existence of abnormal radiation in various flames and the results of the tests are summarized in Table 2.

It is clear from this table, that the excess excitation in the reaction zones of flames is a matter of degree rather than kind. Two variables seem to influence the effect, viz., flame-temperature and reaction velocity. It is proposed here that reactions in hot gases always lead to a disturbance of the Maxwell-Boltmann distribution, because a number of collisions are involved before statistical equilibrium is installed. Whether or not this disturbance is observable will depend on the velocity of the reaction and on temperature. At high temperatures fast particles are present in equilibrium and a small disturbance will not be detected. These two parameters cannot explain all the facts, but provide a basis for a general understanding of the phenomena in both premixed gas and diffusion flames.

A hot diffusion flame has only a small reaction velocity as diffusion is the rate determining factor, the temperature is very high and nonthermal conditions are not observed. If such a flame is highly diluted with inert gas the reaction velocity is not much affected, but the temperature is greatly reduced and nonthermal radiation may be detected by the iron spectrum technique already described. Premixed hydrocarbon-oxygen flames have both a high reaction velocity and a high temperature. The disturbance seems to be so strong that despite the high temperature the effect shows up by a strengthening of the iron lines in the ultraviolet relative to the burned gas. Hydrocarbon-air flames have a lower temperature and a smaller reaction velocity, and the effect is very strong. It seems that at low temperatures iron lines resulting from higher electronic states are thermally excited so little that the method is very sensitive and a small disturbance can be readily detected. The behavior of nitric oxide and nitrogen dioxide flames fits in with this general picture. These flames are even hotter than oxygen flames; despite the greater heat, the burning velocity is only about one-tenth and thus the reaction velocity is only one-hundredth. The effect is clearly not observable as not enough fast particles out of equilibrium are present. Acetylene flames are slightly different because they are quite fast, and therefore the non-thermal radiation becomes observable.

It seems to be possible to explain the thermal or nonthermal nature of most premixed and diffusion flames by considering only the temperature and reaction velocity. There is no doubt that a more quantitative treatment will make it necessary to consider the type of collision and the exact way in which energy is dissipated in the primary act

of reaction. Hydrogen and carbon monoxide flames which show only slight nonthermal behavior will certainly have to be considered in such detail, since they do not easily fit into the simplified picture presented above.

Acknowledgments

Acknowledgment is made to the Chief Scientist, British Ministry of Supply, for permission to publish this paper. Crown copyright Reserved Reproduced with the permission of the Controller of Her Brittanic Majesty's Stationery Office.

REFERENCES

1. Parker, W. G., and Wolfhard, H. G.: *Fourth Symposium (International) on Combustion*, p. 420. Baltimore, The Williams & Wilkins Co., 1953.
2. Adams, G. K., Parker, W. G., and Wolfhard, H. G.: Faraday Soc., *14*, 97 (1935).
3. Wolfhard, H. G., and Parker, W. G.: Proc. Phys. Soc., *A65*, 2 (1952).
4. Gaydon, A. G., and Wolfhard, H. G.: *Third Symposium on Combustion Flame and Explosion Phenomena*, p. 504. Baltimore, The Williams & Wilkins Co., 1949.
5. Gaydon, A. G., and Wolfhard, H. G.: Proc. Roy. Soc., *A205*, 118 (1951).

82

PREDICTION OF THE QUENCHING EFFECT OF VARIOUS SURFACE GEOMETRIES

By A. L. BERLAD and A. E. POTTER, Jr.

Introduction

Recent flame quenching research[1] has indicated that there should be a set of simple relations among the various channel geometries which are capable of just quenching a given flame at a given pressure. The diffusional quenching mechanism proposed by Simon et al. is used there to predict that the quenching effect of a cylindrical tube of a given diameter d_c is equivalent to that displayed by infinitely long plane parallel plates of separation d_p when

$$d_p = \sqrt{12/32}\, d_c$$

An adequate check of this relation was somewhat hindered at that time by the facts that (1) in practice, quenching data associated with infinitely long plane parallel plates can be at best only approximated to by rectangular channels of large length to width ratio, and (2) rectangular slot quenching data[2] are usually obtained with a downward propagating flame, whereas cylindrical tube quenching data[1] are usually obtained with an upward propagating flame.

The objectives of this investigation were essentially twofold:

(1) To derive, on the basis of the average active particle chain length criterion of Simon et al.[1], or on an equivalent thermal basis, a set of equations which predict the relations among the dimension of a number of simple geometries which are capable of just quenching a given flame at a given pressure, and

(2) To test several of these relations by determining experimentally the wall quenching of downward propagating propane-air flames as a function of fuel-air ratio and pressure for rectangular slots, cylinders, and cylindrical annuli.

Nomenclature

The following symbols are used in this paper:

A fraction of molecules present in gas phase which must react for flame to continue to propagate
a inside annulus diameter
B_1 an arbitrary constant
B_2 an arbitrary constant
b_e ellipse major axis
b_r rectangular slot length
C_T total number of active particles
c numerical concentration of active particles
$\bar{c}$ average numerical concentration of active particles
c_0 number of active particles created per unit time per unit volume
D_i diffusion coefficient for active particles of one kind

d quenching distance
d_a outside annulus diameter
d_c cylinder diameter
d_e minor axis of ellipse
d_p plane parallel plate separation
d_r rectangular slot width
d_t side length of equilateral triangle
G quenching geometry factor
k_i specific rate constant for reaction of active particles of one kind with fuel molecules
N_f average number of fuel molecules per unit volume of reaction zone
n power describing the temperature dependence of the diffusion coefficient, $D \propto T^n$
p pressure
r plane polar coordinate
T_0 initial burner wall temperature and temperature of unburned gas
T_R reaction temperature
ν average number of effective collisions of active particle with gas phase molecules before the particle collides with and is destroyed at a wall
τ time between effective colisions
φ equivalence ratio

SUBSCRIPTS

a annulus
c cylinder
e ellipse
G geometry type
i active particle species
p plane parallel plates of infinite extent
r rectangular slot
t equilateral triangle

Theory and Derivations

The diffusional quenching equation of Simon et al.[1] may be written

$$d_G = \sqrt{\frac{A}{k_i}\left(\frac{T_R}{T_0}\right)^n \frac{G}{N_f \sum_i (p_i/D_i)}} \qquad (1)$$

where d_G is the quenching distance for any given geometry and G is a factor associated with that geometry. It is assumed that d^2/G is constant for all quenching gometries and that a flame will be quenched when the average chain length for a given active particle species falls below some critical value[1]. This critical value of ν_G is then the same for all geometries and may be written[3]

$$\nu_G = \frac{d_G^2}{GD_i\tau_i} = \frac{\bar{c}_G}{c_0\tau_i} \qquad (2)$$

For any two geometries, equation (2) gives

$$\frac{d_1^2}{d_2^2} = \frac{G_1}{G_2} \qquad (3)$$

It is thus possible to predict the relative quenching behavior of any two quenching geometries on the basis of the geometry factors obtained from the average chain length calculations.

It should be noted here that a thermal criterion exists for quenching which is fully equivalent to the average active particle chain length criterion of Simon et al.[1]. Equation (2) indicates that ν_G is proportional to $\bar{c}_G$. Also, the concentration term of the differential equation of diffusion is entirely analogous to the temperature excess term of the differential equation of conduction. Thus, it follows that the fully equivalent thermal criterion is one which requires that a given flame be quenched when its average temperature excess falls below some critical value. However, the specific cases treated below will be computed on the basis of the active particle chain length criterion.

QUENCHING BY CYLINDRICAL TUBES AND PLANE PARALLEL PLATES OF INFINITE EXTENT

On the basis of the average chain length calculations of Semenoff[3], a relation between the quenching distances associated with cylindrical tubes and plane parallel plates of infinite extent is given by Simon et al.[1]. For these two geometries, equation (2) yields

$$\nu_c = \frac{d_c^2}{32D_i\tau_i} = \frac{\bar{c}_c}{c_0\tau_i} \qquad (4)$$

and

$$\nu_p = \frac{d_p^2}{12D_i\tau_i} = \frac{\bar{c}_p}{c_0\tau_i} \qquad (5)$$

These two geometries will each just quench a given flame when $\nu_p = \nu_c$. At this condition, then $\bar{c}_c = \bar{c}_p$ and $d_p = \sqrt{12/32}\, d_c$.

QUENCHING BY RECTANGULAR SLOTS

In order to calculate the flame quenching effects of rectangular channels, one may proceed by first solving the diffusion equation subject to the appropriate boundary conditions. Thus, consider a rectangle with center at the origin of the x-y plane. The rectangle is of length b_r and of width d_r. Let this rectangle correspond to a typical cross section of a rectangular channel of infinite extent in which active particles are being

generated uniformly throughout the volume and destroyed on collision with the walls.

The differential equation of diffusion describing this case is

$$\frac{\partial^2 c_r}{\partial x^2} + \frac{\partial^2 c_r}{\partial y^2} = -\frac{c_0}{D_i} \tag{6}$$

subject to the boundary conditions

$$c_r = 0 \text{ at } \begin{Bmatrix} x = \pm d_r/2 \\ y = y \end{Bmatrix} \tag{7a}$$

and

$$c_r = 0 \begin{Bmatrix} x = x \\ y = \pm b_r/2 \end{Bmatrix} \tag{7b}$$

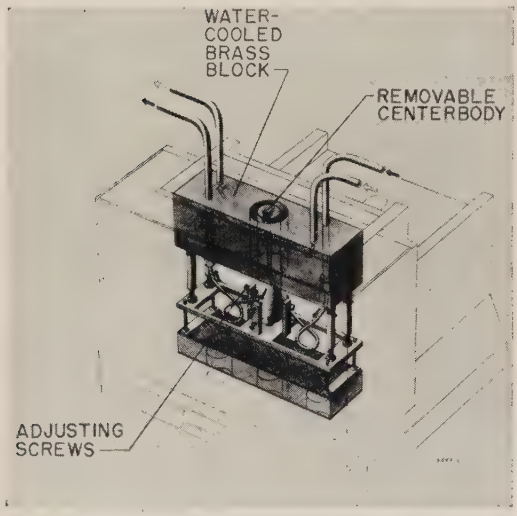

FIG. 1. Slot burner with annular insert.

Considering a unit height, the total number of active particles in the rectangular channel $C_{T,r}$ is given by

$$C_{T,r} = 4 \int_0^{b_r/2} \int_0^{d_r/2} c_r dx dy = \bar{c}_r b_r d_r \tag{8}$$

The formal mathematical problem associated with equations (6) and (7) corresponds to other physical problems which have already been treated and which are presented by Jakob[4] and by Purday[5]. The results given by these authors may be used to calculate relative values of c_r for a range of length-to-width ratios of the rectangular slot. The factor G_r may be evaluated as a function of (d_r/b_r) through the use of these values. The results may then be fitted to a quadratic equation and used with equation (2) to give

$$\nu_r = \frac{\left[1 - 0.300\left(\frac{d_r}{b_r}\right) - 0.047\left(\frac{d_r}{b_r}\right)^2\right] d_r^2}{12 D_i \tau_i} \tag{9}$$

QUENCHING BY CYLINDRICAL ANNULI

Proceeding in a similar manner, consider an annulus of infinite extent that is defined by two concentric cylinders of diameters a and d_a, where $a < d_a$. As before, let this annulus represent a region in which active particles are uniformly generated throughout the volume and destroyed on collision with the walls.

The differential equation of diffusion describing this case is given in plane polar coordinates as

$$\frac{1}{r}\frac{d}{dr}\left(r\frac{dc}{dr}\right) + \frac{c_0}{D_i} = 0 \tag{10}$$

The boundary conditions are

$$\begin{matrix} c = 0 \\ r = a/2 \end{matrix} \tag{11a}$$

and

$$\begin{matrix} c = 0 \\ r = d_a/2 \end{matrix} \tag{11b}$$

It can be shown[6] that equation (10) has the solution

$$c = B_1 + B_2 \log_e r - \frac{1}{4}\frac{r^2 c_0}{D_i} \tag{12}$$

Application of the boundary conditions gives

$$B_1 = \frac{1}{16 D_i}\left[a^2 c_0 - \frac{c_0(a^2 - d_a^2)\log_e (a/2)}{\log_e (a/d_a)}\right] \tag{13a}$$

and

$$B_2 = \frac{c_0(a^2 - d_a^2)}{16 D_i \log_e (a/d_a)} \tag{13b}$$

Thus

$$c = \frac{c_0}{16 D_i}\left[a^2 - 4r^2 + (d_a^2 - a^2)\frac{\log_e (a/2r)}{\log_e (a/d_a)}\right] \tag{14}$$

When a unit height is considered, the total number of active particles in the annulus is given by

$$C_{T,a} = \int_{a/2}^{d_a/2} c(2\pi r)\, dr \tag{15}$$

or

$$C_{T,a} = \frac{\pi c_0(d_a^2 - a^2)}{128 D_i}\left[a^2 + d_a^2 + \frac{d_a^2 - a^2}{\log_e (a/d_a)}\right] \tag{16}$$

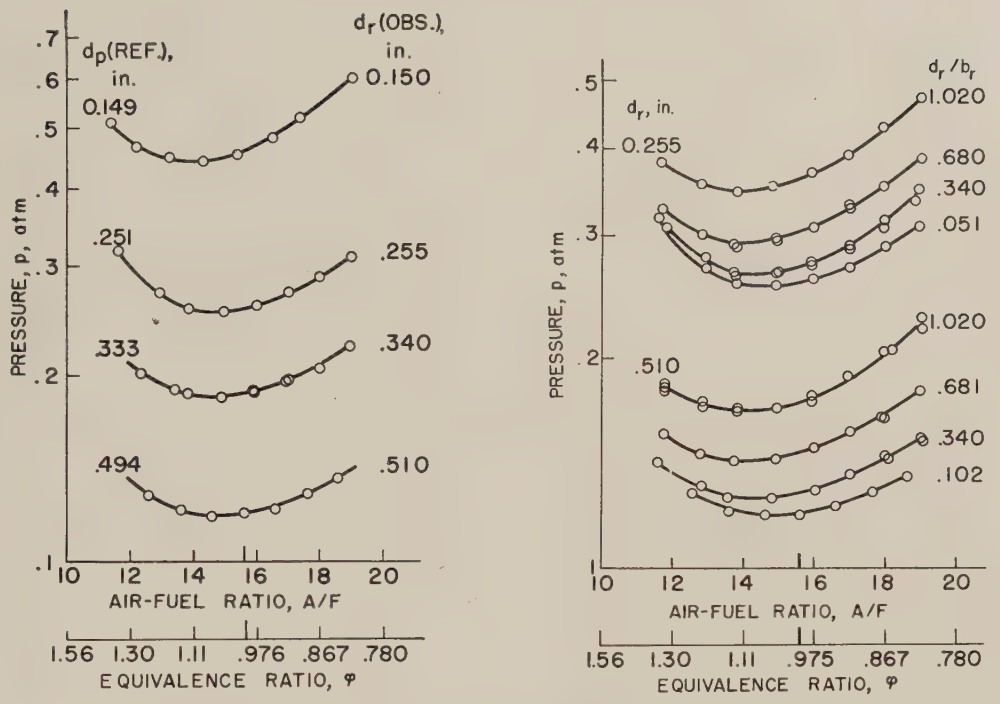

(a) (b)

FIG. 2. Limiting pressure curves for various series of rectangular slots. (a) Full length (5 in.) slots of various widths. (b) Slots of various lengths and widths.

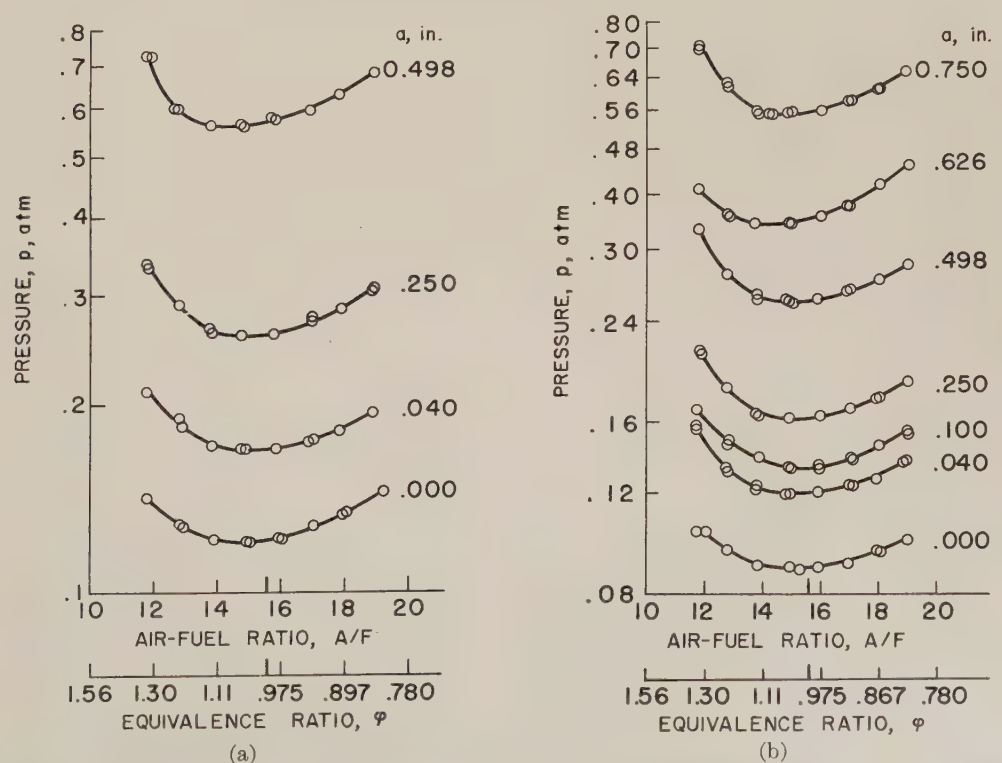

(a) (b)

FIG. 3. Limiting pressure curves for two series of annuli. (a) Outside diameter, 0.750 in. (b) Outside diameter, 1.000 in.

On the basis of the relations given for the reaction velocity[3] it follows that

$$\frac{C_{T,a}}{\tau_i} = \frac{c_0 \pi}{4} (d_a^2 - a^2)\nu_a \tag{17}$$

Equations (16) and (17) then give

$$\nu_a = \frac{d_a^2}{32 D_i \tau_i}\left[1 + \left(\frac{a}{d_a}\right)^2 + \frac{1 - (a/d_a)^2}{\log_e (a/d_a)}\right] \tag{18}$$

To compare the predicted quenching effect of an annulus and that of a cylinder, set $\nu_a = \nu_c$ to get

$$\frac{d_c}{d_a} = \sqrt{1 + \left(\frac{a}{d_a}\right)^2 + \frac{1 - (a/d_a)^2}{\log_e (a/d_a)}} \tag{19}$$

As expected, $d_c = d_a$ for the case where $a = 0$.

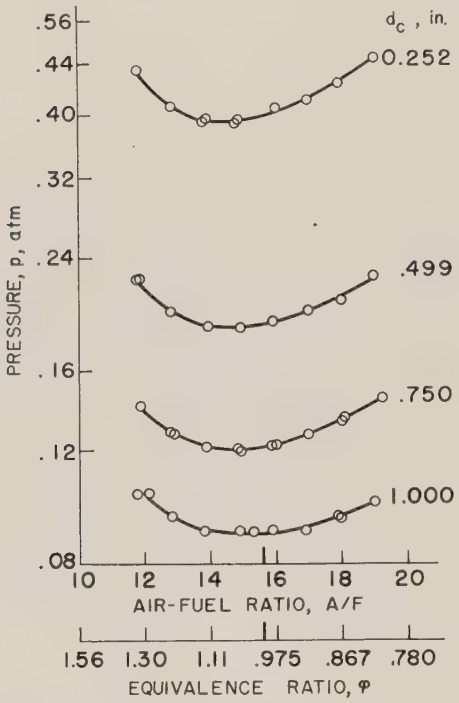

FIG. 4. Limiting pressure curves for series of cylinders.

QUENCHING BY CHANNELS OF ELLIPTICAL AND EQUILATERALLY TRIANGULAR CROSS SECTION

Calculations for geometries other than those discussed previously may be carried out in a similar fashion. Thus, when a channel of elliptical cross section, where d_e and b_e are the minor and major axes, respectively is considered, it follows from Purday[5] that the average chain length is given by

$$\nu_e = \frac{d_e^2}{16\left(\frac{d_e^2}{b_e^2} + 1\right) D_i \tau_i} \tag{20}$$

As expected, this equation reduces to equation (4) for the case where $d_e = b_e$.

Similarly, for a channel with a cross section defined by an equilateral triangle of side length d_t, the results of Purday[5] may be employed to show that

$$\nu_t = \frac{d_t^2}{80 D_i \tau_i} \tag{21}$$

GENERAL RELATIONS

The relations among the dimensions of the six quenching geometries treated may be expressed by the following set of equations

$$\begin{aligned}\frac{d_p^2}{12} &= \frac{d_c^2}{32} = \frac{d_r^2}{12}\left[1 - 0.300\left(\frac{d_r}{b_r}\right) - 0.0470\left(\frac{d_r}{b_r}\right)^2\right]^2 \\ &= \frac{d_a^2}{32}\left[1 + \left(\frac{a}{d_a}\right)^2 + \frac{1 - (a/d_a)^2}{\log_e (a/d_a)}\right] \\ &= \frac{d_e^2}{32}\left[\frac{2}{1 + (d_e/b_e)^2}\right] \\ &= \frac{d_t^2}{80}\end{aligned} \tag{22}$$

Apparatus

The apparatus consisted of a fuel-air metering-and-mixing system, a rectangular slot burner enclosed in a pressure-controlled tank, and various inserts which were placed in the opening of the slot burner so as to alter the geometry of the burner channel. Sonic orifices were employed to meter the propane and the air separately. The slot burner is described elsewhere[7].

Two types of slot burner insert were used—one type was designed to produce rectangular channels, the other to produce annular or cylindrical channels.

The first type of insert consisted of two water-cooled brass blocks placed in the opening of the slot burner in such a way as to produce a rectangular channel. Blocks of various dimensions were made in order to provide various rectangular channels.

The kind of insert used to form channels of annular cross section is shown in Figure 1. The cylindrical opening in the hollow brass block

forms the outer diameter of the annulus. The removable center body forms the inner diameter of the annulus. Both the hollow block and centerbody were water cooled as shown. The position of the centerbody with respect to the cylindrical opening could be adjusted by means of the screws.

Very small centerbodies were made by joining 0.04- or 0.10-in stainless-steel tubing to a short brass tube of large enough diameter to be conveniently held by the positioning screws. These small centerbodies were aircooled, so that it was necessary to extend the centerbody 10 to 12 in above the burner lip to avoid disturbance of the flame by the air blast from the centerbody tip.

The insert used to form annular burner channels was also used to form cylindrical channels simply by removal of the centerbody. To obtain cylindrical channels of different diameters, brass sleeves were slipped into the cylindrical opening. The lips of such sleeves were water cooled.

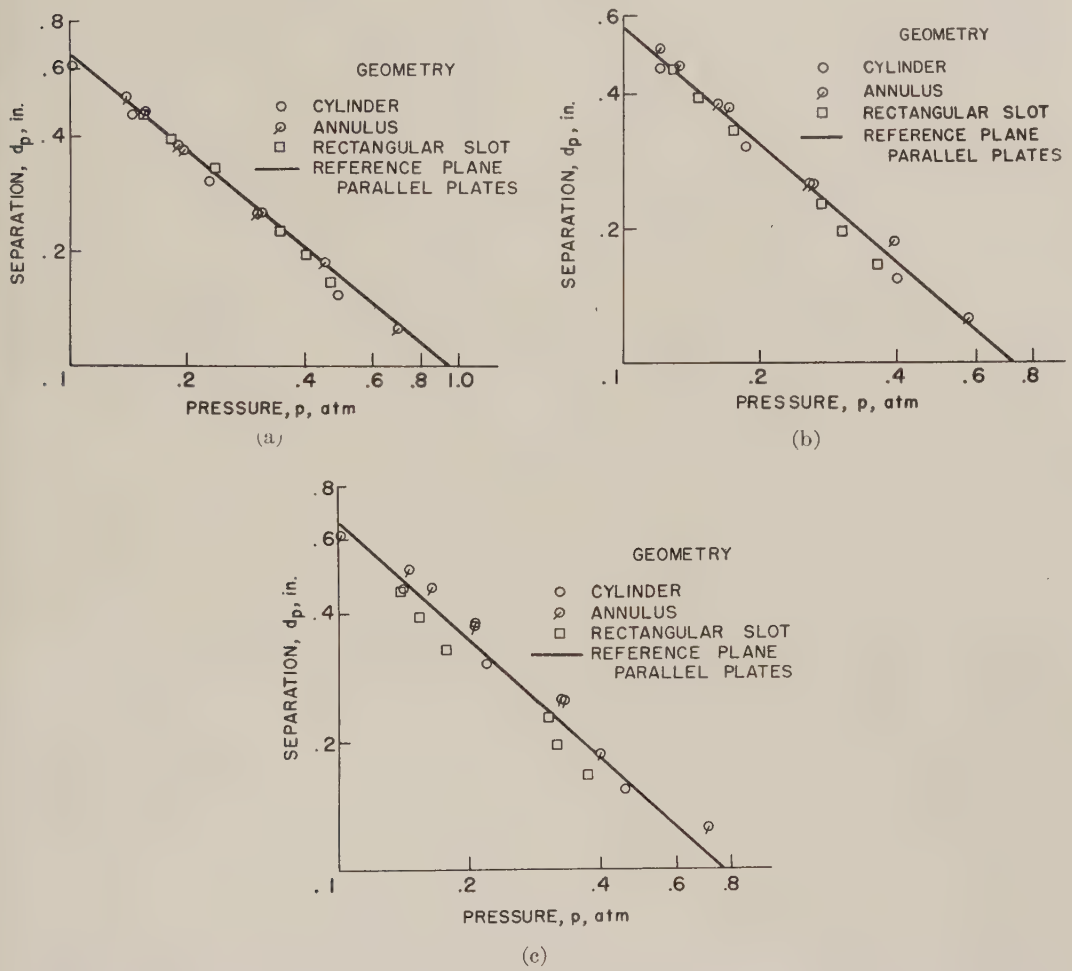

FIG. 5. Calculated plane parallel plate quenching distance as a function of observed limiting pressure for various geometries. (a) Air fuel ratio, 19.0. (b) Air-fuel ratio, 15.6. (c) Air-fuel ratio, 12.0.

Procedure

The limiting pressure for flame propagation through a burner channel of any given geometry was measured in the same manner as described by Berlad[7]. First, a flame was established on the burner. Then, after the pressure in the tank was stabilized, flow to the burner was suddenly interrupted. The flame would either die on the burner lip, or flash back through the burner channel. Generally, the difference between the two pressures which defined the transition from the flashback region to the quenching region could be determined to about 0.02 in of mercury. Flash back

occurred at the upper pressure, quenching at the lower. The limiting pressure was taken to be the average of these two pressures.

The question of whether or not air cooling was sufficient for the small (0.04 and 0.10 in) centerbodies was resolved by decreasing stepwise the flow through the centerbody, measuring the limiting pressure after each step. The limiting pressure remained unchanged until the air flow was decreased to an exceedingly small fraction of the normally used flow. It was concluded that the method of cooling was satisfactory.

Experimental Results

Experimental propane-air quenching data were obtained for three quenching geometries: rectangular slots, cylinders, and cylindrical annuli. Curves of limiting quenching pressure as a function of air-fuel ratio are presented in Figures 2, 3 and 4 for rectangular slots, cylindrical annuli, and cylinders, respectively. In these Figures, an equivalence ratio scale φ, as well as a mass air-fuel ratio scale is given. Stoichiometric air-fuel ratio is indicated in each Figure by a short vertical line placed just above the air-fuel scale at 15.6. The range of φ values examined, 0.82 to 1.3, was deemed sufficiently large to serve the aims and purposes of this research and was actually narrower than the range that could have been obtained with the quenching apparatus for the 0.1–1.0-atm pressure range investigated.

Table 1. Percentage Deviation of Calculated from Reference Plane Parallel Plate Quenching Distances for Various Geometries

A/F mass ratio	Equivalence ratio, φ	Rectangular slot deviation	Annulus deviation	Cylinder deviation
		per cent	*per cent*	*per cent*
19.0	0.822	3.63	1.77	7.48
18.0	.867	3.96	2.39	7.91
15.6	1.00	6.16	3.99	7.07
13.0	1.20	8.50	5.99	6.57
12.0	1.30	11.12	11.33	5.07
$\varphi \leq 1$ range		4.58	2.72	7.48
$\varphi > 1$ range		9.81	8.66	5.82
Total range		6.67	5.09	6.86

Discussion of Results

The observed quenching behavior of the geometries investigated was compared with that predicted by theory, in the following way. The full length (b_r, 5 in) rectangular slot quenching distances need only small end corrections for conversion to quenching distances for plane parallel plates of infinite extent. The appropriate portion of equations (22) was used to calculate d_p values (reference plane parallel plate separations) from the rectangular slot width d_r values for which the length-to-width ratio was greater than 10. The d_r values used and the reference d_p values calculated from them are indicated in Figure 2a. For a given air-fuel ratio, a logarithmic plot of these d_p values against limiting quenching pressure was then made, giving a straight line. For a given air-fuel ratio, this line (Fig. 5) defines the reference d_p values with which the quenching behavior of all other geometries are compared. The calculated plane parallel plate quenching distance for any geometry was then defined to be that wall separation which would, according to equations (22), be as effective a quenching system as the geometry under consideration. These calculated values are indicated in Figure 5 as data points.

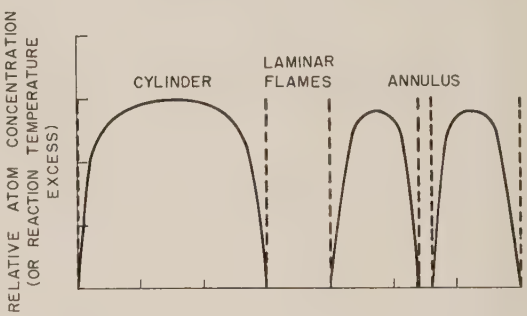

Fig. 6. Relative atom concentration (or reaction temperature excess) as function of position in cylinder and annulus for typical case of laminar flame propagation (qualitative representation).

A comparison of reference and calculated plane parallel plate quenching distances as a function of observed limiting pressures for cylinders, annuli, and rectangular slots is presented in Figure 5 for air-fuel ratios of 19.0, 15.6, and 12.0. In Figure 5, the straight lines are exclusively based on the reference d_p values of Figure 2a.

The agreement of theory and experiment may be seen from Table 1 which presents the percentage deviation of calculated from reference plane parallel plate quenching distances for various geometries.

For rectangular slots and for cylindrical annuli, the agreement between theory and experiment improves systematically as the flame varies from

rich to lean. For the case of quenching by cylinders, systematic improvement occurs when the flame is varied from lean to rich. In practically all cases, however, the deviation of the calculated from the reference plane parallel plate quenching distance appears to depend upon the air-fuel ratio. This deviation may be interpreted to mean that the term

$$\frac{d^2}{G} = \frac{A}{k_i}\left(\frac{T_R}{T_0}\right)^n \left(\frac{1}{N_f \sum_i \frac{p_i}{D_i}}\right)$$

of equation (1) varies slightly with geometry and that the amount of this variation is mildly air-fuel-ratio dependent.

Examination of the data of Figure 5 indicates that the individual deviations for any geometry practically always have the same algebraic sign. Allowing for a small amount of experimental scatter, it is apparent that the calculated plane parallel plate quenching distances for annuli are somewhat larger than anticipated and that those for rectangular slots and cylinders are somewhat smaller than anticipated. This may again be interpreted as meaning that the term d^2/G varies slightly with geometry.

Good agreement between calculated and reference d_p values is obtained even for values of $\varphi > 1$ ($A/F < 15.6$). Because equation (1) does not appear to be entirely suitable for values of $\varphi > 1$[7], this agreement may be attributed to the fact that all terms other than d and G essentially cancel out in the course of the calculations.

The fact that a relatively small cold surface may exhibit a large quenching effect, under proper circumstances, is illustrated by the fact that when a 0.04-in outside diameter cold tube is inserted along the axis of a 1-in inside diameter tube, the unit is found to quench as effectively as a 0.75-in inside diameter cylindrical tube. This large effect may be explained by the fact that even a small surface can serve as a large sink for active particles (Fig. 6). Thus, a small centerbody changes the active-particle concentration field from one with a relative maximum at the center for the cylinder to zero throughout the centerbody for an annulus (Fig. 6). The average concentration of active particles in the channel is thereby sufficiently lowered to cause a large increase in the quenching effect of the unit.

As indicated earlier, the effect of geometry on quenching predicted on the basis of the average chain length calculations may also be predicted through the use of a thermal quenching equation in which the propagation or nonpropagation of a flame is determined by some critical value of the difference between the average reaction temperature and the cold gas temperature. Of course, whether or not such an equation would be generally as satisfactory as equation (1) has yet to be answered. Thus, Figure 6 may also represent the change in the reaction temperature field from one with a maximum at the center for the cylinder to cold gas temperature throughout the centerbody for the annulus.

REFERENCES

1. Simon, D. M., Belles, F. E., and Spakowski, A. E.: *Fourth Symposium (International) on Combustion*, p. 126. Baltimore, The Williams & Wilkins Co., 1953.
2. Friedman, R., and Johnston, W. C.: J. Appl. Phys., *21*, 791 (1950).
3. Semenoff, N.: *Chemical Kinetics and Chain Reactions*. Oxford, Clarendon Press, 1935.
4. Jakob, M.: *Heat Transfer*, vol. 1, pp. 177–180. New York, John Wiley & Sons, Inc., 1949.
5. Purday, H. F. P.: *An Introduction to the Mechanics of Viscous Flow*, pp. 16–18, 28. Dover Pub., Inc., 1949.
6. Carslaw, H. S., and Jaeger, J. C.: *Conduction of Heat in Solids*, p. 168. Oxford, University Press, 1950.
7. Berlad, A. L.: *Flame Quenching by a Variable-Width Rectangular-Channel Burner as a Function of Pressure for Propane-Oxygen-Nitrogen Mixtures*. J. Phys. Chem., *58*, 1023 (1954).

83

STATIONARY FLAMES IN CYLINDRICAL FLOW OF HOMOGENEOUS AIR-HYDROGEN MIXTURES

By C. FOURÉ

Introduction

The theoretical study of the aerothermodynamic development of flows in which chemical reactions occur requires schematic representations[1]. Generally speaking, it is rather difficult to develop experimental setups that meet, even approximately, the requirements for such ideal representations. Accordingly, any device which permits systematic exploration of a reaction zone is of great help in obtaining new data.

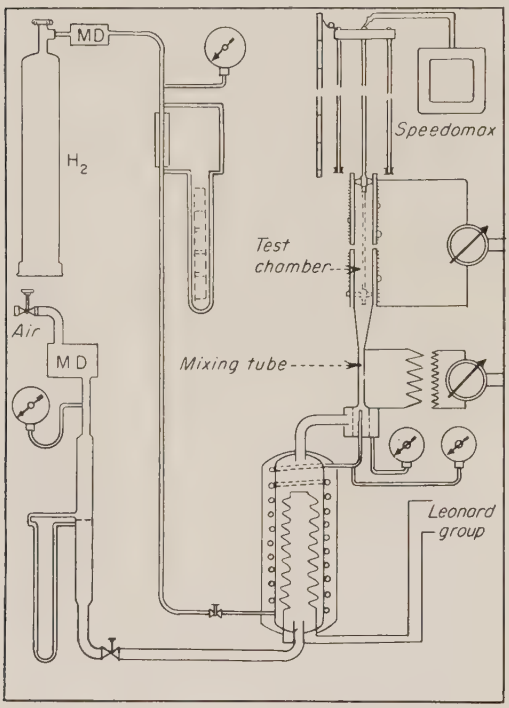

FIG. 1. Diagram of experimental apparatus.

It seemed of interest to obtain combustion in homogeneous cylindrical flow of a combustible mixture (air-hydrogen, for instance) without superposition of the heat transfer phenomena on the chemical reaction of the initial mixture.

The setup used in these experiments is based to some extent on that of Mullins[2], in which the heterogeneous flow prevented any correct interpretation of the chemical reaction of the mixture.

Our purpose was to maintain as homogeneous a flow as possible through a cylindrical tube of a mixture brought to a temperature high enough for spontaneous ignition. With the very lean mixtures used in these experiments, the reaction zone extends over several inches, making temperature change and gas composition readily observable.

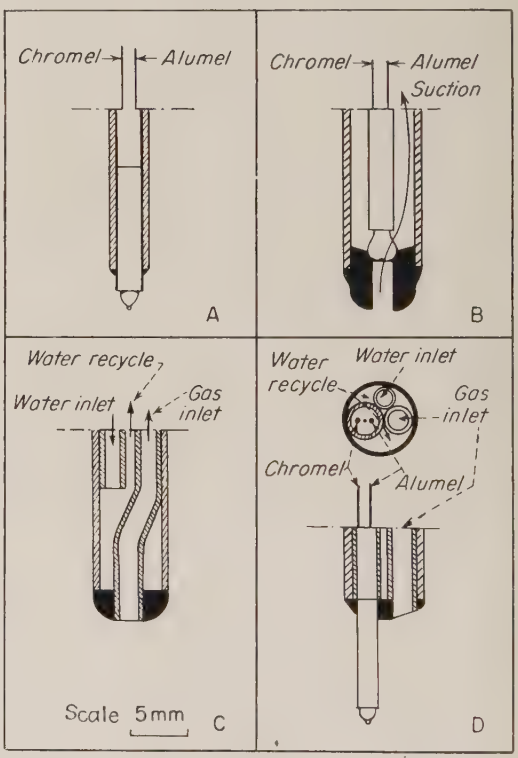

FIG. 2. Probes used. A, thermoelectric probe with exposed junction; B, thermoelectric probe with single flow over the junction; C, water-cooled probe for collecting gas; D, probe combining A and C.

Experimental Procedure

The main difficulty encountered in a setup of this type is the problem of selecting a mixture which can react spontaneously but where the chemical reaction does not set in prematurely. This was solved by using a high-speed mixture and aerodynamic recompression.

Air and hydrogen are supplied from separate

tanks and are preheated separately to about 900°K. The air is accelerated to a high speed (275 m/sec), in a convergent, after which it passes to a mixing tube (inner diameter 0.6 cm, length 50 cm) at the inlet of which hydrogen is injected (Fig. 1). Additional heating of the mixture may be provided through the tube walls without bringing them to the total stagnation temperature.

The mixture which is now homogeneous[a] leaves the mixing tube at approximately sonic velocity.

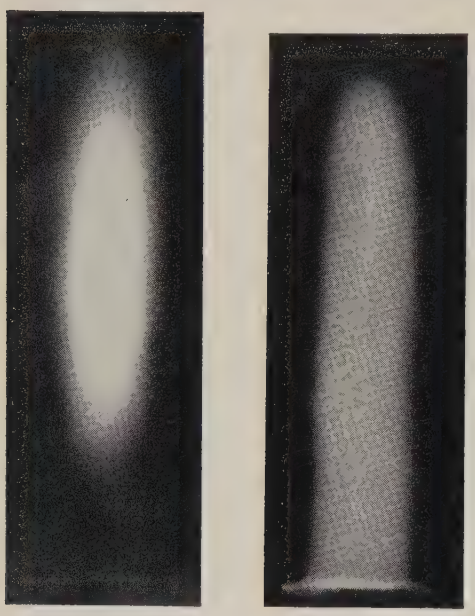

(A) (B)

FIG. 3. Appearance of the chemical reaction zone (A) and the free jet of the mixture just before reaction (B) made visible by increasing the exposure time. In both cases, copper oxide was added to increase emission. (A) exposure 3 seconds; (B) exposure 18 seconds.

During deceleration in a divergent provided at the mixing tube cutlet, the static temperature rises about 150°C, and for the mixtures used (hydrogen concentration, 1 to 3/1000 by weight), a zone of spontaneous reaction appears in the cylindrical experimental tube (length 100 cm, inner diameter 1.9 cm) placed after the divergent.

This reaction zone is investigated by means of a probe-holder, which moves along the axis of the tube at constant speed. Probe readings and signals from electric contacts at 10 cm intervals are recorded simultaneously and indicate the position of the probe.

[a] Length/diameter ratio of 83 and the Reynolds number of 50,000 obtained confirmed this.

The probe-holder was equipped simultaneously or successively with various thermoelectric probes, as well as pressure and gas cocks for determining the local composition of the mixture (Fig. 2).

The electromotive force of the thermocouple is recorded by a Speedomax electronic potentiometer. The proportion of hydrogen in the gas samples is measured with an I.F.P. No. 3 apparatus[3].

Experimental Results

In this experiment, the reaction takes place inside a tube such that neither direct nor photographic observation is possible. In the course of a series of special experiments, the phenomenon was reproduced in the free jet from a shorter tube (5 cm).

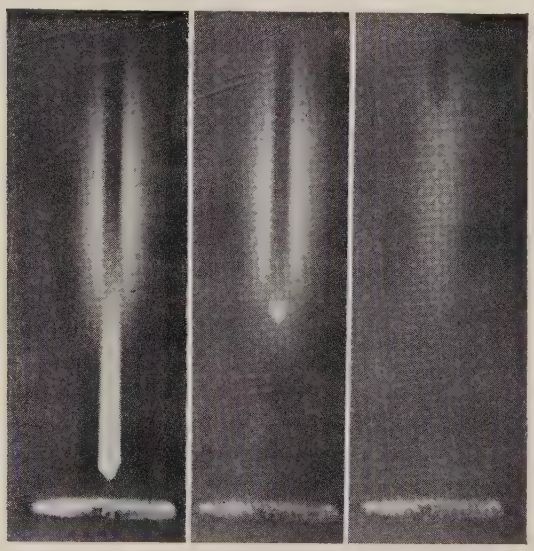

FIG. 4. Reaction as observed for three different positions of the thermoelectric probe (exposure 6 seconds; copper oxide).

The chemical reaction zone is characterized by a pale blue flame whose outline is blurred. To make it possible to observe and photograph this flame, its intensity was increased by the addition of metal salts.

Depending on the exposure time, photographs of the same phenomenon show either the chemical reaction zone alone (Fig. 3, 3 sec) or the entire hot free jet together with the reaction zone (Fig. 3, 18 sec). The appearance of the zone is not affected by the presence of the probe along its axis (Fig. 4). (The picture on the right was taken during a temporary lack of cupric oxide.)

The lack of characterization generally shown by strioscopic images of flame fronts seems to confirm the progressive character of the reaction (Fig. 5).

TEMPERATURE CHANGES INDICATED BY THE PROBE

At initial temperatures below 910°K, there was no noticeable increase in temperature irrespective of the hydrogen concentration of the mixture and the position of the probe in the 100 cm tube. Above this initial value, the temperature was observed to change throughout the length of the tube. Figure 6 is a good example of this and shows a direct Speedomax recording, taken during an upward displacement of the probe (lower half), followed by a downward displacement (upper half). A time scale in msec was added, which was computed on the basis of the flow velocity at the tube inlet.

The following can be observed on this type of recording:

(1) The temperature curve includes a constant temperature section OA, whose length, i.e., time of travel downstream, decreases when the temperature and/or the hydrogen concentration of the initial mixture increases (Fig. 7). Point A, which marks the end of an ignition lag, can be defined only arbitrarily, as for instance in Figure 6. The choice of the tube inlet (point O) as the origin of the abscissae and lags is also arbitrary, but convenient.

(2) Over a region of abscissae of several inches, the temperature increases along the curve AC whose maximum slope (dT/dx or dT/dt) (Fig. 6, line 2) increases with the hydrogen concentration of the initial mixture (Fig. 7).

(3) In the first fractions of the reaction, an unexplained anomaly (B) appears systematically: the slope of the double tangent (Fig. 6, line 1) increases with the hydrogen concentration (Fig. 7).

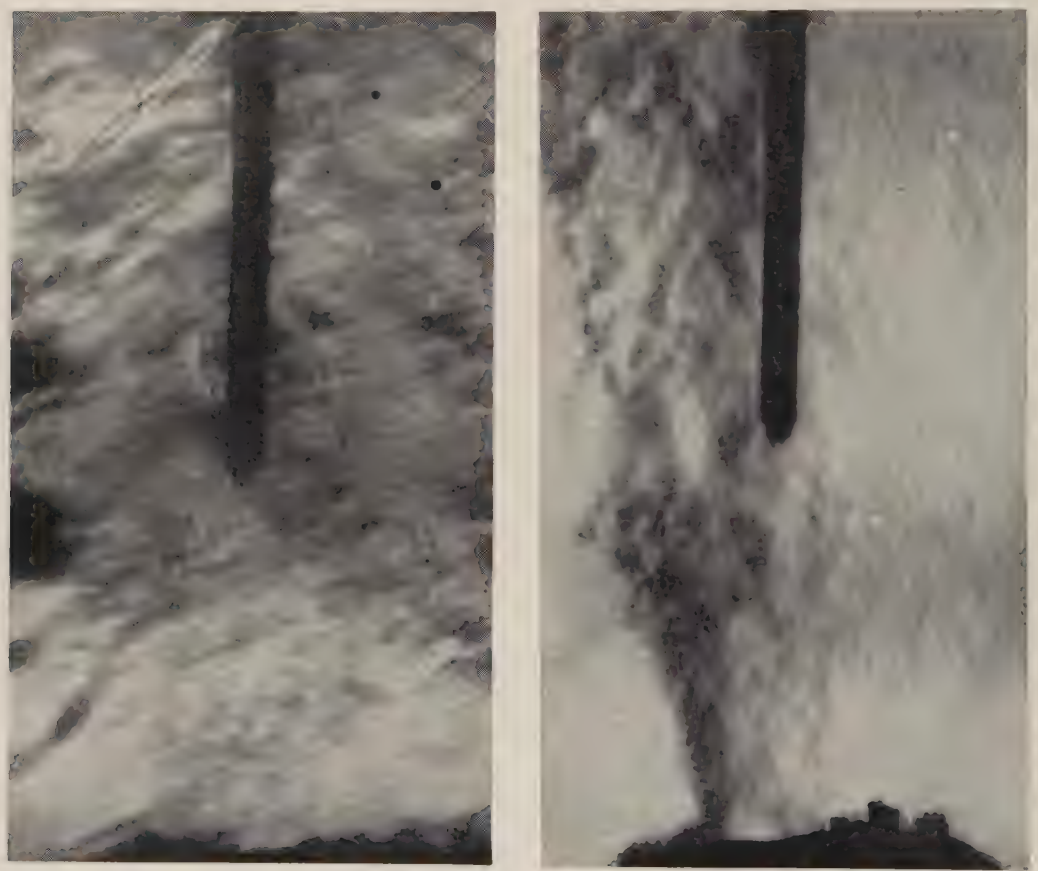

(A) (B)

FIG. 5. Strioscopic pictures of phenomenon. (A) horizontal knife edge; (B) vertical knife edge.

(4) The temperature reaches a maximum (C) and then levels off with a slight downward trend. This decrease in temperature beyond the maximum is due to heat loss by the tube, which is compensated only for the initial temperature of the mixture, and not for temperatures reached after the chemical reaction.

(5) The temperature curves obtained by axial displacement of the probe along increasing and decreasing abscissae coincide if the probe is displaced slowly enough so that there is no effect due to thermal inertia of the probe. For a displacement velocity of 0.37 cm/sec, the thermal inertia effect is slightly perceptible, but it can be corrected by taking the arithmetical value of abscissae and slopes in both directions.

(6) If, for a fixed longitudinal position of the probe, the hot junction is moved along a diameter of the tube, the temperature changes do not exceed 2°C and 10°C respectively, for the region of level stretches and maximum slope of the curve.

PRESSURE CHANGES

A static pressure probe was displaced axially in the tube. As expected in view of the moderate flow velocities (40 m/sec), the small temperature variations (less than 250°C), and the small diameter of the tube, the pressure drop due to the chemical reaction was found to be low, as compared with the drop due to friction at the walls and on the probe itself. This method of experimentation was not precise enough and therefore was abandoned.

VARIATIONS IN THE HYDROGEN CONCENTRATION

Because the overall response time of the apparatus for hydrogen determinations is about 15 to 25 sec, a direct recording cannot be obtained by continuous displacement of the probe. It was necessary to move the probe discontinuously from point to point, maintaining each position long enough for the concentration recorded by the Speedomax to reach equilibrium. The resulting values are plotted against the corresponding abscissae (Fig. 8).

There is no hydrogen reaction in the probe. The small diameter of the sampling tube and the low temperatures maintained by circulating water around it lead to heat losses at the rate of about 10^{6}°C/sec. Moreover, quenching at the cold wall tends to quench any such reaction. The overall hydrogen concentration fluctuates with the temperature (an increase in temperature cor-

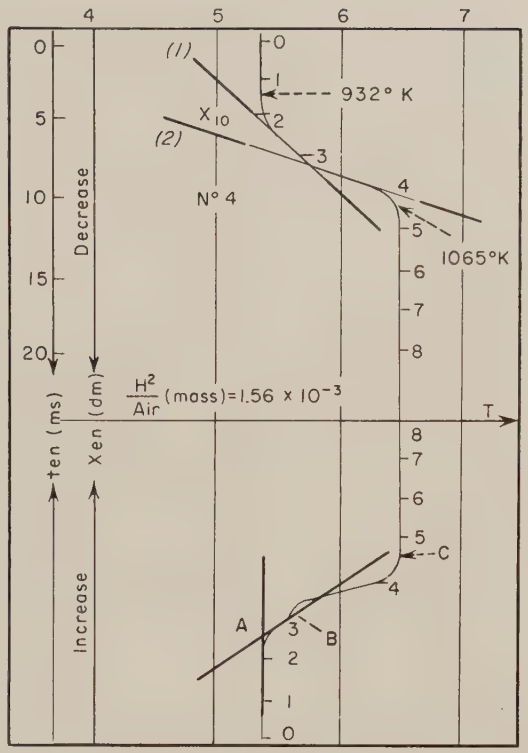

FIG. 6. Temperature curve recorded with probe (Speedomax recording).

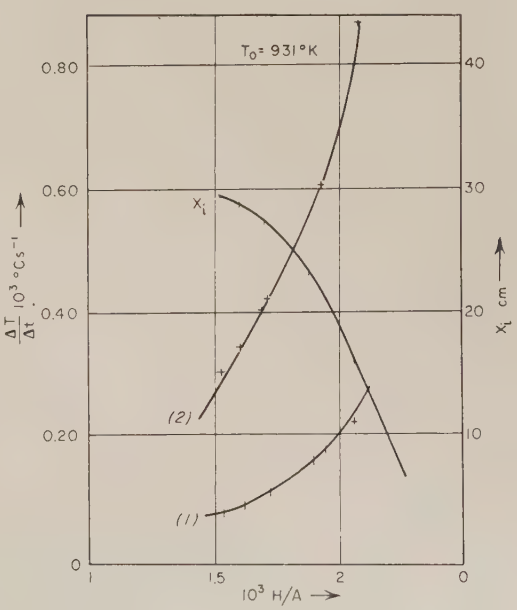

FIG. 7. Effect of initial hydrogen concentration on ignition abscissa and temperature gradients.

responds to a decrease in the hydrogen concentration), except for changes in the slopes of the initial fractions.

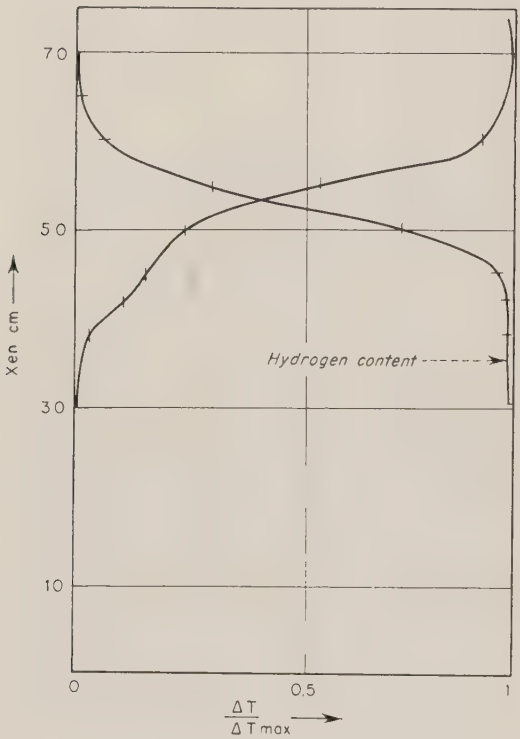

FIG. 8. Temperature and hydrogen concentrations as function of the abscissa.

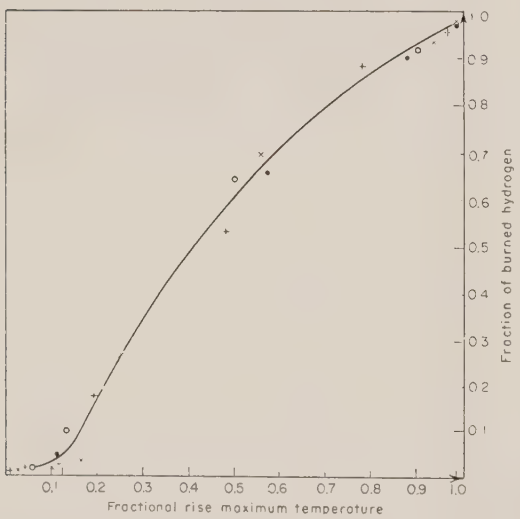

FIG. 9. Correlation between hydrogen combustion and maximum temperature rise.

COMPARISON OF TEMPERATURE AND OF CONCENTRATION CHANGES

To compare these two parameters accurately, a special probe was used (type D, Fig. 2) to make simultaneous measurements, thus eliminating possible discrepancies in the readings. In plotting the points, allowance was made for the longitudinal shift between the junction of thermocouples and the gas sampling outlet. Figure 9 shows the correspondence between these two measurements, with the local temperature increment as abscissa and the fraction of hydrogen consumed as ordinate. The experimental points from a number of experiments fall along a single curve, which is entirely different from the straight line (first bisecting line), which would have been obtained if the reaction had been single and adiabatic, and the measurements had been free of error.

We shall now consider various hypotheses by which this difference can be explained.

Nonadiabaticity of the phenomenon might be a cause. Because of insufficient compensation for heat loss at the wall in the reaction zone, the temperature increments ΔT measured in this zone are all smaller than those which would have been obtained for an adiabatic reaction. It can therefore be assumed, as a first approximation, (if these ΔT remain less than 250°C) that the negative errors for individual ΔT's increase linearly with the value of ΔT. This means that the values of the $\Delta T/\Delta T_{max}$ ratio are not affected by the nonadiabatic character of the phenomenon.

In the simplified case of a single reaction promoted at the surface of the hot junction or in its boundary layer, the curve obtained would be entirely below the first bissecting line, as the temperature increases would have been ahead of the decreases in hydrogen concentration.

In a probable case[4] of a reaction involving intermediate species such as H, O, OH, H_2, O_2, HO_2, the concentration of these species would necessarily increase to a maximum and then decrease within the reaction zone. The heat of formation of these species being positive or lower in absolute value than that of water, the curve obtained for ideal temperature measurements would lie entirely above the first bissecting line.

Subject to reservations, anomaly B which appears on the temperature curve (Figs. 6 and 8) and the lower part of the curve in Figure 9 situated below the first bisecting line might be

explained by chain breaking at the thermocouple junction entailing liberation of energy which affects the measurements. It is to be noted that this perturbation seems to be limited to the first quarter of the evolution.

To make the fullest use of the possibilities of such a flame for the study of the reaction kinetics, it would be interesting to determine the evolution of the intermediate compounds and the temperature by spectro-optical methods.

REFERENCES

1. Roy, M.: *Thermodynamique des systèmes propulsifs à réaction et de le turbine à gaz*, p. 26–41. Paris, Dunod, 1947.
2. Mullins, B. P.: *Third Symposium on Combustion, Flame and Explosion Phenomena*, p. 704–713. Baltimore, The Williams & Wilkins Company, 1949.
3. Monicard, R.: Rev. l'Indust. Française du Pétrole, *6*, 324, 379 (1951).
4. Lewis, B., and von Elbe, G.: *Combustion, Flames and Explosions of Gases*, p. 27. New York, Academic Press, Inc., 1951.

84

KINETICS OF OXYGEN UPTAKE BY CYCLOHEXENE IN THE LIQUID PHASE[a]

By ANIS T. TOUMA and FRANK H. VERHOEK

This chapter reports the results of a study of the oxidation of cyclohexene, both as the pure liquid and in benzene solution, without shaking or stirring. The rates were measured manometrically by measuring pressure changes at constant volume. Oxygen-enriched air was used.

Early experiments were carried out in Pyrex glass vessels. For 10 ml volumes of cyclohexene, the plot of oxygen absorbed against time showed a slowly accelerating rate followed by a period of steady reaction. The length of the period during which the rate was accelerating varied in irregular manner from one experiment to another. If Pyrex beads were placed in the liquid so that they lay partly above and partly below the surface, the length of this period was decreased. When a liquid-gas interface of constant area was maintained, by using Pyrex cylinders of constant cross-section, the reaction for amounts of cyclohexene less than 1 ml proved to be decelerating at the start, with an initially faster reaction, the smaller the volume of cyclohexene used. It was concluded that the glass surface was exerting a catalytic influence on the initial stages of the reaction.

The difficulties encountered in Pyrex vessels were avoided by using Teflon cups, bored out as cylinders of 2.22 cm inside diameter with flat bases, as containers for the hydrocarbon. These were inserted into 125 ml Pyrex flasks, which were in turn connected to mercury manometers. Care had to be taken to avoid contact of liquid with the glass portions of the apparatus, as by condensation, in order to obtain reproducibility. The experiments were started by pipetting the liquid to be studied into the Teflon cylinders in the thermostat, closing the apparatus, and admitting oxygen until the total pressure was of the order of 900 mm. The oxygen-nitrogen ratio in the atmosphere above the liquid was thus of the order of 40:60 depending upon the vapor pressure of the liquid at the temperature used. The surprisingly long time of several hours was required to establish vapor pressure equilibrium; this makes the very early portions of the reaction somewhat uncertain. The pressure was allowed to fall as oxygen was absorbed until near to atmospheric pressure; then more oxygen was added and observations continued. No dependence upon oxygen pressure was observed at partial pressure greater than about 40 mm; all experiments were made in this oxygen-independent region.

[a] This investigation was carried out as one phase of a research project on the mechanism of combustion, directed by Prof. Cecil E. Boord and sponsored by the Air Research and Development Command (Contract No. AF 33(038)22959) in cooperation with The Ohio State University Research Foundation.

The cyclohexene used was a research grade of 99.9 per cent purity. It was freed from peroxide by filtering through silica gel and either used immediately or after short periods of storage in sealed ampoules in an oxygen-free atmosphere.

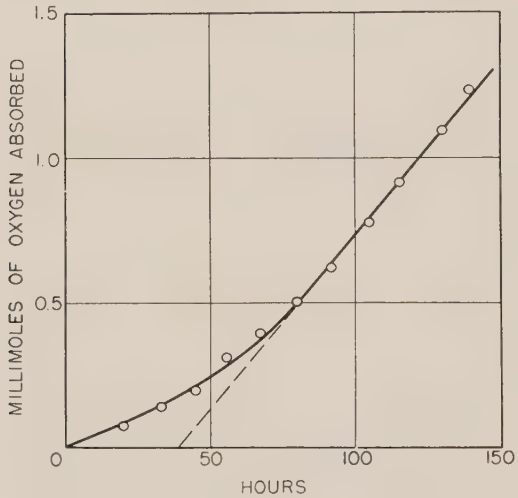

FIG. 1. Absorption of oxygen by cyclohexene at 40°.

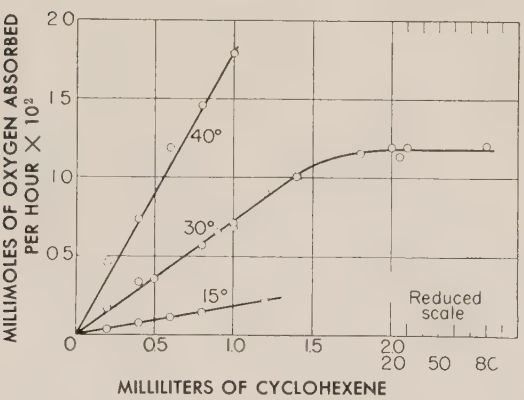

FIG. 2. Variation of steady-state rate with volume of cyclohexene. The point for 1.0 ml at 40° represents the average of nine determinations.

The data obtained may best be interpreted in terms of the mechanism of Bolland and Gee[1].

$$2\text{ROOH} \xrightarrow{k_1} \text{R} + \text{RO}_2 + \text{H}_2\text{O} \qquad (1)$$

$$\text{R} + \text{O}_2 \xrightarrow{k_2} \text{RO}_2 \qquad (2)$$

$$\text{RO}_2 + \text{RH} \xrightarrow{k_3} \text{ROOH} + \text{R} \qquad (3)$$

$$\text{RO}_2 + \text{RO}_2 \xrightarrow{k_6} \text{chain end} \qquad (4)$$

Tobolsky, Metz, and Mesrobian[2] show that this mechanism predicts that oxygen will be absorbed as a function of time as

$$[\text{O}_2] = [\text{ROOH}]_\infty \text{ at} + [\text{ROOH}]_\infty \ln \cdot \left\{ \frac{1 - \left(1 - \frac{[\text{ROOH}]}{[\text{ROOH}]_\infty}\right) e^{-\text{at}}}{1 - \left(1 - \frac{[\text{ROOH}]_\infty}{[\text{ROOH}]_0}\right)} \right\} \qquad (5)$$

where $[\text{ROOH}]_0$ and $[\text{ROOH}]_\infty$ are respectively the initial and steady state concentrations of hydroperoxide, and

$$[\text{ROOH}]_\infty = \frac{k_3}{\sqrt{k_1 k_6}} [\text{RH}]$$

$$\text{and} \quad a = k_3 \sqrt{\frac{k_1}{k_6}} [\text{RH}] \qquad (6)$$

For low initial hydroperoxide concentration, $[\text{ROOH}]_0$, this equation predicts a curve showing initial acceleration followed by a period of steady reaction. Agreement is shown in Figure 1, where the number of millimoles of oxygen absorbed at 40°C by 0.6 ml of cyclohexene initially 0.053 m in hydroperoxide is plotted against the time.

The observed straight line in the later portions of the reaction is predicted by the limiting form of equation (6) for long times

$$[\text{O}_2] = [\text{ROOH}]_\infty \text{ at} - [\text{ROOH}]_\infty \ln \frac{[\text{ROOH}]_\infty}{[\text{ROOH}]_0} \qquad (7)$$

A straight line on a graph corresponding to that of Figure 1 would also be obtained if the rate of oxygen absorption was controlled by the rate of diffusion or solution of oxygen rather than by chemical reaction. That chemical reaction is the controlling step for volumes less than about 1 ml is shown by the plot of the steady state rate against the volume of cyclohexene shown in Figure 2. The curve for 30° shows that chemical reaction is controlling up to 1.4 ml, after which a physical process, no longer dependent upon the amount of hydrocarbon, is rate controlling at that temperature. The highest rate reported at 40° is probably close to the limiting rate at 40°. The slopes of the curves in Figure 2, according to equations (6) and (7), give $(k_3^2[\text{RH}]^2/k_6)$; from them, using 9.84 molar as the concentration of cyclohexene at each temperature, the values of k_3^2/k_6 in Table 1 were calculated.

The three values in Table 1 lie on a straight line on a plot of $\ln k_3/\sqrt{k_6}$ against $1/T$ and the

activation energy difference $E_3 - E_6/2$ was found to be 8.3 kcal. This value is reasonable in comparison with similar activation energy expressions for other hydrogen-abstraction and radical-combination reactions[3].

Equation (7) predicts that the slopes of the straightline portions of curves like that in Figure 1 should be independent of the initial hydroperoxide concentration, at constant volume of hydrocarbon. This is verified by the data for 1 ml at 40° shown in Table 2, column 3. In these experiments the hydroperoxide concentration was changed by mixing with a nearly peroxide free sample various amounts of peroxidized cyclohexene obtained by bubbling oxygen through the liquid at an elevated temperature.

If the straightline portions of the curve in Figure 1 are extrapolated back, the intercept on the time axis, t_0, is obtained from equation (7) as

$$t_0 = \frac{2.303}{a} (\log [\mathrm{ROOH}]_\infty - \log [\mathrm{ROOH}]_0) \quad (8)$$

The intercept should thus be independent of the volume of hydrocarbon used at constant $[\mathrm{ROOH}]_0$, and should form a straight line of negative slope when plotted against log $[\mathrm{ROOH}]_0$; the intercept of this line at $t_0 = 0$ should give log $[\mathrm{ROOH}]_\infty$. The values in the fourth column of Table 2 for 0.053 molar hydroperoxide show that the first prediction is verified, and Figure 3 shows that the points, although scattered, are consistent with the requirement of a straight line of negative slope. If the line shown in Figure 3 is taken as a correct representation of the variation of t_0 with log $[\mathrm{ROOH}]_0$, then $k_3 k_1^{1/2} k_6^{-1/2}$ is obtained from its slope and equation (6) as 8.0×10^{-3} liter mole^{-1} hour^{-1} at 40°. The intercept corresponds to $[\mathrm{ROOH}]_\infty = 0.57$ moles/l. Values of $[\mathrm{ROOH}]_\infty$ obtained by actual titration of the liquid left in the reaction flasks are much larger than this. They show considerable variation from experiment to experiment, due in part to the difficulty of securing valid aliquots from the flasks; the average of eight determinations at 40° was 1.56 molar, with an average deviation of 0.25. The variations in the measured values show no correlation with the volume of cyclohexene or the initial hydroperoxide concentration. The difference between the value obtained from the t_0 variation and the measured value may point to the production of an inhibitor in the reaction mixture.

There is another way in which an estimate of the magnitude of $k_3 k_1^{1/2} k_6^{-1/2}$ can be obtained. Comparison of the amount of hydroperoxide

Table 1. Velocity Constants for the Oxidation of Cyclohexene in the Steady State

Temp	k_3^2/k_6 (liter mole^{-1} hour^{-1} $\times 10^5$)
°C	
15	1.89
30	7.53
40	18.6

Table 2. Oxidation of Cyclohexene at 40°

Volume of cyclohexene	Initial hydroperoxide	Steady state rate	Intercept t_0	$\frac{d \log (O_2 \text{ abs})}{dt}$
ml	*m/l*	*millimoles O_2 per hour* $\times 10^3$	*hr*	*hr*$^{-1}$ $\times 10^3$
0.2	0.053	4.6	—	—
0.4	0.053	7.4	36.5	18.7
0.6	0.053	11.9	38.1	16.7
0.8	0.053	14.6	32.5	14.2
1.0	0.005	15.5	59.0	29.1
1.0	0.008	16.8	51.5	—
1.0	0.014	18.4	39.2	26.5
1.0	0.017	18.4	47.4	19.2
1.0	0.020	18.7	33.4	18.5
1.0	0.130	17.5	23.0	—
1.0	0.184	19.3	17.5	—
1.0	0.210	17.7	9.5	—
1.0	0.250	18.6	6.2	—

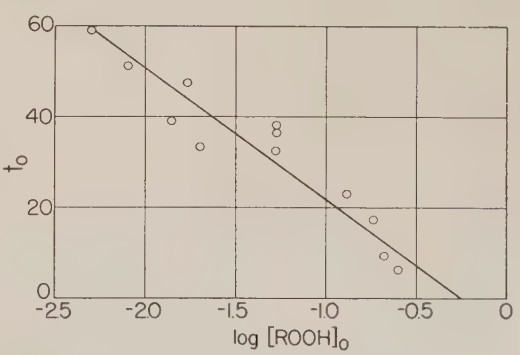

Fig. 3. Variation of t_0 with $(\mathrm{ROOH})_0$.

formed with the amount of oxygen absorbed in early stages shows that, within the experimental error, all the oxygen is used to form hydroperoxide. Hence we may neglect the decomposition

of hydroperoxide in step 1, so that

$$-\frac{d[O_2]}{dt} = \frac{d[ROOH]}{dt} = k_3[RO_2][RH] = a[ROOH] \quad (9)$$

Proportionality between the rate of oxygen uptake by cyclohexene and the concentration of hydroperoxide for low concentrations of hydroperoxide has been shown for large liquid volumes

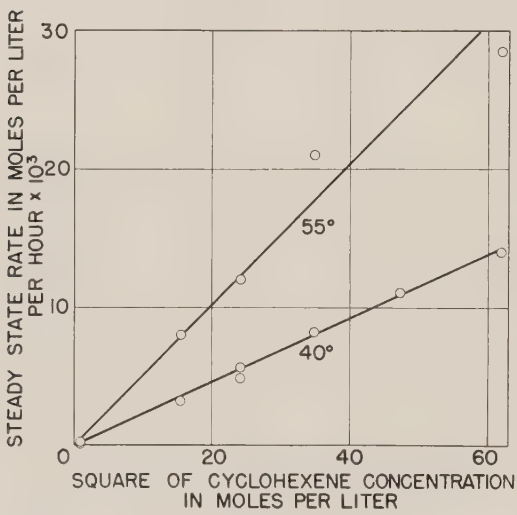

FIG. 4. Dependence of rate of oxygen absorption on cyclohexene concentration.

in stirred systems in Pyrex by Frye, Kretschmer, and Wiebe[4]. Integration of equation (9) gives

$$[ROOH] = [ROOH]_0 e^{at} \quad (10)$$

and

$$-[O_2] = [ROOH]_0(e^{at} - 1) \quad (11)$$

Hence, approximately

$$\log[-O_2] = \log[ROOH]_0 + \frac{a}{2.303}t \quad (12)$$

Thus the logarithm of the amount of oxygen absorbed should be a straight line function of the time in the early part of the reaction. The slope of this line should be independent of the value of $[ROOH]_0$ and of the volume of hydrocarbon used, and the intercept at $t = 0$ should depend upon both. In spite of the uncertain readings at the start of the reaction, the straight-line prediction of equation (12) was observed in experiments with not too small amounts of hydrocarbon and with low initial peroxide content. The slopes of the lines were found to vary widely, however, as shown by the data in column 5 of Table 2, and while the intercepts at $t = 0$ increased with the amount of hydroperoxide at constant hydrocarbon volume and with the volume of hydrocarbon at constant $[ROOH]_0$, no exact dependence upon the logarithms of these quantities could be established.

The average of the values in column 5 of Table 2 is 20.4×10^{-3} with an average deviation 3.0×10^{-3}; the average gives 4.8×10^{-3} liter mole^{-1} hour^{-1} for $k_3 k_1^{1/2} k_6^{-1/2}$. This value is to be compared with 8.0×10^{-3} liter mole^{-1} hour^{-1} obtained from the slope of the curve in Figure 3. The average of twelve values of d log (O_2 abs)$/dt$ at 30° was 9.7×10^{-3}, with an average deviation 1.7×10^{-3}, in reciprocal hours. The temperature coefficient obtained from the first and third values of $k_3 k_1^{1/2} k_6^{-1/2}$ gives $E_3 + \frac{1}{2}E_1 - \frac{1}{2}E_6 = 14.0$ kcal. When this is combined with $E_3 - \frac{1}{2}E_6 = 8.3$ kcal, E_1 is obtained as 11.4 kcal. This seems small for a reaction involving a split into free radicals. If the 30° value is combined with the higher 40° value, E_1 is obtained as 30.8 kcal, which is closer to the values established for other peroxide decompositions.

An estimate of the activation energy of step 1 could also be obtained from the values of $[ROOH]_\infty$ using equation (6). The value of E_1 so obtained is 4.8 kcal, but our values of $[ROOH]_\infty$ vary so widely from experiment to experiment that no weight can be placed upon this value.

Equation (7) requires a second-order dependence of the steady state rate on the concentration of cyclohexene. In order to test this, experiments were made by mixing benzene with cyclohexene containing relatively large amounts of hydroperoxide (to shorten the induction period), in various proportions, and observing the rate of oxygen uptake by 1 ml quantities of these solutions. The experiments showed periods of increasing rate followed by a steady state as for the pure hydrocarbon, but the initial or induction periods were not as reproducible functions of hydroperoxide content as in the former case. The experiments were carried on until 0.1 to 0.2 mole oxygen had been absorbed per mole of cyclohexene, and the slopes in the steady state referred back to the initial cyclohexene concentration. The data, plotted in Figure 4, show that the dependence on the square of the cyclohexene concentration is satisfactorily reproduced.

The slope of the curves in Figure 4 give k_3^2/k_6; the values are 23.0×10^{-5} l/mole/hr at

40° and 50.8 × 10^{-5} l/mole/hr at 55°. The 40° value is appreciably higher than the value obtained from measurements on the pure hydrocarbon, given in Table 1, and the quantity $E_3 - \frac{1}{2}E_6$ obtained from these two temperatures is 5.4 kcal, compared to 8.3 kcal from the data of Table 1. The latter value, from measurements at three temperatures, is believed to be more accurate.

The data reported here, in spite of uncertainties as to the exact values of the quantities calculated, show that the oxidation of liquid cyclohexene is satisfactorily accounted for by the mechanism of Bolland and Gee[1], with second-order hydroperoxide decomposition as the initiating step.

REFERENCES

1. Bolland, J. L., and Gee, G.: Trans. Faraday Soc., *42*, 236, 244 (1936).
2. Tobolsky, A. V., Metz, D. J., and Mesrobian, R. B.: J. Am. Chem. Soc., *72*, 1942 (1950).
3. Steacie, E. W. R., and Trotman-Dickenson, A. F.: J. Phys. Chem., *55*, 908 (1951); Woodward, A. E., and Mesrobian, R. B.: J. Am. Chem. Soc., *75*, 6189 (1953).
4. Frye, C. F., Kretschmer, C. B., and Wiebe, R.: Ind. & Eng. Chem., *46*, 1517 (1954).

Flame Spectra and Dissociation Energies

85

SPECTROPHOTOMETRIC TRAVERSES THROUGH FLAME FRONTS[a]

By K. WOHL AND F. WELTY

A spectrophotometric study of the structure of the burning zone and the postcombustion zone of butane-air flames at 1 atm has been undertaken. A flat flame front has been created which was viewed edgewise by the spectroscope, and the light emission of a gas element has been followed along its path. Measurements in the near infrared yielded the temperature profile, and measurements in the visible and ultraviolet gave information on the rise, and mainly the decay, of the radiation of flame radicals.

(1) Method

The flat flame is maintained in an enclosed burner above a rectangular slit of 3 x 51 mm between quartz plates as shown in Figure 1. The two other sides of the burner are water vapor-cooled. The main flame is stabilized by a pilot flame of the same composition burning from a narrower parallel slit. The central straight section of the main flame has a height of 7 mm. The boundaries of the stream of luminous exhaust gases are shown in the Figure. The burner was tilted to make the flame front parallel to the spectroscopic slit. In order to follow the progress of combustion the burner was moved in such a way that the optical axis of the spectroscope travelled into the postcombustion zone along the line of maximum luminosity of the flame gases (Fig. 1). The flame section which is seen by the spectroscope at one specific instant is also indicated in the Figure.

[a] This research was conducted under the auspices of Project SQUID, jointly sponsored by the Office of Naval Research, Department of the Navy, Office of Scientific Research, Department of the Air Force, and Office of Ordnance Research, Department of the Army, under Contract No. N6-ori-105.

Temperature profiles through the flame have already been determined previously with a very similar instrument[1] from the intensity ratio of two water-vapor band peaks in the near infrared. The receiving instrument used in this range is a lead sulfide cell. For the visible and ultraviolet, a quartz-enclosed photomultiplier tube has been employed. Absolute calibration at all wave lengths has been obtained by comparing the flame signal with that from a standard tungsten-in-quartz lamp.

Three premixed butane-air flames have mainly been studied, containing 2.67 per cent, 3.40 per cent, and 4.00 per cent butane, respectively. The stoichiometric mixture contains 3.13 per cent. The medium concentration chosen is close to the one giving maximum temperature and burning velocity. The flow rate of the cold mixture was kept constant at 267 cc/sec. This yielded approximately a velocity of 330 cm/sec of the hot gases in the post-combustion zone. With the help of this factor the distance behind the flame front can be converted into time.

(2) Temperature Measurements

For the infrared measurements, spectroscopic slit and aperture have been chosen so that the average thickness of the visible flame section was 0.22 mm. The results for the three flames mentioned are shown in Figures 2 to 4. The position of the flame front as defined by the maximum of the CH-radiation is marked on the figures. It is noted that the temperature in the flame front T_{fr} is a few 100°C below the maximum temperature T_m , and that it takes still a distance $d_m \cong 1$ cm, corresponding to a time of 0.003 sec, to reach this maximum. Similar observations have been made by Lewis and von Elbe[2] on the temperature profile above the tip of a Bunsen cone. Table 1

shows that $T_m - T_{fr}$ and d_m decrease from lean to rich.

Apart from the position of the flame front it is noticed that the steepness of temperature rise increases from lean to rich (while the temperature drop behind the maximum is about the same in all cases). This indicates a decrease of heat loss through the flame front with increasing fuel content which is confirmed by the dependence of the difference $T_{ad} - T_m$ on concentration (Table 1, T_{ad} = adiabatic equilibrium temperature). There is a parallelism between these findings and the observation that the quenching distance of rich hydrocarbon flames is smaller than that of lean ones of equal burning velocity[3]. The common cause of these phenomena is probably found in an increase of average chemical reaction rate in the burning zone from lean to rich.

(3) Radical Radiation, Continuous Background

Entrance slit and aperture were adjusted to give a flame section of 0.13 mm thickness in the vicinity of the flame front. At larger distance from the flame front where the radiation gradients and intensities became low the thickness was increased to 0.9 mm at the most. The exit slit was kept constant at 0.3 mm so that the spectral resolution changed only very little with distance. Figure 5 shows a spectrum emitted by a flame front. The wave lengths in Table 2 have been chosen as characteristic of the various radicals.

A continuous background underlies all banded spectra. It is relatively much stronger in the post-combustion zone than in the flame front as is seen from Figure 6. In order to find the radiation intensity due to the radicals the background intensity has to be subtracted from the net signals. This is facilitated by the observation that the background curves obtained by smoothly connecting the minima of the net radiation curves are geometrically similar to each other within 2 per cent for distances from the flame front between 0.5 to 20 mm and for mixtures containing from 2.2 to 4.6 per cent butane. Thus the background radiation is normally only measured at one wave length which is free from other bands and for which 4500 Å has been chosen, and the corrections are made with the help of the fixed ratios of the interpolated background intensities at the wave lengths of interest to the intensity at 4500 Å. The CHO radiation cannot be accurately ascertained in this manner since its intensity is too weak. Therefore only trends will be reported on CHO radiation.

The continuous background spectra of the post-combustion zones of CH_4-air and CO-air flames have the same shape as the background spectrum of the butane-air flame within the limit of errors, and the continuous spectrum of the

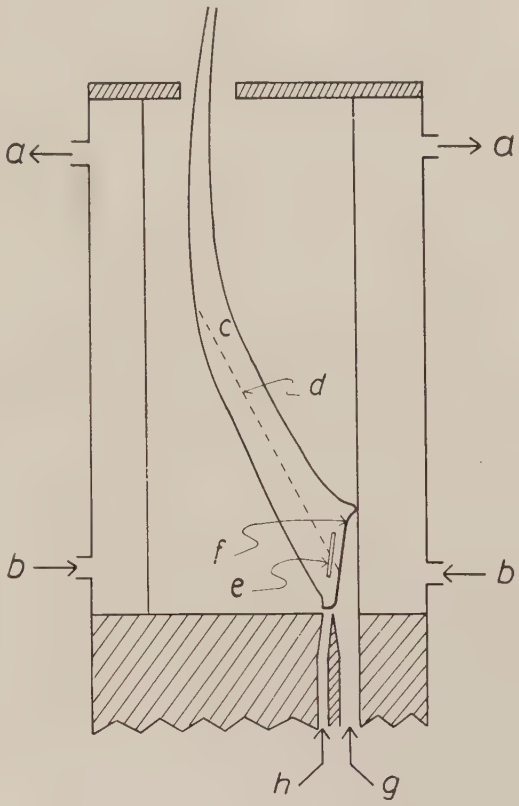

FIG. 1. Cross-section through rectangular burner. a, Water vapor; b, condensate return; c, luminous post-combustion zone; d, traverse path; e, average cross-section of observed flame region; f, flame front; g, main stream of fuel-air mixture; h, pilot gas stream.

flame front of a CO-air flame is at least very similar to that of the butane-air flame as is shown in Figure 6. On the other hand, the weak background radiation of H_2-air flames has an altogether different shape than that of the flames mentioned so far, the intensity being relatively much stronger at small wave lengths[b]. This proves that one and the same process is responsible for the continuum in hydrocarbon and CO-flames. According to Gaydon[4], this process is $O + CO \rightarrow$

[b] Measurements of all flames other than butane-air flames have been carried out by E. T. Child.

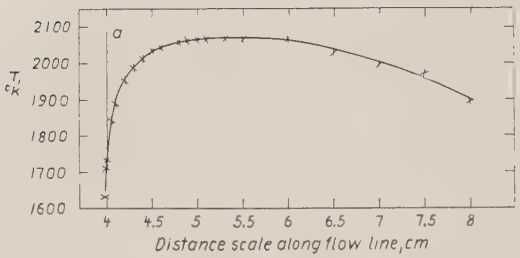

FIG. 2. Temperature through flame front along flow line. Butane-air flame with 2.67% butane. (a) Position of flame front, at 4.006 cm.

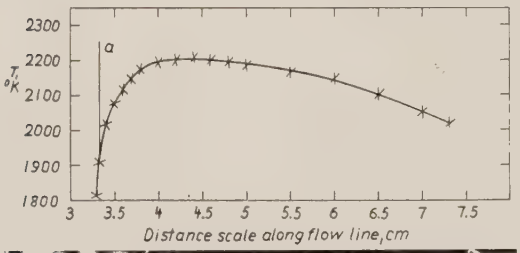

FIG. 3. Temperature through flame front along flow line. Butane-air flame with 3.40% butane. (a) Position of flame front, at 3.327 cm.

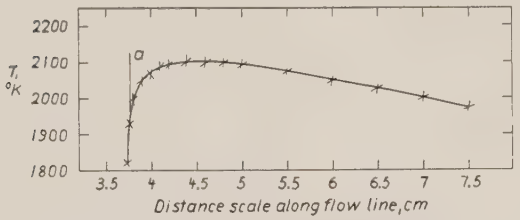

FIG. 4. Temperature through flame front along flow line. Butane-air flame with 4.00% butane. (a) Position of flame front, at 3.762 cm.

TABLE 1. TEMPERATURE RELATIONS

Per cent butane	2.67	3.40	4.00
T_m, °K	2070	2206	2102
T_{fr}, °K	1736	1909	1930
$T_m - T_{fr}$	334	297	172
d_m, mm	15.0	10.7	7.4
$T_{ad} - T_m$	~60	~30	~−10

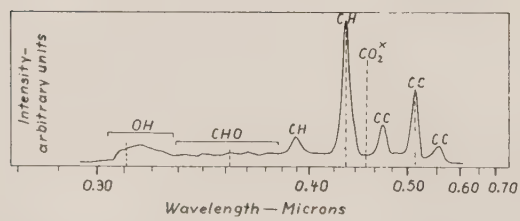

FIG. 5. Spectrum of the flame-front of a butane-air flame with 3.40% butane. Slit widths 0.3 mm. Dotted lines: see Table 2.

$CO_2 + h\nu$. It may be characterized by the symbol CO_2' which designates the short-living energy-rich product of a binary collision between CO and O.

(4) Peak Radiation in the Flame Front

The plane of maximum intensity in the flame front is, within the limit of errors, the same for all emitters except for OH for which this plane is displaced by 0.04–0.05 mm toward the upstream side. The maxima of the radiation intensities of OH, CH, C_2, and CO_2' have been plotted as a function of mixture composition in Figure 7. The unit is watts/cm²/micron/unit solid angle. The resolution for OH at the conditions of experiment is 20 Å, for CH 52 Å, and for C_2 80 Å (see Table 2). But the absolute meaning of the data of Figure 7 is irrelevant for the present discussion. The influence of composition on radiation is such that the effect of the adiabatic equilibrium temperature is superimposed by a preference of the rich side. Only CHO which is not included in Figure 7 radiates preferentially in the lean range which speaks in favor of a participation of a highly oxidative intermediate in the formation of this radical (see, however, Gaydon and Wolfhard[5]). Preferential radiation on the rich side is most outspoken with C_2 as is well known, but it exists even for OH and CO_2', and for both to about an equal degree.

For a discussion of Figure 7 it has to be realized that there exists in the flame front an excess of radicals and atoms in the fundamental state which has been created by chain-branching. In addition, an excess of excited radicals beyond the concentration given by the Boltzmann factor is produced through chemiluminescence and sensitization as mentioned. An important overall-sensitizer probably is the long-living energy-rich CO_2^* which is produced by a ternary collision of $O + CO + M$. Concerning C_2 and CH, the higher radiation intensity on the rich side is due in the first place to an especially high generation of these radicals in the fundamental state from the excess of fuel. The equilibrium concentration of OH is lowest on the rich side, and so is probably the concentration in the flame front. The shift of the OH-radiation curve toward rich will thus be the result of an increase of excitation in this direction[5]. Also the equilibrium value of the product $O \times CO$ is smallest in the rich range. The shift of the CO_2'-radiation toward rich is unexplained. Concerning this radiation, see Broida and Gaydon[6].

(5) Decay of Radical Radiation

(5.1) SURVEY AND INITIAL STAGE OF DECAY

The results of traverses through the flame front and post-combustion zone for the various radicals are shown in Figures 8 through 10 on semi-logarithmic plots. The mutual position of the curves in vertical direction is irrelevant and chosen to make the curves distinguishable from each other. The data points are so numerous and lie so close to the average lines that they have been omitted. The translation of the slopes of these curves into decay rates has been discussed before. Table 3 contains the peak intensities I_0 in the flame front ($d = 0$) and the intensity drops $\frac{I_2}{I_1}$ over various distances behind the flame front. There is a steep initial drop of radiation within 1 mm. The slope increases for a given flame in the direction

$$CO_2' \rightarrow OH \rightarrow \begin{cases} CH \\ C_2 \end{cases}$$

(The slopes discussed are negative; the characterization of magnitude pertains to their absolute values.) Beyond 1 mm the decay slows down considerably. The C_2-radiation in the lean flame (Fig. 8) becomes soon immeasurably small. Eventually the other curves become essentially of the first order, i.e., linear on the plots chosen. The CH-curve in Figure 8 has a pronounced kink at about 1 mm distance and is steeper than the CO_2' and OH curves. The CH-radiation is measurable to 1.4 cm behind the flame front. In the medium rich flame (Fig. 9) C_2 behaves similarly to CH. Both curves show a kink; they drop less steeply than in the lean flame so that the radiation is measurable up to larger distances. Their slopes, however, are still steeper than those of the CO_2'- and OH-curves for the same flame. In the richest flame (Fig. 10) all the four curves show a kink though it is least pronounced with CO_2'. Their slopes are now commensurate. The CH- and C_2-radiation can be followed well up to a distance of 4 cm behind the flame front. At this distance the CH-radiation has dropped to $\frac{1}{370,000}$ of the intensity in the flame front.

A promotion of the radiation of the CHO-radical by oxygen in the post-combustion zone is shown in Table 4 which gives the distance behind the flame front d up to which CHO can be detected, as a function of composition.

It is remarkable that the rate of radiation decay varies for a given radical from mixture to mixture, and partly for a given mixture also from radical to radical, at larger distances qualitatively in the same manner as in the range of strong initial decay (see Figures 8 through 10 and Table

Table 2.

Radical	Wavelength	Transition
	Å	
OH	3110	$^2\Sigma - {}^2\pi$ (0.0)
CH	4315	$^2\Delta - {}^2\pi$ (0.0)
C_2	5147	$^3\pi_g - {}^3\pi_u$ (0.0)
CHO	3505	
(CO_2')	(4500*)	

* See text.

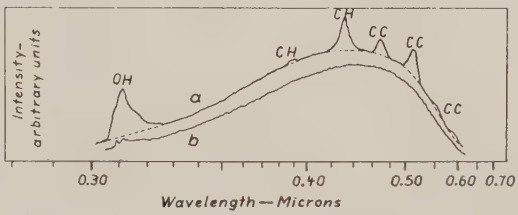

Fig. 6. (a) Spectrum of the post-combustion zone of a 4.00% butane-air flame 10 mm behind the flame front. Slit widths 0.3 mm. Dashed curve represents interpolated curve of background (CO'_2) radiation. (b) Spectrum of the flame front of a stoichiometric CO-air flame. Slit widths 0.1 mm.

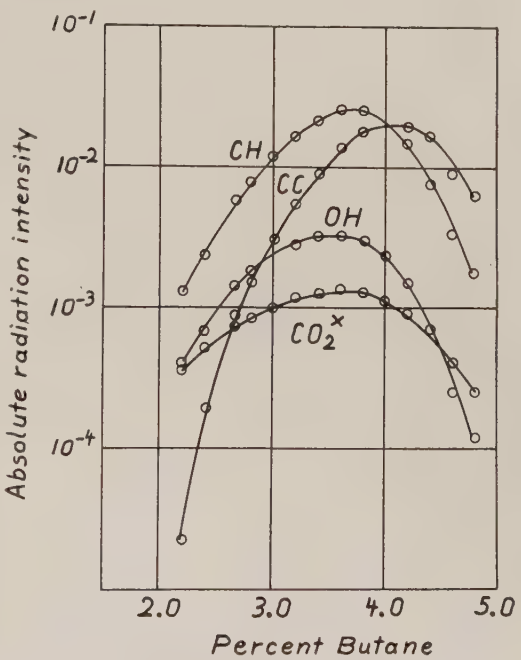

Fig. 7. Absolute intensity (watts/cm²/micron/unit solid angle) emitted by flame radicals at wavelengths given in Table 2. Thickness of observed flame section 0.13 mm.

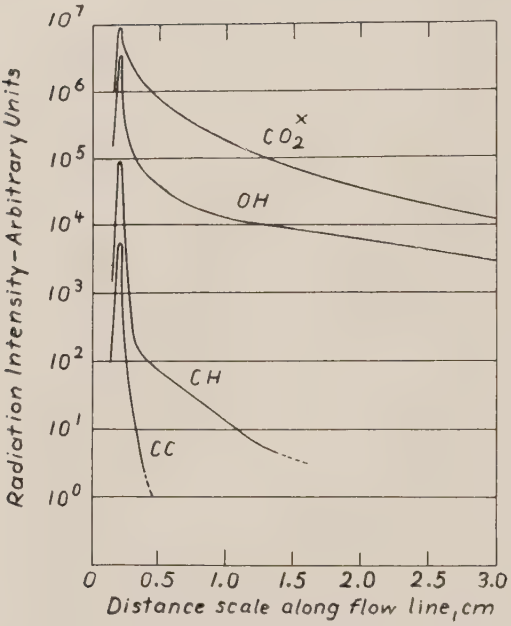

FIG. 8. Radical radiation through flame front along direction of flow. Butane-air flame with 2.67% butane. The vertical positions of the curves with respect to each other are arbitrary. Wavelengths: see Table 2.

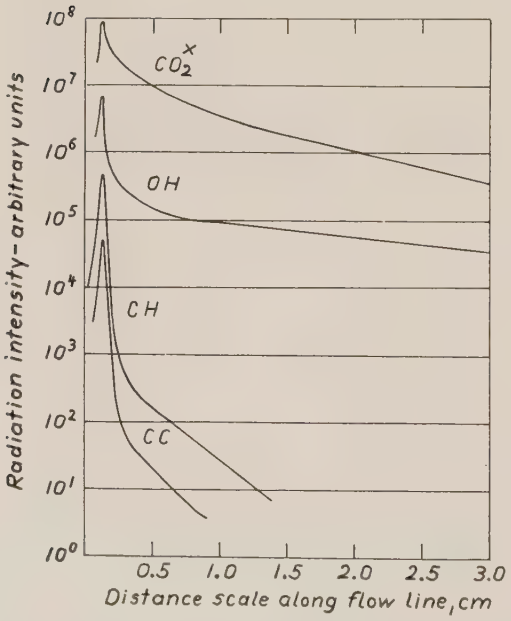

FIG. 9. Radical radiation through flame front along direction of flow. Butane-air flame with 3.40% butane. The vertical positions of the curves with respect to each other are arbitrary. Wavelengths: see Table 2.

3). This seems only possible if the creation of radicals by chain-branching ceases to be a rapid process rather abruptly in the flame front proper. From then on the radicals are essentially swept down by the gas stream while undergoing chemical reactions. Diffusion processes which are of importance to the structure of the cold stream side of the flame front soon become irrelevant on the hot stream side. As long as the concentrations of the radicals are high they react preferably with each other and with atoms. This results in a rapid decrease which also reduces the chance for the processes of chemiluminescence and sensitization. Thus the concentration of excited radicals, and consequently the radiation intensity, will fade out still more rapidly. When the radical concentrations have become lower the reactions with molecules which require a high activation energy will become more and more predominant whenever such reactions are possible. Where the kink shows, the excitation process may have become largely thermal so that the slopes of curves downstream of the kink reflect mostly the disappearance of radicals in the fundamental state. It corresponds to this viewpoint that the OH-curve shows a kink only in the richest mixture where the chemiluminescence mentioned before is strongest.

(5.2) DECAY OF C_2- AND CH-RADIATION

The radicals C_2 and CH are both capable of undergoing exothermal reactions with OH, O_2, H_2O, and CO_2. The decay of C_2-radiation in the lean flame is especially rapid. It is concluded that the reaction between C_2 and O_2 is especially fast (the OH concentration also increases from rich to lean but not very strongly). It is surprising that this holds for the reaction between CH and O_2 only to a very minor degree (Fig. 8 and below). The CH-radiation curves, and for the two rich mixtures also the C_2-radiation curves, become of the first order at a short distance behind the kink. Table 5 contains the logarithmic slopes of the first order decay, $-\Delta \log I/\Delta x$ (I = radiation intensity, x = distance behind the flame front) and the range of distances behind the flame front in which a constant logarithmic slope was observed. For CH and C_2 there are also recorded the differences of the temperatures at the end points of the distance ranges given. The difference is practically zero in case of the richest mixture.

A first order of decay of radiation means that the concentration of excited radicals decays by the first order. This will occur if the excitation is thermal and if the radical in the fundamental

state disappears by a reaction with molecules of constant concentration. This condition is virtually fulfilled for the reactions of C_2 and CH with O_2 in a lean mixture and with H_2O and CO_2 in a rich mixture. However, a contribution to the decay rate in the post-combustion by reaction with OH cannot be excluded.

It is noticed that the dependence of the slopes in Table 5 on fuel concentration is mostly the same as that of the decay rates closer to the flame front according to Table 3. In case of CH the slopes are largest for the mixture with 3.40 per cent butane and smallest for that with 4.00 per cent. It is suggested that the slope at 3.40 per cent is highest because the temperature is highest (see Table 1). Between 3.40 and 4.00 per cent the concentrations of the reaction partners of CH and C_2 in rich mixtures, H_2O and CO_2, change only little, and the concentration of OH decreases. The decay rate of CH at 2.67 per cent butane will be higher than that at 4.00 per cent because the reaction with O_2 is somewhat more rapid than that with H_2O and CO_2, while at the same time the OH concentration is highest in the lean mixture. For C_2 the situation in the two rich mixtures is qualitatively the same as for CH while in lean mixtures the rate of reaction $C_2 + O_2$ seems to be especially high as was mentioned. Beyond the range of constant logarithmic slope the CH-curves, and the C_2-curve in the richest mixture, become gradually flatter.

The slow decay rate of CH and C_2 offers a serious difficulty. We write for the average relative decay rate of a radical R

$$-\frac{\overline{dR}}{dtR} = Z\bar{p}_0 e^{-E/RT} = \frac{-\Delta \log I}{\Delta x}\frac{\Delta x}{\Delta t} 2.303$$

Z = collision number at 1 atm and 2000°K (2.6×10^9), $\bar{p}_0$ = average partial pressure of the reaction partner (0.3 atm), E = activation energy. An average value of slope, $-\Delta \log I/\Delta x$, for CH and C_2 is 1.4 cm^{-1}; $\Delta x/\Delta t$ = 330 cm/sec as mentioned. There follows an activation energy of 54 kcal for reactions of C_2 and CH with H_2O and CO_2 and of CH with O_2; this appears too high. If it is assumed that CH and C_2 disappear by reactions with OH a mole fraction of OH higher than the equilibrium pressure of OH in the rich mixture (which is about 1.4×10^{-4}) has to be employed. There follows $E \geqq 24$ kcal which is also very high for a reaction between radicals.

A gradual approach to equilibrium radiation might possibly be considered for CH in rich flames, but seems out of the question for CH in the lean flame, and for C_2 in general.

(5.3) DECAY OF OH AND CO_2'-RADIATION

The transition from the steep radiation drop right behind the flame front to the final first order decay is more gradual for OH than for CH and C_2, and is still smoother for CO_2' as can be seen from Table 5 by the distance at which the first order decay starts. In between there is a range in

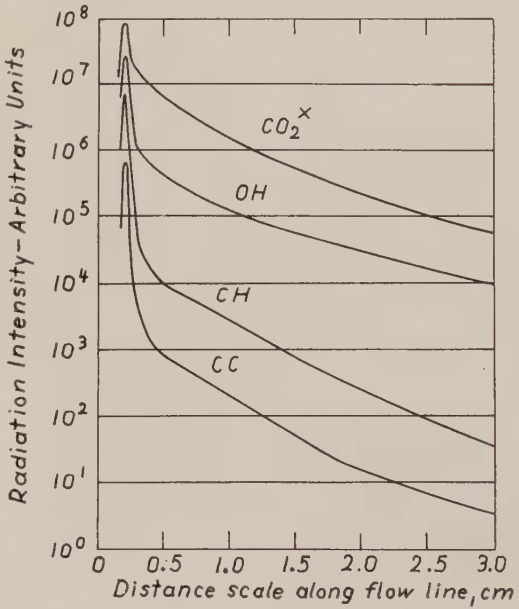

FIG. 10. Radical radiation through flame front along direction of flow. Butane-air flame with 4.00% butane. The vertical positions of the curves with respect to each other are arbitrary. Wavelengths: see Table 2.

which the OH-radiation drops according to a second order reaction:

$$-\frac{dI}{dx} = kI^2, \qquad \text{or integrated}$$

$$\frac{\Delta(I_0/I)}{\Delta x} = kI_0 = \text{const.}$$

The simplest explanation for this observation is that the concentration of the excited OH is proportional to that of OH in the fundamental state, and that the latter disappears by a second order reaction. The second order range is largest for the lean flame and extends in this case with moderate accuracy from 1 to 18 mm behind the flame front.

The OH-radical will disappear by reacting with

Table 3. Peak Radiation Intensities and Radiation Decay

Per cent butane		2.67				3.40				4.00			
Radicals		CO_2'	OH	CH	CC	CO_2'	OH	CH	CC	CO_2	OH	CH	CC
I_0	d = 0 mm	72	142	550	87	128	320	2170	900	114	236	2120	2000
$\frac{I_2}{I_1}$	0–1 mm	0.25	0.040	0.0029	0.0026	0.27	0.53	0.0023	0.0036	0.18	0.024	0.0055	0.0050
	1–2.7 mm	0.40	0.38	0.32	0.046	0.52	0.49	0.20	0.16	0.45	0.58	0.25	0.26
	2.7–7.5 mm	0.29	0.31	0.19		0.35	0.52	0.18	0.13	0.24	0.30	0.29	0.26
	7.5–23.4 mm	0.087	0.28			0.16	0.44			0.058	0.12	0.025	0.030
	23.4–39.7 mm	0.16	0.17			0.19				0.19	0.13	0.27	0.44

Table 4. CHO-Radiation Decay

Per cent butane	2.2	2.5	2.67	3.40	4.00
d, mm	5.0	3.0	1.0	0.7	0.5

second order decay of OH-radiation in the lean flame.

The absolute rate of this decay appears surprisingly slow. In analogy to the first order rate equation in the preceding section we write for

Table 5. Characteristics of First Order Decay

		Per cent butane		
		2.67	3.40	4.00
CO_2'	$-\Delta \log I/\Delta X$, cm^{-1}	0.68	0.38	0.42
	Distance range, mm	18–36	19–33	26–40
	Temperature range, °K	2070–1955	2185–2090	2034–1948
	E, kcal	127	127	127
	$\Delta(E/2.30RT)/\Delta X$, cm^{-1}	0.41	0.41	0.43
OH	$-\Delta \log I/\Delta X$, cm^{-1}	0.32	0.22	0.50
	Distance range, mm	10–30	6–29	14.7–38
	Temperature range, °K	2067–1989	2190–2127	2084–1969
	E, kcal	131	159	159
	$\Delta (E/2.30RT)/\Delta X$, cm^{-1}	0.27	0.20	0.42
CH	$-\Delta \log I/\Delta X$, cm^{-1}	1.48	1.51	1.09
	Distance range, mm	2.8–10.0	3.5–12.5	3.6–17.6
	$T_2 - T_1$	72	57	0
CC	$-\Delta \log I/\Delta X$, cm^{-1}	(8.42)	1.87	1.19
	Distance range, mm	(0.7–2.7)	3.0–7.5	4.6–16.6
	$T_2 - T_1$	(117)	72	0

itself, with H, H_2 and CO. In the flame front the reaction of OH with itself which is likely to yield $H_2O + O$, is followed by a sequence of chain reactions between O and H_2, and H and O_2, which recovers the hydroxyl. But in the post-combustion zone, H_2 or O_2 or both will be scarce, depending on the mixture, so that OH will actually be removed by reacting with itself. In the lean flame, this reaction should be the only one which matters. This explains the large range of

the second order rate equation

$$\frac{\Delta(OH)_0/(OH)}{\Delta x}\frac{\Delta x}{\Delta t} = Z(OH)_0 e^{-E/RT}$$

(OH) = partial pressure of OH,

$(OH)_0$ = partial pressure of OH at the beginning of the second order reaction.

One finds

$$\frac{\Delta(OH)_0/(OH)}{\Delta x} = \frac{\Delta(I_0/I)}{\Delta x} = 290 \text{ cm}^{-1}$$

$(OH)_0$ is assumed to be 0.01 atm

There follows E = 27,000 which again appears

very high. In rich flames the reactions of OH with H + M, H_2 and CO will be predominant.

A pseudomonomolecular reaction which might explain the final first order decay of the OH-radiation is hard to conceive for a lean flame. The first order slopes of all the three flames investigated, however, are rather small, and it appears that the values of these average slopes can be explained by a drop of flame temperature on the assumption that at these large distances from the flame front the OH-radiation is essentially thermal. The intensity of the OH-radiation is then proportional to the equilibrium concentration of excited hydroxyl OH* which depends on temperature chiefly according to the factor $e^{-\Delta H/RT}$ where ΔH is the enthalpy requirement for the formation of OH*. In rich mixtures ΔH equals the sum of the enthalpy changes connected with the processes $H_2O \rightarrow \frac{1}{2}\ H_2 + OH$ (67.8 kcal) and $OH \rightarrow OH^*$ (91 kcal), i.e., 159 kcal. In lean flames the first process has to be replaced by $\frac{1}{2}\ H_2O + \frac{1}{4}\ O_2 \rightarrow OH$ (38.9 kcal) so that a total value of 130 kcal results. A comparison of $(-\Delta \log I/\Delta x)$ with

$$\frac{\Delta(E/2.30RT)}{\Delta x} = \frac{\Delta(E/2.30RT)}{\Delta T}\,\frac{\Delta T}{\Delta x}$$

is given in Table 5. The temperature range ΔT and the distance range Δx are also found in this Table. The agreement is satisfactory. The fact that the experimental slopes are consistently slightly larger than the calculated ones may indicate that the equilibrium is not yet fully reached in the beginning of the range.

The CO_2'-radiation is assumed to be proportional to the product of the concentrations of O and CO. The O atom will disappear by reactions with O + M, H + M, H_2 and CO + M. The latter reaction proceeds via CO_2^* (see p. 748). The analogy with the reactions by which OH disappears is striking. The rate of decrease of CO-concentration can be assumed to be slow compared with that of the O-concentration so that the decrease of the latter determines the decay of CO_2' radiation. This is likely to be true to some degree even for the lean flame so that the general analogy between OH- and CO_2'-radiation decay which is, e.g., evident from Table 3, is understandable.

The CO_2'-radiation also has an extended intermediate range of a reaction order higher than 1, though the order is not the second but the 1.5th and the range is largest for the medium rich flame (1–22 mm behind the flame front). The CO_2'-radiation also seems finally to become thermal, at least in case of the two rich flames. Using for ΔH the heat of dissociation of CO_2 into CO + O (127 kcal), good agreement is obtained for these flames between the logarithmic decay rate of CO_2' radiation and the change of the O-atom concentration at equilibrium with temperature (see Table 5). (It may be mentioned that the production of O-atoms from H_2O requires 117 kcal which is not very different from 127.) For the lean flame the decay rate of radiation is higher than calculated.

The decay rates of OH- and CO_2'-radiation are practically at all distances largest for the richest flame and smallest for the medium rich flame which has the highest temperature. This behavior is exactly opposite to that of the CH-radiation. The increase of the decay rate of the OH- and O-concentrations from the 3.40 per cent to the 4.00 per cent-mixture is probably due to the increase of the concentration of the reaction partners CO and H_2. This effect is larger than a possible decrease of reaction rate by the drop of temperature. (This interpretation does not apply to the very large distances of Table 5 where equilibrium has been assumed to exist.) The increase of decay rate on going from the medium rich to the lean flame may be due to the relatively high concentrations of O and OH in this flame which lead to an especially high rate of the reactions of these radicals with themselves.

All these relationships between the radiation decays at various conditions gain special significance through the observation that almost invariably they are true also for CH_4-air flames[c]. It is plausible that differences between these two flames will show rather in the range of chain-branching than in the following range of straight radical reactions which has been studied here.

REFERENCES

1. Bernath, L., Powell, H. N., Robison, G. A., Welty, F., and Wohl, K.: Proc. Gen. Dission on Heat Transfer, p. 315. London, The Institution of Mechanical Engineers, 1951.
2. Lewis, B., and von Elbe, G.: J. Chem. Phys., *11*, 75 (1943).
3. Wohl, K.: *Fourth Symposium on Combustion*, p. 68. Baltimore, The Williams & Wilkins Co., 1953.
4. Gaydon, A. G., and Wolfhard, H. G.: *Flames*. London, Chapman and Hall, Ltd., 1953.
5. Gaydon, A. G., and Wolfhard, H. G.: *Fourth Symposium on Combustion*, p. 211. Baltimore, The Williams & Wilkins Co., 1953.
6. Broida, H. B., and Gaydon, A. G.: Trans. Faraday Soc., *49*, 1190 (1953).

[c] Measurements by T. E. Child.

86

ATOMIC FLAMES: SPECTRA, "TEMPERATURES", AND PRODUCTS

By R. E. FERGUSON AND H. P. BROIDA

The origin of the anomalies of hydrocarbon flame spectra is still one of the unsolved problems of combustion kinetics. The mechanisms responsible for the nonthermal excitation of some of the species present in the reaction zone of a flame may or may not influence appreciably the rate of the overall reaction occurring in the flame front; however, the question of their kinetic importance will probably be answered only after considerably more is known about these mechanisms and also about the phenomena to which they give rise.

Whether or not nonthermal excitation of a particular radical exists is sometimes difficult to establish, and in cases where the excitation is definitely nonthermal, it may be difficult to determine whether this is due to chemiluminescence (formation in a chemical reaction of the radical in an excited state) or to activation by collision with another excited radical or molecule. Working with reaction systems at low pressure lessens some of these difficulties since, as the pressure is reduced, collisions in the reacting gases become fewer while the radiative lifetimes of the excited species remain constant; hence there is a better chance at low pressure of observing radiation from excited states which have been less altered by collisions occurring during their radiative lifetimes.

Gaydon and Wolfhard[1-6] have studied the visible and ultraviolet spectra of low pressure flames. This work has indicated that there are marked departures from thermal equilibrium in the reaction zone. Similar lack of equilibrium has been observed under certain conditions in hydrocarbon flames burning at atmospheric pressure[7-19]. Recently Gaydon and Wolfhard[10], working with flames supported by free oxygen atoms, observed an abnormal rotational intensity distribution in the OH band at 3064A and excess excitation of iron atoms introduced into the reaction zone. This is of considerable interest, since the use of an atomic flame as a source to supplement the low pressure flame for the study of non-thermal excitation has several advantages. Flames can be maintained at very low pressure (down to 0.1 mm Hg) where one might expect enhancement of the nonequilibrium phenomena. Moreover, the experimental arrangement and conditions are such that partially quenched product samples can be easily obtained.

The work to be described represents for the most part an experimental survey of the spectra and products of the luminous reaction between acetylene and the products of an electric discharge through oxygen. The purpose of the study was, generally, to obtain a useful working knowledge of atomic flames which at present cannot be gained from the literature, and specifically, to determine whether there is any obvious relation between changes in products and changes in the emission due to excited radicals as conditions (pressure, flow rate, and fuel/oxidant flow ratio) are varied. In addition to data on flames with atomic oxygen, information is presented on the spectra and products of flames of acetylene with atomic hydrogen and with the products of a discharge through water vapor[10, 11].

The new (in application to the study of atomic flames) techniques of main interest involve the direct intensity recording of high resolution visible and ultraviolet spectra, the mass spectrometric analysis of stable product samples taken while spectra were being recorded, and the use of a microwave oscillator for exciting the discharge for the production of atoms.

Experimental

The reaction vessel (Fig. 1) was a one-liter Pyrex bulb fitted with quartz windows, Q, with two 13 mm sealed-in inlets, O and A_2, entering at a right angle, and a 30 mm pumping outlet, P. The inlet tube O, through which oxygen was introduced was surrounded by a larger concentric tube, A_1. The apparatus provided in effect two separate burner types with different flow and mixing patterns; with partly dissociated oxygen streaming into the bulb from the inner of the two concentric tubes, acetylene could be introduced either through the outer concentric tube or through the inlet entering at a right angle. It was possible to check quickly, by using one flow arrangement and then the other, the influence of flow pattern on the form and luminosity of the flame.

A large mechanical pump with a free air

capacity of 27 l/sec was used to maintain fast flow at working pressures of 0.5 to 3.0 mm Hg. Pumping speed was controlled with a large stopcock in the pumping line. Pressure was measured accurately to 0.1 mm Hg with a sensitive diaphragm manometer connected to a separate inlet on one side of the reaction bulb.

Acetylene, oxygen, hydrogen, and water flow rates were controlled by stopcocks in the inlet lines and, with the exception of water, were measured on the high pressure side of the control stopcocks (C, Fig. 1) with floating ball type flowmeters. Commercial cylinder gases were used. Oxygen and hydrogen were specified by the supplier to have purities greater than 99.7 per cent and the mass spectrometric data were consistent with this figure. In the first few experiments acetone was removed from tank acetylene by passage through a trap at dry ice temperature. Because of difficulties with rapid solution of acetylene in the acetone condensed in the trap, attempts to purify the acetylene were abandoned in later experiments. No significant changes in the products or spectra due to the presence of acetone were detected. Water vapor was pumped from a tube containing water. After the evaporation rate had stabilized, the flow rate was determined by measuring the change of liquid volume during the time required to obtain spectra and samples. Hydrogen was dried by passing it through a trap filled with glass beads and immersed in liquid nitrogen.

The high frequency electrodeless discharge for the production of atoms and for the dissociation of water vapor was excited by a 2450 megacycle oscillator, the output of which was fed through a coaxial cable to a section of wave guide (W, Fig. 1) used as a cavity through which the inner concentric inlet tube passed a few cm from the reaction bulb. At the beginning of the experiments, the position of the tube and the tuning member of the guide were adjusted visually to give maximum intensity of the discharge, and left in this position during the course of the experiments. The section of inlet tubing containing the discharge was cooled by an air stream. The intensities of atomic flames obtained with this type of discharge were compared with intensities obtained by conventional means with large aluminum electrodes[10] operated at 5000 volts and with 2 kw input power. Although the total electrical power used by the high frequency unit was only 125 watts, the flames were slightly brighter with this unit. In addition to the advantage of greatly reduced power requirements, the electrodeless discharge permits a simpler and cleaner glass system.

Gas samples were taken from the pumping line a few cm from the reaction zone into a separate sampling line previously evacuated with a mercury diffusion pump, and were stored in bulbs at the original flame pressure until analyzed. The rate of flow into the sampling system was low enough that the reaction zone was not visibly disturbed during the sampling period. The gas samples and samples of condensibles collected in a large dry ice cooled trap in the main pumping line were analyzed by mass spectrometer.

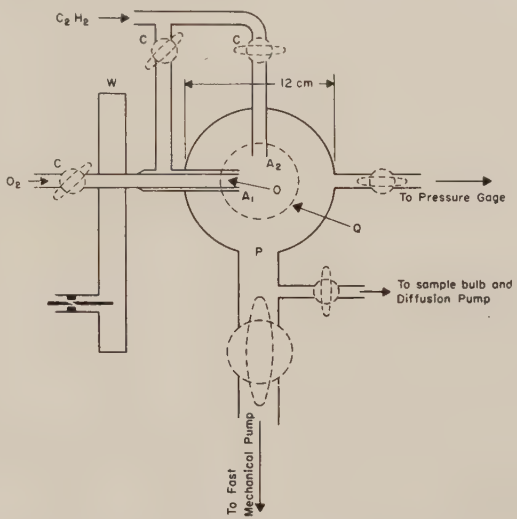

FIG. 1. Reaction vessel. C, control stopcocks; W, waveguide; O, inlet tube for products from discharge; A_1 and A_2, acetylene inlets; Q_1 quartz viewing window; P, pumping line.

A high resolution grating monochromator[a] with photoelectric detection and direct intensity recording[12] was used to obtain the spectra for measuring vibrational and rotational "temperatures". A quartz lens, 35 cm from the monochromator slit, was used to focus the image of the flame without magnification on the slit. The portion of the flame observed was 2 mm from the oxygen inlet tube, O, and at right angles to the direction of flow.

Procedure

Before the range of conditions available and the results obtained with the apparatus are de-

[a] This instrument was constructed by the Research Department of Leeds and Northrup Company and loaned to the National Bureau of Standards on a field trial arrangement.

scribed, it will be helpful to discuss the changes in appearance of the luminous zone of acetylene-atomic oxygen flames with changing conditions.

First, with the mass flow of C_2H_2 and O_2 into the bulb fixed, the luminous zone expands as the pressure is decreased, as would be expected due to the increase in mean free path, until at about 0.2 mm the glow appears to fill the entire bulb. Below 1 mm, the flames (providing that more than a trace of C_2H_2 is added) have the same size and shape regardless of the inlet arrangement used; this indicates that at these pressures the rate of interdiffusion of the reacting gases de-

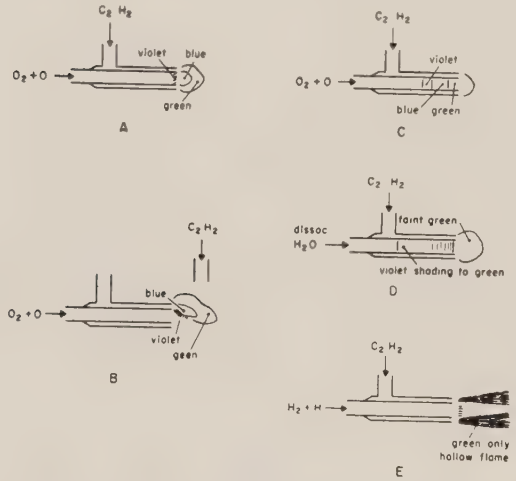

FIG. 2. Sketches of atomic flames with acetylene. A. $C_2H_2/O_2 = 1$, O_2 flow = 2.4 cc/sec NTP, $P = 1$ mm Hg (flame 1B); B. $C_2H_2/O_2 = 0.25$, $P = 3.0$ mm Hg (flame 4C); C. flame showing color separation (see text); D. dissociated water flame. $C_2H_2/H_2O = 1$, H_2O (gas) flow = 0.15 cc/sec NTP, $P = 0.2$ mm Hg.; E. atomic hydrogen flame, $C_2H_2/H_2 = 2$, H_2 flow = 2.3 cc/sec NTP, $P = 0.42$ mm Hg.

termines the size and shape of the flame and that this mixing is so rapid that the linear flow pattern has little or no effect. Thus the flame with equal C_2H_2 and O_2 flow at 1 mm (Fig. 2a) should probably be considered as a predominantly premixed flame in which the mixture ratio (C_2H_2/oxidant) increases continuously from the inner to the outer zones. As the pressure is increased, the reaction zone takes on more of the appearance of a diffusion flame and its position visibly depends upon the inlet arrangement (Fig. 2b).

At a constant pressure of 1 mm and fixed flow of O_2 through the discharge, the luminous zone contracts as the C_2H_2 flow is increased. At equal C_2H_2 and O_2 flow, it is about 2 cm in diameter and has moved 2 to 3 mm inside the oxygen inlet tube (Fig. 2a). If the O_2 flow is now reduced, the luminous zone moves into the oxygen inlet tube, where it exhibits a banded appearance with good color separation. The order of appearance, going from the oxygen to the acetylene side, is violet, blue, and green (Fig. 2c). It is interesting to note that this sequence at first appears to be the reverse of that observed in low pressure premixed flames which have greenish bases. However, it is important to recognize that in both cases the green appears first near the region in which there is the greatest concentration of acetylene.

At constant pressure and flow ratio, an increase of total flow rate slightly elongates the flame shown in Figure 2a. The flame is very slightly displaced downward toward the pumping line when the flow rate is approximately doubled.

At pressures above 3 mm with oxygen flow in excess of acetylene flow, a small increase of acetylene flow caused a marked change in appearance (brightening and fanning out) of the flame. It was found that the change was due to the appearance of a self-supporting diffusion flame which was not extinguished by turning off the discharge. This flame with considerable care in adjustment of flow and flow ratio could be maintained down to about 1.2 mm.

The range of conditions investigated was limited by (1) the desirability of keeping the flame focused on the spectrometer slit, which was kept stationary, (2) the requirement of sufficient intensity to obtain good direct recordings of resolved spectra, and (3) a desire to eliminate the self-supporting flame as a complicating factor. In line with these requirements a standard flame was selected with the following conditions: O_2 flow = 2.4 cc/sec NTP, C_2H_2/O_2 volume flow ratio = 1, and $P = 1$ mm Hg. This flame could be obtained with roughly half the available pumping speed, leaving a reserve for use in increasing the total flow or for decreasing the pressure. The experimental conditions were varied widely about those of the standard flame. For example, in the experiments with atomic oxygen flames, the total gas flow through the bulb, measured at the flame pressure, ranged from 1 to 7.5 l/sec over a pressure range of 0.5 to 3.0 mm, giving linear streaming velocities in the inlet tubes of 8 to 50 m/sec; C_2H_2/O_2 volume flow ratios varied from 0.25 to 5; and the visually estimated volume of the luminous zone ranged from 1 to 33 cc. Conditions were actually set by fixing the flow ratio, total inlet flow, and pressure; the streaming rate and flame volume, of course, could not be independently controlled in the present apparatus.

In all, products and spectra were obtained from thirteen acetylene-atomic oxygen flames and from one flame each of dissociated water and of atomic hydrogen with acetylene. The manner in which conditions were varied for twelve of the atomic oxygen flames is shown in the upper part of Table 1, which will serve as a guide to the discussion of the results. Flame 1B is the standard flame referred to above. The series of measurements were made consecutively over a period of about three weeks.

flow ratios are accurate to ±10 per cent, as are the total flow and streaming rates listed. The flame volumes were obtained from visual scale drawings of each flame and are given to show trends.

The flames with dissociated water were much fainter than those obtainable with atomic oxygen and were more sensitive to adjustment of flow ratio and pressure. The most intense flame was produced in this apparatus with a volume flow ratio C_2H_2/H_2O of 1:1 at a pressure of 0.2 mm

Table 1. Acetylene-Atomic Oxygen Flames: Conditions and Main Products

	1. Effect of flow ratio			2. Effect of Pressure and flow rate					3. Reduced oscillator power	4. Effect of using right angle inlet system		
	1A	1B	1C	2A	2B	2C	2D	2E	3A	4A	4B	4C
Pressure in bulb, mm Hg	1.0	1.0	1.0	0.6	3.0	0.5	3.0	1.0	1.0	1.0	0.4	3.0
C_2H_2/O_2 flow ratio	0.25	1.0	5	1.0	1.0	0.25	0.25	1.0	1.0	1.0	0.25	0.25
Total flow at flame pressure, l/sec	2.4	4.0	7.5	6.4	1.3	4.9	0.8	6.7	4.0	4.0	5.8	0.8
Streaming rate of O_2 in inlet, m/sec	23	23	23	37	7.6	46	7.7	39	23	23	54	7.6
Flame volume, cc	9.2	5.6	2.6	6.4	0.9	17	9	6	2.6	6	33	See fig. 2b
O_2 consumed/C_2H_2 consumed	1.38	1.15	0.97	1.21	†	1.36	1.90	1.13	1.08	0.98	1.38	†
C_2H_2 consumed, per cent	66	18	4.9	16		60	99	17	14	25	57	
O_2 consumed, per cent	24	23	15	20		19	46	19	18	28	18	
CO/CO_2 ratio in products	1.8	6.4	11.5	5.7		2.5	0.15	7.4	6.2	5.4	1.5	
CO*	12.9	15.3	12.8	14.9		14.2	2.6	14.9	15.1	13.7	11.6	
CO_2*	7.1	2.4	1.1	2.6		5.7	17.4	2.0	2.4	2.5	7.7	
H_2*	5.2	2.8	4.2	4.0		4.6	1.6	5.2	5.1	2.5	7.0	
H_2O*	0.4	1.5	0.0	2.3		1.6	0.6	1.1	0.0	0.0	0.0	
H_2CO*	0.0	1.3	4.4	1.7		0.0	0.0	2.3	1.6	1.0	0.8	

* Expressed as moles of product per 10 moles of acetylene consumed.

† Analysis not used because of small air leak into sample bulb; spectra were obtained.

The purpose of each series is indicated in the column heads in Table 1. Series 3, one flame of which is listed, was done in order to examine the effect of decreasing the discharge excitation power, which should decrease the atom concentration in the oxygen stream. The right-angle inlet arrangement (i.e., the C_2H_2 entered the reaction vessel through A_2, Fig. 1) was used for series 4, and conditions were chosen so that these flames could be compared to some of those in series 1 and 2, which were all run with the concentric inlet system (A_1). The oxygen flow was 2.4 cc/sec NTP except in 2E, in which it was 4.0 cc/sec NTP. The pressures listed in Table 1 are *measured* pressures as described above. The

Hg and a water vapor flow of 0.15 cc/sec NTP (Fig. 2d).

Atomic hydrogen with acetylene gave a very faint green flame which could be seen only in a well-darkened room. The luminosity was sensitive to changes of conditions, the maximum being obtained with a volume flow ratio C_2H_2/H_2 of 2:1 at 0.42 mm Hg and a hydrogen flow of 2.3 cc/sec NTP. The form of the luminous zone is shown in Figure 2e. Products and spectra were obtained only for the one set of conditions giving maximum intensity for both the atomic hydrogen and the dissociated water flames.

Products of Atomic Oxygen Flames

The main products as determined by mass spectrometric analysis of the gas samples are shown in the lower part of Table 1 in terms of moles of product per 10 moles of acetylene consumed. The reported total composition of samples from flames 1A, 1B, and 1C (increasing C_2H_2 flow at constant pressure and O_2 streaming rate) are given in Table 2 as examples of the data reported by the Mass Spectrometry Section of the National Bureau of Standards. All of the figures shown are corrected for carbon oxides formed from oxygen in the samples and carbon-containing residues in the ion chamber of the mass spectrometer. The corrections were obtained as follows: four control samples (discharge turned off) were taken covering the range of flow ratios used in the experiments; from the analyses of these samples and a sample of tank oxygen, a plot of spurious CO versus concentration of oxygen in the sample was obtained, and the corrections applied to the reported CO and O_2 concentrations in the reaction products were obtained by interpolation from this curve. The spurious CO_2 was practically the same for all samples, varying from about 0.1 to 0.3 mole per cent. The maximum spurious CO found (this was in the pure oxygen sample) amounted to 10 mole per cent of the sample. As a check on the constancy of this instrumental error, a sample of tank oxygen was run along with each series of gas samples analyzed; the variation in CO reported from series to series was only 1 to 2 per cent of the total spurious CO. Another error, difficult to evaluate, is that due to loss of water from the samples due to adsorption on the walls of the storage bulbs and mass spectrometer inlet system. That this loss was not negligible is shown by the apparent loss of hydrogen from the sample, which in the most extreme case (2D) amounted to 70 per cent of that in the reacted acetylene. In this case, however, as with the other atomic oxygen flames, a back calculation based on the carbon and oxygen balance checked the measured inlet flow ratio within 15 per cent. For the above reasons, the water content listed in Tables 1 and 2 should be considered doubtful.

Table 2. Mass Spectrometric Analyses of Sample from Series 1, Acetylene-Atomic Oxygen Flames*

Constituent	1A	1B	1C
C_2H_2	6.9	42.6	69.6
O_2	57.8	35.5	20.4
CO	17.3	14.1	4.6
CO_2	9.5	2.2	0.4
H_2	7.0	2.6	1.5
H_2O	0.6	1.4	0.0
H_2CO	0.0	1.2	1.6
C_3H_4	0.0	0.2	0.2
CH_3COCH_3†	0.2	0.0	1.6
CH_3CHO	0.4	0.0	0.0
CH_4	0.4	0.2	0.0

* Products are expressed in mole per cent of the sample, based on the partial pressures of the constituents of the sample at a total pressure of 1 mm Hg.

† 2 mole per cent acetone was present in the acetylene used in 1A and 1C; it was removed for flame 1B.

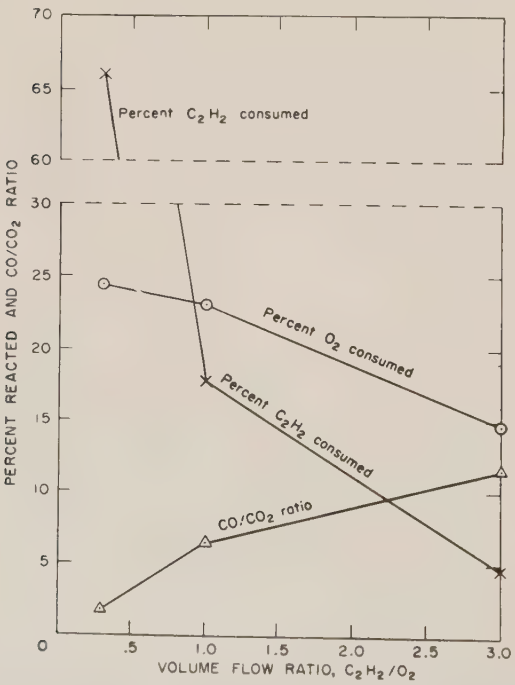

Fig. 3. Effect of flow ratio with O_2 flow = 2.4 cc/sec NTP, P = 1 mm Hg, acetylene-atomic oxygen flame.

Figure 3 illustrates the effect of increasing acetylene flow at constant pressure and constant O_2 flow rate upon the extent of the reaction and upon the CO/CO_2 ratio for the products of flames 1A, 1B, and 1C. For these three flames the oxygen atom concentration at the inlet should be the same; hence the changes in the product distribution are due solely to the change in acetylene flow.

Figure 4 shows the effect of increasing pressure at constant flow ratio. The points on the solid lines represent flames 2C, 1A, and 2D, in order of

increasing pressure. In this series there is the possibility of some change in the oxygen atom concentration since the streaming rate in the discharge changes with pressure in the bulb, but this effect is not expected to be large.

From Figures 3 and 4 it is evident that the CO/CO_2 ratio varies inversely with the extent of the reaction as expressed in terms of the percentages of reactants consumed, regardless of whether a variation of C_2H_2/O_2 flow ratio or pressure is responsible for the change. With the flames used for Figure 3, the change in CO/CO_2 is due chiefly to a decrease in the CO_2 formed at higher C_2H_2/O_2 flow ratios; in Figure 4 the change is due both to a decrease in CO and an increase in CO_2 produced in the reaction. Due to the complexity of the flames (with respect to the concentration gradients existing in the reaction zone, flow pattern, etc.) no attempt will be made here to interpret the trends in product distribution.

The data for 4A and 4B in Table 1 (compare with 1B and 2C) show only a slight influence of flow pattern upon the products and the percentages of reactants consumed.

Condensable products were collected from flames 1B and 1C. For these runs acetone was removed from the tank acetylene. In one hour, during which time about 0.75 mole of mixture 1B passed through the dry ice-cooled trap, 0.5 gm of condensate was obtained, corresponding to 2.2 weight per cent of the products or the original reactants. The amount of condensate from flame 1C was smaller for the same volume of gases pumped through the trap, due mainly to the absence of water as a product of this flame. A control run (condition 1B, discharge off) gave only an estimated 1 to 2 mg of condensate, representing less than a thousandth of that obtained from the reacting mixtures over a comparable running time.

The condensed material from both flames consisted of two fractions, one a liquid at room temperature and one a yellow waxy solid. The entire condensate sample was completely miscible with water. The liquid fractions were distilled in vacuum to sample bulbs for analysis and one sample of the solid was collected on glass wool after pumping off the volatile material and opening the trap. The solid sample and glass wool were placed in a sample bulb and evacuated to 1 micron, then closed off until analyzed. The analysis for the solid thus represents the decomposition products and contaminants of the solid, itself nonvolatile. The composition of the solid residue has not yet been determined. It was not a hydrocarbon polymer since it was water soluble; its water solution was acid and gave a strong starch-iodide test.

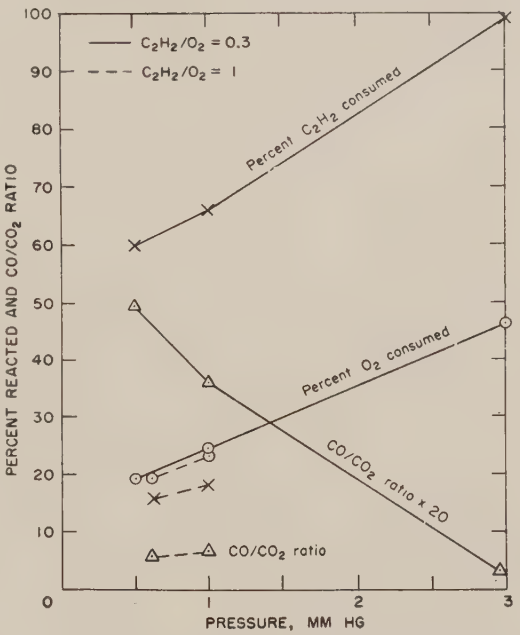

FIG. 4. Effect of pressure at constant flow ratio, O_2 flow = 2.4 cc/sec NTP, acetylene-atomic oxygen flame.

TABLE 3. MASS SPECTROMETRIC ANALYSES OF CONDENSATE SAMPLES, ACETYLENE-ATOMIC OXYGEN FLAMES*

Constituent	Liquid fraction, flame 1B	Liquid fraction, flame 1C	Solid fraction, flame 1C
Carbon monoxide	0.7	2.4	11.5
Carbon dioxide	8.6	17.9	9.5
Hydrogen	1.5	4.2	1.4
Water	78.2	0.0	33.5
Formaldehyde	0.0	2.8	1.2
Formic acid	0.5	0.0	25.5
Acetic acid	4.3	0.0	11.1
Methyl alcohol	3.4	0.0	5.2
Acetaldehyde	0.0	3.2	0.0
Methyl formate	0.0	61.9	0.0

* Products are expressed in mole per cent of the sample and are based on the partial pressures of the components of the liquid phase; the more volatile components are thus favored. The analysis of the solid fraction shows its decomposition products and contaminants.

The condensate analyses (mass spectrometer) are given in Table 3. Only products present in

amounts greater than 1 mole per cent are listed. In addition to these, small amounts of higher aldehydes and traces of allene and propylene were indicated by the mass patterns; the latter two may have been impurities in the acetylene used.

Table 4. Products of the Reaction of Acetylene with Dissociated Water Products.* Flame Pressure 0.2 mm Hg

Constituent	Control sample	Reaction products
C_2H_2	48.1	8.5
H_2O	51.1	3.9
Acetone	1.5	0.2
CO		19.0
CO_2		3.6
H_2		57.3
H_2CO		1.2
CH_4		0.8

* Components are given in mole per cent of the sample, based on the partial pressures of the components in the sample at a total pressure of 0.2 mm Hg.

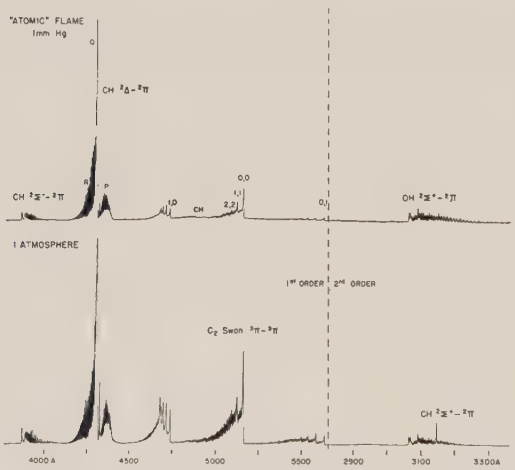

Fig. 5. Comparison of atomic flame and ordinary flame spectra. Atomic flame: $C_2H_2/O_2 = 1$, $P = 1$ mm Hg (flame 1B). Atmospheric pressure flame: $C_2H_2/O_2 = 0.4$. Rapid scans, 240 A/min in first order.

No evidence for the existence of hydrocarbon polymers was found in any of the samples.

Products of Atomic Hydrogen and Dissociated Water Flames

The appearance of these flames has been described above. The analysis of a gas sample from the hydrogen flame showed, as others have found[13], only the original starting materials, and only a minute amount (1–2 mg) of unidentified volatile condensate was recovered over a period in which 2 moles of mixture ($C_2H_2/H_2 = 1$) passed through the cold trap.

The analyses of the products of the water flame (probably supported mainly by OH radicals as initators) and of the unreacted control sample are shown in Table 4. The extent of reaction here, about 60 per cent of the original C_2H_2, is much greater than would be expected for an atomic oxygen flame under comparable conditions of flow and pressure, judging from the trends shown in Figure 4. Of some interest is the indicated efficiency of decomposition of the water vapor passing through the discharge; this may account in part for the relatively large percentage of acetylene consumed in the reaction.

For the dissociated water flame, the element balances calculated from the product sample analysis do not check at all well with those calculated from the reactant sample; the main difference would be accounted for by assuming loss of carbon, whereas the discrepancies with the atomic oxygen flame samples were due mainly to apparent loss of hydrogen. Apparent loss of carbon occurred also with the atomic hydrogen flame.

Spectra of Atomic Oxygen Flames

General Discussion

The visible and ultraviolet radiation from the acetylene-atomic oxygen flames gave the familiar spectrum of hydrocarbon flames due to OH, CH, C_2, and the emitter of the Vaidya hydrocarbon flame bands. A weak continuum also was present in all of these flames.

For the study of changes in relative intensities of bands due to the various species, a rapid scan of the spectrum (240 A per minute in the first order) from 2800 to 5600 A was made for each flame. An example is shown in Figure 5 together with a spectral recording from the inner cone of a flame at atmospheric pressure with a stoichiometric acetylene-oxygen mixture. Both spectra were taken with the same optical arrangement and monochromator slit width. It can be seen that in the atomic flame the $^2\Sigma^+ - {}^2\Pi$ band of CH (3143 A) is not present and that the intensity of the $^2\Sigma^- - {}^2\Pi$ band (3872 A) is reduced relative to that of the $^2\Delta - {}^2\Pi$ band (4315 A). In addition, the line-like structure at 4324 A is relatively low. The other major difference in the two spectra is in the intensity distribution within the

$^2\Sigma^+ - {}^2\Pi$ OH band (3064 A). In the atomic flame the higher K transitions can be seen beyond 3200 A; this is characteristic of a high rotational "temperature". These differences in the two spectra are not striking and cannot be attributed to the effect of pressure, since even at atmospheric pressure the radiation from a cooler acetylene flame would be similar to that from the atomic flame at 1 mm Hg. There is evidence of predissociation in both the CH and OH bands in the atomic oxygen flames. The CH predissociation is shown in Figure 5 by the abrupt breaking off of the rotational lines in the $^2\Sigma^- - {}^2\Pi$ CH band (3872 A).

For the measurement of apparent rotational and vibrational "temperatures", slow scans (12 A per min in the 1st order) with resolution of 0.2 A were made of selected regions of OH, CH, and C_2 bands for each flame. Examples are given in Figures 6, 7 and 8, again with comparison spectra of the atmospheric pressure flame. Figure 6 shows clearly, by the increased relative intensity of lines of the higher K transitions, that the OH rotational "temperature" is much greater in the atomic flames, whereas both CH (Fig. 7) and C_2 (Fig. 8) rotational "temperatures" are lower. In the atomic flame, CH shows a predissociation affecting only one set of levels; this is most easily seen by the absence of one pair of $R19$ lines in the 1,1 transition at 4207 A. The effect of pressure on the perturbation in the $R47$ line of C_2 (5049 A) is interesting but unexplained.

Since the portion of the flame focused on the spectrometer slit varied somewhat with flame size and position, it was necessary to examine the trend of relative intensities and "temperatures" from the center to the edge of the flame. Accordingly, spectra of flame regions 1 mm long were obtained at several positions including the center, halfway to the edge, and at the edge of the luminous zone of flame 1B. Toward the edge both the CH and C_2 intensities decreased relative to that of OH, the CH intensity dropping off more rapidly than that due to C_2, resulting in the green envelope shown in Figure 2. The variation of measured "temperatures" across the flame was small and within the uncertainty of the measurements.

Intensities (arbitrary units) and relative intensities of the different bands were measured as follows: OH intensity from the first line of the R_2 branch of the 0,0 band; CH intensity from the Q heads of the 0,0 bands; and C_2 intensity from the 0,0 band head. Since we were unable to ob-

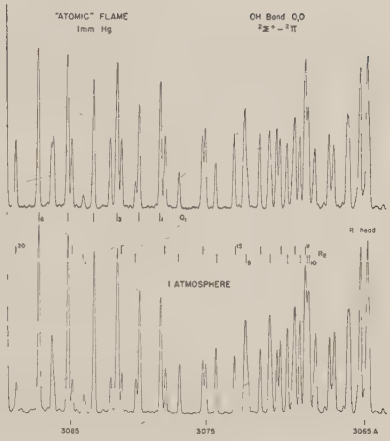

FIG. 6. O,O band of OH. Same flame as in Fig. 5. Slow scans 6A/min in second order.

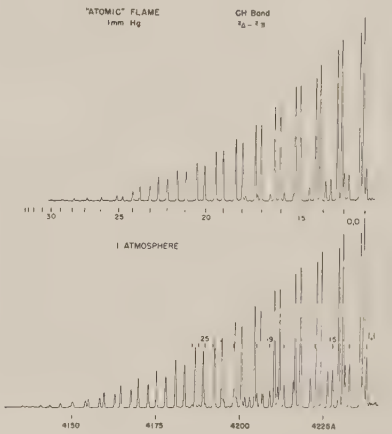

FIG. 7. $^2\Delta - {}^2\Pi$ band of CH. Same flames as in Fig. 5. Slow scans, 12A/min in first order.

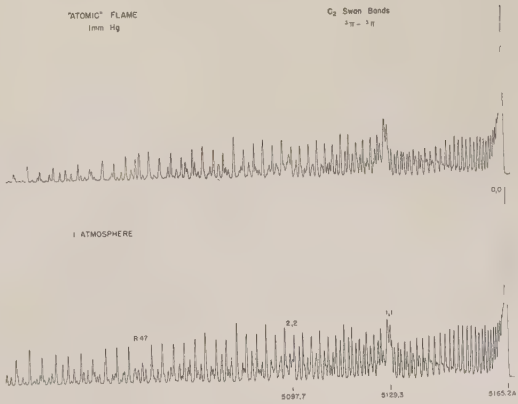

FIG. 8. C_2 Swan bands. Same flames as in Fig. 5. 12A/min.

tain the integrated intensities over the whole flame, the measurements are of doubtful quantitative significance but are of interest qualitatively.

At constant pressure, increasing the C_2H_2/O_2 flow ratio caused the OH, CH, and C_2 intensities to increase at fixed pressures of 1 mm Hg and below; at 3 mm Hg however, the OH and CH intensities did not change when the flow ratio was increased from 0.25 to 1.0. The C_2 intensity did increase, although not as much as at the lower pressures. The C_2 intensity was the most sensitive to variations in flow ratio; even so, the greatest intensity increase observed was by a factor of only 2.5 with a change in C_2H_2/O_2 from 0.25 to 5.0 at 1 mm Hg (flames 1A and 1C). This represents about one fortieth the increase in C_2 intensity for a comparable change in flow ratio in a premixed atmospheric pressure flame[14]. The

Table 5. Apparent Temperatures (°K), Acetylene-Atomic Oxygen Flames

Pressure	OH		CH		C_2	
	Rotation	Vibration	Rotation	Vibration	Rotation	Log $I_{1,1}/I_{0,0}$
mm Hg						
0.5	12,000		2,600	2,350	3,000	1.96
1.0	12,000	>5,000	2,600	2,350	3,000	1.96
3.0	9,200		2,400	2,275	4,000	2.06

relative intensities C_2/CH and C_2/OH showed a change which was at most a twentieth of that for a flame at atmospheric pressure.

At constant flow ratio, the OH, CH, and C_2 intensities increased generally with pressure from 0.5 to 1.0 mm Hg. CH and C_2 appeared to reach a maximum and then to fall off between 1 and 2 mm Hg with $C_2H_2/O_2 = 1$, but OH increased steadily with pressure at this flow ratio. Again, variations in relative intensities were surprisingly small, the extreme variation observed being that of C_2/OH in going from flame 2D to 2E, which represents a large change in pressure, flow ratio, and streaming rates. With this change, C_2/OH increased only by a factor of 6.

As the discharge excitation power (atom concentration) was decreased (flame 3A) the OH and C_2 intensities fell off slightly, but the CH intensity dropped markedly. This effect was probably due to the fact that the flame contracts as the power input to the discharge is decreased so that in this case the edge of the flame was observed.

Rotational and Vibrational "Temperatures"

Rotational "temperatures" for OH, CH, and C_2 were determined in the usual way[15] from plots of $\log I/A\nu^4$ vs. E, where I is the measured intensity of a rotational line, A the transition probability, ν the frequency, and E the energy of the upper state of the transition. The R_2 branch of the 0,0 band of OH ($^2\Sigma^+ - {}^2\Pi$), the R_{cd} branch of the 0,0 band of CH ($^2\Delta - {}^2\Pi$), and the superimposed R lines of the 0,0 band of C_2($^3\Pi - {}^3\Pi$) were used for these intensity measurements. Most of the C_2 rotational "temperature" trends were estimated from the relative intensities of the $R19$ and $P47$ lines by comparison with previously determined temperatures measured as described above.

OH vibrational "temperatures" could be estimated from measured intensities of unblended lines in the 0,0 and 1,1 bands, using the calculated vibrational transition probabilities[16]; those for CH were estimated from the relative intensities of the $K' = 14$ lines in the 0,0 and 1,1 bands[8]; and changes in vibrational "temperatures" for C_2 were estimated from the relative intensities of the 0,0, 1,1, and 2,2 band heads.

The measured "temperatures", which are given only as measures of the abnormality of the rotational and vibrational intensity distribution, are shown in Table 5. The precision of such measurements is approximately 10 per cent. The OH vibrational "temperature" was estimated to be greater than 5000°K in all of the flames. The C_2 vibrational "temperature" trend is shown in terms of $\log I_{1,1}/I_{0,0}$.

There was no significant variation of apparent temperatures with flow ratio, O_2 streaming rate, inlet arrangement, discharge excitation power or position in the flame. Between 0.5 and 1.0 mm Hg the "temperatures" appear to be independent of pressure, but at 3 mm OH and CH "temperatures" have decreased and the C_2 "temperatures" have increased. The precision of the measurements for C_2 is poor, but the increase is real and the rotational "temperature" at 3 mm is at least 30 per cent greater than that at 1 mm Hg. Previous measurements at pressures above 3 mm confirm this trend.

The OH rotational "temperature" is the highest yet reported for a flame. The high "temperature", however, probably represents merely the continuation of the trend, previously observed with ordinary flames, toward a more abnormal rotational intensity distribution as flame pressure is reduced[1]; it probably should not be considered as

being due to reactions peculiar to atomic flames. The CH and C_2 "temperatures" listed are not much different from those that can be observed in ordinary flames at both low and high pressure[2, 3, 8, 14].

Reference to Figure 9, which illustrates a plot of log $I/A\nu^4$ vs. $E_{K'}$, over a rather wide range of $E_{K'}$, will clarify the meaning of the rotational "temperature" measured for OH. If OH were in thermal equilibrium, in respect to its rotational degrees of freedom, with the flame gases at the adiabatic flame temperature, the plot of log $I/A\nu^4$ vs. $E_{K'}$ would be a straight line with slope corresponding to this temperature. A departure from rotational equilibrium will appear as a departure of the points from a straight line; conversely, a departure from a straight line indicates, if self-absorption is absent, rotational non-equilibrium, or an abnormal rotational intensity distribution.

In Figure 9 there are two regions, one below 33,500 cm^{-1} and one between 36,000 and 39,000 cm^{-1}, where the curve approximates a straight line, and so to which "temperatures" may be assigned, 1900°K to one and 12,000°K to the other. It is reasonable to suppose that there are two intensity distributions in this band, one corresponding to a "temperature" comparable to an adiabatic flame temperature and one corresponding to an abnormally high temperature. (The form of the curve in this case is not affected by self-absorption, since the points obtained from the P_1 and R_2 branches fall on or near the same line.) The falling off of the curve above 38,000 cm^{-1} has been explained as a predissociation effect[6]. It should be emphasized that the manner in which this curve has been drawn accentuates the departure from a smooth curve and that the $E_{K'}$ interval used for the high "temperature" determinations is the usual energy interval used for such measurements.

The anomalous rotational intensity distribution is illustrated in Figure 10 in another way by the plot of intensity vs. K', the rotational quantum number of the upper state. Since lines near the first maximum are less overlapped in these branches, the Q_1 and Q_2 branches of the 0,0 band were used for this plot. Points from the other branches are consistent with these curves. The curve can be considered for purposes of discussion as representing the sum of two curves or two intensity distributions, one with a maximum near $K' = 9$ and the other with a maximum near $K' = 18$. If each were a thermal distribution the maximum at lower K' would correspond to a temperature of 4300°K and the other to a temperature of 17,000°K.

For comparison with Figure 10, a comparable plot of the intensity distribution of OH in an electric discharge through water vapor[17] is given in Figure 11. In the plot for the discharge at pressures between 0.025 and 3.2 mm Hg the peaks occur at $K' = 4$ and $K' = 17$, corresponding to temperatures of 800°K and 15,000°K. In this case the second maximum is more pronounced because of the wide separation in K'.

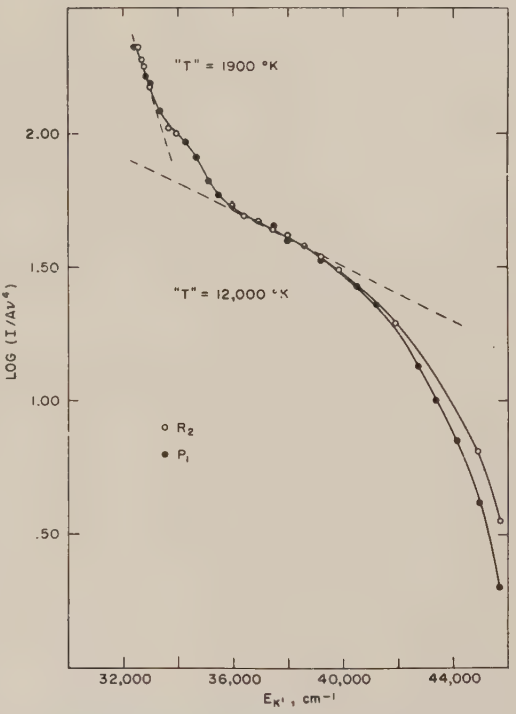

FIG. 9. Logarithmic plot of OH rotational intensity distribution in atomic oxygen flame 1B: $C_2H_2/O_2 - 1$, $P = 1$ mm Hg.

The similarity of the rotational intensity distributions in the flame and in the discharge indicates that the mechanisms responsible for the abnormal distribution may be similar to the two cases. It has been suggested previously that in the discharge the maximum at lower K' is due to thermal OH radiation[17]. In the atomic flame, the "temperature" indicated by the first peak is greater than the adiabatic flame temperature but this may be caused by the superposition of the two intensity distributions, tending to shift the peak to higher K'.

The origin of the maxima at higher K' is not known. It is tempting however, in view of the similarity of the curves in Figures 10 and 11, to regard the abnormal rotational excitation as the result of the same sort of process in both cases. Further work will be necessary to determine whether this supposition is correct.

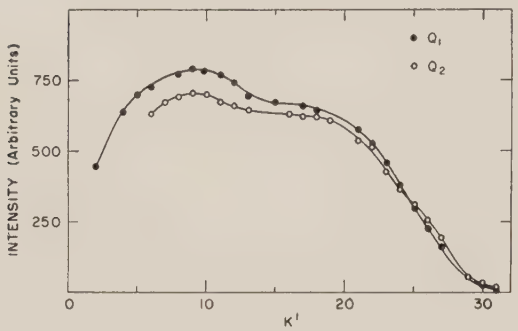

FIG. 10. Intensity distributions in the Q_1 and Q_2 branches in the O,O band ($^2\Sigma^+ - {}^2\Pi$) of OH in atomic oxygen flame 1B.

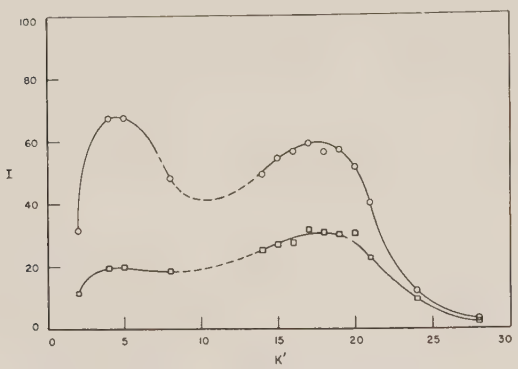

FIG. 11. Intensity distributions in the R_2 branch in the O,O band ($^2\Sigma^+ - {}^2\Pi$) of OH in an electrodeless discharge through water vapor. ○ $P \sim 1$ mm Hg; □ $P \sim 0.1$ mm Hg.

FLAMES WITH DISSOCIATED WATER AND WITH ATOMIC HYDROGEN

The spectrum of the radiation from the flame of acetylene with dissociated water showed, as previously observed[10], bands due to OH, CH, and C_2. It was not possible to obtain usable recordings of the OH spectrum due to reflections of light from the discharge in the water vapor inlet. The ratio of intensities CH/C_2 was 1.2, compared with 1.8 for flame 1B. The measured CH rotational "temperature" was 3000°K, somewhat higher than in the atomic oxygen flames; the vibrational "temperature" was also higher. The C_2 rotational "temperature" was comparatively low, approximately 2000°K, but the estimated vibrational "temperature" was comparable to those in the atomic oxygen flames.

The glow produced by streaming atomic hydrogen into acetylene was extremely faint and showed only the C_2 Swan bands (if CH radiation was present, its intensity was less than a hundredth of the C_2 intensity). The C_2 intensity was sufficient only for identification with the spectrometer used.

Since there is some doubt about the existence of luminous reactions of hydrocarbons with dry atomic hydrogen[10] the following observations may be of some interest. With the tank gases used and a dry system (evacuated overnight with a diffusion pump) we did not obtain the fairly intense flames which are sometimes reported, but did observe a very faint green glow which was reproducible from day to day in the sense that the maximum intensity always occurred at the same pressure and flow ratio. Immersion in liquid nitrogen of an efficient trap in the hydrogen inlet line produced no visible change in the glow, ruling out the presence of traces of water in the hydrogen being the cause, and the blank condensate runs described in the section on products above rule out an explanation in terms of traces of water in the acetylene. There remains the possibility that traces of oxygen are present in one or both of the gases; since no oxygenated products could be collected from the gases downstream from the luminous zone, the concentration of oxygen necessary to produce the glow would have to be exceedingly small, and a fairly elaborate experiment would be necessary to dismiss this possibility.

General Comments

There is no easily discernible relation between the spectra and products of the atomic oxygen flames. It is apparent that in these flames the reactions leading to the electronic excitation of radicals are not related in any simple way to those which determine the composition of the product samples. The relative intensities and "temperatures" vary surprisingly little with changes in flow ratio, atom concentration, streaming rates, and inlet arrangement, whereas the products and the quantity of reactants consumed do vary significantly.

It is well known that the relative intensities of the bands due to OH, CH, and C_2 in ordinary flames and explosions are quite sensitive to

changes in fuel concentration. Hence it would seem that in the flames with atomic oxygen the variation of mixture ratio in the luminous zone itself with a change in inlet flow ratio is small. Put another way, it seems likely that the luminous reaction is confined to a region of reactant concentrations which is roughly the same for all of the flames. Under the conditions of the experiments reported here, this region is probably determined largely by the distance through which oxygen atoms can diffuse before reacting.

From the spectroscopic evidence, however, it appears that the flames are atomic only in the sense that oxygen atoms are known to be the original chain initiators, and that the processes leading to the production of electronically excited species are not different from those occurring in ordinary flames. It is the opinion of the authors that all of the spectroscopic properties of these flames (with the exception of predissociation effects) could be reproduced in ordinary atmospheric pressure flames by selecting appropriate conditions (such as the degree of dilution with inert gases) and by viewing a selected part of the reaction zone.

The products of the atomic oxygen flame are not typical of ordinary flame products. In the first place, the fact that the mixture ratio changes from one part of the luminous zone to another means that no simple comparison of the product distributions for these flames with those for ordinary premixed flames can be made (e.g., CO might be formed throughout the flame whereas CO_2 might be produced in the lean zone, and there is a lean zone in all atomic oxygen flames regardless of the flow ratio). One must also take into account the fact that much of the acetylene may bypass the luminous zone in passing through the reaction bulb, and that some molecular oxygen goes through unchanged. These gases will be heated and can be expected to undergo reactions typical of slow combustion, giving products not ordinarily found in gases from premixed flames. Finally, longer-lived radicals produced in the luminous zone may diffuse out of the zone or be carried in the gas stream into the pumping line where they can undergo low temperature reactions to give products such as were detected in the condensates discussed above.

In the light of information obtained in this study, the reactions which occur in the luminous zone itself, excepting the primary initiation step, can be considered the same as those occurring in the reaction zone of ordinary acetylene-oxygen flames. The unlikely products detected can be explained reasonably as originating in a zone of low temperature reaction surrounding or downstream from the flame. Thus the atomic oxygen flame provides a source to supplement the low pressure flame for the study of the origins of nonthermal excitation. Results obtained with flames supported by atomic oxygen should be applicable to the problem of understanding nonthermal excitation in hydrocarbon flames generally.

Acknowledgment

The authors wish to thank Dr. F. L. Mohler, Dr. V. H. Dibeler, and Miss Edith Quinn of the Mass Spectrometry Section of the National Bureau of Standards for the mass spectrometric analyses and for their help with some of the problems which arose because of the complex nature of the mixtures analyzed.

REFERENCES

1. Gaydon, A. G., and Wolfhard, H. G.: Proc Roy. Soc., *A194*, 169 (1948).
2. Gaydon, A. G., and Wolfhard, H. G.: Proc Roy. Soc., *A199*, 89 (1949).
3. Gaydon, A. G., and Wolfhard, H. G.: Proc. Roy. Soc., *A201*, 561 (1950).
4. Gaydon, A. G., and Wolfhard, H. G.: Proc. Roy. Soc., *A201*, 570 (1950).
5. Gaydon, A. G., and Wolfhard, H. G.: Proc. Roy. Soc., *A205*, 199 (1951).
6. Gaydon, A. G., and Wolfhard, H. G.: Proc. Roy. Soc., *A208*, 63 (1951).
7. Shuler, K. E., and Broida, H. P.: J. Chem. Phys. *20*, 1383 (1952).
8. Broida, H. P.: J. Chem. Phys., *21*, 340 (1953).
9. Kane, W. R., and Broida, H. P.: J. Chem. Phys., *21*, 347 (1953).
10. Gaydon, A. G., and Wolfhard, H. G.: Proc. Roy. Soc., *A213*, 366 (1952).
11. Broida, H. P., and Gaydon, A. G.: Proc. Roy. Soc., *A218*, 60 (1953).
12. Fastie, W.: J. Opt. Soc. Am., *42*, 641 (1952).
13. LeRoy, D. J., and Steacie, E. W. R.: J. Chem. Phys., *12*, 369 (1944).
14. Broida, H. P.: Unpublished data.
15. Herzberg, G.: *Molecular Spectra and Molecular Structure*. I, pp. 122–127, 203–207. New York, D. Van Nostrand Company, Inc., 1950.
16. Shuler, K. E.: J. Chem. Phys., *18*, 1221 (1950).
17. Broida, H. P., and Kane, W. R.: Phys. Rev., *89*, 1053 (1953).

87

INFRARED EMISSION FROM COOL FLAMES

STABILIZED COOL FLAMES; ENGINE COOL FLAME REACTIONS; GAS TEMPERATURES DEDUCED FROM INFRARED EMISSION

By W. G. AGNEW, J. T. AGNEW, AND K. WARK, JR.

Introduction

Low temperature reaction systems have been observed for a great variety of fuels with air. In numerous cases these reactions are accompanied by a visible blue light emission, and in these instances the reactions are termed cool flames. The visible emission spectrum of cool flames was first reported by Emeleus[1] in 1926. The spectrum, consisting of a series of diffuse bands between 3000 and 5000 Å, was the same for a number of different fuels, and in 1935 and 1936 the emitter of Emeleus's band spectrum was identified by Fowler and Pearse (see Ubbelohde)[2] and Kondratjew[3] as excited formaldehyde.

The actual structure of Emeleus's cool flames, formed with diethyl ether, acetaldehyde, propaldehyde, and hexane with air, was not clearly described, but his apparatus included an electrically heated silica reaction tube through which the fuel-air mixture flowed continuously. The flame formed in the heated portion of the tube, and the spectroscope viewed the flame through a quartz window in the direction of gas flow.

Topps and Townend[4] in 1946 arranged a tapered glass reaction tube with ether- and acetaldehyde-oxygen mixtures entering at the small end. Under the proper conditions, a cool flame formed in the tube and moved upstream to a point where stability was reached with the rate of propagation of the cool flame just equal to the gas velocity. Under other conditions in this apparatus two-stage flames were formed. The first stage appeared identical with the cool flames observed previously, but downstream from this flame a second luminous flame, somewhat hotter, and more diffuse than the first stage appeared. The second-stage flame exhibited the same excited formaldehyde spectrum as the first stage but was more intense, particularly at the longer wavelengths. If the term cool flame is considered to define a flame of relatively low temperature (relative to normal flame temperatures of 3000 or 4000°F) exhibiting a spectrum of excited formaldehyde, then both stages in the two-stage flame could be considered as cool flames. Topps and Townend[4], however, preferred to label the second-stage as a blue flame. In any case, the second-stage flame could hardly be associated with a normal flame.

Mullins[5] in 1948 reported further cool flame spectra obtained when liquid kerosene containing 5 per cent ethyl nitrate was injected into a stream of hot combustion products. The spectrum again showed only the emission bands of excited formaldehyde.

These cool flame experiments are of considerable interest to researchers studying fuel-engine relationships at the General Motors Research Laboratories, since it has been demonstrated that reactions of a very similar nature occur in the unburned mixture ahead of the normal flame front in engine cylinders, and it seems probable that these reactions are associated in some way with engine knock. This general type of reaction may also occur adjacent to the cool walls of the engine combustion chamber where quenching causes incomplete combustion. Mass spectrometer studies of the product gases from burner flames conducted at the General Motors Research Laboratories have demonstrated that unburned hydrocarbons do result from wall-quenching. Since the presence of unburned hydrocarbons in automotive exhaust gases has been mentioned as a possible contributor to smog, it is possible that a clearer understanding of low temperature reaction mechanisms may provide valuable information in the very difficult smog problem.

The presence of preflame reactions in engine cylinders has been confirmed by numerous investigators who have detected pressure development resulting from preflame energy release in motored and late-fired engines and radiation emitted from the preflame reactions in motored, late-fired, and normally-fired[6] engines. The energy release data indicate that these reactions are certainly of low order, and since Levedahl and Broida[7] and Downs, Street, and Wheeler[8] have both reported that the emission spectrum of the preflame reactions is that of excited formaldehyde, the preflame reactions would seem to deserve the name cool flame by the definition given above. Levedahl and Broida's experiments with *n*-heptane and Downs, Street, and Wheeler's ex-

periments with diethyl ether were both conducted with motored engines. Withrow and Rassweiler[9] as early as 1933 detected formaldehyde by absorption in the unburned mixture in an engine fired with gasoline and air.

Downs, Street, and Wheeler[8] also show some evidence for the identification of CO in their preflame reaction spectra, but the evidence does not appear conclusive.

All of the work described above has been concerned with the visible and ultraviolet portions of the spectrum, and except for proving the existence of cool flames, there appears to be little further information to be gained from spectral studies in this range. In fact, there is considerable evidence to indicate that the visible luminosity of cool flames represents only a very small part of the complete cool flame reaction story. Reaction is known to occur both before and after the visible luminosity, and different fuels are known to undergo somewhat different reactions, even although all produce the same visible spectrum.

It was believed that considerable additional information about the cool flame reaction story might be obtained by spectroscopic studies in the infrared region, since many of the intermediate and final products of cool flame reactions were expected to show infrared spectra, and temperatures in cool flames were expected to be high enough to cause these compounds to radiate thermally. Therefore, a program was initiated to record the infrared emission spectra of cool flames stabilized in a burner and produced in an engine cylinder. The three specific goals in this work were: (1) The identification of emitters in the cool flame reactions as well as in the dark reactions occurring before and after the cool flame reactions, and the tracing of the distribution of these emitters through the flame; (2) The correlation of cool flames produced in a burner with those produced in an engine cylinder; (3) The development of a method of measuring temperatures in the cool flame regime by infrared radiation means.

Work along these general lines utilizing both emission and absorption measurements is continuing, and the results presented here are of only a preliminary nature.

Stabilized Cool Flames

EQUIPMENT AND PROCEDURE

A convenient method for stabilizing cool and two-stage flames of hydrocarbons for spectroscopic study is provided by the so-called flat-flame burner developed by Powling[10] and by Egerton and Thabet[11]. A sketch of the upper half of such a burner is shown in Figure 1. A fuel-air mixture is caused to flow with almost uniform velocity distribution from an inner burner tube. An outer glass tube supports a stabilizing screen. When the mixture is artificially ignited and the fuel-air ratio made quite rich (in the case of diethyl ether at atmospheric pressure and approximately 20°C) two distinct flame fronts can be established in the positions labeled 1–1 and 3–3 in Figure 1. For these experiments the outer glass tube was a composite structure with a square cross-section. Sodium chloride windows

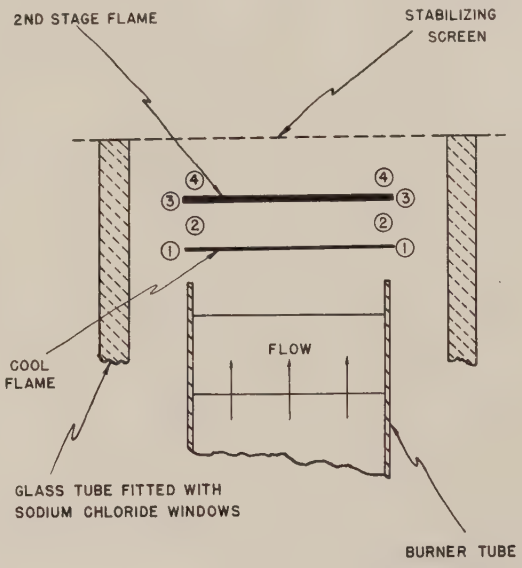

FIG. 1. Diagrammatic sketch of two-stage flat flame.

were fixed at two ends of this assembly. One window allowed the transmission of long wavelength infrared radiation to the monochromator, and the other window, which was also in the line of sight of the monochromator, was installed simply to reduce background radiation.

Figure 2 shows the arrangement of the apparatus used to obtain the infrared emission spectra shown in Figures 3 to 7 inclusive. The burner and a pair of flat mirrors were positioned relative to a spherical mirror and a Model 99 Perkin-Elmer double-pass monochromator with a sodium chloride prism and thermocouple detector. An image of the flame zone was focused on the entrance slit of the monochromator with the two flat mirrors serving as an image rotator so that the horizontal flame appeared verticle on the entrance slit. Normally, the separation between the two flame

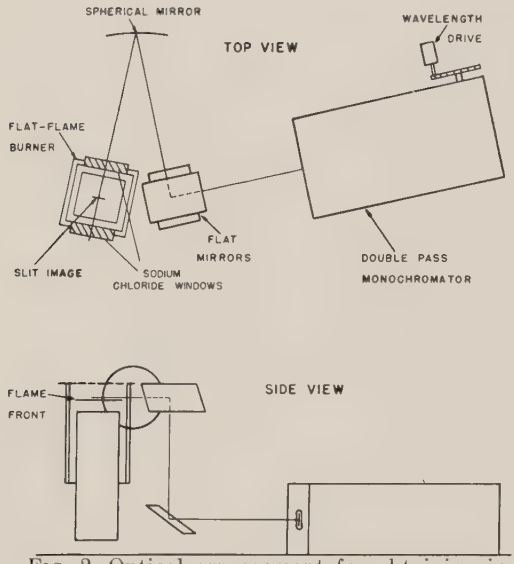

FIG. 2. Optical arrangement for obtaining infrared spectra of stabilized cool flames.

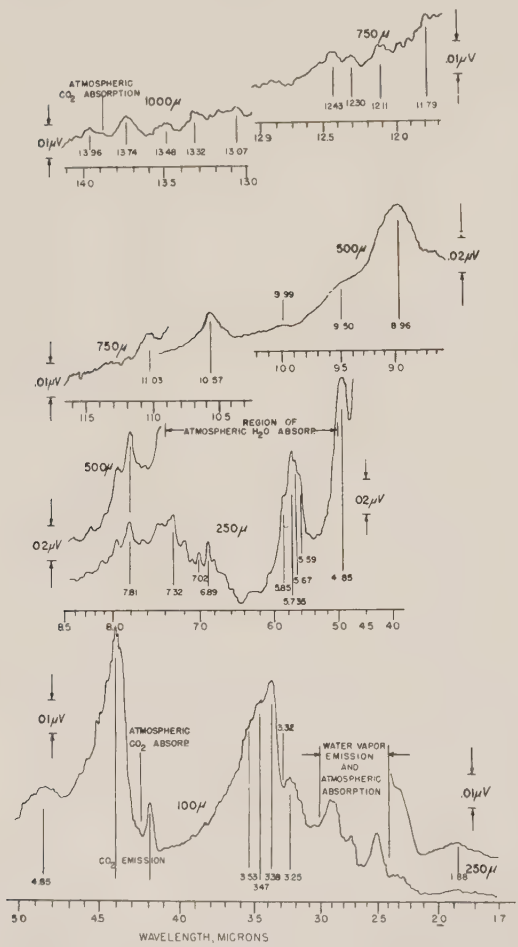

FIG. 3. Composite diagram of infrared emission spectrum of a cool flame from 3.0 to 14.0 microns.

fronts shown in Figure 1 was of the order of ¼ inch, and there was a magnification of the flame zone as it appeared on the entrance slit by a factor of approximately two. Thus there was no difficulty in obtaining satisfactory space resolution of the flame zone.

The results shown in this paper are for four different positions in the flame zone as indicated in Figure 1. All of the spectra are for rich mixtures of diethyl ether and air, with an equivalence ratio of approximately 3.0. Position 1–1 is designated as "in the cool flame". Visible spectra for this flame have not yet been recorded, but the pale blue color is believed to be due to formaldehyde fluorescence, and the flame is thought to be a true cool flame. This flame was a very pale blue, sometimes almost greyish in appearance, and the visible reaction zone was quite thin. The flame in position 3–3 will be referred to as the second-stage flame. This flame was a much brighter blue than the cool flame, and the visible reaction zone appeared to be somewhat thicker. The second-stage flame appeared to be much like that observed by Topps and Townend[4], but until it is definitely established that the blue color of the second-stage flame is due entirely to formaldehyde emission, it will not be called a cool flame. The two remaining positions in the flame zone which were investigated were position 2–2, between the cool flame and second-stage flame, and position 4–4, above the second-stage flame.

RESULTS AND DISCUSSION

It will be of interest to compare the spectra shown in Figures 3 and 4 with infrared emission spectra of normal hot flames produced in a bunsen burner. Such spectra have been determined by Plyler[15] out to wavelengths as long as 24μ. The chief difference between Plyler's spectra and those reported here is the fact that Plyler found no emission bands which were not attributable to either H_2O or CO_2. The emission spectra given here contain many bands which are believed to be due to neither H_2O nor CO_2, but to certain of the intermediate products formed in the cool flame (first stage) and second-stage flame. Figures 3 and 4 are composite diagrams of the infrared emission spectra of radiation from the cool and second-stage flames respectively. In both of these figures, as well as in Figures 5, 6, and 7, the slit width and the electronic amplification used in various regions of the spectrum are indicated. The slit width is given in μ, and the electronic amplification is indicated by the inter-

val corresponding to a certain microvolt output from the thermocouple.

Beginning at the short wavelength region of the spectrum, the first band detected was at 1.88 μ in the second-stage flame (Fig. 4). As is discussed later, this band was also detected in the radiation from compressed air in a motored engine

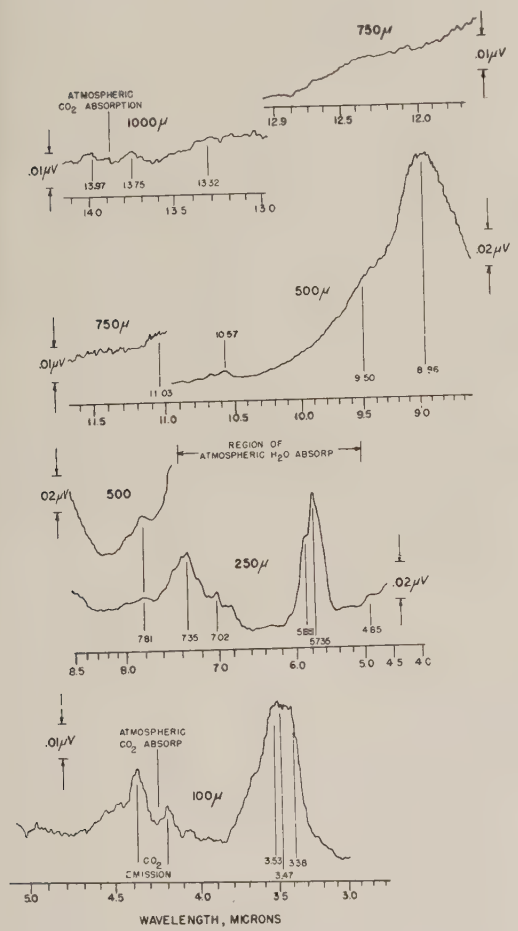

FIG. 4. Composite diagram of infrared emission spectrum of a second-stage flame from 1.7 to 14.0 microns.

as well as in the engine cool flame emission. The 1.88 μ band is probably due to H_2O emission.

The next band of interest is not specifically labelled in Figure 4, but it will be noticed that a small maximum is indicated at approximately 2.32 μ. This is just the wavelength at which radiation was observed from engine cool flames. No identification of the emitter of this radiation has yet been made.

In the second-stage flame (Fig. 4) strong emission of radiation was in evidence in the range 2.5–2.9 μ. It will be seen later from the motored engine experiments that both H_2O and CO_2 contribute radiation in this spectral range. In Figure 4, strong attenuation due to atmospheric absorption is also evident. The water vapor emission was not observable in the burner cool flame spectra.

FIG. 5. Infrared emission spectra from 3.2 to 3.8 microns for four positions in the flame.

Radiation in the spectral range 3.2–3.8 μ was very strong in all four flame positions investigated and has been studied as a function of these flame positions as shown in Figure 5. In the cool flame spectra the maximum intensity in this region appears to be at 3.53 μ with no pronounced secondary maxima. At position 2, between the two flames, the maximum shifted to 3.47 μ, still with no indication of secondary maxima. In the second-stage flame (position 3) marked changes occurred. A weak additional band appeared at

3.25 μ, and also a band began to appear at 3.38 μ. Above the second-stage flame the 3.38 band is quite pronounced, as is the 3.25 band. The shifting of the maxima in this spectral range could be

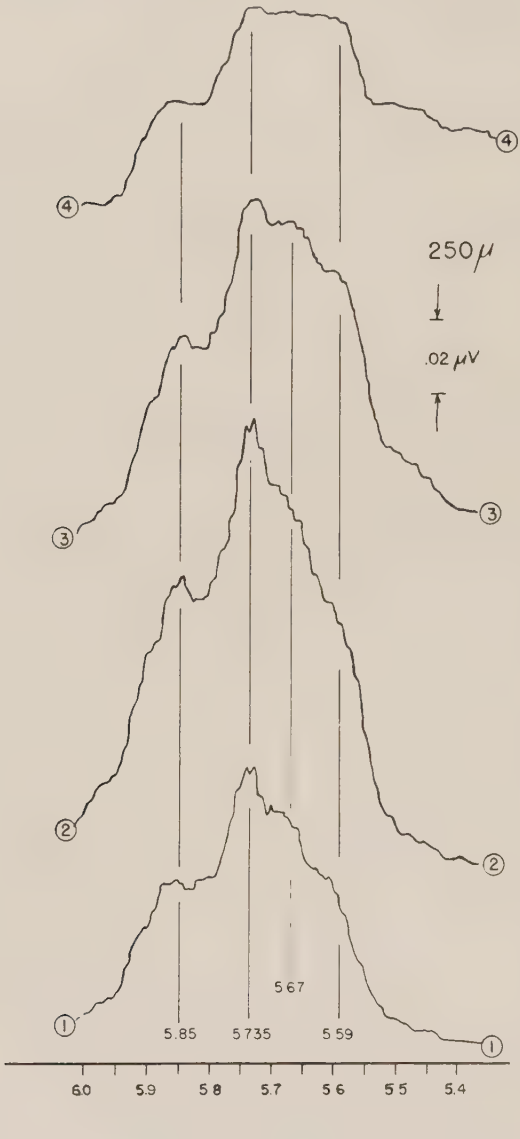

FIG. 6. Infrared emission spectra from 5.4 to 6.0 microns for four positions in the flame.

due either to a variation in concentration of certain molecular species, to a temperature effect, or to a combination of both. It may also be mentioned that the two bands at 3.38 and 3.25 μ have a shape such that actually only one band may be present, with strong re-absorption at 3.32 μ. The strong emission at 3.47 μ just above the cool flame may be due to formaldehyde. Herzberg[12] lists very strong formaldehyde bands (in absorption) at 3.48 and 5.74 μ. Strong emission at both of these wavelengths has been observed, as can be seen in Figures 3, 4, 5, and 6.

The next region of strong emission is the CO_2 region in the vicinity of 4.2–4.7 μ. It can be seen that the CO_2 radiation is much stronger in the second-stage flame than in the cool flame, an effect which could again be the result either of the increased temperature or an increased CO_2 concentration in the second stage.

Adjacent to the CO_2 region is a rather weak band at 4.85 μ. This band is very weak in the cool flame, but of appreciable intensity in the second-stage flame. Carbon monoxide is known to have a strong absorption band at 4.61 μ, which could possibly appear at 4.85 μ in emission. Later, however, it will be mentioned that one of the longer wavelength bands provides a strong indication of the presence of ethylene, which also has a weak absorption band at 4.89 μ. Also, methyl alcohol, a likely intermediate product, has an absorption band at 4.87 μ. Therefore, one or both of these compounds might be responsible for the 4.85 μ radiation observed.

The third region of strong emission is the 5.4–6.0 μ region. The change in the structure of the emission bands in this range as a function of flame position is shown in more detail in Figure 6. The predominant change is the increase in the relative intensity of radiation at 5.59 μ as the second-stage is traversed. A prominent feature of this spectral region is the band at 5.735 μ. This has been tentatively identified as C=O emission from formaldehyde. The identity of an emitter at 5.59 μ has not yet been established. Again, the shift in the bands in this region may be in part a temperature effect.

Proceeding to longer wavelengths, the next region of interest is the wavelength range 6.5 to 8.5 μ. In the cool flame spectrum (Fig. 3) a very prominent band at 7.35 μ is in evidence, and weak bands were observed at 7.02 and 7.81 μ. In the spectrum of the second-stage flame (Fig. 4) a sharp band at 6.89 μ appeared; the band at 7.02 remained; the 7.35 maximum shifted to 7.32 with relatively strong radiation also at 7.47 μ; the band at 7.81 remained, and a sharp band appeared at 7.95 μ. In the second-stage flame, the 6.89 and 7.81 radiation was stronger, relative to the 7.35 radiation, than in the cool flame. Formaldehyde

is known to have a strong absorption band at 7.82 μ. No assignments have been made for emitters at the other wavelengths noticed in this region.

The next spectral range studied in some detail overlapped the region just discussed to some extent, extending from 7.4 to 11.0 μ. Figure 7 shows emission spectra in this range for the four different positions in the flame zone. The principal features of these emission spectra are: The 7.81 band, which grew progressively stronger as the second-stage was approached; a very strong band at 8.96 μ; a weak band at 9.50 μ; and finally, a rather sharp band detected at 10.57 μ. It was interesting to note that the 8.96 μ band appeared relatively the strongest in position 2–2 (between the cool and second-stage flames) while the 10.57 μ band was relatively the strongest in the second-stage flame (position 3–3). A tentative assignment of ethylene has been given to the 10.57 μ band. This assignment is supported by the following facts. Ethylene has strong absorption bands at 3.22 and 3.34 μ, wavelengths which are near the values of 3.25 and 3.38 μ where other bands were also observed to appear in the second-stage flame. In addition, ethylene has strong bands at 4.89 and 6.93 μ in absorption, wavelengths which again are near values (4.85 and 6.89–7.02) at which bands were observed in emission from the second-stage flame. Finally, ethylene has a medium band in absorption at 10.05 μ, a value not too far removed from that for a weak band observed in emission in the second-stage flame (9.99 μ).

The 8.96 μ band persisted even at a considerable distance below the cool flame. This would indicate strongly that it may be due simply to the C—O bond of the preheated fuel, diethyl ether. Since the mixture is rich, the hot fuel possibly could persist even up into the second-stage flame. Alternatively, intermediate products such as formic acid could be formed, which also contain a C—O bond.

Beyond 11.0 μ many weak bands were observed, particularly in the second-stage flame. These bands have been assigned wavelengths of 11.03, 11.79, 12.11, 12.30, 12.43, 13.07, 13.32, 13.48, 13.74, and 13.96 μ. In the cool flame only a few bands could be observed with sufficient regularity to be given assignments of 11.03, 13.32, 13.75, and 13.97 μ. No emitters have been assigned to any of these bands with the possible exception of the 13.74 μ band, which could conceivably be acetylene. Also the region near 13.88 μ may be affected by atmospheric CO_2 absorption.

Much work remains to be done in order to identify the emitters responsible for all the emission bands observed in the burner flames and to trace the concentration of these emitters through the flames. It is believed, however, that improvements in experimental techniques, e.g., an increase in flame depth and the use of combined emission and absorption measurements, will allow more exact information to be obtained concerning the identity and concentration of inter-

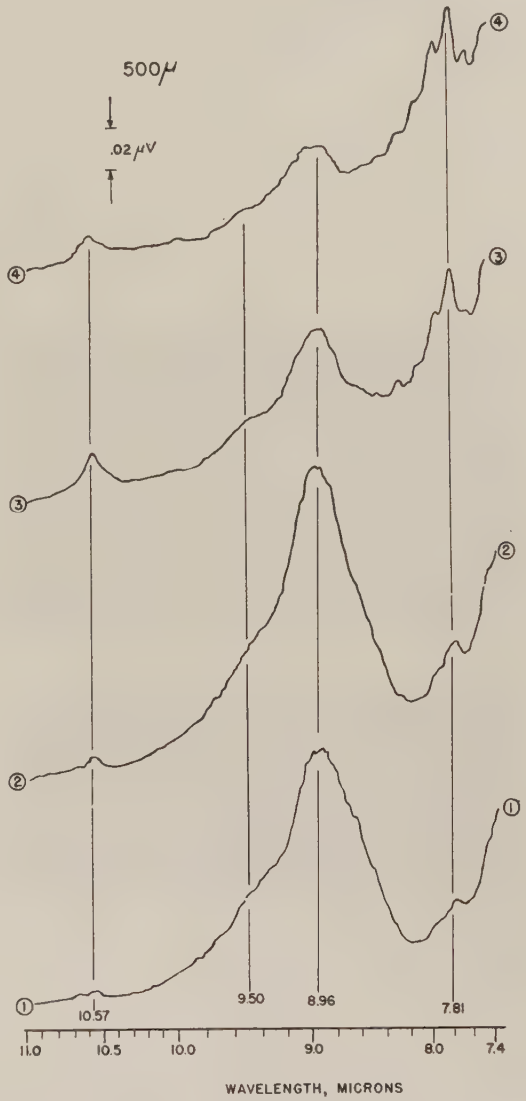

FIG. 7. Infrared emission spectra from 7.4 to 11.0 microns for four positions in the flame.

mediate products formed in the low-temperature reactions which precede normal hot flames in the oxidation of hydrocarbons.

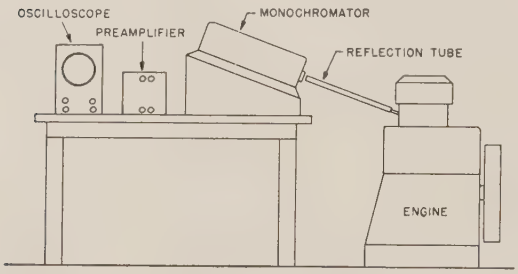

FIG. 8. Arrangement of engine and monochromator.

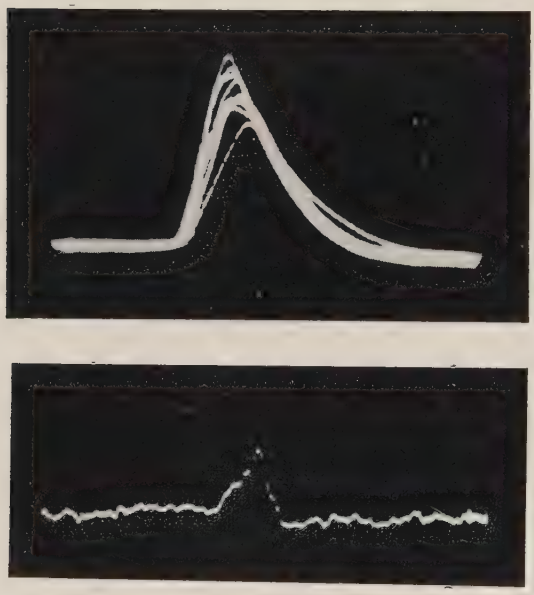

FIG. 9. Typical oscilloscope traces of engine radiation intensity. Above, normal flames; below, cool flame.

Engine Cool Flames

EQUIPMENT AND PROCEDURE

Engine studies were conducted with a single-cylinder research engine of overhead valve design with a compression ratio of 7.5. Airflow to the engine was metered with a closed air-metering system employing critical flow nozzles, and fuel was supplied through a standard automotive carburetor. Fuel-air ratio was determined by exhaust gas analysis and controlled with a needle valve.

The Perkin-Elmer Model 99 Monochromator was again used, but in this case the detector was a lead-sulfide cell and the monochromator was operated as a single-pass instrument without the radiation chopper. The output of the lead-sulfide cell was displayed on an oscilloscope. In most of the work an A.C. preamplifier was used between the lead-sulfide cell and the oscilloscope amplifier. In addition, the signal-to-noise ratio of the detection system was increased by cooling the lead-sulfide cell with a dry ice and acetone bath. Atmospheric absorption in the monochromator was reduced by sealing a desiccant and a CO_2 absorbent in the instrument.

An opening in one side of the engine combustion chamber was provided with a calcium fluoride window $\frac{3}{8}$ inch in diameter, which provided a view of the central portion of the combustion chamber. The window opening was at an angle of 22 degrees with the horizontal, and the monochromator was arranged with respect to the engine as shown in Figure 8. A piece of hard copper tubing, $\frac{7}{16}$ in inside diameter and 13 in long with its interior polished, was placed between the engine window and the monochromator in order to reflect the largest possible amount of radiation into the monochromator entrance slit.

Figure 9 illustrates the type of oscilloscope traces obtained at one particular wavelength setting for an engine normally-fired with 95 octane number fuel and motored with a 70 octane number fuel. In each trace the output of the lead-sulfide cell (radiation intensity) is plotted vertically as a function of time on the horizontal axis. The exposure time for the normal flame traces was one second, and traces of eight engine cycles are superimposed in the photograph to illustrate the cyclic variations. The $\frac{1}{10}$ sec exposure of the cool flame allowed only one cycle to appear. The cool flame trace was recorded with a motored engine, and there was a tendency for two peaks to appear in the radiation intensity under these conditions. One peak (or inflection) appeared at the top center piston position (marker pip in Figure 9) and the other larger peak slightly afterwards. It was later shown that the first peak was associated primarily with radiation from the compressed air in the unreacted mixture, and the second peak was related to the cool flame reaction.

In recording spectra, the engine conditions were first set and allowed to stabilize. Monochromator slit width and amplifier gain settings were made as required, and the height of the signal on the oscilloscope screen (peak deflection) was measured for a series of wavelength settings

on the monochromator. Cyclic variations were averaged by eye, and no account was taken of possible shifts in the time in the cycle at which maximum radiation appeared. However, there was no readily apparent change in the time of occurrence of peak radiation at different wavelengths.

RESULTS AND DISCUSSION

As an aid in the identification of emitters, the engine studies included several reference spectra in addition to the cool flame spectra. These reference spectra included results obtained from normal flames of a fired engine and air compressed in the motored engine with and without H_2O and CO_2 additions. These spectra will be described before presenting the engine cool flame spectra.

Normal flame spectrum

Figure 10 shows the spectrum of a normal flame recorded under the following set of engine conditions:

Engine speed	1000 rpm
Air flow	full throttle
Intake air pressure	atmospheric induction
Fuel-air ratio by weight	0.077 (maximum power)
Spark advance	10° BTC
Inlet mixture temperature	300°F
Coolant temperature	168°F
Fuel	95 per cent iso-octane 5 per cent *n*-heptane

The original data are presented in a number of curves recorded with different amplifier gains and slit widths in order to bring out as far as possible all features of the spectrum. Beside each curve there is given a term indicating the monochromator slit width and oscilloscope gain settings. The first number in this term indicates the monochromator slit width in microns, the second figure the oscilloscope Y-attenuator setting (1000, 100, 10, 1), and the third figure the Y-amplifier gain. Conversion of all the data to a common gain and slit width is not practical because the gain settings are not accurately reproducible, and changes in slit width alter the resolution as well as the aperture of the light path.

It should be pointed out that in this work no distinction has been made between the normal flame front and the hot products of the normal flame. The condition studied was actually that producing maximum cylinder gas radiation.

Figure 10 shows five distinct emission bands in the lead-sulfide 1.0 to 3.0 μ range and two indications of unresolved peaks. The wavelengths of these observed bands and inflections are compared in Table 1 with absorption band data given by Herzberg[12] and a summary of emission data[13, 14, 15] for bunsen flames. The data from different sources appear to be in general agreement and permit the conclusion that nearly all the emission from engine normal flames in the 1.0 to 3.0 μ region results from H_2O and CO_2 formed as products of combustion.

The intense band with a peak at 2.61 μ resulted from overlapping H_2O and CO_2 radiation. Improved resolution in later work actually showed that radiation in the region from 2.4 to 2.67 μ was

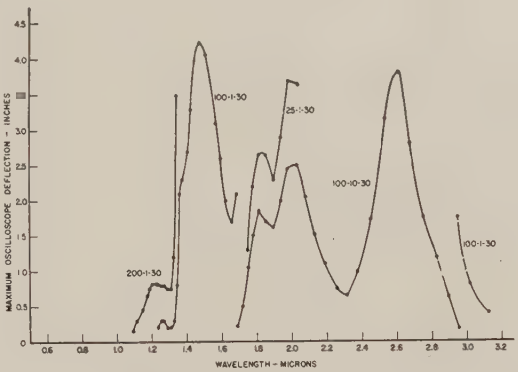

FIG. 10. Emission spectrum of a normal engine flame.

primarily due to H_2O emission, and the radiation at 2.69, 2.73, and 2.78 μ resulted from CO_2, H_2O, and CO_2 respectively. The only indication of this structure in Figure 10 is the small inflection near 2.8 μ. The 1.24 and 2.02 μ CO_2 bands and the 1.48 and 1.83 μ H_2O bands are in fairly good agreement with the absorption band data. The inflection in the side of the 1.48 μ H_2O band at about 1.35 μ (which was completely resolved in later work) also resulted from H_2O emission.

Compressed air spectrum

Figures 11 and 12 show the spectra obtained when air (without fuel) was passed through the motored single-cylinder engine with and without H_2O and CO_2 additions under the following conditions:

Engine speed	1000 rpm
Air flow (full throttle)	0.61 pound per min
Intake air pressure (no additive)	29.26 in Hg
Intake air temperature	300°F
Coolant temperature	115°F

The H_2O was added (Figures 12a and 12b) by introducing steam in the intake air stream from the building steam lines, and CO_2 was supplied from a compressed-gas cylinder. In each case the gas was added in a concentration of about 10 per cent by volume.

added to the air, and even then with only a very low intensity.

Cool flame spectrum

Figures 13 and 14 show the spectra obtained from engine cool flames with and without H_2O

TABLE 1. IDENTIFICATION OF EMITTERS IN ENGINE SPECTRA (WAVELENGTHS OF RADIATION PEAKS IN μ)

Molecule	Absorption bands, Herzberg[12]		Bunsen burner emission[13, 14, 15] wavelength	Engine normal flame emission wavelength	Engine compressed air emission wavelength	Engine cool flame emission wavelength
	Wavelength	Intensity 0–10 scale				
CO_2	2.77	7	2.72–2.88	2.83	2.82	2.82
CO_2	2.69	7	2.69			
CO_2	2.055	5				
CO_2	2.003	5	1.95–1.99	2.02	2.00	2.00
CO_2	1.959	5				
CO_2	1.643	2				
CO_2	1.604	2				
CO_2	1.573	2		1.35–1.65		1.5–1.6
CO_2	1.535	2				
CO_2	1.432	2				
CO_2	1.221	1		1.24		
CO_2	1.208	1				
H_2O	3.17	5				
H_2O	2.738	7	2.72–2.88	2.83	2.82	2.82
H_2O	2.662	10	2.49–2.65	2.61	2.67	2.63
H_2O	1.875	5	1.79–1.87	1.83	1.88	1.87
H_2O	1.453	2	1.40–1.46	1.48	1.45*	1.45
H_2O	1.379	5	1.30–1.40	1.39		
H_2O	1.135	7				
H_2O	0.942	7	0.94			
?						2.3–2.37
?						2.92

* H_2O added.

From the wavelength comparisons in Table 1 and the effects of the additives it is concluded that all of the emission in the compressed air spectrum again resulted from H_2O and CO_2. From Figure 12a it is concluded that the 2.67 μ band was almost entirely due to H_2O, whereas the 2.82 μ band had contributions from both H_2O and CO_2. The unresolved band in the compressed air spectrum near 1.9 μ (Fig. 11), as shown in Figure 12b combined the H_2O emission at 1.88 μ and the CO_2 emission at 2.00 μ. The 1.45 μ H_2O band appeared only when H_2O was and CO_2 additions. Motored engine operating conditions were as follows:

Engine speed	1000 rpm
Air flow (full throttle)	0.69 pound per min
Intake air pressure (no additives)	29.26 in Hg
Fuel-air ratio by weight	.058 (lean)
Inlet mixture temperature	150°F
Coolant temperature	112°F
Fuel	50 per cent diethyl ether 50 per cent isooctane

The blend of diethyl ether and isooctane was chosen because it gave very intense cool flames. The conditions of intake mixture temperature and fuel-air ratio were also selected as those producing the brightest cool flames. The H_2O and CO_2 were added in the same manner as in the compressed air experiments at a concentration of about 10 per cent by volume.

It may be seen from Figure 13 and Table 1 that many of the same bands appeared in the cool flame spectrum as were noted in the normal flame and compressed air spectra. The region from 2.5 to 3.1 μ again contained two peaks at 2.63 and 2.82 μ. The 2.63 μ peak again appeared to result primarily from H_2O emission, and that at 2.82 μ again seemed to be a combination of H_2O and CO_2 emission (as shown in Figure 14a). The 1.87 μ H_2O band was prominent, and the 1.45 μ H_2O band was also easily detected. The 2.00 μ band of CO_2 was nearly overshadowed by the 1.87 μ H_2O band, but still appeared to be present. Also, a small amount of radiation in the region 1.5 to 1.6 μ might be attributed to a number of weak CO_2 bands listed there in absorption (Table 1).

The radiation appearing in the cool flame spectrum between 2.1 and 2.45 μ is at present unidentified. With the smallest slit widths, 100 and 50 μ, this radiation showed a peak near 2.32 μ. The small inflection at 2.92 μ, if it actually represents a distinct emission band, could correspond to an absorption band of H_2O_2 listed by Herzberg[12] at 2.93 μ.

The addition of H_2O increased the intensity of the H_2O emission at 2.67, 1.87, and 1.45 μ, but decreased the CO_2 emission at 2.05 and 1.5–1.6 μ. The addition of CO_2, however, markedly decreased the H_2O emission at 2.67, 1.87, and 1.45 μ, and also slightly decreased the CO_2 emission at 2.85 (allowing for slit width), 2.00, and 1.5–1.6 μ. These results are contrary to those obtained when H_2O and CO_2 additions were made to compressed air, and it is concluded that the major portion of the near infrared radiation emitted from engine cool flames arises from H_2O and CO_2 *produced by* the cool flame reaction. Since little change in the gas temperature was expected to result when H_2O and CO_2 were added from an external source, it appears that these additions decreased the amount of H_2O and CO_2 produced by the cool flame, while at the same time tending to increase the net concentration of the added constituent. With H_2O addition, the added gas apparently over-balanced by a considerable amount the loss of H_2O occasioned by the less extensive cool

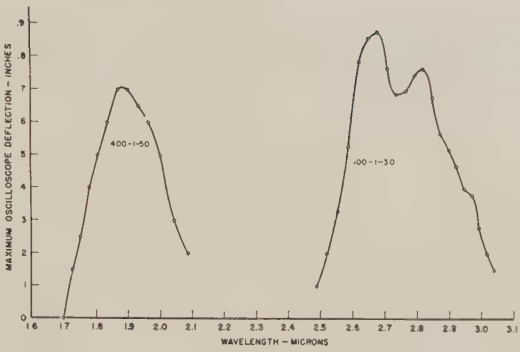

FIG. 11. Emission spectrum of compressed air

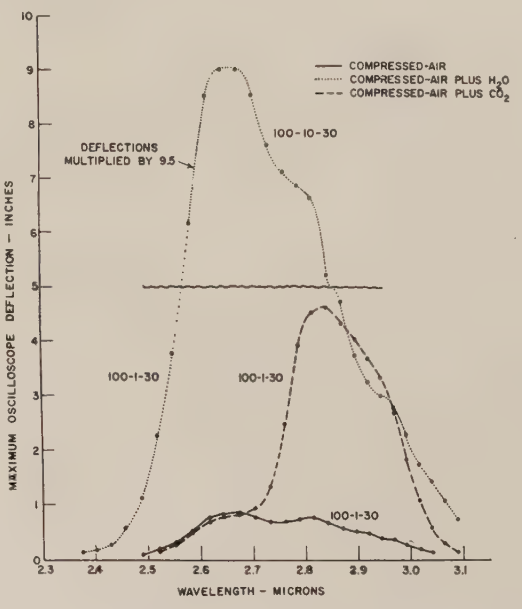

FIG. 12a. Effects of H_2O and CO_2 on compressed air spectrum, 2.3–3.1 microns.

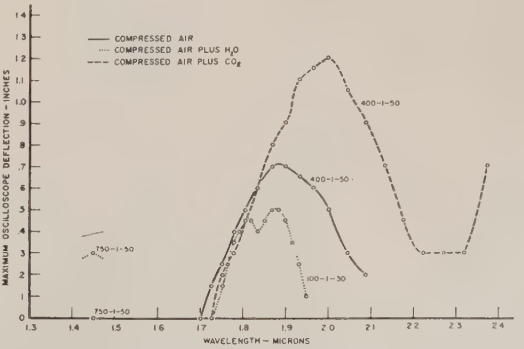

FIG. 12b. Effects of H_2O and CO_2 on compressed air spectrum, 1.3–2.4 microns.

flame reaction. With CO_2 addition, the loss in CO_2 production was apparently not quite balanced by the added gas.

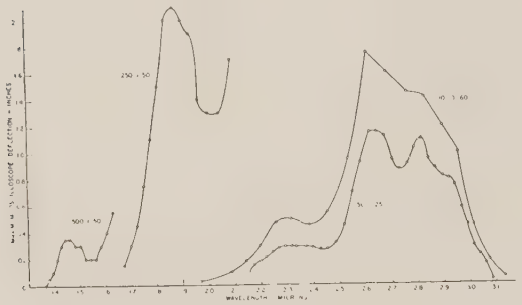

FIG. 13. Emission spectrum of engine cool flame.

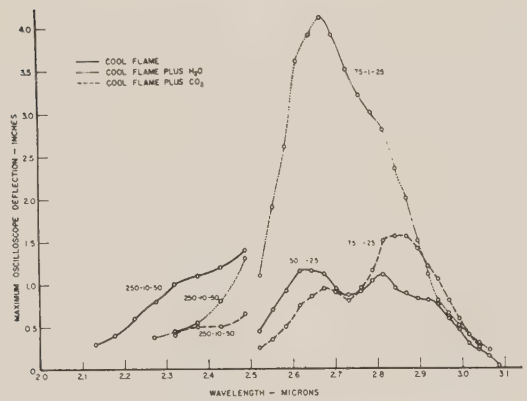

FIG. 14a. Effects of H_2O and CO_2 on cool flame spectrum, 2.0–3.1 microns.

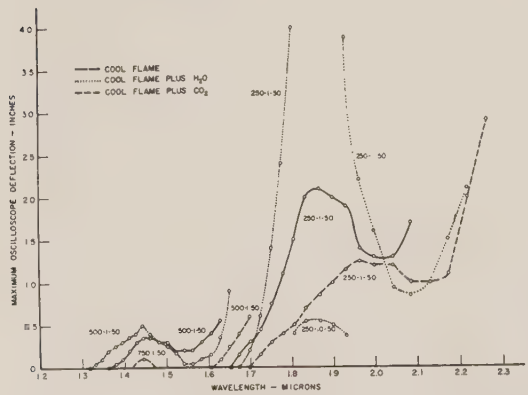

FIG. 14b. Effects of H_2O and CO_2 on cool flame spectrum, 1.2–2.3 microns.

Both the H_2O and CO_2 additions decreased considerably the unidentified radiation at 2.32 μ, and it is thus indicated that this radiation was emitted by some material produced in the cool flame reaction other than H_2O and CO_2.

Comparison of Burner and Engine Cool Flames

A comparison of the two series of spectra reported here is unfortunately made very difficult by the different instrument requirements of the burner and engine. Burner spectra were recorded with a thermocouple detector in the range from 1.7 to 14.0 μ. However, thermocouple detectors do not respond fast enough to follow the variation in radiation with time in an engine cylinder, nor are they considered sensitive enough to integrate the engine radiation. On the other hand, the lead-sulfide cell used in the engine experiments, although having sufficient speed of response and sensitivity, is limited to the wavelength range between 1.0 and 3.0 μ. Future plans include an examination of the burner flames with a lead-sulfide cell, in which case direct comparisons may be made with the engine flames in the wavelength region 1.0 to 3.0 μ. However, since H_2O and CO_2 are the only prominent emitters in this region, it is not expected that this information will provide convincing evidence of the similarity of the reaction mechanisms.

The work reported here already indicates a general similarity between the engine cool flame spectrum and the burner second-stage spectrum. The 1.88 and 2.5 to 2.9 μ H_2O and CO_2 emission appeared in both spectra. Also, the radiation near 2.3 μ was clearly evident in both spectra (Figs. 4 and 13). As was mentioned previously, the emitter of the 2.3 μ band has not yet been identified.

It is perhaps of interest to mention that certain differences in operating conditions which exist in the burner and engine cool flames immediately raise questions as to the similarity of the reaction mechanisms. Most obvious is the fact that cool and two-stage flames with diethyl ether have only been obtained with very rich mixtures (equivalence ratios of 2.5 to 3.5) in the flat-flame burner, whereas the maximum cool flame intensity in the engine was obtained with a lean mixture (equivalence ratio 0.85), and rich mixtures actually caused the engine cool flame to disappear. The much higher pressures (on the order of 150 psi) and possibly higher temperatures (around 1000°F) of the engine cool flames, along with the generally shorter time intervals in the engine, are also to be considered when making comparisons.

Cylinder-Gas Temperatures Deduced from Infrared Emission

Since the engine spectra already provided most of the required data, a brief preliminary check was made of the two-color radiation method for determining gas temperatures. This method requires that the radiation be of thermal origin, and is based on the following relation derived from Planck's equation for blackbody radiation:

$$\frac{D_{\lambda_1}}{D_{\lambda_2}} = \frac{\epsilon_{\lambda_1}}{\epsilon_{\lambda_2}} \left(\frac{\lambda_2}{\lambda_1}\right)^5 \frac{e^{(C_2/\lambda_2 T)} - 1}{e^{(C_2/\lambda_1 T)} - 1}$$

where λ_1 and λ_2 are two wavelengths of radiation

D is the oscilloscope deflection

T is the absolute temperature of the gas

C_2 is a universal constant equal to 14385 μ °K

$\epsilon_{\lambda_1}/\epsilon_{\lambda\epsilon_2}$ is the ratio of emissivities at the two wavelengths, and includes such instrument constants as the spectral slit widths at the two wavelengths.

In order to determine whether the method had any applicability to the present situation, four engine conditions were chosen and estimates were made of the gas temperatures based on prior experience in determining engine temperatures from pressure data and sodium-line reversal measurements. (The estimates were probably within about ±100°K of the true temperature.) The four engine conditions and the estimated temperatures are shown in Table 2. Five different wavelengths corresponding to band peaks of H_2O and CO_2 were selected from the engine spectra, which made possible ten combinations of two different wavelengths. The wavelengths, the emitters, and the relative intensities corrected for wavelength sensitivity of the lead-sulfide cell are shown in Table 3.

It was next assumed that the estimated temperature of 2778°K for condition A was correct, and, using this value, the relative emissivities for the

Table 2. Engine Conditions for Temperature Analysis

	A	B	C	D
Engine condition	Firing high temperature	Firing low temperature	Motoring cool flames	Motoring air
Estimated maximum gas temperature	2778°K	2220°K	777°K	777°K

Table 3. Relative Band Intensities for Four Engine Conditions (Intensities Corrected for PbS Cell Sensitivity)

Engine condition		A	B	C	D	Relative emissivities computed for condition A
Wavelength	Emitter					
μ						
2.61	H_2O	333,700	226,400	396.2	79.24?	1000
2.04	CO_2	90,550	49,800	13.78	1.324	147.15
1.83	H_2O	100,100	57,200	21.78	2.618	129.19
1.48	H_2O	26,200	13,680	1.00	—	23.544
1.25	CO_2	1,978	1,188	—	—	1.4758

Table 4. Calculated Cylinder Gas Temperatures (Condition A Assumed 2778°K)

Wavelengths	Temperatures, engine condition		
	B	C	D
μ	°K	°K	°K
From H_2O bands			
2.61–1.83	2245	893	748
2.61–1.48	2322	830	
1.83–1.48	2420	762	
From CO_2 bands			
2.04–1.25	2959		
From H_2O and CO_2 bands			
2.61–2.04	1930	575	451
2.61–1.25	2615		
2.04–1.83	3292	>3333	>3333
2.04–1.48	2620	1112	
1.83–1.25	2900		
1.48–1.25	3653		

five emission bands were calculated from the equation given above. These relative emissivities in turn were then used to calculate temperatures for the other three engine conditions. From the results in Table 4 it may be seen that the calculated temperatures agreed quite well with the estimated values when only H_2O bands were used, and that for conditions B and C, in which several independent values could be computed from different H_2O bands, the agreement between separate calculations was also fairly good. This would indicate that the H_2O radiation under all four engine conditions was probably of thermal origin, and that the relative emissivities were not greatly affected by changing engine conditions.

Only one temperature calculation was possible using only CO_2 bands, since two CO_2 bands were not detected under conditions C and D. The single value for condition B appears out of line, but there is insufficient data to decide whether this was the result of errors in measurement or whether the result indicates that the CO_2 radiation is nonthermal (CO_2 has been known to exhibit excitation lag which could give the effect of nonthermal radiation[16]).

Temperature calculations using combinations of H_2O and CO_2 bands appear from Table 4 to be inconsistent. These results could arise if the CO_2 radiation were nonthermal, but a more apparent reason exists in the fact that a change in the relative concentrations of H_2O and CO_2 would markedly alter the relative emissivities of bands from these constituents. Small changes in the relative concentrations of H_2O and CO_2 are expected between conditions A and B, and of course, quite large changes are expected in conditions C and D.

It is believed that more refined measurements of the type described here will provide quite accurate determinations of gas temperature, and that the two-color temperature determination method may be a very useful tool in the study of combustion processes.

Summary

In summary it may be stated that infrared spectral studies appear to offer a fruitful line of attack for explaining the complicated reaction mechanisms of low temperature oxidations. The infrared spectrum of cool and two-stage flames contains a large number of easily measured emission bands which are characteristic of the intermediate and final products of reaction. The instrumentation problems which arise in determining engine spectra are somewhat more difficult than in the case of stabilized flames, but these too may be overcome with the application of sufficient effort. Analysis of the infrared radiation from low temperature reactions in terms of blackbody radiation and emissivities would appear to be a useful tool, not only for determining gas temperatures in very complicated systems, but also for indicating the sources of excitation of the various chemical species present.

REFERENCES

1. Emeleus, H. J.: J. Chem. Soc., *128*, 2948 (1926); J. Chem. Soc., *131*, 1733 (1929).
2. Ubbelohde, A. R.: Proc. Roy. Soc., *A152*, 354 (1935).
3. Kondratjew, V. A.: Acta Physicochim. (U.R.S.S.), *4*, 556 (1936).
4. Topps, J. E. C., and Towend, D. T. A.: Trans. Faraday Soc., *42*, 345 (1946).
5. Mullins, B. P.: *Third Symposium on Combustion, Flame, and Explosion Phenomena*, pp. 704–713. Baltimore, The Williams & Wilkins Co., 1949.
6. Wentworth, J. T., and Daniel, W. A.: Unpublished data from the Research Laboratories Division, General Motors Corporation.
7. Levedahl, W. J., and Broida, H. P.: Anal. Chem., *24*, 1776 (1952); See also: Broida, H. P., Levedahl, W. J., and Howard, F. L.: J. Chem. Phys., *19*, 797 (1951).
8. Downs, D., Street, J. C., and Wheeler, R. W.: Fuel, *32*, 279 (1953).
9. Withrow, L. L., and Rassweiler, G. M.: Ind. & Eng. Chem., *25*, 923 (1933); Ind. & Eng. Chem., *25*, 1359 (1933).
10. Powling, J.: Fuel, *28*, 25 (1949).
11. Egerton, A. C. G., and Thabet, S. K.: Proc. Roy. Soc., *A211*, 445 (1952).
12. Herzberg, G.: *Molecular Spectra and Molecular Structure*, Vol. II. New York, D. Van Nostrand Co., 1945.
13. Ellis, J. W.: Phys. Rev., *26*, 469 (1925).
14. Bailey, C. R., and Lih, K. H.: Trans. Faraday Soc., *25*, 29 (1929).
15. Plyler, E. K.: J. Res. Nat. Bur. Standards, *40*, 113 (1948).
16. Gaydon, A. G.: *Spectroscopy and Combustion Theory*, 2nd Ed. London, Chapman & Hall, Ltd., 1948.

88

ULTRAVIOLET SPECTROPHOTOMETRY OF LOW PRESSURE EXPLOSIONS

By G. J. MINKOFF, A. J. EVERETT, AND H. P. BROIDA

As a result of studies of formation of hydrogen peroxide during low pressure, spark ignited explosions of mixtures of hydrogen and oxygen[1], and of methane and oxygen[2], it was decided to examine the ultraviolet absorption spectrum as a function of time, in order to determine whether H_2O_2 or O_3 were formed in the gas phase. The results obtained showed that the method is very suitable for the study of the rapid reactions associated with explosions. Some of these results are therefore described in detail, even though the type of reaction vessel was suited more particularly to the present problems than to general investigations. This communication may thus be considered as an introductory one.

Experimental

A specially selected 1-P28 photomultiplier (with UV transmitting envelope) was fitted to a large aperture Hilger E-518 spectrograph with quartz optics. A very simple power supply was used for the photomultiplier[3]. The signal from the photomultiplier was sent to a cathode ray oscilloscope (Furzehill Type 1648/D), to which a camera was attached. The switch which passed the spark through the explosive mixture also operated another circuit which enabled the CRO spot to traverse the screen simultaneously, at a predetermined speed.

The reaction vessel consisted of a Pyrex tube, 2 cm wide and 30 cm long, with quartz windows. The electrodes were tungsten wires (0.1 mm diam) fused in Pyrex capillaries so that only the cross-section of the wires was exposed to the hot gases. The spark gap was situated in a small chamber to one side of the tube. Condensation on the windows was prevented by surrounding the whole tube with a steam jacket.

OPTICAL ALIGNMENT

The light from the hydrogen arc, which was run on heavy duty accumulators, was focused on the spectrometer slit by one quartz lens, between the arc and the explosion vessel. The latter was thus traversed by a slowly converging beam of light, which should reduce errors due to reflection or channelling inside the walls of the vessel. Such errors were also diminished by using a stop on the lens, and so confining the light to the center of the tube. In order to test for the possibility of changes in light intensity due to overall changes in refractive index of the gases (due to variation of temperature or of composition), experiments were repeated using parallel, diverging and converging beams of light. However, the amount of absorption was unaffected. This does not eliminate the possibility of scattering of light by pockets of burning gas, cellular flames or similar phenomena.

MATERIALS

Hydrogen and oxygen were of commercial purity. The only impurity in the methane, from Point of Ayr Colliery, was 2 per cent nitrogen. Commercial carbon monoxide was freed of moisture and carbonyls by passage through liquid nitrogen. The hydrogen content was shown to be not greater than 3 parts in 10,000 by mass spectrometer analysis (by courtesy of Dr. C. A. Bunton). Mixtures were made up in 5-l flasks at least one day before they were required, to ensure thorough mixing. The compositions used were: $2CO + O_2$; $1.6\ H_2 + O_2$ and $CH_4 + 2O_2$.

Results

ABSORPTION

Wavelength dependence

The explosions of hydrogen-oxygen, carbon monoxide-oxygen and methane-oxygen mixtures all showed absorption beginning below 3000 A and increasing more rapidly as the wavelength decreased to 2100 A. It was found that with all three gases, straight lines were obtained by plotting the logarithm of the optical density ($\log_{10}D$) against the frequency (wave number) of the absorbing light. The slopes of five such lines, which include two pressures each of hydrogen and of carbon monoxide and one of methane, are identical within the experimental error, and have a value of 1.51×10^{-4}.

Although the slopes have a common value, the amount of absorption depends both on the gas and on the pressure. Thus, at 2300 A and a pressure of 10 cm, hydrogen explosions had an optical density of 0.28, carbon monoxide 0.35, while methane had the strongest absorption, with an

optical density of 0.65. If the absorbing species had a concentration which was proportional only to the pressure (p) (e.g., one of the initial reactants), then plots of D/p against p should be straight lines parallel to the pressure axis. A relation of this type was exhibited only by methane explosions above 4 cm pressure. Hydrogen

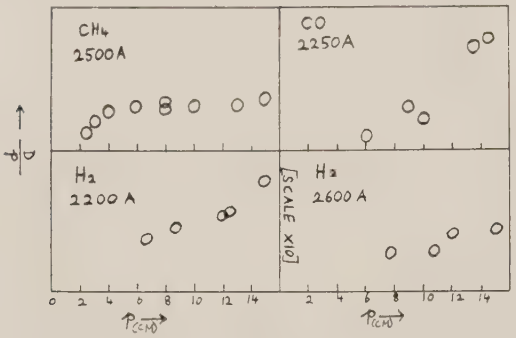

FIG. 1. Pressure dependence of absorption

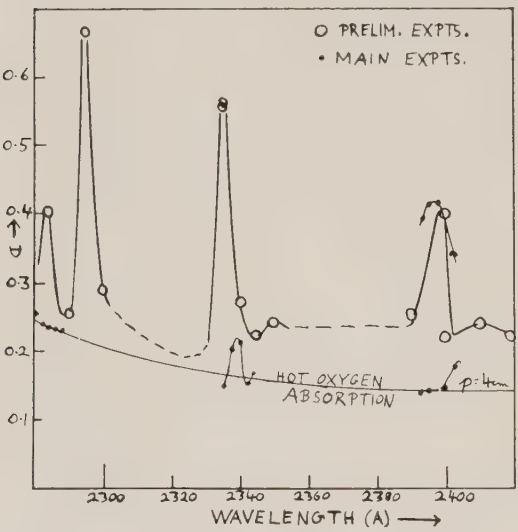

FIG. 2. Absorption of methane explosions

showed a slow, linear increase passing through the origin, while carbon monoxide was associated with a steeper rise beginning at a higher pressure than hydrogen (Fig. 1).

Absorption due to formic acid

Formic acid vapor has a banded absorption system with the most intense maxima at 2285, 2295, 2340 and 2400 A[4]. During the main part of the work, peaks were observed at 2340 and 2400 A, with optical densities which were only about 0.06 above the values of the main absorption slope. In the preliminary series of experiments in which the explosion tube was not heated by the steam jacket, peaks were detected at the four wavelengths corresponding to formic acid within the accuracy of the measurements; however, the optical densities were much greater in relation to neighboring absorption, as is evident from Figure 2, in which the observations in this part of the spectrum are plotted on an extended wavelength scale. The discrepancy was not due to the effect of heating the vessel, since the more intense absorption did not return when the heating was stopped.

Absorption by ozone

Ozone has an absorption system with a maximum at 2550 A[5]. Many readings were taken between 2350 and 2750 A with explosions of both methane and carbon monoxide. No significant absorption was found apart from the continuous absorption already described. The scatter of the experimental points was such that a peak with an optical density of 0.03 would have been just detectable. This would correspond to approximately 0.03 per cent of the original free oxygen in a $2CO:O_2$ mixture at 15 cm pressure.

Although there was no evidence of ozone absorption in the main part of the reaction zone, one series of experiments on the effect of pressure on the absorption at 2500 A in methane explosions suggested that a small quantity of ozone might be formed after the reaction was over and the products were cooling. This was shown by the presence of a very small amount of absorption about 10 millisec after the main absorption peak. Although this phenomenon was not always reproducible, and, in some tests, was obscured by electronic noise, a linear relationship between the pressure (p, in cms) and the time (t, in millisec) which elapsed between the initial sharp rise in absorption and the appearance of the second peak suggested that it was not merely a random phenomenon. The equation of the straight line was

$$t = p + 4$$

Rate of decay

Although there were differences in the appearance of the absorption curves, the rate of decay of absorption was found to be exponential. This suggests the disappearance of an activated or hot species by a process such as cooling, rather than by reaction with another low concentration intermediate.

EMISSION

The emission from the explosion, viewed end-on, was recorded with an appropriate gain setting of the CRO amplifier. No other modifications was necessary. The regions studied were: 3090 (OH) in all explosions, 4300 (CH) and 5150 (C_2) in methane and 3500 A in the carbon monoxide explosions. Under some conditions, e.g., at 2700 A in methane explosions, both emission and absorption were recorded together; the emission appeared first, and lasted approximately half the duration of the absorption. The C_2 region showed an additional feature, consisting of a spike lasting approximately ½ millisec. The decay of the main emission was similar to that of the absorption, i.e., exponential.

The most striking result was the relation between pressure and intensity (measured by the height of the oscilloscope trace). The intensity increased nearly as the square of the pressure, and not, as might have been anticipated, linearly. This relation held for all the emission regions studied.

Pressure effect

The variation of maximum flame temperature with pressure was calculated for H_2 and CO explosions by assuming constant pressure conditions. This was probably more justified for the CO explosions, since the high speed photographs showed no re-illumination, such as is normally observed in closed sphere explosions of CO[6, 7]. The cooling by the walls of the tube presumably chilled the hot gases, a factor which is comparatively unimportant in spherical vessels. Hydrogen and methane explosions, in which a maximum light intensity is observed a millisec or so after the end of the flame travel, are more nearly adiabatic, and the effect of pressure on closed vessel, adiabatic explosions of H_2 are being calculated. Temperatures obtained from the constant pressure calculations are given in Table 1. Clearly, a fourfold increase in pressure gives a temperature rise of the order of 150°. Now, if it be assumed that the light emission is thermal, and that the intensity depends on the fraction of gas with an energy content greater than 100 kcals (of the order of 2500 A), then the ratio of the populations at the two temperatures is approximately 3:1. Since the effect at constant pressure is likely to be smaller than that at constant volume, there is agreement with the observed ratio of 16:1, of which 4:1 is due to the increase in molecules present, and the remaining 4:1 to the effect of the temperature.

THE TIME FACTOR

Hydrogen explosions

Both the absorption and emission rose steeply at first, then more slowly to a maximum, and finally decayed exponentially. The times observed at 15 cm may be compared with those deduced from high speed photography. The film reveals that the flame travel is complete in 0.7 millisec, and the maximum intensity is reached in a total of 1.4 millisec. The decay appears to last for a further 3 millisec. The OH emission rises steeply in 1 millisec, with a slower rise of 2–3 millisec. This, however, may be due to an inequality of flame travel in the two directions. The whole process occupies 5–7 millisec, i.e., of the same order as is indicated by the film. Absorption, at say 2200 and 2600 A, also rises steeply for 1 millisec, with a further slow rise of 3 millisec, and decays for another 10 millisec.

TABLE 1

Gas	Atmos.				
	1.0	0.2	0.1	0.05	0.01
	°K	°K	°K	°K	°K
H_2	3090	2882	2802	2720	2597
CO	2965	2775	2710	2640	2510

Methane

The initial rise, both in absorption and emission, was markedly less steep (except for the C_2 spike). Thus, for an explosion at 15 cms, 1.5 millisec were required to reach the maximum emission, at all three wavelengths. Although this is also the time to maximum intensity indicated by the film, the rate of rise was constant for nearly 2 millisec, while the time of flame travel was 0.7 millisec. The C_2 spike, however, lasted approximately ½ millisec.

The duration of light emission shown by the film was 8.6 millisec, at 15 cm pressure. This was less than the duration of absorption (12 millisec), but double the emission time at 3064, 4300 or 5150 A (all 4 millisec). At lower pressures, however, e.g., 6 cms, the emission time indicated by both methods were 4 millisec, although the absorption still lasted longer (8 millisec). This dependence of the emission times

on the method suggested that possibly a continuum became more important at the higher pressure. The total light received by the film would be increased by contributions of all wavelengths (which could reach the film), while the oscilloscope, receiving energy from only a very short wavelength region, would register hardly any increase. This was later confirmed by photographs of the whole UV emission spectrum (see below).

Carbon monoxide

It has been found by high speed photography that at 15 cm pressure, the explosion in the narrow closed tube propogates rapidly for 5 millisec, and then quite slowly, reaching the ends of tube in a further 18 millisec. Glowing gases were only observed immediately behind the flame front, in contrast to the H_2 and CH_4 explosions. The luminosity disappeared completely in another 7 millisec, giving a total time of 30 millisec. The oscilloscope records, however, showed considerably longer times. Thus, an initial peak, 10–15 millisec long (both at 3090 and 3500 A) was followed by a further 40-millisec rise, then a rapid exponential decay, a total time of 60–65 millisec. Absorption rose rapidly in 5 millisec, then more slowly for another 40 millisec, before decaying for about 40 millisec, a total time of 85 millisec. Even at 10 cm pressure, there was no clear correlation among the three methods of observing the explosions. The emission shown by the oscilloscope trace lasts 80 millisec, while the total light emission was 54 millisec. No explanation of these differences has yet been proposed.

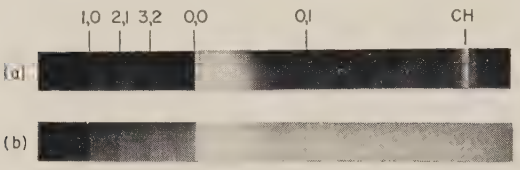

Methane-oxygen explosions
(a) 15 explosions at 5 cm pressure
(b) 1 explosion at 20 cm pressure

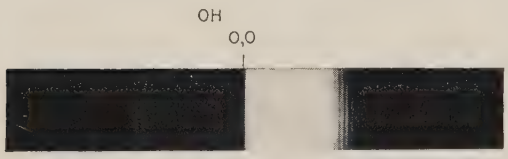

Hydrogen-oxygen explosions
2 explosions at 20 cm pressure

FIG. 3.

EFFECT OF PRESSURE ON APPEARANCE OF UV EMISSION SPECTRA

In order to investigate the effect of pressure on the continuum, photographs were taken of the whole of the UV emission. In order to obtain similar intensities, the spectrum from one or both CO and CH_4, at 20 cm, was compared with that from 15 explosions at 5 cm. As is shown in Figure 3, although the OH bands have similar intensities, the continuum is very much stronger at 20 cm in methane explosions. The difference was less marked in CO explosions, but the explosions at the lower pressure clearly showed the CO flame bands, which were not observable at the high pressure. No appreciable continuum was observed with hydrogen explosions.

The effect of pressure and temperature on the CO flame bands has been observed previously and discussed by Gaydon[8]. The continuum is attributed to the bimolecular association:

$$CO + O \rightarrow CO_2 + h\nu \qquad (1)$$

while the bands have been shown to be due to the reaction of O atoms with CO in 3 body collisions[9]:

$$CO + O + M \rightarrow CO_2^* + M \qquad (2)$$

Although the effect of increasing pressure would be to favor 3 body collisions at the expense of bimolecular, it appears that little activation energy is required for reaction (2); considerable energy is needed, however, for the CO + O system to move sufficiently far up the repulsive curve to attain the configuration necessary for transition to the lower stable potential energy curve. As a consequence of this, the increase in temperature associated with the increase in pressure must be more important in promoting reaction (2) than is the increase in probability of three body collisions.

The OH emission in the H_2 and CH_4 explosions showed, not the equilibrium distribution of vibrational intensity, but the abnormal distribution observed by Kondratjew[10] and by Gaydon and Wolfhard[11] in hydrogen flames. In the low pressure explosions of hydrogen, the (2,1) band was more intense than either the (1,0) or (3,2) bands, these two being of comparable intensities. In methane explosions, the (3,2) was very slightly more intense than the (2,1) band, which

was stronger than the (1,0). However, there must have been a great deal of self-absorption in the (0,0) band, since the (0,1) appears more intense than usual relative to the (0,0) band.

Discussion

ABSORPTION EXPERIMENTS

Continuous absorption

At the present time, the most suitable explanation for the rising absorption below 2800 A is the presence of hot oxygen molecules. The very complex spectrum of this molecule appears almost continuous under low dispersion, and has been observed in absorption by several authors[12].

The presence of this absorption makes it very difficult to decide whether there is any hydrogen peroxide in the gas phase. If all the expected H_2O_2 were present in the gas, the optical density at 2300 A would be 0.21 for explosions of $H_2 + O_2$ at 15 cm pressure (measured at 20°C), but the observed value is more than double, i.e., 0.44. Clearly, a different technique must be employed. There is, however, some indirect evidence of the formation of H_2O_2 without any refrigeration of the vessel. Thus, in preliminary experiments in which no heating jacket was used, visual observation of the CRO trace of methane explosions suggested that up to about 3000 A, the absorption rose very rapidly, fell by a third, then slowly decayed to the residual value of 10 per cent absorption. The latter was observed at all wavelengths. Hydrogen explosions showed an additional feature, which consisted of a second absorption peak preceding the slow fall to the residual value. The second peak, as well as the residual, was observed at wavelengths up to 4350 A. The residual absorption has been shown to be due to the formation of condensate on the windows. The observed facts could be explained by suggesting that the second peak in hydrogen explosions is connected with the condensation of unstable hydrogen peroxide, whose rapid decomposition on the windows leads to a change in drop size and hence of the scattering of light. This is in agreement with the observation that much of the hydrogen peroxide chilled out (at −80°C or below) from hydrogen-oxygen explosions decomposed in less than a second while warming up, while no peroxide at all can be isolated if the reaction vessel is at room temperature[13].

BANDED ABSORPTION

No evidence was found to suggest that more than 0.03 per cent of ozone was formed during the main part of the explosion process. It is just possible that mercury vapor was responsible for the absence of ozone, since some mercury lines appeared in emission in an experiment carried out later; however, this is not considered probable. No definite conclusion about the role of ozone in explosions of carbon monoxide or of methane can be drawn, since it could be argued that its stationary concentration remains very low. Nevertheless, although a low stationary concentration of intermediate is expected in a slow reaction or below an explosion limit, the instantaneous concentration might have been expected to increase considerably during a branched-chain explosion. If the small additional absorption at 2550 A observed after the main absorption can be proved to be due to ozone, formed by the recombination of free oxygen atoms with each other or with oxygen molecules on cooling, then the evidence presented in this communication may be taken to indicate that ozone does not play a major part in the explosive oxidation of carbon monoxide.

The role of formic acid in the explosion of methane will not be discussed in detail at this stage. It has been detected previously in the chilled products of methane explosions[2]. The lack of reproducibility of the formic acid absorption is probably connected with the difficulties encountered in attempts to isolate an organic peroxide from the products of methane explosions in vessels cooled to −180°C. If the latter is shown to contain formyl hydroperoxide, it may then be possible to establish a connection with the formic acid. It seems preferable, however, to defer further discussion until the absorption spectrum has been photographed with a short duration flash lamp, and the spectrum of HCOOH confirmed.

STATE OF THE BURNED GASES

We wish to decide to what extent the hot gases are in equilibrium, both thermal and chemical. The evidence provided by the photographs of the spectra of hydrogen and methane explosions will first be examined, and the $^2\Sigma \leftrightarrow {}^2\Pi$ transition of OH will be considered first.

The resolution of the spectroscope was not sufficient to permit measurements of rotational or vibrational temperatures. Nevertheless, from a

comparison of the intensity of the (0,1) band with that of the tail of the (0,0) band, it was clear that there was no evidence of abnormal rotational distributions in the H_2 or CH_4 explosions. The OH radiation is thus probably due to thermal emission, or possibly to the type of chemiluminescence found in alcohol flames, which results in high intensity of emission, but with normal rotational temperature. There was, however, no experimental evidence of this high intensity. The strength of the OH emission of the methane explosion was within an order of magnitude of that of the hydrogen explosion. Since the latter emission is known to be thermal it seems likely that the OH emission in methane explosions is also thermal rather than chemiluminescent. This is supported by an estimate of the intensity factor made by Gaydon and Wolfhard when studying low pressure flames of hydrogen: when ½ per cent of acetylene was added to the fuel, the OH emission in the flame front became 500 times stronger, and had a very high rotational temperature.

The vibrational distribution within the OH spectrum of the hydrogen explosions is similar to that observed by Gaydon and Wolfhard[11] at the top of low-pressure flames of hydrogen. These authors now attribute this distribution to a combination of two factors. First, the low pressure may lead to radiative non-equilibrium, which weakens all three bands (i.e., (1,0), (2,1) and (3,2)); however, the population of the $v \geqslant 2$ is maintained by pre-association through collisions of H and O atoms. Pre-association may also arise from the presence of excess free H and O atoms, leading to an increase in intensity of the (2,1) (3,2) bands. The excess atoms are left by the flame front reactions, since the atoms are formed in bimolecular reactions, and can only disappear, normally, in much slower three-body collisions. Since similar vibrational distributions were obtained in explosions of hydrogen at 5 and 20 cm pressure, the second factor is probably the more important in the present work.

In methane explosions, the three bands have similar intensities. This was not due to chemiluminescence, since in the flame front of low pressure CH_4-O_2 flames (unpublished spectra kindly made available to authors by Dr. Gaydon), the distribution corresponding to this process was: (1,0) medium (2,1) rather weaker, (3,2) absent. This is in agreement with the usual distribution for chemiluminescence. However, if the emission is thermal in both H_2 and CH_4 explosions, the difference in distribution must be explained satisfactorily. This can be done, at least qualitatively, on the basis of the difference between the concentration of H atoms at equilibrium and in the flame. A larger concentration of free atoms in the hydrogen explosions will account for the greater relative intensity of the (2,0 and 3,2) bands.

The conclusion is thus reached that the bulk of the OH radiation is thermal, and that there is evidence of the presence of excess H and O atoms.

The results obtained with the oscilloscope confirm that the emission is associated with the hot gases, and therefore indicate that the emission spectra are representative of the state of the hot gases, and are not merely an overlapping record of several stages of the process. This is further supported by the similar pressure dependence indicated by the two techniques. An explanation of this dependence has been given in terms of the equilibrium flame temperature. However, both Kondratjew[14], and Gaydon and Wolfhard[15] found a different type of pressure dependance of light emission from the flame fronts of low-pressure flames of carbon monoxide and of acetylene. The radiation, which was chemiluminescent, diminished with increasing pressure, owing to increasing quenching of excited molecules by collision. It is clearly necessary that in work of the present type, there should be a satisfactory separation of the flame front and the hot gases. This has been achieved for the explosions of hydrogen and of methane, since the flame travel is completed in so small a fraction of the time, but not in carbon monoxide explosions. Presumably the increasing intensity with pressure in the latter is due to the relative intensities of the emission from the flame front and from the hot gases.

The emission at 4300 A in methane explosions cannot be interpreted so simply. Although the oscilloscope traces show an increase with pressure, the photographs reveal that the CH radiation is in fact replaced by CO continuum at the higher pressure. Qualitatively, this suggests that the CH band, shown free of continuum at 5 cm, has the same duration as the OH and C_2 and the visible radiation. It is difficult to believe that the CH and C_2 are present in thermal equilibrium. For a satisfactory decision to be possible, a separate study must be made of the photographed spectrum as a function of time.

Finally, it may be concluded that the high

concentrations of free atoms, which have been shown to be present for several millisec, support the suggestion of Norrish and Porter[16] as to the relative inefficiency of three-body recombination processes during the duration of these experiments. These authors concluded that under their experimental conditions, the rate of removal of OH radicals depended on the rate of chemical reactions (bimolecular) rather than on the rate of cooling, although the magnitudes of these effects were of the same order. In the present work, the decays of both the emission of OH and the absorption of hot oxygen, were exponential, which suggests at first sight that cooling was rate determining. However, since it has been shown that thermal equilibrium has been established, the cooling would affect the concentration of excited molecules, since this involves only rapid energy transfers, but not necessarily the concentration of ground state OH radicals, since these can only disappear by chemical reaction. This process would lead to a complicated kinetic type of disappearance of the ground state, without affecting the form of the decrease of OH emission. No evidence regarding the former is provided by the present work; but, clearly, if the rates of cooling and of reaction of OH are comparable, no appreciable nonequilibrium would be introduced between the excited and ground state OH radicals. Our results are thus in accord with those of Norrish and Porter[16].

Acknowledgments

One of us (H. P. B.) is grateful for the award of a John Simon Guggenheim Fellowship. The authors wish to express their indebtedness to Dr. A. G. Gaydon for valuable discussions. The authors wish to thank Messrs. Furzehill Laboratories, Ltd., for the loan of the oscilloscope and camera. They also wish to acknowledge that they are aware of the work in progress in Cambridge, as a result of the visit of one of them (H. P. B.) to Professor Norrish's Laboratory.

REFERENCES

1. Egerton, A. C., and Minkoff, G. J.: Proc. Roy. Soc., *A191*, 145 (1947).
2. Everett, A. J., and Minkoff, G. J.: *Third Symposium on Combustion, Flame and Explosion Phenomena*, p. 390. Baltimore, The Williams & Wilkins Co., 1949.
3. Oldenberg, O., and Broida, H.: J. Opt. Soc. Am., *40*, 381 (1950).
4. Pearse, R. W. B., and Gaydon, A. G.: *The Identification of Molecular Spectra*, 2nd ed. London, Chapman and Hall, 1950.
5. Fabry, C.: *L'ozone Atmospherique*. Paris, C.N.R.S., 1950.
6. Ellis, O. C., and Wheeler, R. V.: J. Chem. Soc., 310 (1927).
7. Bullock, B. W., and Silverman, S.: J. Opt. Soc. Am., *43*, 389 (1953).
8. Gaydon, A. G.: *Spectroscopy and Combustion Theory*, 2nd ed. London, Chapman and Hall, 1948.
9. Broida, H., and Gaydon, A. G.: Trans. Faraday Soc., *49*, 1190 (1953).
10. Kondratjew, V. A., and Ziskin, M.: Acta Phys. Chem. (U.R.S.S.), *6*, 307 (1937).
11. Gaydon, A. G., and Wolfhard, H. G.: Proc. Roy. Soc., *A208*, 63 (1951).
12. Gaydon, A. G.: Proc. Roy. Soc., *A148*, 61 (1941); Norrish, R. G. W., and Porter, G.: Proc. Roy. Soc., *A210*, 439 (1952); Parker, W. G., and Wolfhard, H. G.: Proc. Phys. Soc., *A45*, 2 (1952).
13. Everett, A. J.: *Thesis*, London, 1953.
14. Kondratjew, V. A.: Z. Phys., *63*, 322 (1930).
15. Gaydon, A. G., and Wolfhard, H. G.: Proc. Roy. Soc., *A201*, 570 (1950).
16. Norrish, R. G. W., and Porter, G.: Proc. Roy. Soc., *A210*, 439 (1952).

89

PHOTODECOMPOSITION OF FORMALDEHYDE[a]

By L. SCHOEN

Introduction

The identity of the chemical species acting as chain carriers in a hydrocarbon decomposition or oxidation reaction is often a matter of controversy. It is obviously desirable to establish the thermal stability of a given molecule in the temperature region involved before assignment as a chain carrier in a combustion reaction. The role of the formyl radical in the oxidation of methane, as recently discussed by Lewis and von Elbe[1] illustrates this general situation.

The present investigation of formaldehyde photolysis, employing deuterium as a tracer for hydrogen atoms, was carried out primarily to obtain an independent estimate of the limiting energy of dissociation of the C—H bond in the formyl radical. The photodecomposition of formaldehyde had previously been studied by Norrish and Kirkbride[2], Style and Summers[3], Gorin[4], Calvert and Steacie[5], and others. From the present work, a mechanism compatible with the results of experiment is suggested from which additional information concerning the decomposition may be deduced.

Experimental

Formaldehyde was prepared by the method of Spence and Wild[6]. Alpha polyoxymethylene was utilized as the starting material in place of paraformaldehyde to take advantage of the lesser degree of hydration of the former polymer. The deuterium used was of 99.5-per cent enrichment or better. Formaldehyde-deuterium mixtures were made up and stored in a mixing vessel maintained at about 120°C in order to minimize formaldehyde polymerization. The pressure in the mixing vessel was monitored before each run to correct for the small amounts of polymerization that occurred. The photolysis cell consisted of a quartz cylinder, 25 mm in diameter and 20 cm long, with optically flat windows fused onto the ends. This vessel was placed in a cylindrical brass furnace electronically regulated to ±1°C. All surfaces that came into contact with formaldehyde vapor were wound with chromel wire heated to about 130°C. High-vacuum silicone grease was used to lubricate all stopcocks subjected to high temperatures. Pressure measurements were made with a Pyrex spiral gauge. The light source utilized was a Hanovia high-pressure xenon arc emitting an intense continuum in the visible and ultraviolet. A concave reflector was placed one focal length in back of the source. The wavelengths employed were isolated by means of a Farrand ultraviolet monochromator of $f/4$ aperture. At the conclusion of a run, the products were circulated through a liquid-nitrogen-cooled trap by an automatic Toepler pump to separate the noncondensable gases D_2, H_2, HD and CO from excess formaldehyde and traces of methanol. The noncondensable fraction was then analyzed for the above gases by means of a Consolidated mass spectrometer. In addition to the deuterium experiments, some runs were carried out with dideuterioacetylene-formaldehyde mixtures. The deuterium enrichment of the acetylene exceeded 95 per cent.

Results and Discussion

THE THERMAL REACTION

The products of the thermal reaction at 300°C were found to be carbon monoxide, methyl alcohol, and, to a lesser extent, hydrogen, as reported by Calvert and Steacie[5]. In addition, in the presence of deuterium, an exchange reaction forming HD was noted. The amounts of HD formed thermally were relatively large, necessitating corrections to the photochemical rates of about 20 per cent at 300°C for the runs at λ3130. In the case of the experiments carried out at λ3650, where the light absorption by formaldehyde falls off, corrections for the rate of formation of HD amounted to approximately 50 per cent at 300°C. Corrections to photochemical rates of formation of hydrogen at this temperature reached a maximum of 10 per cent at λ3130 and about 50 per cent at λ3650. To correct photochemical rates of formation of HD and H_2 for thermal reaction, each photochemical run was preceded or followed by a dark reaction carried out at the same temperature and essentially the

[a] This research is a part of the work by the Bureau of Mines on Order No. CS-670-54-9, supported by Headquarters, Air Research and Development Command, Office of Scientific Research, through Project SQUID.

same concentrations of deuterium and formaldehyde, for the same length of time. Photochemical rates determined by this method were generally reproducible to within a range of 20 per cent.

It is suggested that the formation of methanol is due to a heterogeneous process involving the hydrogenation of formaldehyde following thermal decomposition.

$$H_2CO = H_2 + CO, \qquad (A)$$

$$H_2CO + H_2 \overset{\text{wall}}{=} CH_3OH. \qquad (B)$$

This would lead to a $[CO]/[H_2]$ ratio greater than one in agreement with experimental observation. In addition to reactions (A) and (B), the following reactions might occur in the presence of deuterium:

$$H_2CO + D_2 = CH_2DOD, \qquad (C)$$

$$CH_2DOD = HD + HDCO \qquad (D)$$

$$CH_2DOD = D_2 + H_2CO, \qquad (E)$$

where the probability for the occurrence of reaction (D) is approximately twice that for reaction (E). It is believed that these processes may account for HD formation during the thermal reaction.

DETERMINATION OF LIMITING WAVELENGTH FOR FREE RADICAL DISSOCIATION OF FORMALDEHYDE

With the monochromator slits set to pass a band of radiation 100 Å in width, formaldehyde-deuterium mixtures were photolyzed at various wavelengths up to λ3850. Although, as previously mentioned, thermal formation of HD at the longer wavelengths was substantial, there was in every instance a net photochemical rate of production of HD up to and including λ3650, as illustrated by runs 5, 8, 10 and 13 of Table 1. The formation of HD up to λ3650 was taken as a criterion of the photochemical act (I) given below. At λ3750 and λ3850, there was no measurable rate of photochemical formation of HD as evidenced by runs 14 and 30, respectively. The energy resident in light of wavelength 3650A is 78 kcal per mole quantum; therefore, the energy of dissociation of the first C—H bond in formaldehyde may not exceed this value. The primary process involved must then be given by

$$H_2CO + h\nu = H + HCO \qquad \Delta H \leqslant 78 \text{ kcal} \qquad (I)$$

The dissociation of the two C—H bonds in formaldehyde is known to require 105 kcal[7]:

$$H_2CO = 2H + CO \qquad \Delta H = 105 \text{ kcal} \qquad (II)$$

It follows then that the energy of dissociation of the C—H bond in the formyl radical cannot be less than 27 kcal:

$$HCO = H + CO \qquad \Delta H \geqslant 27 \text{ kcal.} \qquad (III)$$

These are also the conclusions reached by Gorin[4] from a study of the photodecomposition of formaldehyde in the presence of iodine.

Table 1. Photolysis of Formaldehyde at 300°C

1 No.	2 λ	3 Time	4 $[H_2CO]$	5 $[D_2]$	6 $\frac{[H_2CO]}{[D_2]}$	7 $[C_2D_2]$	8 [HD]	9 $[H_2]$	10 [H]	11 [D]	12 $\frac{R_{H_2}}{R_{HD}}$	13 $\frac{(12)}{(6)}$ (3.86)
	Å	*min*	*mm*	*mm*		*mm*	*mm*	*mm*	*mm* × 10^7	*mm* × 10^9		
5	3650	190	416	101	4.12	—	0.72	19.4	—	—	26.9	25.2
8	3650	202	343	89	3.86	—	.60	15.3	—	—	25.5	25.5
10	3650	190	299	81	3.69	—	.42	9.4	—	—	22.4	23.4
13	3650	180	244	71	3.44	—	.32	6.5	—	—	20.4	22.9
14	3750	360	218	68	3.21	—	—	7.8	—	—	—	—
30	3850	350	381	87	4.38	—	—	—	—	—	—	—
6	3130	195	394	97	4.06	—	2.7	6.6	8.7	3.6	24.6	23.4
9	3130	181	323	85	3.80	—	1.8	5.1	7.1	3.6	27.4	27.8
12	3130	191	261	74	3.53	—	2.2	4.8	9.5	4.0	23.0	25.2
16	3130	185	195	60	3.26	—	1.5	3.0	8.3	3.5	20.0	23.7
37	3650	120	412	—	—	79	0.066	0.86	—	—	13.0	—
39	3650	140	365	—	—	68	.056	.81	—	—	14.5	—

THE PHOTOLYSIS AT λ3130

The following mechanism, which has been found to be compatible with the results of ex-

periment, is proposed for the photodecomposition at 300°C.

$$H_2CO + h\nu \overset{I_a''}{=} H + HCO, \quad (1)$$

$$H + H_2CO \overset{k_2}{=} H_2 + HCO, \quad (2)$$

$$H + D_2 \overset{k_3}{=} HD + D, \quad (3)$$

$$D + H_2CO \overset{k_4}{=} HD + HCO, \quad (4)$$

$$HCO \overset{k_5}{=} H + CO; \qquad E \geqslant 27 \text{ kcal}, \quad (5)$$

$$HCO \overset{k_6}{=}_{\text{wall}} \text{Prods } (H_2CO; \quad H_2CO + CO). \quad (6)$$

Here the heterogeneous chain-breaking step originally postulated by Calvert and Steacie[5] has been adopted. This step involves the reaction of an adsorbed formyl radical with either a hydrogen atom to reform formaldehyde or with another formyl radical to form formaldehyde and carbon monoxide. The rate expression obtained from this mechanism is given by

$$\left(\frac{R_{H_2}}{R_{HD}}\right)_{3130} = \frac{k_2[F]}{2k_3[D_2]}. \quad (7)$$

Figure 1 is a plot of the ratio of rates on the left side of equation (7) against values of the formaldehyde-deuterium ratio for several runs at a temperature of 300°C. From the slope of this line and the value of k_3 given by Farkas and Farkas[8], it becomes possible to evaluate k_2. Preliminary studies at 100°C indicated that reaction (3) could not at all compete with reaction (2), as judged by the relative amounts of HD and H_2 formed. It was anticipated then that the energy of activation of reaction (2) would be quite small. The values of k_2 obtained at several temperatures between 300° and 375°C listed in Table 2 demonstrate that the energy of activation of reaction (2) is not too far from zero in this temperature range. Assuming the values of k_2 to be uncertain by ± 10 per cent, in the extreme case the value of E_2 may not exceed 4 kcal. This result agrees with the investigations of Geib[9] and Calvert and Steacie[5], in both of which the activation energy of reaction (2) is estimated as equal to or less than 5 kcal.

If the primary process remains unchanged at the lower wavelengths, as found by Gorin[4] down to λ2537, the mechanism furnishes a qualitative explanation of the results of Akeroyd and Norrish[10]. These investigators found that the quantum yield of formaldehyde photolysis in the full light of a mercury arc varies from unity to a value of 100 in the temperature range 100° to 350°C. In accordance with an earlier suggestion of Axford and Norrish[11], this variation in quantum yield may be ascribed to the high energy of activation for reaction (5), together with a relatively low energy of activation for the chain termination process. At the lower temperatures the chain-breaking reaction predominates, the majority of formyl radicals being destroyed at the wall. The chain nature of the reaction is thus not immediately recognizable. At the higher temperatures a larger fraction of formyl radicals react via reaction (5) which serves to regenerate hydrogen atoms. The resulting increase in chain length is then reflected in the quantum yield measurements.

DETERMINATION OF THE STATIONARY HYDROGEN AND DEUTERIUM ATOM CONCENTRATIONS AT λ3130

From reactions (2), (3) and (4),

$$R_{H_2} = k_2[H][H_2CO], \quad (8)$$

$$R_{HD} = k_3[H][D_2] + k_4[D][H_2CO]; \quad (9)$$

and these, together with reaction (7), lead to

$$R_{HD} = 2\,k_3[H][D_2], \quad (10)$$

$$R_{HD} = 2\,k_4[D][H_2CO]. \quad (11)$$

The stationary hydrogen atom concentration may be estimated from reaction (10), and making the assumption that k_4 is the same as k_2 for the corresponding isotopic atom reaction, the stationary deuterium atom concentration may be calculated from reaction (11). Representative values for these quantities at 300°C are tabulated in columns 10 and 11 of Table 1.

THE PHOTOLYSIS AT λ3650

At λ3650, considerable quantities of H_2 as well as HI were observed by Gorin[4]. He therefore postulated the additional primary process

$$H_2CO + h\nu \overset{I_a'}{=} H_2 + CO. \quad (12)$$

If this step is incorporated into the reaction scheme, the rate law becomes

$$\left(\frac{R_{H_2}}{R_{HD}}\right)_{3650} = \left(\frac{I_a' + I_a''}{I_a''}\right)_{3650} \frac{k_2[F]}{2k_3[D_2]}. \quad (13)$$

At the shorter wavelengths, where I_a' goes to

zero, this equation reduces to the rate expression (7) obtained directly for λ3130, whereas at the longer wavelengths, where I_a'' presumably approaches zero, the equation indicates that the rate of formation of HD becomes insignificantly small. In column 13 of Table 1 are tabulated values of $(R_{H_2}/R_{HD})_{3130}$ and $(R_{H_2}/R_{HD})_{3650}$ corrected to an arbitrary $[F]/[D_2]$ ratio of 3.86. It is expected that the values of the ratio R_{H_2}/R_{HD} at λ3650 will exceed that at λ3130 by the amount of the third term in equation (13). Due to an uncertainty of almost 20 per cent in the determination of these ratios, however, it is required that, in order to detect a measurable difference between $(R_{H_2}/R_{HD})_{3130}$ and $(R_{H_2}/R_{HD})_{3650}$,

$$\frac{I_a' + I_a''}{I_a''} \geqslant \frac{6}{5}. \tag{14}$$

As seen in column 13 of Table 1, no such difference between the values of $(R_{H_2}/R_{HD})_{3130}$ and $(R_{H_2}/R_{HD})_{3650}$ could be detected; therefore we conclude that the reverse of equation (14) is true

$$\frac{I_a' + I_a''}{I_a''} \leqslant \frac{6}{5}, \tag{15}$$

or

$$\frac{I_a'}{I_a''} \leqslant 0.2; \tag{16}$$

i.e., at λ3650 the incidence of the primary process proceeding by way of free radical splitting must be at least five times that proceeding by direct intramolecular decomposotion into hydrogen and carbon monoxide. This conclusion does not agree with the results of Gorin[4] at λ3650, where a value of approximately 0.4 was found for the ratio of equation (16), assuming no reaction between formyl radicals and iodine. On the basis of later work by Blacet and Heldman[11], it appears that this assumption is not justified, and Gorin's value becomes too small by approximately a factor of two. The reason for lack of agreement is not immediately obvious; however, one might observe from Table 1 that between λ3650 and λ3750 the amounts of HD formed begin to approach zero. The quantity $(I_a' + I_a''/I_a'')_{3650}$ is thus an extremely sensitive function of wavelength, and it becomes imperative in comparing the results of two photochemical experiments in this region that the wavelength or band of wavelengths utilized be almost identical in both experiments. The use of a mercury arc and chemical filter of diamantfuxin by Gorin[4] to isolate 3650 radiation as compared to the use of a xenon arc-monochromator combination in the present work may account for the disagreement.

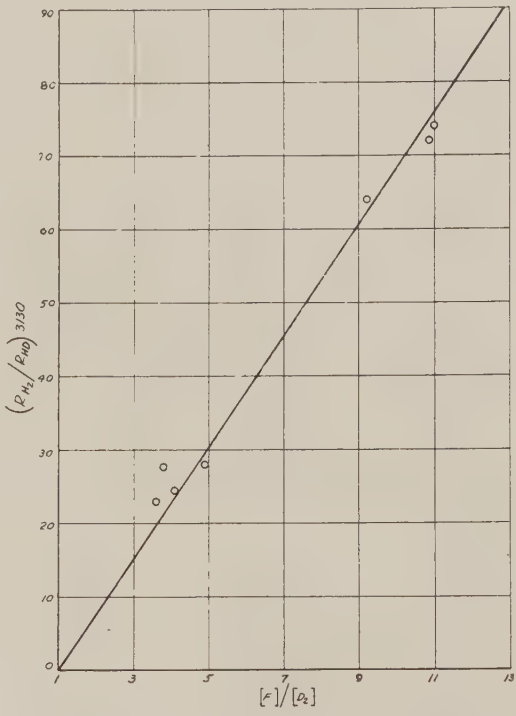

FIG. 1. Dependence of $\frac{R_{H_2}}{R_{HD}}$ 3130 on $\frac{[F]}{[D_2]}$ at 300°C

TABLE 2. TEMPERATURE DEPENDENCE OF k_2 BETWEEN 300° AND 375°C

Temperature	k_2, litmole^{-1} sec^{-1} × 10^{-6}
°C	
303	6.9
324	6.9
348	7.3
375	7.1

THE USE OF DIDEUTERIOACETYLENE AS A TRACER FOR HYDROGEN ATOMS

Several runs were carried out with deuterated acetylene-formaldehyde mixtures at λ3650 to test the initial conclusions regarding the C—H bond dissociation energies arrived at using deuterium as a tracer for hydrogen atoms. In this case, reaction (2) is replaced by

$$H + C_2D_2 = HD + C_2D. \tag{17}$$

Runs 37 and 39 of Table 1 illustrate the nature of the data obtained. As with deuterium, there is a net photochemical rate of production of HD after correction for thermal reaction. The use of deuterated acetylene therefore provides additional evidence in favor of the limiting values of 78 and 27 kcal previously given for the energies of dissociation of the C—H bonds in formaldehyde.

Acknowledgments

The author is indebted to Drs. Bernard Lewis and Guenther von Elbe for suggesting the problem and for their guidance and advice throughout the investigation. He also wishes to thank Drs. R. Klein and M. D. Scheer for numerous provocative discussions, and A. G. Sharkey, Jr., for the mass-spectrographic analyses.

REFERENCES

1. Lewis, B., and von Elbe, G.: *Combustion, Flames and Explosions of Gases*, p. 96. New York, Academic Press, 1951.
2. Norrish, R. G. W., and Kirkbride, F. W.: J. Chem. Soc., 1518 (1932).
3. Style, D. W. G., and Summers, D.: Trans. Faraday Soc., *35*, 899 (1939).
4. Gorin, E.: J. Chem. Phys., *7*, 256 (1939).
5. Calvert, J. G., and Steacie, E. W. R.: J. Chem. Phys., *19*, 176 (1951).
6. Spence, R., and Wild, W.: J. Chem. Soc., 338 (1935).
7. National Bureau of Standards: *Selected Values of Chemical Thermodynamic Properties*. Circular 500, February 1952.
8. Farkas, A., and Farkas, L.: Proc. Roy. Soc. (London), *A152*, 124 (1935).
9. Geib, K. H.: Ergeb. exakt. Naturwiss., *15*, 44 (1936).
10. Akeroyd, E. I., and Norrish, R. G. W.: J. Chem. Soc., 890 (1936).
11. Axford, D. W. E., and Norrish, R. G. W.: Proc. Roy. Soc. (London), *A192*, 518 (1948).
12. Blacet, F. E., and Heldman, J. D.: J. Am. Chem. Soc., *64*, 889 (1942).

90

SPECTROSCOPIC DETERMINATION OF THE DISSOCIATION ENERGY OF THE OH RADICAL

By GEORGE A. HORNBECK

Introduction

The advent of rockets and jet engines of various types has led to an increased interest in combustion reactions in general. Thermodynamic interpretation of the kinetics of such reactions requires an adequate knowledge of the dissociation energy of the molecules and radicals involved in high temperature chemical processes. In particular, dissociation energies along with other pertinent data obtained by spectroscopic means, such as moments of inertia, fundamental vibrational frequencies, statistical weights, and internal partition functions are useful for the calculations of such thermodynamic quantities as heat capacity, enthalpy, equilibrium constants, etc. This is particularly true for some molecular species such as OH and CH for which there are no thermochemical means of obtaining this information. Also, the interpretation of bond energies is considerably aided by accurate values of the dissociation energies of diatomic molecules.

In view of the fact that the OH radical is an intermediate product in the oxidation of hydrogenous fuels, it appears worthwhile to recalculate the dissociation energy of OH from the recent and more reliable data of the ground electronic state obtained by Herman and Hornbeck[1]. The data from this vibration-rotation spectrum should give a better value of the dissociation energy, as the accuracy of extrapolation to high vibrational levels is not likely to be affected by perturbations since the latter do not usually occur in the ground state. In addition, the number of vibrational levels which have been observed in the ground state are about twice the number observed in the electronically excited state from which the

currently accepted value of D_0(OH) was computed[2].

Experimental

An oxyacetylene flame was the source of OH which was used in obtaining the spectroscopic data reported by Herman and Hornbeck[1], and a discussion of the experimental details can be found in their paper. In brief, the spectrograms were taken in the first order of a 2-meter concave grating spectrograph on 1-N hypersensitized plates. The vibration-rotation bands of OH which were analyzed are found in the photographic infrared region in the approximate range from 7450 to 8750 A, and the many measurements of line position are believed to be accurate to about 0.05–0.10 cm^{-1}.

Results and Discussion

D_0 is the dissociation energy which is usually quoted, and in the case of a diatomic species is the energy required to carry a molecule from the lowest vibrational level through the highest level into a state of two normal atoms. Thus, D_0 refers to the energy above the lowest vibrational level of an electronic state and not to the potential minimum as is the case for D_e. The dissociation energy D_e which is required for some calculations, such as potential energy functions, is larger than D_0 by an amount equal to the zero point energy. Although every stable electronic state has a D_0 value, the following discussion concerns the $^2\Pi$ ground state of OH since the D_0 of this state will equal the heat of dissociation of the molecule.

D_0 is equal to the summation of the separation between successive vibrational levels, that is

$$D_0 = \Sigma_v \Delta G_{v+1/2} \tag{1}$$

This summation is readily done once the vibrational term values G_v have been computed. For the vibrational quanta we have

$$\Delta G_{v+1/2} = G(v+1) - G(v) \tag{2}$$

and the customary polynomial for the term values is

$$G(v) = \omega_e(v+\tfrac{1}{2}) - \omega_e X_e(v+\tfrac{1}{2})^2 + \omega_e Y_e(v+\tfrac{1}{2})^3 \tag{3}$$

Here the coefficients are the molecular vibrational constants, and the author believes that the accuracy of the experimental data of Herman and Hornbeck[1] justifies the inclusion of a quartic term in equation (3), viz., $-\omega_e Z_e(v+\tfrac{1}{2})^4$. The term values shown in Table 1 have been computed using the four vibrational constants of the $^2\Pi$ state of OH given by Herman and Hornbeck[1]. These constants are as follows:

$\omega_e = 3738.48\ cm^{-1}$ $\quad \omega_e Y_e = 0.7232\ cm^{-1}$

$\omega_e X_e = 85.482\ cm^{-1}$ $\quad \omega_e Z_e = 0.04544\ cm^{-1}$

Table 1 also lists the calculated separation between levels ($\Delta G_{v+1/2}$) from $v = 0$ to $v_{max} = 19$; and the summation of these is 37340.25 cm^{-1}.

Unfortunately, spectra involving all the vibrational levels have not been observed, nor have those which have been reported been observed with a similar degree of accuracy. The highest level observed with good dispersion and resolving power is $v = 6$. Vibration-rotation spectra of OH, using an oxyacetylene flame as a source, have been studied with relatively high dispersion instruments by several investigators[1, 3, 4, 5]. In general, the measurements of these workers are in good agreement, and transitions involving $v = 0$ to $v = 6$ have been reported. The work of the night-sky investigators[6, 7] has extended the observed transitions to $v = 9$, but the low intensity of this source precludes the use of high resolution spectrographs required for maximum accuracy. A comparison of $\Delta G_{v+1/2}$ as calculated by equation (3) with the observed values is given

TABLE 1

v	$G(v)$	$\Delta G_v + \frac{1}{2}$
	cm^{-1}	cm^{-1}
0	1847.96	3569.64
1	5417.60	3403.87
2	8821.46	3240.25
3	12061.71	3077.71
4	15139.42	2915.13
5	18054.55	2751.43
6	20805.99	2585.57
7	23391.56	2416.39
8	25807.95	2242.81
9	28050.75	2063.77
10	30114.52	1878.17
11	31992.69	1684.89
12	33677.57	1482.87
13	35160.44	1271.02
14	36431.46	1048.24
15	37479.70	813.43
16	38293.13	565.54
17	38858.67	303.43
18	39162.10	26.09
19	39188.19	

in Table 2. The numbers indicated by an asterisk have been averaged from the data of Meinel[6] and

TABLE 2

v	Calc. $\Delta G_{v+1/2}$	Obs. $\Delta G_{v+1/2}$		Obs. − calc.	
	cm^{-1}	cm^{-1}		cm^{-1}	
0	3569.64	3569.63		−0.01	
1	3403.87	3403.95		+0.08	
2	3240.25	3240.25		0.00	
3	3077.71	3077.67		−0.04	
4	2915.13	2915.24	2915.9*	+0.11	+0.8*
5	2751.43	2751.43	2753.5*	0.00	+2.1*
6	2585.57		2582.3*		−3.3*
7	2416.39		2406.0*		−10.4*
8	2242.81		2242.8*		0.0*

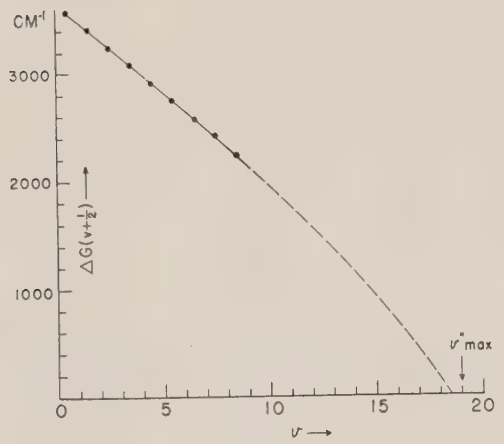

FIG. 1. Curve of $\Delta G(v + \frac{1}{2})$ against v for the ground state of OH.

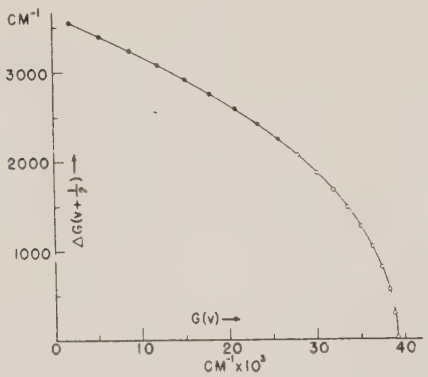

FIG. 2. Curve of $\Delta G(v + \frac{1}{2})$ against total energy of OH ground state.

Chamberlain and Oliver[7], and the others were obtained from data of flame spectra. Although some of the differences between observed and calculated are appreciable in the case of the night-sky data, it is most likely a matter of experimental accuracy; however, it is interesting to note that these discrepancies are even greater if the quartic term in equation (3) is not included in the calculation of the term values.

An examination of Table 1 discloses that the second differences of $G(v)$ are not constant. In a plot of $\Delta G_{v+1/2}$ against v, Figure 1, the curve is at first slightly concave upwards, and then at about $v = 5$, $\Delta_2 G(v)$ begins to increase with v. Although in Figure 1 $\Delta G_{v+1/2}$ does not converge very rapidly with v, the deviation from a straight line is sufficiently great to introduce a rather large error in D_0(OH) if one tries to represent the term values with a two constant formula and then applies a Birge-Sponer[8] linear extrapolation. This would yield a dissociation energy for OH that is much higher than the value calculated from the four constant formula of equation (3).

In Figure 1 the observed energy intervals have been plotted against the vibrational levels v, and the dashed curve extrapolated to v_{max} was computed from equation (3). This extrapolation defines the limit of the upper level at $v''_{max} = 19$. This level is higher than v''_{max} based on the D_0(OH) value from the data of the upper electronic state, and is lower than that which is obtained from a Birge-Sponer linear extrapolation of the ground state.

It is frequently helpful to plot $\Delta G_{v+1/2}$ against the total energy $G(v)$. A graph of this type is shown in Figure 2. This curve takes the general form of a parabola, and the intercept on the $G(v)$ axis gives the total dissociation energy D_e(OH) for the $^2\Pi$ ground state. Here again the solid circles are from observed data, and the open circles are calculated values.

Although there seem to be no peculiarities associated with the potential function of OH, and although more than half of the total energy of the ground state is represented by $v = 0$ through $v = 9$, it is obvious from Figure 2 that until the positions of some of the higher vibrational levels have been verified it is only with a limited degree of certainty that one can depend on the accuracy of any value of D_0(OH).

The calculations with the data from the vibration-rotation spectrum of OH give a higher value for D_0(OH) than the presently accepted value[2] of 4.45 ev which was derived from the data of the upper electronic state of OH, i.e., the $^2\Sigma \rightarrow {}^2\Pi$ transitions. Taking 8065.98 cm^{-1} to be 1 ev from DuMond and Cohen[9], the value of D_0(OH) as

calculated from the ground state data of Herman and Hornbeck[1] is 4.62(9) ev or 106.71 kcal/gm mol, and D_e(OH) is 4.85(8) ev.

Since the potential energy of a molecule is so largely dependent on the dissociation energy it appears worth while to construct a potential energy curve for the ground state of OH using the above calculated value of the dissociation energy. The best known approximation for the potential energy curve of a diatomic molecule was introduced by Morse[10]. A discussion of the merits of the Morse function, as well as other recommended potential functions, has been given by Hulbert and Hirschfelder[11]. Although there is considerable virtue in the other functions, the author has chosen the more general purpose formula of Morse[10] for developing the potential energy curve shown in Figure 3. The mathematical expression for the potential function as proposed by Morse with the notation as set forth by Herzberg[12] is as follows:

$$U(r - r_e) = D_e(1 - e^{-\beta(r-r_e)})^2 \qquad (4)$$

where,

$$\beta = \sqrt{\frac{2\pi^2 c\mu}{D_e h}}\,\omega_e = 1.2177 \times 10^7 \omega_e \sqrt{\frac{\mu_A}{D_e}} \qquad (5)$$

and,

$$r_e = \sqrt{h/8\pi^2 c\mu B_e} = \frac{4.1061}{\sqrt{B_e \mu_A}} \qquad (6)$$

The dissociation energy D_e refers to the energy above the potential minimum instead of the lowest vibrational level, and may be expressed in the following form:

$$\begin{aligned} D_e &= D_0 + G(0) \\ &= D_0 + \tfrac{1}{2}\omega_e - \tfrac{1}{4}\omega_e X_e + \tfrac{1}{8}\omega_e Y_e - \tfrac{1}{16}\omega_e Z_e \end{aligned} \qquad (7)$$

The definition and value of the pertinent symbols in the above equations are as follows:

B_e = 18.86(7) cm^{-1}, rotational constant in the equilibrium position

D_e = 39188.19 cm^{-1}, dissociation energy referred to the minimum of the potential curve

e = natural logarithm base

μ_A = 0.948376 (Atomic-weight units), reduced mass of OH

r = internuclear distance in cm

r_e = 0.9707 × 10^{-8} cm, equilibrium internuclear distance

ω_e = 3738.48 cm^{-1}, fundamental vibrational constant of OH in the ground state

In Figure 3 the energy values have been plotted for r = 0.60–3.00 (10^{-8} cm), and the observed

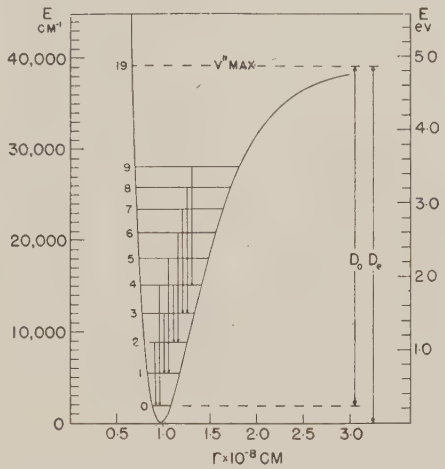

FIG. 3. Potential energy curve for OH ground state.

TABLE 3

r × 10^{-8} cm	E cm^{-1}	r × 10^{-8}	E cm^{-1}
0.60	65571	1.85	29011
0.65	43249	1.90	30017
0.70	27222	1.95	30930
0.75	16003	2.00	31759
0.80	8492	2.05	32509
0.85	3775	2.10	33183
0.90	1153	2.15	33799
0.95	89	2.20	34347
1.00	158	2.25	34848
1.05	1038	2.30	35293
1.10	2476	2.35	35696
1.15	4286	2.40	36063
1.20	6321	2.45	36387
1.25	8472	2.50	36674
1.30	10664	2.55	36941
1.35	12836	2.60	37177
1.40	14948	2.65	37383
1.45	16974	2.70	37574
1.50	18893	2.75	37744
1.55	20695	2.80	37890
1.60	22378	2.85	38029
1.65	23938	2.90	38153
1.70	25375	2.95	38261
1.75	26697	3.00	38362
1.80	27907		

transitions in the $^2\Pi$ ground state have been indicated. In order that the potential energy curve of OH as computed from the Morse[10] formula may

be compared with those computed from other potential functions, a list of the computed values used in Figure 3 is given in Table 3.

Conclusion

The redetermined value of D_0(OH) raises the question of the adequacy of the internal partition functions which may in the past have been used for calculating the thermodynamic quantities of OH. If temperatures high enough to necessitate consideration of the upper electronic state were involved, it may be necessary to evaluate again the vibrational contribution, including the anharmonicity, to the partition function for some of the thermodynamic properties of OH.

REFERENCES

1. Herman, R. C., and Hornbeck, G. A.: Astrophys. J., *118*, 214 (1953).
2. Gaydon, A. G.: *Dissociation Energies.* London, Chapman and Hall, Ltd., 1952.
3. Benedict, W. S., Plyler, E. K., and Humphreys, C. J.: J. Chem. Phys., *21*, 398 (1953).
4. Dejardin, G., Janin, J., and Peyron, M.: C. R. Acad. Sci. (Paris), *234*, 1866 (1952); *235*, 538 (1952).
5. Dejardin, G., Janin, J., and Peyron, M.: Phys. Rev., *90*, 359 (1953).
6. Meinel, A. B.: Astrophys. J., *111*, 555 (1950); *112*, 120 (1950).
7. Chamberlain, J. W., and Oliver, N. J.: Phys. Rev., *90*, 1118 (1953).
8. Birge, R. T., and Sponer, H.: Phys. Rev., *28*, 259 (1926).
9. DuMond, J. W. M., and Cohen, E. R.: Rev. Mod. Phys., *25*, 691 (1953).
10. Morse, P. M.: Phys. Rev. *34*, 57 (1929).
11. Hulbert, H. M., and Hirschfelder, J. O.: J. Chem. Phys. *9*, 61 (1941).
12. Herzberg, G.: *Spectra of Diatomic Molecules*, 2nd ed., New York, D. Van Nostrand Co., Inc., 1950.

Panel Discussions

1

HETEROGENEOUS BURNING

Panel Members

Hoyt C. Hottel, *Chairman*
David Altman
Sabri Ergun
Glenn C. Williams

The chairman introduced the subject with comments on the complications introduced into the combustion process, as encountered in practical devices, by the presence of fuels in liquid or in solid form, then called on Professor Altman for remarks on the burning of liquid droplets.

Professor Altman. "It has been recognized for some time that the gross characteristics of heterogeneous combustion in jet engines and furnaces are determined largely by the physical-chemical constants of the combustibles and the fluid dynamic characteristics of the system rather than the chemical reaction rate data alone. Thus, if one considers a diversified group of combustibles in which the chemical rate constants for the reactions vary by orders of magnitude, the volume requirements of the combustion chambers are found to vary only by small factors, perhaps 2 or 3. The immediate inference is, therefore, that heterogeneous combustion involving liquid droplets has in common a process which is not primarily dependent upon the reaction rates characterizing the combustion reaction. This is not to deny the importance of the chemical aspects in affecting control over certain aspects of combustion, as for instance in the application of tetraethyl lead in internal combustion engines. It appears rather that the overall nondetonative process is one which combines fluid dynamics with chemistry and in which the basic considerations of heat and mass flow appear of greater importance. For this reason the theoretical treatments of burning of droplets as has been developed by Spalding, Godsave and others at this Symposium contain as the essential theme the balance of heat and mass flow, and ignore almost completely kinetics. In one case which I would like to discuss later, Spalding has invoked the qualitative concepts of chemical rates to explain the 'extinction' phenomenon of small burning droplets resulting either from minute size or high flow velocity of air past the droplet.

"There are several interesting aspects of the combustion of liquid droplets which I think could provide further discussion and consideration:

(1) Temperature penetration into the droplet

"A simplified theory for droplet combustion generally assumes steady-state conditions of heat and mass flow and ignores the radiation effects of the flame front. Godsave has investigated the problem of radiation effects and concluded that it could be as high as 20 per cent of the overall heat transfer rate, and has also shown that if a burning droplet surface is assumed to be near its boiling point, the temperature at the center of the droplet should be expected to increase with time resulting from conduction. This phenomenon of heating at the center of the droplet has been observed experimentally by Hottel in hydrocarbon combustibles where tarry residues are observed to exist within the drop near the end of burning. With regard to these two effects, it should be noted that the occurrence of radiation heat transfer cannot be treated by a simple modification of the heat transfer coefficient because the radiative heat flow is governed essentially by Beer's law, and therefore shows a different temperature penetration from heat transfer governed

by a conduction process. The second consideration is that if heat flows into the center of the droplet by conduction then the overall process obviously cannot be steady-state. In some of the fuels studied by Godsave, for instance, it can be shown that the deviations from steady-state amount to 30 per cent or more when the enthalpy of the liquid at the surface temperature, above that at the ambient temperature, is an appreciable fraction of the latent heat. The result of this effect is to cause the burning rate to increase continually during burning and finally exceed the value predicted from steady-state considerations. The droplet lifetime, however, should be little affected because of the cancellation of the burning rate deviations from the theory at earlier and later times.

(2) Flame extinction

"Zeldovich was the first to treat flame extinction for a system of initially unmixed gases as a function of the relative flow velocities of the fuel and oxidizer. The explanation states that the burning would be expected to depend primarily on the rates of mass transfer of fuel and oxidizer to the combustion surface, which would depend largely on the relative flow velocities of the two components. Since chemical kinetics can support only a certain maximum conversion rate which would occur if the fuel and oxidizer combine at a temperature near the flame temperature, there is a limitation to the maximum rate of combustion in such a system. This concept was applied by Spalding to explain the phenomenon of flame 'extinction' which he observed on flow of air past droplets. The concept is based on the fact that the combustion zone is of finite width, and hence fuel and oxidizer coexist for a finite time. Since the chemical rates are finite it is clear that there is a limitation of mass flux of oxidizer and fuel into the combustion zone. It follows from this reasoning that if a relative flow velocity exists requiring a flux of oxidizer into the combustion region exceeding this limit a breakdown of the steady-state must occur. Spalding has expanded this thinking and concluded this limit occurs when the quantity U/d is of the order of 100 sec^{-1}. For a droplet 1000 μ in size this velocity is 10 cm/sec. It is clear, therefore, that in combustion chambers where relative velocities of this magnitude and larger are to be expected, droplets probably burn with a front portion of their surface extinguished. This consideration is therefore important in the application of the droplet burning data to combustion chambers.

"Further consequence of this reasoning indicates that extinction should also occur for droplets that attain very small size. It has been shown both experimentally and theoretically that the burning rate per unit area of surface varies inversely with the droplet radius. Since there is an upper limit to the combustion rate which determines the mass flow rate per unit area, it follows that there must be a lower limit to the droplet radius for steady burning.

(3) Vaporization of multicomponent mixtures

"Since droplet burning is assumed to occur as a vaporization process at the liquid surface, it is interesting to inquire whether multicomponent mixtures vaporize by equilibrium distillation or by flash vaporization in which both low and high boiling constituents vaporize in proportion to their concentration in the liquid phase. It appears from the work of Hottel and coworkers that, for hydrocarbon droplets burning in furnaces where the lifetime is of the order of a few tenths to 1 sec, equilibrium distillation occurs approximately according to Raoult's law. This result implies that diffusion in the liquid phase is rapid enough to keep up with the rate of selective distillation. For small droplets with high characteristic flame temperatures, however, the vaporization rates per unit area of surface are much larger. It may be more difficult to satisfy the requirements of equilibrium distillation. Such a condition may occur for instance in rocket motor chambers where flame temperatures are high and droplet sizes small.

(4) Flame temperature

"From the simple theory of droplet burning where the combustion surface is assumed to be infinitesimal in thickness, the temperature at this surface is determined by balancing the heat generation resulting from the flow of reactants to this surface with the conductive heat loss away from the surface along the temperature gradients. This was shown by Goldsmith and Penner to lead to a nonadiabatic temperature many hundreds of degrees higher than the adiabatic flame temperature in some systems. Such a conclusion is fictitious in that it assumes complete spherical symmetry which is generally not realized in practice, and it assumes infinite reaction rates.

However, since the same principle of heat balance can be applied to real systems it is interesting to inquire what temperatures would realistically occur in a physical system. It seems obvious, however, that in a system with free or forced convection where reaction rates are finite, a small element of combustion products will be essentially at its adiabatic temperature when first formed if molecular diffusion of reactant or inert into the element is small.

(5) Application to combustion volume calculations

"Although the present theory for droplet burning provides a characteristic lifetime for the droplet in the appropriate oxidizing atmosphere, several considerations must be made prior to the application of such data to the estimation of combustion volumes. One such important consideration is the velocity lag of the droplet with respect to the flowing gas stream. Miesse has recently published a calculation of the residence time requirement of liquid droplets in a rocket motor by considering the distance travelled by a burning droplet in an assumed velocity field which was considered characteristic of rocket motors. Miesse used burning rate data given by the theoretical expressions, with a suitable correction for the Reynold's number as given by Frossling. These calculations were interesting and showed that, for drops of representative size, a reasonable residence time for the characteristic length of the rocket motors could be obtained. Such a calculation is simplified because of the neglect of the statistical variation of droplet size and injection velocity and because of the neglect of the influence of the burning rate on the local velocity flow field. However, the work represents a good initial attempt at applying some of the concepts of droplet burning to combustion in an actual engine.

(6) Ignition of drops

"An additional consideration of importance is the ignition time of the droplet. Thus, spontaneous ignition of the droplet may be presumed to occur when the droplet surface has been heated sufficiently to provide the critical concentration of vapor in the oxidizer for ignition at the temperature near the droplet surface. In the experiments performed by Kobayasi and Nishiwaki described at this symposium it was shown that ignition occurs after an appreciable lapse of time when the droplet is subjected to a heated atmosphere. In a jet engine the heated atmosphere is the flame and therefore corresponds to a relatively severe condition for heat flux. It may be presumed, therefore, that the ignition correction for such a condition represents a time which is small compared with the lifetime of the droplet."

Professor Altman's comments were followed by a floor discussion indicating lack of agreement as to whether existing treatments of droplet burning rates, based on assumptions of radial symmetry and allowing for the variation of physical properties through the gas near the liquid surface, are capable of predicting burning times from primary data within a factor closer than 2 or 3.

Professor Williams emphasized the need for identifying drop size in making generalizations concerning individual droplet burning. A graph was presented (reproduced elsewhere in this volume) showing the influence of drop size and furnace temperature on the relative importance of radiation and convection, and indicating a complete reversal of their relative importance within the range of practical interest in droplet burning.

The discussion then turned to the reactions of solid carbon with gas. Dr. Ergun spoke on recent developments in correlating data on the reactions of CO_2 and H_2O with carbons of different reactivity.

Dr. Ergun. "The kinetics of the surface reaction of carbon dioxide with carbons (charcoal, activated carbon, and natural graphite) has been determined at 700 to 1400°C and atmospheric pressure. For the first time it has been demonstrated that carbons of different porosity and crystallinity, regardless of source, can be treated on a common basis. This result was achieved by considering the kinetic problem on fundamental grounds and by solving the ancillary problems arising from fluid flow and diffusion.

"For the case of reaction of carbon dioxide with carbon, the surface reaction involves a labile equilibrium,

$$CO_2 + C_F \underset{k_1'}{\overset{k_1}{\rightleftharpoons}} CO + C_O \qquad (1)$$

where C_F is a bare carbon atom on the surface acting as a site, and C_O is a carbon atom on the surface chemically combined with an oxygen atom. This reaction is accompanied by the conversion of an occupied site to a carbon monoxide

molecule according to the reaction

$$C_O \xrightarrow{k_3} CO. \qquad (2)$$

"Reaction (1) is the oxygen exchange between carbon dioxide and carbon monoxide in the gas phase and occupied and free sites in the solid phase. Experimental results as well as theoretical considerations show that the equilibrium constant of the exchange reaction is independent of the type of carbon. This fact indicates an identity in the energy and chemical nature of the sites of all carbons with trigonal (coplanar) bonds. The heat of reaction of the equilibrium, as calculated from the temperature coefficient, is 23,000 cal/mol. The equilibrium is labile at temperatures both above and below gasification temperatures.

"Reaction (2), the gasification step, is slower than reaction (1). It represents the transfer of carbon atoms from the solid phase to the gas phase. The energy of activation of the gasification step, 59,000 cal/mol, as determined experimentally, was the same for all of the carbons investigated. This agreement also indicates that the energy and chemical nature of the reaction site are identical regardless of source of carbon.

"For the case of reaction of steam with carbon, the surface reaction involves oxygen exchange between steam and hydrogen in addition to that between carbon dioxide and carbon monoxide:

$$H_2O + C_F \underset{k_2'}{\overset{k_2}{\rightleftharpoons}} H_2 + C_O \qquad (3)$$

The gasification step is the same as in the case of carbon dioxide, namely, equation (2). Formation of carbon monoxide, equation (2), and subsequent surface reaction according to equation (1) lead to the formation of carbon dioxide. In the case of gasification with steam, reactions (1) and (3) occur, therefore, simultaneously and result in the water-gas-shift reaction:

$$H_2O + CO \rightleftharpoons H_2 + CO_2. \qquad (4)$$

A simultaneous labile equilibrium of the reactions indicated by equations (1) and (3) results in the water-gas-shift equilibrium in the gas phase. When steam was employed, the energy of activation of the gasification step was found to be the same as in the case of carbon dioxide, and remained the same for all carbons.

"The rate constants k_1, k_1', k_2, k_2', and k_3 are general rate constants, that is, probability factors, and functions of temperature only. The present theoretical development and the experimental results show that the differences in the rates of reactions of various carbons are due to the numbers of reaction sites per unit weight. The relative numbers of these sites for the widely different carbons investigated ranged from 1 to only 100, and yet accounted for the differences in the overall reaction rates in the temperature range of 700 to 1400°C."

Professor Williams then discussed briefly the problem of ignition of carbon in air. Making reasonable assumptions as to the nature of (1) resistance to counterdiffusion of oxygen and combustion products near a carbon surface, (2) rate of chemical reaction at the surface, (3) heat transfer by convection from the carbon surface to the ambient gas, and (4) radiant heat exchange between the carbon and its surroundings, one may show that for a particular set of conditions of gas velocity, carbon type and radiation view-factor, there is a critical ambient gas temperature below which the carbon will not ignite and continue to burn without external addition, no matter what initial temperature it is given. Between this lower critical ambient-gas temperature and a second or upper critical gas temperature, there is a characteristic "ignition" temperature of the carbon surface which is a function of the gas temperature. If an external heat supply is applied to bring the carbon to any point below this ignition line and then withdrawn, the "fire will go out"; if the carbon is brought to any point above the line, sustained burning occurs and the carbon surface reaches a new equilibrium temperature much higher than the ambient-gas temperature[1]. Finally, if the ambient gas temperature is above its second critical value, the carbon will ignite without auxiliary heat addition and come to its equilibrium burning temperature. Thus the concept of an ignition temperature, widely used in industry, needs replacement by an ignition line the shape of which is calculable from a well-designed experiment on the solid fuel in question.

REFERENCE

1. Smith, F. W. *Predicted Combustion Characteristics of Brush Carbon Spheres in High-Velocity Air.* M. I. T. Meteor Report No. 6, January, 1947.

2

STATUS OF THE THEORY OF THE KINETICS OF COMBUSTION REACTIONS

Panel Members

A. R. Ubbelohde, *Chairman*
George Porter
John M. Richardson
Kurt E. Shuler

In addition to the panel members, others taking part in the discussion included Dr. Altman, Dr. Avery, Dr. Anderson, Mr. Bahn, Professor Bawn, Dr. Cullis, Dr. Ferguson, Mr. Grumer, Dr. Bernard Lewis, Mr. Levedahl, Dr. Minkoff, Dr. Matsen, Dr. Napier, Dr. Penner, Dr. Powell, Mr. Robison, Dr. Schultz, Dr. Steinberg, Dr. Wolfhard, Dr. Wise and Dr. Weinberg. Written commentaries supplementing points made in the discussion were also received from Dr. Cassel, Dr. Ferguson and Mr. Robison.

After introducing the discussion leaders to those present in the body of the auditorium, Professor Ubbelohde explained the factors which had determined the choice of themes for discussion. At present, many branches of the kinetic theory of combustion processes have reached a stage where the theoretical concepts are fairly clear, but where new experimental facts are essential before real progress can be made. Though much valuable experimental work is going on, in many cases new experimental techniques seem to be required to provide really novel information, without which theories cannot decide between conflicting views. For example, many studies have been reported on induction period phenomena, and on other build-up processes in a combustion system, such as cool-flame pulses, or the transition from burning to detonation when a flame travels along a tube containing a detonating mixture. It is generally agreed that some kind of physico-chemical transformation is taking place during any build-up period, and in certain cases quite plausible explanations have been suggested. But in these cases conclusive advances in theory seem to require new methods to obtain new facts to establish which transformations are really significant. Another example where theory now seems to have outstripped experiment is in the domain of radical-chain mechanisms of combustion. Quite plausible steps in these mechanisms are widely accepted in interpreting the main features of many combustion processes in the gas phase, and probably also in the liquid phase. But new facts are needed to substantiate the free radicals which are postulated, and to characterize their most important physico-chemical parameters, such as heats of formation, valency states, steric configurations and effective collision diameters.

The present discussion did not aim to echo the perennial demand for new facts to fill out quite plausible theories of combustion. The plan was rather to select branches of theory where even the theoretical possibilities seem to call for new concepts and fresh approaches. Important themes presented to the meeting for consideration included the following:

(1) What are the relationships between combustion kinetics at really high temperatures, and the reactions studied at fairly low temperatures? Are the important steps quite different in the two extremes, or is some kind of extrapolation permissible?

(2) What are the possible mechanisms of carbon formation in combustion systems? Are new theories required to account for the formation of a polymer in gas-phase combustion, or is carbon formation primarily heterogeneous?

(3) What factors determine the stability of those free radicals and labile molecules generally important for combustion? How far is it necessary to have a 3-body encounter to ensure a lifetime for a labile molecule freshly formed by collision which shall be large compared with the duration of the collision?

(4) How important is the transfer of internal energy in combustion kinetics involving chain mechanisms? A closely related problem is to account for the production of labile molecules in combustion, when their internal energy is markedly out of balance with their translational energy.

(5) Does the combustion of aromatic compounds follow the same basic steps as for aliphatic and alicyclic compounds?

In the course of the discussion which followed, it became apparent that themes (3) and (4) often

had a bearing on (1) and (2), although by reason of the many contributions made only the first two themes could be covered. No attempt was made to deal with (5), although it was pointed out that with the newer catalytic processes for transforming crude hydrocarbons, the combustion mechanisms of aromatic compounds would acquire increasing practical importance.

Correlation of low and high temperature kinetics and mechanisms

For the purpose of this discussion, high temperature is taken as the region between 1000 to 3000°K. This is the temperature regime which one usually finds for premixed flames and in which most of the elementary flame reactions take place. There is very little experimental work available on chemical kinetics at these temperatures and hardly any theoretical work has been carried out to determine the possible effects of these high temperatures on the kinetics of elementary processes.

There was some discussion about the theoretical implications of various vector processes which are so characteristic of applications of combustion at high temperatures as in diffusion flames, turbulent combustion systems, explosions, and detonations. Vector processes complicate the study of high temperature kinetics, and in many ways the best hope of experimental advances lies in the study of thermal reaction systems where the effects of vector processes are either absent or have been minimized. Examples of such systems include shock tubes, where the shock intensity is not too large, and stirred homogeneous reactors of the type used by Longwell.

One main feature which would appear to distinguish high temperature kinetics is the much larger amount of energy which is found in the reaction system. This energy may either (1) originate externally from a heat bath, (2) be furnished internally by the exothermicity of the chemical reactions, or (3) appear as heat of compression in a shock wave.

Some of the possible consequences of this high energy content in a reaction system may be listed.

(1) Nonequilibrium energy distributions may appear among reactants and products in fast, high temperature reactions. This may necessitate the reformulation of the theory of reaction rates along nonequilibrium lines.

Certain vector processes, such as diffusion in flames, or mass flow in detonation waves, can disturb the nonequilibrium distribution directionally. While these directional effects are of great practical significance, a chemical rate process is intrinsically a scalar quantity. In the first instance the effects of nonequilibrium distribution should be amenable to theoretical discussion regardless of vector processes.

(2) High concentrations of electronically and/or vibrationally excited species may be formed, possibly in excess of their thermal equilibrium value, with the attending possibility of energy chains.

Although energy chains are likely to be of importance in several combustion processes, little specific information about their role is as yet available. It was agreed to treat energy chains as a principal theme for discussion at a later stage.

(3) Large numbers of atoms and radicals *per se* may be produced either in their equilibrium concentrations or in excess of equilibrium. This may lead to a modification of the commonly accepted low temperature mechanisms owing to the possibility of radical-radical reactions.

One consequence of the much higher proportion of labile molecules at high temperatures is that competition between alternative combustion reactions will depend more markedly on steric factors (the "P" factor in reaction kinetics) than on differences of activation energy.

Specific attention was drawn to the change in oxygen as temperature rises, since oxygen forms the oxidizing agent in so many combustions. Although O_2 can be regarded as a free radical at low temperatures, the bond between the atoms is very strong. Below about 1000°K oxidation processes involving molecular oxygen tend to keep the O—O bond intact, for example by forming hydroperoxides. At higher temperatures the splitting of this bond at a very early stage of the reaction sequence becomes much more likely.

(4) Diatomic and triatomic radicals, such as OH, CH, HCO, NH_2, etc., may be formed at high temperatures, in contrast to the polyatomic radicals which are usually observed in low temperature (cool) flame reactions. The appearance of these radicals in the reaction system may necessitate a modification of the low temperature reaction mechanisms.

Spectroscopic methods of study using ultraviolet emission, which often predominate in experiments on high temperature combustion, tend to reveal the simple labile molecules more readily. Since the presence of the larger polyatomic molecules is not easy to observe spectroscopically, it remains an open question whether in high tem-

perature combustion polyatomic molecules retain some kind of skeleton during a number of steps in the combustion sequence ultimately leading to carbon dioxide and water, or whether they dissociate into smaller fragments at a very early stage. This problem also has some bearing on possible mechanisms of carbon formation, discussed below.

Finally, combustion at high temperatures frequently also involves high pressures in practical applications. High pressures may bias the reaction kinetics in favor of bi-and-ter molecular reactions, and away from chain mechanisms.

Carbon formation

No less than four different theories of carbon formation have been proposed. It is indeed conceivable that different mechanisms may operate under different conditions.

One basic distinction is to determine whether the carbon is formed heterogeneously, on preexisting walls or on the surface of solid particles, or alternatively whether there is a build-up of carbon by formation of a polymer in the gas phase, not unlike the polymerization of vaporized methyl methacrylate, or ethylene. When a surface is necessary, this immediately makes experiments requiring probes very dubious to interpret.

A related question is whether the solid product described as "carbon" or "soot" really is substantially graphitized, or whether the content of hydrogen and other atoms is sufficiently large to make it more realistic to consider the soot as an organic polymer with merely a very high C:H and C:O ratio.

Two of the mechanisms proposed fit the possibility that the product is essentially carbon, and not an organic polymer. However, the proposed reaction (Boudouard and Behrens) $CO + CO \rightleftarrows CO_2 + C_S$ certainly requires a solid phase on which the carbon is to be deposited, to be energetically plausible. It seems unlikely to apply to flames. The hypothesis (Smith) that the first step in carbon formation is the production of the molecule (C_2) gas is again rather improbable energetically, and is not supported by spectroscopic evidence.

Many observations were reported on the color changes in flames accompanying carbon formation, but without spectroscopic analysis the information given by color changes can only be qualitative. There is no spectroscopic evidence against the alternative theory supported by Norrish, in which the fuel breaks down even further to carbon atoms, but thermochemical considerations rule this out with some certainty.

A second pair of mechanisms postulates that a highly unsaturated hydrocarbon is first formed from the fuel. This is supposed to polymerize and to become stripped of hydrogen to form "carbon." Gaydon and Wolfhard prefer the view that the fuel skeleton is preserved and merely becomes so unsaturated that polymerization ensues. Porter assumes that the fuel somehow breaks up to form acetylene. This then polymerizes by a well known exothermic reaction and becomes stripped of its hydrogen.

Some doubt was expressed whether the stripping of hydrogen from off the postulated polymer could really take place in a single collision. The kinetic theory of the supposed stripping process clearly needs elucidation.

These views do not deal with the problem, whether "soot" or "carbon" formed from aromatic hydrocarbons is different in structure from "soot" with an aliphatic origin. If a molecular skeleton is preserved preceding polymerization, it might be expected that aromatic soots would be more highly graphitized and less hydrogenated. Another way of producing soot free from hydrogen is to start with hexachlor-benzene and to treat it with sodium vapor. The abundant production of carbon when hydrocarbons are burned in fluorine would also repay further study. More scientific studies to characterize the soot as to particle size, crystal structure, and occluded atoms seem desirable to elucidate the problem of the origin of the carbon.

Much information from the carbon black industry suggests that when carbon is formed, mainly in diffusion flames, the interior of the particles is more highly graphitized and contains less hydrogen than the surface. The shape of the particles obtained depends on the originating hydrocarbon used, and differs, for example, for benzene or acetylene.

By using propane with the central carbon atom labeled radioactively, with C^{13}, it may be possible to decide how far the fuel skeleton breaks up before polymerizing. In the processes

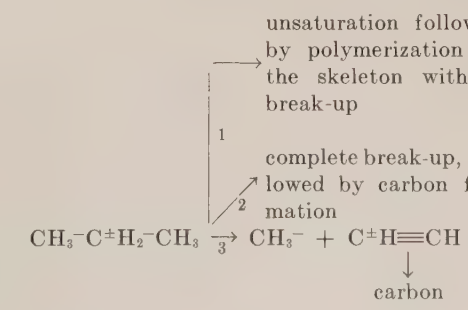

the first two mechanisms would lead to soot with the same ratio of $C^{\pm}$ to C as in the parent hydrocarbon. The third process in which only the acetylene forms carbon should lead to a calculable enhancement of the $C^{\pm}$:C ratio in the soot. Experiments along these lines are in progress at the National Bureau of Standards.

A further theoretical possibility is that oxygen plays a very positive role in inducing polymerization, just as it affects the decomposition of certain organic molecules such as acetaldehyde. Partly oxygenated products may also polymerize to form "soots" much more readily and at lower concentrations than acetylene.

Date Due ONE MONTH AFTER THE LAST DATE STAMPED BELOW

DEC 4 1967				
DEC 5 - 1967				
NOV 18 1969 -HL				

10 002069813
UNIVERSITY OF HAWAII

QD 516
S92
1954

Symposium... 56-1577

University of Hawaii Library

RULES

1. Books may be kept two weeks and may be renewed once.

2. A fine will be charged on each book which is not returned according to the above rule.

3. All injuries to books beyond reasonable wear, and all losses shall be made good to the satisfaction of the Librarian.

4. Each borrower is held responsible for all books drawn on his card and for all fines accruing on the same.